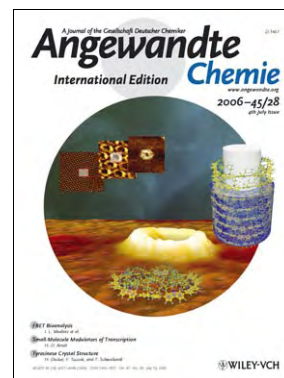


## Cover Picture

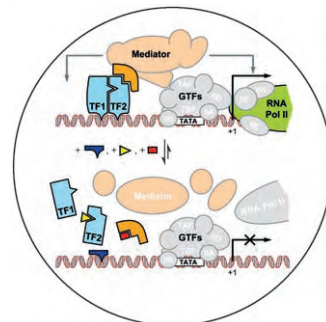
**Sung-Hyun Jung, Wojciech Pisula, Ali Rouhanipour,  
Hans Joachim Räder, Josemon Jacob, and Klaus Müllen\***

***Like the rings of Saturn*** a fully conjugated cyclododeca-2,7-carbazole surrounds a porphyrin template. The macrocycle can be released from the template. The cover shows a single-molecule STM measurement with the structure of cyclododeca-2,7-carbazole in the foreground. The tunneling current is dominated by the conjugated cyclic structure and shows an “electronic hole” in the center. For further details on these molecules and their self-assembly into columnar stacks see the Communication by K. Müllen et al. on page 4685 ff.



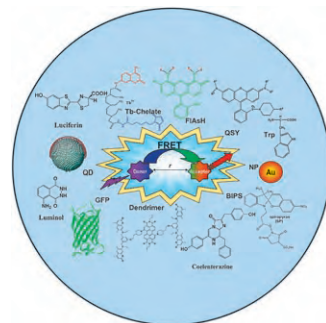
### ***Transcription Factors***

Small-molecule ligands that can modulate gene transcription by interacting with different sites on multiprotein complexes and thereby exerting different functions have been described by H.-D. Arndt in his Minireview on page 4552 ff.



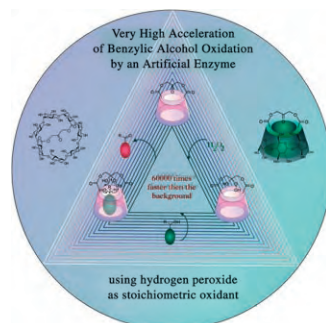
### ***Bioanalysis***

Modern bioanalytical techniques based on fluorescence resonance energy transfer (FRET) are discussed by I. L. Medintz and co-workers in their Review on page 4562 ff. Particular emphasis is given to novel donor and acceptor materials and the combination of different classes of materials.



### ***Supramolecular Chemistry***

In their Communication on page 4590 ff., L. G. Marinescu and M. Bols show that at neutral pH and ambient temperature, hydrogen peroxide and benzyl alcohols meet in the active site of a cyclodextrin-derived ketone and react up to 60000 times faster than they do outside the cyclodextrin.





The following Communications have been judged by at least two referees to be “very important papers” and will be published online at [www.angewandte.org](http://www.angewandte.org) soon:

J. M. Goicoechea, S. C. Sevov\*

[Zn<sub>9</sub>Bi<sub>11</sub>]<sup>5-</sup>: A Ligand-Free Intermetalloid Cluster

W. Su, S. Raders, J. G. Verkade,\* X. Liao, J. F. Hartwig\*

Palladium-Catalyzed  $\alpha$ -Arylation of Trimethylsilyl Enol Ethers with Aryl Bromides and Chlorides: A Synergistic Effect of Two Metal Fluorides as Additives

A. Abo-Riziq, B. O. Crews, M. P. Callahan, L. Grace, M. S. de Vries\*  
Spectroscopy of Isolated Gramicidin Peptides

V. Lemieux, S. Gauthier, N. R. Branda\*

Selective and Sequential Photorelease Using Molecular Switches

C. Ye,\* Y. Bando, G. Shen, D. Golberg

Formation of Single-Crystalline SrAl<sub>2</sub>O<sub>4</sub> Nanotubes by a Roll-Up and Post-Annealing Approach

A. Narayanaswamy, H. Xu, N. Pradhan, X. Peng\*

Single-Crystal Nanoflowers with Different Chemical Compositions and Physical Properties Grown by Limited Ligand Protection

## Meeting Reviews

The Evolution of Stereochemistry

H.-D. Arndt \_\_\_\_\_ 4542

## Books

Nanoscale Assembly

Wilhelm T. S. Huck

reviewed by E. Dujardin \_\_\_\_\_ 4544

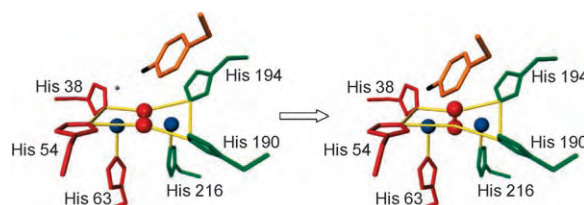
## Highlights

### Metalloenzymes

H. Decker,\* T. Schweikardt,

F. Tuczek\* \_\_\_\_\_ 4546 – 4550

The First Crystal Structure of Tyrosinase:  
All Questions Answered?



**Tyrosinases** are essential enzymes that occur in all organisms and belong to the class of type3 copper proteins. The first crystal structure of a tyrosinase (from *Streptomyces castaneoglobisporus*) has been achieved and offers important

insights into the mechanism of phenol hydroxylation (see scheme; Cu blue, O red, substrate orange; *trans*-axial position on CuA: gray dot), the process of activation, and the incorporation of copper.

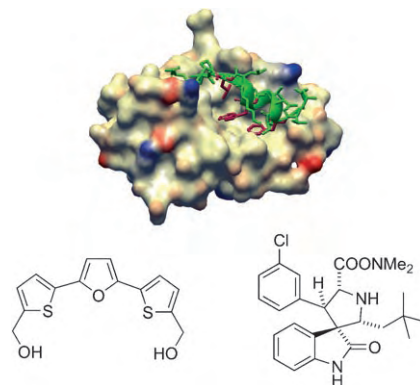
## Minireviews

### Gene Transcription

H.-D. Arndt\* \_\_\_\_\_ 4552 – 4560

Small Molecule Modulators of Transcription

**Small can do too:** Recent research on transcriptional factors has uncovered small-molecule ligands that are able to modulate gene transcription by interacting with multiprotein complexes. Some of these compounds bind to different sites on the target proteins and therefore exert different functions. The picture shows the association of the HDM2 protein (bronze) with the tumor suppressor p53 (green), and two small molecules that influence p53 function positively.

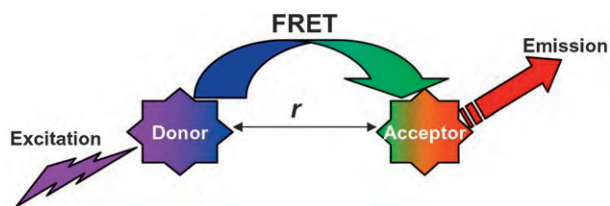


## Reviews

### Bioanalysis

K. E. Sapsford, L. Berti,  
I. L. Medintz\* — 4562–4589

Materials for Fluorescence Resonance  
Energy Transfer Analysis: Beyond  
Traditional Donor–Acceptor  
Combinations



**Dye another day:** Modern donor and acceptor materials for fluorescence resonance energy transfer (FRET) analyses (see picture) comprise photochromic dyes, semiconductor nanocrystals, nanoparticles, fluorescent amino acids, polymers, and genetically encoded protein, in

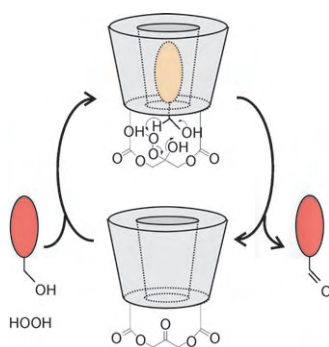
addition to “traditional” organic dyes. The scope and boundaries of such systems, as well as available methods for bioconjugation are discussed, with an emphasis on the combination of different materials.

## Communications

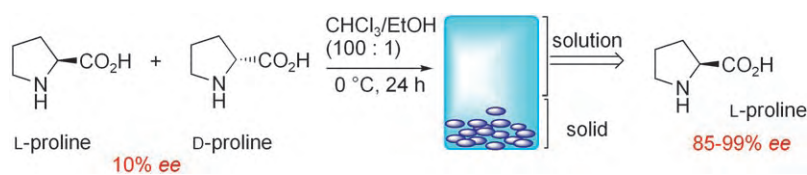
### Artificial Enzymes

L. G. Marinescu, M. Bols\* — 4590–4593

Very High Rate Enhancement of Benzyl  
Alcohol Oxidation by an Artificial Enzyme



**Promoting the atomic dialogue!** At neutral pH and ambient temperature, a cyclodextrin-derived ketone causes hydrogen peroxide and benzyl alcohols to meet in its active site and react up to 60000 times faster than they do outside the cyclodextrin.



**A clue to the origin of chirality?** A solution of proline with high enantiomeric excess (85–99% *ee*) was obtained from solid proline of only 10% *ee* through novel

dissolution and crystallization processes (see scheme). This observation may be an explanation for the origin of chirality on Earth.

### Enantiomeric Enrichment

Y. Hayashi,\* M. Matsuzawa, J. Yamaguchi,  
S. Yonehara, Y. Matsumoto, M. Shoji,  
D. Hashizume, H. Koshino — 4593–4597

Large Nonlinear Effect Observed in the  
Enantiomeric Excess of Proline in Solution  
and That in the Solid State

#### For the USA and Canada:

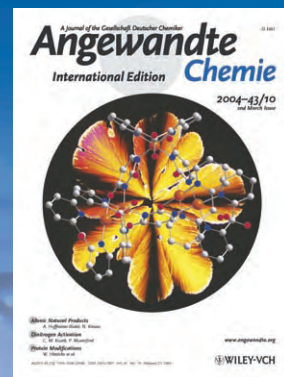
ANGEWANDTE CHEMIE International  
Edition (ISSN 1433-7851) is published weekly  
by Wiley-VCH PO Box 191161, D 69451 Wein-  
heim, Germany. Air freight and mailing in the  
USA by Publications Expediting Inc. 200

Meacham Ave., Elmont, NY 11003. Periodicals  
postage paid at Jamaica NY 11431. US POST-  
MASTER: send address changes to *Angewandte  
Chemie*, Wiley-VCH, 111 River Street, Hoboken,  
NJ 07030. Annual subscription price for insti-  
tutions: US\$ 5685/5168 (valid for print and

electronic / print or electronic delivery); for  
individuals who are personal members of a  
national chemical society prices are available  
on request. Postage and handling charges  
included. All prices are subject to local VAT/  
sales tax.



# The best in chemistry – for more than a hundred years



A Journal of the Gesellschaft Deutscher Chemiker  
**Angewandte Chemie**  
International Edition

[www.angewandte.org](http://www.angewandte.org)

**1888:** The beginning  
of a success story

## Constant Innovations

- 1962:** First issue of the International Edition
- 1976:** Graphical abstracts
- 1979:** Cover pictures
- 1988:** Centenary of Angewandte
- 1989:** Routine use of color
- 1991:** New section: Highlights
- 1992:** Computerized editorial tracking system
- 1995:** Internet service for readers
- 1998:** Regular press service; full-text online
- 2000:** New section: Essays; EarlyView: Communications available online ahead of the printed version
- 2001:** New section: Minireviews
- 2002:** Online submission of manuscripts
- 2003:** Weekly publication; new section: News; new layout
- 2004:** Backfiles (1962-1997); ManuscriptXpress: Online system for authors and referees



## Angewandte's advisors...

**J. Fraser Stoddart**  
University of California,  
Los Angeles

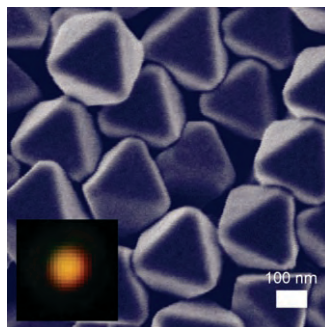
» When it comes to informing myself, I have two weekly fixations. The Economist and **Angewandte Chemie**. Both are compulsive browsing and there are many articles in each that are essential reading. I simply cannot afford not to know what's in every issue of **Angewandte**. Being on the board of **Angewandte Chemie** has been a real pleasure. Whether or not it's true, I have the feeling that I have really been able to influence how some of the most creative chemistry in my time has been presented to the scientific community at large. «

**Angewandte Chemie International Edition** is  
a journal of the German Chemical Society (GDCh)





**A scattering of silver:** Polyhedral silver nanocrystals display complex and distinct scattering signatures dictated by their shape and size (see picture). The ability to engineer specific plasmon modes should have profound consequences for surface-enhanced Raman spectroscopy, subwavelength optics, and plasmonic transport.



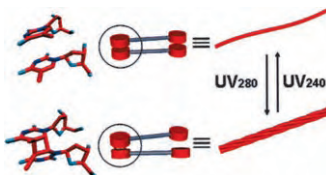
### Silver Nanocrystals



A. Tao, P. Sinsermsuksakul,  
P. Yang\* \_\_\_\_\_ 4597–4601

Polyhedral Silver Nanocrystals with  
Distinct Scattering Signatures

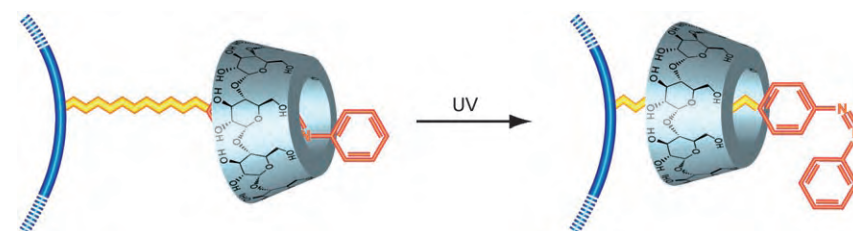
**Light twisting and untwisting:** UV light was found to drive reversible helical-nanofiber formation based on the photo-dimerization and photodissociation of the thymine residue in the 1,ω-thymidylic acid appended bolaamphiphile. <sup>1</sup>H NMR spectroscopy revealed that UV irradiation of the self-assembled nanofibers induces a helical structure through the formation of a *cis-syn* isomer of the thymine moiety.



### Helical Nanofibers

R. Iwaura, T. Shimizu\* \_\_\_\_\_ 4601–4604

Reversible Photochemical Conversion of  
Helicity in Self-Assembled Nanofibers  
from a 1,ω-Thymidylic Acid Appended  
Bolaamphiphile



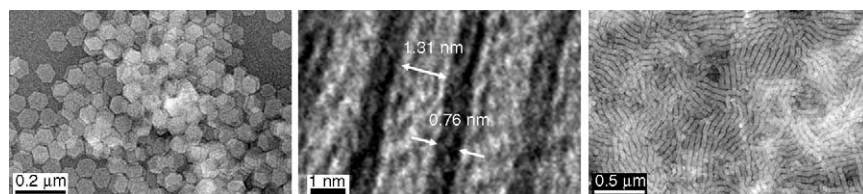
**A bit on the side:** A side-chain polyrotaxane that consists of simple components is successfully constructed and

controlled by using photoisomerization of  
an azobenzene moiety at the terminal of  
the side chain.

### Supramolecular Chemistry

I. Tomatsu, A. Hashidzume,  
A. Harada\* \_\_\_\_\_ 4605–4608

Cyclodextrin-Based Side-Chain  
Polyrotaxane with Unidirectional  
Inclusion in Aqueous Media



**Arrested precipitation** of  $\text{In}_2\text{S}_3$  affords ultrathin hexagonal nanoplates with 0.76-nm thickness and controllable sizes of 22–63 nm. The pictures show (from left to

right) TEM images of 63-nm nanoplates aligned parallel to a support, a side view of nanoplates, and 45-nm nanoplates self-assembled into microwires.

### Inorganic Nanoplates

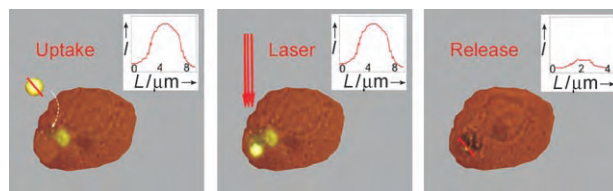
K. H. Park, K. Jang,  
S. U. Son\* \_\_\_\_\_ 4608–4612

Synthesis, Optical Properties, and Self-  
Assembly of Ultrathin Hexagonal  $\text{In}_2\text{S}_3$   
Nanoplates

## Drug Delivery

A. G. Skirtach,\* A. Muñoz Javier, O. Kreft,  
K. Köhler, A. Piera Alberola, H. Möhwald,  
W. J. Parak,\*  
G. B. Sukhorukov ————— 4612–4617

Laser-Induced Release of Encapsulated  
Materials inside Living Cells



**Escape route:** The laser-initiated release of fluorescently labeled polymers from polyelectrolyte-multilayer microcapsules is demonstrated inside living cancer cells. A polymer is incorporated in capsules with metal nanoparticles in their walls, which

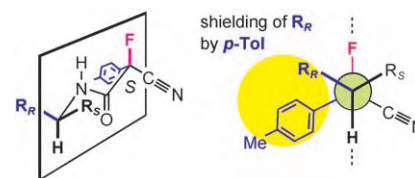
serve as light-absorbing centers. The capsules are internalized by cells and near-infrared light ruptures the walls of the capsules, thus releasing the content into the cells.

## Structure Elucidation

Y. Takeuchi,\* M. Segawa, H. Fujisawa,  
K. Omata, S. N. Lodwig,  
C. J. Unkefer ————— 4617–4619

The CFTA Method: A Reliable Procedure  
for the Determination of the Absolute  
Configuration of Chiral Primary Amines by  
<sup>1</sup>H NMR Spectroscopic Analysis

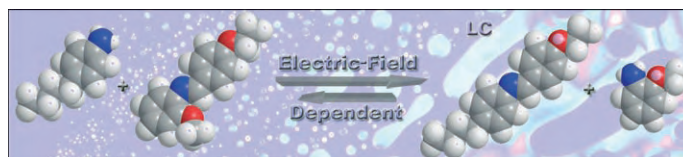
**Surprisingly stable** anti-periplanar conformers of CFTA amides form the basis of a new and very reliable method for determining the absolute configuration of chiral primary amines by <sup>1</sup>H NMR spectroscopy (see picture). CFTA = α-cyano-α-fluoro-*p*-tolylacetic acid.



## Dynamic Combinatorial Chemistry

N. Giuseppone, J.-M. Lehn\* 4619–4624

Electric-Field Modulation of Component  
Exchange in Constitutional Dynamic  
Liquid Crystals



**Playing the field:** Application of an electric field to the thermodynamic equilibria of constitutionally dynamic sets of imines and amines that contain an imine with liquid-crystalline properties and a negative dielectric anisotropy leads to the amplifi-

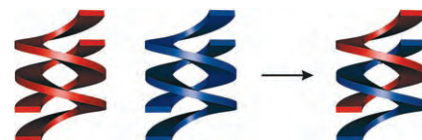
cation of the constituent that couples most strongly to the electric field, namely the liquid crystal (LC, see example). The field can thus induce a liquid to nematic phase transition.

## Helical Structures

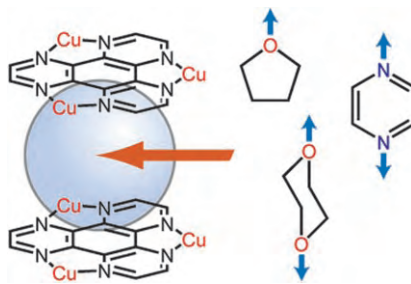
C. Zhan, J.-M. Léger, I. Huc\* 4625–4628

Cross-Hybridization of  
Pyridinedicarboxamide Helical Strands  
and Their *N*-Oxides

**Swapping partners:** The presence of *N*-oxide functions in double-helical dimers formed from oligo(pyridinedicarboxamide)s promotes heterodimerization (see picture). This process mimicks the essence of base pairing and information storage in DNA through heterologous A/T and G/C Watson–Crick base pairing.



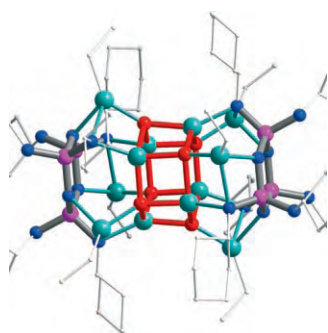
**Neutral organic guest molecules** are confined within the cavities of a porous coordination polymer. The key interaction is that of electron-deficient  $\pi$  planes of the polymer surface with electronegative atoms of the guest molecules (see picture). Evidence from thermogravimetric analysis suggests that guests with two electronegative atoms form more-stable complexes with the polymer than those with one electronegative atom.



### Host–Guest Systems

D. Tanaka, S. Masaoka, S. Horike, S. Furukawa, M. Mizuno, K. Endo, S. Kitagawa\* — 4628–4631

Porous Coordination Polymer with  $\pi$  Lewis Acidic Pore Surfaces,  $\{[\text{Cu}_3(\text{CN})_3\{\text{hat}(\text{CN})_3(\text{OEt})_3\}]\cdot 3\text{THF}\}_n$

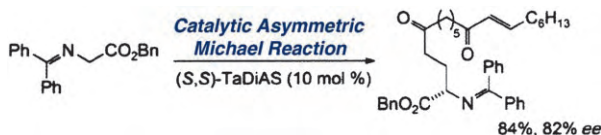


**Casting clusters from the mold:** Tris-(ethylzinc) phosphazenes exhibit a bowl-shaped coordination surface of three Lewis acidic EtZn moieties and three Lewis basic N sites. This surface provides a perfect mold for planar  $\{(\text{ZnO})_3\}$  rings and hexagonal  $\{(\text{ZnO})_6\}$  prisms. The zinc oxide clusters were generated in situ by reaction of phosphazene hydrates with diethylzinc.

### N,P Ligands

R. Boomishankar, P. I. Richards, A. Steiner\* — 4632–4634

Tris(organozinc) Phosphazenes as Templates for Trimeric and Hexameric Zinc Oxide Clusters



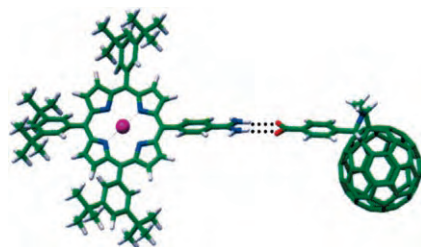
**Two for the price of one:** The total synthesis of (+)-cylindricine C has been achieved in six steps using a catalytic asymmetric Michael reaction and tandem

cyclization. A newly designed two-center organocatalyst gives good selectivity in this Michael reaction. TaDiAS = tartrate-derived diammonium salt.

### Cyclization

T. Shibuguchi, H. Mihara, A. Kuramochi, S. Sakuraba, T. Ohshima, M. Shibasaki\* — 4635–4637

Short Synthesis of (+)-Cylindricine C by Using a Catalytic Asymmetric Michael Reaction with a Two-Center Organocatalyst



**Hooking up:** Self-assembly of a porphyrin amidine and fulleropyrrolidine carboxylic acid based on a two-point amidinium–carboxylate motif leads to supramolecular dyads of high stability ( $K_s \approx 10^7 \text{ M}^{-1}$  in toluene/acetonitrile (9:1)). The synergy of the hydrogen bonds and electrostatic interactions has been shown to be particularly beneficial in terms of electronic coupling between both electroactive components of the dyads.

### Electron Transfer

L. Sánchez, M. Sierra, N. Martín,\* A. J. Myles, T. J. Dale, J. Rebek, Jr.,\* W. Seitz, D. M. Guldi\* — 4637–4641

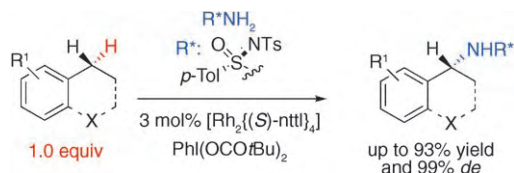
Exceptionally Strong Electronic Communication through Hydrogen Bonds in Porphyrin– $\text{C}_{60}$  Pairs



## Transition-Metal Catalysis

C. Liang, F. Robert-Peillard, C. Fruit,  
P. Müller,\* R. H. Dodd,\*  
P. Dauban\* ————— 4641 – 4644

Efficient Diastereoselective  
Intermolecular Rhodium-Catalyzed C–H  
Amination



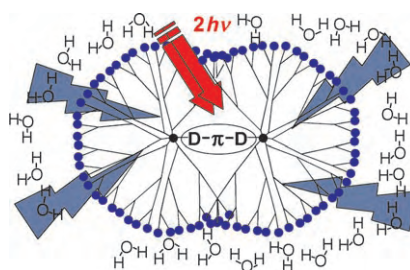
**Successful matchmaking:** The combination of a chiral nitrene precursor with a chiral rhodium(II) catalyst is the key factor that allows efficient intermolecular regioselective C–H amination. Good-to-excel-

lent yields and excellent diastereoselectivities can be obtained with a stoichiometric amount of the C–H bond containing substrate. nttl = *N*-1,8-naphthoyl-*tert*-leucine.

## Contrast Agents

T. R. Krishna, M. Parent, M. H. V. Werts,  
L. Moreaux, S. Gmouh, S. Charpak,  
A.-M. Caminade, J.-P. Majoral,\*  
M. Blanchard-Desce\* ——— 4645 – 4648

Water-Soluble Dendrimeric Two-Photon  
Tracers for In Vivo Imaging

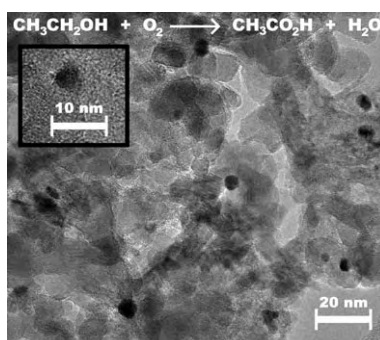


**In a (nut)shell:** Covalently wrapped in a protecting and solubilizing dendrimeric shell (see picture), an initially hydrophobic two-photon fluorophore becomes a biocompatible contrast agent with strong emission for imaging in vivo by multi-photon microscopy.

## Sustainable Chemistry

C. H. Christensen,\* B. Jørgensen,  
J. Rass-Hansen, K. Egeblad, R. Madsen,  
S. K. Klitgaard, S. M. Hansen,  
M. R. Hansen, H. C. Andersen,  
A. Riisager ————— 4648 – 4651

Formation of Acetic Acid by Aqueous-  
Phase Oxidation of Ethanol with Air in the  
Presence of a Heterogeneous Gold  
Catalyst



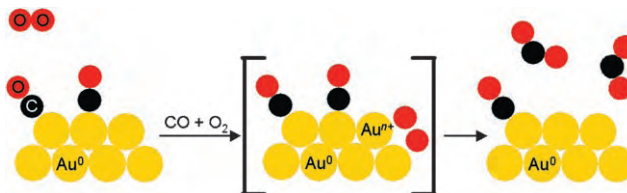
**Wine into vinegar:** It is possible to selectively oxidize ethanol into acetic acid in aqueous solution with air as the oxidant and a heterogeneous gold catalyst (see TEM image of supported gold particles) at temperatures of about 423 K and  $\text{O}_2$  pressures of 0.6 MPa. This reaction proceeds readily in aqueous acidic media with yields of up to 90% and  $\text{CO}_2$  as the only major by-product.



## Oxygen Activation

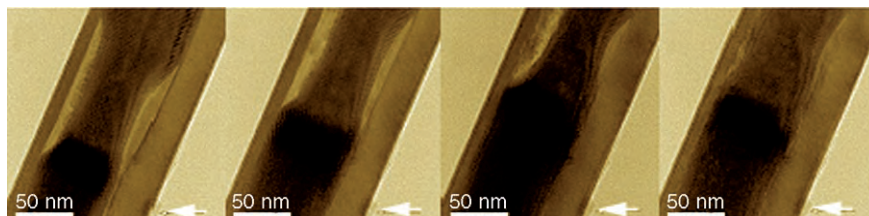
J. A. van Bokhoven,\* C. Louis, J. T. Miller,  
M. Tromp, O. V. Safonova,  
P. Glatzel ————— 4651 – 4654

Activation of Oxygen on Gold/Alumina  
Catalysts: In Situ High-Energy-Resolution  
Fluorescence and Time-Resolved X-ray  
Spectroscopy



**Gold is not so inert after all!** X-ray absorption spectroscopy was used to probe the activation of  $\text{O}_2$  and its reaction with CO over an  $\text{Au}/\text{Al}_2\text{O}_3$  catalyst. The

catalytic activity of small gold particles in the oxidation of CO arises from their ability to transfer charge to oxygen (see picture).



**Tin inside In:** Hollow and tin-filled nanotubes of single-crystalline  $\text{In}(\text{OH})_3$  are grown in a one-step solution–liquid–solid–solid (SLSS) process, and the structural properties of nanotubes synthesized under different growth condi-

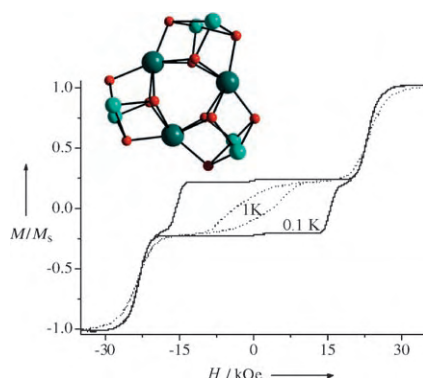
tions characterized and studied. The nanofluidic properties of the interior Sn (see picture) are demonstrated by its response to a rising environmental temperature brought about by electron-beam irradiation.

### Inorganic Nanotubes

Y. Fang, X. Wen, S. Yang\* — 4655–4658

Hollow and Tin-Filled Nanotubes of Single-Crystalline  $\text{In}(\text{OH})_3$  Grown by a Solution–Liquid–Solid–Solid Route

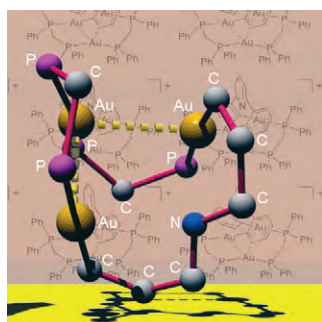
**Highly attractive:** Features typical of a single-molecule magnet (that is, a high anisotropy barrier of 25 K, very slow zero-field relaxation, and a large coercive field of 15 kOe) are exhibited by a  $\text{Dy}^{\text{III}}\text{Cu}^{\text{II}}$  nonanuclear complex, which was synthesized by using a Schiff base ligand. The picture shows the  $\{\text{DyCuO}\}$  core of the cluster (dark green Dy, light green Cu, red O) and low-temperature magnetization curves.



### Single-Molecule Magnets

C. Aronica, G. Pilet, G. Chastanet, W. Wernsdorfer, J.-F. Jacquot, D. Luneau\* — 4659–4662

A Nonanuclear Dysprosium(III)–Copper(II) Complex Exhibiting Single-Molecule Magnet Behavior with Very Slow Zero-Field Relaxation



**A Möbius arrangement** of the bonds directly attached to a metallamacrocycle was observed for the  $\text{Au}^{\text{I}}$  complex  $[\text{Au}_3(\text{CNC})(\mu\text{-Ph}_2\text{PCH}_2\text{PPh}_2)_2]^+$ , which was self-assembled by treating the lithium salt of pyridyl-2,6-diphenyl<sup>2-</sup> (CNC) with  $[\text{Au}_2\text{Cl}_2(\mu\text{-Ph}_2\text{PCH}_2\text{PPh}_2)]$ . The trinuclear  $\text{Au}^{\text{I}}$  complex has intramolecular  $\text{Au}\cdots\text{Au}$  and  $\text{C}\cdots\text{H}\cdots\pi$  interactions, exhibits a remarkable stability in solution, and is cytotoxic toward cancer cell lines.

### CNC Ligands

S. C. F. Kui, J.-S. Huang, R. W.-Y. Sun, N. Zhu, C.-M. Che\* — 4663–4666

Self-Assembly of a Highly Stable, Topologically Interesting Metallamacrocycle by Bridging Gold(I) Ions with Pyridyl-2,6-diphenyl<sup>2-</sup> and Diphosphanes



**A novel spin-polarization mechanism** involving the intramolecular ion pair  $^*\text{A}^+-\text{D}^+-\text{R}$ , which competes with a spin-orbit intersystem crossing, is proposed for the formation of the uniquely spin-polar-

ized quartet photoexcited state observed for **1**, which consists of a bodipy acceptor (A), a phenylanthracene donor (D), and a stable verdazyl radical (R).

### Photoexcited States

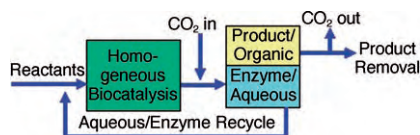
Y. Teki,\* H. Tamekuni, J. Takeuchi, Y. Miura — 4666–4670

First Evidence for a Uniquely Spin-Polarized Quartet Photoexcited State of a  $\pi$ -Conjugated Spin System Generated via the Ion-Pair State

## Catalyst Recycling

J. M. Broering, E. M. Hill, J. P. Hallett,  
C. L. Liotta, C. A. Eckert,  
A. S. Bommarius\* — 4670–4673

Biocatalytic Reaction And Recycling by  
Using CO<sub>2</sub>-Induced Organic–Aqueous  
Tunable Solvents

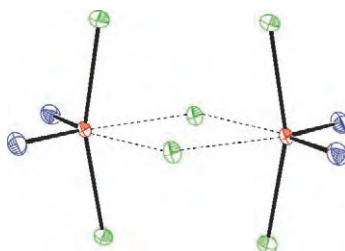


**Tamed OATS:** A scheme that integrates homogeneous biocatalysis in organic–aqueous mixtures with CO<sub>2</sub>-induced separation has been developed. This method allows for simultaneous product recovery and recycling of the homogeneous biocatalyst for reuse.

## Rhenium Chloride Oxides

J. Supek, K. Seppelt\* — 4675–4677

Rhenium Trichloride Dioxide, ReO<sub>2</sub>Cl<sub>3</sub>



**Re-discovery:** The only rhenium(VII)–chlorine compound known previously was ReO<sub>3</sub>Cl, and chloride oxides of composition AO<sub>2</sub>Cl<sub>3</sub> (A = nonmetal or metal) were completely unknown. The synthesis of ReO<sub>2</sub>Cl<sub>3</sub> has now been achieved. The compound exists as a chlorine-bridged dimer (see Figure; Re red, O blue, Cl green) in the solid state, and as a monomer in solution.

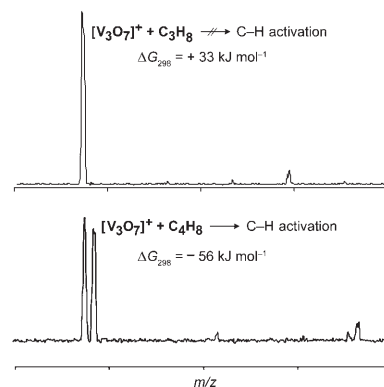
## C–H Activation

S. Feyel, D. Schröder, X. Rozanska,  
J. Sauer,\* H. Schwarz\* — 4677–4681

Gas-Phase Oxidation of Propane and  
1-Butene with [V<sub>3</sub>O<sub>7</sub>]<sup>+</sup>: Experiment and  
Theory in Concert

**A good beginning is half the battle.**

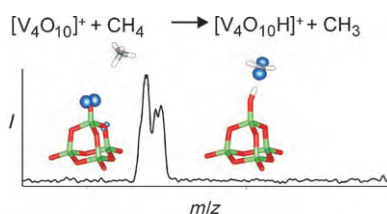
Combined experimental and theoretical studies concerning the dehydrogenation of hydrocarbons by [V<sub>3</sub>O<sub>7</sub>]<sup>+</sup> underline the decisive role of the initial C–H activation step. Propane is found to be unreactive, whereas 1-butene rapidly reacts with [V<sub>3</sub>O<sub>7</sub>]<sup>+</sup> (see picture).



## C–H Activation

S. Feyel, J. Döbler, D. Schröder, J. Sauer,\*  
H. Schwarz\* — 4681–4685

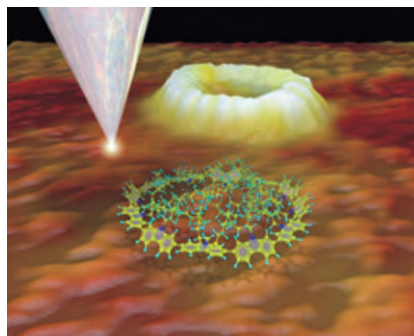
Thermal Activation of Methane by  
Tetranuclear [V<sub>4</sub>O<sub>10</sub>]<sup>+</sup>



**Hand in hand:** In a combination of experimental (mass spectrometry) and theoretical (density functional theory) studies [V<sub>4</sub>O<sub>10</sub>]<sup>+</sup> is described as the first polynuclear transition-metal oxide capable of activating methane at room temperature (see picture). The [V<sub>4</sub>O<sub>10</sub>]<sup>+</sup> cation can be considered a prototype of oxide clusters of early 3d transition metals.



**Round up:** A fully conjugated cyclodeca-2,7-carbazole is prepared around a porphyrin template and the corresponding empty macrocycle then released. Single molecules could be visualized by STM (see image) and their arrangement by atomic force microscopy. The macrocycles self-assemble into a hexagonal array of columns. Efficient energy transfer occurs from the peripheral carbazole  $\pi$  system to the central porphyrin core.



## Macrocycles

S.-H. Jung, W. Pisula, A. Rouhanipour,  
H. J. Räder, J. Jacob,  
K. Müllen\* \_\_\_\_\_ **4685–4690**

A Conjugated Polycarbazole Ring around  
a Porphyrin

## Sources

### Product and Company Directory

You can start the entry for your company in “Sources” in any issue of *Angewandte Chemie*.

If you would like more information, please do not hesitate to contact us.

Wiley-VCH Verlag – Advertising Department

Tel.: 0 62 01 - 60 65 65

Fax: 0 62 01 - 60 65 50

E-Mail: MSchulz@wiley-vch.de

## Service

Keywords \_\_\_\_\_ **4692**

Authors \_\_\_\_\_ **4693**

Angewandte's  
Sister Journals \_\_\_\_\_ **4694–4695**

Vacancies \_\_\_\_\_ **4541**

Preview \_\_\_\_\_ **4697**

## Corrigendum

Supramolecular Chirality in Layered  
Crystals of Achiral Ammonium Salts and  
Fatty Acids: A Hierarchical Interpretation

A. Tanaka, K. Inoue, I. Hisaki, N. Tohnai,  
M. Miyata,\* A. Matsumoto — **4142–4145**

*Angew. Chem. Int. Ed.* **2006**, 45

DOI 10.1002/anie.200504424

In Reference [8] of this Communication, the space group for crystal **1·2** appeared incorrectly and should read as *P*1 (no. 1).

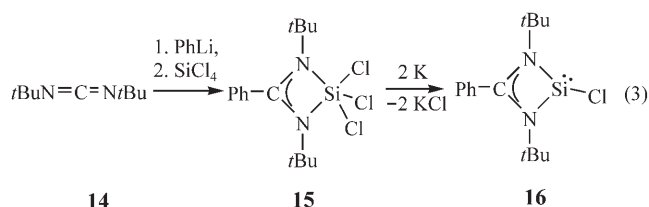
A Stable Silylenoid and a Donor-Stabilized  
Chlorosilylene: Low-Coordinate Silicon  
Compounds—A Never-Ending Story?

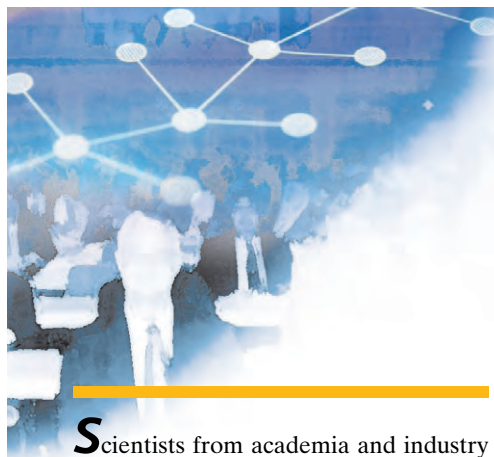
M. Weidenbruch\* \_\_\_\_\_ **4241–4242**

*Angew. Chem. Int. Ed.* **2006**, 45

DOI 10.1002/anie.200601414

In Equation (3) of the Highlight, the carbodiimide **14** incorrectly appeared below the arrow and the *tert*-butyl groups in **15** were inadvertently omitted. The correct equation is shown below.





# The Evolution of Stereochemistry\*\*

Hans-Dieter Arndt

Scientists from academia and industry once again convened at Bürgenstock, above Lake Lucerne (Switzerland), for the 41st EUCHEM Conference on Stereochemistry, chaired by Bernhard Kräutler (University of Innsbruck, Austria). According to a long tradition the program of the conference was not disclosed beforehand, and so an element of surprise lay in store for the 125 participants of this year's meeting.

The President and his organizational committee (Hans-Beat Bürgi, University of Bern; François Diederich, ETH Zürich; E. Peter Kündig, University of Geneva; Klaus Müller, Hoffmann-La Roche; Philippe Renaud, University of Bern; Jay Siegel, University of Zürich) organized a series of lectures that covered the breadth of current research in organic chemistry and encompassed aspects of structure, synthesis, and reactivity, as well as materials science and nanotechnology, functional biological oligomers, chemical biology, and even molecular evolution. Two poster sessions over four afternoons provided the opportunity for additional presentations and comprehensive discussions alike.

The scientific program was opened by Peter Seeberger (ETH Zürich, CH), who presented an insightful analysis of the structural space of oligosaccharides, the scalable syntheses of monosaccharide building blocks, and the scope as well as some limitations of automated oligosaccharide synthesis. He demonstrated, furthermore, how to prepare and utilize microarrays of surface-immobilized oligosaccharides (e.g. heparin sulfates) and how potent synthetic vaccines based on oligosaccharides can be in the prophylaxis against malaria.

Thereafter, Antonio Echavarren (ICIQ Tarragona, Spain) devoted his presentation to noble-metal catalysis. He showed what kind of complex cycloisomerizations and reaction cascades of enynes can be induced by Pt and Au catalysts. Fine tuning of the ligands allowed the reactivities of Au catalysts to be adjusted, and unforeseen reaction pathways could be explained by the intermediacy of Au–carbene complexes.

In the first evening lecture, Rainer Herges (University of Kiel, Germany) drew the participants into the world of Möbius objects. He presented the first synthesis of an isolable Möbius-aromatic compound from tetradehydro-dianthracene and the cyclobutadiene dimer, as well as studies about the  $C_{17}H_{17}^+$  cation, for which he also expects a Möbius-type ground state. The evening was crowned by a performance of the *Crab Canon* from the musical offering (J.-S. Bach), whose score can be deliberately projected onto a Möbius strip to deliver a version that plays continuously by two strings!

The next day was dedicated to the materials sciences. Chad Mirkin (Northwestern University, Evanston, USA) introduced a parallelized concept for dip-pen lithography, which allows the many thousandfold reproduction of micrometer-scaled structures by AFM manipulations. By optimizing the synthesis of DNA-functionalized nanoparticles, his group was able to develop sensitive assay formats for bioanalytical applications. Additionally he reported that such DNA–nanoparticle conjugates

surprisingly penetrate the wall of living cells without transfection reagents and as such can elicit antisense effects.

Collin Nuckolls (Columbia University, New York, USA) then turned to molecular electronics and introduced the investigation of conducting organic single molecules, which had been attached in nanometer-sized “gaps” between conducting electrodes or the ends of carbon nanotubes, both covalently as well as noncovalently. Furthermore, he presented a study on the characterization of carbenes bound on Ru metal surfaces (stable up to 160°C) which enabled the stable cross-linking of Ru nanoparticles by ring-opening metathesis polymerization (ROMP).

In the evening, Hermann Gaub (LMU München, Germany) opened the toolbox of force microscopy, which his group uses to characterize the unfolding of proteins and association of molecules. He reported how DNA oligonucleotides can be used to achieve a higher sensitivity and perform measurements in parallel, and demonstrated with force-coupled azobenzene molecules the principle of a molecular, light-driven motor (a “photo-Otto-cycle”).

On the third day, Donald Hilvert (ETH Zürich, Switzerland) gave an account on catalytic antibodies and their specific optimization and selection by yeast cell surface display techniques. He also reported on the molecular evolution of a chorismate mutase dimer and its “halved” constructs. The monomers thus obtained displayed many properties of a molten globule, with a high level of catalytic activity retained.

The lecture by Morten Meldal (Carlsberg Laboratory, Copenhagen, Denmark) was directed towards combinatorial chemistry. With carefully optimized solid-phase synthesis of small-compound libraries, cell-based assays on beads could be developed. He then described the combinatorial generation of non-natural receptors and metallo-peptides as catalysts, and then introduced a novel technique to encode and automatically identify single polymer

[\*] Dr. H.-D. Arndt  
Universität Dortmund  
Fachbereich Chemie  
Otto-Hahn-Strasse 6  
D-44221 Dortmund (Germany)  
and  
Max-Planck-Institut für molekulare  
Physiologie  
Otto-Hahn-Strasse 11  
D-44227 Dortmund (Germany)  
E-mail: hans-dieter.arndt@mpi-dortmund.mpg.de

[\*\*] 41st EUCHEM Conference on Stereochemistry, April 22–28, 2006, Bürgenstock (Switzerland)

beads by using a “fingerprint” of copolymerized fluorescent particles.

The focus of the fourth day was on synthetic chemistry. Shengming Ma (Institute of Organic Chemistry, Shanghai, China) illustrated how allenes can be utilized for selective transformations. He presented metal-induced reaction cascades that lead to interesting polycyclic skeletons as well as detailed investigations on stereoselective electrophilic additions to allenes. He also showed how allenyl thioethers and sulfides can be used as bifunctional building blocks for synthesis.

Ilan Marek (Technion, Haifa, Israel) continued in this direction with chiral 3,3-disubstituted allyl organometallics for the generation of quaternary stereocenters. He described the development of chiral sulfoxide directing groups to suppress metallotropic shifts and allow for good stereoinduction. The corresponding reagents could even be sequentially formed and reacted in a one-pot organometallic multicomponent reaction (alkenylsulfoxide, organocopper, diethylzinc, diiodomethane, aldehyde).

In the evening, Donna Blackmond (Imperial College, London, UK) gave a provocative yet stimulating account of her kinetic studies of catalytic reaction systems. She reported detailed studies of autocatalytic reactions (Soai reaction, organocatalytic  $\alpha$ -hydroxyamination of aldehydes) and the intricate influence of the solubility of single intermediates. A systematic study of the phase diagrams of stereoisomers of amino acids corro-

borated the frequent enrichment of one isomer in the supernatant (eutectic for serine: 99% *ee* in solution), which could be of relevance for prebiotic organocatalytic reaction networks.

The final day was devoted to biomolecules and especially their molecular evolution. Ronald Breaker (Yale University, New Haven, USA) demonstrated the successful *in vitro* evolution of functional riboswitches on the basis of coupled aptamer and ribozyme domains, respectively, which could even be fused to realize molecular logical gates. He then discussed how biologically important riboswitches can be successfully found and characterized, opening up new aspects of gene regulation with small molecules.

Gerald Joyce (Scripps Research Institute, La Jolla, USA) described thereafter the *in vitro* evolution of RNA-templated RNA polymerases from oligonucleotides, which could even be performed with a reduced set of bases (three or even two) as well as with DNA or RNA. He then presented how up to 280 evolutionary cycles per day can be carried out in a miniaturized microfluidic device, which suggests that “molecular evolution on a chip” may become feasible in the near future.

The scientific program was concluded by Robert Stroud (UC San Francisco, USA), who clarified the transport of water and ammonia molecules by high-resolution crystal structure analyses of membrane-bound transport proteins. The surprising selectivity of aquaporins for water molecule trans-

port versus the intrinsically much more mobile protons could be traced to a pseudo-centrosymmetrically bound water molecule at the center of the channel. On the basis of a high-resolution structure of the ammonia channel AmtB (1.34 Å), Stroud suggested a model to describe the permeation of neutral NH<sub>3</sub> molecules (instead of the charged NH<sub>4</sub><sup>+</sup> ions) through the selectivity filter of this channel and thus explain its extraordinary selectivity.

In his closing talk, Klaus Müller (Hoffmann-La Roche) gave a humorous review in the style of “Dr. Seuss” of the scientific aspects of the meeting and set the scene for lighthearted reflections.

The 41st EUCHEM Conference on Stereochemistry displayed all facets of organic chemistry and served as a cross-disciplinary platform for all participants. Unfortunately, the venerable Bürgenstock Hotel complex will close next year for reconstruction. Nevertheless, the president of next year’s meeting, Samir Zard (Ecole Polytechnique, Palaiseau, France), and the organizing committee have found an alternative nearby, still at Bürgenstock and not far from the traditional location. The 42nd EUCHEM Conference on Stereochemistry will take place on April 14–20, 2007 (<http://www.stereochemistry-buergenstock.ch>). We await with great anticipation to learn what lies in store for the participants at the next “Bürgenstock Conference”.

DOI: 10.1002/anie.200602300



# The First Crystal Structure of Tyrosinase: All Questions Answered?

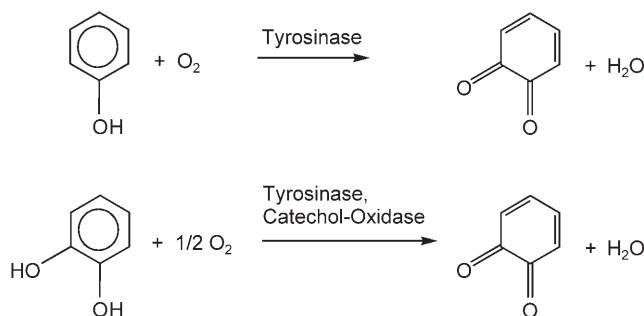
Heinz Decker,\* Thorsten Schweikardt, and Felix Tuczek\*

## Keywords:

bioinorganic chemistry · copper · metalloenzymes · protein structures · tyrosinase

## 1. Introduction

The resolution of the structure of an important protein is always a major event in biological sciences. This applies in particular to the recently published, first crystal structure of tyrosinase, which was determined by Matoba et al. on a bacterial tyrosinase from *Streptomyces castaneoglobisporus* at a resolution of 1.4 Å.<sup>[1]</sup> Tyrosinases are essential copper-containing enzymes that occur in all organisms.<sup>[2–7]</sup> They are involved in browning processes of skin, hair, and fruit, and in wound healing or the immune response. Tyrosinases initiate the synthesis of melanin by catalyzing the hydroxylation of monophenols to *ortho*-diphenols and the subsequent two-electron oxidation to *ortho*-quinones with molecular oxygen (Scheme 1). The latter reaction is also catalyzed by the related enzyme catechol oxidase (Scheme 1), which, however, is unable to mediate the phenol hydroxylation step. Both tyrosinase and catechol oxidase belong to the monophenol oxidase family and possess active sites with two copper atoms (CuA and CuB), both of which are coordinated by three histidine residues (type3 copper proteins). The third group of proteins



**Scheme 1.** Top: Tyrosinases catalyze the conversion of monophenols to *ortho*-quinones via *ortho*-diphenols. Bottom: Catechol oxidase catalyzes only the second step (*ortho*-diphenol → *ortho*-quinone).

that have type3 copper active sites are the hemocyanins, which serve as oxygen carriers in some arthropods and molluscs, analogous to hemoglobin in vertebrates.<sup>[8]</sup> Arthropod hemocyanin and mollusc hemocyanin differ with respect to their sequences and structures, but both exhibit highly cooperative oxygen-binding behavior.<sup>[9]</sup>

Before any X-ray crystallographic information on type3 copper proteins was available, spectroscopic and mechanistic experiments had already shown that the active site of tyrosinase is very similar to that of hemocyanin.<sup>[6,10]</sup> On the basis of spectral comparison with a corresponding model complex from Kitajima and Moro-oka,<sup>[11]</sup> it was further concluded that these metalloproteins in their *oxy* form should bind dioxygen as peroxide in the unique side-on bridging ( $\mu\text{-}\eta^2\text{:}\eta^2$ ) manner, as was later confirmed by crystal structures of *oxy* hemocyanin from arthropods<sup>[12]</sup> and molluscs.<sup>[13]</sup> The existence of the same side-on peroxide-bridged *oxy* form in tyrosinase has now impressively been demonstrated by the new tyrosinase structure from *Streptomyces castaneoglobisporus* (sTy). Al-

though no crystallographically characterized *oxy* structure is available yet for catechol oxidase, data from UV/Vis and resonance Raman spectroscopy indicate that dioxygen is also bound as a side-on bridging peroxide ligand in this enzyme.<sup>[14,15]</sup> Thus, dioxygen binds to all type3 copper proteins in the same way, as has been anticipated for many years.

## 2. Protein Folding and the Active Site

In view of their almost identical active sites, the very different functions of tyrosinase, hemocyanin, and catechol oxidase are remarkable and have aroused the interest of researchers for a very long time. The quaternary structures of these proteins also differ appreciably.<sup>[8]</sup> Depending on the species, hemocyanins of arthropods consist of hexamers and integer multiples thereof (1 × 6, 2 × 6, 4 × 6, 6 × 6, and 8 × 6), whereas hemocyanins from molluscs form decamers or didecamers.<sup>[8a,b,9]</sup> Phenol oxidases, in contrast, occur as monomers (as in sTy), dimers (as in human tyrosi-

[\*] H. Decker, T. Schweikardt  
Institut für Molekulare Biophysik  
Johannes Gutenberg-Universität  
55099 Mainz (Germany)  
Fax: (+49) 6131-3923557  
E-mail: hdecker@uni-mainz.de  
F. Tuczek  
Institut für Anorganische Chemie  
Christian-Albrechts-Universität  
24098 Kiel (Germany)  
Fax: (+49) 431-880-1520  
E-mail: ftuczek@ac.uni-kiel.de

nase),<sup>[2,5]</sup> or hexamers (as found in some arthropods).<sup>[16]</sup> The monomers of type3 copper proteins, in turn, consist of two or three domains with different folding motifs (for three domains: I = N terminal, II = central, III = C terminal).<sup>[16b]</sup> The crystal structures of sTy, catechol oxidase, and molluscan hemocyanin reveal that these proteins have the second domain in common, which folds in a “four  $\alpha$ -helix bundle” motif and bears the active site with the two copper atoms CuA and CuB (Figure 1 a–d). In molluscan hemocyanin, access to the active site is blocked by the C-terminal domain; moreover, in the case of a structurally characterized functional unit of hemocyanin from *Octopus dofleini* (Odg), a leucine group (Leu2830) of

this domain (III) extends into the pocket of the active site. In arthropodan hemocyanin, on the other hand, the active site is shielded by domain I, and additionally, as in the case of hemocyanin from *Limulus*, a phenylalanine residue (Phe49) of this domain extends into the substrate binding site. External substrates thus cannot reach the active site, and the only physiological role of hemocyanin is O<sub>2</sub> binding and transport.<sup>[17]</sup>

For the inactive form of catechol oxidase from the sweet potato, *Ipomoea batatas*, (IbCO) the active site is covered by domain III. After dissociation of this domain the active site is accessible to substrates.<sup>[18]</sup> This finding is in agreement with a recent report on plant and fungal polyphenol oxidases in which

domain III blocks the entrance to the active site with a conserved phenylalanine residue.<sup>[4]</sup> External substrates can thus be converted by the binuclear copper center only after dissociation of this domain. The crystal structure of tyrosinase, finally, has been obtained on a complex of this protein with a caddie protein (ORF378; ORF = open reading frame), which again shields the active site. In this case a tyrosine residue (Tyr98) of ORF378 extends into the substrate binding pocket.<sup>[1]</sup> After dissociation of the caddie protein, the active site of sTy is accessible to substrates.

A comparison of the dinuclear active sites of *Limulus* hemocyanin, *Octopus* hemocyanin, IbCO, and sTy shows that each of the metal centers is coordinated by the N<sub>ε</sub> atoms of three histidine residues. All six histidine residues are conserved among the type3 copper proteins and exhibit a very similar binding geometry (Figure 1 e). In catechol oxidase and *Octopus* hemocyanin, an unusual cysteine–histidine bond stabilizes the second of the histidine residues that coordinate to CuA, the only histidine residue which is located on a flexible loop and is not bonded to a rigid  $\alpha$  helix. This thioether bond also appears to be present in most molluscan hemocyanins and fungal tyrosinases,<sup>[3]</sup> but is absent in sTy, mouse and human tyrosinase,<sup>[19]</sup> and arthropodan hemocyanin.

Besides the *oxy* form, Matoba et al.<sup>[1]</sup> were also successful in obtaining structures of two *met* forms of sTy (*metI* and *metII*) which contain two Cu<sup>II</sup> centers that are bridged by one and two water (hydroxide) ligands, respectively. Furthermore, they structurally characterized the *deoxy* form which contains two Cu<sup>I</sup> centers and is able to bind O<sub>2</sub>, thereby being converted into the *oxy* form. In this way, all relevant intermediates of the tyrosinase catalytic cycle<sup>[6,20]</sup> are now structurally characterized, thus making it possible to draw some important conclusions with respect to the chemistry of the tyrosinase active site.

### 3. Substrate Binding Geometry: Hints from X-ray Crystallography

The most interesting step among the reactions that are catalyzed by tyrosi-

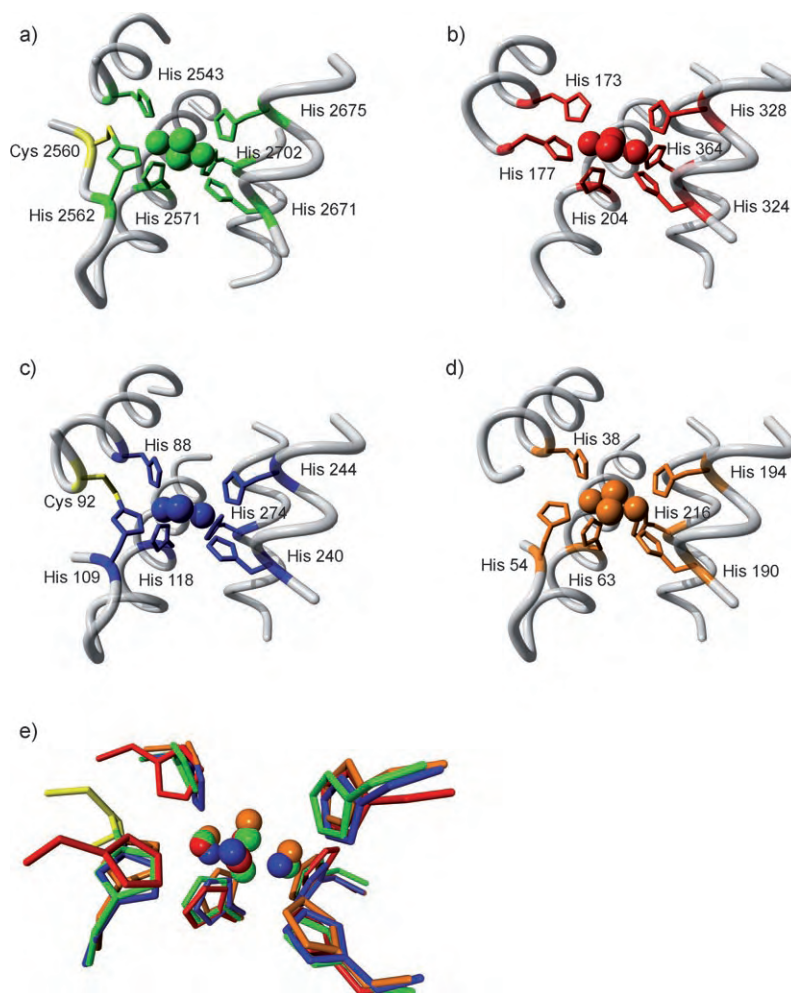


**Figure 1.** a)–d) Active sites of four crystallographically characterized type3 copper proteins: a) *Octopus dofleini* hemocyanin<sup>[13]</sup> (green), b) *Limulus polyphemus* hemocyanin<sup>[12]</sup> (red), c) *Ipomoea batatas* catechol oxidase<sup>[22]</sup> (blue), d) *Streptomyces castaneoglobosporus* tyrosinase<sup>[1]</sup> (orange). The copper-binding histidine residues are bound to  $\alpha$  helices and loops (gray). The Cys–His bonds are colored in yellow; the copper–oxygen complexes are shown by space-filling representations. e) A superposition of the four active sites demonstrates the high degree of structural similarity (color codes as above).

nase is the *ortho* hydroxylation of tyrosine, as mediated by the *oxy* form of this enzyme. Of crucial importance for this reaction is the orientation of the phenolic substrate with respect to the binuclear copper active site. Experimental information on this point has mostly been derived from spectroscopic studies on the bonding of inhibitors to tyrosinase.<sup>[10,21]</sup> Alternatively, it has been proposed that an external tyrosine substrate is oriented at the active site of tyrosinase in the same way as Phe49 in the *Limulus oxy* hemocyanin structure.<sup>[17]</sup> Most interestingly, the new tyrosinase structure reveals a very similar arrangement in which a tyrosine residue (Tyr98) from the associated caddie protein extends into the pocket of the active site like a potential substrate (Figure 2, top). This tyrosine residue, however, is not hydroxylated since all of its atoms are more than 3.4 Å away from the Cu<sub>2</sub>O<sub>2</sub> unit, and a closer approach to the active site is prevented by the attachment to the caddie protein. For a free tyrosine substrate, however, this would be possible, as shown below.

Figure 2 (middle) shows the *Limulus oxy* site along with Phe49 from domain I (see Section 2). In the *para* position of the phenyl ring of Phe49 (which can almost be superimposed with that of Tyr98 in sTy) an oxygen atom has been added to generate a putative tyrosine substrate. The orientation of the phenyl group is further determined by a hydrophobic interaction with one of the histidine residues that coordinate to CuB (His328); an analogous interaction occurs in sTy between the phenyl ring of Tyr98 and His194 (Figure 2, top). For the coordination of diphenols to the active site of catechol oxidase, a substrate bonding geometry has been derived on the basis of the crystallographically characterized, PTU-bound *met* form of IbCO (PTU = phenylthiourea). Specifically, Klabunde et al.<sup>[22]</sup> proposed that the phenyl ring of the diphenol is aligned with the phenyl ring of the inhibitor, which in turn can almost be superimposed with the phenyl ring of Phe49 in *Limulus* hemocyanin and Tyr98 in sTy. This way, a substrate bonding geometry that exhibits one Cu–O bond to CuB and one phenoxo bridge between CuA and CuB is obtained (Figure 2, bottom); a hydropho-

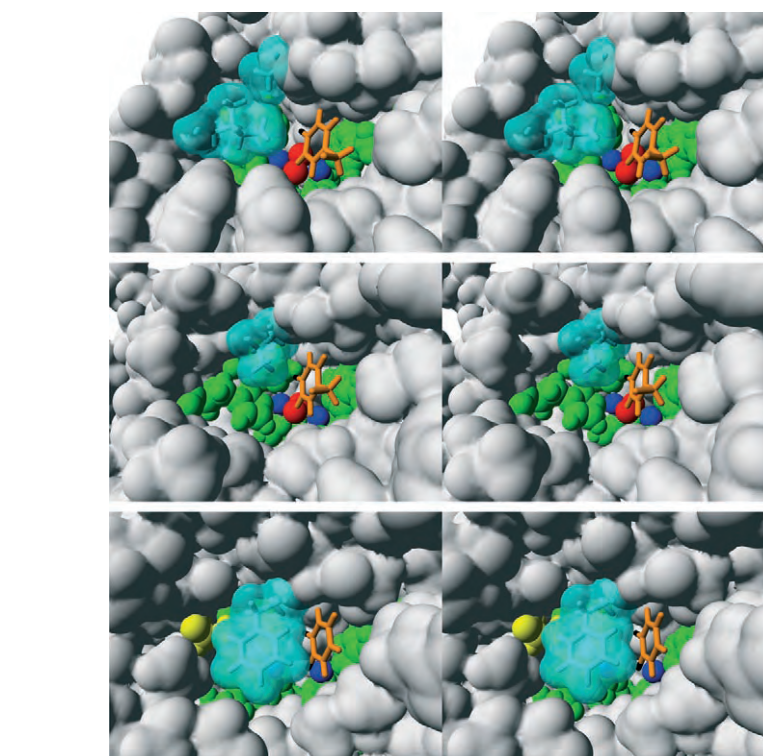


**Figure 2.** Stereoviews of the active sites and substrate binding pockets of sTy (top), *Limulus polyphemus* hemocyanin (middle), and IbCO (bottom). The substrate binding pockets are occupied by Tyr98 (top), Phe49 (augmented by an oxygen atom (black) to generate a tyrosine residue; middle), and a catechol (bottom). The catechol is constructed from the phenyl ring of the inhibitor PTU by adding two oxygen atoms. Cu: blue; O<sub>2</sub>: red; His: green; substrate (tyrosine/catechol): orange; shielding residues: cyan. The hydroxyl groups of the tyrosines are oriented more towards CuA than CuB. In the case of IbCO, CuA cannot be approached because it is shielded by a phenylalanine residue.

bic interaction with His244 further stabilizes the substrate orientation.

Importantly, CuA in IbCO is shielded by a phenylalanine residue (Phe261). At this structural position in sTy there is instead an isoleucine residue; that is, CuA is *not* masked by a bulky residue in sTy. This could indicate that CuA is necessary for the bonding and conversion of monophenols to *o*-quinones which in turn would provide a possible explanation for the functional difference between catechol oxidase and tyrosinase.

#### 4. Substrate Binding Site: CuA or CuB?

There has been considerable debate on whether external substrates of tyrosinase bind to CuA or to CuB.<sup>[1,6,17,21,22]</sup> New information on this point can now be obtained from a detailed analysis of the *metII* and *oxy* structures of sTy. These two forms are very similar, such

that *metII* may be taken to analyze substrate bonding to *oxy* (Figure 3a). In the *metII* structure, the CuA center exhibits a tetragonal-pyramidal geometry, with two bridging water (hydroxide) ligands and two histidine residues in equatorial positions and one histidine residue in an axial position. If a substrate binds to such a copper center, it will coordinate in the position *trans* to the axial histidine residue. The three N<sub>ε</sub>(His)–CuA bond lengths are 2.09 (His38), 2.26 (His54), and 2.43 Å (His63), thus indicating that the former two are equatorial and the latter axial. This assignment disagrees with the analysis of Matoba et al., who assign the axial position of CuA to His54.<sup>[23]</sup> However, the much longer Cu–N bond length of His63 unequivocally indicates that this residue occupies the axial position of CuA.<sup>[24]</sup> Importantly, the position *trans* to His63 (Figure 3a) is freely accessible from the substrate binding pocket, in contrast to the posi-



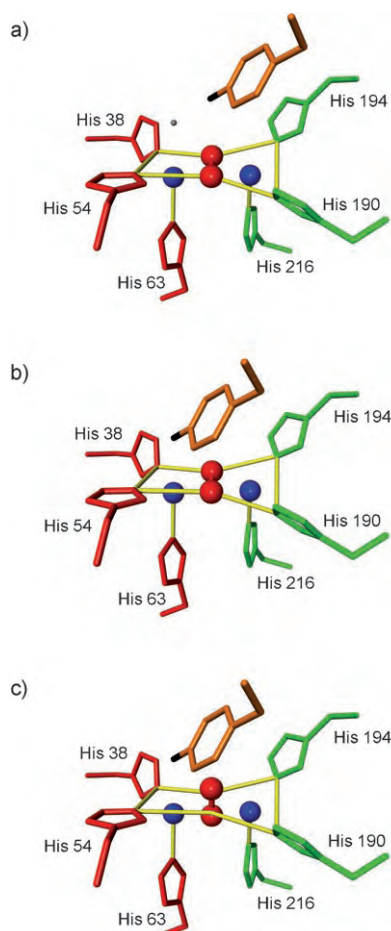


**Figure 3.** Orientation of a tyrosine substrate at the active site of oxy tyrosinase. a) Initial configuration after approach to the active site, as based on the crystal structure of sTy. b) Shift of the substrate to CuA. c) Rotation of the O–O axis towards the aromatic ring and electrophilic attack at the *ortho* position. Cu: blue; His on CuA: red; His on CuB: green; O<sub>2</sub>: red; monophenolic substrate: orange (oxygen atom therein: black); equatorial coordination of CuA and CuB: yellow frame; axial coordination of CuA and CuB: yellow bonds; *trans*-axial coordination of CuA: gray dot. Molecular graphics created with Yasara (<http://www.yasara.org>) and Povray (<http://www.povray.org>).

tion *trans* to His54. If the substrate binds to CuA, it will thus bind *trans*-axially to His63.

The CuB center of *metII* and *oxy* also exhibits a tetragonal-pyramidal geometry, but here the distinction between axial and equatorial histidine residues is somewhat less pronounced. Matoba et al.<sup>[1]</sup> assigned the equatorial positions of CuB to His194 and His216, whereas the axial position is occupied by His190.

This assignment disagrees with the fact that in all three structures (*metI*, *metII*, *oxy*) the N<sub>ε</sub>(His216)–CuB bond is the longest, thereby indicating that His216 is in the axial position. The position *trans* to His216 is also accessible from the substrate binding pocket. Thus, in sTy, a phenolic substrate could in principle also bind to CuB, in the position *trans* to His216. Alternatively, the role of CuB for substrate binding in sTy may be to provide structural guidance to the orientation of the phenyl ring of the substrate through a hydrophobic interaction with His194, as suggested for the interaction between a possible substrate and His244 of IbCO or His328 of *Limulus* hemocyanin.

## 5. Hydroxylation of Tyrosine

On the basis of this concept, the following mechanism for the hydroxylation of tyrosine can be envisaged. After approach to the *oxy* site, the substrate is preoriented through a hydrophobic interaction with His194 on CuB, such that its C–O bond is oriented towards CuA, in analogy to the orientation of Tyr98 (Figure 3a). The substrate is then shifted towards CuA to bind in the position *trans* to His63 (Figure 3b). Then, hydroxylation of the aromatic ring occurs. To this end, the O–O axis of the peroxo ligand rotates to point towards the phenolic ring; moreover, the substrate may rotate slightly around the C–O axis (Figure 3c). The proximity of the *ortho* position of the phenolic ring to the side-on coordinated peroxo group then enables an electrophilic attack of the Cu<sub>2</sub>O<sub>2</sub> moiety on the aromatic ring, whereby concomitant cleavage of the O–O bond occurs.<sup>[17,25]</sup> The *o*-quinone product is formed via a diphenolic intermediate that binds in a bidentate fashion, and is subsequently released from the active site, thus regenerating the *deoxy* form. This sequence of reactions is summarized in Scheme 2.

## 6. Activation Mechanism and Copper Incorporation

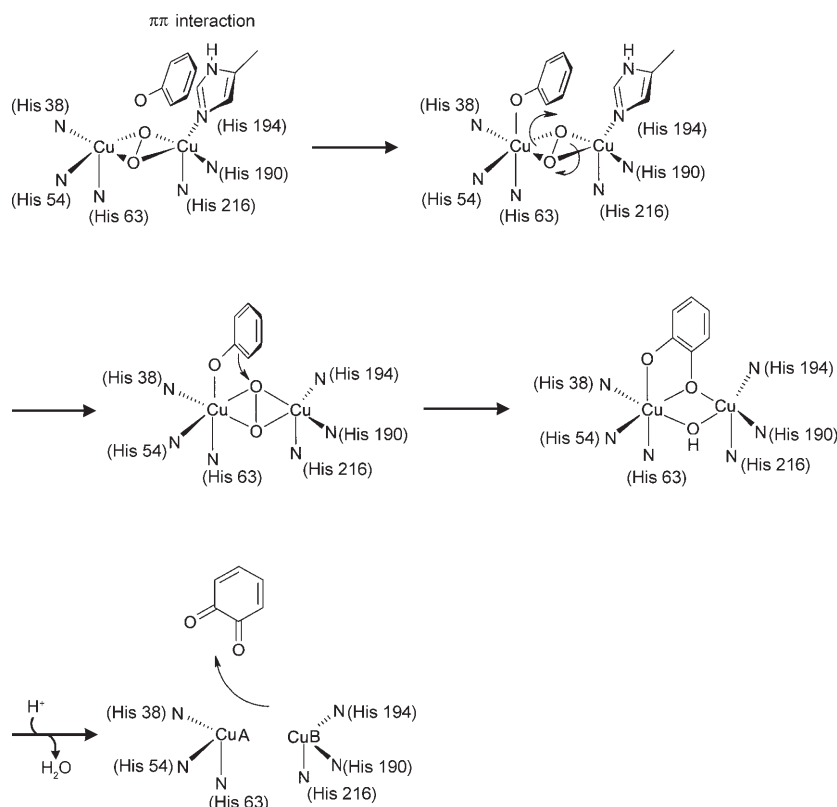
The major difference between hemocyanin on the one hand and tyrosinase/catechol oxidase on the other is the

accessibility of substrates to the active site (see Sections 2 and 3). As long as hemocyanins serve as oxygen carriers, the entrance to the active site in domain II is blocked, and the substrate binding pocket is additionally occupied by a residue from, depending on the organism, domain I or III (for example, Phe49 for *Limulus* hemocyanin). It has been hypothesized that this residue acts as a “placeholder” for monophenolic substrates.<sup>[17]</sup> These substrates can enter the active site after the placeholder has been pulled out of the substrate binding pocket, which occurs by dissociation of domain I or III. In hemocyanin this “activation” step can be achieved artificially by limited proteolysis or conformational movement of the N-terminal domain by treatment with sodium dodecylsulfate (SDS).<sup>[16]</sup> The physiological activation of fungal and plant polyphenol oxidases or IbCO occurs similarly by cleavage of domain III, which blocks the active site.<sup>[3,4]</sup>

In sTy a caddie protein (ORF378) has been cocrystallized which shields the entrance to the active site and contains a tyrosine residue (Tyr98) that extends into the pocket of the active site. Matoba et al.<sup>[1]</sup> found that this caddie protein also binds copper centers through a number of histidine residues. The electron density maps suggest that the copper atoms “jump” from histidine cluster to histidine cluster, from which the authors conclude that the caddie protein is responsible for the incorporation of copper into the metal-free expressed enzyme. Details of this process are, however, unknown,<sup>[7]</sup> and it is unclear how the copper atoms ultimately reach the active site of sTy. The authors even show that upon increase of the copper concentration in solution the caddie protein dissociates from sTy.<sup>[1]</sup> In light of the above considerations, this dissociation can also be interpreted as an activation of the enzyme, thus making the active site accessible to external substrates.

## 7. Conclusions

The first structure of a tyrosinase is a breakthrough in the chemistry and biology of copper proteins. It contributes new and interesting aspects to long-



**Scheme 2.** Hydroxylation of a monophenolic substrate (tyrosine) by tyrosinase.

standing problems related to the properties of type3 copper proteins and supports some of the concepts developed earlier to account for the functional differences observed in this class of proteins. Significant insights have in particular been obtained with respect to the following points:

- Tyrosinase and catechol oxidase: X-ray crystallography indicates that in catechol oxidase the CuA site is shielded whereas in sTy it is not, thus supporting the hypothesis that monophenols should bind to CuA in order to be converted into *o*-quinones. Nevertheless, the crystal structures of sTy also leave open the possibility that monophenols bind to CuB.
- Molecular mechanism of monophenol hydroxylation: The structures provide information regarding the possible orientation of phenolic substrates at the active site, which is the basis for a mechanistic understanding of monophenol hydroxylation.
- Activation and copper incorporation: The Tyr98 residue provided by the cocrystallized caddie protein supports the “placeholder” concept for

the activation of type3 copper enzymes. The caddie protein further appears to be responsible for copper incorporation, but the mechanism of this process remains to be elucidated.

Published online: June 23, 2006

- [1] Y. Matoba, T. Kumagai, A. Yamamoto, H. Yoshitsu, M. Sugiyama, *J. Biol. Chem.* **2006**, 281, 8981.
- [2] J. C. Garcia-Borrón, F. Solano, *Pigment Cell Res.* **2002**, 15, 162.
- [3] S. Halaoui, M. Asther, J. C. Sigoillot, M. Hamdi, A. Lomascolo, *J. Appl. Microbiol.* **2006**, 100, 219.
- [4] C. M. Marusek, N. M. Trobaugh, W. H. Flurkey, J. K. Inlow, *J. Inorg. Biochem.* **2006**, 100, 108.
- [5] N. Wang, D. N. Hebert, *Pigm. Cell Res.* **2006**, 19, 3.
- [6] E. I. Solomon, U. M. Sundaram, T. E. Machonkin, *Chem. Rev.* **1996**, 96, 2563.
- [7] H. Claus, H. Decker, *Syst. Appl. Microbiol.* **2006**, 29, 3.
- [8] a) K. E. van Holde, K. I. Miller, H. Decker, *J. Biol. Chem.* **2001**, 276, 15563; b) H. Decker in *Encyclopedia of Inorganic Chemistry*, Vol. 2, 2nd ed. (Ed.: R. B. King), Wiley, New York, **2006**, pp. 1159–1173.

- [9] K. E. van Holde, K. I. Miller, *Adv. Protein Chem.* **1995**, 47, 1.
- [10] R. S. Himmelwright, N. C. Eickman, C. D. LuBien, E. I. Solomon, K. Lerch, *J. Am. Chem. Soc.* **1980**, 102, 7339.
- [11] N. Kitajima, Y. Moro-oka, *Chem. Rev.* **1994**, 94, 737.
- [12] K. A. Magnus, B. Hazes, H. Ton-That, C. Bonaventura, J. Bonaventura, W. G. Hol, *Proteins Struct. Funct. Genet.* **1994**, 19, 302.
- [13] M. E. Cuff, K. I. Miller, K. E. van Holde, W. A. Hendrickson, *J. Mol. Biol.* **1998**, 278, 855.
- [14] C. Eicken, C. Gerdemann, B. Krebs, *Handbook of Metalloproteins*, Vol. 2 (Eds.: A. Messerschmidt, R. Huber, T. Poulos, K. Wieghardt), Wiley, New York, **2001**, p. 1319.
- [15] a) A. Rempel, H. Fischer, D. Meiwes, K. Büldt-Karentzopoulos, R. Dillinger, F. Tuczek, H. Witzel, B. Krebs, *J. Biol. Inorg. Chem.* **1999**, 4, 56; b) R. Dillinger, A. Magrini, F. Tuczek, B. Krebs, unpublished results.
- [16] a) E. Jaenicke, H. Decker, *Biochem. J.* **2003**, 371, 515; b) E. Jaenicke, H. Decker, *ChemBioChem* **2004**, 5, 163.
- [17] a) H. Decker, F. Tuczek, *Trends Biochem. Sci.* **2000**, 25, 392; b) H. Decker, R. Dillinger, F. Tuczek, *Angew. Chem. Int. Ed.* **2000**, 39, 1591; c) H. Decker, T. Rimke, *J. Biol. Chem.* **1998**, 273, 25889.
- [18] C. Gerdemann, C. Eicken, H. J. Galla, B. Krebs, *J. Inorg. Biochem.* **2002**, 89, 155.
- [19] T. Schweikardt, F. Solano, E. Jaenicke, J. C. Garcia-Borrón, H. Decker, unpublished results.
- [20] a) A. Sanchez-Ferrer, J. N. Rodriguez-Lopez, F. Garcia-Canovas, F. Garcia-Carmona, *Biochim. Biophys. Acta* **1995**, 1247, 1; b) L. Bubacco, M. v. Gastel, E. J. J. Groenen, E. Vijgenboom, G. W. Canters, *J. Biol. Chem.* **2003**, 278, 7381.
- [21] A. W. Tepper, L. Bubacco, G. W. Canters, *J. Am. Chem. Soc.* **2005**, 127, 567.
- [22] T. Klabunde, C. Eicken, J. C. Sacchettini, B. Krebs, *Nat. Struct. Biol.* **1998**, 5, 1084.
- [23] The assignment of Matoba et al. is only correct for the *deoxy* and *metI* forms, which are not relevant for catalysis.
- [24] In the *oxy* form, which is generated by H<sub>2</sub>O<sub>2</sub>, the differences in bond lengths are less distinct, but the Cu–N(His63) bond length is still the longest (2.20 vs. 2.19 and 2.14 Å). In the *oxy* form that is generated in the presence of dithiothreitol, the CuA–N(His63) bond is again much longer than the other ones (2.37 vs. 2.15 and 2.08 Å).
- [25] E. Pidcock, H. V. Obias, C. X. Zhang, K. D. Karlin, E. I. Solomon, *J. Am. Chem. Soc.* **1998**, 120, 7841.

# Small Molecule Modulators of Transcription

Hans-Dieter Arndt\*

## Keywords:

antitumor agents · coactivators · gene expression · protein-protein interactions · transcription factors

**S**ignal transduction cascades ultimately trigger transcriptional programs that are executed by transcription factors interacting with coactivator or corepressor proteins in large multi-protein complexes. Despite the difficulties associated with discovering and verifying potent antagonists (or agonists) of protein–protein interaction events, several small molecules have been identified within the last few years that modulate transcription by directly interacting with transcriptional proteins. Some of these small molecules display surprising selectivity and some even show efficacy *in vivo*. This review summarizes the current status in this developing field to illustrate the emerging opportunities in the chemical biology of transcription.

## 1. Introduction

The genetic information encoded in cellular DNA is only revealed on regulated expression, that is, its transcription into the pre-mRNA. This process is tightly controlled by nuclear factors embedded in complex cellular signaling networks. In higher organisms, an estimated 5–10% of all gene-coding capacity is dedicated to proteins that regulate transcription.<sup>[1]</sup> The expression level of particular genes is associated with specific phenotypes, and aberrant expression of genes is interlinked with a multitude of diseases. Hence, small molecules with the ability to interfere directly with the transcriptional machinery carry great potential not only as therapeutic agents, but also as research tools in chemical biology. Such molecules could be used to clarify the intriguing interplay between chromatin, transcription factors, and gene expression levels.

The most important way to target genes with small molecules is to capitalize on inherently ligand-dependent transcription factors, the so-called nuclear receptors (NRs).<sup>[2,3]</sup> A multitude of steroid- and non-steroid-based effectors (e.g. selective estrogen receptor modulators,

“SERMs”) are currently in scientific and clinical use or development. But unfortunately, their application remains inherently limited to NR-dependent genes or phenotypes.

To open up new activity profiles, it would be desirable to target more components of the transcriptional machinery as specifically as possible. As tools for chemical-biology research, such compounds may allow advancement in our understanding of transcriptional events and complement investigations on upstream signal transduction cascades. With respect to drug development, direct modulation of transcription remains a territory rarely explored (with the prominent exception of nuclear receptors); new findings could therefore open up distinct therapeutic windows, especially in the anticancer field.<sup>[4]</sup> In the following sections, recent advances, mainly in the area of small molecules that directly interact with proteins of the transcriptional machinery will be discussed.<sup>[5]</sup>

## 2. Transcription initiation

The promoter-specific transcription initiation of protein coding genes (Figure 1) requires both gene-specific (TF) and general transcription factors (GTF), which assemble cooperatively on cognate DNA elements upstream of the coding region (“promoter”).<sup>[6]</sup> Transcription factors can recruit coactivator proteins,<sup>[7]</sup> which in turn may stabilize GTFs on the core promoter. Furthermore, they induce chromatin remodeling and recruit additional proteins to form a large bridging multiprotein assembly currently termed “mediator”.<sup>[8]</sup> A unifying nomenclature for the considerable variety of mediator- and mediator-like components has recently been suggested.<sup>[8c]</sup> Altogether they establish a stable preinitiation complex that recruits RNA polymerase II (RNA Pol II) to initiate gene transcription.<sup>[8d]</sup>

[\*] Dr. H.-D. Arndt  
Universität Dortmund, Fachbereich Chemie  
Otto-Hahn-Str. 6, 44221 Dortmund (Germany)  
and  
Max-Planck-Institut für molekulare Physiologie  
Otto-Hahn-Str. 11, 44227 Dortmund (Germany)  
Fax: (+49) 231-133-2498  
E-mail: hans-dieter.arndt@mpi-dortmund.mpg.de



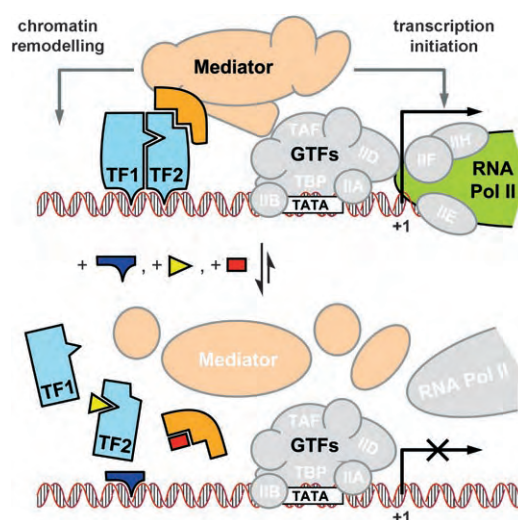


**Figure 1.** Simplified representation of the assembly of the transcription-initiation complex illustrating specific interference with small molecules that target DNA (blue), transcription factors (yellow), or coactivators/mediator (orange). A coactivator may also bind to the GTFs and to chromatin as well as other coactivators (not depicted). TF = transcription factor, GTF = general transcription factors, RNA Pol II = RNA polymerase II, TATA = TATA box, TBP = TATA-box-binding protein, TAF = TBP-associated factor, +1 = transcription start site.

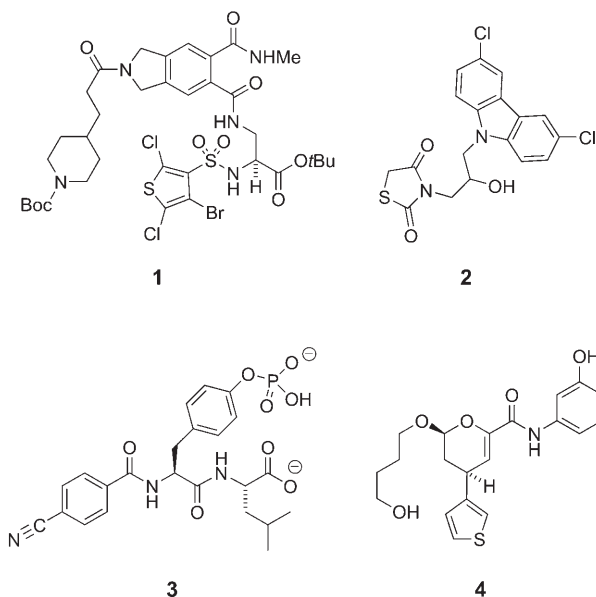
Evidence is mounting that the assembly of nuclear factors on chromatin is highly dynamic (seconds timescale) and may obey a stochastic sensing model.<sup>[9,10]</sup> Statically bound proteins seem to be rare and the exception to the rules. Moreover, even an actively transcribed locus appears to undergo constant dynamic remodeling (minutes timescale).<sup>[10a]</sup> Therefore, although transcription initiation may necessitate the association of several dozen transcription factors and mediating proteins, interception or modulation of this process should be feasible and reasonably fast. Small molecules binding to transcription factors, coactivators, or DNA should lead to destabilization of the multi-protein assembly (Figure 1), reduce RNA Pol II recruitment, and hence lower the expression levels of the encoded gene. This antagonist concept has been experimentally validated in several cases. The alternative stabilization of multi-TF assemblies by small-molecule agonists leading to upregulation has been demonstrated in model systems (see Section 5).



**Hans-Dieter Arndt**, born 1971, studied Chemistry at Ulm, London (Imperial College), and Marburg university. He obtained his doctorate in 2002 with Ulrich Koert at the Humboldt University of Berlin for work on artificial ion channels. After postdoctoral research with Peter B. Dervan at the California Institute of Technology, where he investigated protein-recruiting DNA ligands, he became group leader at the Max Planck Institute for Molecular Physiology in 2004 and Emmy-Noether fellow at the University of Dortmund. His research interests focus on the chemical biology of transcription and translation as well as organic synthesis.

### 3. Inhibitors of transcription-factor association

Transcription factors seldom work as single molecules, but rather function mostly in conjunction with many other transcription factors bound to promoter DNA. As an underlying principle, most transcription factors form homo- or heterodimers as a small subunit and in a cooperative fashion. Often, it is only these dimers that have a high-enough binding affinity and specificity for cognate DNA. Disturbing the dimerization of a crucial TF could be a promising strategy to exert influence on gene expression and curb the dimerization of important transcription factors (Scheme 1).



**Scheme 1.** Chemical structures of the transcription-factor association inhibitors (1–4). Boc = *tert*-butoxycarbonyl.

#### 3.1. Myc/Max

The first such interaction for which a small-molecule antagonist was identified was Myc/Max.<sup>[11]</sup> c-Myc is a basic helix–loop–helix leucine-zipper transcription factor that is involved in cell proliferation and differentiation suppression, and was found to be frequently upregulated in human cancers.<sup>[12]</sup> The activation is however driven by heterodimers formed from c-Myc with the partner protein Max. To identify antagonists of the Myc–Max interaction, Vogt and co-workers utilized fusion proteins of cyan (CFP) and yellow fluorescent protein (YFP) with c-Myc and Max in a fluorescence resonance energy transfer (FRET)-based experiment.<sup>[11]</sup> In a high-throughput dimerization assay, several antagonists were discovered with activities in the medium micromolar range, with isoindoline **1** (Scheme 1) being the most potent (50  $\mu$ M). Furthermore, isoindoline **1** interfered with an oncogenic transformation of cultured chicken-embryo fibroblasts (approximately 20  $\mu$ M), thus providing a proof of principle for targeting this TF dimerization in general.<sup>[11]</sup> After this finding, different compounds that are able to

disrupt the Myc–Max interaction have been disclosed by Prochownik and co-workers.<sup>[13]</sup> In this case, yeast two-hybrid assays were employed to screen for c-Myc–Max disruption. In this way, dichlorocarbazole **2** was uncovered, among other effective inhibitors, from a commercial library. Importantly, **2** was not only reported to prevent c-Myc–Max dimerization in vitro in the low micromolar range but also to inhibit fibroblast proliferation in a c-Myc-dependent manner. Furthermore, growth of tumor xenografts in nude mice was prevented when they were pretreated with **2** (39  $\mu\text{M}$ ) before inoculation. Although the potency of **2** is still not high, it strongly supports the general potential of c-Myc–Max antagonists for anticancer treatment. This is further supported by a very recent study<sup>[14]</sup> in which structurally related naphthols were identified as antagonists (17–36  $\mu\text{M}$ ) of the c-Myc–Max interaction in vitro and also showed activity in cellular transformation assays.

### 3.2. STAT-3

As a second group of TFs of potential interest, STATs (signal transducer and activator of transcription) have been investigated. STATs are unique in their ability to transduce extracellular signals and regulate transcription directly: After phosphorylation events mediated by growth factor and cytokine receptors or non-receptor-associated tyrosine kinases (e.g. Abl or c-Src), the STATs dimerize through reciprocal phosphotyrosine-SH2 domain (src homology 2) interactions. After translocation to the nucleus, these dimers drive diverse transcriptional events associated with immune response, inflammation, proliferation, differentiation, development, and apoptosis.<sup>[15]</sup> STAT signaling in the cell is tightly regulated. However, dysregulation of STAT subtypes is regarded to be important for tumor malignancy, particularly the overactivation of STAT3 and STAT5.<sup>[15b]</sup> In an investigation targeting STAT3, the tripeptide mimic **3** was identified by Turkson et al. as an inhibitor (40  $\mu\text{M}$ ) of STAT3 dimerization,<sup>[16]</sup> with **3** being derived from a STAT-3 binding phosphopeptide. Cell permeability and stability of compound **3** may be critical, but Turkson et al. secured proof for not only STAT3 dimer disruption, but also growth inhibition in cellular assays. This validates the hypothesis that direct inhibition of STAT3 dimerization (and in turn its activating potential) is effective and may become a conceptual alternative to targeting the STAT3 phosphorylating kinases upstream (Abl, c-Src).<sup>[17]</sup>

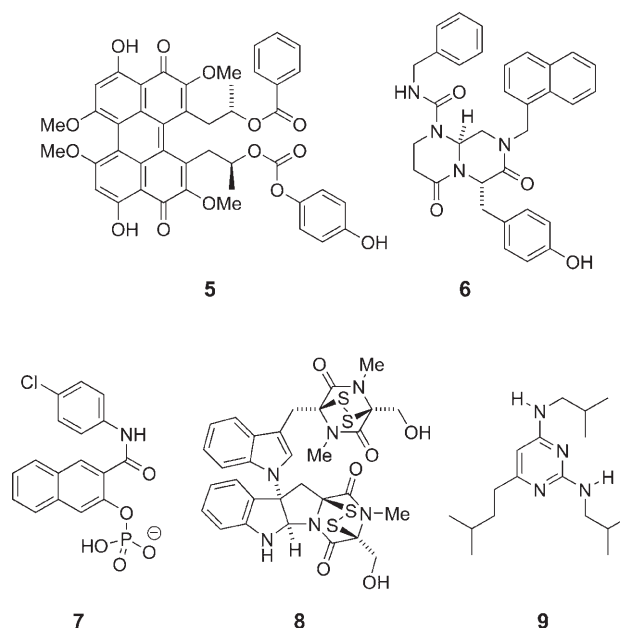
### 3.3. HAP3

In a completely different approach, dihydropyran **4** was identified from a small-molecule microarray to bind to the yeast transcription factor HAP3 (heme-activated protein 3) selectively.<sup>[18]</sup> HAP2/3/5 from yeast, as well as their homologues in higher eukaryotes (NF-Y, CBF), bind as heterotrimers to highly conserved CCAAT DNA sequences with subnanomolar affinities. Data from surface plasmon resonance, reporter assays, and whole-genome profiling in yeast

showed that dihydropyran **4** binds to HAP3 directly (0.3  $\mu\text{M}$ ), can downregulate HAP-dependent transcription (24  $\mu\text{M}$ ), and affects HAP-dependent gene regulation on the genomic scale, respectively. It will be interesting to see how dihydropyran **4** will affect the NF-Y complex, which serves more general and diverse purposes in mammalian genomes than its HAP homologue in yeast.<sup>[19]</sup>

## 4. Interference with cofactor interactions

Transcription factors are always endowed with at least two functional domains: Primarily they bind to genomic DNA to allow readout and processing of genomic programs that are dependent on promoter sequences. On the other hand, they interact with further cofactors to execute their function and may therefore be regarded as quasi-combinatorial adaptor proteins that mediate the DNA sequence context.<sup>[20]</sup> Many of the proteins targeted by TFs are coactivator proteins necessary for chromatin reorganization and transcription initiation, or corepressor proteins that silence a gene or even a whole locus. Interactions may also extend to basal transcription factors or mediator components. Hence apart from TF–TF interactions, a further possibility to affect transcription would be modulating the communication of transcription factors with coregulators as can be seen in Scheme 2. The progress in



**Scheme 2.** Chemical structures of the transcription-cofactor association modulators (**5–8**).

this area has been notable, and efficacy in animal models could even be demonstrated in several cases. Furthermore, some of these molecules show clear selectivity for one binding site within a multivalent protein (i.e. a protein with several binding positions).

#### 4.1. $\beta$ -Catenin

The multifunctional protein,  $\beta$ -catenin, transduces the signals from the Wnt pathway as a transcriptional coactivator and often becomes slightly hyperactive as a result of oncogenic mutations.<sup>[21]</sup> On the molecular level,  $\beta$ -catenin forms complexes in the nucleus, most importantly with the T-cell factor (TCF) and lymphoid enhancer factor (LEF) family of transcription factors, to become functional. This dimerization event utilizes a large flat surface provided by the 12 mer “armadillo repeat” of  $\beta$ -catenin ( $>3600 \text{ \AA}^2$ )<sup>[22]</sup> and may therefore be regarded as extremely difficult to be targeted directly with small molecules. Nevertheless, in a high-throughput screening experiment of natural products (7000 compounds), several small molecules were identified and investigated in detail.<sup>[23]</sup> The planar quinone **5** (Scheme 2), a fungal metabolite, emerged as one interesting candidate. Quinone **5** disrupts the complex of pure  $\beta$ -catenin–TCF ( $3 \mu\text{M}$  ELISA) in vitro as well as in cell extracts, inhibits cancer cell proliferation that is dependent on cell type ( $0.4\text{--}3.4 \mu\text{M}$ ), suppresses the levels of  $\beta$ -catenin dependent targets (cyclin D1, c-myc) in HCT116 cells, and displays a strong influence on  $\beta$ -catenin-dependent development in *xenopus* embryos. Although the authors have cautioned that **5** may have additional targets, quinone **5** remains a strong candidate for direct  $\beta$ -catenin–TCF disruption. This becomes especially noteworthy when considering that 45 000 compounds from a synthetic library did not yield any hits in the same high-throughput screen.<sup>[24]</sup>

#### 4.2. CREB binding protein (CBP) and p300

CBP and the highly homologous protein p300 are high-molecular-weight (300 kDa) multidomain coactivator proteins that function synergistically to reorganize chromatin and activate transcription after recruitment by TFs.<sup>[25]</sup> Within the transcriptional networks, CBP/p300 is generally considered a limiting factor in terms of both rate and concentration. CBP/p300 carries at least six interaction domains that are able to interact with a plethora of TFs and mediator subunits. This makes it a very complex target. However, recently three different molecules have been found to interfere with TFs that bind to CBP/p300 and yet target three distinct interactions (Scheme 2).

In a 5000-compound library screen, piperazinone **6** was found to downregulate  $\beta$ -catenin/TCF signaling.<sup>[26]</sup> In contrast to quinone **5**, however, it could be shown by affinity chromatography that piperazinone **6** selectively binds to CBP where it directly competes with  $\beta$ -catenin binding. Mapping studies showed **6** to bind to the N terminus of CBP (AA 1–111), which is also the site of recruitment for nuclear receptors (RAR/RXR). Interestingly, compound **6** does not bind to the highly homologous coactivator p300. Several oncogenic targets downstream of  $\beta$ -catenin (e.g. survivin and cyclin-D1) were found to be significantly downregulated after treatment with piperazinone **6** both in cultured colon cancer cells ( $25 \mu\text{M}$ ) and in mice ( $150 \text{ mg kg}^{-1}$  delivered intravenously), showing that this approach is effective in vivo.

For the binding of the prototypical CBP effector, the molecule CREB (cAMP response element binding protein) was recently reported as an antagonist.<sup>[27]</sup> Naphthol phosphate **7** was identified as a small-molecule antagonist of the CREB–CBP interaction by NMR-spectroscopic-based screening. Detailed NMR spectroscopic experiments led the authors to the conclusion that **7** targets a binding site distal to the CREB binding groove on the CBP KIX domain and hence functions through an allosteric mechanism. Reported assays confirmed the attenuation of CREB association in vivo ( $10 \mu\text{M}$ ). CREB is involved in hepatic gluconeogenesis and therefore a possible diabetes type II target. Furthermore, as the KIX domain on CBP serves as a binding platform for various transcription factors, compounds like **7** indicate that this binding platform can be influenced with varied outcomes.

The natural product chetomin (**8**) was identified in a high-throughput screen for molecules able to interfere with p300–HIF-1 $\alpha$  binding.<sup>[28]</sup> HIF-1 $\alpha$  is a key transcription factor in the response of tissues to hypoxic (low  $\text{O}_2$ ) conditions and therefore considered as an important potential antiangiogenesis target. Indeed, it is the coactivator p300 that mediates the potential of HIF-1 $\alpha$  by docking it with its TAZ1 domain (also called the CH1 domain). Chetomin **8** seems to disrupt the TAZ1-domain fold on p300; hence HIF-1 $\alpha$  is impaired in its activity as it is necessary that p300 binding occurs at this domain. This is also the case for other TFs that are attached to this domain (demonstrated for HIF-2 $\alpha$  and STAT2). This was further corroborated by the fact that disulfide **8** does not lead to covalent modification of the potentially reactive Cys-800 in the crucial HIF-1 $\alpha$  activation domain. The exact binding site of chetomin **8** on p300 remains to be elucidated, but its high potency in cellular assays (low nM) as well as nude-mouse tumor xenografts ( $1 \text{ mg kg}^{-1}$  delivered intravenously) carries high promise that exploiting this novel mode of action may become fruitful in the future.

#### 4.3. Nuclear receptors

A nuclear receptor will generally adjust the conformation of its ligand-binding domain in response to the binding of a ligand (e.g. a steroid) and present a remodeled binding surface that favors coactivator (for agonists) or corepressor recruitment (antagonist or apo form).<sup>[29]</sup> Coactivators have been shown to bind on top of the ligand-binding domain through a highly conserved helical LxxLL motif, often termed a “nuclear-receptor interaction box”. A high level of sophistication has been reached in targeting this interface with conformationally restrained peptides and peptidomimetics.<sup>[30]</sup> Katzenellenbogen and co-workers have, however, recently demonstrated that a small molecule is able to inhibit coactivator-peptide binding to the estrogen receptor  $\alpha$  (ER- $\alpha$ ) as well.<sup>[31]</sup> Following the rationale outlined above, the authors designed various molecules presenting three leucine-like side chains and investigated them for ER- $\alpha$ -coactivator peptide complex disruption. Despite the modest effectiveness of their optimal compound **9** ( $K_d \approx 30 \mu\text{M}$ ), it is the first nonpeptidic molecule that is able to reversibly disrupt the binding of coactivators to an agonist-bound nuclear receptor.

If this important proof of principle could be extended to more potent ligands, selective interference with steroid-like NR ligands could be realized in a novel fashion. Very recent results from a high-throughput screen for thyroid hormone receptor (TR) coregulator antagonists lead in this direction: Guy and co-workers have uncovered vinyl-aryl ketones as covalently reacting ligands of the TR that abrogate binding of coactivators to the TR in the submicromolar range.<sup>[32]</sup>

#### 4.4. p53

Certainly most intensively investigated in this field is the tumor suppressor p53.<sup>[33,34]</sup> This potent transcription factor integrates diverse stress signals and affects cell-cycle control, senescence, and apoptosis pathways. Owing to its “cellular gatekeeper” role, the p53 pathway is a hot spot for oncogenic mutations that compromise p53 function. In healthy cells, tight control of p53 levels is ensured by the regulator protein HDM2 in humans (or the respective MDM2 homologue in mice), which can shield the crucial p53 activation domain as well as induce p53 degradation by its intrinsic RING-finger and E3-type ubiquitin ligase activity. Blocking HDM2 should therefore result in restoring and/or promoting of the beneficial p53 activity in compromised cells.

In pursuing this goal, three independent groups have recently reported potent small-molecule ligands that target the p53 binding interface on HDM2/MDM2. Binding of p53 has been shown to occur in a cleft on HDM2 in which an  $\alpha$ -helical segment of p53 projects three side chains (Phe-19, Trp-23, Leu-26) into a largely hydrophobic cavity (Figure 2).<sup>[35]</sup>

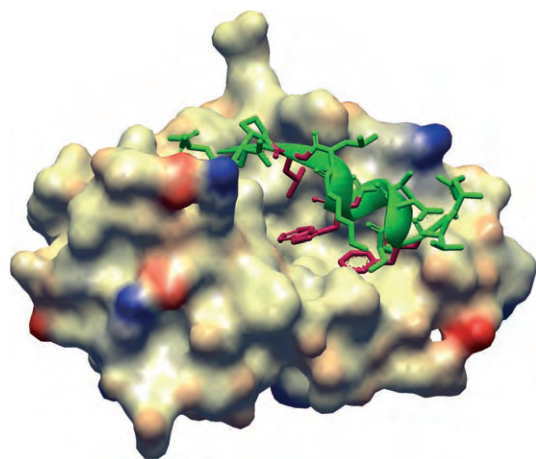
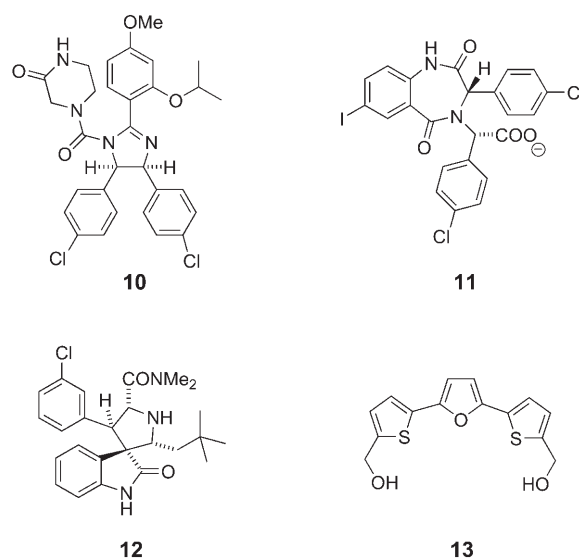


**Figure 2.** Rendering of the HDM2 protein (bronze) crystal structure associated with a p53 transactivation domain peptide (green).<sup>[35]</sup> The residues crucial for binding are highlighted in purple (PDB-1YCR).

The first potent and selective small-molecule inhibitor of the MDM2–p53 interaction was reported by a Roche group,<sup>[36]</sup> which identified *cis* imidazolines as MDM2–p53-antagonists after high-throughput screening and structure-based optimization with affinities in the high nanomolar range (Scheme 3). “Nutlin 3” (**10**) was found to bind MDM2 (0.1  $\mu\text{M}$ ) to inhibit cancer-cell growth (1–3  $\mu\text{M}$ ) and to



**Scheme 3.** Chemical structures of p53-modulating compounds (**9–12**).

annihilate tumor growth in mouse xenograft models after oral administration (400 mg kg<sup>−1</sup>/day). In these models, imidazoline **10** compared well with the approved anti-cancer drug doxorubicin.

In turn, a Johnson & Johnson group disclosed benzodiazepinones as an HDM2 antagonists, with benzodiazepine **11** as the most active in in vitro and cell-based assays.<sup>[37]</sup> Despite considerable shape similarity to the *cis* imidazolines, the reported benzodiazepinones seem to be less potent but could still suppress cancer-cell growth at around 30  $\mu\text{M}$ . Both the nutlins **10** and benzodiazepine **11** were characterized by X-ray crystallography while bound to their respective target. They were shown to target the p53 binding cleft on MDM2 (**10**) or HDM2 (**11**).

Recently, spiro-oxindoles were reported as potent MDM2 antagonists by an academic team.<sup>[38]</sup> Interestingly, these compounds were designed by substructure comparison with natural-product-derived scaffolds as well as molecular modeling, and synthesized by using an enantioselective dipolar azomethinyliide cycloaddition. Despite the few derivatives so far reported, compound **12** compared favorably with the *cis*-imidazolines as far as in vitro potency is concerned (see Section 6, Table 1).

On the other hand, a distinct type of p53 activator was recently described by Selivanova and co-workers.<sup>[39]</sup> Bisthiophenylfuran **13** (“RITA”) was identified by a library screen with a pair of isogenic colon-cancer cell lines that differed only in p53 status. The activity of RITA was later confirmed in several experimental setups. Most importantly, RITA **13** was found to completely stop tumor growth in mouse xenografts at 10 mg kg<sup>−1</sup>/day when the dose was delivered intravenously. Although it interferes with HDM2–p53 complex formation, **13** seemingly does not bind to HDM2, but directly to p53 with very high affinity ( $K_d = 1.5$  nM). The authors concluded that **13** likely targets an as-yet unmapped allosteric site on p53. In this way, **13** possibly blocks a conformational transition involved in the complex formation with HDM2 and/or stabilizes a conformation that recruits further cofactors.



Given the complex biology of p53, this new paradigm requires further confirmation.

Interestingly, native p53 was recently found by NMR spectroscopy<sup>[40]</sup> to remain largely unstructured even when bound to MDM2, and hence may require additional regulators to fold into its activated state. As a caveat, this same study reported that the strength of aggregation and precipitation of MDM2 can vary depending on the small-molecule ligand. Nevertheless, the high potency of heterocycle **13** in p53<sup>+</sup> tumor tissues and its novel mode of action highlight the potential for unbiased screening setups.

### 5. Modular non-peptidic activators

A completely different approach to target transcription would be not to destabilize but to promote preinitiation complex formation. This in turn should lead to more-frequent transcription initiation events and elevated gene-expression levels. Two- and three-hybrid setups utilize artificial activation for detection by transcriptional readout of reporter constructs, and fusions proteins composed of activators and DNA-binding domains from TFs have been shown to act as artificial activators with novel properties.<sup>[41]</sup> Small molecules endowed with stabilizing properties of transcriptional complexes have not been reported to date. However, small molecules that target components of the transcriptional machinery allow non-peptidic, small-molecule activators to be reached by the chemical biologist when modular design is deliberately applied.

After identification of a suitable ligand for coactivator or mediator proteins, for example, by screening for TF-cofactor complex dissociation<sup>[42]</sup> or cofactor binding,<sup>[43]</sup> covalent attachment to a module with high DNA affinity should generate a novel activating entity (Figure 3). Activation of a specific

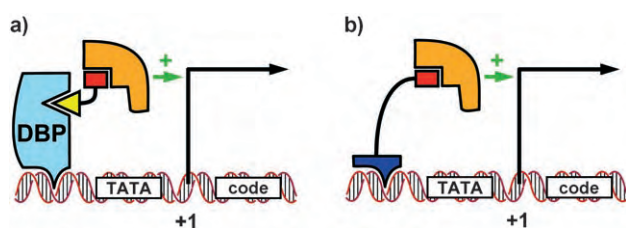


**Figure 3.** Schematic representation of modular artificial activators. a) Activating module (red) attached to a ligand for a DNA-binding protein (DBP, yellow), b) Activating module attached to a DNA-binding molecule (blue). Code: coding region, TATA = TATA-box, +1 = transcription start site.

gene of interest can be ensured either thorough targeting a DNA-binding protein (natural or artificial; Figure 3A) or targeting the DNA itself with a sequence-specific small-molecule ligand (Figure 3B). Such activation leads to small-molecule protein–protein or protein–DNA dimerizers, respectively. Along this line, three distinct molecules have validated the feasibility of the concept with non-peptidic activator modules (Scheme 4).

Isoxazolidine **14** and related compounds were found by Mapp and co-workers to upregulate transcription of a target gene 5–7-fold in vitro.<sup>[44]</sup> DNA affinity was conferred by the attachment of methotrexate, which binds to an artificial fusion protein composed of dihydrofolate reductase and the DNA-binding domain of the yeast transcription factor, LexA. Interestingly, both the stereochemistry and the substituent distribution around the isoxazoline core seem to be variable to some degree, a property that is likewise found in most natural activator domains.<sup>[44b]</sup> The cellular target protein(s) of the isoxazolidine activator as well as the degree of influence of the accessory fusion protein on the activation process have not been detailed, however.

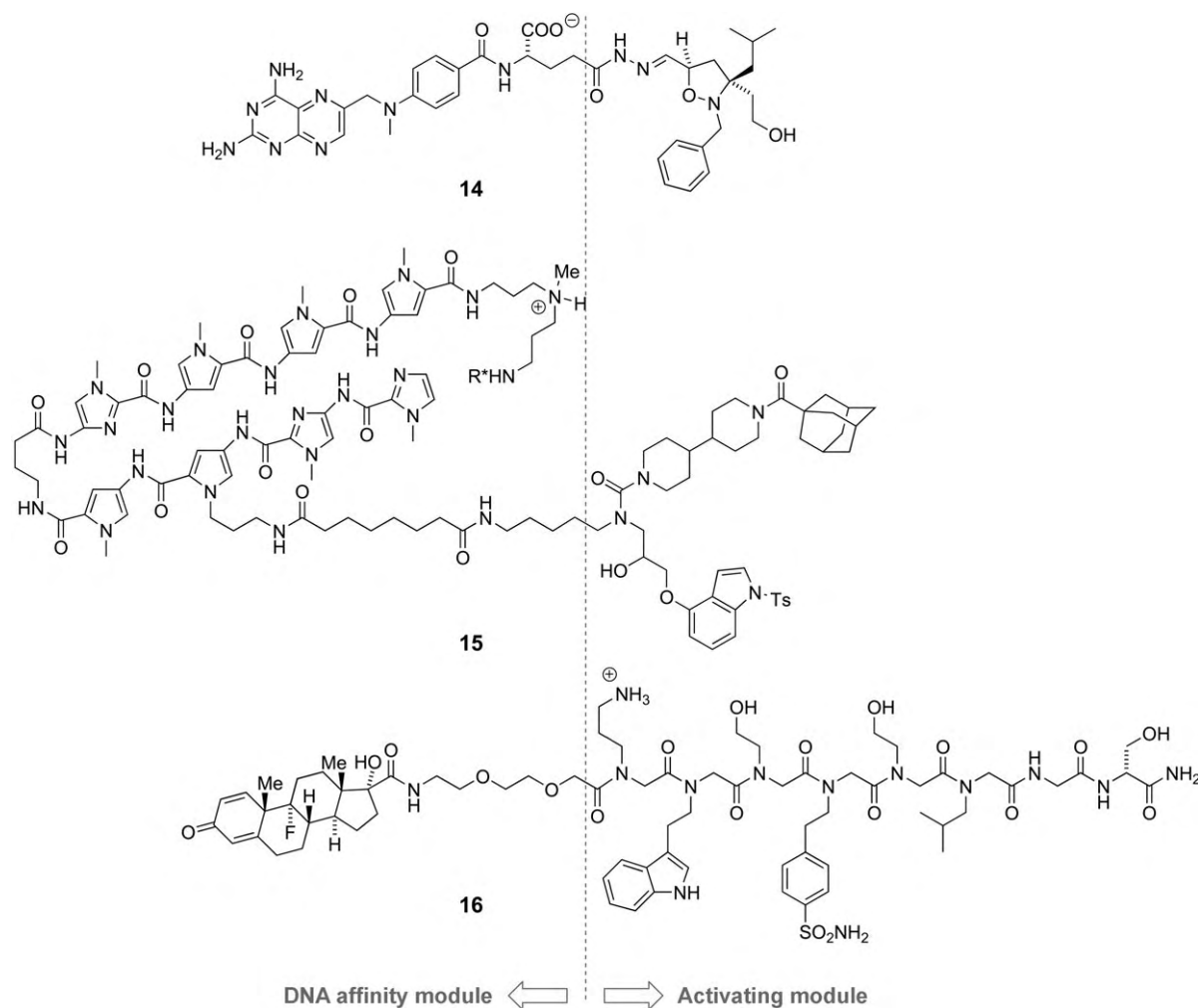
Subsequently, Uesugi, Dervan, and co-workers reported a conjugate (**15**) of wrenchnolol and a DNA-binding polyamide that sequence specifically activated DNA transcription in vitro without the need for an artificial DNA-binding protein.<sup>[45]</sup> The compound wrenchnolol had previously been identified and optimized as a micromolar ligand for Sur-2, a Ras-linked subunit of the human mediator complex.<sup>[42]</sup> The wrenchnolol conjugate **15** features a sequence specific DNA-binding polyamide,<sup>[46]</sup> and both Sur-2 and RNA Pol II were demonstrated to be recruited to target DNA. This corroborated the reconstitution of the transcription-competent preinitiation complex from its presumed molecular components in vitro.

From a library of 100000 peptoids, Kodadek and co-workers have recently identified three potent ligands for the KIX domain of CBP that have the potential for recruiting this general coactivator.<sup>[47]</sup> Conjugation to dexamethasone gave compound **16**, which was found to be cell permeable despite its considerable size. The authors demonstrated that the peptoid conjugate **16** functions as a strong activator in cellular assays in vivo in which a fusion protein of the glucocorticoid-receptor ligand-binding domain and the Gal4 DNA-binding domain ensured specificity for an artificial reporter gene. Notably, other CBP ligands identified would not deliver potent activators as dexamethasone conjugates. Therefore, the binding-site location and orientation within the coactivator seem to be crucial variables for function here.

### 6. Discussion and Outlook

Relevant data for compounds **1–13** are summarized in Table 1. What conclusions can be drawn from these findings? First, these various examples demonstrate that it is indeed possible to identify potent and selective small molecules that act on transcriptional processes, with some moving towards the regime of drug-like potency in vivo. Second, potent modulators for transcriptional cofactors may be easier to generate than small molecules that target transcription factors directly. Finally, it is possible to identify small molecules that are able to target different regions of the same macromolecular target to give different outcomes.

Most of the compounds discussed here (**1–13**) share one common structural feature: they project lipophilic residues in a predefined 3D orientation, often almost star-like. This is commonly deemed to mimic the 3D shape of a confined protein domain (e.g., an  $\alpha$ -helix or  $\beta$ -turn). Nevertheless, only



**Scheme 4.** Chemical structures of modular non-peptidic activator compounds (**13–15**). Activating modules are located on the right side. R<sup>+</sup> = 5-thioureido fluorescein, Ts = tosyl.

a few of the compounds described herein are functional “nonconventional peptidomimetics” like the cleft binders for

the HDM ligands (**10**, **11**). The majority of the molecular parameters of interactions are only coarsely defined, but a

complex, even allosteric influence on protein structure is emerging in some of the cases. In other words, they indirectly modulate protein–protein interactions by using the structural plasticity of the binding interfaces. This plasticity may be especially characteristic for transcriptional proteins with their multimodal, multivalent nature.

Even more conventional interactions of small molecules with proteins have unearthed surprises in this regard.<sup>[48]</sup> A more precise, molecular understanding of these transcriptional proteins and their interaction with the small molecule modulators is hence anxiously awaited. Nevertheless, it has been conclusively demonstrated that identifying potent small molecules that target transcriptional proteins directly is fundamentally feasible. Many exciting

**Table 1:** Activities of small molecules in transcription modulation.

Compound	Name	Source <sup>[a]</sup>	Target <sup>[b]</sup>	IC <sub>50</sub> /K <sub>d</sub> <sup>[c]</sup> [μM]
1	IIA6B17	COM	Myc/Max	50–125/n.d.
2	10074A4	COM	c-Myc/Max	n.d./≈5
3	ISS-610	SGD	STAT3	42/n.d.
4	haptamide B	COM	HAP3	24/0.33
5	PKF115-584	NAT	TCF/β-catenin	3.2/n.d.
6	ICG-001	COM	CBP/β-catenin	3/n.d.
7	KG-501	COM	CBP/CREB	10/50
8	chetomin	NAT	p300/HIF-1α	≈0.01 <sup>[d]</sup> /n.d.
9	–	SGD	ER-α <sup>[e]</sup>	n.d./29
10	nutlin-3	COM	MDM2/p53	1–3/0.09 <sup>[f]</sup>
11	–	COM	HDM2/p53	30/0.4 <sup>[f]</sup>
12	–	SGD	MDM2/p53	0.8–10/0.09 <sup>[f]</sup>
13	RITA	COM	p53	0.05–13/0.0015

[a] SGD = structure guided design, COM = combinatorial chemistry or library, NAT = natural product or derivative. [b] Identified primary binding partners are shown underlined. [c] All values are strongly assay- and cell-type dependent and should be compared only with great caution, even when the same mode of action is likely. n.d. = not determined. [d] Reporter and two-hybrid assays under hypoxic conditions. [e] The ER-ligand binding site was saturated with estradiol. [f] K<sub>d</sub> from p53 peptide competition assays.

advancements are likely to arise from the field: Most of the compounds should serve as excellent molecular probes for transcriptional regulation and some of them may even lead the way to new therapeutic applications.

*Funding by the Fonds der Chemischen Industrie (Liebig scholarship) and the DFG (AR493-I) is gratefully acknowledged. I thank Prof. Dr. H. Waldmann for support and encouragement.*

Received: January 23, 2006

- [1] M. Levine, R. Tjian, *Nature* **2003**, *424*, 147–151.
- [2] For recent reviews, see: a) A. Ananda, A. Pascual, *Physiol. Rev.* **2001**, *81*, 1269–1304; b) N. J. McKenna, B. W. O'Malley, *Cell* **2002**, *108*, 465–474; c) V. Perissi, M. G. Rosenfeld, *Nat. Rev. Mol. Cell Biol.* **2005**, *6*, 542–554.
- [3] a) H. Gronemeyer, J.-A. Gustafsson, V. Laudet, *Nat. Rev. Drug Discovery* **2004**, *3*, 950–964; b) K. W. Nettles, G. L. Greene, *Annu. Rev. Physiol.* **2005**, *67*, 309–333.
- [4] J. E. Darnell Jr., *Nat. Rev. Cancer* **2002**, *2*, 740–749.
- [5] This account focuses on non-oligomeric compounds. Targeting protein–protein interactions in general has been recently reviewed, see: a) T. Berg, *Angew. Chem.* **2003**, *115*, 2566–2586; *Angew. Chem. Int. Ed.* **2003**, *42*, 2462–2481; b) M. R. Arkin, J. A. Wells, *Nat. Rev. Drug Discovery* **2004**, *3*, 301–317; c) H. Yin, A. D. Hamilton, *Angew. Chem.* **2005**, *117*, 4200–4235; *Angew. Chem. Int. Ed.* **2005**, *44*, 4130–4163.
- [6] T. I. Lee, R. A. Young, *Annu. Rev. Genet.* **2000**, *34*, 77–137.
- [7] A. M. Näär, B. D. Lemon, R. Tjian, *Annu. Rev. Biochem.* **2001**, *70*, 475–501.
- [8] a) M. Boubé, L. Joulia, D. L. Cribbs, H. M. Bourbon, *Cell* **2002**, *110*, 143–150; b) R. D. Kornberg, *Trends Biochem. Sci.* **2005**, *30*, 235–239; c) H.-M. Bourbon, A. Aguilera, A. Z. Ansari, F. J. Asturias, A. J. Berk, S. Bjorklund, T. K. Blackwell, T. Borggreffe, M. Carey, M. Carlson, J. W. Conaway, R. C. Conaway, S. W. Emmons, J. D. Fondell, L. P. Freedman, T. Fukasawa, C. M. Gustafsson, M. Han, X. He, P. K. Herman, A. G. Hinnebusch, S. Holmberg, F. C. Holstege, J. A. Jaehning, Y.-J. Kim, L. Kuras, A. Leutz, J. T. Lis, M. Meisterernest, A. M. Naar, K. Nasmyth, J. D. Parvin, M. Ptashne, D. Reinberg, H. Ronne, I. Sadowski, H. Sakurai, M. Sipiczki, P. W. Sternberg, D. J. Stillman, R. Strich, K. Struhl, J. Q. Svejstrup, S. Tuck, F. Winston, R. G. Roeder, R. D. Kornberg, *Mol. Cell* **2004**, *14*, 553–557; d) Certain conditions allow transcription without a mediator: X. Fan, D. M. Chou, K. Struhl, *Nat. Struct. Mol. Biol.* **2006**, *13*, 117–120.
- [9] a) H. Kimura, K. Sugaya, P. R. Cook, *J. Cell Biol.* **2002**, *159*, 777–782; b) R. T. Phair, P. Scaffidi, C. Elbi, J. Vecerová, A. Dey, K. Ozato, D. T. Brown, G. Hager, M. Bustin, T. Misteli, *Mol. Cell Biol.* **2004**, *24*, 6393–6402.
- [10] a) R. Métivier, G. Penot, M. R. Hübner, G. Reid, H. Brand, M. Koš, F. Gannon, *Cell* **2003**, *115*, 751–763; b) Review: X. Darzacq, R. H. Singer, Y. Shav-Tal, *Curr. Opin. Cell Biol.* **2005**, *17*, 332–339.
- [11] T. Berg, S. B. Cohen, J. Desharnais, C. Sonderegger, D. J. Maslyar, J. Goldberg, D. L. Boger, P. K. Vogt, *Proc. Natl. Acad. Sci. USA* **2002**, *99*, 3830–3835.
- [12] a) C. E. Nesbitt, J. M. Tersak, E. V. Prochownik, *Oncogene* **1999**, *18*, 3004–3016; b) S. K. Oster, C. S. Ho, E. L. Soucie, L. Z. Penn, *Adv. Cancer Res.* **2002**, *84*, 81–154.
- [13] X. Yin, C. Giap, J. S. Lazo, E. V. Prochownik, *Oncogene* **2003**, *22*, 6151–6159.
- [14] Y. Xu, J. Shi, N. Yamamoto, J. A. Moss, P. K. Vogt, K. D. Janda, *Bioorg. Med. Chem.* **2006**, *14*, 2660–2673.
- [15] Reviews: a) G. R. Stark, I. M. Kerr, B. R. Williams, R. H. Silverman, R. D. Schreiber, *Annu. Rev. Biochem.* **1998**, *67*, 227–264; b) H. Yu, R. Jove, *Nat. Rev. Cancer* **2004**, *4*, 97–105.
- [16] J. Turkson, J. S. Kim, S. Zhang, J. Yuan, M. Huang, M. Glenn, E. Haura, S. Sebti, A. D. Hamilton, R. Jove, *Mol. Cancer Ther.* **2004**, *3*, 261–269.
- [17] Peptidomimetics with submicromolar affinities for STAT3 in vitro have recently been reported, see: D. R. Coleman, Z. Y. Ren, P. K. Mandal, A. G. Cameron, G. A. Dyer, S. Muranjan, M. Campbell, X. M. Chen, J. S. McMurray, *J. Med. Chem.* **2005**, *48*, 6661–6670.
- [18] A. N. Koehler, A. F. Shamji, S. L. Schreiber, *J. Am. Chem. Soc.* **2003**, *125*, 8420–8421.
- [19] R. Mantovani, *Gene* **1999**, *239*, 15–27.
- [20] For reviews, see: a) C. Wolberger, *Annu. Rev. Biophys. Biomol. Struct.* **1999**, *28*, 29–56; b) K. Ogata, K. Sato, T. Tahirov, *Curr. Opin. Struct. Biol.* **2003**, *13*, 40–48; c) R. Marmorstein, M. X. Fitzgerald, *Gene* **2003**, *304*, 1–12.
- [21] a) V. Korinek, N. Barker, P. J. Morin, D. van Wichen, R. de Weger, K. W. Kinzler, B. Vogelstein, H. Clevers, *Science* **1997**, *275*, 1784–1787; b) P. Polakis, *Curr. Opin. Genet. Dev.* **1999**, *9*, 15–21; c) M. Bienz, H. Clevers, *Cell* **2000**, *103*, 311–320.
- [22] T. A. Graham, C. Weaver, F. Mao, D. Kimelman, W. Xu, *Cell* **2000**, *103*, 885–896.
- [23] M. Lepourcelet, Y.-N. P. Chen, D. S. France, H. Wang, P. Crews, F. Petersen, C. Bruseo, A. W. Wood, R. A. Shivdasani, *Cancer Cell* **2004**, *5*, 91–102.
- [24] In an earlier screening effort, piperazinones were reported to depress LEF-1/β-catenin mediated transcription: D. L. Boger, J. Goldberg, S. Satoh, Y. Ambroise, S. B. Cohen, P. K. Voigt, *Helv. Chim. Acta* **2000**, *83*, 1825–1845. The exact target of these compounds remains unresolved at present; a different piperazinone (**6**) was reported to bind to CBP (see reference [26]).
- [25] N. Vo, R. H. Goodman, *J. Biol. Chem.* **2001**, *276*, 13505–13508.
- [26] K. H. Emami, C. Nguyen, H. Ma, D. H. Kim, K. W. Jeong, M. Eguchi, R. T. Moon, J. L. Teo, S. W. Oh, H. Y. Kim, S. H. Moon, J. R. Ha, M. Kahn, *Proc. Natl. Acad. Sci. USA* **2004**, *101*, 12682–12687.
- [27] J. L. Best, C. A. Amezcua, B. Mayr, L. Flechner, C. M. Murawsky, B. Emerson, T. Zor, K. H. Gardner, M. Montminy, *Proc. Natl. Acad. Sci. USA* **2004**, *101*, 17622–17627.
- [28] A. L. Kung, S. D. Zabudoff, D. S. France, S. J. Freedman, E. A. Tanner, A. Vieira, S. Cornell-Kennon, J. Lee, B. Wang, J. Wang, K. Memmert, H.-U. Naegeli, F. Petersen, M. J. Eck, K. W. Bair, A. W. Wood, D. M. Livingston, *Cancer Cell* **2004**, *6*, 33–43.
- [29] L. Nagy, J. W. R. Schwabe, *Trends Biochem. Sci.* **2004**, *29*, 317–324.
- [30] a) T. R. Geistlinger, R. K. Guy, *J. Am. Chem. Soc.* **2001**, *123*, 1525–1526; b) T. R. Geistlinger, R. K. Guy, *J. Am. Chem. Soc.* **2003**, *125*, 6852–6853; c) A. M. Leduc, J. O. Trent, J. L. Wittliff, K. S. Bramlett, S. L. Briggs, N. Y. Chirgadze, Y. Wang, T. P. Burris, A. F. Spatola, *Proc. Natl. Acad. Sci. USA* **2003**, *100*, 11273–11278.
- [31] A. L. Rodriguez, A. Tamrazi, M. L. Collins, J. A. Katzenellenbogen, *J. Med. Chem.* **2004**, *47*, 600–611.
- [32] L. A. Arnold, E. Estébanez-Perpiña, M. Togashi, N. Jouvarel, A. Shelat, A. C. McReynolds, E. Mar, P. Nguyen, J. D. Baxter, R. J. Fletterick, P. Webb, R. K. Guy, *J. Biol. Chem.* **2005**, *280*, 43048–43055.
- [33] K. H. Vousden, X. Lu, *Nat. Rev. Cancer* **2002**, *2*, 594–604.
- [34] P. Chène, *Nat. Rev. Cancer* **2003**, *3*, 102–109.
- [35] P. H. Kussie, S. Gorina, V. Marechal, B. Elenbaas, J. Moreau, A. J. Levine, N. P. Pavletich, *Science* **1996**, *274*, 948–953.
- [36] L. T. Vassilev, B. T. Vu, B. Graves, D. Carvajal, F. Podlaski, Z. Filipovic, N. Kong, U. Kammlott, C. Lukacs, C. Klein, N. Fotouhi, E. A. Liu, *Science* **2004**, *303*, 844–848.
- [37] B. L. Grasberger et al., *J. Med. Chem.* **2005**, *48*, 909–912.

- [38] K. Ding, Y. Lu, Z. Nikolovska-Coleska, S. Qiu, Y. Ding, W. Gao, J. Stuckey, K. Krajewski, P. P. Roller, Y. Tomita, D. A. Parrish, J. R. Deschamps, S. Wang, *J. Am. Chem. Soc.* **2005**, *127*, 10130–10131.
- [39] N. Issaeva, P. Bozko, M. Enge, M. Protopopova, L. G. G. C. Verhoef, M. Masucci, A. Pramanik, G. Selivanova, *Nat. Med.* **2004**, *10*, 1321–1328.
- [40] L. D'Silva, P. Ozdowy, M. Krajewski, U. Rothweiler, M. Singh, T. A. Holak, *J. Am. Chem. Soc.* **2005**, *127*, 13220–13226.
- [41] a) J. Ma, M. Ptashne, *Cell* **1987**, *51*, 113–119; b) O. Nyanguile, M. Uesugi, D. J. Austin, G. L. Verdine, *Proc. Natl. Acad. Sci. USA* **1997**, *94*, 13402–13406; c) For a review, see: A. Z. Ansari, A. K. Mapp, *Curr. Opin. Chem. Biol.* **2002**, *6*, 765–772.
- [42] H. Shimogawa, Y. Kwon, Q. Mao, Y. Kawazoe, Y. Choi, S. Asada, H. Kigoshi, M. Uesugi, *J. Am. Chem. Soc.* **2004**, *126*, 3461–3471.
- [43] Z. Wu, G. Belanger, B. B. Brennan, J. K. Lum, A. R. Minter, S. P. Rowe, A. Plachetka, C. Y. Majmudar, A. K. Mapp, *J. Am. Chem. Soc.* **2003**, *125*, 12390–12391.
- [44] a) A. R. Minter, B. B. Brennan, A. K. Mapp, *J. Am. Chem. Soc.* **2004**, *126*, 10504–10505; b) S. J. Buhrhage, B. B. Brennan, A. R. Minter, A. K. Mapp, *J. Am. Chem. Soc.* **2005**, *127*, 12456–12457.
- [45] Y. Kwon, H.-D. Arndt, Q. Mao, Y. Choi, Y. Kawazoe, P. B. Dervan, M. Uesugi, *J. Am. Chem. Soc.* **2004**, *126*, 15940–15941.
- [46] Review on DNA-binding hairpin polyamides: P. B. Dervan, B. S. Edelson, *Curr. Opin. Struct. Biol.* **2003**, *13*, 284–299.
- [47] B. Liu, P. G. Alluri, P. Yu, T. Kodadek, *J. Am. Chem. Soc.* **2005**, *127*, 8254–8255.
- [48] S. J. Teague, *Nat. Rev. Drug Discovery* **2003**, *2*, 527–541.

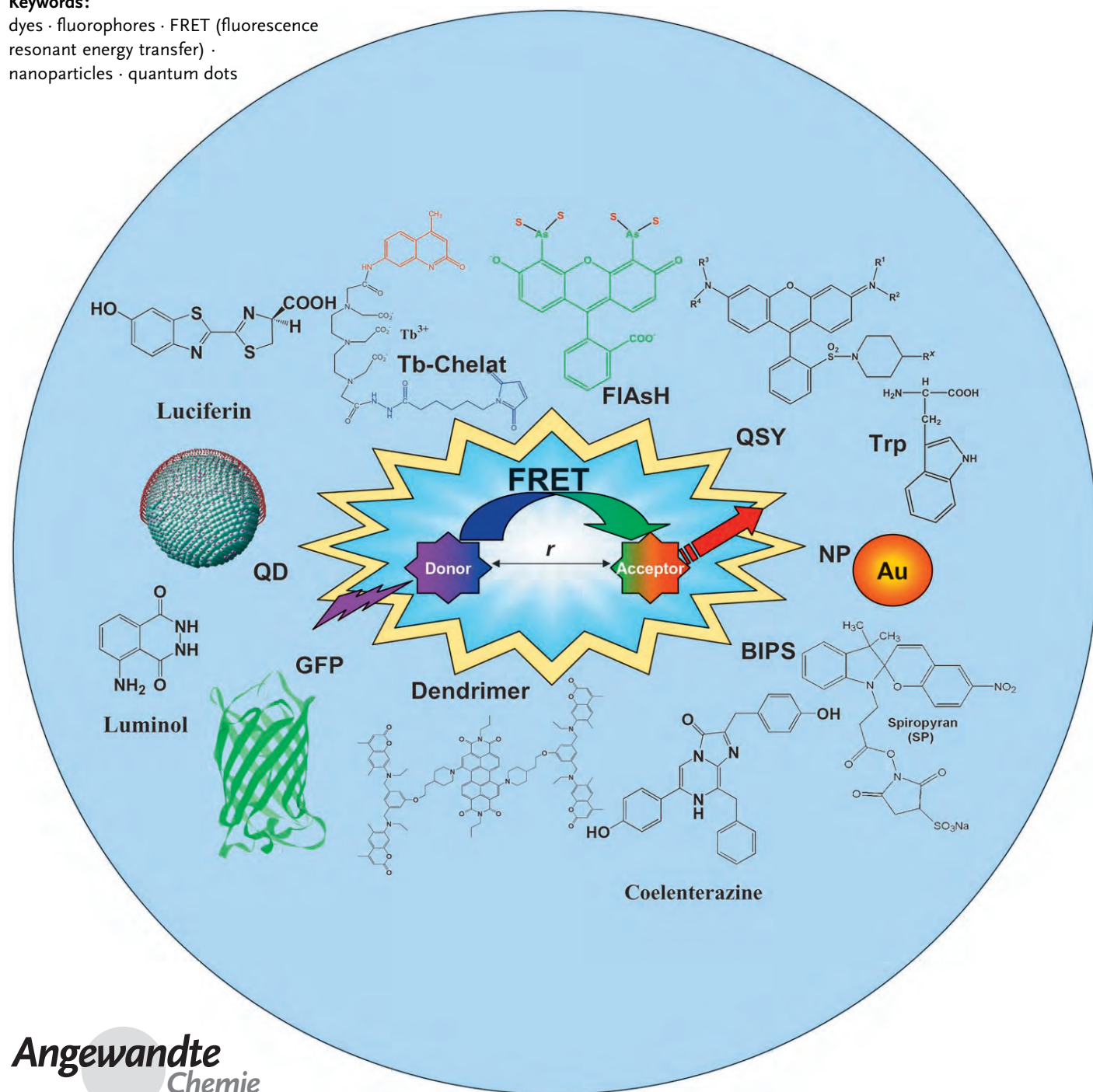


# Materials for Fluorescence Resonance Energy Transfer Analysis: Beyond Traditional Donor–Acceptor Combinations\*\*

Kim E. Sapsford, Lorenzo Berti, and Igor L. Medintz\*

**Keywords:**

dyes · fluorophores · FRET (fluorescence resonant energy transfer) · nanoparticles · quantum dots



**The use of Förster or fluorescence resonance energy transfer (FRET) as a spectroscopic technique has been in practice for over 50 years. A search of ISI Web of Science with just the acronym “FRET” returns more than 2300 citations from various areas such as structural elucidation of biological molecules and their interactions, in vitro assays, in vivo monitoring in cellular research, nucleic acid analysis, signal transduction, light harvesting and metallic nanomaterials. The advent of new classes of fluorophores including nanocrystals, nanoparticles, polymers, and genetically encoded proteins, in conjunction with ever more sophisticated equipment, has been vital in this development. This review gives a critical overview of the major classes of fluorophore materials that may act as donor, acceptor, or both in a FRET configuration. We focus in particular on the benefits and limitations of these materials and their combinations, as well as the available methods of bioconjugation.**

## 1. Introduction

### 1.1. The FRET Process

Fluorescence resonance energy transfer (FRET) is a nonradiative process whereby an excited state donor D (usually a fluorophore) transfers energy to a proximal ground state acceptor A through long-range dipole–dipole interactions (Figure 1).<sup>[1,2]</sup> The acceptor must absorb energy at the emission wavelength(s) of the donor, but does not necessarily have to reemit the energy fluorescently itself (i.e. dark quenching). The rate of energy transfer is highly dependent on many factors, such as the extent of spectral overlap, the relative orientation of the transition dipoles, and, most importantly, the distance between the donor and acceptor molecules.<sup>[2]</sup> An intensive description of the physical basis of FRET, which is beyond the scope of this review, can be found in reference [2].

FRET usually occurs over distances comparable to the dimensions of most biological macromolecules, that is, about 10 to 100 Å. Although configurations in which multiple donors and acceptors interact are increasingly common (see, for example, references [3–5]), the following equations consider energy transfer between a single linked D/A pair separated by a fixed distance  $r$  and originate from the theoretical treatment of Förster.<sup>[2,6,7]</sup> The energy transfer rate  $k_T(r)$  between a single D/A pair is dependent on the distance  $r$  between D and A and can be expressed in terms of the Förster distance  $R_0$ .  $R_0$  is the distance between D and A at which 50 % of the excited D molecules decay by energy transfer, while the other half decay through other radiative or nonradiative channels.  $R_0$  can be calculated from the spectral properties of the D and A species [Eq. (1)].

$$R_0 = 9.78 \times 10^3 [\kappa^2 n^{-4} Q_D J(\lambda)]^{1/6} \text{ (in Å)} \quad (1)$$

The factor  $\kappa^2$  describes the D/A transition dipole orientation and can range in value from 0 (perpendicular) to 4 (collinear/parallel). There has been much debate about which

## From the Contents

<b>1. Introduction</b>	<b>4563</b>
<b>2. Organic Materials</b>	<b>4565</b>
<b>3. Biological Materials</b>	<b>4571</b>
<b>4. Inorganic Materials</b>	<b>4576</b>
<b>5. Multi-FRET Systems</b>	<b>4582</b>
<b>6. New Materials</b>	<b>4583</b>
<b>7. Summary and Outlook</b>	<b>4584</b>

dipole orientation value to assign for particular FRET formats. Only in few cases can the crystal structure of the D/

A molecules be determined; there is no other reliable experimental method to measure absolute or fixed  $\kappa^2$  values, which leads to potential uncertainties in subsequent calculations.<sup>[2,8,9]</sup> Fortunately, the accumulated evidence has shown that the mobility and statistical dynamics of the dye linker lead to a  $\kappa^2$  value of approximately 2/3 in almost all biological formats. This also sets an upper error limit of 35 % on any calculated distance.<sup>[2]</sup> Excellent discussions of this issue are provided by dos Remedios and Moens<sup>[9]</sup> as well as Stryer.<sup>[10]</sup> The refractive index  $n$  of the medium is ascribed a value of 1.4 for biomolecules in aqueous solution.  $Q_D$  is the quantum yield (QY) of the donor in the absence of the acceptor and  $J(\lambda)$  is the overlap integral, which represents the degree of spectral overlap between the donor emission and the acceptor absorption. The values for  $J(\lambda)$  and  $R_0$  increase with higher acceptor extinction coefficients and greater overlap between the donor emission spectrum and the acceptor absorption spectrum. Whether FRET will be effective at a particular distance  $r$  can be estimated by the “rule of thumb”  $R_0 \pm 50\%$   $R_0$  for the upper and lower limits of the

[\*] Dr. K. E. Sapsford,<sup>[†]</sup> Dr. I. L. Medintz  
Center for Bio/Molecular Science and Engineering  
U.S. Naval Research Laboratory, Code 6910  
4555 Overlook Ave, SW Washington, DC 20375 (USA)  
Fax: (+1) 202-767-9594  
E-mail: imedintz@cbmse.nrl.navy.mil  
Dr. K. E. Sapsford<sup>[†]</sup>  
George Mason University  
10910 University Blvd, MS 4E3, Manassas, VA 20110 (USA)  
Dr. L. Berti<sup>[†]</sup>  
S3-INFM-CNR  
National Research Center on nanoStructures and bioSystems at Surfaces  
Via Campi 213/A, 41100 Modena (Italy)

[†] These authors contributed equally.

[\*\*] Supporting information for this article (a list of companies whose products are mentioned in this review) is available on the WWW under <http://www.angewandte.org> or from the author.

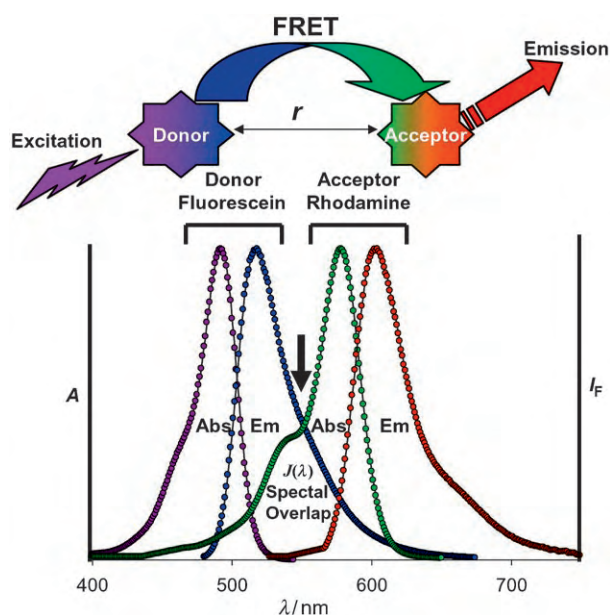


**Figure 1.** Schematic of the FRET process: Upon excitation, the excited-state donor molecule transfers energy nonradiatively to a proximal acceptor molecule located at distance  $r$  from the donor. The acceptor releases the energy either through fluorescence or nonradiative channels. The spectra show the absorption (Abs) and emission (Em) profiles of one of the most commonly used FRET pairs: fluorescein as donor and rhodamine as acceptor.<sup>[309]</sup> Fluorescein can be efficiently excited at 480 nm and emits at around 520 nm. The spectral overlap between fluorescein emission and rhodamine absorption, as defined by  $J(\lambda)$ , is observed at 500–600 nm. The Förster distance  $R_0$  for this pair is 55 Å. Thus, in an optimal configuration ( $r < 55$  Å), excitation of fluorescein at under 500 nm can result in significant FRET emission of the rhodamine at above 600 nm.  $A$  = normalized absorption,  $I_F$  = normalized fluorescence.

Förster distance.<sup>[8,9]</sup> The efficiency of the energy transfer can be determined from either steady-state [Eq. (2)] or time-resolved [Eq. (3)] measurements.

$$E = 1 - \frac{F_{DA}}{F_D} \quad (2)$$

$$E = 1 - \frac{\tau_{DA}}{\tau_D} \quad (3)$$

$F$  is the relative donor fluorescence intensity in the absence ( $F_D$ ) and presence ( $F_{DA}$ ) of the acceptor, and  $\tau$  is the fluorescent lifetime of the donor in the absence ( $\tau_D$ ) and presence ( $\tau_{DA}$ ) of the acceptor.

FRET is very appealing for bioanalysis because of its intrinsic sensitivity to nanoscale changes in D/A separation distance (proportional to  $r^6$ ). This property is exploited in FRET techniques ranging from the assay of interactions of an antigen with an antibody *in vitro* to the real-time imaging of protein folding *in vivo*.<sup>[11,12]</sup> The myriad FRET configurations and techniques currently in use are covered in many reviews.<sup>[8,13,14]</sup> Herein, we focus primarily on the fluorophore materials utilized in bioanalytical FRET rather than the process itself. The materials can be divided into various classes: organic materials, which includes “traditional” dye fluorophores, dark quenchers, and polymers; inorganic materials such as metal chelates, and metal and semiconductor nanocrystals; fluorophores of biological origin such as fluorescent proteins and amino acids; and biological compounds that exhibit bioluminescence upon enzymatic catalysis. These materials may function as either FRET donors, FRET acceptors, or both, depending upon experimental design. A major focus is on FRET between disparate classes of materials; selected examples will be discussed for this purpose. We also focus on potential FRET materials that have not yet found practical application. Given the myriad examples available, we cannot do justice to all developments and we extend our apologies for any omissions.

## 1.2. Methods of Conjugating Fluorophores to Biomolecules

Fluorophore conjugation to biomolecules at known distinct locations is the most desirable FRET configuration; thus techniques for accomplishing this deserve some discussion. The most commonly used reagents for site-specific biolabeling are commercially available fluorophores with a succinimidyl ester or maleimide reactive group that targets the primary amino or thiol groups, respectively, on biomolecules such as proteins or DNA. As proteins have many primary amino groups (mostly lysine residues), the coupling is relatively unspecific and variable dye-to-protein (D/P) ratios result. Targeting thiol groups on cysteine residues with maleimide chemistry is more specific as these can be easily



Igor L. Medintz, born 1968, studied chemistry and forensic science at John Jay College of Criminal Justice, City University of New York. In 1998, he received his PhD in molecular biology under Prof. Corinne Michels of Queens College (also CUNY). He carried out postdoctoral research under Prof. Richard A. Mathies (UC Berkeley) on the development of FRET-based assays for microfabricated devices for genetic analysis. Since 2002 he has been at the Center for Bio/Molecular Science and Engineering of the US Naval Research Laboratory where he is working in collaboration with Dr. Hedi Mattoussi on creating biosensors with quantum dots.



Kim E. Sapsford, born 1974, studied chemistry at the University of East Anglia (Norwich, UK) and in 2001 received her PhD in analytical chemistry under Prof. David A. Russell. Since 2001 she has been at the Center for Bio/Molecular Science and Engineering of the US Naval Research Laboratory, where she is working on creating fluorescent-based biosensors using the array biosensor technology that was developed by Dr. Frances Ligier.



introduced into proteins recombinantly for this purpose.<sup>[15]</sup> However, this too can be problematic, since disulfide bridges already present in proteins may be critical to the conformation, and additional cysteine residues could destroy the protein structure. Additionally, proteins expressing even a single surface-exposed thiol group will form dimers when purified, so that a reduction step is necessary prior to labeling. The original chemistry for protein labeling was developed by Gregorio Weber, and many of the probes he developed are still in use today.<sup>[2]</sup> In general DNA and RNA labeling is less challenging, as these can be synthesized with site-specific thiol or amine groups, as well as nucleotides modified with a variety of fluorophores and quenchers.<sup>[16,17]</sup> Thus, both differential labeling and the exact placement of fluorophores within the oligonucleotide structure are possible. Table 1 lists some of the commonly available reactive groups on fluorophores designed for labeling biomolecules, along with their targets.

A variety of protocols exist for introducing specific functional groups onto biomolecules. Perhaps the best available resource on this subject is Hermanson's *Bioconjugate Techniques*.<sup>[18]</sup> *A Guide to Fluorescent Probes and Labeling Technologies* by Haugland is another good source (available free of charge from Molecular Probes).<sup>[19]</sup> Strategies exist that employ noncovalent or electrostatic interactions for associating fluorophores with biomolecules, although these are not so attractive for FRET applications.<sup>[2,19]</sup>

Several emerging technologies offer alternatives for site-specific fluorescent labeling of proteins; most are geared towards applications in vivo. Fluorescent proteins (FPs) such

as the green fluorescent protein (GFP) can be appended onto existing proteins by using recombinant techniques, thus allowing the endogenous expression of fluorescent protein chimeras (see Section 3.2).<sup>[14,20,21]</sup> The FAsH method (FAsH = 4',5'-bis(1,3,2-dithioarsolan-2-yl)fluorescein) developed by Tsien allows in vivo coupling of nonfluorescent, cell-permeable biarsenical fluorophores to proteins expressing an optimized Cys-Cys-Pro-Gly-Cys-Cys sequence. Only the reacted fluorophore is emissive. This labeling technique has already been used for in vivo FRET applications (Figure 2).<sup>[21–24]</sup>

The HaloTag method utilizes a fusion protein with a dehalogenase domain, on which a fluorescent ligand is conjugated through substitution of a chloride function.<sup>[25]</sup> Another fusion protein based system, which allows both in vivo and solution labeling of target proteins, is the SNAP tag. This system utilizes a modified alkylguanine–DNA alkyl transferase, which reacts with a *p*-benzylguanine-modified fluorophore to form a thioether bond. Hellinga and co-workers have also described a method for the sequential/orthogonal labeling of multiple thiol groups on purified proteins by exploiting metal coordination and disulfide bond formation to protect cysteine residues in a Cys<sub>2</sub>His<sub>2</sub> zinc-finger domain.<sup>[26]</sup> Future strategies may include in vivo incorporation of unnatural amino acids as unique labeling sites.<sup>[27]</sup> Regardless of the FRET method chosen, having both the donor and acceptor at known, distinct locations on biomolecule(s) is most desirable for analysis of the experimental data. It is also the most technically challenging to accomplish on a single molecular entity.

**Table 1:** Common reactive groups and methods for attaching fluorophores to biomolecules.<sup>[18,19]</sup>

Target	Reactive Group	Comment
thiol	maleimide, iodoacetyl, pyridyldisulfide <sup>[a]</sup>	site-specific but requires a free cysteine on proteins
primary amine	succinimidyl esters (NHS), sulfonyl chlorides, iso(thio)cyanates, carbonyl azides <sup>[a]</sup>	proteins may have many primary amines
carboxyl	carbonyldiimidazoles, carbodiimides <sup>[b]</sup>	allows further coupling to amines
hydroxyl	carbonyldiimidazoles, periodate, disuccinimidyl carbonate <sup>[b]</sup>	allows further coupling to amines
carbohydrates	periodate <sup>[b]</sup>	oxidizes sugars to create reactive aldehydes, which couple to amines
intracellular proteins	FAsH <sup>[22]</sup>	requires cloning
intracellular proteins	SNAP-tag/HaloTag <sup>[25]</sup>	requires cloning and commercial ligands
intracellular proteins	fluorescent proteins <sup>[14,20,21]</sup>	requires cloning and formation of a chimera

[a] Reactivity can also target amine- or thiol-modified DNA. [b] Multistep modifications.



Lorenzo Berti, born 1971, studied Chemistry at the University of Bologna (Italy) and obtained his PhD in organic chemistry from the same university in 2000. He carried out postdoctoral research under Prof. Richard A. Mathies at UC Berkeley, where he developed universal FRET tags for DNA sequencing and genotyping. Since 2003 he has been a Research Scientist at the INFN-CNR in Modena, Italy. His research interests include developing linking strategies for conjugating biomolecules to inorganic materials and exploiting the potential of DNA for engineering nanostructures.

## 2. Organic Materials

### 2.1. UV-, Vis-, and IR-Emitting Dyes

Organic dyes that emit in the ultraviolet (UV), visible (Vis), and near-infrared (IR) region are considered “traditional” FRET dyes. They represent the majority of D/A pairs currently used in FRET applications and are also the first type of dye usually tested with new or “nontraditional” materials. The most common are several structurally related classes of dyes whose emissions span the UV-to-IR spectrum (Figure 3). Such dyes are available in reactive form from commercial sources activated with *N*-hydroxysuccinimide (NHS) ester,



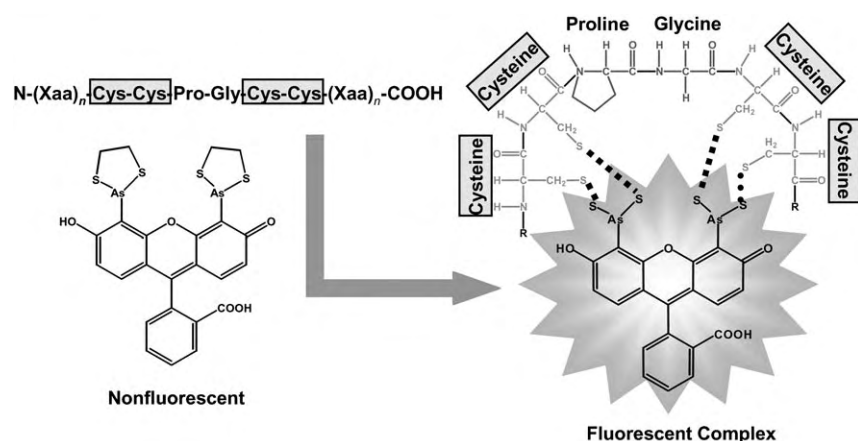


**Figure 2.** Structure of the fluorescein derivative FIAsh in its nonfluorescent form and the optimized hairpin motif with target cysteine residues highlighted (Xaa = generic amino acid). After conjugating with this peptide sequence in vivo, the bound fluorophore becomes emissive.<sup>[22,23]</sup>

Members of some dye families, such as the cyanines (Cy), are closely related in structure, whereas others, such as the AlexaFluor compounds, are quite diverse. All dye families are typically characterized by closely spaced, broad absorption/emission profiles (small Stokes shift) and all have both associated advantages and disadvantages depending on the intended application. For example, fluorescein dyes are popular because of their high quantum yields, solubility, and ease of bioconjugation, and fluorescence is readily obtained by excitation with a standard argon-ion laser (488 nm). However, fluorescein has a high rate of photobleaching, is pH-sensitive (which is sometimes advantageous, see Section 2.3), and can self-quench at high degrees of substitution. Alternatives such as Oregon Green dyes (fluorinated fluorescein analogues), the AlexaFluor compounds, the Cy family, and the

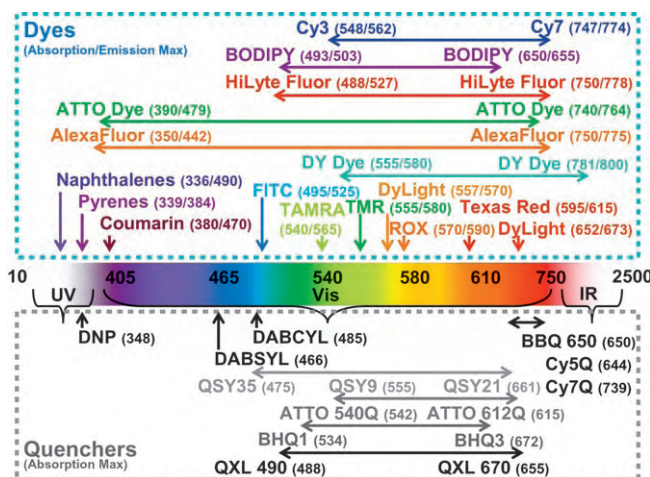
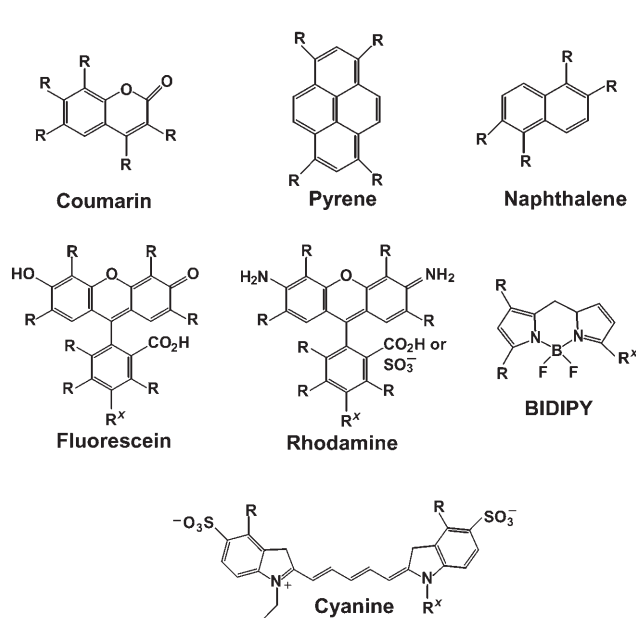


**Figure 3.** Examples of available fluorescent dye and quencher families, almost all of which have been used for FRET measurements. Absorbance and emission maxima along with spectral regions covered by a particular dye family are highlighted. Tetramethylrhodamine (TMR), carboxytetramethylrhodamine (TAMRA), and carboxy-X-rhodamine (ROX) are all rhodamine-based dyes. The most common D/A dye combinations are coumarin/fluorescein, fluorescein/rhodamine, and Cy3.5/Cy5. Popular dye/quencher combinations include rhodamine/Dabcyl and Cy3/QSY9. Major suppliers are the companies Molecular Probes (fluorescein, rhodamine, AlexaFluor, BODIPY Oregon Green, Texas Red, and QSY quenchers), Amersham Biosciences (Cy dyes and Cy5Q/Cy7Q quenchers), AnaSpec (HiLyte Fluors, QXL quenchers), ATTO-TEC (ATTO dyes and quenchers), and Molecular Biotechnology (DY dyes), Pierce (DyLight 547 and DyLight 647 dyes), Berry and Associates (BlackBerry), and Biosearch Technologies (Black Hole). FITC = fluorescein isothiocyanate.

maleimide, hydrazide, or amine functionalities for bioconjugation. The UV dyes are typically pyrene-, naphthalene-, and coumarin-based structures, while the Vis/near-IR dyes include a variety of fluorescein-, rhodamine-, and cyanine-based derivatives (Scheme 1).



**Scheme 1.** Structures of common UV/Vis fluorescent dyes. Typical substituents at the R position include CO<sub>2</sub><sup>-</sup>, SO<sub>3</sub><sup>-</sup>, OH, OCH<sub>3</sub>, CH<sub>3</sub>, and NO<sub>2</sub>; R' marks the typical position of the bioconjugation linker.

BODIPY compounds may alleviate some of these issues. Low solubility in aqueous environments can be an issue for some of the redder dyes, for which overlabeling can induce protein precipitation. For FRET applications in particular, the broad absorption/emission profiles and small Stokes shifts often lead to direct excitation of the acceptor, which complicates subsequent analysis. In general, their advantages include: the availability from commercial sources, their relatively low cost, the availability of established methods for bioconjugation, and, most importantly, the extensive description of their FRET properties in the literature.

There are many resources available to aid in choosing suitable D/A pairs, including a number of reviews.<sup>[2, 15, 28, 29]</sup> Wu and Brand<sup>[30]</sup> offer an extensive list of donor-acceptor dye pairs and their respective  $R_0$  values. Haugland's *Handbook* is another excellent resource.<sup>[19]</sup> The web-based programs of Invitrogen (<http://probes.invitrogen.com/resources/spectraviewer/>) and BioRad (<http://microscopy.biorad.com/fluorescence/fluorophoreDatab.htm>) allow the researcher to plot multiple dye absorption/emission profiles to optimize spectral overlap as well as choose appropriate filters. Buschmann et al. also give an excellent comparison of the physical and spectroscopic properties of a number of red-absorbing dyes.<sup>[31]</sup>

Dye-to-dye FRET combinations still remain state-of-the-art for many applications.<sup>[2, 8]</sup> Enzymes, designed substrates, and cell surface receptors labeled with these organic D/A dye pairs have been used both in vitro and in vivo to monitor various biochemical processes, such as 3',5' cyclic monophosphate (cAMP) production,<sup>[32]</sup> phosphodiesterase activity,<sup>[33]</sup>  $\beta$ -lactamase activity,<sup>[34]</sup> integrin binding,<sup>[35, 36]</sup> as well as conformational and electrical processes in single-ion channels.<sup>[37]</sup> Similar dye combinations are also useful for FRET-based biosensors, for examples, hydrogel-encapsulated glucose sensors<sup>[38]</sup> and sensors for lysozyme,<sup>[39]</sup> zinc,<sup>[40]</sup> and cholera toxin.<sup>[41]</sup>

One area in which FRET applications with donor-acceptor dye combinations has had tremendous impact is nucleic acid analysis, particularly DNA sequencing and genotyping.<sup>[16, 28, 29, 42]</sup> Mathies, Glazer, and co-workers realized that the use of a FRET system could simplify the instrumentation needed for DNA sequencing. By utilizing a common donor and four different acceptors (one for each of the DNA bases) attached to common DNA primers, they created four well-separated spectral emission windows that were excited at only a single wavelength.<sup>[43–45]</sup> The use of FRET could increase the acceptor emission with these primers by over 20 times with respect to directly excited non-FRET controls. This FRET strategy became the backbone of the DNA analysis technology that has revolutionized genomics and is found in derivative genotyping technology such as the Taqman assay.<sup>[16]</sup> A cassette version of the ET primers was created for attachment to any desired thiolated primer or oligonucleotide (Figure 4).<sup>[17]</sup> FRET-based DNA sensors have also been used to monitor pH variations in living cells during apoptosis.<sup>[46]</sup>

Interestingly, the use of DNA scaffolds has helped address fundamental questions about the dependence of the FRET efficiency on the orientation of the D/A dyes.<sup>[47]</sup> The immobilization of FRET-based DNA probes onto glass<sup>[48]</sup> and gold<sup>[49]</sup> has recently been tested and will be important

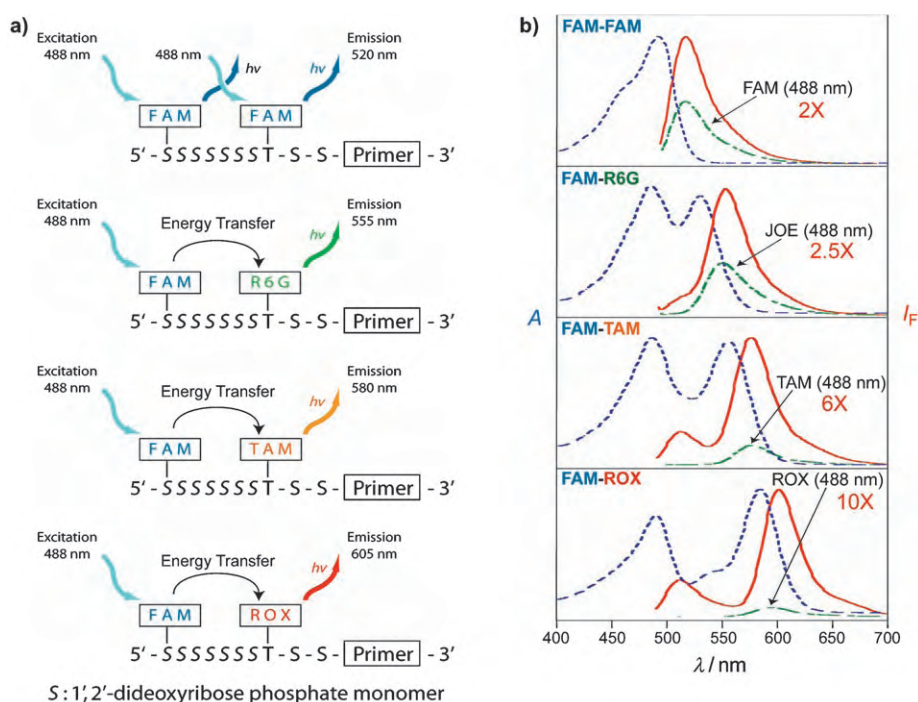


**Figure 4.** a) Schematic of energy-transfer cassette primers.<sup>[17]</sup> Each of the cassettes is built upon a common modified sugar-nucleotide backbone. The use of different acceptors creates four spectrally separated emission windows centered at 520, 550, 580, and 605 nm. The energy-transfer cassettes are attached to thiolated primers through thiol bridges. R6G = 6-carboxyrhodamine-6-G, TAM = carboxy-*tr*-methylrhodamine. b) Normalized absorbance and emission spectra (488-nm excitation) for each of the four colors of an ET cassette compared with direct excitation of the corresponding control acceptor dye at the same concentration. The factor by which the emission is increased in the FRET system relative to the single dye control assay is indicated in red. Figure generously provided by R. Mathies, UC Berkeley.

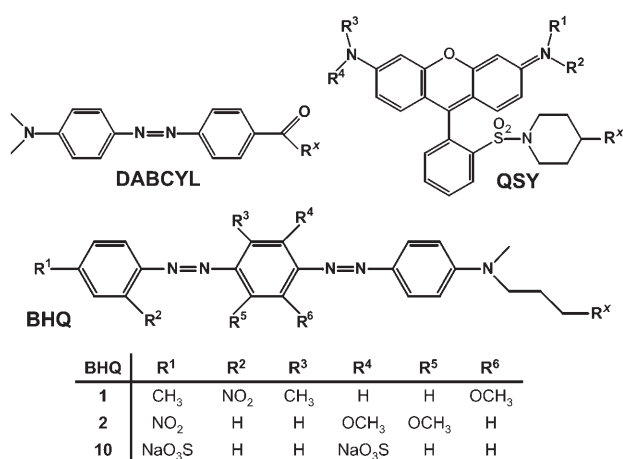
for utilizing such probes in high-throughput parallel detectors (analogues of DNA microarrays).

It is clear that traditional dye-to-dye FRET systems will continue to play an important role. The substitution of the donor and acceptor with other classes of fluorophore will be driven by addressing deficiencies of organic dyes and creating new applications.

## 2.2. Quencher Molecules

The use of quenching acceptors is becoming increasingly popular in FRET systems. The principal advantage that these molecules offer over their fluorescent counterparts is the elimination of background fluorescence originating from direct acceptor excitation or re-emission.

Quenchers can take the form of organic molecules or metallic materials such as gold (Section 4.2). There are a variety of organic quencher families available commercially (Figure 3 and Scheme 2). Dabcyl (4-(4'-dimethylaminophenylazo)benzoic acid) and Dabsyl (4-dimethylaminoazobenzene-4'-sulfonyl) are two of the most common nonfluorescent acceptors, with absorption maxima centered at 485 and 466 nm, respectively. Other quencher families include the QSY, QXL, ATTO, BlackBerry, and Black Hole quenchers.



**Scheme 2.** Structures of common organic quencher molecules. The substituents R are listed; R<sup>x</sup> marks the typical position of the bioconjugation linker.

These generally tend to have broad absorption spectra, which allow them to function as acceptors for many dyes. Quenchers are often applied to DNA analysis, in particular, in molecular beacons in the form of acceptors paired with organic dye donors (see review articles by Tan et al.<sup>[28,29]</sup> and Didenko<sup>[16]</sup>). The principal advantage of this configuration is that it allows monitoring of the donor channel alone and if sufficient spectral separation is achieved opens the possibility of “multiplexing” with other donor/quencher pairs. Besides DNA-based diagnostics, molecular beacons incorporating quencher species have been used to measure DNA permeability of polyelectrolyte thin films,<sup>[50]</sup> and catalytic DNA biosensors have detected lead ions.<sup>[51]</sup> Quencher-labeled substrate analogues have been used in conjunction with dye-labeled proteins for FRET-based displacement biosensing of nutrients.<sup>[52]</sup> One of the few examples of a FRET system in which organic quencher molecules are coupled to a non-organic fluorophore involves quantum dot (QD) donors (see Section 4.3).

### 2.3. Environmentally Sensitive Fluorophores

Environmentally sensitive fluorophores exhibit some change in their absorbance and emission properties in response to a change in their environment such as pH, ionic strength or type, (e.g., Ca<sup>2+</sup>, Cl<sup>−</sup>), O<sub>2</sub> saturation, solvation, or polarity. It is difficult to define them as a completely discrete class of fluorophores, as almost all fluorophores respond to some perturbation in their environment.<sup>[2,19]</sup> Thus, these fluorophores are usually defined by the analyte or condition to which they respond most favorably (e.g., pH or calcium indicator dyes).<sup>[19]</sup> Perhaps the best known example is fluorescein (FAM; Scheme 1), whose absorption and emission change in response to pH as a function of ionization equilibria (Figure 5).<sup>[19]</sup> This property has been extensively exploited to monitor intracellular pH, and a variety of FAM ester derivatives are available and are retained intracellularly following delivery and ester hydrolysis. The most commonly

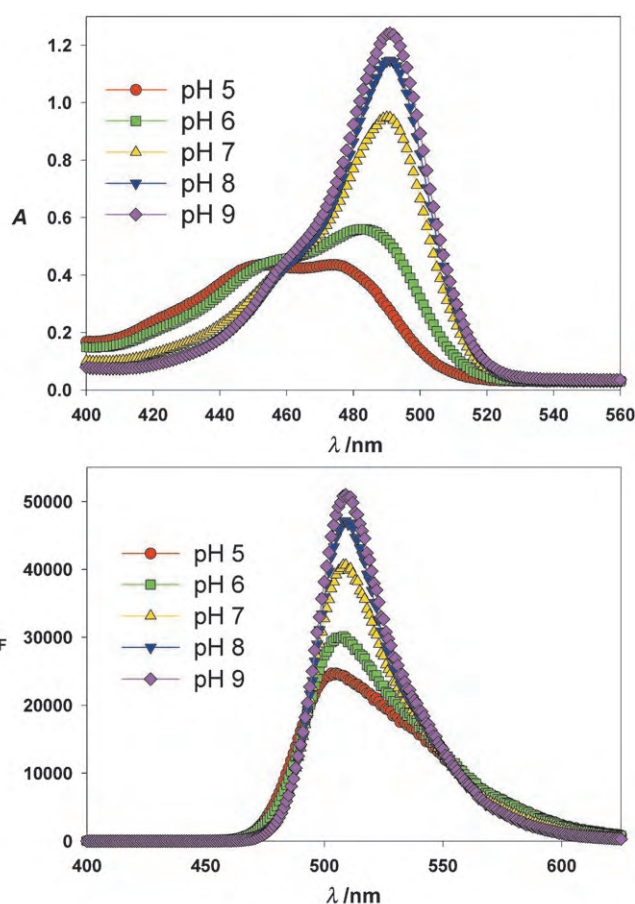


**Figure 5.** pH-dependent absorption (top) and emission (bottom) spectra of fluorescein. The largest change is between pH 6 and pH 7.

used probe for estimating intracellular pH is the polar BCECF derivative developed by Tsien and co-workers.<sup>[53]</sup> For pH monitoring, Molecular Probes offers a variety of reactive FAM analogues and proprietary seminaphthorhodafluors (SNARF), seminaphthofluoresceins (SNAFL), and their ester derivatives.<sup>[19]</sup> The optimal working range of these fluorophores is around pH 5–9. For acidic solutions, Oregon Green and LysoSensors are more appropriate.<sup>[19]</sup> However, the emission of these dyes is confined to the visible and near-IR region, and many are not available with reactive groups, so extensive chemical modification may be necessary to attach them to biomolecules or other dyes. Again, Haugland's *Handbook*<sup>[19]</sup> is a good reference for probes optimized for monitoring pH, NO<sub>2</sub>, Ca<sup>2+</sup>, Mg<sup>2+</sup>, Zn<sup>2+</sup>, Na<sup>+</sup>, Cl<sup>−</sup>, K<sup>+</sup>, and membrane potential.

Several other dyes such as acrylodan and pyrene have also been used as biosensors for changes in the environment of the coupled protein.<sup>[15]</sup> Lakowicz and co-workers have utilized FRET with environmentally sensitive acceptors to measure pH values, as well as CO<sub>2</sub> and NH<sub>3</sub> concentrations by using phase modulation fluorometry,<sup>[54,55]</sup> a technique that requires specialized equipment and expertise. In general, FRET configurations with environmentally sensitive fluorophores have not been utilized extensively as most of the fluorophores function adequately alone. Future applications of FRET-



based environmental sensors could facilitate spatiotemporal-correlated multicolor measurements of intracellular conditions by working in conjunction with other dyes.

#### 2.4. Dye-Labeled Microspheres/Nanoparticles

One of the limitations of conventional fluorescent assays is the difficulty in conjugating more than one fluorophore to a target. Conjugation to multiple fluorophores can increase the signal and achieve lower limits of detection; however, it can alter the function of the target biomolecule. To overcome these limitations, functionalized polymeric microspheres have been “soaked” with fluorophores, resulting in highly fluorescent nano- and microscale particles. Besides the increase in fluorescence intensity, fluorescent microspheres present other advantages. For instance, fluorophores that are water-insoluble or lack a reactive group can be loaded into microspheres. Fluorescent microspheres that absorb and emit from the UV to the near IR and whose sizes can range from 2  $\mu\text{m}$  down to around 20 nm are available from, for example, Molecular Probes, Bangs Laboratories, and Polysciences. Molecular Probes also offer TransFluospheres, which are microspheres loaded with a proprietary combination of dyes that optimize internal FRET to yield large Stokes shifts.<sup>[56]</sup> Fluorescent microspheres are also provided with a variety of surface functionalities (e.g., biotin, avidin, collagen, amines, aldehydes, sulfates, and carboxylates) that allow facile bioconjugation to targets of interest. Functionalized spheres can also be purchased and soaked with dyes by following published procedures.<sup>[57,58]</sup>

Fluorescent microspheres have been extensively employed in FRET-based analytical assays, especially flow cytometry<sup>[59–61]</sup> and SNP genotyping.<sup>[62]</sup> Besides standard fluorophores, fluorescent microspheres loaded with Eu-based fluorophores are available which can be used for time-resolved measurements of the energy transfer (Section 4.1).<sup>[63]</sup> Apart from flow cytometry, the use of fluorescent microspheres for FRET-based assays is still in their infancy. However, their high fluorescence intensity, wide absorption with multiple emission colors, multifaceted chemistry, and commercial availability make them promising as donors, especially for multiplex FRET assays.

#### 2.5. Dendrimers and Polymers

Dendrimers are highly-branched polymers that are obtained by stepwise synthesis.<sup>[64]</sup> A typical dendrimer contains a core monomer from which multiple branches stem. Each branch can be further expanded by adding other layers of monomers.<sup>[65]</sup> The principal utility in the current context is that multiple fluorophores and other chemical functionalities, which may be modified further, can be conjugated or adsorbed to the external shell to create highly fluorescent dendrimers.<sup>[66–71]</sup> Inherently fluorescent dendrimers have also been synthesized.<sup>[72,73]</sup>

The oriented placement of dyes can allow the energy absorbed at the periphery of the dendrimer to be funneled

through intramolecular energy transfer to a common acceptor positioned at the core; thus the dendrimer effectively acts as an artificial light-harvesting antenna (Figure 6, top).<sup>[74–77]</sup> The

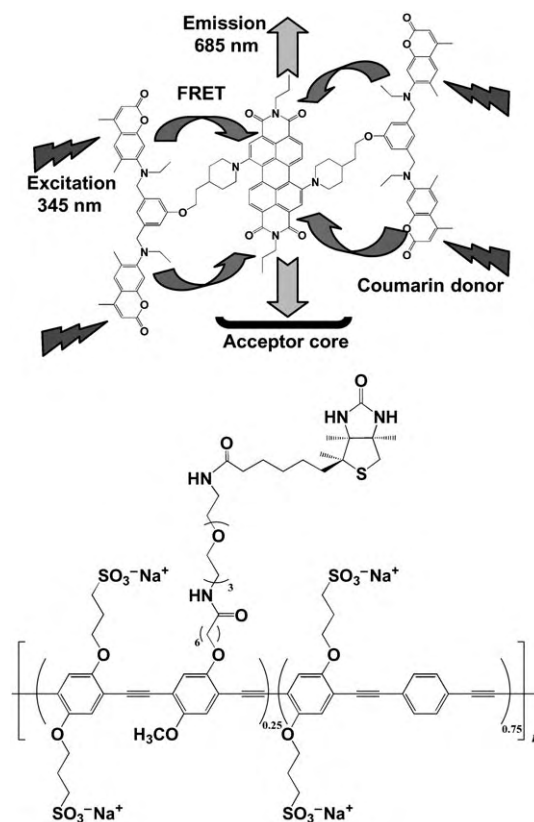


**Figure 6.** Top) Structure of a FRET dendrimer derived from a perylene bis(dicarboximide) acceptor as the core and a coumarin functionalized shell as the donor.<sup>[76]</sup> UV light (345 nm) is absorbed at the periphery, transferred as electronic energy to the acceptor in the core, and from there emitted in the near-IR (685 nm; 99% ET efficiency). Bottom) Structure of a biotin–polymer conjugate, employed in the detection of DNA hybridization.<sup>[98]</sup>

major advantages of dendrimer-based fluorophores in bioassays are the increased absorption cross section and higher fluorescence intensity.<sup>[78,79]</sup> Furthermore, as the solubility is determined by the dendrimer, it is possible to deliver a drug or a fluorophore to an environment in which it would otherwise be insoluble.<sup>[80]</sup> Dendrimers have been used, for example, as carriers for a variety of labels including metal nanoparticles<sup>[81,82]</sup> and oligonucleotides,<sup>[83]</sup> as well as for in vitro probes and in drug-delivery assays.<sup>[84,85]</sup> Intermolecular energy transfer between dendrimers and other donors or acceptors are known but not common. Examples include FRET from dendrimers to pyrene polymers in Langmuir–Blodgett multilayers<sup>[86]</sup> and between dendrimers.<sup>[87]</sup>

Dendrimers with functionalities that can be further modified by the end user are commercially available (Dendritech and Dendritic Nanotechnologies). Genisphere commercializes DNA-based dendrimers that can be used in hybridization and detection of low-copy target genes. Qiagen



offers dendrimers functionalized to bind both DNA and cells for cellular transfection. Glen Research commercializes monomers for generating multibranched synthetic DNA dendrimers<sup>[88,89]</sup> that can be employed for labeling oligonucleotides with multiple fluorophores. Such multilabeled dendrimeric primers can also be employed for high-sensitivity, multiplex PCR analysis (PCR = polymerase chain reaction). The corresponding synthetic methods are also available.<sup>[64]</sup>

Fluorescent polymers are a related class of fluorophores that can be either intrinsically fluorescent (e.g., conjugated polymers) or functionalized with multiple fluorophores.<sup>[90–94]</sup> Similar to dendrimers, fluorescent polymers are characterized by high molar absorption coefficients and are effective light-harvesting antennas. Disadvantages for their use as fluorescent labels for bioconjugation are their size and polydispersity. The emission of fluorescent polymers is not localized, since energy transfer occurs along the whole chain and thus the emission is diffuse.<sup>[95]</sup> Polymers therefore cannot be used as point donors in FRET systems. Nonetheless, fluorescent polymers have found broad application as fluorescent layers and in thin films for biosensors.<sup>[96,97]</sup>

Polymer-based FRET systems have been successfully employed in developing highly sensitive bioassays by exploiting a phenomenon known as superquenching. Superquenching is a photophysical phenomenon whereby certain fluorescent polymers act as strong fluorescence quenchers when associated through electrostatic interactions with small molecules.<sup>[98]</sup> It occurs by a very efficient energy-transfer mech-

anism that is possible in solution and on surfaces. The effect has been used in DNA hybridization (Figure 6, bottom),<sup>[98]</sup> SNP analysis,<sup>[99]</sup> and protease detection.<sup>[100]</sup> Swager and co-workers have harnessed this phenomenon to develop “amplified fluorescent polymer sensors” for a variety of explosives and biological moieties.<sup>[97,101,102]</sup> Superquenching also occurs in conjugates of gold nanoparticles and fluorescent polymers;<sup>[103]</sup> such systems may be exploitable for bioassays.

## 2.6. Photochromic Dyes

Jovin and co-workers define photochromic compounds as “having the ability to undergo a reversible transformation—in response to illumination at appropriate wavelengths—between two different structural forms having different absorption (and in some cases, fluorescence) spectra”.<sup>[104]</sup> The primary attraction of using photochromic dyes as FRET acceptors is the possibility of reversibly switching the acceptor (and hence the FRET effect) “on” and “off” with light. Many interesting FRET configurations can be constructed with this concept.

Spiropyrans and functionally related molecules are among the more prominent photochromic compounds. These molecules exist in closed spiro forms (absorbance < 400 nm) that undergo a light-driven intramolecular rearrangement to an open merocyanine form (absorbance 500–700 nm; Figure 7a).<sup>[105]</sup> Jovin and co-workers have synthesized a family of substituted diheteroarylethenes as photoswitchable accept-

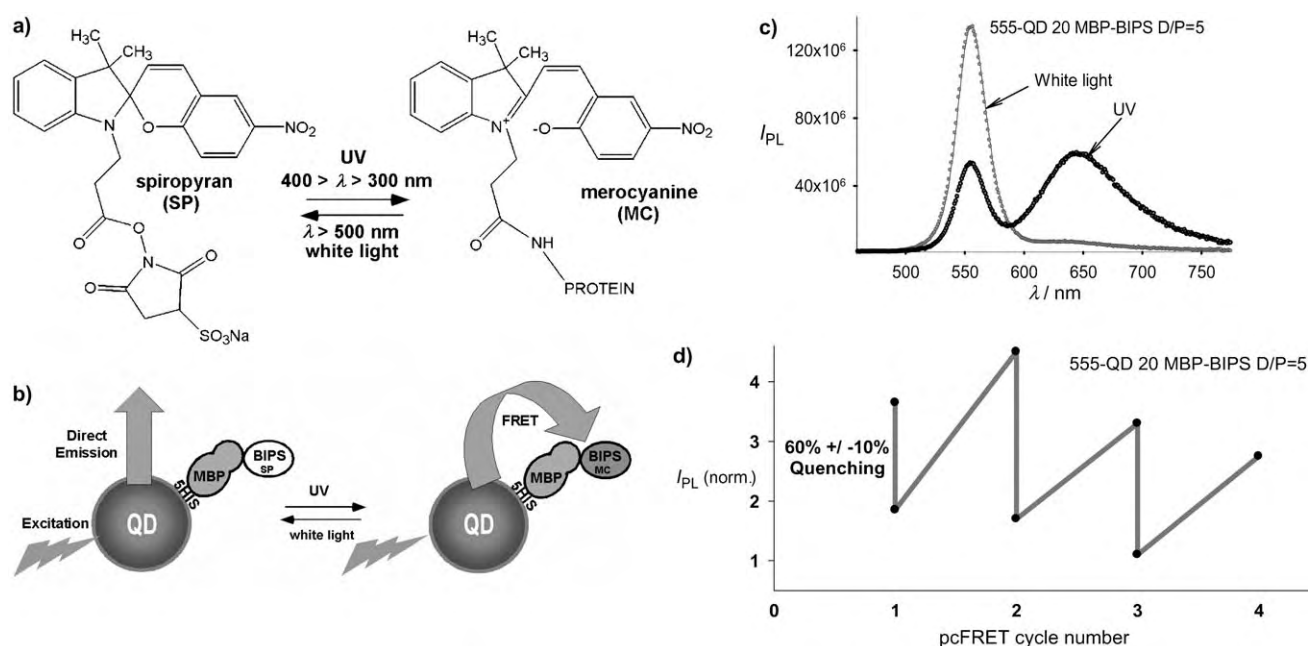


**Figure 7.** a) Structure of sulfo-NHS-BIPS (sulfo-NHS = *N*-hydroxysulfosuccinimide sodium salt; BIPS = 1',3',3'-trimethylspiro[2H-1-benzopyran-2,2'-indoline]) in the spiropyran (SP) form before (left) and merocyanine (MC) form after (right) conjugation to a protein. b) Schematic representation of quantum dot (QD) modulation by photochromic FRET after interacting with MBP-BIPS (MBP = maltose-binding protein). When BIPS is converted to the MC form by UV light, the QD emission is reduced through FRET quenching. After photoconversion with white light to the SP form, the direct emission of the QD is substantially increased. c) Photoluminescence spectra of the 555-nm luminescing QD 20 MBP-BIPS system with a dye/protein ratio of 5 after photoconversion from the SP to the MC form. d) Effect of pcFRET on QD photoluminescence (initial change from white light to UV). Figure adapted from reference [106] with permission of the American Chemical Society.

ors for what they term photochromic FRET (pcFRET). Using Lucifer Yellow as a donor, they demonstrate 100% FRET efficiency in 40 consecutive pcFRET switching cycles without photophysical fatigue.<sup>[104]</sup> A further pcFRET system consisted of a nitrospiropyran acceptor linked to a porphyrin donor as a free base or complexed to zinc.<sup>[105]</sup>

A system consisting of a QD donor surrounded by multiple spiropyran acceptors has also been investigated for pcFRET (Figure 7b–d).<sup>[106]</sup> Altering the number of acceptors around the central QD donor modulated the pcFRET efficiency to between 25 and 50%. Other photochromic dyes include substituted perfluorocyclopentene, dithienylethenes, substituted oxazolyfulgides, and bismuth vanadate pigments.<sup>[107–109]</sup> A variety of spironaphthoxazines and naphthopyrans (known as Reversacols) are available in more than 20 different colors from the company James Robinson.

There are inherent benefits to pcFRET. As a result of the switching properties, two interconvertible FRET sensors with different photophysical characteristics can be obtained from a single configuration. The choice of switching wavelength can be such that it does not overlap with the absorbance of the donor. Jovin and co-workers have postulated that the use of pcFRET could overcome problems in quantitative cell-based FRET analysis (high local sensor densities, irreversible photobleaching with continuous monitoring).<sup>[104]</sup> Although the pcFRET process remains fascinating, a realistic biological system has not yet been demonstrated.

### 3. Biological Materials

#### 3.1. Natural Fluorophores

There are many naturally occurring, intrinsically fluorescent biomolecules, including several enzymatic cofactors and the aromatic amino acids, tryptophan (Trp), tyrosine (Tyr), and phenylalanine (Phe), which are the focus of this review (Scheme 3).<sup>[2]</sup> Perhaps the single biggest benefit from using these residues for fluorescence is their endogenous presence in proteins/peptides and the ease with which they can either be introduced into proteins recombinantly or synthesized into nascent peptides. The strong UV absorbance of proteins at 280 nm (commonly used for quantitation) as well as the emission at 340–360 nm originate mostly from the indole ring

of the tryptophan residue; tyrosine and phenylalanine contribute to a much lesser extent.<sup>[2]</sup> The negligible quantum yield (ca. 0.02) of phenylalanine makes it less amenable to FRET, except perhaps in intraprotein configurations. Tyrosine is prone to quenching and energy transfer to tryptophan. This leaves tryptophan as the most reliable residue for FRET (see review articles and references [2,30,110]). A potential drawback to FRET applications with Trp is that the excitation lines and any D/A dyes will be confined to the UV region. The fluorescence from these residues is also environmentally sensitive and so placement of these residues deep within a protein structure will produce results that differ from those at the terminus of a small peptide. As an example of protein fluorescence, the absorption and emission spectra of the maltose-binding protein (MBP) are shown in Figure 8. MBP is a well-characterized member of the bacterial periplasmic binding protein (bPBP) superfamily and contains 8 Trp, 15 Tyr, and 15 Phe residues.<sup>[15]</sup>

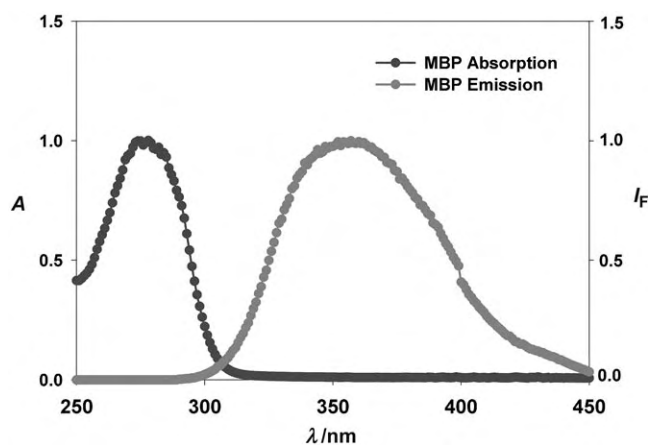
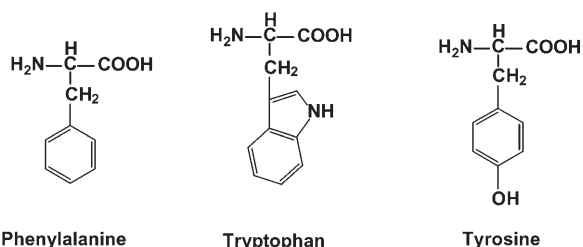


**Figure 8.** Normalized absorption and emission profile ( $\lambda_{\text{ex}} \approx 280$  nm) of maltose-binding protein (MBP;  $M_r \approx 44,000$ ).<sup>[4,15,129]</sup>

Myriad examples highlighting the versatility of these endogenous fluorophores abound. These include a FRET system with a Trp donor and dansyl acceptor to estimate the helix–helix association of bacterioopsin.<sup>[111]</sup> A Trp donor has also been used to measure the binding affinities for the *E. coli* DEAD-Box RNA helicase DbpA with fluorescent nucleotide analogues as acceptor.<sup>[112]</sup> A Trp located within the core of a reductase protein functioning in conjunction with a NADPH coenzyme quencher was used for measuring binding affinities.<sup>[113]</sup> Trp residues within the *E. coli* melibiose permease acting as energy donors for a fluorescent sugar analogue were identified through their sequential mutagenesis.<sup>[114]</sup> A FRET system consisting of a fixed Trp residue as donor and a modified 3-nitrotyrosine as acceptor within the human  $\alpha$ -synuclein protein was used to demonstrate that the elongated structure of a mutant is associated with Parkinson's disease.<sup>[115]</sup> Trp has also been used as an acceptor for a nitrile-derivatized phenylalanine donor to study the conformation of a 14-residue amphipathic peptide.<sup>[116]</sup> The distance between helices in the M13 transmembrane procoat protein was



**Scheme 3.** Structures of the three naturally fluorescent aromatic amino acids phenylalanine (Phe: QY = 0.02,  $\tau \approx 7$  ns,  $\lambda_{\text{ex}} \approx 260$  nm,  $\lambda_{\text{em}} \approx 282$  nm), tryptophan (Trp: QY = 0.13,  $\tau \approx 3$  ns,  $\lambda_{\text{ex}} \approx 295$  nm,  $\lambda_{\text{em}} \approx 353$  nm), and tyrosine (Tyr: QY = 0.14,  $\tau \approx 3$ –4 ns,  $\lambda_{\text{ex}} \approx 275$  nm,  $\lambda_{\text{em}} \approx 304$  nm).<sup>[2,110]</sup>

measured by FRET with a Tyr donor and a Trp acceptor.<sup>[117]</sup> Other FRET configurations include a Trp donor and a chromium(III) acceptor,<sup>[118]</sup> and a homotransfer system between Trp residues.<sup>[119]</sup>

Residue-to-residue FRET is more advantageous for smaller distances (<5 nm) and is ideal for intraprotein studies. The  $R_0$  values reported by Wu and Brand for 14 combinations with Trp as the donor and a dye as the acceptor range from 12 to 40 Å, which also represents a good estimate of the viable FRET range with dye acceptors.<sup>[30]</sup> From this range one can generalize that Trp residues almost anywhere within a “smaller” protein (diameter <3 nm;  $M_r$  < 30 000) will probably function as either a donor or an acceptor for an appropriate dye implanted within the protein structure. Indeed, if several Trp residues are present they will contribute to FRET to different extents on the basis of their separation distance. In view of the relative ease of introducing mutations into proteins, it should not be difficult to design modules with fluorescent residues for appending onto proteins of interest. These modules could function as efficient donors with large absorption cross sections to augment a FRET-based biosensing protein or as a tandem donor for a fluorescent protein or in a light-harvesting complex. With the growing interest in the structure and function of proteins, these endogenous fluorophores clearly remain underutilized.

### 3.2. Fluorescent Proteins

Fluorescent proteins (FPs) are being used increasingly in FRET systems, and the technologies and materials are continually improving. There are clear conceptual benefits to a fluorophore that is genetically appended onto the gene coding for a protein of interest to create a fluorescent chimera: the fluorophore and protein can then be co-expressed intracellularly and, when visualized, reveal the location and relative expression level.<sup>[14,20,21]</sup> The green fluorescent protein (GFP; Figure 9) derived from the jellyfish *Aequorea victoria* is the prototypical fluorophore of this protein family and has been used to revolutionize many aspects of cell biology.<sup>[120]</sup> Tsien provides an excellent monograph on this protein and its photophysical function.<sup>[20]</sup>



Figure 9. Ribbon structure of the green fluorescent protein (GFP).

The GFP was first described more than 40 years ago but was not cloned until the early 1990s. Key to its widespread use was the demonstration that this gene could be expressed in other organisms, since the coding sequence alone contains everything needed for the chromophore to mature and function.<sup>[20]</sup> Key internal residues are modified during maturation to form the *p*-hydroxybenzylideneimidazolinone chromophore, located in the central helix and surrounded by 11  $\beta$  strands ( $\beta$ -can structure).

Many GFP variants exist that differ in protein and chromophore structure and hence also in their absorbance and emission profiles.<sup>[20]</sup> Through mutation and selection, a more enhanced and stable GFP was produced, as well as blue, cyan, and yellow fluorescent proteins (BFP, CFP, YFP).<sup>[21]</sup> The red fluorescent protein (DS Red) was cloned in 1999 and revealed to be an obligate tetramer that matured slowly from green to red.<sup>[21,121,122]</sup> Tsien and co-workers developed a monomeric red fluorescent protein (mRFP) and various other red fluorophores, which they named after the fruit colors they resemble.<sup>[21,123]</sup> Other colors of FPs have been cloned from coral; these also appear to be tetrameric.<sup>[21]</sup> Figure 10 shows the absorption and emission profiles of representative FPs.

There are also commercially available FPs, such as the red/green series of phycobilisome-derived PBXL fluorophores.<sup>[124]</sup> These are stabilized multichromophore supramolecular protein complexes that can be linked to proteins. The increased number of fluorophores provides significantly higher sensitivity.

FPs are primarily being used for in vivo labeling of cells. FPs encoded in plasmids are available that are optimized for cloning proteins at either the N- or C-terminal. The plasmids allow controlled expression in a variety of cells and organisms including bacteria, yeast, and eukaryotes. The quantum yields of these proteins are generally good, ranging from 0.17 for a BFP to around 0.79 for a wild-type GFP, and largely depend upon which mutations are present and the final chromophore structure.<sup>[21]</sup> These benefits do, however, come with liabilities. Most FPs are large ( $M_r \approx 25$  to 30 kD and larger); appending a protein of this size onto another protein while maintaining the desired function can be problematic.<sup>[24]</sup> An FP can also be placed in the center of a protein or on the intra- or extracellular membrane; however, the correct folding, insertion, and fluorescence are never guaranteed. FPs that form dimers and tetramers can compound issues of creating bifunctional chimeras.<sup>[21,121]</sup> It can take several hours for FPs to mature and for the final chromophore to be formed, and the absorption and emission may shift during this process. These proteins are also susceptible to pH, temperature,  $O_2$  concentration, and other environmental conditions.<sup>[20]</sup> Although many FPs may be sensitive to photobleaching, this need not be a liability, since advanced imaging techniques such as fluorescence recovery after photobleaching (FRAP) can exploit these phenomena.<sup>[125]</sup> As can be seen in Figure 10, the generally broad absorption/emission profiles of an FP may preclude multiplex analysis.

The strategy of Tsien and co-workers for FRET-based FP indicators created a new class of genetically encoded sensors for monitoring intracellular analytes.<sup>[126,127]</sup> The original constructs (termed “cameleons”) were designed to sense calcium



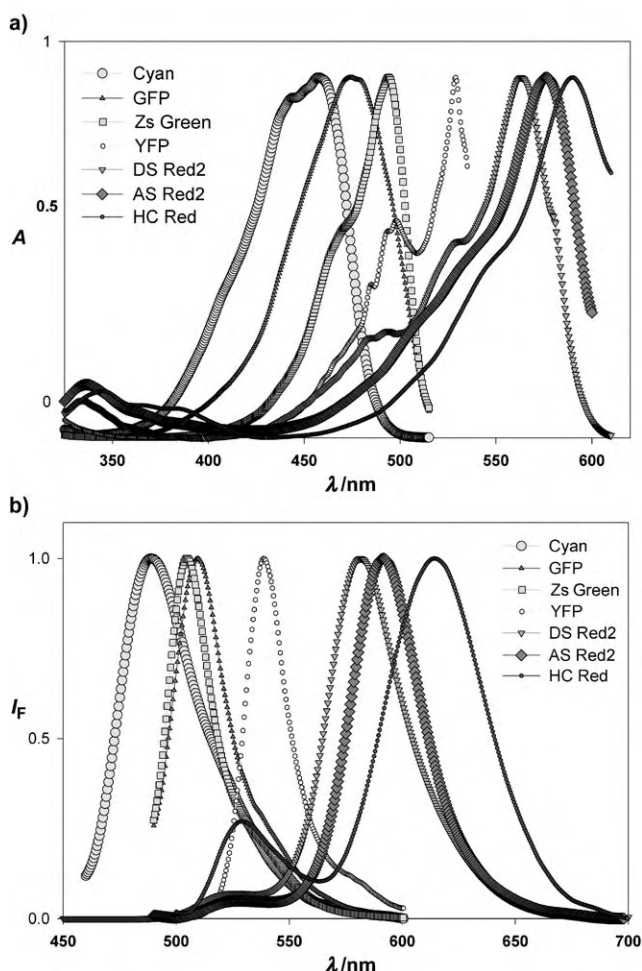


**Figure 10.** a) Normalized absorption and b) fluorescence profiles of representative fluorescent proteins: cyan fluorescent protein (cyan), GFP, Zs Green, yellow fluorescent protein (YFP), and three variants of red fluorescent protein (DS Red2, AS Red2, HC Red). Figure courtesy of Clontech.<sup>[14]</sup>

and consisted of linear fusions of BFP or CFP donors and enhanced GFP or YFP acceptors, which flanked calmodulin and the calmodulin-binding peptide.<sup>[127]</sup> Upon  $\text{Ca}^{2+}$  binding, calmodulin wraps around the peptide, so that the distance between the flanking FPs is reduced and the FRET increased. Following this strategy, the group of Frommer developed an elegant series of intracellular sensors that consist of FPs fused to the N- and C-termini of bPBPs.<sup>[128–130]</sup> The prototype consisted of MBP with an enhanced CFP (ECFP) donor fused to the N-terminus and a YFP acceptor fused to the C-terminus (Figure 11).<sup>[129]</sup> MBP belongs to the superfamily of hinge-binding proteins. Upon binding maltose, it undergoes a conformational change around the central hinge. This movement causes the two FPs to move closer together, thus altering the FRET efficiency and allowing transduction by a change in emission ratio of the donor and acceptor (Figures 11 and 12).

Additional sensors target glucose and ribose; however, the FPs in these sensors move apart in response to binding, thus resulting in a decrease in the D/A fluorescent ratio.<sup>[128,130]</sup> The overlap of the absorption and emission spectra of

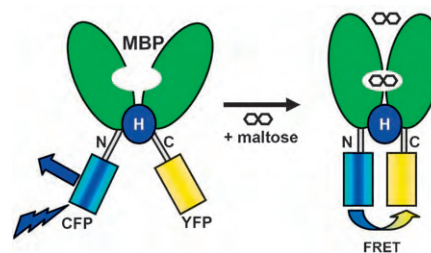


**Figure 11.** Modified MBP fluorescent indicator. ECFP as donor was fused to the N terminus of MBP, and YFP as a FRET acceptor was fused to the C terminus. H indicates the portion of protein functioning as a hinge between the two lobes of the MBP. The central binding pocket of the MBP is located between the two lobes. In the absence of maltose, the two FPs are at their maximum distance from each other and FRET is minimal. Upon binding maltose, the MBP undergoes a conformational change that brings the two FPs into close proximity and increases FRET, which can be monitored by the change in ratio of the YFP and CFP emission (see Figure 12).<sup>[129]</sup>

multiple-FP fusions results in small dynamic changes in FRET configurations; therefore sensitive optical equipment and spectral deconvolution are necessary. Biosensors that are based on this tandem-FP consensus design have now been developed to target kinases, lipases, various intracellular second messengers, and proteases.<sup>[120]</sup>

Rice created a kinesin C-terminal GFP fusion and labeled the kinesin with tetramethylrhodamine to allow FRET monitoring of the conformational changes of the protein upon binding nucleotides.<sup>[131]</sup> Hoffman et al. demonstrated a novel combination of CFP and the FLaSH system to label a G-

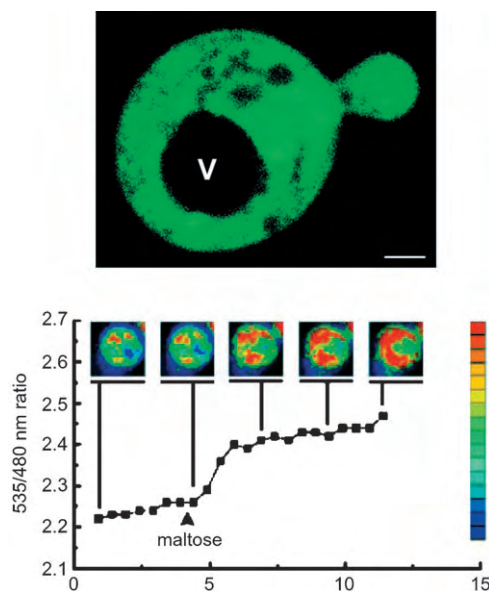


**Figure 12.** a) Confocal image of a maltose-FP sensor expressed in yeast. Fluorescence is detected in the cytosol but not in the vacuole. Scale bar = 1 μm. b) Changes of the maltose concentration in the cytosol of yeast that expresses a maltose sensor with a  $K_d$  value of 25 μM. The graph indicates emission ratio as a function of maltose uptake for a single yeast cell. Figure generously provided by W. Frommer, Stanford University; reproduced with permission of the National Academy of Sciences USA.<sup>[129]</sup>



protein-coupled receptor system.<sup>[24]</sup> Dual labeling of the same receptor with CFP and YFP maintained receptor activation but disrupted downstream signaling. Replacing YFP with a FIAsh dye allowed normal downstream signaling.<sup>[24]</sup>

Those interested in using these proteins can now consult several guides.<sup>[21,132]</sup> The increased interest in utilizing FPs for FRET and other intracellular applications has stimulated their continual improvement, and enhanced GFPs that are more tolerant to pH and environment have been created.<sup>[20]</sup> Through mutational selection, monomeric RFPs have been developed from the original tetramers and dimers.<sup>[123,133]</sup> For optimal FRET pairing, Nguyen and Daugherty developed a CFP–YFP pair that exhibited a 20-fold change in the FRET signal ratio (compared with a 3-fold change for the original construct).<sup>[134]</sup> This new D/A pair should enable FP FRET sensors in which the donor and acceptor have less than optimal configuration. FPs from different species have also been cloned with new colors and interesting properties such as photoconversion.<sup>[135]</sup>

### 3.3. Enzyme-Generated Bioluminescence

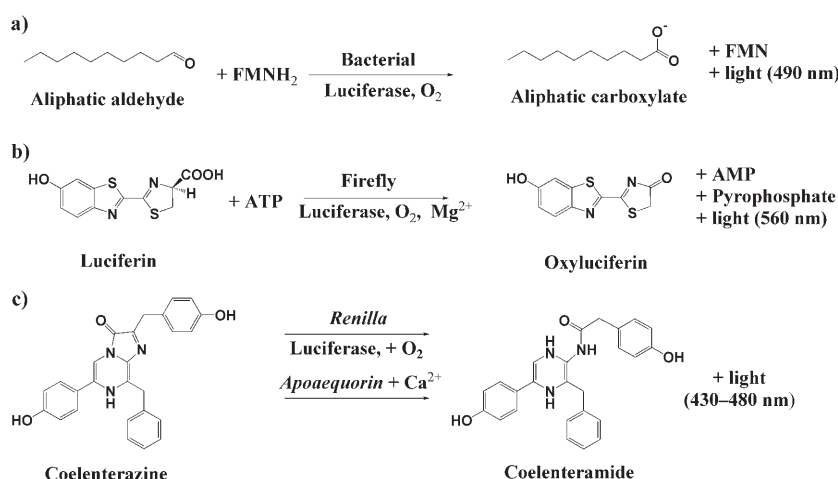
Enzyme-generated bioluminescence (BL) is a natural phenomenon found in certain beetles, bacteria, and marine species. In BL, the substrate luciferin is oxidized by a luciferase enzyme in the presence of O<sub>2</sub> and sometimes a cofactor such as ATP.<sup>[136–139]</sup> The oxidation of luciferin yields an excited-state molecule that decays with light emission (Scheme 4). BL has found applications as a reporter in many bioassays.<sup>[140–143]</sup> The light emitted from a BL system can also be exploited for energy transfer to an appropriate acceptor.<sup>[144–147]</sup> This process, known as bioluminescence resonance energy transfer (BRET), is a variant of FRET and is similarly efficient for D/A separation distances from 10 to 100 Å.<sup>[141]</sup> Luciferase acts as the donor in a BRET system, and the acceptor is usually GFP, which is also the physiological acceptor in luminescent organisms.<sup>[148,149]</sup> The principal

advantage offered by BRET is that no excitation light source is required to excite the donor, which avoids problems such as light scattering, high background noise, and direct acceptor excitation.<sup>[146]</sup> Additionally, since the donor or both the donor and acceptor can be co-expressed in the cell as fusion proteins and the excitation follows a localized event (luciferin delivery), the target of interest can be excited specifically, which is especially important for applications in vivo.<sup>[145]</sup>

BRET reporter pairs have been utilized for in vivo monitoring of protein–protein interactions including the interactions between circadian clock proteins,<sup>[144]</sup> insulin receptor activity,<sup>[150–152]</sup> and the real-time monitoring of intracellular ubiquitination.<sup>[145,153]</sup> Whereas the acceptor is usually conserved as GFP or one of its variants, a variety of related donor enzymes have been employed. The most commonly exploited luciferases are the terrestrial and marine bacterial luciferases and the eukaryotic firefly and *Renilla* (Sea Pansy) luciferases (Table 2). Luciferases catalyze the oxidation of reduced flavin mononucleotide (FMNH<sub>2</sub>) and a long-chain aliphatic aldehyde in the presence of O<sub>2</sub> to yield blue light (Scheme 4a).<sup>[154,155]</sup> Because FMNH<sub>2</sub> is rapidly oxidized in air, this luciferase cannot provide continuous emission, but instead generates only short bursts of light.<sup>[137]</sup> Also, since these genes are not easily expressed in mammalian cells, bacterial luciferases have found limited applications. No BRET application of bacterial luciferase has been reported to date.

The firefly luciferase/luciferin pair is the most commonly exploited BL reporter system. This luciferase catalyzes the oxidation of luciferin in the presence of ATP with emission of green-yellow light (Scheme 4b).<sup>[156]</sup> The light emitted initially is highly intense, but then decays to a sustained low-intensity luminescence. The addition of coenzyme A can help to yield a more-stable, high-intensity luminescence that decays over several minutes.<sup>[157]</sup> Caged luciferin, which is designed for intracellular delivery, is commercially available.<sup>[158]</sup> Once inside the cell, this luciferin can be activated either by UV light or by the action of intracellular esterases. The firefly luciferase/luciferin system is probably the best candidate for a BRET-based donor, as it shows a high quantum yield (0.88) and is easily expressed in *E. coli*. However, as its emission maximum is around 560 nm, GFP and some of its variants are not suitable as acceptors. Alternative acceptors such as Cy3/Cy5 and the fluorescent protein DS Red have already been used with this protein donor to monitor antigen–antibody binding<sup>[159]</sup> and protein–protein interactions.<sup>[160]</sup>

*Renilla* luciferase (RLuc) catalyzes the oxidation of coelenterazine to coelenteramide with the emission of blue light (Scheme 4c).<sup>[138]</sup> Although the quantum yields of RLuc are low (0.07) in comparison with those of firefly luciferase, the assays are simpler to perform as cofactors are not required. Unfortunately, RLuc exhibits a certain amount of autoluminescence, which results in a less sensitive assay. Even with this limitation, the *Renilla* luciferase/coelenterazine system is the first and probably most exploited donor for BRET systems.<sup>[144]</sup> Exam-



**Scheme 4.** Bioluminescent substrates and enzymatic reactions of several common luciferases: a) the aliphatic aldehyde substrate of bacterial luciferase; b) structure and reaction of luciferin, the substrate of firefly luciferase; c) coelenterazine, the substrate for *Renilla* luciferase and also part of *apoequorin*.

**Table 2:** Characteristics of common enzymes that catalyze bioluminescent and chemiluminescent reactions, along with their substrates.

Enzyme	Gene	$M_w$ [kDa]	Substrate	Cofactor(s)	$\lambda_{em}$	Notes	References
<b>Bioluminescence</b>							
bacterial luciferase ( <i>Vibrio</i> , <i>Photobacterium</i> , <i>Xenorhabdus</i> genera)	<i>Lux</i>	80 (dimer)	aliphatic aldehyde	FMNH <sub>2</sub> , O <sub>2</sub>	490	limited applications	[136, 154, 155]
firefly luciferase ( <i>Photinus pyralis</i> )	<i>Luc</i>	61 (monomer)	luciferin <sup>[a]</sup> , caged luciferin <sup>[b]</sup>	ATP	560	coenzyme A increases luminescence; BRET acceptors: Cy3/Cy5, DS Red.	[156–160]
<i>Renilla</i> luciferase	<i>Ruc</i> , <i>hRluc</i>	35 (monomer)	coelenterazine, coelenterazine ( <i>h</i> , <i>n</i> ), <sup>[c]</sup> coelenterazine <i>cp</i> , <i>f</i> , <sup>[d]</sup> DeepBlueC	none	475 442–473 395	autoluminescence	[138, 147, 164, 165]
<i>Gaussia</i> luciferase	<i>hGluc</i>	20 (monomer)	coelenterazine	none	480	[e]	[167–169]
<i>Aequorin</i> (from jellyfish <i>Aequorea victoria</i> or recombinant)		22 (monomer)	coelenterazine, <i>f</i> , <i>h</i> , <i>hcp</i> , <i>cp</i> , and <i>n</i>	Ca <sup>2+</sup>	445–475	[f]	[139, 172]
<b>Chemiluminescence</b>							
horseradish peroxidase ( <i>Armoracia rusticana</i> )		44 (glycoprotein)	luminol, isoluminol, lumigen, acridan	H <sub>2</sub> O <sub>2</sub> <sup>[g]</sup>	411–425	[h]	[183–185]
alkaline phosphatase ( <i>Pandalus borealis</i> )		106 (homodimer)	1,2-dioxetanes (lumigen, Lumi-Phos, CDP-Star)		480, 530	[i]	[191, 192]

[a] D-(–)-2-(6'-hydroxy-2'-benzothiazolyl)thiazoline-4-carboxylic acid. [b] Available from Molecular Probes, Promega. [c] Molecular Probes, Biotium. [d] Available from Perkin Elmer (BRET<sup>2</sup>). [e] Available from Prolume and NEB. [f] Available from Lux Biotech. and Molecular Probes. [g] Enhancers: luciferin, fluorescein, phenolic compounds. [h] Aureon Biosystems, Vector Labs and Alpha Innotech. [i] Michigan Diagnostics.

ples of its use include the monitoring of the dimerization of the  $\beta$ -adrenergic receptor<sup>[161, 162]</sup> and the binding of the insulin-like growth factor II to the insulin-like growth factor binding protein in living cells.<sup>[163]</sup> Two new *Renilla* genes (*hRluc*) that are optimized for expression in mammalian cells have also been created (Table 2). The emission of *Renilla* luciferase can also be modulated by choosing the appropriate coelenterazine substrate, and several analogues with different emissions are available.<sup>[164, 165]</sup>

Perkin-Elmer has developed a proprietary BRET2 assay that utilizes *Renilla* luciferase, a coelenterazine substrate named DeepBlueC (emission at 395 nm), and an optimized GFP2 acceptor. This configuration functions like a standard BRET assay, but has greater spectral resolution between the donor and acceptor pair.

Another luciferase from *Gaussia* (*hGluc*), has been optimized for expression in both bacterial and mammalian cells.<sup>[166, 167]</sup> With a molecular mass of only 20 kDa (compared with 35 kDa for *Renilla*), *hGluc* displays spectral characteristics similar to *Rluc* while also addressing problems associated with steric constraints in chimeric fusions. *Gaussia* luciferase expressed in mammalian cells generates up to 1000-fold brighter light than native *Renilla*.<sup>[168]</sup> Although *hGluc* has been employed as a reporter label for following DNA hybridization<sup>[167]</sup> and for monitoring bacterial cells,<sup>[169]</sup> there are no reports of its use as a BRET donor. Other isolated luciferases include the 19-kDa luciferase from the luminous

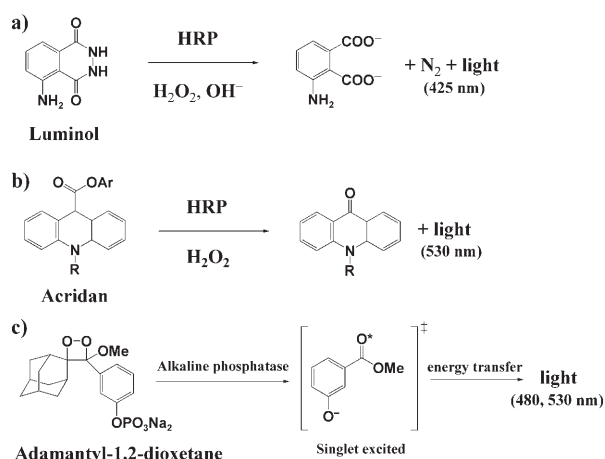
shrimp *Oplophorus gracilirostris*, which catalyzes the oxidation of coelenterazine and emits light at 454 nm with high quantum yield at temperatures up to 40°C.<sup>[170]</sup>

*Aequorin*, derived from jellyfish, is a Ca<sup>2+</sup>-sensitive bioluminescent photoprotein consisting of the luciferase apoaquorin complexed to its coelenterazine substrate (Scheme 4c)<sup>[171]</sup>. The blue bioluminescence of *Aequorin* is triggered by Ca<sup>2+</sup> ions; hence, its principal application is as a reporter for Ca<sup>2+</sup> ions.<sup>[139, 172]</sup> *Aequorin* has been employed as a BRET donor to monitor the interaction between Streptavidin (fused with *Aequorin*) and a biotin carboxyl carrier protein (fused with an EGFP acceptor).<sup>[173]</sup> In a modified BRET assay, the bioluminescence of biotinylated *Aequorin* was quenched by Dabcyl or QSY-7-labeled avidin upon exposure to Ca<sup>2+</sup> ions.<sup>[174]</sup>

In general, BRET systems with the described enzymatic donors have been exploited mostly for in vivo assays. However, it is foreseeable that applications such as biosensors that do not require an excitation source can be developed.

### 3.4. Enzyme-Generated Chemiluminescence

Enzyme-generated chemiluminescence (CL) is closely related to BL, with the difference being that the luminophore in this case is a synthetic substrate that is excited through an enzymatically catalyzed reaction.<sup>[143]</sup> Scheme 5 and Table 2



**Scheme 5.** Chemiluminescent substrates and the enzymatic reactions of horseradish peroxidase (HRP) and alkaline phosphatase. a) Luminol; b) Acridan (also available as an ester); c) Adamantyl-1,2-dioxetane (substrate for alkaline phosphatase and other enzymes).

describe some common CL substrates along with their processing enzymes. In general, the quantum yields for CL are lower than for BL. CL has found broad applications as a sensitive reporter system in drug screening, capillary electrophoresis, and immunoassays.<sup>[140–143,175–177]</sup> Although examples of chemiluminescent resonance energy transfer (CRET) are known,<sup>[178–182]</sup> this concept remains relatively underexplored. Akin to BRET systems, CL labels are potential donors in CRET-based assays.

Horseradish peroxidase (HRP) is probably the most commonly used enzyme for CL detection. Although a variety of chemiluminescent substrates exist for this enzyme, luminol and its luminogenic derivatives remain the most popular (Scheme 5a).<sup>[183–185]</sup> In the presence of hydrogen peroxide, HRP oxidizes luminol to give a luminescent species that emits blue light (425 nm). Luminol is usually employed in conjunction with an enhancer, such as luciferin, fluorescein, or a phenolic compound.<sup>[186,187]</sup> Exposing acridan substrates to HRP generates luminescent acridinium ester intermediates, which decay with emission of yellow light (530 nm) at a higher luminescent intensity than that of luminol (Scheme 5b).<sup>[188–190]</sup> Alkaline phosphatase is also commonly used to catalyze the oxidation of 1,2-dioxetanes as a luminogenic substrate (Scheme 5c).<sup>[191,192]</sup> Since 1,2-dioxetanes are inherently unstable four-membered cyclic peroxides, more-stable substrates such as adamantyl-1,2-dioxetane phosphate were developed. Dioxetanes are usually delivered in combination with proprietary enhancers that increase the stability and luminosity, and also expand the spectral range through energy transfer to another fluorophore; in this way, two emission wavelengths are obtained (480 and 530 nm). Dioxetanes can also be luminogenic substrates for other enzymes such as  $\beta$ -D-galactosidase,  $\beta$ -glucosidase,  $\beta$ -glucuronidase, arylesterase, arylsulfatase, and neuramidase.

Although CRET systems have been utilized predominantly as reporters, the large number of recombinant enzymes available, coupled with the low cost of commercial substrates

and the ability to control the emission wavelength, opens up the possibility of exploring CRET applications in biosensors.

## 4. Inorganic Materials

### 4.1. Metal Chelate Complexes and Long-Lifetime Dyes

Luminescent lanthanides are the most prominent class of long-lifetime dyes used for energy-transfer applications in biophysical research. Selvin's group has been at the forefront of developing these probes for biological studies.<sup>[193]</sup> Four lanthanides emit in the visible region: terbium, europium, samarium, and dysprosium. Because of the high intensity of their emission, Tb and Eu cations are most commonly used.

For biophysical applications, lanthanide cations are typically complexed within a chelate ligand, whose design must fulfill several functional requirements (Figure 13): 1) The

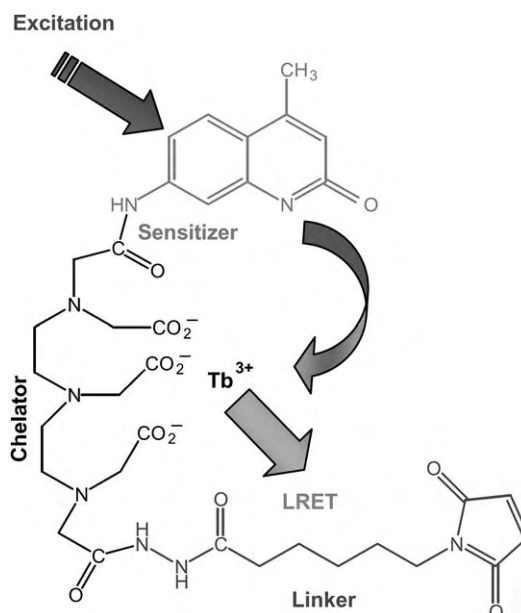


**Figure 13.** Structure of the Lanthascreen Tb probe from Invitrogen with the functionalities highlighted. The linker group is typically either an NHS ester or isothiocyanate/maleimide group.

lanthanide ion must form a tightly bound complex with the ligand, so that high thermodynamic and photochemical stability is achieved and the lanthanide ion is shielded from the quenching effects of the surrounding solution. Chelate ligands often take the form of polyaminocarboxylates, pyridines, or salicylic acid derivatives.<sup>[193,194]</sup> 2) Relative to common dyes, lanthanide ions have very low extinction coefficients ( $\approx 1\text{M}^{-1}\text{cm}^{-1}$ ), which makes them difficult to excite directly. Thus, the chelate label must contain an organic chromophore in close proximity to the ion which functions as a light-harvesting antenna or sensitizer. The sensitizer molecule absorbs incident light and transfers this energy to the lanthanide ion. 3) The chelate label should possess a reactive group to allow bioconjugation.

Research continues on the improvement of antennas and development of methods for the direct coupling of antennas and chelators to the termini or side chains of nascent peptides.<sup>[195,196]</sup> The currently available linkers for coupling these probes are relatively long and flexible, which leads to some uncertainty in the analysis. Direct attachment of the probes should improve the accuracy of measurements of the D/A distance. Sources for lanthanide probes include CIS-Bio International (cryptate-based probes), Perkin-Elmer, Invitrogen (LanthaScreen), and Amersham Biosciences (europium-TMT chelates).

Long-lifetime donors (fluorescent lifetime  $\tau > 100$  ns to several ms) have a number of technical advantages over conventional fluorescent dyes ( $\tau = 1\text{--}5$  ns). The principal benefit arises from the ability, through time-resolved measurements, to eliminate background fluorescence (from direct excitation of dyes, scattering, and autofluorescence from cells and biomolecules), thereby dramatically improving sensitivity. Lanthanide probes also possess multiple distinct, sharp emission bands and large Stokes shifts, so that D/A emission can be detected far from the excitation wavelength (Figure 14). Together these properties allow lanthanide probes to be coupled to a wide range of acceptor dyes. Terbium, for example, has good spectral overlap with fluorescein, rhodamine, and Cy3. Selvin's review article has a list of matching dyes along with their corresponding  $R_0$  values.<sup>[193]</sup>

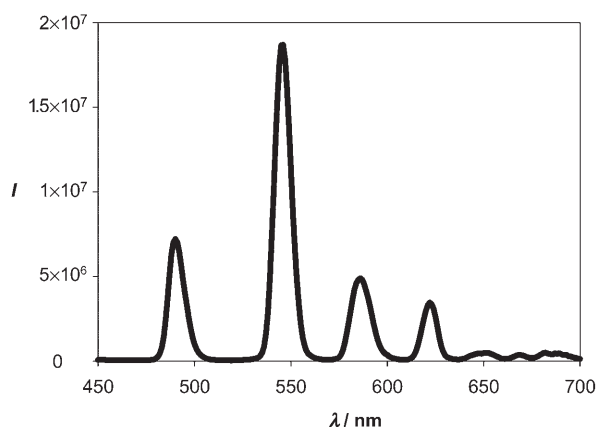


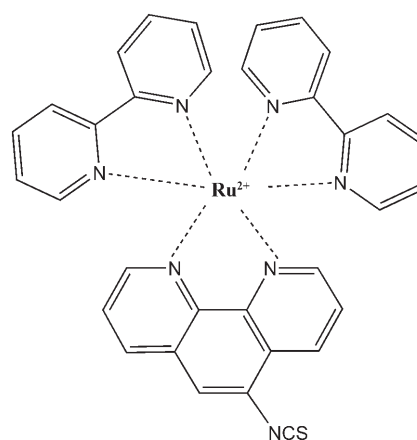
**Figure 14.** The unique sharp emission profile of the LanthaScreen Tb probe ( $\lambda_{\text{exc,max}} \approx 343$  nm).

Resonance energy transfer using lanthanide donors is (more correctly) referred to as luminescent resonance energy transfer (LRET), since technically lanthanide emission is not considered fluorescence. However, it originates from the same electric dipole transitions as conventional organic dyes and is therefore governed by the same  $r^6$  distance dependence as for FRET. The high quantum yields of the lanthanide probes (0.1–0.4) translates into  $R_0$  values up to 100 Å. Care should be taken in the determination of the spectral overlap, since some emission bands arise from both magnetic and electric dipole transitions, whereas only the electrical transitions allow significant energy transfer.<sup>[197]</sup> Time-based meas-

urements require more-complex equipment than that needed for steady-state measurements. However, because the dyes have long lifetimes ( $\mu\text{s}$  to ms), the instrumentation is typically less costly than that required for measurements with conventional dyes (ns lifetimes). In fact, many microtiter well-plate readers are available that allow gated lifetime measurements in this timescale.

LRET studies with lanthanide probes typically use conventional dyes as acceptors.<sup>[193]</sup> Lanthanide-based LRET has been used to study the activity of enzymes such as telomerase, caspase, helicase, and phosphatase.<sup>[198,199]</sup> An Eu–Cy5 D/A pair has also been used in high-throughput screening of potential antimicrobial drugs.<sup>[200]</sup> The same Eu–Cy5 pair was also used for competitive immunoassays of urinary albumin and noncompetitive assays of morphine.<sup>[201,202]</sup> Tsourkas et al. developed molecular beacons with Tb- and Eu-labeled DNA donors and demonstrated that time-resolved measurements with this LRET pair required neither a quencher nor a hairpin structure on the lanthanide-labeled probe.<sup>[203]</sup> An LRET system with a Tb donor and a Cy3 acceptor has also been used to monitor DNA hybridization.<sup>[204]</sup> Lanthanide probes have also been used in elucidating biological structures, for example, for measuring conformational changes in ion channels and enzymes, monitoring transmembrane signal transmission through voltage-sensitive segments within a functional potassium channel, and measuring distances across thin muscle filaments.<sup>[193,205–207]</sup>

Sigma–Aldrich offers a series of reactive ruthenium complexes (Scheme 6) that were originally developed by



**Scheme 6.** Structure of the commercially available ruthenium complex that is typically used in long-lifetime fluorescent studies.

Lakowicz and co-workers as anisotropy labels for measuring the rotational dynamics of proteins.<sup>[208,209]</sup> These Ru complexes have lifetimes of approximately 500 ns and are thus closer to organic dyes than lanthanides. As with the lanthanide probes the main advantage is the ability to monitor fluorescence selectively after the background fluorescence has decayed. Ru complexes have relatively small extinction coefficients ( $14\,500\text{ M}^{-1}\text{ cm}^{-1}$ ) and low quantum yields (0.05), but these disadvantages are again offset by their long lifetimes, high photostability, fairly large Stokes shift, and



absorption across almost the entire visible spectrum (Figure 15). Ru complexes have been applied as LRET donors in direct and competitive immunoassays for human serum albumin.<sup>[209]</sup> In another case, an environmentally

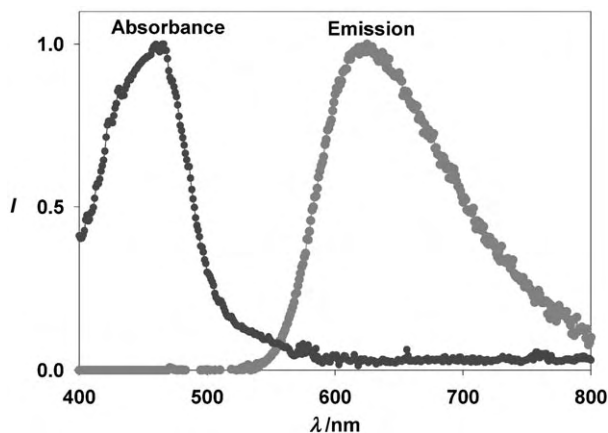


**Figure 15.** Absorption and emission profiles of the ruthenium complex shown in Scheme 6.

sensitive Sudan III diazo acceptor dye was coupled to a Ru complex in silica gel and used for the LRET-based detection of CO<sub>2</sub>.<sup>[210]</sup> In a rare example of the use of the complex as an acceptor, a glucose-binding protein was labeled with an environmentally sensitive acrylodan dye and a Ru complex.<sup>[211]</sup> The acrylodan was affected indirectly by glucose (which altered the protein conformation), whereas the Ru complex was not affected and thus served as an internal standard for ratiometric measurements.

Other types of materials for LRET applications have hardly been explored. All long-lifetime probes could quite easily be paired with dark quenchers. However, time-gated detection obviates this. As time-resolved fluorimeters become more accessible, long-lifetime probes will see increased use in LRET assays, driven mainly by the dramatic increase in signal-to-noise ratio afforded.

## 4.2. Gold, Metal, and Silicon Nanoparticles

### 4.2.1. Gold

Gold nanoparticles (NPs) are increasingly used in FRET-based applications, mostly because of their exceptional quenching ability. Gold and other noble metals have unique properties, such as plasmon resonances in the visible range (typically with large extinction coefficients around 10<sup>5</sup> cm<sup>-1</sup>M<sup>-1</sup>), stable, unfluctuating signal intensities, and resistance to photobleaching. Daniel and Astruc provide an excellent review of almost all properties of gold NPs,<sup>[212]</sup> including the somewhat murky distinction between clusters and colloids (the latter have size polydispersity).

Besides standard FRET considerations, the size and shape of the gold NPs also play an important role in FRET systems. Detailed studies have characterized the fluorescence quenching of dyes attached at a fixed distance from the surface of

various sized gold NPs (1–30 nm) as well as dyes attached at varying distances (2–16 nm) from the surface of 6-nm gold NPs.<sup>[213]</sup> Almost all the gold NPs were found not only to increase the nonradiative rate of decay of the dye, but also to decrease the radiative rate—even 1-nm gold NPs were capable of greater than 99 % quenching efficiency.

Gold NPs can be produced in various sizes by using either the citrate-reduction (diameter 16–147 nm) or the Brust–Schiffrin method (diameter 1.5–5.2 nm).<sup>[212]</sup> One of the intrinsic benefits of using gold NPs is that biomolecules containing exposed thiol groups can be attached to the NPs directly through gold–sulfur bonds. Gold NPs can also be treated with sulfur-containing ligands that possess distinct terminal groups (e.g., carboxylic acids or amines) that in turn can be used for subsequent bioconjugation. Alternatively, Nanoprobes offer 1.4-nm gold nanoclusters that are activated with either a single succinimidyl ester or maleimide.

Gold NPs have been used successfully in FRET applications with molecular beacons for the sensing of DNA (Figure 16). These were 100-fold more sensitive than previous

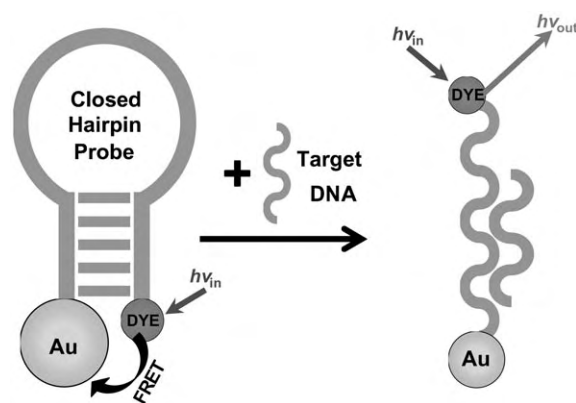


**Figure 16.** Schematic of a gold nanoparticle probe: In the closed hairpin structure, the D/A pair are in close proximity and the fluorescence is quenched.<sup>[214]</sup> Hybridization of the target single strand DNA opens up the structure of the molecular beacon, which increases the distance between the gold NP and the dye and results in a significant increase in fluorescence.

dye combinations.<sup>[214,215]</sup> The research group of Krauss developed a system in which molecular beacons are immobilized onto gold surfaces.<sup>[49,216]</sup> Both surface- and NP-based molecular beacons using organic dye donors demonstrate a high sensitivity for single base-pair mismatches. Seidel et al. demonstrated a FRET-based immunoassay for the detection of the pesticide atrazine by using gold-coated well plates (Figure 17).<sup>[217]</sup> Recently, gold NPs have also been tested as quenchers for semiconductor QDs (see Section 4.3). The hybridization of two complementary pieces of single-strand DNA, one attached to a QD and the other coupled to a 1.4-nm gold NP, was monitored by FRET (Figure 18).<sup>[218,219]</sup> The formation of nanoscale assemblies between oppositely charged QDs and gold NPs in solution has also been monitored by FRET.<sup>[220]</sup> An inhibition assay with streptavidin-coated QDs and biotin-functionalized gold NPs has also been reported (Figure 19).<sup>[221]</sup> The results from these studies

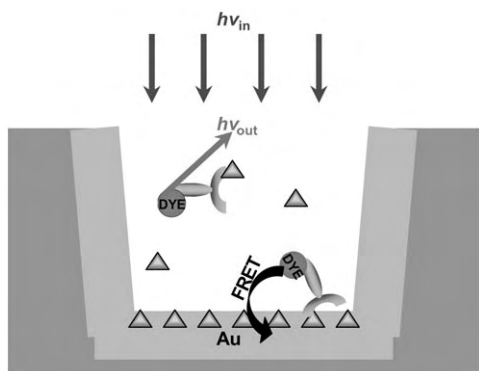


**Figure 17.** Gold-coated well plates for the competitive immunoassay detection of atrazine.<sup>[217]</sup> The binding of dye-labeled antibodies to the atrazine immobilized on the gold surface results in FRET quenching of the dye. Free atrazine in solution competes with the toxin on the gold, prevents the binding of the antibody to the surface, and thus increases the fluorescence.

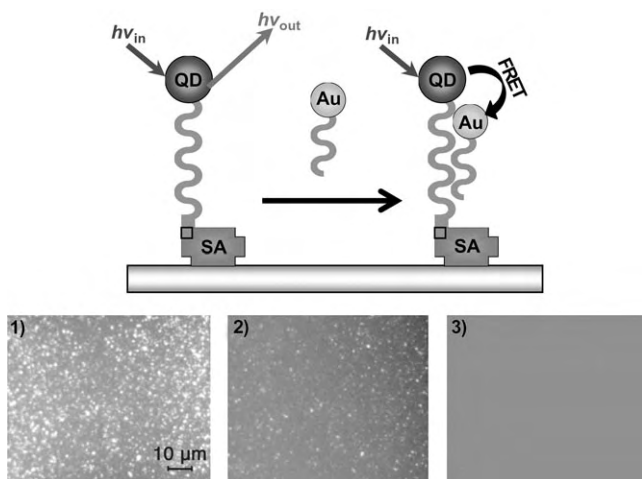


**Figure 18.** Detection of DNA hybridization by quenching upon binding of a gold-labeled single strand of target DNA. 1–3) Fluorescence signal of the surface after introduction of the gold target;  $t=0$  min (1), 5 min (2), 15 min (3). Images generously supplied by T. Melvin and reproduced with permission from the Royal Society of Chemistry.<sup>[218]</sup>

suggest that such FRET configurations have tremendous potential. The main advantages are the lower background signal, the improved sensitivity, and the ability to label both the gold NP and QD with multiple biologically active groups.

Gold is typically used for its quenching abilities; another possible use in which highly fluorescent gold QDs are used was described recently by Dickson and co-workers.<sup>[222,223]</sup> Much like their semiconductor counterparts, these gold QDs have size-tunable emission maxima, which shift to longer wavelengths with increasing nanocluster size. Fluorescent gold QDs can be used in FRET applications as both donors and acceptors; also, since the surface is stabilized with poly(amidoamine) dendrimers (PAMAM), the free amines on the dendrimer could be used in bioconjugation. It is quite clear that the use of gold NPs and surfaces for FRET

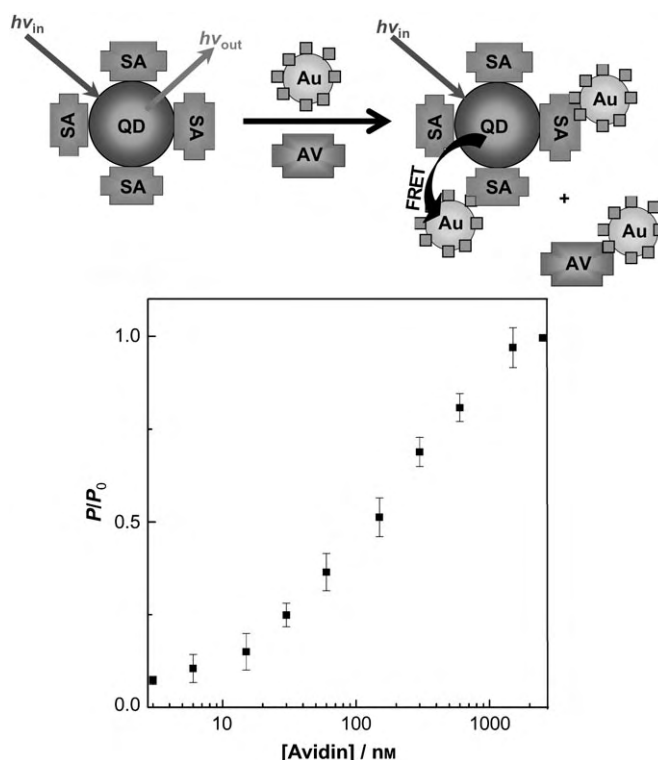


**Figure 19.** Top: Competitive inhibition assay for the detection of avidin on the basis of quenching of QDs by gold nanoparticles. Binding of the biotin-functionalized gold particle brings it into proximity of the streptavidin-labeled QD, which results in FRET and loss of QD photoluminescence. Avidin in solution competes with the streptavidin-labeled QDs for the biotin-gold particles and thus changes the FRET. Bottom: The resulting dose response for the assay. Figure generously supplied by E. Ohand; reproduced with permission from the American Chemical Society.<sup>[221]</sup>

measurements is still in its infancy, but many new applications can be expected in the near future.

#### 4.2.2. Metal and Silicon Nanoparticles

Interest in single-molecule optoelectronic materials has driven research into the fluorescence properties of small metallic NPs.<sup>[222,224]</sup> Clusters constituted of just a few noble-metal atoms show interesting emission properties, provided they are appropriately stabilized.<sup>[225,226]</sup> The fluorescence of noble-metals NPs can be intense; however, it is difficult to control the emission wavelength.<sup>[227]</sup> Besides gold NPs, silver NPs have also been shown to have interesting optical properties such as shape-dependent absorption and highly intense fluorescence.<sup>[228–233]</sup> Copper nanoparticles have been less studied; they display a large plasmon resonance peak in the visible range and interesting nonlinear optical properties.<sup>[234–236]</sup>

Silicon NPs have equally interesting optical characteristics, such as bright size-dependent photoluminescence and broad excitation spectra.<sup>[237–240]</sup> Because of their brightness and resistance to photobleaching, Si NPs have been investigated as fluorescent tags for DNA<sup>[241,242]</sup> and potentially nontoxic alternatives to semiconductor materials for in vivo

imaging.<sup>[243]</sup> The synthesis and stabilization of Si NPs remains tricky, although viable methods exist.<sup>[244,245]</sup> Wiesner and co-workers developed hybrid nanoparticles with a fluorescent core and a silicon shell which they refer to as CU dots (Cornell University).<sup>[246]</sup> These hybrids are synthesized by covalent conjugation of dye molecules to a silicon precursor and condensation to form a dye-rich core. Finally, silicon sol-gel monomers are added to form a denser outer silicon network. Because of their photostability, tunability, and ease of surface modification, applications of Si-based NPs as FRET donors can be expected.

Extensive studies on metal NPs coated with fluorescent dyes have confirmed plasmonic enhancement effects.<sup>[247–251]</sup> This effect involves energy transfer from the excited-state fluorophore to the plasmon resonance of the proximal metal surface/particle, which results in significantly different fluorophore excitation and emission properties.<sup>[249,251]</sup> Plasmon enhancement also decreases the excited-state lifetime of the fluorophore, which may increase stability by reducing photobleaching. The type of metal, size of the NP, and the fluorophore all have an influence in this complex process, but the general effect is that the quantum yield of the fluorophore increases dramatically, particularly for fluorophores with low quantum yield.<sup>[253–259]</sup> For plasmon enhancement to function, the spacing between fluorophore and metal must be carefully tuned.<sup>[256–259]</sup> The effect has already been exploited to increase the FRET efficiency between DNA-bound fluorophores,<sup>[260]</sup> and it is just a matter of time before more viable configurations are found.

### 4.3. Semiconductor Nanocrystals

Pioneering studies demonstrated that colloidal luminescent semiconductor nanocrystals or QDs could be used for the detection of proteins or DNA.<sup>[261,262]</sup> Extensive reviews can be found in references [263–268]. QDs have several unique intrinsic photophysical properties which make them attractive biolabels: relatively high quantum yields, molar extinction coefficients 10 to 100 times those of organic dyes, as well as high resistance to photobleaching and chemical degradation.<sup>[263–265]</sup> In direct comparison with organic dyes, several properties of QDs stand out: 1) size-tunable photoluminescent emission; 2) broad absorption spectra and large Stokes shifts, which allow excitation of mixed QD populations at a wavelength far from their emission wavelengths (Figure 20).<sup>[263–265,269,270]</sup> For FRET applications in particular, this means that QDs can be size-tuned or “dialed in” to give better spectral overlap with a particular acceptor dye (Figure 21).<sup>[271]</sup> As the spectral overlap increases, there is a proportional increase in the value of  $R_0$ , which, together with the high quantum yield of the QDs, permit FRET systems with longer separation distances. Since QDs can be excited at almost any wavelength below their emission wavelength, an excitation wavelength can be chosen that corresponds to the absorption minimum of the acceptor so that direct excitation is minimized.

QDs for biological assays are commercially available (Quantum Dot Corporation and Evident Technologies).

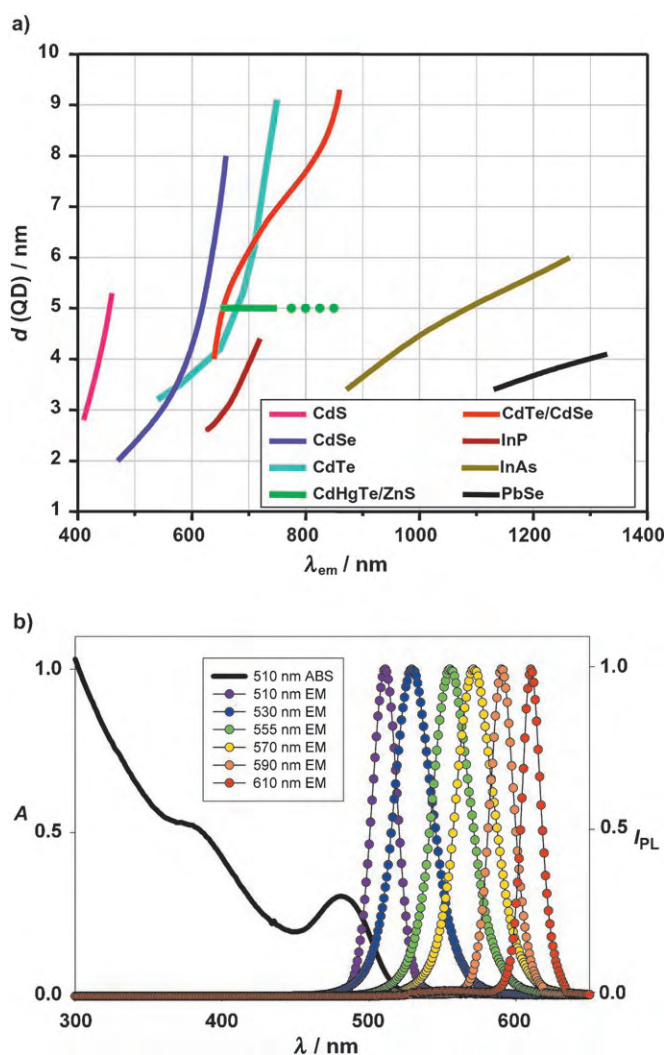


**Figure 20.** a) Correlation of emission maxima with the size of QDs composed of different binary and ternary semiconductors. b) Absorption and emission of six different QDs (in buffer) that have been utilized in several assays.<sup>[263]</sup> The black line shows the representative absorption of the QDs that emit at 510 nm. Note that the absorption increases steadily towards the UV. Figure generously provided by X. Michalet, UCLA, and reproduced with permission from reference [265].

These materials are available precoated with avidin or other proteins to facilitate bioconjugation. There are also several detailed monographs describing QD synthesis.<sup>[227,270,272–274]</sup> The best available QDs for biological applications consist of a CdSe core material coated with a ZnS shell (Figure 22). The shell passivates the core, protects it from oxidation and leeching, and at the same time significantly improves the photoluminescence.<sup>[263–265,270]</sup> Since QDs are typically synthesized from insoluble salts, they are also not water-soluble. Therefore, the native organic ligands used for synthesis must be exchanged with a bifunctional cap that attaches to the QD with one functionality and provides solubility and possible bioconjugation sites with the other. A wide variety of ligands can be used; each have their own advantages and disadvantages. For example, some limit dispersions of QDs to the basic pH range, whereas others increase the size considerably.<sup>[263,265]</sup>



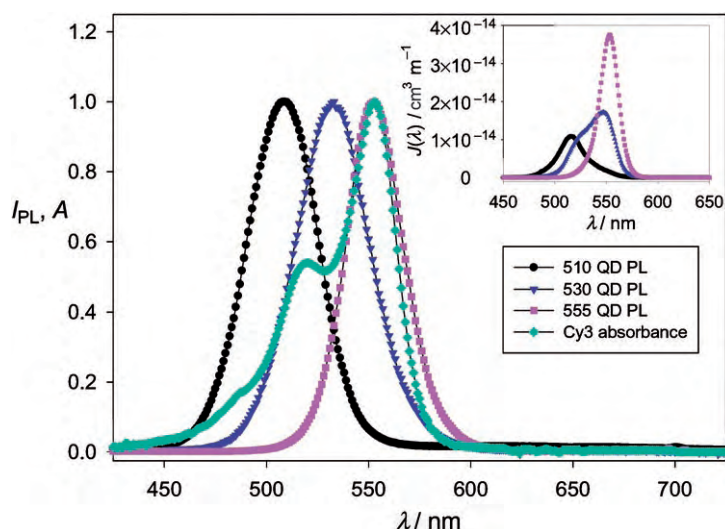


**Figure 21.** Normalized absorption spectrum of Cy3 and emission spectra of three QD solutions. The inset shows a plot of the resulting overlap functions  $J(\lambda)$ , which highlight the ability to tune the emission of the QD by changing its size to improve the spectral overlap with this acceptor.<sup>[271]</sup> Reproduced with permission from the American Chemical Society.

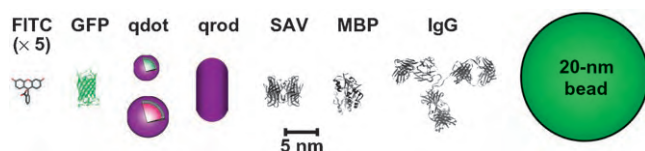


**Figure 22.** Comparison of the size of QDs and several comparable objects: FITC (fluorescein isothiocyanate), CdSe/ZnS QD (green: 4-nm diameter; red: 6.5-nm diameter), qrod (rod-shaped QD), SAV (streptavidin), IgG (immunoglobulin G). Figure generously provided by X. Michalet, UCLA, and reproduced with permission from reference [265].

Diverse strategies also exist for attaching biomolecules to QDs, for example, covalent coupling,<sup>[261,262]</sup> electrostatic or metal-affinity-driven self-assembly, and biotin-avidin chemistry.<sup>[263,265,267,268,275,276]</sup> QDs consisting of various other binary and ternary semiconductor materials including ZnS, CdS, CdTe, PbSe, and CdHgTe with emissions ranging from the UV to the IR have also been synthesized (Figure 20 a).<sup>[263–265]</sup>

The finite size of QDs presents an interesting predicament, since it can be both a benefit and a liability for FRET applications. The diameters of the CdSe/ZnS QDs shown in Figure 20 b range from approximately 50 Å for the 510-nm QDs to more than 80 Å for the 610-nm QDs (not including the capping ligand, which can add between 20 and 100 Å to the overall size).<sup>[263,271,276,277]</sup> For many bioconjugates with a QD donor and a dye-labeled protein as acceptor, the  $R_0$  value may actually fall within the radius of the QD, which results in a FRET efficiency that is relatively low for a D/A pair consisting of a single QD and a single acceptor.<sup>[4,271]</sup> However, it has been shown that by loading a central QD donor with multiple protein-based acceptors, the FRET efficiency can be increased in proportion with the cross section of the FRET acceptor.<sup>[263,271]</sup>

Mattoussi's group has been at the forefront of exploring QD FRET for bioassays. They have characterized and reported on D/A pairs of QD and dye-labeled proteins,<sup>[271,277]</sup> QD-based sensors for maltose and TNT,<sup>[4,278]</sup> surface-attached QD nanoassemblies,<sup>[279]</sup> QD-FRET-based reagentless biosensors,<sup>[280]</sup> the control of QD-donor FRET by a photochromic dye,<sup>[106]</sup> and the FRET-based structural elucidation of QD-protein bioconjugates (Figure 23).<sup>[281]</sup> These studies also demonstrate how FRET can be used with two different classes of fluorophores that differ in size by many orders of magnitude.

Other FRET applications with QDs include using DNA complementarity to attach gold quenchers to QDs<sup>[219]</sup> and using the quenching of these QDs to monitor avidin-biotin interactions.<sup>[221]</sup> The dynamics of DNA replication and telomerization have been monitored with QD donors that were conjugated to DNA primers and fluorescent nucleotide acceptors.<sup>[282]</sup> QDs have also been investigated as possible FRET donors in molecular beacons.<sup>[283]</sup> QDs located deep within lipid vesicles have been used as donors for

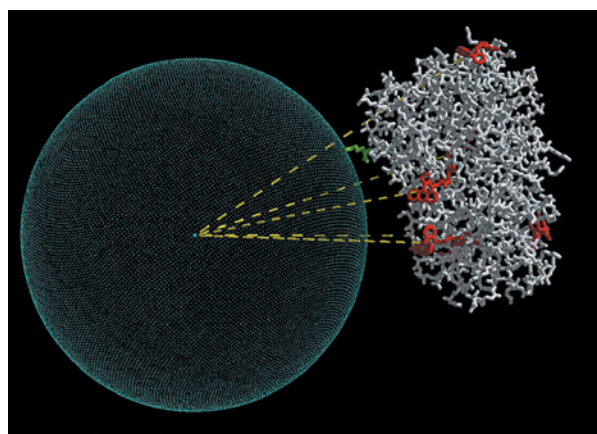


**Figure 23.** Side view of the structure of MBP as it self-assembles onto the surface of a QD. Six rhodamine red structures are highlighted in red. The distances from the center of the QD to each dye were determined by FRET (yellow). The crystallographic coordinates of the MBP were used in conjunction with these six distances to solve the structure of the MBP bioconjugate. Reproduced with permission from National Academy of Sciences USA.<sup>[281]</sup>

assaying interactions with other lipid-soluble and water-soluble dyes.<sup>[284]</sup> There is also a continuing discussion about using QDs as FRET-donating photosensitizers in photodynamic cancer therapy.<sup>[285,286]</sup>

There are far fewer examples of QDs as acceptors in biological contexts. There are two possible factors for this: 1) The broad absorbance profile, high extinction coefficients, and the large size of QDs cause QD to be excited as well as or better than any potential donor. 2) QDs have a longer lifetime ( $\tau = 10$  to 50 ns) than typical fluorescent dyes ( $\tau = 1$  to 5 ns).<sup>[277]</sup> Thus, the opportunity exists to use a different class of fluorophores, such as long-lifetime lanthanide chelates, as



donors in a FRET system, so as to exploit properties not found in “conventional” organic dyes. In view of the unique photophysical properties of QDs, we can expect their continued utilization in many FRET-based biological assays.

## 5. Multi-FRET Systems

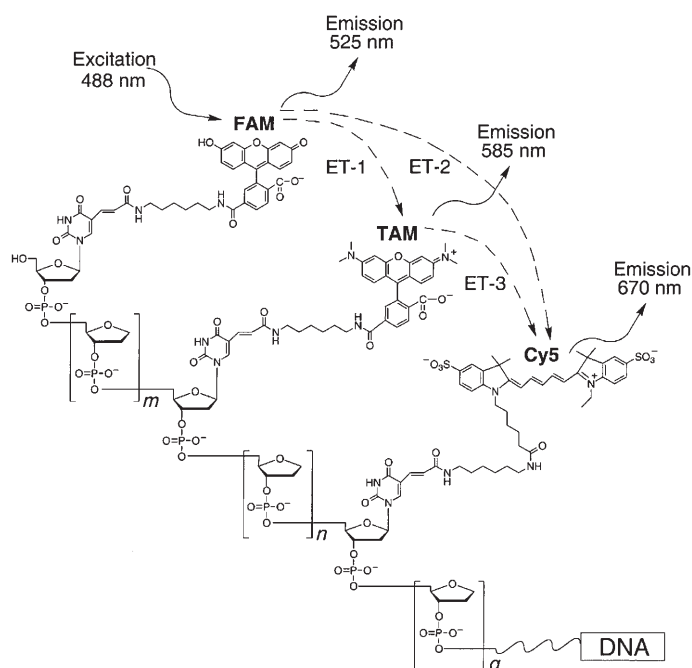
The naturally occurring multi-FRET biological systems are exemplified by the light-harvesting phycobilisomes.<sup>[287–291]</sup> These supramolecular complexes, found in blue-green cyanobacteria, red algae, and cryptomonad algae, function to extend the wavelength range for photosynthesis in the marine environment. Phycobilisomes consist of multiple phycobiliprotein subunits that can be pigmented or colorless; their composition varies widely depending on the light quality and the organism.<sup>[287–291]</sup>

An example of a multi-FRET function within a phycobilisome is the absorption of light by the phycobiliprotein R-phycoerythrin with subsequent energy transfer to C-phyco-cyanin and from there to allophycocyanin. The latter is connected through a linker chromophore to the photosystem II of the photosynthesis complex. Glazer and Stryer demonstrated that these tandem FRET probes could be adapted for sensitive cellular labeling and immunoassays.<sup>[292,293]</sup> Individually, these same fluorophores are also commercially available in the PBXL series.<sup>[123]</sup> The energy-transfer efficiency in this system approaches 100%—both the complexity and the efficiency of this naturally occurring energy-harvesting system are yet to be matched experimentally.

Biologically inspired synthetic multi-FRET systems have generally been used in two almost complementary configurations. In one case, defined biological structures are used to space or orient the fluorophores precisely.<sup>[5,47,294–296]</sup> In the converse case, multiple fluorophores are used to elucidate biological structures.<sup>[3,297]</sup> DNA is perhaps the most attractive biological platform for multi-FRET configurations for a number of reasons: 1) its predictable structure and chemistry; 2) the inherent ability to introduce fluorophores at specific sites;<sup>[5]</sup> 3) the ability to hybridize multiple dye-labeled oligonucleotides to a complementary strand;<sup>[298]</sup> 4) the ability to control the orientation of the attached fluorophores.<sup>[47]</sup>

DNA can be synthesized with multiple fluorophores or thiol, amine, biotin, and other modifications at specific terminal or internal sites. A change in the D/A spacing is facile in this configuration and allows fine tuning of FRET efficiency.<sup>[299,300]</sup> Such multilabeled DNA structures have been proposed as combinatorial fluorescence energy transfer (CFET) tags for information encoding. Tong et al. constructed eight CFET tags by altering the spacing between three fluorophores on a deoxyribose backbone to create different emission ratios of each color (Scheme 7).<sup>[295,296]</sup> In this configuration it is possible to excite at a single wavelength and use the different emission ratios as unique FRET signatures. The CFET tags have already been demonstrated in genotyping assays.

MBP has also been used to test different protein-based multi-FRET configurations.<sup>[26,52]</sup> Hellenga used orthogonal



**Scheme 7.** Structure of a CFET tag, which is constructed through attachment of chromophores to the modified thymidine residues of a nucleotide backbone. The FAM donor is excited at 488 nm and transfers energy to the proximal TAM and the terminal Cy5. TAM acts as a relay to forward energy to the Cy5. The spacing between FAM and TAM is controlled by the number of sugar phosphates  $m$ , and  $n$  defines the spacing between TAM and Cy5. Through changing the spacings, the emission can be tuned so that a unique ratiometric signature is produced. The CFET tag can be attached to DNA at point  $q$ , whose spacing can also be controlled. Figure courtesy of A. Tong.<sup>[295,296]</sup>

protein labeling to create a triply labeled MBP: the labels, FAM, tetramethylrhodamine (TMR), and Cy5, form a FRET relay that responds to maltose according to the change in the FRET ratio between FAM and Cy5, while the central TMR acts as a relay.<sup>[26]</sup> In another approach, a Cy3–MBP conjugate was used as a relay between a QD and a Cy3.5-labeled analogue of maltose, bound in the central binding pocket of the MBP (Figure 24). Although maltose sensing in this QD–MBP displacement sensor is based on changes in the ratio of FRET emission from MBP–Cy3 and Cy3.5, the sensor is “driven” by the QD, which is the primarily excited participant (Figure 25). This approach was helpful in overcoming inherent limitations of the D/A distance.<sup>[52]</sup> A multi-FRET format with 148 donors and 24 acceptors has been used to elucidate the structure of tarantula hemocyanin.<sup>[301]</sup> A FRET system with three fluorophores for a high-throughput drug screening format has also been reported.<sup>[302]</sup> Recently, Wang and Tan incorporated a combination of three organic dyes into silicon nanoparticles and varied the ratio of these tandem dyes to tune the FRET-mediated emission signatures.<sup>[303]</sup> This strategy represents an interesting functional hybrid that combines elements of silicon NPs,<sup>[237–240]</sup> CU dots,<sup>[246]</sup> and TransFluospheres.<sup>[56]</sup>

Multi-FRET systems have tremendous potential for elucidating protein structures and interactions, and a worth-

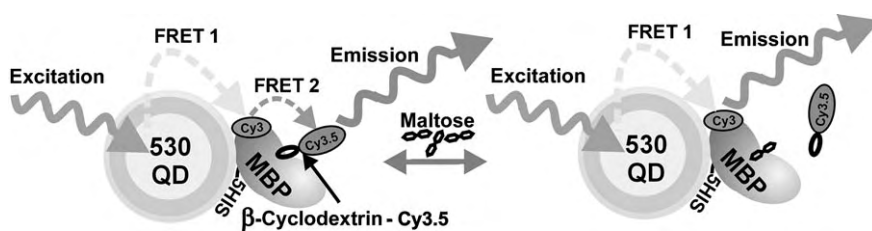


**Figure 24.** Schematic function of a multi-FRET QD maltose sensor. A 530-nm QD is surrounded by about 10 MBPs (only one shown), each labeled with a single Cy3 molecule (absorption maximum 556 nm, emission maximum 570 nm).  $\beta$ -Cyclodextrin, an analogue of the primary maltose analyte, is labeled with Cy3.5 ( $\beta$ -CD-Cy3.5, absorption maximum 575 nm, emission maximum 595 nm); it binds specifically in the binding pocket of MBP to complete the sensor complex. Excitation of the QD results in excitation of the MBP-Cy3 (FRET 1), which in turn excites the  $\beta$ -CD-Cy3.5 (FRET 2). Added maltose displaces  $\beta$ -CD-Cy3.5 and leads to increased emission of Cy3.

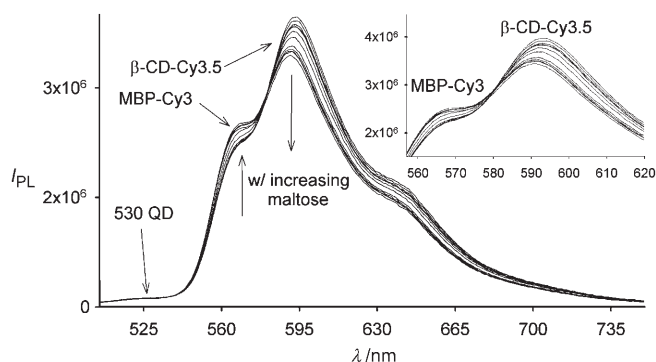


**Figure 25.** Maltose sensing using the configuration shown in Figure 24. Inset: Close up of the MBP-Cy3 and  $\beta$ -CD-Cy3.5 fluorescence portions. Reproduced with permission of the Nature Publishing Group.<sup>[4]</sup>

while strategy for their construction is in particular the combination of different types of functionalized fluorophores.

## 6. New Materials

With the growth in recent years of our understanding of FRET and its applications, possibilities have arisen for moving beyond the distance limitations of traditional FRET applications ( $R_0 = 60\text{--}90\text{ Å}$ ,  $r = 100\text{--}120\text{ Å}$ ). For example, Jares-Erijman and Jovin<sup>[13]</sup> point out that certain FRET parameters, including  $R_0$ , may be more plastic depending upon experimental configuration than previously thought. Specifically, the distance dependence of energy-transfer from a point to a plane could vary with the fourth

power of separation rather than the sixth.<sup>[13]</sup> Strouse and co-workers investigated this aspect by using variable-length DNA that was labeled at one end with FAM and at the other with a 1.4-nm Au cluster (Figure 26).<sup>[304]</sup> The Au cluster acts as a dipole surface and demonstrates  $1/R^4$  distance dependence of the surface energy transfer (SET). An SET radius  $d_0$  (analogous to  $R_0$ ) can be extrapolated.<sup>[304]</sup> SET may provide a distance resolution of up to 220 Å or more, which is twice the distance resolution measurable with traditional dye-based FRET pairs.

In a related approach, which is admittedly not directly based on energy transfer, Alivisatos and co-workers demonstrated a “molecular ruler” based on the plasmon coupling of single Au or Ag nanoparticles.<sup>[305]</sup> Plasmon coupling allows single pairs of nanoparticles separated by distances up to 700 Å to be monitored. However, deducing absolute distance values is complicated by factors such as the refractive index and light scattering. Interestingly, these two processes specifically necessitate the use of fluorophores distinct from traditional organic dyes.

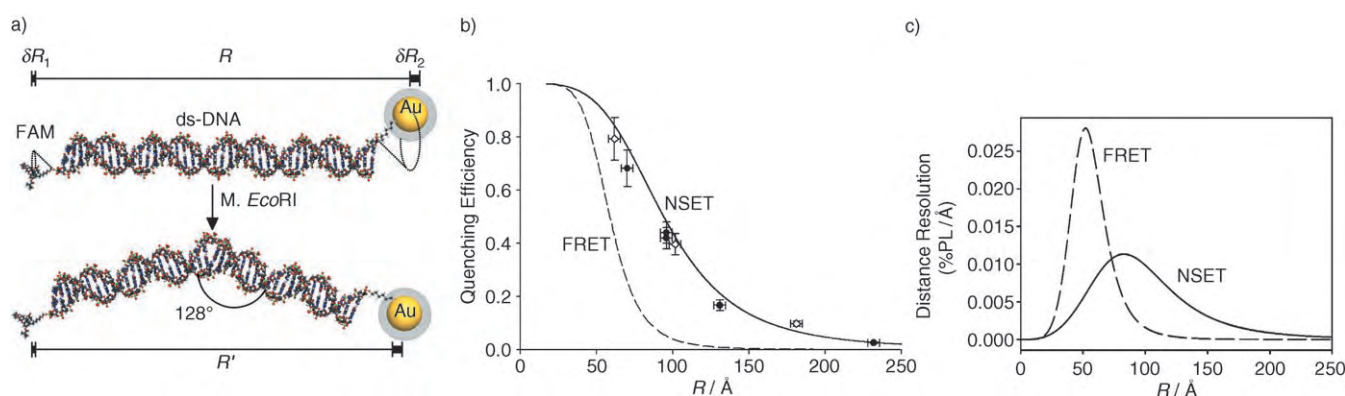


**Figure 26.** a) Schematic of the FAM-DNA-Au system: FAM is appended to DNA with a 1.4-nm Au particle attached at the other end. Flexible  $C_6$  linkers produce cones of uncertainty ( $\delta R$ ) for both appended moieties. Binding of *M. EcoRI* methyltransferase bends the DNA by  $128^\circ$ , which alters distance  $R$  to  $R'$  and results in a new D/A distance. b) Energy-transfer efficiency plotted against distance of separation  $R$  between FAM and Au. Filled circles represent DNA lengths of 15 bp, 20 bp, 30 bp, and 60 bp. Efficiencies after *M. EcoRI* binding are shown in open symbols. The dashed line is the theoretical FRET efficiency and the solid line is the theoretical SET efficiency. c) Distance-dependent length resolution of FRET and SET mechanisms. The intersection of the curves is the distance at which the two methods have identical resolution. Figure generously provided by G. Strouse F.S.U. and reproduced from reference [304] with permission from the American Chemical Society.

## 7. Summary and Outlook

Despite the numerous examples of FRET systems with divergent materials presented in this Review, FRET remains an underused and underappreciated analytical tool. Possible applications are numerous; for example, most commercial DNA sequencers utilize energy-transfer primers or terminators for fluorescent labeling as this simplifies the instrumental optical systems needed yet few realize this realiance.<sup>[16,306–308]</sup> There are few other bioanalytical techniques that can in so many different experimental formats consistently provide accurate intramolecular distance measurements in the nanometer range. We are fortunate to be part of an era in which not only is sensitive detection equipment available, but there are also many disparate materials that can be used as donors and acceptors in FRET systems, and numerous methods to label biomolecules. In particular, the use of nontraditional combinations with materials other than the usual organic donor and acceptor dyes will expand the applicability of FRET analysis. We predict six areas that will benefit the most in the near future: 1) studies of protein and peptide folding kinetics; 2) the elucidation of macromolecular interactions; 3) multicolor analysis, especially in vivo; 4) clinical and in vitro assays; 5) novel nanomaterials; 6) single-molecule FRET analyses.<sup>[310,311]</sup>

## Addendum

During the production of this Review, several pertinent papers were published which deserve mention. In a fascinating example of FRET between disparate classes of materials, So et al. used BRET to illuminate QDs in the absence of external excitation and demonstrated this for in vivo deep tissue imaging.<sup>[312]</sup> A multi-FRET construct consisting of five perylene bisimide dyes on a calixarene backbone was demonstrated for potential use in light-harvesting arrays.<sup>[313]</sup> Simultaneous multiplex FRET with up to four QD donors was demonstrated,<sup>[314]</sup> and a very informative review article on BRET applications for determining protein–protein interactions was published.<sup>[315]</sup>

## Abbreviations

BFP	blue fluorescent protein
BL	bioluminescence
BRET	bioluminescent resonance energy transfer
CFET	combinatorial fluorescence energy transfer
CFP	cyan fluorescent protein
CL	chemiluminescence
CRET	chemiluminescent resonance energy transfer
D/A	donor/acceptor
FAM	fluorescein
FRET	Förster or fluorescence resonance energy transfer
FP	fluorescent protein
GFP	green fluorescent protein
HRP	horseradish peroxidase
MBP	maltose-binding protein

NP	nanoparticle
pcFRET	photochromic FRET
QD	quantum dot
QY	quantum yield
$R_0$	Förster distance
SNP	single nucleotide polymorphism
SET	surface energy transfer
$\tau$	excited-state fluorescent lifetime
YFP	yellow fluorescent protein

I.M. and K.S. acknowledge the US Naval Research Laboratory.

Received: November 2, 2005

- [1] “10th Spiers Memorial Lecture. Transfer mechanisms of electronic excitation”: T. Förster, *Discuss. Faraday Soc.* **1959**, 27, 7.
- [2] J. R. Lakowicz, *Principles of Fluorescence Spectroscopy*, 2nd ed., Kluwer/Plenum, New York, **1999**.
- [3] H. M. Watrob, C. P. Pan, M. D. Barkley, *J. Am. Chem. Soc.* **2003**, 125, 7336.
- [4] I. L. Medintz, A. R. Clapp, H. Mattoussi, E. R. Goldman, B. Fisher, J. M. Mauro, *Nat. Mater.* **2003**, 2, 630.
- [5] A. K. Tong, S. Jockusch, Z. M. Li, H. R. Zhu, D. L. Akins, N. J. Turro, J. Y. Ju, *J. Am. Chem. Soc.* **2001**, 123, 12923.
- [6] T. Förster, *Z. Naturforsch. A* **1949**, 4, 321.
- [7] T. Förster, *Ann. Phys.* **1948**, 2, 55.
- [8] K. E. Sapsford, L. Berti, I. L. Medintz, *Minerva Biol.* **2005**, 16, 253.
- [9] C. G. dos Remedios, P. D. Moens, *J. Struct. Biol.* **1995**, 115, 175.
- [10] L. Stryer, *Annu. Rev. Biochem.* **1978**, 47, 819.
- [11] U. Schobel, H. J. Egelhaaf, A. Brecht, D. Oelkrug, G. Gauglitz, *Bioconjugate Chem.* **1999**, 10, 1107.
- [12] M. P. Lillo, B. K. Szpikowska, M. T. Mas, J. D. Sutin, J. M. Beechem, *Biochemistry* **1997**, 36, 11273.
- [13] E. Jares-Erijman, T. Jovin, *Nat. Biotechnol.* **2003**, 21, 1387.
- [14] A. Miyawaki, A. Sawano, T. Kogure, *Nat. Cell Biol.* **2003**, S1.
- [15] R. M. De Lorimier, J. J. Smith, M. A. Dwyer, L. L. Looger, K. M. Sali, C. D. Paavola, S. S. Rizk, S. Sadigov, D. W. Conrad, L. Loew, H. W. Hellinga, *Protein Sci.* **2002**, 11, 2655.
- [16] V. V. Didenko, *Biotechniques* **2001**, 31, 1106.
- [17] L. Berti, J. Xie, I. L. Medintz, A. N. Glazer, R. A. Mathies, *Anal. Biochem.* **2001**, 292, 188.
- [18] G. T. Hermanson, *Bioconjugate Techniques*, Academic Press, San Diego, **1996**.
- [19] R. P. Haugland, *The Handbook. A Guide to Fluorescent Probes and Labeling Technologies*, 10th ed., Invitrogen, San Diego, **2005**.
- [20] R. Y. Tsien, *Annu. Rev. Biochem.* **1998**, 67, 509.
- [21] R. Y. Tsien, *FEBS Lett.* **2005**, 579, 927.
- [22] B. A. Griffin, S. R. Adams, R. Y. Tsien, *Science* **1998**, 281, 269.
- [23] S. R. Adams, R. E. Campbell, L. A. Gross, B. R. Martin, G. K. Walkup, Y. Yao, J. Llopis, R. Y. Tsien, *J. Am. Chem. Soc.* **2002**, 124, 6063.
- [24] C. Hoffmann, G. Gaietta, M. Bunemann, S. R. Adams, S. Oberdorff-Maass, B. Behr, J. P. Vilardaga, R. Y. Tsien, M. H. Eisman, M. J. Lohse, *Nat. Methods* **2005**, 2, 171.
- [25] G. V. Los, A. Darzins, N. Karassina, C. Zimprich, R. Learish, M. G. McDougall, L. P. Encell, R. Friedman-Ohana, M. Wood, G. Vidugiris, K. Zimmerman, P. Otto, D. H. Klaubert, K. V. Wood, *Cell Notes* **2005**, 11, 2.
- [26] J. J. Smith, D. W. Conrad, M. J. Cuneo, H. W. Hellinga, *Protein Sci.* **2005**, 14, 64.
- [27] I. Chen, A. Y. Ting, *Curr. Opin. Biotechnol.* **2005**, 16, 35.



- [28] L. Tan, Y. Li, T. J. Drake, L. Moroz, K. M. Wang, J. Li, A. Munteanu, C. Y. J. Yang, K. Martinez, W. H. Tan, *Analyst* **2005**, *130*, 1002.
- [29] W. H. Tan, K. M. Wang, T. J. Drake, *Curr. Opin. Chem. Biol.* **2004**, *8*, 547.
- [30] P. G. Wu, L. Brand, *Anal. Biochem.* **1994**, *218*, 1.
- [31] V. Buschmann, K. D. Weston, M. Sauer, *Bioconjugate Chem.* **2003**, *14*, 195.
- [32] S. R. Adams, A. T. Harootunian, Y. J. Buechler, S. S. Taylor, R. Y. Tsien, *Nature* **1991**, *349*, 694.
- [33] H. Takakusa, K. Kikuchi, Y. Urano, S. Sakamoto, K. Yamaguchi, T. Nagano, *J. Am. Chem. Soc.* **2002**, *124*, 1653.
- [34] G. Zlokarnik, P. A. Negulescu, T. E. Knapp, L. Mere, N. Burrell, L. X. Feng, M. Whitney, K. Roemer, R. Y. Tsien, *Science* **1998**, *279*, 84.
- [35] A. Chigaev, T. Buranda, D. C. Dwyer, E. R. Prossnitz, L. A. Sklar, *Biophys. J.* **2003**, *85*, 3951.
- [36] R. S. Larson, T. Davis, C. Bologa, G. Semenuk, S. Vijayan, Y. Li, T. Oprea, A. Chigaev, T. Buranda, C. R. Wagner, L. A. Sklar, *Biochemistry* **2005**, *44*, 4322.
- [37] P. R. Selvin, *Biophys. J.* **2003**, *84*, 1.
- [38] R. J. Russell, M. V. Pishko, C. C. Gefrides, M. J. McShane, G. L. Cote, *Anal. Chem.* **1999**, *71*, 3126.
- [39] H. Ueda, K. Kubota, Y. Wang, K. Tsumoto, W. Mahoney, I. Kumagai, T. Nagamune, *Biotechniques* **1999**, *27*, 738.
- [40] H. A. Godwin, J. M. Berg, *J. Am. Chem. Soc.* **1996**, *118*, 6514.
- [41] X. D. Song, J. Shi, J. Nolan, B. Swanson, *Anal. Biochem.* **2001**, *291*, 133.
- [42] D. Klostermeier, D. Millar, *Biopolymers* **2002**, *61*, 159.
- [43] A. N. Glazer, R. A. Mathies, *Curr. Opin. Biotechnol.* **1997**, *8*, 94.
- [44] J. Y. Ju, C. C. Ruan, C. W. Fuller, A. N. Glazer, R. A. Mathies, *Proc. Natl. Acad. Sci. USA* **1995**, *92*, 4347.
- [45] J. Y. Ju, A. N. Glazer, R. A. Mathies, *Nat. Med.* **1996**, *2*, 246.
- [46] T. Ohmichi, Y. Kawamoto, P. Wu, D. Miyoshi, H. Karimata, N. Sugimoto, *Biochemistry* **2005**, *44*, 7125.
- [47] F. D. Lewis, L. Zhang, X. Zuo, *J. Am. Chem. Soc.* **2005**, *127*, 10002.
- [48] O. Piester, H. Barsch, V. Buschmann, T. Heinlein, J. P. Knemeyer, K. D. Weston, M. Sauer, *Nano Lett.* **2003**, *3*, 979.
- [49] H. Du, C. M. Strohsahl, J. Camera, B. L. Miller, T. D. Krauss, *J. Am. Chem. Soc.* **2005**, *127*, 7932.
- [50] A. P. R. Johnston, F. Caruso, *J. Am. Chem. Soc.* **2005**, *127*, 10014.
- [51] J. W. Liu, Y. Lu, *Anal. Chem.* **2003**, *75*, 6666.
- [52] I. L. Medintz, E. R. Goldman, M. E. Lassman, J. M. Mauro, *Bioconjugate Chem.* **2003**, *14*, 909.
- [53] A. M. Paradiso, R. Y. Tsien, T. E. Machen, *Proc. Natl. Acad. Sci. USA* **1984**, *81*, 7436.
- [54] Q. Chang, J. Sipior, J. R. Lakowicz, G. Rao, *Anal. Biochem.* **1995**, *232*, 92.
- [55] J. R. Lakowicz, H. Szmajda, M. Karakelle, *Anal. Chim. Acta* **1993**, *272*, 179.
- [56] D. V. Roberts, B. P. Wittmershaus, Y. Z. Zhang, S. Swan, M. P. Klinosky, *J. Lumin.* **1998**, *29*, 225.
- [57] S. Niehren, W. Kinzelbach, S. Seeger, J. Wolfrum, *Anal. Chem.* **1995**, *67*, 2666.
- [58] J.-S. Hsiao, S. E. Webber, *J. Phys. Chem.* **1993**, *97*, 8289.
- [59] J. Szollosi, S. Damjanovich, L. Matyus, *Cytometry* **1998**, *34*, 159.
- [60] G. Horvath, M. Petras, G. Szentesi, A. Fabian, J. W. Park, G. Vereb, J. Szollosi, *Cytometry Part A* **2005**, *65*, 148.
- [61] E. Zahavi, M. Fisher, A. Bromberg, U. Olshevsky, *Appl. Environ. Microbiol.* **2003**, *69*, 2330.
- [62] K. V. N. Rao, P. W. Stevens, J. G. Hall, V. Lyamichev, B. P. Neri, D. M. Kelso, *Nucleic Acids Res.* **2003**, *31*, e66.
- [63] A. Valanne, H. Lindroos, T. Lovgren, T. Soukka, *Anal. Chim. Acta* **2005**, *539*, 251.
- [64] S. M. Grayson, J. M. J. Frechet, *Chem. Rev.* **2001**, *101*, 3819.
- [65] C. Gorman, *Nature* **2002**, *415*, 487.
- [66] G. M. Stewart, M. A. Fox, *J. Am. Chem. Soc.* **1996**, *118*, 4354.
- [67] A. Andronov, P. R. L. Malenfant, J. M. J. Frechet, *Chem. Mater.* **2000**, *12*, 1463.
- [68] T. Gensch, J. Hofkens, A. Herrmann, K. Tsuda, W. Verheijen, T. Vosch, T. Christ, T. Basche, K. Müllen, F. De Schryver, *Angew. Chem.* **1999**, *111*, 3970; *Angew. Chem. Int. Ed.* **1999**, *38*, 3752.
- [69] S. Onclin, J. Huskens, B. J. Ravoo, D. N. Reinhoudt, *Small* **2005**, *1*, 852.
- [70] V. Balzani, P. Ceroni, S. Gestermann, M. Gorka, C. Kaufmann, F. Vögtle, *Tetrahedron* **2002**, *58*, 629.
- [71] V. Vicinelli, P. Ceroni, M. Maestri, V. Balzani, M. Gorka, F. Vögtle, *J. Am. Chem. Soc.* **2002**, *124*, 6461.
- [72] B. R. Kaafarani, B. Wex, F. Wang, O. Catanescu, L. C. Chien, D. C. Neckers, *J. Org. Chem.* **2003**, *68*, 5377.
- [73] D. Wang, T. Imae, *J. Am. Chem. Soc.* **2004**, *126*, 13204.
- [74] V. Balzani, P. Ceroni, M. Maestri, C. Saudan, V. Vicinelli, *Top. Curr. Chem.* **2003**, *288*, 159.
- [75] V. Balzani, P. Ceroni, M. Maestri, V. Vicinelli, *Curr. Opin. Chem. Biol.* **2003**, *7*, 657.
- [76] J. M. Serin, D. W. Brousmiche, J. M. J. Frechet, *J. Am. Chem. Soc.* **2002**, *124*, 11848.
- [77] J. M. Serin, D. W. Brousmiche, J. M. J. Frechet, *Chem. Commun.* **2002**, 2605.
- [78] A. W. Bosman, H. M. Janssen, E. W. Meijer, *Chem. Rev.* **1999**, *99*, 1665.
- [79] Y. Kim, S. C. Zimmerman, *Curr. Opin. Chem. Biol.* **1998**, *2*, 733.
- [80] H. Yoo, R. L. Juliano, *Nucleic Acids Res.* **2000**, *28*, 4225.
- [81] H. C. Choi, W. Kim, D. Wang, H. Dai, *J. Phys. Chem. B* **2002**, *106*, 12361.
- [82] K. R. Gopidas, J. K. Whitesell, M. A. Fox, *J. Am. Chem. Soc.* **2003**, *125*, 6491.
- [83] P. Chaltin, A. Margineanu, D. Marchand, A. Van Aerschot, J. Rozenski, F. De Schryver, A. Herrmann, K. Müllen, R. L. Juliano, M. H. Fisher, H. Kang, S. De Feyter, P. Herdewijn, *Bioconjugate Chem.* **2005**, *16*, 827.
- [84] J. R. Morgan, M. J. Cloninger, *Curr. Opin. Drug Discovery Dev.* **2002**, *5*, 966.
- [85] U. Boas, P. M. Heegard, *Chem. Soc. Rev.* **2004**, *33*, 43.
- [86] U. Oertel, D. Appelhans, P. Friedel, D. Jehnichen, H. Komber, B. Pilch, B. Hänel, B. Voit, *Langmuir* **2002**, *18*, 105.
- [87] U. Hahn, M. Gorka, F. Vögtle, V. Vicinelli, P. Ceroni, M. Maestri, V. Balzani, *Angew. Chem.* **2002**, *114*, 3747; *Angew. Chem. Int. Ed.* **2002**, *41*, 3595.
- [88] M. Shchepinov, K. U. Mir, J. K. Elder, M. D. Frank-Kamenetskii, E. M. Southern, *Nucleic Acids Res.* **1999**, *27*, 3035.
- [89] M. S. Shchepinov, I. A. Udalo, A. J. Bridgman, E. M. Southern, *Nucleic Acids Res.* **1999**, *27*, 4447.
- [90] S. Yamaguchi, T. M. Swager, *J. Am. Chem. Soc.* **2001**, *123*, 12087.
- [91] S. C. Ng, H. F. Lu, H. S. O. Chan, A. Fujii, T. Laga, K. Yoshino, *Macromolecules* **2001**, *34*, 6895.
- [92] G. Lange, B. Tieke, *Macromol. Chem. Phys.* **1999**, *200*, 106.
- [93] M. D. Disney, J. Zheng, T. M. Swager, P. H. Seeberger, *J. Am. Chem. Soc.* **2004**, *126*, 13343.
- [94] C. Ego, D. Marsitzky, S. Becker, J. Y. Zhang, A. C. Grimsdale, K. Müllen, J. D. MacKenzie, C. Silva, R. H. Friend, *J. Am. Chem. Soc.* **2003**, *125*, 437.
- [95] M. Wohlgenannt, W. Graupner, F. P. Wenzl, S. Tasch, E. J. W. List, G. Leising, M. Graupner, A. Hermetter, U. Rohr, P. Schlichting, Y. Geerts, U. Scherf, K. Müllen, *Chem. Phys.* **1998**, *227*, 99.
- [96] V. V. Didenko, V. C. Moore, D. S. Baskin, R. E. Smalley, *Nano Lett.* **2005**, *5*, 1563.
- [97] J. S. Yang, T. M. Swager, *J. Am. Chem. Soc.* **1998**, *120*, 5321.



- [98] S. A. Kushon, K. D. Ley, K. Bradford, R. M. Jones, D. McBranch, D. Whitten, *Langmuir* **2002**, *18*, 7245.
- [99] S. A. Kushon, K. Bradford, V. Marin, C. Suhrada, B. A. Armitage, D. McBranch, D. Whitten, *Langmuir* **2003**, *19*, 6456.
- [100] S. Kumarasamy, T. Bergstedt, X. B. Shi, F. Rininsland, S. A. Kushon, W. S. Xia, K. D. Ley, K. Achyuthan, D. McBranch, *Proc. Natl. Acad. Sci. USA* **2004**, *101*, 7511.
- [101] S. W. Thomas, J. P. Amara, R. E. Bjork, T. M. Swager, *Chem. Commun.* **2005**, 4572.
- [102] D. T. McQuade, A. E. Pullen, T. M. Swager, *Chem. Rev.* **2000**, *100*, 2537.
- [103] C. Fan, S. Wang, J. Hong, G. C. Bazan, K. W. Plaxco, A. J. Heeger, *Proc. Natl. Acad. Sci. USA* **2003**, *100*, 6297.
- [104] L. Giordano, T. M. Jovin, M. Irie, E. A. Jares-Erijman, *J. Am. Chem. Soc.* **2002**, *124*, 7481.
- [105] J. L. Bahr, G. Kodis, L. de la Garza, S. Lin, A. L. Moore, T. A. Moore, D. Gust, *J. Am. Chem. Soc.* **2001**, *123*, 7124.
- [106] I. L. Medintz, S. A. Trammell, H. Mattoussi, J. M. Mauro, *J. Am. Chem. Soc.* **2004**, *126*, 30.
- [107] A. Tucks, H. P. Beck, *J. Solid State Chem.* **2005**, *178*, 1145.
- [108] S. Z. Pu, T. S. Yang, J. K. Xu, L. Shen, G. Z. Li, Q. Xiao, B. Chen, *Tetrahedron* **2005**, *61*, 6623.
- [109] R. Matsushima, H. Morikane, Y. Kohno, *Chem. Lett.* **2003**, *32*, 302.
- [110] A. P. Demchenko, *Ultraviolet Spectroscopy of Proteins*, Springer, New York, **1981**.
- [111] S. J. Nannepaga, R. Gawalapu, D. Velasquez, R. Renthal, *Biochemistry* **2004**, *43*, 550.
- [112] M. A. Talavera, E. M. De La Cruz, *Biochemistry* **2005**, *44*, 959.
- [113] H. E. Townley, R. B. Sessions, A. R. Clarke, T. R. Dafforn, W. T. Griffiths, *Proteins Struct. Funct. Genet.* **2001**, *44*, 329.
- [114] E. Cordat, I. Mus-Veteau, G. Leblanc, *J. Biol. Chem.* **1998**, *273*, 33198.
- [115] J. C. Lee, R. Langen, P. A. Hummel, H. B. Gray, J. R. Winkler, *Proc. Natl. Acad. Sci. USA* **2004**, *101*, 16466.
- [116] M. J. Tucker, R. Oyola, F. Gai, *J. Phys. Chem. B* **2005**, *109*, 4788.
- [117] M. Eisenhawer, S. Cattarinussi, A. Kuhn, H. Vogel, *Biochemistry* **2001**, *40*, 12321.
- [118] H. Y. Shrivastava, B. U. Nair, *J. Inorg. Biochem.* **2004**, *98*, 991.
- [119] P. D. J. Moens, M. K. Helms, D. M. Jameson, *Protein J.* **2004**, *23*, 79.
- [120] J. A. Schmid, H. Neumeier, *ChemBioChem* **2005**, *6*, 1149.
- [121] G. S. Baird, D. A. Zacharias, R. Y. Tsien, *Proc. Natl. Acad. Sci. USA* **2000**, *97*, 11984.
- [122] M. V. Matz, A. F. Fradkov, Y. A. Labas, A. P. Savitsky, A. G. Zarausky, M. L. Markelov, S. A. Lukyanov, *Nat. Biotechnol.* **1999**, *17*, 969.
- [123] R. E. Campbell, O. Tour, A. E. Palmer, P. A. Steinbach, G. S. Baird, D. A. Zacharias, R. Y. Tsien, *Proc. Natl. Acad. Sci. USA* **2002**, *99*, 7877.
- [124] J. P. Morseman, M. W. Moss, S. J. Zoha, F. C. T. Allnut, *Biotechniques* **1999**, *26*, 559.
- [125] D. Sinnecker, P. Voigt, N. Hellwig, M. Schaefer, *Biochemistry* **2005**, *44*, 7085.
- [126] A. Miyawaki, O. Griesbeck, R. Heim, R. Y. Tsien, *Proc. Natl. Acad. Sci. USA* **1999**, *96*, 2135.
- [127] A. Miyawaki, J. Llopis, R. Heim, J. M. McCaffery, J. A. Adams, M. Ikura, R. Y. Tsien, *Nature* **1997**, *388*, 882.
- [128] M. Fehr, D. W. Ehrhardt, S. Lalonde, W. B. Frommer, *Curr. Opin. Plant Biol.* **2004**, *7*, 345.
- [129] M. Fehr, W. B. Frommer, S. Lalonde, *Proc. Natl. Acad. Sci. USA* **2002**, *99*, 9846.
- [130] M. Fehr, S. Lalonde, I. Lager, M. W. Wolff, W. B. Frommer, *J. Biol. Chem.* **2003**, *278*, 19127.
- [131] K. G. Rice, *Anal. Biochem.* **2001**, *297*, 117.
- [132] N. C. Shaner, P. A. Steinbach, R. Y. Tsien, *Nat. Methods* **2005**, *2*, 905.
- [133] N. C. Shaner, R. E. Campbell, P. A. Steinbach, B. N. G. Giepmans, A. E. Palmer, R. Y. Tsien, *Nat. Biotechnol.* **2004**, *22*, 1567.
- [134] A. W. Nguyen, P. S. Daugherty, *Nat. Biotechnol.* **2005**, *23*, 355.
- [135] V. V. Verkhusha, K. A. Lukyanov, *Nat. Biotechnol.* **2004**, *22*, 289.
- [136] E. A. Meighen, *Microbiol. Rev.* **1991**, *55*, 123.
- [137] K. V. Wood, *Promega Notes* **1998**, *65*, 14.
- [138] W. W. Lorenz, R. O. McCann, M. Longiaru, M. J. Cormier, *Proc. Natl. Acad. Sci. USA* **1991**, *88*, 4438.
- [139] J. M. Kendall, M. N. Badminton, *Trends Biotechnol.* **1998**, *16*, 216.
- [140] A. Roda, M. Guardigli, E. Michelini, M. Mirasoli, P. Pasini, *Anal. Chem.* **2003**, *75*, 462A.
- [141] A. Roda, M. Guardigli, P. Pasini, M. Mirasoli, *Anal. Bioanal. Chem.* **2003**, *377*, 826.
- [142] A. Roda, P. Pasini, M. Mirasoli, E. Michelini, M. Guardigli, *Trends Biotechnol.* **2004**, *22*, 295.
- [143] C. Dodeigne, L. Thunus, R. Lejeune, *Talanta* **2000**, *51*, 415.
- [144] Y. Xu, D. W. Piston, C. H. Johnson, *Proc. Natl. Acad. Sci. USA* **1999**, *96*, 151.
- [145] Y. Xu, A. Kanauchi, A. G. von Arnim, D. W. Piston, C. H. Johnson, *Biophotonics Part A* **2003**, *360*, 289.
- [146] N. Boute, R. Jockers, T. Issad, *Trends Pharmacol. Sci.* **2002**, *23*, 351.
- [147] N. Boute, K. Pernet, T. Issad, *Mol. Pharmacol.* **2001**, *60*, 640.
- [148] Y. Ohmiya, T. Hirano, *Chem. Biol.* **1996**, *3*, 333.
- [149] J. G. Morin, J. W. Hastings, *J. Cell. Physiol.* **1971**, *77*, 313.
- [150] "Cell Signaling, Transcription, and Translation as Therapeutic Targets": T. Issad, N. Boute, K. Pernet, *Ann. N. Y. Acad. Sci.* **2002**, *973*, 120.
- [151] T. Issad, N. Boute, K. Pernet, *Biochem. Pharmacol.* **2002**, *64*, 813.
- [152] L. S. Laursen, C. Oxvig, *Biochem. Pharmacol.* **2005**, *69*, 1723.
- [153] J. Perroy, S. Pontier, P. G. Charest, M. Aubry, M. Bouvier, *Nat. Methods* **2004**, *1*, 203.
- [154] W. A. Francisco, H. M. Abu-Soud, T. O. Baldwin, F. M. Raushel, *J. Biol. Chem.* **1993**, *268*, 24734.
- [155] T. O. Baldwin, J. A. Christopher, F. M. Raushel, J. F. Sinclair, M. M. Ziegler, A. J. Fisher, I. Rayment, *Curr. Opin. Struct. Biol.* **1995**, *5*, 798.
- [156] J. R. de Wet, K. V. Wood, D. R. Helinski, M. DeLuca, *Proc. Natl. Acad. Sci. USA* **1985**, *82*, 7870.
- [157] R. L. Airth, W. C. Rhodes, W. D. McElroy, *Biochim. Biophys. Acta* **1957**, *27*, 519.
- [158] J. Yang, D. B. Thomason, *Biotechniques* **1993**, *15*, 848.
- [159] Y. Yamakawa, H. Ueda, A. Kitayama, T. Nagamune, *J. Biosci. Bioeng.* **2002**, *93*, 537.
- [160] R. Arai, H. Nakagawa, A. Kitayama, H. Ueda, T. Nagamune, *J. Biosci. Bioeng.* **2002**, *94*, 362.
- [161] S. Angers, A. Salahpour, E. Joly, S. Hilairat, D. Chelsky, M. Dennis, M. Bouvier, *Proc. Natl. Acad. Sci. USA* **2000**, *97*, 3684.
- [162] J. F. Mercier, A. Salahpour, S. Angers, A. Breit, M. Bouvier, *J. Biol. Chem.* **2002**, *277*, 44925.
- [163] Y. Wang, G. Wang, D. J. O'Kane, A. A. Szalay, *Mol. Gen. Genet.* **2001**, *264*, 578.
- [164] S. Inouye, O. Shimomura, *Biochem. Biophys. Res. Commun.* **1997**, *233*, 349.
- [165] C. Wu, H. Nakamura, A. Murai, O. Shimomura, *Tetrahedron Lett.* **2001**, *42*, 2997.
- [166] B. J. Bryan, C. S. Szent-Gyorgyi, US Patent 6232107, **2001**.
- [167] M. Verhaegen, T. K. Christopoulos, *Anal. Chem.* **2002**, *74*, 4378.
- [168] B. A. Tannous, D. E. Kim, J. L. Fernandez, R. Weissleder, X. O. Breakefield, *Mol. Ther.* **2005**, *11*, 435.
- [169] S. Wiles, K. Ferguson, M. Stefanidou, D. B. Young, B. D. Robertson, *Appl. Environ. Microbiol.* **2005**, *71*, 3427.

- [170] S. Inouye, K. Watanabe, H. Nakamura, O. Shimomura, *FEBS Lett.* **2000**, *481*, 19.
- [171] A. Chiesa, E. Rapizzi, V. Tosello, P. Pinton, M. De Virgilio, K. E. Fogarty, R. Rizzuto, *Biochem. J.* **2001**, *355*, 1.
- [172] J. Alvarez, M. Montero, *Cell Calcium* **2002**, *32*, 251.
- [173] A. Y. Gorokhovatsky, N. V. Rudenko, V. V. Marchenkov, V. S. Skosyrev, M. A. Arzhanov, N. Burkhardt, M. V. Zakharov, G. V. Semisotnov, L. M. Vinokurov, Y. B. Alakhov, *Anal. Biochem.* **2003**, *313*, 68.
- [174] M. Adamczyk, J. A. Moore, K. Shreder, *Org. Lett.* **2001**, *3*, 1797.
- [175] L. J. Kricka, *Anal. Chim. Acta* **2003**, *500*, 279.
- [176] Y. M. Liu, J. K. Cheng, *J. Chromatogr. A* **2002**, *959*, 1.
- [177] I. Weeks, M. L. Sturgess, J. S. Woodhead, *Clin. Sci.* **1986**, *70*, 403.
- [178] M. L. Grayeski, P. A. Moritzen, *Langmuir* **1997**, *13*, 2675.
- [179] E. J. Williams, A. K. Campbell, *Anal. Biochem.* **1986**, *155*, 249.
- [180] A. K. Campbell, A. Patel, *Biochem. J.* **1983**, *216*, 185.
- [181] A. Patel, A. K. Campbell, *Clin. Chem.* **1983**, *29*, 1604.
- [182] A. Patel, C. J. Davies, A. K. Campbell, F. McCapra, *Anal. Biochem.* **1983**, *129*, 162.
- [183] I. Durrant, *Methods Mol. Biol.* **1994**, *31*, 147.
- [184] G. Messeri, A. Orlandini, M. Pazzagli, *J. Biolumin. Chemilumin.* **1989**, *4*, 154.
- [185] S. J. Richards, F. S. Wusteman, *J. Biolumin. Chemilumin.* **1989**, *3*, 175.
- [186] P. M. Easton, A. C. Simmonds, A. Rakishev, A. M. Egorov, L. P. Candeias, *J. Am. Chem. Soc.* **1996**, *118*, 6619.
- [187] A. N. Diaz, F. G. Sanchez, J. A. G. Garcia, *Anal. Chim. Acta* **1996**, *327*, 161.
- [188] H. Akhavan-Tafti, R. de Silva, R. A. Eickholt, R. S. Handley, M. Mazelis, M. Sandison, *Talanta* **2003**, *60*, 345.
- [189] H. Akhavan-Tafti, R. DeSilva, Z. Arghavani, R. A. Eickholt, R. S. Handley, B. A. Schoenfelner, K. Sugioka, Y. Sugioka, A. P. Schaap, *J. Org. Chem.* **1998**, *63*, 930.
- [190] A. M. Osman, G. Zomer, C. Laane, R. Hilhorst, *Luminescence* **2000**, *15*, 189.
- [191] S. Beck, H. Koster, *Anal. Chem.* **1990**, *62*, 2258.
- [192] A. P. Schaap, H. Akhavan-Tafti, L. J. Romano, *Clin. Chem.* **1989**, *35*, 1863.
- [193] P. R. Selvin, *Annu. Rev. Biophys. Biomol. Struct.* **2002**, *31*, 275.
- [194] C. X. Sun, J. H. Yang, L. Li, X. Wu, Y. Liu, S. F. Liu, *J. Chromatogr. B* **2004**, *803*, 173.
- [195] C. F. W. Becker, D. Clayton, G. Shapovalov, H. A. Lester, G. G. Kochendoerfer, *Bioconjugate Chem.* **2004**, *15*, 1118.
- [196] H. K. Lee, H. Cao, T. M. Rana, *J. Comb. Chem.* **2005**, *7*, 279.
- [197] P. R. Selvin, J. E. Hearst, *Proc. Natl. Acad. Sci. USA* **1994**, *91*, 10024.
- [198] M. Gabourdes, V. Bourguine, G. Mathis, H. Bazin, W. Alpha-Bazin, *Anal. Biochem.* **2004**, *333*, 105.
- [199] J. Karvinen, V. Laitala, M. L. Makinen, O. Mulari, J. Tamminen, J. Hermonen, P. Hurskainen, I. Hemmila, *Anal. Chem.* **2004**, *76*, 1429.
- [200] V. Bergendahl, T. Heyduk, R. R. Burgess, *Appl. Environ. Microbiol.* **2003**, *69*, 1492.
- [201] T. Pulli, M. Hoyhtya, H. Soderlund, K. Takkinen, *Anal. Chem.* **2005**, *77*, 2637.
- [202] Q. P. Qin, O. Peltola, K. Pettersson, *Clin. Chem.* **2003**, *49*, 1105.
- [203] A. Tsourkas, M. A. Behlke, Y. Q. Xu, G. Bao, *Anal. Chem.* **2003**, *75*, 3697.
- [204] S. Sueda, J. L. Yuan, K. Matsumoto, *Bioconjugate Chem.* **2002**, *13*, 200.
- [205] X. D. Chen, X. B. Wang, L. Liu, D. C. Yang, L. Fan, *Anal. Chim. Acta* **2005**, *542*, 144.
- [206] T. Heyduk, *Curr. Opin. Biotechnol.* **2002**, *13*, 292.
- [207] D. J. Posson, P. H. Ge, C. Miller, F. Bezanilla, P. R. Selvin, *Nature* **2005**, *436*, 848.
- [208] E. Terpetschnig, H. Szmazinski, H. Malak, J. R. Lakowicz, *Biophys. J.* **1995**, *68*, 342.
- [209] H. J. Youn, E. Terpetschnig, H. Szmazinski, J. R. Lakowicz, *Anal. Biochem.* **1995**, *232*, 24.
- [210] C. von Bultzingslowen, A. K. McEvoy, C. McDonagh, B. D. MacCraith, *Anal. Chim. Acta* **2003**, *480*, 275.
- [211] X. D. Ge, L. Tolosa, G. Rao, *Abstr. Pap. Am. Chem. Soc.* **2004**, *227*, U128.
- [212] M. C. Daniel, D. Astruc, *Chem. Rev.* **2004**, *104*, 293.
- [213] E. Dulkeith, M. Ringler, T. A. Klar, J. Feldmann, A. M. Javier, W. J. Parak, *Nano Lett.* **2005**, *5*, 585.
- [214] B. Dubertret, M. Calame, A. J. Libchaber, *Nat. Biotechnol.* **2001**, *19*, 680.
- [215] D. J. Maxwell, J. R. Taylor, S. M. Nie, *J. Am. Chem. Soc.* **2002**, *124*, 9606.
- [216] H. Du, M. D. Disney, B. L. Miller, T. D. Krauss, *J. Am. Chem. Soc.* **2003**, *125*, 4012.
- [217] M. Seidel, D. M. Dankbar, G. Gauglitz, *Anal. Bioanal. Chem.* **2004**, *379*, 904.
- [218] L. Dyadyusha, H. Yin, S. Jaiswal, T. Brown, J. J. Baumberg, F. P. Booy, T. Melvin, *Chem. Commun.* **2005**, 3201.
- [219] Z. Gueroui, A. Libchaber, *Phys. Rev. Lett.* **2004**, *93*, 166108.
- [220] R. Wagnier, A. V. Baranov, V. G. Maslov, V. Stsiapura, M. Artemyev, M. Pluot, A. Sukhanova, I. Nabiev, *Nano Lett.* **2004**, *4*, 451.
- [221] E. Oh, M. Y. Hong, D. Lee, S. H. Nam, H. C. Yoon, H. S. Kim, *J. Am. Chem. Soc.* **2005**, *127*, 3270.
- [222] T. H. Lee, J. I. Gonzales, J. Zheng, R. M. Dickson, *Acc. Chem. Res.* **2005**, *38*, 534.
- [223] J. Zheng, C. W. Zhang, R. M. Dickson, *Phys. Rev. Lett.* **2004**, *93*, 077402.
- [224] J. Zheng, J. T. Petty, R. M. Dickson, *J. Am. Chem. Soc.* **2003**, *125*, 7780.
- [225] J. Zheng, R. M. Dickson, *J. Am. Chem. Soc.* **2002**, *124*, 13982.
- [226] L. A. Peyser, A. E. Vinson, A. P. Bartko, R. M. Dickson, *Science* **2001**, *291*, 103.
- [227] C. Burda, X. B. Chen, R. Narayanan, M. A. El-Sayed, *Chem. Rev.* **2005**, *105*, 1025.
- [228] A. Maali, T. Cardinal, M. Treguer-Delapierre, *Phys. E* **2003**, *17*, 559.
- [229] J. T. Petty, J. Zheng, N. V. Hud, R. M. Dickson, *J. Am. Chem. Soc.* **2004**, *126*, 5207.
- [230] D. D. Evanoff, G. Chumanov, *ChemPhysChem* **2005**, *6*, 1221.
- [231] C. Felix, C. Sieber, W. Harbich, J. Buttet, I. Rabin, W. Schulze, G. Ertl, *Chem. Phys. Lett.* **1999**, *313*, 105.
- [232] C. Felix, C. Sieber, W. Harbich, J. Buttet, I. Rabin, W. Schulze, G. Ertl, *Phys. Rev. Lett.* **2001**, *86*, 2992.
- [233] J. P. Gao, J. Fu, C. K. Lin, J. Lin, Y. C. Han, X. Yu, C. Y. Pan, *Langmuir* **2004**, *20*, 9775.
- [234] R. A. Ganeev, A. I. Rysanyansky, A. L. Stepanov, T. Usmanov, *Phys. Solid State* **2004**, *46*, 351.
- [235] H. H. Huang, F. Q. Yan, Y. M. Kek, C. H. Chew, G. Q. Xu, W. Ji, P. S. Oh, S. H. Tang, *Langmuir* **1997**, *13*, 172.
- [236] N. A. Dhas, C. P. Raj, A. Gedanken, *Chem. Mater.* **1998**, *10*, 1446.
- [237] G. Belomoin, J. Therrien, M. Nayfeh, *Appl. Phys. Lett.* **2000**, *77*, 779.
- [238] G. Belomoin, J. Therrien, A. Smith, S. Rao, R. Twisten, S. Chaieb, M. H. Nayfeh, L. Wagner, L. Mitas, *Appl. Phys. Lett.* **2002**, *80*, 841.
- [239] V. Kapaklis, C. Politis, P. Pouloupoulos, P. Schweiss, *Appl. Phys. Lett.* **2005**, *87*.
- [240] S. Prusty, H. S. Mavi, A. K. Shukla, *Phys. Rev. B* **2005**, *71*.
- [241] L. Wang, V. Reipa, J. Blasic, *Bioconjugate Chem.* **2004**, *15*, 409.
- [242] D. P. Singh, A. K. Singh, N. Srivastava, *Indian J. Sci. Ind. Sect. A* **2004**, *78*, 197.
- [243] Z. F. Li, E. Ruckenstein, *Nano Lett.* **2004**, *4*, 1463.

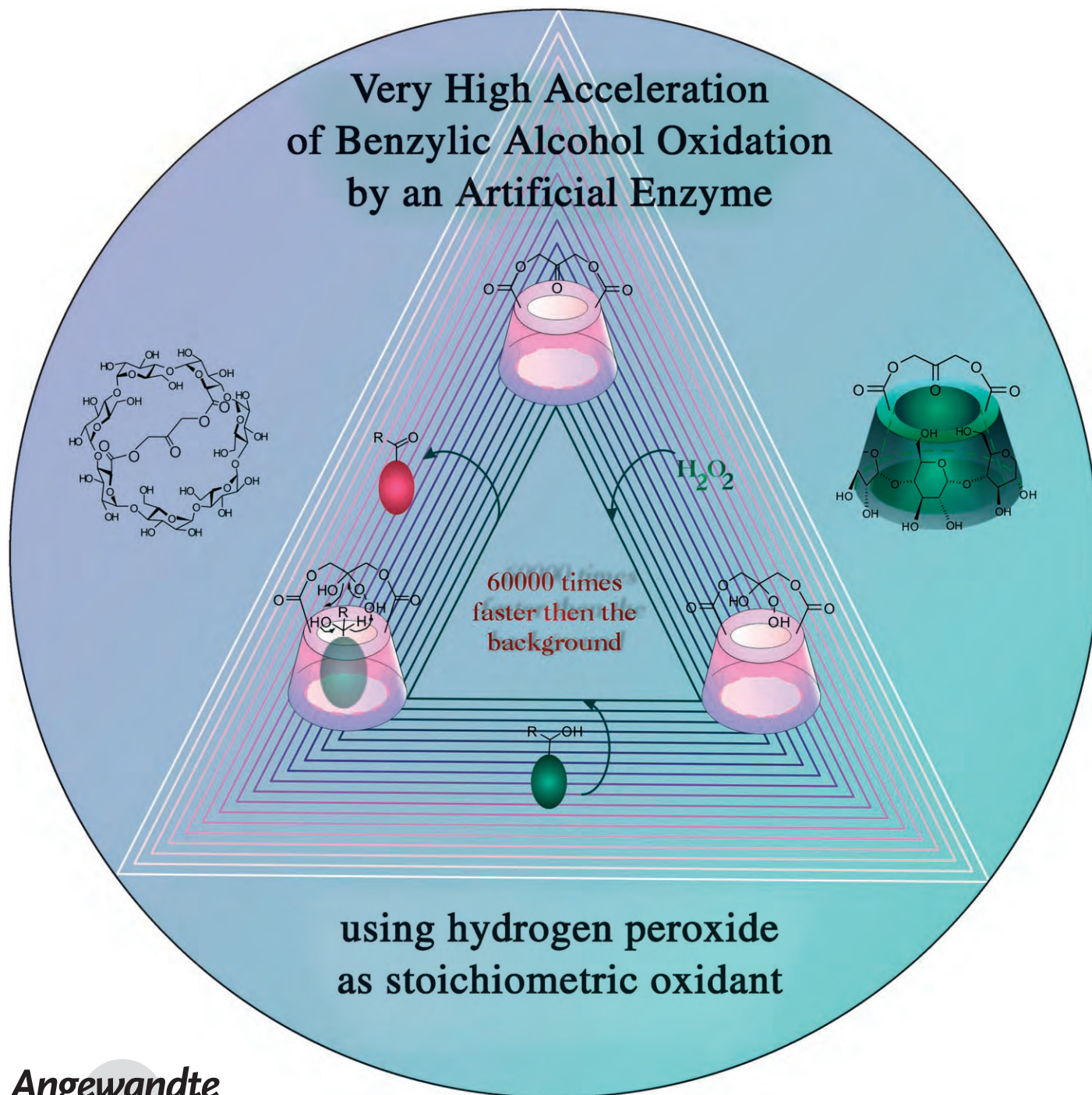
- [244] X. G. Li, Y. Q. He, S. S. Talukdar, M. T. Swihart, *Langmuir* **2003**, *19*, 8490.
- [245] J. Zou, R. K. Baldwin, K. A. Pettigrew, S. M. Kauzlarich, *Nano Lett.* **2004**, *4*, 1181.
- [246] H. Ow, D. R. Larson, M. Srivastava, B. A. Baird, W. W. Webb, U. Wiesner, *Nano Lett.* **2005**, *5*, 113.
- [247] H. G. Craighead, A. M. Glass, *Opt. Lett.* **1981**, *6*, 248.
- [248] I. Cohanoschi, F. E. Hernandez, *J. Phys. Chem. B* **2005**, *109*, 14506.
- [249] K. Aslan, I. Gryczynski, J. Malicka, E. Matveeva, J. R. Lakowicz, C. D. Geddes, *Curr. Opin. Biotechnol.* **2005**, *16*, 55.
- [250] K. Aslan, J. R. Lakowicz, C. D. Geddes, *Anal. Bioanal. Chem.* **2005**, *382*, 926.
- [251] D. S. Wang, M. Kerker, *Phys. Rev. B* **1982**, *25*, 2433.
- [252] O. Stranik, H. M. McEvoy, C. McDonagh, B. D. MacCraith, *Sens. Actuators B* **2005**, *107*, 148.
- [253] J. Zhang, J. R. Lakowicz, *J. Phys. Chem. B* **2005**, *109*, 8701.
- [254] J. Zhang, J. Malicka, I. Gryczynski, J. R. Lakowicz, *J. Phys. Chem. B* **2005**, *109*, 7643.
- [255] J. Lukomska, J. Malicka, I. Gryczynski, Z. Leonenko, J. R. Lakowicz, *Biopolymers* **2005**, *77*, 31.
- [256] J. Malicka, I. Gryczynski, J. Y. Fang, J. R. Lakowicz, *Anal. Biochem.* **2003**, *317*, 136.
- [257] J. Malicka, I. Gryczynski, C. D. Geddes, J. R. Lakowicz, *J. Biomed. Opt.* **2003**, *8*, 472.
- [258] J. Malicka, I. Gryczynski, Z. Gryczynski, J. R. Lakowicz, *Biophys. J.* **2003**, *84*, 290 A.
- [259] J. R. Lakowicz, J. Malicka, I. Gryczynski, *Photochem. Photobiol.* **2002**, *77*, 604.
- [260] J. Malicka, I. Gryczynski, J. Fang, J. Kusba, J. R. Lakowicz, *Anal. Biochem.* **2003**, *315*, 160.
- [261] M. Bruchez, Jr., M. Moronne, P. Gin, S. Weiss, A. P. Alivisatos, *Science* **1998**, *281*, 2013.
- [262] W. C. W. Chan, S. Nie, *Science* **1998**, *281*, 2016.
- [263] I. Medintz, H. Uyeda, E. Goldman, H. Mattoussi, *Nat. Mater.* **2005**, *4*, 435.
- [264] C. J. Murphy, *Anal. Chem.* **2002**, *74*, 520A.
- [265] X. Michalet, F. F. Pinaud, L. A. Bentolila, J. M. Tsay, S. Doose, J. J. Li, G. Sundaresan, A. M. Wu, S. S. Gambhir, S. Weiss, *Science* **2005**, *307*, 538.
- [266] P. Alivisatos, *Nat. Biotechnol.* **2004**, *22*, 47.
- [267] W. J. Parak, D. Gerion, T. Pellegrino, D. Zanchet, C. Micheel, S. C. Williams, R. Boudreau, M. A. Le Gros, C. A. Larabell, A. P. Alivisatos, *Nanotechnology* **2003**, *14*, R15.
- [268] W. J. Parak, T. Pellegrino, C. Plank, *Nanotechnology* **2005**, *16*, R9.
- [269] C. A. Leatherdale, W. K. Woo, F. V. Mikulec, M. G. Bawendi, *J. Phys. Chem. B* **2002**, *106*, 7619.
- [270] B. O. Dabbousi, J. Rodríguez-Viejo, F. V. Mikulec, J. R. Heine, H. Mattoussi, R. Ober, K. F. Jensen, M. G. Bawendi, *J. Phys. Chem. B* **1997**, *101*, 9463.
- [271] A. R. Clapp, I. L. Medintz, J. M. Mauro, B. R. Fisher, M. G. Bawendi, H. Mattoussi, *J. Am. Chem. Soc.* **2004**, *126*, 301.
- [272] H. Mattoussi, K. Kuno, E. R. Goldman, G. P. Anderson, J. M. Mauro in *Optical Biosensors: Present and Future* (Eds.: F. S. Ligler, C. A. Rowe Tait), Elsevier, San Diego, **2002**, p. 537.
- [273] M. A. Hines, P. Guyot-Sionnest, *J. Phys. Chem.* **1996**, *100*, 468.
- [274] Z. A. Peng, X. Peng, *J. Am. Chem. Soc.* **2001**, *123*, 183.
- [275] F. Pinaud, D. King, H.-P. Moore, S. Weiss, *J. Am. Chem. Soc.* **2004**, *126*, 6115.
- [276] H. Mattoussi, J. M. Mauro, E. R. Goldman, G. P. Anderson, V. C. Sundar, F. V. Mikulec, M. G. Bawendi, *J. Am. Chem. Soc.* **2000**, *122*, 12142.
- [277] A. R. Clapp, I. L. Medintz, R. B. Fisher, G. P. Anderson, H. Mattoussi, *J. Am. Chem. Soc.* **2005**, *127*, 1242.
- [278] E. Goldman, I. Medintz, J. Whitley, A. Hayhurst, A. Clapp, H. Uyeda, J. Deschamps, M. Lassman, H. Mattoussi, *J. Am. Chem. Soc.* **2005**, *127*, 6744.
- [279] K. E. Sapsford, I. L. Medintz, J. P. Golden, J. R. Deschamps, H. T. Uyeda, H. Mattoussi, *Langmuir* **2004**, *20*, 7720.
- [280] I. L. Medintz, A. R. Clapp, J. S. Melinger, J. R. Deschamps, H. Mattoussi, *Adv. Mater.* **2005**, *17*, 2450.
- [281] I. L. Medintz, J. H. Konnert, A. R. Clapp, I. M. Stanish, M. E. Twigg, H. Mattoussi, J. M. Matthew, J. R. Deschamps, *Proc. Natl. Acad. Sci. USA* **2004**, *101*, 9612.
- [282] F. Patolsky, R. Gill, Y. Weizmann, T. Mokari, U. Banin, I. Willner, *J. Am. Chem. Soc.* **2003**, *125*, 13918.
- [283] J. H. Kim, D. Morikis, M. Ozkan, *Sens. Actuators B* **2004**, *102*, 315.
- [284] J. A. Kloepper, N. Cohen, J. L. Nadeau, *J. Phys. Chem. B* **2004**, *108*, 17042.
- [285] A. C. S. Samia, X. Chen, C. Burda, *J. Am. Chem. Soc.* **2003**, *125*, 15736.
- [286] R. Bakalova, H. Ohba, Z. Zhelev, M. Ishikawa, Y. Baba, *Nat. Biotechnol.* **2004**, *22*, 1360.
- [287] A. N. Glazer, *J. Appl. Physiol.* **1994**, *6*, 105.
- [288] A. N. Glazer, *Methods Enzymol.* **1988**, *167*, 291.
- [289] A. N. Glazer, J. H. Clark, *Biophys. J.* **1986**, *49*, 115.
- [290] A. N. Glazer, *Annu. Rev. Biophys. Biophys. Chem.* **1985**, *14*, 47.
- [291] D. J. Lundell, R. C. Williams, A. N. Glazer, *J. Biol. Chem.* **1981**, *256*, 3580.
- [292] A. N. Glazer, L. Stryer, *Biophys. J.* **1983**, *43*, 383.
- [293] A. N. Glazer, L. Stryer, *Trends Biochem. Sci.* **1984**, *9*, 323.
- [294] Y. Ohya, K. Yabuki, M. Hashimoto, A. Nakajima, T. Ouchi, *Bioconjugate Chem.* **2003**, *14*, 1057.
- [295] A. K. Tong, J. Y. Ju, *Nucleic Acids Res.* **2002**, *30*.
- [296] A. K. Tong, Z. M. Li, G. S. Jones, J. J. Russo, J. Y. Ju, *Nat. Biotechnol.* **2001**, *19*, 756.
- [297] G. F. Schröder, H. Grubmüller, *Comp. Phys. Commun.* **2004**, *158*, 150.
- [298] S. Kawahara, T. Uchimaru, S. Murata, *Chem. Commun.* **1999**, 563.
- [299] S. C. Hung, R. A. Mathies, A. N. Glazer, *Anal. Biochem.* **1997**, *252*, 78.
- [300] S. C. Hung, R. A. Mathies, A. N. Glazer, *Anal. Biochem.* **1998**, *255*, 32.
- [301] W. Erker, R. Hubler, H. Decker, *Eur. Biophys. J. Biophys. Lett.* **2004**, *33*, 386.
- [302] D. Klostermeier, P. Sears, C. H. Wong, D. P. Millar, J. R. Williamson, *Nucleic Acids Res.* **2004**, *32*, 2707.
- [303] L. Wang, W. Tan, *Nano Lett.* **2006**, *6*, 84.
- [304] C. S. Yun, A. Javier, T. Jennings, M. Fisher, S. Hira, S. Peterson, B. Hopkins, N. O. Reich, G. F. Strouse, *J. Am. Chem. Soc.* **2005**, *127*, 3115.
- [305] C. Sonnichsen, B. J. Reinhard, J. Liphardt, A. P. Alivisatos, *Nat. Biotechnol.* **2005**, *23*, 741.
- [306] L. J. Kricka, *Ann. Clin. Biochem.* **2002**, *39*, 114.
- [307] I. G. Gut, *Hum. Mutat.* **2001**, *17*, 475.
- [308] I. Kheterpal, R. A. Mathies, *Anal. Chem.* **1999**, *71*, 31A.
- [309] C. S. Lim, J. N. Miller, J. W. Bridges, *Anal. Chim. Acta* **1980**, *114*, 183.
- [310] P. Tinnefeld, M. Sauer, *Angew. Chem.* **2005**, *117*, 2698; *Angew. Chem. Int. Ed.* **2005**, *44*, 2642.
- [311] S. Weiss, *Nat. Struct. Biol.* **2000**, *7*, 724.
- [312] M. K. So, C. Xu, A. M. Loening, S. S. Gambhir, J. Rao, *Nat. Biotechnol.* **2006**, *24*, 339.
- [313] C. Hipplius, F. Schlosser, M. O. Vysotsky, V. Böhmer, F. Würthner, *J. Am. Chem. Soc.* **2006**, *128*, 3870.
- [314] A. R. Clapp, I. L. Medintz, H. T. Uyeda, B. R. Fisher, E. R. Goldman, M. G. Bawendi, H. Mattoussi, *J. Am. Chem. Soc.* **2005**, *127*, 18212.
- [315] K. D. Pflieger, K. A. Eidne, *Nat. Methods* **2006**, *3*, 165.



# Very High Rate Enhancement of Benzyl Alcohol Oxidation by an Artificial Enzyme\*\*

Lavinia G. Marinescu and Mikael Bols\*

## Very High Acceleration of Benzylic Alcohol Oxidation by an Artificial Enzyme

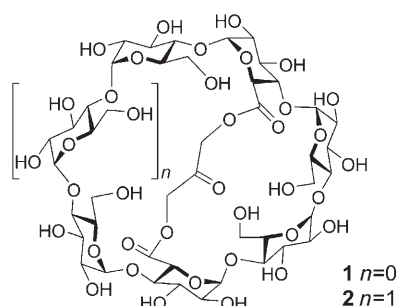


Angewandte  
Chemie



**E**nzymes have fascinated scientists since their discovery, and, over some decades, one aim in organic chemistry has been to create molecules that mimic the active sites of enzymes and promote catalysis.<sup>[1–6]</sup> Nevertheless even today there are relatively few examples of enzyme models that actually perform Michaelis–Menten catalysis under enzymatic conditions (i.e., water, pH 7, ambient temperature),<sup>[7]</sup> and very high rate accelerations under these conditions are rare.<sup>[8]</sup> On the other hand progress in synthetic chemistry, in this context, in carbohydrate chemistry,<sup>[9]</sup> now makes it possible to prepare more sophisticated rigid catalysts.

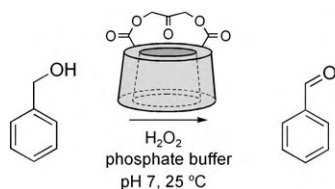
Recently we reported the bridged ketocyclodextrins **1** and **2** (Scheme 1)<sup>[10]</sup> and that they catalyze the oxidation of



**Scheme 1.** Catalysts **1** and **2**, which consist of a core of either  $\alpha$ - or  $\beta$ -cyclodextrin with dihydroxyacetone attached to the primary rim through ester bonds.

anilines to nitrobenzenes in the presence of hydrogen peroxide ( $\text{H}_2\text{O}_2$ ) in a reaction with enzyme kinetics and with a ratio  $k_{\text{cat}}/k_{\text{uncat}}$  up to 1070.<sup>[11]</sup> The cup-shaped compounds **1** and **2** bind the aromatic amino group in their hydrophobic cavities ( $K_{\text{m}} \approx 1\text{--}5\text{ mM}$ ), while the ketone functionality is believed to form a hydroperoxide adduct with  $\text{H}_2\text{O}_2$  that is responsible for the oxidation of the bound amine.<sup>[11]</sup> We have now found that **1** and **2** also catalyze the oxidation of benzylic alcohols to aldehydes, and that for this reaction the rate acceleration for the catalyzed reaction is very high.

The cyclodextrins **1** and **2** catalyze the transformation of benzylic alcohols into aldehydes (or ketones) in the presence of hydrogen peroxide (72 mM) in aqueous solution, at room temperature, and at pH 7.0 [Eq. (1)]. The reaction rate of the



(1)

[\*] Dr. L. G. Marinescu, Prof. Dr. M. Bols  
Department of Chemistry  
University of Aarhus  
8000 Aarhus (Denmark)  
Fax: (+45) 8619-6199  
E-mail: mb@chem.au.dk

[\*\*] We thank the Lundbeck foundation and the SNF (FNU) for support.

catalyzed reaction is observable even at cyclodextrin concentrations that are 10000 times lower than the substrate concentration and as low as  $1\text{ }\mu\text{M}$ . GC-MS analysis revealed that complete oxidation of the starting material can be achieved. The reaction follows Michaelis–Menten kinetics (Figure 1), can be inhibited by addition of cyclopentanol, and

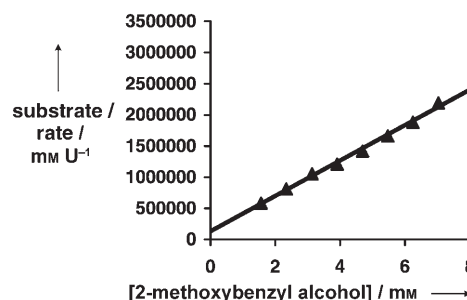


**Figure 1.** Hanes plot of the **2**-catalyzed ( $[\mathbf{2}] = 0.38\text{ mM}$ ) oxidation of 2-methoxybenzyl alcohol to 2-methoxybenzaldehyde in the presence of 72 mM  $\text{H}_2\text{O}_2$ , 25 °C.

is catalyzed neither by  $\beta$ -cyclodextrin nor by 1,3-dichloroacetone (DCA, Table 1). 1,3-Diacetoxyacetone (DAA) catalyzes the reaction slightly (Table 1). Under these reaction conditions **1** and **2** are stable and preincubation with hydrogen peroxide for a couple of hours does not decrease the catalytic activity.

The kinetic data ( $K_{\text{m}}$  and  $k_{\text{cat}}$ ) for a range of benzyl alcohol substrates were obtained from  $v_{\text{cat}}$  vs.  $[S]$  data ( $v_{\text{cat}}$ : velocity of the catalyzed reaction,  $S$ : substrate) in the usual manner using nonlinear least-squares fitting and are shown in Table 1. For pH 7 and 25 °C, the  $K_{\text{m}}$  values range from  $(0.21 \pm 0.07)$  to  $(5.0 \pm 1.6)\text{ mM}$  which are typical values for the binding of small aromatic molecules by cyclodextrins. The  $k_{\text{cat}}$  constants vary from about  $10^{-6}$  to about  $2.5 \times 10^{-4}\text{ s}^{-1}$  and since the first-order rate constant for the background oxidation ( $k_{\text{uncat}}$ ) under these condition is  $10^{-8}\text{--}10^{-9}\text{ s}^{-1}$  the ratio between the reaction rates for the reactions inside and outside the cavity ( $k_{\text{cat}}/k_{\text{uncat}}$ ) varies from about 400 to about 29 000 at 25 °C. The comparison with diacetoxyacetone is also significant: DAA catalysis gives a second-order rate constant  $k_{\text{cat},2}$  of  $4 \times 10^{-4}\text{ M}^{-1}\text{ s}^{-1}$ , which has to be compared to the  $k_{\text{cat}}/K_{\text{m}}$  values for **1** and **2** that are  $1.35 \times 10^{-2}$  and  $1.75 \times 10^{-2}\text{ M}^{-1}\text{ s}^{-1}$ , respectively; it follows that the supramolecular catalysts are 30 to 45 fold more efficient than DAA. As can be seen from Table 1 secondary alcohols (Me or Ph substituents) are oxidized as well. A range of substituents on the aromatic ring is tolerated though with variations in the catalysis rate.

For three reactions, a study of pH and temperature effects was performed (see Table 1, entries marked with [a]). The reaction rate increases with temperature and pH value, but above pH 9 the catalyst starts to decompose, presumably as a result of the lability of the esters. At pH 8.0 and 45 °C the rate increase observed for the oxidation of 2-hydroxybenzyl alcohol is approximately  $6.3 \times 10^4$ . Though this value still is lower than that found for natural enzymes, where rate increases have been calculated<sup>[12]</sup> to lie between  $10^6$  and  $10^{18}$ , it is fascinating to consider that since **2** has a  $10^2$  times

**Table 1:** Kinetic data for the oxidation of various benzylic alcohols to aldehydes catalyzed by **1** or **2** and compared with those of other potential catalysts. Except otherwise noted the experiments were performed in a 95 mM phosphate buffer at 25 °C and pH 7 with a H<sub>2</sub>O<sub>2</sub> concentration of 72 mM and with a concentration of the catalyst of 0.38 mM.

Substrate	A or X	Catalyst	$k_{\text{cat}} [\times 10^6 \text{ s}^{-1}]$	$K_{\text{m}} [\text{mM}]$	$k_{\text{cat}}/k_{\text{uncat}}$
		<b>1</b>	$26.9 \pm 3.2$	$2.0 \pm 0.7$	$1690 \pm 230$
		<b>2</b>	$26.3 \pm 2.0$	$1.5 \pm 0.4$	$1650 \pm 150$
		<b>2</b> <sup>[a]</sup>	$244 \pm 6$	–	$989 \pm 28$
		<b>2</b> <sup>[c]</sup>	no catalysis	$2.2 \pm 0.2$	1
		DCA	no catalysis	–	1
		DAA <sup>[d]</sup>	–	–	–
	<sup>1</sup> H	<b>1</b>	$24.4 \pm 1.5$	$0.72 \pm 0.30$	$5930 \pm 360$
	<sup>1</sup> H	<b>2</b>	$22.6 \pm 1.7$	$5.0 \pm 1.6$	$5490 \pm 420$
	<sup>2</sup> H	<b>2</b>	$15.8 \pm 1.4$	$0.77 \pm 0.63$	not determined
		<b>1</b>	$18.6 \pm 0.3$	$1.1 \pm 0.1$	$973 \pm 22$
		<b>2</b>	$18.3 \pm 0.4$	$0.84 \pm 0.1$	$960 \pm 34$
		β-CD	no catalysis	–	1
		<b>2</b>	$6.24 \pm 0.63$	$1.3 \pm 0.2$	$28\,600 \pm 9200$
		<b>2</b> <sup>[a]</sup>	$62.1 \pm 0.8$	$1.20 \pm 0.15$	$62\,900 \pm 5500$
		<b>2</b> <sup>[b]</sup>	no catalysis	–	1
		DCA	no catalysis	–	1
	OMe	<b>2</b>	$3.41 \pm 0.07$	$0.52 \pm 0.08$	$2740 \pm 130$
	Cl	<b>2</b>	$8.90 \pm 0.35$	$0.61 \pm 0.17$	$971 \pm 76$
	Br	<b>2</b>	$66.8 \pm 4.5$	$0.71 \pm 0.19$	$366 \pm 27$
	Br	<b>2</b> <sup>[a]</sup>	$591 \pm 62$	$1.2 \pm 0.4$	$82 \pm 13$
		<b>1</b>	$5.62 \pm 0.44$	$1.83 \pm 0.51$	$748 \pm 106$
		<b>2</b>	$4.55 \pm 0.47$	$1.09 \pm 0.56$	$887 \pm 103$
	OMe	<b>1</b>	$9.63 \pm 0.60$	$2.52 \pm 0.43$	$6760 \pm 570$
	OMe	<b>2</b>	$3.85 \pm 0.12$	$0.97 \pm 0.16$	$2700 \pm 110$
	OMe	<b>2</b> <sup>[a]</sup>	$159 \pm 12$	$6.1 \pm 0.8$	$1760 \pm 130$
	OH	<b>2</b>	$1.28 \pm 0.08$	$0.09 \pm 0.08$	not determined
	F	<b>2</b>	$9.10 \pm 0.49$	$0.66 \pm 0.23$	$402 \pm 41$
	Cl	<b>2</b>	$21.5 \pm 0.4$	$0.37 \pm 0.05$	$707 \pm 155$
	Br	<b>1</b>	$33.7 \pm 0.9$	$1.15 \pm 0.12$	$1030 \pm 30$
	Br	<b>2</b>	$24.2 \pm 0.1$	$0.93 \pm 0.02$	$739 \pm 4$
	Me	<b>2</b>	$3.93 \pm 0.98$	$0.78 \pm 0.93$	$945 \pm 236$
	OMe	<b>2</b>	$1.57 \pm 0.03$	$0.50 \pm 0.06$	$2120 \pm 86$
	Cl	<b>2</b>	$16.0 \pm 0.8$	$0.21 \pm 0.07$	$446 \pm 81$
		<b>2</b>	$293 \pm 51$	$11.8 \pm 2.3$	$539 \pm 94$

[a]  $T = 45^\circ\text{C}$ , pH 8. [b] Cyclopentanol (109 mM) was added as inhibitor. [c] H<sub>2</sub>O<sub>2</sub> was replaced with *tert*-butyl hydroperoxide. [d]  $k_{\text{cat},2} = 0.4 \text{ mM}^{-1} \text{ s}^{-1}$ ;  $k_{\text{cat}}/k_{\text{uncat}} = 9.8 \text{ mM}^{-1}$ .

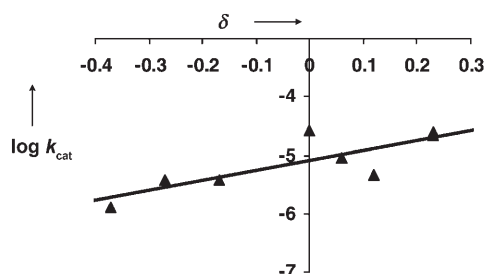
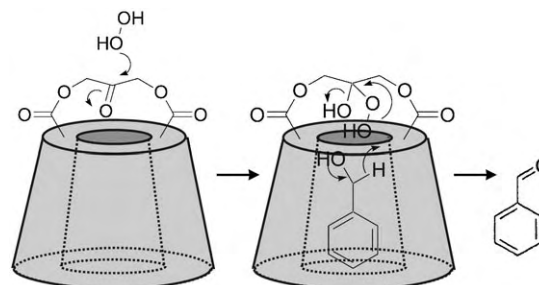


**Figure 2.** Hammett plot of the **2**-catalyzed oxidation of *p*-substituted benzyl alcohols at pH 7.0 in the presence of 72 mM H<sub>2</sub>O<sub>2</sub>, 25 °C. The plot has a slope ( $\rho$ ) of 1.93 and a correlation  $r^2$  of 0.82.



**Scheme 2.** Proposed mechanism of the catalytic process. First hydrogen peroxide is added to the ketone, and then bound substrate is oxidized. The oxidation step may be assisted by a hydrogen bond.

smaller molecular weight than a typical enzyme, the efficiency per mass unit is in the same range.

From the series of *p*-substituted benzyl alcohols (see Table 1) one can construct a Hammett plot (Figure 2), which gives a correlation between  $k_{\text{cat}}$  and  $\sigma$  of  $r^2 = 0.82$ , and 1.9 as the reaction constant ( $\rho$ ).<sup>[13]</sup> This value suggests that the transition state is ionic and has some negative charge at the reaction center. A comparison of 1-phenylethanol with its 1-deuterated analogue (Table 1) reveals a small isotope effect ( $k_{\text{H}}/k_{\text{D}} = 1.4$ ). Based on this we suggest a mechanism (Scheme 2) related to what has been formulated for the tungsten-catalyzed H<sub>2</sub>O<sub>2</sub>-oxidation of alcohols, which also gives a relatively low isotope effect ( $k_{\text{H}}/k_{\text{D}} = 2$ ).<sup>[14]</sup> This mechanism is also similar to what we have proposed for amine oxidation.<sup>[11]</sup> The somewhat high  $\rho$  value<sup>[15]</sup> could be an indication that the reaction is facilitated by hydrogen bonding between the proton of the benzylic alcohol and a Lewis base, such as the keto hydroxy group, thus invoking the cyclic mechanism outlined. The remarkable supramolecular catalysis displayed by **1** and **2** under mild aqueous conditions is, as discussed above, in the best case as efficient per mass-unit catalyst as that of some natural enzymes. When this level of catalysis can be achieved, practical applications of such molecules are not far away.

## Experimental Section

**Determining the rate of oxidation:** Each reaction was performed on 4–16 samples (2 mL each) of the appropriate substrate at different concentrations in 95 mM phosphate buffer containing 72 mM H<sub>2</sub>O<sub>2</sub> and either **1** or **2** (1 mg) or nothing (as control). The reactions were followed at 25 °C using UV absorption at an appropriate wavelength<sup>[16]</sup> and typically monitored for 5 h. Velocities were determined as the slope of the progress curve of each reaction. The velocities of the

uncatalyzed reactions were obtained directly from the control samples, those of the catalyzed reactions were calculated by subtracting the uncatalyzed rate from the total rate of the appropriate cyclodextrin-containing sample. The  $v_{\text{cat}}$  values were used to construct Hanes plots ( $[S]/v$  vs.  $[S]$ ) to ensure that the reaction follows Michaelis–Menten kinetics. In that case  $K_m$  and  $v_{\text{max}}$  were determined using least-squares nonlinear regression fitting to the  $v_{\text{max}}$  vs.  $[S]$  curve.  $k_{\text{cat}}$  was calculated as  $v_{\text{max}}/[\text{cyclodextrin}]$ .  $k_{\text{uncat}}$  was determined as the slope from a plot of  $v_{\text{uncat}}$  vs.  $[S]$ .<sup>[16]</sup>

GC-MS experiments: A pseudo-preparative experiment was performed by mixing 0.5 mmol substrate with 0.02 mmol catalyst **1** or **2** in 1.5 mL  $\text{H}_2\text{O}$  and slowly adding 1.5 mL  $\text{H}_2\text{O}_2$ , 35%. The mixture was incubated at 25 °C from 3 h to several days. After extraction of the mixture with dichloromethane and evaporation the sample was analyzed in a Hewlett-Packard 5890A gas chromatograph equipped with a 5971A MSD mass-selective detector.

Received: March 2, 2006

Published online: June 21, 2006

**Keywords:** biomimetics · cyclodextrins · Michaelis–Menten kinetics · supramolecular chemistry

[16] The following extinction coefficients  $\epsilon$  [ $\text{mm}^{-1}\text{cm}^{-1}$ ] (25 °C, pH 7) and wavelengths  $\lambda$  [nm] of the products were determined and used: benzaldehyde (1.23, 285), acetophenone (0.32, 300), benzophenone (4.03, 280), 2-hydroxybenzaldehyde (2.92, 325), 2-methoxybenzaldehyde (2.75, 323), 2-chlorobenzaldehyde (1.24, 300), 2-bromobenzaldehyde (0.47, 292), 3-methoxybenzaldehyde (2.48, 313), 4-methoxybenzaldehyde (7.53, 300), 4-hydroxybenzaldehyde (6.1, 329), 4-fluorobenzaldehyde (0.88, 292), 4-chlorobenzaldehyde (1.09, 286), 4-bromobenzaldehyde (1.59, 295), 4-methylbenzaldehyde (3.37, 285), 2,6-dimethoxybenzaldehyde (3.63, 323), 2,6-dichlorobenzaldehyde (1.03, 309), acetylferrocene (1.68, 345 nm).

- [1] A. J. Kirby, *Angew. Chem.* **1996**, *108*, 770–790; *Angew. Chem. Int. Ed. Engl.* **1996**, *35*, 706–724.
- [2] R. Breslow, S. D. Dong, *Chem. Rev.* **1998**, *98*, 1997–2012.
- [3] E. E. Karakhanov, A. L. Maksimov, E. A. Runova, Y. S. Kardasheva, M. V. Terenina, T. S. Buchneva, A. Y. Guchkova, *Macromol. Symp.* **2003**, *204*, 159–173.
- [4] S. Sasaki, K. Koga, *Stud. Org. Chem.* **1992**, *45*, 265–310.
- [5] W. B. Motherwell, M. J. Bingham, Y. Six, *Tetrahedron* **2001**, *57*, 4663–4686.
- [6] R. Breslow, *Science* **1982**, *218*, 532–537.
- [7] For some recent examples, see: a) M. J. Han, S. K. Yoo, J. Y. Chang, T.-K. Ha, *Angew. Chem.* **2000**, *112*, 355–357; *Angew. Chem. Int. Ed.* **2000**, *39*, 347–349; b) R. Breslow, X. Zhang, Y. Huang, *J. Am. Chem. Soc.* **1997**, *119*, 4535–4536; c) M. Kunishima, K. Yoshimura, H. Morigaki, R. Kawamata, K. Terao, S. Tani, *J. Am. Chem. Soc.* **2001**, *123*, 10760–10761; d) S. H. Yoo, B. J. Lee, H. Kim, J. Suh, *J. Am. Chem. Soc.* **2005**, *127*, 9593–9602; e) L. Jiang, Z. L. Liu, Z. Liang, Y. Gao, *Bioorg. Med. Chem.* **2005**, *13*, 3673–3680; f) N. M. Milovic, J. D. Badjic, N. M. Kostic, *J. Am. Chem. Soc.* **2004**, *126*, 696–697.
- [8] High rate acceleration has however been observed in the transacylation of cyclodextrins at high pH, see: G. L. Trainer, R. Breslow, *J. Am. Chem. Soc.* **1981**, *103*, 154–158.
- [9] A. J. Pearce, P. Sinaĳ, *Angew. Chem.* **2000**, *39*, 3610–3611; *Angew. Chem. Int. Ed.* **2000**, *39*, 3610–3611.
- [10] C. Rousseau, B. Christensen, M. Bols, *Eur. J. Org. Chem.* **2005**, 2734–2739.
- [11] L. Marinescu, M. Mølbach, C. Rousseau, M. Bols, *J. Am. Chem. Soc.* **2005**, *127*, 17578–17579.
- [12] R. Wolfenden, M. J. Snider, *Acc. Chem. Res.* **2001**, *34*, 938–945.
- [13] A plot of  $k_{\text{cat}}/K_m$  vs.  $\sigma$  (not shown) gave a poorer correlation ( $r^2 = 0.55$ ) and 1.2 as  $\rho$ .
- [14] S. E. Jacobson, D. A. Muccigrosso, F. Mares, *J. Org. Chem.* **1979**, *44*, 921–924.
- [15] Ruthenium- and palladium-catalyzed oxidation of benzylic alcohols gives reaction constants that are small and negative ( $\rho \approx -0.5$ ; see: a) A. Dijksman, A. Marino-Gonzalez, A. Mairata I Payeras, I. W. C. E. Arends, R. A. Sheldon, *J. Am. Chem. Soc.* **2001**, *123*, 6826–6833; b) J. A. Mueller, C. P. Goller, M. S. Sigman, *J. Am. Chem. Soc.* **2004**, *126*, 9724–9734). As the present reaction does not involve formation of a positively charged metal center, its high  $\rho$  value is not surprising.

## Enantiomeric Enrichment

DOI: 10.1002/anie.200601506

# Large Nonlinear Effect Observed in the Enantiomeric Excess of Proline in Solution and That in the Solid State\*\*

Yujiro Hayashi,\* Masayoshi Matsuzawa,  
Junichiro Yamaguchi, Sayaka Yonehara,  
Yasunobu Matsumoto, Mitsuru Shoji,  
Daisuke Hashizume, and Hiroyuki Koshino

How homochiral amino acids and sugars arose out of a presumably prochiral prebiotic environment is a puzzling question,<sup>[1]</sup> to which many answers have been proposed: for example, absolute asymmetric synthesis with circularly polarized light, photoreactions in chiral crystals, and asymmetric automultiplication with asymmetric autocatalysis, as exemplified by the recent work of Soai et al.<sup>[2]</sup> There are reports describing a connection between the chirality of amino acids and sugars: Amplification of *ee* was observed in the  $\alpha$ -aminooxylation of an aldehyde using proline as catalyst to generate a key intermediate of sugars,<sup>[3]</sup> while amino acids

[\*] Prof. Dr. Y. Hayashi, M. Matsuzawa, J. Yamaguchi, S. Yonehara,  
Y. Matsumoto, Dr. M. Shoji  
Department of Industrial Chemistry  
Faculty of Engineering  
Tokyo University of Science  
Kagurazaka, Shinjuku-ku, Tokyo 162-8601 (Japan)  
Fax: (+81) 3-5261-4631  
E-mail: hayashi@ci.kagu.tus.ac.jp  
Dr. D. Hashizume, Dr. H. Koshino  
RIKEN  
2-1 Hirosawa, Wako, Saitama 351-0198 (Japan)

[\*\*] This work was partially supported by Toray Science Foundation and a Grant-in-Aid for Scientific Research on Priority Areas 16073219 from MEXT. We thank Professors K. Soai (Tokyo University of Science) and K. Saigo (The University of Tokyo) for helpful discussions.



Supporting information for this article is available on the WWW under <http://www.angewandte.org> or from the author.



have been proposed as asymmetric catalysts for the synthesis of sugars.<sup>[4]</sup> Recently, Cordova et al. demonstrated the synthesis of a hexose (55% *ee*) from proline with low *ee* (20% *ee*), with a nonlinear effect.<sup>[5]</sup> Herein, we demonstrate experimentally a connection between an amino acid with low *ee* (10% *ee*) and a chiral sugar intermediate of high enantiomeric purity (96% *ee*).

Amino acids promote several organic transformations, and proline, a widely distributed amino acid, is one of the most effective organic catalysts.<sup>[6]</sup> In 1971, Hajos and Parrish, as well as Eder et al., reported an intramolecular aldol reaction catalyzed by proline.<sup>[7]</sup> Following the observation of the intermolecular version of this reaction by List, Lerner, and Barbas in 2000,<sup>[8]</sup> other highly enantioselective catalytic reactions using proline have been developed, including aldol<sup>[9]</sup> and Mannich<sup>[10]</sup> reactions, and  $\alpha$ -amination<sup>[11]</sup> and  $\alpha$ -aminooxylation<sup>[12]</sup> of carbonyl compounds.

We have observed that a solution of proline with high *ee* can be obtained from solid proline of low optical purity during the dissolution process. As proline is only very sparingly soluble in pure  $\text{CHCl}_3$ , and as the addition of EtOH increases its solubility therein, we employed  $\text{CHCl}_3$  containing 1% EtOH as solvent.  $\text{CHCl}_3$  stabilized with amylene (*not* with EtOH) was distilled from  $\text{CaH}_2$  before use, and then EtOH was added (1%). At first, reproducibility of the solubility was poor. After several experiments, both the surface and the particle size of the solid proline were found to be important. Proline that had been recrystallized from EtOH and ground with a mortar under an Ar atmosphere was employed.

The experiment using 10% *ee* L-rich proline was performed as follows:  $\text{CHCl}_3$  (20 mL) containing 1% EtOH was added to a mixture of L-proline (550 mg) and D-proline (450 mg; 10% *ee* combined) at 0°C, and the suspension was stirred for 24 h at this temperature under an Ar atmosphere. After filtration of the insoluble proline, a solution (17–19 mL) containing proline (40–65 mg) was obtained, the *ee* value of which was very high (85–99% *ee*). It is particularly unusual that a proline solution with very high *ee* was obtained from proline of low *ee*; this phenomenon is not observed in other solvents such as EtOH and dimethyl sulfoxide.

A solution of proline with very high *ee* (97–99% *ee*) was also obtained from proline with even lower *ee* (1.0% *ee*). Even by using nearly racemic proline (< 0.4% *ee*), which was prepared from L-proline ( $250 \pm 1$  mg) and D-proline ( $250 \pm 1$  mg), the optical purity of proline in solution was found to be very high. With the exception of phenylalanine (Phe), we were unable to demonstrate any enrichment of *ee* in  $\text{CHCl}_3$  solution with other amino acids (Val, Met, and Tyr) because of their extremely low solubility in that solvent. In the case of Phe, although it is only very sparingly soluble in  $\text{CHCl}_3$ , a solution of Phe with 10% *ee* was obtained from a solid of 40% *ee*. This observation also indicates that there is something special in the dissolution of proline.

To clarify the reason for these phenomena, the crystal structures of L-proline<sup>[13]</sup> and DL-proline,<sup>[14]</sup> recrystallized from EtOH, were analyzed (Figure 1, Figure 2). The powder X-ray diffraction (XRD) method was used to confirm that the crystal forms of the powdered L- and DL-prolines were the same as those of the corresponding single crystals. Both

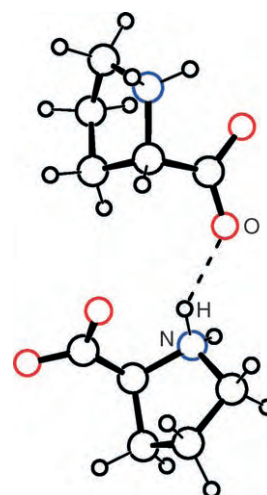


**Figure 1.** Hydrogen-bonded dimer structure formed between the columns in a crystal of L-proline.<sup>[13]</sup>

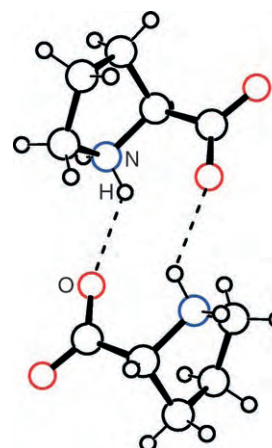


**Figure 2.** Hydrogen-bonded dimer structure formed between the columns in a crystal of DL-proline.

crystals have very similar structural motifs, forming a column structure with  $\text{N-H}\cdots\text{O}$  hydrogen bonds. However, the joining modes of these columns are quite different: In the chiral crystal, the columns align antiparallel and each molecule in the column connects with those in two neighboring columns through hydrogen bonds to form a 2D sheet structure (Figure 3). On the other hand, in the racemic crystal each molecule in the column forms two centrosymmetric hydrogen bonds with the nearest neighboring enantiomeric column to form a ladder structure (Figure 4). These ladders are linked by rather weak  $\text{C-H}\cdots\text{O}$  interactions. As the heterochiral molecules bind together with two hydrogen bonds, their association is energetically preferable to that of homochiral molecules, and this causes racemic crystals to be much less soluble than those of the pure enantiomers ( $0.01\text{--}0.09\text{ g L}^{-1}$  versus  $6.1\text{--}6.3\text{ g L}^{-1}$  at 0°C in  $\text{CHCl}_3$  containing 1% EtOH). Therefore, crystals of DL-proline precipitate preferably from a mixture of enantiomers in solution.

To shed more light on the reaction mechanism, the following experiments were performed: 1)  $\text{CHCl}_3$  (100 mL)

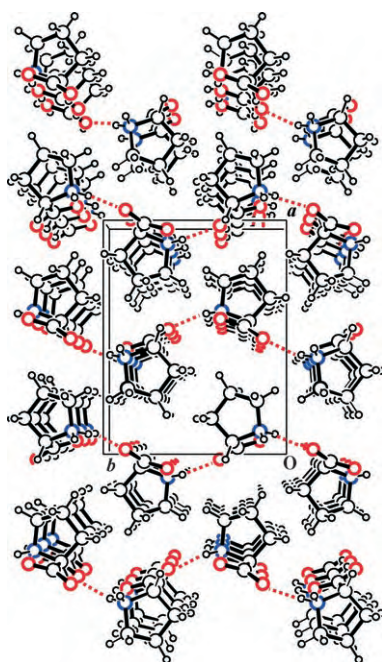


**Figure 3.** Crystal structure of L-proline.<sup>[13]</sup> O red, N blue, C black (large), H black (small).

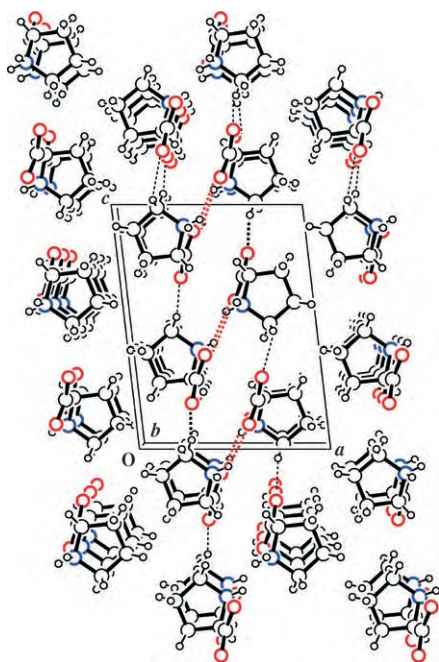


**Figure 4.** Crystal structure of DL-proline. O red, N blue, C black (large), H black (small).

and EtOH (1 mL) were added to a mixture of L-proline (2.25 g) and D-proline (2.75 g; total 10% *ee* D-rich), and the reaction mixture was stirred for a certain time. 2) D-proline (2.75 g, total 10% *ee* D-rich) was added to a CHCl<sub>3</sub>/EtOH suspension (100 mL:1 mL) of L-proline (2.25 g) at 0°C, and the reaction mixture was stirred for a certain time. In these two reactions, the *ee* of proline in solution was measured while the content of DL-proline in the solid was analyzed by

XRD (the results are summarized in Table 1 and Table 2, respectively). Both experiments show an increase in DL-proline content of the solid with reaction time. After 12 h,

**Table 1:** The effect of time on the *ee* of proline in solution and on the content of the DL isomer in the solid.<sup>[a]</sup>

Entry	<i>t</i> [h]	Solubility [mg mL <sup>-1</sup> ] <sup>[b]</sup>	<i>ee</i> [%] <sup>[c]</sup>	Content [%] <sup>[d]</sup>
1	0.17	2.9	7 <sup>[e]</sup>	7
2	1	0.3	57 <sup>[e]</sup>	46
3	6	1.3	96 <sup>[e]</sup>	77
4	12	3.5	95 <sup>[e]</sup>	84

[a] CHCl<sub>3</sub> containing 1% EtOH was added to a mixture of L- and D-proline; see text for details. [b] Solubility of proline in CHCl<sub>3</sub>/EtOH (100:1). [c] *ee* of proline in solution. [d] Content of DL-proline in solid. [e] D-enantiomer rich.

**Table 2:** The effect of time on the *ee* of proline in solution and on the content of the DL isomer in the solid.<sup>[a]</sup>

Entry	<i>t</i> [h]	Solubility [mg mL <sup>-1</sup> ] <sup>[b]</sup>	<i>ee</i> [%] <sup>[c]</sup>	Content [%] <sup>[d]</sup>
1	0	6.7	−100 <sup>[e]</sup>	0
2	0.17	3.9	76 <sup>[f]</sup>	33
3	1	0.65	68 <sup>[f]</sup>	54
4	6	2.6	90 <sup>[f]</sup>	83
5	12	3.7	92 <sup>[f]</sup>	92

[a] D-proline was added to a suspension of L-proline in CHCl<sub>3</sub> containing 1% EtOH; see text for details. [b] Solubility of proline in CHCl<sub>3</sub>/EtOH (100:1). [c] *ee* of proline in solution. [d] Content of DL-proline in solid. [e] L-enantiomer rich. [f] D-enantiomer rich.

most of the L- and D-proline had been converted into DL-proline and the *ee* of proline in solution was very high (> 90% *ee*). In the second experiment, the proline isomer in excess in solution changed from the L to the D enantiomer within 1 h, with the formation of solid DL-proline. Thus, the highly selective dissolution of one enantiomer of proline is caused not by a simple extraction of the excess enantiomer but by the following dissolution and crystallization mechanism: Soluble L- and D-prolines dissolve in the solvent, and the less-soluble racemic DL-proline, but not a conglomerate, precipitates.

The dissolution and crystallization process is also different from that of standard recrystallization. Although the recrystallization of proline from EtOH or from EtOH/Et<sub>2</sub>O<sup>[15]</sup> has been known for a long time, there are no reports describing a change in the *ee* value of proline by recrystallization, either in solution or in the solid state. We thus examined the recrystallization of proline (10% *ee*) in different solvents and analyzed the *ee* of proline in the filtrate (Table 3). CHCl<sub>3</sub> could not be used as solvent owing to the low solubility of proline in this solvent alone. No increase in *ee* was observed in H<sub>2</sub>O. Though a substantial increase in *ee* was observed in EtOH or in *i*PrOH and water (1:1), it was not so large relative to that observed with CHCl<sub>3</sub> containing 1% EtOH.

For some compounds, homochiral crystals have been obtained from solutions of low *ee* by the preferential

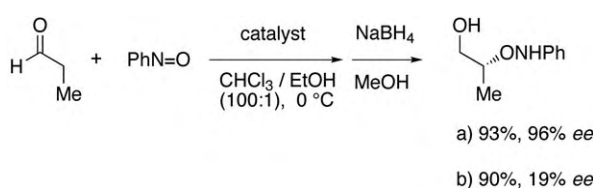
**Table 3:** The effect of solvent on the *ee* of proline in solution through recrystallization.<sup>[a]</sup>

Entry	Solvent	<i>ee</i> [%]
1	H <sub>2</sub> O	14
2	EtOH	43
3	<i>i</i> PrOH/H <sub>2</sub> O (1:1)	39

[a] Proline (10% *ee*) was recrystallized from the indicated solvent, and the *ee* of proline in the filtrate was determined.

crystallization of conglomerates,<sup>[16]</sup> a process that is distinct from the present phenomena in which a solution with very high *ee* is obtained from a solid of low *ee*. Though several examples are known for which a chiral crystal is more soluble than the corresponding racemic one, there is only one report describing the enrichment of an enantiomer in solution during recrystallization, a special case in which polymorphic transformation occurs during crystallization.<sup>[17]</sup> In the present case, a solution of proline with very high *ee* is obtained from a solid of low *ee* during the processes of dissolution and crystallization, a mechanism which is completely different to that of any other known resolution.

As optically pure proline is known to promote several asymmetric reactions, one possible application of the solution of proline of high *ee* obtained from proline solid of low *ee* is  $\alpha$ -aminoxylation of propanal.<sup>[12a,b,c]</sup> As shown in Scheme 1, the

**Scheme 1.**  $\alpha$ -Aminoxylation of propanal using proline as catalyst. A solution of proline prepared from solid proline (10% *ee*) used a) after filtration gave the product with 96% *ee* and b) without filtration gave the product with only 19% *ee*.

product was obtained in 96% *ee*, demonstrating that this proline solution can be applied to other useful asymmetric transformations. When proline with 10% *ee* was employed in  $\alpha$ -aminoxylation without filtration, the *ee* of the product was low (19% *ee*) and a slight nonlinear effect was observed, as reported by Blackmond and co-workers.<sup>[3]</sup> This slight increase in *ee* can be explained in some part as follows: The initial *ee* of proline in solution is very high, but as the reaction proceeds the *ee* of proline in solution begins to decrease because the generated product acts as a polarized solvent to bring both D- and L-proline from the solid into the organic phase. That is, while the *ee* of proline in the initial solution is extremely high, this *ee* in solution decreases as the reaction progresses owing to the increased solubility of both L- and D-proline in the mixture of solvent, propanal, and forming products.<sup>[18,19]</sup>

The fact that a solution of proline of high *ee* was obtained from solid proline with low *ee* may be involved in the origin of chirality on Earth. Proline has been used as the catalyst in a short synthesis of sugars<sup>[4,5]</sup> and in the synthesis of  $\alpha$ -hydroxyaldehydes, key molecules for sugar synthesis, by

reaction of aldehydes with molecular oxygen under photo-irradiation—plausible prebiotic conditions.<sup>[20]</sup> As an enantiomerically enriched solution of proline might be separated from solid proline by filtration through strata, one can speculate that in the prebiotic era a similar mechanism involving proline of very low *ee* was involved in the generation of other biologically important homochiral organic molecules.

Some amino acids have been found in meteorites with significant enantiomeric excess.<sup>[21]</sup> Though proline is scarcely present in meteorites, it was found in the room-temperature residue of an interstellar ice analogue that had been irradiated with UV light under high vacuum at 12 K, which indicates that proline may have been produced in the prebiotic era.<sup>[22]</sup> Therefore, it seems possible that asymmetric photolysis in interstellar clouds may produce optically active proline. Under certain circumstances the imbalance thus generated could be amplified into an optically enriched solution of proline by selective dissolution. Such a solution can promote many organic transformations and generate important intermediates of sugar synthesis with very high optical purity, as demonstrated in the present report. Though the present reaction is only successful under certain limited conditions, it may indicate a possible mechanism by which an amino acid of low *ee* generated homochirality in biologically important organic molecules in the prebiotic environment.<sup>[23]</sup>

Received: November 28, 2004

Revised: May 9, 2006

**Keywords:** amino acids · asymmetric catalysis · carbohydrates · chirality · proline

- [1] a) S. Mason, *Chem. Soc. Rev.* **1988**, 17, 347; b) W. A. Bonner, *Origins Life Evol. Biosphere* **1991**, 21, 59; c) B. L. Feringa, R. A. van Delden, *Angew. Chem.* **1999**, 111, 3624; *Angew. Chem. Int. Ed.* **1999**, 38, 3418; d) M. Avalos, R. Babiano, P. Cintas, J. L. Jimenez, J. C. Palacios, *Chem. Commun.* **2000**, 887; e) H. Buschmann, R. Thede, D. Heller, *Angew. Chem.* **2000**, 112, 4197; *Angew. Chem. Int. Ed.* **2000**, 39, 4033; f) J. Podlech, *Cell. Mol. Life Sci.* **2001**, 58, 44.
- [2] a) K. Soai, T. Shibata, H. Morioka, K. Choji, *Nature* **1995**, 378, 767; b) K. Soai, T. Shibata, I. Sato, *Acc. Chem. Res.* **2000**, 33, 382; c) K. Soai, I. Sato, T. Shibata, *Chem. Rec.* **2001**, 1, 321; d) K. Soai, T. Shibata, I. Sato, *Bull. Chem. Soc. Jpn.* **2004**, 77, 1063.
- [3] S. P. Matthew, H. Iwamura, D. G. Blackmond, *Angew. Chem.* **2004**, 116, 3379; *Angew. Chem. Int. Ed.* **2004**, 43, 3317.
- [4] a) S. Pizzarello, A. L. Weber, *Science* **2004**, 303, 1151; b) A. B. Northrup, D. W. C. MacMillan, *Science* **2004**, 305, 1752; c) D. Enders, C. Grondal, *Angew. Chem.* **2005**, 117, 1235; *Angew. Chem. Int. Ed.* **2005**, 44, 1210; d) J. T. Suri, D. B. Ramachary, C. F. Barbas III, *Org. Lett.* **2005**, 7, 1383; e) A. Cordova, I. Ibrahim, J. Casas, H. Sunden, M. Engqvist, E. Reyes, *Chem. Eur. J.* **2005**, 11, 4772; f) D. Enders, J. Palecek, C. Grondal, *Chem. Commun.* **2006**, 655; g) C. Grondal, D. Enders, *Tetrahedron* **2006**, 62, 329; h) I. Ibrahim, A. Cordova, *Tetrahedron Lett.* **2005**, 46, 3363; i) N. S. Chowdari, D. B. Ramachary, A. Cordova, C. F. Barbas III, *Tetrahedron Lett.* **2002**, 43, 9591; j) for a review of proline-catalyzed synthesis of carbohydrates, see: D. Enders, M. Voith, A. Lenzen, *Angew. Chem.* **2005**, 117, 1330; *Angew. Chem. Int. Ed.* **2005**, 44, 1304.



- [5] A. Cordova, M. Engqvist, I. Ibrahim, J. Casas, H. Sunden, *Chem. Commun.* **2005**, 2047.
- [6] Reviews: a) P. I. Dalko, L. Moisan, *Angew. Chem.* **2001**, *113*, 3840; *Angew. Chem. Int. Ed.* **2001**, *40*, 3726; b) M. Movassaghi, E. N. Jacobsen, *Science* **2002**, *298*, 1904; c) B. List, *Acc. Chem. Res.* **2004**, *37*, 548; d) P. I. Dalko, L. Moisan, *Angew. Chem.* **2004**, *116*, 5248; *Angew. Chem. Int. Ed.* **2004**, *43*, 5138; e) A. Berkessel, H. Groger, *Asymmetric Organocatalysis*, Wiley-VCH, Weinheim, **2005**; f) for reviews on the utilization of amino acids in stereoselective synthesis, see: K. Drauz, A. Kleeman, J. Martens, *Angew. Chem.* **1982**, *94*, 590; *Angew. Chem. Int. Ed. Engl.* **1982**, *21*, 584; g) J. Martens, *Top. Curr. Chem.* **1984**, *125*, 165.
- [7] a) Z. G. Hajos, D. R. Parrish, German Patent DE 2102623, **1971**; b) U. Eder, G. Sauer, R. Wiechert, *Angew. Chem.* **1971**, *83*, 492; *Angew. Chem. Int. Ed. Engl.* **1971**, *10*, 496.
- [8] B. List, R. A. Lerner, C. F. Barbas III, *J. Am. Chem. Soc.* **2000**, *122*, 2395.
- [9] For selected studies of proline-catalyzed aldol reactions, see: a) W. Notz, B. List, *J. Am. Chem. Soc.* **2000**, *122*, 7386; b) K. Sakthivel, W. Notz, T. Bui, C. F. Barbas III, *J. Am. Chem. Soc.* **2001**, *123*, 5260; c) A. B. Northrup, D. W. C. MacMillan, *J. Am. Chem. Soc.* **2002**, *124*, 6798; d) for a review, see: B. List in *Modern Aldol Reactions*, Vol. 1 (Ed.: R. Mahrwald), Wiley-VCH, Weinheim, **2004**, p. 161.
- [10] A. Cordova, *Acc. Chem. Res.* **2004**, *37*, 102.
- [11] R. O. Duthaler, *Angew. Chem.* **2003**, *115*, 1005; *Angew. Chem. Int. Ed.* **2003**, *42*, 975.
- [12] a) G. Zhong, *Angew. Chem.* **2003**, *115*, 4379; *Angew. Chem. Int. Ed.* **2003**, *42*, 4247; b) S. P. Brown, M. P. Brochu, C. J. Sinz, D. W. C. MacMillan, *J. Am. Chem. Soc.* **2003**, *125*, 10808; c) Y. Hayashi, J. Yamaguchi, K. Hibino, M. Shoji, *Tetrahedron Lett.* **2003**, *44*, 8293; d) A. Bøgevig, H. Sunden, A. Cordova, *Angew. Chem.* **2004**, *116*, 1129; *Angew. Chem. Int. Ed.* **2004**, *43*, 1109; e) Y. Hayashi, J. Yamaguchi, T. Sumiya, M. Shoji, *Angew. Chem.* **2004**, *116*, 1132; *Angew. Chem. Int. Ed.* **2004**, *43*, 1112; f) A. Cordova, H. Sunden, A. Bøgevig, M. Johansson, F. Himo, *Chem. Eur. J.* **2004**, *10*, 3673; g) Y. Hayashi, J. Yamaguchi, T. Sumiya, K. Hibino, M. Shoji, *J. Org. Chem.* **2004**, *69*, 5966; h) for a review, see: P. Merino, T. Tejero, *Angew. Chem.* **2004**, *116*, 3055; *Angew. Chem. Int. Ed.* **2004**, *43*, 2995.
- [13] R. L. Kayushina, B. K. Vainshtein, *Kristallografiya* **1965**, *10*, 834.
- [14] A CIF file for D,L-proline was deposited with the Cambridge Crystallographic Data Centre. CCDC 254728 contains the supplementary crystallographic data for this paper. These data can be obtained free of charge from The Cambridge Crystallographic Data Centre via [www.ccdc.cam.ac.uk/data\\_request/cif](http://www.ccdc.cam.ac.uk/data_request/cif).
- [15] D. D. Perrin, W. L. F. Armarego, *Purification of Laboratory Chemicals*, Pergamon Press, Oxford, England, **1988**.
- [16] J. Jacques, A. Collet, S. H. Wilen, *Enantiomers, Racemates and Resolutions*, Wiley, New York, **1981**.
- [17] R. Tamura, D. Fujimoto, Z. Lepp, K. Misaki, H. Miura, H. Takahashi, T. Ushio, T. Nakai, K. Hirotsu, *J. Am. Chem. Soc.* **2002**, *124*, 13139.
- [18] When *N,N*-dimethylformamide was used as a solvent in  $\alpha$ -aminooxylation, a linear effect was observed.
- [19] Blackmond and co-workers proposed an increase in solubility of proline caused by product, owing to a hydrogen-bonding interaction, see: H. Iwamura, D. H. Wells, Jr., S. P. Mathew, M. Klusmann, A. Armstrong, D. G. Blackmond, *J. Am. Chem. Soc.* **2004**, *126*, 16312.
- [20] A. Cordova, H. Sunden, M. Engqvist, I. Ibrahim, J. Casas, *J. Am. Chem. Soc.* **2004**, *126*, 8914.
- [21] S. Pizzarello, M. Zolensky, K. A. Turk, *Geochim. Cosmochim. Acta* **2003**, *67*, 1589.
- [22] G. M. M. Caro, U. J. Meierhenrich, W. A. Schutte, B. Barbier, A. A. Segovia, H. Rosenbauer, W. H.-P. Thiemann, A. Brack, J. M. Greenberg, *Nature* **2002**, *416*, 403.
- [23] *Note added in proof (June 12, 2006)*: Since this manuscript was accepted for publication, a paper by Blackmond and co-workers has appeared that describes a similar phenomenon (M. Klusmann, H. Iwamura, S. P. Mathew, D. H. Wells, Jr., U. Pandya, A. Armstrong, D. G. Blackmond, *Nature* **2006**, *441*, 621). The results in our present Communication explain the greater stability of crystals of D,L-proline over those of the separate enantiomers and provide a rationale for the nonlinear effects observed in the *ee* of proline in solution and hence in the aldol reaction.



DOI: 10.1002/anie.200601277

**Polyhedral Silver Nanocrystals with Distinct Scattering Signatures\*\****Andrea Tao, Prasert Sinsermsuksakul, and Peidong Yang\**

Subwavelength silver nanoparticles display a variety of unrivaled optical properties in the visible and near-IR regime, including scattering cross-sections that are orders of magnitude higher than the fluorescence emission from organic dyes as well as intense local amplification of electromagnetic fields. These phenomena result from localized surface plasmons (LSPs), where the plasma oscillations of free electrons in the metal are bound by nanoparticle geometry. Plasmon excitation occurs when a photon is absorbed at a metal–dielectric interface, transferring energy into the collective oscillations of conduction electrons, which are coupled in-phase with incident radiation. For silver and gold nanoparticles, these resonant frequencies occur at wavelengths in the visible region, giving rise to the brilliant colors that are characteristic of their colloidal solutions.

For silver particles with diameter  $d \ll \lambda$ , a single dipolar plasmon mode is allowed.<sup>[1]</sup> However, for particles with lower symmetry or anisotropic dielectric surroundings, the nature of

[\*] A. Tao, P. Sinsermsuksakul, Prof. P. Yang  
Department of Chemistry  
University of California, Berkeley  
Materials Science Division  
Lawrence Berkeley National Laboratory  
Berkeley, CA 94720 (USA)  
Fax: (+1) 510-642-7301  
E-mail: p\_yang@berkeley.edu

[\*\*] We thank Tevye Kuykendall and Susan Habas for technical assistance and helpful discussions. This work was supported by the Office of Basic Science, Department of Energy. A.R.T. gratefully acknowledges the National Science Foundation for a graduate research fellowship. We thank the National Center for Electron Microscopy for the use of their facilities.



Supporting information for this article is available on the WWW under <http://www.angewandte.org> or from the author.

these LSP modes is more difficult to map. Elongated shapes such as nanowires and rods experience a “lightning-rod effect”, whereby the metal structure acts as an antenna for electromagnetic field amplification as a result of highly polarized LSPs.<sup>[2]</sup> Nanostructures that contain sharp vertexes, such as triangular plates<sup>[3]</sup> and icosahedra,<sup>[4]</sup> have also been shown to exhibit multipolar plasmon modes. Principally, polyhedral shapes with well-defined facets and corners are predicted to have distinct scattering signatures in addition to scattering efficiencies that are orders of magnitude higher than those of their spherical counterparts.<sup>[5]</sup> Scanning near-field<sup>[6]</sup> and TEM-correlated darkfield experiments<sup>[7]</sup> are among the few experimental attempts to spatially resolve these shape-dependent plasmons. Here, we employ a strategic synthetic approach to correlate nanocrystal geometry with specific LSP modes, investigating the systematic shape evolution of polyhedral nanocrystals.

We synthesized monodisperse colloidal solutions of silver nanocrystals with regular polyhedral shapes and bound entirely by {100} and {111} facets of the fcc crystal lattice (Figure 1a). These nanocrystals were synthesized using the polyol method,<sup>[8]</sup> where the metal salt is reduced by a diol solvent at near-reflux temperatures ( $\approx 180^\circ\text{C}$ ) in the presence of a polymeric stabilizing agent. We used poly(vinyl pyrrolidone) (PVP) as the capping polymer as it has been demonstrated to be a successful shape control agent for fcc metals.<sup>[9,10]</sup> We adapted the synthetic procedure first developed by Sun and Xia,<sup>[9]</sup> who reported the use of PVP for the formation of silver nanocubes. In a typical synthesis, silver

nitrate and PVP were dissolved separately and then injected periodically into a solution of hot pentanediol. Depending on how long these sequential additions are continued, specific polyhedral shapes can be obtained in high yield.

As seen in the scanning electron microscopy (SEM) images in Figure 1 b–f, we synthesized a variety of nanocrystal shapes with uniform sizes: cubes ( $d \approx 80$  nm), truncated cubes ( $d \approx 120$  nm), cuboctahedra ( $d \approx 150$ – $200$  nm), truncated octahedra ( $d \approx 200$ – $250$  nm), and octahedra ( $d \approx 250$ – $300$  nm). Transmission electron microscopy images (see Supporting Information) confirm that the polyhedra are single-crystalline and exhibit atomically defined facets with sharp edges and corners. Although similar truncated shapes have been previously observed,<sup>[11]</sup> this is the first observation of metallic octahedral nanocrystals as the majority product. On the basis of energetic considerations, the optimal particle shape for an fcc metal is a truncated octahedron with regular hexagonal faces.<sup>[12]</sup> Thus, the formation of octahedra suggests that the polyhedral nanocrystals observed here result from a kinetically limited reaction equilibrium.

To investigate this growth mechanism, we employed UV/Vis absorption spectrometry (Agilent, UV/Visible Chemstation) to probe shape-specific LSPs in the optical frequencies. Figure 2 displays a plot of the dipolar plasmon wavelength as

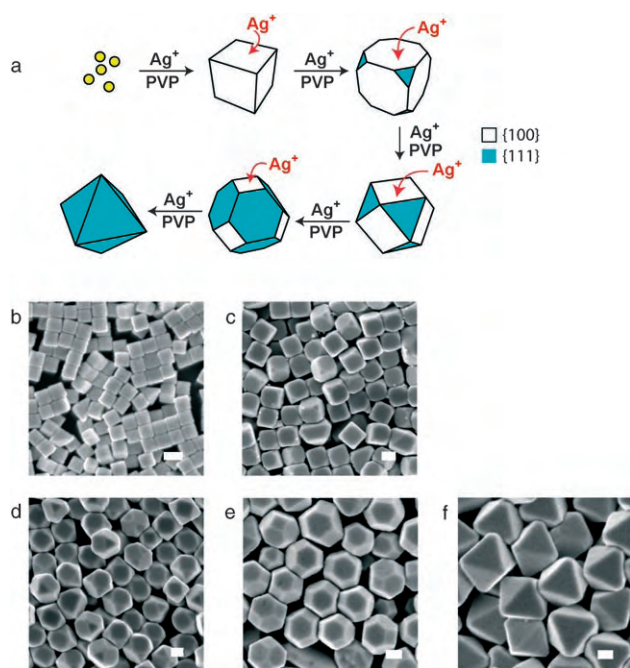


**Figure 1.** By extending the polyol reaction for a given time period, various polyhedral shapes capped with {100} and {111} faces can be obtained in high yield. a) A schematic of the nucleation and growth process, in which silver continuously deposits onto the {100} facet to eventually result in a completely {111}-bound octahedron. b–f) SEM images of cubes, truncated cubes, cuboctahedra, truncated octahedra, and octahedra, respectively (scale bar: 100 nm).

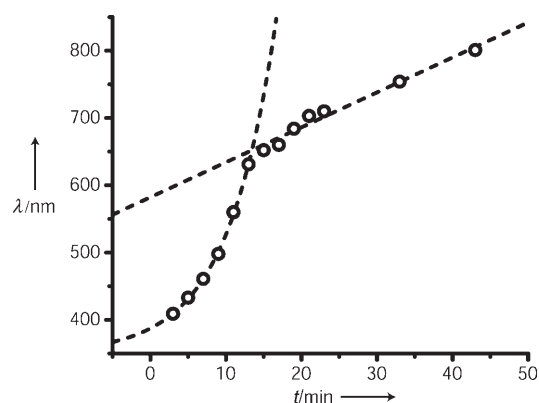


**Figure 2.** Plot of reaction time versus dipolar surface plasmon wavelength, which is correlated to nanocrystal volume. Exponential nanocrystal growth corresponds to the nucleation process, whereas the linear regime corresponds to slow layer-by-layer growth.

a function of reaction time. This LSP mode is associated with nanoparticle volume and undergoes a red shift with increasing diameter. The graph indicates that shape evolution occurs in two steps: fast nucleation, which occurs at an exponential rate, and slow growth, which occurs at a linear rate. Initially, small silver particles ( $< 10$  nm) nucleate and develop into nanocubes bound by {100} planes, which are thought to be selectively stabilized by adsorbed PVP. As the reaction is continued, silver deposits selectively onto the {100} nanocrystal facets rather than growing in a layer-by-layer fashion (Figure 1a). The {111}-capped corners of the nanocube are stabilized during this growth period in which the nanocrystal evolves from a {100}-bound cube to a {111}-bound octahedron. The stability of both {100} and {111} planes in the presence of PVP indicates that shape control may not be

explicitly dictated by the capping polymer. Rather, preferential crystal growth seems to result from a kinetically limited equilibrium influenced heavily by reaction parameters such as temperature, reactant concentration, and reactant molar ratios.

UV/Vis spectra were obtained after the colloidal solutions were repeatedly washed with ethanol to remove excess polymer and filtered (Millipore, DVPP Durapore Membrane Filters). The extinction spectra (extinction = scattering + absorption) in Figure 3a show the differences in LSP modes for colloidal suspensions of cubes, cuboctahedra, and octahedra, all of which exhibit highly complex plasmon signatures as a result of their geometric anisotropy. These LSPs can be assigned by comparing experimental extinction spectra with theoretical extinction cross-section curves calculated using the discrete dipole approximation (DDA).<sup>[13]</sup> DDA is an analytical method used to model light scattering by small particles, whose optical properties experience strong variation with particle size, shape, and local environment. We used an algorithm developed by Draine and Flatau<sup>[14]</sup> in which the nanocrystal is represented by a scattering target composed of point dipoles and is subjected to an incident plane wave. As seen in Figure 3b,c, the theoretical curves obtained with this method agree remarkably well with our experimental data.

Note that because DDA calculations were performed for a vacuum environment, the experimental resonances appear slightly red-shifted ( $< 10$  nm) as expected for a higher dielectric medium.

With this data, we can begin to relate optical signature with the physical geometry of each silver nanocrystal shape. The optical properties of silver nanocubes with an edge length  $a = 30$  nm have been studied in depth in Reference [15] with respect to different refractive media, but only two resonances were observed for these particles. For nanocubes with  $a = 80$  nm, the theoretical curve predicts six strong LSP resonances. The lowest frequency (first and second) modes at  $\lambda \approx 480$  nm and  $\lambda \approx 550$  nm correspond to quadrupolar and dipolar LSP modes, respectively. The quadrupolar mode is the sharpest and the strongest LSP mode. For truncated cubes whose corners are replaced by a flat {111} facet, this LSP mode disappears (see Supporting Information). This indicates that for the quadrupolar mode, amplitude is particularly high at the eight corners of the cube. As the cube truncates and develops increasingly larger {111} facets, the third and fourth plasmon modes increasingly dominate the scattering spectrum. For a cuboctahedron with  $a = 151$  nm, these modes are red-shifted and appear at  $\lambda \approx 430$  nm and  $\lambda \approx 480$  nm. Thus, for the third and fourth LSP modes, amplitude is strongly

associated with the edges of the polyhedra. Previous calculations in which the optical absorption of NaCl crystals was predicted qualitatively agree with these spatial assignments.<sup>[16]</sup>

The characteristic optical signature for octahedral-shaped nanocrystals is much greater in complexity compared to the other polyhedral shapes, despite their shared  $O_h$  symmetry. Octahedral particles exhibit several strong LSP modes as well as fine structure in the form of many less-intense resonances (Figure 3a). This fine structure is well-resolved in the UV/Vis spectrum in the 400–600 nm range, where no less than six LSP bands can be clearly distinguished. DDA calculations (Figure 3b) assign these higher frequency LSPs as hexapolar and higher-order modes, while the resonances at  $\lambda \approx 800$  nm are mainly quadrupolar in nature.

Extinction measurements for colloidal solutions, however, are bulk measurements which rely on sample homogeneity. To investigate shape-

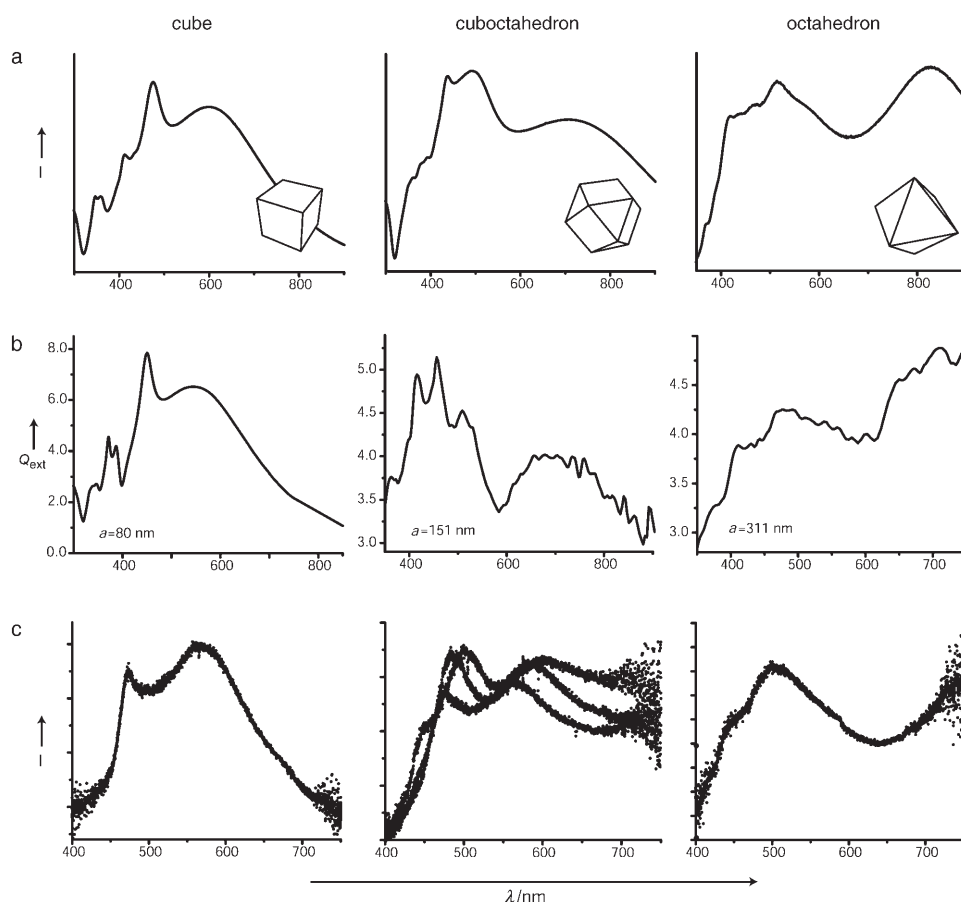


**Figure 3.** Silver nanocubes, cuboctahedra, and octahedra display distinct scattering signatures despite possessing the same point group symmetry. a) UV/Vis spectra of colloidal dispersions. b) DDA simulations for single particles of each shape, where  $a$  is the edge length for the polyhedron. c) Darkfield scattering spectra for single nanocrystals. For cuboctahedra, varying degrees of truncation exist within the sample.

dependent scattering at the single-particle level, we also collected darkfield Rayleigh scattering signals from individual nanocrystals. In these experiments, a drop of the colloidal solution was cast onto a glass coverslip and irradiated with a tungsten lamp. The scattering colors of the silver nanocrystals were observed by using an inverted microscope (Olympus IX71) equipped with a darkfield condenser and collection objective. The images in Figure 4 are real colors captured by a

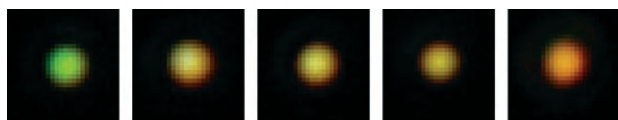


**Figure 4.** Real color images taken with a digital camera displaying the different colors that result from plasmon-mediated scattering. Each spot corresponds to the light scattered from a single nanocrystal. From left to right: cube, truncated cube, cuboctahedron, truncated octahedron, and octahedron. The color evolves from green to orange with increasing degrees of truncation.

digital camera (Olympus DP70, 12MP). Each colored circle is the total scattered light from a single nanocrystal. Cubes ( $a \approx 80$  nm) strongly scatter green light, given that their strongest LSP resonances occur around  $\lambda \approx 500$ –550 nm. As the nanocrystal shape increases in volume and evolves into its truncated forms, the scattering color changes from green to yellow and eventually to the red-orange color characteristic of octahedra ( $a \approx 300$  nm).

Scattering spectra from single nanocrystals can be obtained by directing scattered light to an imaging CCD and spectrometer. The sample preparation is identical to the aforementioned experiments, in which the nanocrystals are cast onto a glass substrate. This sampling geometry, however, is conducive to substrate effects because the particle is in intimate contact with two different media: glass and air. This anisotropic dielectric environment can greatly influence LSPs.<sup>[17]</sup> To prevent this effect, we prepared our nanocrystals with a thick ( $\approx 50$  nm) silica shell to ensure a homogenous dielectric surrounding (see Supporting Information). In general, increasing the refractive index of the nanocrystal environment leads to a red shift in the frequencies of allowed plasmon modes but the overall line shape is unaffected, which can be confirmed experimentally by UV/Vis measurements. Figure 3c shows representative scattering signatures for single nanocrystals with cubic, cuboctahedral, and octahedral shapes. Although only the most intense LSP bands appear, the spectra for the cube and octahedron agree well with UV/Vis extinction measurements (absorption effects are negligible above 400 nm) and DDA calculations. Three representative scattering spectra for cuboctahedral nanocrystals are shown in Figure 3c because varying degrees of truncation exist within the same sample. It is perhaps this shape variance that accounts for the lack of fine structure predicted by theory and a broadening of LSP peaks in the UV/Vis spectrum of the colloidal solution.

Thus far, we have investigated LSPs for different polyhedral nanocrystals for both isotropically distributed colloidal suspensions and isolated single particles. From both a

theoretical and experimental standpoint, the nature of these modes is of great interest given their ability to spatially confine light to a metal–dielectric interface. The ability to engineer metallic nanocrystals that allow the excitation of specific localized surface plasmon modes should have profound consequences for research fields such as surface-enhanced Raman spectroscopy<sup>[18,19]</sup> or plasmonic transport.<sup>[20]</sup> Future experiments may further elucidate the mechanism for local field amplification and electromagnetic coupling, in addition to providing important optical characterization of these metallic nanoscale building blocks.

## Experimental Section

**Nanocrystal synthesis:** Silver nitrate (0.50 g) and copper(II) chloride (0.86  $\mu$ g) were dissolved in 1,5-pentanediol (12.5 mL) in a glass vial. In a separate vial, PVP ( $M_w = 55\,000$  amu, 0.25 g) was dissolved in 1,5-pentanediol (12.5 mL). Using a temperature-controlled silicone oil bath, 1,5-pentanediol (20 mL) was heated for 10 min. The two precursor solutions were then injected into the hot reaction flask at different rates: 500  $\mu$ L of the silver nitrate solution every minute and 250  $\mu$ L of the PVP solution every 30 s. For nanocubes, this addition was stopped once the solution turned opaque ( $\approx 6$  min). For truncated cubes, cuboctahedra, and octahedra, the addition of precursor solutions was continued for a longer period of time ( $\approx 120$  min for octahedral nanocrystals).

**Silica coating:** 5 mL of colloidal solution was diluted with propan-2-ol (15 mL) and deionized water (5 mL). While stirring vigorously, tetraethoxysilane (400  $\mu$ L) and ammonium hydroxide (400  $\mu$ L) were added to the mixture. The reaction was allowed to proceed for 10 min before the solution was centrifuged and the precipitate was collected.

**Darkfield scattering measurements:** A dilute colloidal solution of nanocrystals was drop-cast onto a clean glass coverslip and then dried under vacuum ( $\approx 10^{-2}$  Torr). Samples were then illuminated with a 100-W halogen bulb using a darkfield condenser (NA = 1.2–1.4) with immersion oil. Light was collected through a 60 $\times$  microscope objective lens (NA = 0.7) and captured by a 1340  $\times$  400-pixel back-illuminated CCD (Princeton Instruments, Spec-10:400B) and spectrometer (Princeton Instruments, SpectraPro 2300i).

Received: April 1, 2006

Published online: June 22, 2006

**Keywords:** colloids · nanostructures · silver · surface plasmon resonance

- [1] C. F. Bohren, D. R. Huffman, *Absorption and Light Scattering of Light by Small Particles*, Wiley-Interscience, New York, **1983**.
- [2] C. Sonnichsen, T. Franzl, T. Wilk, G. von Plessen, J. Feldmann, O. Wilson, P. Mulvaney, *Phys. Rev. Lett.* **2002**, *88*, 077402/1.
- [3] J. E. Millstone, S. Park, K. L. Shuford, L. Qin, G. C. Schatz, C. A. Mirkin, *J. Am. Chem. Soc.* **2005**, *127*, 5312.
- [4] A. S. Kumbhar, M. K. Kinnan, G. Chumanov, *J. Am. Chem. Soc.* **2005**, *127*, 12444.
- [5] I. O. Sosa, C. Noguez, R. G. Barrera, *J. Phys. Chem. B* **2003**, *107*, 6269.
- [6] S. Kawata, *Top. Appl. Phys.* **2001**, *81*, 1.
- [7] J. J. Mock, M. Barbic, D. R. Smith, D. A. Schultz, S. Schultz, *J. Chem. Phys.* **2002**, *116*, 6755.
- [8] F. Fievet, J. P. Lagier, B. Blin, B. Beaudoin, M. Figlarz, *Solid State Ionics* **1989**, 198.
- [9] Y. Sun, Y. Xia, *Science* **2002**, *298*, 2176.



- [10] F. Kim, S. Connor, H. Song, T. Kuykendall, P. Yang, *Angew. Chem.* **2004**, *116*, 3759–3763; *Angew. Chem. Int. Ed.* **2004**, *43*, 3673.
- [11] B. Wiley, T. Herricks, Y. Sun, Y. Xia, *Nano Lett.* **2004**, *4*, 1733.
- [12] J. W. M. Frenken, P. Stoltze, *Phys. Rev. Lett.* **1999**, *82*, 3500.
- [13] E. M. Purcell, C. R. Pennypacker, *Astrophys. J.* **1973**, *361*, 705.
- [14] B. T. Draine, P. J. Flatau, *J. Opt. Soc. Am.* **1994**, *A11*, 1491.
- [15] L. J. Sherry, S.-H. Chang, B. J. Wiley, Y. Xia, G. C. Schatz, R. P. Van Duyne, *Nano Lett.* **2005**, *5*, 2034.
- [16] R. Fuchs, *Phys. Rev. B* **1975**, *11*, 1732.
- [17] K. L. Kelly, E. Coronado, L. L. Zhao, G. C. Schatz, *J. Phys. Chem. B* **2003**, *107*, 668.
- [18] R. G. Freeman, K. C. Grabar, K. J. Allison, R. M. Bright, J. A. Davis, A. P. Guthrie, M. B. Hommer, M. A. Jackson, P. C. Smith, D. G. Walter, M. J. Natan, *Science* **1995**, *267*, 1629.
- [19] M. Moskovits, *Rev. Mod. Phys.* **1985**, *57*, 783.
- [20] W. L. Barnes, A. Dereux, T. W. Ebbesen, *Nature* **2003**, *424*, 824.

because of the large photoinduced changes in their molecular geometry.

UV light is also known to cause diverse chemical reactions, such as photodimerization in the nucleobase moieties of DNA.<sup>[9,10]</sup> The major photoproduct is a *cis-syn* cyclobutane pyrimidine dimer. Except for our previous study,<sup>[11]</sup> there have been no reports of direct visualization focusing on the effect of thymine photodimerization on the morphologies of self-assembled nanofibers. Moreover, no one has ever addressed reversible induction of helical and non-helical morphologies, driven by light or photoreaction, in molecular self-assemblies consisting of bilayer or monolayer membranes. Here we describe for the first time the reversible conversion of helicity, driven by a photochemical process of the thymine moiety with UV light, in self-assembled nanofibers from a 1, $\omega$ -thymidylic acid appended bolaamphiphile, **1** (Scheme 1).

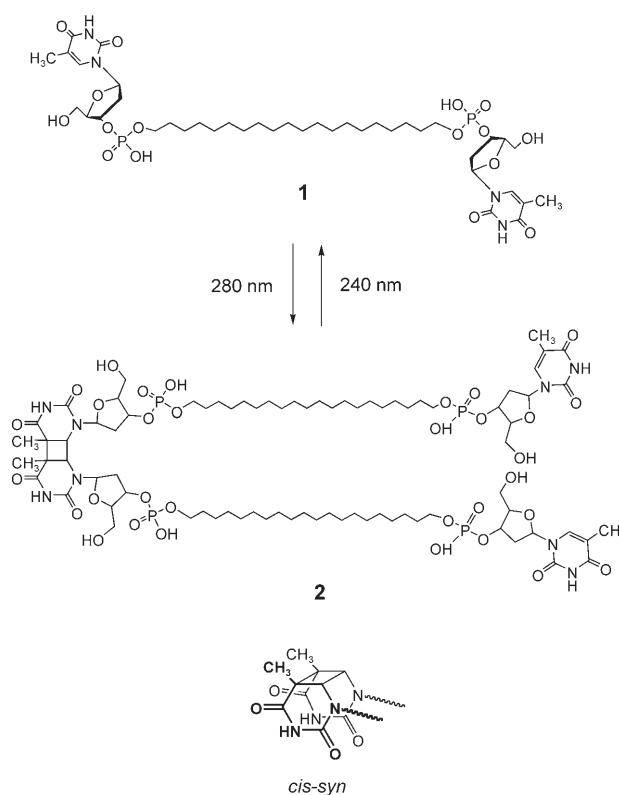
## Helical Nanofibers

DOI: 10.1002/anie.200601173

### Reversible Photochemical Conversion of Helicity in Self-Assembled Nanofibers from a 1, $\omega$ -Thymidylic Acid Appended Bolaamphiphile

Rika Iwaura and Toshimi Shimizu\*

Activation of photoreactive compounds, such as azobenzene-containing derivatives,<sup>[1–3]</sup> stilbene-containing compounds,<sup>[4]</sup> dithienylcyclopentene,<sup>[5]</sup> maleic acid amide derivatives,<sup>[6]</sup> and 2*H*-chromene-containing compounds,<sup>[7]</sup> is known to induce changes in the self-assembly behavior of the molecules. For example, UV light can act as a switching trigger not only to drive a change in the self-assembled morphology from spheres to rods<sup>[1]</sup> but also to induce gel-to-sol phase transitions.<sup>[2,4,6,7]</sup> Sometimes, linearly polarized light allows a single film of a liquid crystal network containing an azobenzene chromophore to bend in any direction.<sup>[8]</sup> In all cases, configurational or conformational changes in the molecular structures lead to a substantial change in the self-assembled morphologies based on each molecule. The most widely used photoswitching molecules are azobenzene derivatives



**Scheme 1.** Conversion of the monomer **1** into the photodimer **2** and the structure of the *cis-syn* isomer.

Scanning electron microscopy (SEM) and atomic force microscopy (AFM) provided evidence that the bolaamphiphile **1** self-assembles in aqueous solutions into fiber structures with 10-nm thickness and 80-nm width as typical dimensions.<sup>[12]</sup> A field emission (FE) SEM<sup>[13]</sup> image of the self-assembled nanofibers from **1** revealed the presence of nonhelical nanorod or nanofiber structures with diameters ranging from 100–300 nm (Figure 1a). A high-magnification image allowed us to observe a bundle formation of four fibers, each 50 nm in diameter (Figure 1b). UV irradiation at  $\lambda = 280$  nm (UV<sub>280</sub>) for 2–3 h gave helical features to parts of the

[\*] Dr. R. Iwaura, Dr. T. Shimizu  
Nanoarchitectonics Research Center (NARC)  
National Institute of Advanced Industrial Science and Technology (AIST)  
Tsukuba Central 5, 1-1-1 Higashi, Tsukuba, Ibaraki 305-8565 (Japan)  
Fax: (+81) 29-861-4545  
E-mail: tshimz-shimizu@aist.go.jp  
Dr. T. Shimizu  
SORST  
Japan Science and Technology Agency (JST)  
Tsukuba Central 5, 1-1-1 Higashi, Tsukuba, Ibaraki 305-8565 (Japan)  
Supporting information for this article is available on the WWW under <http://www.angewandte.org> or from the author.

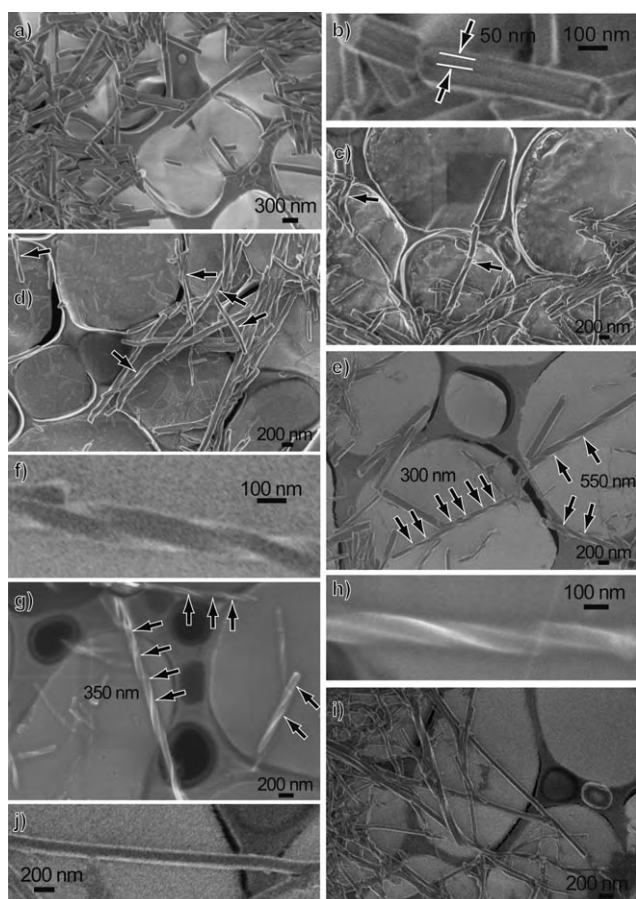


**Figure 1.** FE-SEM images of the self-assembled nanofibers from **1** in aqueous solution. a,b) Images before UV irradiation. c–h) Images after UV irradiation at  $\lambda = 280$  nm for c) 2 h, d) 3 h, e) and f) 4 h, and g) and h) 3 days. i,j) Images after the successive UV irradiation at  $\lambda = 280$  nm for 5 h and then at  $\lambda = 240$  nm for 3 h.

self-assembled nanofibers (Figures 1 c,d, indicated by arrows). The helical structures stood out clearly after 4 h of UV<sub>280</sub> irradiation. The helical pitches of the self-assemblies were estimated to be 300–550 nm (Figures 1 e,f). Finally, 3 days of UV<sub>280</sub> irradiation caused all of the nanofibers to form helical structures with pitches of 350–400 nm (Figures 1 g,h). The number of helical nanofibers increases with time after UV<sub>280</sub> irradiation. We thus found that exposure to UV light strongly affects the self-assembled morphologies of **1** and eventually induces helical twisting in the nanofiber structures. The helicity observed by FE-SEM was found to be right-handed for all of the nanofibers. Interestingly, irradiation of this sample with UV light at  $\lambda = 240$  nm (UV<sub>240</sub>) for 3 h converted the helical fibers to intrinsically nonhelical ones (Figures 1 i,j).

To examine the photodimerization behavior of the thymine moiety in **1**, we carried out UV spectroscopy and matrix-assisted laser desorption/ionization time-of-flight mass spectrometry (MALDI-TOF MS) measurements for the self-assembled nanofibers. The UV<sub>280</sub> irradiation gradually caused a decrease in the absorption intensity at 270 nm<sup>[9]</sup> to 30 % of the original value for the self-assembled nanofibers of **1** over a period of 5 h (Figures 2 a,b). This finding gives strong evidence for the formation of thymine photodimers in

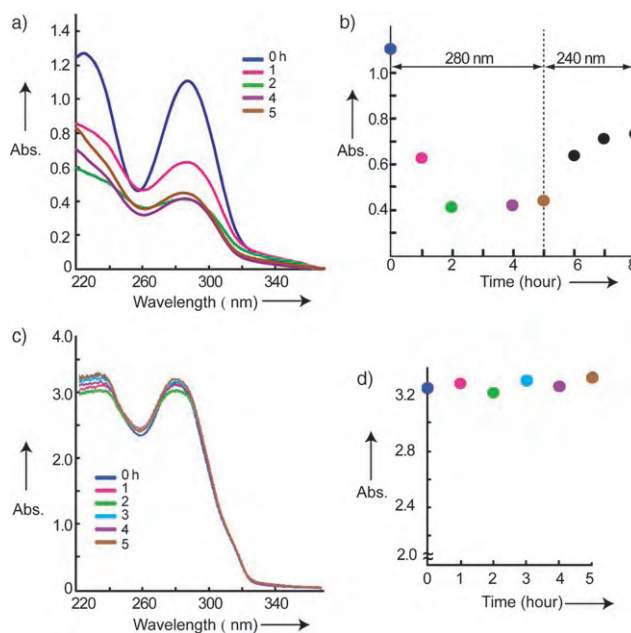


**Figure 2.** a) Time dependence of UV-spectral changes for the self-assemblies of **1** in aqueous solution ( $2.2 \times 10^{-3}$  M) on UV irradiation at  $\lambda = 280$  nm. b) Time dependence of UV absorbance at  $\lambda = 270$  nm on UV irradiation at  $\lambda = 280$  nm (0–5 h) and then at  $\lambda = 240$  nm (5–8 h). c) Time dependence of the UV-spectral changes for the binary mixture of **1** and dA<sub>6</sub> in aqueous solution ( $2.2 \times 10^{-3}/7 \times 10^{-5}$  M) upon UV irradiation at  $\lambda = 280$  nm. d) Time dependence of the UV absorbance at  $\lambda = 270$  nm for the binary mixture of **1** and dA<sub>6</sub> upon UV irradiation at  $\lambda = 280$  nm.

the self-assembly of **1**. MALDI-TOF MS measurements also support this fact. The spectrum for the nanofibers after UV<sub>280</sub> irradiation for 3 days gave the peak ascribable to the dimerized component **2** (Scheme 1) at  $m/z$  1844, in addition to the peak assignable to the monomer **1** at  $m/z$  922. We were unable to observe any peaks corresponding to other high-mass components such as trimers or oligomers. Therefore, we concluded that the dimerization of the thymine moiety takes place between one end of two molecules in the self-assembly of **1**.

On the other hand, UV<sub>240</sub> irradiation of previously UV<sub>280</sub>-irradiated nanofibers for 3 h induced the recovery of up to 60 % of the absorption intensity of the thymine moiety (Figure 2 b). This finding clearly indicates that photodissociation of the thymine dimer occurs in the self-assembly system.

Next, we performed UV<sub>280</sub> irradiation on the self-assembled nanofibers of **1** in the presence of complementary 6-mer oligoadenylic acid, dA<sub>6</sub>. The UV absorption maximum of the nucleic acids, that is, thymine and adenine, scarcely changed upon UV<sub>280</sub> irradiation (Figures 2 c,d), which means that no thymine photodimers form in the presence of the complementary component dA<sub>6</sub>.

Figure 3 shows partial <sup>1</sup>H NMR spectra for the self-assembled nanofibers before and after UV irradiation. Two additional peaks appeared at  $\delta = 1.22$  and 1.23 ppm in the methyl-proton region after UV irradiation (Figure 3 b); these peaks were ascribable to the C5 position of the thymine photodimer. The appearance of these two signals after the

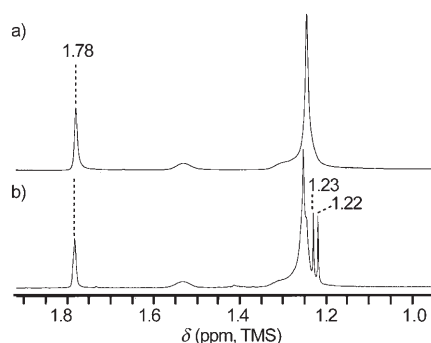


**Figure 3.** Partial  $^1\text{H}$  NMR spectra (600 MHz, at  $80^\circ\text{C}$  in  $[\text{D}_6]\text{DMSO}$ ) of a) the self-assembled nanofibers from **1** before UV irradiation and b) those after UV irradiation at  $\lambda = 280$  nm for 3 days.

$\text{UV}_{280}$ -irradiated self-assembly of **1** is compatible with the previous results on related *cys-syn* photodimers.<sup>[14,15]</sup> Thus, the MS and  $^1\text{H}$  NMR measurements strongly support the conclusion that the major photodimer product from **1** is the *cis-syn* isomer **2**, in which one end of the bolaamphiphile is associated with the end of another molecule.

CD spectra for the self-assembly of **1** before and after exposure to UV light gave two relatively strong CD bands (positive and negative ones at 290 and 235 nm, respectively), in addition to zero crossing at 246 nm (Figure 4). Similar split

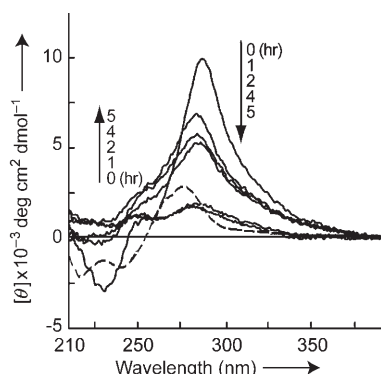


**Figure 4.** CD spectral changes for the diluted self-assemblies from **1** in aqueous solution ( $2.2 \times 10^{-3}$  M) upon UV irradiation at  $\lambda = 280$  nm (black lines). For reference, the CD spectrum of 3'-thymidine mono-phosphate in aqueous solution is shown as a dashed line ( $4.3 \times 10^{-3}$  M).

patterns were also observed for the CD spectrum of right-handed oligo- and polynucleotides.<sup>[16,17]</sup>  $\text{UV}_{280}$  irradiation induced the blue shift of the positive band from 290 to 285 nm and a reduction in the intensities of both bands. The large alterations in the CD spectra indicate the different molecular orientation of the thymidylic acid moieties associated with the photodimerization.<sup>[17]</sup> Interestingly, the CD intensities at 285 nm gradually decreased over a period of 4 h of  $\text{UV}_{280}$  irradiation, whereas the reduction in the UV absorption intensities at around 270 nm was complete even after 2 h (Figures 2a,b). CD spectroscopy is more sensitive to the observed helical-nanofiber formation than the UV measure-

ments and probes the later changes in molecular packing owing to the photodimerization (Figures 1e,f).

The self-assembled nanofibers from **1** consist of monolayer sheets with a long period of 3.59 nm (Figure 5a).<sup>[12]</sup>

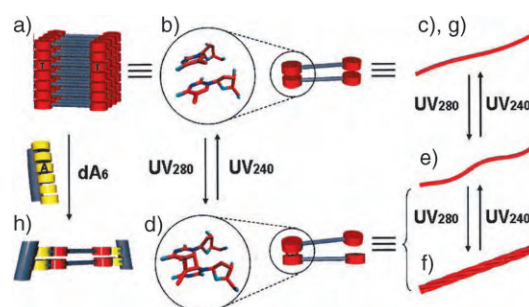


**Figure 5.** A proposed mechanism for the reversible photochemical conversion by UV irradiation in the self-assembled nanofibers from **1**. a) Monolayer sheets of the self-assembly of **1** with a long period of 3.59 nm. b) Molecular model of two thymidine moieties and schematic illustration of the two **1** molecules in the monolayer sheets before UV irradiation. c) Self-assembled nonhelical nanofiber from **1** before UV irradiation. d) Molecular model of a thymidine photodimer and schematic illustration of the dimer molecule **2** in the monolayer sheets after UV irradiation. e) Twisted monolayer. f) The resultant helical nanofiber. g) Recovery of the nonhelical nanofiber after  $\text{UV}_{240}$  irradiation of the *cis-syn* thymine dimer in the self-assembly from **1**. h) Inhibition of the photodimerization of thymine moieties in **1** in the presence of complementary  $\text{dA}_6$  by the formation of A-T base pairs. The molecular structures of the models in (b) and (d) were drawn by using the VMD software<sup>[22]</sup> on the basis of information in ref. [10] and the Protein Databank (<http://www.pdb.org/>; PDB file code: 1T4L).

Before  $\text{UV}_{280}$  irradiation, the molecules hold together, stabilized by noncovalent interactions, such as base stacking between the thymine moieties and hydrophobic interactions between the oligomethylene chains (Figures 5b,c).<sup>[12]</sup> The stacking features of the thymine moieties in the self-assembly of **1**<sup>[12]</sup> should be favorable for effective photodimerization, even in the absence of a triplet photosensitizer such as acetone.<sup>[9]</sup> Actually,  $\text{UV}_{280}$  irradiation of the self-assembly of **1** causes the photodimerization of the thymine moieties with the formation of covalent bonds partially in the monolayer sheets. The generation of a *cis-syn* derivative after the UV irradiation is compatible with the fact that the *cis-syn* isomer is a major product when the stacked thymine bases in DNA or dinucleotide are exposed to UV light.<sup>[9]</sup> The UV absorption change (Figure 2a) indicated the amount of photodimerized thymine to be 63%. The estimated quantity is enough to convert all of the molecular packing of the self-assembly of **1** into helical-nanofiber structures. The formation of the *cis-syn* isomer generates no chiral centers, which are commonly seen in the molecular building blocks of helical assemblies.<sup>[18]</sup> Therefore, we think that the role of the *cis-syn* isomer is to enhance and to stabilize the chirality of the D-sugar moiety in **1**.

After  $\text{UV}_{280}$  irradiation, each thymine base tilts to form a nonparallel orientation with the central cyclobutane ring puckering by  $20^\circ$ , as seen in the DNA crystal structure<sup>[10]</sup>



(Figure 5d, molecular models). Therefore, the photodimerization of the thymine moieties should greatly affect the molecular packing in the self-assembly of **1**. The covalent formation of a *cis-syn* cyclobutane pyrimidine dimer allows a half molecule of the dimer to pack at a nonzero angle with respect to their nearest neighbors. This feature leads us to suppose that the chiral molecular packing induces twisting in the monolayer sheets, which results in twisting of the resultant nanofibers (Figures 5d–f).<sup>[19]</sup> The nanofiber structures with no helical features were recovered after the UV<sub>240</sub> irradiation on the *cis-syn* thymine dimer in the self-assembly system of **1** (Figure 5g). FE-SEM and UV measurements clearly evidenced the photolysis of the thymine dimer into the thymine monomer. On the other hand, the presence of the complementary dA<sub>6</sub> molecule acts to effectively suppress the photodimerization of the thymine moiety in **1**. The nucleotide bolaamphiphile **1** and the complementary oligoadenylic acids form binary complexes through the complementary A–T base pair. We have indeed found the formation of intertwined, nonhelical nanofibers based on binary self-assembly of **1** and dA<sub>6</sub>.<sup>[20]</sup> The complementary base pairing will provide the self-assembled structures of **1** with molecular packing that is resistant to the photodimerization of the thymine moiety.<sup>[21]</sup>

In conclusion, we have demonstrated that UV light directs the reversible photochemical conversion between self-assembled helical nanofibers and nonhelical ones from the 1,ω-nucleotide bolaamphiphile **1**. The photodimerization of a part of the thymine moiety of **1** produces a *cis-syn* photodimer, **2**, in the self-assemblies and this results in right-handed helical nanofibers. Photodissociation of the dimer **2** converts the helical fibers into nonhelical ones again. These findings are of great importance in terms of the photochemical switching of nanofiber morphologies.

### Experimental Section

**1** was synthesized by coupling 1,20-icosanediol with thymidylic acid by use of phosphoramidite methods, as reported elsewhere.<sup>[12]</sup> The self-assembly of **1** ( $2.2 \times 10^{-3}$  M) was irradiated with monochromated light (Bunkoh-keiki, SM-5) at  $\lambda = 280$  or  $240$  nm for photodimerization and photodissociation, respectively. For the UV irradiation at  $\lambda = 280$  nm, a UV 28 colored optical glass (Hoya) was used to cut off the light below  $\lambda = 280$  nm. To prepare the binary self-assembly solutions for UV irradiation, we added dA<sub>6</sub> to the aqueous solution of **1** and adjusted the concentrations of **1** and dA<sub>6</sub> to  $2.2 \times 10^{-2}$  and  $0.7 \times 10^{-3}$  M, respectively. This aqueous solution was treated in the same manner as the self-assembly of **1** mentioned above. FE-SEM observation was conducted on a JEOL S-4800 instrument (accelerate voltage 0.5–1.8 kV, working distance 4 mm). UV, <sup>1</sup>H NMR, and CD spectroscopy and MALDI-TOF mass spectrometry were carried out by using UV-3300 (Hitachi), LA600 (600 MHz, JEOL), J-820 (Jasco), and Kratos Kompact-MALDI III (Shimadzu) instruments, respectively. See the Supporting Information for further details of the experiments.

Received: March 24, 2006

Published online: June 22, 2006

**Keywords:** amphiphiles · fibers · nucleotides · photochemical reactions · self-assembly

- [1] T. Kunitake, N. Nakashima, M. Shimomura, Y. Okahata, K. Kano, T. Ogawa, *J. Am. Chem. Soc.* **1980**, *102*, 6642–6644.
- [2] a) K. Murata, M. Aoki, T. Suzuki, T. Harada, H. Kawabata, T. Komori, F. Ohseto, K. Ueda, S. Shinkai, *J. Am. Chem. Soc.* **1994**, *116*, 6664–6676; b) N. Koumura, M. Kudo, N. Tamaoki, *Langmuir* **2004**, *20*, 9897–9900.
- [3] a) X. Song, J. Perlstein, D. G. Whitten, *J. Am. Chem. Soc.* **1997**, *119*, 9144–9159; b) K. Aoki, M. Nakagawa, K. Ichimura, *J. Am. Chem. Soc.* **2000**, *122*, 10997–11004; c) S. Yagai, T. Karatsu, A. Kitamura, *Chem. Eur. J.* **2005**, *11*, 4054–4063.
- [4] J. Eastoe, M. Sánchez-Dominguez, P. Wyatt, R. K. Heenan, *Chem. Commun.* **2004**, 2608–2609.
- [5] J. J. D. de Jong, P. R. Hania, A. Pugžlys, L. N. Lucas, M. de Loos, R. M. Kellogg, B. L. Feringa, K. Duppen, J. H. van Esch, *Angew. Chem.* **2005**, *117*, 2425–2428; *Angew. Chem. Int. Ed.* **2005**, *44*, 2373–2376.
- [6] L. Frkanec, M. Jokic, J. Makarevic, K. Wolsperger, M. Zinic, *J. Am. Chem. Soc.* **2002**, *124*, 9716–9717.
- [7] S. A. Ahmed, X. Sallenave, F. Fages, G. Mieden-Gundert, W. M. Müller, U. Müller, F. Vögtle, J. L. Pozzo, *Langmuir* **2002**, *18*, 7096–7101.
- [8] a) Y. Yu, M. Nakano, T. Ikeda, *Nature* **2003**, *425*, 145–145; b) T. Ikeda, T. Sasaki, K. Ichimura, *Nature* **1993**, *361*, 428–430.
- [9] S. Y. Wang, *Photochemistry and Photobiology of Nucleic Acids*, Academic Press, New York, **1976**.
- [10] H. Park, K. Zhang, Y. Ren, S. Nadji, N. Sinha, J.-S. Taylor, C. Kang, *Proc. Natl. Acad. Sci. USA* **2002**, *99*, 15965–15970.
- [11] T. Shimizu, R. Iwaura, M. Masuda, T. Hanada, K. Yase, *J. Am. Chem. Soc.* **2001**, *123*, 5947–5955.
- [12] R. Iwaura, K. Yoshida, M. Masuda, K. Yase, T. Shimizu, *Chem. Mater.* **2002**, *14*, 3047–3053.
- [13] a) Y. Zhou, Q. Ji, M. Masuda, S. Kamiya, T. Shimizu, *Chem. Mater.* **2006**, *18*, 403–406; b) Q. Ji, S. Kamiya, J. H. Jung, T. Shimizu, *J. Mater. Chem.* **2005**, *15*, 743–748.
- [14] a) K. Kondo, T. Sato, K. Takemoto, *Chem. Lett.* **1973**, 967–968; b) M. J. Moghaddam, S. Hozumi, Y. Inaki, K. Takemoto, *J. Polym. Sci. Polym. Chem. Ed.* **1988**, *26*, 3297–3308.
- [15] J. Cadet, L. Voituriez, F. E. Hruska, L. S. Kan, F. A. A. M. Deleeuw, C. Altona, *Can. J. Chem.* **1985**, *63*, 2861–2868.
- [16] Y. Inoue, S. Aoyagi, K. Nakanishi, *J. Am. Chem. Soc.* **1967**, *89*, 5701–5706.
- [17] I. Tinoco, Jr., *J. Am. Chem. Soc.* **1964**, *86*, 297–298.
- [18] J.-H. Fuhrhop, W. Helfrich, *Chem. Rev.* **1993**, *93*, 1565–1582.
- [19] a) T. Shimizu, M. Masuda, H. Minamikawa, *Chem. Rev.* **2005**, *105*, 1401–1443; b) M. S. Spector, J. V. Selinger, A. Singh, J. M. Rodriguez, R. R. Price, J. M. Schnur, *Langmuir* **1998**, *14*, 3493–3500.
- [20] a) R. Iwaura, M. Ohnishi-Kameyama, M. Yoshida, T. Shimizu, *Chem. Commun.* **2002**, 2658–2659; b) R. Iwaura, K. Yoshida, M. Masuda, M. Ohnishi-Kameyama, M. Yoshida, T. Shimizu, *Angew. Chem.* **2003**, *115*, 1039–1042; *Angew. Chem. Int. Ed.* **2003**, *42*, 1009–1012.
- [21] a) T. Schultz, E. Samoylova, W. Radloff, I. V. Hertel, A. L. Sobolewski, W. Domcke, *Science* **2004**, *306*, 1765–1768; b) C. E. Crespo-Hernández, B. Cohen, B. Kohler, *Nature* **2005**, *436*, 1141–1144.
- [22] W. Humphrey, A. Dalke, K. Schulten, *J. Mol. Graphics* **1996**, *14*, 33–38.

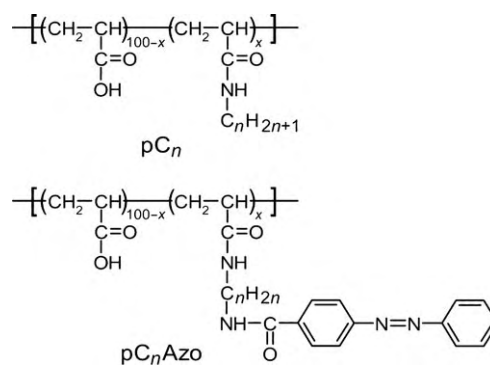
# Cyclodextrin-Based Side-Chain Polyrotaxane with Unidirectional Inclusion in Aqueous Media\*\*

Itsuro Tomatsu, Akihito Hashidzume, and Akira Harada\*

Recently, polyrotaxanes have attracted much interest from researchers from the viewpoint of nanotechnological applications.<sup>[1]</sup> In particular, well-defined polyrotaxanes that consist of simple components are becoming important for the construction of more sophisticated molecular machines. There are a number of designs and strategies for the preparation of polyrotaxanes.<sup>[2]</sup> Among these approaches, the side-chain polyrotaxane is one of the simplest architectures, but there are only a few examples of side-chain polyrotaxanes that contain cyclodextrin (CD),<sup>[3]</sup> apart from those of Ritter and co-workers.<sup>[4]</sup> Extensive studies by Ritter<sup>[4]</sup> demonstrated the successful synthesis of side-chain polyrotaxanes primarily in organic media from methylated  $\beta$ -CD and various polymers.

Over the past decade, we have been studying the interaction of cyclodextrins with polymer side chains attached to water-soluble polymers.<sup>[5]</sup> Herein, we report an example of the successful construction of CD-based side-chain polyrotaxanes in aqueous media, in which CD includes polymer side chains preferentially from the side with the secondary hydroxy functionality, by using a combination of simple components,  $\alpha$ -CD and hydrophobically modified poly-(acrylic acid) (pAA).

We have reported that CD interacts with polymer side chains and forms inclusion complexes.<sup>[5]</sup> For example,  $\alpha$ -CD forms 1:1 inclusion complexes with alkyl side chains attached to the pAA backbone in aqueous media at lower  $\alpha$ -CD concentrations.<sup>[6]</sup> The structure of 1:1 complexes of  $\alpha$ -CD with hexyl- and dodecyl-modified pAAs (pC<sub>n</sub>,  $n = 6$  and 12, respectively; Scheme 1) were investigated in detail by 2D NOESY analysis (Figure 1). Both the spectra exhibit clear correlation peaks between the inner protons in the  $\alpha$ -CD cavity and protons in the alkyl side chains, indicative of the



Scheme 1. Structures of the polymers used in this study.

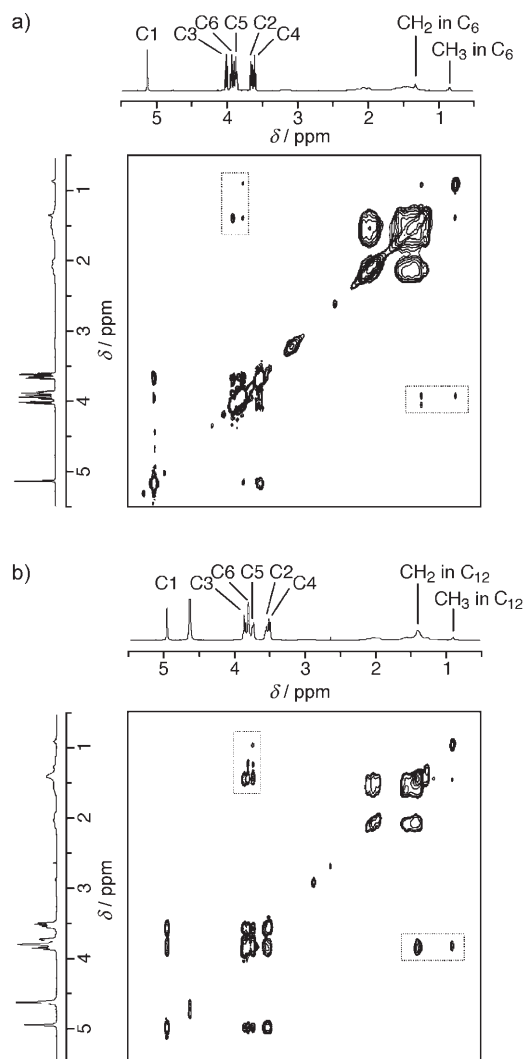


Figure 1. 2D NOESY spectra of solutions of a) pC<sub>6</sub> and b) pC<sub>12</sub> (5 g L<sup>−1</sup>) in the presence of  $\alpha$ -CD (10 g L<sup>−1</sup>).

formation of inclusion complexes of  $\alpha$ -CD with the alkyl side chains. It is of note that both the spectra also exhibit significant correlation peaks between the protons at the 5-position in  $\alpha$ -CD and the protons of the terminal methyl group in the alkyl side chains. These data indicate that  $\alpha$ -CD includes the side chains preferentially from the side of the secondary hydroxy group. In other words, we have success-

[\*] I. Tomatsu, Dr. A. Hashidzume, Prof. Dr. A. Harada  
Department of Macromolecular Science  
Graduate School of Science  
Osaka University Toyonaka  
Osaka 560-0043 (Japan)  
Fax: (+81) 6-6850-5445  
E-mail: harada@chem.sci.osaka-u.ac.jp

[\*\*] We thank Prof. Dr. Tatsuki Kitayama, Associate Professor Dr. Koichi Ute, and Takashi Nishimura for pulsed-field-gradient NMR measurements and analyses. I.T. appreciates Research Fellowships for Young Scientists from the Japan Society for the Promotion of Science.

Supporting information for this article is available on the WWW under <http://www.angewandte.org> or from the author.

fully obtained unidirectionally included side-chain pseudorotaxanes by using a combination of simple components. At present, we are not sure of the driving force for the unidirectional inclusion, but it should be thermodynamically driven: certain interactions between the hydroxy groups in  $\alpha$ -CD and the carboxylate groups in the pAA backbone may lead to a stronger interaction between the side of the secondary hydroxy group that bears more hydroxy groups with the pAA backbone. Thus, this observation may be in contrast to the cases of kinetically driven unidirectional inclusion reported recently.<sup>[7,8]</sup>

These observations motivated us to construct unidirectionally included side-chain polyrotaxanes in aqueous media. For this purpose, we prepared two azobenzene-carrying pAAs, namely, pAAs modified with azo moieties through hexamethylene and dodecamethylene linkers ( $pC_nAzo$ ,  $n = 6$  and 12, respectively; Scheme 1). As azobenzene derivatives are isomerized from *trans* to *cis* under irradiation with UV light,<sup>[9]</sup> it is expected that side-chain polyrotaxanes can be controlled by utilizing photoisomerization of the azo moiety in  $pC_nAzo$ .<sup>[10]</sup>

The formation of inclusion complexes of  $\alpha$ -CD with  $pC_nAzo$  was confirmed by UV/Vis absorption spectroscopy (see the Supporting Information). The structure of inclusion complexes of  $\alpha$ -CD with  $pC_nAzo$  was also explored by 2D NOESY analysis. The spectrum for the  $\alpha$ -CD/ $pC_6Azo$  mixture exhibits correlation peaks between the inner protons in the  $\alpha$ -CD cavity and protons in the azo and  $C_6$  moieties, thus indicating that  $\alpha$ -CD includes both the moieties in the polymer side chain (Figure 2a). The correlation peaks between  $\alpha$ -CD and the azo moiety are stronger than those between  $\alpha$ -CD and the  $C_6$  linker, thus indicating that  $\alpha$ -CD interacts with the azo moiety more favorably than with the  $C_6$  linker. The spectrum for the  $\alpha$ -CD/ $pC_{12}Azo$  mixture also indicates that  $\alpha$ -CD included both the azo and  $C_{12}$  moieties (Figure 3a). The correlation peaks between  $\alpha$ -CD and the  $C_{12}$  linker are much stronger than those between  $\alpha$ -CD and the azo moiety, thus indicating that  $\alpha$ -CD interacts with the  $C_{12}$  linker much more favorably than with the azo moiety.

When we irradiated the  $\alpha$ -CD/ $pC_nAzo$  mixtures with UV light, more than 75 % of the azo moieties were isomerized into the *cis* form. The formation of the side-chain polyrotaxane was investigated by 2D NOESY analysis. The spectrum for the  $\alpha$ -CD/ $pC_6Azo$  mixture after UV irradiation exhibits no significant correlation peaks between the protons in  $\alpha$ -CD and those in the azo moiety and in the  $C_6$  linker, thus indicating that the inclusion complex of  $\alpha$ -CD with the side chain is dissociated by *trans*-to-*cis* photoisomerization (Figure 2b). This observation implies that the  $C_6$  linker is so short that side-chain polyrotaxanes are not formed. On the other hand, the spectrum for the  $\alpha$ -CD/ $pC_{12}Azo$  mixture after UV irradiation exhibits correlation peaks between the inner protons in  $\alpha$ -CD and those in the  $C_{12}$  linker (Figure 3b). This observation means that  $\alpha$ -CD stays on the  $C_{12}$  linker, even after *trans*-to-*cis* photoisomerization of the azo moiety, which is indicative of the formation of the side-chain polyrotaxane. The formation of the side-chain polyrotaxane was confirmed by pulsed-field-gradient NMR spectroscopy, which demonstrated two diffusion modes of the signals as a

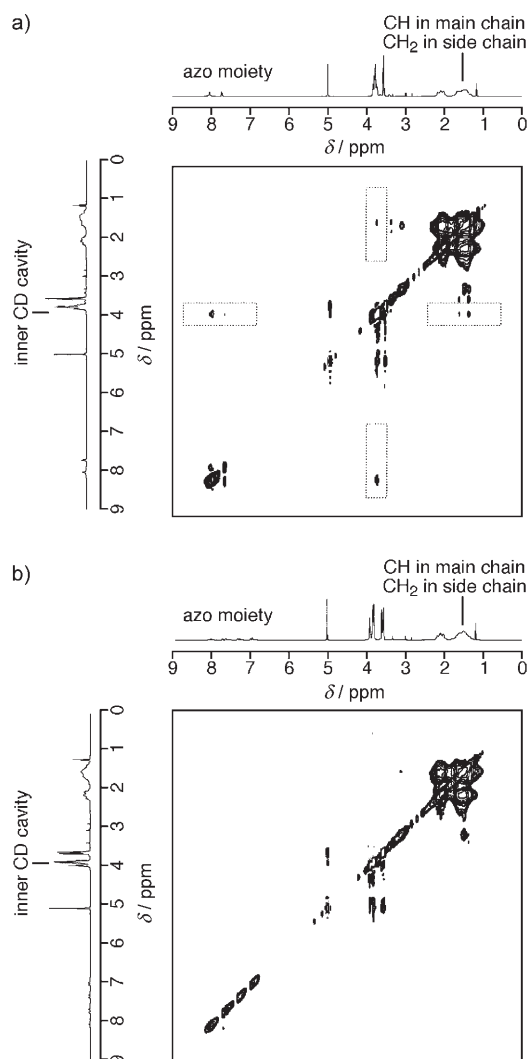


**Figure 2.** 2D NOESY spectra of a solution of  $pC_6Azo$  ( $10 \text{ g L}^{-1}$ ) in the presence of  $\alpha$ -CD ( $10 \text{ g L}^{-1}$ ) measured a) before and b) after UV irradiation.

result of  $\alpha$ -CD with diffusion constants  $6.8 \times 10^{-12}$  (complexed  $\alpha$ -CD) and  $1.7 \times 10^{-10}$  (free  $\alpha$ -CD)  $\text{m}^2 \text{s}^{-1}$  (see the Supporting Information). As shown in Figure 4a, the expanded 2D NOESY spectrum for the  $\alpha$ -CD/ $pC_{12}Azo$  mixture exhibits a weak but clear correlation peak between protons of the 5-position in  $\alpha$ -CD and the proton e of the *cis* azo moiety. This spectrum indicates that the  $C_{12}$  linker is included by  $\alpha$ -CD, in which the primary hydroxy side is close to the azo moiety (Figure 4b).

In conclusion, we have successfully constructed a CD-based side-chain polyrotaxane with unidirectional inclusion in aqueous media by using a combination of the simple components,  $\alpha$ -CD and  $pC_{12}Azo$ . We are investigating the driving force for the unidirectional inclusion.

## Experimental Section

**Materials:** Poly(acrylic acid) (pAA; Wako Pure Chemical Industries, Ltd.) was used as supplied. The average molecular weight of pAA was reported to be 250000 by the supplier.  $\alpha$ -Cyclodextrin ( $\alpha$ -CD) was

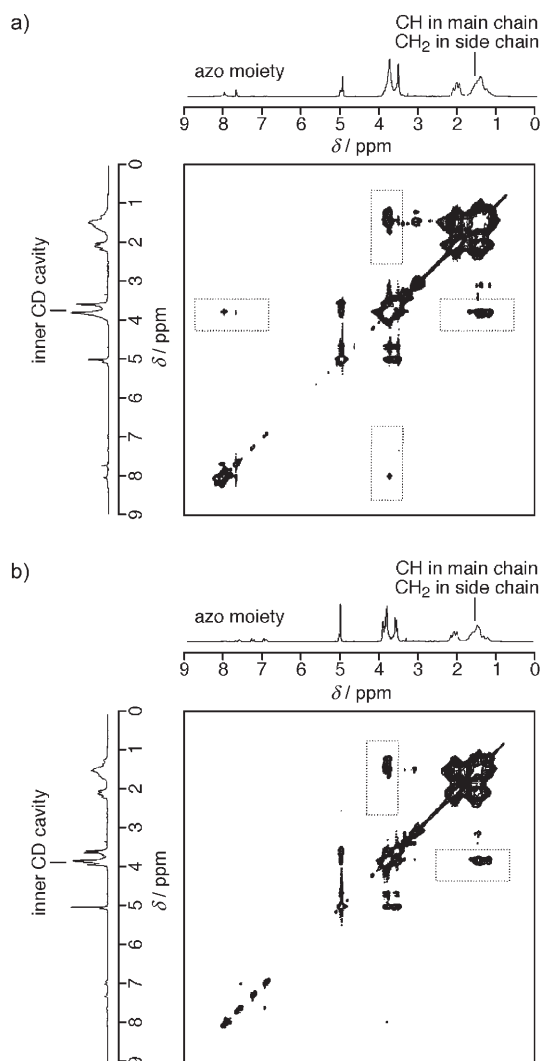


**Figure 3.** 2D NOESY spectra of a solution of pC<sub>12</sub>Azo (10 g L<sup>-1</sup>) in the presence of  $\alpha$ -CD (10 g L<sup>-1</sup>) measured a) before and b) after UV irradiation.

recrystallized twice from water. Milli-Q water was used for preparation of aqueous solutions. Other reagents were used as received.

**Preparation of hydrophobically modified pAAs:** Alkyl-modified pAAs (pC<sub>n</sub>, *n* = number of carbon atoms in the alkyl chain) were prepared from pAA and respective amines in the presence of *N,N'*-dicyclohexylcarbodiimide (DCC) according to the procedure of Iliopoulos and co-workers.<sup>[11]</sup> The preparation details are described elsewhere.<sup>[6]</sup> The degrees of modification (*x*) were determined to be 5.4 and 5.2 mol% for pC<sub>6</sub> and pC<sub>12</sub>, respectively, by <sup>1</sup>H NMR spectroscopic analysis. Azobenzene-modified pAAs (pC<sub>n</sub>Azo, *n* = number of carbon atoms in the alkylene linker) were also prepared by the same procedure. The preparation details are described elsewhere.<sup>[12]</sup> The degrees of modification (*x*) were determined to be 3.8 and 2.7 mol% for pC<sub>6</sub>Azo and pC<sub>12</sub>Azo, respectively, by <sup>1</sup>H NMR spectroscopic analysis.

**NMR:** Two-dimensional NOESY NMR spectra were recorded with a VARIAN UNITY INOVA PLUS 600 NMR or JEOL JNM LA500 NMR spectrometer at 30 °C. Sample solutions were prepared with D<sub>2</sub>O containing 0.05 M sodium carbonate and 0.05 M sodium bicarbonate. Sample solutions were heated at 60 °C for 1 day, and then the solution was irradiated with UV light for 12 h. Pulsed-field-gradient NMR measurements were performed on a VARIAN

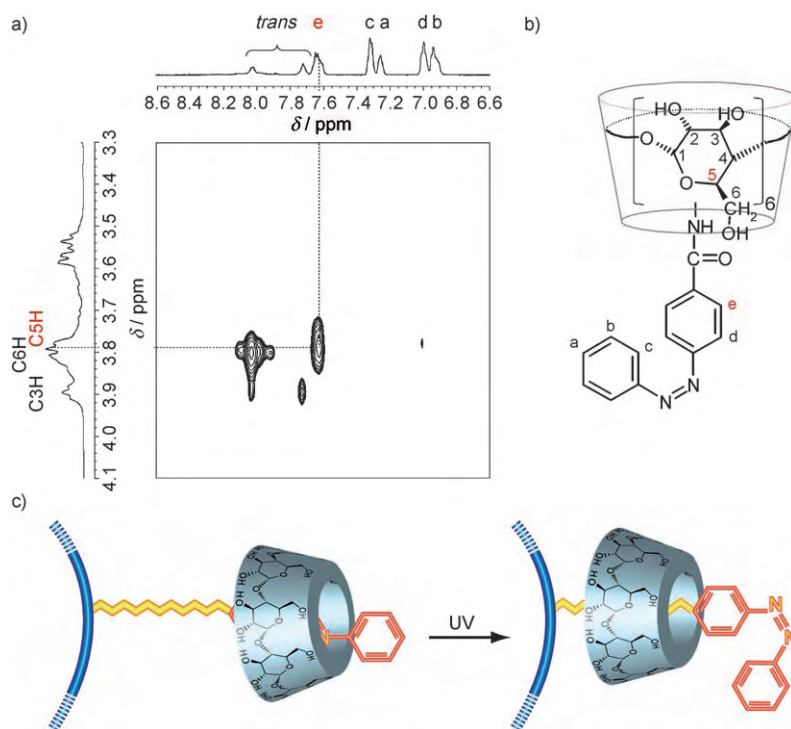


**Figure 4.** Expanded 2D NOESY spectra of a solution of pC<sub>12</sub>Azo (10 g L<sup>-1</sup>) in the presence of  $\alpha$ -CD (10 g L<sup>-1</sup>) measured after UV irradiation (a). Schematic representation of side-chain polyrotaxane with unidirectional inclusion (b) and (c).

UNITY INOVA 750 NMR spectrometer at 25 °C. Diffusion constants were calculated using the direct exponential curve resolution algorithm and the maximum entropy method. The experimental details are described elsewhere.<sup>[13]</sup>

**UV/Vis absorption spectroscopy:** UV/Vis absorption spectra were recorded with a Shimadzu UV-2500PC spectrophotometer using a 1-cm path length quartz cuvette. Sample solutions were prepared with a carbonate buffer solution containing 0.05 M sodium carbonate and 0.05 M sodium bicarbonate, and the solution was heated at 60 °C for 1 day.

**Photoisomerization:** pC<sub>6</sub>Azo and pC<sub>12</sub>Azo were isomerized from *trans* to *cis* isomers by UV irradiation with a 500-W Xe lamp (Ushio Inc.) equipped with a cutoff filter (Hoya UV34) and a band-pass filter (Hoya U340). The distance between the sample cell and the lamp was fixed at 40 cm.

Received: March 20, 2006

Published online: June 22, 2006

**Keywords:** cyclodextrins · inclusion compounds · polymers · rotaxanes · supramolecular chemistry

- [1] For example: a) G. Wenz, B.-H. Han, A. Müller, *Chem. Rev.* **2006**, *106*, 782–817; b) “Supramolecular Technology”: J. L. Atwood, J. E. D. Davies, D. D. MacNicol, F. Vögtle, J.-M. Lehn in *Comprehensive Supramolecular Chemistry*, Vol. 10 (Ed.: D. N. Reinhoudt), Pergamon, Oxford, UK, **1996**.
- [2] For example: F. M. Raymo, J. F. Stoddart, *Chem. Rev.* **1999**, *99*, 1643–1664.
- [3] I. Yamaguchi, K. Osakada, T. Yamamoto, *Macromolecules* **1997**, *30*, 4288–4294.
- [4] a) M. Born, H. Ritter, *Makromol. Chem. Rapid Commun.* **1991**, *12*, 471–476; b) M. Born, T. Koch, H. Ritter, *Acta Polym.* **1994**,



- 45, 68–72; c) H. Ritter, *Angew. Makromol. Chem.* **1994**, 223, 165–175; d) M. Born, H. Ritter, *Angew. Chem.* **1995**, 107, 342–344; *Angew. Chem. Int. Ed. Engl.* **1995**, 34, 309–311; e) M. Born, T. Koch, H. Ritter, *Macromol. Chem. Phys.* **1995**, 196, 1761–1767; f) M. Born, H. Ritter, *Adv. Mater.* **1996**, 8, 149–151; g) M. Born, H. Ritter, *Macromol. Rapid Commun.* **1996**, 17, 197–202; h) O. Noll, H. Ritter, *Macromol. Rapid Commun.* **1997**, 18, 53–58; i) O. Noll, H. Ritter, *Macromol. Chem. Phys.* **1998**, 199, 791–794.
- [5] For example: a) A. Harada, H. Adachi, Y. Kawaguchi, M. Kamachi, *Macromolecules* **1997**, 30, 5181–5182; b) A. Harada, F. Ito, I. Tomatsu, K. Shimoda, A. Hashidzume, Y. Takashima, H. Yamaguchi, S. Kamitori, *J. Photochem. Photobiol. A* **2006**, 179, 13–19; c) I. Tomatsu, A. Hashidzume, A. Harada, *Macromol. Rapid Commun.* **2006**, 27, 238–241; d) A. Hashidzume, A. Harada, *Polymer* **2006**, 47, 3448–3454.
- [6] a) I. Tomatsu, A. Hashidzume, A. Harada, *Macromol. Rapid Commun.* **2005**, 26, 825–829; b) I. Tomatsu, A. Hashidzume, A. Harada, *Macromolecules* **2005**, 38, 5223–5227.
- [7] A. J. Baer, D. H. Macartney, *Org. Biomol. Chem.* **2005**, 3, 1448–1452.
- [8] T. Oshikiri, Y. Takashima, H. Yamaguchi, A. Harada, *J. Am. Chem. Soc.* **2005**, 127, 12186–12187.
- [9] For example: a) F. Cramer, H. Hettler, *Naturwissenschaften* **1967**, 54, 625–632; b) P. Bortolus, S. Monti, *J. Phys. Chem.* **1987**, 91, 5046–5050.
- [10] T. Ikeda, T. Ooya, N. Yui, *Polym. J.* **1999**, 31, 658–663.
- [11] K. T. Wang, I. Iliopoulos, R. Audebert, *Polym. Bull.* **1988**, 20, 577–582.
- [12] I. Tomatsu, A. Hashidzume, A. Harada, *J. Am. Chem. Soc.* **2006**, 128, 2226–2227.
- [13] T. Kanematsu, T. Sato, Y. Imai, K. Ute, T. Kitayama, *Polym. J.* **2005**, 37, 65–73.

## Inorganic Nanoplates

DOI: 10.1002/anie.200601031

Synthesis, Optical Properties, and Self-Assembly of Ultrathin Hexagonal  $\text{In}_2\text{S}_3$  Nanoplates\*\*

Kang Hyun Park, Kwonho Jang, and Seung Uk Son\*

Anisotropic nonspherical nanomaterials have attracted a special attention in material science because of their unique chemical, physical, and optical properties, which are greatly

affected by their shape and size.<sup>[1]</sup> Thus, many efforts have been made to synthesize nanorods and nanowires.<sup>[2]</sup> Compared with one-dimensional (1D) structures, 2D nanomaterials such as nanoplates and nanodisks have been relatively little explored and require further investigation. To date the following nanoplates have been prepared: hexagonal<sup>[3]</sup> ( $\text{Co}(\text{OH})_2$ ,  $\text{Cu}_2\text{S}$ ,  $\text{SbTe}_3$ ,  $\text{Bi}_2\text{Te}_3$ , etc.), trigonal<sup>[4]</sup> ( $\text{Au}$ ,  $\text{Ag}$ ,  $\text{Pd}$ ,  $\text{Bi}$ ,  $\text{Se}$ ,  $\text{LaF}_3$ , etc.), square<sup>[5]</sup> (rare earth metals,  $\text{Bi}_2\text{WO}_6$ , etc.), and circular<sup>[6]</sup> ( $\text{Ag}$ ,  $\text{Co}$ , etc.).

Over the last two decades, the chemical and physical properties of diverse semiconductor nanocrystals have been investigated.<sup>[7]</sup> Compared to the corresponding conventional bulk materials, semiconductor nanomaterials show unique optical, mechanical, electronic, and catalytic properties which are highly dependent on size and shape. Of the known semiconductor nanomaterials, perhaps the semiconducting metal chalcogenides have been studied most widely. In particular, most studies have focused on II–VI quantum dots (QDs) such as  $\text{CdS}$ ,  $\text{ZnS}$ , and  $\text{CdSe}$ .<sup>[8]</sup> Moreover, I–VI QDs such as  $\text{Ag}_2\text{S}$  and  $\text{Cu}_2\text{S}$  have received significant attention.<sup>[9]</sup> Compared with the semiconductor nanomaterials mentioned above, the optical and electronic properties of metal chalcogenides which have 1:1.5 molar ratio of metal to chalcogenide in their unit cells have received comparatively little attention. These include  $\text{In}_2\text{S}_3$ ,  $\text{Bi}_2\text{S}_3$ , and  $\text{Sb}_2\text{S}_3$  nanocrystals.<sup>[10]</sup>

Indium sulfide ( $\text{In}_2\text{S}_3$ ) exists in three different crystalline forms:  $\alpha$ - $\text{In}_2\text{S}_3$  (defect cubic),  $\beta$ - $\text{In}_2\text{S}_3$  (defect spinel), and  $\gamma$ - $\text{In}_2\text{S}_3$  (layered structure).<sup>[11]</sup> Of these,  $\beta$ - $\text{In}_2\text{S}_3$  is an n-type semiconductor with a band gap of 2.0–2.3 eV and is stable above 420 °C.<sup>[12]</sup> Moreover, the unique luminescence properties of  $\beta$ - $\text{In}_2\text{S}_3$  have enabled its use as a phosphor in display devices.<sup>[13]</sup> Furthermore, its photoconductive properties<sup>[14]</sup> make it a promising candidate for photovoltaic applications such as solar cells. Recently, it was reported that solar cell devices prepared by using  $\beta$ - $\text{In}_2\text{S}_3$  as a buffer layer show 16.4 % conversion efficiency, which is very close to that of the standard  $\text{CdS}$  buffer layer.<sup>[15]</sup> Much effort has been made to replace highly toxic cadmium with other metals for environmental reasons.<sup>[16]</sup>

A number of synthetic methods<sup>[17]</sup> have been developed to prepare  $\beta$ - $\text{In}_2\text{S}_3$ , for example, direct reacting of the elements at high temperature, heating  $\text{In}_2\text{O}_3$  in  $\text{H}_2\text{S}$ , thermal decomposition of organometallic precursors, and metathesis reaction between  $\text{InCl}_3$  and  $\text{Li}_2\text{S}$ . To fabricate thin films of  $\beta$ - $\text{In}_2\text{S}_3$  for solar cell applications, several deposition techniques, such as organometallic chemical deposition, spray pyrolysis, and chemical bath deposition, have been developed.<sup>[18]</sup>  $\beta$ - $\text{In}_2\text{S}_3$  can also be prepared by a wet chemical approach,<sup>[19]</sup> that is, by reaction between aqueous  $\text{InCl}_3$  and  $\text{H}_2\text{S}$ ,  $(\text{NH}_4)_2\text{S}$ , or  $\text{NaSH}$ ; by laser-induced formation of  $\text{In}_2\text{S}_3$  from sodium polysulfide in aqueous solution; by using red light and  $\text{Na}_2\text{S}$ ; by forming colloidal particles in reverse micelles; by injecting  $\text{H}_2\text{S}$  into  $\text{In}(\text{ClO}_4)_3$  solution; by hydrothermal treatment of an acidic sol of  $\text{InCl}_3$  and  $\text{Na}_2\text{S}$ ; or by sonochemical synthesis from  $\text{InCl}_3$  and  $\text{MeCSNH}_2$ . Recently, 3-nm  $\beta$ - $\text{In}_2\text{S}_3$  nanocrystals were prepared by an arrested-precipitation method using aqueous  $\text{InCl}_3$  solution and a thiol stabilizer.<sup>[20]</sup> However, as far as we are aware, the synthesis of  $\beta$ - $\text{In}_2\text{S}_3$  in organic media

[\*] Dr. K. H. Park, K. Jang, Prof. S. U. Son  
Department of Chemistry  
Sungkyunkwan University  
Suwon 440-746 (Korea)  
Fax: (+82) 31-299-4572  
E-mail: sson@skku.edu

[\*\*] This work was supported by the Korea Research Foundation Grant funded by the Korean Government (MOEHRD, KRF-2005-005J11901) and through a Faculty Research Fund-2005 funded by Sungkyunkwan University. We thank J. S. Ju at Cooperative Center for Research Facilities at Sungkyunkwan University for TEM studies.



Supporting information for this article is available on the WWW under <http://www.angewandte.org> or from the author.

has received little attention, although it is well recognized that various organic surfactants can be excellent reaction media for synthesis of high-quality nanocrystals.<sup>[21]</sup>

Herein we report on the synthesis of monodisperse hexagonal  $\beta$ - $\text{In}_2\text{S}_3$  nanoplates of 0.76-nm thickness in organic media at high temperature by using the arrested-precipitation method. In a typical synthesis, oleylamine was used as a stabilizer and solvent. Anhydrous  $\text{InCl}_3$  and sulfur powder were dissolved in well-dried oleylamine (9–18 mL), and the mixture was then heated to 215 °C and held at this temperature for 1 h. A bright yellow precipitate formed during the aging step. The TEM images of these precipitates revealed hexagonal nanoparticles (Figure 1 a–c). More detailed TEM

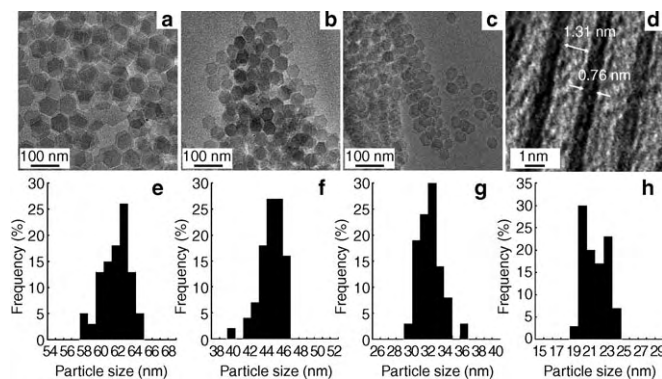


**Figure 1.** TEM images of a) 63-nm, b) 45-nm, and c) 33-nm  $\beta$ - $\text{In}_2\text{S}_3$  nanoplates; d) side view of nanoplates; and histograms illustrating the particle size distributions for e) 63-nm, f) 45-nm, g) 33-nm, and h) 22-nm  $\beta$ - $\text{In}_2\text{S}_3$  nanoplates.

investigation showed the synthesized nanoparticles to have a hexagonal plate form. Side views of these plates were obtained on grids, and high-resolution (HR) TEM revealed a plate thickness of 0.76 nm (Figure 1 d), which makes them, as far as we are aware, the thinnest nanoplates known.<sup>[22]</sup>

Moreover, by changing the concentration of the precursor in oleylamine, we were able to control the size of these hexagonal nanoplates, as shown in Figures 1 a–c and e–h. Using 0.10 M precursor solution, we obtained 63-nm hexagonal nanoplates, and when its concentration was reduced to 0.050 M, the nanoplate size decreased to 45 nm. Also we obtained 33- and 22-nm hexagonal nanoplates using 0.025 M and 0.00125 M precursor solutions, respectively. Interestingly, the nanoplate thickness remained constant throughout the above experiments, and this implies that growth along one plane is much slower than along the others. Unfortunately, numerous trials to determine the retarded-growth direction by HRTEM were unsuccessful because of the extreme thinness of the plates. However, we could get some information about this retarded-growth direction from X-ray diffraction patterns.

Figure 2 shows representative powder X-ray diffraction (XRD) and electron diffraction (ED) patterns of 33-nm hexagonal nanoplates. The powder XRD patterns revealed three sharp peaks at 27.2, 47.9, and 55.8° originating from (109), (400), and (533), which are very close to those reported for  $\beta$ - $\text{In}_2\text{S}_3$  (JCPDS card 25-390).<sup>[23]</sup> From the Debye–Scherrer

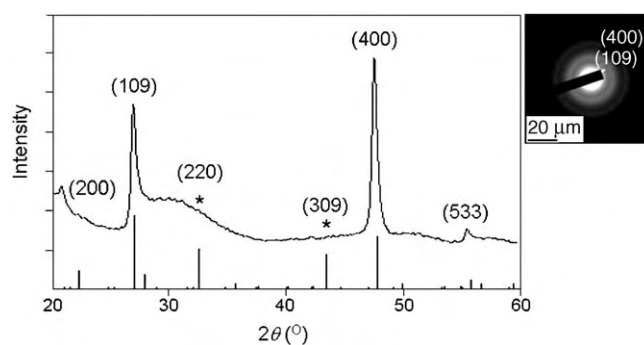


**Figure 2.** Powder XRD (left) and ED (right) patterns of 33-nm  $\text{In}_2\text{S}_3$  nanoplates.

equation, the size of the nanoplates was calculated to be 37 nm from the half-width of the (400) diffraction peak, which is consistent with the size determined by TEM. We could not find the (220) and (309) diffraction peaks, which were expected at 32 and 44° correspondingly. According to a library spectrum<sup>[23]</sup> of bulk  $\beta$ - $\text{In}_2\text{S}_3$ , the (220) and (309) peaks should be of high intensity. Thus, we suggest that the retarded growth direction may be related to these two lattice planes. The ED pattern shows two broad diffraction circles, which correspond to  $d$  spacings of 3.10 and 1.94 Å, respectively. These are consistent with the literature values of 3.241 and 1.912 Å originating from the (109) and (400) reflections of  $\beta$ - $\text{In}_2\text{S}_3$ .<sup>[23]</sup>

To confirm the chemical stoichiometry of the synthesized nanoplates, we performed energy dispersive spectroscopy (EDS) for indium and sulfur on four samples. All samples showed In:S = 1:1.5 (see Supporting Information for EDS spectra of all samples). Figure 3 shows a representative EDS spectrum of 45-nm nanoplates. It is noteworthy that  $\text{In}_2\text{S}_3$  remained the sole product when the amount of sulfur was reduced to 0.075 equivalents versus indium.

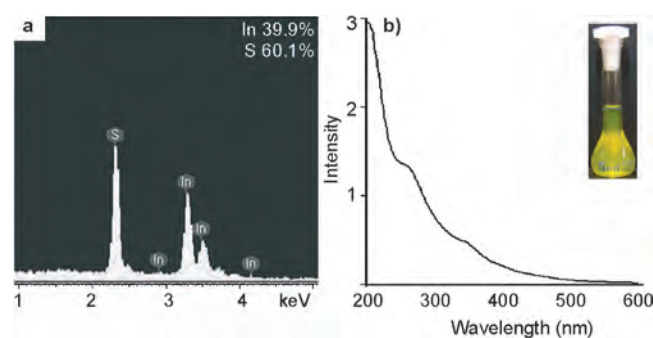


**Figure 3.** a) EDS and b) UV/Vis absorption spectra of 45-nm  $\text{In}_2\text{S}_3$  nanoplates, inset: photo of sample.

We carried out UV/Vis absorption and photoluminescence (PL) studies to investigate the optical properties of the ultrathin hexagonal nanoplates. Dispersed hexane solutions of nanoplates had a slightly luminescent yellow color (inset in Figure 3 b). Figure 3 b shows a representative UV/Vis absorption spectrum of 45-nm hexagonal nanoplates. Compared to the absorption peak of 3.0-nm nanoparticles,<sup>[20]</sup> that of 45-nm

nanoplates was red-shifted by 30 nm. In addition, the UV/Vis spectra of nanoplates showed a steplike shape, which was mentioned to be an indicator of conduction and valence band transition in  $\beta\text{-In}_2\text{S}_3$ .<sup>[20]</sup> Interestingly, we observed no significant differences between the UV/Vis spectra of 63-, 45-, 33-, and 22-nm nanoplates (see Supporting Information for UV/Vis spectra of 63-, 45-, and 22-nm nanoplates), which implies that the sizes (22–63 nm) of the nanoplates are beyond the quantum confinement range. Detailed optical characterizations including emission, quantum yields, and decay kinetics will be reported elsewhere. In addition, the electroluminescence properties of nanoplates will be characterized after layering on indium tin oxide (ITO)/glass by the Langmuir–Blodgett technique.

For applications in various optical devices, including solar cells, thin-film fabrication techniques are needed.<sup>[18]</sup> Since the hexagonal nanoplates are extremely thin, we believe that these nanomaterials can be used as building blocks to prepare subnanometer films by self-assembly. The high surface area of the 2D nanoplates, as compared with 0D or 1D nanomaterials, is interesting from the aspect of self-assembly behavior. Recently, the formation of spherulike macrostructures by self-assembly of hexagonal nanoplates was reported.<sup>[24]</sup>

Hexagonal  $\text{In}_2\text{S}_3$  nanoplates showed two self-assembly patterns in TEM studies: parallel alignment to a solid support and upright alignment due to interactions with other nanoplates. Interestingly, these self-assembly behaviors depend on nanoplate size and concentration. When nanoplate size was reduced from 63 to 22 nm, upright alignment was favored, and when the concentration of nanoplates in the mother solution was reduced, parallel alignment was favorable, as sketched in Figure 4.

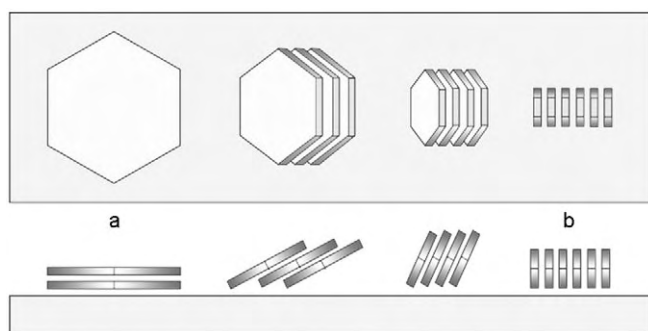


**Figure 4.** Sketch of size-dependent self-assembly of  $\text{In}_2\text{S}_3$  nanoplates. a) Parallel alignment and b) upright alignment.

The 63-nm nanoplates showed a preference toward parallel alignment to a solid support (Figure 5a), and we also observed a regular parallel packing structure (Figure 5b). For 45-nm nanoplates, the self-assembly process was strongly concentration dependent. When we used a dilute solution (ca. 5 mg of nanoplates in 2 mL of dichloromethane) to induce self-assembly by drop casting on a grid, we observed substantial parallel alignment to the solid support (Figure 5c). In some regions of the grid, we observed both parallel and upright alignments of 45-nm nanoplates (Figure 5d). When we used a relatively concentrated sample of 45-nm nanoplates

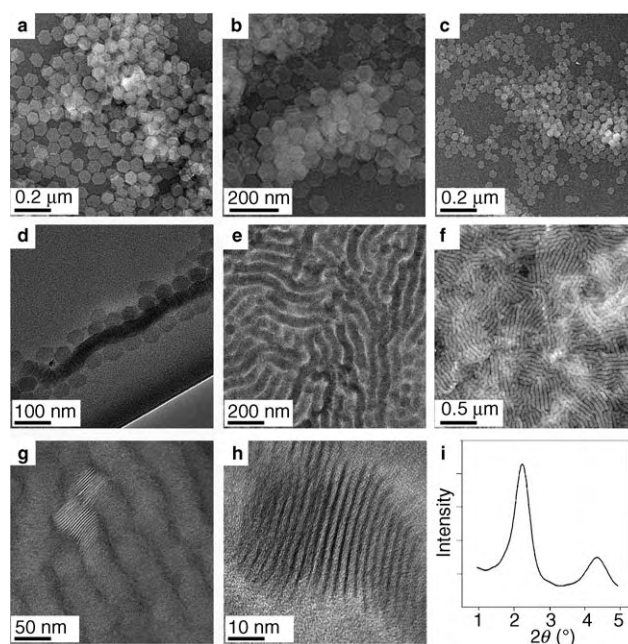


**Figure 5.** TEM images of a, b) parallel-aligned 63-nm nanoplates, c–f) 45-nm nanoplates at relatively low (c, d) and high (e, f) concentration, and g, h) 33-nm nanoplates at relatively high concentration; i) low-angle powder XRD pattern of self-assembled 45-nm nanoplates.

(ca. 20 mg in 1 mL of dichloromethane), we observed upright alignment in almost all regions (Figure 5e, f). In the case of 33- and 22-nm nanoplates, the upright alignment was strongly favored. It can be speculated that this behavior is due to greater attraction between larger nanoplates and the carbon film on the grid. Interestingly, more hexagonal nanoplates which are perpendicular to the surface of the grid (parallel to electron beam of the TEM) were observed for 33- and 22-nm nanoplates. (Figure 5g, h) Using HRTEM, we measured the thicknesses of and the distances between aligned nanoplates. The inside distance between two aligned nanoplates was about 1.3 nm and nanoplate thickness was 0.76 nm. (Figure 1d) Low-angle powder XRD studies also provided information about distances in the self-assembled structures. The two peaks in the low-angle XRD pattern in Figure 5i correspond to 2.7 and 1.3 nm, which agree well with the results of HRTEM studies. This understanding of the self-assembly behavior of nanoplates could be helpful for future applications of these materials to photovoltaic devices.

In conclusion, we have synthesized ultrathin hexagonal  $\beta\text{-In}_2\text{S}_3$  nanoplates of unprecedented thinness by an arrested-precipitation method from organic media and characterized them using TEM, powder XRD, and EDS studies. These nanoplates showed intriguing optical properties and self-assembly behavior.  $\beta\text{-In}_2\text{S}_3$  is a common material for solar cell applications,<sup>[18]</sup> and many efforts have been made to fabricate this material in thin-film form on a suitable support. The  $\beta\text{-In}_2\text{S}_3$  nanoplates are 0.76 nm thick and show size- and concentration-dependent self-assembly behavior. We are now trying to assemble a monolayer on a solid support such as ITO. We believe that these self-assembling nanoplates can



be used for the development of diverse ultrathin nano-devices,<sup>[25]</sup> such as solar cells.

## Experimental Section

All spectroscopic studies were performed on as-prepared nanoplates without employing any size-selection process. TEM and HRTEM images were recorded with a JEOL 2100F unit operated at 200 kV. The self-assembly of nanoplates was carried out on carbon-coated copper grids by drop casting nanoplates dispersed in dichloromethane. EDS was performed on a FE-SEM (JSM6700F). Powder XRD patterns were obtained on a Rigaku MAX-2200 with filtered Cu<sub>Kα</sub> radiation. UV/Vis absorption spectra of hexagonal nanoplates were recorded on a Jasco V-500 spectrophotometer. For UV/Vis experiments, solutions of 4 mg of nanoplates in hexane (HPLC grade, Burdick & Jackson, 100 mL) were used.

In a typical synthetic procedure, anhydrous InCl<sub>3</sub> and 1.5 equivalents of sulfur powder were added to 9–18 mL of oleylamine. After heating the mixture at 110°C for 1 h, the temperature was increased to 215°C and held for 1 h. After cooling the solution to 35°C, methanol was added to the reaction mixture and the precipitate formed was retrieved by centrifugation. After repeating this washing procedure twice, the obtained precipitates were dried under vacuum. Using 0.10, 0.050, 0.025, 0.0125 M solutions of indium chloride in oleylamine, we obtained 63-, 45-, 33-, and 22-nm hexagonal nanoplates.

Received: March 15, 2006

Published online: June 22, 2006

**Keywords:** indium · nanostructures · self-assembly · semiconductors · sulfur

- [1] Selected literature: a) J. T. Hu, T. W. Odom, C. M. Lieber, *Acc. Chem. Res.* **1999**, 32, 435; b) Y. Sun, Y. Xia, *Science* **2002**, 298, 2176; c) B. Nikoobakht, M. A. El-Sayed, *Chem. Mater.* **2003**, 15, 1957; d) special issue on nanowires: *Adv. Mater.* **2003**, 15, 351–466.
- [2] a) Y. Cui, C. M. Lieber, *Science* **2001**, 291, 851; b) M. Huang, S. Mao, H. Feick, H. Yan, Y. Wu, H. Kind, E. Weber, R. Russo, P. Yang, *Science* **2001**, 292, 1897; c) T. Hanrath, B. A. Korgel, *J. Am. Chem. Soc.* **2002**, 124, 1424; d) F. Dumestre, B. Chaudret, C. Amiens, M.-C. Fromen, M.-J. Casanove, M. Respaud, P. Zurcher, *Angew. Chem.* **2002**, 114, 4462; *Angew. Chem. Int. Ed.* **2002**, 41, 4286; e) W. U. Huynh, J. J. Dittmer, A. P. Alivisatos, *Science* **2002**, 295, 2425; f) C. Qian, F. Kim, L. Ma, F. Tsui, P. Yang, J. Liu, *J. Am. Chem. Soc.* **2004**, 126, 1195.
- [3] a) M. B. Sigman, Jr., A. Ghezelbash, T. Hanrath, A. E. Sanuders, F. Lee, B. A. Korgel, *J. Am. Chem. Soc.* **2003**, 125, 16050; b) H.-T. Zhang, G. Wu, X.-H. Chen, *Langmuir* **2005**, 21, 4281; c) W. Wang, B. Poudel, J. Yang, D. Z. Wang, Z. F. Ren, *J. Am. Chem. Soc.* **2005**, 127, 13792; d) Y. Hou, H. Kondoh, M. Shimojo, T. Kogure, T. Ohta, *J. Phys. Chem. B* **2005**, 109, 19094; e) W. Lu, Y. Ding, Y. Chen, Z. L. Wang, J. Fang, *J. Am. Chem. Soc.* **2005**, 127, 10112; f) S. S. Garje, D. J. Eisler, J. S. Ritch, M. Afzaal, P. O'Brien, T. Chivers, *J. Am. Chem. Soc.* **2006**, 128, 3120.
- [4] a) S. Chen, D. L. Carroll, *J. Phys. Chem. B* **2004**, 108, 5500; b) Y.-W. Zhang, X. Sun, R. Si, L.-P. You, C.-H. Yan, *J. Am. Chem. Soc.* **2005**, 127, 3260; c) Y. He, G. Shi, *J. Phys. Chem. B* **2005**, 109, 17503; d) Y. Xiong, J. M. McLellan, J. Chen, Y. Yin, Z.-Y. Li, Y. Xia, *J. Am. Chem. Soc.* **2005**, 127, 17118; e) K. Aslan, J. R. Lakowicz, C. D. Geddes, *J. Phys. Chem. B* **2005**, 109, 6247; f) B. Liu, J. Xie, J. Y. Lee, Y. P. Ting, J. P. Chen, *J. Phys. Chem. B* **2005**, 109, 15256.
- [5] a) Y. C. Cao, *J. Am. Chem. Soc.* **2004**, 126, 7456; b) R. Si, Ya.-W. Zhang, L.-P. You, C.-H. Yan, *Angew. Chem.* **2005**, 117, 3320; *Angew. Chem. Int. Ed.* **2005**, 44, 3256; c) T. Yu, J. Joo, Y. I. Park, T. Hyeon, *J. Am. Chem. Soc.* **2006**, 128, 1786.
- [6] a) V. F. Puentes, K. M. Krishnan, A. P. Alivisatos, *Science* **2001**, 291, 2115; b) V. F. Puentes, D. Zanchet, C. K. Erdonmez, A. P. Alivisatos, *J. Am. Chem. Soc.* **2002**, 124, 12874; c) S. Chen, Z. Fan, D. L. Carroll, *J. Phys. Chem. B* **2002**, 106, 10777.
- [7] a) H. Weller, *Angew. Chem.* **1993**, 105, 43; *Angew. Chem. Int. Ed. Engl.* **1993**, 32, 41; b) A. P. Alivisatos, *J. Phys. Chem.* **1996**, 100, 13226; c) S. Empedocles, M. Bawendi, *Acc. Chem. Res.* **1999**, 32, 389; d) M. Nirmal, L. Brus, *Acc. Chem. Res.* **1999**, 32, 407; e) Z. A. Peng, X. Peng, *J. Am. Chem. Soc.* **2002**, 124, 3343; f) D. J. Milliron, S. M. Hughes, Y. Cui, L. Manna, J. Li, L.-W. Wang, A. P. Alivisatos, *Nature* **2004**, 430, 190.
- [8] Selected examples: a) Z. A. Peng, X. Peng, *J. Am. Chem. Soc.* **2001**, 123, 183; b) Y.-W. Jun, S.-M. Lee, N.-J. Kang, J. Cheon, *J. Am. Chem. Soc.* **2001**, 123, 5150; c) J. Joo, H. B. Na, T. Yu, J. H. Yu, Y. W. Kim, F. Wu, J. Z. Zhang, T. Hyeon, *J. Am. Chem. Soc.* **2003**, 125, 11100; d) Y. C. Cao, J. Wang, *J. Am. Chem. Soc.* **2004**, 126, 14336.
- [9] a) L. Motte, M. P. Pileni, *J. Phys. Chem. B* **1998**, 102, 4104; b) X. Wen, W. Zhang, S. Yang, Z. R. Dai, Z. L. Wang, *Nano Lett.* **2002**, 2, 1397; c) L. Chen, Y.-B. Chen, L.-M. Wu, *J. Am. Chem. Soc.* **2004**, 126, 16334; d) Z. Liu, D. Xu, J. Liang, J. Shen, S. Zhang, Y. Quan, *J. Phys. Chem. B* **2005**, 109, 10699.
- [10] a) N. M. Dimitrijevic, P. V. Kamat, *Langmuir* **1987**, 3, 1004; b) R. Vogel, P. Hoyer, H. Weller, *J. Phys. Chem.* **1994**, 98, 3183; c) R. Suarez, P. K. Nair, P. V. Kamat, *Langmuir* **1998**, 14, 3236.
- [11] a) R. Diehl, R. Nitsche, *J. Cryst. Growth* **1975**, 28, 306; b) S.-H. Yu, L. Shu, Y.-S. Wu, J. Yang, Y. Xie, Y.-T. Qian, *J. Am. Ceram. Soc.* **1999**, 82, 457.
- [12] T. Asikainen, M. Ritala, M. Leskela, *Appl. Surf. Sci.* **1994**, 82/83, 122.
- [13] a) Japanese patent application, *Chem. Abstr.* **1981**, 95, 107324x; b) S. Yu, L. Shu, Y. Qian, Y. Xie, J. Yang, L. Yang, *Mater. Res. Bull.* **1998**, 33, 717.
- [14] a) W.-T. Kim, C.-D. Kim, *J. Appl. Phys.* **1986**, 60, 2631; b) R. Nomura, S. Inazawa, K. Kanaya, H. Matsuda, *Appl. Organomet. Chem.* **1989**, 3, 195.
- [15] a) E. Dalas, S. Sakkopoulos, E. Vitoratos, G. Maroulis, L. Kobotiatas, *J. Mater. Sci.* **1993**, 28, 5456; b) N. Naghavi, S. Spiering, M. Powalla, B. Cavana, D. Lincot, *Prog. Photovoltaics Res. Appl.* **2003**, 11, 437; c) J. Sterner, J. Malmstrom, L. Stolt, *Prog. Photovoltaics Res. Appl.* **2005**, 13, 179.
- [16] a) D. Braunger, D. Hariskos, T. Walter, H. W. Schock, *Solar Energy Mater. Solar Cells* **1996**, 40, 97; b) A. Ennaoui, C. D. Lokhande, M. Weber, R. Scheer, H. J. Lawrenz, *14th European Photovoltaic Solar Energy Conference (EPSEC)*, Barcelona, **1997**.
- [17] a) H. B. Richard, H. M. William, *J. Phys. Chem. Solids* **1959**, 10, 333; b) C. Kaito, Y. Saito, K. Fujita, *J. Cryst. Growth* **1989**, 94, 967; c) J. C. Fitzmaurice, I. P. Parkin, *Main Group Met. Chem.* **1994**, 17, 481.
- [18] a) R. Nomura, K. Konishi, H. Matsuda, *Thin Solid Films* **1991**, 198, 339; b) C. D. Lokhande, A. Ennaoui, P. S. Patil, M. Giersig, K. Diesner, M. Muller, H. Tributsch, *Thin Solid Films* **1999**, 340, 18.
- [19] a) P. N. Kumta, P. P. Phule, S. H. Risbud, *Mater. Lett.* **1987**, 5, 401; b) P. V. Kamat, N. M. Dimitrijevic, R. W. Fessenden, *J. Phys. Chem.* **1988**, 92, 2324; c) Y. Nosaka, N. Ohta, H. Miyama, *J. Phys. Chem.* **1990**, 94, 3752; d) S. Avivi, O. Palchik, W. Palchick, M. A. Slifkin, A. M. Weiss, A. Gedanken, *Chem. Mater.* **2001**, 13, 2195.
- [20] D. K. Nagesha, X. Liang, A. A. Mamedov, G. Gainer, M. A. Eastman, M. Giersig, J.-J. Song, T. Ni, N. A. Kotov, *J. Phys. Chem. B* **2001**, 105, 7490.
- [21] a) S. U. Son, Y. Jang, J. Park, H. B. Na, H. M. Park, H. J. Yun, J. Lee, T. Hyeon, *J. Am. Chem. Soc.* **2004**, 126, 5026; b) S. U. Son, U. K. Park, J. Park, T. Hyeon, *Chem. Commun.* **2004**, 778;

- c) S. U. Son, Y. Jang, K. Y. Yoon, C. An, Y. Hwang, J.-G. Park, H.-J. Noh, J.-Y. Kim, J.-H. Park, T. Hyeon, *Chem. Commun.* **2005**, 86.
- [22] For  $\beta$ - $\text{In}_2\text{S}_3$ , the parameters of the tetragonal crystal lattice are  $a = b = 7.62 \text{ \AA}$ ,  $c = 32.32 \text{ \AA}$ .
- [23] Powder Diffraction File Sets 1–5 (Revised), Joint Committee on Powder Diffraction Standards, Philadelphia, **1967**, pp. 5-0729–5-0731.
- [24] Z. R. Tian, J. A. Voigt, J. Liu, B. McKenzie, M. J. Mcdermott, M. A. Rodriguez, H. Konishi, H. Xu, *Nat. Mater.* **2003**, 2, 821.
- [25] *Physics of Quantum Well Devices* (Ed.: B. R. Nag), Kluwer, Dordrecht, **2000**.

## Drug Delivery

DOI: 10.1002/anie.200504599

**Laser-Induced Release of Encapsulated Materials inside Living Cells\*\***

Andre G. Skirtach,\* Almudena Muñoz Javier,  
Oliver Kreft, Karen Köhler, Alicia Piera Alberola,  
Helmuth Möhwald, Wolfgang J. Parak,\* and  
Gleb B. Sukhorukov

Drug delivery into biological cells is an important and growing area of application.<sup>[1]</sup> Among other systems, such as gels,<sup>[2]</sup> polymeric micelles,<sup>[3]</sup> liposomes,<sup>[4a,b]</sup> and colloids,<sup>[4c]</sup> nanoengineered polyelectrolyte multilayer microcapsules<sup>[5]</sup>

offer a unique opportunity to combine surface multifunctionality with design flexibility for the delivery of encapsulated materials into designated compartments and cells.<sup>[6]</sup> Furthermore, microcapsules can be arranged in arrays for imaging,<sup>[7a,b]</sup> could be appropriate candidates for a cell-sorting system,<sup>[7c,d]</sup> and serve as fluorescence markers for the characterization of cells by fluorescence-activated cell sorting (FACS).<sup>[7e]</sup> The capsules are fabricated using the layer-by-layer (LbL) method<sup>[8]</sup> by alternately adsorbing oppositely charged polymers on colloidal templates followed by core dissolution. In this regard, proteins and biocompatible polymers have also received increased interest.<sup>[9]</sup> The main advantage of such a method is the precise control over the chemical composition of the surfaces.

In the area of biomedical applications, polyelectrolyte-multilayer capsules are envisioned for the delivery of encapsulated materials into biological cells.<sup>[6]</sup> Recently, we have presented the real-time monitoring and remote release of encapsulated materials from polyelectrolyte-multilayer capsules on the single-capsule level.<sup>[10]</sup> Such an approach<sup>[10]</sup> is different from the studies reported by other research groups<sup>[11]</sup> in that it is performed on a single-capsule level, which is the method ideally suited to applications where precise control is necessary. In addition, the distinctive feature reported in reference [10b] is the measurement of the temperature rise induced locally by absorption of laser light by nanoparticles.

In general, nanoparticles<sup>[12]</sup> are becoming ubiquitous components that link chemistry and physics with biology and biochemistry. They can be embedded in the walls of capsules to provide functionality,<sup>[6a]</sup> and they are also finding increasing interest for biological imaging.<sup>[13]</sup> Herein, we show that polyelectrolyte-multilayer capsules containing metallic nanoparticles in their walls can be remotely activated to release encapsulated material inside living cells. Fluorescently labeled polymers were chosen as a model system for encapsulated materials. The remote-release experiments were conducted according to the following scheme. The polyelectrolyte-multilayer shells were doped with metal nanoparticles, which served as absorption centers for energy supplied by a laser beam. These absorption centers cause local heating that disrupts the local polymer matrix and allows the encapsulated material to leave the interior of the capsule.

When using lasers with biological objects, it is important to minimize the absorption of laser light by cells and tissue. This can be accomplished by choosing the laser wavelength in the biologically "friendly" window<sup>[14a,b]</sup>—the near-infrared (NIR) part of the spectrum. Usually the spectral properties of water<sup>[14c]</sup> serve as a good criterion, as it constitutes 80–85 % of eukaryotic cells. Indeed, in water the temperature rise in the focus of a laser diode with wavelength 850 nm and operating at optical powers up to 100 mW during less than 1 s exposure time was reported to be under 1 K.<sup>[14d]</sup> Other important parameters that control the interaction of laser light with the absorption centers are the size of the nanoparticles and their concentration on the microcapsules.<sup>[10b]</sup> The concentration of metal nanoparticles plays an important role for two reasons: 1) when the distance between the two adjacent nanoparticles is of the order of their size, the thermal effects produced by

[\*] Dr. A. G. Skirtach, Dr. O. Kreft, K. Köhler, Prof. Dr. H. Möhwald, Prof. Dr. G. B. Sukhorukov  
Institut für Grenzflächen  
Max-Planck-Institut für Kolloid- und Grenzflächenforschung  
Am Mühlenberg 1, 14424 Golm/Potsdam (Germany)  
Fax: (+49) 331-567-9202  
E-mail: andre.skirtach@mpikg-golm.mpg.de

A. Muñoz Javier, A. Piera Alberola, Dr. W. J. Parak  
Center for NanoScience  
Ludwig-Maximilians-Universität München  
Amalienstrasse 54, 80799 München (Germany)  
Fax: (49) 89-2180-2050  
E-mail: wolfgang.parak@physik.uni-muenchen.de  
Prof. Dr. G. B. Sukhorukov  
IRC/Department of Materials  
Queen Mary University of London  
Mile End Road, London E1 4NS (UK)

[\*\*] We thank Dr. A. L. Rogach and Dr. A. S. Susa for providing nanoparticles, Annegret Praast for technical assistance, Anne Heilig for AFM measurements, and Rona Pitschke for TEM measurements. We gratefully acknowledge the Volkswagen-Stiftung (I/80-051-054) and the 6th FP EU projects STREP NMP3-CT-2005-516922 "SelectNANO" and STREP 01428 "NANOCAPS". Support by NATO grant no. CLG981299 and the Emmy Noether Program of the Deutsche Forschungsgemeinschaft is also acknowledged.

Supporting information for this article is available on the WWW under <http://www.angewandte.org> or from the author.

adjacent nanoparticles add up; and 2) the interaction of nanoparticles located in close proximity to each other results in an increase of absorption at lower energies or higher wavelengths (causing the so-called red shift) compared to the surface plasmon resonance band of stand-alone nanoparticles.<sup>[15]</sup> In this regard, spatial arrangement of the nanoparticles is essential<sup>[16a-c]</sup> and control of their distribution is paramount.<sup>[16d]</sup>

In the present studies we used silver nanoparticles<sup>[10a]</sup> for the remote activation of microcapsules, defined as deformation of their shape upon laser illumination, inside the cells. These nanoparticles were chosen because they provide dark contrast in transmission microscopy as a result of their high concentration on the capsules. Most of the silver nanoparticles were larger than 20 nm. These features lead to nonvanishing absorption<sup>[10a]</sup> in the NIR part of the spectrum as a consequence of dipolar and higher-order multipolar contributions<sup>[15b,c]</sup> and interaction between the nanoparticles.<sup>[15a]</sup> This finding is consistent with the visible–NIR spectral characteristics of silver nanoparticles with larger sizes<sup>[15b]</sup> located in clusters.<sup>[15c]</sup> Further studies were conducted of the release of encapsulated polymers from microcapsules containing gold and gold sulfide nanoparticles.<sup>[17]</sup> These nanoparticles absorb in the NIR part of the spectrum,<sup>[17]</sup> and the nature of the NIR absorption is the subject of continuing research.<sup>[17c]</sup>

Encapsulation of macromolecules can be performed, for example, by pH-controlled<sup>[18]</sup> swelling and shrinking of capsules<sup>[19]</sup> or with a matrix polyelectrolyte system.<sup>[20]</sup> We encapsulated an Alexa Fluor 488 (AF-488) dextran conjugate by a thermal<sup>[21]</sup> treatment method developed by Köhler et al.<sup>[21b]</sup> and based on the size reduction of strong polyelectrolyte sodium poly(styrene sulfonate)(PSS)/poly(diallyldimethylammonium chloride) (PDADMAC) microcapsules upon heating. Indeed, temperature was shown to affect the polyelectrolyte multilayers.<sup>[22]</sup> The heat-induced shrinking of microcapsules with a balanced charge ratio of polyelectrolytes is attributed to the reduced water/polyelectrolyte interface and subsequently lower surface energy.<sup>[21b]</sup> Therefore, the heat treatment of microcapsules applied in our study was accompanied by a reduction in size from about 4.5 to about 3  $\mu\text{m}$ , which entrapped the dextran.

Figure 1 presents AFM images of a typical dried capsule before and after heat treatment. Upon heat treatment, the thickness of the walls of the capsules increases from about 14 to about 42 nm. Furthermore, the polymers incorporated inside the capsules smooth the surfaces of their walls. Peaks and valleys in the range of 55–120 nm can be seen in the thermally treated capsules without encapsulated polymer (Figure 1d–f). In contrast, the thermally treated capsules containing encapsulated polymer exhibit a uniform thickness of about 40 nm. The presence of polymers inside the microcapsules leaves the average wall thickness virtually unchanged but alters the texture and reduces the roughness (Figure 1g–i). Nanoparticles embedded in the walls of the capsules can also be seen after heat treatment (inset to Figure 1i). The capsules were constructed on silica templates, which have a negligible effect on polyelectrolyte multilayers.<sup>[21b]</sup>

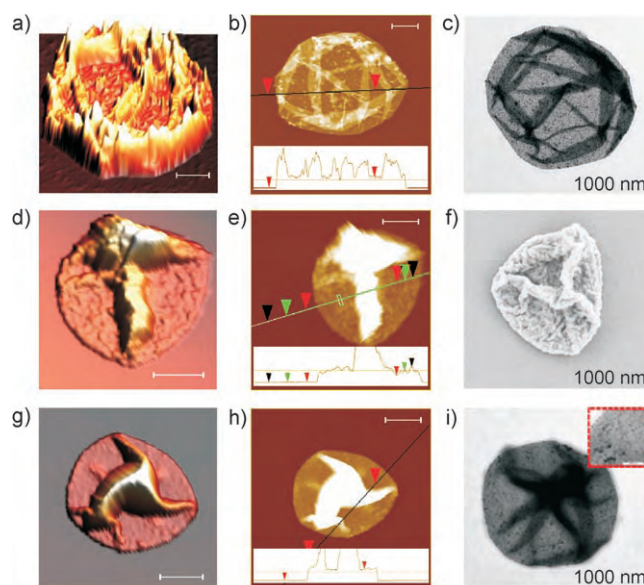


**Figure 1.** a,b) AFM and c) TEM images of (PSS/PDADMAC)<sub>4</sub> polyelectrolyte-multilayer capsules with gold and gold sulfide nanoparticles embedded in their walls before thermal treatment; the height marked by the red arrows in the inset to (b) corresponds to 28 nm. d,e) AFM and f) SEM images of a similar capsule after thermal treatment without encapsulated polymer; the heights marked by the green, red, and black arrows in the inset to (e) are 55, 87, and 120 nm, respectively. g,h) AFM and i) TEM images of a similar capsule after thermal treatment with encapsulated AF-488 dextran. The height marked by the red arrows in the inset to (h) is 82 nm; the inset to (i) shows a magnified area. All values for heights correspond to the double wall thickness. The scale bars in all images correspond to 1  $\mu\text{m}$ .

The mechanical properties of the polyelectrolyte microcapsules<sup>[23a–f]</sup> and multilayers<sup>[23g–j]</sup> have been the subject of extensive research. The studies conducted by AFM<sup>[23b,c]</sup> revealed that forces in the range of hundreds of piconewtons are sufficient to induce buckling of capsules that were not thermally treated. The study of the mechanical properties of thermally treated PSS/PDADMAC capsules at room temperature demonstrated<sup>[23e]</sup> that after heating for 20 min at 50 °C, the stiffness increased by four times (from  $\approx 220$  to  $\approx 870$   $\text{pN nm}^{-1}$ ) and, even more remarkably, by more than ten times (from  $\approx 220$  to  $\approx 2600$   $\text{pN nm}^{-1}$ ) upon heat treatment at 55 °C. Such an enhancement of the stiffness is attributed to the increase of the wall thickness that accompanies the heat shrinking. The improvement of the mechanical integrity of thermally treated capsules was also consistent with our observations,<sup>[6c]</sup> as the thickness of the walls has an important influence on the percentage of capsules that are deformed upon ingestion by cells. Capsules with thicker walls are less likely to be deformed, and are thus more suited to the delivery of encapsulated materials.

All encapsulation and release experiments were performed with the AF-488 dextran conjugate because it is significantly brighter and more photostable than other green fluorophores,<sup>[24a,b]</sup> which is a required condition for experiments under physiological conditions. The pH stability of encapsulated AF-488 dextran at different pH values was



investigated in comparison to that of fluorescein isothiocyanate (FITC) dextran (see Supporting Information), which is a commonly used, strongly pH-dependent, fluorescently labeled polymer that exists in four forms in solution.<sup>[24c–f]</sup> At pH > 5, both phenol and carboxylic groups of the FITC dye molecules are ionized, whereas at pH < 5 the majority of them are in their neutral or cationic, predominantly nonfluorescent, state. This results in decreasing fluorescence at lower pH values (see Supporting Information). A sharp contrast between the pH stability of AF-488 and FITC dextran is observed. Therefore, AF-488 can be used in experiments where stability is required, whereas FITC is intended for pH and other sensors. In addition, experiments were performed to determine both the mechanical integrity of capsules without nanoparticles and the photostability of encapsulated AF-488 dextran.

In fluorescent dyes the excitation from the ground state to the first singlet state  $S_1$  dominates the absorption processes,<sup>[25]</sup> while higher-order photon excitation may influence the signal only at high photon fluxes (typically with femtosecond lasers).<sup>[25b]</sup> The laser wavelength (830 nm) is located outside the 450–510 nm absorption band of AF-488 dextran (see Supporting Information). Notwithstanding this fact, a control experiment was conducted in which microcapsules without embedded nanoparticles were exposed to laser light with intensities and conditions similar to those used in the release studies (see Supporting Information). It served to test both the photostability (or exclude the possibility of photobleaching) and the mechanical integrity of microcapsules filled with AF-488 dextran but without nanoparticles in their walls upon laser excitation. Illumination was performed by a laser operating in the continuous wave (CW) mode at 830 nm with an incident intensity of 50 mW. Notably, although the laser operated in a CW mode, the shutter of the laser was opened for a short pulse (on the order of seconds or less) during the illumination. No fluorescence intensity changes were observed before and after illumination. In addition to test the photostability, this experiment also provides evidence that a capsule without nanoparticles is not deformed upon illumination with laser light. Note that the laser beam was directed from the top, thus pushing the capsule against the cover slide as a result of the radiation pressure of light<sup>[26]</sup> so that the capsule remained in the focus. Further studies were conducted with capsules containing nanoparticles in their walls.

Before the release studies, we performed experiments on the remote activation of capsules inside living cells. For this purpose, we fed living cells with capsules containing silver nanoparticles in their walls. These capsules were prepared according to the method described previously;<sup>[10a]</sup> they had no encapsulated material inside and were chosen for dark contrast in transmission. An ingested capsule was illuminated with a CW laser beam directed from the bottom and operating at 830 nm with a power of 50 mW. Figure 2 demonstrates that a capsule can be opened or activated remotely inside a cell. The rupture of the capsule (Figure 2c) demonstrates that a laser–nanoparticle interaction through thermal processes<sup>[10b]</sup> is responsible for its activation. Other processes, for example transport of protons or electron

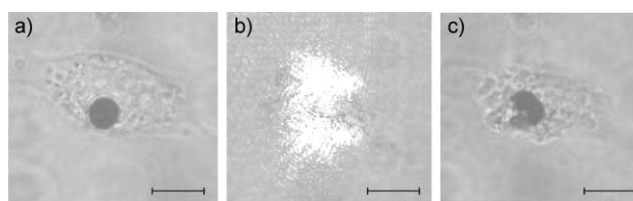


**Figure 2.** Remote activation of a capsule containing silver nanoparticles in its walls. The capsule was ingested by a living MDA-MB-435S cancer cell. The images show the cell before (a), during (b), and after (c) illumination with a laser. The scale bars correspond to 10  $\mu\text{m}$ .

redistribution around the nanoparticles,<sup>[27]</sup> do not determine the activation of and eventual release from microcapsules, because the polyelectrolyte multilayers were shown to be permeable for protons<sup>[24c]</sup> and the local redistribution of electrons cannot cause the rupture of the capsules. In the next step, release experiments were conducted with AF-488 dextran-filled capsules containing gold and gold sulfide nanoparticles in the walls.

Figure 3 demonstrates the release of encapsulated AF-488-labeled dextran inside a living cell upon laser illumination. The fluorescence image of the capsules is presented in

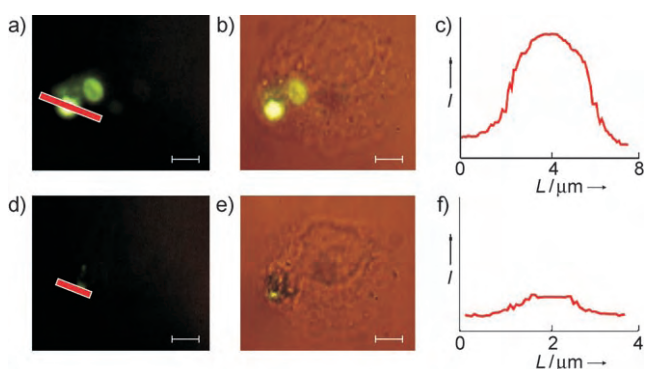


**Figure 3.** Sequence of images showing the release of fluorescent AF-488 dextran inside a living MDA-MB-435S cell. a) Fluorescence image of a filled capsule; b) superimposed fluorescence and transmission images of the capsule inside the same cell; c) fluorescence intensity  $I$  profile plotted along the length  $L$  of the red line in (a). d)–f) Similar data after exposure of the cell to a laser beam. The scale bars in all images correspond to 5  $\mu\text{m}$ .

Figure 3a, while Figure 3b shows the superimposed fluorescence and transmission signals from the same cell and the same capsules before illumination by laser light. The capsule appears filled (Figure 3c) before illumination. Similar images of the same capsule after illumination (Figure 3d–f) show that, although there is some leftover fluorescence in the walls of the capsules, most polymer molecules had left the interior of the capsule. The leftover fluorescence traces in the walls of the capsule are consistent with earlier reported experiments.<sup>[10b]</sup> Notably, the rise in temperature during laser illumination of capsules with embedded nanoparticles is several degrees and it is concentrated in the vicinity of the capsules.<sup>[10b]</sup> In our experiments, the cells adhered to the substrate both before and after the release of the encapsu-

lated polymer, which indicates that this method is feasible for the delivery of encapsulated materials into cells.

In the activation and release experiments, contrary to the photostability tests, the laser beam was directed from the bottom onto the chamber containing the living cells because of its design. In such a geometry, capsules not taken up by cells are pushed up by the laser beam and away from the field of view as a result of the radiation pressure of light.<sup>[26]</sup> This effect is demonstrated in Figure 4, which shows that capsules

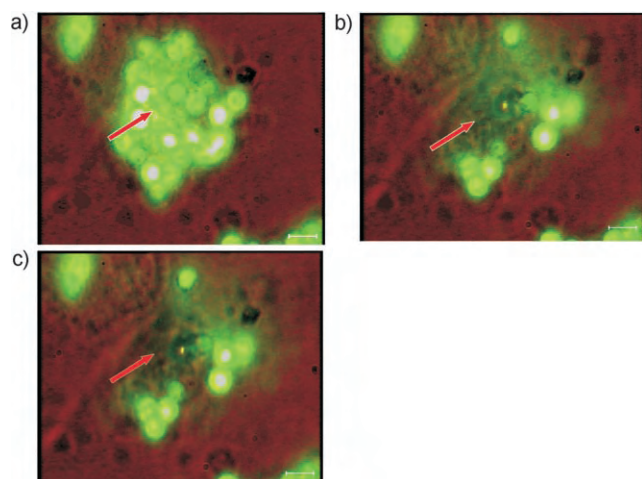


**Figure 4.** Fluorescence images demonstrating the lifting up of non-internalized capsules located on top of a living MDA-MB-435S cell above and away from the imaging plane or the focus a) before, b) during, and c) after the laser beam illuminated the chamber from the bottom. The capsules were lifted up with a laser power of 50 mW. The red arrows indicate the locations of the capsules that were lifted up. The scale bars in all images correspond to 5  $\mu\text{m}$ .

situated on top of a cell are pushed out of the field of view by the laser. Figure 4a shows that an agglomerate of capsules is located in the field of view slightly above the cell, whose contours can also be seen. Figure 4b shows the same cell and the same agglomerate of capsules during laser illumination, while Figure 4c presents the same cell after liftoff of the capsules. The agglomerate of the capsules is not a heavy aggregate, as part of it can still be seen in Figure 4c. Besides, the cell itself did not undergo changes, which is consistent with the data reported for the temperature rise during laser illumination.<sup>[14d]</sup> These experiments with “flying capsules” demonstrate that the release of encapsulated material can be carried out only from capsules internalized by the cells; capsules merely adherent to the outer membrane were lifted up and away from the imaging plane.

In conclusion, the release of encapsulated material from polyelectrolyte-multilayer capsules has been demonstrated inside living cells. Metal nanoparticles were incorporated inside the walls of the capsules, and served as energy-absorbing centers for illumination by laser light. AF-488 dextran was successfully incorporated into the capsules using a novel heat-shrinking method. The capsules obtained by such a method exhibit improved mechanical stability—properties important for the delivery of encapsulated material. Upon illumination by laser light, the encapsulated dextran leaves

the interior of a capsule inside a living cancer cell. Capsules not internalized by the cells are pushed up by the laser and move away from the field of view upon laser illumination from the bottom. The study presented herein serves as a significant step toward the use of polyelectrolyte-multilayer capsules for the delivery of medicine into biological cells, and is, therefore, relevant to research on drug delivery.<sup>[1]</sup> The presented method is different from previous, albeit also important, studies in that it is conducted on an individual-capsule level and offers an improved degree of control and monitoring.

### Experimental Section

Polyelectrolyte-multilayer capsules were prepared according to the previously described method.<sup>[5,21]</sup> Silica particles ( $\text{SiO}_2$ , 4.55  $\mu\text{m}$ ; Microparticles GmbH, Berlin, Germany) were alternately coated with four double layers of PDADMAC ( $M_w \approx 200\text{--}350$  kDa; Sigma-Aldrich, Munich, Germany) and PSS ( $M_w = 70$  kDa; Sigma-Aldrich). FITC dextran (Sigma-Aldrich) was used in pH stability tests. All chemicals were used without further purification. The water used in all experiments was prepared in a three-stage Millipore Milli-Q Plus 185 purification system and had a resistivity higher than 18.2  $\text{M}\Omega\text{cm}$ .

For activation studies, silver-containing microcapsules were prepared according to the method described earlier.<sup>[10a]</sup> For release studies, gold and gold sulfide<sup>[17]</sup> nanoparticles were deposited in the layers according to the method described earlier.<sup>[10b]</sup> After deposition of eight polyelectrolyte monolayers, silica cores were dissolved in 0.1M HF.<sup>[21b]</sup> Alexa Fluor 488 dextran conjugate (AF-488 dextran,  $M_w = 10$  kDa; Invitrogen, Karlsruhe, Germany) was encapsulated in (PDADMAC/PSS)<sub>4</sub> capsules according to the thermal treatment method.<sup>[21b,c]</sup>

The optical setup used in the experiments was similar to that described previously.<sup>[10]</sup> The laser was operated in CW mode, and the shutter was opened during illumination for brief pulses of the order of seconds or less. MDA-MB-435S cancer cell lines were used in the experiments; they were seeded on the substrate overnight, then approximately 30 capsules per cell were added and the experiments were carried out after incubation for 4 h as previously reported.<sup>[6c]</sup>

Received: December 27, 2005

Revised: April 13, 2006

Published online: June 22, 2006

**Keywords:** drug delivery · multilayers · nanoparticles · photoactivation · polymers

- [1] a) R. Langer, *Nature* **1998**, 392, 5–10; b) M. Ferrari, *Nat. Rev. Cancer* **2005**, 5, 161–171; c) H. Ai, S. A. Jones, M. M. de Villiers, Y. M. Lvov, *J. Controlled Release* **2003**, 86, 59–68.
- [2] a) A. P. Nowak, V. Breedveld, L. Pakstis, B. Ozbas, D. J. Pine, D. Pochan, T. J. Deming, *Nature* **2002**, 417, 424–428; b) M. Das, S. Mardiyani, W. C. W. Chan, E. Kumacheva, *Adv. Mater.* **2006**, 18, 80–83.
- [3] a) G. S. Kwon, T. Okano, *Adv. Drug Delivery Rev.* **1996**, 21, 107–116; b) C. Allen, A. Eisenberg, J. Mrcic, *Drug Delivery* **2000**, 7, 139–145; c) R. Duncan, *Nat. Rev. Drug Discovery* **2003**, 2, 347–360.
- [4] a) B. Chaize, J. P. Colletier, M. Winterhalter, D. Fournier, *Artif. Cells Blood Substitutes Biotechnol.* **2004**, 32, 67–75; b) M. Michel, M. Winterhalter, L. Darbois, J. Hemmerle, J.-C. Voegel, P. Shaaf, V. Ball, *Langmuir* **2004**, 20, 6127–6133; c) S. Faraassen,

- J. Vörös, G. Csucs, M. Textor, H. P. Merkle, E. Walter, *Pharm. Res.* **2003**, *20*, 237–246.
- [5] a) E. Donath, G. B. Sukhorukov, F. Caruso, S. A. Davies, H. Möhwald, *Angew. Chem.* **1998**, *110*, 2324–2327; *Angew. Chem. Int. Ed.* **1998**, *37*, 2202–2205; b) C. Peyratout, L. Dähne, *Angew. Chem.* **2004**, *116*, 3850–3873; *Angew. Chem. Int. Ed.* **2004**, *43*, 3762–3783.
- [6] a) G. B. Sukhorukov, A. L. Rogach, B. Zebli, T. Liedl, A. G. Skirtach, K. Köhler, A. A. Antipov, N. Gaponik, A. S. Sussha, M. Winterhalter, W. Parak, *Small* **2005**, *1*, 194–200; b) B. G. De Geest, C. Dégunat, G. B. Sukhorukov, K. Braeckmans, S. C. De Smedt, J. Demeester, *Adv. Mater.* **2005**, *17*, 2357–2361; c) A. Muñoz Javier, O. Kreft, A. Piera Alberola, C. Kirchner, B. Zebli, A. S. Sussha, E. Horn, S. Kempner, A. G. Skirtach, A. L. Rogach, J. Rädler, G. B. Sukhorukov, M. Benoit, W. J. Parak, *Small* **2006**, *2*, 394–400; d) M. Fischlechner, L. Toellner, P. Messner, R. Grabherr, E. Donath, *Angew. Chem.* **2006**, *118*, 798–803; *Angew. Chem. Int. Ed.* **2006**, *45*, 784–789; e) B. G. De Geest, R. E. Vandenbroucke, A. M. Guenther, G. B. Sukhorukov, W. E. Hennink, N. N. Sanders, J. Demeester, S. C. De Smedt, *Adv. Mater.* **2006**, *18*, 1005–1009.
- [7] a) M. Nolte, A. Fery, *Langmuir* **2004**, *20*, 2995–2998; b) B. Wang, Q. Zhao, F. Wang, C. Gao, *Angew. Chem.* **2006**, *118*, 1590–1593; *Angew. Chem. Int. Ed.* **2006**, *45*, 1560–1563; c) S. C. Grover, A. G. Skirtach, R. C. Gauthier, C. P. Grover, *J. Biomed. Opt.* **2001**, *6*, 14–22; d) P. S. Dittrich, P. Schwill, *Anal. Chem.* **2003**, *75*, 5767–5774; e) S. Hiller, A. Schnackel, E. Donath, *Cytometry A* **2005**, *64*, 115–127.
- [8] a) G. Decher, J. D. Hong, J. Schmitt, *Thin Solid Films* **1992**, *210*, 831–835; b) Y. Lvov, G. Decher, H. Möhwald, *Langmuir* **1993**, *9*, 481–486; c) G. Decher, *Science* **1997**, *277*, 1232–1237; d) P. Bertrand, A. Jonas, A. Laschewsky, R. Legras, *Macromol. Rapid Commun.* **2000**, *21*, 319–348; e) M. Schönhoff, *J. Phys. Condens. Matter* **2003**, *15*, R1781–R1808; f) D. M. Delongchamp, P. T. Hammond, *Chem. Mater.* **2003**, *15*, 1165–1173; g) E. Blomberg, E. Poptoshev, P. M. Claesson, F. Caruso, *Langmuir* **2004**, *20*, 5432–5438; h) S. A. Sukhishvili, *Curr. Opin. Colloid Interface Sci.* **2005**, *10*, 37–44; i) C. Jiang, V. V. Tsukruk, *Adv. Mater.* **2006**, *18*, 829–840.
- [9] a) Y. Lvov, K. Ariga, I. Ichinose, T. Kunitake, *J. Am. Chem. Soc.* **1995**, *117*, 6117–6123; b) C. Delgado, G. E. Francis, D. Fisher, *Crit. Rev. Ther. Drug Carrier Syst.* **1992**, *9*, 249–304; c) J. Rieger, K. V. Bernaerts, F. E. Du Prez, R. Jerome, C. Jerome, *Macromolecules* **2004**, *37*, 9738–9745.
- [10] a) A. G. Skirtach, A. A. Antipov, D. G. Shchukin, G. B. Sukhorukov, *Langmuir* **2004**, *20*, 6988–6992; b) A. G. Skirtach, C. Déjournat, D. Braun, A. S. Sussha, A. L. Rogach, W. J. Parak, H. Möhwald, G. B. Sukhorukov, *Nano Lett.* **2005**, *5*, 1371–1377.
- [11] a) S. Serksen, S. L. Westcott, N. J. Halas, J. L. West, *J. Biomed. Mater. Res.* **2000**, *51*, 293–298; b) B. Radt, T. A. Smith, F. Caruso, *Adv. Mater.* **2004**, *16*, 2184–2189; c) A. S. Angelatos, B. Radt, F. Caruso, *J. Phys. Chem. B* **2005**, *109*, 3071–3076; d) X. F. Yuan, K. Fischer, W. Scharlt, *Langmuir* **2005**, *21*, 9374–9380.
- [12] a) C. A. Mirkin, R. L. Letsinger, R. C. Mucic, J. J. Storhoff, *Nature* **1996**, *382*, 607–609; b) A. P. Alivisatos, K. P. Johnsson, X. G. Peng, T. E. Wilson, C. J. Loweth, M. P. Bruchez, P. G. Schultz, *Nature* **1996**, *382*, 609–611; c) D. I. Gittins, F. Caruso, *Angew. Chem.* **2001**, *113*, 3089–3092; *Angew. Chem. Int. Ed.* **2001**, *40*, 3001–3004; d) M. El-Sayed, *Acc. Chem. Res.* **2001**, *34*, 257–264; e) W. J. Parak, T. Pellegrino, C. M. Micheel, D. Gerion, S. C. Williams, A. P. Alivisatos, *Nano Lett.* **2003**, *3*, 33–36; f) L. Manna, D. J. Milliron, A. Meisel, F. C. Scher, A. P. Alivisatos, *Nat. Mater.* **2003**, *2*, 382–385; g) M. K. Corbierre, N. S. Cameron, M. Sutton, S. G. J. Mochrie, L. B. Lurio, A. Ruhm, R. B. Lennox, *J. Am. Chem. Soc.* **2004**, *126*, 2867–2873; h) E. Katz, I. Willner, *Angew. Chem.* **2004**, *116*, 6166–6235; *Angew. Chem. Int. Ed.* **2004**, *43*, 6042–6108; i) J. Lee, A. O. Govorov, N. A. Kotov, *Angew. Chem.* **2005**, *117*, 7605–7608; *Angew. Chem. Int. Ed.* **2005**, *44*, 7439–7442; j) W. J. Parak, T. Pellegrino, C. Planck, *Nanotechnology* **2005**, *16*, R9–R25; k) C. J. Murphy, N. R. Jana, *Adv. Mater.* **2002**, *14*, 80–82; l) D. V. Guzatov, A. A. Oraevsky, A. N. Oraevsky, *Quantum Electron.* **2003**, *33*, 817–822; m) M. C. Daniel, C. Astruc, *Chem. Rev.* **2004**, *104*, 293–346.
- [13] a) J. A. Copland, M. Eghtedari, V. L. Popov, N. Kotov, N. Mamedova, M. Motamedi, A. A. Oraevsky, *Mol. Imaging Biol.* **2004**, *6*, 341–349; b) K. Sokolov, M. Follen, J. Aaron, I. Pavlova, A. Malpica, R. Lotan, R. Richards-Kortum, *Cancer Res.* **2003**, *63*, 1999–2004; c) M. Eghtedari, J. A. Copland, N. A. Kotov, A. A. Oraevsky, M. Motamedi, *Lasers Surg. Med.* **2004**, *164* Suppl. S16; d) D. Pissuwan, S. M. Valenzuela, M. B. Cortie, *Trends Biotechnol.* **2006**, *24*, 62–67.
- [14] a) A. Roggan, M. Friebel, K. Dorschel, A. Hahn, G. Müller, *J. Biomed. Opt.* **1999**, *4*, 36–46; b) A. N. Yaroslavsky, I. V. Yaroslavsky, T. Goldbach, H. J. Schwarzmaier, *Proc. SPIE-Int. Soc. Opt. Eng.* **1996**, *2678*, 314–324; c) G. M. Hale, M. R. Querry, *Appl. Opt.* **1973**, *12*, 555–563; d) A. Schönle, S. W. Hell, *Opt. Lett.* **1998**, *23*, 325–327.
- [15] a) U. Kreibig in *Physics and Chemistry of Finite Systems: From Clusters to Crystals* (Eds.: P. Jenna, S. N. Khanna, B. K. Rao), Kluwer Academic Publishers, London, **1991**; b) U. Kreibig, B. Schmitz, H. D. Breuer, *Phys. Rev. B* **1987**, *36*, 5027–5030; c) T. Kahlau, M. Quinten, U. Kreibig, *Appl. Phys. A* **1996**, *62*, 19–27.
- [16] a) L. Lu, R. Capek, A. Kornowski, N. Gaponik, A. Eychmüller, *Angew. Chem.* **2005**, *117*, 6151–6155; *Angew. Chem. Int. Ed.* **2005**, *44*, 5997–6001; b) M. Morikawa, N. Kimizuka, *Chem. Commun.* **2005**, *38*, 4866–4868; c) G. Zhang, D. Y. Wang, H. Möhwald, *Angew. Chem.* **2005**, *117*, 7945–7948; *Angew. Chem. Int. Ed.* **2005**, *44*, 7767–7770; d) A. G. Skirtach, C. Déjournat, D. Braun, A. S. Sussha, A. L. Rogach, G. B. Sukhorukov, unpublished results.
- [17] a) H. S. Zhou, I. Honma, H. Komiyama, J. W. Haus, *Phys. Rev. B* **1994**, *50*, 12052–12056; b) R. D. Averitt, D. Sarkar, N. J. Halas, *Phys. Rev. Lett.* **1997**, *78*, 4217–4220; c) T. Norman, Jr., C. D. Grant, D. Magana, J. Z. Zhang, J. Liu, D. Cao, F. Bridges, A. van Buuren, *J. Phys. Chem. B* **2002**, *106*, 7005–7012; d) G. Raschke, S. Brogl, A. S. Sussha, A. L. Rogach, T. A. Klar, J. Feldman, B. Fieres, N. Petkov, T. Bein, A. Nichtl, K. Kürzinger, *Nano Lett.* **2004**, *4*, 1853–1857; e) J. Z. Zhang, A. M. Schwartzberg, T. Norman, Jr., C. D. Grant, J. Liu, F. Bridges, T. Van Buuren, *Nano Lett.* **2005**, *5*, 809–810.
- [18] a) D. Yoo, S. S. Shiratori, M. Rubner, *Macromolecules* **1998**, *31*, 4309–4318; b) J. D. Mendelsohn, C. J. Barrett, V. V. Chan, A. J. Pal, A. M. Mayes, M. F. Rubner, *Langmuir* **2000**, *16*, 5017–5023; c) S. Sukhishvili, S. Granick, *J. Am. Chem. Soc.* **2000**, *122*, 9550–9551; d) H. H. Rmaile, J. B. Schlenoff, *Langmuir* **2002**, *18*, 8263–8265; e) L. Richert, F. Boulmedias, P. Laval, J. Mutterer, E. Ferreux, G. Decher, P. Schaaf, J.-C. Voegel, C. Picart, *Biomacromolecules* **2004**, *5*, 284–294; f) S. E. Burke, C. J. Barrett, *Macromolecules* **2004**, *37*, 5375–5384.
- [19] a) A. A. Antipov, G. B. Sukhorukov, S. Leporatti, I. L. Radtchenko, E. Donath, H. Möhwald, *Colloids Surf. A* **2002**, *535*, 198–200; b) T. Mauser, C. D. Déjournat, G. B. Sukhorukov, *Macromol. Rapid Commun.* **2004**, *25*, 1781–1785; c) C. D. Déjournat, D. Halozan, G. B. Sukhorukov, *Macromol. Rapid Commun.* **2005**, *26*, 961–967; d) Z. An, H. Möhwald, J. Li, *Biomacromolecules* **2006**, *7*, 580–585.
- [20] a) D. V. Volodkin, A. I. Petrov, M. Prevot, G. B. Sukhorukov, *Langmuir* **2004**, *20*, 3398–3406; b) A. I. Petrov, D. V. Volodkin, G. B. Sukhorukov, *Biotechnol. Prog.* **2005**, *21*, 918–925.
- [21] a) K. Köhler, D. Shchukin, H. Möhwald, G. B. Sukhorukov, *Macromolecules* **2004**, *37*, 9546–9550; b) K. Köhler, D. G. Shchukin, H. Möhwald, G. B. Sukhorukov, *J. Phys. Chem. B*



- 2005**, *109*, 18250–18259; c) K. Köhler, G. B. Sukhorukov, unpublished results.
- [22] a) V. A. Izumrudov, H. O. Ortiz, A. B. Zevin, V. A. Kabanov, *Macromol. Chem. Phys.* **1998**, *199*, 1057–1062; b) S. Leporatti, C. Gao, A. Voight, E. Donath, H. Möhwald, *Eur. Phys. J. E* **2001**, *5*, 13–20; c) C. Gao, S. Leporatti, S. Moya, E. Donath, H. Möhwald, *Chem. Eur. J.* **2003**, *9*, 915–920; d) J. F. Quinn, F. Caruso, *Langmuir* **2004**, *20*, 20–22; e) M. Salomaki, I. A. Vinokurov, J. Kankare, *Langmuir* **2005**, *21*, 11232–11240.
- [23] a) C. Gao, S. Leporatti, S. Moya, E. Donath, H. Möhwald, *Langmuir* **2001**, *17*, 3491–3495; b) C. Y. Gao, S. Moya, E. Donath, H. Möhwald, *Macromol. Chem. Phys.* **2002**, *203*, 953–960; c) F. Dubreuil, N. Elsner, A. Fery, *Eur. Phys. J. E* **2003**, *12*, 215–221; d) A. Fery, F. Dubreuil, H. Möhwald, *New J. Phys.* **2004**, *6*, 1–13; e) R. Müller, K. Köhler, R. Weinkamer, G. Sukhorukov, A. Fery, *Macromolecules* **2005**, *38*, 9766–9771; f) V. V. Lulevich, S. Nordschild, O. I. Vinogradova, *Macromolecules* **2004**, *37*, 7736–7741; g) O. Mermut, J. Lefebvre, D. G. Gray, C. J. Barrett, *Macromolecules* **2003**, *36*, 8819–8824; h) D. Collin, P. Laval, J. M. Garza, J.-C. Voegel, P. Schaaf, P. Martinoty, *Macromolecules* **2004**, *37*, 10195–10198; i) A. J. Nolte, M. F. Rubner, R. E. Cohen, *Macromolecules* **2005**, *38*, 5367–5370; j) J. A. Jaber, J. B. Schlenoff, *J. Am. Chem. Soc.* **2006**, *128*, 2940–2947.
- [24] a) R. P. Haugland in *Handbook of Fluorescent Probes and Research Chemicals*, 7th ed., Molecular Probes, Eugene, OR, **1999**; b) N. Panchuk-Voloshina, R. P. Haugland, J. Bishop-Stewart, M. K. Bhalat, P. J. Millard, F. Mao, W. Leung, R. P. Haugland, *J. Histochem. Cytochem.* **1999**, *47*, 1179–1188; c) R. von Klitzing, H. Möhwald, *Langmuir* **1995**, *11*, 3554–3559; d) N. Klonis, W. H. Sawye, *J. Fluoresc.* **1996**, *6*, 147–157; e) R. Sjöback, J. Nygren, M. Kibuta, *Spectrochim. Acta A* **1995**, *51*, L7–L21; f) M. M. Marin, L. Lindqvist, *J. Lumin.* **1975**, *10*, 381–390.
- [25] a) P. S. Dittrich, P. Schwill, *Appl. Phys. B* **2001**, *73*, 829–837; b) C. Eggeling, A. Volkmer, C. A. M. Seidel, *ChemPhysChem* **2005**, *6*, 791–804.
- [26] a) P. Lebedew, *Ann. Phys.* **1901**, *6*, 433–458; b) A. Ashkin, *Biophys. J.* **1992**, *61*, 569–582; c) R. C. Gauthier, *Appl. Phys. Lett.* **1995**, *67*, 2269–2271; d) S. C. Grover, R. C. Gauthier, A. G. Skirtach, *Opt. Express* **2000**, *7*, 533–539.
- [27] a) R. E. Holmin, R. F. Ismagilov, R. Haag, V. Mujica, M. A. Ratner, M. A. Rampi, G. M. Whitesides, *Angew. Chem.* **2001**, *113*, 2378–2382; *Angew. Chem. Int. Ed.* **2001**, *40*, 2316–2325; b) J. Zhang, R. M. Lahtinen, K. Kontturi, P. R. Unwin, D. J. Schiffrin, *Chem. Commun.* **2001**, *18*, 1818–1819; c) J. J. Zhao, C. R. Bradbury, S. Huclova, I. Potapova, M. Carrara, D. J. Fermin, *J. Phys. Chem. B* **2005**, *109*, 22985–22994.

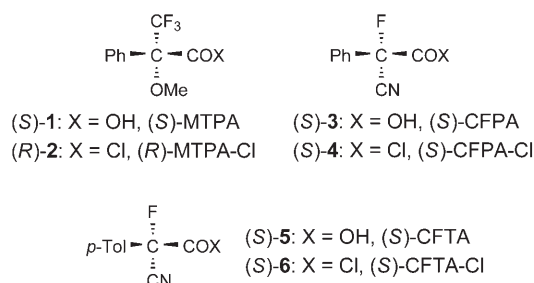


DOI: 10.1002/anie.200600157

# The CFTA Method: A Reliable Procedure for the Determination of the Absolute Configuration of Chiral Primary Amines by $^1\text{H}$ NMR Spectroscopic Analysis\*\*

Yoshio Takeuchi,\* Masaru Segawa, Hidehito Fujisawa, Kenji Omata, Siegfried N. Lodwig, and Clifford J. Unkefer

Methods for the determination of the absolute configuration of chiral molecules are indispensable in modern organic chemistry, especially in asymmetric synthesis and in studies of the structures of complex natural products.<sup>[1]</sup> Although the modified Mosher method<sup>[2]</sup> with  $\alpha$ -methoxy- $\alpha$ -trifluoromethylphenylacetic acid (MTPA, **1**)<sup>[3]</sup> is often employed for this



purpose, many cases have been identified in which the MTPA procedure can not be applied, either because of the low reactivity of MTPA chloride (**2**)<sup>[4]</sup> or because of the number of complex conformers observed in the MTPA derivatives.<sup>[5]</sup> To overcome these limitations, we developed  $\alpha$ -cyano- $\alpha$ -fluoro-phenylacetic acid (CFPA, **3**), in which the fluorine atom is

[\*] Prof. Dr. Y. Takeuchi, M. Segawa, H. Fujisawa

Faculty of Pharmaceutical Sciences

University of Toyama

Sugitani, Toyama 930-0194 (Japan)

Fax: (+81) 76-434-5053

E-mail: takeuchi@pha.u-toyama.ac.jp

Dr. K. Omata

Department of Chemistry

Graduate School of Science, Tohoku University

Aramaki, Aoba-ku, Sendai 980-8578 (Japan)

Dr. S. N. Lodwig, Dr. C. J. Unkefer

National Stable Isotope Resource

Bioscience Division, MS E529

Los Alamos National Laboratory

Los Alamos, NM 87544 (USA)

[\*\*] The authors are grateful to Dr. K. Kabuto of Tohoku University for his helpful suggestion. This work was partially supported by the National Stable Isotope Resource at Los Alamos (NIH 5P41 EB002166). CFTA =  $\alpha$ -cyano- $\alpha$ -fluoro-*p*-tolylacetic acid.



Supporting information for this article is available on the WWW under <http://www.angewandte.org> or from the author.

located on the stereogenic center. We found that CFPA chloride (**4**) reacts with nucleophiles 500 times faster than MTPA chloride (**2**), and even undergoes condensation with hindered nucleophiles, such as pinacolyl alcohol.<sup>[6]</sup>

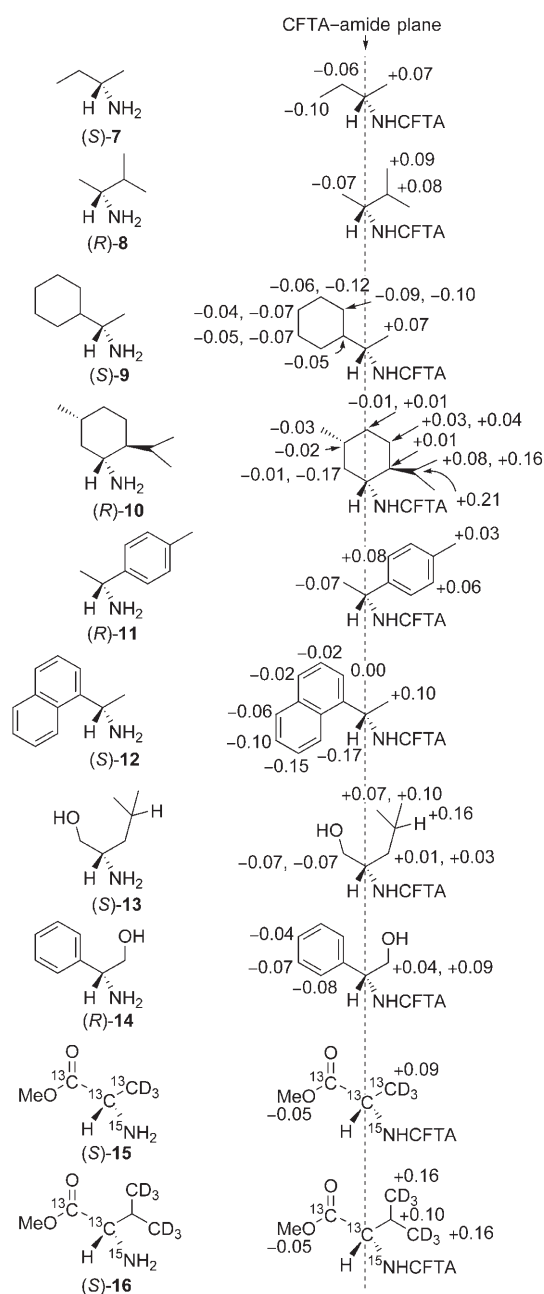
The phenyl hydrogen atoms of CFPA give rise to a complex multiplet in the <sup>1</sup>H NMR spectrum, which can often complicate the analysis of the <sup>1</sup>H NMR spectra of substrates with aromatic substituents. We therefore decided to search for a derivatizing agent with more readily distinguishable aromatic proton signals to simplify the assignment of proton signals to the derivatized diastereomers.<sup>[7]</sup> This approach led to our development of  $\alpha$ -cyano- $\alpha$ -fluoro-*p*-tolylacetic acid (CFTA, **5**; Tol = tolyl),<sup>[8]</sup> a reagent that can be used in the determination of the absolute configuration of chiral carbinols,<sup>[9]</sup> even those with two essentially identical substituents.<sup>[10]</sup> Herein, we report that the CFTA method is also reliably applicable to the determination of the absolute configuration of various chiral amine compounds.

We measured the chemical-shift difference,  $\Delta\delta_{\text{H}}$  ( $\delta_{\text{S}} - \delta_{\text{R}}$ ),<sup>[11]</sup> for corresponding protons of the diastereomeric (*S*)- and (*R*)-CFTA amides of chiral primary amines **7–14** of known absolute configuration (Scheme 1).<sup>[12]</sup> All proton signals for the amine residue were assigned for both the (*S*)- and (*R*)-CFTA diastereomers by means of COSY and other NMR spectroscopic techniques. Thus, a  $\Delta\delta_{\text{H}}$  value was readily obtained for each hydrogen atom of the diastereomers.

The CFTA–amide plane is defined as the plane with an all-*anti* (F–C)–(C=O)–(N–H)–(C–H) conformation<sup>[12]</sup> (Scheme 2). When the CFTA amides are depicted in a manner such that the two substituents at the stereogenic center adjacent to the N atom are in the plane of the page (which is perpendicular to the CFTA–amide plane) and the  $\alpha$  hydrogen atom is coming out of the plane of the page, the hydrogen atoms with negative  $\Delta\delta_{\text{H}}$  values are invariably on the left-hand side of the CFTA–amide plane and those with positive  $\Delta\delta_{\text{H}}$  values are on the right-hand side of the CFTA–amide plane (Scheme 1). In general, greater  $\Delta\delta_{\text{H}}$  values were observed for the CFTA amides than for the MTPA amides. Thus, the CFTA method enables the determination of the absolute configuration of chiral amines by <sup>1</sup>H NMR spectroscopy much more readily and accurately than the method with MTPA.

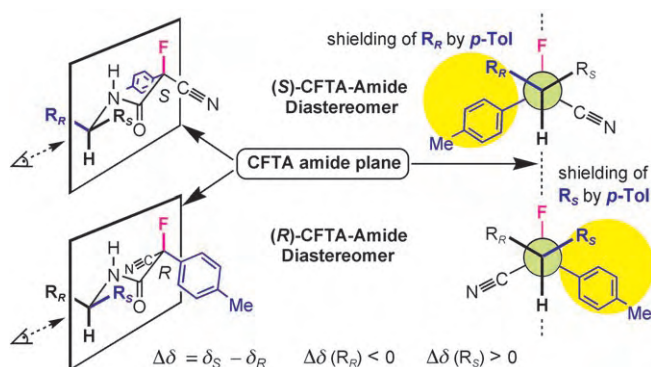
To investigate the scope and limitations of the CFTA method, we applied our procedure to the multiply labeled amino acid derivatives **15** and **16**. From the  $\Delta\delta$  values obtained by <sup>1</sup>H and <sup>2</sup>H NMR spectroscopy, we found that both **15** and **16** have the *S* absolute configuration, as was expected from the synthetic route used for their preparation.<sup>[13]</sup> X-ray analysis of the CFTA amide of **15** confirmed the *S* configuration for this derivative.<sup>[14]</sup>

The signs of  $\Delta\delta$  on each side of the CFTA–amide plane were opposite for the CFTA amides to those observed for the CFTA esters<sup>[9]</sup> and also opposite to those observed with MTPA amides. Therefore, we propose that the stable conformation for the amides is that in which the C–F bond occupies an anti-periplanar position with respect to the C=O bond (Scheme 2), in contrast to the syn-periplanar conformation that is favored in the case of the CFTA esters. The amides of the chiral amines  $\text{R}_\text{S}\text{R}_\text{R}\text{CHNH}_2$  can be viewed from the left-



**Scheme 1.**  $\Delta\delta_{\text{H}}$  or  $\Delta\delta_{\text{D}}$  values for CFTA amide diastereomers of chiral amines **7–16**.

hand side in an extended Newman projection, in which the amide linkage is omitted for convenience. Conformational arguments can be used to explain the algebraic signs of the  $\Delta\delta$  values. In the case of the (*S*)-CFTA diastereomer, the signals for the hydrogen atoms of the  $\text{R}_\text{R}$  group should always be shifted upfield as a result of the anisotropic shielding of the aromatic ring. In contrast, for the *R* diastereomer, the hydrogen atoms of the  $\text{R}_\text{S}$  group are shielded, and these signals should therefore appear upfield. Thus, the  $\Delta\delta$  values for the protons on the left-hand side of the CFTA–amide plane should be negative and those for the protons on the right-hand side of the plane should be positive. This conformation was supported by X-ray crystallographic analysis of the CFTA



**Scheme 2.** Conformations of (S)- and (R)-CFTA amides of chiral primary amines  $R_5R_6CHNH_2$ .

amide of 1-phenylethylamine<sup>[8a]</sup> and ab initio calculations (GAUSSIAN98, RHF/6-31 + G\*) of the CFPA amide of Val-OMe as a similar molecule.<sup>[8b]</sup>

In summary, we have presented the CFTA method as a new and reliable procedure for the determination of the absolute configuration of chiral amines. This method has important advantages over other conceptually similar procedures available because of the very high reactivity of the agent<sup>[6]</sup> and because the C–F bond at the stereocenter exerts strong conformational control on the amides.<sup>[12b]</sup> For these reasons we feel this method should be widely applicable.

Received: January 14, 2006

Published online: June 21, 2006

**Keywords:** CFTA diastereomers · configuration determination · NMR spectroscopy · reactivity

- Sasaki, K. Omata, C. Kabuto, K. Kabuto, Y. Takeuchi, *Tetrahedron: Asymmetry* **2004**, *15*, 555; d) (S)- and (R)-CFTA-Cl are both commercially available from Kanto Denka Kogyo Co., Ltd.
- [9] T. Takahashi, A. Fukushima, Y. Tanaka, Y. Takeuchi, K. Kabuto, C. Kabuto, *Chem. Commun.* **2000**, 787.
- [10] Y. Takeuchi, H. Fujisawa, R. Noyori, *Org. Lett.* **2004**, *6*, 4607.
- [11] The  $\Delta\delta$  values are defined as  $\delta_S - \delta_R$ , in which  $\delta_S$  and  $\delta_R$  are the chemical shifts of the corresponding protons in the (S)- and (R)-CFTA amides, respectively.
- [12] a) S. K. Latypov, J. M. Seco, E. Quiñoá, R. Riguera, *J. Org. Chem.* **1995**, *60*, 1538; b) C. R. S. Briggs, D. O'Hagan, J. A. K. Howard, D. S. Yufit, *J. Fluorine Chem.* **2003**, *119*, 9.
- [13] S. N. Ludwig, C. J. Unkefer, *J. Labelled Compd. Radiopharm.* **1998**, *XLI*, 983; see also the Supporting Information.
- [14] CCDC-291185 and CCDC-291186 contain the supplementary crystallographic data for this paper. These data can be obtained free of charge from The Cambridge Crystallographic Data Centre via [www.ccdc.cam.ac.uk/data\\_request/cif](http://www.ccdc.cam.ac.uk/data_request/cif).

- [1] J. M. Seco, E. Quiñoá, R. Riguera, *Chem. Rev.* **2004**, *104*, 17, and references therein.
- [2] a) I. Ohtani, T. Kusumi, Y. Kashman, H. Kakisawa, *J. Org. Chem.* **1991**, *56*, 1296; b) I. Ohtani, T. Kusumi, Y. Kashman, H. Kakisawa, *J. Am. Chem. Soc.* **1991**, *113*, 4092.
- [3] a) J. A. Dale, D. L. Dull, H. S. Mosher, *J. Org. Chem.* **1969**, *34*, 2543; b) J. A. Dale, H. S. Mosher, *J. Am. Chem. Soc.* **1973**, *95*, 512; c) G. R. Sullivan, J. A. Dale, H. S. Mosher, *J. Org. Chem.* **1973**, *38*, 2143.
- [4] a) J. S. Dutcher, J. G. Macmillan, C. H. Heathcock, *J. Org. Chem.* **1976**, *41*, 2663; b) L. Hietaniemi, E. Pohjala, P. Malkonen, M. L. Riekkola, *Finn. Chem. Lett.* **1989**, *16*, 67; c) A. Svatos, I. Valterova, D. Samon, J. Vrkoc, *Collect. Czech. Chem. Commun.* **1990**, *55*, 485; d) Y. Takeuchi, N. Itoh, S. Kawahara, T. Koizumi, *Tetrahedron* **1993**, *49*, 1861.
- [5] J. M. Seco, S. K. Latypov, E. Quiñoá, R. Riguera, *J. Org. Chem.* **1997**, *62*, 7569.
- [6] Y. Takeuchi, M. Itoh, T. Koizumi, *J. Chem. Soc. Chem. Commun.* **1992**, 1514; see also: Y. Takeuchi, M. Itoh, T. Koizumi, *Chem. Ind.* **1992**, 874.
- [7] The assignment of the AB-quartet-like proton signals for the p-Tol group is much easier than that of the complex multiplet signals for the Ph group, especially for those chiral amines with aromatic residues.
- [8] a) Y. Takeuchi, M. Konishi, H. Hori, T. Takahashi, T. Kometani, K. L. Kirk, *Chem. Commun.* **1998**, 365; b) T. Fujiwara, K. Omata, K. Kabuto, C. Kabuto, T. Takahashi, M. Segawa, Y. Takeuchi, *Chem. Commun.* **2001**, 2694; c) T. Fujiwara, M.

## Dynamic Combinatorial Chemistry

DOI: 10.1002/anie.200600430

**Electric-Field Modulation of Component Exchange in Constitutional Dynamic Liquid Crystals\*\***
*Nicolas Giuseppone and Jean-Marie Lehn\**

Dynamic combinatorial chemistry (DCC) forms the covalent domain of constitutional dynamic chemistry (CDC)<sup>[1,2]</sup> which covers reversible constitutional reorganization on both the molecular (covalent) and supramolecular (noncovalent) levels. It gives access to all possible combinations of the available components, which are connected through reversible covalent bonds. It thus generates constitutional dynamic libraries (CDLs) that, at thermodynamic equilibrium, display all the constituents or leave some of them virtual, depending on the conditions.<sup>[1a]</sup> Such systems can be driven either by internal organization (self-recognition) or by external interaction (species binding). As a result, the equilibrium may shift to the over-expression of selected products through an adaptative process. To date, the discrimination between the constituents of dynamic libraries has centered on the utilization of target recognition as a driving force, in particular as a result of applications in drug discovery.<sup>[3]</sup> In the course of our

[\*] Dr. N. Giuseppone, Prof. Dr. J.-M. Lehn  
Institut de Science et d'Ingénierie Supramoléculaires  
8 Allée Gaspard-Monge, BP 70028, 67083 Strasbourg (France)  
Fax: (+33) 390-245-140  
E-mail: lehn@isis.u-strasbg.fr

[\*\*] We thank Dr. Jean-Louis Schmitt for checking the experimental results. We are grateful to Dr. Daniel Guillon, Dr. Jacques Malthête, and Dr. Jacques Prost for their constructive remarks on the manuscript.



investigations toward the design of adaptative chemical systems that respond to a wide array of environmental parameters, we have become interested in the potential offered by the possibility to drive constituent reorganization and amplification/selection by component exchange, by external physical (temperature,<sup>[4a]</sup> phase transition<sup>[5]</sup>), or chemical (protons,<sup>[4]</sup> metal ions<sup>[4b,c,6]</sup>) triggers. Changes in the composition of the members of a constitutional dynamic library (CDL) represent an adaptation of the dynamic system in response to the perturbation. Such effects are of special interest in terms of developing dynamic materials that respond to environmental effectors.<sup>[7,8]</sup>

To extend the range of physical external triggers for inducing selection processes, we have explored the possibility of using an electric field to influence the thermodynamic equilibrium in a mixture of constitutionally interrelated compounds. To this end, the development of dynamic liquid crystals (LCs) appeared particularly well-suited for three main reasons: 1) the wide use of LCs as materials, in particular for display technology;<sup>[9]</sup> 2) the potential existence of various LC phases—such as nematic, smectic, etc.—depending on the constitution of the mixtures and molecular structure of the components;<sup>[10]</sup> and 3) the well-known behavior of LCs to become macroscopically oriented and stabilized in either electric<sup>[11]</sup> or magnetic fields.<sup>[12]</sup>

We herein describe the perturbations imposed by an electric field on mixtures of imines and amines containing an LC-type imine with a negative dielectric anisotropy, namely MBBA (**1**) or EBBA (**5**, Scheme 1). Two distinct phenomena have been observed that are linked to the transitions between isotropic and nematic phases. The first one consists of the expulsion from the LC, upon application of an electric field, of compounds that do not participate in the formation of a nematic phase; the second is based on a direct effect of the electric field on the thermodynamic equilibria in a CDL by the coupling of the field to the LC-forming entity and its subsequent stabilization/amplification.

The effect of constitutional modifications by component exchange on the isotropic/nematic phase transition temperatures ( $T_{IN}$ ) of MBBA (**1**) was investigated by following UV/Vis spectroscopic changes upon introduction of various amounts of several additives (Figure 1).<sup>[13]</sup>

The value of  $T_{IN}$  decreased linearly as a function of the amount of additive and the slopes of the lines fall into two sets. In one set are the additives which cannot lead to a new imine by constitutional reorganization (triethylamine, cyclopentanol, *N,N*-dimethylaniline) and where the addition of 15 mol % of compound results in a decrease in the  $T_{IN}$  value to close to room temperature. The second set contains the additives which can react with MBBA (**1**) by transimination reactions<sup>[14]</sup> (cyclopentylamine, aniline, 2,4-dimethoxybenzylamine) with formation of new imines, and where the addition of only 3 mol % of compound is enough to give a  $T_{IN}$  value

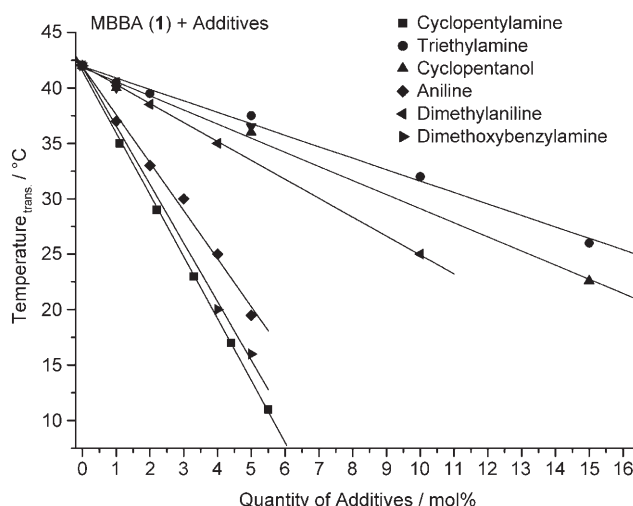
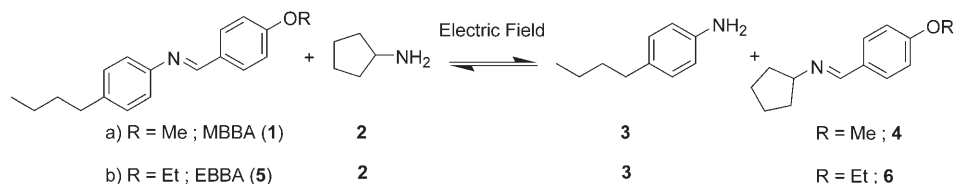


**Figure 1.** Representation of the evolution of the phase-transition temperature ( $T_{IN}$ ) of MBBA (**1**) as a function of increasing amounts of various additives. Phase-transition temperatures were determined by using variable temperature UV/Vis spectroscopy as the average of the transitions recorded in the heating/cooling cycles of 10  $\mu$ m thickness films ( $\lambda = 400$  nm and  $V_{\Delta T} = 1$  °C/min). NMR spectroscopic observation was used to ensure that equilibrium was reached.

close to room temperature. This differential behavior suggested that it was the generation of recombinant imines that led to marked changes in the value of  $T_{IN}$ .

We then investigated whether an electric field would influence the equilibria involving compounds **1**, **2**, **3**, and **4** as well as **5**, **2**, **3**, and **6**, respectively, where the imines **1** and **5** are LCs, but **4** and **6** are not (Scheme 1) and should result in changes in the  $T_{IN}$  value.



**Scheme 1.** Component exchange between MBBA (**1**) or EBBA (**5**) and cyclopentylamine (**2**) leading to a constitutional dynamic equilibrium with 4-butaniline (**3**) and imines **4** or **6**, respectively, modulated by an applied electric field.

The experiments were performed on thin films of 21- ( $\pm 5$  %)  $\mu$ m thickness between transparent indium tin oxide (ITO) plates so that sufficiently high voltages could be applied to the systems. Under these conditions, the maximum voltage applied was  $3.5 \times 10^4$  V cm<sup>-1</sup> ( $\pm 0.15 \times 10^4$  V cm<sup>-1</sup>) which enabled a high resistivity ( $R \geq 6 \times 10^7$   $\Omega$  cm<sup>-1</sup>) to be maintained and to avoid fast degradation of the compounds as well as heating-induced phenomena arising from the electric current.<sup>[15]</sup> The phase transition could be observed both with the naked eye (as a consequence of the opacity of the nematic phase under a high electric field in the dynamic scattering mode, DSM)<sup>[16]</sup> and by using a polarized light microscope (Figure 2A).

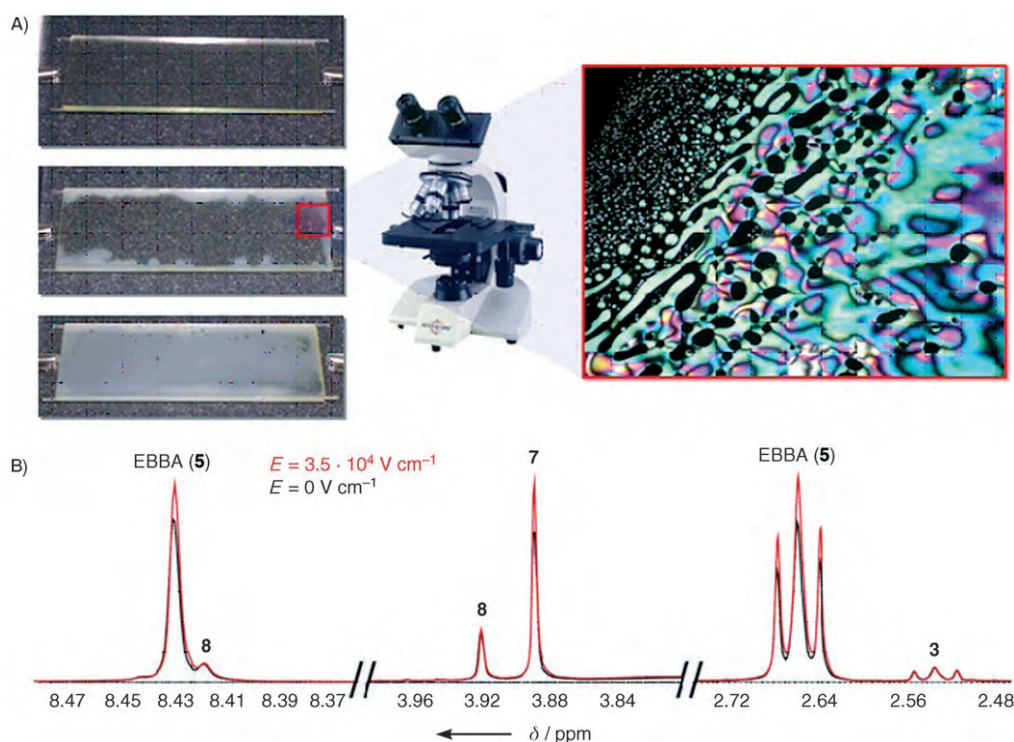


**Figure 2.** A) Left: Typical appearance of the ITO plates ( $7.25 \times 2.5$  cm) as a function of time in an experiment using MBBA (1) in the presence of additives and under the influence of an electric field (when the applied voltage is superior to the minimum necessary for observing the changes through the dynamic scattering mode<sup>[16]</sup>): top: liquid mixture; middle: coexistence between liquid and nematic phases; bottom: nematic phase over the entire ITO plate. Right: Microscopy observation, using a polarized light microscope in transmission mode ( $\times 40$ ), which shows the expansion of the nematic phase into the liquid one under the influence of an electric field ( $E = 0$  V at the instant of the snapshot). B) Partial 400 MHz  $^1\text{H}$  NMR spectra showing the changes in chemical composition induced by the application of an electric field ( $E = 3.5 \times 10^4 \text{ V cm}^{-1}$  ( $\pm 5\%$ )) at  $24^\circ\text{C}$  for 2 h on the equilibrium described in Scheme 2 (red spectrum), compared to the control experiment without field (black line).

The molecular composition of the system described in Scheme 1 at equilibrium was obtained from the  $^1\text{H}$  NMR spectra of the solutions of complete mixtures in  $\text{CDCl}_3$  set between the ITO plates, and by superimposition of the NMR spectra of the pure compounds. Under neat conditions, the rate of the transimination reaction was slow enough ( $V_0 = 1.84 \text{ M h}^{-1}$ ,  $t_{1/2} = 64$  min; for a 1:2 ratio of 1:0.64 and for  $T = 22.7^\circ\text{C}$ ) to allow accurate measurements by NMR spectroscopy.<sup>[17]</sup> A static electric field was applied to the two dynamic mixtures illustrated in Scheme 1 and the evolution of the equilibrium amounts (namely, expression) of MBBA (1) and EBBA (5) was followed as a function of field strength (Figure 3).

The data showed a nonlinear displacement of the equilibrium, which shifts towards the generation of MBBA and EBBA, respectively, as the field strength increases. That this change (about 6%) was not a result of a variation in

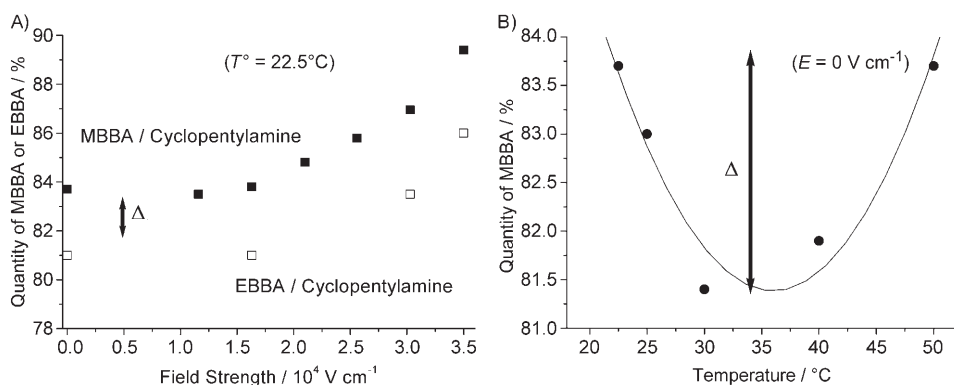


**Figure 3.** A) Effect of the strength of the electric field, at  $22.5^\circ\text{C}$  after 24 h, on the equilibria described in Scheme 1 for an initial molar ratio of MBBA:cyclopentylamine of  $1:0.2 \pm 1.1\%$  (■) and for an initial molar ratio of EBBA:cyclopentylamine of  $1:0.25 \pm 1.1\%$  (□). B) Effect of the temperature, after 24 h, on the equilibrium of the reaction described in Scheme 1 with MBBA (initial molar ratio of MBBA:2 1:0.2).  $\Delta$  shows the scale change for comparing the effect of electric field (A) and temperature (B) on the equilibrium.

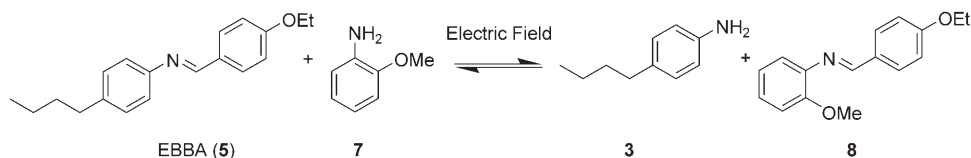
temperature is indicated by the fact that heating the ITO plates (even by tens of degrees) led to a much smaller displacement of the equilibrium (about 2%) than that observed with the electric field.<sup>[15,18]</sup> Several other mixtures involving aniline, benzylamine, isopentylamine, and allylamine, and even libraries containing all these amines together led to similar observations. In all these cases an accelerated

loss of the volatile amines by evaporation occurred (Figure 3A), which led to irreversible systems. To confirm these findings, we studied a nondynamic system consisting of a mixture of MBBA (**1**) and cyclopentanol in which component exchange does not occur; a similar enhanced loss of cyclopentanol by evaporation under the influence of the electric field was observed.<sup>[19]</sup> The behavior of the present systems may be related to some electrohydrodynamic effects in the DSM that result from the coupling of the LC molecules (of negative dielectric anisotropy) to the electric field, and that lead to an extrusion (and subsequent evaporation) of the foreign (volatile) substances not involved in the LC molecules.<sup>[20]</sup> It could also present interesting applications, for example, for the controlled release of molecules or for the design of sensors.

The next step was to design a fully reversible system to examine the direct influence of the electric field on the equilibrium itself. A proof of principle was finally obtained using EBBA (**5**) and (the nonvolatile) 2-methoxyaniline (**7**; b.p. 225 °C) in the process described in Scheme 2, which led through transimination to an equilibrating reaction with **3** and the non-LC imine **8**.

The <sup>1</sup>H NMR spectra of mixtures of EBBA (**5**) and **7**, chosen so as to correspond to a  $T_{1/N}$  value close to room temperature (molar ratio **5**:**7** = 79.3:20.7 ± 1.2 %) were determined in the absence and in the presence of an applied electric field ( $E = 3.5 \times 10^4 \text{ V cm}^{-1}$  (±5 %)) after 2 h equilibration at 24 °C (Figure 2B). The relative variation of the percentage of 4-butylaniline (**3**) with respect to the initial molar ratio of **5**:**3** (93:7) for various strengths of the electric field is shown in Figure 4, together with kinetic data for reaching equilibrium in the presence of the electric field and after switching it off.

The spectra in Figure 2B show an increase in the amount of **5** and **7** at equilibrium under the applied electric field, and a concomitant decrease of **3** and **8**. The increase in **7** is of particular importance: as it is nonvolatile relative to cyclo-



**Scheme 2.** Transimination reaction between EBBA (**5**) and 2-methoxyaniline (**7**) leading to an equilibrium with 4-butylaniline (**3**) and imine **8**, modulated by the presence of an electric field.

pentylamine (**2**), loss by evaporation cannot here be the driving force for the evolution of the system, thus the changes observed may be ascribed to the direct effect of the electric field on the equilibrium. Moreover, there is an exponential correlation between the strength of the field and the equilibrium displacement (Figure 4A). Furthermore, the field-induced perturbation was fully reversible, as shown in Figure 4B by the evolution of the system as a function of time under applied electric field, compared to the control experiment, and after the field had been shut off. Whereas the equilibrium was attained in about 2 h in the presence of the

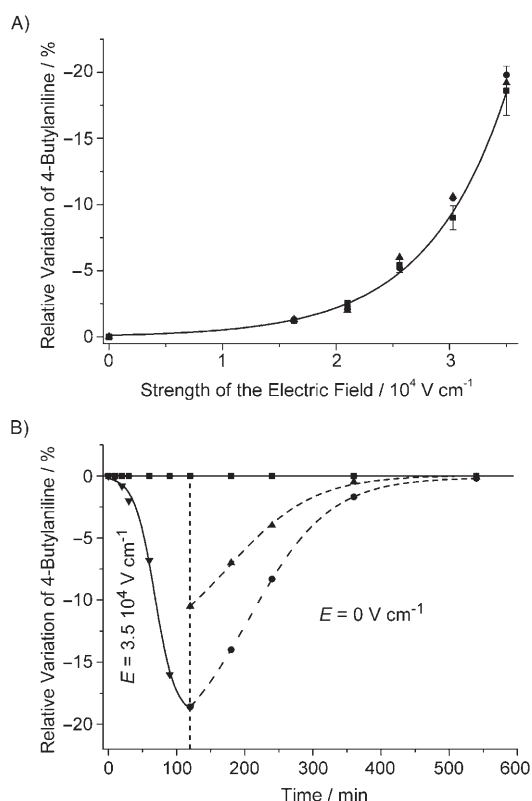


**Figure 4.** A) Effect of the strength of the electric field, at 24 °C for 2 h on the equilibrium described in Scheme 2 (molar ratio of EBBA:**7** 79.3:20.7 ± 1.2 %); each reaction was repeated three times and the error bars represent values between ± 10 %. B) Kinetics of the variation of the equilibrium between ITO plates under a field  $E = 3.5 \times 10^4 \text{ V cm}^{-1}$  (± 5 %; ▲; solid line curve); kinetics of equilibration after stopping the electric field and dissolution ( $C = 3.84 \text{ M}$  in  $\text{CDCl}_3$ ; ●, dashed line curve); and kinetics of equilibration after stopping the electric field and dissolution, for an initial applied field of  $E = 3.03 \times 10^4 \text{ V cm}^{-1}$  (± 5 %; ▲, dashed line curve). The values are given using the relative variation in the percentage of amine **3** (experiments with and without field (■; solid line curve)), and corrected for the dilution effect.

field, after switching it off, the initial position of the equilibrium was restored after about 6 h in a  $\text{CDCl}_3$  solution at 24 °C. The reversibility between the ITO plates at 24 °C was a very slow process in the absence of DSM (more than several days), while heating the plates without field at 45 °C for 4 h led to the return of the equilibrium to its initial position. Thus, a faster interconversion over several cycles would require acting on both parameters: electric field and temperature.

Finally, we investigated whether, in the absence of an applied field, a temperature-induced phase transition would by itself have an effect on the constitutional equilibrium (Figure 5).

The changes in composition remained very minor compared to those observed under an applied electric field, with relative variations in the fraction of 4-butylaniline of less than 3 % both inside a single phase and at the phase transitions.

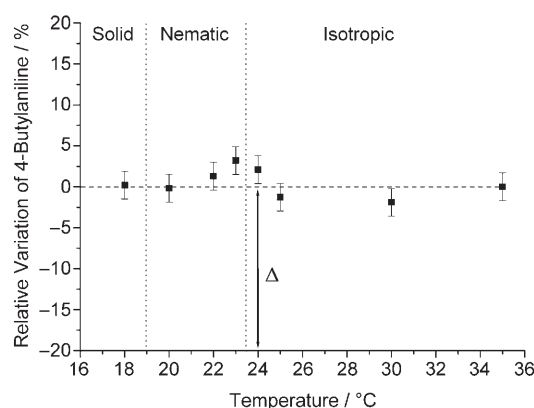


**Figure 5.** Effect of the temperature, after two hours, on the equilibrium described in Scheme 2 (molar ratio of EBBA:6 79.3:20.7 ± 1.2%) and under slight mechanical stirring; the error bars represent values between ± 2.5%, which is close to the accuracy of the  $^1\text{H}$  NMR method. The  $\Delta$  symbol shows on the same scale the change of the equilibrium in presence of an electric field ( $E = 3.5 \times 10^4 \text{ V cm}^{-1}$  (± 5%), after two hours, Figure 4).

When the same system was studied at higher temperatures, the liquid to nematic phase transition was observed up to 55 °C, when the mixture starts losing its electric resistance.<sup>[21]</sup>

It is known that applying an electric field to genuine liquid crystals with either positive<sup>[11,15b]</sup> or negative<sup>[22]</sup> dielectric anisotropy leads only to a small change in the  $T_{\text{IN}}$  values (typically ≤ 1 K for an applied field of  $2 \times 10^5 \text{ V cm}^{-1}$ ). The marked change in the  $T_{\text{IN}}$  values observed here must result from a specific property of the present system, namely its constitutional variation under application of an electric field. Furthermore, when the mixture described in Scheme 2 was studied under a field of  $3.5 \times 10^4 \text{ V cm}^{-1}$  (± 5%) for 2 h at a 5:7 ratio of 69.5:30.5 (± 1.3%), which does not allow a phase transition from liquid to nematic at 24 °C, a comparable change occurred in the composition at equilibrium (18% for the relative variation of 3). This observation indicates the coupling of EBBA (5) to the electric field even in the liquid paranematic phase, as a result of the electric field induced formation of cybotactic groups—small sets of locally organized molecules.

In conclusion, we have shown that the interaction between an electric field and LC molecules having a negative dielectric anisotropy can lead to two different phenomena: 1) a purification of the system by extrusion of the molecules that do not couple to the electric field, probably through electrohydrodynamic processes; and 2) a direct action of the electric field on a constitutional dynamic equilibrium involving LC molecules formed from components connected through reversible imine-type bonds.<sup>[23]</sup> The amplified constituent is that which couples the strongest to the electric field (the liquid crystal), and this amplification can consequently result in a phase transition from liquid to nematic. The processes described here broaden the scope of CDC by demonstrating the influence of a particularly interesting environmental parameter, the electric field, and illustrate the adaptation of the dynamic mixtures to a physical effector through the

formation of the “fittest” constituent, that presenting the strongest coupling to the field.<sup>[24]</sup> This approach may in principle be applied 1) to more complex mixtures, in particular containing several different dynamic LC molecules, 2) to systems involving different reversible covalent processes, as well as 3) to supramolecular LCs or LC polymers.<sup>[8]</sup> The phenomena discovered could also be of potential interest for practical applications in various areas, such as the fine-tuning of a given material or controlled release processes.

## Experimental Section

**General aspects:** All reagents were purchased at the highest commercial quality and used without further purification except for EBBA (5) which was recrystallized by slow cooling from a hot saturated solution in heptane, and for 2-methoxyaniline (7) which was distilled two times, immediately prior to use. The phase-transition temperatures (42.5 °C for MBBA and 78.5 °C for EBBA) agreed with those reported in the literature.  $^1\text{H}$  NMR spectra were recorded on a Bruker Avance 400 MHz spectrometer. To avoid the catalysis of the transimination reaction, traces of acid in the deuterated chloroform were removed by flash chromatography through neutral alumina immediately prior to use. The ITO plates were purchased from Aldrich (70–100 ohm; ref: 576352) and the electric field was applied with a TTI EX752M multimode PSU generator. The resistivity of the thin films was measured with a Keithley 6517A instrument. The temperature of the samples was regulated by placing the ITO plates on a thermostated surface, controlled by a Polystat cc2 Huber system, and checked at the surface of the glass slides using a thermocouple (Bead Probe Keithley 6517-TP).

**General procedure for cross-over experiments and determinations of thermodynamic and kinetic data:** In a typical protocol the compounds to exchange were mixed in a closed vial. The mixture was heated up to 60 °C for 5 min, then cooled down to room temperature, and left for 2 h at that temperature. Then, 38  $\mu\text{L}$  (± 5%) of the neat mixture was placed between two ITO plates by using a microsyringe, and the glass plates were gently pressed to get a thin film (21  $\mu\text{m}$ , ± 5%) over the entire surface (18.1  $\text{cm}^2$ ; see Figure 2A). The plates were thermostated, and then connected to the cathode and the anode of the generator; electric fields between 0 and 75 V were applied (for an applied field of 75 V, the experimental errors will lead to a value of  $3.5 \times 10^4 \text{ V cm}^{-1}$  (±  $0.15 \times 10^4 \text{ V cm}^{-1}$ ). After a given time, the electric field was shut off, and the whole mixture contained between the two plates was dissolved in  $\text{CDCl}_3$  (2 mL), immediately prior to  $^1\text{H}$  NMR measurements (within 5 minutes). The  $^1\text{H}$  NMR spectra were recorded until stabilization of the equilibria for both the experiment with the field as well as the thermostated control experiment (without field but with the same initial mixture). The values for the changes in sample composition were obtained from comparison of the spectra for the two corresponding experiments after the same time of equilibration in solution.

Received: February 1, 2006

Published online: June 21, 2006

**Keywords:** dynamic combinatorial chemistry · electrochemistry · imines · liquid crystals · phase transitions

- [1] a) J.-M. Lehn, *Chem. Eur. J.* **1999**, *5*, 2455; b) R. L. Cousins, S. A. Poulsen, J. K. M. Sanders, *Curr. Opin. Chem. Biol.* **2000**, *4*, 270; c) S. J. Rowan, S. J. Cantrill, G. R. L. Cousins, J. K. M. Sanders, J. F. Stoddart, *Angew. Chem.* **2002**, *114*, 938; *Angew. Chem. Int. Ed.* **2002**, *41*, 898.



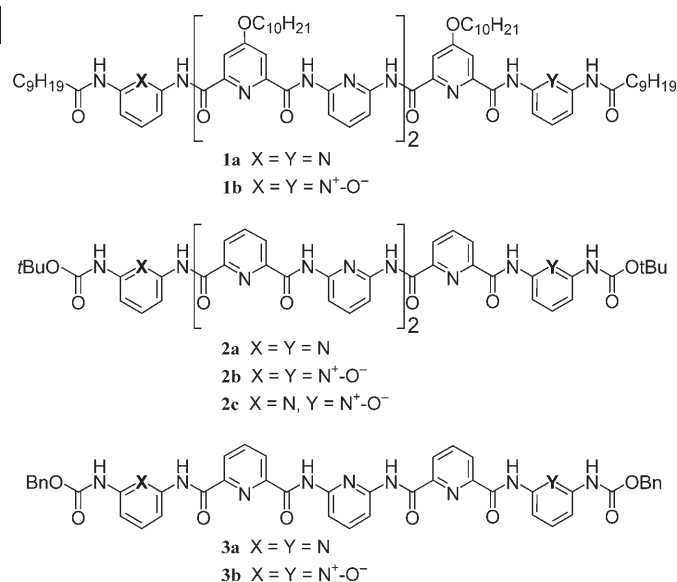
- [2] a) J.-M. Lehn, *Proc. Natl. Acad. Sci. USA* **2002**, 99, 4763; b) J.-M. Lehn, *Science* **2002**, 295, 2400.
- [3] O. Ramström, J.-M. Lehn, *Nat. Rev. Drug Discovery* **2001**, 1, 26.
- [4] a) N. Giuseppone, J.-M. Lehn, *Chem. Eur. J.* **2006**, 12, 1715; b) N. Giuseppone, J.-M. Lehn, *J. Am. Chem. Soc.* **2004**, 126, 11448; c) N. Giuseppone, G. Fuks, J.-M. Lehn, *Chem. Eur. J.* **2006**, 12, 1723.
- [5] S. Nampally, J.-M. Lehn, *Proc. Natl. Acad. Sci. USA* **2005**, 102, 5938.
- [6] N. Giuseppone, J.-L. Schmitt, J.-M. Lehn, *Angew. Chem.* **2004**, 116, 5010; *Angew. Chem. Int. Ed.* **2004**, 43, 4902.
- [7] J.-M. Lehn in *Supramolecular Science: Where It Is and Where It Is Going* (Eds.: R. Ungaro, E. Dalcanele), Kluwer, Dordrecht, The Netherlands, **1999**, 287.
- [8] J.-M. Lehn, *Polym. Int.* **2002**, 51, 825, and references therein.
- [9] For a recent review on the use of liquid crystals for display technology, see: P. Kirsch, M. Bremer, *Angew. Chem.* **2000**, 112, 4384; *Angew. Chem. Int. Ed.* **2000**, 39, 4216.
- [10] P.-G. de Gennes, *The Physics of Liquid Crystals* Clarendon, Oxford, **1973**.
- [11] a) C.-P. Fan, M. J. Stephen, *Phys. Rev. Lett.* **1970**, 25, 500; b) I. Lelidis, M. Nobili, G. Durand, *Phys. Rev. E* **1993**, 48, 3818; c) I. Lelidis, G. Durand, *Phys. Rev. E* **1993**, 48, 3822; d) I. Lelidis, G. Durand, *Phys. Rev. Lett.* **1994**, 73, 672; e) I. Lelidis, G. Durand, *Phys. Rev. Lett.* **1996**, 76, 1868.
- [12] a) J. Tang, S. Fraden, *Phys. Rev. Lett.* **1993**, 71, 3509; b) M. I. Boamfä, K. Viertel, A. Wewerka, F. Stelzer, P. C. M. Christensen, J. C. Maan, *Phys. Rev. E* **2003**, 67, 050701.
- [13] a) To improve the reliability of LC displays, some studies addressed the influence of traces of water in mixtures of imine-type liquid crystals.<sup>[13b]</sup> The presence of residual water was demonstrated, as well as subsequent changes in the  $T_{IN}$  values of the mixtures; however, the use of mixtures of LCs as dynamic systems, has not been explored; b) H. Sorkin, A. Denny, *RCA Rev.* **1973**, 34, 308.
- [14] The choice of transimination as the exchange reaction is of crucial importance to avoid the presence of water (that would be formed in amine-carbonyl condensations) in the present systems so as to maintain high resistance to the electric current upon application of a high voltage. For catalyzed and noncatalyzed transimination reactions, see: N. Giuseppone, J.-L. Schmitt, E. Schwartz, J.-M. Lehn, *J. Am. Chem. Soc.* **2005**, 127, 5528, and references therein.
- [15] a) Under these conditions the heating appeared negligible (ca. 1 °C measured at the surface of the ITO plates), in agreement with literature results; b) W. Helfrich, *Phys. Rev. Lett.* **1970**, 24, 201; c) A. J. Nicastro, P. H. Keys, *Phys. Rev. A* **1981**, 30, 3156.
- [16] G. H. Heilmeyer, L. A. Zoanoni, L. A. Barton, *Appl. Phys. Lett.* **1968**, 13, 46.
- [17] The rate of the reaction in a  $CDCl_3$  solution ( $C = 3.84\text{ M}$ ) was found to be  $t_{1/2} = 60\text{ min}$  at 22.5 °C and  $t_{1/2} = 30\text{ min}$  at 30 °C, which is also suitable for NMR measurements.
- [18] The change in the direction of the displacement of the equilibrium above 30 °C (Figure 3B, right-hand part of the curve) was found to arise from evaporation of cyclopentylamine. Thus, the effect of heating on the equilibrium is in the opposite direction (left-hand part of the curve, Figure 3B) than that caused by the field before evaporation takes over.
- [19] For example, the use of a molar ratio of MBBA:cyclopentanol of 55:45 leads to an evaporation of 7.5% of the cyclopentanol without field, and of 38.5% with a field of  $3.5 \times 10^4\text{ V cm}^{-1}$ , after 18 h at 23 °C. Moreover, if MBBA is replaced by pentaethylene glycol (with no liquid-crystal properties and similar viscosity), no differential evaporation was observed.
- [20] The effect amounts to a sort of purification under high voltage; for electrohydrodynamic effects in the MBBA-type nematic phases, see: D. Jin, H. Kim, S. H. Kim, S. K. Kim, *J. Phys. Chem. B* **1997**, 101, 10757.
- [21] The coexistence between liquid-crystalline and liquid domains is observed between the ITO plates.
- [22] S. Dhara, N. V. Madhusudana, *Europhys. Lett.* **2004**, 67, 411.
- [23] For a theoretical study of the effect of an external electric field on bond activation reactions, see: S. Shaik, S. P. de Visser, D. Kumar, *J. Am. Chem. Soc.* **2004**, 126, 11746.
- [24] We thank a referee for comments concerning the origin of the chemical effects observed by application of the electric field. In particular, the “coupling to the field” merely indicates that the observed effects result from the interaction of the electric field with the liquid-crystalline species. Such coupling may involve several factors/mechanisms. The energy necessary to displace the equilibrium as described in Scheme 2 and Figure 4 is calculated to be about  $\Delta\Delta G \approx 80\text{ cal mol}^{-1}$ . The electric interaction energy with the system is too weak to explain the observations, even if a contribution from flexoelectricity<sup>[10]</sup> is taken into account. When the field is applied close to the phase transition, the effect could be in the correct range, but should change on varying the temperature, which appears not to be the case. The heat capacity associated with the isotropic/nematic phase transition is known to be also in the range required to shift the equilibrium,<sup>[25]</sup> however, the lack of a temperature effect (Figure 5) indicates that it is not a major factor. Finally, electrohydrodynamic instabilities observed in the DSM mode are known to be caused by ionic currents;<sup>[26]</sup> the contribution of the field heterogeneity related to the motions of ionic particles throughout the sample could be more than enough to displace the equilibrium with the experimentally measured values of the conductivity. Ionic motions and the conceivable accumulation of charges on the electrode surfaces would lead to high local field values, capable of sufficient interaction with the liquid crystal to result in its amplification from the DCL.
- [25] R. Chang, F. B. Jones, J. J. Ratto, *Mol. Cryst. Liq. Cryst.* **1976**, 33, 13 ( $\Delta H_{(\text{Nematic-Isotropic})} = 0.10\text{ kcal mol}^{-1}$ ;  $T = 45.8^\circ\text{C}$ ).
- [26] a) E. F. Carr, *Mol. Cryst. Liq. Cryst.* **1969**, 7, 253; b) W. Helfrich, *J. Chem. Phys.* **1969**, 51, 4093; c) S. Hirata, T. Tako, *Jpn. J. Appl. Phys. Part 2* **1982**, 21, L607; d) S. J. Tavener, T. Mullin, G. I. Blake, K. A. Cliffe, *Phys. Rev. E* **2000**, 63, 011708.

# Cross-Hybridization of Pyridinedicarboxamide Helical Strands and Their *N*-Oxides\*\*

Chuanlang Zhan, Jean-Michel Léger, and Ivan Huc\*

Chemists have exploited the ability of nucleic acids to form sequence-selective double-stranded hybrids and have turned it into an incredibly powerful tool to direct chemical synthesis<sup>[1]</sup> and to create well-defined discrete nanoarchitectures and two-dimensional patterns.<sup>[2]</sup> Non-natural double-stranded molecules held together by noncovalent interactions which mimic nucleic acid hybridization<sup>[3]</sup> may potentially be useful in a similar way. For example, hydrogen-bonded duplexes based on linear oligoamide strands have recently been used to template cross-olefin metathesis.<sup>[4]</sup> Such applications require the hybridization of two *different* strands to form a cross-hybrid so that each strand can selectively bring a given functionality or a given structural unit to the duplex. In DNA, this is expressed by the fact that the basic level of complementarity—canonical A/T and G/C base pairing—is indeed heterologous and not homologous. However, most synthetic oligomers that hybridize into double-stranded structures reported to date are homodimers, including most of the numerous helicates,<sup>[5]</sup> hydrogen-bonded linear tapes<sup>[6–10]</sup> and helices,<sup>[11]</sup> as well as the aromatic oligoamides (AOAs) derived from 2,6-diaminopyridine and 2,6-pyridinedicarboxylic acid that we have been studying.<sup>[12,13]</sup> There are only a few examples of heterodimerized oligomeric strands that form helicates<sup>[14]</sup> and hydrogen-bonded structures,<sup>[4,15,16]</sup> as well as of hybrids based on the assembly of electron-poor and electron-rich aromatic compounds,<sup>[17]</sup> but among these, less than a handful (two to our knowledge)<sup>[14,16]</sup> possess a well-characterized structure. Herein, we describe our discovery of a cross-hybridization between double helices formed by AOAs and their *N*-oxide derivatives.

In solution, oligomers such as **1a**, **2a**, and **3a** (Scheme 1) form single helices<sup>[18]</sup> that can extend like springs and intertwine into double-helical homodimers.<sup>[12,19]</sup> The single



Scheme 1. Oligomers studied. Bn = benzyl.

and double helices are in slow exchange on the NMR timescale, thus giving rise to two sets of signals for heptamer **1a** (Figure 1a) and for heptamer **2a** (Figure 2a). The

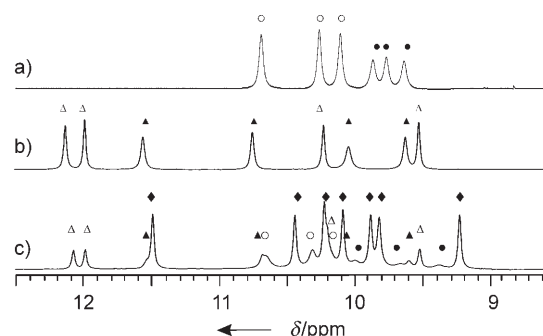


Figure 1. Partial 400 MHz <sup>1</sup>H NMR spectra at 25°C showing the amide resonances of: a) **1a** (8 mm), b) **1b** (8.5 mm), and c) **1a** + **1b** (8 mm each). The resonances were assigned to **1a** (○), (**1a**)<sub>2</sub> (●), **1b** (△), (**1b**)<sub>2</sub> (▲), and **1a**·**1b** (◆). The signal of the peripheral amide NH protons of **1a** within single or within double helices appears at higher field in the aromatic region.

proportions of these signals allow calculation of the dimerization constants as  $K_{\text{dim}}(\mathbf{1a})_2 = 30 \text{ L mol}^{-1}$  ( $\Delta G_{\text{dim}}(\mathbf{1a})_2 = -8.4 \text{ kJ mol}^{-1}$ ) and  $K_{\text{dim}}(\mathbf{2a})_2 = 120 \text{ L mol}^{-1}$  ( $\Delta G_{\text{dim}}(\mathbf{2a})_2 = -11.9 \text{ kJ mol}^{-1}$ ) in CDCl<sub>3</sub> at 25°C—the difference between the two being assigned to effects of terminal substituents (decanoylamino versus *tert*-butylcarbamate) and side chains (decyloxy versus hydrogen). Recently, we showed that oligomers possessing 2,6-diaminopyridines as their terminal residues can be cleanly converted into the corresponding bis(pyridine *N*-oxide)s in the presence of *meta*-chloroperbenzoic acid (MCPBA), with only the terminal residues oxidized.<sup>[13]</sup> Specifically, **1a** was converted into **1b** and pentamer **3a** into **3b**. Furthermore, the *N*-oxidized oligomers also possess the ability to hybridize into double-helical dimers:

[\*] Dr. C. Zhan, Dr. I. Huc  
Institut Européen de Chimie et Biologie  
2 rue Robert Escarpit  
33607 Pessac (France)  
Fax: (+33) 540-00-22-15  
E-mail: i.huc@iecb.u-bordeaux.fr  
Prof. J.-M. Léger  
Laboratoire de Pharmacochimie  
146 rue Léo Saignat  
33076 Bordeaux (France)

[\*\*] This work was supported by the CNRS, the University of Bordeaux I, the University of Bordeaux II, and by the French Ministry of Research and Education. We thank J. Lefeuvre for performing ab initio calculations.

Supporting information for this article is available on the WWW under <http://www.angewandte.org> or from the author.

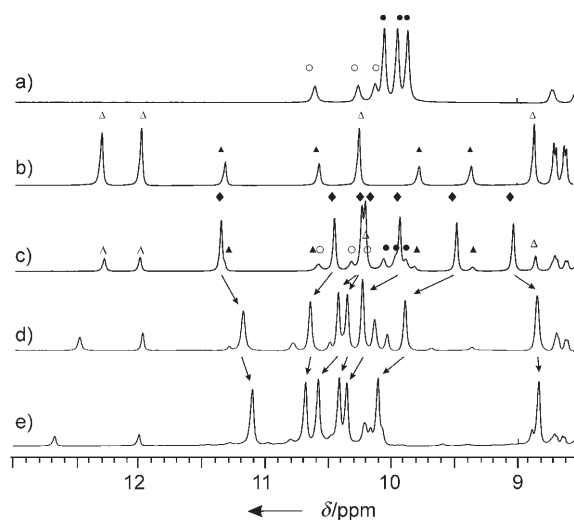


**Figure 2.** Partial 400 MHz  $^1\text{H}$  NMR spectra showing the amide resonances of: a) **2a** at 25°C (32 mm), b) **2b** at 25°C (32 mm), c) **2a+2b** at 25°C (32 mm each), d) **2a+2b** at 0°C (32 mm each), and e) **2a+2b** at -25°C (32 mm each). The resonances were assigned to **2a** (○), (**2a**)<sub>2</sub> (●), **2b** (△), (**2b**)<sub>2</sub> (▲), and **2a-2b** (◆). The signal of the peripheral amide NH protons of **1a** within single or within double helices appears at higher field in the aromatic region.

spectra such as that shown in Figure 1b allow calculation of  $K_{\text{dim}}(\mathbf{1b})_2 = 125 \text{ L mol}^{-1}$  ( $\Delta G_{\text{dim}}(\mathbf{1b})_2 = -12.0 \text{ kJ mol}^{-1}$ ); this value is about four times higher than  $K_{\text{dim}}(\mathbf{1a})_2$ .<sup>[13]</sup>

The AOAs are amenable to chemical transformations but still retain their ability to hybridize, which prompted us to explore the possibility of cross-hybridization between chemically different oligomers. Thus when **1a** and its di-*N*-oxide **1b** are mixed in stoichiometric amounts (8 mm each), the NMR spectrum (Figure 1c) shows minor signals of both monomers and both homodimers, but the spectrum is dominated by new signals, the multiplicity of which exactly corresponds to that expected for heterodimer **1a-1b**. The variation in the intensities of these signals, which decrease upon diluting or heating the solution, and their low chemical shifts are consistent with this assignment. Most importantly, the cross-hybrid seems considerably more stable than either of the homodimers:  $K_{\text{assoc}}(\mathbf{1a-1b}) = 1140 \text{ L mol}^{-1}$ , which corresponds to  $\Delta G_{\text{assoc}}(\mathbf{1a-1b}) = -17.4 \text{ kJ mol}^{-1}$ . In the hypothetical case where each individual strand would bring the same stabilization energy to a duplex regardless of its nature, the expected value would have been  $\Delta G_{\text{assoc}}(\mathbf{1a-1b}) = (\Delta G_{\text{dim}}(\mathbf{1a})_2 + \Delta G_{\text{dim}}(\mathbf{1b})_2)/2 - RT \ln(2) = -11.5 \text{ kJ mol}^{-1}$  (the second term accounts for the statistical factor that favors cross-hybridization at the expense of homodimerization). The heterodimer is thus stabilized by  $5.9 \text{ kJ mol}^{-1}$  relative to this theoretical value.

Oligomers **1a** and **1b** have long alkyl chains and do not crystallize. Unsubstituted heptamer **2a**, however, is highly crystalline and has been characterized in the solid state, both as a single helix and as a double helix.<sup>[12]</sup> We thus prepared heptamer bis-*N*-oxide **2b** and heptamer mono-*N*-oxide **2c** from **2a** in the hope that crystals of the heterodimer could be grown. This proved unsuccessful and only single helical **2b** could be characterized (in several crystalline forms).<sup>[20]</sup>

However, the behavior of **2a**, **2b**, and **2c** in solution is fully consistent with that of **1a** and **1b**. As shown in Figure 2b and c, bis-*N*-oxide dimerizes with  $K_{\text{dim}}(\mathbf{2b})_2 = 22 \text{ L mol}^{-1}$  ( $\Delta G_{\text{dim}}(\mathbf{2b})_2 = -7.6 \text{ kJ mol}^{-1}$ )<sup>[21]</sup> while **2a** and **2b** cross-hybridize with  $K_{\text{assoc}}(\mathbf{2a-2b}) = 650 \text{ L mol}^{-1}$  ( $\Delta G_{\text{assoc}}(\mathbf{2a-2b}) = -16.1 \text{ kJ mol}^{-1}$ ). The cross-hybrid is more stable by  $5.1 \text{ kJ mol}^{-1}$  relative to the theoretical value of  $(\Delta G_{\text{dim}}(\mathbf{2a})_2 + \Delta G_{\text{dim}}(\mathbf{2b})_2)/2 - RT \ln(2) = -11.0 \text{ kJ mol}^{-1}$ . Cross-hybrid **2a-2b** prevails at 25°C (Figure 2c) and even more so at lower temperatures (Figure 2d,e), although the other species then become too minor to determine the  $K_{\text{assoc}}$  values accurately.

Heptamer **2c**, which contains only one *N*-oxide function, can in principle form parallel and antiparallel dimers, depending on whether the *N*-oxide functions of the two strands reside at the same end or at opposite ends of the duplex. Figure 3

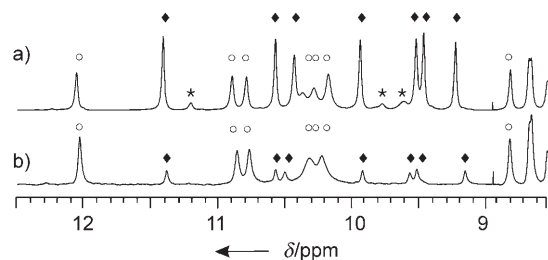


**Figure 3.** Partial 400 MHz  $^1\text{H}$  NMR spectra at 25°C showing the amide resonances of **2c** at a) 32 mm and b) 2 mm. The resonances were assigned to **2c** (○), antiparallel (**2c**)<sub>2</sub> (◆), and parallel (**2c**)<sub>2</sub> (\*). The signal of one of the two peripheral carbamate NH protons of **2c** appears at higher field in the aromatic region.

shows that two sets of signals can indeed be assigned to two different dimers, but that their amounts differ by a factor of 7.8, which represents an energy difference between the two dimers of  $\Delta \Delta G_{\text{dim}}(\mathbf{2c}) = 5.1 \text{ kJ mol}^{-1}$ . The NMR spectra alone do not allow an unambiguous assignment of the two sets of signals. However, it seems reasonable to assign the major species to antiparallel (**2c**)<sub>2</sub> and the minor species to parallel (**2c**)<sub>2</sub> on the basis of the stability of **1a-1b** and **2a-2b**, in which only one *N*-oxide function is found at each end of the duplex.

Complete solid-state characterization of the homo- and heterodimerization products was obtained with pentamers **3a** and **3b**. As shown in Figure 4, the homodimer was obtained when either **3a** or **3b** was left to crystallize alone,<sup>[12,13]</sup> but cocrystals of the two strands (a heterodimer) were obtained when an equimolar mixture of the two was left to crystallize.<sup>[22]</sup> The structure of **3a-3b** is remarkably similar to that of (**3b**)<sub>2</sub> (Figure 4) despite the fact that the unit cells, the space groups, and the crystallization solvent (and thus the included solvent molecules) of the two crystals are different. The relative positions of the two strands and the interactions between them (for example, aromatic...aromatic distances and a single interstrand NH...ON hydrogen bond) are identical in **3a-3b** and (**3b**)<sub>2</sub>. These findings corroborate the solution studies and supports the complete compatibility between the hybridization of the two series of AOAs. However, it does little to clarify the origin of the larger stability of heterodimers which presumably lies in electro-

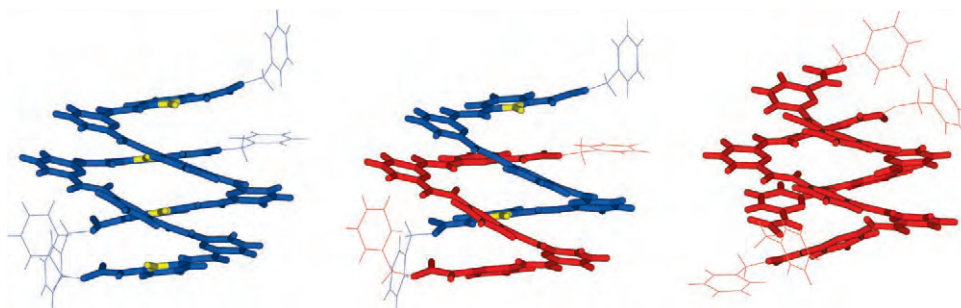


**Figure 4.** Stick representation of the crystal structures of **(3b)<sub>2</sub>** (left), **3a·3b** (center), and **(3a)<sub>2</sub>** (right). The N-oxide functions are shown in yellow. Included solvent molecules are omitted for clarity.

static interactions between amide, pyridine, and pyridine *N*-oxide moieties. Specifically, the surprising stack of four pyridine *N*-oxides rings with all their dipoles in a parallel orientation, as observed in the structure of **(3b)<sub>2</sub>**, certainly causes unfavorable electrostatic interactions that are relieved in the structure of **3a·3b**. We performed ab initio density functional theory calculations (RHF, 6-31G\* basis set) using GAMESS<sup>[23]</sup> to evaluate the electrostatics of the pyridine and pyridine *N*-oxide molecules. The dipole moment of pyridine is estimated as 2.31 D, whilst that of pyridine *N*-oxide is more than twice as large (5.24 D) and has the same orientation. In addition to dipolar interactions, local charges certainly come into play. The partial charge on the pyridine nitrogen atom is −0.51 whilst that on the pyridine *N*-oxide nitrogen atom is only −0.07, with the electrons being located on the oxygen atom (−0.62). One may actually wonder why the pyridine *N*-oxide oligomers hybridize at all. Orbital electron densities show that the  $\pi$  clouds of pyridine *N*-oxide are not as electron-rich as those of pyridine, which probably favors face-to-face  $\pi$ – $\pi$  interactions with the *N*-oxides.

It is worth noting that each aromatic ring within the **3a·3b** duplex interacts directly with two other aromatic rings, one below and one above. The stability of a given duplex may thus be affected in a complex way, depending on whether the rings above and below each aromatic unit are oxidized or not. In DNA, base-pairing energy is known to vary significantly depending on the nature of the neighboring base pairs; such effects could be even more pronounced in heptameric or pentameric molecular duplexes such as **1a·1b** and **3a·3b**.

The tendency of *N*-oxide AOAs to hybridize with their precursors rather than with themselves represents an original example of cross-hybridization. It contrasts with other experiments where self-recognition was reported to prevail over heterologous recognition.<sup>[24]</sup> The hybridization of AOAs may provide a means to elaborate complex sequence-selective hybridization of longer oligomers and more than two *N*-oxide functions per duplex.

Received: February 28, 2006

Published online: June 21, 2006

**Keywords:** helical structures · molecular recognition · supramolecular chemistry

- [1] X. Li, D. R. Liu, *Angew. Chem.* **2005**, *116*, 4956; *Angew. Chem. Int. Ed.* **2004**, *43*, 4848; T. M. Snyder, D. R. Liu, *Angew. Chem.* **2005**, *117*, 7545; *Angew. Chem. Int. Ed.* **2005**, *44*, 7379.

- [2] N. C. Seeman, *Angew. Chem.* **1998**, *110*, 3408; *Angew. Chem. Int. Ed.* **1998**, *37*, 3220; P. W. K. Rothemund, A. Ekani-Nkodo, N. Papadakis, A. Kumar, D. K. Fygenon, E. Winfree, *J. Am. Chem. Soc.* **2004**, *126*, 16344; M. Endo, N. C. Seeman, T. Majima, *Angew. Chem.* **2005**, *117*, 6228; *Angew. Chem. Int. Ed.* **2005**, *44*, 6074; A. Y. Koyfman,

G. Braun, S. Magonov, A. Chworos, N. O. Reich, L. Jaeger, *J. Am. Chem. Soc.* **2005**, *127*, 11886; S. H. Park, C. Pistol, S. J. Ahn, J. H. Reif, A. R. Lebeck, C. Dwyer, T. H. LaBean, *Angew. Chem.* **2006**, *118*, 749; *Angew. Chem. Int. Ed.* **2006**, *45*, 735.

- [3] M. Albrecht, *Angew. Chem.* **2005**, *117*, 6606; *Angew. Chem. Int. Ed.* **2005**, *44*, 6448.
- [4] X. Yang, B. Gong, *Angew. Chem.* **2005**, *117*, 1376; *Angew. Chem. Int. Ed.* **2005**, *44*, 1352.
- [5] M. Albrecht, *Chem. Rev.* **2001**, *101*, 3457; C. Piguet, G. Bernardinelli, G. Hopfgartner, *Chem. Rev.* **1997**, *97*, 2005.
- [6] E. A. Archer, M. J. Krische, *J. Am. Chem. Soc.* **2002**, *124*, 5074; H. Gong, M. J. Krische, *J. Am. Chem. Soc.* **2005**, *127*, 1719; E. A. Archer, A. E. Sochia, M. J. Krische, *Chem. Eur. J.* **2001**, *7*, 2059.
- [7] A. P. Bisson, F. J. Carver, D. S. Eggleston, R. C. Haltiwanger, C. A. Hunter, D. L. Livingstone, J. F. MacCabe, C. Rotger, A. E. Rowan, *J. Am. Chem. Soc.* **2000**, *122*, 8856.
- [8] B. Gong, Y. Yan, H. Zeng, E. Skrzypczak-Jankun, Y. Wah Kim, J. Zhu, H. Ickes, *J. Am. Chem. Soc.* **1999**, *121*, 5607; H. Zeng, R. S. Miller, R. A. Flowers II, B. Gong, *J. Am. Chem. Soc.* **2000**, *122*, 2635.
- [9] P. S. Corbin, S. C. Zimmerman, *J. Am. Chem. Soc.* **2000**, *122*, 3779; P. S. Corbin, S. C. Zimmerman, P. A. Thiessen, N. A. Hawryluk, T. J. Murray, *J. Am. Chem. Soc.* **2001**, *123*, 10475.
- [10] C. Schmuck, W. Wienand, *Angew. Chem.* **2001**, *113*, 4493; *Angew. Chem. Int. Ed.* **2001**, *40*, 4363; C. Schmuck, W. Wienand, *J. Am. Chem. Soc.* **2003**, *125*, 452.
- [11] B. Di Blasio, E. Benedetti, V. Pavone, C. Pedone, *Biopolymers* **1989**, *28*, 203.
- [12] V. Berl, I. Huc, R. Khoury, M. J. Krische, J.-M. Lehn, *Nature* **2000**, *407*, 720; V. Berl, I. Huc, R. Khoury, J.-M. Lehn, *Chem. Eur. J.* **2001**, *7*, 2810; V. Maurizot, J.-M. Léger, P. Guionneau, I. Huc, *Russ. Chem. Bull.* **2004**, *113*, 1572; H. Jiang, V. Maurizot, I. Huc, *Tetrahedron* **2004**, *60*, 10029.
- [13] C. Dolain, C. Zhan, J.-M. Léger, I. Huc, *J. Am. Chem. Soc.* **2005**, *127*, 2400.
- [14] B. Hasenknopf, J.-M. Lehn, G. Baum, D. Fenske, *Proc. Est. Acad. Sci. Eng. Proc. Natl. Acad. Sci. USA* **1996**, *93*, 1397; J.-M. Lehn, *Chem. Eur. J.* **2000**, *6*, 2097.
- [15] H. Zeng, H. Ickes, R. A. Flowers II, B. Gong, *J. Org. Chem.* **2001**, *66*, 3574.
- [16] Y. Tanaka, H. Katagiri, Y. Furusho, E. Yashima, *Angew. Chem.* **2005**, *117*, 3935; *Angew. Chem. Int. Ed.* **2005**, *44*, 3867.
- [17] G. J. Gabriel, B. L. Iverson, *J. Am. Chem. Soc.* **2002**, *124*, 15174; Q.-Z. Zhou, X.-K. Jiang, X.-B. Shao, G.-J. Chen, M.-X. Jia, Z.-T. Li, *Org. Lett.* **2003**, *5*, 1955.
- [18] V. Berl, I. Huc, R. Khoury, J.-M. Lehn, *Chem. Eur. J.* **2001**, *7*, 2798; I. Huc, V. Maurizot, H. Gornitzka, J.-M. Léger, *Chem. Commun.* **2002**, 578; C. Dolain, A. Grélaud, M. Laguerre, H. Jiang, V. Maurizot, I. Huc, *Chem. Eur. J.* **2005**, *11*, 6135.
- [19] A. Acocella, A. Venturini, F. J. Zerbetto, *J. Am. Chem. Soc.* **2004**, *126*, 2362.



- [20] See the Supporting Information.
- [21] The presence of two *N*-oxide groups in **2a** slightly lowers its ability to hybridize whereas the contrary occurs for **1a**, thus suggesting that side-chain and terminal-group effects are complex and do not operate in the same manner on the oxidized oligomers as they do on their precursors.
- [22] Crystal data for **3a·3b**:  $C_{108}H_{82}N_{30}O_{24} \cdot CHCl_3 \cdot C_3H_7NO \cdot 2H_2O$ ,  $M_r = 2412.53$ , crystal size  $0.10 \times 0.10 \times 0.05$ , monoclinic, space group  $P2_1/n$ ,  $Z = 4$ ,  $a = 26.0433(12)$ ,  $b = 14.5247(3)$ ,  $c = 26.6580(10)$  Å,  $\beta = 115.935(2)^\circ$ ,  $V = 9068.4(6)$  Å<sup>3</sup>,  $\rho_{\text{calcd}} = 1.767 \text{ mg m}^{-3}$ ,  $T = 163(2)$  K,  $\theta_{\text{min}} = 6.33^\circ$ ,  $\theta_{\text{max}} = 50.43^\circ$ ,  $\lambda = 1.54180$  Å. Radiation type  $\text{Cu K}\alpha$ ,  $\mu(\text{Cu K}\alpha) = 1.871 \text{ mm}^{-1}$ . Data collected on a Rigaku MM007-Rapid R-Axis diffractometer with confocal optics. Of 95321 reflections measured, 9455 were unique ( $R_{\text{int}} = 0.2080$ ), 5092 with  $I > 2\sigma(I)$ , 1271 parameters in the final refinement. The structure was solved by direct methods and refined by full-matrix least-squares on  $F^2$  (SHELXL version 6.12). The final  $R$  indices were  $R_1$  ( $I > 2\sigma(I)$ ) = 0.1218,  $wR_2(F^2) = 0.3439$  (all data). CCDC-299505 contains the supplementary crystallographic data for this paper. These data can be obtained free of charge from The Cambridge Crystallographic Data Centre via [www.ccdc.cam.ac.uk/data\\_request/cif](http://www.ccdc.cam.ac.uk/data_request/cif).
- [23] M. W. Schmidt, K. K. Baldrige, J. A. Boatz, S. T. Elbert, M. S. Gordon, J. H. Jensen, S. Koseki, N. Matsunaga, K. A. Nguyen, S. J. Su, T. S. Windus, M. Dupuis, J. A. Montgomery, *J. Comput. Chem.* **1993**, *14*, 1347.
- [24] A. Wu, L. Isaacs, *J. Am. Chem. Soc.* **2003**, *125*, 4831; D. Bilgiçer, X. Xing, K. Kumar, *J. Am. Chem. Soc.* **2001**, *123*, 11815.

## Host–Guest Systems

DOI: 10.1002/anie.200600973

**Porous Coordination Polymer with  $\pi$  Lewis Acidic Pore Surfaces,  $[[\text{Cu}_3(\text{CN})_3\{\text{hat}(\text{CN})_3(\text{OEt})_3]\}_n \cdot 3\text{THF}]_n^{**}$** *Daisuke Tanaka, Shigeyuki Masaoka, Satoshi Horike, Shuhei Furukawa, Motohiro Mizuno, Kazunaka Endo, and Susumu Kitagawa\**

Modification of chemical properties of porous coordination polymers (PCPs) is very topical in the area of materials

[\*] Dr. D. Tanaka, Dr. S. Masaoka, S. Horike, Dr. S. Furukawa, Prof. Dr. S. Kitagawa

Department of Synthetic Chemistry and Biological Chemistry  
Graduate School of Engineering, Kyoto University  
Katsura, Nishikyo-ku, Kyoto 615-8510 (Japan)  
Fax: (+81) 75-383-2732

E-mail: kitagawa@sbchem.kyoto-u.ac.jp

Prof. Dr. M. Mizuno, Prof. Dr. K. Endo

Department of Chemistry, Graduate School of Natural Science and  
Technology, Kanazawa University  
Kakuma, Kanazawa, Ishikawa 920-1192 (Japan)

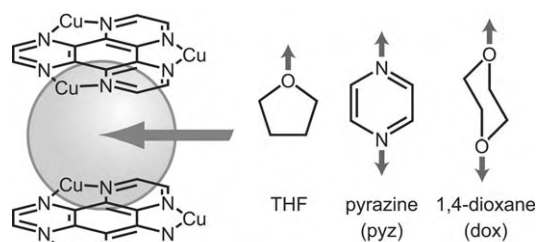
[\*\*] hat = hexaazatriphenylene. This work was supported by a Grants-in-Aid for Scientific Research in a Priority Area "Chemistry of Coordination Space" (#434) and a Grant-in-Aid for Young Scientists (B) (#17750125) from the Ministry of Education, Culture, Sports, Science and Technology, Government of Japan.

Supporting information for this article is available on the WWW under <http://www.angewandte.org> or from the author.

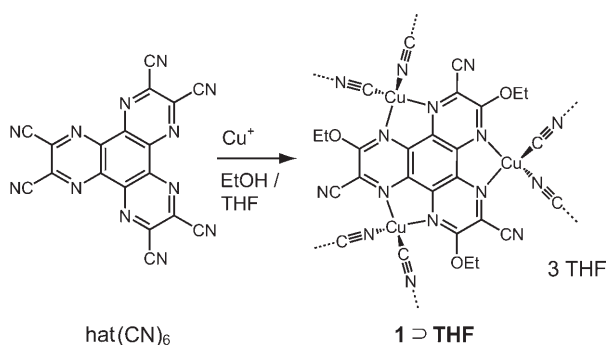
chemistry.<sup>[1]</sup> PCPs with functional groups such as open metal sites or metal-free organic groups in the pores have attracted attention because of their versatile applicability to gas storage, ion exchange, heterogeneous catalysis, and selective guest adsorption. There is no doubt that an adsorption system specific to a target molecule can be realized when multiple interaction sites are located at suitable positions on a regular micropore.<sup>[2]</sup> To obtain such systems, aromatic  $\pi$  moieties could be a key component for the effective confinement of guest molecules that is not only shape-selective but also site-selective due to their large surface area and feasibly modifiable functionality, which is responsible for their interaction with guests.<sup>[3]</sup> In general, aromatic  $\pi$  faces, such as those of benzene, interact with positively charged groups or hydrogen atoms as a Lewis base (so-called, cation– $\pi$ <sup>[4]</sup> and XH– $\pi$ -type interactions, in which X is O, N, C<sup>[5]</sup>). These interactions play important roles in chemical and biological recognition as well as in the construction of protein structures.<sup>[6]</sup> In contrast, interactions of negatively charged atoms with aromatic rings (i.e., anion– $\pi$  interactions) are rare. However, several recent reports claimed that electron-deficient  $\pi$  systems could operate as receptors capable of binding an anion or molecule with electronegative atoms.<sup>[7,8]</sup> In spite of the importance of this interaction and the interest that it has generated, experimental studies within porous frameworks are still rare and recent reports have focused on interaction of discrete anion receptors.<sup>[8,9]</sup> The investigation and discovery of PCPs with neutral  $\pi$  Lewis acidic sites is significant to the design of a new type of interaction site that makes the surface functionality of the pores useful.

To realize PCPs with electron-deficient  $\pi$  systems, hexaazatriphenylene (hat) derivatives were chosen as building units<sup>[10–12]</sup> as they have electron-deficient heterocyclic cores responsible for anion– $\pi$  interactions<sup>[11]</sup> and three chelating sites, which are useful for the construction of a coordination network.<sup>[10]</sup> Previously, we reported anion-trapping host systems constructed from hat derivatives,<sup>[12a]</sup> and a recent theoretical investigation demonstrated that hat derivatives could be used for the molecular recognition of anions.<sup>[11c]</sup> Herein, we report a 3D PCP of a hat derivative, which incorporates neutral guest molecules that have electronegative atoms with the aid of an electron-deficient  $\pi$  surface (Scheme 1).

A coordination polymer,  $[[\text{Cu}^{\text{I}}_3(\text{CN})_3\{\text{hat}(\text{CN})_3(\text{OEt})_3\}_n \cdot 3\text{THF}]_n$  (**1**·3THF), was prepared by the slow intermixing of a solution of  $[\text{Cu}^{\text{I}}_2(\mu\text{-}\eta^2, \eta^2\text{-benzoquinone})(\text{OAc})_2]$  in ethanol and a solution of hat(CN)<sub>6</sub> in THF.<sup>[13]</sup> This reaction affords C<sub>3</sub> symmetrical hat(CN)<sub>3</sub>(OEt)<sub>3</sub> and CN<sup>−</sup> ions through the substitution of an ethoxy for a cyano group (Scheme 2).<sup>[14]</sup> Single-crystal X-ray diffraction measurements confirmed that the distorted tetrahedron around the Cu<sup>I</sup> cation consists of two nitrogen atoms from hat(CN)<sub>3</sub>(OEt)<sub>3</sub>, one nitrogen atom, and one carbon atom from the cyanide anions. These cyanide ligands link the two tetrahedral copper ions to form a 3D (8,3)-c type network (Figure 1).<sup>[15]</sup> There are two kinds of pores in this structure: one is a large 1D channel running along the *c* axis with a cross section of  $10 \times 10 \text{ \AA}^2$  (Figure 1a); the other pore is just a pocket located along the channel, in which the hat units form a floor and a ceiling and whose



**Scheme 1.** Inclusion of solvent guest molecules into pores comprising  $\pi$  planes.



**Scheme 2.** Synthesis of **1**⊃THF.

portals open to three adjacent channels (Figure 1b). The crystal structure in Figure 1c,d reveals that the three THF molecules are accommodated in the cavity. Interestingly, the THF molecules do not sit parallel but perpendicular to the hat plane, and the vertical distance between the hat plane and the oxygen atom is 2.97 Å,<sup>[16]</sup> which indicates that there is an attractive interaction between the oxygen atom and the hat  $\pi$  plane that is attributed to an anion- $\pi$  type interaction.

Thermogravimetric analysis (TGA) of **1**⊃THF shows that the removal of two THF molecules in the temperature range 30–80 °C is accompanied by a severe broadening of the X-ray powder diffraction (XRPD) pattern (see Supporting Information).<sup>[17]</sup> Complete removal of three THF molecules was accomplished by putting **1**⊃THF in a vacuum at 50 °C or by washing with EtOH to afford an amorphous guest-free solid, **1**. However, by soaking **1** in THF, a porous framework identical to that of **1**⊃THF returns, as demonstrated by XRPD (see Supporting Information). This phenomenon also occurs with 1,4-dioxane (dox), *N,N*-dimethylformamide (DMF) or in an ethanol solution of pyrazine (pyz; see Supporting Information). Such an amorphous-to-crystal phase transition is associated with the guest (G) inclusion as shown in Equation (1).



In contrast, when **1** is soaked in hydrocarbons (hexane, cyclohexane, and benzene), linear ethers and alcohols (diethylether, methanol, and ethanol), and a large-molecule compound (4,4'-bipyridyl), there are no sharp peaks in the corresponding XRPD patterns. The structural recovery occurs only for guest molecules with at least one electro-

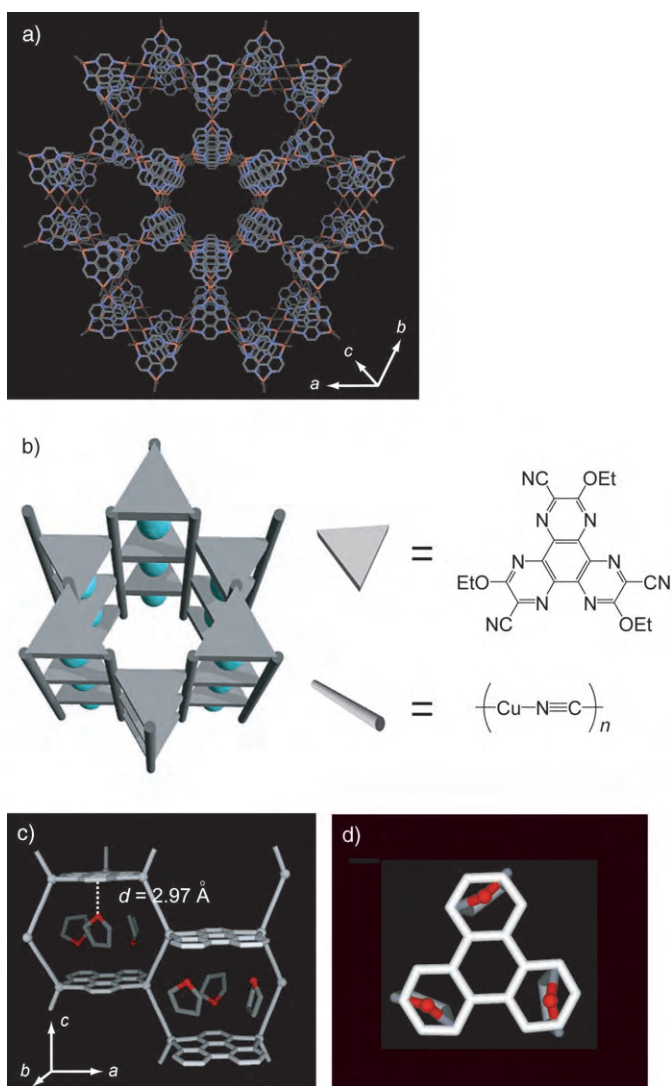


**Figure 1.** Structural representation of **1**⊃THF. a) 1D channel structure constructed by Cu<sup>I</sup>, hat(CN)<sub>3</sub>(OEt)<sub>3</sub>, and cyanide anions (Cu, red; C, gray; N, blue). The ethoxy and cyano groups of hat and the THF molecules are omitted for clarity. b) Schematic representation of the pore structure of **1**⊃THF. c) Crystal structure of the cavity defined by two hat molecules. (O, red; C, gray) d) View of hat with THF along the *c* axis. Disordered THF molecules are omitted for clarity in (c) and (d).

negative atom, X, and which are the right size for the cavity, thus indicating that the origin of the guest-responsive phase transformation is the guest-selective inclusion in the cavity promoted by X- $\pi$ (hat) interactions.

To determine the crystal structures of **1** with other guests, single crystals were obtained by the crystal-to-crystal guest exchange of **1**⊃THF with pyz and dox. When single crystals of **1**⊃THF were immersed in an ethanol solution of pyz (0.1 M) at room temperature for several days, the THF molecules in the cavity were replaced by pyz to give **1**⊃pyz without loss of crystallinity. Similarly, single crystals of **1**⊃dox were obtained by immersing single crystals of **1**⊃THF in a mixture of dox/EtOH (1:1 v/v).

The crystallographic analysis reveals that the framework of **1**⊃pyz is isomorphous to that of **1**⊃THF; the pyz molecules

are accommodated within the cavity in place of the THF molecules. The accommodation of pyz involves elongation of the crystal dimension along the crystallographic  $c$  axis ( $8.7244(9) \text{ \AA} \rightarrow 8.791(2) \text{ \AA}$ ;  $\Delta = 0.07 \text{ \AA}$ ) and shrinking along the  $a$  and  $b$  axes ( $18.1226(19) \text{ \AA} \rightarrow 18.034(5) \text{ \AA}$ ;  $\Delta = -0.09 \text{ \AA}$ ). In the cavity, the edge-to-face contact between a nitrogen atom of pyz and the hat  $\pi$  plane is easily identified, with a separation of  $3.02 \text{ \AA}$  (Figure 2a). The pyz plane disorders over two positions around the  $C_2$  axes with an angle,  $\theta$ , of  $40^\circ$  (Figure 2b). The short  $\pi(\text{hat})\text{--N}(\text{pyz})$  separations indicate that two nitrogen atoms of the pyz molecule interact with the two  $\pi$  planes of the hat moieties.

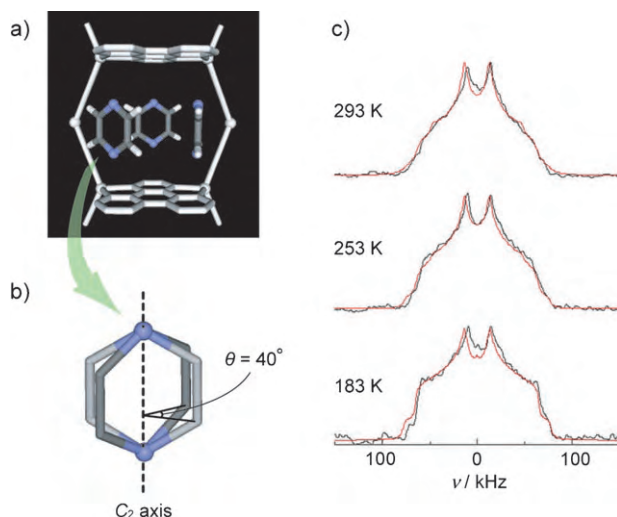


**Figure 2.** a) Crystal structure of the cavity of **1Dpyz**. The ethoxy and cyano groups and disordered pyz molecules are omitted for clarity. b) Schematic illustration of disordered structure of pyz. c) Selected  $^2\text{H}$  NMR spectra (black line: experimental; red line: simulation) of the  $[\text{D}_4]\text{pyz}$  molecule of **1D** $[\text{D}_4]\text{pyz}$  (see Supporting Information).

Similarly, the single crystal structure of **1Ddox** shows that the dox molecules are accommodated within the cavity. The  $\text{O}\text{--}\pi$  separations are  $2.93\text{--}2.95 \text{ \AA}$  (see Supporting Information). In all cases of **1DG**, the  $\text{X}\text{--}\pi$  separations indicate that the electronegative atoms of the guest molecules interact with the hat  $\pi$  planes, and the lone pair of X is directed towards the  $\pi$  face as in the case of hexafluorobenzene complexes.<sup>[7c,18]</sup> It is worth noting that there are no recognizable specific host–guest interactions except for the  $\text{X}\text{--}\pi$  plane contact in the crystal structures of **1DG**. These results confirm that the origin of the guest-selective inclusion of **1** is the interaction between  $\pi$  Lewis acid and electronegative atoms.

Information about the dynamics of the confined guest molecules in the host framework is important for an in-depth understanding of how strongly the guest molecules are accommodated. We acquired solid-state  $^2\text{H}$  NMR spectra of **1D** $[\text{D}_4]\text{pyz}$  between 183 and 293 K, which show doublet patterns of  $[\text{D}_4]\text{pyz}$  in the cavity over the whole temperature range. The simulation of the signal affords an anisotropic motion of the  $[\text{D}_4]\text{pyz}$ , which is a pyz ring rotation around the molecular NN axis perpendicular to the hat plane. The motion has two kinds of frequencies and moves over four sites

with angles of  $0^\circ$ ,  $40^\circ$ ,  $180^\circ$  and  $220^\circ$ . This result is consistent with the crystallographic structure of disordered pyz shown in Figure 2b. The restricted motion is caused by the interaction between two nitrogen atoms of pyz and hat  $\pi$  planes.

TGA and XRPD measurements of heated samples of **1DTHF** show that the crystallinity of **1DG** is not retained upon the loss of the guest molecules (Supporting Information).<sup>[17]</sup> Therefore, the presence of guest molecules is essential to maintain the framework. Unlike results obtained from the analysis of **1DTHF**, the results of crystallographic analysis and solid-state  $^2\text{H}$  NMR spectra of **1Dpyz** reveal that the pyz molecules behave as if the two nitrogen atoms at both ends of the molecule bind with the two  $\pi$  planes of hat moieties. The multiple interactions in **1Dpyz** could influence the stability of the framework. Indeed, XRPD measurements with heating and TGA show that **1Dpyz** is stable up to  $120^\circ\text{C}$  (Supporting Information). Interestingly, placing **1Dpyz** under vacuum or washing the compound with ethanol does not result in the removal of pyz molecules and there is no significant loss in crystallinity. In contrast, **1DTHF** gradually collapses upon the removal of THF molecules under ambient temperature and pressure. Such strong accommodation and enhanced stability of the crystal phase of **1Dpyz** is ascribed to the pillar support of the pyz within the cavity, which arises from the two-point N– $\pi$  interactions.

In conclusion, we have demonstrated that neutral organic guest molecules can be confined within the cavities of a porous coordination polymer through the interaction between electronegative atoms and electron-deficient  $\pi$  planes, the so-called anion– $\pi$  interaction. This interaction could be exploited to design a new family of PCPs.

## Experimental Section

**Synthesis of 1DTHF:** hat(CN)<sub>6</sub> was prepared according to reported procedures.<sup>[19]</sup> An ethanol solution of  $[\text{Cu}^{\text{I}}_2(\mu\text{--}\eta^2, \eta^2\text{--benzoquinone})\text{--}(\text{OAc})_2]$  (10 mM, 2 mL), prepared by the in situ reaction of copper (II) acetate with hydroquinone in ethanol,<sup>[13]</sup> was carefully layered on a hat(CN)<sub>6</sub> solution in THF, where a mixed solvent of THF/ethanol (1:1 v/v) was placed between the two layers. Dark brown crystals suitable for single-crystal X-ray analysis were obtained after one week. For elemental analysis, these crystals were collected, washed with EtOH and dried in vacuo. Elemental analysis of guest-free solid, **1**, calcd for  $\text{C}_{24}\text{H}_{15}\text{Cu}_3\text{N}_{12}\text{O}_3$  (%): C 40.59, H 2.13, N 23.67; found: C 39.65, H 2.42, N 22.72. IR (Nujol):  $\tilde{\nu} = 2236 \text{ cm}^{-1}$  (CN from hat(CN)<sub>3</sub>–(OEt)<sub>3</sub>),  $2138 \text{ cm}^{-1}$  (cyanide anion).

**Physical measurements:** XRPD data were collected on a Rigaku RINT 2000 (Ultima) diffractometer by using  $\text{CuK}\alpha$  radiation. Elemental analyses were measured on Thermo Finnigan EA1112. TGA was carried out with a Rigaku Instrument TG8120 in a nitrogen atmosphere at  $2^\circ\text{C min}^{-1}$ . IR spectra were recorded on a Perkin-Elmer 2000 FTIR spectrophotometer with samples prepared with Nujol. Solid-state  $^2\text{H}$  NMR spectra were measured by a Varian Chemagnetics CMX-300 spectrometer operated at  $45.826 \text{ MHz}$  and the quadrupole pulse sequence was used for the measurements. Simulated spectra were produced by using home-written FORTRAN programs.

**X-ray structure determination:** X-ray structures were determined on a Rigaku Mercury CCD system with  $\text{MoK}\alpha$  radiation. In all cases, the structure was solved by direct methods (SIR 97) and refined on  $F^2$  in SHELXL-97. Crystal data for **1DTHF**,  $\text{C}_{12}\text{Cu}_4\text{N}_4\text{O}_2$ ,  $M_r = 295.70$ , hexagonal, space group  $P6_3/mmc$ , (no. 194),  $a = 18.1226(19)$ ,  $c =$



8.7244(9) Å,  $V = 2481.5(4)$  Å<sup>3</sup>,  $Z = 6$ ,  $\rho_{\text{calc}} = 1.187$  g cm<sup>-3</sup>,  $F(000) = 870$ ,  $\mu(\text{Mo}_{\text{K}\alpha}) = 1.321$  cm<sup>-1</sup>,  $T = -50^\circ\text{C}$ ,  $2\theta_{\text{max}} = 50.0^\circ$ ,  $\lambda(\text{Mo}_{\text{K}\alpha}) = 0.71070$  Å, reflections collected/unique 17476/858,  $R(R_w) = 0.077$  (0.218), GOF = 1.220 and 66 parameters. The residual electron density (min./max.) is  $-0.41/0.48$  e Å<sup>-3</sup>. Solvent molecules and some disordered molecules were refined isotropically, whereas other atoms were refined anisotropically. The C–C and C–O bond lengths in THF were restrained to 1.54 Å. Crystal data for **1**⌐pyz, C<sub>12</sub>H<sub>4</sub>CuN<sub>6</sub>O,  $M_r = 311.75$ , hexagonal, space group  $P6_3/mmc$ , (no. 194),  $a = 18.034(5)$ ,  $c = 8.791(2)$  Å,  $V = 2476.0(11)$  Å<sup>3</sup>,  $Z = 6$ ,  $\rho_{\text{calc}} = 1.254$  g cm<sup>-3</sup>,  $F(000) = 930$ ,  $\mu(\text{Mo}_{\text{K}\alpha}) = 1.326$  cm<sup>-1</sup>,  $T = -50^\circ\text{C}$ ,  $2\theta_{\text{max}} = 50.0^\circ$ ,  $\lambda(\text{Mo}_{\text{K}\alpha}) = 0.71070$  Å, reflections collected/unique 17608/859,  $R(R_w) = 0.060$  (0.172), GOF = 1.166 and 67 parameters. The residual electron density (min./max.) is  $-0.50/0.59$  e Å<sup>-3</sup>. Disordered atoms were refined isotropically, whereas other non-hydrogen atoms were refined anisotropically. Hydrogen atoms of pyz were placed geometrically and refined by using a riding model with  $U_{\text{iso}}$  constrained to be 1.2 times  $U_{\text{eq}}$  of the carrier atom. Crystal data for **1**⌐dox, C<sub>12</sub>H<sub>4</sub>CuN<sub>6</sub>O,  $M_r = 311.75$ , hexagonal, space group  $P6_3/mmc$ , (no. 194),  $a = 18.421(5)$ ,  $c = 8.537(5)$  Å,  $V = 2508.8(18)$  Å<sup>3</sup>,  $Z = 6$ ,  $\rho_{\text{calc}} = 1.238$  g cm<sup>-3</sup>,  $F(000) = 918$ ,  $\mu(\text{Mo}_{\text{K}\alpha}) = 1.314$  cm<sup>-1</sup>,  $T = -50^\circ\text{C}$ ,  $2\theta_{\text{max}} = 50.0^\circ$ ,  $\lambda(\text{Mo}_{\text{K}\alpha}) = 0.71070$  Å, reflections collected/unique 14492/866,  $R(R_w) = 0.067$  (0.175), GOF = 1.137 and 75 parameters. The residual electron density (min./max.) is  $-0.53/0.57$  e Å<sup>-3</sup>. Solvent molecules and some of disordered molecules were refined isotropically, whereas other atoms were refined anisotropically. CCDC-600740, CCDC-600741 and CCDC-600742 contain the supplementary crystallographic data for this paper. These data can be obtained free of charge from The Cambridge Crystallographic Data Centre via [www.ccdc.cam.ac.uk/data\\_request/cif](http://www.ccdc.cam.ac.uk/data_request/cif).

Received: March 13, 2006

Published online: June 22, 2006

**Keywords:** coordination polymers · copper · crystal engineering · host–guest systems ·  $\pi$  interactions

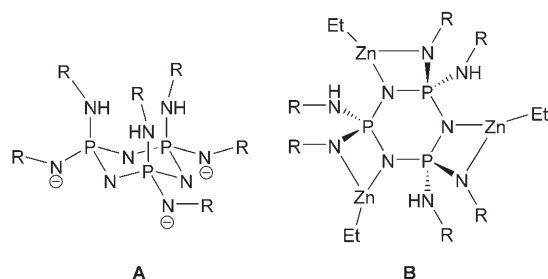
- [1] a) P. J. Langley, J. Hulliger, *Chem. Soc. Rev.* **1999**, 28, 279–291; b) B. Moulton, M. J. Zaworotko, *Chem. Rev.* **2001**, 101, 1629–1658; c) O. M. Yaghi, M. O’Keeffe, N. W. Ockwig, H. K. Chae, M. Eddaoudi, J. Kim, *Nature* **2003**, 423, 705–714; d) G. S. Papaefstathiou, L. R. MacGillivray, *Coord. Chem. Rev.* **2003**, 246, 169–184; e) M. J. Rosseinsky, *Microporous Mesoporous Mater.* **2004**, 73, 15–30; f) R. J. Hill, D. L. Long, N. R. Champness, P. Hubberstey, M. Schröder, *Acc. Chem. Res.* **2005**, 38, 337–350; g) S. Kitagawa, R. Kitaura, S. Noro, *Angew. Chem.* **2004**, 116, 2388–2430; *Angew. Chem. Int. Ed.* **2004**, 43, 2334–2375.
- [2] R. Matsuda, R. Kitaura, S. Kitagawa, Y. Kubota, R. V. Belosludov, T. C. Kobayashi, H. Sakamoto, T. Chiba, M. Takata, Y. Kawazoe, Y. Mita, *Nature* **2005**, 436, 238–241.
- [3] P. Sozzani, S. Bracco, A. Comotti, L. Ferretti, R. Simonutti, *Angew. Chem.* **2005**, 117, 1850–1854; *Angew. Chem. Int. Ed.* **2005**, 44, 1816–1820.
- [4] J. C. Ma, D. A. Dougherty, *Chem. Rev.* **1997**, 97, 1303–1324.
- [5] M. Nishio, *CrystEngComm* **2004**, 6, 130–158.
- [6] E. A. Meyer, R. K. Castellano, F. Diederich, *Angew. Chem.* **2003**, 115, 1244–1287; *Angew. Chem. Int. Ed.* **2003**, 42, 1210–1250.
- [7] a) D. Quinonero, C. Garau, C. Rotger, A. Frontera, P. Ballester, A. Costa, P. M. Deya, *Angew. Chem.* **2002**, 114, 3539–3542; *Angew. Chem. Int. Ed.* **2002**, 41, 3389–3392; b) M. Mascal, A. Armstrong, M. D. Bartberger, *J. Am. Chem. Soc.* **2002**, 124, 6274–6276; c) Y. Danten, T. Tassaing, M. Besnard, *J. Phys. Chem. A* **1999**, 103, 3530–3534.
- [8] For a recent experimental study on anion receptors with electron-deficient  $\pi$  systems, see: a) R. M. Fairchild, K. T. Holman, *J. Am. Chem. Soc.* **2005**, 127, 16364–16365; b) S. Demeshko, S. Dechert, F. Meyer, *J. Am. Chem. Soc.* **2004**, 126, 4508–4509; c) Y. S. Rosokha, S. V. Lindeman, S. V. Rosokha, J. K. Kochi, *Angew. Chem.* **2004**, 116, 4750–4752; *Angew. Chem. Int. Ed.* **2004**, 43, 4650–4652; d) P. de Hoog, P. Gamez, I. Mutikainen, U. Turpeinen, J. Reedijk, *Angew. Chem.* **2004**, 116, 5939–5941; *Angew. Chem. Int. Ed.* **2004**, 43, 5815–5817; e) O. B. Berryman, F. Hof, M. J. Hynes, D. W. Johnson, *Chem. Commun.* **2006**, 506–508.
- [9] M. Yoshizawa, T. Kusukawa, M. Kawano, T. Ohhara, I. Tanaka, K. Kurihara, N. Niimura, M. Fujita, *J. Am. Chem. Soc.* **2005**, 127, 2798–2799.
- [10] a) B. E. Abrahams, P. A. Jackson, R. Robson, *Angew. Chem.* **1998**, 110, 2801–2804; *Angew. Chem. Int. Ed.* **1998**, 37, 2656–2659; b) H. S. Grove, J. Julve, F. Lloret, *Dalton Trans.* **2001**, 1029–1034; c) M. Shatruk, A. Chouai, A. V. Prosvirin, K. R. Dunbar, *Dalton Trans.* **2005**, 1897–1902; d) X. H. Bu, K. Biradha, T. Yamaguchi, M. Nishimura, T. Ito, K. Tanaka, M. Shionoya, *Chem. Commun.* **2000**, 1953–1954; e) S. Kitagawa, S. Masaoka, *Coord. Chem. Rev.* **2003**, 246, 73–88.
- [11] a) J. T. Rademacher, A. W. Czarnik, *J. Am. Chem. Soc.* **1993**, 115, 3018–3019; b) E. O. Arikainen, N. Boden, R. J. Bushby, O. R. Lozman, J. G. Vinter, A. Wood, *Angew. Chem.* **2000**, 112, 2423–2426; *Angew. Chem. Int. Ed.* **2000**, 39, 2333–2336; c) A. Frontera, F. Sączewski, M. Gdaniec, E. Dziemidowicz-Borys, A. Kurland, P. M. Deya, D. Quinonero, C. Garau, *Eur. J. Org. Chem.* **2005**, 179–183.
- [12] a) T. Okubo, S. Kitagawa, M. Kondo, H. Matsuzaka, T. Ishii, *Angew. Chem.* **1999**, 111, 980–983; *Angew. Chem. Int. Ed.* **1999**, 38, 931–933; b) S. Furukawa, T. Okubo, S. Masaoka, D. Tanaka, H. C. Chang, S. Kitagawa, *Angew. Chem.* **2005**, 117, 2760–2764; *Angew. Chem. Int. Ed.* **2005**, 44, 2700–2704.
- [13] S. Masaoka, G. Akiyama, S. Horike, S. Kitagawa, T. Ida, K. Endo, *J. Am. Chem. Soc.* **2003**, 125, 1152–1153.
- [14] This nucleophilic displacement reaction is characteristic of N-heterocyclic chelate ligands such as 2,2'-bipyridyl (bpy) and 1,10-phenanthroline (phen). Coordination of N-heterocyclic chelate ligands to a metal ion activates the  $\alpha$  carbon atoms of the ligands towards nucleophilic attack. For details of this type of reaction, see: a) R. D. Gillard, *Coord. Chem. Rev.* **1975**, 16, 67–94; b) X. M. Zhang, M. L. Tong, X. M. Chen, *Angew. Chem.* **2002**, 114, 1071–1073; *Angew. Chem. Int. Ed.* **2002**, 41, 1029–1031.
- [15] A. F. Wells, *Three-Dimensional Nets and Polyhedra*, Wiley, New York, **1977**.
- [16] This distance is slightly shorter than the sum of van der Waals radii. The van der Waals radii of carbon, nitrogen, and oxygen are 1.7, 1.5 and 1.5 Å, respectively.
- [17] The XRPD patterns of heated **1**⌐THF show that the Bragg peaks become broad and disappear with elongation of the  $a$  and  $b$  axes and shrinking along the  $c$  axis in the temperature range 30–80°C. These observations and the results of TGA demonstrate that the guest molecules play an important role in stabilizing the crystal structures.
- [18] I. Alkorta, I. Rozas, M. L. Jimeno, J. Elguero, *Struct. Chem.* **2001**, 12, 459–464.
- [19] J. T. Rademacher, K. Kanakarajan, A. W. Czarnik, *Synthesis* **1994**, 378–380.

## Tris(organozinc) Phosphazenes as Templates for Trimeric and Hexameric Zinc Oxide Clusters\*\*

Ramamoorthy Boomishankar, Philip I. Richards, and Alexander Steiner\*

Molecular metal oxide complexes can serve as valuable models in various areas, including surface–substrate interactions in heterogeneous catalysis, metal oxide particles in porous solids, deposition, precipitation, and condensation reactions that lead to  $M_xO_y$  framework structures.<sup>[1]</sup> High oxidation-state metal oxide complexes  $[(R_mM_xO_y)_n]$  exhibit a variety of frameworks  $[(M_xO_y)_n]$  that comprise ring or cage structures.<sup>[2]</sup> While the metal centers are shielded by anionic organic ligands, R, the oxygen centers, as a result of their low basicity, can occupy corner positions of the framework. In contrast, complex oxides of +I and +II metal ions are fairly basic. Hence, their oxide ions are located at interstitial sites surrounded by excess metal ions, and complexes bearing more than two oxide centers are rare.<sup>[3]</sup> A notable exception is a complex reported by Mulvey and co-workers that contains six oxide ions. It comprises an  $\{(MgO)_6\}$  core enclosed by six  $NaNR_2$  moieties.<sup>[4]</sup>

Over the past years, we have studied the coordination behavior of multianionic phosphazenate ligands.<sup>[5]</sup> The trianionic ligand **A** features three anionic N centers at equatorial positions ( $N_{eq}$ ) of the chair-shaped  $\{P_3N_3\}$  ring and offers three chelating  $N_{eq}$ – $N_{ring}$  sites (Scheme 1).<sup>[6]</sup> Herein, we report that

Scheme 1. Trianionic ligand **A** and tris(ethylzinc) complex **B**.

the tris(ethylzinc) complex **B** can act as a template for trimeric and hexameric zinc oxide clusters through the bowl-shaped coordination surface of three Lewis basic  $N_{eq}$  functions and three Lewis acidic Zn centers. The *n*-propyl

derivative was obtained by deprotonation of the phosphazene  $(nPrNH)_6P_3N_3$  (**1**) with three equivalents of  $Et_2Zn$  in hexane. The resulting complex **2** shows a singlet at  $\delta = 26.4$  ppm in the  $^{31}P$  NMR spectrum. Compound **2** exists as a dimeric complex of molecular  $D_3$  symmetry in the solid state (Figure 1).<sup>[7]</sup> Two **B** segments are linked through six short  $Zn$ – $N_{eq}$  interactions (av: 2.038 Å). Although the  $Zn$ – $N_{ring}$  bonds are also short (av: 2.046 Å), the  $Zn$ – $N_{eq}$  interactions inside **B** appear to be rather loose (av: 2.390 Å).

Recently, we found that phosphazenes  $(RNH)_6P_3N_3$  crystallize in the presence of water as distinct hydrates,  $(RNH)_6P_3N_3 \cdot xH_2O$ , which display hydrogen-bonded networks in the solid state.<sup>[8]</sup> This behavior suggested to us that we should treat these hydrates with  $3 + x$  equivalents of  $Et_2Zn$  in anticipation that three equivalents of  $Et_2Zn$  deprotonate the phosphazene to form **B**. The  $ZnO$ , generated by the in situ hydrolysis of  $x$  equivalents of  $Et_2Zn$  by  $x$  equivalents of water, might then be trapped within the molecular complex. Compound **1**·1.5  $H_2O$  crystallized from a solution of **1** in hexane exposed to moist air. Subsequently, it was treated with 4.5 equivalents of  $Et_2Zn$  in hexane, thus giving a singlet at  $\delta = 26.1$  ppm in the  $^{31}P$  NMR spectrum. The crystal structure of the product complex **3** shows a planar  $\{(ZnO)_3\}$  ring sandwiched between two **B** segments (Figure 1).<sup>[7]</sup> The cyclohexyl (Cy) derivative  $(CyNH)_6P_3N_3$  (**4**) crystallized as the pentahydrate **4**·5  $H_2O$  from THF/water. Proceeding in the same manner as in the synthesis of **3**, we treated **4**·5  $H_2O$  with eight equivalents of  $Et_2Zn$  in hexane. The reaction solution was filtered from a small amount of precipitate (presumably excess  $ZnO$ ). The crystal structure of the product complex **5** comprises a hexagonal  $\{(ZnO)_6\}$  prism sandwiched between two **B** segments (Figure 1).<sup>[7]</sup> To the best of our knowledge, zinc oxide clusters that contain more than two oxide ions have not been reported. There is one example of a planar  $\{(ZnO)_3\}$  ring with hydroxide ions,<sup>[9]</sup> but there are no precedents for  $\{(ZnO)_6\}$  prisms.

Complexes **3** and **5** display molecular  $D_3$  and  $S_6$  symmetries, respectively. Both are derived from the insertion of zinc oxide clusters into the dimeric arrangement of two **B** segments. The coordination surface of **B** provides a perfect mold for trimeric and hexameric  $ZnO$  clusters that bind Zn ions through  $N_{eq}$  centers and oxide ions to the  $EtZn$  units. As a result, the  $\{(ZnO)_3\}$  ring structure of **3** demands the phosphazenate ligands to be eclipsed, whereas the  $\{(ZnO)_6\}$  prism of **5** is supported by a staggered ligand arrangement. The selection of either the ring or prism assembly is largely determined by the steric demand of the R substituents. The cyclohexyl groups are too bulky to maintain the eclipsed conformation, but they are able to interdigitate in the staggered conformation of **5**. When **4**·1.5  $H_2O$ <sup>[10]</sup> was treated with 4.5 equivalents of  $Et_2Zn$  with the aim of producing a  $\{(ZnO)_3\}$  ring complex, only an indistinct product mixture was obtained. On the other hand, when the trihydrate of  $(iBuNH)_6P_3N_3$  (**6**·3  $H_2O$ ),<sup>[10]</sup> which features the less bulky isobutyl groups, was treated with six equivalents of  $Et_2Zn$  to form a  $\{(ZnO)_6\}$  complex, the product **7** contained a  $\{(ZnO)_3\}$  unit similar to that found in **3**.<sup>[7]</sup>

The eclipsed ligand arrangement forces the  $\{(ZnO)_3\}$  ring of **3** into a planar conformation that shows minimal deviation

[\*] Dr. R. Boomishankar, Dr. P. I. Richards, Dr. A. Steiner  
Department of Chemistry  
University of Liverpool  
Liverpool, L69 7ZD (UK)  
Fax: (+44) 151-794-388  
E-mail: a.steiner@liv.ac.uk

[\*\*] This work was supported by EPSRC.

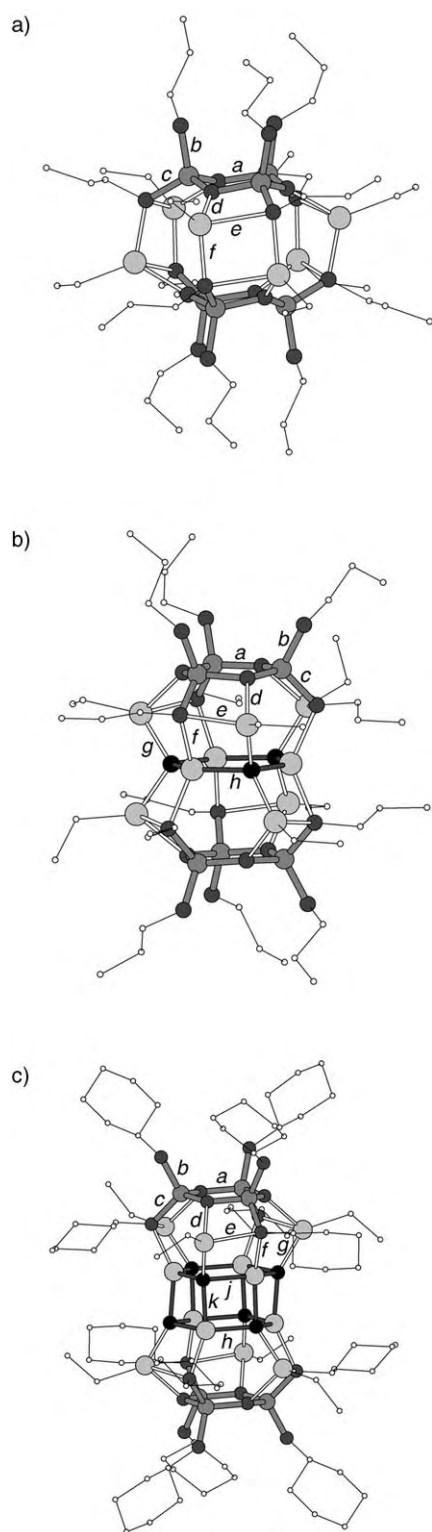


**Figure 1.** Crystal structures of a) **2**, b) **3**, and c) **5**. Zn light gray, P medium gray, N dark gray, O black, C white. H atoms are omitted for clarity. Selected bond lengths [Å] averaged over topologically equivalent bonds: **2**: P–N(a) 1.629, P–N(b) 1.654, P–N(c) 1.626, Zn–N(d) 2.046, Zn–N(e) 2.390, Zn–N(f) 2.038; **3**: P–N(a) 1.623, P–N(b) 1.647, P–N(c) 1.636, Zn–N(d) 2.115, Zn–N(e) 2.292, Zn–N(f) 2.067, Zn–O(g) 1.966, Zn–O(h) 1.968; **5**: P–N(a) 1.622, P–N(b) 1.650, P–N(c) 1.641, Zn–N(d) 2.176, Zn–N(e) 2.290, Zn–N(f) 2.021, Zn–O(g) 1.949, Zn–O(h) 1.963, Zn–O(i) 1.984, Zn–O(j) 2.034.

from the mean plane (0.007(1) Å), whereas the staggered arrangement in **5** enables the six-membered rings of the  $\{(ZnO)_6\}$  prisms to pucker slightly into a chair-conformation (0.054(1) Å). The  $\{(PN)_3\}$  rings of **3** and **5** show very little puckering (0.052(2) and 0.063(1) Å, respectively), whereas those of **2** exhibit a more pronounced chair-conformation (0.162(1) Å). This behavior suggests that there is some flexibility within the ligand to adapt to the host structure by tightening or widening its grip. The average distance between the  $N_{eq}$  sites within **B** provides a useful ligand grip parameter that measures 5.22 Å in **2** and that tightens upon coordination of zinc oxide to 4.77 and 4.80 Å in **3** and **5**, respectively.

The bond lengths of the  $\{(ZnO)_3\}$  ring in **3** fall within a narrow range of 1.962(2)–1.974(2) Å. The bond angles in the  $\{(ZnO)_3\}$  ring are much wider at the Zn (av: 126.4°) than at the O center (av: 113.6°). The  $\{(ZnO)_6\}$  cage of **5** contains three types of topologically unique Zn–O bonds (labeled *h*, *j*, and *k* in Figure 1 c). Bonds *h* and *k* alternate around both six-membered Zn–O rings. The slightly longer bonds *h* are parallel to  $EtZn-N_{eq}$  bonds of the adjacent **B** segment. Bulk ZnO (zincite) exhibits the hexagonal wurtzite structure,<sup>[11]</sup> whereas its high pressure phase (*hp*ZnO) adapts the cubic structure of rock salt.<sup>[12]</sup> Zn–O bond lengths in zincite compare well with those found in **3** and **5**. Figure 2 illustrates

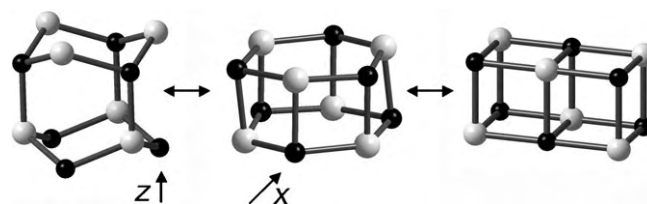


**Figure 2.** The  $\{(ZnO)_6\}$  segments of **5** (center), zincite (left), and *hp*ZnO (right).

how the  $\{(ZnO)_6\}$  prism of **5** relates to the open  $\{(ZnO)_6\}$  segment of zincite and also to the corresponding  $\{(ZnO)_6\}$  segment of *hp*ZnO. The prism can be regarded as an intermediate along the pathway of a hypothetical transformation: Compression of the open zincite-type segment along the *z* axis gives the prism, which furnishes the cubic arrangement of *hp*ZnO when squashed along the *x* axis.

In conclusion, we have shown that tris(ethylzinc) phosphazenes can act as templates for the construction of novel zinc oxide clusters. Their bowl-shaped coordination surface of three Lewis acidic and three Lewis basic sites provides a perfect mold for planar  $\{(ZnO)_3\}$  rings and hexagonal  $\{(ZnO)_6\}$  prisms. The availability of well-defined phosphazene hydrates  $(RNH)_6P_3N_3 \cdot xH_2O$  offers a convenient route for reactions of reactive metal reagents with stoichiometric amounts of water in situ. In principle, other small substrates that form distinct adducts  $(RNH)_6P_3N_3 \cdot yH_2X$  could react in a similar fashion, thus producing small molecular frameworks that are trapped inside organometal phosphazenate complexes.



## Experimental Section

All operations were performed in an inert-gas atmosphere. Compounds **1**, **4**, and **6** were prepared as described previously.<sup>[13]</sup> Et<sub>2</sub>Zn was applied as a 1.0 M solution in hexane. NMR spectra were taken from [D<sub>8</sub>]toluene solutions.

**2:** Et<sub>2</sub>Zn (6.2 mmol) in hexane (6.2 mL) was added to a solution of **1** (1 g, 2.07 mmol) in hexane (20 mL). The reaction mixture was stirred for 12 h, filtered, and concentrated. Colorless crystals formed after 3 days at 5 °C (1.32 g, 84 %). M.p. > 275 °C (decomp); <sup>1</sup>H NMR (400 MHz): δ = 0.66 (q, ZnCH<sub>2</sub>), 1.58 (t, ZnCH<sub>2</sub>CH<sub>3</sub>), 0.8–2.3 (m, *n*Pr-H), 3.2–3.4 ppm (m, NCH<sub>2</sub>); <sup>13</sup>C NMR (100 MHz): δ = 12.9, 21.7, 24.4, 25.0, 30.7, 35.5, 48.7, 61.50 ppm; <sup>31</sup>P NMR (162 MHz): δ = 26.4 ppm; IR (Nujol):  $\tilde{\nu}$  = 3393 w, 1256 s, 1084 vs, 1021 vs, 948 w, 862 w, 799 s cm<sup>-1</sup>.

**3:** Et<sub>2</sub>Zn (3.5 mmol) in hexane (3.5 mL) was added to a suspension of **1**·1.5H<sub>2</sub>O (0.40 g, 0.78 mmol) in hexane (10 mL). The reaction mixture was stirred for 12 h, filtered, and concentrated. Colorless crystals formed after 2 days at –20 °C (0.46 g, 67 %). M.p. > 162 °C (decomp); <sup>1</sup>H NMR (400 MHz): δ = 0.73 (q, CH<sub>2</sub>Zn), 0.84 (t, NHCH<sub>2</sub>CH<sub>2</sub>CH<sub>3</sub>), 1.68 (t, CH<sub>3</sub>CH<sub>2</sub>Zn), 1.03 (t, NCH<sub>2</sub>CH<sub>2</sub>CH<sub>3</sub>), 1.34 (q, NHCH<sub>2</sub>CH<sub>2</sub>), 1.87 (m, NCH<sub>2</sub>CH<sub>2</sub>), 2.08 (m, NH), 2.86 (m, NHCH<sub>2</sub>), 3.06 (m, NCH<sub>2</sub>); <sup>13</sup>C NMR (100 MHz): δ = 1.1, 11.1, 11.9, 13.7, 25.4, 31.6, 43.1, 50.5 ppm; <sup>31</sup>P NMR (162 MHz): δ = 26.1 ppm; IR (Nujol):  $\tilde{\nu}$  = 1286 w, 1261 w, 1227 s, 1112 vs, 1051 s, 888 w, 800 s cm<sup>-1</sup>.

**5:** Et<sub>2</sub>Zn (4.9 mmol) in hexane (4.9 mL) was added to a suspension of **4**·5H<sub>2</sub>O (0.25 g, 0.31 mmol) in hexane (10 mL). The reaction mixture was stirred for 12 h, filtered, and concentrated. Colorless crystals formed after 5 days at –20 °C (0.27 g, 71 %). M.p. > 240 °C (decomp); <sup>1</sup>H NMR (400 MHz): δ = 0.68 (q, CH<sub>2</sub>Zn), 1.63 (t, CH<sub>3</sub>CH<sub>2</sub>Zn), 0.8–1.95 (m, CH<sub>2</sub>), 2.09 (m, NH), 3.1–3.4 ppm (m, NCH); <sup>13</sup>C NMR (100 MHz): δ = 1.3, 12.9, 21.7, 24.0, 21.4, 24.9, 25.9, 30.7, 35.4 ppm; <sup>31</sup>P NMR (162 MHz): δ = 21.6 ppm; IR (Nujol):  $\tilde{\nu}$  = 3411 w (N–H), 1405 w, 1291 m, 1291 m, 1261 m, 1229 s, 1186 w, 1146 m, 1078 vs, 915 s, 888 m, 846 m, 805 s cm<sup>-1</sup>.

**7:** Et<sub>2</sub>Zn (5.3 mmol) in hexane (5.3 mL) was added to a mixture of **6** (0.50 g, 0.88 mmol) and H<sub>2</sub>O (0.048 mL, 2.65 mmol) in hexane (15 mL). The reaction mixture was stirred for 12 h, filtered, and concentrated. Colorless crystals formed after 2 days at –20 °C (0.48 g, 56 %). M.p. > 180 °C (decomp); <sup>1</sup>H NMR (400 MHz): δ = 0.72 (q, CH<sub>2</sub>Zn), 0.91 (d, NHCH<sub>2</sub>CH(CH<sub>3</sub>)<sub>2</sub>), 1.14 (d, NCH<sub>2</sub>CH(CH<sub>3</sub>)<sub>2</sub>), 1.63 (t, CH<sub>3</sub>CH<sub>2</sub>Zn), 1.67–1.89 (m, CH<sub>2</sub>CH(CH<sub>3</sub>)<sub>2</sub>), 2.09 (m, NH), 2.84 (m, NHCH<sub>2</sub>), 3.11 ppm (m, 12H, NCH<sub>2</sub>); <sup>13</sup>C NMR (100 MHz): δ = 1.3, 14.1, 14.6, 22.4, 23.4, 30.8, 32.4, 49.8 ppm; <sup>31</sup>P NMR (162 MHz): δ = 26.8 ppm; IR (Nujol):  $\tilde{\nu}$  = 3404 br, 1401 w, 1279 w, 1231 s, 1200 s, 1130 vs, 1089 s cm<sup>-1</sup>.

Received: March 22, 2006

Published online: June 22, 2006

**Keywords:** metal oxides · N,P ligands · phosphazenes · phosphazenes · zinc

- [4] A. M. Drummond, L. T. Gibson, A. R. Kennedy, R. E. Mulvey, C. T. O'Hara, R. B. Rowlings, T. Weightman, *Angew. Chem.* **2002**, *114*, 2488; *Angew. Chem. Int. Ed.* **2002**, *41*, 2382.
- [5] A. Steiner, S. Zacchini, P. I. Richards, *Coord. Chem. Rev.* **2002**, *227*, 193.
- [6] G. T. Lawson, F. Rivals, M. Tascher, C. Jacob, J. F. Bickley, A. Steiner, *Chem. Commun.* **2000**, 341.
- [7] Crystal data were measured on a Bruker Apex diffractometer at *T* = 100 K using MoK $\alpha$  radiation. Crystal structures were refined against *F*<sup>2</sup> using all data.<sup>[14]</sup> **2:** C<sub>48</sub>H<sub>120</sub>N<sub>18</sub>P<sub>6</sub>Zn<sub>6</sub>, *M<sub>r</sub>* = 1527.7, *C2/c*, *a* = 22.0843(11), *b* = 13.8929(7), *c* = 23.6468(12) Å,  $\beta$  = 95.3500(10)°, *V* = 7223.6(6) Å<sup>3</sup>, *Z* = 4, *R*<sub>1</sub> (*I* > 2σ(*I*)) = 0.028, *wR*<sub>2</sub> (all data) = 0.074; **3:** C<sub>48</sub>H<sub>120</sub>N<sub>18</sub>O<sub>3</sub>P<sub>6</sub>Zn<sub>9</sub>, *M<sub>r</sub>* = 1771.8, *P2<sub>1</sub>/c*, *a* = 16.5237(9), *b* = 15.2248(9), *c* = 29.8265(17) Å,  $\beta$  = 91.7800(10)°, *V* = 7499.8(7) Å<sup>3</sup>, *Z* = 4, *R*<sub>1</sub> (*I* > 2σ(*I*)) = 0.038, *wR*<sub>2</sub> (all data) = 0.100; **5:** 1.5C<sub>6</sub>H<sub>14</sub>: C<sub>93</sub>H<sub>189</sub>N<sub>18</sub>O<sub>6</sub>P<sub>6</sub>Zn<sub>12</sub>, *M<sub>r</sub>* = 2625.9, *P1̄*, *a* = 14.164(2), *b* = 14.976(2), *c* = 16.602(2) Å,  $\alpha$  = 113.405(2),  $\beta$  = 100.528(3),  $\gamma$  = 96.041(2)°, *V* = 3115.2(8) Å<sup>3</sup>, *Z* = 1, *R*<sub>1</sub> (*I* > 2σ(*I*)) = 0.035, *wR*<sub>2</sub> (all data) = 0.102; **7:** C<sub>60</sub>H<sub>144</sub>N<sub>18</sub>O<sub>6</sub>P<sub>6</sub>Zn<sub>6</sub>, *M<sub>r</sub>* = 1940.1, *R3̄c*, *a* = 18.8839(10), *c* = 50.977(6) Å, *V* = 15 743(2) Å<sup>3</sup>, *Z* = 6, *R*<sub>1</sub> (*I* > 2σ(*I*)) = 0.099, *wR*<sub>2</sub> (all data) = 0.35. Crystals of **7** diffracted very weakly and refined poorly, thus structural parameters are not discussed; however, the data quality was sufficient to confirm the connectivity of **7**. Crystallographic data in CIF format (CCDC-602267 (**2**), -602268 (**3**), -602269 (**5**), -602266 (**7**)) contain the supplementary crystallographic data for this paper. These data can be obtained free of charge from The Cambridge Crystallographic Data Centre via [www.ccdc.cam.ac.uk/data\\_request/cif](http://www.ccdc.cam.ac.uk/data_request/cif).
- [8] A detailed account on phosphazene hydrates will be reported elsewhere. Selected data for **1**·1.5H<sub>2</sub>O: m.p. 55 °C, *P2<sub>1</sub>/n*, *a* = 9.3162(5), *b* = 24.704(1), *c* = 24.810(1) Å,  $\beta$  = 92.460(1)°; **4**·5H<sub>2</sub>O: m.p. 162 °C, *P2<sub>1</sub>/n*, *a* = 16.736(3), *b* = 19.977(2), *c* = 27.476(3) Å,  $\beta$  = 104.46(2)°.
- [9] I. B. Gorrell, A. Looney, G. Parkin, A. L. Rheingold, *J. Am. Chem. Soc.* **1990**, *112*, 4068.
- [10] Complexes **6**·3H<sub>2</sub>O and **4**·1.5H<sub>2</sub>O were prepared by grinding phosphazenes with stoichiometric amounts of water.
- [11] a) J. Albertsson, S. C. Abrahams, Å. Kvik, *Acta Crystallogr. Sect. B* **1989**, *45*, 34; b) S. C. Abrahams, J. L. Bernstein, *Acta Crystallogr. Sect. B* **1969**, *25*, 1233.
- [12] a) C. H. Bates, W. B. White, R. Roy, *Science* **1962**, *137*, 993; b) S. Desgreniers, *Phys. Rev. B* **1998**, *58*, 14102.
- [13] J. F. Bickley, R. Bonar-Law, G. T. Lawson, P. I. Richards, F. Rivals, A. Steiner, S. Zacchini, *Dalton Trans.* **2003**, 1235.
- [14] G. M. Sheldrick, SHELX-97, Universität Göttingen, 1997.

- [1] a) J.-P. Jolivet, *Metal Oxide Chemistry and Synthesis: From Solution to Solid State*, Wiley, Chichester, **2000**; b) C. N. R. Rao, B. Raveau, *Transition Metal Oxides: Structure, Properties, and Synthesis of Ceramic Oxides*, Wiley-VCH, Weinheim, **1998**; c) J. M. Thomas, W. J. Thomas, *Principles and Practice of Heterogeneous Catalysis*, Wiley-VCH, Weinheim, **1997**.
- [2] a) H. W. Roesky, I. Haiduc, N. S. Hosmane, *Chem. Rev.* **2003**, *103*, 2579; b) H. W. Roesky, M. G. Walawalkar, R. Murugavel, *Acc. Chem. Res.* **2001**, *34*, 201; c) V. Chandrasekhar, S. Nagen-dran, V. Baskar, *Coord. Chem. Rev.* **2002**, *235*, 1.
- [3] A. E. H. Wheatley, *Chem. Soc. Rev.* **2001**, *30*, 265.



## Cyclization

DOI: 10.1002/anie.200601722

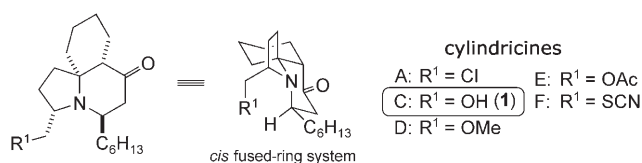
## Short Synthesis of (+)-Cylindricine C by Using a Catalytic Asymmetric Michael Reaction with a Two-Center Organocatalyst\*\*

Tomoyuki Shibuguchi, Hisashi Mihara,  
Akiyoshi Kuramochi, Shun Sakuraba,  
Takashi Ohshima, and Masakatsu Shibasaki\*

Present syntheses of natural products and medicinally relevant compounds require high efficiency in terms of the number of synthetic steps. Tandem reactions that combine several transformations in a single procedural step are powerful tools for minimizing synthetic steps.<sup>[1]</sup> In addition to time–cost benefits, they can allow selective reactions of unstable species and side reactions to be minimized by the rapid successive formation and consumption of intermediates. Catalytic asymmetric reactions have also enabled more efficient syntheses of various highly versatile chiral compounds that allow for the development of new or more practical retrosynthetic analyses of complex natural products.<sup>[2]</sup> The combination of tandem reactions and catalytic asymmetric reactions leads to more efficient synthetic routes. Herein, we report a short total synthesis of (+)-cylindricine C by a tandem cyclization and catalytic asymmetric Michael reaction with a newly designed two-center organocatalyst.

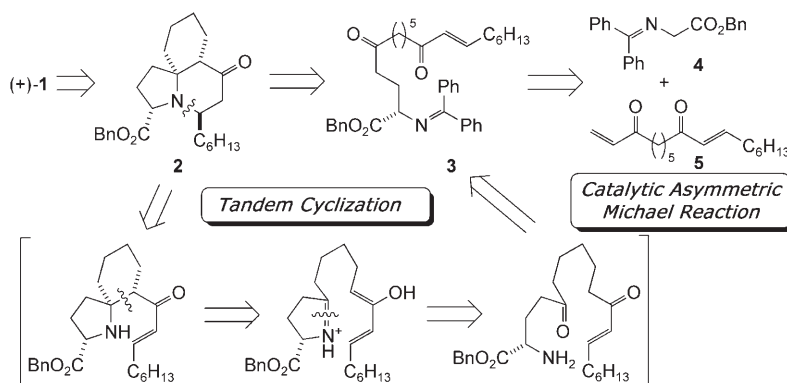
The cylindricines were isolated from the marine ascidian *Clavelina cylindrica* by Blackman et al. between 1993 and 1995.<sup>[3]</sup> These structurally related compounds exhibit bioactivity against a DNA-repair-deficient yeast strain<sup>[4]</sup> and also inhibit the growth of murine leukemia and human solid-tumor cell lines.<sup>[5]</sup> Their tricyclic ring system (see Scheme 1) is comprised of a spirocyclic amine that makes them an attractive target for total synthesis.<sup>[6]</sup>

The first total synthesis of optically active cylindricine C was reported by Molander and Ronn,<sup>[7a]</sup> and several groups also succeeded in its total synthesis.<sup>[7b–e]</sup> Because they used stepwise strategies to construct the tricyclic ring system, their synthesis required several steps (9–14 steps). We planned to



Scheme 1. Structure of the cylindricines.

construct a tricyclic ring system from **3** in a one-pot reaction by using tandem cyclization through imine formation, the Mannich reaction, and the aza-Michael reaction (Scheme 2). The required compound **3** is a highly functionalized  $\alpha$ -amino



Scheme 2. Retrosynthetic analysis of (+)-cylindricine C. Bn = benzyl.

acid derivative. Recently, we developed a two-center organocatalyst **6** (TaDiAS; tartrate-derived diammonium salt) that efficiently catalyzes phase-transfer alkylation,<sup>[8a,b]</sup> Michael reactions,<sup>[8a,b]</sup> and Mannich-type reactions of the glycine Schiff base.<sup>[8c]</sup> We planned to synthesize **3** by using a catalytic asymmetric Michael reaction<sup>[9,10]</sup> with TaDiAS.

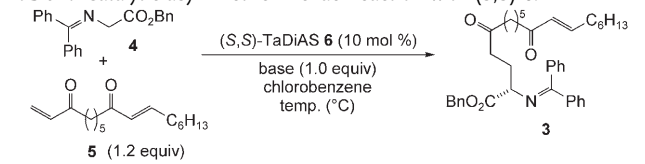
First, we examined the catalytic asymmetric Michael reaction of glycine Schiff base **4** to dienone **5**, which was prepared from pimelic acid in two steps (Table 1). Based on our previous results,<sup>[8a,b]</sup> the reaction was performed with 10 mol% of (*S,S*)-**6a** (the best catalyst for the Michael reaction to  $\alpha,\beta$ -unsaturated esters). In contrast to the Michael reaction to  $\alpha,\beta$ -unsaturated esters, the addition of **4** to  $\alpha,\beta$ -unsaturated ketones (enone) proceeds with more modest selectivity.<sup>[8a,b]</sup> As expected from previous work, the reaction with **5** was only moderately enantioselective (entry 1). Nevertheless, we were pleased to observe clean formation of the monoaddition product. Next we examined the catalyst structure to improve the enantioselectivity. Previous conformational analysis of **6a**<sup>[8c]</sup> suggested that the acetal moiety regulates the chiral environment around the two ammonium cations. We designed a new catalyst **6b** that has a 2,6-disubstituted cyclohexane structure at the acetal moiety to affect the chiral environment more strongly. Among the three diastereomers that originate from the relative stereochemistry of the acetal moiety, *C*<sub>2</sub>-symmetric **6b** was found to be most effective in the preceding investigations (see the Supporting Information). When **6b** was applied to the reaction of **4** with **5**, enantioselectivity was improved to 63% *ee* (entry 2). At lower temperature (–30°C) both reactivity and selectivity

[\*] T. Shibuguchi, H. Mihara, A. Kuramochi, S. Sakuraba, Dr. T. Ohshima, Prof. Dr. M. Shibasaki  
Graduate School of Pharmaceutical Sciences  
The University of Tokyo  
Hongo, Bunkyo-ku, Tokyo 113-0033 (Japan)  
Fax: (+81) 3-5684-5206  
E-mail: mshibasa@mol.f.u-tokyo.ac.jp

[\*\*] This work was supported by RFTF, a Grant-in-Aid for the Encouragement of Young Scientists (A), and a Grant-in-Aid for Specially Promoted Research from the Japan Society for the Promotion of Science (JSPS) and the Ministry of Education, Culture, Sports, Science and Technology (MEXT).

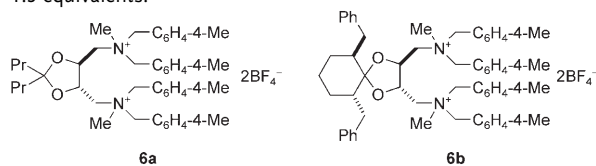
Supporting information for this article is available on the WWW under <http://www.angewandte.org> or from the author.

**Table 1:** Catalytic asymmetric Michael reaction with (S,S)-**6**.



Entry	Catalyst	Base	T [°C]	t [h]	Yield [%] <sup>[a]</sup>	ee [%] <sup>[b]</sup>
1	<b>6a</b>	K <sub>2</sub> CO <sub>3</sub>	4	14	96	48
2	<b>6b</b>	K <sub>2</sub> CO <sub>3</sub>	4	14	96	63
3	<b>6b</b>	K <sub>2</sub> CO <sub>3</sub>	−30	36	86	61
4	<b>6b</b>	Cs <sub>2</sub> CO <sub>3</sub>	−30	24	72	74
5 <sup>[c,d]</sup>	<b>6b</b>	Cs <sub>2</sub> CO <sub>3</sub>	−40	66	84	82

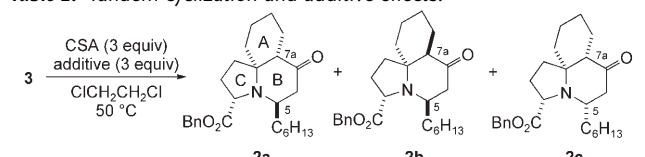
[a] Yield of the isolated product. [b] Determined by chiral stationary phase HPLC. [c] 3-Fluorotoluene was used as the solvent. [d] Cs<sub>2</sub>CO<sub>3</sub>: 1.5 equivalents.



were lowered (entry 3). Enantioselectivity was improved to 74% ee by using Cs<sub>2</sub>CO<sub>3</sub> as the base (entry 4). Further investigations revealed that the use of 1.5 equivalents of Cs<sub>2</sub>CO<sub>3</sub> and 3-fluorotoluene as the solvent at −40 °C **3** could be obtained in 84% yield of isolated product and 82% ee (entry 5).

We next examined tandem cyclization (Table 2). Tricyclic compound **2** was obtained when **3** was treated with 3 equivalents of camphorsulfonic acid (CSA) in 1,2-dichloroethane. The reaction provided three diastereomers (**2a–c**), as determined by NMR spectroscopic analysis, whose configurations were identified as shown in Table 2 (**2a**: desired *cis* fused AB ring; **2b**: *trans*-fused AB ring; **2c**: *cis* fused AB ring and *epi* C5 position). Under these conditions, the chemical yield was moderate (47%) and **2b** was obtained as the major product (entry 1, **2a/2b/2c** = 33:63:4). Several different solvents and acids were examined, but the reactivity and diastereoselectivity were insignificantly affected. When AlCl<sub>3</sub> was used as an additive, the diastereoselectivity was greatly improved, thus selectively

**Table 2:** Tandem cyclization and additive effects.

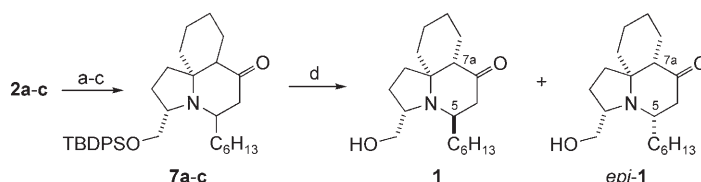


Entry	Additive	t [h]	d.r. [2a/2b/2c] <sup>[a]</sup>	Yield [%] <sup>[b]</sup>
1	–	18	33:63:4	47
2	AlCl <sub>3</sub>	24	87:13:trace	47
3	[La(OTf) <sub>3</sub> ]	12	27:65:8	57
4	MgCl <sub>2</sub>	12	84:9:7	65
5	MgBr <sub>2</sub> ·(Et <sub>2</sub> O) <sub>2</sub>	18	82:13:5	61
6	LiCl	18	89:6:5	57

[a] Determined by <sup>1</sup>H NMR spectroscopic analysis. [b] Yield of the isolated product.

affording the desired **2a** (entry 2, **2a/2b/2c** = 87:13:trace). Several other additives were examined under the optimized conditions (entries 3–6). The reaction with [La(OTf)<sub>3</sub>] (OTf = triflate) afforded **2b** as the major product (entry 3), whereas MgCl<sub>2</sub>, MgBr<sub>2</sub>·(Et<sub>2</sub>O)<sub>2</sub>, and LiCl gave better reactivity and **2a** as the major product (entries 4–6). The mechanism of the additive effects is unclear, but we assume that additives operate as Lewis acids and organize the reacting centers through chelation.<sup>[11]</sup>

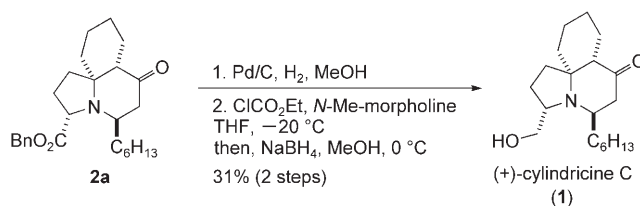
The obtained tricyclic compounds **2a–c** were transformed into (+)-cylindricine C (Scheme 3). The product mixture from entry 4 in Table 2 (**2a/2b/2c** = 84:9:7) was converted into **7a–c** in three steps. Cylindricine C (**1**) and 5-*epi*-cylindricine C (*epi-1*)<sup>[7c,11]</sup> were obtained in 80 and 8% yield, respectively, after treatment of **7a–c** with tetrabutylammonium fluoride (TBAF). The *trans*-fused AB ring of **7b** was isomerized at the C7a position to the desired *cis* fused AB ring under basic conditions.<sup>[7d,e]</sup> Computational studies also supported this result.<sup>[11]</sup> Optically pure **1** was obtained in 59% yield after three recrystallizations of the picric acid salt of **1** from EtOH.



**Scheme 3.** Synthesis of (+)-cylindricine C. Reagents and conditions:

a) LiAlH<sub>4</sub>, THF, reflux; b) *tert*-butyldiphenylsilyl chloride (TBDPSCl), Et<sub>3</sub>N, CH<sub>2</sub>Cl<sub>2</sub>; c) Dess–Martin periodinane, CH<sub>2</sub>Cl<sub>2</sub> (71%; 3 steps); d) TBAF, THF, RT (**1**: 80%; *epi-1*: 8%).

Thus, we succeeded in the synthesis of enantiomerically pure **1** from pimelic acid in nine steps, including the recrystallization process. The number of synthetic steps required to obtain **1** could be further decreased by using a mixed anhydride reduction process.<sup>[12]</sup> Thereby, **1** was obtained in two steps from **2a** (Scheme 4; total 6 steps).



**Scheme 4.** Shorter approach to (+)-cylindricine C from **2a**.

In conclusion, we have achieved a short synthesis of (+)-cylindricine C (6 steps) using a catalytic asymmetric Michael reaction of a glycine Schiff base and subsequent tandem cyclization. Further improvement of each step and the expansion of current strategies are in progress.

Received: May 2, 2006

Published online: June 21, 2006

**Keywords:** cyclization · Michael addition · phase-transfer catalysis · spiro compounds · total synthesis

- [1] For representative reviews of tandem reactions in organic synthesis, see: a) J. D. Winkler, *Chem. Rev.* **1996**, 96, 167; b) P. J. Parsons, C. S. Penkett, A. J. Shell, *Chem. Rev.* **1996**, 96, 195; c) K. C. Nicolaou, T. Montagnon, S. A. Snyder, *Chem. Commun.* **2003**, 551; d) J. C. Wasilke, S. J. Obrey, R. T. Baker, G. C. Bazan, *Chem. Rev.* **2005**, 105, 1001.
- [2] For general reviews, see: a) R. Noyori, *Asymmetric Catalysis in Organic Synthesis*, Wiley, New York, **1994**; b) *Comprehensive Asymmetric Catalysis* (Eds.: E. N. Jacobsen, A. Pfaltz, H. Yamamoto), Springer, New York, **1999**; c) I. Ojima, *Catalytic Asymmetric Synthesis*, 2nd ed., Wiley, New York, **2000**.
- [3] a) A. J. Blackman, C. Li, D. C. R. Hockless, B. H. Skelton, *Tetrahedron* **1993**, 49, 8645; b) A. J. Blackman, C. Li, *Aust. J. Chem.* **1994**, 47, 1355; c) A. J. Blackman, C. Li, *Aust. J. Chem.* **1995**, 48, 955.
- [4] a) A. D. Patil, A. J. Freyer, R. Reichwein, B. Carte, L. B. Killmer, L. Faucette, R. K. Johnson, D. J. Faulkner, *Tetrahedron Lett.* **1997**, 38, 363; b) S. Dutta, H. Abe, S. Aoyagi, C. Kibayashi, K. S. Gates, *J. Am. Chem. Soc.* **2005**, 127, 15004.
- [5] M. F. Raub, J. H. Cardellina, M. I. Choudhary, C.-Z. Ni, J. Clardy, M. C. Alley, *J. Am. Chem. Soc.* **1991**, 113, 3178.
- [6] For a review of the synthesis of cylindricines, see: J. Liu, R. P. Hsung, *ChemTracts* **2005**, 18, 321.
- [7] a) G. A. Molander, M. Ronn, *J. Org. Chem.* **1999**, 64, 5183; b) B. M. Trost, M. T. Rudd, *Org. Lett.* **2003**, 5, 4599; c) S. Canesi, D. Bouchu, M. A. Ciufolini, *Angew. Chem.* **2004**, 116, 4436; *Angew. Chem. Int. Ed.* **2004**, 43, 4336; d) T. Arai, H. Abe, S. Aoyagi, C. Kibayashi, *Tetrahedron Lett.* **2004**, 45, 5921; e) J. Liu, R. P. Hsung, S. D. Peter, *Org. Lett.* **2004**, 6, 3989.
- [8] a) T. Shibuguchi, Y. Fukuta, Y. Akachi, A. Sekine, T. Ohshima, M. Shibasaki, *Tetrahedron Lett.* **2002**, 43, 9539; b) T. Ohshima, T. Shibuguchi, Y. Fukuta, M. Shibasaki, *Tetrahedron* **2004**, 60, 7743; c) A. Okada, T. Shibuguchi, T. Ohshima, H. Masu, K. Yamaguchi, M. Shibasaki, *Angew. Chem.* **2005**, 117, 4640; *Angew. Chem. Int. Ed.* **2005**, 44, 4564.
- [9] For recent reviews of asymmetric phase-transfer catalysis (PTC) reactions, see: a) K. Maruoka, T. Ooi, *Chem. Rev.* **2003**, 103, 3013; b) M. J. O'Donnell, *Acc. Chem. Res.* **2004**, 37, 506; c) B. Lygo, B. I. Andrews, *Acc. Chem. Res.* **2004**, 37, 518.
- [10] For the catalytic asymmetric phase-transfer Michael reaction of the glycine Schiff base, see: a) E. J. Corey, M. C. Noe, F. Xu, *Tetrahedron Lett.* **1998**, 39, 5347; b) M. J. O'Donnell, F. Delgado, E. Dominguez, J. de Blas, W. L. Scott, *Tetrahedron: Asymmetry* **2001**, 12, 821; c) S. Arai, R. Tsuji, A. Nishida, *Tetrahedron Lett.* **2002**, 43, 9535; d) T. Akiyama, M. Hara, K. Fuchibe, S. Sakamoto, K. Yamaguchi, *Chem. Commun.* **2003**, 1734; e) B. Lygo, B. Albutt, E. H. M. Kirton, *Tetrahedron Lett.* **2005**, 46, 4461; f) P. V. Ramachandran, S. Madhi, L. Bland-Berry, M. V. R. Reddy, M. J. O'Donnell, *J. Am. Chem. Soc.* **2005**, 127, 13450.
- [11] a) K. M. Werner, J. M. de los Santos, S. M. Weinreb, M. Shang, *J. Org. Chem.* **1999**, 64, 8263; b) J. J. Swidorski, J. Wang, R. P. Hsung, *Org. Lett.* **2006**, 8, 777.
- [12] a) K. Ishizumi, K. Koga, S. Yamada, *Chem. Pharm. Bull.* **1968**, 16, 492; b) G. Kokotos, *Synthesis* **1990**, 299.

DOI: 10.1002/anie.200601264

# Exceptionally Strong Electronic Communication through Hydrogen Bonds in Porphyrin-C<sub>60</sub> Pairs\*\*

Luis Sánchez, Maria Sierra, Nazario Martín,\*  
Andrew J. Myles, Trevor J. Dale, Julius Rebek, Jr.,\*  
Wolfgang Seitz, and Dirk M. Guldi\*

*In memory of Roger Taylor*

Proton pumping in the photosynthetic reaction center and conduction of electrons in cytochrome C are significant examples of biological processes governed by supramolecular interactions.<sup>[1]</sup> The key function of these examples is electron transfer, which is powered through a network of hydrogen bonds. As a result, hydrogen-bonded donor-acceptor assemblies have emerged as a benchmark for biomimetic model systems: they provide the means for understanding and controlling the role of hydrogen-bonding networks either as a simple molecular interface or, more interestingly, as an actively functioning motif (namely, by assisting more efficient electron-transfer events). These effects largely result from the high efficiency that this supramolecular motif offers in controlling through-bond-mediated electron-transfer processes as well as long-range electronic coupling between donors and acceptors.<sup>[2]</sup> Pioneering work carried out by Sessler and

[\*] Dr. L. Sánchez, M. Sierra, Prof. Dr. N. Martín  
Departamento de Química Orgánica  
Facultad de Química  
Universidad Complutense de Madrid, 28040 Madrid (Spain)  
Fax: (+ 34) 91-394-4103  
E-mail: nazmar@quim.ucm.es

Dr. A. J. Myles, T. J. Dale, Prof. Dr. J. Rebek, Jr.  
The Skaggs Institute for Chemical Biology and Department of Chemistry  
The Scripps Research Institute  
10550 North Torrey Pines Road (MB26), La Jolla, CA 92037 (USA)  
Fax: (+ 34) 91-394-4103  
E-mail: jrebek@scripps.edu

W. Seitz, Prof. Dr. D. M. Guldi  
Institut für Physikalische und Theoretische Chemie  
Universität Erlangen-Nürnberg  
Egerlandstrasse 3, 91058 Erlangen (Germany)  
Fax: (+ 49) 9131-852-830  
E-mail: dirk.guldi@chemie.uni-erlangen.de

[\*\*] This work was supported by the MEC of Spain and Comunidad de Madrid (CTQ2005-02609/BTQ and P-PPQ-000225-0505), the Deutsche Forschungsgemeinschaft (SFB 583), FCI, the Office of Basic Energy Sciences of the US Department of Energy (contribution No. NDRL-4670 from the Notre Dame Radiation Laboratory), and the Skaggs Institute for Chemical Biology. M.S. is indebted to MEC of Spain for a PhD fellowship, A.J.M. is a NSERC postdoctoral fellow, and T.J.D. is a Skaggs predoctoral fellow.



Supporting information for this article is available on the WWW under <http://www.angewandte.org> or from the author.

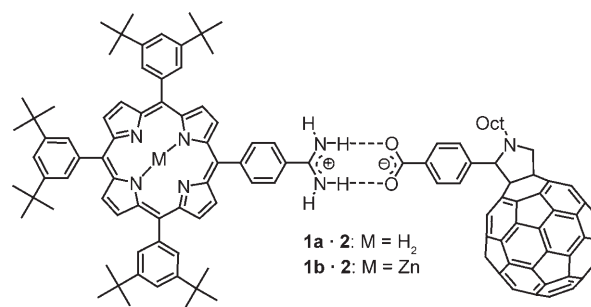


Therien have demonstrated that the electronic communication through hydrogen-bonding interfaces is more efficient than those found in comparable  $\sigma$ - or  $\pi$ -bonding networks.<sup>[3]</sup> Electron-transfer events also impart on the function of artificial devices, such as organic photovoltaics.<sup>[4]</sup> The incentives for creating (supra)molecular heterojunctions by, for example, integrating photo-/electroactive donors and acceptors that bear complementary binding sites into functional architectures are 1) facilitation of charge transport and 2) increase in energy conversion efficiency.<sup>[5]</sup>

The relevance of fullerenes as spherical electron acceptors in the construction of novel artificial photosynthetic models and in high-performance organic solar cells is incontestable.<sup>[4–6]</sup> The combination of the characteristic selectivity and directionality of hydrogen bonds with an efficient electron-transfer process through a noncovalent framework is expected to set new milestones, especially in terms of achieving longer-lived radical-ion-pair states. In fact, a plethora of covalent  $C_{60}$ -donor conjugates have stimulated evolutionary advances and revolutionary breakthroughs in the context of converting light into high-energy chemical products or electrical currents.<sup>[7]</sup> Very little is, however, known about noncovalent  $C_{60}$ -based hybrid ensembles.<sup>[8]</sup> To our knowledge, no  $C_{60}$ -based examples of electron-transfer processes that occur exclusively through hydrogen-bonded networks have been reported. We present herein a set of noncovalently associated  $C_{60}$ -porphyrin ensembles (**1–2**) interfaced by a two-point amidinium–carboxylate pair that facilitates an efficient charge-separation process to afford microsecond-lived  $P^{+}-C_{60}^{-}$  radical pairs. The latter is particularly stable, even in highly polar solvents, as a result of the synergy of hydrogen bonds and electrostatic interactions.<sup>[9]</sup> Beneficial effects also materialize from other salt pairs, that is, guanidinium–carboxylate, especially in terms of structural aspects.<sup>[10]</sup> Notably, the noncovalent binding motif utilized herein, amidinium–carboxylate, diminishes the possible bonding modes and, therefore, favors the linearity of the final interfaced pair. In addition, the rational design, that is, placing the amidinium and carboxylate functionalities at the porphyrins and  $C_{60}$ , respectively, reinforces the strength of the hydrogen-bonding network and ensures an optimal pathway for the motion of charges and the electronic coupling between both electroactive units.<sup>[9a]</sup>

The synthesis of the new **1–2** ensembles started from a previously reported porphyrin amidine donor **1a, b**<sup>[11]</sup> and fulleropyrrolidine carboxylic acid **2**.<sup>[12]</sup> Directly mixing both components readily yields target ensembles, namely, noncovalently bonded hybrids **1–2** (see Scheme 1 and the Supporting Information).

Complex formation between **1a** and **2** was monitored by  $^1H$  NMR spectroscopy (3 mm,  $[D_8]THF$ ). Upon titration of one equivalent of **2** into a solution of **1a**, a series of resonance shifts are observed (Figure 1). The most dramatic shift involves the aryl protons *ortho* to the amidine functionality ( $\Delta\delta = 0.35$  ppm).<sup>[13]</sup> Although the amidine protons are not resolved in the  $^1H$  NMR spectrum of **1a**, formation of **1a–2** resolves two broad downfield resonances at  $\delta = 9.4$  and 13.1 ppm. These new peaks each integrate for two protons and are attributed to the two different amidine protons.



**Scheme 1.** Amidinium–carboxylate interfaced porphyrin– $C_{60}$  assemblies (**1–2**).

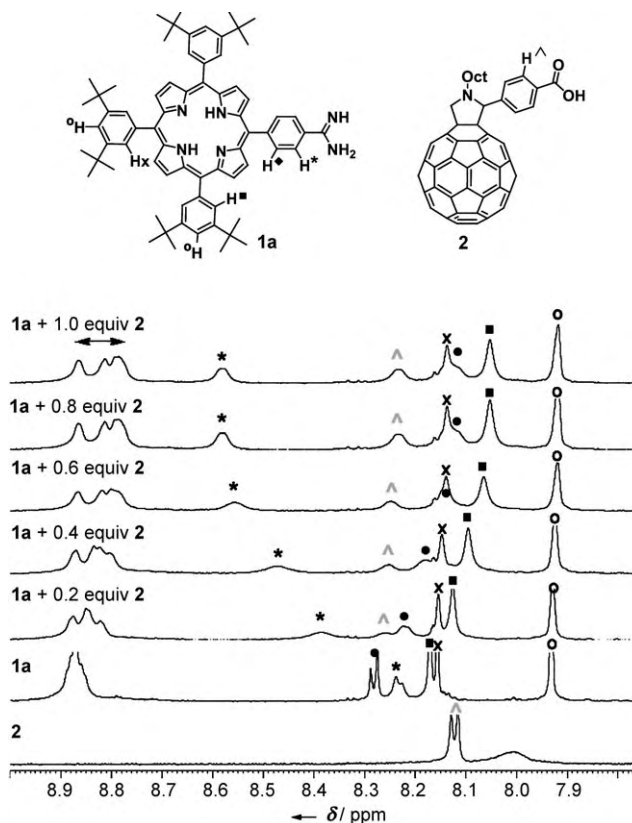


**Figure 1.**  $^1H$  NMR shifts upon titration of **2** into a solution of **1a** in  $[D_8]THF$ .

Importantly, no further changes are observed upon addition of more than one equivalent of **2**, thus confirming the exclusive presence of a strong 1:1 complex.<sup>[14]</sup>

Further details on the formation of **1a–2** and **1b–2** were obtained from experiments in which dilute solutions of **1a** and **1b** in toluene/acetonitrile (9:1, v/v) or THF were titrated with variable amounts of **2** and probed by absorption and fluorescence spectroscopy (see Figure 2 and the Supporting Information in which a typical example for an absorption measurement is given). Relative to the component spectra (**1b** and **2**), a number of differences are apparent. For **1b**, Soret- and Q-band transitions at 428 and 558 nm, respectively, shift incrementally to the red (431 and 560 nm). Moreover, the presence of isosbestic points indicate the transformation

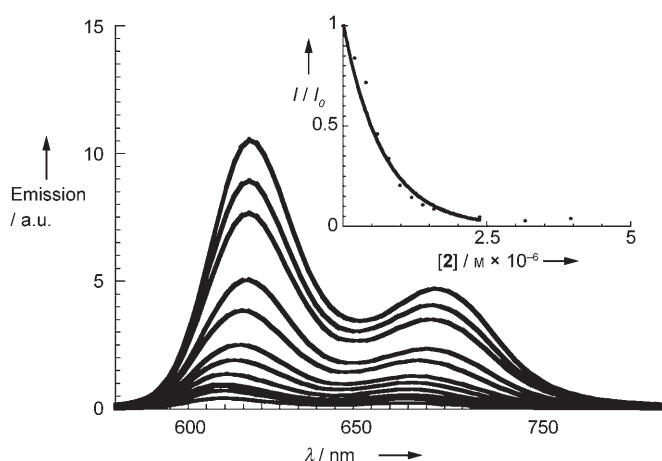


**Figure 2.** Fluorescence spectra ( $\lambda_{\text{exc}} = 433 \text{ nm}$ ) of **1b** ( $1.08 \times 10^{-6} \text{ M}$ ) and variable concentration of **2** (0, 0.2, 0.4, 0.6, 0.8, 1.0, 1.2, 1.4, 1.6, 2.4, 3.9, 9.1, and  $23.7 \times 10^{-6} \text{ M}$ ) in toluene/acetonitrile (9:1, v/v) at room temperature. Insert displays the relationship of  $I/I_0$  versus  $[2]$  that was used to determine the association constant.  $I$  = current intensity in relative units.

of **1b** (the starting point of the titration) into **1b·2** (the end point of the titration). The changes in absorption were further employed to confirm the stoichiometry of **1a·2** and **1b·2** through Job plots. In this light, Gaussian relationships with maxima at 0.5 unequivocally confirm the 1:1 complex stoichiometries that were evoked from the  $^1\text{H}$  NMR experiments (see the Supporting Information).

In excitation experiments with **1a** and **1b**, strong fluorescence emissions are seen in the red region, with quantum yields of 0.2 and 0.04, respectively. When variable concentrations of **2** are present, the fluorescence emission intensities decreased exponentially (see Figure 2 and the Supporting Information). Nonlinear least-square analyses, that is, fluorescence intensity versus concentration of **2**, allowed the evaluation of the binding constants of **1·2**, which are exceptionally high. In solvents that do not interfere significantly with either the electrostatic or the hydrogen-bonding interactions (toluene or toluene/acetonitrile (9:1, v/v)), binding constants as high as  $2.1 \times 10^7 \text{ M}^{-1}$  were deduced. The binding constants in THF, in which interactions are mostly based on electrostatic attractions, showed values between  $1.3 \times 10^5 \text{ M}^{-1}$  (**1a·2**) and  $3.3 \times 10^5 \text{ M}^{-1}$  (**1b·2**).

Potential  $\text{C}_{60}$  interactions with **1a** or **1b** were tested in a series of reference assays. For example, in the absence of the amidine and carboxylic acid functionalities, the absorption spectra remain virtually as the superimpositions of the component spectra throughout the titrations. The lack of mutually interacting systems was also confirmed in fluorescence experiments. Overall, only a quenching of less than 5 % is noted, relative to > 95 % quenching in **1a·2** or **1b·2**.

The redox features of interfaced **1·2** pairs were determined by cyclic voltammetry in THF at room temperature (see the Supporting Information). These values provide useful information about the energies of the radical ion pairs formed upon photoexcitation (see below). The cyclic voltammograms of both porphyrins, free base (**1a**) and zinc (**1b**) at concentrations of  $5 \times 10^{-4} \text{ M}$ , show sets of reversible

reduction and oxidation steps (Figure 3). For **2**, three reduction steps are discernable. The corresponding zinc complex **1b·2** reveals cathodic shifts of the reduction and oxidation steps relative to the free-base complex **1a·2** (see the Supporting Information). In both **1·2** complexes, the redox patterns of the two constituents, namely porphyrin amidines **1** and  $\text{C}_{60}$  carboxylic acid **2**, are essentially preserved (Figure 3).

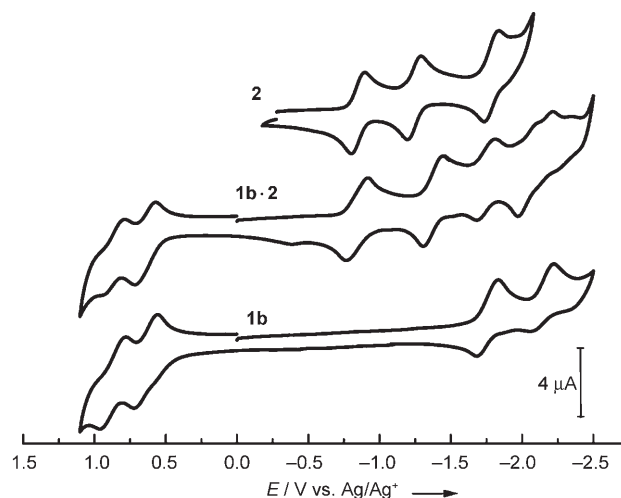


**Figure 3.** Cyclic voltammograms of **1b·2** and its precursors **1b** and **2**, measured in THF ( $5 \times 10^{-4} \text{ M}$ ) at  $100 \text{ mVs}^{-1}$  (V vs.  $\text{Ag}/\text{Ag}^+$ ).

The observed slight shifts in the redox potentials of the **1·2** assemblies could be accounted for by a pronounced electronic coupling between both electroactive components (see below). Neglecting significant electronic interactions, we estimate values of the radical-ion-pair-state energies as the sum of the first reduction potential of **2** and the first oxidation potential of either **1a** or **1b** to be 1.9 and 1.62 eV for **1a·2** and **1b·2**, respectively. In other words, radical-ion-pair formations that evolve from the singlet excited states are highly exothermic.

Finally, transient absorption studies showed the fate of the porphyrin excited states and the identification of the photo-products. Pumping light into the ground state of **1a** or **1b** with short 387-nm (namely, 150 fs) or 532-nm (namely, 6 ns) laser pulses led to the population of their singlet excited states. The latter undergo intersystem crossing ( $\approx 10^8 \text{ s}^{-1}$ ) to the long-lived and molecular-oxygen-sensitive triplet states. Triplet spectra of **1a** or **1b** reveal, besides bleaching in the Soret- and Q-band region, characteristic triplet maxima at 780 (**1a**) or 840 nm (**1b**).<sup>[6d]</sup>

Initially, the porphyrin chromophores in **1a·2** and **1b·2** produce notable singlet fingerprints for **1a** and **1b** upon photoexcitation. This behavior attests to the successful excitation of **1a** and **1b**. However, instead of the slow intersystem crossings, the singlet excited states decay with rates of about  $10^{10} \text{ s}^{-1}$ , from which we deduce an electronic coupling of  $36 \text{ cm}^{-1}$  between both electroactive elements (that is, **1b·2**). At the end of the intrinsically fast decay, differential absorption changes in the visible region are governed by broad absorptions at 600–800 nm, thus indicating **1a**- or **1b**-centered oxidation products. In the near-infrared region, on the other hand, the signature of a **2**-centered

reduction is seen at 1000 nm.<sup>[15]</sup> Figure 4 exemplifies the spectral changes seen in the cases of **1b-2** and **1a-2**, respectively (see the Supporting Information also). The decay kinetics of both signatures—on the nanosecond

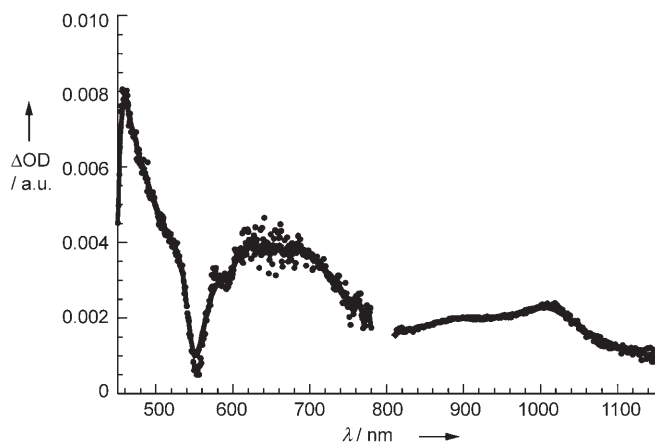


**Figure 4.** Transient absorption spectrum (NIR part) of **1b-2** in toluene at room temperature recorded 50 ps following a 150 fs laser pulse ( $\lambda_{\text{exc}} = 387 \text{ nm}$ ).

scale—reflect the return of the radical-ion-pair states to the electronic ground states. The lifetime of the newly formed radical-ion-pair state, as derived by analyzing several wavelengths under unimolecular conditions, are  $9.3 \pm 0.1$  and  $7.9 \pm 0.5 \mu\text{s}$  for **1a-2** and **1b-2**, respectively, in THF (see the Supporting Information).

In summary, the two-point amidinium–carboxylate binding motif guarantees an extraordinary stabilization for a set of noncovalently interfaced ensembles (**1-2**). Association constants reach up to  $10^7 \text{ M}^{-1}$ . Exceptionally strong electronic couplings stem from such binding, which in turn facilitate a faster, more efficient, and longer-lived formation of radical-ion-pair states (that is,  $\approx 10 \mu\text{s}$  in THF) relative to similar covalent  $\text{C}_{60}$  conjugates (namely,  $\approx 1 \mu\text{s}$  in THF).<sup>[15]</sup> Most importantly, such remarkable radical-ion-pair lifetimes outperform previously reported ensembles based on 1) a non-amidinium–carboxylate binding motif<sup>[8]</sup> or 2) non-fullerene electron acceptors<sup>[2,9]</sup> by several orders of magnitude. These results point unmistakably to the fundamental advantages of strong and highly directional hydrogen-bonding networks in assisting electron-transfer processes and pave the way to the construction of efficient photovoltaic devices inspired by biomimetic principles.

Received: March 31, 2006  
Published online: June 22, 2006

**Keywords:** electron transfer · electronic coupling · fullerenes · hydrogen bond

- [1] a) J. A. Stubbe, D. G. Nocera, C. S. Yee, M. C. Y. Chang, *Chem. Rev.* **2003**, *103*, 2167–2201; b) A. Namslawer, A. Aagaard, A. Katsonouri, P. Brzezinski, *Biochemistry* **2003**, *42*, 1488–1498.  
[2] a) A. P. H. J. Schenning, J. V. Herrikhuyzen, P. Jonkheijm, Z. Chen, F. Würthner, E. W. Meijer, *J. Am. Chem. Soc.* **2002**, *124*,

- 10252–10253; b) J. L. Sessler, M. Sathiosatham, C. T. Brown, T. A. Rhodes, G. Wiederrecht, *J. Am. Chem. Soc.* **2001**, *123*, 3655–3660; c) A. J. Myles, N. R. Branda, *J. Am. Chem. Soc.* **2001**, *123*, 177–178; d) R. K. Castellano, S. L. Craig, C. Nuckolls, J. Rebek, Jr., *J. Am. Chem. Soc.* **2000**, *122*, 7876–7882; e) T. H. Ghaddar, E. W. Castner, S. S. Isied, *J. Am. Chem. Soc.* **2000**, *122*, 1233–1234.  
[3] a) J. L. Sessler, B. Wang, A. Harriman, *J. Am. Chem. Soc.* **1993**, *115*, 10418–10419; b) P. J. F. De Rege, S. A. Williams, M. J. Therien, *Science* **1995**, *269*, 1409–1413.  
[4] a) W. Ma, C. Yang, X. Gong, K. Lee, A. J. Heeger, *Adv. Funct. Mater.* **2005**, *15*, 1617–1622; b) G. Li, V. Shrotriya, J. Huang, Y. Yao, T. Moriarty, K. Emery, Y. Yang, *Nat. Mater.* **2005**, *4*, 864–868; c) I. Riedel, E. von Hauff, J. Parisi, N. Martín, F. Giacalone, V. Dyakonov, *Adv. Funct. Mater.* **2005**, *15*, 1979–1987; d) M. W. Wienk, J. M. Kroon, W. J. H. Verhees, J. Knol, J. C. Hummelen, P. A. van Hal, R. A. J. Janssen, *Angew. Chem.* **2003**, *115*, 3493–3497; *Angew. Chem. Int. Ed.* **2003**, *42*, 3371–3375; e) C. J. Brabec, N. S. Sariciftci, J. C. Hummelen, *Adv. Funct. Mater.* **2001**, *11*, 15–26.  
[5] a) C.-H. Huang, N. D. McClenaghan, A. Kuhn, J. W. Hofstraat, D. M. Bassani, *Org. Lett.* **2005**, *7*, 3409–3412; b) J. L. Brédas, D. Beljonne, V. Coropceanu, J. Cornil, *Chem. Rev.* **2004**, *104*, 4971–5003; c) M. A. Fox, *Acc. Chem. Res.* **1999**, *32*, 201–207.  
[6] a) H. Imahori, Y. Sakata, *Adv. Mater.* **1997**, *9*, 537–546; b) N. Martín, L. Sánchez, B. Illescas, I. Pérez, *Chem. Rev.* **1998**, *98*, 2527–2548; c) D. M. Guldi, N. Martín, *J. Mater. Chem.* **2002**, *12*, 1978–1992; d) D. M. Guldi, *Chem. Soc. Rev.* **2002**, *31*, 22–36; e) J.-F. Nierengarten, *Top. Curr. Chem.* **2003**, *228*, 87–110; f) J. L. Segura, N. Martín, D. M. Guldi, *Chem. Soc. Rev.* **2005**, *34*, 31–47; g) D. M. Guldi, G. M. A. Rahman, C. Ehli, V. Sgobba, *Chem. Soc. Rev.* **2006**, *35*, 471–487.  
[7] For recent examples, see: a) C. M. Atienza, G. Fernández, L. Sánchez, N. Martín, I. Sá Dantas, M. W. Wienk, R. A. J. Janssen, G. M. A. Rahman, D. M. Guldi, *Chem. Commun.* **2006**, 514–516; b) G. Kodis, Y. Terazono, P. A. Liddell, J. Andréasson, V. Garg, M. Hambourger, T. A. Moore, A. L. Moore, D. Gust, *J. Am. Chem. Soc.* **2006**, *128*, 1818–1827; c) L. Sánchez, M. Sierra, N. Martín, D. M. Guldi, M. W. Wienk, R. A. J. Janssen, *Org. Lett.* **2005**, *7*, 1691–1694; d) T. Oike, T. Kurata, K. Takimiya, T. Otsubo, Y. Aso, H. Zhang, Y. Araki, O. Ito, *J. Am. Chem. Soc.* **2005**, *127*, 15372–15373; e) D. M. Guldi, F. Giacalone, G. de la Torre, J. L. Segura, N. Martín, *Chem. Eur. J.* **2005**, *11*, 7199–7210; f) L. Sánchez, M. A. Herranz, N. Martín, *J. Mater. Chem.* **2005**, *15*, 1409–1421; g) R. S. Iglesias, C. G. Claessens, T. Torres, G. M. A. Rahman, D. M. Guldi, *Chem. Commun.* **2005**, 2113–2115; h) K. Ohkubo, H. Kotani, J. Shao, Z. Ou, K. M. Kadish, G. Li, R. K. Pandey, M. Fujitsuka, O. Ito, H. Imahori, S. Fukuzumi, *Angew. Chem.* **2004**, *116*, 871–874; *Angew. Chem. Int. Ed.* **2004**, *43*, 853–856; i) F. Giacalone, J. L. Segura, N. Martín, D. M. Guldi, *J. Am. Chem. Soc.* **2004**, *126*, 5340–5341; j) M. Gutierrez-Nava, G. Accorsi, P. Masson, N. Armadori, J. F. Nierengarten, *Chem. Eur. J.* **2004**, *10*, 5076–5086.  
[8] a) F. Diederich, M. Gómez-López, *Chem. Soc. Rev.* **1999**, *28*, 263–278; b) L. Sánchez, N. Martín, D. M. Guldi, *Angew. Chem.* **2005**, *117*, 5508–5516; *Angew. Chem. Int. Ed.* **2005**, *44*, 5374–5382; c) *Special Issue on Supramolecular Chemistry of Fullerenes* (Eds.: N. Martín, J. F. Nierengarten), *Tetrahedron* **2006**, *62*, 1905–2132; d) U. Hahn, M. Elhabiri, A. Trabolsi, H. Herschbach, E. Leize, A. Van Dorsselaer, A.-M. Albrecht-Gary, J.-F. Nierengarten, *Angew. Chem.* **2005**, *117*, 5472–5475; *Angew. Chem. Int. Ed.* **2005**, *44*, 5338–5341; e) N. D. McClenaghan, Z. Grote, K. Darriet, M. Zimine, R. M. Williams, L. De Cola, D. M. Bassani, *Org. Lett.* **2005**, *7*, 807–810; f) J. L. Sessler, J. Jayawickramarajah, A. Gouloumis, T. Torres, D. M. Guldi, S. Maldonado, K. J. Stevenson, *Chem. Commun.* **2005**, 1892–1894.

- [9] a) J. P. Kirby, J. A. Roberts, D. G. Nocera, *J. Am. Chem. Soc.* **1997**, *119*, 9230–9236; b) N. H. Damrauer, J. M. Hodgkiss, J. Rosenthal, D. G. Nocera, *J. Phys. Chem. B* **2004**, *108*, 6315–6321.
- [10] a) M. Haj-Zaroubi, N. W. Mitzel, F. P. Schmidtchen, *Angew. Chem.* **2002**, *114*, 111–114; *Angew. Chem. Int. Ed.* **2002**, *41*, 104–107; b) V. Král, F. P. Schmidtchen, K. Lang, M. Berger, *Org. Lett.* **2002**, *4*, 51–54; c) M. Berger, F. P. Schmidtchen, *Angew. Chem.* **1998**, *110*, 2840–2842; *Angew. Chem. Int. Ed.* **1998**, *37*, 2694–2694.
- [11] J. Otsuki, K. Iwasaki, Y. Nakano, M. Itou, Y. Araki, O. Ito, *Chem. Eur. J.* **2004**, *10*, 3461–3466.
- [12] M. Segura, L. Sánchez, J. de Mendoza, N. Martín, D. M. Guldi, *J. Am. Chem. Soc.* **2003**, *125*, 15093–15100.
- [13] 2D ROESY spectrometry was performed to confirm peak assignments in the 1D <sup>1</sup>H NMR spectrum of **1a**.
- [14] The high stability of the **1a**·**2** complex prevents reliable determination of the association constants using NMR techniques; see Ref. [9].
- [15] H. Imahori, H. Yamada, D. M. Guldi, Y. Endo, A. Shimomura, S. Kundu, K. Yamada, T. Okada, Y. Sakata, S. Fukuzumi, *Angew. Chem.* **2002**, *114*, 2450–2453; *Angew. Chem. Int. Ed.* **2002**, *41*, 2344–2347.



## Transition-Metal Catalysis

DOI: 10.1002/anie.200601248

## Efficient Diastereoselective Intermolecular Rhodium-Catalyzed C–H Amination\*\*

Chungen Liang, Fabien Robert-Peillard, Corinne Fruit, Paul Müller,\* Robert H. Dodd,\* and Philippe Dauban\*

In memory of Pierre Potier

The selective functionalization of a C–H bond is an area of intense investigation as such a reaction leads to the formation

[\*] Dr. C. Fruit, Prof. Dr. P. Müller  
Department of Organic Chemistry  
University of Geneva  
30 quai Ernest Ansermet, 1211 Geneva 4 (Switzerland)  
Fax: (+41) 223-287-396  
E-mail: paul.muller@chiorg.unige.ch

Dr. C. Liang, F. Robert-Peillard, Dr. R. H. Dodd, Dr. P. Dauban  
Institut de Chimie des Substances Naturelles  
CNRS  
Avenue de la Terrasse, 91198 Gif-sur-Yvette (France)  
Fax: (+33) 1-6907-7247  
E-mail: dodd@icsn.cnrs-gif.fr  
dauban@icsn.cnrs-gif.fr

[\*\*] We wish to thank the Institut de Chimie des Substances Naturelles and the Swiss National Science Foundation for financial support and fellowships. Support and sponsorship concerted by COST Action D24 “Sustainable Chemical Processes: Stereoselective Transition Metal-Catalyzed Reactions” are kindly acknowledged.

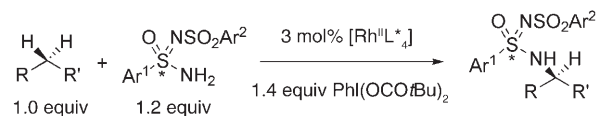
Supporting information for this article is available on the WWW under <http://www.angewandte.org> or from the author.

of valuable building blocks from simple molecules.<sup>[1]</sup> Considering the ubiquity of C–H bonds in organic compounds, the search for a process that allows their selective transformation remains challenging. Methodologies have been recently developed for regioselective C–C,<sup>[2]</sup> C–O,<sup>[3]</sup> or C–N<sup>[4,5]</sup> bond formations that have found applications in total synthesis.<sup>[6]</sup>

In the case of C–H amination, significant results have been obtained by using transition-metal-catalyzed nitrene transfer that starts from iminodanes.<sup>[5,7]</sup> This field, pioneered by Breslow<sup>[8]</sup> and Mansuy,<sup>[9]</sup> has progressed considerably over the last five years with the discovery of new methodologies for the generation<sup>[5a,d,10]</sup> of these hypervalent iodine(III) reagents in situ. Thus, PhI(OAc)<sub>2</sub>-mediated C–H amination has been shown to be catalyzed by ruthenium,<sup>[5a-c]</sup> manganese,<sup>[5a]</sup> rhodium,<sup>[5d-g]</sup> and silver<sup>[5i]</sup> complexes with sulfonamides, sulfamates, or carbamates as nitrene precursors. However, although the intramolecular process occurs efficiently, the intermolecular version suffers from low conversions or the need for a large excess of the starting alkane (5–100 equivalents) to obtain good yields.<sup>[1g,5a,b,h,11]</sup> The involvement of transition-metal catalysts has also allowed the development of enantioselective nitrene C–H insertions.<sup>[12]</sup> Although good enantioselectivities have been reported for intramolecular C–H aminations, an excess of alkane in the intermolecular version is again required to reach satisfactory selectivities.<sup>[12a,b,g]</sup> It is therefore in this context that we report herein an efficient diastereoselective intermolecular C–H amination that occurs under stoichiometric conditions and starts from an enantiomerically pure nitrene precursor (that is, (*S*)-*N*-(*p*-toluenesulfonyl)-*p*-toluenesulfonimidamide (**1a**)).

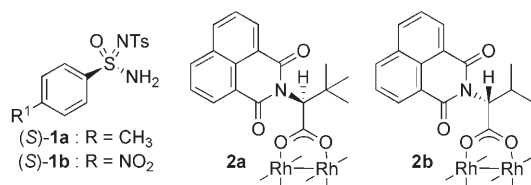
We recently reported the generation of chiral iminodanes from sulfonimidamides in situ.<sup>[13]</sup> It was found that the nitrene intermediates generated from these chiral sulfur(VI) reagents are highly reactive species that add to various olefins in the presence of copper(I) catalysts to afford aziridines in good yields but with moderate diastereoselectivities.<sup>[13a]</sup> Rhodium(II) complexes have also been found to catalyze the aziridination of alkenes, and in particular the use of chiral ligands has been shown to improve diastereoselectivities.<sup>[13b]</sup> Given the greater ability of rhodium(II) tetracarboxylates to mediate C–H amination and the high reactivity of sulfonimidamide-derived nitrenes, we thus decided to combine these properties with the aim of developing an efficient intermolecular C–H amination (Scheme 1).

Initial experiments were aimed at screening various rhodium(II) complexes and enantiomerically pure substituted sulfonimidamides **1** in the presence of PhI(OAc)<sub>2</sub> and MgO in dichloromethane.<sup>[5d]</sup> We found that a combination of (–)-(*S*)-*N*-(*p*-toluenesulfonyl)-*p*-nitrobenzenesulfonimidamide (**1b**)<sup>[13a,b,14]</sup> and the chiral rhodium carboxylate catalysts



**Scheme 1.** Intermolecular C–H amination under stoichiometric conditions.

$[\text{Rh}_2((S)\text{-nttl})_4]$  (**2a**;<sup>[15]</sup> nttl = *N*-1,8-naphthoyl-*tert*-leucine; Scheme 2) gave good results with indane **3** as a model substrate. Starting with one equivalent of **3**, the *p*-nitro analogue of the C–H amination product **3a** was isolated in 45% yield and with >90% diastereoisomeric excess, as estimated by <sup>1</sup>H NMR spectroscopic analysis. However, when applied to other substrates, such as tetrahydronaphthalene **4**, these conditions led to lower yields.



**Scheme 2.** Structures of the *S* enantiomer of the sulfonimidamides **1** and of the rhodium catalysts **2**. Ts = tosyl.

Thus, we decided to study the influence of other reaction parameters. We were very surprised to observe that C–H amination with (*S*)-**1a** takes place in methanol, albeit in moderate yields.<sup>[16]</sup> A possible explanation is that methanol, contrary to dichloromethane, allows the solubilization of **1a**. We also discovered that the reaction works equally well in the absence of MgO. These observations prompted us to run the reaction in mixtures of CH<sub>2</sub>Cl<sub>2</sub> and MeOH without a base. We thus found that a 1:3 mixture of MeOH/CH<sub>2</sub>Cl<sub>2</sub> gives better conversions; consequently, compound **4a** could be isolated starting from tetrahydronaphthalene in 48% yield. Further improvements were obtained by replacing CH<sub>2</sub>Cl<sub>2</sub> with 1,1,2,2-tetrachloroethane and PhI(OAc)<sub>2</sub> with the more soluble PhI(OCO*t*Bu)<sub>2</sub>.<sup>[17]</sup> The C–H amination product **4a** is formed in 80% yield with 96% *de* (Table 1, entry 2) under these conditions and at –35 °C.<sup>[18]</sup>

Application of this optimized procedure to electron-rich C–H bonds is particularly efficient (entries 1–6 and 8–11), whereas the reactivity drops slightly in the presence of an electron-withdrawing group, as observed with *p*-nitroethylbenzene (**8**) (entry 7). Therefore, except in the latter case, this stoichiometric intermolecular C–H amination leads to the formation of a single product in 62–93% yield with nearly complete diastereoselectivity (≥ 93% *de*).<sup>[19]</sup> These results, in terms of reactivity and selectivity, are superior to those reported so far, even in the presence of an excess of substrate.<sup>[1g,12]</sup> Moreover, with 2-methoxyindane (**11**), only the *trans* isomer **11a** was isolated in 62% yield with 99% *de*, as indicated by NOESY experiments (entry 10). This result illustrates the synthetic utility of the intermolecular C–H amination, as it stands in contrast to the intramolecular version that affords only the corresponding *cis* isomer.<sup>[5c–e,j]</sup>

The high efficiency of this stereoselective C–H functionalization, which occurs with retention of configuration through a concerted nitrene insertion,<sup>[5d,20]</sup> is correlated to a dramatic matched effect between the chiral rhodium catalyst **2a** and the sulfonimidamide (*S*)-**1a**. On one hand, reaction of the latter with [Rh<sub>2</sub>(OAc)<sub>4</sub>] leads to very poor conversions

and selectivities. On the other hand, the mismatched combination of the enantiomer (*R*)-**1a** and catalyst **2a** gives *ent*-**4a** in only 10% yield with 53% *de*, whereas the same reaction starting from racemic **1a** affords **4a** in 33% yield with 97% *de*.<sup>[21]</sup> It should also be mentioned that the presence of methanol has a major influence on the matched effect. This result was applied to the preparation of *ent*-**4a**, obtained in 83% yield with 99% *de* (entry 3) from the matched combination of the sulfonimidamide (*R*)-**1a** and the rhodium catalyst [Rh<sub>2</sub>((*R*)-ntv)<sub>4</sub>] (**2b**; ntv = *N*-1,8-naphthoylvaline).<sup>[22]</sup>

Substrates with allylic C–H bonds were also studied to enhance the scope of the reaction. The reaction still occurred efficiently in 55–75% yield, but the diastereoselectivities were moderate (38–50%, entries 12–14). These results, however, compare favorably with those described in previous studies.<sup>[1g,12]</sup> More interestingly, competitive rhodium-catalyzed aziridination does not take place in the case of cyclohexene (**13**) and cyclopentene (**14**), contrary to previous reports of the use of sulfonamides and sulfamates<sup>[23]</sup> or of rhodium acetate with sulfonimidamides.<sup>[13b]</sup> This result is likely to be the consequence of the matched effect which favors C–H insertion as the reaction of racemic **1a** with the chiral catalyst **2a** affords a mixture of C–H amination product **13a** and aziridine in the case of cyclohexene. Finally, the high reactivity of the sulfonimidamide-derived nitrenes has been confirmed by application of the procedure to simple alkanes (entries 15 and 16). Adamantane **16** gives rise to the corresponding C–H insertion product **16a** in 69% yield, whereas the use of five equivalents of cyclohexane **17** affords **17a** in 65% yield, which is identical to the highest yield obtained so far with cyclohexane as the solvent.<sup>[5b]</sup>

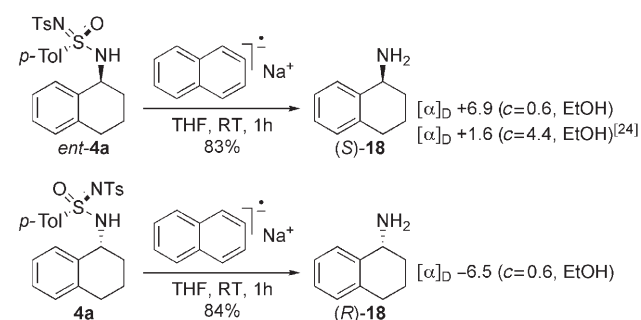
As both enantiomers of **1a** are resolved with (*S*)- or (*R*)- $\alpha$ -methylbenzylamine,<sup>[13a,b]</sup> the absolute configuration at the newly created asymmetric center for the C–H insertion product **5a**, and by analogy for **3a–12a**, was readily determined. Thus, the use of (*S*)-**1a** with rhodium catalyst **2a** leads to the *R* configuration at the benzylic center. This result was confirmed after removal of the sulfonimidoyl moiety from *ent*-**4a**. The free amine **18**, whose optical rotation corresponds to the *S* isomer,<sup>[24]</sup> was produced in 84% yield by using sodium naphthalenide in THF at room temperature; whereas, application of these conditions to **4a** afforded (*R*)-**18**, as indicated by the opposite optical rotation (Scheme 3). Importantly, chiral HPLC indicated that removal of the sulfonimidoyl group takes place without epimerization at the benzylic center.

In conclusion, we have discovered a highly efficient rhodium-catalyzed intermolecular C–H amination procedure with a sulfonimidamide as the nitrene precursor and the C–H-bond-containing substrate as the limiting component. This reaction occurs with good-to-excellent diastereoselectivities of up to 99%, particularly at secondary benzylic positions, and can be applied with equal success to the synthesis of both isomers of the resulting amine. The high reactivity and selectivity have been shown to be the consequence of a pronounced matched effect between the enantiomerically pure sulfonimidamide and the chiral rhodium catalyst. Such a procedure is of high interest for the total synthesis of natural products, for example, colchicine<sup>[25]</sup> or biologically active

**Table 1:** Intermolecular C–H amination with sulfonimidamide (*S*)-**1a** and catalyzed by  $[\text{Rh}_2\{(\text{S})\text{-nttl}\}_4]$  **2a**.<sup>[a]</sup>

Entry	Substrate	Product	Yield [%] <sup>[b]</sup>	<i>de</i> [%] <sup>[c]</sup>	Entry	Substrate	Product	Yield [%] <sup>[b]</sup>	<i>de</i> [%] <sup>[c]</sup>
1			88	> 99	9			62	99
2			80	96	10			62	99
3			83 <sup>[d]</sup>	99 <sup>[d]</sup>	11			78	98
4			73	97	12			75	38
5			87	96	13			72	50
6			93	98	14			55	50
7			51	80	15			69	–
8			80	93	16			65 <sup>[e]</sup>	–

[a] All reactions were conducted at  $-35^\circ\text{C}$  in  $\text{Cl}_2\text{CHCHCl}_2/\text{MeOH}$  (3:1) with (*S*)-**1a** (1.2 equiv),  $\text{PhI}(\text{OCO}t\text{-Bu})_2$  (1.4 equiv), and **2a** (3 mol %). [b] Yield of the isolated products. [c] The *de* values were determined by HPLC (Hypercarb or Symmetry Shield Column). [d] *ent*-**4a** was obtained using 3 mol % of  $[\text{Rh}_2\{(\text{R})\text{-ntv}\}_4]$  (**2b**) and 1.2 equivalents of (*R*)-**1a**. [e] With 5.0 equivalents of cyclohexane.


**Scheme 3.** Deprotection of the C–H insertion products under reductive racemization-free conditions.

compounds, such as sertraline.<sup>[26]</sup> Studies are in progress in this area.

Received: March 30, 2006  
Published online: June 21, 2006

**Keywords:** amination · C–H insertion · hypervalent iodine · nitrenes · rhodium

- [1] For recent reviews, see: a) C. Jia, T. Kitamura, Y. Fujiwara, *Acc. Chem. Res.* **2001**, *34*, 633–639; b) J. A. Labinger, J. E. Bercaw, *Nature* **2002**, *417*, 507–514; c) V. Ritleng, C. Sirlin, M. Pfeffer, *Chem. Rev.* **2002**, *102*, 1731–1769; d) F. Kakiuchi, N. Chatani, *Adv. Synth. Catal.* **2003**, *345*, 1077–1101; e) H. M. L. Davies,

- R. E. J. Beckwith, *Chem. Rev.* **2003**, *103*, 2861–2903; f) A. S. Goldman, K. I. Goldberg in *Activation and Functionalization of C–H Bonds* (Eds.: K. I. Goldberg, A. S. Goldman), ACS Symposium Series 885, American Chemical Society, Washington, DC, **2004**, pp. 1–43; g) A. R. Dick, M. S. Sanford, *Tetrahedron* **2006**, *62*, 2439–2463.
- [2] For recent examples, see: a) F. Kakiuchi, S. Kan, K. Igi, N. Chatani, S. Murai, *J. Am. Chem. Soc.* **2003**, *125*, 1698–1699; b) O. Baudoin, A. Herrbach, F. Guéritte, *Angew. Chem.* **2003**, *115*, 5914–5918; *Angew. Chem. Int. Ed.* **2003**, *42*, 5736–5740; c) R. K. Thalji, J. A. Ellman, R. G. Bergman, *J. Am. Chem. Soc.* **2004**, *126*, 7192–7193; d) D. Kalyani, N. R. Deprez, L. V. Desai, M. S. Sanford, *J. Am. Chem. Soc.* **2005**, *127*, 7330–7331.
- [3] For recent examples, see: a) S. Lee, P. L. Fuchs, *J. Am. Chem. Soc.* **2002**, *124*, 13978–13979; b) L. V. Desai, K. L. Hull, M. S. Sanford, *J. Am. Chem. Soc.* **2004**, *126*, 9542–9543; c) R. Giri, J. Liang, J.-G. Lei, J.-J. Li, D.-H. Wang, X. Chen, I. C. Naggar, C. Guo, B. M. Foxman, J.-Q. Yu, *Angew. Chem.* **2005**, *117*, 7586–7590; *Angew. Chem. Int. Ed.* **2005**, *44*, 7420–7424; d) B. H. Brodsky, J. Du Bois, *J. Am. Chem. Soc.* **2005**, *127*, 15391–15393.
- [4] For recent examples, see: a) J. L. Brice, J. E. Harang, V. I. Timokhin, N. R. Anastasi, S. S. Stahl, *J. Am. Chem. Soc.* **2005**, *127*, 2868–2869; b) W. C. P. Tsang, N. Zheng, S. L. Buchwald, *J. Am. Chem. Soc.* **2005**, *127*, 14560–14561; c) H. Lebel, K. Huard, S. Lectard, *J. Am. Chem. Soc.* **2005**, *127*, 14198–14199; d) T. Katsuki, *Chem. Lett.* **2005**, *34*, 1304–1309.
- [5] For the most relevant examples using iminoiodanes, see: a) X.-Q. Yu, J.-S. Huang, X.-G. Zhou, C.-M. Che, *Org. Lett.* **2000**, *2*, 2233–2236; b) S.-M. Au, J.-S. Huang, C.-M. Che, W.-Y. Yu, *J. Org. Chem.* **2000**, *65*, 7858–7864; c) J.-L. Liang, S.-X. Yuan, J.-S. Huang, C.-M. Che, *J. Org. Chem.* **2004**, *69*, 3610–3619; d) C. G. Espino, J. Du Bois, *Angew. Chem.* **2001**, *113*, 618–620; *Angew. Chem. Int. Ed.* **2001**, *40*, 598–600; e) C. G. Espino, P. M. Wehn, J. Chow, J. Du Bois, *J. Am. Chem. Soc.* **2001**, *123*, 6935–6936; f) P. M. Wehn, J. Lee, J. Du Bois, *Org. Lett.* **2003**, *5*, 4823–4826; g) M. Kim, J. V. Mulcahy, C. G. Espino, J. Du Bois, *Org. Lett.* **2006**, *8*, 1073–1076; h) M. M. Diaz-Requejo, T. R. Belderrain, M. C. Nicasio, S. Trofimenko, P. J. Perez, *J. Am. Chem. Soc.* **2003**, *125*, 12078–12079; i) Y. Cui, C. He, *Angew. Chem.* **2004**, *116*, 4306–4308; *Angew. Chem. Int. Ed.* **2004**, *43*, 4210–4212.
- [6] a) J. A. Johnson, N. Li, D. Sames, *J. Am. Chem. Soc.* **2002**, *124*, 6900–6903; b) A. Hinman, J. Du Bois, *J. Am. Chem. Soc.* **2003**, *125*, 11510–11511; c) S. J. O'Malley, K. L. Tan, A. Watzke, R. G. Bergman, J. A. Ellman, *J. Am. Chem. Soc.* **2005**, *127*, 13496–13497.
- [7] For general reviews, see: a) P. Müller, C. Fruit, *Chem. Rev.* **2003**, *103*, 2905–2919; b) P. Dauban, R. H. Dodd, *Synlett* **2003**, 1571–1586; c) J. A. Halfen, *Curr. Org. Chem.* **2005**, *9*, 657–669; d) C. G. Espino, J. Du Bois in *Modern Rhodium-Catalyzed Organic Reactions* (Ed.: P. A. Evans), Wiley-VCH, Weinheim, **2005**, pp. 379–416; e) H. M. L. Davies, M. S. Long, *Angew. Chem.* **2005**, *117*, 3584–3586; *Angew. Chem. Int. Ed.* **2005**, *44*, 3518–3520.
- [8] a) R. Breslow, S. H. Gellman, *J. Chem. Soc. Chem. Commun.* **1982**, 1400; b) R. Breslow, S. H. Gellman, *J. Am. Chem. Soc.* **1983**, *105*, 6728–6729.
- [9] D. Mansuy, J.-P. Mahy, A. Dureault, G. Bedi, P. Battioni, *J. Chem. Soc. Chem. Commun.* **1984**, 1161–1162.
- [10] P. Dauban, L. Sanière, A. Tarrade, R. H. Dodd, *J. Am. Chem. Soc.* **2001**, *123*, 7707–7708.
- [11] C. G. Espino, K. W. Fiori, M. Kim, J. Du Bois, *J. Am. Chem. Soc.* **2004**, *126*, 15378–15379.
- [12] a) Y. Kohmura, T. Katsuki, *Tetrahedron Lett.* **2001**, *42*, 3339–3342; b) M. Yamawaki, H. Tsutsui, S. Kitagaki, M. Anada, S. Hashimoto, *Tetrahedron Lett.* **2002**, *43*, 9561–9564; c) J.-L. Liang, J.-S. Huang, X.-Q. Yu, N. Zhu, C.-M. Che, *Chem. Eur. J.* **2002**, *8*, 1563–1572; d) J.-L. Liang, S.-X. Yuan, J.-S. Huang, W.-Y. Yu, C.-M. Che, *Angew. Chem.* **2002**, *114*, 3615–3618; *Angew. Chem. Int. Ed.* **2002**, *41*, 3465–3468; e) J. Zhang, P. W. Hong Chan, C.-M. Che, *Tetrahedron Lett.* **2005**, *46*, 5403–5408; f) C. Fruit, P. Müller, *Helv. Chim. Acta* **2004**, *87*, 1607–1615; g) C. Fruit, P. Müller, *Tetrahedron: Asymmetry* **2004**, *15*, 1019–1026.
- [13] a) P. Di Chenna, F. Robert-Peillard, P. Dauban, R. H. Dodd, *Org. Lett.* **2004**, *6*, 4503–4505; b) C. Fruit, F. Robert-Peillard, G. Bernardinelli, P. Müller, R. H. Dodd, P. Dauban, *Tetrahedron: Asymmetry* **2005**, *16*, 3484–3487; for a recently reported analogous diastereoselective copper-catalyzed nitrene transfer, see: c) D. Leca, A. Toussaint, C. Mareau, L. Fensterbank, E. Lacôte, M. Malacria, *Org. Lett.* **2004**, *6*, 3573–3575.
- [14] For previous preparations of sulfonimidamides, see: a) E. S. Levchenko, N. Y. Derkach, A. V. Kirsanov, *Zh. Obshch. Khim.* **1962**, *32*, 1208–1212; b) S. Tsushima, Y. Yamada, T. Onami, K. Oshima, M. O. Chaney, N. D. Jones, J. K. Swartzendruber, *Bull. Chem. Soc. Jpn.* **1989**, *62*, 1167–1178.
- [15] P. Müller, Y. Allenbach, E. Robert, *Tetrahedron: Asymmetry* **2003**, *14*, 779–785.
- [16] This result is unexpected as it has been shown that protic solvents induce hydrolysis of the (presumably formed) iminoiodane in the presence of transition-metal complexes; see: a) R. E. White, *Inorg. Chem.* **1987**, *26*, 3916–3919; b) D. A. Evans, M. M. Faul, M. T. Bilodeau, *J. Am. Chem. Soc.* **1994**, *116*, 2742–2753.
- [17] J. Du Bois, *Chemtracts: Org. Chem.* **2005**, *18*, 1–13.
- [18] Under these conditions, the sulfonimidamide (*S*)-**1b** is less soluble than **1a**, thus leading to lower yields.
- [19] It is also worth mentioning that no competitive sulfimidation takes place with 2-ethylthiophene (entry 11). T. Otani, Y. Sugihara, A. Ishii, J. Nakayama, *Tetrahedron Lett.* **1999**, *40*, 5549–5552.
- [20] I. Nägeli, C. Baud, G. Bernardinelli, Y. Jacquier, M. Moran, P. Müller, *Helv. Chim. Acta* **1997**, *80*, 1087–1105.
- [21] This result strongly suggests a kinetic resolution of **1a**, the scope and application of which are currently under investigation.
- [22] P. Müller, G. Bernardinelli, Y. Allenbach, M. Ferri, H. D. Flack, *Org. Lett.* **2004**, *6*, 1725–1728.
- [23] a) K. Guthikonda, J. Du Bois, *J. Am. Chem. Soc.* **2002**, *124*, 13672–13673; b) P. Müller, C. Baud, Y. Jacquier, M. Moran, I. Nägeli, *J. Phys. Org. Chem.* **1996**, *9*, 341–347.
- [24] O. Cervinka, V. Dudek, *Collect. Czech. Chem. Commun.* **1973**, *38*, 1159–1164.
- [25] T. Graening, H.-G. Schmalz, *Angew. Chem.* **2004**, *116*, 3292–3318; *Angew. Chem. Int. Ed.* **2004**, *43*, 3230–3256.
- [26] G. J. Quallich, *Chirality* **2005**, *17*, 3230–3256.



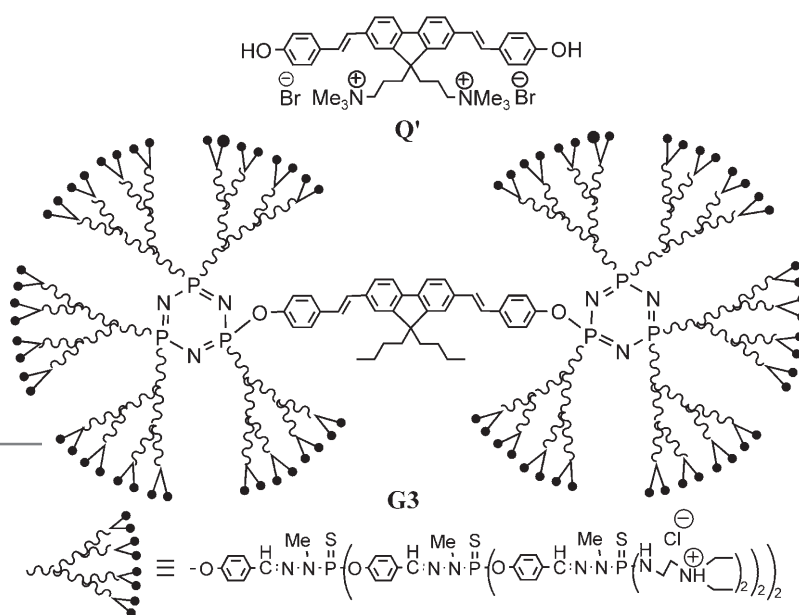
# Water-Soluble Dendrimeric Two-Photon Tracers for In Vivo Imaging\*\*

Thatavarathy R. Krishna, Manuel Parent, Martinus H. V. Werts, Laurent Moreaux, Said Gmouh, Serge Charpak, Anne-Marie Caminade, Jean-Pierre Majoral,\* and Mireille Blanchard-Desce\*

Novel microscopies based on nonlinear optical (NLO) phenomena such as two-photon excited fluorescence (TPEF)<sup>[1]</sup> are rapidly gaining popularity in biological imaging owing to the many advantages they provide. These include a capacity for a highly spatially confined excitation and intrinsic three-dimensional resolution, as well as the ability to image at an increased penetration depth in tissue with reduced photodamage and background fluorescence by operating with excitation radiation in the near-infrared (NIR) region. At first, TPEF was developed using conventional fluorophores whose two-photon absorption (TPA) characteristics were not optimized,<sup>[2]</sup> but it was soon realized that molecules specifically engineered for TPEF can significantly outperform standard fluorophores optimized for one-photon excitation. This realization triggered the search for fluorophores combining a high fluorescence quantum yield ( $\Phi$ ) and a high TPA cross-section ( $\sigma_2$ ) in the spectral region of interest for bioimaging (typically 700–1000 nm, corresponding to

the combination of reduced absorption and scattering). Molecular engineering of optimized chromophores with large TPEF cross-sections has been particularly active in the last decade<sup>[3–5]</sup> and has led, for example, to bolamphiphilic TP markers of interest for imaging of biological membranes and cells or pH sensing.<sup>[4–6]</sup> However, water-soluble TP fluorophores that maintain both a high fluorescence quantum yield and a large TPA cross-section in the spectral range of interest are still rare. In addition, fluorophores with a high TPA cross-section in toluene (that is, in a lipophilic environment) have been reported to undergo a significant decrease of their TPA characteristics in water as a result of molecular aggregation.<sup>[7]</sup>

Herein, we report a general route for the design of water-soluble TP markers from lipophilic TP fluorophores that could be applied to a variety of TP chromophores. To prevent aggregation while ensuring water solubility, we included a TP-active lipophilic chromophoric unit in the core of a dendrimer whose periphery is covered with cationic groups<sup>[8]</sup> (**G3** in Scheme 1). The dendritic sheaths should, in principle, provide



**Scheme 1.** Chromophore **Q'** and a schematized structure of dendrimer **G3**.

isolation of the central chromophore from the outer environment, thus preventing fluorescence quantum yield decrease by nonradiative processes mediated by water molecules, as well as aggregation processes that are detrimental to the TPA response. An alternative (and simpler) route consisting in grafting water-solubilizing cationic groups directly onto the TP-active lipophilic chromophore (chromophore **Q'** in Scheme 1) was also tested to evaluate the relevance of the dendrimer approach.

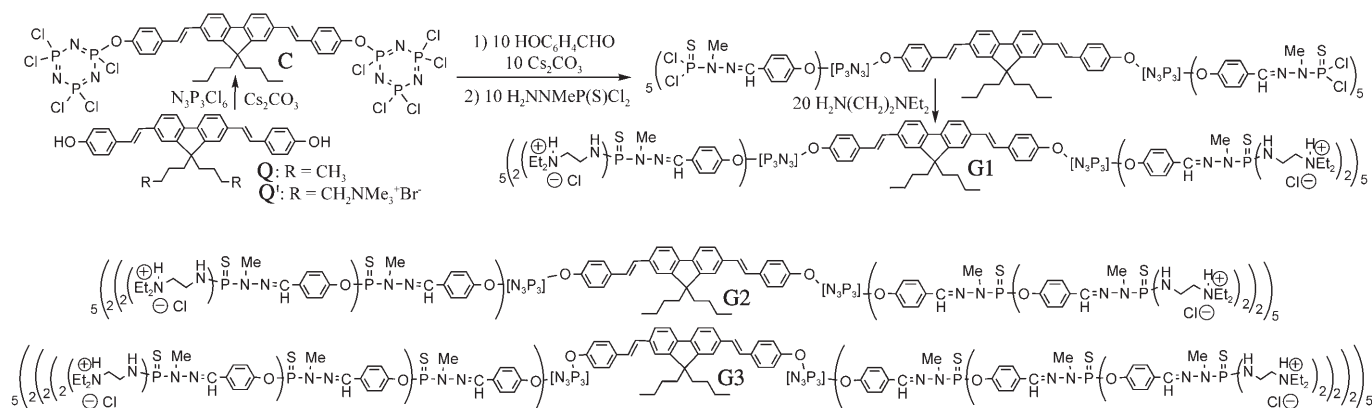
We will show herein that the strategy to incorporate a lipophilic chromophore in a protecting dendrimer shell is indeed successful and leads to nanometric water-soluble fluorescent TP-active tracers. These molecules were built from the core reagent **C** by successive repetition of nucleophilic substitution and condensation reactions. The water solubility is ensured by the ammonium groups that are linked to the surface of **G1–G3** in the last step by reaction with *N,N*-diethylethylenediamine (Scheme 2).

[\*] Dr. T. R. Krishna, Dr. A.-M. Caminade, Dr. J.-P. Majoral  
Laboratoire de Chimie de Coordination  
CNRS  
205 route de Narbonne, 31077 Toulouse Cedex 4 (France)  
Fax: (+33) 5-6155-3003  
E-mail: majoral@lcc-toulouse.fr

M. Parent, Dr. M. H. V. Werts, Dr. S. Gmouh, Dr. M. Blanchard-Desce  
Synthèse et ElectroSynthèse Organiques (CNRS, UMR 6510)  
Institut de Chimie  
Université de Rennes 1  
Campus de Beaulieu, Bât. 10A, 35042 Rennes Cedex (France)  
Fax: (+33) 2-2323-6277  
E-mail: mireille.blanchard-desce@univ-rennes1.fr  
Dr. L. Moreaux, Prof. S. Charpak  
Neurophysiology & New Microscopies Laboratory  
INSERM U603–CNRS FRE 2500  
45 rue des Saints Pères, 75006 Paris (France)

[\*\*] Financial support from the Rennes Métropole and Région Bretagne ("Renouvellement des Compétences" Program) is gratefully acknowledged. J.-P.M. thanks the Ministère de la Recherche (France) for a postdoctoral grant to T.R.K. The authors wish to thank Fayçal Ksar for his experimental contribution.

Supporting Information for this article (synthesis of chromophores **Q** and **Q'**; preparation of dendrimers **G1–G3**; experimental details of spectroscopic measurements; comparison of emission spectra of **G1–G3** in water and ethanol (Figure S1); fluorescence anisotropy results) is available on the WWW under <http://www.angewandte.org> or from the author.



**Scheme 2.** Synthesis of **G1** from **Q**, and structures of **G2** and **G3**. The core reagent **C** was prepared from the bisphenol quadrupolar chromophore **Q** by treatment with  $\text{N}_3\text{P}_3\text{Cl}_6$  under basic conditions.

Dendrimers **G1–G3** show strong one-photon absorption in the near UV and strong emission in the blue-visible region (Figure 1). Interestingly, their photoluminescence (PL) effi-

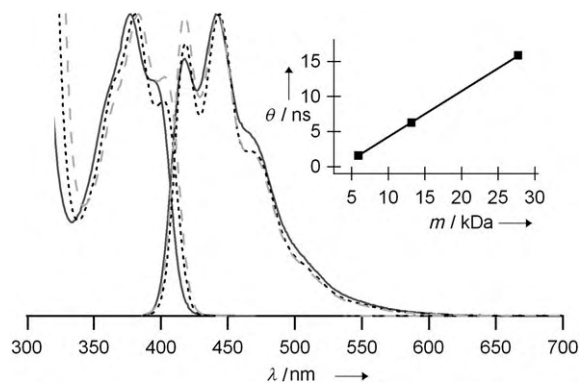


**Figure 1.** Absorption and emission spectra of **G1** (—), **G2** (----), and **G3** (---) in water. Inset: rotational correlation time,  $\theta$ , as a function of molecular weight  $m$  for dendrimers **G1–G3** in water ( $T=298\text{ K}$ ), calculated from the steady-state fluorescence anisotropy and the fluorescence lifetime using the Perrin equation. These anisotropy data indicate that **G1–G3** behave as isolated globular objects as their rotational correlation times increase linearly with the molecular weight. The hydrodynamic diameters of **G1–G3** were estimated from the rotational correlation times to be approximately 2.4, 3.8, and 5.2 nm, respectively.

ciencies are similar in water and ethanol. This indicates that the dendrimeric approach is efficient in providing water solubility while maintaining high PL efficiency. In contrast, adding water-solubilizing ammonium groups directly to the aliphatic chain of the quadrupolar chromophore **Q** (to give the water-soluble chromophore **Q'**) does not lead to retention of the PL efficiency in water (Table 1). This decrease in PL efficiency is most probably related to molecular aggregation phenomena. Indeed, the PL is restored upon addition of a surfactant (sodium dodecylsulfate) to a water solution of **Q'**.

Interestingly, the differences in relative vibronic intensities in the emission spectra of dendrimers **G1–G3** in ethanol

**Table 1:** Photophysical properties of compounds **Q**, **Q'**, and **G1–G3**.

	Solvent	$\lambda_{\text{abs,max}}$ [nm]	$\epsilon_{\text{max}}$ [ $10^4\text{ M}^{-1}\text{ cm}^{-1}$ ]	$\lambda_{\text{em}}$ [nm]	$\Phi^{\text{[a]}}$	$\sigma_2$ [GM] <sup>[b]</sup>
<b>Q</b>	EtOH	379	7.80	435	0.79	155 <sup>[5]</sup>
<b>Q'</b>	water	349	—	354	0.22	8
<b>G1</b>	water	377	7.27	442	0.53	104
<b>G2</b>	water	381	6.24	444	0.71	119
<b>G3</b>	water	383	6.31	443	0.66	127

[a] Fluorescence quantum yield determined relative to fluorescein in 0.1 N NaOH. [b] At 705 nm; 1 GM =  $10^{-50}\text{ cm}^4\text{ s photon}^{-1}$ .

and water tend to disappear with increasing generation number (see the Supporting Information). As a result, the emission spectra of the highest-generation dendrimer **G3** show similar vibronic intensities in ethanol and water, thereby indicating that the dendritic branches provide shielding layers that isolate the core chromophore from interactions with the external environment.

TPA measurements were conducted by investigating the TPEF of dendrimers **G1–G3** as well as model chromophores **Q** and **Q'** in solution. TPEF measurements allow for direct determination of the TPEF action cross-section  $\sigma_2\Phi$ , the relevant figure of merit for imaging applications and from which the TPA cross-sections can be derived.<sup>[9,10]</sup> In addition, the TPEF method has been recognized to be more reliable than nonlinear transmission measurements.<sup>[11]</sup> The quadratic dependence of the TPEF signal on the excitation intensity was checked for each data point and indicated that no photodegradation or saturation occurs. We should stress that the reported values, although moderate, are non-one-photon resonant values, which means that these chromophores could actually allow for the 3D resolution offered by selective two-photon excitation in the NIR region. This is not the case when even a small one-photon absorption is present at the excitation wavelength, which is the case in a number of chromophores with a giant resonant TPA reported recently.<sup>[12,13]</sup>

Strikingly, the water-soluble quadrupole **Q'** undergoes a marked decrease of its TPA characteristics (Table 1) in water as compared to **Q** in ethanol. As a result, although being water-soluble and based on a quadrupolar chromophore that

shows reasonable TPA efficiency in nonaqueous protic media, **Q'** has a low TPEF cross-section in water. In contrast, dendrimers **G1–G3** maintain a significant TPA cross-section in water, thereby confirming that the dendritic branches indeed isolate the chromophoric core, thus preventing aggregation and PL quenching. Interestingly, the TPA characteristics appear to increase slightly with increasing generation. This effect could be related to the slight increase of local polarity at the core with increasing generation due to the nature of the dendritic branches, which provide a somewhat polar environment.<sup>[14]</sup> Recent calculations and experiments<sup>[15]</sup> have shown that increasing solvent polarity, in a certain range, can lead to TPA enhancement.

Our results demonstrate that water-soluble, luminescent two-photon markers can be obtained by incorporating a lipophilic two-photon chromophoric unit within shielding layers built by a dendritic approach. This covalent layer-by-layer approach allows us to modulate the solubility by varying the nature of the peripheral groups while isolating the core TP chromophore from deleterious effects. This route allows us to overcome the drawbacks encountered when solubilizing groups are grafted directly onto a TP chromophore and provides a unique modular approach. In particular, replacing the core unit by more efficient TP chromophores<sup>[3]</sup> and taking advantage of the polar environment provided by the dendritic environment should lead to more efficient TP tracers, while further surface functionalization opens up a route for further functionality (such as recognition or targeting). This strategy can, in principle, be applied to various lipophilic chromophores that show high TPA cross-sections and large fluorescence quantum yields as long as phenol moieties can be grafted onto them, thus allowing for the building of the dendritic sheath.

This is of particular interest for biological applications due to the low toxicity detected for phosphorus-based dendrimers.<sup>[16]</sup> This is a major advantage—in addition to the accessibility for both inner and surface functionalization using covalent chemistry—over semiconductor quantum dots (QD). These inorganic nano-objects have gained a lot of popularity as photonic imaging agents<sup>[17]</sup> but their toxicity is still a main concern. Taking into account potential risks is one of the most important issues in nanoscience. With this aim in mind, we have demonstrated that the organic-nanodots route can provide a promising alternative in terms of two-photon brilliance,<sup>[18]</sup> and that it allows us to maintain excellent PL properties while conveying water solubility, which leads to water-soluble tracers that can indeed be used for in vivo imaging (Figure 2). This is an important step that establishes that organic nanodots definitely merit consideration as an alternative to semiconductor QDs for two-photon imaging, although further studies focusing on toxicity and (photo)-stability are needed. In this respect, it is important to add that in preliminary experiments we have found that polycationic phosphorus dendrimers bearing the same ammonium end groups are stable for months towards hydrolysis and that the photostability of dendrimers **G1** and **G2** is significantly higher than that of chromophore **Q'** in water, thus indicating that this strategy is also of interest in terms of photostability improvement.

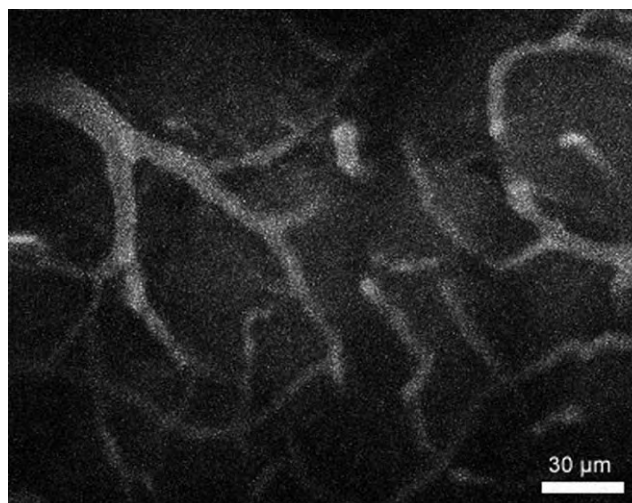


**Figure 2.** Two-photon imaging of the vascular network in the dorsal part of the rat olfactory bulb. Vessels were labeled after injecting intravenously a small bolus of 500  $\mu\text{m}$  of dendrimer **G2** in water. The fluorescence was excited at 710 nm, epi-collected, and band-pass filtered (440/40 nm). The image was taken at a depth of about 200  $\mu\text{m}$ . No obvious toxic effects were observed during the experiment (for technical details, see reference [19]).

Received: March 30, 2006

Published online: June 21, 2006

**Keywords:** chromophores · contrast agents · dendrimers · fluorescence · two-photon absorption

- [1] W. Denk, J. H. Strickler, W. W. Webb, *Science* **1990**, *248*, 73–76.
- [2] C. Xu, W. W. Webb, *J. Opt. Soc. Am. B* **1996**, *13*, 481–491.
- [3] a) S.-J. Chung, K.-S. Kim, T.-C. Lin, G. S. He, J. Swiatkiewicz, P. N. Prasad, *J. Phys. Chem. B* **1999**, *103*, 10741–10745; b) L. Ventelon, L. Moreaux, J. Mertz, M. Blanchard-Desce, *Chem. Commun.* **1999**, 2055–2056; c) M. Rumi, J. E. Ehrlich, A. A. Heikal, J. W. Perry, S. Barlow, Z.-Y. Hu, D. McCord-Maughon, T. C. Parker, H. Röckel, S. Thayumanavan, S. R. Marder, D. Beljonne, J.-L. Brédas, *J. Am. Chem. Soc.* **2000**, *122*, 9500–9510; d) B. R. Cho, K. H. Son, S. H. Lee, Y.-S. Song, Y.-K. Lee, S.-J. Jeon, J. H. Choi, H. Lee, M. Cho, *J. Am. Chem. Soc.* **2001**, *123*, 10039–10045; e) O. Mongin, L. Porrès, L. Moreaux, J. Mertz, M. Blanchard-Desce, *Org. Lett.* **2002**, *4*, 719–722; f) W. J. Yang, D. Y. Kim, C. H. Kim, M.-Y. Jeong, S. K. Lee, S.-J. Jeon, B. R. Cho, *Org. Lett.* **2004**, *6*, 1389–1392; g) L. Porres, O. Mongin, C. Katan, M. Charlot, T. Pons, J. Mertz, M. Blanchard-Desce, *Org. Lett.* **2004**, *6*, 47–50; h) C. Le Droumaguet, O. Mongin, M. H. V. Werts, M. Blanchard-Desce, *Chem. Commun.* **2005**, 2802–2804.
- [4] L. Ventelon, S. Charier, L. Moreaux, J. Mertz, M. Blanchard-Desce, *Angew. Chem.* **2001**, *113*, 2156–2159; *Angew. Chem. Int. Ed.* **2001**, *40*, 2098–2101.
- [5] M. H. V. Werts, S. Gmouh, O. Mongin, T. Pons, M. Blanchard-Desce, *J. Am. Chem. Soc.* **2004**, *126*, 16294–16295.
- [6] M. Blanchard-Desce, *C. R. Phys.* **2002**, *3*, 439–448.
- [7] H. Y. Woo, J. W. Hong, B. Liu, A. Mikhailovsky, D. Korystov, G. C. Bazan, *J. Am. Chem. Soc.* **2005**, *127*, 820–821.
- [8] J. Leclaire, Y. Coppel, A.-M. Caminade, J.-P. Majoral, *J. Am. Chem. Soc.* **2004**, *126*, 2304–2305.
- [9] TPEF measurements were performed by excitation with 150-fs pulses from a Ti:sapphire laser, using the protocol of Xu and Webb,<sup>[2]</sup> taking into account refractive index effects.<sup>[10]</sup>

- [10] M. H. V. Werts, N. Nerambourg, D. Pelegry, Y. Le Grand, M. Blanchard-Desce, *Photochem. Photobiol. Sci.* **2005**, *4*, 531–538.
- [11] D. A. Oulianov, I. V. Tomov, A. S. Dvornikov, P. M. Rentzepis, *Opt. Commun.* **2001**, *191*, 235–243.
- [12] R. Misra, R. Kumar, T. K. Chandrashekar, A. Nag, D. Goswami, *Org. Lett.* **2006**, *8*, 629–631..
- [13] D. Y. Kim, T. K. Ahn, J. H. Kwon, D. Kim, T. Ikeue, N. Aratani, A. Osuka, M. Shigeiwa, S. Maeda, *J. Phys. Chem. A* **2005**, *109*, 2996–2999.
- [14] J. Leclaire, R. Dagiral, S. Fery-Forgues, Y. Coppel, B. Donnadieu, A.-M. Caminade, J.-P. Majoral, *J. Am. Chem. Soc.* **2005**, *127*, 15762–15770.
- [15] A. Masunov, S. Tretiak, J. W. Hong, G. C. Bazan, *Abstracts of Papers, 229th ACS National Meeting, San Diego, CA, March 13–17, 2005*, COMP-295.
- [16] a) M. Maszewska, J. Leclaire, M. Cieslak, B. Nawrot, A. Okruszek, A.-M. Caminade, J.-P. Majoral, *Oligonucleotides* **2003**, *13*, 193–205; b) J. Solassol, C. Crozet, V. Perrier, J. Leclaire, F. Béranger, A.-M. Caminade, B. Meunier, D. Dormont, J. P. Majoral, S. Lehmann, *J. Gen. Virol.* **2004**, *85*, 1791.
- [17] D. R. Larson, W. R. Zipfel, R. M. Williams, S. W. Clark, M. P. Bruchez, F. W. Wise, W. W. Webb, *Science* **2003**, *300*, 1434–1437.
- [18] O. Mongin, T. R. Krishna, M. H. V. Werts, A.-M. Caminade, J.-P. Majoral, M. Blanchard-Desce, *Chem. Commun.* **2006**, 915–917.
- [19] E. Chaigneau, M. Oheim, E. Audinat, S. Charpak, *Proc. Natl. Acad. Sci. USA* **2003**, *100*, 13081–13086.



## Sustainable Chemistry

DOI: 10.1002/anie.200601180

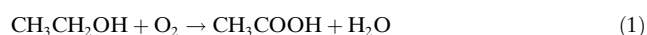
**Formation of Acetic Acid by Aqueous-Phase Oxidation of Ethanol with Air in the Presence of a Heterogeneous Gold Catalyst\*\****Claus H. Christensen,\* Betina Jørgensen, Jeppe Rass-Hansen, Kresten Egeblad, Robert Madsen, Søren K. Klitgaard, Stine M. Hansen, Mike R. Hansen, Hans C. Andersen, and Anders Riisager*

Bioethanol is produced by fermentation of biomass in increasing amounts to meet the growing demands for CO<sub>2</sub>-neutral transportation fuels and to eventually remove the dependence on fossil fuels. However, bioethanol could also find use as a versatile, sustainable chemical feedstock. Herein,

it is shown that it is possible to selectively oxidize ethanol into acetic acid in aqueous solution using air as the oxidant with a heterogeneous gold catalyst at temperatures of about 423 K and O<sub>2</sub> pressures of 0.6 MPa. This reaction proceeds readily in aqueous acidic media and yields of up to 90% are achieved, with CO<sub>2</sub> as the only major by-product. Thus, it constitutes a very simple, green route to acetic acid.

The oxidation of ethanol by air into acetic acid over platinum was among the first heterogeneously catalyzed reactions to be reported. The initial discovery was made by Döbereiner about two centuries ago, even before the term catalysis was coined.<sup>[1]</sup> So far, the reaction has not been used for large-scale production of acetic acid. Instead, three other routes to acetic acid have found industrial application: fermentation (vinegar), catalytic liquid-phase oxidation of butane, naphtha, or acetaldehyde, and the carbonylation of methanol, which has recently become the most important.<sup>[2]</sup>

In the most widely used industrial processes today, the feedstock is almost exclusively derived from fossil fuels. Thus, the production of acetic acid consumes fossil fuels and therefore contributes slightly to increasing CO<sub>2</sub> levels in the atmosphere, and, more importantly, the cost of acetic acid is strongly dependent on the price of the fossil fuels. Therefore, it is interesting that the cost of renewable feedstocks has decreased dramatically relative to fossil fuel feedstocks over the last four decades. Specifically, the cost of corn relative to oil has decreased fivefold from 1950 to 2005. Today, bioethanol is mostly produced by fermentation of starch-containing crops, such as corn or sugar cane, but it seems likely that cellulose-rich agricultural waste will gain importance as a feedstock in the future.<sup>[3]</sup> Therefore, and also because of the continuing technological improvements of the production process, the cost of bioethanol is expected to decrease.<sup>[4]</sup> Thus, with increasing fossil fuel prices, the production of acetic acid from bioethanol will become increasingly favorable compared to current fossil fuel-based methods. Clearly, this development requires that an active and selective catalyst for oxidation of ethanol with dioxygen to form acetic acid [Eq. (1)] is available.



So far, primarily palladium and platinum catalysts have received attention as catalysts for ethanol oxidation.<sup>[5]</sup> However, with these catalysts it has proven difficult to reach sufficient selectivities at high conversions.

Here, it is reported for the first time that gold catalysts are both very active and selective catalysts for aqueous-phase oxidation of ethanol with air into acetic acid at 373–473 K with O<sub>2</sub> pressures of 0.5–1 MPa. Interestingly, metallic gold was for many years considered too unreactive to be useful as a catalyst.<sup>[6]</sup> However, this view was challenged in the seminal studies of Haruta and co-workers,<sup>[7,8]</sup> who showed that gold very efficiently catalyzed the room-temperature oxidation of CO with O<sub>2</sub> to form CO<sub>2</sub>, and by Hutchings, who studied acetylene hydrochlorination with gold catalysts.<sup>[9]</sup> Since then, numerous reports of different gold-catalyzed reactions have appeared and the field has recently been reviewed and highlighted.<sup>[10–12]</sup>

[\*] Prof. C. H. Christensen, B. Jørgensen, J. Rass-Hansen, K. Egeblad, Prof. R. Madsen, S. K. Klitgaard, S. M. Hansen, M. R. Hansen, H. C. Andersen, Prof. A. Riisager  
Center for Sustainable and Green Chemistry  
Department of Chemistry  
Technical University of Denmark  
Kemitorvet building 207, 2800 Kgs. Lyngby (Denmark)  
Fax: (+45) 4525-2235  
E-mail: chc@kemi.dtu.dk

[\*\*] The Center for Sustainable and Green Chemistry is sponsored by the Danish National Research Foundation. Financial support from the Danish Research Agency (grant 2104-04-0003) is acknowledged.

The catalytic oxidation of alcohols with air has also attracted significant attention as a “green” reaction.<sup>[13]</sup> Among the heterogeneous catalysts, mainly Pd and Pt have shown promising result.<sup>[14,15]</sup> Rossi and co-workers were the first to show that alcohols, specifically diols and sugars, can be oxidized to the corresponding acids with gold catalysts but only when a base is present.<sup>[16,17]</sup> Later, the oxidation of glycerol to glycerate using Au/C was similarly demonstrated.<sup>[18]</sup> Recently, it was shown that heterogeneous ceria-supported gold catalysts are able to oxidize several higher alcohols into the corresponding carboxylic acids using air as oxidant.<sup>[19]</sup> In these experiments, the support played an active role in the catalytic cycle. However, it has also been shown that solvent-free oxidations of primary alcohols can selectively yield aldehydes.<sup>[20]</sup> Thus, it is noteworthy that the gold-catalyzed aqueous-phase oxidation of ethanol with air into acetic acid reported here proceeds readily in acidic aqueous solution.

Bioethanol is typically produced in a series of steps, namely fermentation in a batch process (yielding 3–15 vol % aqueous ethanol), distillation to obtain the azeotrope (containing 96 vol % ethanol), and further distillation to achieve the anhydrous ethanol that is required as a fuel additive.<sup>[21]</sup> Therefore, we decided to study the oxidation of ethanol in a batch process with ethanol concentrations corresponding to those obtained during fermentation, as this is expected to represent the easiest scheme for acetic acid production from bioethanol. All catalysts were prepared on a porous support of MgAl<sub>2</sub>O<sub>4</sub> (65 m<sup>2</sup> g<sup>−1</sup>) using HAuCl<sub>4</sub>·3H<sub>2</sub>O, PtCl<sub>4</sub>, and PdCl<sub>2</sub> as metal precursors. The catalytic experiments were conducted in stirred reactors (50 mL, Parr Autoclaves, stainless steel). Liquid samples were drawn from the reactor periodically using the sampling system and analyzed by gas chromatography (GC). Similarly, gas samples were also analyzed by GC. No reaction was observed in the absence of catalyst or when using the pure supports without gold. The metal content of all catalysts was analyzed by atomic absorption spectroscopy (AAS). The gold catalysts were also characterized by transmission electron microscopy (TEM) before and after testing. Typically, 20 images were recorded for each catalyst sample.

Initially, we studied whether gold could catalyze the selective oxidation of ethanol into acetic acid with air in aqueous solution, and how such a catalyst would compare with previously reported systems based on platinum and palladium. Table 1 compares the performance of Au, Pt, and Pd catalysts on a MgAl<sub>2</sub>O<sub>4</sub> support. Previously, the nature of the support has been shown to be critically important for gold

catalysts.<sup>[19,22]</sup> MgAl<sub>2</sub>O<sub>4</sub> was chosen as the support material here since it is stable at high water pressures and because it can be considered completely inactive in redox processes. Thus, the observed activity can be attributed solely to the metal nanoparticles, and no synergistic effect with the support is expected. Other supports might be found to affect the catalytic performance.

Remarkably, the gold catalyst not only exhibits similar or higher catalytic activity than palladium or platinum but, in particular, a significantly higher selectivity towards acetic acid than both of these well-known catalysts. The major by-product for the gold catalyst is CO<sub>2</sub>, whereas the Pd and Pt catalysts also produce significant amounts of acetaldehyde. Thus, we decided to further investigate the performance of gold catalysts for ethanol oxidation to gain a more detailed insight into this reaction and to identify suitable reaction conditions.

Figure 1 shows representative TEM images of the 1 wt % Au/MgAl<sub>2</sub>O<sub>4</sub> catalyst used in this study. Generally, gold particle sizes of 3–6 nm are observed both before and after testing, with no sign of sintering. Figure 1 also illustrates how the ethanol conversion and the acetic acid yield depend on the reaction time. The reaction is conducted with only a slight excess of oxygen and therefore the reaction rate does not obey pseudo-first-order kinetics.

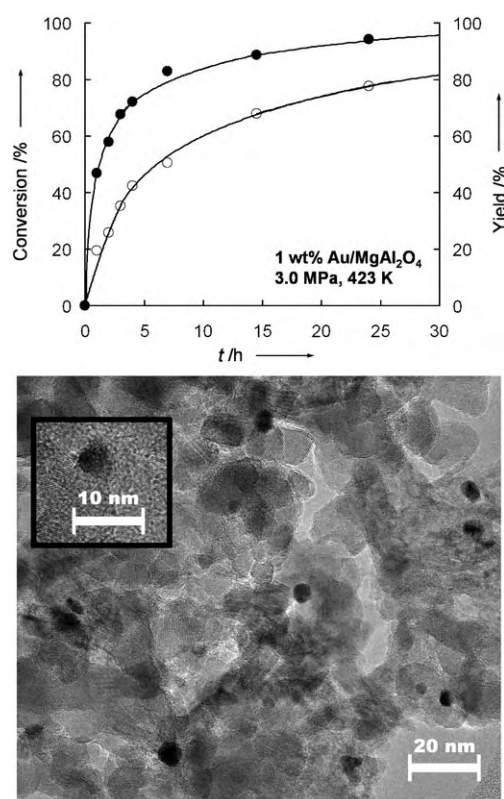


**Figure 1.** Top: Performance of 150 mg of 1 wt % Au/MgAl<sub>2</sub>O<sub>4</sub> catalyst in the oxidation of 10 mL of aqueous 5 wt % ethanol with air at 423 K and 3.0 MPa (● ethanol conversion, ○ acetic acid yield). Bottom: TEM images of the 1 wt % Au/MgAl<sub>2</sub>O<sub>4</sub> catalyst used for ethanol oxidation. The inset shows a high-resolution image of a gold particle with a diameter of about 5 nm.

**Table 1:** Comparison of MgAl<sub>2</sub>O<sub>4</sub>-supported Au, Pt, and Pd catalysts for oxidation of aqueous ethanol to acetic acid with air.<sup>[a]</sup>

Cat.	T [K]	p [MPa]	t [h]	Conv. [%]	Yield [%]	STY <sup>[b]</sup> [mol h <sup>−1</sup> L <sup>−1</sup> ]
Au <sup>[c]</sup>	453	3	4	97	83	0.21
Pt	453	3	4	82	16	0.047
Pd	453	3	4	93	60	0.15

[a] Conditions: 150 mg catalyst, 1 wt % of metal, 10 mL of 5 wt % aqueous ethanol, [b] Space-time yield, [c] Corresponding to 0.07 mol % Au.

Figure 2 shows how the performance of the catalyst depends on temperature and pressure. It is noteworthy that yields above 80% are obtained without any special effort to optimize the reaction conditions or catalyst composition. It can also be seen that the reaction rate and selectivity are only slightly influenced by the total pressure when oxygen is present in excess.

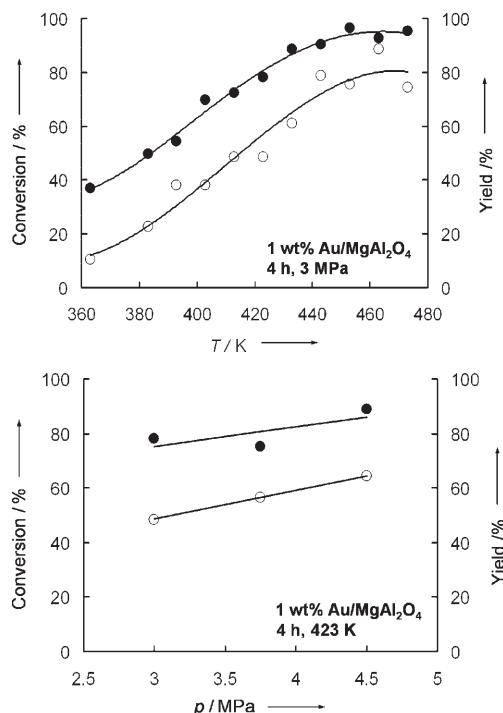


**Figure 2.** Ethanol conversion (●) and acetic acid yield (○) with 10 mL of 5 wt% aqueous ethanol after 4 h in the presence of 150 mg of 1 wt% Au/MgAl<sub>2</sub>O<sub>4</sub> catalyst. Top: temperatures of 363–473 K and an air pressure of 3 MPa. Bottom: pressures of 3–4.5 MPa and a temperature of 423 K.

As the reaction progresses, the solution becomes more and more acidic, but this does not influence the catalyst's performance. By more careful selection of reaction conditions, for example by increasing the reaction time at 423 K or at 453 K and 3.5 MPa, it is possible to achieve acetic acid yields of over 90% (e.g., 92% yield after 8 h at 453 K and 3.5 MPa). The spinel is found to be quite stable under the present reaction conditions. After a typical reaction run, less than 1% is lost according to ICP-MS. Additionally, only phase-pure spinel is found by powder X-ray diffraction. This is in agreement with the previous finding that magnesium aluminum hydroxide (Al/Mg=2) transforms into spinel under hydrothermal conditions.<sup>[23]</sup>

Thus, it is seen that gold catalysts are indeed able to selectively oxidize ethanol to acetic acid in air at moderate temperatures and dioxygen pressures with very high yields. This suggests that it might prove viable to produce aqueous acetic acid in a gold-catalyzed process using aqueous bioethanol as the feedstock. Acetic acid can also be obtained directly by fermentation, however this also represents a challenge since the bacteria do not thrive under the highly

acidic reaction conditions.<sup>[2]</sup> Here, the very high stability of the gold-on-MgAl<sub>2</sub>O<sub>4</sub> catalyst allows the use of high temperatures and pressures, which results in high rates. Recently, bioethanol has also received attention as a feedstock for renewable dihydrogen by steam-reforming<sup>[24]</sup> or autothermal reforming.<sup>[25]</sup> Figure 3 illustrates some proven possibilities for using bioethanol, including both fuel and feedstock applications.

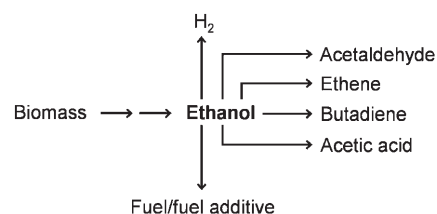


**Figure 3.** Possible uses of bioethanol as a fuel or as a feedstock for important bulk chemicals.<sup>[26]</sup>

A future challenge for chemists could be to find efficient routes from bioethanol to fuels and chemicals. Such processes will also compete with other new processes that allow direct conversion of carbohydrates into, for example, dihydrogen<sup>[27,28]</sup> or synfuels,<sup>[28,29]</sup> which are currently being explored. Here, we have focused on synthesizing acetic acid from ethanol in a simple, green process since acetic acid has a significantly higher value than fuels (including dihydrogen) and also than ethene, acetaldehyde, and butadiene, for example. Therefore, this might represent the currently most efficient use of part of the available bioethanol.

## Experimental Section

The gold catalysts were prepared by deposition-precipitation<sup>[30]</sup> of H<sub>2</sub>AuCl<sub>4</sub>·3H<sub>2</sub>O (supplied by Aldrich) on MgAl<sub>2</sub>O<sub>4</sub>. Stoichiometric MgAl<sub>2</sub>O<sub>4</sub>, calcined at 1000 °C,<sup>[31]</sup> was tabletized, crushed, and sieved to a particle size of 100–250 μm prior to use. For comparative purposes, Pd and Pt catalysts supported on MgAl<sub>2</sub>O<sub>4</sub> were prepared by incipient-wetness impregnation of hydrochloric acid solutions of PdCl<sub>2</sub> and PtCl<sub>4</sub>, respectively. The resulting catalyst precursors were dried at 120 °C for 6 h and calcined at 773 K for 2 h. The pure, stoichiometric, and calcined spinel used here is neutral and causes essentially no change of pH (less than ±0.05) when suspended in water or treated hydrothermally in water.

The reactor (total free volume of 55 mL) was charged with 5 wt% aqueous ethanol (10 mL), and the catalyst (150 mg) was added. After closing the autoclave, it was charged with technical air (80 vol% N<sub>2</sub>, 20 vol% O<sub>2</sub>) at the required pressure (2.5–5.0 MPa) and sealed. No dioxygen was added to replace that consumed by the reaction and consequently only a limited excess of oxygen is present after reaction. The reactor was then heated to a reaction temperature between 373 and 473 K where it was kept for the desired time period (4 to 45 h). The time required to reach the reaction temperature varied slightly. The pressure was monitored during the reaction and the pH was determined in the product. After the reaction, the autoclave was cooled to about 278 K. After each run, the reactor and internal components were cleaned by polishing and washing with water. The catalyst was separated by ultrafiltration and used up to three times. At this point it had lost most of its activity, which corresponds to TONs of more than 10000. The content of Al, Mg, and Au in solution after each run was measured by ICP-MS. In a separate experiment, pure spinel was treated under hydrothermal conditions (150 °C, 3.0 MPa)

with 5 wt% acetic acid. No acetic acid was found to be lost onto the support.

The GC apparatus was equipped with both FID and TCD detectors to allow identification of all liquid and gaseous products present in amounts above about 1 vol%. Product compositions and concentrations were determined using standard solutions. In some cases, the entire reaction mixture was also titrated with aqueous sodium hydroxide after the reaction run to validate the GC results. In all cases, the analyses gave identical results within the experimental uncertainties.

Received: March 24, 2006

Published online: June 22, 2006

**Keywords:** acetic acid · bioethanol · gold · heterogeneous catalysis · oxidation

- 
- [1] J. W. Döbereiner, *Ann. Phys.* **1822**, 72, 193.
  - [2] H. Cheung, R. S. Tanke, G. P. Torrence, *Ullmann's Encyclopedia of Industrial Chemistry*, Wiley-VCH, Weinheim, **2005**.
  - [3] S. Kim, B. E. Dale, *Biomass Bioenergy* **2004**, 26, 361.
  - [4] R. Wooley, M. Ruth, D. Glassner, J. Sheehan, *Biotechnol. Prog.* **1999**, 15, 794.
  - [5] Y. Obana, H. Uchida, K.-i. Sano, US Patent 6,867,164, **2005**.
  - [6] J. Schwank, *Gold Bull.* **1983**, 16, 103.
  - [7] M. Haruta, T. Kobayashi, H. Sano, N. Yamada, *Chem. Lett.* **1987**, 405.
  - [8] M. Haruta, N. Yamada, T. Kobayashi, S. Iilima, *J. Catal.* **1989**, 115, 301.
  - [9] G. J. Hutchings, *J. Catal.* **1985**, 96, 292.
  - [10] T. Mallat, A. Baiker, *Catal. Today* **1994**, 19, 247.
  - [11] G. J. Hutchings, M. Haruta, *Appl. Catal. A* **2005**, 291, 2.
  - [12] G. J. Hutchings, *Catal. Today* **2005**, 100, 55.
  - [13] G.-J. ten Brink, I. W. C. E. Arends, R. A. Sheldon, *Science* **2000**, 287, 1636.
  - [14] K. Mori, T. Hara, T. Mizugaki, K. Ebitani, K. Kaneda, *J. Am. Chem. Soc.* **2004**, 126, 10657.
  - [15] T. Nishimura, N. Kakiuchi, M. Inoue, S. Uemura, *Chem. Commun.* **2000**, 1245.
  - [16] L. Prati, M. Rossi, *J. Catal.* **1998**, 176, 552.
  - [17] C. Bianchi, F. Porta, L. Prati, M. Rossi, *Top. Catal.* **2000**, 13, 231.
  - [18] S. Carretin, P. McMorn, P. Johnston, K. Griffin, C. J. Kiely, G. J. Hutchings, *Chem. Commun.* **2002**, 696.
  - [19] A. Abad, P. Concepción, A. Corma, H. Garcia, *Angew. Chem.* **2005**, 117, 4134; *Angew. Chem. Int. Ed.* **2005**, 44, 4066.
  - [20] D. I. Enache, D. W. Knight, G. J. Hutchings, *Catal. Lett.* **2005**, 103, 43.
  - [21] G. Soboëan, P. Glaviè, *Appl. Therm. Eng.* **2000**, 20, 529.
  - [22] M. S. Chen, D. W. Goodman, *Science* **2004**, 306, 252.
  - [23] G. Fornasari, R. Glöckler, M. Livi, A. Vaccari, *Appl. Clay Sci.* **2005**, 20, 258.
  - [24] A. Haryanto, S. Fernando, N. Murali, S. Adhikari, *Energy Fuels* **2005**, 19, 2098.
  - [25] G. A. Deluga, J. R. Salge, L. Schmidt, X. E. Verykios, *Science* **2004**, 303, 993.
  - [26] Bioethanol, acetaldehyde, ethene, butadiene, acetic acid, and gasoline are currently produced in quantities of about 30, 1.4, 120, 7.5, 8.5, and 1100 million tonnes per year, respectively.
  - [27] R. D. Cortright, R. R. Davda, J. A. Dumesic, *Nature* **2002**, 418, 964.
  - [28] J. R. Rostrup-Nielsen, *Science* **2005**, 308, 1421.
  - [29] G. W. Huber, J. N. Cheeda, C. J. Barrett, J. A. Dumesic, *Science* **2005**, 308, 1446.
  - [30] M. Haruta, *Catal. Today* **1997**, 36, 153.
  - [31] J. Dohrup, C. J. H. Jacobsen, C. Olsen, US Patent 6,416,731, **2002**.



DOI: 10.1002/anie.200601184

**Activation of Oxygen on Gold/Alumina Catalysts:  
In Situ High-Energy-Resolution Fluorescence and  
Time-Resolved X-ray Spectroscopy\*\****Jeroen A. van Bokhoven,\* Catherine Louis,  
Jeffrey T. Miller, Moniek Tromp, Olga V. Safonova, and  
Pieter Glatzel*

Catalysis by gold has received considerable attention in recent years. Particles of gold that are unsupported or supported on oxidic carriers have been reported to be very active in various oxidation reactions. Examples include the oxidation of CO in the presence or absence of hydrogen,<sup>[1]</sup> the water gas shift reaction,<sup>[2]</sup> and the oxidation of hydrocarbons.<sup>[3]</sup> The particle size greatly influences the catalytic activity of gold particles, and with decreasing particle size the activity increases. Moreover, the type of support also affects the catalytic activity: reducible supports lead to more active catalysts than nonreducible ones,<sup>[4]</sup> however, deviations from this trend have been reported.<sup>[5]</sup> Addition of reducible oxides to gold catalysts increased the catalytic activity of small gold particles considerably.<sup>[6]</sup> Correlated to this observation may be the enhanced stability of gold particles after the addition of transition-metal oxides.<sup>[7]</sup>

The origin of the high catalytic activity of gold catalysts has been strongly debated and various models have been presented. Goodman and co-workers<sup>[1b]</sup> suggested that the

[\*] Prof. Dr. J. A. van Bokhoven  
Institute for Chemical and Bioengineering  
ETH Zürich  
8093 Zürich (Switzerland)  
Fax: (+41) 43-362-1162  
E-mail: j.a.vanbokhoven@chem.ethz.ch  
Dr. C. Louis  
Laboratoire de Réactivité de Surface  
UMR 7609 CNRS  
Université Pierre et Marie Curie  
4 place Jussieu, 75252, Paris, Cedex 05 (France)  
Dr. J. T. Miller  
BP Research Center  
150 W. Warrenville Rd., Naperville, IL 60565-8406 (USA)  
Dr. M. Tromp  
University of Southampton  
School of Chemistry  
Southampton, SO17 1BJ (UK)  
Dr. O. V. Safonova, Dr. P. Glatzel  
European Synchrotron Radiation Facility (ESRF)  
BP22, 6 rue Jules Horowitz, 38043 Grenoble (France)

[\*\*] We thank Dr. I. N. Remediakis and Prof. Dr. J. K. Nørskov for providing the coordinates of the calculated gold structures, Dr. F. Krumeich for taking the EM images, Dr. L. Delannoy for making the sample, the SNF (J.A.v.B.), the EPSRC (M.T.), and the ESRF for provision of facilities at ID26 and ID24 (mass spectrometer).



Supporting information for this article is available on the WWW under <http://www.angewandte.org> or from the author.

catalytic activity of small gold particles is paralleled by the loss of metallic character. Moreover, a double layer of gold atoms on a planar titania support was shown to be much more active than thicker layers of gold.<sup>[1c]</sup> Various authors proposed oxidic gold or a combination of reduced and oxidic gold as the active species in oxidation reactions by gold.<sup>[8]</sup> In addition, negatively charge gold atoms have been proposed to be the active centers.<sup>[9]</sup>

Initial theoretical calculations on the mechanism indicated that the support interface is responsible for the oxidation of CO.<sup>[10]</sup> Recently, however, a reaction path that only takes place on a gold particle was proposed.<sup>[11,1c]</sup> The major question that remains is the activation of the oxygen molecule which has been suggested to take place on the support.<sup>[12]</sup> The mechanism proposed by Bond and Thompson<sup>[8]</sup> involves the adsorption of CO on the gold particle at a low-coordinated gold atom. A hydroxy group from the support moves to a Au<sup>III</sup> cation, meanwhile creating an anionic vacancy. These two species react to form a carboxylate group. The anionic vacancy on the support activates an oxygen molecule as O<sub>2</sub><sup>-</sup>, which then is responsible for abstraction of a hydrogen atom, and CO<sub>2</sub> is formed. The hydroperoxide ion reacts with a second carboxylate species to form another CO<sub>2</sub> molecule and restores two hydroxy groups on the support.

Herein, we introduce in situ time-resolved and high-energy-resolution fluorescence-detected (HERFD) X-ray spectroscopy at the Au L<sub>3</sub> edge to determine the activation of oxygen on the gold particle. We studied gold supported on a nonreducible support, Al<sub>2</sub>O<sub>3</sub>. X-ray absorption near-edge structure (XANES) studies probe the local geometry and the oxidation state of the absorption atom. XANES is sensitive to adsorbates on the surface of metallic particles, and the spectral shape is affected by the mode of bonding.<sup>[13]</sup> The intensity of the first feature in the L<sub>3</sub> edge spectrum, which is called whiteline, reveals the number of holes in the d band and therefore reflects charge transfer after adsorption of molecules. Application of high-energy-resolution emission spectroscopy greatly enhances the resolution in the spectra.<sup>[14]</sup> Selective detection of a fluorescence channel with an instrumental broadening below the core hole lifetime greatly enhances the spectral resolution,<sup>[15]</sup> thus resulting in much sharper features in the X-ray absorption spectra. In addition to high-energy-resolution XAS, a time resolution of seconds can be achieved using normal fluorescence detection at beamline ID26 at the ESRF (Grenoble). The response of the system to changes in the gas composition, from oxidizing to reducing and back, can be determined.

The enhancement in spectral resolution when using high-energy-resolution fluorescence detection is illustrated in Figure 1 a, which shows the X-ray absorption spectrum of gold foil measured simultaneously in normal transmission mode and with the high-energy-resolution fluorescence detector. A small whiteline at 11929 eV is visible in the transmission spectrum. The whiteline is very prominent in the spectrum that was recorded with the high-resolution fluorescence detector. Furthermore, all other features are much more pronounced. Any changes that occur after the adsorption of reactants, in the oxidation state of the gold or in its

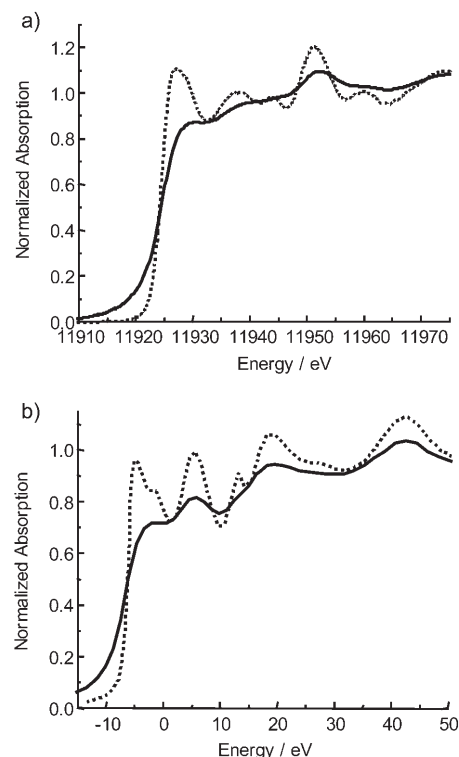


**Figure 1.** a) Experimental and b) theoretically simulated L<sub>3</sub> XANES of Au foil detected in transmission mode (—) and by using high-energy-resolution fluorescence detection (----).

coordination, will be detected with much higher accuracy in the high-resolution data. Although the electron configuration of a gold atom is Xe4f<sup>14</sup>5d<sup>10</sup>6s<sup>1</sup>, in bulk gold the s, p, and d orbitals overlap, which causes orbital hybridization and results in a 5d<sup>10-x</sup>6sp<sup>1+x</sup> electron configuration. The whiteline reflects this hole in the d band. Theoretically simulated spectra using the FEFF8 code are shown in Figure 1 b. Spectra of bulk gold using the full L<sub>3</sub> core hole lifetime and reduced by 1.6 eV showed all the features that were experimentally observed, though the exact positions and relative intensities of the features varied. Theory predicted a double whiteline in the high-energy-resolution data which is observed as a slight asymmetry in the experimental whiteline.

The Au L<sub>3</sub> near-edge spectra of Au/Al<sub>2</sub>O<sub>3</sub> measured in various gas atmospheres using high-energy-resolution emission detection is shown in Figure 2 a. The size of the gold particles is 1–3 nm as determined by scanning transmission electron microscopy (see Supporting Information). The XANES spectrum of the catalyst recorded at room temperature under helium after reduction shows the typical features of a fully reduced gold particle: a small whiteline and further features at similar positions as those in the spectrum of bulk gold. All these features have much less pronounced intensity compared to those in the spectrum of bulk gold (Figure 1). The whiteline has lower intensity than that in the spectrum of bulk gold because of the more atomic-like character in the small particles and the reduced spd hybridization, as the band widths are smaller and show less overlap.

The spectrum of the Au/Al<sub>2</sub>O<sub>3</sub> catalyst measured under 20% oxygen in helium shows an increased whiteline intensity

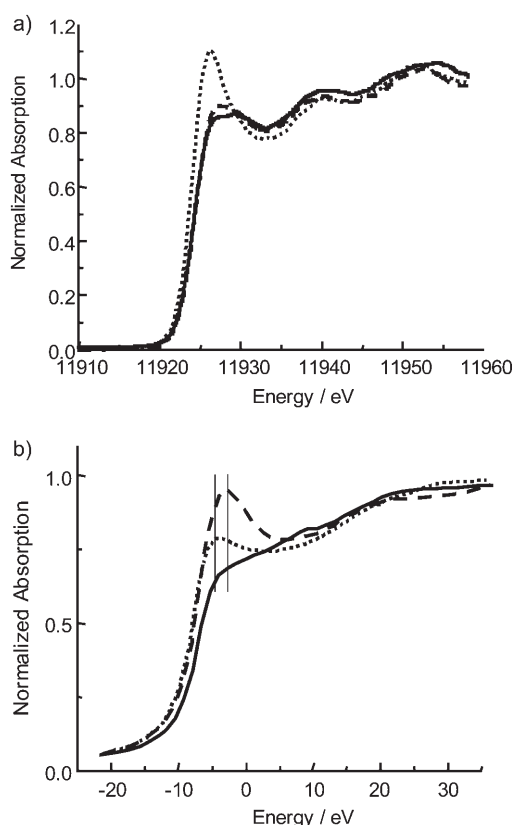


**Figure 2.** a) High-resolution Au L<sub>3</sub> XANES of 4% Au/Al<sub>2</sub>O<sub>3</sub> in various atmospheres applied subsequently: He (—); 20% O<sub>2</sub> in He (---); and 1% CO in He (····). b) FEFF8-calculated Au L<sub>3</sub> XANES of gold clusters (—) with adsorbed oxygen (····) or CO (---).

which reflects charge transfer from the d band to the 2π\* orbital of oxygen, decreasing the gold d-orbital electron count and activating the oxygen molecule. This result agrees with previously reported partial oxidation of small gold particles in air.<sup>[16]</sup> On the basis of the intensity of the whiteline, the fraction of oxidized gold is about 15%, which is very similar to the amount reported by Miller et al.<sup>[16]</sup> Oxygen reacts with the surface of the small gold particles to form a surface oxide. Subsequent exposure of the partially oxidized catalyst to 1% CO in helium resulted in a decreased whiteline intensity. However, the whiteline intensity was higher than that measured in He and the energy of the maximum intensity was shifted to higher energy relative to the spectrum measured under oxygen. This behavior is ascribed to the bonding of CO on the surface of reduced gold particles.<sup>[17,13d]</sup> Simulation of spectra using the full multiple scattering code FEFF8 (Figure 2b) indicated that CO adsorption causes enhanced intensity of the whiteline at a higher energy than adsorbed oxygen (the clusters are taken from Reference [11]). Electron back-donation into the anti-bonding orbitals of CO is responsible for the charge transfer.

The evolution of the spectra, measured in conventional fluorescence mode, after switching the gas flow from 20% oxygen in helium to 1% CO in He is shown in Figure 3. Spectra were recorded every 2 s. The reduction is very fast and was complete after 14 s (seven scans). Meanwhile, small amounts of CO<sub>2</sub> were observed in the mass spectrometer. The

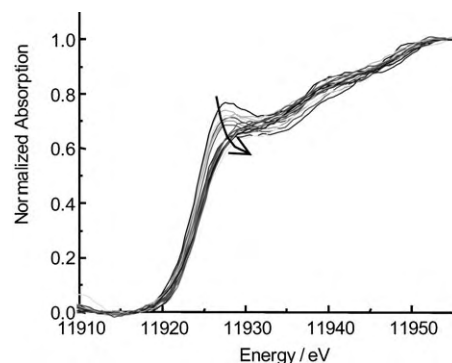


**Figure 3.** Kinetics of re-reduction in CO: Time-resolved XANES spectra measured in normal fluorescence mode.

reduction of partially oxidized gold catalysts is much faster than their oxidation, which took over 5 min to complete (spectra not shown).

One of the main questions regarding the mechanism is how oxygen is activated on the catalyst.<sup>[5,12]</sup> Various reports suggest that the metal-support interface plays a role and that the support activates oxygen and serves as a supply of oxygen that recombines with CO on the gold particle to form CO<sub>2</sub>. Our in situ XANES study clearly showed that charge transfer from small gold particles to oxygen occurs when exposed to oxygen, along with partial depletion of the Au d band. A fraction of the surface atoms react with oxygen. Small gold particles on a nonreducible oxidic support activate oxygen, meanwhile forming partially oxidized gold: Au<sup>0</sup> + O<sub>2</sub> → Au<sub>y</sub>O<sub>x</sub>. Miller et al. observed oxidation of gold by air with Au/Al<sub>2</sub>O<sub>3</sub> catalysts by changes in the near-edge structure, which was confirmed by a decrease in the Au–Au coordination number and an increase in the Au–O contribution in a full EXAFS analysis.<sup>[16]</sup> The partially oxidized gold is reduced very quickly by CO to form CO<sub>2</sub> (Figure 3), showing that the partially oxidized gold particles readily react with CO to form CO<sub>2</sub>, thus closing a catalytic cycle: Au<sub>y</sub>O<sub>x</sub> + CO → Au<sup>0</sup> + CO<sub>2</sub>. After the full reduction, adsorbed CO is observed on the surface by the broadening of the whiteline (Figure 2).<sup>[17,13d]</sup> Clearly, the reduction is much faster than the reoxidation and the rate-limiting step is the activation of oxygen on the gold surface.<sup>[8]</sup> In a mixed O<sub>2</sub>/CO gas environment, fully reduced gold is expected,<sup>[18]</sup> probably with adsorbed CO on its surface.<sup>[17]</sup> In this mechanism, partially oxidized gold is formed upon reaction with oxygen and is present as a short-lived species under catalytic conditions.

In situ high-energy-resolution and time-resolved X-ray spectroscopy identified a possible reaction mechanism for the oxidation of CO over the gold particles in supported gold catalysts. On Au/Al<sub>2</sub>O<sub>3</sub>, there is a reaction channel that has partially oxidized gold as reaction intermediate. Charge transfer from a reduced gold particle to oxygen activates the oxygen molecule. The thermodynamic redox behavior of small gold particles is distinctly different from that of bulk gold, which is inert and unreactive.<sup>[19]</sup> The difference likely originates from the different electronic properties of the small gold particles, which have more d electrons at a different energy to those in bulk gold and which contain a large fraction of corners and edges. Exposure of the activated oxygen to CO

rapidly leads to formation of CO<sub>2</sub> and fully reduced gold. We propose that reduced gold and its ability to transfer charge to oxygen are essential for high catalytic activity in the oxidation of CO.

In situ HERFD X-ray spectroscopy is likely to become a valuable tool in determining the structures of catalysts under catalytically relevant conditions. High-energy-resolution data with time-resolution and the possibility of in situ measurement in combination with mass spectrometry at synchrotrons makes it a promising tool in determining the structures of catalytically active sites.

## Experimental Section

A solution of HAuCl<sub>4</sub> ( $2.1 \times 10^{-3}$  M) was prepared by dissolving the appropriate amount of HAuCl<sub>4</sub>·3H<sub>2</sub>O in deionized water (300 mL). The solution was warmed to 353 K, and 3 g each of support  $\gamma$ -Al<sub>2</sub>O<sub>3</sub> (Condea) and urea (0.21 M) were added. The suspension was kept away from light and stirred during 16 h while maintaining the temperature at 353 K. The suspension was then centrifuged, and the solid was isolated, washed three times with deionized water, and dried under vacuum at room temperature overnight. The fraction of powder containing particles of 90–125  $\mu$ m was separated and introduced into the in situ reactor for X-ray absorption measurements. Transmission electron microscopy showed small gold particles of 1–3 nm.

The experimental setup consists of a reactor, which is a quartz tube with a diameter of 5 mm and a wall thickness of 100  $\mu$ m, and a blower, which was used as a heater. The gas atmosphere in the reactor was controlled by five mass-flow controllers (Bronkhorst). Highly pure He, H<sub>2</sub>, 1% CO in He, and 20% O<sub>2</sub> in He (Air Liquide) were used as the initial gas mixtures. The exhaust of the reactor was connected to a mass spectrometer (Pfeiffer QMS200). After reduction of the catalyst in H<sub>2</sub> at 423 K, the reactor was purged with He and cooled down to room temperature. The catalyst was put in contact with different CO- and O<sub>2</sub>-containing gas mixtures at 298 K. All X-ray spectroscopic measurements were performed in situ under constant flux ( $10 \text{ mL min}^{-1}$ ) of a particular gas atmosphere through the reactor. The studies were performed at the high-brilliance XAFS-XES beamline ID26 at the European Synchrotron Radiation Facility (ESRF) in Grenoble, France. The electron energy was 6.0 GeV, and the ring current varied between 50 and 90 mA. The measurements were performed using the third harmonic of two u35 undulators. The monochromator was equipped with a pair of Si(220) single crystals. Higher harmonics were suppressed by two Cr-coated mirrors operating at 3 mrad relative to the incident beam. The X-ray beam measured 0.3 mm horizontal and 1 mm vertical, with a total flux on the order of  $5 \times 10^{12}$  photon s<sup>-1</sup> on the sample. The energy was calibrated using a gold foil. The high-energy-resolution fluorescence detection was performed using a horizontal-plane Rowland circle spectrometer and an avalanche photodiode (APD, Perkin Elmer) as detector. The spectrometer was tuned to the Au L<sub>α1</sub> (9713 eV) fluorescence line by using the (660) Bragg reflection of one spherically bent Ge wafer with  $R = 1$  m and a diameter of 89 mm. The energy resolution of the spectrometer was 0.6 eV. A Canberra Si photodiode was mounted to measure the total fluorescence yield simultaneously. During XANES scans, the undulators were kept at a fixed gap and only the monochromator angle was changed. To measure fast kinetics, conventional XANES spectra were recorded every 2 s between 11 900 at 11 960 eV with energy steps of 0.5 eV. The statistics were insufficient to perform these measurements in the high-energy-resolution fluorescence detection mode. The XANES spectra in high-resolution mode were measured after the catalyst had reached steady-state conditions. The corresponding spectra were measured during 30 s from 11 880 to 11 980 eV with steps of 0.1 eV and

averaging of 60 scans. Full XAS spectra over a 1000 eV range were also measured under steady-state conditions and used to normalize the XANES data.

Received: March 24, 2006

Published online: June 21, 2006

**Keywords:** gold · oxidation · reaction mechanisms · supported catalysts · X-ray absorption spectroscopy

- [1] a) M. Haruta, T. Kobayashi, T. Sano, N. Yamada, *Chem. Lett.* **1987**, 405; b) M. Valden, X. Lai, D. W. Goodman, *Science* **1998**, *281*, 1647; c) M. S. Chen, D. W. Goodman, *Science* **2004**, *306*, 252; d) P. Landon, J. Ferguson, B. E. Solsona, T. Garcia, A. F. Carley, A. A. Herzing, C. J. Kiely, S. E. Golunski, G. J. Hutchings, *Chem. Commun.* **2005**, 3385.
- [2] J. Breen, R. Burch, J. Gomez-Lopez, A. Ameiro, J. Fisher, D. Thompsott, R. Holliday, D. Thompson, *Proc. Fuel Cell Symposium*, San Antonio, USA, November **2004**.
- [3] M. D. Hughes, Y.-J. Xu, P. Jenkins, P. McMorn, P. Landon, D. I. Enache, A. F. Carley, G. A. Attard, G. J. Hutchings, F. King, E. H. Stitt, P. Johnston, K. Griffin, C. J. Kiely, *Nature* **2005**, *437*, 1131.
- [4] M. M. Schubert, S. Hackenberg, A. C. Van Veen, M. Muhler, V. Plzak, R. J. Behm, *J. Catal.* **2001**, *197*, 113.
- [5] M. Comotti, W.-C. Li, B. Spliethoff, F. Schüth, *J. Am. Chem. Soc.* **2006**, *128*, 917.
- [6] A. C. Gluhoi, N. Bogdanchikova, B. E. Nieuwenhuys, *J. Catal.* **2005**, *229*, 154.
- [7] A. C. Gluhoi, N. Bogdanchikova, B. E. Nieuwenhuys, GOLD2003, Vancouver, September–October **2003**.
- [8] G. C. Bond, D. T. Thompson, *Gold Bull.* **2000**, *33*, 41; C. K. Costello, M. C. Kung, H.-S. Oh, Y. Wang, H. H. Kung, *Appl. Catal. A* **2002**, *232*, 159; J. Guzman, B. C. Gates, *J. Am. Chem. Soc.* **2004**, *126*, 2672; R. J. Davis, *Science* **2003**, *301*, 926.
- [9] B. Yoon, H. Häkkinen, U. Landman, A. S. Wörz, J.-M. Antonietti, S. Abbet, K. Judai, U. Heiz, *Science* **2005**, *307*, 403; H. Häkkinen, S. Abbet, A. Sanchez, U. Heiz, U. Landman, *Angew. Chem.* **2005**, *117*, 1858; *Angew. Chem. Int. Ed.* **2003**, *42*, 1297; .
- [10] L. M. Molina, M. D. Rasmussen, B. Hammer, *J. Chem. Phys.* **2004**, *120*, 7673; Z.-P. Liu, X.-Q. Gong, J. Kohanoff, C. Sanchez, P. Hu, *Phys. Rev. Lett.* **2003**, *91*, 266102.
- [11] I. N. Remediakis, N. Lopez, J. K. Nørskov, *Angew. Chem.* **2005**, *117*, 1858; *Angew. Chem. Int. Ed.* **2005**, *44*, 1824.
- [12] M. Haruta, *Nature* **2005**, *437*, 1098.
- [13] a) M. K. Oudenhuijzen, J. A. van Bokhoven, J. T. Miller, D. E. Ramaker, D. C. Koningsberger, *J. Am. Chem. Soc.* **2005**, *127*, 1530; b) D. E. Ramaker, M. Teliska, Y. Zhang, A. Stakheev, D. C. Koningsberger, *Phys. Chem. Chem. Phys.* **2003**, *5*, 4492; c) D. E. Ramaker, D. C. Koningsberger, *Phys. Rev. Lett.* **2002**, *89*, 139701; d) A. L. Ankudinov, J. J. Rehr, J. J. Low, A. R. Bare, *Phys. Rev. Lett.* **2002**, *89*, 139702; e) N. Weiher, E. Bus, L. Delannoy, C. Louis, D. E. Ramaker, J. A. van Bokhoven, *J. Catal.* **2006**, *240*, 100.
- [14] P. Glatzel, U. Bergmann, *Coord. Chem. Rev.* **2005**, *249*, 65.
- [15] a) K. Hämäläinen, D. P. Siddons, J. B. Hastings, L. E. Berman, *Phys. Rev. Lett.* **1991**, *67*, 2850; b) F. M. F. de Groot, K. H. Krish, J. Vogel, *Phys. Rev. B* **2002**, *66*, 195112; c) F. M. F. de Groot, *Coord. Chem. Rev.* **2005**, *249*, 31.
- [16] J. T. Miller, A. J. Kropf, Y. Zha, J. R. Regalbuto, L. Delannoy, C. Louis, E. Bus, J. A. van Bokhoven, *J. Catal.* **2006**, *240*, 222.
- [17] C. Winkler, A. J. Carew, S. Haq, R. Raval, *Langmuir* **2003**, *19*, 717.
- [18] C. K. Costello, J. Guzman, J. H. Yang, Y. M. Wang, M. C. Kung, B. C. Gates, H. H. Kung, *J. Phys. Chem. B* **2004**, *108*, 12529.
- [19] B. Hammer, J. K. Nørskov, *Nature* **1995**, *376*, 238.



# Hollow and Tin-Filled Nanotubes of Single-Crystalline $\text{In}(\text{OH})_3$ Grown by a Solution–Liquid–Solid–Solid Route\*\*

Yueping Fang, Xiaogang Wen, and Shihe Yang\*

A variety of methods have been employed in recent years to produce nanowires and nanorods of metals/semiconductors with heterostructures such as coaxial core–shell<sup>[1]</sup> and composite<sup>[2]</sup> nanostructures, which appear promising for the nanoscale manipulation of particles/quasi-particles such as electrons and photons. However, these methods often involve tedious procedures, harsh conditions, or expensive instrumentation. For example, multi-step depositions involving sequential charging of desired source materials<sup>[3]</sup> or surface modification by ambient species<sup>[4]</sup> are necessary for the preparation of coaxial core–shell nanowires. Herein, we demonstrate an extension of the solution–liquid–solid (SLS) method for the first synthesis of Sn-filled  $\text{In}(\text{OH})_3$  nanotubes in what is essentially a one-step solution–liquid–solid–solid (SLSS) growth process.

The solution–liquid–solid (SLS) growth of nanowires was first reported by Buhro and co-workers, who used nanoparticles of a low melting point metal (e.g., In and Ga, etc.) in an organic solution to induce the growth of GaAs nanowires with a narrow diameter distribution.<sup>[5]</sup> In a related work, Korgel et al. successfully synthesized carbon nanotubes and defect-free Si nanowires by SLS growth in supercritical fluids.<sup>[6]</sup> However, the SLS method has not been used for the growth of inorganic nanotubes up till now. We are able to assemble Sn-filled  $\text{In}(\text{OH})_3$  nanotubes using liquid droplets of an In–Sn mixture, which serves as both catalyst and reagents for the nanotube growth, from an ethanol-containing aqueous solution under an oxidative atmosphere.

Indium hydroxide is a rather interesting material due to its special semiconducting and optical properties. Ishida and Kuwabara,<sup>[7]</sup> for example, have shown that the conductivity of  $\text{In}(\text{OH})_3$  thin-films varies from  $10^{-7}$  to  $10^{-3} \text{ Scm}^{-2}$  depending on the experimental conditions, which is typical for a wide-bandgap semiconductor, and the optical bandgap,  $E_g$ , of needle-like nanoparticles of indium hydroxide has been estimated to be 5.15 eV by diffuse reflectance spectroscopy

(DRS) using the Kubelka–Munk (KM) technique.<sup>[8]</sup> Although nanowires of  $\text{In}(\text{OH})_3$  have been reported recently,<sup>[9]</sup> currently available approaches have been unable to produce  $\text{In}(\text{OH})_3$  nanotubes or their heterostructural derivatives or analogues.

An SEM image of the as-collected product is shown in Figure 1 A. Numerous rod-like nanostructures are formed in

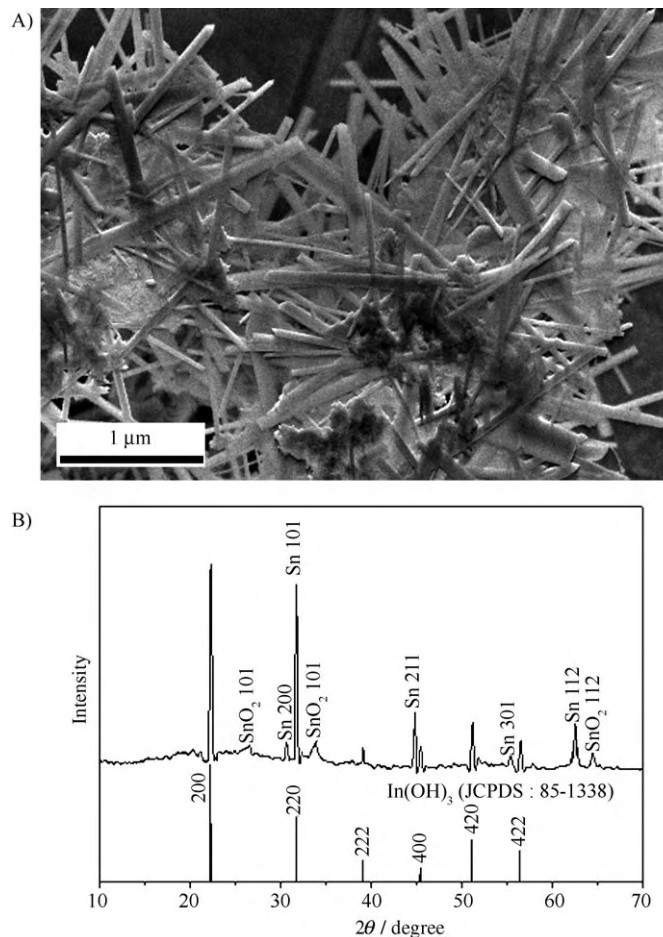


**Figure 1.** A) SEM image and B) XRD pattern of the as-collected product.

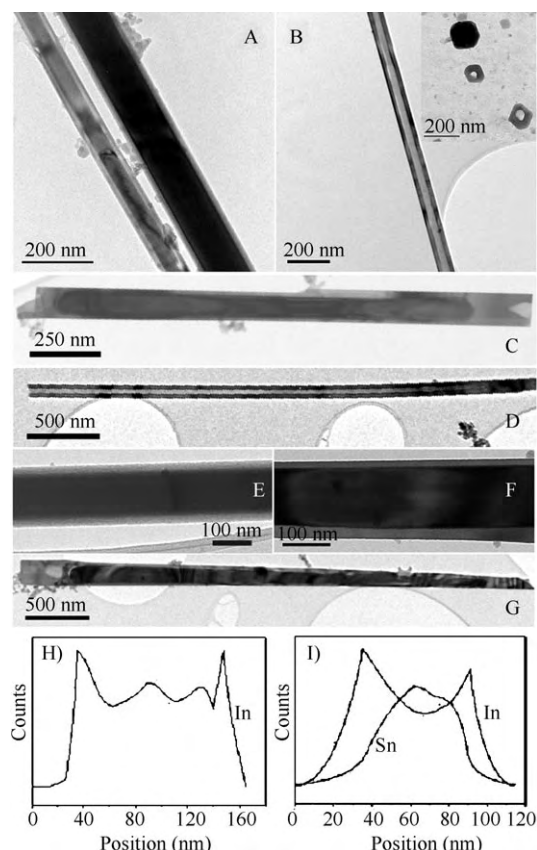
high yield (>80%), most of which are straight and have diameters of 70–250 nm and lengths of 2–5 μm. The XRD pattern in Figure 1 B provides clear evidence that the product nanostructures are composed of two crystalline phases, namely body-centered cubic (bcc)  $\text{In}(\text{OH})_3$  (JCPDS: 85-1338;  $a = 7.979 \text{ Å}$ ) and tetragonal Sn (JCPDS: 86-2265;  $a = 5.831$  and  $c = 3.181 \text{ Å}$ ). Several characteristic peaks from impurities of tetragonal  $\text{SnO}_2$  are also detected in the XRD pattern, probably because of oxidation of Sn outside the nanotubes.

Figure 2 reveals more details about the nanostructures of the products, which are primarily Sn-filled  $\text{In}(\text{OH})_3$  nanotubes (Figure 2 A) along with a few empty  $\text{In}(\text{OH})_3$  nanotubes (Figure 2 B). The cross-sections of the nanotubes appear faceted (inset of B), and most filled nanotubes have uniform diameters and wall thicknesses throughout their whole

[\*] Dr. Y. Fang, X. Wen, Prof. Dr. S. Yang  
Department of Chemistry  
The Hong Kong University of Science and Technology  
Clear Water Bay, Kowloon, Hong Kong (China)  
Fax: (+852) 2358-1594  
E-mail: chsyang@ust.hk

[\*\*] We are grateful to the Hong Kong University of Science and Technology for financial support under the grant HIA05/06.SC02. S.Y. also wishes to thank the Hong Kong Young Scholar Cooperation Research Foundation of NSFC.

Supporting Information for this article is available on the WWW under <http://www.angewandte.org> or from the author.



**Figure 2.** TEM characterizations of empty and filled nanotubes: A) two filled nanotubes; B) an empty nanotube and cross-sections of nanotubes (inset); C) a nanotube with two ends closed; D) a nanotube with one end open; E) a filled nanotube with walls of equal thickness; F) a filled nanotube with walls of unequal thickness; G) a filled nanotube whose diameter gradually decreases along the tube length; H) and I) line-scan EDS elemental profiles recorded for an empty nanotube and for a filled nanotube, respectively.

lengths (Figure 2A). It is interesting to note that the filled nanotubes are more abundant (about 80%) and always have their two ends closed (Figure 2C), whereas the empty nanotubes account for only around 20% of the tubes and have at least one of the ends open (Figure 2D). The TEM images show both symmetrical (Figure 2E) and lopsided (Figure 2F) thicknesses of the two side-walls of the filled nanotubes. This is consistent with the fact that the  $\text{In}(\text{OH})_3$  nanotubes are faceted and thus not cylindrically symmetric. A handful of filled nanotubes whose diameters and wall thicknesses gradually decrease along their lengths, for example from about 220 and 50 nm at the thicker end to about 80 and 20 nm at the thinner end (Figure 2G), are also observed. X-ray energy-dispersive spectroscopy (EDS) of the empty nanotubes gives an elemental ratio of In to O of about 1:3, whereas that of the filled nanotubes contain Sn as well as In and O ( $\text{In}:\text{O}:\text{Sn} \approx 19:57:24$ ). The empty nanotubes are made up of  $\text{In}(\text{OH})_3$ , whereas the filled nanotubes consist of walls of  $\text{In}(\text{OH})_3$  and interiors filled with Sn. This was corroborated by line-scan EDS elemental profiles. One example is for an empty  $\text{In}(\text{OH})_3$  nanotube with a diameter of 140 nm and a wall thickness of about 30 nm (Figure 2H), and the other is

for an  $\text{In}(\text{OH})_3$  shell about 10–20 nm thick with a filling of Sn about 70 nm across (Figure 2I).

The nanotube structures were further examined by recording high-resolution TEM images and electron diffraction patterns, as shown in Figure 3. One can immediately see

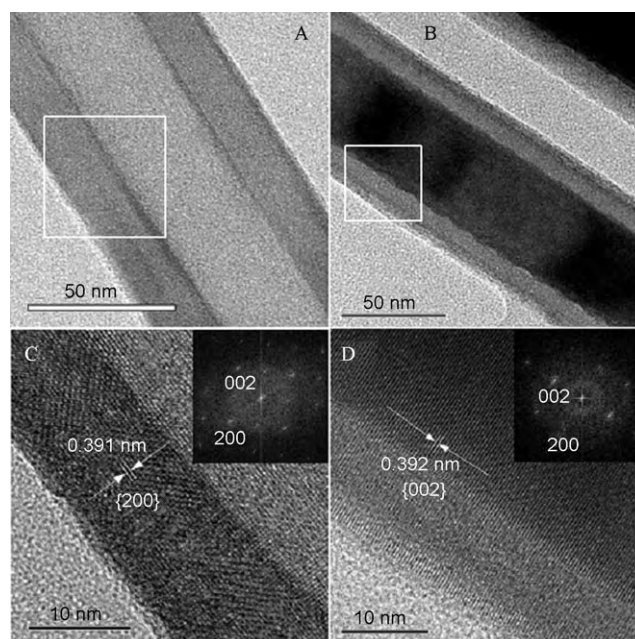


**Figure 3.** HRTEM images and the corresponding FFT patterns (insets) of an empty  $\text{In}(\text{OH})_3$  nanotube (A and C) and a Sn-filled  $\text{In}(\text{OH})_3$  nanotube (B and D). C and D are taken from the squares in A and B, respectively.

the uniform, well-defined single-crystalline structure of the  $\text{In}(\text{OH})_3$  nanotubes both without (Figure 3A) and with the Sn filling (Figure 3B). The HRTEM image in Figure 3C, taken for the area marked by a square in Figure 3A, shows clear lattice fringes for the (200) planes parallel to the tube axis, with a  $d$  spacing of 0.391 nm. The fast Fourier transform (FFT) pattern (inset in Figure 3C) can be indexed to bcc  $\text{In}(\text{OH})_3$  and the nanotubes grow along the  $a$ ,  $b$ , or  $c$  axes of the  $\text{In}(\text{OH})_3$  crystal. A similar HRTEM image, taken from the area highlighted by the square in Figure 3B, is given in Figure 3D for a Sn-filled  $\text{In}(\text{OH})_3$  nanotube. Clear fringes perpendicular to the nanotube axis can be seen here as well. These fringes have an interplanar spacing of 0.392 nm, in accordance with the distance between the (002) crystal planes of  $\text{In}(\text{OH})_3$ , which suggests the same growth direction as for the empty nanotubes. This observation is also mirrored in the FFT pattern (inset of Figure 3D) of this HRTEM image.

During TEM observations, we found that electron-beam irradiation in the microscope could induce fluidic movement of the Sn filling in the  $\text{In}(\text{OH})_3$  nanotubes. Figure 4 shows consecutive TEM images recorded during electron-beam irradiation of the imaged portion of the nanotube. Upward movement of the molten Sn core (by about 60 nm) inside the nanotube is vividly portrayed as a wavy form, which means that the Sn filling undergoes a melting phase transition upon electron-beam irradiation. It appears that part of the driving

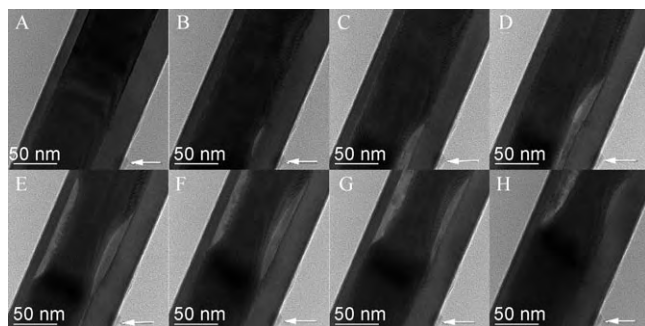
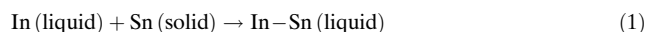


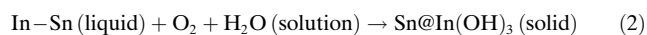
**Figure 4.** Consecutive TEM images (A to H) taken during electron-beam irradiation of the imaged portion of the nanotube. The arrows point to the same overhanging feature of the nanotube and indicate that the molten Sn moves upward.

force for the movement of the molten Sn core is its thermal expansion and non-wetting contact with the  $\text{In}(\text{OH})_3$  nanotube at the low base pressure of the TEM chamber. With better control, this effect could be developed into a nanoscale thermometer. A similar phenomenon has been observed previously for nanotube-encapsulated metals under electron-beam irradiation.<sup>[10]</sup> A significant melting point depression has also been observed for Ge semiconductor nanowires confined in carbon nanotubes, which could be the case for our Sn-filled  $\text{In}(\text{OH})_3$  nanotubes as well.<sup>[11]</sup> It is envisaged that the electron irradiation method may be a useful tool for tailoring the metal filling inside the nanotubes. For example, one could divide the metallic core into uniform nanoparticles to form a 1D array with controlled inter-particle spacings.

In order to shed light on the growth mechanism of the heterostructured  $\text{Sn}@\text{In}(\text{OH})_3$  nanowires, we resort to the binary phase-diagram of In and Sn shown in Figure 5 A. Since the melting points,  $T$ , of In and Sn are 156.6 and 231.86°C, respectively, Sn is expected to dissolve slowly in the molten In to form In–Sn liquid droplets (Figure 5 A) at 180°C with less than 65% Sn (point X), above which solid Sn starts to precipitate [see Eq. (1)].



As the reduction potential of In is more negative (ca. –1.00 V) than that of Sn (ca. –0.91 V) in weakly basic solution,<sup>[12]</sup> In is preferentially oxidized to  $\text{Sn}@\text{In}(\text{OH})_3$  (solid) in the form of a core–shell nanostructure by the oxygen in solution [Eq. (2)].



A critical step in the nanotube formation is the initial elongation. This is achieved by the right combination of materials. Specifically, the nucleation of solid  $\text{In}(\text{OH})_3$  is accompanied by the deposition of solid Sn, both of which are necessarily in contact with the In–Sn droplet during growth so as to ensure a lowest energy path. This is only possible in a tube geometry, as illustrated in Figure 5 B. Note that the reaction/deposition takes place on the surface of the In–Sn droplet to form an  $\text{In}(\text{OH})_3$  shell surrounding a solid Sn rod. After the liquid droplet has been consumed, assembly of the

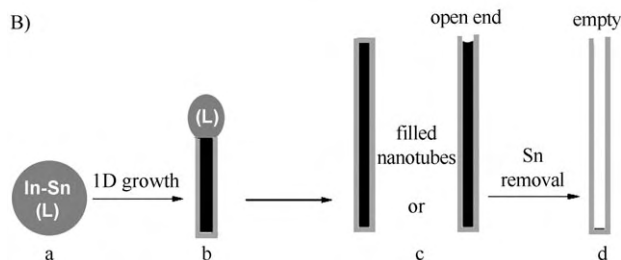
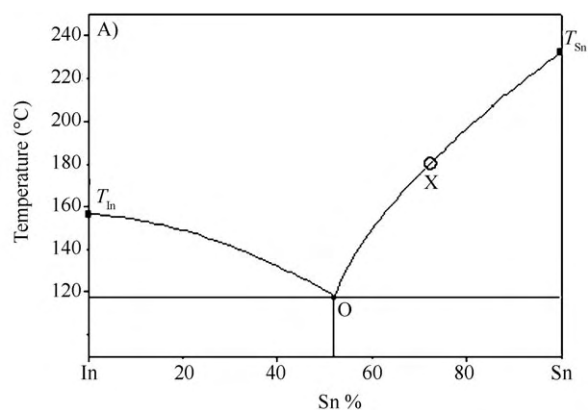


**Figure 5.** A) Binary phase diagram of In–Sn. B) Illustration of the growth process of Sn-filled  $\text{In}(\text{OH})_3$  nanotubes and the formation of empty  $\text{In}(\text{OH})_3$  nanotubes. The molten In reacts with solid Sn to form In–Sn liquid droplets (a). The reaction in Equation (2) then takes place on the surface of these liquid In–Sn droplets to form solid  $\text{In}(\text{OH})_3$ , which is accompanied by the deposition of solid Sn. This leads to the elongation of a solid  $\text{Sn}@\text{In}(\text{OH})_3$  core/shell nanostructure (b). Finally, continuous 1D growth consumes the liquid droplet, thereby completing the SLSS assembly of the  $\text{Sn}@\text{In}(\text{OH})_3$  core/shell nanostructure (c). The empty  $\text{In}(\text{OH})_3$  nanotubes may be formed by dissolution of the Sn core of the  $\text{Sn}@\text{In}(\text{OH})_3$  nanotubes, which have at least one end open, in weakly basic aqueous ethanol solution (d).

Sn-filled  $\text{In}(\text{OH})_3$  nanotube is completed either with the top end closed or open depending on the availability of the necessary shell materials. Empty  $\text{In}(\text{OH})_3$  nanotubes may arise from dissolution of the Sn cores of the  $\text{Sn}@\text{In}(\text{OH})_3$  nanotubes with at least one end open in the weakly basic aqueous ethanol solution. This is in excellent agreement with the observation that the filled nanotubes always have their two ends closed, whereas the empty nanotubes have at least one of the ends open. We coin this unique 1D core–shell growth mode a solution–liquid–solid–solid (SLSS) process (see Figure 5 B for details). This is an interesting extension of the SLS method with the difference of employing an alloy droplet and an additional solid deposition process to form the 1D core–shell nanostructure.

Control experiments have shown that the  $\text{Sn}@\text{In}(\text{OH})_3$  nanotubes can only be formed with the right combination of materials and reaction conditions. The aqueous ethanol solution provides the weakly basic environment necessary for the smooth precipitation of  $\text{In}(\text{OH})_3$ , deposition of Sn, and the subsequent 1D growth guided by the In–Sn droplets. A solution that is either too acidic or too basic would be apt to dissolve the deposited  $\text{In}(\text{OH})_3$  shell, which would eventually



halt the 1D growth (see Supporting Information). We also found that a solution of urea results in the formation of a dandelion-like architecture made up from a single layer of radially oriented  $\text{In}(\text{OH})_3$  nanorods surrounding a Sn core (see Supporting Information). We have therefore established some of the materials and environmental requirements for the 1D growth of the core-shell nanostructure.

To conclude, a one-step SLSS growth mode has been discovered that allows the first synthesis of empty single-crystalline  $\text{In}(\text{OH})_3$  nanotubes as well as nanotubes filled with Sn. The shells of the nanotubes have a cubic structure and grow along the  $a$ ,  $b$ , or  $c$  axes of the  $\text{In}(\text{OH})_3$  crystal. It might be possible to convert the  $\text{In}(\text{OH})_3$  nanostructures into nanostructures of  $\text{In}_2\text{O}_3$  which is a more common semiconductor, by annealing at elevated temperatures. The 1D SLSS growth mode is distinguished from the SLS method by the presence of an alloy droplet, on which reaction and deposition occur to form a solid shell and a solid core at the same time. A nanofluidic flow of the internal Sn has been observed when the environmental temperature is increased by electron-beam irradiation. This property could be exploited to engineer desired nanostructures inside the nanotubes. Our work suggests a new, general working mechanism for the growth of heterostructured core-shell nanowires by a simple solution procedure. With a judicious choice of alloy droplet and reaction and process conditions, one should be able to fabricate nanotubes with different compositions, sizes, morphologies, and heterostructures.

### Experimental Section

The synthesis was carried out by lapping a piece of indium foil ( $7 \times 7 \times 0.25 \text{ mm}^3$ , 99.9%, Aldrich) with a piece of Sn foil ( $10 \times 10 \times 0.25 \text{ mm}^3$ , 99.9%, Aldrich) with a gentle press and placing the two at the bottom of a Teflon-lined stainless steel autoclave (25 mL) containing a solution of 0.5 M NaOH (0.5 mL), ethanol (10 mL), and distilled water (10 mL). The foils were carefully washed with ethanol before loading. The solution was heated to  $180^\circ\text{C}$  and kept at this temperature for 30 h to give a gray powder and a chunk of incompletely reacted Sn foil. This was discarded and the gray powder was rinsed with ethanol and dried in air for characterizations. The structures were determined by powder X-ray diffraction (XRD, Philips PW-1830 X-ray diffractometer with  $\text{Cu}_{K\alpha}$  irradiation,  $\lambda = 1.5406 \text{ \AA}$ , at a scan speed of  $0.025 \text{ deg s}^{-1}$  over the  $2\theta$  range  $10\text{--}70^\circ$ ). Morphologies were examined by scanning electron microscopy characterizations (SEM, JEOL 6300 and JEOL 6700F at an accelerating voltage of 15 kV). TEM observations were carried out with a JEOL 2010F microscope operating at an accelerating voltage of 200 kV. For both SEM and TEM characterizations the powder sample was dispersed in ethanol—the powder samples were embedded in epoxy resin and ultramicrotomed to obtain a cross-sectional view—and the suspension sonicated for 20 min. A drop of the suspension was then placed onto a silicon substrate or a copper grid coated with a holey carbon film and the solvent allowed to evaporate in air.

Received: March 15, 2006

Published online: June 22, 2006

**Keywords:** crystal growth · indium · nanotubes · semiconductors · tin

- [1] a) L. J. Lauhon, M. S. Gudiksen, D. Wang, C. M. Lieber, *Nature* **2002**, 420, 57; b) J. Q. Hu, Q. Li, X. M. Meng, C. S. Lee, S. T. Lee, *Chem. Mater.* **2003**, 15, 305; c) W. Han, A. Zettl, *Adv. Mater.* **2002**, 14, 1560; d) J. Hu, Y. Bando, Z. Liu, *Adv. Mater.* **2003**, 15, 1000; e) Y. B. Li, Y. Bando, D. Golberg, *Adv. Mater.* **2003**, 15, 581; f) Y. H. Gao, Y. Bando, *Nature* **2002**, 415, 599.
- [2] a) J. J. Wu, T. C. Wong, C. C. Yu, *Adv. Mater.* **2002**, 14, 1643; b) K. K. Lew, L. Pan, E. C. Dickey, J. M. Redwing, *Adv. Mater.* **2003**, 15, 2073.
- [3] a) Y. Xie, P. Yan, J. Lu, Y. Qian, S. Zhang, *Chem. Commun.* **1999**, 1969; b) Y. G. Guo, L. J. Wan, C. L. Bai, *J. Phys. Chem. B* **2003**, 107, 5441; c) J. Cao, J. Z. Sun, J. Hong, H. Y. Li, H. Z. Chen, M. Wang, *Adv. Mater.* **2004**, 16, 84.
- [4] a) A. M. Morales, C. M. Lieber, *Science* **1998**, 279, 208; b) H. M. Lin, Y. L. Chen, J. Yang, Y. C. Liu, K. M. Yin, J. J. Kai, F. R. Chen, L. C. Chen, Y. F. Chen, C. C. Chen, *Nano Lett.* **2003**, 3, 537; c) A. Kolmakov, Y. Zhang, M. Moskovits, *Nano Lett.* **2003**, 3, 1125.
- [5] a) T. J. Trentler, K. M. Hickman, S. C. Goel, A. M. Viano, P. C. Gibbons, W. E. Buhro, *Science* **1995**, 270, 1791; b) H. Yu, W. E. Buhro, *Adv. Mater.* **2003**, 15, 416; c) H. Yu, J. B. Li, R. A. Loomis, L. W. Wang, W. E. Buhro, *Nat. Mater.* **2003**, 2, 517.
- [6] a) D. C. Lee, F. V. Mikulec, B. A. Korgel, *J. Am. Chem. Soc.* **2004**, 126, 4951; b) D. C. Lee, B. A. Korgel, *Mol. Simul.* **2005**, 31, 637; c) J. D. Holmes, K. P. Johnston, R. C. Doty, B. A. Korgel, *Science* **2000**, 287, 1471; d) T. Hanrath, B. A. Korgel, *J. Am. Chem. Soc.* **2002**, 124, 1424; e) X. M. Lu, T. K. Hanrath, P. Johnston, B. A. Korgel, *Nano Lett.* **2003**, 3, 93.
- [7] T. Ishida, K. Kuwabara, *J. Ceram. Soc. Jpn.* **1998**, 106, 381.
- [8] S. Avivi, Y. Mastai, A. Gedanken, *Chem. Mater.* **2000**, 12, 1229.
- [9] a) H. L. Zhu, K. H. Yao, Y. H. Wo, N. Y. Wang, L. N. Wang, *Semicond. Sci. Technol.* **2004**, 19, 1020; b) X. H. Zhang, S. Y. Xie, Z. M. Ni, X. Zhang, Z. Y. Jiang, Z. X. Xie, R. B. Huang, L. S. Zheng, *Inorg. Chem. Commun.* **2003**, 6, 1445; c) D. B. Yu, S. H. Yu, S. Y. Zhang, J. Zuo, D. B. Wang, Y. T. Qian, *Adv. Funct. Mater.* **2003**, 13, 497.
- [10] a) W. K. Hsu, M. Terrones, H. Terrones, N. Grobert, A. I. Kirkland, J. P. Hare, K. Prassides, P. D. Townsend, H. W. Kroto, D. R. M. Walton, *Chem. Phys. Lett.* **1998**, 284, 177; b) J. Q. Hu, Y. Bando, J. H. Zhan, D. Golberg, *Angew. Chem.* **2004**, 116, 4706; *Angew. Chem. Int. Ed.* **2004**, 43, 4606.
- [11] Y. Y. Wu, P. D. Yang, *Adv. Mater.* **2003**, 15, 520.
- [12] a) *Inorganic Chemistry*, 3rd ed. (Eds.: X. Z. Cao, T. Y. Song, X. Q. Wang), Higher Education, Beijing, China, **2005**; b) *Lange's Handbook of Chemistry*, 15th ed. (Ed.: J. A. Dean), McGraw-Hill, New York, **1999**.



# A Nonanuclear Dysprosium(III)–Copper(II) Complex Exhibiting Single-Molecule Magnet Behavior with Very Slow Zero-Field Relaxation\*\*

Christophe Aronica, Guillaume Pilet,  
Guillaume Chastanet, Wolfgang Wernsdorfer,  
Jean-François Jacquot, and Dominique Luneau\*

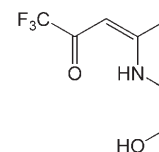
The discovery that some metal coordination clusters may behave as single-molecule magnets (SMMs)<sup>[1–4]</sup> is currently stimulating abundant research in relation to potential applications in information processing and storage.<sup>[5]</sup> Indeed, SMMs are molecules that can be magnetized in a magnetic field and retain the magnetization when it is switched off. As a consequence, they may show hysteresis loops reminiscent of magnets.<sup>[2]</sup> In metal clusters, such behavior results from a strong magnetic ground state with large negative axial anisotropy ( $D < 0$ )<sup>[6,7]</sup> and induces two possible orientations (up and down), between which the magnetization can fluctuate. The fluctuation rate, also named relaxation, depends on the energy barrier  $U$  that separates the orientations. In the case of an ideal ground spin state  $S$  well separated from the excited states,  $U$  is equal to  $-DS^2$  for an integer spin and  $-D(S^2 - 1/4)$  for a half-integer spin ( $D < 0$ ). Therefore, the larger the  $D$  and  $S$  values are, the higher the barrier is and the longer the magnetization is retained. This barrier can be thermally overcome or shortcut by quantum tunneling of magnetization (QTM).<sup>[8]</sup> This tunneling through the barrier contributes to accelerating the overall relaxation process. In practice, coexistence of the two processes leads to an experimental effective barrier  $U_{\text{eff}}$  defined by an Arrhenius law:  $\tau = \tau_0 \exp(U_{\text{eff}}/kT)$ .<sup>[9]</sup> One of the main goals of current research is to achieve long relaxation times  $\tau$ , which are crucial for information storage applications.<sup>[10,11]</sup>

In this context, the use of lanthanide ions, such as Dy<sup>III</sup> and Tb<sup>III</sup>, has many advantages. Indeed, their large spins and pronounced spin–orbit coupling result in strong Ising-type magnetic anisotropy.<sup>[12]</sup> Recent reports have shown that even some of their mononuclear complexes may behave as SMMs.<sup>[13,14]</sup> During this work, a Dy<sup>III</sup><sub>3</sub> trinuclear cluster was also reported to exhibit slow relaxation despite its near diamagnetic ground state.<sup>[15]</sup> Moreover, the combination of 3d and 4f transition-metal ions may increase the ground spin state through d–f magnetic interactions.<sup>[16–20]</sup> Lanthanides have high coordination numbers and geometries, which may be useful for engineering large polynuclear clusters, and their potential optical properties are of interest to prospective multifunctional materials.<sup>[21,22]</sup>

With this in mind, and as part of our work on polynuclear metal complexes,<sup>[23,24]</sup> we chose the Schiff base 1,1,1-trifluoro-7-hydroxy-4-methyl-5-azahept-3-en-2-one (LH<sub>2</sub>, Scheme 1). Such Schiff bases are known to give cubane-like clusters with Cu<sup>II</sup> ions.<sup>[25,26]</sup> By using a mixture of copper(II) and lanthanide(III) ions, we succeeded in synthesizing a family of heterobimetallic nonanuclear clusters [Ln<sup>III</sup><sub>3</sub>Cu<sup>II</sup><sub>6</sub>] for most lanthanide ions. Herein, we report the synthesis, crystal structure, and magnetic properties of the nonanuclear Dy<sup>III</sup>Cu<sup>II</sup> compound [Dy<sup>III</sup><sub>3</sub>Cu<sup>II</sup><sub>6</sub>L<sub>6</sub>(μ<sub>3</sub>-OH)<sub>6</sub>(H<sub>2</sub>O)<sub>10</sub>]Cl<sub>2</sub>·ClO<sub>4</sub>·3.5 H<sub>2</sub>O ([Dy<sub>3</sub>Cu<sub>6</sub>]), which exhibits SMM behavior.

The crystal structure of [Dy<sub>3</sub>Cu<sub>6</sub>] consists of cationic entities [Dy<sup>III</sup><sub>3</sub>Cu<sup>II</sup><sub>6</sub>L<sub>6</sub>(μ<sub>3</sub>-OH)<sub>6</sub>(μ<sub>1</sub>-H<sub>2</sub>O)<sub>10</sub>]<sup>3+</sup> (Figure 1a), uncoordinated chloride and perchlorate anions for charge balance, and water molecules of crystallization. The cationic cluster [Dy<sup>III</sup><sub>3</sub>Cu<sup>II</sup><sub>6</sub>L<sub>6</sub>(μ<sub>3</sub>-OH)<sub>6</sub>(H<sub>2</sub>O)<sub>10</sub>]<sup>3+</sup> (Figure 1a) is built from three Dy<sup>III</sup> ions arranged in a triangular fashion with {Cu<sup>II</sup><sub>2</sub>L<sup>2-</sup><sub>2</sub>} dimer units on each edge of the triangle (Figure 1b,c). Six alkoxo oxygen atoms of the deprotonated ligands L<sup>2-</sup> and six OH groups bridge the different metal ions in a μ<sub>3</sub> fashion (Figure 1c). The six OH groups connect the Dy<sup>III</sup> ions within the triangular framework {Dy<sup>III</sup><sub>3</sub>(OH)<sub>6</sub>} and with the Cu<sup>II</sup> ions of adjacent {Cu<sup>II</sup><sub>2</sub>L<sup>2-</sup><sub>2</sub>} dimer units. One alkoxo bridge connects the Cu<sup>II</sup> ions within the {Cu<sup>II</sup><sub>2</sub>L<sup>2-</sup><sub>2</sub>} dimer units and the second bridge with adjacent Dy<sup>III</sup> ions (Figure 1b). This behavior affords distorted {Cu<sub>2</sub>L<sub>2</sub>Dy<sub>2</sub>(OH)<sub>2</sub>} cubane-like moieties in a similar way to homometallic cubane-like compounds.<sup>[25,26]</sup> The cationic entity can also be described as resulting from condensation of three distorted {Dy<sub>2</sub>Cu<sub>2</sub>O<sub>4</sub>} cubane-like moieties that share the Dy<sup>III</sup> ions in a triangular fashion. The structural features of the {Cu<sub>2</sub>L<sub>2</sub>Dy<sub>2</sub>(OH)<sub>2</sub>} moieties (Figure 1c) are reminiscent of those reported for a [Dy<sub>2</sub>Cu<sub>2</sub>] complex, but in our case the Cu<sup>II</sup> moieties form dimers.<sup>[27]</sup> The {Dy<sub>2</sub>Cu<sub>2</sub>O<sub>4</sub>} cubane-like moieties have small (av.: 3.4 Å) and large (av.: 3.7 Å) Dy...Cu distances. The cationic entities are well isolated from each other, as no relevant hydrogen bonds were found between them.

The three Dy<sup>III</sup> ions have the same eight-coordinate environment formed by the oxygen atoms of two coordinated water molecules, four bridging OH groups, and two bridging alkoxo groups of the ligand L<sup>2-</sup>. The Dy<sup>III</sup>–O bond lengths



**Scheme 1.** Schiff base LH<sub>2</sub>.

[\*] C. Aronica, Dr. G. Pilet, Dr. G. Chastanet, Prof. D. Luneau  
Université Claude Bernard Lyon-1  
Laboratoire des Matériaux et Interfaces (UMR 5615)  
Campus de La Doua, 69622 Villeurbanne Cedex (France)  
Fax: (+33) 472-431-160  
E-mail: luneau@univ-lyon1.fr  
Dr. W. Wernsdorfer  
Laboratoire Louis Néel, CNRS-BP 166  
25 Avenue des Martyrs, 38042 Grenoble, Cedex 9 (France)  
J.-F. Jacquot  
CEA-Grenoble, DRFMC, Service de Chimie Inorganique et Biologique  
17 rue des Martyrs, 38054 Grenoble, Cedex 9 (France)

[\*\*] Supports from the “Région Rhône-Alpes”, Network of excellence MAGMANet (FP6-NMP3-CT-2005-515767-2) and “Commissariat à l’Energie Atomique” (LRC N° DSM-03-31) are gratefully acknowledged.

Supporting information for this article is available on the WWW under <http://www.angewandte.org> or from the author.

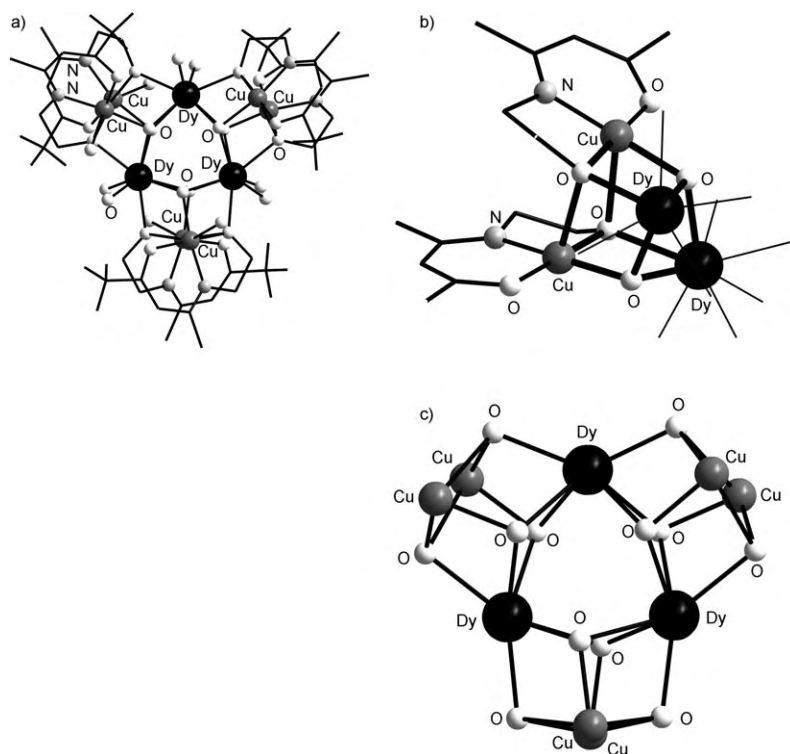


**Figure 1.** Structure of the cation  $[\text{Dy}^{\text{III}}_3\text{Cu}^{\text{II}}_6(\mu_3\text{-OH})_6(\text{H}_2\text{O})_{10}]^{3+}$  (a) with fragments showing the  $\{\text{Cu}_2\text{L}_2\text{Dy}_2(\text{OH})_2\}$  cubane-like moieties (b) and the alkoxo/hydroxo-bridged metal framework  $\{\text{Cu}_6\text{Dy}_3\text{O}_{12}\}$  (c). Selected distances [Å]: Dy...Dy 3.7885(6), 3.8165(5), 3.8201(6); Dy...Cu 3.390(1), 3.401(1), 3.624(1), 3.685(1), 3.399(1), 3.410(1), 3.676(1), 3.703(1), 3.389(1), 3.401(1), 3.632(1), 3.646(1); Cu...Cu 3.195(2), 3.138(2), 3.150(2).

(2.287(6)–2.45(6) Å, av.: 2.38 Å) are normal and in good agreement with calculated values.<sup>[28]</sup> Within the triangular framework  $\{\text{Dy}^{\text{III}}_3(\text{OH})_6\}$  the Dy<sup>III</sup>...Dy<sup>III</sup> distances are in the range 3.7885(6)–3.8201(6) Å.

The six Cu<sup>II</sup> ions all have the same basic five-coordinate environment. The basal plane is made up of two oxygen atoms and one nitrogen atom from the ligand  $\text{L}^{2-}$  plus one oxygen atom of an hydroxo group with Cu–O and Cu–N bond lengths of 1.905(7)–1.989(6) and 1.942(8)–1.954(8) Å, respectively. The axial position is occupied by an oxygen atom from the bridging alkoxo group belonging to the second  $\{\text{Cu}^{\text{II}}\text{L}^{2-}\}$  moiety of the  $\{\text{Cu}^{\text{II}}_2\text{L}^{2-}_2\}$  dimer. As is generally found in cubane-like compounds,<sup>[25,26,29]</sup> this axial Cu–O(alkoxo) bond is long (2.505(8)–2.748(7) Å) and the Cu–O(alkoxo)–Cu bond angles are close to orthogonality (82.6–90.5(3)°). Moreover, among the six Cu<sup>II</sup> ions, four have an additional coordinated water molecule in the sixth position with a long bond (2.84(2)–2.579(8) Å) to form an elongated octahedron. No such sixth ligand was found for two of the Cu<sup>II</sup> ions, and coordination of perchlorate or chloride anions to the two other Cu<sup>II</sup> ions is excluded, as the smallest Cu...O<sub>4</sub>Cl and Cu...Cl distances are 5.490 and 5.233 Å, respectively. Within the three  $\{\text{Cu}_2^{\text{II}}\text{L}^{2-}_2\}$  dimer units (Figure 1b), the Cu...Cu distances are in the range 3.138(2)–3.195(2) Å.

The temperature dependence of the magnetic susceptibility was measured on a polycrystalline sample in the temperature range 2–300 K at 1 kOe (Figure 2). At 300 K,

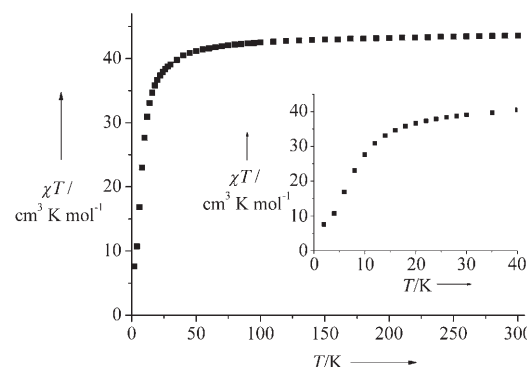


**Figure 2.** Temperature dependence of  $\chi T$  for  $[\text{Dy}_3\text{Cu}_6]$ . The inset shows the low-temperature behavior.

the  $\chi T$  value of  $43.56 \text{ cm}^3 \text{ K mol}^{-1}$  is close to that of  $44.75 \text{ cm}^3 \text{ K mol}^{-1}$  expected for six Cu<sup>II</sup> ( $2.25 \text{ cm}^3 \text{ K mol}^{-1}$ ) plus three Dy<sup>III</sup> ions ( $42.5 \text{ cm}^3 \text{ K mol}^{-1}$ ) in a  $\text{H}_{15/2}$  ground state ( $J = 15/2$ ,  $g = 4/3$ ). On cooling,  $\chi T$  decreases slowly down to 50 K and then drops sharply to reach  $7.57 \text{ cm}^3 \text{ K mol}^{-1}$  at 2 K, at which it shows an inflection. This behavior is ascribed to the effect of the exchange interactions between the metal ions (Cu...Cu, Cu...Dy, and Dy...Dy) combined with the crystal-field effect, which is important for Dy<sup>III</sup>. At present, it is not possible to quantify the different contributions, but the field effect is expected to be dominant. The Cu...Cu exchange should be zero or weakly ferromagnetic. Indeed, considering the structural features (see above) the Cu–O(alkoxo)–Cu bridges within the  $\{\text{Cu}_2^{\text{II}}\text{L}_2\}$  dimer units should not favor strong overlap<sup>[30]</sup> and, in agreement with homometallic Cu<sup>II</sup> cubane-like compounds, this should give weak ferromagnetic coupling.<sup>[25,26,29]</sup> The Dy...Dy and Dy...Cu interactions are expected to be small, as is generally the case for exchange coupling with lanthanides and as has been argued for the related  $[\text{Dy}_2\text{Cu}_2]$ ,<sup>[27]</sup> in which the structural features are comparable with those found for  $[\text{Dy}_3\text{Cu}_6]$  (av.: Dy...Dy 3.94, av.: Cu...Dy 3.32 and 3.70 Å). Previously, it was found that weak antiferromagnetic interactions between lanthanide(III) ions arranged in a triangular configuration may lead to a diamagnetic ground state.<sup>[15,31]</sup> This is not the case in  $[\text{Dy}_3\text{Cu}_6]$ , and we believe that the Cu...Cu and moreover the Cu...Dy couplings while small are responsible for the non-vanishing susceptibility at low temperature and the peculiar magnetic behavior.

At 2 K, the field dependence of the magnetization of polycrystalline samples exhibits an unusual two-step feature (Figure 3a). The first step, which reaches an approximate magnetization of  $6\text{--}7 \mu_{\text{B}}$  at 10 kOe, is followed by a second step that slowly increases to  $19 \mu_{\text{B}}$  at 50 kOe. This value is consistent with that expected for six Cu<sup>II</sup> and three Dy<sup>III</sup> ions with an effective spin of  $S = 1/2$  and a  $g$  value between 8 and 10 at low temperature. The intermediate saturation value of about  $6 \mu_{\text{B}}$ , which corresponds to a fraction of the overall value ( $19 \mu_{\text{B}}$ ), is reminiscent of “canting” in bulk magnets. It is ascribed to the interplay of the different exchange couplings (Cu...Cu, Dy...Cu, and Dy...Dy) being overcome at higher

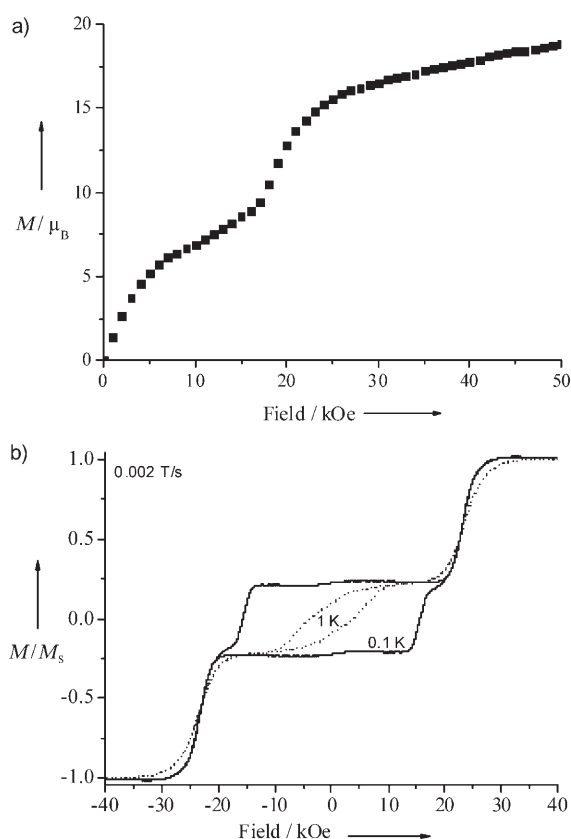


**Figure 3.** Magnetization curves for  $[\text{Dy}_3\text{Cu}_6]$ . a) Polycrystalline sample at 2 K; b) single crystal ( $\mu$ -SQUID) at 1 K (dashed) and 0.1 K (solid line). Scan rate:  $0.002 \text{ T s}^{-1}$ .

field. This value ( $6 \mu_B$ ) is in agreement with the  $\chi T$  value at low temperature (ca.  $7 \text{ cm}^3 \text{ K mol}^{-1}$ ) for a ground state with  $S \approx 3$ .

Single crystals of  $[\text{Dy}_3\text{Cu}_6]$  were further studied by the Micro-SQUID technique<sup>[7]</sup> in the temperature range 1.1–0.04 K. A stepped shape of the magnetization curve is also observed (Figure 3b), in agreement with measurements on polycrystalline samples. Below 1.1 K, hysteresis loops are observed, but only for the first step, with large coercive field widening on cooling ( $H_c = 15 \text{ kOe}$  at 0.1 K). This behavior is typical of an SMM with very slow zero-field relaxation. The absolute value of the magnetization, which is not accessible with this technique, was estimated from the measurement at 2 K on the polycrystalline sample (see above). At this temperature, complete saturation was not reached, but we can estimate the magnetization of the first step to be close to  $6\text{--}7 \mu_B$ . Again the presence of this step exhibiting hysteresis loops at low temperature is quite unusual. It is in contrast with  $[\text{Dy}^{\text{III}}_3]$ .<sup>[15]</sup> Despite the difficulty in quantifying the contributions of the different interactions, this behavior may be ascribed to the anisotropy of the  $\text{Dy}^{\text{III}}\text{--Cu}^{\text{II}}$  magnetic exchange, which could force the resulting anisotropy to be out of the plane. It is in agreement with previous studies on  $[\text{DyCu}_4]$  and  $[\text{Dy}_2\text{Cu}]$  complexes showing that  $\text{Dy}^{\text{III}}\text{--Cu}^{\text{II}}$  exchange coupling causes strong anisotropy.<sup>[19,32]</sup> This anisotropy can lead to strong “canting”, responsible for the nonvanishing magnetic moment in contrast to  $[\text{Dy}^{\text{III}}_3]$ .<sup>[15]</sup>

Studying the magnetization relaxation by ac susceptibility revealed a strong frequency dependence of  $\chi'$  and  $\chi''$  below 5 K, as expected for an SMM (Figure 4). The relaxation time  $\tau$

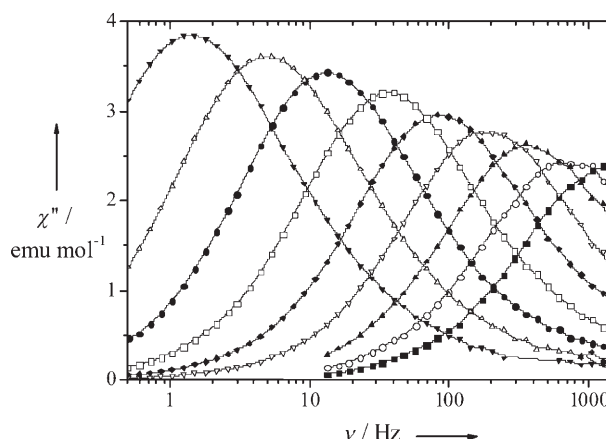


**Figure 4.** Frequency dependence of the out-of-phase magnetic susceptibility  $\chi''$  at different temperatures.

was extracted from the maximum of  $\chi''$  at different frequencies ( $\tau = 1/\omega$ ) between 1.8 and 4 K and by decay measurements of the dc magnetization at different temperatures in the range 1.8–0.04 K.<sup>[33]</sup> (See the Supporting Information for a plot of  $\tau$  values versus  $1/T$ .) A linear fit performed in the high-temperature regime to the Arrhenius equation  $\tau = \tau_0 \exp(U_{\text{eff}}/k_B T)$  gave the dynamical parameters  $U_{\text{eff}} = 25 \text{ K}$  and  $\tau_0 = 1.5 \times 10^{-7} \text{ s}$ .

In summary, the dysprosium–copper nonanuclear complex reported herein exhibits features typical of SMMs, that is, both hysteretic behavior of the magnetization and frequency dependence of the ac magnetic susceptibility. From prior studies the ground spin state of  $[\text{Dy}_3\text{Cu}_6]$  is expected to be  $S = 3$  with an anisotropy barrier of 25 K associated with a slow zero-field relaxation and a large coercive field. Further experiments are underway to quantify the different contributions to this behavior, such as studies on analogues with diamagnetic lanthanide ions, by EPR spectroscopy, with polarized neutrons, and theoretical calculations. Such understanding is required to improve the synthetic strategy. Nevertheless,  $[\text{Dy}_3\text{Cu}_6]$  is at present one of the best single-molecule magnets and demonstrates the ability of the 3d–4f heterometallic strategy to increase  $S$  and  $D$  and consequently the relaxation time.

## Experimental Section

**Synthesis:** All chemicals and solvents were used as received; all preparations and manipulations were performed under aerobic conditions. The Schiff base ligand  $\text{LH}_2$  was obtained by condensation of ethanolamine with 1,1,1-trifluoro-2,4-pentanedione in methanol by a previously reported method.<sup>[34,35]</sup>

$[\text{Dy}_3\text{Cu}_6]$  was obtained in a one-pot reaction by mixing  $\text{LH}_2$ ,  $[\text{Dy}(\text{ClO}_4)_3]$ , and  $\text{CuCl}_2$  in methanol in the presence of triethylamine.  $\text{LH}_2$  (0.2 g, 1.02 mmol) was dissolved in methanol (10 mL) and  $[\text{Dy}(\text{ClO}_4)_3] \cdot 6\text{H}_2\text{O}$  (0.26 g, 0.56 mmol) in methanol (10 mL) was added dropwise with stirring over 10 min. A solution of  $\text{CuCl}_2 \cdot 2\text{H}_2\text{O}$

(85 mg, 0.50 mmol) in methanol (5 mL) was added to the resulting clear yellow solution. The solution turned clear green and stirring was maintained for 5 min. Finally, triethylamine (0.2 mL) was added to the reaction mixture to give a deep-blue solution. One week of slow evaporation gave 125 mg of square-plate blue single crystals suitable for X-ray diffraction, which were isolated by filtration and washed with a small amount of methanol (60% yield based on Cu). Elemental analysis (%) calcd for  $C_{42}H_{81}Cl_3Cu_6Dy_3F_{18}N_6O_{35.50}$ : C 19.74, H 3.20, Cl 4.16, Cu 14.92, Dy 19.08, F 13.38, N 3.29; found: C 19.86, H 2.94, Cl 3.72, Cu 14.23, Dy 18.34, F 12.31, N 3.21.

**Caution:** Although we have not experienced any problems in this work, perchlorate salts may be explosive and should be handled with great care.

Crystal data for  $[Dy_3Cu_6] \cdot C_{42}H_{81}Cl_3Cu_6Dy_3F_{18}N_6O_{35.50}$ ,  $M = 2555.2 \text{ g mol}^{-1}$ , space group  $P2_1/c$  (No. 14),  $a = 17.7136(4)$ ,  $b = 20.6244(4)$ ,  $c = 24.5220(5) \text{ \AA}$ ,  $\beta = 108.352(1)^\circ$ ,  $V = 8503.0(3) \text{ \AA}^3$ ,  $Z = 4$ ,  $\rho = 1.996 \text{ g cm}^{-3}$ ,  $\mu = 4.283 \text{ mm}^{-1}$ ,  $F(000) = 4976$ . 33465 measured reflections<sup>[36]</sup> collected ( $R_{int} = 0.033$ ) at 150 K on a Nonius KappaCCD diffractometer with monochromatic  $MoK_{\alpha}$  radiation ( $\lambda = 0.71073 \text{ \AA}$ ). 1027 refined parameters for 10701 unique reflections. Solution with SIR97;<sup>[37]</sup> refinements with CRYSTALS.<sup>[38]</sup> Final  $R$  indices ( $I > 3\sigma(I)$ ):  $R(F) = 0.0518$ ,  $R_w(F^2) = 0.0619$ . CCDC 297249 contains the supplementary crystallographic data for this paper. These data can be obtained free of charge from The Cambridge Crystallographic Data Centre via [www.ccdc.cam.ac.uk/data\\_request/cif](http://www.ccdc.cam.ac.uk/data_request/cif).

Magnetic measurements: dc measurements were performed on polycrystalline samples with a Quantum Design SQUID magnetometer. To avoid orientation in the magnetic field, the dysprosium samples were pressed in a teflon sample holder equipped with a piston. The magnetic susceptibility was measured in the temperature range 2–300 K in a field of 1 kOe. The magnetization was measured at 2 K in the range 0–5.5 kOe.

Received: February 7, 2006

Revised: April 13, 2006

Published online: June 22, 2006

**Keywords:** cluster compounds · copper · dysprosium · magnetic properties · N,O ligands

- [1] R. Sessoli, H.-L. Tsai, A. R. Schake, S. Wang, J. B. Vincent, K. Folting, D. Gatteschi, G. Christou, D. N. Hendrickson, *J. Am. Chem. Soc.* **1993**, *115*, 1804–1816.
- [2] R. Sessoli, D. Gatteschi, A. Caneschi, M. Novak, *Nature* **1993**, *365*, 149.
- [3] D. Gatteschi, A. Caneschi, L. Pardi, R. Sessoli, *Science* **1994**, *265*, 1054–1058.
- [4] S. M. J. Aubin, M. W. Wemple, D. M. Adams, H.-L. Tsai, G. Christou, D. N. Hendrickson, *J. Am. Chem. Soc.* **1996**, *118*, 7746–7754.
- [5] S. K. Ritter, *Chem. Eng. News* **2004**, *82*(50), 29–32.
- [6] D. Gatteschi, R. Sessoli, *Angew. Chem.* **2003**, *42*, 278–309; *Angew. Chem. Int. Ed.* **2003**, *42*, 268–297.
- [7] W. Wernsdorfer, *Adv. Chem. Phys.* **2001**, *118*, 99–189.
- [8] A. Bencini, D. Gatteschi, *EPR of Exchange Coupled Systems*, Springer, Berlin, **1990**.
- [9] J. Villain, F. Hartman-Boutron, R. Sessoli, A. Rettori, *Europhys. Lett.* **1994**, *27*, 159.
- [10] E. M. Chudnovsky, *Science* **1996**, *274*, 938–939.
- [11] M. N. Leuenberger, D. Loss, *Nature* **2001**, *410*, 789–793.
- [12] R. L. Carlin, *Magnetochemistry*, Springer, Berlin, **1986**.
- [13] N. Ishikawa, M. Sugita, T. Ishikawa, S. Koshihara, Y. Kaizu, *J. Am. Chem. Soc.* **2003**, *125*, 8694–8695.
- [14] N. Ishikawa, M. Sugita, W. Wernsdorfer, *J. Am. Chem. Soc.* **2005**, *127*, 3650–3651.
- [15] J. Tang, I. Hewitt, N. T. Madhu, G. Chastanet, W. Wernsdorfer, C. E. Anson, C. Benelli, R. Sessoli, A. K. Powell, *Angew. Chem.* **2006**, *118*, 1761–1765; *Angew. Chem. Int. Ed.* **2006**, *45*, 1729–1733.
- [16] S. Osa, T. Kido, N. Matsumoto, N. Re, A. Pochaba, J. Mrozinski, *J. Am. Chem. Soc.* **2004**, *126*, 420–421.
- [17] C. M. Zaleski, E. C. Depperman, J. W. Kampf, M. L. Kirk, V. L. Pecoraro, *Angew. Chem.* **2004**, *116*, 4002–4004; *Angew. Chem. Int. Ed.* **2004**, *43*, 3912–3914.
- [18] A. Mishra, W. Wernsdorfer, S. Parsons, G. Christou, E. K. Brechin, *Chem. Commun.* **2005**, 2086–2088.
- [19] F. Mori, T. Nyui, T. Ishida, T. Nogami, K.-Y. Choi, H. Nojiri, *J. Am. Chem. Soc.* **2006**, *128*, 1440–1441.
- [20] J. P. Costes, F. Dahan, W. Wernsdorfer, *Inorg. Chem.* **2006**, *45*, 5–7.
- [21] C. Lescop, D. Luneau, G. Bussiere, M. Triest, C. Reber, *Inorg. Chem.* **2000**, *39*, 3740–3741.
- [22] C. Lescop, D. Luneau, P. Rey, G. Bussiere, C. Reber, *Inorg. Chem.* **2002**, *41*, 5566–5574.
- [23] C. Desroches, G. Pilet, S. A. Borshch, S. Parola, D. Luneau, *Inorg. Chem.* **2005**, *44*, 9112–9120.
- [24] C. Desroches, G. Pilet, P. Á. Szilágyi, G. Molnár, S. A. Borshch, A. Bousseksou, S. Parola, D. Luneau, *Eur. J. Inorg. Chem.* **2006**, 357–365.
- [25] W. J. Jones, S. Gupta, L. J. Theriot, F. T. Helm, W. A. Baker, Jr., *Inorg. Chem.* **1978**, *17*, 87–90.
- [26] L. Merz, W. Haase, *Z. Naturforsch. A* **1976**, *31*, 177–182.
- [27] C. Benelli, A. Caneschi, D. Gatteschi, L. Guilou, L. Pardi, *Inorg. Chem.* **1990**, *29*, 1750.
- [28] R. D. Shannon, *Acta Crystallogr. Sect. A* **1976**, *32*, 751–767.
- [29] M. Nikei, N. Hoshino, T. Ito, H. Oshio, *Polyhedron* **2003**, *22*, 2359–2362.
- [30] W. E. Hatfield, *Comments Inorg. Chem.* **1981**, *1*, 105–121.
- [31] J.-P. Costes, F. Dahan, F. Nicodème, *Inorg. Chem.* **2001**, *40*, 5285–5287.
- [32] J. Sanz, L. R. Ruiz, A. Gleizes, F. Lloret, J. Faus, M. Julve, J. Borrás-Almenar, J. Y. Journaux, *Inorg. Chem.* **1996**, *35*, 7384–7393.
- [33] C. Sangregorio, T. Ohm, C. Paulsen, R. Sessoli, D. Gatteschi, *Phys. Rev. Lett.* **1997**, *78*, 4645–4648.
- [34] E. S. Ibrahim, S. A. Sallam, A. S. Orabi, B. A. El-Shetary, A. Lentz, *Monatsh. Chem.* **1998**, *129*, 159–171.
- [35] E. G. Jäger, *Z. Chem.* **1966**, *6*, 111.
- [36] Nonius, Kappa CCD Program Package: COLLECT, DENZO, SCALEPACK, SORTAV, Nonius B.V., Delft, The Netherlands, **1999**.
- [37] G. Cascarano, A. Altomare, C. Giacovazzo, A. Guagliardi, A. G. G. Moliterni, D. Siliqi, M. C. Burla, G. Polidori, M. Camalli, *Acta Crystallogr. Sect. A* **1996**, *52*, C-79.
- [38] D. J. Watkin, C. K. Prout, J. R. Carruthers, P. W. Betteridge, CRISTAL Issue 11, Chemical Crystallography Laboratory, Oxford, UK, **1999**.

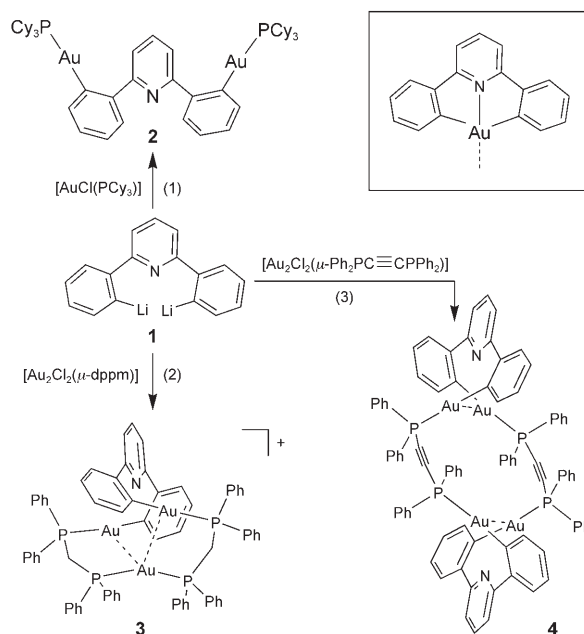


# Self-Assembly of a Highly Stable, Topologically Interesting Metallamacrocycle by Bridging Gold(I) Ions with Pyridyl-2,6-diphenyl<sup>2-</sup> and Diphosphanes\*\*

Steven C. F. Kui, Jie-Sheng Huang, Raymond Wai-Yin Sun, Nianying Zhu, and Chi-Ming Che\*

Metallamacrocycles constructed through self-assembly play an important role in the development of molecular architecture and topology.<sup>[1]</sup> There have been numerous reports on fascinating molecular assemblies that consist of metallamacrocycles, from catenanes,<sup>[1a]</sup> pseudorotaxanes,<sup>[1a,c]</sup> and helicates<sup>[1a,b,d]</sup> to molecular polygons/polyhedrons.<sup>[1d]</sup> The Möbius strip is another intriguing topology that has attracted considerable attention from chemists<sup>[2]</sup> but remains rarely seen in synthetic molecular assemblies. Previous reports are almost all confined to Möbius arrangements of electronic orbitals or spins, including many theoretical studies on Möbius aromaticity or delocalization,<sup>[2]</sup> together with the syntheses of a Möbius aromatic hydrocarbon<sup>[3]</sup> and a magnetic Möbius strip.<sup>[4]</sup> The synthesis of a molecular Möbius strip, an organic molecule consisting of three crown ether rings, was first realized in 1982.<sup>[5]</sup> Recently, a Möbius strip of NbSe<sub>3</sub> single crystals was reported.<sup>[6]</sup> Herein, we report the formation of a molecular assembly that contains a highly robust metallamacrocycle, with the bonds directly attached to the metallamacrocycle adopting a Möbius arrangement.

We have been exploring the chemistry of gold complexes with a pyridyl-2,6-diphenyl<sup>2-</sup> (CNC) ligand. Our previous work led to the isolation of several Au<sup>III</sup>–CNC complexes<sup>[7]</sup> that contain the tridentate CNC ligand (see the inset of Scheme 1). In the course of developing the chemistry of Au<sup>I</sup>–CNC complexes, we conceived that [Li<sub>2</sub>(CNC)(tmeda)] (**1**; tmeda = *N,N,N',N'*-tetramethylethylenediamine)<sup>[8]</sup> would be a useful alkylating agent. Treatment of **1** with [Au(PCy<sub>3</sub>)Cl] (Cy = cyclohexyl) in dry toluene gave [Au<sub>2</sub>(CNC)(PCy<sub>3</sub>)<sub>2</sub>] (**2**; reaction 1, Scheme 1) in 80 % yield. Complex **2** is thermally stable and undergoes decomposition to give metallic gold at > 325 °C. The <sup>31</sup>P NMR spectrum of **2** in CD<sub>2</sub>Cl<sub>2</sub> shows one



**Scheme 1.** Syntheses of **2–4** from **1** (note the omission of the tmeda ligands in **1** for clarity). The inset depicts the coordination mode of the CNC ligand in previously reported gold complexes.

sharp singlet at  $\delta = 57.35$  ppm. The X-ray crystal structure of **2**<sup>[9]</sup> (see the Supporting Information) features a CNC ligand that bridges two Au<sup>I</sup> ions, an unreported coordination mode of the CNC dianion in its coordination chemistry.<sup>[10]</sup>

In view of the propensity of the CNC ligand to bridge Au<sup>I</sup> ions, we envisioned that this ligand could have a unique application in constructing Au<sup>I</sup> metallamacrocycles. Previously, a wide variety of Au<sup>I</sup> metallamacrocycles had been prepared by employing isocyanide-, acetylide-, pyridine-, carboxylate-, and phosphane-based bridging ligands,<sup>[11]</sup> notable examples of which are the singly and doubly braided [2]catenanes reported by Puddephatt and co-workers.<sup>[11b,c]</sup>

Our strategy for constructing the metallamacrocycles presented herein is through self-assembly from **1** and Au<sup>I</sup>–diphosphane complexes (reactions 2 and 3, Scheme 1). Reaction of **1** with [Au<sub>2</sub>Cl<sub>2</sub>( $\mu$ -dppm)] (dppm = bis(diphenylphosphanyl)methane) in dry toluene for 24 h gave a yellow suspension. Removal of the solvent followed by extraction with dry CHCl<sub>3</sub> and slow evaporation of the CHCl<sub>3</sub> extract afforded [Au<sub>3</sub>(CNC)( $\mu$ -dppm)<sub>2</sub>]Cl (**3-Cl**) as yellow crystals in 86 % yield. Under similar conditions, the reaction of **1** with [Au<sub>2</sub>Cl<sub>2</sub>( $\mu$ -Ph<sub>2</sub>PC $\equiv$ CPh<sub>2</sub>)] resulted in the formation of [Au<sub>4</sub>(CNC)<sub>2</sub>( $\mu$ -Ph<sub>2</sub>PC $\equiv$ CPh<sub>2</sub>)<sub>2</sub>] (**4**), which was isolated as yellow crystals in 75 % yield by diffusion of Et<sub>2</sub>O into a solution of CHCl<sub>3</sub>. Treatment of **3-Cl** with excess LiClO<sub>4</sub> and LiPF<sub>6</sub> produced [Au<sub>3</sub>(CNC)( $\mu$ -dppm)<sub>2</sub>]ClO<sub>4</sub> (**3-ClO<sub>4</sub>**) and [Au<sub>3</sub>(CNC)( $\mu$ -dppm)<sub>2</sub>]PF<sub>6</sub> (**3-PF<sub>6</sub>**), respectively, in about 95 % yield. In the solid state, complexes **3-Cl**, **3-ClO<sub>4</sub>**, and **3-PF<sub>6</sub>** exhibited a high thermal stability similar to that of **2**; complex **4** is less stable and decomposed at 150 °C and subsequently gave metallic gold at 250 °C.

X-ray crystal-structure determinations of **3-Cl**·8.5 CHCl<sub>3</sub>, **3-PF<sub>6</sub>**·CH<sub>2</sub>Cl<sub>2</sub>·5 CHCl<sub>3</sub>, and **4**·3 CHCl<sub>3</sub><sup>[9]</sup> revealed a 16-mem-

[\*] Dr. S. C. F. Kui, Dr. J.-S. Huang, Dr. R. W.-Y. Sun, Dr. N. Zhu, Prof. Dr. C.-M. Che  
Department of Chemistry and Open Laboratory of Chemical Biology  
Institute of Molecular Technology for Drug Discovery and Synthesis  
The University of Hong Kong  
Pokfulam Road, Hong Kong (P.R. China)  
Fax: (+852) 2857-1586  
E-mail: cmche@hku.hk

[\*\*] This study was supported by The University of Hong Kong (University Development Fund), the Hong Kong Research Grants Council, and the University Grants Committee of the Hong Kong SAR of China (Area of Excellence Scheme, AoE/P-10/01).

Supporting information for this article is available on the WWW under <http://www.angewandte.org> or from the author.

bered  $C_8NP_4Au_3$  metallamacrocycle in **3** and a 26-membered  $C_{16}N_2P_4Au_4$  metallamacrocycle in **4** (see Figure 1 and the Supporting Information). The Au atoms in **3** and **4** form a  $\{Au_3\}$  triangle and a  $\{Au_4\}$  parallelogram, respectively, with

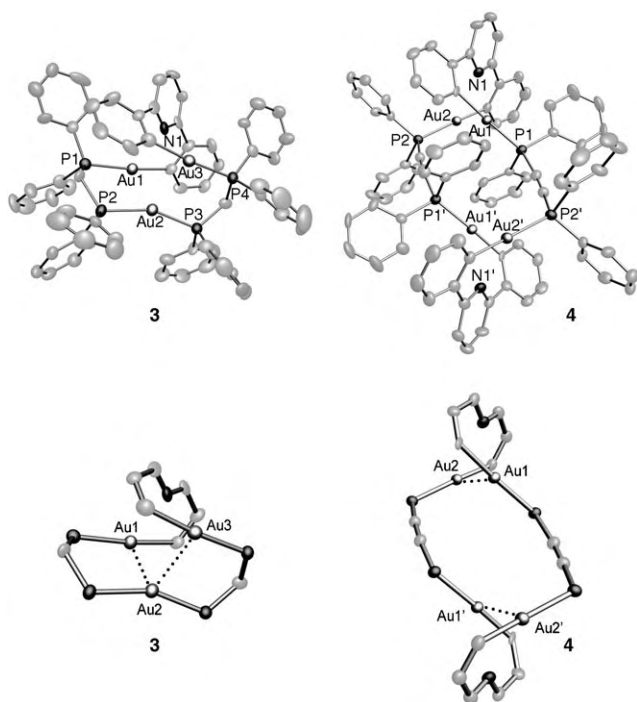


**Figure 1.** Perspective structures of **3-Cl** and **4** determined by X-ray crystallography along with the metallamacrocycles in the two complexes. For **4**, there is a crystallographic center of symmetry located in the center of the molecule.

intramolecular Au...Au contacts of 3.015(29)–3.040(29) Å for **3** (Au1...Au2, Au2...Au3) and 3.178(10) Å for **4** (Au1...Au2, Au1'...Au2'), which fall within the range of 2.9–3.2 Å expected for the occurrence of weak Au<sup>I</sup>...Au<sup>I</sup> interactions.<sup>[12]</sup> The Au–C bond lengths of 2.034(14)–2.070(16) Å in **3** and 2.077(39)–2.091(14) Å in **4** are comparable to those in **2** (2.053(9)–2.059(13) Å).

Interestingly, the bonds directly attached to the 16-membered metallamacrocycle  $C_8NP_4Au_3$  in **3** adopt a Möbius arrangement. The Möbius strip that passes through the  $C_8NP_4Au_3$  ring and the P–C and C–C bonds directly attached to the ring is depicted in Figure 2. As a Möbius strip is chiral, the crystal structure of **3** contains pairs of *P* and *M* enantiomers (see the Supporting Information), thus rendering **3** to be racemic.

Further examination of the structures of **3-Cl**·8.5CHCl<sub>3</sub> and **3-PF<sub>6</sub>**·CH<sub>2</sub>Cl<sub>2</sub>·5CHCl<sub>3</sub> revealed the existence of intramolecular C–H...π interactions, as indicated by the close contacts (2.787–3.113 Å) between one of the methylene hydrogen atoms in each dpmm ligand (see the Supporting Information) and the carbon atoms of the nearest phenyl rings of the CNC ligand. In both crystal structures, **3** exists as dimers, each of which consists of a pair of *P* and *M* enantiomers linked by two intermolecular C–H...π interactions (a C–H bond of a dpmm phenyl group with the nearest phenyl



**Figure 2.** Arrangement of the bonds directly attached to the 16-membered metallamacrocycle  $C_8NP_4Au_3$  of **3** along a Möbius strip. A Möbius strip is a unique single-sided surface, as evident by following the track of the arrows.

ring of the CNC ligand; closest H...C distances: 2.826 Å for **3-Cl**·8.5CHCl<sub>3</sub> and 2.848 Å for **3-PF<sub>6</sub>**·CH<sub>2</sub>Cl<sub>2</sub>·5CHCl<sub>3</sub>). For each of the dimers in **3-Cl**·8.5CHCl<sub>3</sub>, there are also four intermolecular C–H...π interactions that arise from the C–H bonds of four CHCl<sub>3</sub> molecules (two inside and two outside the dimers) and the nearest CNC phenyl rings (closest H...C distances: 2.540 and 2.739 Å for the interactions outside and inside the dimers, respectively).

The structure of **3** remains intact in solution, as revealed by mass-spectrometric and NMR spectroscopic analysis; for example, complex **3-Cl** exhibits a prominent cluster peak at *m/z* 1589 in the FAB mass spectrum, which is assignable to  $[Au_3(CNC)(\mu\text{-dpmm})_2]^+$ . The <sup>31</sup>P NMR spectra of **3-Cl**, **3-ClO<sub>4</sub>**, and **3-PF<sub>6</sub>** each show two multiplets (AA'BB' system) with  $\delta \approx 30$  (P<sup>1</sup> and P<sup>4</sup>) and 37 ppm (P<sup>2</sup> and P<sup>3</sup>; assignment based on the <sup>31</sup>P, <sup>1</sup>H HOESY NMR spectra shown in the Supporting Information), which is consistent with the C<sub>2</sub>-symmetric structure of the molecule of **3**. In the <sup>1</sup>H NMR spectra of **3-Cl**, **3-ClO<sub>4</sub>**, and **3-PF<sub>6</sub>**, the H<sup>a</sup> signal ( $\delta \approx 1.2$  ppm) is substantially upfield from that of H<sup>b</sup> ( $\delta \approx 4.0$  ppm; see the Supporting Information for an example), a phenomenon attributable to the shielding of H<sup>a</sup> by the phenyl ring of the CNC ligand. The NOESY NMR spectrum of **3-Cl** shows a cross peak between H<sup>a</sup> and H<sup>3</sup> (see the Supporting Information). These data are in agreement with the intramolecular C–H...π interactions in the crystal structures of **3-Cl** and **3-PF<sub>6</sub>**.

In contrast, the 26-membered metallamacrocycle  $C_{16}N_2P_4Au_4$  in **4**, which consists of a pair of *P*- and *M*-[Au<sub>2</sub>(CNC)P<sub>2</sub>] moieties,<sup>[13]</sup> exhibits a fluxional behavior in solution. This is evident from the variable-temperature <sup>1</sup>H NMR (60 to –53 °C)<sup>[14]</sup> and <sup>31</sup>P NMR spectra of **4** in CDCl<sub>3</sub> (see the Supporting Information for further details). We propose that **4** is partially changed to its conformer **5** upon dissolution in CDCl<sub>3</sub>, and there is an equilibrium between **4** and **5** in solution (Figure 3).<sup>[15]</sup> Indeed, the EXSY spectrum of **4** at –53 °C shows cross signals of H<sup>3</sup>–H<sup>3'</sup>, H<sup>4</sup>–H<sup>4'</sup>, H<sup>5</sup>–H<sup>5'</sup>,

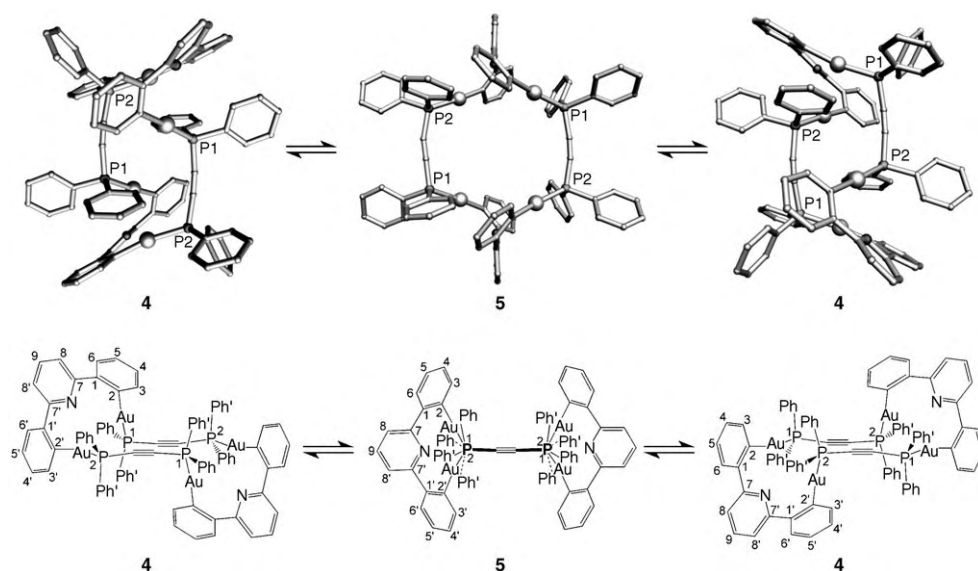


**Figure 3.** Proposed conformational changes of **4** in solution viewed from the top (upper) and side (lower) of the molecules. The structure of **5** was built using Chem3D 5.0 on the basis of the crystal structure of **4**.

$H^6-H^{6'}$ ,  $H^8-H^{8'}$ , and  $Ph-Ph'$  pairs (see Figure 3 and the Supporting Information), together with the cross signals that possibly arise from the exchanges between **4** and **5**, in accordance with the conformational changes shown in Figure 3. Notably, the  $H^3$ ,  $H^4$ , and  $H^{3'}$  signals of **4** ( $\delta = 5.7$ – $6.3$  ppm) are considerably upfield from the corresponding signals of **3** ( $\delta \approx 6.9$ – $7.1$  ppm), which could result from intramolecular  $C-H \cdots \pi$  interactions (see the Supporting Information). Such  $C-H \cdots \pi$  interactions do not exist in **5**, consistent with the downfield shift of these signals, particularly for  $H^3$ , upon increasing temperature (which increases the **5/4** molar ratio).

Complexes **3-Cl**, **3-ClO<sub>4</sub>**, and **3-PF<sub>6</sub>** are remarkably stable both in organic solvents (such as  $CH_2Cl_2$ ,  $CHCl_3$ , dimethylformamide (DMF), and dimethylsulfoxide (DMSO)) and under physiologically relevant conditions (see the Supporting Information). The high stability of **3-Cl** in solution relative to most self-assembled polynuclear  $Au^I$  compounds, including **4** (which decomposed within several days in a solution of  $CHCl_3$  at room temperature), prompted us to examine its cytotoxic properties; gold compounds not only have long been used as antiarthritic drugs but also are promising antitumor agents,<sup>[16]</sup> and stability is an important issue in the design of new  $Au^I$  therapeutic agents. The cytotoxicities of **3-Cl** toward cancer cell lines (including cervical epithelioid carcinoma (HeLa) and nasopharyngeal carcinoma (SUNE1 and its cisplatin-resistant variant CNE1)) and normal lung fibroblast cells (CCD-19Lu) were determined by the 3-(4,5-dimethylthiazol-2-yl)-2,5-diphenyltetrazolium bromide (MTT) assay. From the cytotoxicity profiles (see the Supporting Information), the corresponding  $IC_{50}$  values (dose required for the inhibition of 50 % cellular growth) of the cancer cell lines were determined to be  $6.53$ – $8.20$   $\mu M$ , which are comparable to those of the clinically used cisplatin ( $IC_{50} = 14.8$  (HeLa),  $2.3$  (SUNE1), and  $8.9$   $\mu M$  (CNE1)). Importantly, **3-Cl** was found to be almost equally cytotoxic to SUNE1 and its cisplatin-resistant

variant CNE1, with a resistance factor of 1.2 ( $IC_{50}$ -(CNE1)/ $IC_{50}$ -(SUNE1) ratio) less than one third of that observed for cisplatin (3.9). The  $IC_{50}$  value of **3-Cl** for normal human cells CCD-19Lu was determined to be  $19.1$   $\mu M$ , thus indicating that this  $Au^I$  compound is 2.3–2.9-fold less toxic to normal cells than to the forging cancer cells.

In summary, we have observed a new coordination mode of the pyridyl-2,6-diphenyl<sup>2-</sup> ligand and isolated two  $Au^I$  compounds that contain unprecedented types of gold metallamacrocycles. Both types of metallamacrocycles have intramolecular  $Au^I \cdots Au^I$  and  $C-H \cdots \pi$

$H \cdots \pi$  interactions; the metallamacrocycles with stronger  $Au^I \cdots Au^I$  and  $C-H \cdots \pi$  interactions is highly robust in solution and shows interesting topological and cytotoxic properties, whereas the other exhibits a unique fluxional behavior in solution. The present work demonstrates that polydentate cyclometalating ligands, such as pyridyl-2,6-diaryl<sup>2-</sup>, together with  $Au^I$  could be useful for constructing new classes of molecules with unprecedented topology and properties.

Received: March 1, 2006

Published online: June 22, 2006

**Keywords:** aurophilicity · gold · metallacycles · Möbius strip · structure elucidation

- [1] a) D. B. Amabilino, J. F. Stoddart, *Chem. Rev.* **1995**, *95*, 2725; b) C. Piguet, G. Bernardinelli, G. Hopfgartner, *Chem. Rev.* **1997**, *97*, 2005; c) F. M. Raymo, J. F. Stoddart, *Chem. Rev.* **1999**, *99*, 1643; d) S. Leininger, B. Olenyuk, P. J. Stang, *Chem. Rev.* **2000**, *100*, 853.
- [2] H. S. Rzepa, *Chem. Rev.* **2005**, *105*, 3697.
- [3] a) D. Ajami, O. Oeckler, A. Simon, R. Herges, *Nature* **2003**, *426*, 819; b) T. Kawase, M. Oda, *Angew. Chem.* **2004**, *116*, 4496; *Angew. Chem. Int. Ed.* **2004**, *43*, 4396.
- [4] O. Cadot, D. Gatteschi, R. Sessoli, F. K. Larsen, J. Overgaard, A.-L. Barra, S. J. Teat, G. A. Timco, R. E. P. Winpenny, *Angew. Chem.* **2004**, *116*, 5308; *Angew. Chem. Int. Ed.* **2004**, *43*, 5196.
- [5] D. M. Walba, R. M. Richards, R. C. Haltiwanger, *J. Am. Chem. Soc.* **1982**, *104*, 3219.
- [6] a) S. Tanda, T. Tsuneta, Y. Okajima, K. Inagaki, K. Yamaya, N. Hatakenaka, *Nature* **2002**, *417*, 397; b) G. R. Patzke, *Angew. Chem.* **2003**, *115*, 1002; *Angew. Chem. Int. Ed.* **2003**, *42*, 972.
- [7] a) K.-H. Wong, K.-K. Cheung, M. C.-W. Chan, C.-M. Che, *Organometallics* **1998**, *17*, 3505; b) C.-M. Che, C. K.-L. Li, R. W.-Y. Sun, S. C.-F. Kui, N. Zhu, *Chem. Eur. J.*, DOI: 10.1002/chem.200600117.
- [8] Prepared by treating 2,6-bis(2'-bromophenyl)pyridine with *n*BuLi, followed by addition of TMEDA; see: S. C. F. Kui,

- PhD dissertation, The University of Hong Kong, **2005** (see the Supporting Information for the X-ray crystal structure of **1**<sup>[9]</sup>).
- [9] CCDC 294396–294400 contain the supplementary crystallographic data for this paper. These data can be obtained free of charge from The Cambridge Crystallographic Data Centre via [www.ccdc.cam.ac.uk/data\\_request/cif](http://www.ccdc.cam.ac.uk/data_request/cif).
- [10] For other examples of metal complexes with the CNC dianion, see: a) M. Maestri, C. Deuschel-Cornioley, A. von Zelewsky, *Coord. Chem. Rev.* **1991**, *111*, 117; b) G. W. V. Cave, N. W. Alcock, J. P. Rourke, *Organometallics* **1999**, *18*, 1801; c) W. Lu, M. C. W. Chan, K.-K. Cheung, C.-M. Che, *Organometallics* **2001**, *20*, 2477; d) W. Lu, N. Zhu, C.-M. Che, *Chem. Commun.* **2002**, 900; e) V. W.-W. Yam, R. P.-L. Tang, K. M.-C. Wong, X.-X. Lu, K.-K. Cheung, N. Zhu, *Chem. Eur. J.* **2002**, *8*, 4066; f) M. Polson, S. Fracasso, V. Bertolasi, M. Ravaglia, F. Scandola, *Inorg. Chem.* **2004**, *43*, 1950; g) A. J. Wilkinson, A. E. Goeta, C. E. Foster, J. A. G. Williams, *Inorg. Chem.* **2004**, *43*, 6513; h) J. D. Crowley, I. M. Steele, B. Bosnich, *Inorg. Chem.* **2005**, *44*, 2989.
- [11] Selected examples: a) J. C. Vickery, M. M. Olmstead, E. Y. Fung, A. L. Balch, *Angew. Chem.* **1997**, *109*, 1227; *Angew. Chem. Int. Ed. Engl.* **1997**, *36*, 1179; b) C. P. McArdle, M. J. Irwin, M. C. Jennings, R. J. Puddephatt, *Angew. Chem.* **1999**, *111*, 3571; *Angew. Chem. Int. Ed.* **1999**, *38*, 3376; c) C. P. McArdle, J. J. Vittal, R. J. Puddephatt, *Angew. Chem.* **2000**, *112*, 3977; *Angew. Chem. Int. Ed.* **2000**, *39*, 3819; d) R. J. Puddephatt, *Coord. Chem. Rev.* **2001**, *216–217*, 313; e) J. H. K. Yip, J. Prabhavathy, *Angew. Chem.* **2001**, *113*, 2217; *Angew. Chem. Int. Ed.* **2001**, *40*, 2159; f) F. Mohr, M. C. Jennings, R. J. Puddephatt, *Angew. Chem.* **2004**, *116*, 987; *Angew. Chem. Int. Ed.* **2004**, *43*, 969; g) R. Lin, J. H. K. Yip, K. Zhang, L. L. Koh, K.-Y. Wong, K. P. Ho, *J. Am. Chem. Soc.* **2004**, *126*, 15852.
- [12] a) H. Schmidbaur, *Chem. Soc. Rev.* **1995**, *24*, 391; b) H. Schmidbaur, *Gold: Progress in Chemistry, Biochemistry, and Technology*, Wiley, Chichester, **1999**.
- [13] Although it is possible to generate the *P,P* or *M,M* analogues of **4**, no such structures were observed. Modeling studies revealed that the *P,P* or *M,M* structure renders all the phenyl groups of the two diphosphane ligands in an unfavorable eclipsed arrangement, in contrast with the favorable staggered arrangement of the phenyl groups of each diphosphane ligand in **4** (see the Supporting Information). The molecules of **4** in the crystal structure are linked by intermolecular C–H $\cdots$  $\pi$  interactions (a C–H bond of a dpmp phenyl group with the nearest dpmp phenyl ring; closest H $\cdots$ C distances: 2.841 Å) to give 2D sheets.
- [14] Further decrease in temperature resulted in freezing of the CDCl<sub>3</sub> solvent, which, together with the poor solubility of **4** in other solvents, hampered NMR measurements at lower than –53 °C.
- [15] No molecules of **5** were observed in the crystal structure of **4**. The molecular symmetry of **4** (*C<sub>i</sub>*) and **5** (*C<sub>2h</sub>*) would result in the appearance of two singlets and one singlet, respectively, in their <sup>31</sup>P NMR spectra. The observation of only one singlet at 0 °C or above (see the Supporting Information) could arise from the rapid conformational changes depicted in Figure 3. Lowering the temperature to –40 °C causes the signals of **4** ( $\delta$  = 17.8, 14.7 ppm) and **5** ( $\delta$  = 17.0 ppm) to be resolved. The change from **4** to **5** can be effected by breaking the Au<sup>I</sup> $\cdots$ Au<sup>I</sup> interactions (note the longer Au<sup>I</sup> $\cdots$ Au<sup>I</sup> contact of 3.178(10) Å in **4** than that of 3.015(29)–3.040(29) Å in **3**), accompanied by intramolecular rotations to render the phenyl groups of each Ph<sub>2</sub>PC $\equiv$ CPPH<sub>2</sub> ligand in an eclipsed arrangement. Therefore, **5** should be energetically less favored than **4**, consistent with the increase in the amount of **4** but decrease in the amount of **5** upon lowering the temperature (see the Supporting Information).
- [16] a) C. F. Shaw III, *Chem. Rev.* **1999**, *99*, 2589; b) M. J. McKeage, L. Maharaj, S. J. Berners-Price, *Coord. Chem. Rev.* **2002**, *232*, 127.



DOI: 10.1002/anie.200600898

**First Evidence for a Uniquely Spin-Polarized Quartet Photoexcited State of a  $\pi$ -Conjugated Spin System Generated via the Ion-Pair State\*\****Yoshio Teki,\* Hirotaka Tamekuni, Jun Takeuchi, and Yozo Miura*

Switching of physical properties by external stimuli has attracted much attention in investigations on functional materials.<sup>[1]</sup> Manipulation of the magnetic properties of organic molecules in the spin ground state has been intensively studied by using electron-hole doping<sup>[2]</sup> and photochromic molecules.<sup>[3]</sup> Recently, photoswitching between diamagnetic and paramagnetic phases was realized in a 1,3,5-trithia-2,4,6-triazapentalenyl (TTTA) organic crystal.<sup>[4]</sup> Studying spin alignment in photoexcited states will give key knowledge for the photocontrol of magnetic properties. We have reported photoexcited quartet ( $S = 3/2$ ) and quintet ( $S = 2$ ) high-spin states of  $\pi$ -conjugated organic compounds<sup>[5–7]</sup> constructed from aromatic hydrocarbons and pendant stable radicals.  $\pi$ -Conjugated spin systems lead to robust spin alignment compared with other triplet/radical-pair systems ( $\sigma$ -bonded systems<sup>[8]</sup> and coordination complexes<sup>[9]</sup>). In the quintet state,<sup>[5,6]</sup> photoinduced spin alignment between two pendant radicals was achieved through the triplet excited state of a diphenylanthracene moiety, and exchange coupling between the two radicals changes from antiferromagnetic to ferromagnetic on photoexcitation. This example is the first of spin manipulation of  $\pi$  radicals in the photoexcited state.

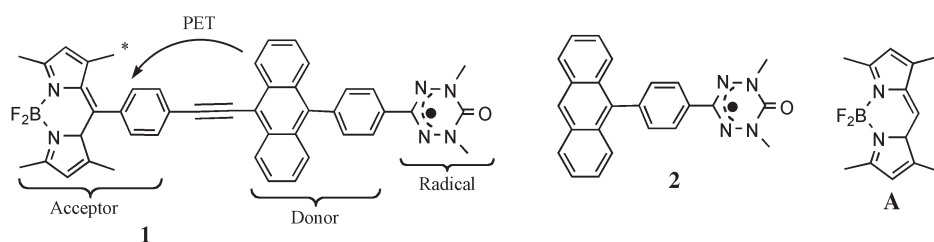
Coupling spin alignment to photoinduced electron transfer (PET) or energy transfer is the next important fundamental research target for the photocontrol of organic magnetism. As a model compound, we designed **1**, in which a 4,4-difluoro-4-bora-3a,4a-diaza-*s*-indacene (bodipy) acceptor moiety (A),<sup>[10]</sup> is covalently linked through an

[\*] Prof. Dr. Y. Teki, H. Tamekuni  
Department of Material Science  
Graduate School of Science  
Osaka City University  
3-3-138 Sugimoto, Sumiyoshi-ku, Osaka 558-8585 (Japan)  
Fax: (+81) 6-6605-2559  
E-mail: teki@sci.osaka-cu.ac.jp  
J. Takeuchi, Prof. Dr. Y. Miura  
Department of Applied Chemistry  
Graduate School of Engineering  
Osaka City University  
3-3-138 Sugimoto, Sumiyoshi-ku, Osaka 558-8585 (Japan)

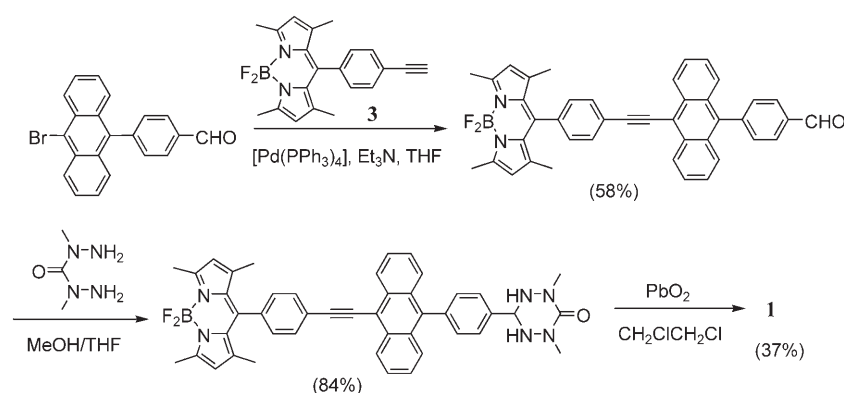
[\*\*] This work was supported by a Grant-in-Aid for Scientific Research on the General (No. 16350079) and Priority Area "Application of Molecular Spin" (Area 769, Prop. No. 15087208) from the Ministry of Education, Culture, Sports, Science and Technology (MEXT), Japan.



Supporting information for this article is available on the WWW under <http://www.angewandte.org> or from the author.



anthracene moiety, as a donor (D) to the verdazyl  $\pi$  radical (R).  $\pi$ -Conjugated system **2** (D–R) has a quartet ( $S = 3/2$ ) photoexcited state. The bodipy moiety is well known as an efficient through-bond energy acceptor for anthracene.<sup>[10]</sup> Herein, we present the first evidence of a uniquely spin-polarized quartet photoexcited state generated by a novel spin-polarization mechanism via the ion-pair state. Compound **1** was synthesized according to Scheme 1.<sup>[11]</sup>



**Scheme 1.** Synthesis of **1**.

The UV/Vis spectrum of a solution of **1** in toluene showed a sharp band at 505 nm (Figure 1) that arises from the acceptor A. This band overlaps with the weak  $n \rightarrow \pi$  transition of the verdazyl radical R. The absorption bands characteristic

of the anthracene moiety are red-shifted by about 40 nm relative to **2** (320–420 nm bands), indicative of an interaction between D and A. The oxidation potential of phenylanthracene is slightly higher than that of component A.<sup>[10]</sup> Thus, there is no charge transfer (CT) character in the ground state. However, if one-electron photoexcitation from the highest occupied molecular orbital (HOMO) of A is carried out, the orbital becomes lower in energy because the on-site Coulomb repulsion is removed. Therefore, A\* will act as an electron acceptor for D and PET occurs immediately in **1** through  $\pi$  conjugation. In the photoexcited state of **1**, the bodipy component will act as an “electron acceptor” (A\*) and the phenylanthracene moiety plays the role of an electron donor (D).

To learn more about the photoexcited state, we measured time-resolved electron spin resonance (TRESR) and pulsed ESR spectra synchronized to pulsed laser excitation. The TRESR spectrum of **1** (Figure 2a) was observed 0.3  $\mu$ s after laser excitation of the absorption band ( $\lambda = 505$  nm) of component A. Almost the same spectrum was obtained by excitation of the absorption band ( $\lambda = 447$  nm) of the anthracene moiety. The emission spectrum characteristic of bodipy (see the Supporting Information) was obtained by excitation of D as well as of component A. These findings show that efficient energy transfer occurs from the anthracene moiety D to A. The spin Hamiltonian parameters of **1** were determined to be  $S = 3/2$ ,  $g = 2.0035$ ,  $D = 0.0215$  cm<sup>−1</sup>, and  $E = 0.001$  cm<sup>−1</sup> by spectral simulation (Figure 2b), with the hybrid eigenfield/exact diagonalization method taking

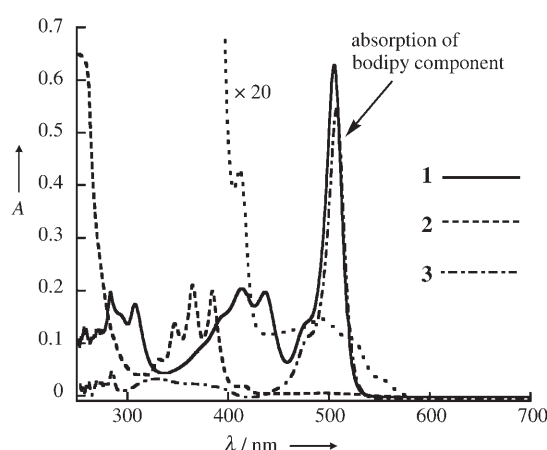


**Figure 1.** UV/Vis absorption spectra of solutions of **1** and **3** in toluene and **2**<sup>[6]</sup> in 2-methyltetrahydrofuran. The absorbance of **1** and **3** is not well-reproduced in the range 250–285 nm as a result of overlap with absorptions from the toluene solvent.

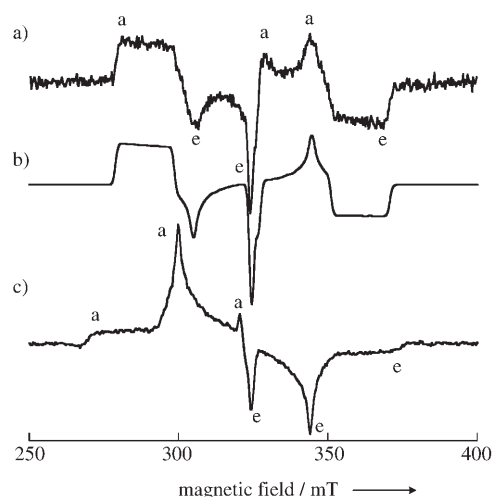


**Figure 2.** TRESR spectra of **1** and **2** at 30 K in glass matrices; a: absorptions; e: emissions of microwaves. a) Observed spectrum of **1**; b) simulation; c) observed spectrum of **2**.

dynamic electron polarization (DEP) into account.<sup>[12]</sup> This magnitude of  $D$  is about 7% smaller than that of **2**<sup>[6]</sup> and indicates delocalization of the unpaired electron toward acceptor moiety A. Comparison with the TRESR spectrum of **2** (Figure 2c) clearly shows that the DEP phase pattern of **1** (aeaaae) is different to that of **2** (aaaeae). This unique DEP is generated by attachment of the bodipy functional group.

To confirm the spin state, spin-echo-detected transient nutation (TN) spectroscopy<sup>[13]</sup> was carried out. Figure 3

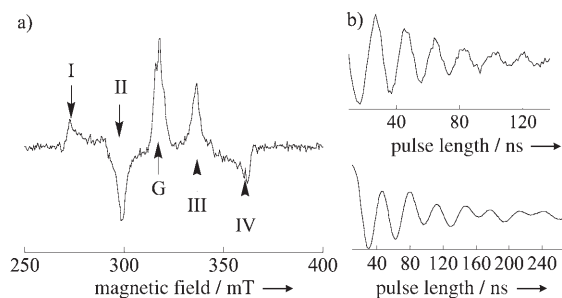


**Figure 3.** Pulsed ESR spectra of **1**. a) Echo-detected ESR spectrum; b) typical TN behavior (top: quartet signal at 337 mT; bottom: ground-state signal without photoexcitation).

depicts the echo-detected ESR spectrum observed 0.3  $\mu$ s after pulsed laser excitation and typical TN behavior of the photoexcited and ground states. The strong center signal is a superposition of the  $M_s = -1/2 \leftrightarrow +1/2$  transition arising from the ground and photoexcited states. Other signals come from the photoexcited state, as was confirmed by the spectrum without photoexcitation. The spectral pattern of the signals as a result of the photoexcited state is almost the same as that of the TRESR spectrum, in that all signals have similar phase-memory times and spin–lattice relaxation times.<sup>[7]</sup> Under the condition  $\omega_1 \ll \omega_{\text{ZFS}}$ , the TN frequency  $\omega_{\text{TN}}$  of the  $M_s \leftrightarrow (M_s + 1)$  transition is given by Equation (1),<sup>[13]</sup> where  $\omega_1 = g\beta B_1/\hbar$ ,

$$\omega_{\text{TN}} = \sqrt{S(S+1) - M_s(M_s+1)} \omega_1 \quad (1)$$

$\omega_{\text{ZFS}} = D/\hbar$ , and  $B_1$  is the microwave-field strength. Therefore, in the quartet state, the expected TN frequencies for  $M_s = \pm 1/2 \leftrightarrow \pm 3/2$  and  $M_s = -1/2 \leftrightarrow +1/2$  allowed transitions are  $\sqrt{3}\omega_1$  and  $2\omega_1$ , respectively. For the ground state,  $\omega_{\text{TN}}^{\text{G}}$  is equal to  $\omega_1$ , because **1** has a doublet ground state ( $S = 1/2$ ).

The observed ratios  $\omega_{\text{TN}}^{\text{EX}}/\omega_{\text{TN}}^{\text{G}}$  for each transition indicated in Figure 3 by arrows are close to  $\sqrt{3}$  (Table 1), which is expected for the ratio of the TN frequencies between the quartet and the doublet states. The TN experiments show unambiguously that all signals indicated by arrows are assigned to  $M_s = \pm 1/2 \leftrightarrow \pm 3/2$  transitions of the quartet state. The center signal attributed to  $M_s = -1/2 \leftrightarrow +1/2$  transitions showed a complicated TN behavior. Fourier transformation gave a power spectrum with multifrequencies,

**Table 1:** Ratios  $\omega_{\text{TN}}^{\text{EX}}/\omega_{\text{TN}}^{\text{G}}$  of TN frequencies of each transition of **1** (see Figure 3).

I	II	III	IV
1.75	1.66	1.76	1.74

which consist of  $2\omega_1$ ,  $\omega_1$ , and lower-frequency signals (possible off-resonance transition).

The quartet photoexcited states of triplet/radical pairs reported so far in the solid phase are formed by spin–orbit intersystem crossing (SO-ISC) of the parent triplet state,<sup>[8,9]</sup> or by enhanced SO-ISC by  $\pi$  conjugation with the pendant radical.<sup>[5–7]</sup> In such cases, the SO-ISC mechanism generates selective population of the zero-field (ZF) wave functions of the quartet spin states, thus leading to an A/E (aaaeae) or E/A (eeaeae) pattern. In contrast, for the two-spin system, it is well-known that the radical-pair (RP) mechanism<sup>[14]</sup> in solution leads to selective population of the high-field (HF) wave functions of the  $M_s$  sublevels by singlet–triplet mixing  $S \rightarrow T_0$  (or  $S \rightarrow T_{\pm 1}$ ). The DEP depends on the pathway that leads to the observed state. Thus, the DEP pattern gives evidence for the dynamic process generating the observed state. Spectral simulation (Figure 2b) was carried out by assuming selective population both for the ZF and HF wave functions (ZF/HF = 0.45:0.55). Judging from the resonance field, the central peak at 325 mT is a superposition of the polarized ground-state signal, which is included in the simulation (see the Supporting Information). Thus, a competition between SO-ISC and other mechanisms occurs in **1**. Similar competitions between SO-ISC and RP mechanisms have been observed only in the reaction centers of photosystems I and II<sup>[15]</sup> and in their model systems via the ion-pair (IP) state.<sup>[16]</sup>

We propose a model to understand the unique spin polarization of the quartet photoexcited state of **1**. Immediately after photoexcitation, component A reaches the singlet photoexcited state ( $S_1$ ). In this state, PET occurs immediately from D to A through the  $\pi$  conjugation in **1**<sup>[17]</sup> and leads to the charge-separated IP state  $A^{\cdot-} \cdots D^{\cdot+} \cdots R$ , in which  $A^{\cdot-}$  is the doublet state and ab initio MO calculations show that the cation of **2** ( $D^{\cdot+} \cdots R$ ) becomes the triplet ground state ( $|T\rangle$ ). In this charge-separated IP state, the electron spins of  $A^{\cdot-}$  and  $D^{\cdot+}$  are far apart and their exchange coupling is very weak (Figure 4). As a consequence, the wave functions of the doublet and quartet states are mixed as given in Equations (2).

$$\phi_1; |T_{+1}, \alpha\rangle = |Q_{3/2}\rangle \quad (2a)$$

$$\phi_2; |T_{+1}, \beta\rangle = \sqrt{\frac{1}{3}}|Q_{1/2}\rangle + \sqrt{\frac{2}{3}}|D_{1/2}\rangle \quad (2b)$$

$$\phi_3; |T_{0}, \alpha\rangle = \sqrt{\frac{2}{3}}|Q_{1/2}\rangle - \sqrt{\frac{1}{3}}|D_{1/2}\rangle \quad (2c)$$

$$\phi_4; |T_{0}, \beta\rangle = \sqrt{\frac{2}{3}}|Q_{-1/2}\rangle + \sqrt{\frac{1}{3}}|D_{-1/2}\rangle \quad (2d)$$

$$\phi_5; |T_{-1}, \alpha\rangle = \sqrt{\frac{1}{3}}|Q_{-1/2}\rangle - \sqrt{\frac{2}{3}}|D_{-1/2}\rangle \quad (2e)$$

$$\phi_6; |T_{-1}, \beta\rangle = |Q_{-3/2}\rangle \quad (2f)$$

The sublevels  $\phi_2$ – $\phi_5$  will be selectively populated, because the initial state generated by photoexcitation is the doublet excited state. During the charge-recombination process, these weakly coupled wave functions  $\phi_2$ – $\phi_5$  change to the strongly

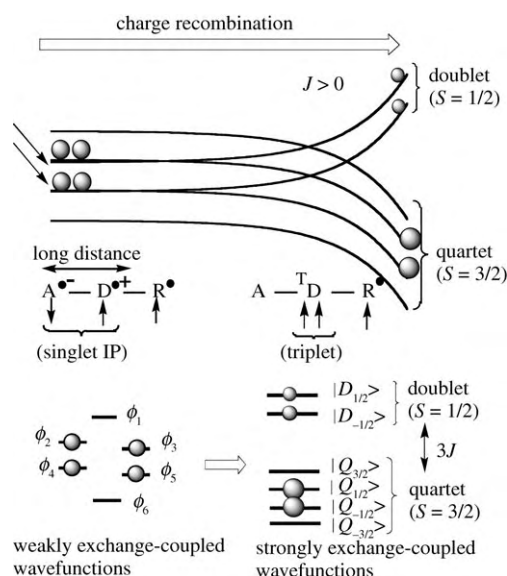


**Figure 4.** Mechanism of DEP generation in the quartet excited state of **1** through the IP state.  $J$  is the magnitude of the effective exchange coupling between unpaired electrons. The magnitude of population transfer from the weakly coupled wave functions to those of the pure quartet and doublet states depends on the duration of the charge-recombination process and the  $\Delta g$  value.

exchange-coupled pure doublet ( $|D_{\pm 1/2}\rangle$ ) and quartet wave functions ( $|Q_{\pm 1/2}\rangle$ ), thus leading to DEP (Figure 4). The ISC and the selective population (DEP) of the high-field wave functions of the quartet state are also expected to depend on D-Q mixing driven by the difference in  $g$  values  $\Delta g$  and in hyperfine interactions, similar to S- $T_0$  mixing of the triplet/radical pair. In other words, as a result of  $M_s$  conservation, population of the charge-separated IP state (left side of Figure 4) can selectively move to the  $M_s = \pm 1/2$  spin sublevels  $|D_{\pm 1/2}\rangle$  and  $|Q_{\pm 1/2}\rangle$  (right side of Figure 4), which leads to a non-Boltzmann population (DEP). This mechanism via the intramolecular doublet-triplet IP state will occur in the solid, liquid, and gas phases and compete with the enhanced SO-ISC mechanism derived from the pendant radical. Unfortunately, direct detection of the IP state by transient absorption spectroscopy was unsuccessful, because strong emission from the bodipy component masks the absorption band of the anthracene radical cation. However, the unique spin polarization pattern observed by both TRESR and pulsed ESR spectroscopy gives clear evidence of the IP state  $A^{\bullet-}D^{\bullet+}R$  as the photoexcited state. This observation is the first of a photoexcited quartet state generated through the IP state of an organic molecule with unpaired spins.

## Experimental Section

Optical, TRESR, and pulsed ESR measurements: UV/Vis spectra were measured on a JASCO V-570 spectrometer at room temperature. A conventional X-band ESR spectrometer (JEOL TE300) was used without field modulation in the TRESR measurements. Signals were amplified by a wide-band preamplifier, transferred to a high-speed digital oscilloscope (LeCroy 9350C), and accumulated for each point. Excitation of **1** was carried out at 505 nm with light from an optical parametric oscillator (OPO) system pumped by a YAG laser

(Continuum Surelite II-10 and Surelite OPO). The temperature was controlled by an Oxford ESR 910 cold He gas flow system. All TRESR and pulsed ESR experiments were carried out with toluene as the glass matrix or solvent. Samples were degassed by repeated freeze-pump-thaw cycles. The pulsed ESR measurements were performed on an X-band ESR spectrometer equipped with a pulsed microwave unit (JEOL ES-PX1150) and a high-speed digital oscilloscope (Tektronix TDS5034). The pulsed microwaves were amplified with a 1-kW traveling wave tube amplifier (TWTa). The Hahn  $\pi/2$ - $\tau$ - $\pi$  pulse sequence was used for spin-echo detection. The microwave pulse was synchronized with the laser excitation by using a delay-pulse generator (Stanford Research DG535). In the echo-detected nutation experiment, the first microwave pulse length was varied.

**Materials:** The stable radical **1** was synthesized according to the procedures shown in Scheme 1.<sup>[11]</sup> Compound **3** was prepared according to the literature method.<sup>[10]</sup> Other reagents were used as purchased. Column chromatography was performed on silica gel (Merk Silica 60) or alumina (Merk Alum. Ox. 60).

Received: March 8, 2006

Published online: June 22, 2006

**Keywords:** donor-acceptor systems · EPR spectroscopy · ion pairs · photochemistry · radicals

- [1] See: *Proceedings of the 9th International Conference on Molecule-based Magnets (Polyhedron* **2005**, *24*, 2063–2912).
- [2] A. Izuoka, M. Hiraishi, T. Abe, T. Sugawara, K. Sato, T. Takui, *J. Am. Chem. Soc.* **2000**, *122*, 3234.
- [3] a) K. Matsuda, M. Irie, *J. Am. Chem. Soc.* **2001**, *123*, 9896; b) K. Takayama, K. Matsuda, M. Irie, *Chem. Eur. J.* **2003**, *9*, 5605.
- [4] H. Matsuzaki, W. Fujita, K. Awaga, H. Okamoto, *Phys. Rev. Lett.* **2003**, *91*, 017403.
- [5] a) Y. Teki, S. Miyamoto, K. Iimura, M. Nakatsuji, Y. Miura, *J. Am. Chem. Soc.* **2000**, *122*, 984; b) Y. Teki, S. Miyamoto, K. Iimura, M. Nakatsuji, Y. Miura, *J. Am. Chem. Soc.* **2001**, *123*, 294.
- [6] Y. Teki, M. Nakatsuji, Y. Miura, *Mol. Phys.* **2002**, *100*, 1385.
- [7] Y. Teki, T. Toichi, S. Nakajima, *Chem. Eur. J.* **2006**, *12*, 2329, and references therein.
- [8] a) C. Corvaja, M. Maggini, M. Prato, G. Scorrano, M. Venzin, *J. Am. Chem. Soc.* **1995**, *117*, 8857; b) J. Fujiwara, Y. Iwasaki, Y. Ohba, S. Yamauchi, N. Koga, S. Karasawa, M. Fuhs, K. Möbius, S. Weber, *Appl. Magn. Reson.* **2001**, *21*, 483, and references therein.
- [9] a) K. Ishii, J. Fujiwara, Y. Ohba, S. Yamauchi, *J. Am. Chem. Soc.* **1996**, *118*, 13079; b) K. Ishii, Y. Hirose, N. Kobayashi, *J. Phys. Chem.* **1999**, *103*, 1986.
- [10] C. W. Wan, A. Burghart, J. Chen, F. Bergström, L. Joansson, M. F. Wolford, T. G. Kim, M. R. Topp, R. M. Hochstrasser, K. Burgess, *Chem. Eur. J.* **2003**, *9*, 4430.
- [11] **1**: Elemental analysis (%) calcd for  $C_{45}H_{36}BF_2N_6O$ : C 74.49, H 5.00, N 11.58; found: C 73.95, H 4.79, N 11.14; HRMS (FAB<sup>+</sup>, 3-NBA matrix):  $m/z$  calcd for  $[M]^+$ : 725.3012; found: 725.3007.
- [12] The details of the spectral simulation are similar to those described in reference [5b], with Equation (6) from reference [5b] being modified as follows:  $P_{MS} = w1 P_{M_s}^{zero\ field} + w2 P_{M_s}^{high\ field}$ ,  $w1 = 0.45$ , and  $w2 = 0.55$ , as described in the text.  $P_{M_s}^{zero\ field}$  is the expectation value of the density matrix, which represents the populations of the zero-field spin sublevels and  $P_{M_s}^{high\ field}$  is that of the high-field spin sublevels ( $|S, M_s\rangle$ ). The doublet ground state was independently simulated using the  $g$  value determined experimentally and superimposed to the quartet spectrum (see the Supporting Information). More details will be published in a full paper.



- [13] a) J. Isoya, H. Kanda, J. R. Norris, J. Tang, M. K. Bowman, *Phys. Rev. B* **1990**, *41*, 3905; b) A. V. Astashkin, A. Schweiger, *Chem. Phys. Lett.* **1990**, *174*, 595.
- [14] F. J. Adrian, *J. Chem. Phys.* **1974**, *54*, 3918.
- [15] H. Levanon, J. R. Norris, *Chem. Rev.* **1978**, *78*, 185.
- [16] a) K. Hasharoni, H. Levanon, S. R. Greenfield, D. J. Gosztola, W. A. Svec, M. R. Wasielewski, *J. Am. Chem. Soc.* **1995**, *117*, 8055; b) K. Hasharoni, H. Levanon, S. R. Greenfield, D. J. Gosztola, W. A. Svec, M. R. Wasielewski, *J. Am. Chem. Soc.* **1996**, *118*, 10228.
- [17] The  $\pi$  conjugation leads to the wavelength shift (ca. 40 nm) of the anthracene moiety in the absorption spectrum shown in Figure 1. The magnitude of the interaction between D and A is estimated to be about  $2300\text{ cm}^{-1}$  from the shift. Such a large interaction cannot be a through-space interaction. Therefore, it is clear that PET is a through-bond effect in this case.

## Catalyst Recycling

DOI: 10.1002/anie.200600862

**Biocatalytic Reaction And Recycling by Using CO<sub>2</sub>-Induced Organic–Aqueous Tunable Solvents\*\****James M. Broering, Elizabeth M. Hill, Jason P. Hallett, Charles L. Liotta, Charles A. Eckert, and Andreas S. Bommarius\**

Enzymes display high substrate specificity and can catalyze reactions that are not possible in a single step through

traditional synthesis.<sup>[1]</sup> In addition, biocatalysts usually function at relatively mild aqueous conditions with moderate temperature, pressure, and pH, and thus can allow for process routes that can potentially replace less environmentally friendly steps in chemical synthesis. The ability, or in many cases, the need to function in relatively mild reaction media can also limit the utility of biocatalysts. Many interesting, often prochiral, compounds are water insoluble and thus unavailable to biocatalytic conversion. Numerous schemes have been developed to use biocatalysts to transform water-insoluble substrates.<sup>[2]</sup> These schemes employ soluble and immobilized enzymes in simple one- and two-phase organic–aqueous mixtures or more-complex mixtures by using reversed micelles,<sup>[3]</sup> supercritical fluids, and ionic liquids.<sup>[4]</sup> Two-phase approaches, either liquid–liquid or solid–liquid (as in the case of immobilized enzymes), can suffer from reduced reaction rates owing to interphase mass-transfer limitations. Furthermore, immobilized enzymes are susceptible to activity loss owing to the immobilization process and leaching of the enzyme from the solid support. Monophasic systems can avoid these limitations; however, recovery and reuse of the biocatalyst, which is imperative for large-scale processes or the isolation of pharmaceutical products, is more challenging.

Herein, we demonstrate an approach to take advantage of the higher reaction rates of homogeneous biocatalysis while providing a simple method for biocatalyst recycling by using organic–aqueous tunable solvent (OATS) systems. OATS mixtures are engineered to couple a reaction and separation as shown in Figure 1. As in other latent biphasic systems,<sup>[5]</sup>

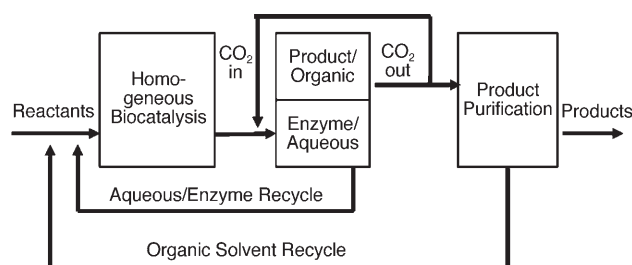


**Figure 1.** A Proposed OATS process for biocatalyst recycling.

OATS mixtures allow homogeneous reactions between hydrophobic and hydrophilic components, therefore eliminating mass-transfer limitations. CO<sub>2</sub> can be added to split the reaction mixture into a gas-expanded liquid organic phase containing hydrophobic components and an aqueous phase containing the hydrophilic catalyst<sup>[6,7]</sup> The CO<sub>2</sub>-induced separation allows for a one-pot reaction and separation scheme.

The successful application of CO<sub>2</sub> as a reversible switch to modulate miscibility of aqueous and organic phases and the phase-separation behavior for a number of OATS systems has previously been studied with solvents such as acetonitrile, THF, and dioxane.<sup>[6,7]</sup> Recent investigation of this miscibility switch as a vehicle for catalyst recovery was tested on the hydrophobic substrate 1-octene with a water-soluble Rh–triphenylphosphine tris-sulfonated salt (TPPTS) complex as the catalyst. The use of an OATS system increased the

[\*] J. M. Broering, Prof. A. S. Bommarius  
School of Chemical and Biomolecular Engineering  
Parker H. Petit Institute for Bioengineering and Bioscience  
Georgia Institute of Technology  
315 Ferst Drive, Atlanta, GA 30332-0363  
Fax: (+1) 404-894-2291  
E-mail: andreas.bommarius@chbe.gatech.edu

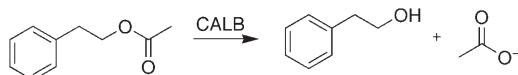
E. M. Hill, Dr. J. P. Hallett, Prof. C. L. Liotta, Prof. C. A. Eckert  
School of Chemical and Biomolecular Engineering  
Specialty Separations Center  
Georgia Institute of Technology  
311 Ferst Drive, Atlanta, GA 30332-0100  
Prof. C. L. Liotta, Prof. C. A. Eckert, Prof. A. S. Bommarius  
School of Chemistry and Biochemistry  
Specialty Separations Center  
Georgia Institute of Technology  
311 Ferst Drive, Atlanta, GA 30332-0100

[\*\*] We gratefully acknowledge the financial support of a National Science Foundation Graduate Fellowship (J.M.B.) and Dept. of Education GAANN fellowships (J.M.B. and E.M.H.). Additional funding was provided by the National Science Foundation (NSF-CTS-0328019) and the J. Erskine Love, Jr., Institute Chair in Engineering. We also thank David Rozzell (Biocatalytics, Pasadena, CA) for providing soluble CALB and helpful discussions, as well as Nazanin Ruppender and Stuart Terrett for assistance in the lab.

Supporting information for this article is available on the WWW under <http://www.angewandte.org> or from the author.

catalytic efficiency by a factor of 65 as compared to the industrially used aqueous biphasic system, which is limited by the substrate solubility.<sup>[8]</sup>

We tested the feasibility of OATS mixtures for biocatalytic reactions and separations with soluble *Candida antarctica* lipase B (CALB) (E.C. 3.1.1.3). This versatile enzyme has been used to catalyze esterifications of hydrophobic acids and alcohols as well as ester hydrolyses in a range of solvents<sup>[9]</sup> and supercritical CO<sub>2</sub>.<sup>[10]</sup> This therefore renders it an attractive choice for use in an OATS process. The hydrolysis of 2-phenethyl acetate (PEA) to 2-phenylethanol (2PE) and acetate (Scheme 1) was selected as a model reaction as both PEA and 2PE both have extremely low water solubility and can be easily detected with gas chromatography to assay the reaction progress.



**Scheme 1.** CALB test reaction.

An OATS process will be most effective when three requirements are met: 1) The use of an OATS mixture must provide acceptable enzyme reactivity in the reaction medium; 2) The biocatalyst must survive the CO<sub>2</sub>-pressurized separation process; 3) The biocatalyst should be retained in the aqueous phase and reaction products should partition favorably into the organic phase. Thus, the reactivity, pH stability, recycleability of the biocatalyst, and partitioning behavior of the substrate and product in a water–dioxane OATS mixture were tested. By satisfying these requirements, we have developed a system that allows 80% recovery of reaction products in the organic phase, and displays less than 10% apparent biocatalyst activity loss after recycling six times.

Enzymatic reaction rates in aqueous buffer–dioxane mixtures were evaluated to choose a suitable solvent composition for future recycling experiments (Figure 2). Since PEA is nearly insoluble in water, monophasic reaction rates in buffer alone are negligible. By taking advantage of the higher substrate solubility afforded by the addition of water-miscible organic solvents, higher specific reaction rates can be

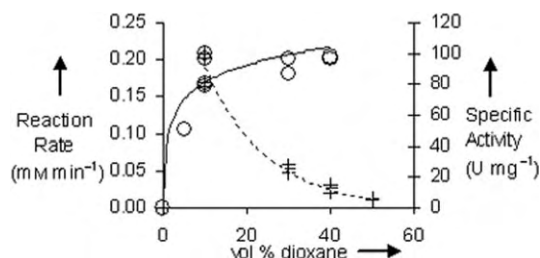


**Figure 2.** Monophasic reaction rates in dioxane OATS mixtures containing 8 mM (+) and near-saturating concentrations (O) of PEA (4, 8, 32, 56 mM for 5, 10, 30, 40% dioxane, respectively). Assumed trend lines for 8 mM (-----) and near-saturating PEA mixtures (—) have been added. Note that 8 mM PEA is also the near-saturation concentration in 10% dioxane mixtures. The specific reaction rates ( $\text{U mg}^{-1} = \mu\text{mol min}^{-1} \text{mg enzyme}^{-1}$ ) are shown on the secondary axis.

obtained than in purely aqueous solvent. Although the rates seen in 8 mM PEA in water–dioxane mixtures decreased as the dioxane content increased, the specific rate in water–dioxane mixtures that are nearly saturated with PEA substrate improved over the range of dioxane content tested owing to the higher substrate solubility (up to 56 mM PEA in 40% dioxane).

A 40% dioxane mixture was chosen for use in further experiments because this mixture provides increased substrate solubility and achieves the highest observable reaction rate. The 40% dioxane mixture is also favorable for the phase separation—upon CO<sub>2</sub> addition it provides a larger organic-phase volume to aid extraction of reaction products than lower dioxane levels, thus improving separation. At greater than 40% dioxane concentration, buffer precipitated out of solution and further study is needed to see if this lower buffer concentration can adequately maintain sufficiently high pH levels. The importance of adequately buffering the reaction mixture is discussed below.

To survive the CO<sub>2</sub>-pressurized separation process, the enzyme must withstand the pressure used for separation as well as the associated pH fluctuations. The pressure required to unfold enzymes ( $> 2000 \text{ bar}$ )<sup>[11]</sup> is one to two orders of magnitude higher than that required to separate OATS mixtures (10–50 bar), so it is unlikely that hydrostatic pressure alone will damage the enzyme. However, it is well documented that CO<sub>2</sub> addition to aqueous mixtures leads to a dramatic drop in solution pH owing to the formation of carbonic acid.<sup>[12]</sup> Such low pH values can have detrimental effects on enzyme activity and stability. We measured pH values of the aqueous phase of CO<sub>2</sub>-separated OATS mixtures as a function of CO<sub>2</sub> pressure by using a method similar to Holmes et al.,<sup>[13]</sup> as shown in Figure 3. In unbuffered

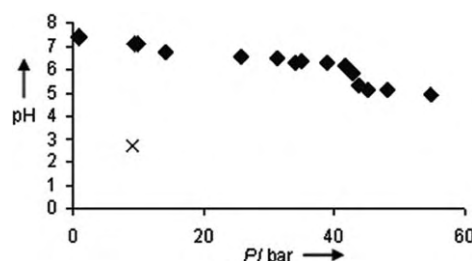


**Figure 3.** The pH of unbuffered (x) and buffered (150 mM phosphate buffer solution ( $\text{NaH}_2\text{PO}_4$ ) (♦) dioxane/water (30:70%) solutions

mixtures, the addition of 9.5 bar of CO<sub>2</sub> lowers the pH to below 3. With 150 mM sodium phosphate buffer solution in the aqueous component, the pH decreases only to  $\approx 5$  under 50 bar CO<sub>2</sub>. A similar result was also found in previous work.<sup>[13]</sup> As the typical time required to pressurize, mix, and separate OATS mixtures with CO<sub>2</sub> is approximately 30 min, the aqueous phase containing enzyme is exposed to pH 5 for a similar amount of time. Enzyme tolerance to low-pH exposure was tested by incubating CALB samples in buffered low-pH solutions and assaying for activity at pH 7 (see the Supporting Information). Even after 2 h of exposure to a solution of pH 4, CALB samples showed no loss in activity.

Clearly, use of 150 mM phosphate buffer solution is sufficient to prevent the pH of the pressurized aqueous phase from decreasing to low levels, and CALB is not detrimentally affected by short exposures to pH 5 that are encountered during phase separation.

As the addition of CO<sub>2</sub> and accumulation of acetate ions (a reaction product) can lower the pH value of the reaction mixture, CALB activity was tested in OATS mixtures with varying pH. As the reaction pH was reduced from 8.2 to 4.8, the conversions observed after two hours decreased from 55% to 40%, respectively. So to attain the highest possible reaction rates in OATS, the pH should be carefully controlled.

Having demonstrated improved reaction rates in dioxane–aqueous mixtures that were nearly saturated with substrate and the absence of adverse effects on CALB resulting from pH changes during separation, the feasibility of implementing a process with dioxane–OATS mixtures and CO<sub>2</sub> for separation and recycling of the homogeneous biocatalyst was tested in 40:60 dioxane/buffer (v/v) mixtures containing PEA. After two hours of reaction, CO<sub>2</sub> was added to separate the mixture. The organic layer was decanted under pressure, and after CO<sub>2</sub> was removed from the cell, the next cycle began by adding buffer solution and dioxane containing PEA (300 mM) to the remaining reaction mixture. The cycle time, from the beginning of one reaction to the next, averaged three hours. Two trials of six consecutive reactions and separations were conducted. In each trial, the reaction mixture remaining in the cell was left overnight after the fourth separation, and the fifth reaction was initiated the following morning by adding more buffer and PEA (300 mM) in dioxane. Exact experimental details can be found in the Supporting Information.

The observed conversion for each two-hour reaction of both trials is shown in Figure 4. Over the concentration ranges

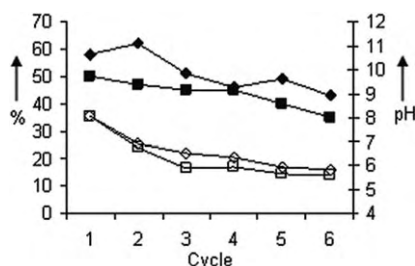


**Figure 4.** Conversions (◆, ■) and initial pH (◇, □) of recycled OATS reactions for trial A (◆) and trial B (■).

seen during the reactions, the CALB-catalyzed reaction in 40% dioxane mixtures is first order with respect to PEA concentration, with an apparent rate constant of 0.0067 min<sup>-1</sup>. This indicates that the enzyme kinetics are not substrate saturated at these concentrations (see the Supporting Information). With the given rate constant, a conversion of 55% is predicted for two hours of reaction, and the observed conversions for the first reaction of both trials are very close to this value (58% and 54%, respectively). Conversion of 100% is observed in both trials when the reaction mixture was allowed to stand overnight between reactions 4 and 5. An

overall process conversion (total moles of 2PE formed/total moles of PEA added) of 61% was obtained for both runs.

The conversion in each trial decreased by 10 to 15 percent by the sixth reaction, suggesting deactivation of CALB. However, since some enzyme is removed as the reactor contents are sampled, the total enzyme concentration in the reactor will be diluted as new solution is added to begin new cycles. This dilution accounts for 11 of the 15 percent of conversion lost by the sixth reaction. Furthermore, the pH of the reaction mixture decreased from 8 to 5.5 over six cycles (Figure 4). This was most likely owing to residual CO<sub>2</sub> that remains saturated in the OATS mixture following the initial separation and accumulation of acetate in the aqueous phase during successive runs. As discussed earlier, CALB reaction rates decrease by up to 20% when reducing the pH from 8 to 5; thus, the pH drift likely explains the remaining observed conversion loss, and better pH control should reduce this effect.

The concentration of PEA and 2PE in the separated organic and aqueous layers was measured as well as the concentration of water in the organic layer. The organic layer, in agreement with previous results, contained approximately 4 wt % water for all cycles.<sup>[6]</sup> The distribution of PEA and 2PE between the separated organic and aqueous phases in each cycle was measured in both trials and is shown in Figure 5.

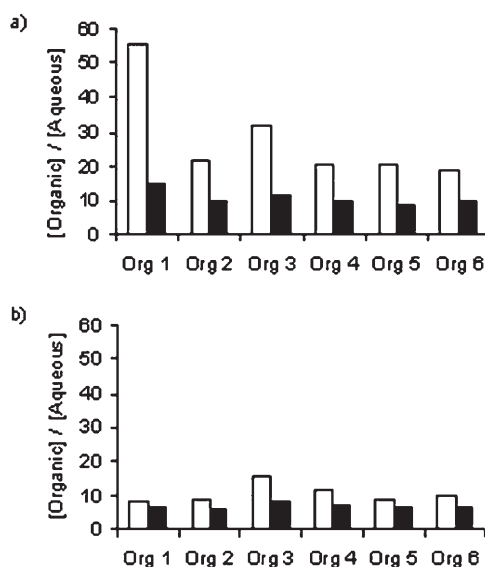


**Figure 5.** OATS distribution coefficients for recycling experiments beginning with 72 mM (A) and 52 mM PEA (B).

Distribution coefficients in trial A ranged between 20 and 55 for PEA and between 11 and 15 for the more hydrophilic 2PE. Trial B showed lower distribution coefficients for both PEA (8–16) and 2PE (6–9). A higher starting concentration of PEA was used in trial A (72 mM) as compared to trial B (56 mM); so it appears that the distributions may be concentration dependent. As 72 mM is above the solubility of PEA in 40% dioxane mixtures, it is likely that excess (insoluble) PEA partitions to the organic phase might explain the larger distribution coefficients for trial A. This and other factors



contributing to variability are currently being investigated. Regardless, the observed distribution coefficients are favorable and show that the separated organic phase can be used to extract product from the reaction mixture: we recovered 80 % of the 2PE product in the organic layer for both trials.

By addressing concerns of reactivity, enzyme stability in separated media, and favorable partitioning, a biocatalytic OATS scheme for processing hydrophobic substrates with product separation and biocatalyst recycling has been developed. Given a cycle time of three hours, 56 mM starting concentration for PEA in buffer–dioxane (40 %) OATS, and an average of 50 % conversion per cycle, we calculated a volumetric productivity, expressed by the space–time yield, of  $27.4 \text{ g L}^{-1} \text{ d}^{-1}$ . Even with an equivalent residence time of 2 h in the reactor and assuming a best case scenario of complete conversion, the space–time yield in a PEA-saturated (4 mM) dioxane (5 %) mixture cannot exceed  $5.9 \text{ g L}^{-1} \text{ d}^{-1}$ . This is almost five-times less than that observed in the OATS system. The space–time yield in pure buffer will be even lower as the substrate is nearly insoluble. Furthermore, we find that the enzyme can be recycled with very little activity loss between cycles. The activity loss observed is entirely due to dilution of the enzyme and pH decrease of the reaction medium. A larger reaction volume, decreased sampling, and improved pH control should minimize activity loss even further. Even better product recoveries could be obtained by using a reaction with more hydrophobic products.

Biocatalytic OATS reaction–separation schemes fulfill an identified need<sup>[14]</sup> to develop new options to meet current challenges in biochemical synthesis. By integrating reaction and separation, simpler and simultaneously more efficient processes with a reduced physical footprint can be designed. The work here shows, for the first time, that biocatalysis in OATS is feasible and can be an effective option for designing biocatalytic processes, especially when hydrophobic substrates are involved. This also opens the door to combining OATS with other biocatalysts and their array of unique chemistries to efficiently synthesize chiral products.

## Experimental Section

*Candida antarctica* lipase B (SOL-101) was a kind gift from Biocatalytics (Pasadena, CA) and was diluted 100 times by volume with 150 mM sodium phosphate buffer solution ( $\text{NaH}_2\text{PO}_4$ ; pH 7.12) before addition to reactions. Supercritical fluid chromatography (purity > 99.9999 %) grade  $\text{CO}_2$  was purchased from Airgas (Radnor, PA) and used without further purification.

OATS reaction mixtures containing the desired amount of dioxane (99 %, Sigma), PEA (99 %, Alfa Aesar), and 150 mM sodium phosphate were prepared and 1:100 diluted CALB was added in a ratio of 0.5 mL enzyme per 9.5 mL OATS mixture. 0.25 mL samples were removed periodically and immediately mixed 1:1 with a mixture of 1:1 glacial acetic acid/dioxane to quench the reaction. Reaction progress was followed by measuring the PEA and 2PE

content of samples by using an Agilent GC-FID with a DB17 column (Agilent model 6890).

Received: March 6, 2006

Published online: June 21, 2006

**Keywords:** catalyst recycling · enzyme catalysis · green chemistry · homogeneous catalysis

- [1] I. C. Cotterill, P. B. Cox, A. F. Drake, D. M. Legrand, E. J. Hutchinson, R. Latouche, R. B. Pettman, R. J. Pryce, S. M. Roberts, G. Ryback, V. Sik, J. O. Williams, *J. Chem. Soc. Perkin Trans. 1* **1991**, 3071; K. Miyamoto, H. Ohta, *J. Am. Chem. Soc.* **1990**, *112*, 4077; K. Matoishi, M. Ueda, K. Miyamoto, H. Ohta, *J. Mol. Catal. B* **2004**, *10*, 161; Y. Ijima, K. Matoishi, Y. Terao, N. Doi, H. Yanagawa, H. Ohta, *Chem. Commun.* **2005**, 877; G. DeSantis, K. Wong, B. Farwell, K. Chatman, Z. L. Zhu, G. Tomlinson, H. J. Huang, X. Q. Tan, L. Bibbs, P. Chen, K. Kretz, M. J. Burk, *J. Am. Chem. Soc.* **2003**, *125*, 11 476; P. Fernandes, A. Cruz, B. Angelova, H. M. Pinheiro, J. M. S. Cabral, *Enzyme Microb. Technol.* **2003**, *32*, 688.
- [2] A. M. Klivanov, *Curr. Opin. Biotechnol.* **2003**, *14*, 427; A. M. Klivanov, *Nature* **2001**, *409*, 241; A. M. Klivanov, *Trends Biochem. Sci.* **1989**, *14*, 141.
- [3] A. S. Bommaris, T. A. Hatton, D. I. C. Wang, *J. Am. Chem. Soc.* **1995**, *117*, 4515; J. W. Shield, H. D. Ferguson, A. S. Bommaris, T. A. Hatton, *Ind. Eng. Chem. Fundam.* **1986**, *25*, 603; C. M. L. Carvalho, J. M. S. Cabral, *Biochimie* **2000**, *82*, 1063; N. W. Fadnavis, A. Deshpande, *Curr. Org. Chem.* **2002**, *6*, 393.
- [4] R. A. Sheldon, *Green Chem.* **2005**, *7*, 267; F. van Rantwijk, R. M. Lau, R. A. Sheldon, *Trends Biotechnol.* **2003**, *21*, 131.
- [5] D. E. Bergbreiter, P. L. Osburn, T. Smith, C. M. Li, J. D. Frels, *J. Am. Chem. Soc.* **2003**, *125*, 6254.
- [6] M. J. Lazzaroni, D. Bush, R. Jones, J. P. Hallett, C. L. Liotta, C. A. Eckert, *Fluid Phase Equilib.* **2004**, *224*, 143.
- [7] J. Lu, J. Lazzaroni, J. P. Hallett, A. S. Bommaris, C. L. Liotta, C. A. Eckert, *Ind. Eng. Chem. Res.* **2004**, *43*, 1586.
- [8] R. Jones, PhD thesis, Georgia Institute of Technology, Atlanta, GA, **2005**.
- [9] F. Secundo, G. Carrea, C. Soregaroli, D. Varinelli, R. Morrone, *Biotechnol. Bioeng.* **2001**, *73*, 157; M. C. Parker, S. A. Brown, L. Robertson, N. J. Turner, *Chem. Commun.* **1998**, 2247; C. Orrenius, T. Norin, K. Hult, G. Carrea, *Tetrahedron: Asymmetry* **1995**, *6*, 3023.
- [10] M. C. Almeida, R. Ruivo, C. Maia, L. Freire, T. C. de Sampaio, S. Barreiros, *Enzyme Microb. Technol.* **1998**, *22*, 494; N. N. Gandhi, N. S. Patil, S. B. Sawant, J. B. Joshi, P. P. Wangikar, D. Mukesh, *Catal. Rev. Sci. Eng.* **2000**, *42*, 439; P. Lozano, T. de Diego, D. Carrie, M. Vaultier, J. L. Iborra, *Chem. Commun.* **2002**, 692; D. Wiktelius, M. J. Johansson, K. Luthman, N. Kann, *Org. Lett.* **2005**, *7*, 4991.
- [11] T. W. Randolph, M. Seefeldt, J. F. Carpenter, *Biochim. Biophys. Acta* **2002**, *1595*, 224.
- [12] K. L. Toews, R. M. Shroll, C. M. Wai, N. G. Smart, *Anal. Chem.* **1995**, *67*, 4040; K. N. West, C. Wheeler, J. P. McCarney, K. N. Griffith, D. Bush, C. L. Liotta, C. A. Eckert, *J. Phys. Chem. A* **2001**, *105*, 3947.
- [13] J. D. Holmes, K. J. Ziegler, M. Audriani, C. T. Lee, P. A. Bhargava, D. C. Steytler, K. P. Johnston, *J. Phys. Chem. B* **1999**, *103*, 5703.
- [14] R. D. Noble, R. Agrawal, *Ind. Eng. Chem. Res.* **2005**, *44*, 2887.

# Rhenium Trichloride Dioxide, $\text{ReO}_2\text{Cl}_3$ \*\*

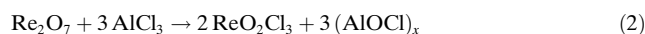
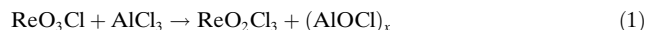
Joanna Supel and Konrad Seppelt\*

Rhenium(VII) is widespread, for example, in  $\text{ReO}_4^-$  and  $\text{ReF}_7$ . Of the binary rhenium chlorides, the highest is  $\text{ReCl}_5$ ; a postulated  $\text{ReCl}_6$  was also revealed to be  $\text{ReCl}_5$ .<sup>[1,2]</sup> However, hexavalent rhenium is found in  $\text{ReOCl}_4$ .<sup>[3]</sup> The only known rhenium(VII)–chlorine compound is  $\text{ReO}_3\text{Cl}$ , which can be prepared in several ways and in large quantities.<sup>[4,5]</sup> A compound richer in chlorine would be  $\text{ReO}_2\text{Cl}_3$ ; interestingly, no examples of chloride oxides of composition  $\text{AO}_2\text{Cl}_3$  (A = nonmetal or metal) have yet been reported. In contrast, several of the corresponding oxide fluorides  $\text{AO}_2\text{F}_3$  (A = Cl, I, Re, Os, Tc) have been described.

In the 1930s, attempts were made to prepare  $\text{ReO}_2\text{Cl}_3$  (for example, through the reaction of rhenium with  $\text{O}_2$  and  $\text{Cl}_2$ )<sup>[6]</sup>; however, they are now known to have been unsuccessful. The properties of the product obtained at that time are not consistent with those of  $\text{ReO}_2\text{Cl}_3$ , presented herein. We were also unable to confirm the results of a 1974 publication, in which the isolation of  $\text{ReO}_2\text{Cl}_3$  by vacuum sublimation from the reaction of  $\text{ReO}_3\text{Cl}$  with  $\text{ReOCl}_4$ ,  $\text{WOCl}_4$ , or  $\text{MoOCl}_4$  was reported.<sup>[7]</sup> We attempted to reproduce the most promising reaction, that of  $\text{ReO}_3\text{Cl}$  with  $\text{WOCl}_4$ , and did indeed obtain a red-brown sublimate, as previously described. However, this product was unambiguously characterized as  $\text{ReO}_3\text{Cl} \cdot \text{ReOCl}_4$  by single-crystal X-ray diffraction.<sup>[8,9]</sup> The reaction conditions, namely heating at 100 or 180 °C for several hours, are also inconsistent with the thermal properties of our  $\text{ReO}_2\text{Cl}_3$ , which decomposes at lower temperatures.

In attempts to produce a largely uncoordinated  $\text{ReO}_3^+$  ion by chloride-ion abstraction from  $\text{ReO}_3\text{Cl}$ , we treated  $\text{ReO}_3\text{Cl}$  with  $\text{AlCl}_3$  [Eq. (1)]. This reaction was already tried in 1979, but only the adduct  $\text{ReO}_3\text{Cl} \cdot \text{AlCl}_3$  was identified by elemental analysis at that time.<sup>[10]</sup> We observed a slow reaction at room temperature in  $\text{CFCl}_3$ , with the formation of an orange-colored solution of  $\text{ReO}_2\text{Cl}_3$  ( $\text{ReO}_3\text{Cl}$  is colorless, and  $\text{AlCl}_3$  is nearly insoluble). At elevated temperatures,  $\text{ReOCl}_4$  is formed, as evidenced by the intense dark red color of the solution. Alternatively,  $\text{Re}_2\text{O}_7$  can be treated with  $\text{AlCl}_3$  to produce  $\text{ReO}_2\text{Cl}_3$  [Eq. (2)]. Moreover, the use of  $\text{BCl}_3$  instead of  $\text{AlCl}_3$  is advantageous, as the reaction proceeds homogeneously without solvent, and  $\text{ReO}_2\text{Cl}_3$  can be recrystallized

directly from the excess  $\text{BCl}_3$  [Eq. (3)]. The orange-colored product solutions contain  $\text{ReO}_2\text{Cl}_3$ , as well as small amounts of  $\text{ReOCl}_4$ . Purification can be accomplished by fractional crystallization.



The large orange crystals of  $\text{ReO}_2\text{Cl}_3$  are easily distinguished from the dark red needles of  $\text{ReOCl}_4$  and its adducts, and from the colorless platelets of  $\text{ReO}_3\text{Cl}$ . According to the single-crystal structure determination,  $\text{ReO}_2\text{Cl}_3$  is composed of cyclic chlorine-bridged  $\{\text{ReO}_2\text{Cl}_3\}_2$  dimers with nearly perfect  $D_{2h}$  symmetry (Figure 1). The *cis* orientation of the

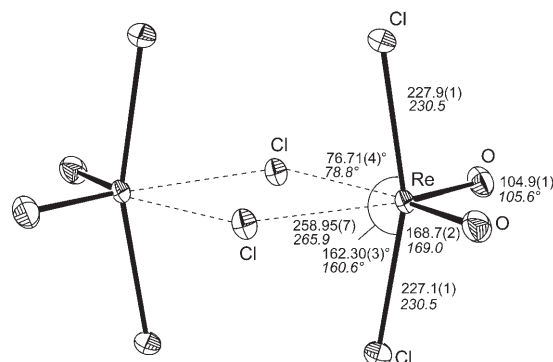


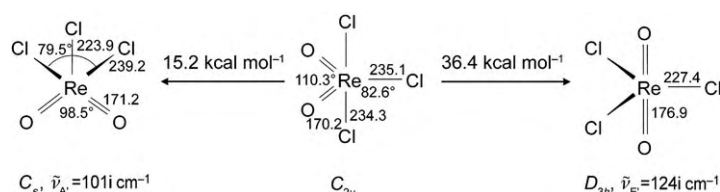
**Figure 1.** Molecular structure of  $\text{ReO}_2\text{Cl}_3$  (ORTEP representation, with thermal ellipsoids set at 50% probability). Selected interatomic distances [pm] and angles [°], along with their calculated values (italics), are indicated.

two double-bonded oxygen atoms at each rhenium center is typical for dioxo compounds of transition metals. Terminal chlorine atoms complete the (distorted) octahedral environments of the rhenium atoms. The melting point of 35–38 °C is reached without decomposition. Further heating results in decomposition and dark coloring. A congruent boiling point is not observed. Upon longer storage at room temperature, progressively more  $\text{ReOCl}_4$  is formed.

The vibrational spectra of the solid are in accord with the  $D_{2h}$  molecular structure and, thus, with the mutual exclusion rule. The structure and vibrational spectra of  $\text{ReO}_2\text{Cl}_3$  can be reproduced well with a density functional theory (DFT) calculation.<sup>[11]</sup> If the calculated energy values are assumed to be similarly trustworthy, an energy of dimerization of  $\Delta H = -0.3 \text{ kcal mol}^{-1}$  is obtained for the equilibrium  $2 \text{ReO}_2\text{Cl}_3 (C_s) \rightleftharpoons \text{Re}_2\text{O}_4\text{Cl}_6 (D_{2h})$ . This low value indicates that the monomer could be observed as well. Indeed, the compound seems to be monomeric in  $\text{CCl}_4$  or  $\text{Cl}_2$  solutions, as the Raman spectra of dissolved  $\text{ReO}_2\text{Cl}_3$  are considerably different from that of the solid. The calculated structure of monomeric  $\text{ReO}_2\text{Cl}_3$  is trigonal bipyramidal, with the double-bonded oxygen atoms in equatorial positions (Scheme 1). A square-pyramidal structure, and a trigonal-bipyramidal structure with the double-bonded oxygen atoms in the axial

[\*] Dipl.-Chem. J. Supel, Prof. Dr. K. Seppelt  
FB Bio/Chem/Pharm, Institut für Chemie  
Anorganische und Analytische Chemie  
Freie Universität Berlin  
Fabeckstrasse 34–36, 14195 Berlin (Germany)  
Fax: (+49) 30-8385-3310  
E-mail: seppelt@chemie.fu-berlin.de

[\*\*] We thank the Deutsche Forschungsgemeinschaft and the Fonds der Chemischen Industrie for financial support.



**Scheme 1.** Calculated structures of monomeric  $\text{ReO}_2\text{Cl}_3$ . Selected interatomic distances [pm] and angles [°] are indicated.

positions are transition states with considerably higher energies.

In the presence of small amounts of water, the monohydrate  $\text{ReO}_2\text{Cl}_3 \cdot \text{H}_2\text{O}$  is formed (Figure 2). The ability to

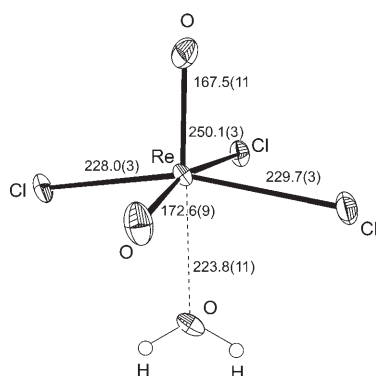


**Figure 2.** Molecular structure of the hydrate  $\text{ReO}_2\text{Cl}_3 \cdot \text{H}_2\text{O}$  (ORTEP representation, with thermal ellipsoids set at 50% probability). Hydrogen atoms are in assumed positions. Selected interatomic distances [pm] are indicated.

form a detectable hydrate, in spite of hydrolytic sensitivity, is common to  $\text{ReO}_2\text{Cl}_3$  and  $\text{ReOCl}_4$ .<sup>[12]</sup> If the reaction temperature is too high, a large amount of  $\text{ReOCl}_4$  is produced as a byproduct, and the adduct  $\text{ReO}_2\text{Cl}_3 \cdot \text{ReOCl}_4$  crystallizes. This adduct also contains a  $\{\text{ReO}_2\text{Cl}_3\}_2$  dimer, in this case with slightly asymmetric chlorine bridges (Figure 3). Two  $\{\text{ReOCl}_4\}$  molecules are coordinated by oxygen atoms from the dimer to form a  $\{\text{ReO}_3\text{Cl} \cdot \text{ReOCl}_4\}_2$  tetramer.

A preference for a coordination number of 6 is often observed in oxide halides of the transition metals, especially in the oxide fluorides:  $\text{ReO}_2\text{F}_3$  exists as a fluorine-bridged

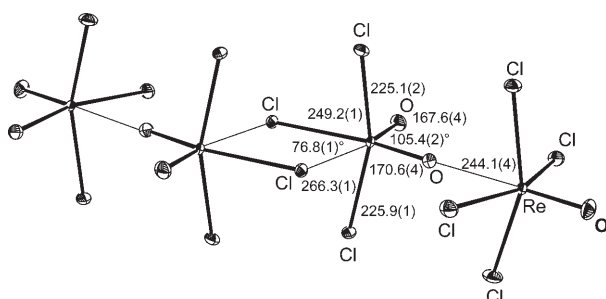


**Figure 3.** Molecular structure of the adduct  $\text{ReO}_2\text{Cl}_3 \cdot \text{ReOCl}_4$  (ORTEP representation, with thermal ellipsoids set at 50% probability). Selected interatomic distances [pm] and angles [°] are indicated.

polymer, and also as cyclic fluorine-bridged trimers and tetramers;<sup>[13,14]</sup> in  $\text{ReO}_3\text{F}$ , the rhenium atoms reach a coordination number of 6 through oxygen and fluorine bridges.<sup>[14]</sup> It is anticipated that  $\text{ReO}_2\text{Cl}_3$  can be transformed into a  $\text{ReO}_2\text{Cl}_2^+$  cation and a  $\text{cis-ReO}_2\text{Cl}_4^-$  anion.

## Experimental Section

$\text{ReO}_2\text{Cl}_3$ : a)  $\text{ReO}_3\text{Cl}$  (1 mmol, 270 mg), prepared according to reference [4], was combined with excess  $\text{AlCl}_3$  (10–15 mmol, 1.3–2 mg). Upon mixing, the color of the solution changed to orange. After 30 min, the components that are volatile at room temperature were transferred under dynamic vacuum into a trap at  $-196^\circ\text{C}$ .  $\text{CFCl}_3$  (3 mL) was then condensed onto the mixture. By slowly cooling the solution to  $-78^\circ\text{C}$ , large orange crystals of  $\text{ReO}_2\text{Cl}_3$  (ca. 100 mg, 31%) were obtained, which could be easily separated from unreacted  $\text{ReO}_3\text{Cl}$  (colorless platelets) and  $\text{ReOCl}_4$  (dark red needles). M.p.  $35\text{--}38^\circ\text{C}$ , with color change to red. Elemental analysis (%) found for  $\text{ReO}_2\text{Cl}_3$ : Cl 32.95; calcd: 32.74. b)  $\text{Re}_2\text{O}_7$  and  $\text{AlCl}_3$  were mixed in the molar ratio 1:15 and shaken at room temperature. The product was isolated as described above, but with poorer yield and purity. c)  $\text{ReO}_3\text{Cl}$  (0.55 mmol, 150 mg) and  $\text{BCl}_3$  (256 mmol, 3 g; free of HCl) were condensed into a glass ampoule. The mixture was briefly warmed and mixed at room temperature. Slow cooling of the red-green  $\text{BCl}_3$  solution to  $-60^\circ\text{C}$  afforded orange crystals of  $\text{ReO}_2\text{Cl}_3$  (175 mg, 97%). Longer reaction times and the presence of HCl led to the formation of  $\text{ReOCl}_4$ , which crystallizes as red needles that are easily distinguished from  $\text{ReO}_2\text{Cl}_3$ .

IR (solid, NaCl, polyethylene):  $\tilde{\nu} = 964.1$  (m),  $934.9$  (s),  $371$   $\text{cm}^{-1}$  (s, br); calculated values:<sup>[11]</sup>  $\tilde{\nu} = 1013.6$  (228),  $993.3$  (206),  $371.5$  (125),  $365.1$  (9.6),  $348.7$   $\text{cm}^{-1}$  (1.6), and eight other absorptions in the range  $278\text{--}76$   $\text{cm}^{-1}$ . Raman (solid):  $\tilde{\nu} = 979$  (100),  $948$  (40),  $385$  (95),  $357$  (30),  $283$  (45),  $261$  (90),  $255$  (sh),  $180$  (sh),  $164$  (25),  $123$  (45),  $105$  (10),  $82$   $\text{cm}^{-1}$  (14); calculated values:  $\tilde{\nu} = 1016.5$  (136),  $981.9$  (76),  $366.3$  (24.4),  $356.1$  (0.7),  $348.7$  (27.2),  $266$  (24.5),  $246.6$  (5.4),  $245.6$  (0.1),  $175.1$  (0.14),  $149.4$  (9.7),  $122.7$  (4.5),  $107.2$  (2.1),  $90.5$  (1.1),  $46.9$   $\text{cm}^{-1}$  (0.26). Raman ( $\text{Cl}_2$  solution):  $\tilde{\nu} = 1000$  (40, p),  $950$  (5, dp),  $539$ ,  $546$  ( $\text{Cl}_2$ ),  $400$  (100, p),  $338$  (20, p),  $309$  (10, dp),  $264$  (30, dp),  $215$  (2, dp),  $195$  (15, dp),  $158$   $\text{cm}^{-1}$  (30, p); calculated values:  $\tilde{\nu} = 1016.7$  (48.3, p),  $982.2$  (14.3, dp),  $381.8$  (20.8, p),  $354.4$  (0.0, dp),  $321.1$  (9.3, p),  $292.5$  (8.1, p),  $272.7$  (7.5, dp),  $263.9$  (9.1, dp),  $213.2$  (0.2, dp),  $191$  (1.7, dp),  $145.7$  (4.0, p),  $36.5$   $\text{cm}^{-1}$  (1.3, dp). MS: most abundant fragment at  $m/z = 308$  [ $^{187}\text{Re}^{35}\text{Cl}_3\text{O}]^+$ , as well as isotopomers of  $^{185/187}\text{Re}$  and  $^{35/37}\text{Cl}$ .

Crystal structures: crystals were mounted at  $-100^\circ\text{C}$  on a Smart CCD diffractometer; full spheres of data were collected, 1800 frames separated by  $\Delta\omega = 0.3^\circ$ ; the structures were solved and refined with the SHELX programs.<sup>[15]</sup>  $\text{ReO}_2\text{Cl}_3$ : orange crystal;  $2\theta_{\text{max}} = 61^\circ$ , 8385 measured, 822 independent reflections;  $a = 797.3(1)$ ,  $b = 813.2(1)$ ,  $c = 774.1(1)$  pm,  $Pnmm$ ,  $Z = 4$ ,  $R = 0.014$ ,  $wR_2 = 0.039$ .  $\text{ReO}_2\text{Cl}_3 \cdot \text{H}_2\text{O}$ : brown needle;  $2\theta_{\text{max}} = 61.0^\circ$ , 3459 measured, 1657 independent reflections;  $a = 543.4(2)$ ,  $b = 616.9(2)$ ,  $c = 944.5$  pm,  $\alpha = 93.42(1)$ ,  $\beta = 104.39(1)$ ,  $\gamma = 98.0(1)^\circ$ ,  $P\bar{1}$ ,  $Z = 2$ ,  $R = 0.067$ ,  $wR_2 = 0.166$ .  $\text{ReO}_2\text{Cl}_3 \cdot \text{ReOCl}_4$ : black needle;  $2\theta_{\text{max}} = 83.6^\circ$ , 29579 measured, 7210 independent reflections;  $a = 615.7(1)$ ,  $b = 1087.7(1)$ ,  $c = 1617.0(2)$  pm,  $\beta = 94.939(4)^\circ$ ,  $P2_1/n$ ,  $Z = 4$ ,  $R = 0.048$ ,  $wR_2 = 0.097$ . Further details on the crystal structure investigations may be obtained from the Fachinformationszentrum Karlsruhe, 76344 Eggenstein-Leopoldshafen, Germany (fax: (+49)7247-808-666; e-mail: crysdata@fiz-karlsruhe.de), on quoting the depository numbers CSD-416056 ( $\text{ReO}_2\text{Cl}_3$ ), CSD-416057 ( $\text{ReO}_2\text{Cl}_3 \cdot \text{H}_2\text{O}$ ), CSD-416053 ( $\text{ReO}_2\text{Cl}_3 \cdot \text{ReOCl}_4$ ), and CSD-416429 ( $\text{ReO}_3\text{Cl} \cdot \text{ReOCl}_4$ ,  $P\bar{1}$ ).

Received: December 16, 2005

Revised: March 16, 2006

Published online: June 21, 2006

**Keywords:** rhenium oxide halides · rhenium · structure elucidation · synthetic methods

- [1] J. H. Canterford, A. B. Wagh, *Inorg. Nucl. Chem. Lett.* **1971**, 7, 395–399; R. Colton, *Nature* **1962**, 194, 374–375; D. Brown, R. Colton, *J. Chem. Soc.* **1964**, 714–717.
- [2] J. Burgess, C. J. Fraser, I. Haigh, R. D. Peacock, *J. Chem. Soc. Dalton Trans.* **1973**, 501–504; C. J. L. Lock, A. Guest, *Can. J. Chem.* **1971**, 49, 603–610.
- [3] A. Brukl, K. Ziegler, *Ber. Dtsch. Chem. Ges.* **1932**, 65, 916–918.
- [4] K. Dehnicke, W. Liese, *Chem. Ber.* **1977**, 110, 3959–3960.
- [5] W. A. Herrmann, R. M. Kratzer, R. W. Fischer, *Angew. Chem.* **1997**, 109, 2767–2768; *Angew. Chem. Int. Ed. Engl.* **1997**, 36, 2652–2654; W. A. Herrmann, F. E. Kühn, C. C. Romão, M. Kleine, J. Mink, *Chem. Ber.* **1994**, 127, 47–54.
- [6] H. V. A. Brisco, P. L. Robinson, A. J. Rudge, *J. Chem. Soc.* **1932**, 1104–1107.
- [7] I. A. Glukhov, N. A. El'manova, S. S. Eliseev, M. T. Temurova, *Zh. Neorg. Khim.* **1974**, 19, 314–318; M. T. Temurova, N. A. El'manova, R. A. Bukharizoda, *Dokl. Akad. Nauk Tadzh. SSR* **1990**, 33, 176–179; A. M. Makhmadmurodov, M. T. Temurova, N. A. El'manova, I. A. Glukhov, *Dokl. Akad. Nauk Tadzh.* **1982**, 25, 225–227.
- [8] Crystal structures of  $\text{ReO}_3\text{Cl}\cdot\text{ReOCl}_4$ :  $a = 576.7(1)$ ,  $b = 593.4(1)$ ,  $c = 773.9(1)$  pm,  $\alpha = 70.159(3)$ ,  $\beta = 79.918(3)$ ,  $\gamma = 85.225(3)^\circ$ ,  $P1$ ,  $Z = 1$ ,  $-100^\circ\text{C}$ ,  $R = 0.049$ ,  $wR_2 = 0.11$ , Flack parameter = 0.047(23). This structure is equivalent to that published in reference [9] ( $a = 578$ ,  $b = 602$ ,  $c = 779.2$  pm,  $\alpha = 70.268$ ,  $\beta = 79.669$ ,  $\gamma = 84.99^\circ$ ,<sup>[9a]</sup> after transformation by (100 0-10 0-1-1)). The compound also exists in a centrosymmetric form:  $a = 521.2(1)$ ,  $b = 876.9(1)$ ,  $c = 1100.2(1)$  pm,  $\alpha = 67.774(4)$ ,  $\beta = 81.311(4)$ ,  $\gamma = 79.973(5)^\circ$ ,  $P\bar{1}$ ,  $Z = 2$ ,  $-100^\circ\text{C}$ ,  $R = 0.023$ ,  $wR_2 = 0.054$ .
- [9] a) A. J. Edwards, *J. Chem. Soc. Dalton Trans.* **1976**, 2419–2421; b) K. I. Petrov, V. V. Kravchenko, D. V. Drobot, V. A. Aleksandrova, *Zh. Neorg. Khim.* **1971**, 16, 1749–1750; c) D. V. Drobot, B. G. Korshunov, V. A. Aleksandrova, *Zh. Neorg. Khim.* **1971**, 16, 2295–2298.
- [10] R. Lössberg, K. Dehnicke, *Z. Naturforsch. B* **1979**, 34, 1040–1041.
- [11] Calculation methods: B3LYP functional; effective core potential (ECP) and a 6s5p3d valence basis set from the Institut für Theoretische Chemie der Universität Stuttgart, were used for the rhenium atoms; 6-31 + G(d,p) basis sets, as implemented in the program Gaussian, were used for the chlorine and oxygen atoms; Gaussian03, Revision B.04, M. J. Frisch, G. W. Trucks, H. B. Schlegel, G. E. Scuseria, M. A. Robb, J. R. Cheeseman, J. A. Montgomery, Jr., T. Vreven, K. N. Kudin, J. C. Burant, J. M. Millam, S. S. Iyengar, J. Tomasi, V. Barone, B. Mennucci, M. Cossi, G. Scalmani, N. Rega, G. A. Petersson, H. Nakatsuji, M. Hada, M. Ehara, K. Toyota, R. Fukuda, J. Hasegawa, M. Ishida, T. Nakajima, Y. Honda, O. Kitao, H. Nakai, M. Klene, X. Li, J. E. Knox, H. P. Hratchian, J. B. Cross, C. Adamo, J. Jaramillo, R. Gomperts, R. E. Stratmann, O. Yazyev, A. J. Austin, R. Cammi, C. Pomelli, J. W. Ochterski, P. Y. Ayala, K. Morokuma, G. A. Voth, P. Salvador, J. J. Dannenberg, V. G. Zakrzewski, S. Dapprich, A. D. Daniels, M. C. Strain, O. Farkas, D. K. Malick, A. D. Rabuck, K. Raghavachari, J. B. Foresman, J. V. Ortiz, Q. Cui, A. G. Baboul, S. Clifford, J. Cioslowski, B. B. Stefanov, G. Liu, A. Liashenko, P. Piskorz, I. Komaromi, R. L. Martin, D. J. Fox, T. Keith, M. A. Al-Laham, C. Y. Peng, A. Nanayakkara, M. Challacombe, P. M. W. Gill, B. Johnson, W. Chen, M. W. Wong, C. Gonzalez, J. A. Pople, Gaussian, Inc., Pittsburgh, PA, **2003**.
- [12] P. W. Fraiss, C. J. L. Lock, *Can. J. Chem.* **1972**, 50, 1811–1818.
- [13] N. Le Blond, G. Schrobilgen, *Inorg. Chem.* **2001**, 40, 1245–1249.
- [14] J. Supel, R. Marx, K. Seppelt, *Z. Anorg. Allg. Chem.* **2005**, 631, 2979–2986.
- [15] G. M. Sheldrick, SHELXS-86, Program for crystal structure solution, Universität Göttingen, **1986**; G. M. Sheldrick, SHELXS-97, Program for crystal structure solution, Universität Göttingen, **1997**.



## C–H Activation

DOI: 10.1002/anie.200600045

**Gas-Phase Oxidation of Propane and 1-Butene with  $[V_3O_7]^+$ : Experiment and Theory in Concert\*\***

Sandra Feyel, Detlef Schröder, Xavier Rozanska, Joachim Sauer,\* and Helmut Schwarz\*

Dedicated to Professor Siegfried Blechert on the occasion of his 60th birthday

Vanadium oxides are employed as efficient oxidation catalysts in various processes such as the oxidative dehydrogenation of propane and the formation of maleic anhydride from butane.<sup>[1]</sup> Nevertheless, mechanistic details of the surface reactions, in particular of the initial C–H activation remain to be elucidated. To obtain more information about intrinsic structure–reactivity correlations of vanadium oxides, a number of vanadium oxide ions have been studied in the gas phase both theoretically<sup>[2–4]</sup> and experimentally.<sup>[5–13]</sup> Here, we report experimental results on the oxidation of propane and 1-butene by mass-selected  $[V_3O_7]^+$ , corroborated by quantum chemical calculations using density functional theory (DFT). The cation  $[V_3O_7]^+$  was chosen because it represents the smallest polynuclear V/O cluster cation containing only formal  $V^{V[2b,3c]}$ . In addition to propane, 1-butene was selected as a representative of a small hydrocarbon that binds more strongly with  $[V_3O_7]^+$ . In general, oxidative

[\*] Dr. X. Rozanska, Prof. Dr. J. Sauer  
Institut für Chemie  
Humboldt Universität zu Berlin  
Unter den Linden 6, 10099 Berlin (Germany)  
Fax: (+49) 30-2093-7136  
E-mail: js@chemie.hu-berlin.de

Dipl.-Chem. S. Feyel, Dr. D. Schröder, Prof. Dr. Drs. h.c. H. Schwarz  
Institut für Chemie  
Technische Universität Berlin  
Strasse des 17. Juni 135, 10623 Berlin (Germany)  
Fax: (+49) 30-314-21102  
E-mail: helmut.schwarz@mail.chem.tu-berlin.de

[\*\*] Financial support by the Fonds der Chemischen Industrie and the Deutsche Forschungsgemeinschaft (SFB 546) is acknowledged. X.R. and S.F. were supported by an Alexander von Humboldt fellowship and a GRK 352 fellowship, respectively.



Supporting information for this article is available on the WWW under <http://www.angewandte.org> or from the author.

dehydrogenation (ODH) of hydrocarbons involves reduction of the metal center ( $[\text{V}_3\text{O}_7]^+ + 2\text{H}^+ + 2\text{e}^- \rightarrow [\text{V}_3\text{O}_7\text{H}_2]^+$ ). This is brought about by transfer of two hydrogen atoms (or equivalently, two protons and two electrons), thus resulting in the dehydrogenation of propane to give propene ( $\text{C}_3\text{H}_8 \rightarrow \text{C}_3\text{H}_6 + 2\text{H}$ ) and of 1-butene to butadiene ( $\text{C}_4\text{H}_8 \rightarrow \text{C}_4\text{H}_6 + 2\text{H}$ ). In a mass spectrometric experiment, two alternative product channels could indicate ODH. Either propene and butadiene are lost as neutrals concomitant with two hydrogen atoms being transferred to  $[\text{V}_3\text{O}_7]^+$  to form  $[\text{V}_3\text{O}_7\text{H}_2]^+$ , or neutral water may be eliminated while the dehydrogenated hydrocarbon remains bound at the metal oxide cation to yield  $[\text{V}_3\text{O}_6(\text{C}_3\text{H}_6)]^+$  and  $[\text{V}_3\text{O}_6(\text{C}_4\text{H}_6)]^+$ , respectively.

The experimental investigation of the  $[\text{V}_3\text{O}_7]^+$ /hydrocarbon systems uses a quadrupole-based mass spectrometer equipped with an electrospray-ionization source.<sup>[14]</sup> Ion-molecule reactions (IMRs) of mass-selected  $[\text{V}_3\text{O}_7]^+$  with propane formally result in molecular addition of the hydrocarbon to the vanadium oxide ion to form  $[\text{V}_3\text{O}_7(\text{C}_3\text{H}_8)]^+$  (Figure 1a) and yields no products indicative for an ODH process. In contrast, oxidative dehydrogenation to yield  $[\text{V}_3\text{O}_7\text{H}_2]^+$  concomitant with formation of neutral butadiene is indeed observed in the reaction of mass-selected  $[\text{V}_3\text{O}_7]^+$  with 1-butene (Figure 1b, Table 1). In addition, four minor

**Table 1:** Experimentally observed, normalized intensities and relative reaction rates for various ion-molecule reactions relevant in the present context.

Reactants	Products <sup>[a]</sup>	$k_{\text{rel}}$
$[\text{V}_3\text{O}_7]^+ + \text{C}_3\text{H}_8 \rightarrow$	$[\text{V}_3\text{O}_7(\text{C}_3\text{H}_8)]^+ (100)$	0.03
$[\text{V}_3\text{O}_6]^+ + n\text{-C}_3\text{H}_7\text{OH} \rightarrow$	$[\text{V}_3\text{O}_7\text{H}_2]^+ + \text{C}_3\text{H}_6 (75)$ $[\text{V}_3\text{O}_6(\text{C}_3\text{H}_7\text{OH})]^+ (25)$	1.00 <sup>[b,c]</sup>
$[\text{V}_3\text{O}_6]^+ + i\text{-CH}_3\text{C}(\text{OH})\text{HCH}_3 \rightarrow$	$[\text{V}_3\text{O}_7\text{H}_2]^+ + \text{C}_3\text{H}_6 (82)$	0.63 $[\text{V}_3\text{O}_6(\text{C}_3\text{H}_7\text{OH})]^+ (18)$
$[\text{V}_3\text{O}_7\text{H}_2]^+ + \text{C}_3\text{H}_6 \rightarrow$	$[\text{V}_3\text{O}_7\text{H}_2(\text{C}_3\text{H}_6)]^+ (100)$	0.24
$[\text{V}_3\text{O}_7]^+ + \text{C}_4\text{H}_8 \rightarrow$	$[\text{V}_3\text{O}_7\text{H}_2]^+ + \text{C}_4\text{H}_6 (64)^{[d]}$	0.24 $[\text{V}_3\text{O}_7(\text{C}_2\text{H}_4)]^+ + \text{C}_2\text{H}_4 (8)$ $[\text{V}_3\text{O}_7(\text{C}_4\text{H}_8)]^+ (7)$ $[\text{C}_4\text{H}_8]^+ + [\text{V}_3\text{O}_7] (4)$ $[\text{C}_4\text{H}_7]^+ + [\text{V}_3\text{O}_7\text{H}] (17)$

[a] Branching ratios in brackets. [b] Relative rates normalized to this reaction. [c] The reaction of bare  $\text{Pt}^+$  with  $\text{CH}_4$  was used as a reference to convert the relative rate constant ( $k_{\text{rel}}$ ) into absolute values, which leads for the reaction of  $[\text{V}_3\text{O}_6]^+$  with  $\text{C}_3\text{H}_7\text{OH}$  to  $k_r = (1.3 \pm 0.2) \times 10^{-9} \text{ cm}^3 \text{ s}^{-1}$ .<sup>[18]</sup> The collision rate constant amounts to  $1.4 \times 10^{-9} \text{ cm}^3 \text{ s}^{-1}$ .<sup>[19]</sup> [d] The primary ionic products rapidly add butene to yield  $[\text{V}_3\text{O}_7\text{H}_2(\text{C}_4\text{H}_8)]^+$ ; see Figure 1b.

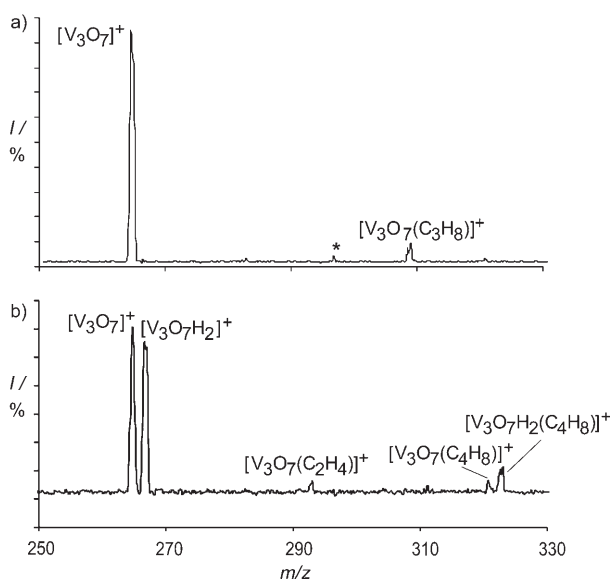
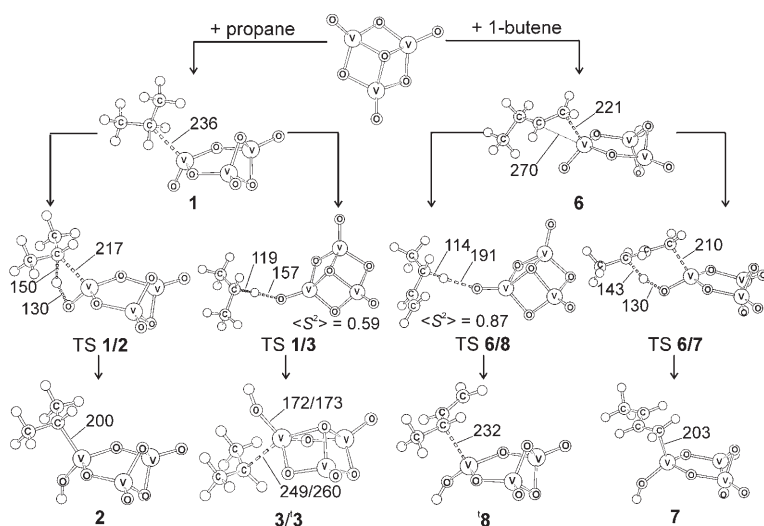


**Figure 1.** IMRs of  $[\text{V}_3\text{O}_7]^+$  with a) propane and b) 1-butene.  $p(\text{hydrocarbon}) = 2.5 \times 10^{-4} \text{ mbar}$ . The signal denoted with an asterisk in Figure 1a is due to residual gases present in the hexapole.

product channels are associated with C–C bond cleavage to lead to the corresponding  $[\text{V}_3\text{O}_7(\text{C}_2\text{H}_4)]^+$  cation with parallel elimination of ethene, mere association to form  $[\text{V}_3\text{O}_7(\text{C}_4\text{H}_8)]^+$ , and electron as well as hydride transfers to yield purely organic cations and neutral vanadium species.<sup>[14]</sup> For the oxidative dehydrogenation of 1-butene, labeling experiments demonstrate that the two hydrogen atoms transferred to  $[\text{V}_3\text{O}_7]^+$  originate specifically from the C3 and C4 positions of 1-butene. We note in passing that the product ion  $[\text{V}_3\text{O}_7\text{H}_2]^+$  displays a dihydroxide structure rather than that of a water complex, that is,  $[\text{V}_3\text{O}_5(\text{OH})_2]^+$  rather than  $[\text{V}_3\text{O}_6(\text{OH}_2)]^+$ .

To understand why ODH is not observed when  $[\text{V}_3\text{O}_7]^+$  reacts with propane, but occurs for 1-butene, we apply density functional theory (DFT). Calculations show that the reactivity difference can be traced back to the initial C–H activation step. It is not the aim of this communication to discuss the entire mechanism, which forms the subject of a separate computational full paper.<sup>[15]</sup>

The reaction of propane with  $[\text{V}_3\text{O}_7]^+$  starts with formation of the remarkably stable ( $-107 \text{ kJ mol}^{-1}$ ) ion-molecule complex **1** (Scheme 1, Figure 2). The secondary carbon atom of propane attaches to a vanadium site, and the  $[\text{V}_3\text{O}_7]^+$  structure deforms such that one oxygen atom of the cluster changes its coordination from three- to twofold. The next step corresponds to a formal [2+2] addition of a secondary C–H bond onto the  $\text{V}=\text{O}$  unit yielding intermediate **2** ( $-166 \text{ kJ mol}^{-1}$ ). These steps involve only closed-shell singlet species. The transition structure **TS 1/2** lies  $13 \text{ kJ mol}^{-1}$  above the separated reactants. In the reaction of ethane and propane with the formal  $\text{V}^{\text{V}}$  compound  $[\text{VO}_2]^+$ , addition of C–H bonds across a  $\text{V}=\text{O}$  unit has also been identified as an initial step, although in these systems the transition structures are below the respective entrance channels because  $[\text{VO}_2]^+$  binds alkanes more strongly.<sup>[12b,13a]</sup> In a thermal gas-phase reaction, **TS 1/2** constitutes a bottleneck because dissociation of the



**Scheme 1.** Reaction intermediates and transition structures in the oxidative dehydrogenation of propane and of 1-butene by  $[\text{V}_3\text{O}_7]^+$ . Selected distances are given in pm, and triplets are indicated by a superscript t.  $\langle S^2 \rangle$ : spin operator value (see the Experimental Section and the Supporting Information).

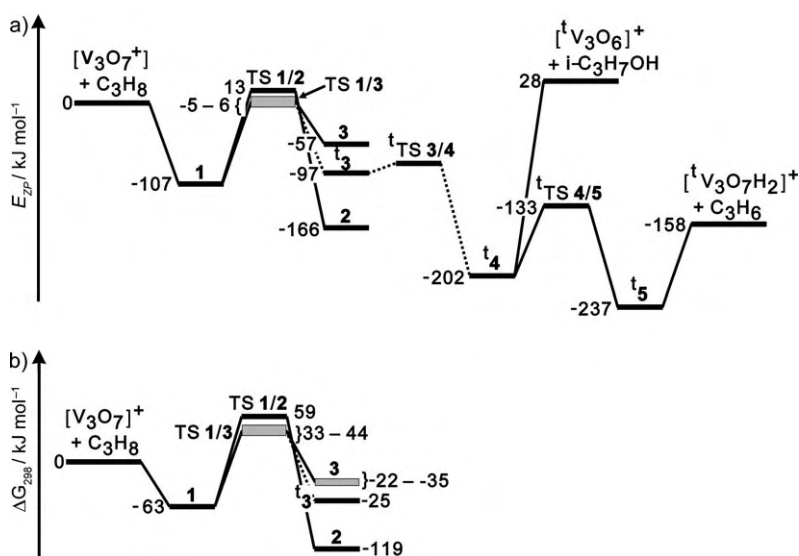


**Figure 2.** a) Relative energies ( $E_{zp}$  at 0 K) for the reaction pathways for oxidative dehydrogenation of propane by  $[\text{V}_3\text{O}_7]^+$ . The transition from  $\mathbf{3}$  to  $\mathbf{4}$  involves a complex rearrangement over several steps which will be described elsewhere.<sup>[15]</sup> b) Free energies ( $\Delta G_{298}$ ) for the initial C–H activation steps. Triplets are indicated by a superscript t.

reactant complex  $\mathbf{1}$  ( $\Delta G_{298} = -63 \text{ kJ mol}^{-1}$ ) into the reactants ( $\Delta G_{298} = 0 \text{ kJ mol}^{-1}$ ) is entropically favored compared to passage via  $\text{TS1/2}$  ( $\Delta G_{298} = 59 \text{ kJ mol}^{-1}$ ; see the Supporting Information).

Another conceivable mechanism commences by abstraction of a hydrogen atom from a secondary C–H bond by a  $\text{V}=\text{O}$  unit of  $[\text{V}_3\text{O}_7]^+$ . This requires decoupling of the electron pair in the C–H bond and proceeds via a biradicaloid  $\text{TS1/3}$  to give the radical pair  $[\text{V}_3\text{O}_7\text{H}^+\cdots\text{C}_3\text{H}_7\cdot]$  (structure  $\mathbf{3}$  in Scheme 1). With the exception of an elongated V–C bond (249 instead of 200 pm), structure  $\mathbf{3}$  is similar to  $\mathbf{2}$ . The existence of two minima along the V–C bond coordinate can

be attributed to an avoided crossing of the potential energy surface (PES) for the dissociation of the C–V  $\sigma$  bond into two  $\sigma$  radicals,  $\text{C}-\text{V} \rightarrow \text{C}\cdot + \cdot\text{V}$ , and that for formation of the  $[\text{V}_3\text{O}_7\text{H}^+\cdots\text{C}_3\text{H}_7\cdot]$  pair from the separated radicals with the single electron on  $[\text{V}_3\text{O}_7\text{H}]^{+\cdot}$  occupying a stable d orbital instead of a  $\sigma$  hybrid orbital, thus creating a  $\text{V}^{\text{IV}}(\text{d}^1)$  site.

On the singlet PES, the energy barrier for this step is computed to be in the range of  $-5$  to  $6 \text{ kJ mol}^{-1}$  relative to the entrance channel. The Gibbs free energy barrier amounts to a range of  $33$  to  $44 \text{ kJ mol}^{-1}$ ; this also implies that back dissociation of  $\mathbf{1}$  into the reactants is favored over crossing  $\text{TS1/3}$ . Whereas the triplet analogue of intermediate  $\mathbf{3}$  has a lower energy (triplets are indicated by a superscript t), in the region of  $\text{TS1/3}$  the triplet surface is located ca.  $50 \text{ kJ mol}^{-1}$  above the singlet PES. Hence, we expect the minimum-energy crossing point from the singlet to the triplet surface to be located between  $\text{TS1/3}$  and  $\mathbf{3}$ , but we did not calculate it explicitly.<sup>[16]</sup>

Starting from the triplet biradical  $\mathbf{3}$  a low-energy intermediate  $\mathbf{4}$  (Figure 3) is reached in a complex, but energetically facile rearrangement. Again, complete details will be given elsewhere.<sup>[15]</sup> Here, it may suffice to note that the highest point between  $\mathbf{3}$  and  $\mathbf{4}$  is  $90 \text{ kJ mol}^{-1}$  below the entrance channel of separated  $[\text{V}_3\text{O}_7]^+ + \text{C}_3\text{H}_8$ .

In conclusion and in agreement with the experimental observations, neither of the two pathways of initial C–H activation allow the system to cross the barrier. The DFT calculations further suggest that the observed formal  $[\text{V}_3\text{O}_7(\text{C}_3\text{H}_8)]^+$  adduct does indeed correspond to the association complex  $\mathbf{1}$  and does not contain new subunits, such as a propene ligand together with two OH groups.

For the reactions of 1-butene with  $[\text{V}_3\text{O}_7]^+$  (Figure 1b), DFT calculations for the closed-shell singlet state predict the reaction to be more exothermic than for propane ( $-174$ <sup>[15]</sup> vs.  $-158 \text{ kJ mol}^{-1}$ ) and also predict formation of a substantially much stronger association complex with  $[\text{V}_3\text{O}_7]^+$  ( $\mathbf{6}$ , Scheme 1, Figure 4). The

intrinsic barrier for the [2+2] addition to the  $\text{V}=\text{O}$  bond is also lower for the allylic C–H bond in 1-butene ( $\text{TS6/7}$ , Scheme 1) than for the secondary C–H bond of propane (91 vs.

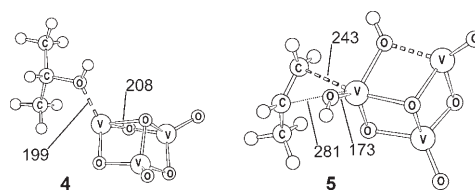


**Figure 3.** Structures of intermediates  $\mathbf{4}$  and  $\mathbf{5}$ .

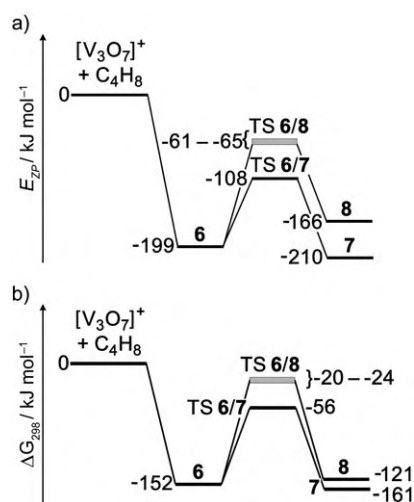


**Figure 4.** Initial C–H activation steps in the reaction of 1-butene with  $[V_3O_7]^+$ . a) Relative energies ( $E_{ZP}$  at 0 K) and b) free energies ( $\Delta G_{298}$ ).

$120 \text{ kJ mol}^{-1}$ ). As a result, TS6/7 is so much below the entrance channel of  $[V_3O_7]^+ + 1\text{-butene}$  (Figure 4) that this energy difference is not compensated for by the entropy gain for the back decomposition into reactants as seen from a strongly negative  $\Delta G_{298} = -56 \text{ kJ mol}^{-1}$ . This computational result is in perfect agreement with the experimentally observed efficient ODH of 1-butene by  $[V_3O_7]^+$  (Table 1). For completeness we note that the open-shell transition structure for hydrogen abstraction, TS6/8, is higher in energy than TS6/7, but is also still significantly below the entrance channel (Figure 4).

In order to further test the DFT-based predictions experimentally, the potential energy surface of the  $[V_3O_7]^+/\text{propane}$  system has also been approached from the product side. Thus, exclusive formation of  $[V_3O_7H_2]^+$  concomitant with neutral propene is observed in the reactions of  $[V_3O_6]^+$  with 1- and 2-propanol (Table 1). The slightly enhanced reactivity of 1-propanol is consistent with linear alcohols being less sterically hindered than branched alcohols. The complementary process, that is, addition of the propene ligand to  $[V_3O_6]^+$  concomitant with loss of neutral water, is not observed with either of the isomeric alcohols. This result can be attributed to the fact that an electron-deficient species such as a high-valent metal oxide cation prefers coordination with water as a better  $\sigma$ -donor ligand rather than with a typical  $\pi$  ligand such as an alkene.<sup>[17]</sup> Furthermore, the reaction of mass-selected  $[V_3O_7H_2]^+$  with propene leads to mere molecular addition of the olefin. These results fully support the computational predictions, in that the reaction of  $[V_3O_6]^+$  and propanol can smoothly proceed from the entrance channel to the products  $[V_3O_7H_2]^+$  and propene, while deoxygenation of the alcohol to yield  $[V_3O_7]^+ + C_3H_8$  via the entropically disfavored TS1/2 ( $\Delta G_{298} = 59 \text{ kJ mol}^{-1}$ ) is unable to compete (Figure 2).

In summary, although the ODH reaction of propane by  $[V_3O_7]^+$  is exothermic, this vanadium oxide cation is not capable of dehydrogenating propane because of the presence of a significant barrier associated with the initial C–H activation. In marked contrast, 1-butene reacts with  $[V_3O_7]^+$

at thermal energies. These experimental results perfectly agree with the DFT calculations, which predict C–H activation as the rate-determining step. The differences between propane and 1-butene can mostly be traced back to the energy gained upon initial coordination of the hydrocarbon by the vanadium oxide cation and the more facile activation of an allylic C–H bond.

### Experimental Section

The experiments were carried out using a tandem mass spectrometer with QHQ configuration (Q: quadrupole, H: hexapole) equipped with an electrospray-ionization (ESI) source as described elsewhere.<sup>[20]</sup> Briefly,  $[V_mO_n]^+$  clusters of interest were generated by ESI of  $V_6O_7(OCH_3)_{12}$  dissolved in  $CD_3OD$ ,<sup>[21,22]</sup> mass-selected using Q1, allowed to interact with propane or 1-butene, at pressures on the order of  $10^{-4}$  mbar, which approximately corresponds to single-collision conditions, and the ionic products were then mass-analyzed using Q2. Ion-reactivity studies were performed at an interaction energy in the hexapole ( $E_{lab}$ ) nominally set to 0 eV. The reaction products formed rapidly decline at elevated collision energies, thereby justifying the assumption that these processes occur at quasi-thermal energies.<sup>[14]</sup>

The calculations were performed using the hybrid density functional B3LYP<sup>[23]</sup> with triple- $\zeta$  plus polarization basis sets (TZVP)<sup>[24]</sup> employing Turbomole 5.7.<sup>[25]</sup> B3LYP was shown previously to describe  $[V_mO_n]$  clusters in good agreement with available experimental data as well as quantum chemical methods that explicitly include electron correlation.<sup>[3c]</sup> The unrestricted Kohn–Sham scheme was used to deal with triplet spin states. For open-shell singlets, broken-symmetry calculations were performed,<sup>[26]</sup> and the low-spin energy was obtained from the triplet and broken-symmetry energies by spin projection.<sup>[27]</sup> When the expectation value of  $S^2$  significantly deviated from one (indicating an increasing overlap between the unpaired electrons), as was the case for TS1/3, spin-projection was questioned<sup>[28]</sup> and both energies were then taken as limiting estimates, as indicated by the gray-shaded boxes in Figures 2 and 4. All intermediates and transition structures were characterized by frequency analysis, and the energies include corrections for zero-point vibrations. Energies, entropies, and Gibbs free energies at room temperature can be found in the Supporting Information.

Received: January 5, 2006

Published online: June 21, 2006

**Keywords:** gas-phase reactions · C–H activation · density functional theory · mass spectrometry · vanadium oxides

[1] G. Centi, F. Cavani, F. Trifirù, *Selective Oxidation by Heterogeneous Catalysis*, Plenum, New York, **2001**.

[2] a) M. Calatayud, B. Silvi, J. Andres, A. Beltran, *Chem. Phys. Lett.* **2001**, 333, 493–503; b) M. Calatayud, J. Andres, A. Beltran, *J. Phys. Chem. A* **2001**, 105, 9760–9775; c) M. Calatayud, J. Andres, A. Beltran, B. Silvi, *Theor. Chem. Acc.* **2001**, 105, 299–308; d) L. Gracia, J. Andres, V. S. Safont, A. Beltran, J. R. Sambrano, *Organometallics* **2004**, 23, 730–739.

[3] a) S. F. Vyboishchikov, J. Sauer, *J. Phys. Chem. A* **2000**, 104, 10913–10922; b) S. F. Vyboishchikov, J. Sauer, *J. Phys. Chem. A* **2001**, 105, 8588–8598; c) J. Sauer, J. Doeblner, *Dalton Trans.* **2004**, 3116–3121.

[4] J. R. T. Johnson, I. Panas, *Inorg. Chem.* **2000**, 39, 3192–3204.

[5] G. K. Koyanagi, D. K. Böhme, I. Kretzschmar, D. Schröder, H. Schwarz, *J. Phys. Chem. A* **2001**, 105, 4259–4271.



- [6] a) G. C. Nieman, E. K. Parks, S. C. Richtsmeier, K. Liu, L. G. Pobo, S. J. Riley, *High Temp. Sci.* **1986**, 22, 115–138; b) R. C. Bell, K. A. Zemski, K. P. Kerns, H. T. Deng, A. W. Castleman, *J. Phys. Chem. A* **1998**, 102, 1733–1742; c) M. Foltin, G. J. Stueber, E. R. Bernstein, *J. Chem. Phys.* **1999**, 111, 9577–9586; d) L. Gracia, J. R. Sambrano, J. Andrés, A. Beltrán, *Organometallics* **2006**, 25, 1643–1653.
- [7] a) R. C. Bell, K. A. Zemski, A. W. Castleman, *J. Phys. Chem. A* **1998**, 102, 8293–8299; b) K. A. Zemski, D. R. Justes, A. W. Castleman, *J. Phys. Chem. B* **2002**, 106, 6136–6148; c) D. R. Justes, R. Mitric, N. A. Moore, V. Bonacic-Koutecky, A. W. Castleman, *J. Am. Chem. Soc.* **2003**, 125, 6289–6299.
- [8] A. Dinca, T. P. Davis, K. J. Fisher, D. R. Smith, G. D. Willett, *Int. J. Mass Spectrom.* **1999**, 182/183, 73–84.
- [9] a) K. R. Asmis, M. Brümmer, C. Kaposta, G. Santambrogio, G. von Helden, G. Meijer, K. Rademann, L. Wöste, *Phys. Chem. Chem. Phys.* **2002**, 4, 1101–1104; b) K. R. Asmis, G. Meijer, M. Brümmer, C. Kaposta, G. Santambrogio, L. Wöste, J. Sauer, *J. Chem. Phys.* **2004**, 120, 6461–6470; c) K. R. Asmis, G. Santambrogio, M. Brümmer, J. Sauer, *Angew. Chem.* **2005**, 117, 3182–3185; *Angew. Chem. Int. Ed.* **2005**, 44, 3122–3125.
- [10] L. Holmgren, A. Rosén, *J. Chem. Phys.* **1999**, 110, 2629–2636.
- [11] J. Xu, M. T. Rodgers, J. B. Griffin, P. B. Armentrout, *J. Chem. Phys.* **1998**, 108, 9339–9350.
- [12] a) L. Gracia, J. R. Sambrano, V. S. Safont, M. Calatayud, A. Beltrán, J. Andrés, *J. Phys. Chem. A* **2003**, 107, 3107–3120; b) J. N. Harvey, M. Diefenbach, D. Schröder, H. Schwarz, *Int. J. Mass Spectrom.* **1999**, 182/183, 85–97.
- [13] a) M. Engeser, M. Schlangen, D. Schröder, H. Schwarz, Y. Takashi, Y. Kazunari, *Organometallics* **2003**, 22, 3933–3943; b) M. Engeser, D. Schröder, T. Weiske, H. Schwarz, *J. Phys. Chem. A* **2003**, 107, 2855–2859.
- [14] S. Feyel, D. Schröder, H. Schwarz, *J. Phys. Chem. A* **2006**, 110, 2647–2654.
- [15] X. Rozanska, J. Sauer, in preparation.
- [16] a) J. L. Carreón-Macedo, J. N. Harvey, *J. Am. Chem. Soc.* **2004**, 126, 5789–5797; b) for a review on the role of different spin states in gas-phase ion–molecule reactions, see: H. Schwarz, *Int. J. Mass Spectrom.* **2004**, 237, 75–103; c) J. M. Mercero, J. M. Matxain, X. Lopez, D. M. York, A. Largo, L. A. Eriksson, J. M. Ugalde, *Int. J. Mass Spectrom.* **2005**, 240, 37–99.
- [17] S. Bärsch, D. Schröder, H. Schwarz, *J. Phys. Chem. A* **2000**, 104, 5101–5110.
- [18] a) U. Achatz, C. Berg, S. Joos, B. S. Fox, M. K. Beyer, G. Niedner-Schatteburg, V. E. Bondybey, *Chem. Phys. Lett.* **2000**, 320, 53–58; b) X. G. Zhang, R. Liyanage, P. B. Armentrout, *J. Am. Chem. Soc.* **2001**, 123, 5563–5575; c) D. Schröder, H. Schwarz, *Can. J. Chem.* **2005**, 83, 1936–1944.
- [19] a) T. Su, W. J. Chesnavich, *J. Chem. Phys.* **1982**, 76, 5183–5185; b) T. Su, *J. Chem. Phys.* **1988**, 88, 4102–4103; c) T. Su, *J. Chem. Phys.* **1988**, 89, 5355.
- [20] D. Schröder, T. Weiske, H. Schwarz, *Int. J. Mass Spectrom.* **2002**, 219, 729–738.
- [21] J. Spandl, C. Daniel, I. Brudgam, H. Hartl, *Angew. Chem.* **2003**, 115, 1195–1198; *Angew. Chem. Int. Ed.* **2003**, 42, 1163–1166.
- [22] D. Schröder, M. Engeser, M. Brönstrup, C. Daniel, J. Spandl, H. Hartl, *Int. J. Mass Spectrom.* **2003**, 228, 743–757.
- [23] a) A. D. Becke, *J. Chem. Phys.* **1993**, 98, 5648–5652; b) C. Lee, W. Yang, R. G. Parr, *Phys. Rev. B* **1988**, 37, 785–789.
- [24] A. Schäfer, C. Huber, R. Ahlrichs, *J. Chem. Phys.* **1994**, 100, 5829–5835.
- [25] a) R. Ahlrichs, M. Bär, M. Häser, H. Horn, C. Kölmel, *Chem. Phys. Lett.* **1989**, 162, 165–169; b) O. Treutler, R. Ahlrichs, *J. Chem. Phys.* **1995**, 102, 346–354; c) K. Eichkorn, F. Weigend, O. Treutler, R. Ahlrichs, *Theor. Chem. Acc.* **1997**, 97, 119–124; d) M. von Arnim, R. Ahlrichs, *J. Chem. Phys.* **1999**, 111, 9183–9190.
- [26] L. Noodleman, *J. Chem. Phys.* **1981**, 74, 5737–5743.
- [27] R. Caballol, O. Castell, F. Illas, I. de P. R. Moreira, J. P. Malrieu, *J. Phys. Chem. A* **1997**, 101, 7860–7866.
- [28] J. Gräfenstein, A. M. Hjerpe, E. Kraka, D. Cremer, *J. Phys. Chem. A* **2000**, 104, 1748–1761.

## C–H Activation

DOI: 10.1002/anie.200600188

Thermal Activation of Methane by Tetranuclear  
[V<sub>4</sub>O<sub>10</sub>]<sup>++</sup>

Sandra Feyel, Jens Döbler, Detlef Schröder,  
Joachim Sauer,\* and Helmut Schwarz\*

Dedicated to Professor Ernst-Ludwig Winnacker  
on the occasion of his 65th birthday

Selective activation of C–H bonds and functionalization of hydrocarbons, in particular of methane, have been referred to as one of the “holy grails” in chemistry.<sup>[1]</sup> A number of factors make the activation of saturated hydrocarbons quite difficult, for example, the significant energies required for both heterolytic and homolytic bond cleavage, negligibly small (if not negative) electron affinities, large ionization energies, huge HOMO/LUMO gaps, and the extremely high pK<sub>a</sub> values of the organic substrates.<sup>[2]</sup> However, in the past two decades researchers have found that transition-metal complexes can be used to surmount some of these obstacles<sup>[1b,2,3]</sup> to the extent that “with detailed knowledge of the underlying reaction mechanisms, the rational design of C–H activation and functionalization systems can become a realistic goal instead of a ‘holy grail’.”<sup>[4]</sup> Nevertheless, the large-scale use of, for example, methane as a chemical feedstock and its selective functionalization by affordable and environmentally benign reagents, avoiding harsh and expensive reaction conditions,<sup>[5a,b]</sup> is still limited by currently available technol-

[\*] Dr. J. Döbler, Prof. Dr. J. Sauer  
Institut für Chemie  
Humboldt Universität Berlin  
Unter den Linden 6, 10099 Berlin (Germany)  
Fax: (+49) 30-2093-7136  
E-mail: js@chemie.hu-berlin.de

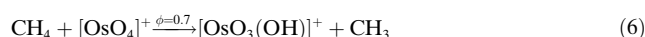
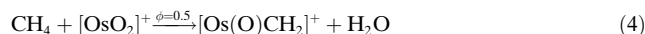
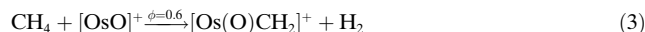
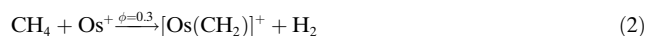
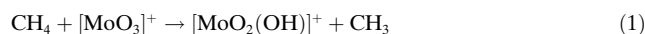
Dipl.-Chem. S. Feyel, Dr. D. Schröder, Prof. Dr. Drs. h.c. H. Schwarz  
Institut für Chemie  
Technische Universität Berlin  
Strasse des 17. Juni 135, 10623 Berlin (Germany)  
Fax: (+49) 30-314-21102  
E-mail: helmut.schwarz@mail.chem.tu-berlin.de

[\*\*] Financial support from the Fonds der Chemischen Industrie and the Deutsche Forschungsgemeinschaft (SFB 546) is acknowledged. S.F. was supported by a GRK352 fellowship.

ogy, and economically competitive and attractive processes have yet to be developed.<sup>[5a,d]</sup>

Greater progress has been made in understanding the elementary steps involved in these reactions.<sup>[1b]</sup> Detailed insight has been obtained into the particular role of electronic structures of transition metals in C–H bond activation, and mechanistic aspects have been studied in well-designed gas-phase experiments using advanced mass-spectrometric techniques in conjunction with theoretical studies,<sup>[6]</sup> in which relativistic effects were demonstrated to be crucial.<sup>[7]</sup>

These effects, which may also explain the unique role platinum ions play in the Shilov and related systems,<sup>[3c]</sup> are also responsible for the different behavior of 5d versus 3d transition-metal oxides. For example, [PtO]<sup>+</sup> reacts with CH<sub>4</sub> at the collisional limit (reaction efficiency,  $\phi = 1$ ) to yield the carbene complex [Pt(CH<sub>2</sub>)]<sup>+</sup> and H<sub>2</sub>O as the predominant products,<sup>[8]</sup> whereas the isoelectronic [NiO]<sup>+</sup> reacts five times more slowly and gives rise to Ni<sup>+</sup> and CH<sub>3</sub>OH only.<sup>[9]</sup> Similarly, [FeO]<sup>+</sup> oxygenates methane,<sup>[9]</sup> while its third-row congener [OsO]<sup>+</sup> ( $\phi = 0.6$ ) exclusively dehydrogenates methane to yield [Os(O)CH<sub>2</sub>]<sup>+</sup>.<sup>[10]</sup> With regard to the role of formal oxidation states of [MO]<sub>*n*</sub><sup>+</sup> ions (*n* = 1–3), Kretzschmar et al. discovered a strong dependence on the number of oxygen atoms: Whereas the bare metal cation Mo<sup>+</sup> and the lower valent oxides [MoO]<sub>*n*</sub><sup>+</sup> (*n* = 1, 2) do not react at all with CH<sub>4</sub>, the radical cation [MoO<sub>3</sub>]<sup>+</sup> promotes homolytic C–H bond activation [Eq. (1)].<sup>[11]</sup> Similar results were reported by Irikura and Beauchamp for gas-phase reactions of [OsO]<sub>*n*</sub><sup>+</sup> (*n* = 0–4) with CH<sub>4</sub>,<sup>[10]</sup> [Eq. (2)–(6)].



Clearly, the driving force in the osmium reactions [Eq. (2)–(4)] is the tremendous energy of the Os<sup>+</sup>–CH<sub>2</sub> bond. In contrast to [MoO<sub>3</sub>]<sup>+</sup>,<sup>[11]</sup> [ReO<sub>3</sub>]<sup>+</sup>,<sup>[10]</sup> and [OsO<sub>4</sub>]<sup>+</sup>, [OsO<sub>3</sub>]<sup>+</sup> is not capable of methane activation. Undoubtedly, in reactions with CH<sub>4</sub> the particular electronic structures of [MO]<sub>*n*</sub><sup>+</sup> are important;<sup>[6d,7b,12]</sup> in a different context<sup>[6c]</sup> the cluster size of the transition-metal oxides was proposed to play a role. In this communication we focus on the latter aspect.

Here, we will describe the reactivity of vanadium oxide cluster cations as a prototypical example for early 3d transition-metal oxides. Not unexpectedly, owing to their large M<sup>+</sup>–O bond energies,<sup>[12]</sup> practically none of the diatomic 3d early-transition-metal oxides react with CH<sub>4</sub> under thermal conditions or at best only sluggishly.<sup>[13]</sup> As will be demonstrated, this finding cannot be extrapolated to polynuclear oxide clusters, which have been suggested to be more appropriate models for surface-mediated hydrocarbon bond-activation processes.<sup>[9,14]</sup>

We performed our experiments with a quadrupole-based mass spectrometer equipped with an electrospray ionization (ESI) source. The latter is used to generate various di-, tri-, and tetranuclear vanadium oxide ions of the general formula [V<sub>*m*</sub>O<sub>*n*</sub>H<sub>*o*</sub>]<sup>+</sup> (*m* = 1–4, *n* = 1–11, *o* = 0–1).<sup>[15]</sup> Of the numerous mass-selected vanadium oxide and hydroxide cations investigated, only the d<sup>0</sup> radical cation [V<sub>4</sub>O<sub>10</sub>]<sup>+</sup> reacts spontaneously with methane [Eq. (7)], resulting in the abstraction of



one hydrogen atom to produce the hydroxide cluster oxide [V<sub>4</sub>O<sub>9</sub>(OH)]<sup>+</sup> and a neutral methyl radical (Figure 1a). Like-

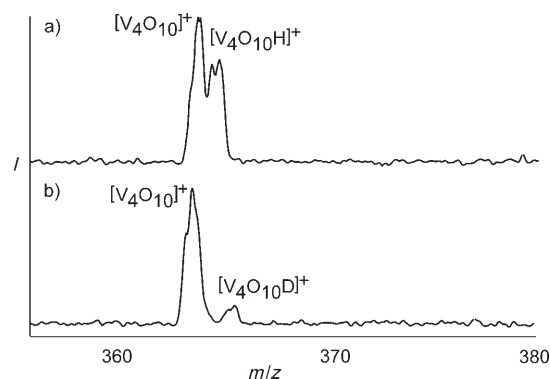
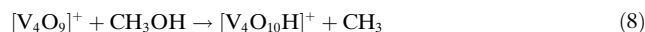


Figure 1. Reaction of mass-selected [V<sub>4</sub>O<sub>10</sub>]<sup>+</sup> with a) CH<sub>4</sub> and b) CD<sub>4</sub>.

wise, labeling experiments using CD<sub>4</sub> (Figure 1b) yielded [V<sub>4</sub>O<sub>9</sub>(OD)]<sup>+</sup> and CD<sub>3</sub>. Further, an intramolecular kinetic isotope effect (KIE) of  $1.35 \pm 0.28$  can be derived from the ratio of the products [V<sub>4</sub>O<sub>10</sub>H]<sup>+</sup> and [V<sub>4</sub>O<sub>10</sub>D]<sup>+</sup> from the reaction of [V<sub>4</sub>O<sub>10</sub>]<sup>+</sup> with CH<sub>2</sub>D<sub>2</sub>. A slightly larger KIE of 2.0 was reported for the [MoO<sub>3</sub>]<sup>+</sup>/CH<sub>2</sub>D<sub>2</sub> system,<sup>[11]</sup> thus pointing to a common bond-activation mechanism. In the multipole set-up used for the present experiments, absolute rate constants (*k<sub>r</sub>*) for the reactions cannot be determined directly. Therefore, we used the well-studied reaction of bare Pt<sup>+</sup> with methane as a reference to convert the relative rate constant *k<sub>rel</sub>* into absolute values. We found *k<sub>r</sub>*(V<sub>4</sub>O<sub>10</sub><sup>+</sup>) =  $(5.5 \pm 0.69) \times 10^{-10} \text{ cm}^3 \text{ s}^{-1}$  ( $\phi = 0.6$ ).<sup>[8a,16]</sup>

Further, we attempted to enter the potential energy surface of the reaction from a different entry by reacting mass-selected [V<sub>4</sub>O<sub>9</sub>]<sup>+</sup> with neutral methanol. The channel affording [V<sub>4</sub>O<sub>10</sub>H]<sup>+</sup> + CH<sub>3</sub> is also observed here, although it is a minor contributor [ $< 3\%$ ; Eq. (8)]. The predominant



reaction was molecular addition to generate [V<sub>4</sub>O<sub>9</sub>–(CH<sub>3</sub>OH)]<sup>+</sup> (38%). Other reactions include oxygen transfer to form [V<sub>4</sub>O<sub>8</sub>]<sup>+</sup> possibly with concomitant formation of CH<sub>2</sub>O + H<sub>2</sub>O (12%), elimination of formaldehyde to form [V<sub>4</sub>O<sub>9</sub>H<sub>2</sub>]<sup>+</sup> (9%), liberation of dihydrogen to generate [V<sub>4</sub>O<sub>9</sub>–(CH<sub>2</sub>O)]<sup>+</sup> (8%), elimination of water to produce [V<sub>4</sub>O<sub>9</sub>CH<sub>2</sub>]<sup>+</sup> (21%), addition of methane concomitant with loss of one oxygen atom (9%), and formation of [V<sub>4</sub>O<sub>10</sub>H]<sup>+</sup> concomitant with generation of CH<sub>3</sub> (3%). The occurrence of reaction (7)

implies that the bond energy of the newly formed O–H bond in the ionic cluster exceeds the C–H bond energy of methane ( $439 \text{ kJ mol}^{-1}$ );<sup>[17]</sup> further, OH abstraction from methanol in reaction (8) implies a lower limit of  $367 \text{ kJ mol}^{-1}$  for the strength of the V–(OH) bond in the  $[\text{V}_4\text{O}_{10}\text{H}]^+$  cluster.<sup>[18]</sup>

As insight into the mechanistic details of the C–H bond-activation step is difficult to obtain by experimental means, computational studies were carried out. According to B3LYP calculations, the most stable isomer of the  $[\text{V}_4\text{O}_{10}]^+$  ion has a slightly distorted tetrahedral cage structure with  $C_s$  symmetry. This structure was previously predicted to be the most stable isomer among many different structures for neutral  $\text{V}_4\text{O}_{10}$ <sup>[19]</sup> and confirmed by IR spectroscopy for the corresponding anion,  $[\text{V}_4\text{O}_{10}]^-$ .<sup>[20]</sup> In the radical cation  $[\text{V}_4\text{O}_{10}]^+$  one valence electron is missing from one V=O bond, leading to an elongation of the vanadyl bond (see Figure 2). The spin density has the shape of a p orbital and is mainly localized at the vanadyl oxygen atom. A small amount of the spin density is also delocalized over the two closest framework oxygen atoms.

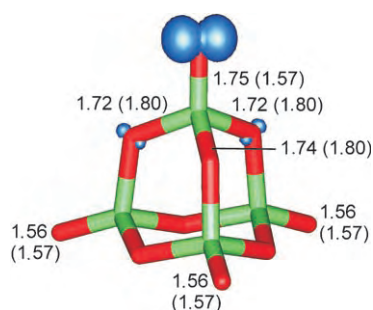


**Figure 2.** Structure of the most stable isomer of  $[\text{V}_4\text{O}_{10}]^+$  with spin density (blue areas). V–O distances for  $[\text{V}_4\text{O}_{10}]^+$  and  $\text{V}_4\text{O}_{10}$  (in parentheses) are given in Å.

The coordination of methane to the cluster and smooth hydrogen-atom abstraction is associated with a remarkably large gain of energy,  $122 \text{ kJ mol}^{-1}$  (Figure 3). It has to be noted no encounter complexes of the type  $[\text{V}_4\text{O}_{10}]^+ \cdot \text{CH}_4$  were found

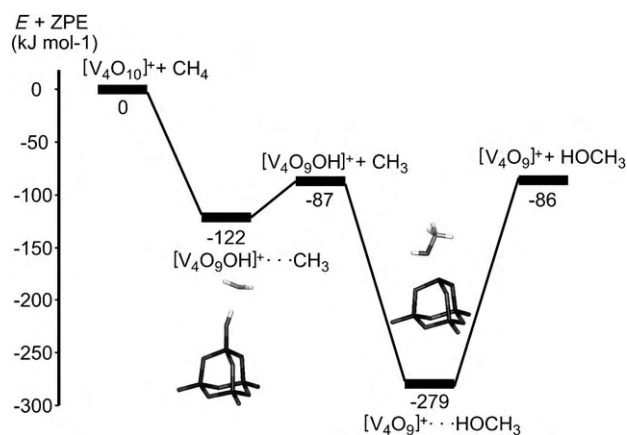


**Figure 3.** Energy diagram for the reaction of  $[\text{V}_4\text{O}_{10}]^+$  and methane. The values are relative to the entrance channel, corrected for zero-point energy, and given in  $\text{kJ mol}^{-1}$ .

in the structure optimizations, suggesting that the reaction proceeds without a noticeable reaction barrier by direct H-atom abstraction to form the intermediate  $[\text{V}_4\text{O}_{10}\text{H}]^+ \cdot \text{CH}_3$ . In the latter, the methyl group is very loosely coordinated to the hydrogen atom of the newly formed, metal-bound hydroxy group (C–H distance:  $1.819 \text{ Å}$ ), and the reaction is completed by loss of a methyl radical concomitant with formation of  $[\text{V}_4\text{O}_{10}\text{H}]^+$  as the ionic product. The computed reaction exothermicity of  $87 \text{ kJ mol}^{-1}$  and the absence of barriers are in full accordance with the experimentally observed occurrence of the ion–molecule reaction under thermal conditions. According to the calculations, the reaction of  $[\text{V}_4\text{O}_9]^+$  with methanol yields a very stable addition complex with an interaction energy of  $-193 \text{ kJ mol}^{-1}$ . This high energy gain is attributed to solvation of the unfavorable threefold-coordinated vanadium atom in  $[\text{V}_4\text{O}_9]^+$ . The energy of separated  $[\text{V}_4\text{O}_9\text{OH}]^+ + \text{CH}_3$  is virtually equal to the entrance channel energy of separated  $[\text{V}_4\text{O}_9]^+ + \text{HOCH}_3$ ; thus loss of a methyl radical can hardly compete with the other observed reaction channels, and it is expected that  $[\text{V}_4\text{O}_9]^+ + \text{HOCH}_3$  yields  $[\text{V}_4\text{O}_9\text{OH}]^+$  merely as a marginal product, in agreement with the experimental findings.

To clarify whether reaction (7) is indeed barrierless, molecular dynamics (MD) simulation was performed (Figure 4). The starting point is an optimized structure of

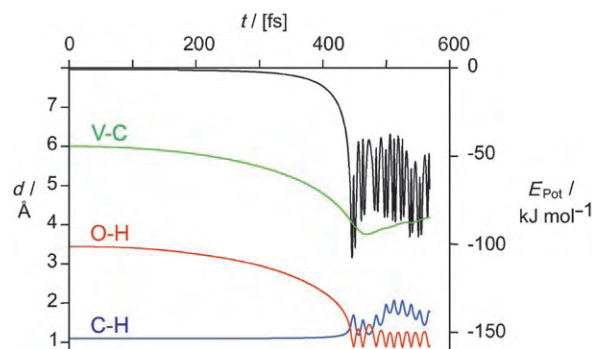


**Figure 4.** Evolution of the potential energy and bond lengths in the MD simulation of the reaction of  $[\text{V}_4\text{O}_{10}]^+$  and methane. The energy is shown in black,  $d(\text{C-H})$  in blue,  $d(\text{O-H})$  in red, and  $d(\text{V-C})$  in green. The fluctuations after 450 fs result from vibrational motions, mainly of the OH group.

$[\text{V}_4\text{O}_{10}]^+$  and  $\text{CH}_4$  in which the V–C distance is constrained to  $6 \text{ Å}$  to prevent the methane from reacting with the cluster. The simulation is started with zero initial velocities when this constraint is lifted. Thus the reaction is driven only by the small attractive forces between methane and the cluster; vibrational and rotational energies are nonexistent. For the first 450 fs of the simulation the potential energy decreases steadily, indicating a barrierless process. In parallel the O–H and V–C distances decrease and the C–H distance increases, indicating the progress of the reaction. After 450 fs when the system contains  $102 \text{ kJ mol}^{-1}$  of kinetic energy, energy is transferred into CH and OH stretching vibrations, corresponding to an oscillation of the hydrogen atom between the vanadyl O atom and the methyl C atom. This is evident as fluctuations of the potential energy. The plot in Figure 4 also



shows the V–C distance, which decreases up until  $t = 470$  fs and then slowly increases. This indicates the beginning of the expulsion of the  $\text{CH}_3$  radical, which would be completed only after significantly longer simulation times.

The progression of the reaction can also be seen by inspection of the spin densities shown in Figure 5. In the

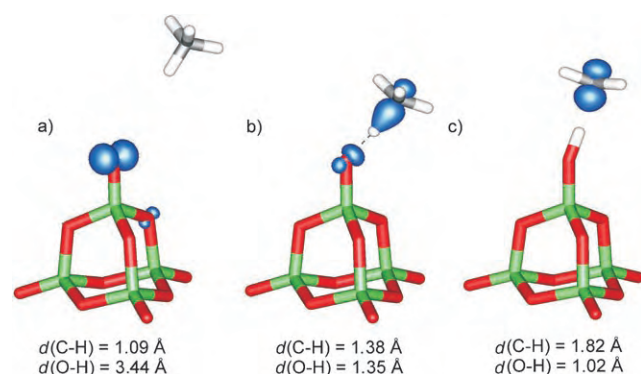


**Figure 5.** Spin density for the reaction of  $[\text{V}_4\text{O}_{10}]^+$  and methane after a) 0 fs and b) 443 fs. c) Spin density of the optimized product structure. C–H and O–H distances are given below the structures.

initial state (structure a in Figure 5), the spin density is similar to that of the isolated  $[\text{V}_4\text{O}_{10}]^+$  ion (Figure 2) and only slightly more delocalized. Structure b was obtained from MD simulation after 443 fs. The O–H and C–H distances are almost identical, and the spin density is distributed between the vanadyl oxygen and the carbon atoms and polarized along the O–H–C axis. Finally, in product c the spin density is completely transferred to the methyl radical, and the shape is again p-orbital-like with only slight distortion towards the newly formed OH group. One explanation of the lack of energy barriers in this reaction is that  $[\text{V}_4\text{O}_{10}]^+$  is highly reactive owing to its radical-cation nature.<sup>[21]</sup>

Our combined experimental and theoretical studies provide the first example for the thermal activation of methane by a polynuclear transition-metal oxide. This observation is not trivial, for it had been noted earlier<sup>[9,14a]</sup> that the often extremely reactive mononuclear metal oxides<sup>[12]</sup> are not ideal model systems relevant for an understanding of a real-life oxidation catalyst; larger systems, that is, cluster oxides, are better suited to serve this purpose.

## Experimental Section

The experiments were carried out using a tandem mass spectrometer with QHQ configuration (Q: quadrupole, H: hexapole) equipped with an electrospray ionization (ESI) source as described elsewhere.<sup>[22]</sup> Briefly, vanadium oxide clusters were generated by ESI of a solution of  $\text{V}_6\text{O}_7(\text{OCH}_3)_{12}$  in  $\text{CD}_3\text{OD}$ . Then,  $\text{V}_4\text{O}_{10}^+$  was mass-selected using Q1 and reacted with methane in the hexapole at pressures on the order of  $10^{-4}$  mbar, which approximately corresponds to single-collision conditions. The reaction was followed by detection of the ionic products using Q2. Ion-reactivity studies were performed at an interaction energy in the hexapole ( $E_{\text{lab}}$ ) nominally set to 0 eV.<sup>[15,23]</sup>

Calculations were performed using the hybrid density functional theory method B3LYP<sup>[24]</sup> with triple- $\zeta$  plus polarization basis sets

(TZVP)<sup>[25]</sup> employing Turbomole 5.7.<sup>[26]</sup> B3LYP has been shown previously to describe vanadium oxides in good agreement with available experimental data and the results of quantum chemical methods that explicitly include electron correlation.<sup>[27]</sup> MD simulation was performed with zero initial velocities from an optimized structure with a fixed distance between the vanadium and carbon atoms.

Received: January 17, 2006

Published online: May 26, 2006

**Keywords:** C–H activation · density functional calculation · mass spectrometry · molecular dynamics · vanadium oxides

- a) D. H. R. Barton, *Aldrichimica Acta* **1990**, 23, 3; b) B. A. Arndtsen, R. G. Bergman, T. A. Mobley, T. H. Peterson, *Acc. Chem. Res.* **1995**, 28, 154.
- A. A. Fokin, P. R. Schreiner, *Chem. Rev.* **2002**, 102, 1551.
- For selected reviews and original contributions, see: a) P. L. Watson, G. W. Parshall, *Acc. Chem. Res.* **1985**, 18, 51; b) C. Hall, R. N. Perutz, *Chem. Rev.* **1996**, 96, 3125; c) A. E. Shilov, G. B. Shul'pin, *Chem. Rev.* **1997**, 97, 2879; d) A. Sen, *Acc. Chem. Res.* **1998**, 31, 550; e) S. S. Stahl, J. A. Labinger, J. E. Bercaw, *Angew. Chem.* **1998**, 110, 2298; *Angew. Chem. Int. Ed.* **1998**, 37, 2180; f) H. Chen, S. Schlecht, T. C. Semple, J. F. Hartwig, *Science* **2000**, 287, 1995; g) J. H. Lunsford, *Catal. Today* **2000**, 63, 165; h) W. D. Jones, *Science* **2000**, 287, 1942; i) R. H. Crabtree, *J. Chem. Soc. Dalton Trans.* **2001**, 2437; j) C. Jia, T. Kitamura, Y. Fujiwara, *Acc. Chem. Res.* **2001**, 34, 633; k) P. Gelin, M. Primet, *Appl. Catal. B* **2002**, 39, 1; l) J. A. Labinger, J. E. Bercaw, *Nature* **2002**, 417, 507; m) J. A. Labinger, *J. Mol. Catal.* **2004**, 220, 27; n) M. Lersch, M. Tilset, *Chem. Rev.* **2005**, 105, 2471.
- U. Fekl, K. I. Goldberg, *Adv. Inorg. Chem.* **2003**, 54, 259.
- a) J. Haggin, *Chem. Eng. News* **1993**, 71, 27; b) R. H. Crabtree, *Chem. Rev.* **1995**, 95, 987; c) G. A. Olah, A. Molnar, *Hydrocarbon Chemistry*, Wiley, New York, **1995**; d) R. A. Periana, D. J. Taube, S. Gamble, H. Taube, T. Sato, H. Fuji, *Science* **1998**, 280, 560.
- For selected reviews, see: a) P. B. Armentrout, J. L. Beauchamp, *Acc. Chem. Res.* **1989**, 22, 315; b) H. Schwarz, D. Schröder, *Pure Appl. Chem.* **2000**, 72, 2319; c) P. Chen, *Angew. Chem.* **2003**, 115, 2938; *Angew. Chem. Int. Ed.* **2003**, 42, 2832; d) H. Schwarz, *Int. J. Mass Spectrom.* **2004**, 237, 75; e) D. K. Böhme, H. Schwarz, *Angew. Chem.* **2005**, 117, 2388; *Angew. Chem. Int. Ed.* **2005**, 44, 2336.
- For reviews, see: a) P. Pyykkö, *Chem. Rev.* **1988**, 88, 563; b) H. Schwarz, *Angew. Chem.* **2003**, 115, 4580; *Angew. Chem. Int. Ed.* **2003**, 42, 4442.
- a) R. Wesendrup, D. Schröder, H. Schwarz, *Angew. Chem.* **1994**, 106, 1232; *Angew. Chem. Int. Ed. Engl.* **1994**, 33, 1174; b) M. Pavlov, M. R. A. Blomberg, P. E. M. Siegbahn, R. Wesendrup, C. Heinemann, H. Schwarz, *J. Phys. Chem. A* **1996**, 104, 4642.
- D. Schröder, H. Schwarz, *Angew. Chem.* **1995**, 107, 2126; *Angew. Chem. Int. Ed. Engl.* **1995**, 34, 1973.
- K. K. Irikura, J. L. Beauchamp, *J. Am. Chem. Soc.* **1989**, 111, 75.
- I. Kretzschmar, A. Fiedler, J. N. Harvey, D. Schröder, H. Schwarz, *J. Phys. Chem. A* **1997**, 101, 6252.
- D. Schröder, H. Schwarz, S. Shaik, *Structure and Bonding* (Ed.: B. Meunier), Springer, Berlin, **2000**, p. 97.
- a) M. M. Kappes, R. H. Staley, *J. Am. Chem. Soc.* **1981**, 103, 1286; b) Y. M. Chen, D. E. Clemmer, P. B. Armentrout, *J. Am. Chem. Soc.* **1994**, 116, 7815; c) M. F. Ryan, A. Fiedler, D. Schröder, H. Schwarz, *Organometallics* **1994**, 13, 4072.
- a) K. A. Zemski, D. R. Justes, A. W. Castleman, Jr., *J. Phys. Chem. B* **2002**, 106, 6136 b) for the particular role of vanadium oxides as selective oxidation catalysts, see: G. Centi, F. Cavani, F.

- Triviró, *Selective Oxidation by Heterogeneous Catalysis*, Plenum Publishers, New York, **2001**.
- [15] S. Feyel, D. Schröder, H. Schwarz, *J. Phys. Chem. A* **2006**, *110*, 2647.
- [16] a) U. Achatz, C. Berg, S. Joos, B. S. Fox, M. K. Beyer, G. Niedner-Schatteburg, V. E. Bondybey, *Chem. Phys. Lett.* **2000**, *320*, 53; b) X. G. Zhang, R. Liyanage, P. B. Armentrout, *J. Am. Chem. Soc.* **2001**, *123*, 5563; c) D. Schröder, H. Schwarz, *Can. J. Chem.* **2005**, *83*, 1936.
- [17] J. Berkowitz, G. B. Ellison, D. Gutman, *J. Phys. Chem. B* **1994**, *98*, 2744.
- [18] H. T. Thümmel, *J. Phys. Chem. B* **1998**, *102*, 2002.
- [19] S. F. Vyboishchikov, J. Sauer, *J. Phys. Chem. A* **2001**, *105*, 8588.
- [20] K. R. Asmis, G. Santambrogio, M. Brümmer, J. Sauer, *Angew. Chem.* **2005**, *117*, 3182; *Angew. Chem. Int. Ed.* **2005**, *44*, 3122.
- [21] More generally speaking, the fact that  $[V_4O_{10}]^+$  [Eq. (7)],  $[MoO_3]^+$  [Eq. (1)], and  $[OsO_4]^+$  [Eq. (6)] bring about homolytic C–H activation of  $CH_4$  while  $[OsO_3]^+$  does not [Eq. (5)] underlines the particular role of the radical character of oxygen in this reaction. This conjecture is further supported by the notion that Li-doped MgO, which contains an  $O^-$  radical anion, is also predicted to bring about methane activation: a) D. J. Driscoll, W. Martir, J.-X. Wang, J. H. Lunsford, *J. Am. Chem. Soc.* **1985**, *107*, 58; b) S. J. Korf, J. A. Roos, N. A. De Bruijn, J. G. Van Ommen, J. R. H. Ross, *Catal. Today* **1988**, *2*, 535–545; c) S. J. Korf, J. A. Roos, N. A. De Bruijn, J. G. Van Ommen, J. R. H. Ross, *Appl. Catal.* **1990**, *58*, 131–146; d) V. R. Choudhary, S. T. Chaudhari, M. Y. Pandit, *J. Chem. Soc. Chem. Commun.* **1991**, 1158–1159; e) R. Orlando, F. Cora, R. Millini, G. Perego, R. Dovesi, *J. Chem. Phys.* **1996**, *105*, 8937–8943; f) C. R. A. Catlow, S. A. French, A. A. Sokol, J. M. Thomas, *Philos. Trans. R. Soc. London Ser. A* **2005**, *363*, 913–936.
- [22] D. Schröder, T. Weiske, H. Schwarz, *Int. J. Mass Spectrom.* **2002**, *219*, 729.
- [23] D. Schröder, M. Engeser, M. Brönstrup, C. Daniel, J. Spandl, H. Hartl, *Int. J. Mass Spectrom.* **2003**, *228*, 743.
- [24] a) C. Lee, W. Yang, R. G. Parr, *Phys. Rev. B* **1988**, *37*, 785; b) A. D. Becke, *J. Chem. Phys.* **1993**, *98*, 5648.
- [25] A. Schäfer, C. Huber, R. Ahlrichs, *J. Chem. Phys.* **1994**, *100*, 5829.
- [26] a) R. Ahlrichs, M. Bär, M. Häser, H. Horn, C. Kölmel, *Chem. Phys. Lett.* **1989**, *162*, 165; b) O. Treubler, R. Ahlrichs, *J. Chem. Phys.* **1995**, *102*, 346; c) K. Eichhorn, F. Weigand, O. Treubler, R. Ahlrichs, *Theor. Chem. Acc.* **1997**, *97*, 119; d) M. von Arnim, R. Ahlrichs, *J. Chem. Phys.* **1999**, *111*, 9183.
- [27] J. Sauer, J. Döbler, *Dalton Trans.* **2004**, *19*, 3116.

DOI: 10.1002/anie.200601131

## A Conjugated Polycarbazole Ring around a Porphyrin\*\*

Sung-Hyun Jung, Wojciech Pisula, Ali Rouhanipour,  
Hans Joachim Räder, Josemon Jacob, and  
Klaus Müllen\*

The construction of a  $\pi$ -conjugated macrocycle around a central  $\pi$ -system raises fascinating opportunities for energy or charge transfer between the core and periphery. Further, if the ring–core dyad assembles to a columnar superstructure, it can form a so-called coaxial cable. This is a long sought-after motif in materials science,<sup>[1]</sup> since it gives rise, for example, to separate energy- and charge-transport pathways along the column. In view of the difficulties in efficiently synthesizing large macrocycles, the core might also serve as a template for the build-up of the ring. Shape-persistent macrocycles with porous cavities, capable of forming ordered columnar structures have been synthesized both by a geometry-driven and a templated approach,<sup>[2–10]</sup> however, only few of them possess an extended  $\pi$ -conjugation.<sup>[11,12]</sup>

Poly(9-alkyl-2,7-carbazol)s (Scheme 1) are stable and processable conjugated polymers with favorable optical properties, such as emission with high color stability.<sup>[13–15]</sup> The inherently bent shape of the monomer allows for the formation of macrocycles with low torsional strain and extended  $\pi$ -conjugation, a situation which does not hold for many cyclic oligophenylenes and cyclic 3,6-oligocarbazoles<sup>[16,17]</sup> owing to the presence of *meta*-phenylene units. A prerequisite for the formation of hollow supramolecular columnar structures is to prevent the macrocyclic building blocks from collapsing, which in flexible ring systems can be avoided by the creation of host–guest complexes.<sup>[18]</sup> The formation of a tubular structure from a rigid carbazole macrocycle is particularly attractive as its inside can be functionalized through the introduction of functional groups at the carbazole nitrogen atoms.<sup>[8,10,19]</sup>

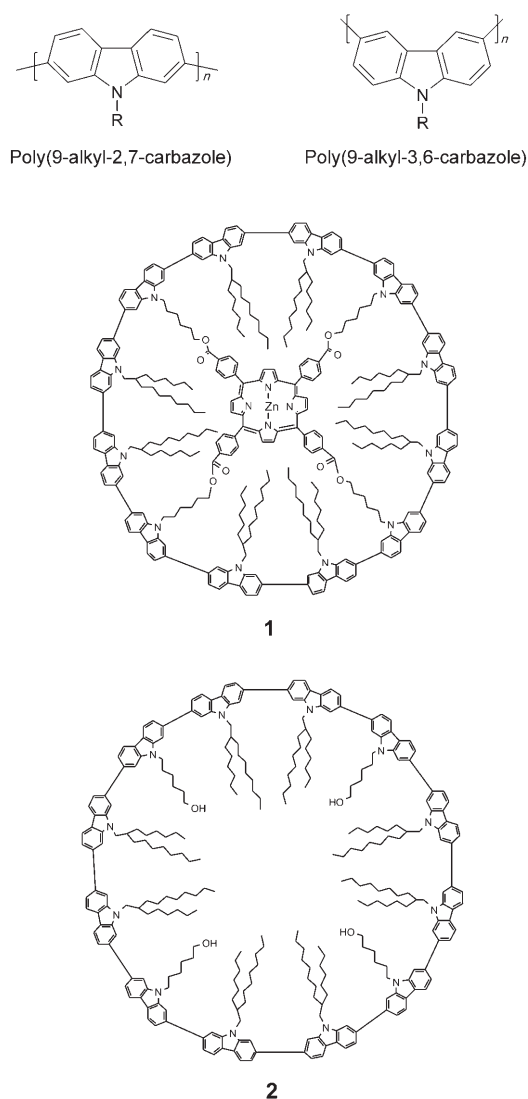
Herein, the template-assisted synthesis of a fully conjugated cyclododeca-2,7-carbazole around a *meso*-tetraphenylporphyrin template is presented, to afford **1** (Scheme 1).

[\*] Dr. S.-H. Jung, Dr. W. Pisula, A. Rouhanipour, Dr. H. J. Räder, Dr. J. Jacob, Prof. K. Müllen  
Max-Planck-Institut für Polymerforschung  
Ackermannweg 10, 55128 Mainz (Germany)  
Fax: (+49) 6131-379-350  
E-mail: muellen@mpip-mainz.mpg.de

[\*\*] This work was financially supported by the Post-doctoral Fellowship Program of Korea Science & Engineering Foundation (04-09-06-1). The authors would like to thank Dr. Martin Baumgarten for computational simulation and helpful discussions, Dr. Rüdiger Berger for introduction and support in AFM and STM measurements and Dr. Roland Bauer for graphical presentations.



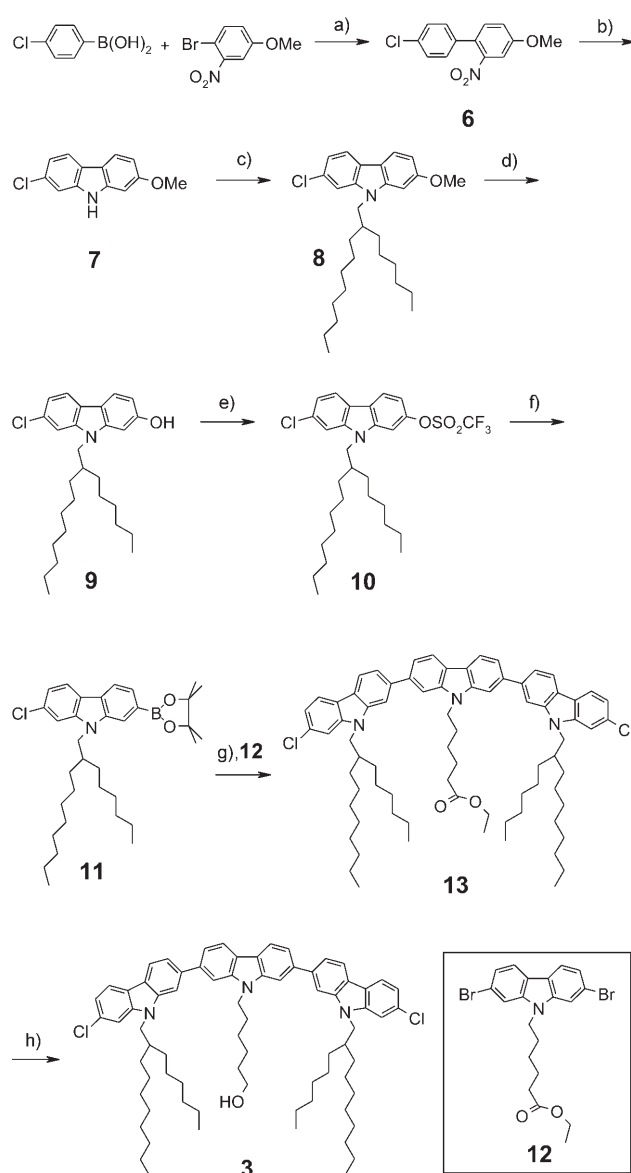
Supporting information for this article is available on the WWW under <http://www.angewandte.org> or from the author.



**Scheme 1.** Structures of poly(9-alkylcarbazole)s, templated cyclodeca-2,7-cabazole **1**, and corresponding vacant macrocyclic carbazole ring **2**.

Removal of the porphyrin template from the interior by hydrolytic cleavage of the ester groups of the spacers yields the vacant macrocycle **2**. Although its flexible alkyl chains only point towards the interior, columnar superstructures can be formed by fiber extrusion. Single-molecule detection of the new macrocycle and visualization of its doughnut shape are possible by scanning tunneling microscopy (STM).<sup>[20]</sup>

The key to the synthesis of the tris(carbazole) building block **3** is the hetero functionalization of a 2,7-disubstituted carbazole derivative, to yield the intermediate **8** (Scheme 2). From the commercially available 4-chlorobenzenboronic acid and 2-bromo-5-methoxynitrobenzene, a Suzuki coupling generated the biphenyl derivative **6** in 87% yield. Cadogan-type reductive amination gave the 2-chloro-7-methoxycarbazole which could be isolated in 58% yield.<sup>[8]</sup> Alkylation of the nitrogen atom (97%), and subsequent deprotection of the methoxy group with  $\text{BBr}_3$  (74%) and esterification, afforded 2-chloro-7-trifluoromethanesulfonyl-*N*-(2-hexyldecyl)carba-

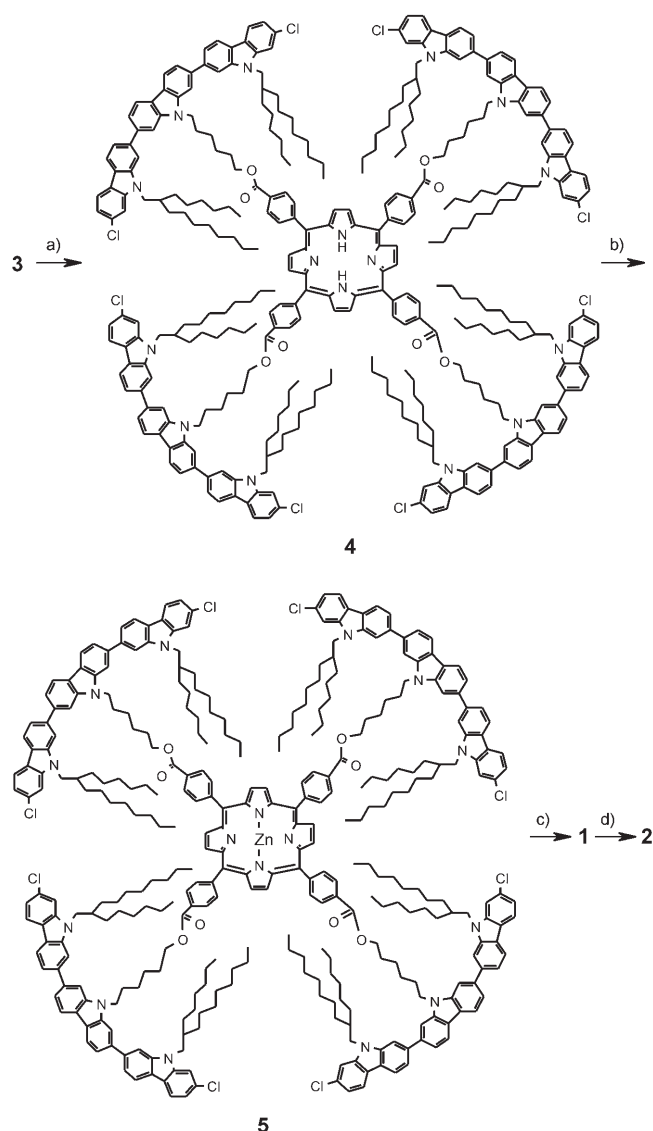


**Scheme 2.** a)  $[(\text{PPh}_3)_4\text{Pd}^0]$ , aqueous  $\text{K}_2\text{CO}_3$  (2 M), toluene, reflux for 12 h, 87%; b) triethylphosphite, reflux for 15 h, 58%; c) 1-bromo-2-hexyldecane, NaH, DMF, 97%; d)  $\text{BBr}_3$ , dichloromethane,  $-78^\circ\text{C}$  for 3 h, RT for 12 h, 74%; e) trifluoromethanesulfonyl anhydride, dimethylaminopyridine, pyridine,  $0^\circ\text{C}$  for 2 h, RT for 24 h, 86%; f) bis(pinacolato)diboron,  $[\text{PdCl}_2(\text{dppf})]$ , potassium acetate, DMF,  $80^\circ\text{C}$  for 12 h, 86%; g)  $[(\text{PPh}_3)_4\text{Pd}^0]$ , aqueous  $\text{K}_2\text{CO}_3$  (2 M), toluene, reflux for 12 h, 67%; h)  $\text{LiAlH}_4$ , THF, RT for 1 h, 94%. dppf = 1,1'-bis(diphenylphosphanyl)ferrocene.

zole (**10**) in 86% yield.<sup>[21]</sup> The triflate group underwent selective conversion into the corresponding boronate ester **11** (86%) under palladium-catalyzed conditions. The functionalized tris(carbazole) **13** was synthesized by a Suzuki coupling of **11** with **12** (67%). Reduction of **13** with  $\text{LiAlH}_4$  gave the carbazole trimer **3** with a hydroxy tether on the central carbazole (94%).

Four equivalents of **3** were coupled with *meso*-tetra(4-carboxyphenyl)porphyrin in the presence of diethylazodicarboxylate and triphenylphosphine to afford the porphyrin **4** (73% yield; Scheme 3), which was then complexed with zinc





**Scheme 3.** a) *meso*-Tetra(4-carboxyphenyl)porphine, diethyl azodicarboxylate, PPh<sub>3</sub>, THF, RT overnight, 73%; b) ZnOAc<sub>2</sub>·2H<sub>2</sub>O, CH<sub>3</sub>OH, dichloromethane, reflux for 2 h, 94%; c) bis(1,5-cyclooctadiene)-nickel(0), 2,2'-bipyridine, cyclooctadiene, toluene, DMF, 70°C for 3 h, 80°C for 3 h, 100°C for 8 h, 9%; d) KOH, H<sub>2</sub>O, CH<sub>3</sub>OH, THF, reflux for 24 h, 18%.

by heating under reflux with zinc acetate to generate **5** (94%). The final cyclization of **5** was performed by a nickel-mediated Yamamoto coupling reaction for which two experimental details are crucial: 1) high dilution ( $8 \times 10^{-5}$  M) to prevent the intermolecular aryl–aryl coupling, and 2) use of a microwave reactor to increase the efficiency of the Yamamoto reaction. Separation of the desired compound from the mixture of products by preparative thin-layer chromatography (TLC) resulted in the isolation of **1** (9%). The MALDI-TOF mass spectrum of the product exhibited one intense signal corresponding to the calculated mass of **1** (see Supporting Information). The template was readily removed from the ring by hydrolysis with KOH to generate the fully conjugated macrocyclic carbazole dodecamer **2** which is soluble in

common organic solvents, thus enabling purification by preparative TLC and HPLC (18% yield).

Compounds **1** and **2** were characterized by UV/Vis and fluorescence spectroscopy, MALDI-TOF, atomic force microscopy (AFM), STM, two-dimensional wide angle X-ray scattering (2D WAXS), and <sup>1</sup>H and <sup>13</sup>C NMR spectroscopy measurements. Figure 1a illustrates the MALDI-TOF spec-

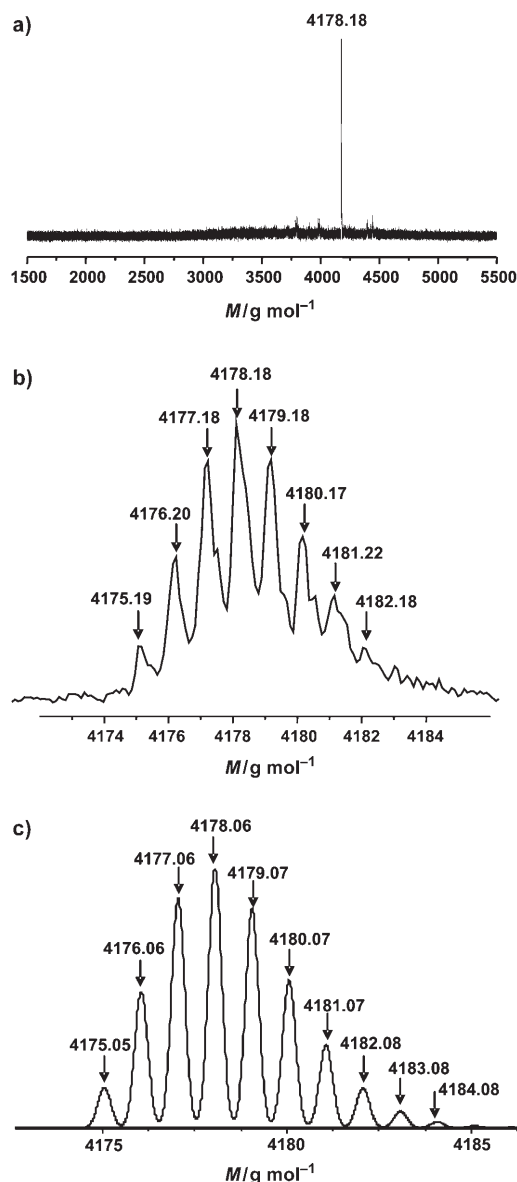


**Figure 1.** a) MALDI-TOF spectrum of **2** b) section of the experimental spectrum b) section of the simulated spectrum.

trum of **2** together with an expanded view of the molecular-ion region. A comparison of the measured (Figure 1b) and the calculated (Figure 1c) isotopic distributions of **2** shows a good agreement.<sup>[22]</sup>

The absorption and emission spectra of **1**, **2**, and poly[9-(2-decyltetradecyl)-2,7-carbazole] ( $M_n = 1.9 \times 10^4$ , polyparaphenylene (PPP) standard), as a linear model compound, in dichloromethane ( $10^{-6}$  M) are shown in Figure 2. Compound **2**

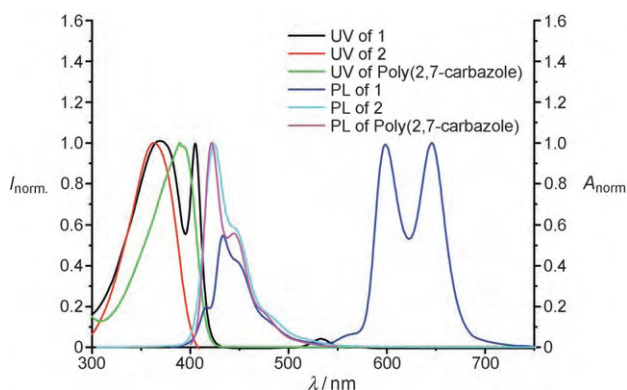


**Figure 2.** Comparison of normalized absorption ( $A_{\text{norm}}$ ) and emission ( $I_{\text{norm}}$ ) spectra of templated **1**, **2**, and poly[9-(2-decyltetradecyl)-2,7-carbazole] in dichloromethane. PL = photoluminescence.

gives an absorption maximum at 363 nm, which is blue-shifted by 27 nm compared to the linear polymer. This shift is attributed to a stronger twist between successive carbazole units in the macrocycle, since all the carbazole moieties are arranged in a *cis* fashion. However, the emission spectra of both **2** and the linear polymer are almost identical, which indicates similar excited state geometries. Compound **1** gives an absorption at 369 nm, corresponding to the  $\pi$ - $\pi^*$  transition of the carbazole macrocycle, and at 405 nm, corresponding to the Soret band of the zinc-complexed porphyrin, with the Q-band absorptions at 533 nm and 571 nm. The  $\pi$ - $\pi^*$  transition of **1** is slightly red shifted (6 nm) compared with **2**. This shift indicates that the “anchored” carbazole macrocycle around the porphyrin template is slightly planarized owing to the restricted torsion. Upon excitation of **1** ( $\lambda_{\text{ex}} = 370$  nm), emission is observed from both the carbazole ring, at 433 nm, and the porphyrin template, at 600 nm and 647 nm. The spectral overlap between the emission of the carbazole ring and the absorption of the porphyrin core demonstrates that there is Förster energy transfer from the peripheral carbazole  $\pi$  system to the central porphyrin core (calculated energy transfer efficiency 83 %).<sup>[23]</sup>

Information on the size and shape of **2** was obtained after spin coating its dilute THF solution on a freshly cleaved, highly oriented pyrolytic graphite (HOPG) surface and visualization of the ad-layer by AFM.<sup>[24]</sup> Figure 3 shows two- and three-dimensional presentations of self-assembled molecules of **2** forming extended domains with an average height of 0.3 nm (determined from the difference between the domains and the smooth and flat regions of the uncovered HOPG surface between the domains). The constant thickness of 0.3 nm as well as the hexagonal lattice of spots having a uniform size distribution gives evidence that the domains are composed of a monolayer of single-molecules facing the surface. The average center-to-center distance of 4.1 nm between the molecules and their compact and round shape confirm the cyclic structure and suggest that the alkyl chains are directed towards the center of the macrocycle. The bulky alkyl chains seem to fill the inner space (see Supporting Information), which explains why the macrocycles in Figure 3 do not appear flat or empty in the center. This result is in

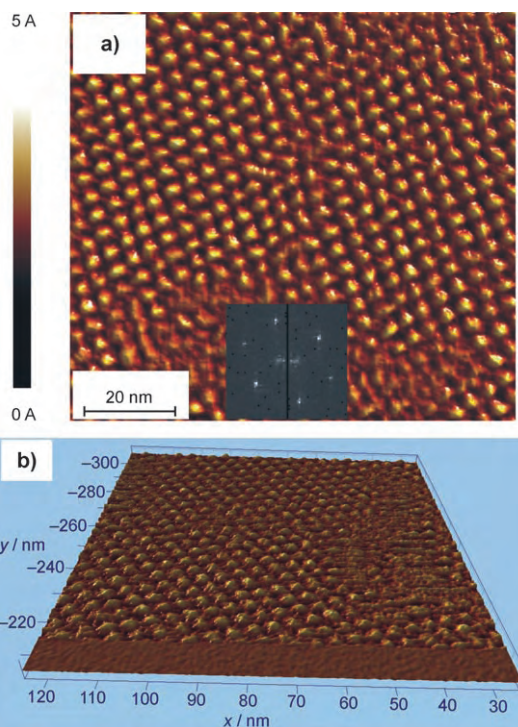


**Figure 3.** a) 2D and b) 3D-AFM images of a monolayer **2** on a HOPG surface.

agreement with the calculated molecular structure; semi-empirical calculation at the AM1 level showed that **2** has a diameter of 3.6 nm (see Supporting Information).

A submolecular resolution of **2** was obtained by STM investigations at the solid/air interface. Similar to AFM, the STM sample was prepared by spincoating a dilute THF solution of **2** on a fresh HOPG surface. Figure 4b,c illustrate three-dimensional representations of single-molecules of **2** on a partially covered HOPG surface. Remarkably, the thermal movement of some molecules at the surface is slow enough relative to the scan speed to achieve measurements of single-molecules even at room temperature. The picture in Figure 4b shows additional unresolved objects which originate from the measurement of moving macrocycles. On the same sample, small domains of macromolecules pack in a hexagonal arrangement (Figure 4a). The average diameter of the ring-shaped objects is 4.0 nm. The contrast in the STM pictures of **2** is provided by the conjugated cyclic aromatic  $\pi$  system, as aromatic moieties show a higher tunneling efficiency than the aliphatic parts.<sup>[25]</sup> Thus, the STM pictures give clear evidence for the perfect cyclic structure and visualize the  $\pi$  system composed of carbazole subunits with an “electronic hole” in the core.

The 3D-supramolecular organization of **2** was investigated by 2D-WAXS experiments on a mechanically aligned sample.<sup>[26]</sup> The equatorial reflections at ambient temperatures (Figure 5a) indicate a self-assembly of the macrocycles into a hexagonal array of columns with a packing parameter of 4.7 nm (Figure 5c). In these structures the ring-shaped molecules have their molecular planes orthogonal to the columnar axis. The appearance of multiple meridional

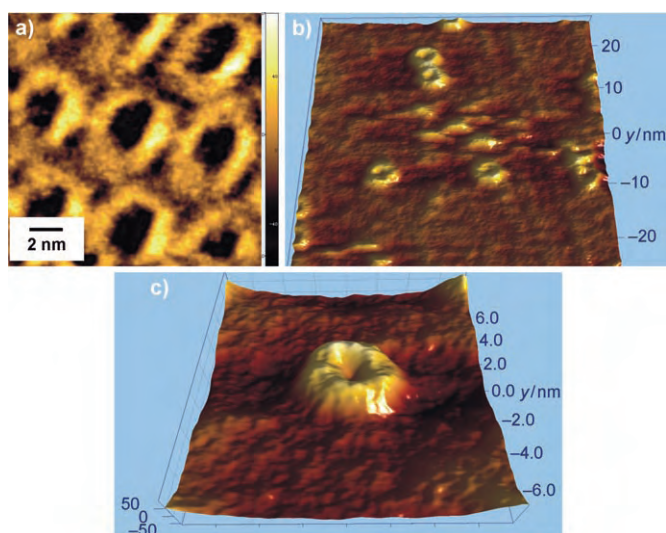


**Figure 4.** STM images of **2** on a HOPG surface at solid/air interface (tunneling current: 1.3 pA, bias voltage: 800 mV). a) 2D view of a monolayer with hexagonal packing of **2**. b) 3D view of individual macrocycles. The unresolved objects originate from the movement of molecules. c) 3D view of a single macrocycle showing the “electronic hole” in the center.

reflections indicates a complex intracolumnar arrangement.<sup>[27]</sup> The first meridional reflection and the stacking distance of 0.4 nm between neighboring cycles implies a correlation between every fourth molecule along the columns. Therefore, each macrocycle is rotated by 22.5° towards the adjacent building block leading to an identical positional order after rotation by 90°. This structure is in good agreement with the molecular structure, where every third carbazole unit in the 12-membered ring has a hydroxyalkyl chain on the nitrogen atom. This helical arrangement is the result of an intracolumnar packing optimization arising from the nonplanarity of the core. In contrast to discotic and macrocyclic columnar systems,<sup>[9,26]</sup> the space between rigid stacks of **2** cannot be filled by the flexible aliphatic side chains, as the side chains point towards the molecular center. The optimal columnar arrangement should be hexagonal, which is indeed observed. This remarkable self-organization of the macrocycles into superstructures occurs in spite of the nonplanarity of the molecular rings. This arrangement opens the opportunity for a charge-carrier transport along the  $\pi$ -stacking direction as observed for many columnar thermotropic discotic compounds, but with the difference that in this case the columnar periphery is not filled by the insulating alkyl substituents. The charge carriers are not necessarily transported on only one column, they are able to change their percolation pathways spontaneously thereby decreasing the influence of single defects.

In conclusion, the synthesis of a fully conjugated, monodisperse, 2,7-carbazole-based macrocyclic dodecamer, using a template approach, is presented. AFM measurements of a monolayer of **2** on HOPG displayed a hexagonal lattice composed of spots of uniform size distribution. Additional evidence for the conjugated ring-shaped structure of **2** was obtained by STM investigations. It is remarkable that even

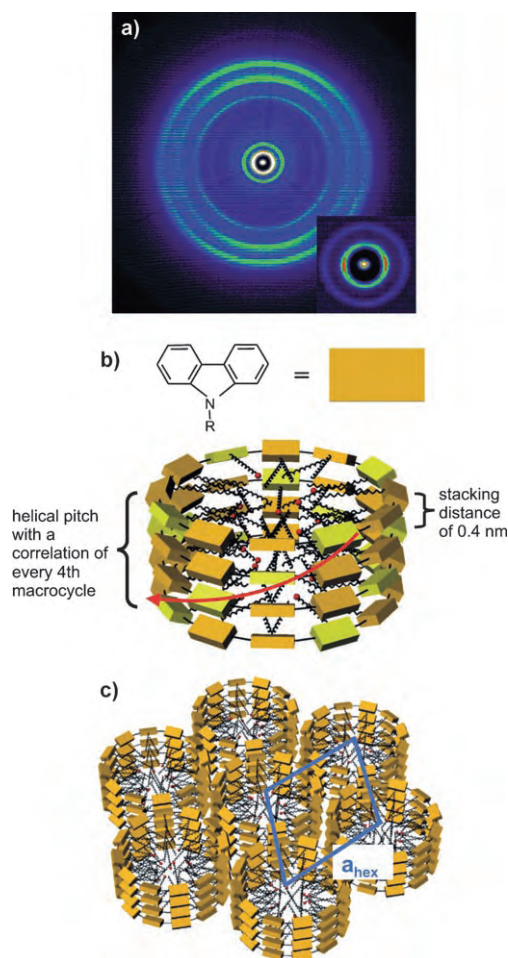


**Figure 5.** a) 2D-WAXS of **2** at ambient temperature (inset: small-angle region at different contrast), b) schematic illustration of the helical organized macrocycles (the units containing the hydroxyalkyl chain are indicated in yellow), c) hexagonal arrangement of the columnar structures with 4.7 nm as the 2D lateral packing parameter.

single-molecules and small domains with ordered structures can be measured at ambient conditions; this provides evidence that **2** is perfectly round with a conjugated cyclic  $\pi$ -system. 2D-WAXS experiments on a mechanically aligned sample indicated self-assembly of the macrocycles into columnar structures. The molecules are rotated laterally towards each other, as induced by the molecular geometry. Our template approach towards conjugated macrocyclic oligocarbazoles holds promise for the design of further nanoscale  $\pi$ -systems: 1) as a result of the functionalized cavities of **2**, guest molecules, such as electron acceptors, can be introduced by noncovalent interactions or chemical reactions, 2) thanks to the low mobility of **2** on surfaces STM characterization of similar systems should be possible, and 3) other templates can pave the way to larger oligocarbazole macrocycles.

Received: March 22, 2006

Published online: June 21, 2006



**Keywords:** macrocycles · oligocarbazoles · scanning probe microscopy · template synthesis · X-ray diffraction

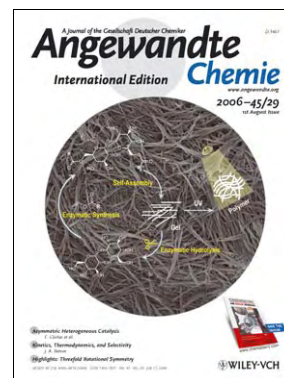
- [1] J. S. Wu, M. Baumgarten, M. G. Debije, J. M. Warman, K. Müllen, *Angew. Chem.* **2004**, *116*, 5445–5449; *Angew. Chem. Int. Ed.* **2004**, *43*, 5331–5335.
- [2] S. Höger, A. D. Meckenstock, S. Müller, *Chem. Eur. J.* **1998**, *4*, 2423–2434.
- [3] S. Höger, *Chem. Eur. J.* **2004**, *10*, 1320–1329.
- [4] D. H. Zhao, J. S. Moore, *Chem. Commun.* **2003**, 807–818.
- [5] W. Zhang, J. S. Moore, *J. Am. Chem. Soc.* **2004**, *126*, 12796–12796.
- [6] S. Höger, *J. Polym. Sci. Part A* **1999**, *37*, 2685–2698.
- [7] S. Höger, K. Bonrad, A. Mourran, U. Beginn, M. Möller, *J. Am. Chem. Soc.* **2001**, *123*, 5651–5659.
- [8] M. Fischer, S. Höger, *Eur. J. Org. Chem.* **2003**, 441–446.
- [9] M. Fischer, G. Lieser, A. Rapp, I. Schnell, W. Mamdouh, S. De Feyter, F. C. De Schryver, S. Höger, *J. Am. Chem. Soc.* **2004**, *126*, 214–222.
- [10] S. Höger, A. D. Meckenstock, *Chem. Eur. J.* **1999**, *5*, 1686–1691.
- [11] G. Fuhrmann, J. Krömer, P. Bäuerle, *Synth. Met.* **2001**, *119*, 125–126.
- [12] J. Krömer, I. Rios-Carreras, G. Fuhrmann, C. Musch, M. Wunderlin, T. Debaerdemaeker, E. Mena-Osteritz, P. Bäuerle, *Angew. Chem.* **2000**, *112*, 3623–3628; *Angew. Chem. Int. Ed.* **2000**, *39*, 3481–3486.
- [13] J. F. Morin, M. Leclerc, *Macromolecules* **2001**, *34*, 4680–4682.
- [14] J. F. Morin, M. Leclerc, *Macromolecules* **2002**, *35*, 8413–8417.
- [15] J. F. Morin, P. L. Boudreault, M. Leclerc, *Macromol. Rapid Commun.* **2002**, *23*, 1032–1036.
- [16] J. Ostrauskaite, P. Stroehriegl, *Macromol. Chem. Phys.* **2003**, *204*, 1713–1718.
- [17] S. Maruyama, H. Hokari, T. Wada, H. Sasabe, *Synthesis* **2001**, 1794–1799.
- [18] A. Liebmann, C. Mertesdorf, T. Plesnivý, H. Ringsdorf, J. H. Wendorff, *Angew. Chem.* **1991**, *103*, 1358–1361; *Angew. Chem. Int. Ed. Engl.* **1991**, *30*, 1375–1377.
- [19] M. Fischer, S. Höger, *Tetrahedron* **2003**, *59*, 9441–9446.
- [20] O. Shoji, H. Tanaka, T. Kawai, Y. Kobuke, *J. Am. Chem. Soc.* **2005**, *127*, 8598–8599.
- [21] F. Dierschke, A. C. Grimsdale, K. Müllen, *Synthesis* **2003**, 2470–2472.
- [22] The small signals in the region below 4000 g mol<sup>-1</sup> can be explained by fragmentation of one or two branched alkyl chains (–C<sub>16</sub>H<sub>33</sub>, 225 g mol<sup>-1</sup>). Such fragmentations in MALDI-TOF experiments are related to the strong UV absorption of the macrocycle at the wavelength of the nitrogen desorption laser (337 nm), which causes a high internal energy of the analyte molecules in the gas phase and thus a higher tendency for fragmentation. L. Przybilla, J. D. Brand, K. Yoshimura, H. J. Räder, K. Müllen, *Anal. Chem.* **2000**, *72*, 4591–4597.
- [23] T. Förster, *Ann. Phys.* **1948**, *2*, 55–75.
- [24] M. Namba, M. Sugawara, P. Buhlmann, Y. Umezawa, *Langmuir* **1995**, *11*, 635–638.
- [25] S. De Feyter, A. Gesquière, M. M. Abdel-Mottaleb, P. C. M. Grim, F. C. De Schryver, C. Meiners, M. Sieffert, S. Valiyaveetil, K. Müllen, *Acc. Chem. Res.* **2000**, *33*, 520–531.
- [26] W. Pisula, Ž. Tomovic, C. D. Simpson, M. Kastler, T. Pakula, K. Müllen, *Chem. Mater.* **2005**, *17*, 4296–4303.
- [27] J. S. Wu, M. D. Watson, L. Zhang, Z. H. Wang, K. Müllen, *J. Am. Chem. Soc.* **2004**, *126*, 177–186.



# Cover Picture

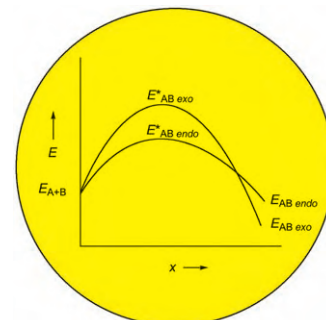
George John, Guangyu Zhu, Jun Li, and Jonathan S. Dordick\*

**Enzymatically synthesized** symmetrical trehalose diesters self-assemble into fibrous gel networks in a wide range of organic solvents and at very low gelator concentrations. Gels containing acrylate functionalities can be further stabilized through polymerization. In the presence of added water and the same enzyme, the gels degrade into trehalose, as shown in the cover picture. In their Communication on page 4772 ff., J. S. Dordick et al. describe how combining the principles of supramolecular chemistry and the selectivity of biocatalysis represents a powerful strategy to develop defined functional materials.



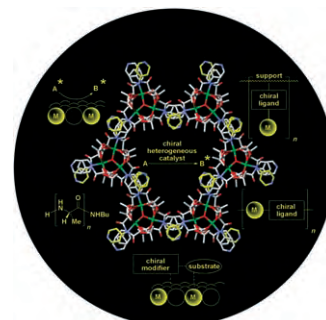
## Concept of Selectivity

In his Essay on page 4724 ff., J. A. Berson describes the reception by the scientific community in the first half of the 20th century of the principles of kinetic versus thermodynamic control and explains the physical basis of selectivity.



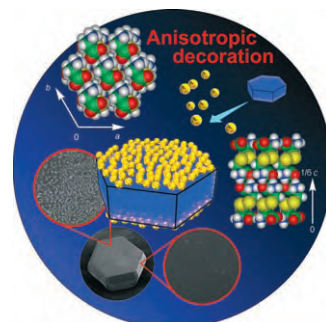
## Asymmetric Heterogeneous Catalysis

An overview of the concepts of asymmetric heterogeneous catalysis is given in the Review by F. Glorius et al. on page 4732 ff. The central themes are metal–organic catalysts, chiral modifiers, noncovalent immobilization, and the application of solid supports.



## Composite Materials

In their Communication on page 4764 ff., K. Sada, S. Shinkai, and co-workers describe how the anisotropy of L-cystine single crystals leads to their face-selective decoration by gold nanoparticles.





The following Communications have been judged by at least two referees to be "very important papers" and will be published online at [www.angewandte.org](http://www.angewandte.org) soon:

C. P. Gros, Jean-M. Barbe,\* E. Espinosa, R. Guillard\*  
Room-Temperature Autoconversion of Free-Base Corrole to Free-Base Porphyrin

S. Cobo, G. Molnár, J. A. Real, A. Bousseksou\*  
Multilayer Sequential Assembly of Thin Films Displaying Room-Temperature Spin Crossover with Hysteresis

R. J. Wright, M. Brynda, P. P. Power\*  
Synthesis and Structure of "Dialuminyne"  $\text{Na}_2\text{Ar}'\text{AlAlAr}'$  and "Cyclotrialuminene"  $\text{Na}_2(\text{Ar}''\text{Al})_3$ : Al–Al Bonding in  $\text{Al}_2\text{Na}_2$  and  $\text{Al}_3\text{Na}_2$  Clusters

J. M. Goicoechea, S. C. Sevov\*  
 $[\text{Zn}_9\text{Bi}_{11}]^{5-}$ : A Ligand-Free Intermetalloid Cluster

W. Su, S. Raders, J. G. Verkade,\* X. Liao, J. F. Hartwig\*  
Palladium-Catalyzed  $\alpha$ -Arylation of Trimethylsilyl Enol Ethers with Aryl Bromides and Chlorides: A Synergistic Effect of Two Metal Fluorides as Additives

A. Abo-Riziq, B. O. Crews, M. P. Callahan, L. Grace, M. S. de Vries\*  
Spectroscopy of Isolated Gramicidin Peptides

## Meeting Reviews

From Abyssomicin to Zaragozaic Acid: Chemical Synthesis and Drug Innovation

S. A. Snyder \_\_\_\_\_ 4714

## Books

Oxidation and Antioxidants in Organic Chemistry and Biochemistry

Evgeny T. Denisov, Igor B. Afanas'ev

reviewed by G. Pedulli \_\_\_\_\_ 4715

## Highlights

### Threefold Symmetry (1)

S. E. Gibson,\* M. P. Castaldi 4718–4720

$C_3$  Symmetry: Molecular Design Inspired by Nature

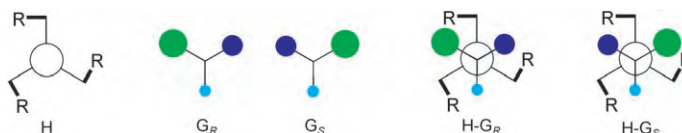


**Symmetry and molecular recognition:** The presence of  $C_3$  symmetry in nature has recently inspired the first biomimetic  $C_3$ -symmetric catalyst for asymmetric syntheses (see picture). Threefold symmetry also features in a recent approach to modulating the function of the tumor necrosis factor receptor superfamily.

### Threefold Symmetry (2)

C. Moberg\* \_\_\_\_\_ 4721–4723

Can  $C_3$ -Symmetric Receptors Differentiate Enantiomers?



**Symmetry and chiral recognition:** In contrast to previous arguments, recent reports have demonstrated that  $C_3$ -symmetric receptors can bind chiral sub-

strates with high enantioselectivity (see picture: H = host, G = (*S*) or (*R*)-configured guest; colored spheres represent different-sized substituents).

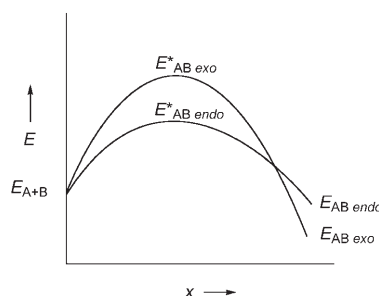
## Essays

### History of Science

J. A. Berson\* \_\_\_\_\_ 4724–4729

Kinetics, Thermodynamics, and the Problem of Selectivity: The Maturation of an Idea

**Why so slow?** Why did it take several decades for the concept of selectivity to develop into a fundamental consideration in organic chemistry? The Essay describes the reception by the scientific community in the first half of the 20th century of the principles of kinetic versus thermodynamic control and explains the physical basis of selectivity (see picture: energy diagram for the reaction of pentamethylenefulvene (A) and maleic anhydride (B)).

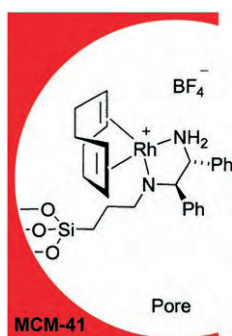


## Reviews

### Catalysis

M. Heitbaum, F. Glorius,\*  
I. Escher \_\_\_\_\_ 4732–4762

Asymmetric Heterogeneous Catalysis



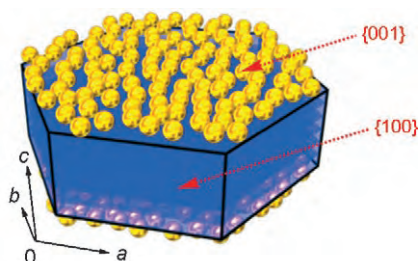
**Mirror, mirror** on the wall, who is the best asymmetric catalyst of all? The field of heterogeneous asymmetric catalysis is multifarious, vibrant, and creates new possibilities. For example, the use of mesoporous solids (see picture) allows selective immobilization in the pores, which results in improved catalytic properties in a number of cases. The most important methods are discussed in the Review.

## Communications

### Composite Materials

Y. Fujiki, N. Tokunaga, S. Shinkai,  
K. Sada\* \_\_\_\_\_ 4764–4767

Anisotropic Decoration of Gold Nanoparticles onto Specific Crystal Faces of Organic Single Crystals



**Face to face:** The hexagonal {001} or {00 $\bar{1}$ } faces of single crystals of L-cystine were selectively decorated by dipping them into a solution of gold nanoparticles (see picture). The selectivity results from an anisotropic molecular packing of L-cystine in the single crystal.

#### For the USA and Canada:

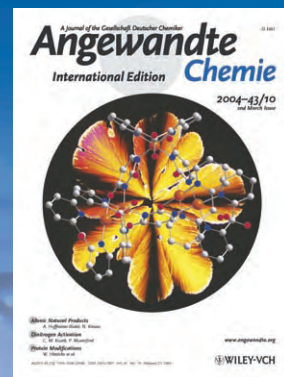
ANGEWANDTE CHEMIE International Edition (ISSN 1433-7851) is published weekly by Wiley-VCH PO Box 191161, D 69451 Weinheim, Germany. Air freight and mailing in the USA by Publications Expediting Inc. 200

Meacham Ave., Elmont, NY 11003. Periodicals postage paid at Jamaica NY 11431. US POSTMASTER: send address changes to *Angewandte Chemie*, Wiley-VCH, 111 River Street, Hoboken, NJ 07030. Annual subscription price for institutions: US\$ 5685/5168 (valid for print and

electronic / print or electronic delivery); for individuals who are personal members of a national chemical society prices are available on request. Postage and handling charges included. All prices are subject to local VAT/sales tax.



# The best in chemistry – for more than a hundred years



A Journal of the Gesellschaft Deutscher Chemiker  
**Angewandte Chemie**  
International Edition

[www.angewandte.org](http://www.angewandte.org)

**1888:** The beginning  
of a success story

## Constant Innovations

- 1962:** First issue of the International Edition
- 1976:** Graphical abstracts
- 1979:** Cover pictures
- 1988:** Centenary of Angewandte
- 1989:** Routine use of color
- 1991:** New section: Highlights
- 1992:** Computerized editorial tracking system
- 1995:** Internet service for readers
- 1998:** Regular press service; full-text online
- 2000:** New section: Essays; EarlyView: Communications available online ahead of the printed version
- 2001:** New section: Minireviews
- 2002:** Online submission of manuscripts
- 2003:** Weekly publication; new section: News; new layout
- 2004:** Backfiles (1962-1997); ManuscriptXpress: Online system for authors and referees



## Angewandte's advisors...

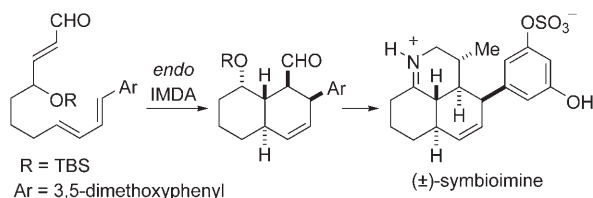
**Hartmut Wiezer**  
Clariant International AG,  
Sulzbach am Taunus

» *Angewandte Chemie* is a highly acknowledged international chemical journal. Its attraction is based on excellence in content and presentation. It is a pleasure to commit myself to further the quality and success of **Angewandte Chemie**.«

Angewandte Chemie International Edition is  
a journal of the German Chemical Society (GDCh)







**An inside job:** A Lewis acid induced intramolecular Diels–Alder (IMDA) reaction is used as the key step in the formation of symbioimine, an iminium alkaloid. The intermediate octahydronaphthalene is obtained from the IMDA

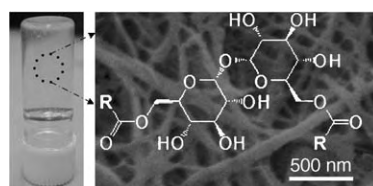
reaction, after which extension of the aldehyde to a nitrile, alkylation of the nitrile, and imine formation allows for an efficient route to the target compound (see scheme; TBS = *tert*-butyldimethylsilyl).

## Cycloaddition

G. N. Varseev, M. E. Maier\* 4767–4771

Total Synthesis of (±)-Symbioimine

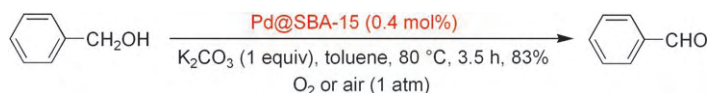
**The long and short of it:** A regioselective enzyme-catalyzed acylation of the disaccharide trehalose generated a family of low-molecular-weight gelators with unprecedented properties. The selectivity of enzymatic catalysis enables direct control over gelation properties by simply varying the acyl-chain length to give gelation in solvents ranging from the highly hydrophilic acetonitrile to the highly hydrophobic cyclohexane.



## Organogels

G. John, G. Zhu, J. Li,  
J. S. Dordick\* 4772–4775

Enzymatically Derived Sugar-Containing Self-Assembled Organogels with Nanostructured Morphologies



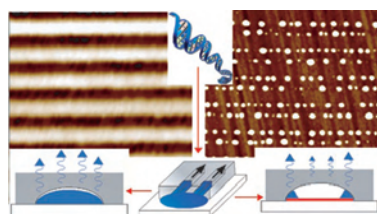
**Scaling down the activity:** An efficient recyclable palladium-based catalyst has been developed for the aerobic oxidation of alcohols (see scheme). The combination of a substituted bipyridyl ligand and ordered mesoporous channels (in SBA)

causes a synergistic effect that results in enhanced activity, the prevention of agglomeration of the palladium nanoparticles, and the generation of a durable catalyst.

## Aerobic Oxidation

B. Karimi,\* S. Abedi, J. H. Clark,  
V. Budarin 4776–4779

Highly Efficient Aerobic Oxidation of Alcohols Using a Recoverable Catalyst: The Role of Mesoporous Channels of SBA-15 in Stabilizing Palladium Nanoparticles



**DNA deposits** with submicrometer features can be prepared by micromolding in capillaries on a mica plate (see picture). Upon evaporation, surface properties of the DNA solution and the support come to the fore. The morphology of the DNA deposit can be controlled simply by adjusting the concentrations of the DNA solution and added salt.

## DNA on Surfaces

E. Bystrenova, M. Facchini, M. Cavallini,  
M. G. Cacace, F. Biscarini\* 4779–4782

Multiple Length-Scale Patterning of DNA by Stamp-Assisted Deposition

## Efficient Hydrogenation

A. B. Hungria, R. Raja, R. D. Adams,\*  
B. Captain, J. M. Thomas,\* P. A. Midgley,  
V. Golovko, B. F. G. Johnson **4782–4785**

Single-Step Conversion of Dimethyl  
Terephthalate into Cyclohexane-  
dimethanol with Ru<sub>5</sub>PtSn, a Trimetallic  
Nanoparticle Catalyst

**Highly active and selective:** A supported Ru<sub>5</sub>PtSn nanoparticle cluster (the picture shows an axial projection of a tomogram), prepared from the carbonyl cluster [PtRu<sub>5</sub>(CO)<sub>15</sub>(μ-SnPh<sub>2</sub>)(μ<sub>6</sub>-C)], is an excellent catalyst in the single-step hydrogenation of dimethyl terephthalate to cyclohexanedimethanol under mild conditions (100 °C, 20 bar H<sub>2</sub>).

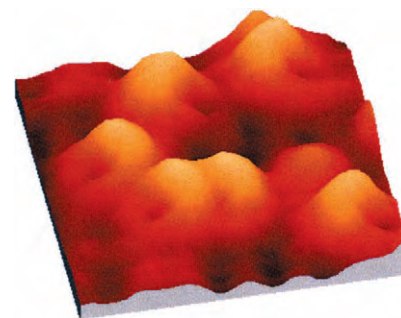


## Oxide Clusters

O. Bondarchuk, X. Huang, J. Kim,  
B. D. Kay, L.-S. Wang, J. M. White,\*  
Z. Dohnálek\* **4786–4789**

Formation of Monodisperse (WO<sub>3</sub>)<sub>3</sub>  
Clusters on TiO<sub>2</sub>(110)

**In groups of three:** Monodisperse clusters of WO<sub>3</sub> were prepared on a TiO<sub>2</sub>(110) surface through direct sublimation of WO<sub>3</sub> onto the substrate at 300 K followed by annealing to 600 K (see image). Combined evidence from scanning tunneling microscopy, X-ray photoelectron spectroscopy, quartz crystal mass balance, and density functional theory strongly indicates that the clusters are cyclic (WO<sub>3</sub>)<sub>3</sub> species.

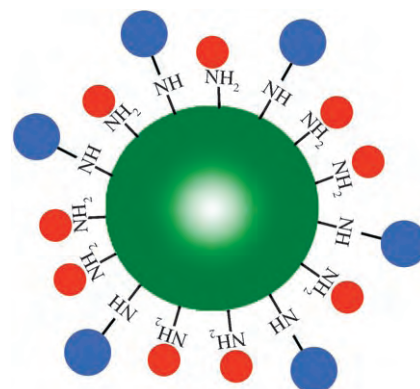


## Nanoparticle Assemblies

J. Kim, J. E. Lee, J. Lee, Y. Jang, S.-W. Kim,  
K. An, J. H. Yu, T. Hyeon\* **4789–4793**

Generalized Fabrication of  
Multifunctional Nanoparticle Assemblies  
on Silica Spheres

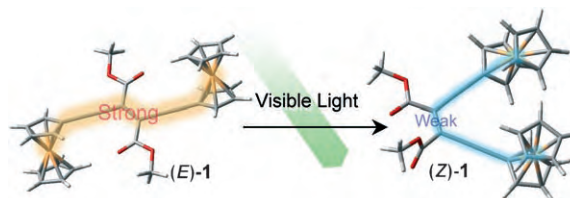
**Sequential decoration** of silica spheres by covalent bonding of magnetite nanoparticles (blue) and attachment of functional nanoparticles of Au, CdSe/ZnS, or Pd (red) afforded multifunctional assemblies exhibiting combinations of magnetism with surface plasmon resonance (Au), luminescence (CdSe/ZnS), and catalytic activity (Pd), respectively.



## Ferrocene Derivatives

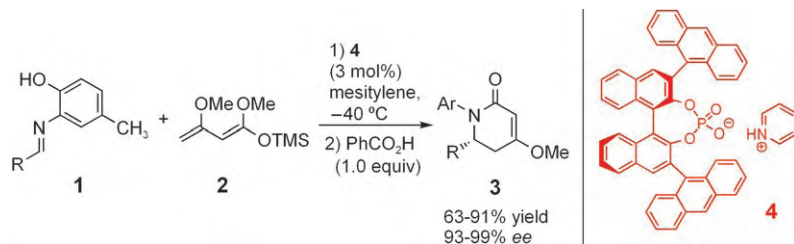
R. Sakamoto, M. Murata,  
H. Nishihara\* **4793–4795**

Visible-Light Photochromism of  
Bis(ferrocenylethynyl)ethenes Switches  
Electronic Communication between  
Ferrocene Sites



**Communicating better over a long distance:** The bis(ferrocenylethynyl)ethene **1** undergoes *E*→*Z* photoisomerization upon excitation of a charge-transfer band

with visible light (546 nm). This structural change leads to a decrease in the “through-bond” mixed-valence interaction between the two ferrocene units.



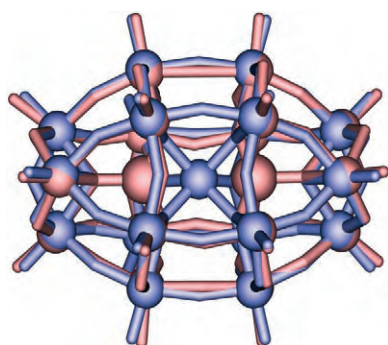
**Brønsted, Brassard, Diels, and Alder:** Aldimines **1** undergo aza-Diels–Alder reactions with Brassard's diene **2** in the presence of a chiral cyclic phosphate

pyridinium salt **4** as a chiral Brønsted acid to give  $\alpha,\beta$ -unsaturated  $\delta$ -lactams **3** with excellent enantioselectivity.

## Organocatalysis

J. Itoh, K. Fuchibe,  
T. Akiyama\* 4796–4798

Chiral Brønsted Acid Catalyzed  
Enantioselective Aza-Diels–Alder  
Reaction of Brassard's Diene with Imines

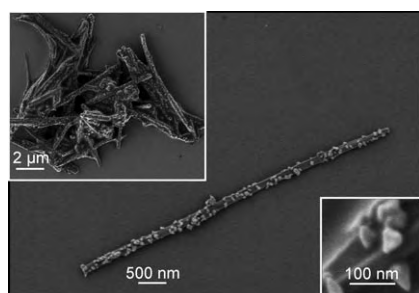


**Caged up:** A family of isopolyoxotungstate clusters of the form  $[H_4W_{19}O_{62}]^{6-}$  with a cluster cage (blue) identical to that of the Dawson-type heteropolyacids (red) has been discovered. These comprise a single trigonal-prismatic or octahedral  $\{WO_6\}^{6-}$  moiety in place of the two heteroanions found in the Dawson structure.

## Cluster Compounds

D.-L. Long,\* P. Kögerler, A. D. C. Parenty,  
J. Fielden, L. Cronin\* 4798–4803

Discovery of a Family of  
Isopolyoxotungstates  $[H_4W_{19}O_{62}]^{6-}$   
Encapsulating a  $\{WO_6\}$  Moiety within a  
 $\{W_{18}\}$  Dawson-like Cluster Cage



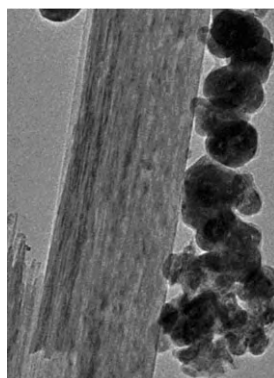
**Biofunctionalized ceramic nanowires:** A reactive ester polymer has been used to immobilize silicatein, a hydrolytic enzyme involved in the biomineralization of  $SiO_2$ , on the surface of  $TiO_2$  nanowires. The surface-bound protein retains its original hydrolytic properties and also acts as a reductant for  $AuCl_4^-$  in the synthesis of hybrid  $TiO_2$ /silicatein/Au nanocomposites.

## Nanotechnology

M. N. Tahir, M. Eberhardt, H. A. Therese,  
U. Kolb, P. Theato, W. E. G. Müller,  
H.-C. Schröder, W. Tremel\* 4803–4809

From Single Molecules to Nanoscopically  
Structured Functional Materials: Au  
Nanocrystal Growth on  $TiO_2$  Nanowires  
Controlled by Surface-Bound Silicatein

**Deck the walls:** The principles of coordination chemistry and multidentate ligand design have been used to functionalize the surface of highly inert  $MoS_2$  nanoparticles. In this approach the tetradentate nitrilotriacetic acid ligand was coupled either to a fluorescent ligand (for detection) or to a reactive polymer, which serves as an anchor to the sulfide and oxide surfaces of inorganic fullerene/ $MoS_2$  and  $TiO_2$  nanorods, respectively (see picture).



## Nanocomposites

M. N. Tahir, N. Zink, M. Eberhardt,  
H. A. Therese, U. Kolb, P. Theato,  
W. Tremel\* 4809–4815

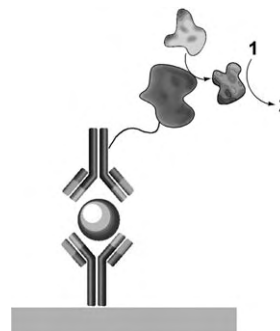
Overcoming the Insolubility of  
Molybdenum Disulfide Nanoparticles  
through a High Degree of Sidewall  
Functionalization Using Polymeric  
Chelating Ligands

## Immunosensors

B. Shlyahovsky, V. Pavlov, L. Kaganovsky,  
I. Willner\* — 4815–4819

Biocatalytic Evolution of a Biocatalyst  
Marker: Towards the Ultrasensitive  
Detection of Immunoconjugates and  
DNA Analysis

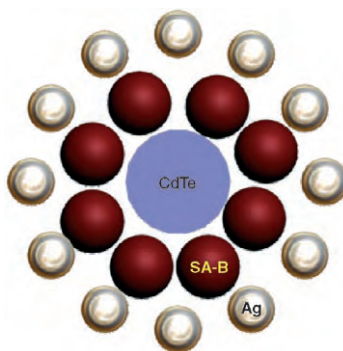
**Sensitive ELISA:** A new enzyme-labeled immunosorbant assay (ELISA) protocol has been developed that makes use of two enzymatic reactions to detect antibody–antigen interactions: 1) the conversion of prothrombin to thrombin by ecarin and 2) the hydrolysis of a nonfluorescent substrate **1** to a fluorescent product **2** by thrombin. The system was used to detect bovine serum albumin, telomerase, and DNA with high sensitivity.



## Metamaterials

J. Lee, T. Javed, T. Skeini, A. O. Govorov,  
G. W. Bryant, N. A. Kotov\* — 4819–4823

Bioconjugated Ag Nanoparticles and  
CdTe Nanowires: Metamaterials with  
Field-Enhanced Light Absorption

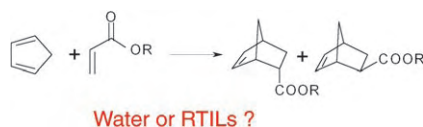


**Shiny silver:** A superstructure consisting of Ag nanoparticles and CdTe nanowires connected by a streptavidin (SA) and D-biotin (B) affinity pair displays twofold enhancement of the nanowire luminescence. The optical process involved could also be operative in other metamaterials and could serve as a basis for applications in a variety of optoelectronic devices.

## Ionic Liquids

S. Tiwari, A. Kumar\* — 4824–4825

Diels–Alder Reactions Are Faster in Water  
than in Ionic Liquids at Room  
Temperature



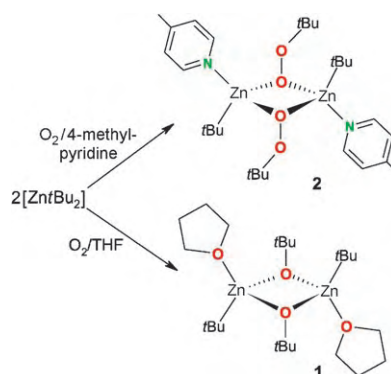
**Nobody does it better:** A comparative study indicates that water, rather than room-temperature ionic liquids (RTILs), is still the solvent of choice for accelerating Diels–Alder reactions. Both the hydrogen-bonding ability and the viscosity of the solvent are thought to play a role.

## Dioxygen Activation

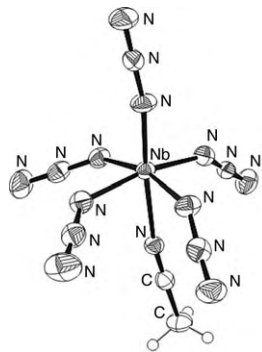
J. Lewiński,\* W. Śliwiński, M. Dranka,  
I. Justyniak, J. Lipkowski — 4826–4829

Reactions of  $[ZnR_2(L)]$  Complexes with  
Dioxygen: A New Look at an Old Problem

**OR or OOR?** The oxygenation of  $Zn(tBu)_2$  in the presence of donor ligands demonstrates the tendency of zinc dialkyls to undergo oxidation of only one Zn–C bond under controlled conditions (see scheme). The formation of alkoxide or peroxide species is influenced by the type of donor ligand employed, and these divergent pathways offer a glimpse into the general mechanism of dioxygen activation.







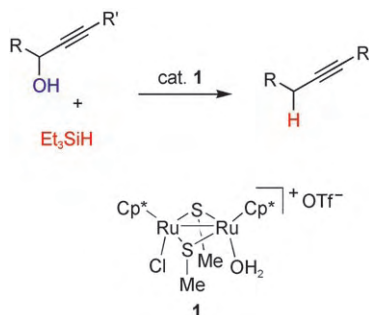
**Straightened out:** The first binary Group 5 azides were prepared by fluoro-azido exchange starting from  $\text{MF}_5$  ( $\text{M} = \text{Nb}, \text{Ta}$ ) and characterized by vibrational spectroscopy. The crystal structure of the acetonitrile adduct  $[\text{Nb}(\text{N}_3)_5(\text{CH}_3\text{CN})]$  (see picture) provides the first experimental evidence for the existence of linear M-N-N coordination for azido complexes.

### Azido Ligands

R. Haiges,\* J. A. Boatz, T. Schroer, M. Yousufuddin, K. O. Christe\* ————— **4830–4835**

Experimental Evidence for Linear Metal–Azido Coordination: The Binary Group 5 Azides  $[\text{Nb}(\text{N}_3)_5]$ ,  $[\text{Ta}(\text{N}_3)_5]$ ,  $[\text{Nb}(\text{N}_3)_6]^-$ , and  $[\text{Ta}(\text{N}_3)_6]^-$ , and 1:1 Acetonitrile Adducts  $[\text{Nb}(\text{N}_3)_5(\text{CH}_3\text{CN})]$  and  $[\text{Ta}(\text{N}_3)_5(\text{CH}_3\text{CN})]$

**$\text{Ru}_2$  can do it!** Substitution of the OH moiety in propargylic alcohols by hydride proceeds smoothly with triethylsilane by catalysis with the thiolate-bridged diruthenium complex **1** (see scheme;  $\text{Cp}^* = \eta^5\text{-C}_5\text{Me}_5$ ). This reaction gives the corresponding alkynes in good to high yields with complete selectivity, in contrast to a monoruthenium-catalyzed hydrosilylation of propargylic alcohols with silanes.

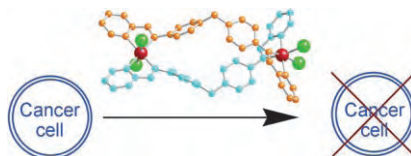


### Synthetic Methods

Y. Nishibayashi,\* A. Shinoda, Y. Miyake, H. Matsuzawa, M. Sato — **4835–4839**

Ruthenium-Catalyzed Propargylic Reduction of Propargylic Alcohols with Silanes

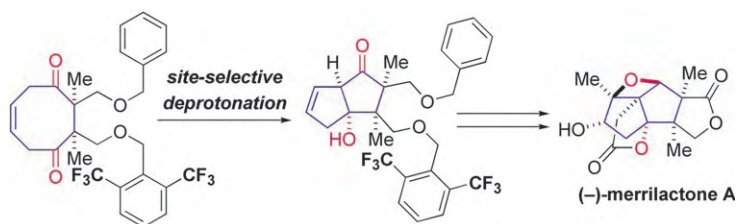
**Just add a twist:** Metallosupramolecular architecture design is used to create anticancer agents with high activities in human breast cancer cell lines. Three isomers, which comprise a nonhelical metallocyclophane, an unsaturated double helicate, and a new type of double helicate, bridge the fields of metallosupramolecular architecture and anticancer drug design (picture: double-helical *trans/cis* isomer; red Ru, green Cl).



### Helical Structures

A. C. G. Hotze, B. M. Kariuki, M. J. Hannon\* ————— **4839–4842**

Dinuclear Double-Stranded Metallosupramolecular Ruthenium Complexes: Potential Anticancer Drugs



**Designer elegance:** The transannular aldol reaction of a cyclooctene diketone is the key step in this total synthesis of the natural enantiomer of merrilactone A (see scheme). The configuration of the two

stereocenters generated in the formation of the central bicyclo[3.3.0]octane framework of the natural product was established using a specially designed bulky protecting group.

### Total Synthesis

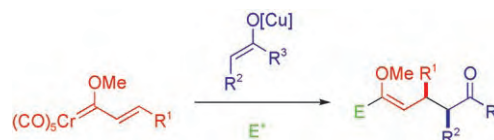
M. Inoue,\* T. Sato, M. Hirama ————— **4843–4848**

Asymmetric Total Synthesis of (–)-Merrilactone A: Use of a Bulky Protecting Group as Long-Range Stereocontrolling Element

## C–C Coupling

J. Barluenga,\* A. Mendoza, A. Diéguez,  
F. Rodríguez, F. J. Fañanás – 4848–4850

Umpolung Reactivity of Alkenyl Fischer  
Carbene Complexes, Copper Enolates,  
and Electrophiles



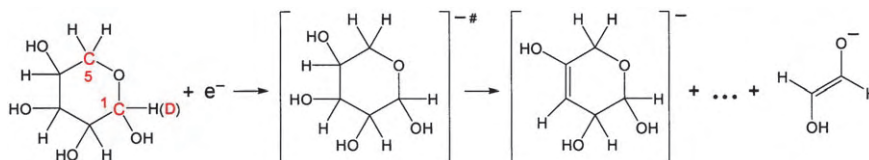
**Copper makes the difference:** An umpolung reactivity of Michael acceptors is observed when alkenyl carbene complexes react with copper ketone enolates and electrophiles. This reaction allows the

straightforward synthesis of functionalized three-component coupling products in a completely regio- and diastereoselective way.

## DNA Damage

I. Bald, J. Kopyra,  
E. Illenberger\* – 4851–4855

Selective Excision of C5 from D-Ribose in  
the Gas Phase by Low-Energy Electrons  
(0–1 eV): Implications for the Mechanism  
of DNA Damage



**Attachment of low-energy electrons** to D-ribose triggers a series of complex decomposition reactions associated with the loss of neutral water molecules as well as the excision of C-containing units leading to the degradation of the cyclic

structure of the sugar. This excision of C-containing neutral fragments involves C5 exclusively. The sugar unit is thought to play a key role in the mechanism of DNA damage by low-energy electrons.

## Allylation

U. Kazmaier,\* J. Deska,  
A. Watzke – 4855–4858

Highly Stereoselective Allylic Alkylations  
of Peptides



**Help from the neighbors:** Palladium-catalyzed allylic alkylations are extremely suitable for the stereoselective introduction of unsaturated side chains to peptides (see scheme; TFA = trifluoroac-

tate). The chiral information of the peptide can be used to control the formation of the new stereogenic center. In general, S amino acids induce the formation of R-configured amino acids.

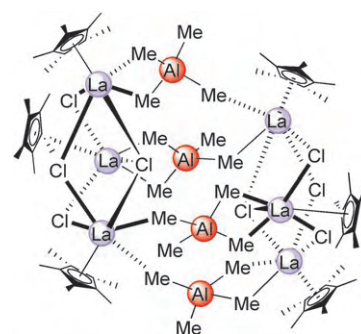


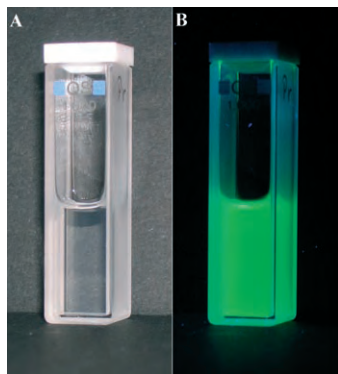
## Cluster Compounds

H. M. Dietrich, O. Schuster,  
K. W. Törnroos,  
R. Anwander\* – 4858–4863

Heterobimetallic Half-Lanthanidocene  
Clusters: Novel Mixed  
Tetramethylaluminato/Chloro  
Coordination

**Size does matter:** When treated with  $\text{Me}_2\text{AlCl}$ , highly soluble bis(aluminate) complexes  $[\text{Cp}^*\text{Ln}(\text{AlMe}_4)_2]$  ( $\text{Ln} = \text{Y}, \text{La}, \text{Nd}$ ;  $\text{Cp}^* = \text{C}_5\text{Me}_5$ ) undergo intrinsic alkyl/chloro ligand-exchange reactions to give products of variable Ln nuclearity, depending on the size of the  $\text{Ln}^{\text{III}}$  metal. The reproducible formation of  $\text{Y}_2\text{Al}_2$ ,  $\text{La}_6\text{Al}_4$ , and  $\text{Nd}_5\text{Al}$  heterobimetallic alkyl clusters leads to novel  $\text{AlMe}_4$  coordination modes (see picture:  $\text{La}_6\text{Al}_4$  cluster).





**Illuminating results:** A novel microwave-assisted synthesis in ionic liquids produces highly luminescent and dispersible  $\text{LaPO}_4\text{:Ce,Tb}$  nanocrystals (see picture: ethanol dispersion of the nanocrystals in daylight (A) and with UV excitation (B)). This preparation method offers the possibility of synthesis-independent surface conditioning of the nanocrystals.

### Synthetic Methods

G. Bühler, C. Feldmann\* — 4864–4867

Microwave-Assisted Synthesis of Luminescent  $\text{LaPO}_4\text{:Ce,Tb}$  Nanocrystals in Ionic Liquids

The issues for July 2006 appeared online on the following dates  
Issue 25: June 8. • Issue 26: June 16. • Issue 27: June 28. • Issue 28: July 3

## Sources

### Product and Company Directory

You can start the entry for your company in “Sources” in any issue of *Angewandte Chemie*.

If you would like more information, please do not hesitate to contact us.

Wiley-VCH Verlag – Advertising Department

Tel.: 0 62 01 - 60 65 65

Fax: 0 62 01 - 60 65 50

E-Mail: MSchulz@wiley-vch.de

### Service

Keywords — 4868

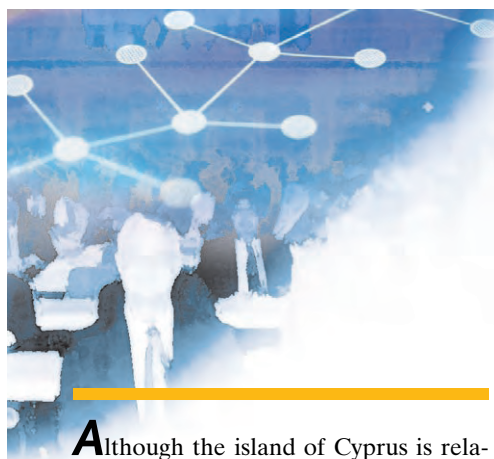
Authors — 4869

Angewandte's  
Sister Journals — 4870–4871

Preview — 4873



For more information on  
*Chemistry—An Asian Journal* see  
[www.chemasianj.org](http://www.chemasianj.org)



# From Abyssomicin to Zaragozic Acid: Chemical Synthesis and Drug Innovation\*\*

Scott A. Snyder

Although the island of Cyprus is relatively small, its position in the Mediterranean Sea at the crossroads of three continents has assured it a starring role throughout the course of recorded human history, both as a locus for the spread of ideas between disparate cultures and as a strategic base of operations for those empires seeking to expand their conquests into neighboring territories. Indeed, over the centuries many nations and nationalities—from the Greeks, Romans, Persians, Egyptians, Italians, and British, to the European Union—have shaped, and been shaped by, Cyprus.

A few weeks ago, the scientific community had the opportunity to follow suit when nearly 400 participants gathered at the Elysium Beach Resort in the coastal town of Paphos for an international symposium organized to honor Cypriot-native K. C. Nicolaou on the occasion of his 60th birthday. The theme of the meeting, one with a broadness befitting Cyprus' history, was to explore the increasingly interrelated fields of chemistry, biology, and medicine from both academic and industrial perspectives.

Each of the four days of the conference featured a series of engaging lectures covering the most exciting areas of research being pursued today along the chemistry, biology, and medicine con-

tinuum. Academic speakers described some of the latest developments in asymmetric catalysis, biocatalysis, transition-metal catalysis, supported synthesis, structure-based drug design, and target-oriented synthesis (see Table 1). A theme shared by many of these talks was the unique capability of natural products to serve as catalysts for innovation, not only for discovering reactivity but also as a means to identify novel ways to modulate and eradicate disease. Speakers from industry, many of whom were former graduate or postdoctoral researchers with Nicolaou (see Table 1), talked about a number of research programs at leading pharmaceutical companies to discover small molecules that can selectively engage essential biological targets, as well as efforts to develop technologies to speed up the entire drug-discovery process.

In between sessions, participants had the opportunity to peruse over 100 posters, to explore the surrounding countryside and take in Cyprus' history through organized excursions, and to participate in an informative panel discussion on new trends in chemical outsourcing.

K. C. Nicolaou offered the final words of the conference in a plenary lecture covering his entire career—one which has made an impact on the fields of chemistry, biology, and medicine through natural product synthesis. His

lecture took the audience on a journey encompassing virtually every class of natural product architecture known, including complex carbohydrates, enediynes, heterocycles, and macrolides, showcasing how each target molecule afforded his group with opportunities to discover new reactions and novel synthetic strategies and make fundamental contributions to our understanding of human biology. Special focus was paid to the topic of cascade reactions leading to complex architectures, a subject that will be discussed in a forthcoming Review in *Angewandte Chemie*.

Without doubt, the lecture was a fitting close to a conference sure to be long-remembered by those who participated, especially the 80 or so former students of Nicolaou who had the opportunity to share in the occasion. Whether the conference will become a regular event remains to be seen (whispers to that effect were heard), but, in any event, this symposium has set a high standard for future efforts to discuss these diverse fields in a single meeting. And, though I dare not suggest that its participants left an indelible impression of Cyprus, the island certainly left its mark on those who visited its shores for the first time.

DOI: 10.1002/anie.200602427

**Table 1:** List of speakers.

Phil Baran (Scripps Research Institute); Stefan Bräse (University of Karlsruhe); François Diederich (ETH Zürich); Peter Garratt (University College London); Rodney Kip Guy (St. Jude Children's Research Hospital, Memphis); Steven Hanessian (University of Montreal); Madeleine Joullie (University of Pennsylvania); Steven Ley (Cambridge University); Nicos Petasis (University of Southern California); Floris Rutjes (Radboud University); Masakatsu Shibasaki (University of Tokyo); Nigel Simpkins (University of Nottingham); Erik Sorensen (Princeton University); David Tanner (Technical University of Denmark); Emmanuel Theodorakis (University of California, San Diego); F. Dean Toste (University of California, Berkeley); Jun-ichi Uenishi (Kyoto Pharmaceutical University); Nicolas Winssinger (Université Louis Pasteur, Strasbourg); Zhen Yang (Peking University).

Magid Abou-Gharbia (Wyeth Research, Princeton); Mark Bunnage (Pfizer, Kent); David Claremon (Vitae Pharmaceuticals); Rolf Jautelat (Schering AG, Berlin); Philippe Nantermet (Merck and Co., West Point); Swaminathan Ravi Natarajan (Merck and Co., Rahway).

[\*] Prof. Dr. S. A. Snyder  
Columbia University  
Department of Chemistry  
Havemeyer Hall – Mail Code 3129  
3000 Broadway  
New York, NY 10027 (USA)  
E-mail: sas2197@columbia.edu

[\*\*] International Symposium on Chemistry, Biology, and Medicine at Paphos, Cyprus, May 28–June 1, 2006



# C<sub>3</sub> Symmetry: Molecular Design Inspired by Nature

Susan E. Gibson\* and M. Paola Castaldi

## Keywords:

asymmetric catalysis · biomimetic design · molecular recognition · molecular symmetry · trivalent systems

The principles of symmetry have inspired and directed the design of molecules for many years.<sup>[1]</sup> While twofold rotational symmetry has been successfully employed in a large number of chiral ligands and catalysts,<sup>[2]</sup> there is still comparatively little known about the efficiency of systems of higher rotational symmetry in this and other areas. For this reason there is an ongoing interest in the application of C<sub>3</sub>-symmetric molecules in areas as diverse as asymmetric catalysis,<sup>[3]</sup> molecular recognition,<sup>[4]</sup> and materials science.<sup>[5]</sup>

In the area of asymmetric catalysis, for example, the current state of the art is typified by the use of a Ti<sup>IV</sup> complex of the chiral C<sub>3</sub>-symmetric ligand **1** to catalyze an enantioselective alkynylation of aldehydes (up to 92% *ee*) (Figure 1).<sup>[6]</sup> However, a significant development in the use of C<sub>3</sub> symmetry in asymmetric catalysis, which was inspired by nature, was described recently by Gade and co-workers.<sup>[7]</sup> Guided by the use of tripodal N-donor ligands as models of the tris(histidine) binding sites found in many zinc-containing enzymes,<sup>[8]</sup> Gade and co-workers considered chiral tris(oxazolines) to be good candidates for mimics of zinc-dependent transesterases. Although the C<sub>3</sub>-symmetric dinuclear zinc complex **2**, derived from ligand **3**, showed only modest enantioselectivity in the kinetic resolution of various phenyl ester derivatives of N-protected amino acids by transesterification with methanol, the

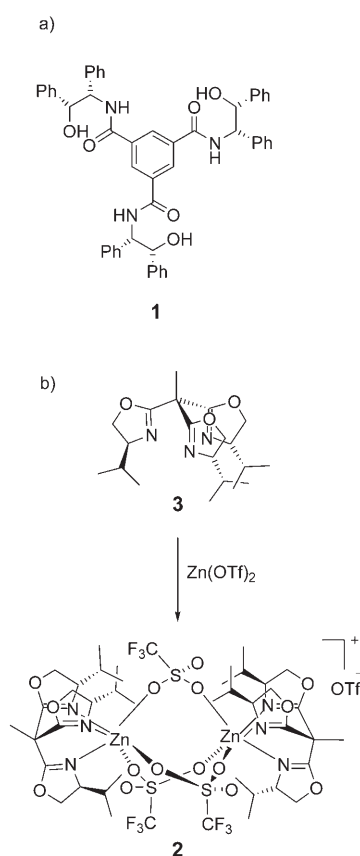


**Figure 1.** a) The C<sub>3</sub>-symmetric tris(β-hydroxy amide) ligand **1**. b) Synthesis of the dinuclear complex **2** from C<sub>3</sub>-symmetric tris(oxazoline) ligand **3**.<sup>[6,7]</sup> OTf = trifluoromethanesulfonate.

principle of using C<sub>3</sub>-symmetric ligands to mimic C<sub>3</sub>-symmetric active sites found in enzymes to inspire the design of new asymmetric catalysts was established and is predicted to lead to exciting developments in the future.

In the area of molecular recognition, several key studies that feature architectures constructed around C<sub>3</sub>-symmetric cores suggest that C<sub>3</sub> symmetry has an important role to play in this area. Moreover, a recent report by Guichard

and co-workers<sup>[9]</sup> that was inspired by C<sub>3</sub> symmetry found in nature perhaps points the way to exciting future developments. For example, an early demonstration of the power of C<sub>3</sub> symmetry in a biological context was provided by Whitesides and co-workers, who showed that tris(vancomycin carboxamide) (Figure 2) binds a trivalent ligand derived from D-Ala-D-Ala with exceptionally high affinity: its binding constant is 25 times higher than that for the biotin-avidin interaction, which is one of the strongest known in biological systems.<sup>[10]</sup> Whitesides and co-workers recognized that trivalent systems (and indeed polyvalent systems in general) are fundamentally different from monovalent systems in that dissociation of the complex, which occurs in stages, can be accelerated by addition of competing monovalent ligand, thus adding an extra degree of flexibility to potential applications of such systems.

Precedent for a somewhat different use of C<sub>3</sub> symmetry in a biological context was provided by the studies of Nishida et al. on carriers for the Lewis<sup>x</sup> antigen.<sup>[11]</sup> Widespread interest in polyvalent structures that carry human oligosaccharide antigens led to the synthesis of **4** (Figure 3), in which three Lewis<sup>x</sup> antigen trisaccharides are attached to a C<sub>3</sub>-symmetric core. The Lewis<sup>x</sup> antigen is typically located on cell-membrane lipids and leads to association in the presence of calcium ions;<sup>[12]</sup> it is thus of interest to develop probes to investigate this recognition phenomenon. Although other polyvalent systems including dimers, liposomes, gold nanoparticles, and self-assembling monolayers have previously been used as multivalent probes in this area, it was reasoned that C<sub>3</sub>-symmetric probes were attractive because they

[\*] Prof. S. E. Gibson, M. P. Castaldi  
Department of Chemistry  
Imperial College London  
South Kensington Campus  
London SW72AY (UK)  
Fax: (+44) 207-594-5804  
E-mail: s.gibson@imperial.ac.uk

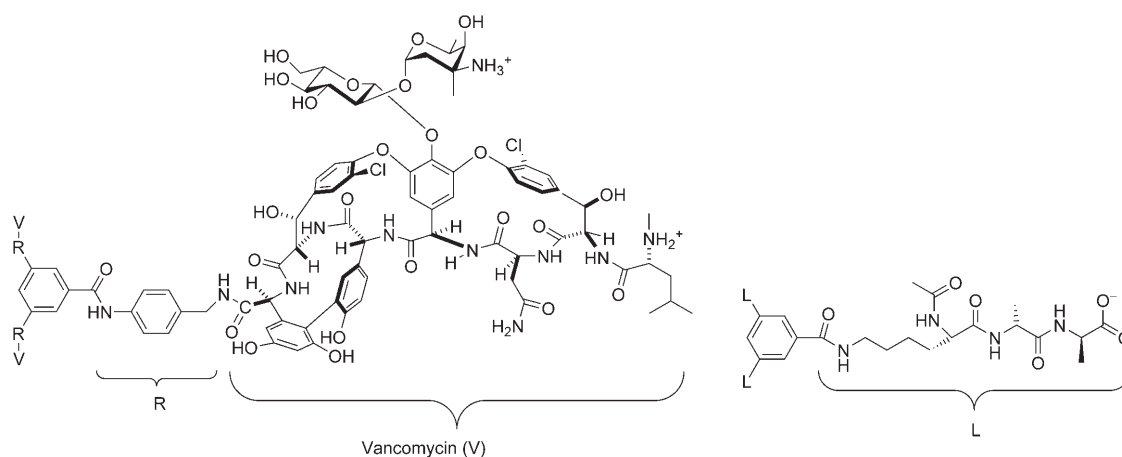


**Figure 2.** Structures of the trivalent derivatives of vancomycin (left) and of D-Ala-D-Ala (right).<sup>[10]</sup>

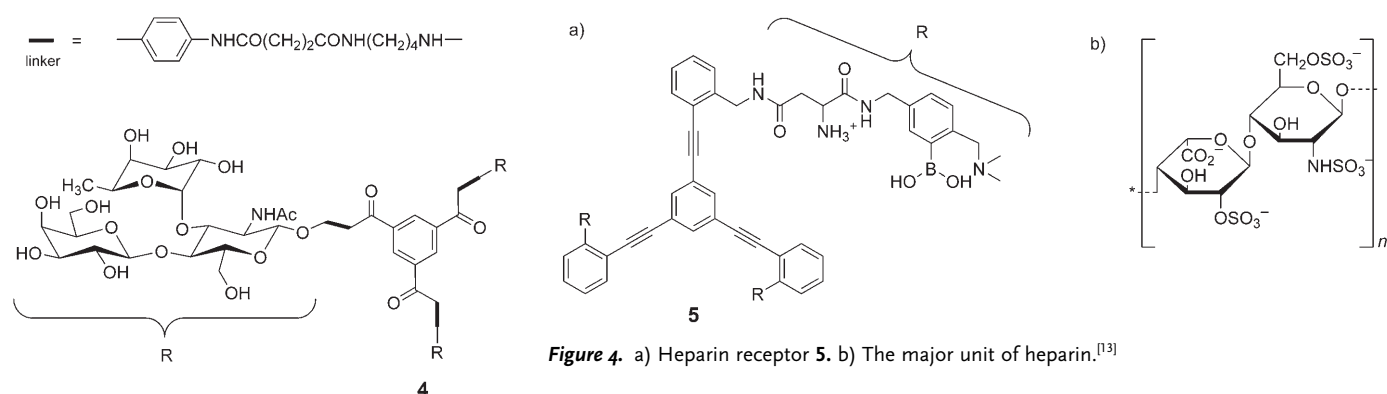


**Figure 4.** a) Heparin receptor **5**. b) The major unit of heparin.<sup>[13]</sup>

**Figure 3.** A  $C_3$ -symmetric Lewis<sup>x</sup> antigen trisaccharide.<sup>[11]</sup>

should produce significant multivalent effects without generating the complex analysis problems associated with non-symmetric or dendritic models. The preliminary analytical results reported were encouraging, and more detailed analyses derived from this system are awaited with anticipation.

The high affinity and selectivity that can be achieved using trivalent complexes has been exploited by Anslyn and co-workers in the design of a very promising assay for heparin.<sup>[13]</sup> The concentration of the clinical anticoagulant heparin is routinely monitored during and after surgery to prevent complications such as hemorrhages, but cheaper, more reliable, and more practical methods for analyzing heparin concentrations than those currently available are desirable. The large cavity receptor **5** (Figure 4) was designed to envelop a large surface of the oligosaccharide, thus

maximizing affinity and specificity by maximizing the number of possible interactions. Use of a fluorescent scaffold, 1,3,5-triphenylethynylbenzene, enabled Anslyn and co-workers to generate calibration curves for heparin in serum at clinically relevant dosing levels, thus demonstrating that synthetic receptors of this type function successfully under physiological conditions and can be used to target complex bioanalytes.

The examples of the uses of  $C_3$  symmetry in a biological context described above are based on the inventive introduction of  $C_3$  symmetry into molecular design to enhance or create desirable characteristics, for example, high affinity, good selectivity, and relatively easy analysis. The report by Guichard and co-workers<sup>[9]</sup> describes the design of a system that benefits from all of these advantages but differs from previous studies inasmuch as the inspiration for the use of  $C_3$  symmetry is derived from nature itself.

Signaling through receptors of the tumor necrosis factor receptor superfamily relies strongly on the formation of  $C_3$ -symmetric complexes.<sup>[14]</sup> One member of the family, the receptor CD40, interacts with its natural ligand CD40L by self-assembly of CD40L around a threefold symmetry axis to form a noncovalent homotrimer that binds to three CD40 receptor molecules (Figure 5). The geometry of the resulting 3:3 complex favors the formation of a signaling complex, which ultimately leads to a range of regulatory effects. Moreover, CD40 antibodies with agonist activity were previously used to increase immune response in infectious diseases, and in cancer immunotherapy.<sup>[15]</sup> It was thus postulated that the development of small-molecule CD40 agonists that mimic the action of the 39-kDa natural ligand CD40L may lead to important therapeutic applications.

Guichard and co-workers designed low-molecular-weight CD40L mimetics with  $C_3$ -symmetric architectures not only to provide the correct geometry for

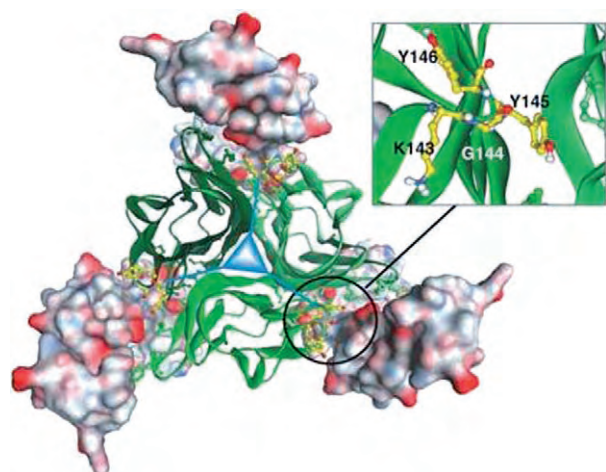


**Figure 5.** Model of the 3:3 complex between CD40 (surface representation) and CD40L (ribbon) viewed down the  $C_3$  axis, and a magnified view of the polar CD40-binding surface and the “hot-spot” region Lys143–Tyr146 of CD40L identified as the CD40-binding motif.<sup>[9,16]</sup>

receptor binding and subsequent signaling but also to achieve tight binding between the small low-surface-area ligand and the receptor CD40.<sup>[9]</sup> A  $C_3$ -symmetric D,L- $\alpha$ -hexapeptide and a  $\beta^3$ -tripeptide were used as core structures

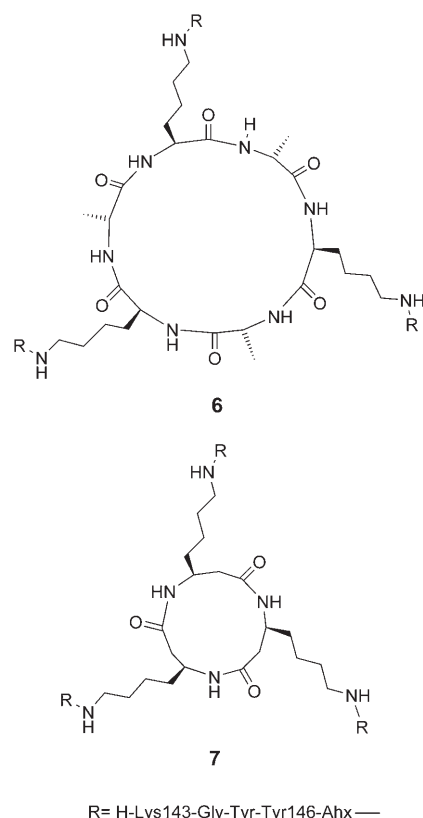


**Figure 6.** Synthetic  $C_3$ -symmetric CD40L mimetics.

to distribute receptor-binding elements with geometries and distances that could match those of the homotrimer form of CD40L. The CD40-interacting region Lys143–Gly–Tyr–Tyr146 of CD40L was selected as a CD40-binding motif and tethered by an aminohexanoic acid (Ahx) residue spacer to the central core structures to give compounds **6** and **7** (Figure 6).

A range of in vitro experiments revealed that these molecules interact with CD40, compete with the binding of CD40L to CD40, and reproduce, to a certain extent, the functional properties of the much larger natural ligand CD40L. This work not only

paves the way to using relatively small  $C_3$ -symmetric CD40 ligands to amplify immune responses in vivo, but also suggests that modulation of the functions of other members of the tumor necrosis factor receptor superfamily may be successfully achieved by using  $C_3$ -symmetrical small molecules.

To conclude,  $C_3$ -symmetrical functional molecules provide perhaps an optimum balance between enhanced properties, such as binding and selectivity, and ease of synthesis and analysis. The work of Guichard and co-workers, inspired by nature's exploitation of  $C_3$  symmetry, has provided interesting and exciting results and suggests that biomimetic applications of  $C_3$  symmetry in the area of molecular recognition may lead to further significant advances in the future. In parallel, recognition of nature's use of  $C_3$  symmetry in enzymes has inspired the first biomimetic  $C_3$ -symmetric asymmetric catalyst, and the approach of Gade and co-workers is predicted to stimulate many new developments in this area in the future.

Published online: June 23, 2006

- [1] See, for example: R. Noyori, *Asymmetric Catalysis in Organic Synthesis*, Wiley, New York, **1994**.  
 [2] See, for example: W. Tang, X. Zhang, *Chem. Rev.* **2003**, *103*, 3029–3070.

- [3] See, for example: a) G. Bringmann, R.-M. Pfeifer, C. Rummey, K. Hartner, M. Breuning, *J. Org. Chem.* **2003**, *68*, 6859–6863; b) S. Bellemin-Lapomnaz, L. H. Gade, *Angew. Chem.* **2002**, *114*, 3623–3625; *Angew. Chem. Int. Ed.* **2002**, *41*, 3473–3475.  
 [4] See, for example: a) J. Chin, C. Walsdorff, B. Stranix, J. Oh, H. J. Chung, S.-M. Park, K. Kim, *Angew. Chem.* **1999**, *111*, 2923–2926; *Angew. Chem. Int. Ed.* **1999**, *38*, 2756–2759; b) S.-G. Kim, K.-H. Kim, Y. K. Kim, S. K. Shin, K. H. Ahn, *J. Am. Chem. Soc.* **2003**, *125*, 13819–13824.  
 [5] See, for example: a) J. van Gestel, A. R. A. Palmans, B. Titulaer, J. A. J. M. Vekemans, E. W. Meijer, *J. Am. Chem. Soc.* **2005**, *127*, 5490–5494; b) M. L. Bushey, T.-Q. Nguyen, W. Zhang, D. Horoszewski, C. Nuckolls, *Angew. Chem.* **2004**, *116*, 5562–5570; *Angew. Chem. Int. Ed.* **2004**, *43*, 5446–5453.  
 [6] T. Fang, D.-M. Du, S.-F. Lu, J. Xu, *Org. Lett.* **2005**, *7*, 2081–2084.  
 [7] C. Dro, S. Bellemin-Lapomnaz, R. Welter, L. H. Gade, *Angew. Chem.* **2004**, *116*, 4579–4582; *Angew. Chem. Int. Ed.* **2004**, *43*, 4479–4482.  
 [8] G. Parkin, *Chem. Rev.* **2004**, *104*, 699–767.  
 [9] S. Fournel, S. Wieckowski, W. Sun, N. Troouche, H. Dumortier, A. Bianco, O. Chaloin, M. Habib, J.-C. Peter, P. Schneider, B. Vray, R. E. Toes, R. Offringa, C. J. M. Melief, J. Hoebeke, G. Guichard, *Nat. Chem. Biol.* **2005**, *7*, 377–382.  
 [10] J. Rao, J. Lahiri, L. Isaacs, R. M. Weiss, G. M. Whitesides, *Science* **1998**, *280*, 708–711.  
 [11] Y. Nishida, T. Tsurumi, K. Sasaki, K. Watanabe, H. Dohi, K. Kobayashi, *Org. Lett.* **2003**, *5*, 3775–3778.  
 [12] S. Hakomori, *Cancer Res.* **1996**, *56*, 5309–5318.  
 [13] A. T. Wright, Z. Zhong, E. V. Anslyn, *Angew. Chem.* **2005**, *117*, 5825–5828; *Angew. Chem. Int. Ed.* **2005**, *44*, 5679–5682.  
 [14] J.-L. Bodmer, P. Schneider, J. Tschopp, *Trends Biochem. Sci.* **2002**, *27*, 19–26.  
 [15] See, for example: a) L. Diehl, A. T. den Boer, S. P. Schoenberger, E. I. H. van der Voort, T. N. M. Schumacher, C. J. M. Melief, R. Offringa, R. E. M. Toes, *Nat. Med.* **1999**, *5*, 774–779; b) D. Chaussabel, F. Jacobs, J. de Jonge, M. de Veerman, Y. Carlier, K. Thielemans, M. Goldman, B. Vray, *Infect. Immun.* **1999**, *67*, 1929–1934.  
 [16] J. Singh, E. Garber, H. V. Vlijmen, M. Karpusas, Y. M. Hsu, Z. Zheng, J. H. Naismith, D. Thomas, *Protein Sci.* **1998**, *7*, 1124–1135.

# Can $C_3$ -Symmetric Receptors Differentiate Enantiomers?\*

Christina Moberg\*

**Keywords:**

chiral recognition · enantioselectivity · host–guest systems · molecular symmetry · receptors

Chiral recognition is a key issue in both living and artificial systems. It is essential for biological function and has a central role in asymmetric synthesis and chiral separation. A combination of attractive and repulsive interactions, the former including hydrogen bonds, ion–dipole and dipole–dipole interactions,  $\pi$  stacking, and hydrophobic interactions, is responsible for such chiral recognition.

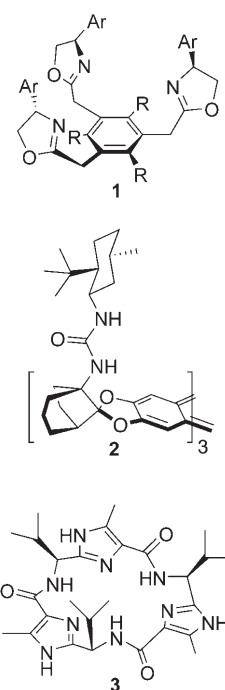
Synthetic receptors that can differentiate enantiomers have been the subject of recent intensive studies. Symmetry properties of the receptor may play an important role in the recognition process. Artificial chiral receptors endowed with rotational axes have been frequently employed as a result of their ability to simplify the procedure for their preparation and occasionally also to improve the selectivity by reducing the number of diastereomeric substrate–receptor interactions.

The role of threefold rotational symmetry in chiral recognition has been a matter of some confusion. The ability of  $C_3$ - or  $D_3$ -symmetric receptors to differentiate the two enantiomers of a chiral ammonium (or some other analogous) guest molecule was questioned some time ago.<sup>[1]</sup> It was argued that the steric requirements of the two host–

guest complexes obtained from the two enantiomers of the guest and the chiral receptor are the same and that chiral recognition therefore must be absent or at least poor. Although this statement might have hampered the development of receptors with threefold symmetry, a number of  $C_3$ -symmetric artificial receptors have recently been described.<sup>[2]</sup> Over the last few years, Ahn and co-workers have presented a number of tripodal oxazoline-based artificial receptors of general structure **1** by employing 1,3,5-*R*-2,4,6-*R'*-hexasubstituted arenes as a platform, thereby taking advantage of the alternating ababab geometric pattern that favors proper organization.<sup>[3]</sup> Contrary to their expectations,<sup>[4]</sup> the receptors exhibited high enantioselectivity in their complexation to  $\alpha$ -chiral primary ammonium ions. That  $C_3$ -symmetric receptors are capable also of enantiofacial discrimination was demonstrated upon complexation of caffeine to **2** by Waldvogel and co-workers.<sup>[5]</sup>

A different strategy for the preparation of tripodal receptors was presented by Haberhauer et al. Instead of using an achiral platform for the construction of the receptor, chiral arms were attached by means of N-alkylation to a chiral platform, **3** (in similar fashion to the construction of the siderophore enterobactin).<sup>[6]</sup> Also, a chiral tren derivative (tren = tris(2-aminoethyl)amine) was recently used as a platform for a calix-[6]arene, thereby producing a pseudo- $C_3$ -symmetric receptor.<sup>[7]</sup>

Successful examples of enantiodiscrimination by chiral receptors with threefold symmetry prompted a reconsideration of the previous statements.<sup>[1]</sup> The arguments for the predicted failure



of this type of receptors to differentiate enantiomeric guests were as follows: If we take a  $C_3$ - or  $D_3$ -symmetric receptor **H** (Figure 1) and the two enantiomers of a chiral guest molecule ( $G_R$  and  $G_S$ ), then these compounds form the two diastereomeric complexes  $H\text{-}G_R$  and  $H\text{-}G_S$ . In the analysis of the steric requirements of the two complexes, the environment of the small, medium, and large groups of the guest were compared and evidently found to be the same (Figure 2).

It is indeed obvious that the segments compared are isometric and even identical. However, this simple analysis does not take into account the chirality of the guest molecule. One substituent of a chiral compound is compared to the

[\*] Prof. C. Moberg  
Department of Chemistry  
KTH School of Chemical Science and Engineering  
SE 100 44 Stockholm (Sweden)  
Fax: (+46) 8-791-2333  
E-mail: kimo@kth.se

[\*\*] The European Community's Human Potential Program under contract HPRN-CT-2001-00187, [AC3S], is gratefully acknowledged.



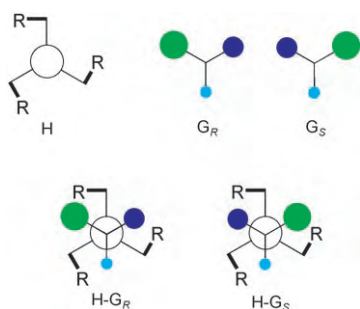


**Figure 1.** C<sub>3</sub>-symmetric host (H), enantiomeric guests (G<sub>R</sub> and G<sub>S</sub>), and diastereomeric host-guest complexes. The green, dark blue, and pale blue spheres represent large, medium, and small substituents, respectively, in the guest.

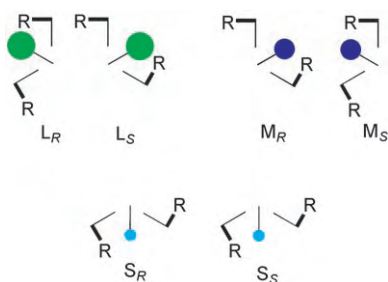


**Figure 2.** Isolated, isometric segments of diastereomeric host-guest complexes. L, M, and S denote large, medium, and small, respectively.

same substituent in its enantiomer. This situation is like comparing a methyl group in L-alanine with the methyl group in D-alanine; obviously they are identical. Instead, the order in space—the direction—of the three substituents of the guest has to be taken into account. The interactions of the large substituents in G<sub>R</sub> and G<sub>S</sub> and their clockwise neighbors, as well as the interaction of the large and small substituents in the two complexes with the chiral host, are shown in Figure 3. The latter segments are obviously non-isometric (diastereomeric).

All the segments that should be compared in the two complexes are shown in Figure 4. It is clear that the steric requirements in the two complexes are different and that the number of favorable and unfavorable interactions is different. Some favorable interactions are more important than others, and some unfavorable interactions are more severe than others, with the interactions that involve the large and small

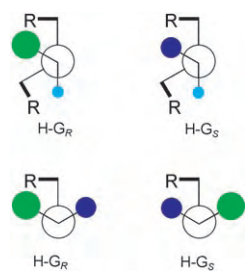


**Figure 3.** Non-identical segments of diastereomeric host-guest complexes.

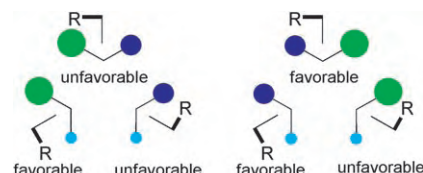
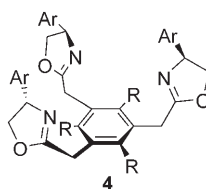


**Figure 4.** A guest exhibits one favorable and two unfavorable interactions with the host, while its enantiomer exhibits two favorable and one unfavorable interactions.

substituents probably being more important than those that involve other pairs of substituents.

There is thus no principal reason why C<sub>3</sub>- or D<sub>3</sub>-symmetric hosts would not be able to recognize chiral ammonium ions. This argument was indeed stressed by Ahn and co-workers upon observing the high selectivity of the trisoxazoline receptors **1**.<sup>[4]</sup> It may certainly be the case that the energy difference between the host-guest complexes of enantiomeric ammonium ions with a host with lower symmetry (C<sub>1</sub> or C<sub>2</sub>) is larger, but there is no fundamental rule governing these differences. To further study the role of symmetry, Ahn and co-workers recently prepared a receptor, **4**, with reduced symmetry in which one of the substituents was replaced by one



with opposite chirality.<sup>[8]</sup> This led to lower selectivity but also to a different type of binding (2:1 host-guest complex) owing to the different structures of

the ligands. Conclusions regarding the influence of symmetry alone are difficult to make.

One advantage of C<sub>3</sub>-symmetric ligands is that their host-guest complexes give rise to three identical situations, that is, only one complex (Figure 5), thereby frequently resulting in more efficient discrimination of the enantiomeric guests.

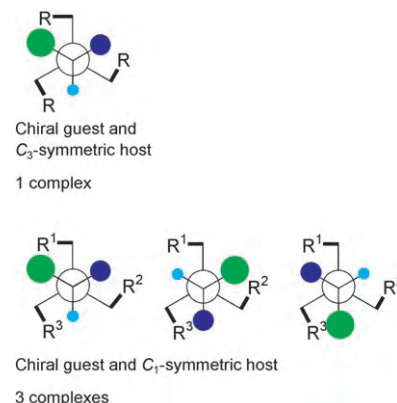


**Figure 5.** C<sub>3</sub> symmetry reduces the number of different complexes as compared to C<sub>1</sub> and C<sub>2</sub> symmetry.

Symmetry is not in itself a property that determines the ability of a receptor to recognize a chiral guest. However, symmetry reduces the number of different complexes obtained from a receptor and a substrate. This factor may, but does not necessarily have to, lead to improved selectivity.<sup>[9]</sup> Rules based exclusively on the symmetry properties of host compounds are therefore irrelevant.

Published online: June 23, 2006

- [1] H.-G. Löhr, F. Vögtle, *Acc. Chem. Res.* **1985**, *18*, 65–72; See also: X. X. Zhang, J. S. Bradshaw, R. M. Izatt, *Chem. Rev.* **1997**, *97*, 3313–3361.
- [2] There are a few earlier examples, such as the enantioselective binding of peptides to C<sub>3</sub>-symmetric synthetic receptors: D. Q. McDonald, W. C. Still, *J. Am. Chem. Soc.* **1996**, *118*, 2073–2077.
- [3] a) J. Kim, B. Raman, K. H. Ahn, *J. Org. Chem.* **2006**, *71*, 38–45; b) J. Kim, D. Ryu, Y. Sei, K. Yamaguchi, K. H. Ahn, *Chem. Commun.* **2006**, 1136–1138.
- [4] S.-G. Kim, K.-H. Kim, J. Jung, S. K. Shin, K. H. Ahn, *J. Am. Chem. Soc.* **2002**, *124*, 591–596.

- [5] M. C. Schopohl, C. Siering, O. Kataeva, S. R. Waldvogel, *Angew. Chem.* **2003**, *115*, 2724–2727; *Angew. Chem. Int. Ed.* **2003**, *42*, 2620–2623; for the preparation of the receptors, see: M. C. Schopohl, A. Faust, D. Mirk, R. Fröhlich, O. Kataeva, S. R. Waldvogel, *Eur. J. Org. Chem.* **2005**, 2987–2999.
- [6] a) G. Haberhauer, T. Oeser, F. Rominger, *Chem. Commun.* **2005**, 2799–2801; b) G. Haberhauer, T. Oeser, F. Rominger, *Chem. Eur. J.* **2005**, *11*, 6718–6726.
- [7] E. Garrier, S. Le Gac, I. Jabin, *Tetrahedron: Asymmetry* **2005**, *16*, 3767–3771.
- [8] J. Kim, S.-G. Kim, H. R. Seong, K. H. Ahn, *J. Org. Chem.* **2005**, *70*, 7227–7231.
- [9] For additional applications of  $C_3$ -symmetric compounds, see: S. E. Gibson, M. P. Castaldi, *Angew. Chem.* **2006**, *118*, 4834–4837; *Angew. Chem. Int. Ed.* **2006**, *45*, 4718–4720.



**WILEY InterScience®**  
DISCOVER SOMETHING GREAT

Access some of the finest full text journals, reference works, books, and databases from around the globe. It's just what you need to make some important discoveries of your own.

[ABOUT US](#)  
[VIEW DEMO](#)  
[CONTACT US](#)  
[HELP](#)

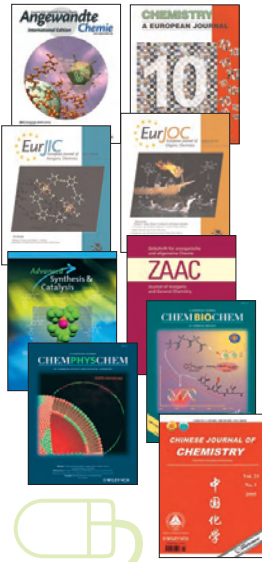
Access your saved titles, articles, queries and alerts in My Profile.

☐ Remember Me

[Register Now](#) | [Athens Link](#)  
[Forgot My Password](#)

## Manage your access easily with “MY PROFILE”

Simply register. Registration is fast and free to all internet users.



### Easy Access

- Save Titles, Articles & Queries for quick access
- Set up roaming access to access content outside of your institutions network
- Get free online sample copies
- Get free online trial subscriptions
- View a complete list of your subscriptions and accessible products

### Enhanced Tools

- Receive E-Mail Alerts when new content is available
- Purchase Article Select Tokens online
- Purchase individual articles online with Pay-Per-View



**WILEY InterScience®**  
DISCOVER SOMETHING GREAT

www.interscience.wiley.com

# Kinetics, Thermodynamics, and the Problem of Selectivity: The Maturation of an Idea

Jerome A. Berson\*

## Keywords:

history of science · kinetics · reaction mechanisms · selectivity · thermodynamics

**T**his Essay examines the response of organic chemists to the need for application of the principles of physical chemistry to competing reactions. Both mechanistic investigations and multistep chemical synthesis benefited through the eventual establishment of those principles.

## 1. Understanding Selectivity Requires Physical Chemistry

New ideas in science typically develop on the basis of previous theories and observations. There is much we can learn by examining that process. This Essay examines the problem of selectivity in organic chemistry and how chemists' awareness of it grew over decades. That advance required the incorporation of some important theoretical ideas from physical chemistry, namely the concepts of reaction rate and equilibrium that control the ratios of products in competing reactions. Thus, the selectivity may be determined either by competing rates (if under kinetic control) or by the position of the equilibrium among the products (if under thermodynamic control). The concept is commonplace today and one that every student in organic chemistry is required to learn.

However, that was emphatically not the case even as late as my student years

in the 1940s. Many undergraduate and even graduate textbooks of that period, although concerned with the problem of selectivity, make no mention of this critically important distinction. Although one can point to instances in which a kind of rough-and-ready perception of kinetic versus thermodynamic control was helpful in the work of a few chemists, the organic chemistry community on the whole did not alert itself to the broad reach of these ideas until the late 1950s. This left chemists with only dim insights into the physical and chemical consequences of the interrelationships of energy, rate, and equilibrium. Of course, it would be the height of condescension to claim on behalf of today's chemists that we are more able than our predecessors to handle issues on the forward edge of discovery. Accordingly, I believe that we can be instructed by imagining ourselves in the surroundings of that time.

## 2. From Affinity to Rate and Free Energy

During the first half of the 19th century, chemists used the rather vague and highly controversial concept of affinity to explain the course of reactions.<sup>[1,2]</sup> The malleability of the idea lent it a spurious utility in systematizing experimental facts, but because the underlying physical basis was unknown the concept was not suited to make quantitative conclusions and was open to a variety of oppositional arguments.

The modern formulation of rates and equilibria began to emerge as early as the 1860s and continued well into the next century. These advances were thor-

oughly reviewed, publicized, and employed by some of the founders of modern physical chemistry, notably van't Hoff,<sup>[3-5]</sup> Arrhenius,<sup>[6]</sup> and Ostwald,<sup>[7]</sup> who acted as advocates for the new ideas by virtue of their positions among the leading researchers in the field. Among the most significant developments were the differential formulation of the rate equation and the subsequent quantitative expression of the relationships of rate, temperature, and activation energy. These equations provided the means to compare reaction rates on a common basis. Similarly, the thermodynamic driving force of a reaction, that is, the physical reason why some reactants are transformed to products essentially completely whereas others reach equilibrium short of completion, could be explained by the concept of free energy.

## 3. Kinetic or Thermodynamic Control of Selectivity?

The fundamental laws of physical chemistry led to a number of statements, some of which will be of particular relevance in our examination of selectivity:

### Corollary 1

If the competing reactions are each essentially irreversible, the products will be formed in the same ratios as the ratios of the respective rate constants, provided that Corollary 2 is fulfilled and provided that the products are not differentially consumed by other side reactions.

[\*] Prof. J. A. Berson  
Department of Chemistry  
Yale University  
P.O. Box 208107  
New Haven, CT 06520-8107 (USA)  
Fax: (+1) 203-432-6144  
E-mail: jerome.berson@yale.edu

**Corollary 2**

Those relative rates, however, will only be time-independent if the competing reactions are all of the same kinetic order. To my knowledge, this idea was first stated by Ingold et al. in 1931.<sup>[8]</sup> If the rates are of different orders, the product ratio in general will change with time, as not all of the concentration terms in the rate equations for the competition will cancel.

**Corollary 3**

If the reactions are reversible, a channel exists through which products can interconvert with each other by reverting to starting materials.

a) If this interconversion process is fast compared to the initial reaction, the product ratio will be the same as the equilibrium ratio.

b) If the interconversion is only moderately fast, the product ratio will change with time.

**Corollary 4**

However, the products may interconvert by some other independent process, even if the reactions by which they are formed are essentially irreversible.

a) If this other process is fast compared to the initial reaction, the product ratio will be the same as the equilibrium ratio.

b) If the interconversion is only moderately fast, the product ratio will change with time.

Corollaries 1 and 2 are the basis of kinetically controlled reactions, whereas corollaries 3 and 4 come into play for thermodynamically controlled (3a and 4a) or thermodynamically influenced (3b and 4b) reactions. These corollaries were not set out in detail in the early reports, but they were implied by the basic theory. In the following years, chemists sometimes invoked one or another of the corollaries to justify their procedures. However, it is difficult to find a statement of the complete set of corollaries in books or journal articles of the time.

**4. A Slow Learning Process**

Thus, whether chemists were aware of it or not, they had proper intellectual tools at hand since about 1900 or even earlier to think clearly about these concepts. Looking back on the subsequent developments, one asks why then did another half-century have to pass for them to diffuse broadly throughout the organic chemical community. We return to this question later. First, we address how slow the learning process was.

The basis for a (very crude) estimate of how slowly the process occurred can be derived from *Chemical Abstracts*, which covers the period from 1907 to the present. A search therein for the term “kinetic control” during the period 1907–1930 gleans only one hit, whereas for the term “thermodynamic control” no hits are obtained. These results increase only to two and 18, respectively, during 1930–1950, but by 1950–1970 an exponential growth is apparent, with 65 and 124 references, respectively. Of course, too much cannot be read into this data; the apparent increase in hits may overestimate the true extent of cognitive growth if some of them simply reflect an autocatalytic expansion of the community’s familiarity with the specific identifying terms “kinetic control” and “thermodynamic control.” On the other hand, there would be a countervailing deficiency of the search for those terms if there were instances (as we will discuss later) in which the investigators were fully aware of the concept but used other nomenclature or simply did not include the term in the abstract.

With the exception of Walter Hückel, no author of textbooks before about 1940 seems to have incorporated any systematic discussion of the corollaries. Even Hückel’s treatment in the 1935 version (2nd edition) of his *Theoretische Grundlagen der Organischen Chemie*<sup>[9]</sup> is fragmentary, as he states that the ratio of the rates of two competing reactions is given by the ratio of the products, provided that the reactions are irreversible. The statement is literally correct, but it is incomplete in defining the selectivity because it overlooks the proviso of Corollary 2. In the postwar translation<sup>[10]</sup> of the *Grundlagen*, this flaw was pointed out by the translator, Rathmann. Such important pedagogical texts

as Hammett’s *Physical Organic Chemistry*<sup>[11]</sup> and Frost and Pearson’s *Kinetics and Mechanism*<sup>[12]</sup> do not treat competitive reactions as a general category at all, although Hammett does give a very brief mention of one group of them in a discussion of the Friedel–Crafts reaction (see Section 6).

**5. Kinetically Controlled Aromatic Substitutions**

Holleman at the University of Amsterdam was one of the first organic chemists to incorporate the new concepts. He made important progress in determining product ratios in aromatic substitutions, mostly through the construction and use of Gibb’s phase diagrams.<sup>[13,14]</sup> His strength in physical chemistry, probably gained in his experience as an assistant in the laboratory of van’t Hoff,<sup>[15]</sup> led him to adopt the working principle that the product ratios were measures of the *relative rates* of the competing reactions. This idea, which now seems obvious to the modern chemist, apparently was a substantial intellectual leap in the first decade of the 20th century. Following on from the earlier work of van’t Hoff<sup>[4]</sup> and Lapworth,<sup>[16]</sup> it was one of the first applications of the new quantitative concept of reaction velocity to organic chemical phenomena. Beginning in about 1910, Holleman and co-workers studied the absolute reaction rates of various substitutions to make quantitative the generalizations that *meta*-directing groups deactivate the ring (decrease the rate of substitution), whereas *ortho/para*-directing groups activate the ring (increase the rate of substitution). Subsequently, Holleman and Caland<sup>[17]</sup> showed that the sulfonation of toluene is kinetically controlled. It was a rare and perhaps unprecedented instance in which the explicit attention of the investigators to the central issue of selectivity was clearly manifested.

Note, however, that the experiments by Holleman and Caland did not come to grips with the requirement of identity of kinetic order of the competing reactions (Corollary 2). Also, a modern chemist might be concerned about the sensitivity of Holleman’s analytical method for determining the product



ratios by phase diagrams. Nevertheless, the sophisticated level of reasoning in this early mechanistic study is impressive; very few other experiments of comparable quality were to be found during that era. Despite that, the insights reported by Holleman did not seem to make much impact on organic chemists for many years to come.

## 6. Thermodynamically Controlled Aromatic Substitutions

Not all aromatic substitutions are kinetically controlled, as can be seen in the literature regarding Friedel–Crafts alkylation of aromatic compounds<sup>[18–20]</sup> which provides compelling examples of thermodynamically controlled systems. The reaction of benzene with chloromethane in the presence of aluminum chloride is difficult to stop at the stage of monomethylation to toluene because the product is quickly alkylated further to dimethylbenzenes (xylenes) and higher alkylation products.<sup>[21,20]</sup> However, the significant point in the present context is that the distribution of the three xylene products (*ortho*, *meta*, and *para*) changes during the time they are allowed to remain in contact with the aluminum chloride. Similarly, in the methylation of toluene, the three products initially comprise mostly *ortho*- and *para*-xylene, together with small amounts of *meta*-xylene, but over time the amount of the *meta* product increases, mainly at the expense of the *ortho* derivative.

It was only in 1939 that the Lewis acid facilitated interconversion of the isomeric xylenes was examined in some detail by Norris and co-workers. Their work had an empirical and preparative motivation, not a mechanistic one.<sup>[22,23]</sup> The papers by Norris and co-workers report the influence of time, temperature, and other variables on the ratio of xylene isomers but do not attempt to discuss the results in kinetic or thermodynamic terms. Even later (1946) in a review article on Friedel–Crafts reactions,<sup>[19]</sup> Price gives no discussion in terms of physical chemistry principles and describes the variations in product composition by the following statement: “[...] in general, the more vigorous the conditions with respect to the activity of

*the catalyst or the alkylating agent or the severity of the time and temperature factors, the greater is the tendency for the formation of the abnormal m-derivatives.”*

This terminology invoking the “vigour” of the conditions was quite widespread, even if not universal,<sup>[24]</sup> during that period, but it is seen to be lacking a precise physical foundation. The review by Price even omits any mention of the landmark study by Pitzer and Scott in 1943<sup>[25]</sup> which definitively showed that some of the Norris–Vaala<sup>[23]</sup> xylene mixtures corresponded closely in composition to the *equilibrium mixture* predicted directly from the measured thermodynamic properties of the individual components.

Despite the clearly laggard pace of adoption of the underlying physical principles of selectivity in aromatic substitutions, it should not be assumed that the entire community of chemists failed to recognize the importance of those ideas. A few early examples may be found in which one or more of the concepts were fully understood. Among these were several studies of allylic rearrangements.<sup>[26,8,27–30]</sup> In the interest of brevity, we omit a detailed description of those important results in order to focus on a stereochemical issue of broad significance (Section 7).

## 7. Kinetics versus Thermodynamics in Other Systems: The Puzzle of the Walden Inversion

Walden’s astonishing discoveries, which were reviewed in 1911,<sup>[31]</sup> of stereochemical inversion of configuration in several substitution reactions (for example, OH replacing Cl or vice versa) of aliphatic compounds are now well understood, as a result of studies carried out by Phillips, Kenyon, Hughes, and Ingold, among others.<sup>[32]</sup> Modern chemists therefore must exert some imagination to reproduce the widespread confusion that prevailed when the results were new. In both his review<sup>[31]</sup> and book,<sup>[33]</sup> Walden considers several now-abandoned theories proposed by his contemporaries, some of which were imaginative but none of which survived further examination.

From the point of view of this Essay, the most interesting of those abandoned theories was a proposal by Noyes and Potter<sup>[34]</sup> in 1912 which was essentially a restatement of a hypothesis that Walden had already considered and rejected. Noyes and Potter stated: “*The rational view seems to be that the Walden inversion is merely a limiting case of ordinary rearrangements, where the interatomic forces are such that the equilibrium in the formation of two possible forms lies far on the side toward the formation of one of these.*”

Walden criticized this proposal on the following grounds: “*This conclusion of Noyes, however, is only another formulation of the facts as those which Walden first established and has presented as inexplicably opposed to theory. The question of course remains open as to what kind of force must exist by which this extreme case of equilibrium, which defies kinetic and thermodynamic considerations, can be kept in place when otherwise it should strive to exit from this state and lead to a true equilibrium.*”<sup>[33]</sup>

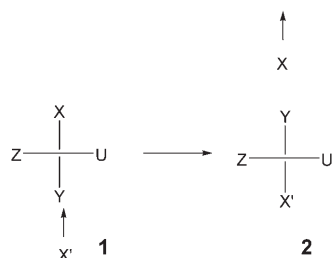
Apparently, the idea that “direct” displacement of one group by another could be accompanied by clean inversion of configuration was so strange that Walden could not conceptualize it and therefore thought that it amounted to a complete overshoot of the equilibrium position, which of course was a thermodynamic impossibility.

Walden ended his review<sup>[31]</sup> with a comparison of the views of two of the leaders of physical chemistry. Ostwald,<sup>[35]</sup> Walden’s postdoctoral mentor, asserted that “[...] *this phenomenon appears to me in opposition to the fundamental principles of stereochemistry. One cannot invoke here the assistance of a transposition, which in principle, always gives only the racemic combination but not the optical inverse. Obviously, one cannot pretend that the problem does not permit of a solution, but each worthy solution actually considered shakes or modified the bases of stereochemistry.*”

In contrast, Arrhenius was not ready to abandon the fundamentals, as he put it in his book:<sup>[6]</sup> “*It is even more probable that from the consequences of more extensive research, a new hypothesis in agreement with the principles of stereochemistry will explain the Walden*

inversion [...] allowing for the formation of intermediate products, this singular result will no longer remain inexplicable.”

A direct challenge to Walden’s pessimistic position of 1911 on the inversion phenomenon appeared later that same year, when Le Bel wrote a short note<sup>[36]</sup> based on a private letter sent earlier from Le Bel to Walden, proposing what turned out to be a prescient explanation. Le Bel began by saying that the phenomenon of Walden inversion “[...] astonished me like everyone by its novelty, but I do not believe that one must see it as being in disagreement with the principles of stereochemistry.” He imagined that in certain cases the attacking reagent, X’, could approach the asymmetric carbon center which bears the groups X, Y, Z, and U (**1**, Scheme 1)



**Scheme 1.** The Walden inversion according to Le Bel.

from the direction opposite to the position occupied by the leaving group X, rather than from the same side. In effect, if X’ pushes Y in front of itself with sufficient force, racemization need not result but instead the restoration of the tetrahedral structure may take place, with Y occupying the place originally held by X and with X’ occupying the original place of Y, as in **2**. A similar argument appeared in a paper by Emil Fischer in the same year.<sup>[37]</sup>

Le Bel and Fischer both went on to consider, as a plausible but not obligatory possibility, that the actual mechanism may involve a “product of addition” as an intermediate stage. Although neither of them used the specific term, the context of their remarks seem to point to a pentavalent carbon atom as the key structural feature of the intermediate. Le Bel ended his discussion, “I therefore conclude that the Walden in-

version [...] does not modify the bases of stereochemistry.”

Eight years later, in his book<sup>[33]</sup> Walden still held to his doubts that his inversions could be reconciled with fundamental physical theory. Regarding Le Bel’s idea, he remarked that “[...] it has the merit of simplicity which is inherent in the chosen mechanical picture. One can hardly claim that it also possesses the characteristic of completeness.”

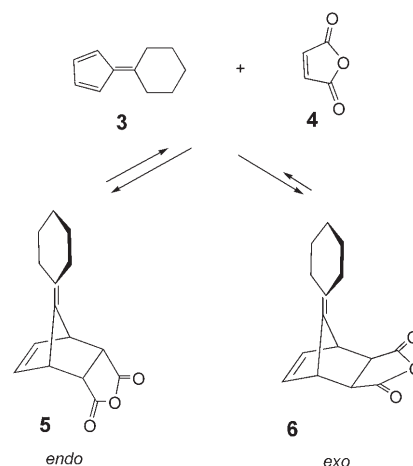
Missing from the theory, according to Walden, was an explanation of why some substitutions at asymmetric centers gave largely retention, others gave inversion, and still others gave some of each or even a near-racemic mixture, even when after-the-fact racemization could be shown to be absent.

To the present-day chemist, the Le Bel–Fischer hypothesis bears a strong resemblance to the later ideas about Walden inversion pioneered primarily by Ingold and the English school during the period 1920–1940.<sup>[32]</sup> What was the insight that Walden needed to grasp in order to accept the Le Bel–Fischer hypothesis as the basis for further progress in elucidating the mechanism of inversion? In my view, it was precisely the necessity to distinguish between kinetic and thermodynamic factors. Walden met an impasse at the point in his argument when he could not understand how one could overshoot equilibrium. Possibly he was influenced by his former mentor Ostwald, who also was confused by the problem. What both of them apparently failed to recognize was that the substitution reactions are under *kinetic control*. If the product ratio is determined by the ratio of competing rates, one does not reach equilibrium. This point had been made, notably by Holleman for aromatic substitutions (Section 5), but Walden did not make the conceptual connection of that work to his own.

## 8. The Pedagogy of Selectivity

Scattered evidence of awareness of the kinetics versus thermodynamics problem in selectivity is evident during the period up to 1940, notably in several papers on allylic rearrangements from several different laboratories.<sup>[26,38,8,27–30]</sup>

However, formal attempts to communicate the general principles in a concise way were rare until the appearance of a paper on the Diels–Alder reaction by Woodward and Baer,<sup>[39]</sup> who reported in 1944 that the addition of pentamethylenefulvene **3** to maleic anhydride **4** (Scheme 2) gives both *endo* and *exo* ad-



**Scheme 2.** Addition of pentamethylenefulvene (**3**) to maleic anhydride (**4**) to give the *endo* adduct **5** and *exo* adduct **6**.

ducts (**5** and **6**, respectively). The *endo* adduct **5** is formed in greater amount at low temperature, but the product composition gives increasing proportions of *exo* product at higher temperatures. Furthermore, even in cold solution, the *endo* adduct, but not the *exo* product, dissociates to the addends—a reaction that is readily visible because of the yellow color of the fulvene. They proposed that the rate of formation of the *endo* adduct is faster than that of the *exo* adduct at low temperature, but the *exo* adduct is more stable than the *endo* adduct and therefore accumulates at equilibrium. Woodward and Baer summarized their proposal in the energy diagram shown in Figure 1.

Alder and Trimborn had made similar observations and interpretations, perhaps as early as 1943, during the war in Germany, but apparently they were unaware of Woodward and Baer’s paper. Eventually a referee called it to Alder’s attention,<sup>[40]</sup> and Alder and Trimborn finally published in 1950, after the end of the war, the results of Trimborn’s dissertation from 1943.<sup>[41]</sup> They

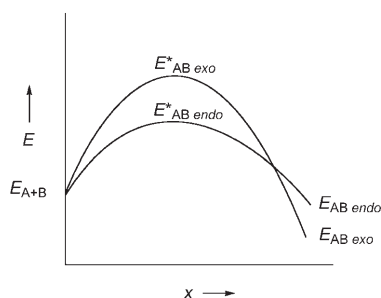


**Figure 1.** Diagram of energy versus reaction coordinate for the reaction of pentamethylene-fulvene (A) and maleic anhydride (B). Adapted from Ref. [39] with permission of the American Chemical Society.

reported essential agreement with Woodward and Baer in all of the relevant experimental and interpretive points.

Obviously, these events raise a question of priority for the discovery of the temperature dependence of the Diels–Alder reactions of fulvenes, but of greater interest here is the appearance of the energy diagram shown in Figure 1. This diagram is one of the first—perhaps the very first—pictorial aid expressing the problem of kinetic versus thermodynamic control in chemical selectivity.

Although the Woodward–Baer diagram preceded by four years a paper on allylic rearrangements by Catchpole, Hughes, and Ingold,<sup>[42]</sup> the latter authors were apparently unaware of the earlier work and presented an essentially equivalent diagram representing selectivity in allylic rearrangements. A number of chemists had mastered the basic concepts of the selectivity problem, but it is curious that, as far as I can determine, the actual terms themselves did not make an appearance until the paper by Ingold in 1948.<sup>[42]</sup> By then, Ingold apparently was concerned to teach chemists the basic ideas in a pedagogically compelling way. The abstract of that paper contains the statement, “the distinctions between the kinetic and thermodynamic control of the rearrangement are emphasized.” Still later, Zimmerman used essentially the same kind of graphic illustration to display the energy relationships that control the stereochemistry of ketonization of enols, again with no mention of either of the previous published diagrams.<sup>[43]</sup>

I believe that the repeated presentations plausibly represent the urgency the authors felt to disseminate the basics of kinetic–thermodynamic principles to the community. This illustrates how spotty they must have seen the recognition of these principles to be at that time.

## 9. Why so Slow?

One of the reasons for the slow learning curve may have been sociological. Segregation of organic and physical chemistry was endemic during the 19th century, especially in Germany, where the traditional academic organization of chemistry into separate institutes for each disciplinary unit prevailed. A more practical issue before 1950 was the difficulty of analyzing product mixtures to obtain accurate product ratios. Although solutions to this problem ultimately could be found in carefully chosen cases (see Section 5), there were no accurate analytical methods of general applicability until the advent of sophisticated chromatographic methods and of nuclear magnetic resonance spectroscopy, among other powerful tools. Still another stimulus to productive thinking about kinetic and thermodynamic issues after 1950 was the tremendous flowering of multistep organic synthesis, a discipline for which control of selectivity is required at every step. Examples of successful regiospecific applications abound in the recent literature on synthetic organic chemistry, but also worthy of mention are the numerous enantiospecific syntheses now appearing in response to government requirements that a chiral drug be enantiomerically pure. Satisfaction of this requirement can be achieved only by the choice of conditions that avoid the thermodynamic trap of racemization.

Published online: June 21, 2006

- [1] J. R. Partington, *A History of Chemistry*, Vol. 4, Macmillan, New York, **1964**, p. 569.
- [2] S. Weininger in *Tools and Modes of Representation in the Laboratory Sciences*. Boston Studies in the Philosophy of

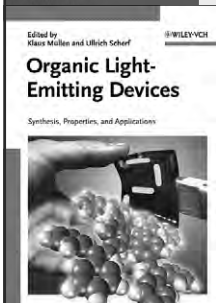
Science (Ed.: U. Klein), Kluwer, Dordrecht, **2001**, p. 237.

- [3] J. H. van't Hoff, *Studies in Chemical Kinetics*, Williams and Norgate, London, **1896**. Revised and enlarged from the original 1883 French edition, *Etudes de Dynamique Chimique* by E. Cohen (translated by T. Ewan).
- [4] J. H. van't Hoff, *Lectures in Theoretical and Physical Chemistry. Part I. Chemical Dynamics*, Edward Arnold, London, **1899**. Lectures from a course given by van't Hoff at the University of Berlin.
- [5] J. H. van't Hoff, *Physical Chemistry in the Service of the Sciences*, University of Chicago, Chicago, **1903**. Lectures given at the University of Chicago, June 20–24, 1901, in celebration of the decennial of its founding. Translated by A. Smith.
- [6] S. Arrhenius, *Theories of Chemistry, Being Lectures Delivered at the University of California, in Berkeley*, Longmans, Green, London, **1907**.
- [7] W. Ostwald, *Klassiker der exakten Wissenschaften*, Akademische Verlagsgesellschaft Geest & Portig, Leipzig, **1889**. A series of articles including important developments in physical chemistry.
- [8] C. K. Ingold, A. Lapworth, E. Rothstein, D. Ward, *J. Chem. Soc.* **1931**, 1959.
- [9] W. Hückel, *Theoretische Grundlagen der Organischen Chemie*, Akademische Verlagsgesellschaft, Leipzig, **1935**.
- [10] W. Hückel, *Theoretical Principles of Organic Chemistry*, Elsevier, New York, **1955–1958**. Translated from the 7th edition by F. H. Rathmann.
- [11] L. P. Hammett, *Physical Organic Chemistry*, McGraw-Hill, New York, **1940**.
- [12] A. A. Frost, R. G. Pearson, *Kinetics and Mechanism: A Study of Homogeneous Chemical Reactions*, Wiley, New York, **1953**.
- [13] A. F. Holleman, *Die Direkte Einführung von Substituenten in den Benzolkern*, Veit, Leipzig, **1910**.
- [14] A. F. Holleman, *Chem. Rev.* **1924**, *1*, 187. This paper was based upon a lecture Holleman gave at the dedication of the Sterling Chemistry Laboratory of Yale University.
- [15] J. P. Wibaut, *Chem. Weekbl.* **1929**, *26*, 441.
- [16] A. Lapworth, *J. Chem. Soc.* **1904**, 85, 30.
- [17] A. F. Holleman, P. Caland, *Ber. Dtsch. Chem. Ges.* **1911**, *44*, 2519. With contributions from J. P. Wibaut and T. van der Linden.
- [18] G. A. Olah, *Friedel–Crafts Chemistry*, Wiley, New York, **1973**, pp. 70–72.
- [19] C. C. Price, *Organic Reactions*, Vol. III, Wiley, New York, **1946**, pp. 8–10.
- [20] R. M. Roberts, A. A. Khalaf, *Friedel–Crafts Alkylation Chemistry: A Century*



- of Discovery, Marcel Dekker, New York, **1984**, pp. 674–700.
- [21] D. A. McCauley, A. P. Lien, *J. Am. Chem. Soc.* **1952**, *74*, 6246.
- [22] J. F. Norris, D. Rubenstein, *J. Am. Chem. Soc.* **1939**, *61*, 1163.
- [23] J. F. Norris, G. T. Vaala, *J. Am. Chem. Soc.* **1939**, *61*, 2131.
- [24] C. M. Suter, A. W. Weston in *Organic Reactions, Vol. III*, Wiley, New York, **1946**, pp. 141.
- [25] K. S. Pitzer, D. W. Scott, *J. Am. Chem. Soc.* **1943**, *65*, 813.
- [26] H. Burton, C. K. Ingold, *J. Chem. Soc.* **1928**, 904.
- [27] R. P. Linstead, *J. Chem. Soc.* **1927**, 129, 2579.
- [28] J. D. Roberts, S. Winstein, W. G. Young, *J. Am. Chem. Soc.* **1942**, *64*, 2157.
- [29] S. Winstein, W. G. Young, *J. Am. Chem. Soc.* **1936**, *58*, 104.
- [30] W. G. Young, S. Winstein, *J. Am. Chem. Soc.* **1935**, *57*, 2013.
- [31] P. Walden, *J. Chim. Phys.* **1911**, *9*, 160.
- [32] J. A. Berson, *Chemical Creativity: Ideas from the Work of Woodward, Huckel, Meerwein, and Others*, Wiley-VCH, Weinheim, **1999**, chap. 5.
- [33] P. Walden, *Optische Umkehrerscheinungen (Waldensche Umkehrung)*, Vieweg & Sohn, Braunschweig, **1919**, pp. 138–139.
- [34] W. A. Noyes, R. S. Potter, *J. Am. Chem. Soc.* **1912**, *34*, 1071.
- [35] W. Ostwald, *Leitlinien der Chemie*, **1906**, Akademische Verlagsgesellschaft, Leipzig, p. 152. As cited by Walden.
- [36] J.-A. Le Bel, *J. Chim. Phys.* **1911**, *9*, 325.
- [37] E. Fischer, *Justus Liebigs Ann. Chem.* **1911**, *381*, 126.
- [38] W. E. Hugh, G. A. R. Kon, R. P. Linstead, *J. Chem. Soc.* **1927**, 129, 2585.
- [39] R. B. Woodward, H. Baer, *J. Am. Chem. Soc.* **1944**, *66*, 645.
- [40] K. Alder, R. Rühmann, *Justus Liebigs Ann. Chem.* **1950**, *566*, 1.
- [41] K. Alder, W. Trimborn, *Justus Liebigs Ann. Chem.* **1950**, *566*, 58.
- [42] A. G. Catchpole, E. D. Hughes, C. K. Ingold, *J. Chem. Soc.* **1948**, 8.
- [43] H. E. Zimmerman, *J. Org. Chem.* **1955**, *20*, 549.

# Wiley-VCH BOOK SHOP



K. Müllen / U. Scherf (eds.)

## Organic Light Emitting Devices Synthesis, Properties and Applications

Reflecting a decade of intense research, the contributions here from academic and industrial leaders combine the fundamentals and latest research results with application know-how and examples of functioning displays, covering all four important aspects.

ISBN 3-527-31218-8, 426 pp, cl, € 139.00



N. E. Schore

## Arbeitsbuch Organische Chemie

Wer die didaktischen Qualitäten des „Vollhardt“ wirklich ausschöpfen und sich gründlich auf die Prüfung vorbereiten will, braucht zur Selbstkontrolle und zur Vertiefung dieses Ergänzungswerk. Das Lehrbuch und das Arbeitsbuch: Auch in der 4. Auflage ein bewährtes Gespann.

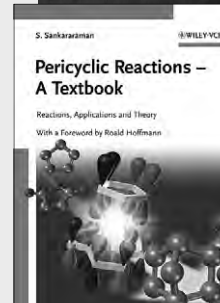
ISBN 3-527-31526-8, approx. 340 pp, pr, approx. € 34.90

S. Sankararaman

## Pericyclic Reactions – A Textbook Reactions, Applications and Theory

This long awaited textbook presents Diels-Alder reactions, electrocyclic reactions, sigma-tropic rearrangements plus many more topics in a highly didactic way, with both classical and new examples explained in detail. With a foreword by Nobel Laureate Roald Hoffmann.

ISBN 3-527-31439-3, 432 pp, pr, € 49.90



B. Tiede

## Makromolekulare Chemie Eine Einführung

Für Chemiker, Polymerchemiker und besonders für Chemiestudenten ist der „Tiede“ ein gelungenes und ausgewogenes Lehrbuch über das Basiswissen in der Makromolekularen Chemie. Mit bereits bewährter Didaktik wird der Stoff in verständlicher Form und klar gegliedert dargestellt.

ISBN 3-527-31379-6, 391 pp, pr, € 39.90



You can order online via <http://www.wiley-vch.de>

Wiley-VCH Verlag GmbH & Co. KGaA · POB 10 11 61 · D-69451 Weinheim, Germany

Phone: 49 (0) 6201/606-400 · Fax: 49 (0) 6201/606-184 · E-Mail: [service@wiley-vch.de](mailto:service@wiley-vch.de)



BS\_0512\_OC3\_1c\_1-2h\_gu



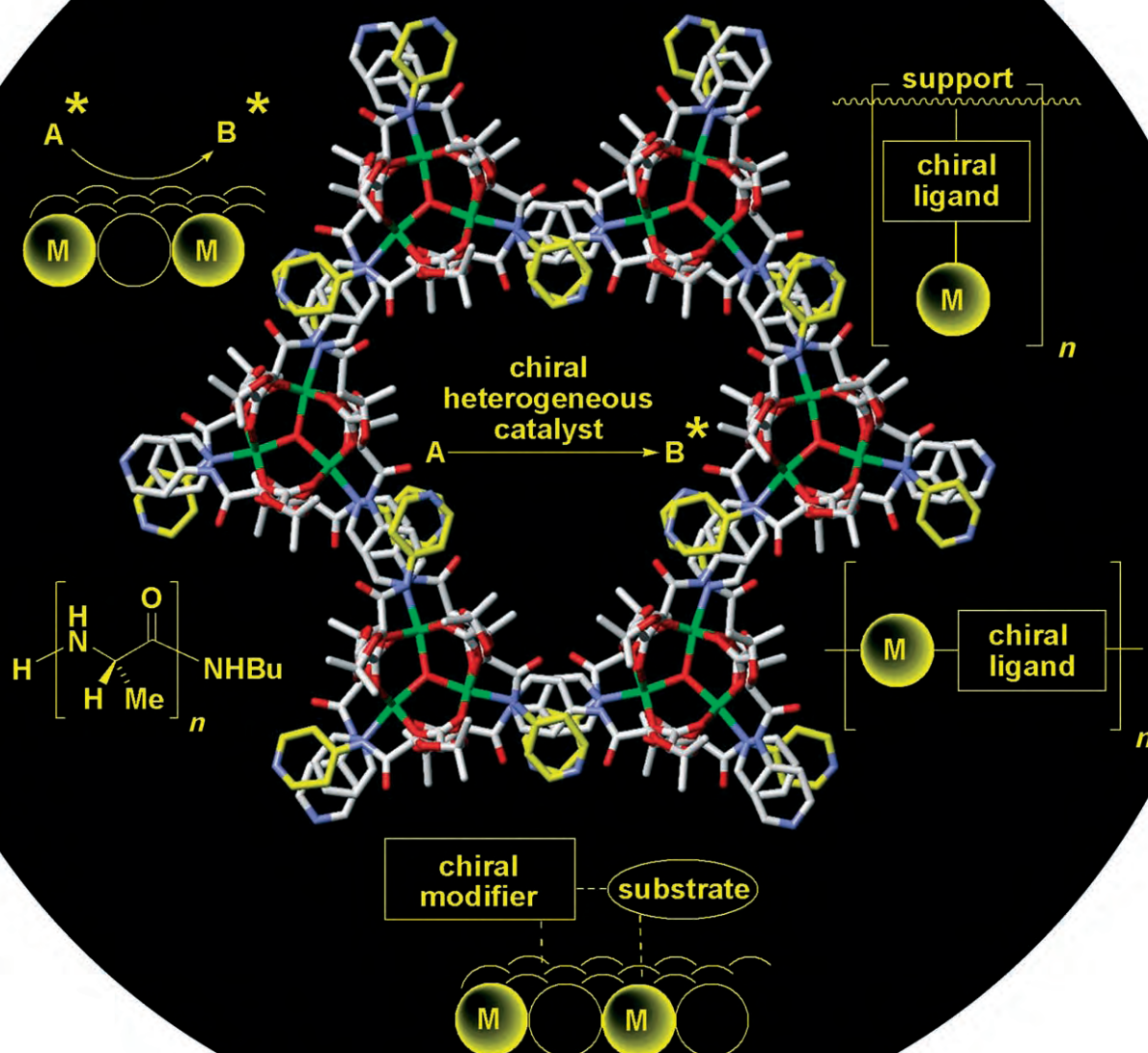
# Asymmetric Heterogeneous Catalysis

Maja Heitbaum, Frank Glorius,\* and Iris Escher

**Keywords:**

asymmetric catalysis · coordination compounds · heterogeneous catalysis · metal–organic frameworks · supported catalysts

*Dedicated to Professor Albert Eschenmoser on the occasion of his 80th birthday*



**L**imited natural resources and an increasing demand for enantio-merically pure compounds render catalysis and especially heterogeneous asymmetric catalysis a key technology. The field has rapidly advanced from the initial use of chiral biopolymers, such as silk, as a support for metal catalysts to the modern research areas. Mesoporous supports, noncovalent immobilization, metal–organic catalysts, chiral modifiers: many areas are rapidly evolving. This Review shows that these catalysts have more to them than facile separation or recycling. Better activities and selectivities can be obtained than with the homogeneous catalyst and novel, efficient reaction mechanisms can be employed. Especially fascinating is the outlook for highly ordered metal–organic catalysts that might allow a rational design, synthesis, and the unequivocal structural characterization to give tailor-made catalysts.

## 1. Introduction

Catalysis of organic reactions is key for an efficient synthesis and, thus, represents one of the most economically important technologies.<sup>[1]</sup> The growing demand for enantio-pure compounds in the life sciences has stimulated an increased interest in asymmetric catalysis.<sup>[2]</sup> Although homogeneous catalysts are often expensive and their separation and recycling troublesome, the field of asymmetric catalysis has been dominated for a long time by homogeneous catalysis because of the excellent selectivities and activities obtained. In more recent years, significant developments in the area of solid-phase chemistry has resulted in enormous progress being made in interdisciplinary research on stereoselective heterogeneous catalysis.<sup>[3]</sup> The potential advantages of heterogeneous catalysis, such as easy separation, efficient recycling, minimization of metal traces in the product, and an improved handling and process control, that finally result in overall lower costs are well known. Furthermore, in some cases heterogeneous catalysts are even more selective than their homogeneous counterparts. Ideally, the advantages of homogeneous and heterogeneous catalysis, such as high activity and selectivity on one hand and separation and recycling on the other, should be combined.<sup>[4]</sup> However, the different areas of asymmetric heterogeneous catalysis have reached widely different levels of maturity. Whereas the immobilization of homogeneous catalysts on solid supports represents an established field that is on the verge of being applied in industry, the young field of metal–organic catalysts is in a rapidly growing development phase.

It is the goal of this Review to give an overview of asymmetric heterogeneous catalysis from the point of view of an organic chemist—presenting the state of the art and discussing their potential and limitations. Heterogeneous asymmetric catalysis has been subdivided into three major categories: 1) application of immobilized homogeneous catalysts (Sections 2 and 3), 2) catalysis on surfaces that are chiral themselves or modified with chiral modifiers (Sections 4 and 5), and 3) diastereoselective reactions of chiral substrates promoted by achiral catalysts (Section 6).

## From the Contents

1. Introduction	4733
2. Immobilization of Chiral Homogeneous Catalysts	4733
3. Chiral Metal–Organic Catalysts	4747
4. Chiral Modifiers	4750
5. Di- and Polypeptides as Chiral Macromolecular Catalysts	4754
6. Diastereoselective Heterogeneous Catalysis	4755
7. Conclusion	4757

In contrast to the first group of catalysts, whose profile closely resembles that of homogeneous catalysts, those of groups two and three show unique mechanisms that do not have a counterpart in homogeneous catalysis. A simplified overview of the advantages and disadvantages of the different methodologies is given in Table 1.

## 2. Immobilization of Chiral Homogeneous Catalysts

Homogeneous asymmetric catalysis<sup>[5]</sup> has already proven its usefulness in a number of industrial applications, and the chemists involved in the pioneering breakthroughs were recently awarded the Nobel prize.<sup>[6]</sup> Nevertheless, the efficiency of these processes can be improved even further through the employment of the corresponding heterogeneous catalysts that are derived from their homogeneous counterparts by immobilization, since the catalyst can be easily separated and recycled, and contamination with metal traces minimized. Immobilization occurs by covalent or noncovalent attachment of the chiral ligand, the metal, or the preassembled complex to the support (Figure 1). The ligand can even be synthesized on the support, thus allowing the efficient synthesis and screening of a library of ligands.<sup>[7]</sup> The choice of a suitable support plays an important, although not fully understood, role and remains challenging. Numerous prob-

[\*] Dipl.-Chem. M. Heitbaum, Prof. Dr. F. Glorius  
Philipps-Universität Marburg  
Fachbereich Chemie  
Hans-Meerwein-Strasse, 35032 Marburg (Germany)  
Fax: (+49) 6421-282-5562  
E-mail: glorius@chemie.uni-marburg.de  
Dr. I. Escher  
Bayer CropScience AG  
Chemistry Frankfurt  
Industriepark Höchst, 65926 Frankfurt am Main (Germany)

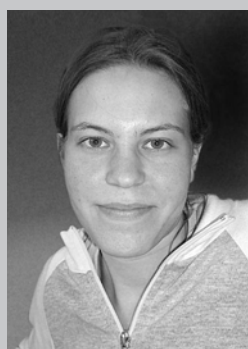
**Table 1:** Evaluation of the different types of asymmetric heterogeneous catalysts.

Advantages	Disadvantages
immobilized homogeneous catalysts	
<ul style="list-style-type: none"> <li>+ many homogeneous systems known for immobilization</li> <li>+ a variety of linking techniques exist</li> <li>+ various supports to choose from</li> <li>+ suited for fast ligand screening</li> <li>+ a few ligands are commercially available</li> <li>+ broad spectrum of reactions</li> <li>+ in some cases higher selectivities can be obtained with the heterogeneous than with the homogeneous catalyst</li> <li>+ rather mature methodology giving predictable results</li> </ul>	<ul style="list-style-type: none"> <li>– additional functionalization of ligands renders their synthesis more costly</li> <li>– limited access to the active catalysts decreases the reaction rate</li> <li>– low catalyst loadings</li> <li>– leaching possible</li> <li>– restriction of degrees of freedom of the catalyst can result in decreased enantioselectivities</li> </ul>
metal–organic systems	
<ul style="list-style-type: none"> <li>+ relatively easy immobilization technique</li> <li>+ no support necessary</li> <li>+ high density of active catalyst centers</li> <li>+ crystalline catalyst (still rare), structure can be determined by X-ray structural analysis</li> <li>+ high levels of porosity</li> <li>+ often no leaching</li> </ul>	<ul style="list-style-type: none"> <li>– synthesis of modified ligands necessary</li> <li>– structure of the network is hard to predict</li> </ul>
chiral modifier	
<ul style="list-style-type: none"> <li>+ synthetically rather facile</li> <li>+ inexpensive</li> <li>+ unique mechanisms that have no counterpart in homogeneous catalysis</li> </ul>	<ul style="list-style-type: none"> <li>– only a few successful modifier/catalyst systems are known</li> <li>– the high complexity of the catalyst system complicates the de novo design</li> <li>– challenging analysis of the mechanism makes optimization of reaction conditions difficult</li> <li>– limited substrate scope</li> </ul>
macromolecular catalysts	
<ul style="list-style-type: none"> <li>+ simple synthesis of catalyst, suited for scale-up (polypeptides)</li> <li>+ unique mode of action</li> </ul>	<ul style="list-style-type: none"> <li>– only a few successful systems known</li> <li>– relatively low turnover frequencies (TOFs)</li> <li>– challenging analysis of mechanisms</li> <li>– substrate limitations</li> </ul>
diastereoselective catalysis	
<ul style="list-style-type: none"> <li>+ known mechanism</li> <li>+ robust and reliable</li> <li>+ often rationally designed</li> </ul>	<ul style="list-style-type: none"> <li>– cost of the chiral auxiliary</li> <li>– demanding substrate synthesis</li> <li>– additional steps for the attachment and cleavage of the auxiliary necessary</li> </ul>

lems can occur during the immobilization of a homogeneous catalyst and diminish its performance:

- undesired interactions between the support and the metal–ligand complex,
- the optimal geometry of the catalyst, crucial for high enantioinduction, is disturbed by the support,

- unsatisfactory stability of the linkage between the catalyst and support or the catalyst itself which results in leaching,
- limited accessibility of the active site,
- undesired isolation of catalyst centers that need to cooperate during the reaction.<sup>[8]</sup>



Maja Heitbaum was born in Frankfurt (Germany) in 1981. She studied chemistry at the Philipps-Universität in Marburg and obtained her diploma in 2005. She is currently working as a PhD student in the group of Prof. Frank Glorius on asymmetric hydrogenation reactions of aromatic and heteroaromatic compounds.



Frank Glorius studied chemistry at the Universität Hannover, Stanford University (Prof. Paul A. Wender), the Max-Planck-Institut für Kohlenforschung and Universität Basel (Prof. Andreas Pfaltz), and Harvard University (Prof. David A. Evans). In 2001 he began his independent research career at the Max-Planck-Institut für Kohlenforschung in Germany (Prof. Alois Fürstner). Since 2004 he has been a Professor for Organic Chemistry at the Philipps-Universität Marburg. His research focuses on the development of new concepts for catalysis and their implementation in organic synthesis.

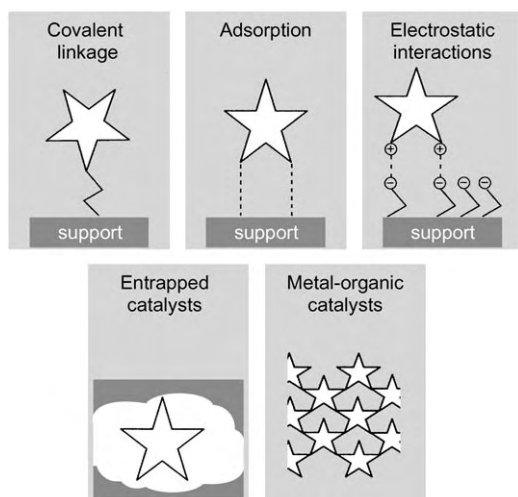


**Figure 1.** Strategies for the immobilization of chiral homogeneous catalysts (symbolized by stars).

In this section, the different strategies of immobilization are introduced briefly, followed by modern, representative examples of immobilized privileged ligands.<sup>[5c]</sup> There are numerous relevant examples, but only a few have been selected in which the selectivities that were obtained were comparable or superior to the homogeneously catalyzed reaction. The article focuses on immobilized metal–ligand complexes,<sup>[9]</sup> while immobilized enzymes,<sup>[10]</sup> soluble polymer-bound,<sup>[9c,11]</sup> and dendritic catalysts,<sup>[12]</sup> which have all shown remarkable results in recent years, are not included.

## 2.1. Covalently Immobilized Catalysts

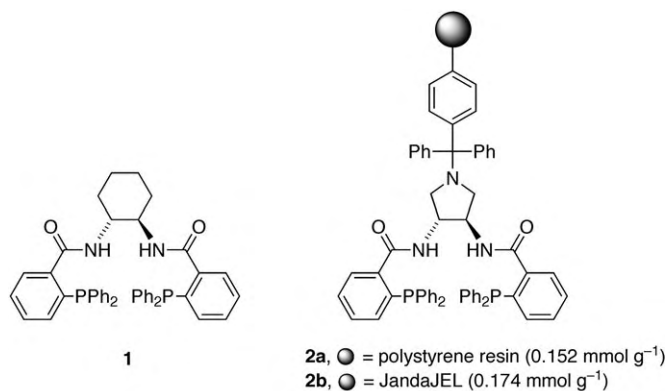
A classical method to immobilize a chiral homogeneous ligand or its metal complex is copolymerization with a monomer, or its covalent linkage to a suitable support, such as functionalized polymers, inorganic oxides, nanotubes, etc. The modification of the chiral ligand, the length and flexibility of the linker, as well as the catalyst loading, the accessibility of the active catalyst center, and the choice of the solvent are only a few parameters that influence the immobilization of a metal complex.

Interestingly, two opposite strategies—the avoidance and the willful causation of interactions of the catalyst with the solid support—can be advantageous for the performance of the catalyst. To achieve minimal levels of interaction, which has been the predominant strategy, the anchoring point in the ligand structure should be as far away from the active site of the catalyst as possible. Furthermore, a long and flexible polymer should be chosen. However, the catalyst can also be attached to the support in proximity to the active site, which has led to improved catalytic performances in a few cases.

### 2.1.1. Covalent Immobilization on Polymeric Resins

The success of the solid-phase peptide synthesis developed by Merrifield in the 1960s has resulted in the covalent attachment of chiral ligands onto a functionalized polymer becoming a popular approach. In addition to only slightly cross-linked Merrifield resins (poly(styrenedivinylbenzene)-polymers),<sup>[13]</sup> other resins such as JandaJEL (polystyrene polymers containing a tetrahydrofuran-derived cross-linker),<sup>[14]</sup> TentaGel (polystyrene-poly(ethyleneglycol-OC<sub>2</sub>H<sub>4</sub>-NHCOC<sub>2</sub>H<sub>5</sub>)),<sup>[15]</sup> and other PS-PEG (polystyrene-polyethyleneglycol) resins<sup>[16]</sup> have been employed successfully for anchoring metal–ligand complexes.

Han and co-workers developed ligand **2**, a variation of the chiral Trost ligand **1**, in which the cyclohexyldiamine moiety was replaced by a pyrrolidinediamine unit so as to allow facile anchoring onto the support and minimal disturbance to the catalytic site (Scheme 1).<sup>[17]</sup> It was shown that the use of



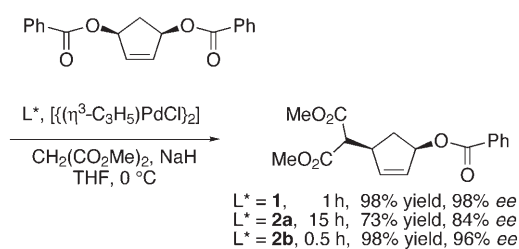
**Scheme 1.** Trost ligand **1** and immobilized variants **2a** and **b**.

different resins results in significantly different catalytic performances in the palladium-catalyzed desymmetrization of 1,4-bis(benzoyloxy)cyclopent-2-ene with dimethyl malonate (Scheme 2). The JandaJEL-supported ligand **2b** gave results comparable to those obtained with the homogeneous catalyst, whereas the polystyrene-bound catalyst derived from ligand **2a** was clearly less active and selective. In contrast to the classical Merrifield resin, the JandaJEL resin contains long and flexible, tetrahydrofuran-derived cross-linkers. It is assumed that the resulting higher swellability of the resin in organic solvents gives the attached complex more degrees of



Iris Escher studied chemistry at the Universität Hannover (Diploma), Stanford University (DAAD exchange, Dr. J. Griffin), the Max-Planck Institut für Kohlenforschung and Universität Basel (PhD in the group of Prof. Andreas Pfaltz), and Harvard University (post-doctoral research with Prof. G. Verdine). In 2001 she became team leader for the Bayer AG (Zentrale Forschung). She joined the Bayer CropScience AG in 2002, where she is currently a scientist in herbicide chemistry. Her main research interests are the synthesis of active ingredients for crop protection.

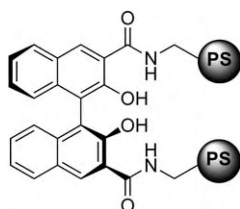




**Scheme 2.** Palladium-catalyzed desymmetrization.

freedom and consequently allows it to perform more like a homogeneous catalyst.

In one of the rare examples in which interactions with the polymeric support were found to be beneficial, Chan and co-workers chose an amide linkage in proximity to the catalytically active site to anchor a modified binol (1,1'-bi-2-naphthol) through its 3,3'-position to polystyrene (Scheme 3).<sup>[18]</sup> Clearly higher *ee* values were obtained at full



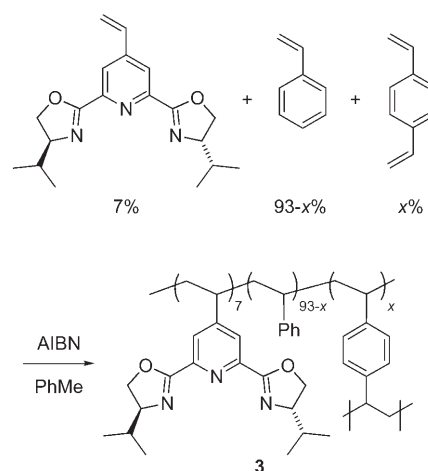
**Scheme 3.** Binol, attached through its 3,3'-position to polystyrene (PS).

conversion in the titanium-catalyzed addition of diethylzinc to aldehydes in the presence of this ligand than with homogeneous binol (benzaldehyde: 97 versus 91.5% *ee*, respectively). The authors attribute the positive effect of the polymer to its proximity to the catalytically active site, thus resulting in an increased conformational rigidity of the metal complex. However, the ligand's bite angle might also be affected by the performance of the polymer.

#### 2.1.2. Covalent Immobilization by Copolymerization

Copolymerization of suitable monomers allows for the introduction of the chiral information into the backbone of the heterogeneous catalyst. Radical polymerization of vinyl-modified ligands with styrene and divinylbenzene<sup>[19]</sup> (Scheme 4) or polymerization of amines with isocyanates to polyurethanes<sup>[20]</sup> are commonly used methods. The accessibility of the active site, which depends heavily on the degree of cross-linkage in the copolymer, is crucial for the activity and selectivity of the final catalyst. In general, the swellability of the copolymer in organic solvents decreases as the degree of cross-linkage increases.

Alternatively, a ligand library can be synthesized efficiently by first preparing a functionalized copolymer which can be used as the key building block in the final synthesis of the chiral ligands. For example, the opening of enantiomerically pure epoxides immobilized on a copolymer with different amines gave a series of immobilized amino alcohols.



**Scheme 4.** Radical copolymerization of a PyBox derivative. AIBN = azobisisobutyronitrile.

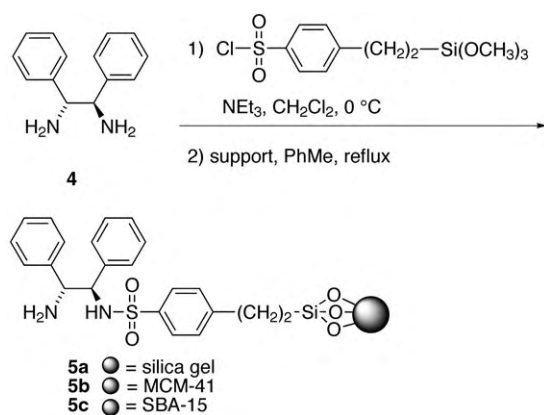
These ligands were screened successfully in the ruthenium-catalyzed asymmetric transfer hydrogenation of acetophenone.<sup>[21]</sup>

#### 2.1.3. Covalent Immobilization on an Inorganic Support

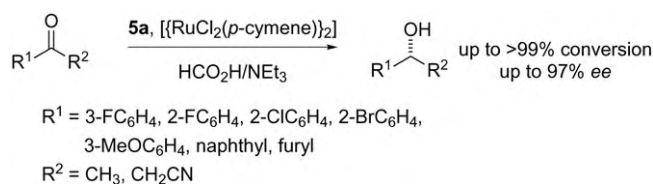
The application of inorganic materials as heterogeneous supports offers a number of advantages: their rigid structure does not allow the aggregation of active catalysts, they do not swell, and are insoluble in organic solvents.<sup>[22]</sup> The last two properties are interesting in regard to their application as stationary chiral phases in a continuous process. In addition, inorganic supports possess better thermal and mechanical stability under catalysis conditions.

Among others, zeolites and other mesoporous materials (pore size between 2 and 50 nm),<sup>[23]</sup> which are characterized by their high surface area and easily accessible pores, have been used successfully for the covalent immobilization of asymmetric catalysts.<sup>[24]</sup> Prominent examples are MCM-41 ("mobile crystalline material", ordered hexagonal, usually 30–40 Å pore diameter; its very high porosity renders it less mechanically stable than other inorganic materials),<sup>[23d]</sup> MCM-48 (ordered cubic), Grace 332 (ca. 19 Å pore diameter), USY ("ultrastabilized zeolite y", 12–30 Å pore diameter), SBA 15 (ordered hexagonal, 46–300 Å pore diameter),<sup>[23b]</sup> and nonporous silica such as carbosil. The linker (for example, a trialkoxysilane) is attached through the silanol moieties on the surface or at the inner walls of the pores of the support. Afterwards, the ligand or metal–ligand complex is attached. Alternatively, a presynthesized linker–ligand building block can be used to allow for a rapid immobilization on different supports (Scheme 5).<sup>[25]</sup> In the case of ligands **5**, the best results in the ruthenium-catalyzed transfer hydrogenation of various aromatic ketones were obtained with the ligand immobilized on silica gel (**5a**; Scheme 6).<sup>[26]</sup>

In the case of mesoporous supports, the catalyst can be immobilized on the surface or in the pores of the inorganic support. The ligand can be immobilized only in the pores by treating the surface silanol groups with a silylating agent such



**Scheme 5.** Immobilization on different inorganic supports.

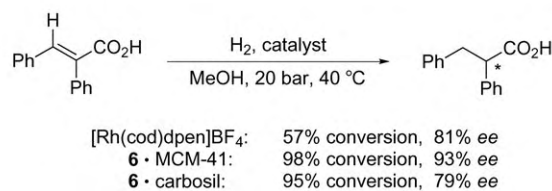
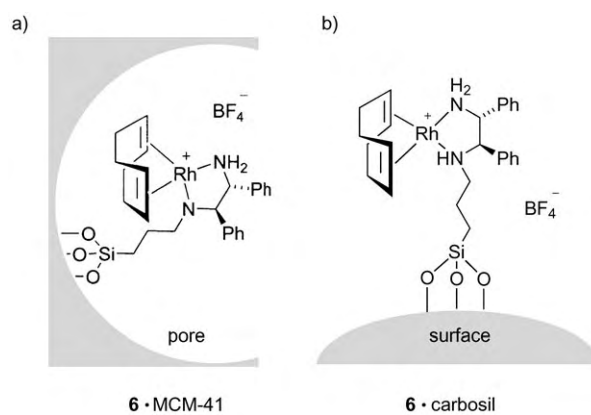


**Scheme 6.** Ruthenium-catalyzed transfer hydrogenation.

as diphenylsilyl dichloride prior to attaching the chiral ligand. Such a site-selective immobilization of the catalyst can have a positive effect on the selectivity of the catalysis. Either the active complex is conformationally confined by the interior of the pore<sup>[27,28]</sup> or the access of the substrates to the catalyst is restricted.<sup>[29]</sup> Remarkably, Thomas and co-workers found that the chiral ligand (*R,R*)-diphenylethylenediamine (dpen) anchored to the inner walls of porous MCM-41 led to enhanced enantiomeric excess in the Rh-catalyzed asymmetric hydrogenation of phenylcinnamic acid relative to that of the homogeneously catalyzed reaction (93 versus 81% ee, respectively; Scheme 7a).<sup>[29]</sup> This improvement was not observed with the catalyst immobilized on the convex surface of nonporous silica (carbosil, Scheme 7b) and was attributed to the restricted approach of the reactant to the active catalyst in the concave pore. Furthermore, **6**·MCM-41 was recycled and reused two times (90% ee).

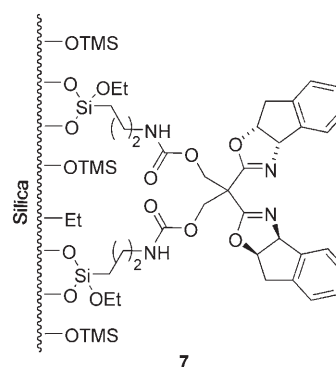
The influence of the pore diameter on the performance of the immobilized chiral, cationic rhodium and palladium complexes was investigated. These complexes were bound electrostatically to a number of commercially available silicates with various pore sizes (38–250 Å pore diameter) by a surface-supported triflate counterion. Interestingly, the selectivity of the asymmetric hydrogenation of methyl benzoylformate decreased as the pore size increased.<sup>[30]</sup>

Not only can passivation be used to block all of the surface silanol groups and to direct the immobilization to the pores, but it can also be used to modify the surrounding of the anchored catalyst and improve the properties of the catalyst. Very recently, Lemaire and co-workers showed a linear correlation between the increasing degree of passivation and the enantioselectivity obtained in the Diels–Alder reaction of cyclopentadiene with *N*-acryloyloxazolidinone catalyzed by



**Scheme 7.** Asymmetric hydrogenation of phenylcinnamic acid. cod = cycloocta-1,5-diene.

the bisoxazoline **7** immobilized on silica gel (increase from 58 to 80% ee, Scheme 8).<sup>[31]</sup> This improvement in selectivity has been observed before,<sup>[32]</sup> but can not be generalized.<sup>[33]</sup> The

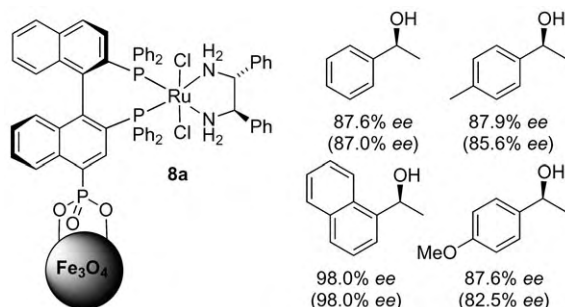


**Scheme 8.** A bisoxazoline ligand immobilized on a passivated silica surface. TMS = trimethylsilyl.

authors speculate that the silylation of the free OH groups on the silica prevents the formation of catalytically active, achiral metal–silanol complexes.

In addition to these mesoporous supports, crystalline nanoparticles possessing a high surface area have also been employed. Very recently, Lin et al. used super-paramagnetic magnetite nanoparticles ( $\text{Fe}_3\text{O}_4$ ) as a support for the  $[\text{Ru}(\text{binap})(\text{dpen})]$  complex (binap: 2,2'-bis(diphenylphosphine)-1,1'-binaphthyl).<sup>[34]</sup> These magnetite nanoparticles are intrinsically not magnetic, but can readily be magnetized by an external magnet. Two different types of nanoparticle were employed: one obtained by thermal decomposition (**8a**) and the other by co-precipitation (**8b**). Slightly higher enantioselectivity

lectivities were obtained in all cases when catalyst **8a** was used in the asymmetric hydrogenation of ketones compared to those obtained with the homogeneous [Ru(binap)(dpen)] catalyst (Scheme 9).<sup>[34]</sup> In the asymmetric hydrogenation of 1-



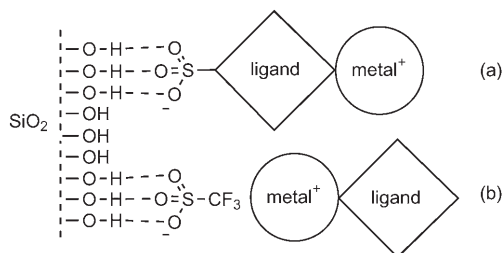
**Scheme 9.** Asymmetric hydrogenation of acetophenone derivatives with magnetically separable, immobilized catalysts (results of the homogeneous [Ru(binap)(dpen)] complex are given in brackets).

acetophenone, the heterogeneous catalyst **8b** could be separated by simple “magnetic” decantation and was recycled up to 14 times without a decrease in the conversion or enantioselectivity (100% conversion, 97–98% ee).

## 2.2. Noncovalently Immobilized Catalysts

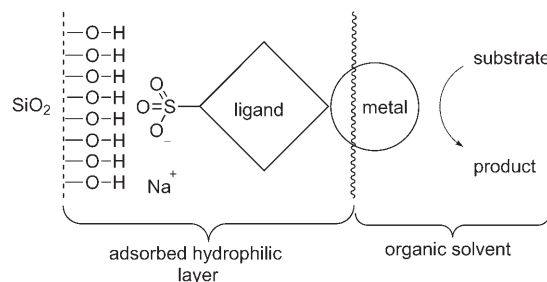
### 2.2.1. Immobilization by Adsorption

The simple physisorption of a chiral ligand or metal–ligand complex on a support through van der Waals interactions is an attractive approach, since it renders a synthetic modification of the chiral ligand unnecessary. However, this concept has only had limited success, because the complexes are only weakly bound. Therefore, the optimization of the reaction conditions, especially the choice of the right solvent, is a difficult task. The stability can be improved significantly if the chiral metal–ligand complex is immobilized by hydrogen bonding<sup>[35]</sup> on a polar support such as silica. Hydrogen acceptors such as sulfonates need to be introduced into the ligand structure to make use of hydrogen bonding with the polar silanol moieties (Scheme 10a). Alternatively, a cationic complex can be bound by a surface-supported counterion, such as a triflate. In this case no modification of the ligand structure is necessary. (Scheme 10b).<sup>[36]</sup>



**Scheme 10.** Immobilization of metal–ligand complexes by hydrogen bonding of the support with a) the ligand or b) the counterion.

In an interesting alternative approach, a hydrophilic phase, such as water or ethylene glycol, in which the chiral complex has been dissolved is immobilized on a hydrophilic support such as silica gel or controlled pore glass (SAPC: supported aqueous-phase catalyst).<sup>[37]</sup> The catalysis takes place at the interface of the immobilized hydrophilic layer and the immiscible organic solvent. The heterogeneous support promotes the reaction by increasing the surface contact area between the two phases significantly. The appropriate chiral ligand needs to be hydrophilic, which can be achieved by the incorporation of sulfonate groups into the ligand structure (Scheme 11).<sup>[38]</sup> The immobilized complex



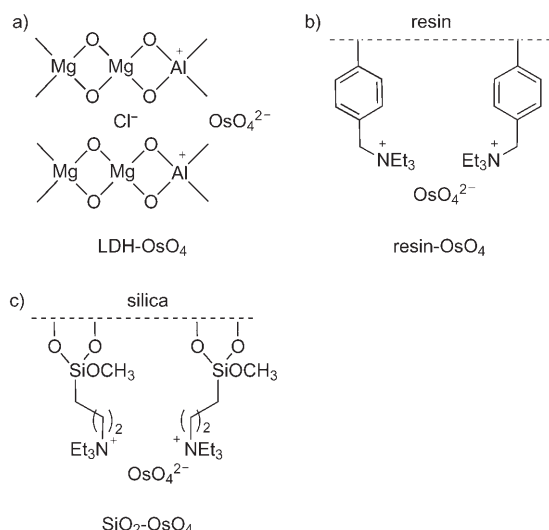
**Scheme 11.** Mode of action of an SAP catalyst.

can be recycled by simple filtration and reused immediately. Even if only a few asymmetric applications of SAPCs have been reported so far, for example, in the synthesis of naproxen (Section 2.3.1.2), this technique is likely to become more and more popular in transition-metal catalysis.

### 2.2.2. Immobilization by Ion Exchange

Ion exchange between a chiral, cationic metal–ligand complex and an acidic resin represents an elegant method for immobilization through electrostatic interactions. For example, this methodology has been applied successfully in copper-catalyzed aziridination of alkenes,<sup>[39]</sup> enantioselective dehydrogenation,<sup>[40]</sup> Diels–Alder reactions,<sup>[41]</sup> and imino–ene reactions<sup>[42]</sup> (see also Section 2.3.3.2). Moreover, ion exchange is the only method that allows the direct immobilization of the metal itself. Therefore, it is a method of choice for the recycling of expensive or very toxic metal derivatives such as osmium tetroxide.<sup>[43]</sup> Choudary et al. were the first to immobilize  $\text{OsO}_4^{2-}$  in layered double hydroxides (LDHs).<sup>[44]</sup> LDHs contain alternating cationic  $\text{M(II)}_{1-x}\text{M(III)}_x(\text{OH})_2^{x+}$  and anionic  $\text{A}^{n-} \cdot z\text{H}_2\text{O}$  layers.<sup>[45]</sup> The exchange of chloride anions for  $\text{OsO}_4^{2-}$  in  $\text{Mg}_{1-x}\text{Al}_x(\text{OH})_2(\text{Cl})_x \cdot z\text{H}_2\text{O}$  crystals ( $x = 0.25$ ) gives the LDH- $\text{OsO}_4$  catalyst. Interestingly, the metal is localized on the surface and not in the interlamellar space of the LDH (Scheme 12a).

The LDH- $\text{OsO}_4$  catalyst did not only show very high activity and selectivity in the asymmetric dihydroxylation reaction of *trans*-stilbene (96% yield, 99% ee), but also gave excellent results with cinnamates (93–96% yield, 99% ee) and 1-naphthyl allyl ether (94% yield, 77% ee) that were comparable to those obtained with the homogeneous catalyst. LDH- $\text{OsO}_4$  could be recycled in the presence of *N*-methyl-



**Scheme 12.** Immobilization of  $\text{OsO}_4^{2-}$  by ion exchange.

morpholine-*N*-oxide (NMO) as cooxidant three times without loss of selectivity in the asymmetric dihydroxylation of  $\alpha$ -methylstyrene. The significant deactivation observed when using  $\text{K}_3[\text{Fe}(\text{CN})_6]$  or molecular oxygen as the cooxidant was explained by a competitive exchange of the  $\text{OsO}_4^{2-}$  ions for ferrocyanide or phosphate ions.<sup>[46]</sup> Catalysts prepared by the immobilization of  $\text{OsO}_4^{2-}$  on quaternary ammonium groups supported on a polymer such as chloromethylated styrenedi-vinylbenzene copolymers (Merrifield resin, resin- $\text{OsO}_4$ ; Scheme 12b) or silica gel ( $\text{SiO}_2$ - $\text{OsO}_4$ ; Scheme 12c) did not show any undesired leaching of osmium in the presence of  $\text{K}_3[\text{Fe}(\text{CN})_6]$  (Table 2). A higher activity was observed with

**Table 2:** Asymmetric dihydroxylation with LDH- $\text{OsO}_4$  and resin- $\text{OsO}_4$ .

$\text{Ph}-\text{CH}=\text{CH}-\text{Ph} \xrightarrow[\text{K}_3\text{Fe}(\text{CN})_6/\text{K}_2\text{CO}_3 \text{ or NMO}]{\text{catalyst (1 mol \%)} \text{ (DHQD)}_2\text{AQN (1 mol \%)} \text{ tBuOH/H}_2\text{O}}$ $\text{Ph}-\text{CH}(\text{OH})-\text{CH}(\text{OH})-\text{Ph}$					
Entry	Olefin	Catalyst	Cooxidant	Yield [%]	<i>ee</i> [%]
1	$\text{Ph}-\text{CH}=\text{CH}-\text{Ph}$	LDH- $\text{OsO}_4$	NMO	96	99
2	$\text{Ph}-\text{CH}=\text{CH}-\text{Ph}$	resin- $\text{OsO}_4$	$\text{K}_3[\text{Fe}(\text{CN})_6]$	95	99
3	$\text{Ph}-\text{CH}=\text{CH}-\text{Ph}$	LDH- $\text{OsO}_4$	NMO	97	97
4	$\text{Ph}-\text{CH}=\text{CH}-\text{Ph}$	resin- $\text{OsO}_4$	$\text{K}_3[\text{Fe}(\text{CN})_6]$	92	98
5	$\text{CH}_3(\text{CH}_2)_7\text{CH}=\text{CH}_2$	resin- $\text{OsO}_4$	$\text{K}_3[\text{Fe}(\text{CN})_6]$	85	82

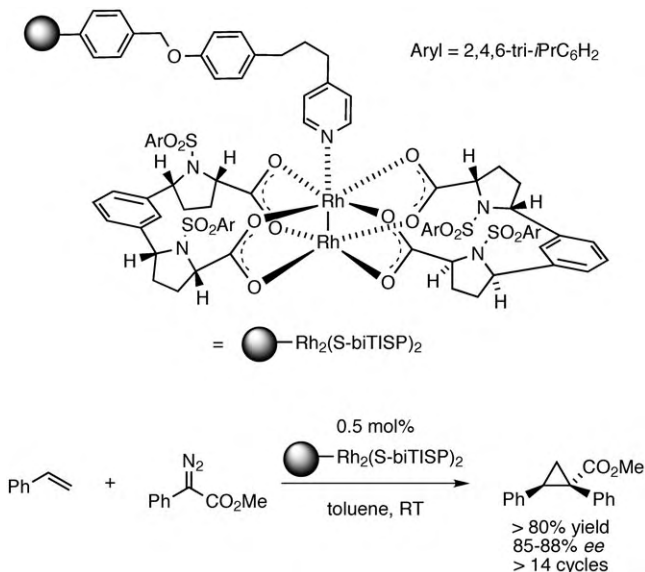
resin- $\text{OsO}_4$  than with  $\text{SiO}_2$ - $\text{OsO}_4$ , which was attributed to the better swelling properties of the polymer in organic solvents. Resin- $\text{OsO}_4$  is also an excellent catalyst for the asymmetric dihydroxylation of aliphatic olefins such as 1-octene (90 % yield, 84 % *ee*).<sup>[47]</sup> LDH- $\text{OsO}_4$  has also been applied in the asymmetric oxidation of sulfides (up to 51 % *ee*).<sup>[48]</sup>

### 2.2.3. Other Noncovalent Interactions

The encapsulation of chiral catalysts in a support, often referred to as “ship in a bottle”, is the only type of immobilization that does not require any favorable interac-

tion between the metal–ligand complex and the support. In general, chiral complexes can either be successively assembled in the pores of a mesoporous material<sup>[49]</sup> or the presynthesized complex is entrapped by polymerization in a sol–gel process or in a polydimethylsiloxane (PDMS) film. In both cases, synthetic methods are required that are well tolerated by the support and the metal–ligand complex. If the support is assembled around the presynthesized complexes, the diameter and the openings of the pores formed can differ significantly, often accompanied by a negative impact on the selectivity of the immobilized catalyst. The openings of the pores of the support need to be smaller than the enclosed complex to avoid leaching (Figure 1). As a consequence, the accessibility of the active complex is generally limited and results in significantly longer reaction times.<sup>[50]</sup> For these reasons, only a few highly selective encapsulated catalysts can be found in the literature. An example is the application of a Rh-Meduphos complex embedded in a PDMS membrane for the asymmetric hydrogenation of C=C bonds. This catalyst still resulted in high enantioselectivity (96 % versus 98 % *ee* for the homogeneously catalyzed reaction), however, the reactions were ten-times slower (Section 2.3.2.1).<sup>[51]</sup>

A different, very effective approach was developed by Davies et al. They immobilized dirhodium complexes by coordination and employed them in the asymmetric, intermolecular cyclopropanation and C–H activation of donor/acceptor-substituted carbenoids.<sup>[52]</sup> Specifically, a pyridine tethered to a highly cross-linked polymer (argopore) by the Wang linker binds to the catalytically active chiral dirhodium complex (Scheme 13). Part of the immobilization was attrib-



**Scheme 13.** Coordinatively immobilized dirhodium complex used in asymmetric cyclopropanation.

uted to microencapsulation, whereas a capture-release (boomerang) mechanism could be excluded. An immobilization by coordination has the advantage that: 1) no modification of the chiral ligands on the rhodium is necessary, thus the



structure of the chiral complex that is necessary for the selectivity is not impaired, 2) although one rhodium atom is deactivated by coordination, the other remains active for catalysis, and 3) this methodology can be applied successfully to numerous chiral dirhodium complexes.<sup>[53]</sup> For example, the immobilized catalyst used in the cyclopropanation of styrene was recycled up to 15 times without loss of selectivity and yield—only a slight decrease in the reactivity was observed (Scheme 13). Coordinative metal–ligand interactions are also used for immobilization in metal–organic frameworks (see Section 3).

### 2.3. Immobilization of Privileged<sup>[5d]</sup> Chiral Catalysts

The following chapters are organized according to the order used for the different immobilization techniques described in Sections 2.1 and 2.2.

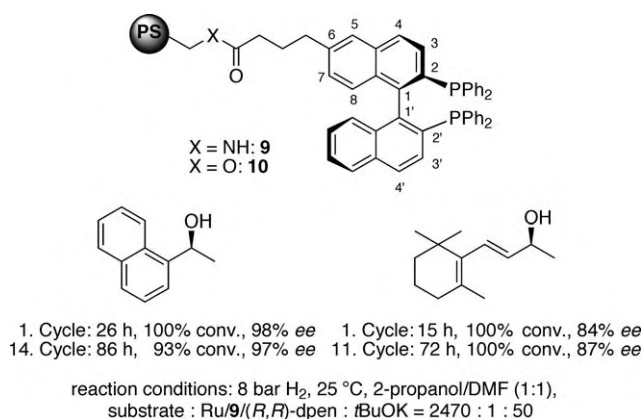
#### 2.3.1. Metal–Binap Complexes

##### 2.3.1.1. Covalent Immobilization of Binap

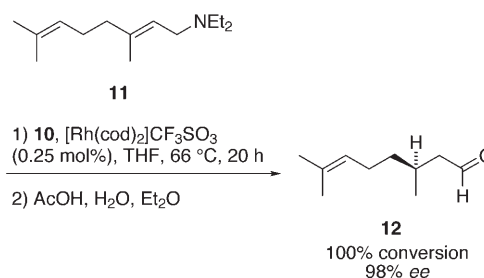
The binap ligand is arguably one of the most prominent and successful chiral ligands for asymmetric catalysis, and therefore it has often been used for the investigation of new immobilization techniques. Bayston et al. obtained high activities and enantioselectivities in the ruthenium-catalyzed hydrogenation of  $\beta$ -ketoesters (for example, for  $\text{CH}_3\text{CH}_2\text{COCH}_2\text{CO}_2\text{Me}$ , 99% yield, 97% *ee*)<sup>[54]</sup> with binap **9** connected to polystyrene (PS) through an alkyl amide at its 6-position.<sup>[54]</sup> Using the same PS–binap ligand **9**, Noyori and co-workers obtained excellent enantioselectivities and also high turnover numbers (TON) in the ruthenium-(*R,R*)-dppe-catalyzed hydrogenation of ketones; for example, in the hydrogenation of acetophenone a TON of 33 000 was obtained in a total of 14 experiments (Scheme 14).<sup>[55]</sup>

Immobilized binap on polystyrene (**10**) is commercially available and has been applied successfully in many reactions such as the palladium-catalyzed Mukaiyama–aldol reaction and the asymmetric Mannich reaction.<sup>[56]</sup> In the industrially interesting isomerization of (*E*)-diethylgeranylamine (**11**) to (*S*)-citronellal (**12**), catalyst **10** did not only give activities and selectivities comparable to the homogeneous system (100% conversion, 98% *ee*) but could also be recycled and reused up to 37 times by simple decantation or filtration (Scheme 15).<sup>[57]</sup>

Although good results have been obtained with binap-derived catalysts that are anchored to polymers such as polyesters and PEG that are soluble under the reaction conditions, they are not covered in this Review.<sup>[9c,11]</sup>

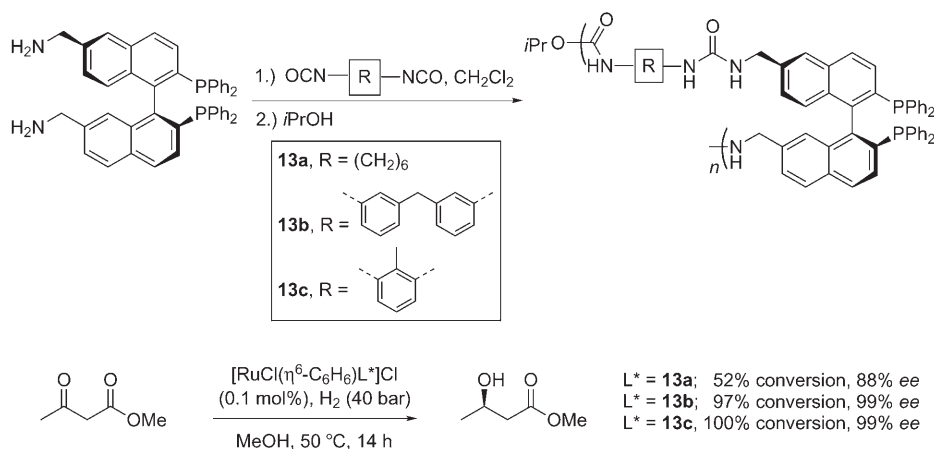


**Scheme 14.** Enantioselective ruthenium-catalyzed hydrogenation with the PS-bound binap ligand **9**.



**Scheme 15.** Isomerization of (*E*)-diethylgeranylamine (**11**) to (*S*)-citronellal (**12**).

Lemaire and co-workers favored the immobilization of 6,6'-diaminomethyl-binap by copolymerization with diisocyanates to polyureas (**13**, Scheme 16) instead of tethering the complex to an existing polymer.<sup>[20,58]</sup> As the rigidity of the linker moiety *R* increased, the enantioselectivities obtained with the Ru complexes in the asymmetric hydrogenation of methyl acetoacetate increased from good to excellent. Moreover, polymer **13c** could be recycled three times without loss

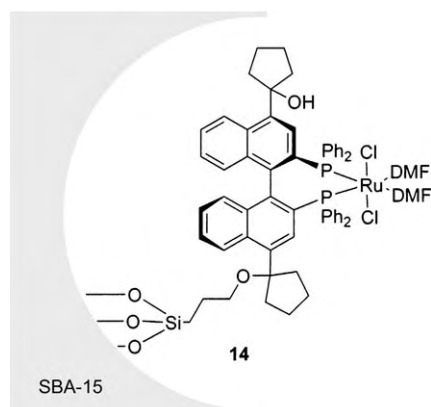


**Scheme 16.** Immobilization of 6,6'-diaminomethyl-binap by copolymerization with diisocyanates.

of activity and reactivity. Additional cross-linking with triisocyanatotoluene (30 %) resulted in a significant decrease in the activity and selectivity (35 % yield, 9 % *ee*). These polyureas also sometimes gave good results in the ruthenium-catalyzed hydrogenation of olefinic double bonds.<sup>[59]</sup>

Pu and co-workers utilized poly(binap) (prepared by Suzuki–Miyaura coupling of 1,4-dibromo-2,5-dialkylbenzene with a chiral binap-boronic ester) in the ruthenium-catalyzed reduction of aryl methyl ketone in the presence of (*R,R*)-diphenylethylenediamine (99 % conversion, 90 % *ee*).<sup>[60]</sup>

Sterically demanding substituents in the 4,4'-position of binap derivatives can improve the asymmetric induction in the ruthenium-catalyzed hydrogenation of  $\beta$ -ketoesters.<sup>[61]</sup> Anchoring binap through the 4,4'-position to the inner surface of a mesoporous SBA-15 pore (BJH-measured pore size after immobilization of **14**: 96 Å) has also been shown to be especially rewarding (**14**, Scheme 17). Methyl acetoacetate was hydrogenated with 98.6 % *ee* and the chiral catalyst **14** could be recycled three times with full conversion and a slightly reduced *ee* value (96.2–98.6 %).<sup>[62]</sup>

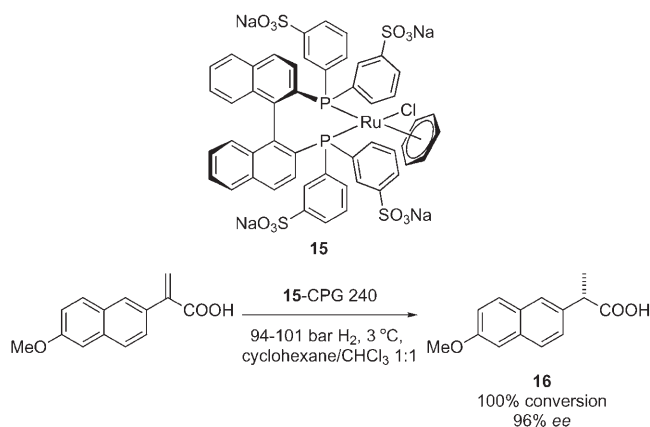


**Scheme 17.** Ru complex **14** immobilized in a pore of SBA-15.

Convincing results have also been afforded with chiral porous binap-zirconium phosphonates in the ruthenium-catalyzed asymmetric hydrogenation of  $\beta$ -ketoesters (see Section 2.3).<sup>[63]</sup>

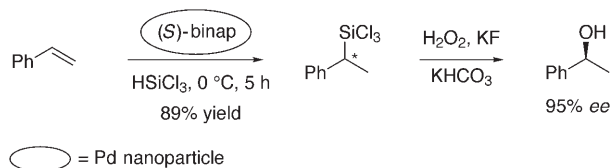
### 2.3.1.2. Noncovalently Immobilized Binap

Compared to the homogeneous catalysts, attempts to immobilize binap complexes by noncovalent methods such as embedding in membranes,<sup>[50b,64]</sup> by sol-gel polymerization,<sup>[65]</sup> or by impregnation of silica gel<sup>[66]</sup> were accompanied by a loss in activity or enantioselectivity. However, the binap complex **15** dissolved in ethylene glycol and adsorbed on glass (CPG-240, controlled pore glass-240, pore diameter 242 Å) gave good results in the ruthenium-catalyzed hydrogenation.<sup>[67]</sup> Similar to the homogeneous catalyst, this binap-SAP catalyst afforded 96 % *ee* in the synthesis of naproxen (**16**; TOF = 41 h<sup>-1</sup> (heterogeneous); 131 h<sup>-1</sup> (homogeneous); Scheme 18).



**Scheme 18.** Synthesis of naproxen (**16**).

Binap-palladium nanoparticles have also been prepared by the reduction of K<sub>2</sub>PdCl<sub>4</sub> with sodium borohydride in the presence of binap (dispersity 2.0 ± 0.5 nm). Strikingly, whereas the homogeneous palladium-binap complex does not promote the reaction, the nanoparticle-based catalyst gave up to 95 % *ee* in the hydrosilylation of styrene (the *ee* value was determined after oxidation to the alcohol, Scheme 19).<sup>[68]</sup>



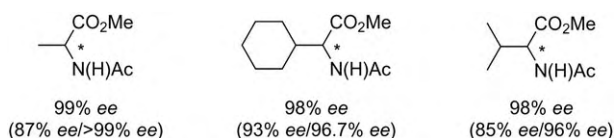
**Scheme 19.** Asymmetric hydrosilylation of styrene.

### 2.3.2. [Rh{(R,R)-Meduphos}] Complexes

Both covalent<sup>[69]</sup> and noncovalently immobilized duphos complexes have been used successfully in asymmetric catalysis. Noncovalently immobilized strategies have proved to be especially successful, and will be discussed in more detail in the following section.

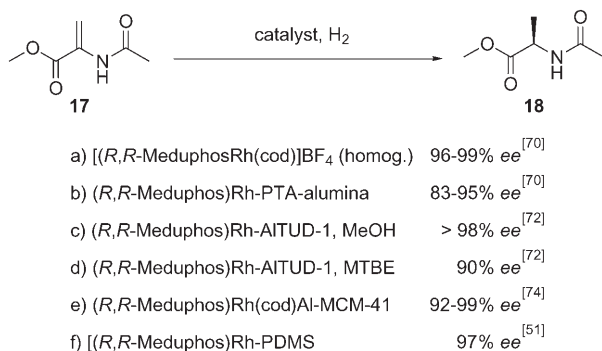
#### 2.3.2.1. Noncovalently Supported [Rh{(R,R)-Meduphos}] Complexes

The immobilized cationic [(*R,R*)-Meduphos]Rh(cod)]OTf complex was prepared by simple mixing the complex with MCM-41 in CH<sub>2</sub>Cl<sub>2</sub>. Presumably, it is bound through the hydrogen bonding of the triflate counterion to the support.<sup>[36a]</sup> In the asymmetric hydrogenation of olefins in hexane, the heterogeneous catalyst gave superior selectivities than the homogeneous system that performed in methanol (Scheme 20). Remarkably, this impregnated, heterogeneous catalyst could be recycled and reused up to four times without loss of activity and selectivity.



**Scheme 20.** Asymmetric hydrogenation with impregnated  $[(R,R)\text{-Meduphos}]\text{Rh}(\text{cod})\text{OTf}$ ; results obtained with the homogeneous catalyst are given in brackets (in hexane/methanol). Tf = triflate.

In a different approach Augustine et al. used phosphotungstic acid (PTA) as the linker between the support and the chiral metal–ligand complex.<sup>[70]</sup> The immobilization is based on the interaction of both the metal–ligand complex as well as the support with an oxygen atom or a hydroxy group of the PTA. Therefore, a synthetic modification of the ligand structure is not necessary for the immobilization. In the Rh-catalyzed asymmetric hydrogenation of methyl 2-acetamidoacrylate (**17**) similarly high selectivities were obtained using  $[\text{Rh}(\text{Meduphos})]\text{-PTA-alumina}$  as under homogeneous conditions (up to 95 % *ee* after three cycles, Scheme 21 b).



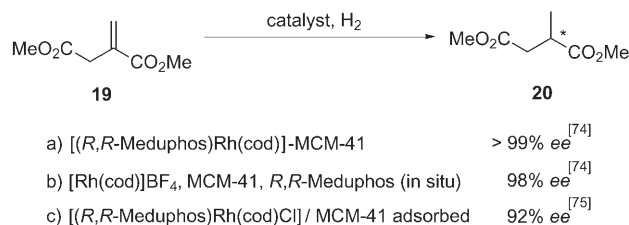
**Scheme 21.** Hydrogenation of methyl 2-acetamidoacrylate (**17**).

Remarkably, the enantioselectivity obtained increased with the progressing recycling in up to 15 cycles going from 67 to 97 % *ee* (homogeneous 76 % *ee*) by using  $[\text{Rh}(\text{dipamp})]$  immobilized by PTA on montmorillonite K<sup>[71]</sup> without any decrease in activity.<sup>[49]</sup>

Rh-Meduphos complexes have also been supported successfully by ion exchange. By utilizing tetraethylene glycol as a template Maschmeyer and co-workers prepared a mesoporous, Brønsted acidic aluminosilicate (AITUD-1, pore diameter 20–500 Å) with an unusually low Si/Al ratio of 4:1 to allow for a tetrahedral coordination of aluminum (Si/Al<sub>tet</sub> 9:1).<sup>[72]</sup> After ion exchange with  $[(R,R)\text{-Meduphos}]\text{Rh}(\text{cod})\text{BF}_4$ , the resulting catalyst afforded > 98 % *ee* in the asymmetric reduction of methyl 2-acetamidoacrylate (**17**) in methanol, similar to the homogeneous counterpart. Unfortunately, a significant leaching of ruthenium was observed (4.9 mg L<sup>−1</sup>, 17 %). The leaching could be reduced to 0.01 mg L<sup>−1</sup> by using the apolar solvent methyl *tert*-butyl ether (MTBE) without affecting the conversion and reaction rate (100 % conversion, TOF > 350 h<sup>−1</sup>, 90 % *ee*, Scheme 21 c,d). Nevertheless, it was not possible to recycle the catalyst successfully. This was attributed to an intrinsic

instability<sup>[73]</sup> of the Rh-duphos complex under the reaction conditions.

In contrast, Hutchings and co-workers were able to prepare a stable  $[(R,R)\text{-Meduphos}]\text{Rh}(\text{cod})\text{Al-MCM-41}$  catalyst by ion exchange of  $[(R,R)\text{-Meduphos}]\text{Rh}(\text{cod})\text{BF}_4$  with acidic (H<sup>+</sup>)Al-MCM-41. Excellent enantioselectivities and activities were reported for the asymmetric hydrogenation of dimethyl itaconate (substrate/Rh = 250:1, cycle 1 to 5: 1 h, > 99 % conversion, > 99 % *ee*, Scheme 22 a). Moreover,



**Scheme 22.** Hydrogenation of dimethyl itaconate (**19**).

the catalyst was recycled up to eight times (cycle 8: 1 h, 99 % conversion, 95 % *ee*).<sup>[74]</sup> Similarly good results were obtained in the reduction of methyl 2-acetamidoacrylate (**17**; 92–99 % *ee* in five cycles compared to 99 % *ee* under homogeneous conditions, Scheme 21 a,e). Instead of having to exchange the presynthesized chiral complex, an in situ synthesis of the complex in the pore of MCM-41 is feasible. First  $[\text{Rh}(\text{cod})_2]\text{BF}_4$  is exchanged, followed by treatment with the chiral Meduphos ligand (dimethyl itaconate/rhodium = 1000:1, 100 % conversion, 98 % *ee*, Scheme 22 b). In general, this in situ synthesis allows a rapid and efficient catalyst screening of multiple chiral ligands.

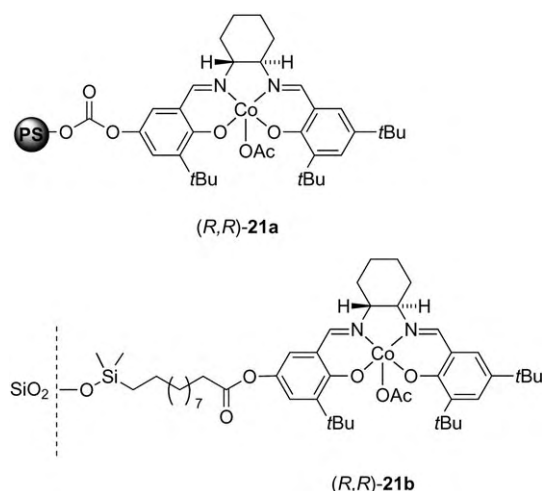
The adsorption of  $[(R,R)\text{-Meduphos}]\text{Rh}(\text{cod})\text{Cl}$  in the pores of Al-MCM-41 led to active and stable heterogeneous catalysts that could be recycled up to four times. However, only 92 % *ee* was obtained in the hydrogenation of dimethyl itaconate (**19**; 100 % conversion, TON > 4000, Scheme 22 c).<sup>[75]</sup>

$\{\text{Ru}(\text{Meduphos})\}$  occluded in a polydimethylsiloxane matrix catalyzes the hydrogenation of methyl 2-acetamidoacrylate in water with good enantioselectivity (heterogeneous 96.9 %, homogeneous 99 %), but with significantly reduced activity (TOF<sub>PDMS/water</sub> = 12.6 h<sup>−1</sup>; TOF<sub>homogeneous/MeOH</sub> = 320 h<sup>−1</sup>, Scheme 21 f) as a result of mass transfer limitations.<sup>[51]</sup>

### 2.3.3. Metal–Salen Complexes

#### 2.3.3.1. Covalently Anchored Salen Complexes

Salen is yet another privileged ligand in asymmetric catalysis and has been immobilized frequently, most often through covalent binding. Jacobsen and co-workers attached chiral  $[\text{Co}(\text{salen})]$  complexes through a carbonate linker<sup>[76]</sup> to polystyrene (**21a**, 160 μmol  $[\text{Co}(\text{salen})]$  per gram polymer) and through a bifunctional linker to silica gel<sup>[77]</sup> (**21b**, scheme 23). Very good results were obtained with these catalysts in the kinetic hydrolytic resolution of epoxides in up to five reaction cycles (Table 3).<sup>[78]</sup>



**Scheme 23.** Immobilized [Co(salen)] complexes.

**Table 3:** Kinetic resolution with immobilized [Co(salen)] complexes.

Entry	Catalyst (mol %)	R	Yield of <b>23</b> (Conversion) [%]	ee (S)- <b>23</b> [%]	ee (R)- <b>22</b> [%]
1	<b>21 a</b> (0.25)	CH <sub>2</sub> Cl	41 (51–52)	92–95 <sup>[a]</sup>	> 99 <sup>[a]</sup>
2	<b>21 a</b> (0.5)	CH <sub>2</sub> Br	94 <sup>[b]</sup>	96 <sup>[a]</sup>	–
3	<b>21 a</b> (0.4)	(CH <sub>2</sub> ) <sub>2</sub> OH	36 (40)	94 <sup>[a]</sup>	59 <sup>[a]</sup>
4	<b>21 b</b> (0.3)	Ph	(50)	96	90
5	<b>21 b</b> (0.4)	(CH <sub>2</sub> ) <sub>2</sub> OH	(34)	93	48
6	<b>21 b</b> (0.5) <sup>[c]</sup>	(CH <sub>2</sub> ) <sub>2</sub> OH	(36–39)	94	54–61
7	[Co( <b>24</b> )]PF <sub>6</sub> (0.5)	Ph	32	96	98
8	[Co( <b>25</b> )]PF <sub>6</sub> (0.5)	CH <sub>2</sub> Cl	43	98	99

[a] Result over 5 cycles. [b] Dynamic kinetic resolution of epibromohydrin. [c] Applied as a stationary phase in a continuous flow reactor.

The inflexibility and noncompressibility of the silica support renders **21b** the catalyst of choice for application as a stationary phase in a continuous flow reactor (Table 3, entry 6). Overall, better results were obtained with highly loaded silica gel. This result supports the assumption that the reaction proceeds by a cooperative bimetallic mechanism that profits from a high local concentration of catalyst (highly loaded silica gel) or a flexible support (polystyrene).

Kwon and Kim polymerized existing salen derivatives by a nucleophilic substitution or built up the salen moiety by imine formation through the reaction of suitable dialdehydes with chiral diaminocyclohexane in the polymerization step (**24** and **25**, Scheme 24).<sup>[79,80]</sup> Very good results were obtained in the cobalt-catalyzed hydrolytic kinetic resolution of epoxides with these catalysts (Table 3, entries 7 and 8). Remarkably, these copolymers can be

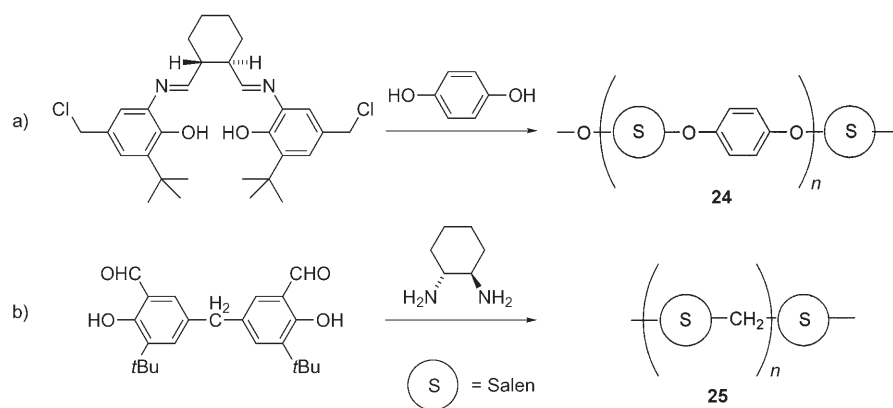
recycled and reused up to seven times without any loss of activity and selectivity, and do not need to be regenerated.

In addition, epoxides can be opened highly enantioselectively with phenols in the presence of catalyst **21a** (Scheme 25). This transformation was the key step in a parallel synthesis of a small, pharmaceutically interesting library of compounds.<sup>[81]</sup>

Immobilized [Mn(salen)] complexes have been utilized repeatedly in the epoxidation of alkenes, but recycling has often proved to be a problem because of the intrinsic instability of the complex under the reaction conditions.<sup>[78,82]</sup> However, Li and co-workers were able to immobilize [Mn(salen)] complexes **26** by binding them axially to phenoxy or phenylsulfone ligands on a highly cross-linked PS (Scheme 26). These catalysts were reused up to three times without any loss in activity or selectivity in the epoxidation of olefins.<sup>[83]</sup>

Seebach and co-workers used radical copolymerization of salen dendrimers **27** with styrene to give spherical beads of cross-linked polystyrene (400 μm diameter; swelling factor: 2.5 (CH<sub>2</sub>Cl<sub>2</sub>) and 4 (THF)).<sup>[84]</sup> The polymers generated by this method contain cavities around the active site within the polymer matrix that are likely to be chiral.<sup>[85]</sup> After conversion into the corresponding Mn and Cr complexes, good results were obtained in the asymmetric epoxidation of olefins (Scheme 27) and also in the hetero-Diels–Alder reaction of Danishefsky's diene with different aldehydes (50–70% ee). Interestingly, and in contrast to homogeneous Mn-salen catalysts, the catalyst prepared by copolymerization of monomer **28** could be stored and was stable to air. Thus, it could be reused up to 10 times without any loss of activity and selectivity in the asymmetric epoxidation of styrene (quantitative conversion after 30 min; 62% ee).

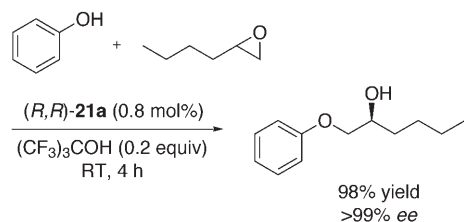
Garcia and co-workers compared salen ligands **29** covalently bound to different supports in the vanadium-catalyzed asymmetric cyanosilylation of aldehydes (Table 4).<sup>[86]</sup> For the



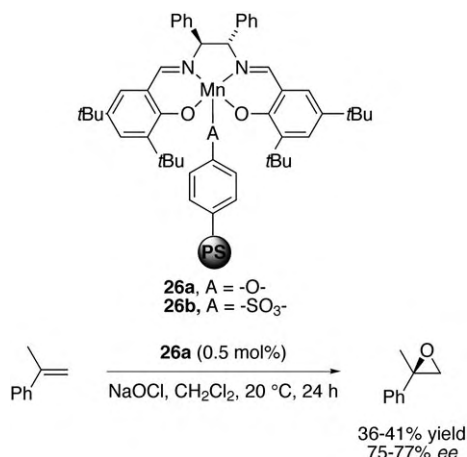
**Scheme 24.** Salen copolymers.

first time, the corresponding [VO(salen)] complexes were attached to the tip of single-walled nanotubes (SWNT,  $\varnothing$  = 1.4 nm, lengths of bundles = 5 μm). Compared to the results obtained under homogeneous conditions with SWNT-[VO-





**Scheme 25.** Asymmetric opening of an epoxide with phenol.



**Scheme 26.** Epoxidation of an unfunctionalized olefin.

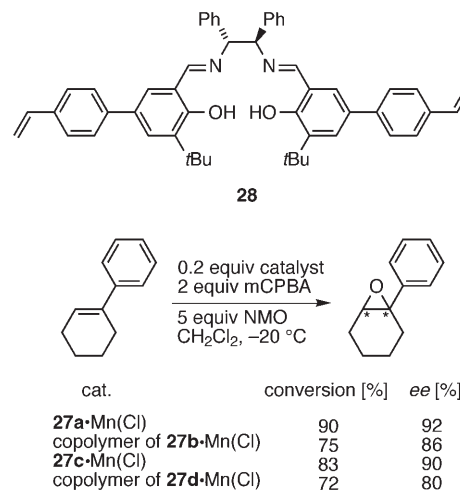
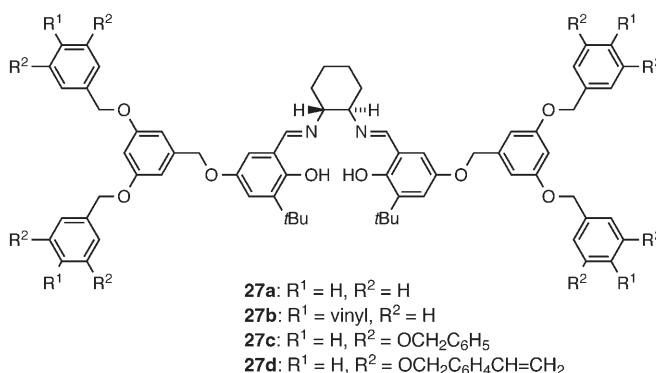
(salen)], similar TOFs but reduced enantioselectivities were obtained in the cyanosilylation of benzaldehyde, while silica gel-[VO(salen)] afforded similar enantioselectivities (Table 4).

### 2.3.3.2. Noncovalent Immobilization of Salen Complexes

Since the synthesis of metal–salen complexes is high yielding, this class of ligands is especially suited for immobilization by assembly within the pores of a mesoporous material such as zeolites.<sup>[87]</sup> However, the selectivities and reaction rates so far reported are reduced compared to those obtained with the corresponding homogeneous catalysts.

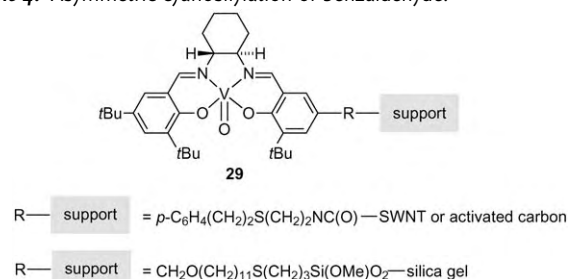
The physisorption of salen complexes on silica gel was also investigated. The impregnated heterogeneous catalysts were shown to have stability problems that were accompanied by a continuous fragmentation of the silica support as a result of severe abrasive forces in the stirred reactor.<sup>[88]</sup> The deterioration of the silica support not only increased significantly the time needed for separation of the catalyst but also led to increased leaching. Therefore, a recovery of the [Cr(salen)] catalyst by desorption followed by impregnation on new silica gel was favored.

Choi and Kim circumvented these kinds of problems by using a membrane reactor. They reported the kinetic resolution of epoxides with the [Co<sup>III</sup>(salen)] complex **33** immobilized in a membrane (Schemes 28 and 29).<sup>[89]</sup> The membrane consists of a ZSM-5-zeolite film on porous anodisc47. The chiral metal complex is impregnated on anodisc47. It is in contact with the aqueous phase while the



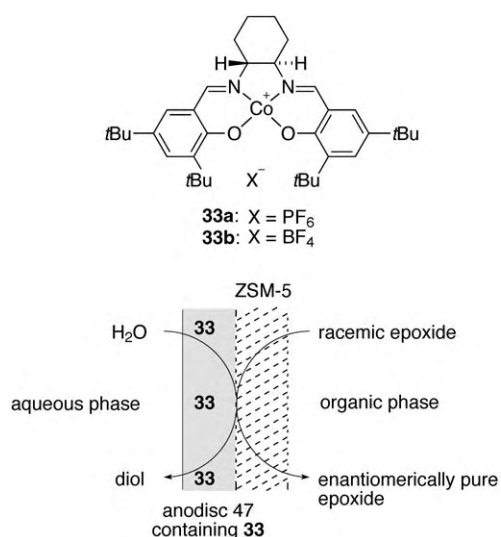
**Scheme 27.** Epoxidation of 1-phenylcyclohexene. mCPBA = *meta*-chloro-perbenzoic acid.

**Table 4:** Asymmetric cyanosilylation of benzaldehyde.

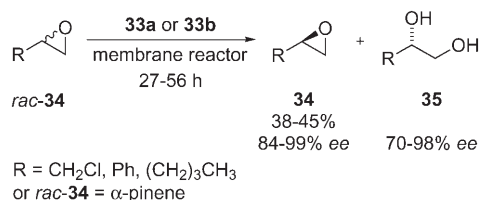


Entry	Catalyst	Conversion [%]	TOF [h <sup>-1</sup> ]	ee [%]
1	[VO(salen)], homogeneous	85	3.5	89
2	SWNT-[VO(salen)]	67	3.1	66
3	activated carbon-[VO(salen)]	81	3.75	48
4	silica gel-[VO(salen)]	78	2.7	85

ZSM-5-zeolite film is adjacent to the organic phase (CH<sub>2</sub>Cl<sub>2</sub>), in which the racemic epoxide is dissolved. No leaching is observed because complex **33** is insoluble in water and also too large to diffuse through the pores of the ZSM-5 film. The



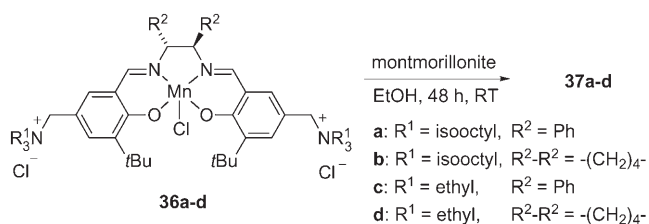
**Scheme 28.** Anodic 47/ZSM-5-membrane reactor for the kinetic resolution of epoxides.



**Scheme 29.** Kinetic resolution of epoxides in a membrane continuous flow reactor.

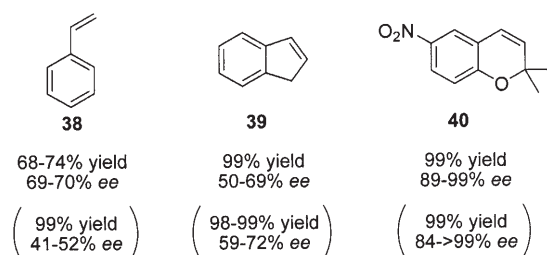
membrane is necessary to immobilize the catalyst and at the same time allows the separation of organic compounds with significantly different polarities by continuous extraction. In this case the hydrophilic diol, which diffuses through the membrane into the aqueous phase, is separated elegantly from the epoxide during the course of the reaction. Various terminal epoxides were converted with high yield and selectivity (Scheme 29). The membrane could be reused up to four times without loss of activity and selectivity in a continuous-type membrane reactor, in which the aqueous and the organic phase were circulated in a countercurrent flow. It can be expected that membrane reactors will be applied more frequently in asymmetric catalysis.

Kureshy et al. immobilized dicationic [Mn<sup>III</sup>(salen)] complexes by ion exchange in the interlayers of montmorillonite (Scheme 30).<sup>[90]</sup>



**Scheme 30.** Immobilization by ion exchange.

The heterogeneous catalyst gave reduced yields but improved enantioselectivities in the epoxidation of styrene compared to the results obtained under homogeneous conditions (Scheme 31). The improved enantioselectivity was



**Scheme 31.** Substrates for the asymmetric epoxidation with **37a-d** (results obtained with the homogeneous catalyst are given in brackets).

explained in terms of the unique spatial environment of the confined medium. Furthermore, the flexibility of the lamellar structure of the montmorillonite allows for the selective conversion of sterically more demanding substrates such as **39** and **40**, with results comparable to those obtained with the homogeneous catalyst.

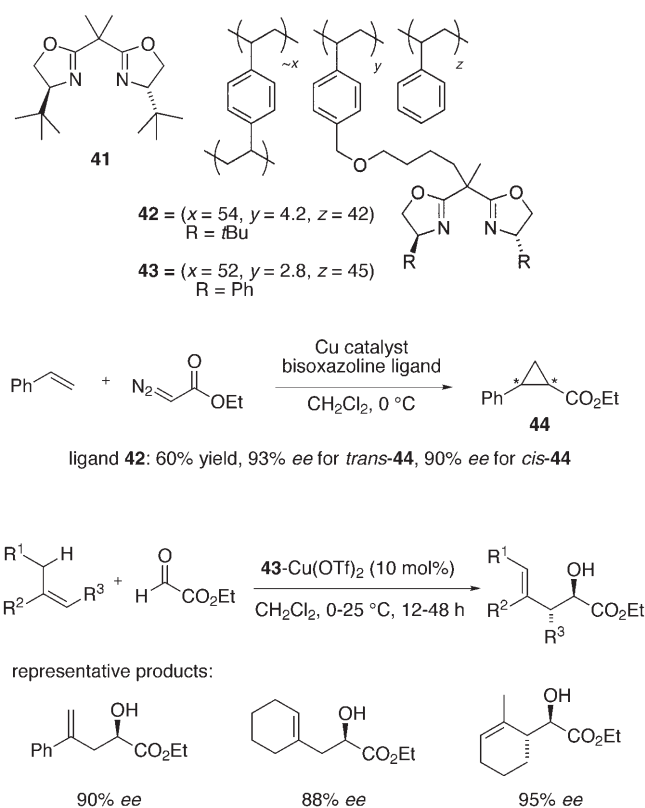
### 2.3.4. Metal-Bisoxazoline Complexes

Chiral bisoxazolines have proven to be excellent catalysts for a number of transition-metal-catalyzed processes.<sup>[5a]</sup> However, the often relatively high catalyst concentrations required (up to 10 mol%) demand for an efficient recycling strategy.<sup>[91]</sup>

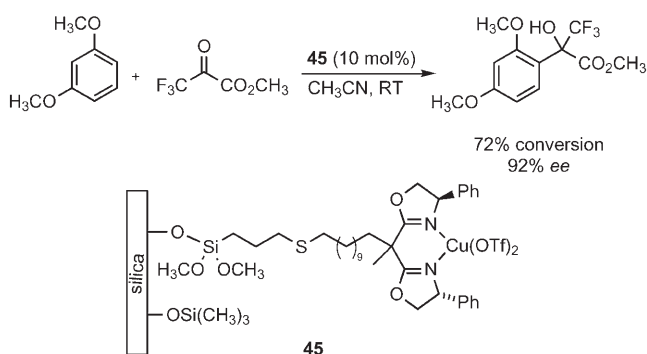
#### 2.3.4.1. Covalently Immobilized Bisoxazoline Complexes

Bisoxazolines have often been immobilized by copolymerization with styrene.<sup>[92]</sup> Salvadori and co-workers obtained > 90% ee (in up to 5 cycles) in the copper-catalyzed cyclopropanation of styrene with ethyl diazoacetate by using the highly cross-linked (ca. 54%), heterogeneous, chiral ligand **42** (Scheme 32).<sup>[92e]</sup> Although the C<sub>2</sub> symmetry of the ligand is lost upon attachment to the support, the results obtained are comparable to those obtained with the homogeneous catalyst. Similarly good results were obtained with **43** in the copper-catalyzed glyoxylate-ene reaction (Scheme 32).<sup>[93]</sup>

Bisoxazolines covalently anchored to silicates have been applied among others in the asymmetric Diels-Alder reaction<sup>[29,94]</sup> and cyclopropanation.<sup>[95]</sup> Corma et al. immobilized bisoxazolines on silica gel (Scheme 33) and MCM-41 through a long flexible linker to minimize spatial restrictions by the support. Application of catalyst **45**, which exhibits a high degree of conformational freedom, in a Friedel-Crafts hydroxyalkylation resulted in up to 92% ee, compared to 72% ee under analogous homogeneous conditions.<sup>[96]</sup>



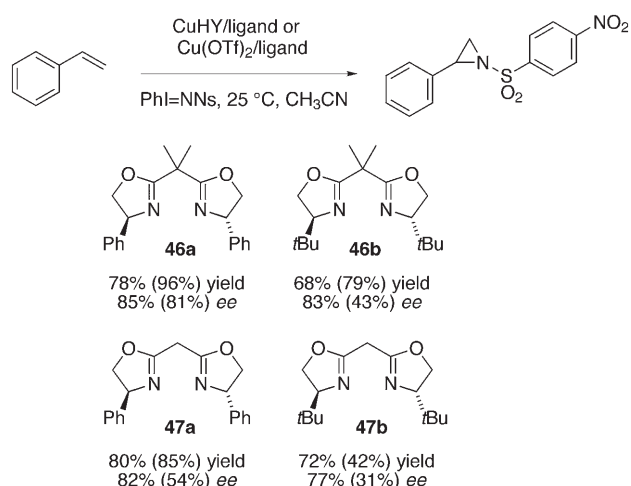
**Scheme 32.** Copolymerized bisoxazolines in the cyclopropanation and glyoxylate-ene reactions.



**Scheme 33.** Enantioselective Friedel-Crafts alkylation with heterogeneous catalyst **45**.

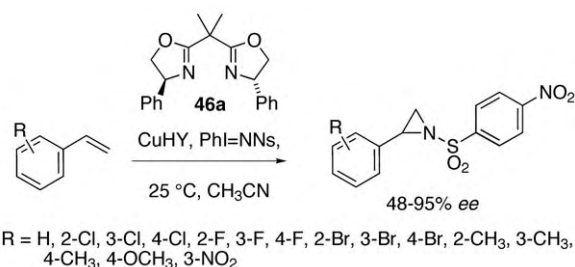
### 2.3.4.2. Noncovalently Immobilized Bisoxazoline Complexes

The immobilization of a chiral metal-ligand complex by ion exchange is an attractive strategy, since no structural modification of the chiral ligand is required.<sup>[97]</sup> This important methodology was intensively investigated by using chiral bisoxazolines and has been applied successfully to many asymmetric catalysts. Hutchings and co-workers immobilized chiral copper(bisoxazoline) complexes on zeolite Y through the electrostatic interactions of the copper cations with the anionic support. These catalysts proved to give comparably high or improved selectivities as the homogeneous catalysts in the copper-catalyzed aziridination of styrene (Schemes 34 and



**Scheme 34.** Effect of the zeolite on the ee value (results obtained with the corresponding homogeneous catalysts are given in brackets).

35),<sup>[39b,98]</sup> the Diels-Alder reaction,<sup>[99]</sup> as well as the carbonyl- and imino-ene reactions.<sup>[42]</sup> EPR spectroscopic studies indicate that the copper(bisoxazoline) complexes are located in



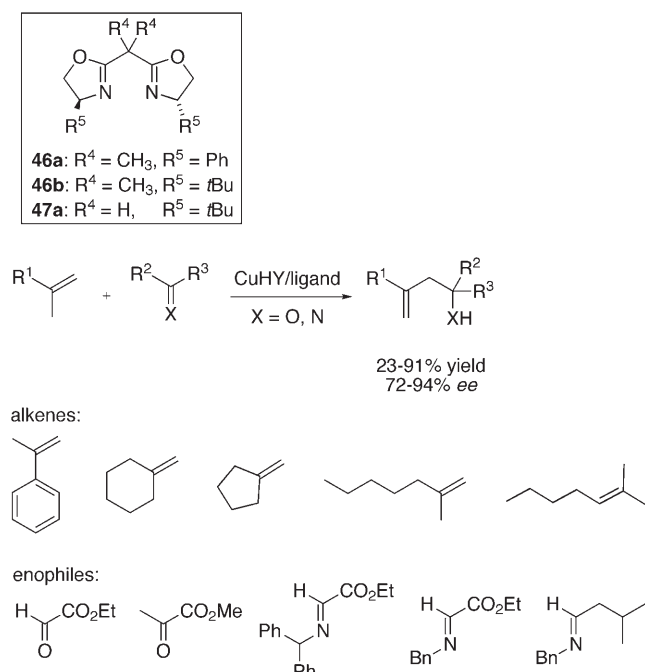
**Scheme 35.** Enantioselective aziridination of styrene derivatives with immobilized ligand **46a**.

the pores of the zeolite. Depending on the reaction, the improved enantiodifferentiation has been attributed to either the enhanced confinement of the substrate<sup>[98c]</sup> or the catalyst.<sup>[100]</sup>

Similar or higher enantioselectivities (72–99%), but with reduced yields (Scheme 36), could be obtained in the carbonyl- and imino-ene reaction with the heterogeneous catalyst compared to the homogeneously catalyzed reaction. In contrast to the homogeneously catalyzed reaction, the imino-ene reaction surprisingly did not require imine substrates with electron-deficient substituents under heterogeneous conditions.<sup>[101]</sup> Also, the heterogeneous catalyst could be recovered and reused up to four times without any loss of activity and selectivity.

### 2.4. Conclusion

For a long time, the immobilization of homogeneous chiral catalysts had been accompanied by a loss in activity and selectivity. Today, by choosing a suitable support, especially



**Scheme 36.** Carbonyl- and imino-ene reactions.

mesoporous materials, a heterogeneous catalyst can be prepared that gives similar or even enhanced selectivities and activities. In other words, the role of the support has changed from an inevitable appendage to a well-defined material that can be used to beneficially influence the outcome of a catalyzed reaction. This has been demonstrated impressively by Thomas and co-workers in the enantioselective hydrogenation of phenylcinnamic acid (Section 2.1.3).<sup>[29]</sup> However, more mechanistic investigations are needed for a better understanding of the interactions between the chiral complex, substrate, and support. Nevertheless, industrial applications, improved overall properties, as well as a rational design of immobilized homogeneous catalysts are becoming realistic.

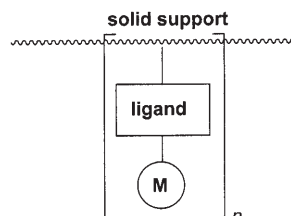
Is a covalent or a noncovalent immobilization of the catalyst preferential? For a long time, covalent immobilization of chiral complexes was unrivaled because of the stability and recyclability of the resulting catalysts. In contrast, catalysts prepared by the often synthetically more facile noncovalent immobilization strategy most often suffered from severe stability problems. However, recent results with cationic complexes immobilized by surface-supported counteranions (Section 2.2.1)<sup>[36]</sup> or ion exchange (Section 2.3.2.1)<sup>[74]</sup> have demonstrated that these noncovalently immobilized catalysts can show good stabilities, can be recycled several times, and in addition result in good selectivities and activities.

### 3. Chiral Metal–Organic Catalysts

In the last five years another exciting class of immobilized catalysts has emerged. In the classical immobilization approach described in the previous sections, the chiral

ligand is anchored covalently or noncovalently to the support. This new immobilization technique is based on the skillful application of multitopic ligands and metals and allows for a simple and efficient assembly of solid metal–organic structures by complexation without the need for an additional

supported homogeneous catalysts:



metal–organic catalysts:

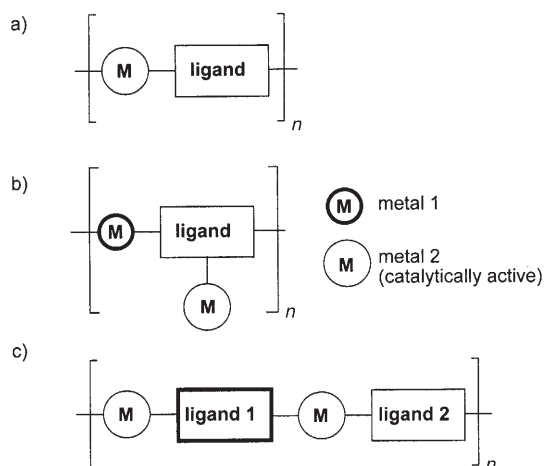


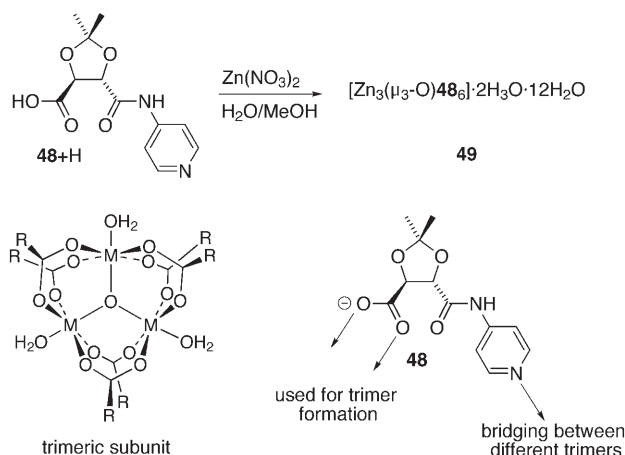
**Figure 2.** Comparison of a supported homogeneous catalyst and metal–organic polymers.

support (Figure 2). This self-assembly can give highly porous, in some cases very regular, coordination polymers that mainly consist of the metal and the chiral ligand.<sup>[102]</sup> Numerous reports show that inorganic–organic networks are suitable achiral catalysts.<sup>[102b,103,104]</sup> Very recently this fascinating class of immobilized catalysts has been applied in enantioselective catalysis.<sup>[102c]</sup> Since this area showed high potential and developed rapidly from the beginning, it will be discussed in greater detail in this Review. The catalyst systems reported so far can be subdivided into three categories (Figure 2a–c).

In the most simple scenario the metal–organic polymer consists of one metal ion and one ligand, both possessing at least two coordination sites (Figure 2, type a). Polymeric chains, layers, or networks are formed depending on the number of these coordination sites. In 2000, Kim and co-workers were the first to report the application of such a metal–organic material in enantioselective catalysis.<sup>[105]</sup> The chiral carboxylic acid **48** + H functions as the organic ligand and can easily be prepared from tartaric acid. The chiral ligand reacts with  $\text{Zn}^{2+}$  ions to give the metal–organic polymer **49**. It is characterized by trimeric subunits, in which three zinc ions are connected by six carboxylate groups of the



building block **48** and one additional oxygen atom (Scheme 37). The formation of a three-dimensional network is realized by linking these subunits through the coordination



**Scheme 37.** Synthesis of the metal–organic polymer **49** and analysis of its structural elements.

of the pyridine nitrogen atoms to the zinc ions of neighboring trimers.

The resulting porous polymer **49** (Figure 3) has been tested in the transesterification of ester **50** with alcohols and

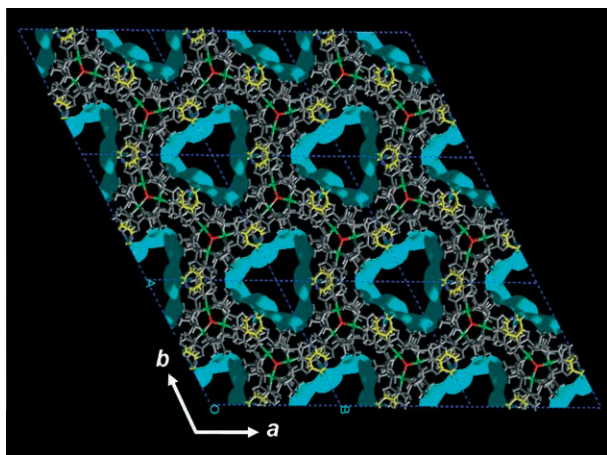
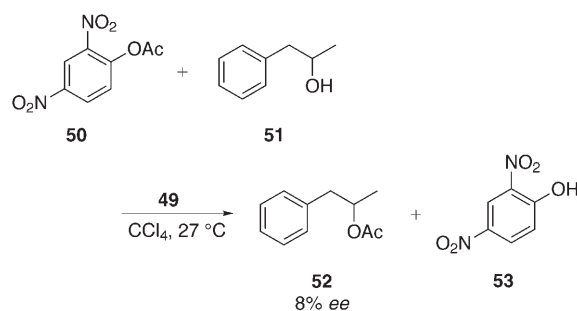


**Figure 3.** View along the *c*-axis of **49**. Clearly visible are the large chiral channels, with the accessible surface highlighted. (Reproduced from Ref. [105].)

gave enantioselectivities up to 8% *ee* (Scheme 38). Despite this low level of enantioinduction, this report was the starting point for the rapidly growing field of asymmetric metal–organic catalysts.

The research groups of Sasai and Ding later developed chiral, heterogeneous catalysts of type a that gave good to excellent enantioselectivities in the carbonyl–ene reaction (Scheme 39).<sup>[106]</sup> Both research groups used differently connected dimeric binol units as ligands and titanium as the



**Scheme 38.** Enantioselective transesterification with catalyst **49**.

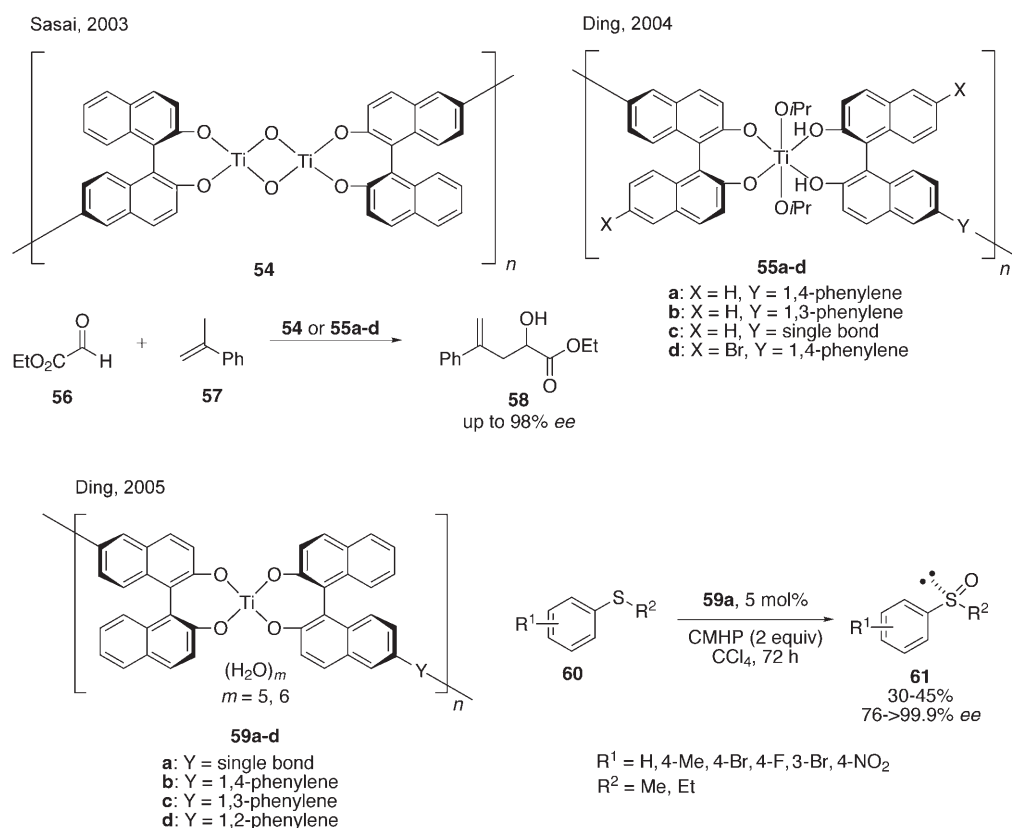
catalytically active metal (**54** and **55**). Sasai and co-workers were able to carry out the reaction of aldehyde **56** with  $\alpha$ -methylstyrene in air and reuse the coordination polymer **54**.<sup>[106a]</sup> Furthermore, the catalyst could be recycled and reused up to five times without affecting the enantioselectivity. Modification of the metal–organic networks **59** by addition of water resulted in catalysts that effected the asymmetric oxidation of aryl sulfides **60** with up to 99.9% *ee* (Scheme 39).<sup>[106c]</sup>

Wang and Ding used this self-assembly strategy to immobilize monodentate phosphoramidites (Scheme 40).<sup>[102d]</sup> The chiral polymeric catalyst **62** was shown to catalyze the asymmetric hydrogenation of olefins with higher enantioselectivity (Scheme 40) than the corresponding homogeneous monophos/Rh catalyst ( $R^1 = H$ ,  $R^2 = Ph$ ; homogeneous: 89% *ee*).

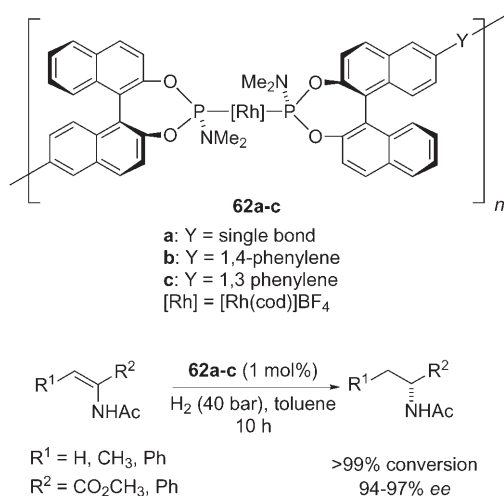
Ding and co-workers treated differently linked binol ligands **63** (Scheme 41) with  $La(OiPr)_3$  to give heterogeneous analogues of the Shibasaki catalyst.<sup>[107]</sup> These catalysts epoxidized numerous chalcones **64** with excellent yields and enantioselectivities in the presence of molecular sieves and triphenylphosphine oxide as additives (Scheme 42). Interestingly, the structure of the linker has a strong influence on the performance of the catalyst. Decreasing the length of the linker which reduces the angle between the ligands is detrimental to the enantioselectivity. High activities and enantioselectivities were obtained (92–95% *ee* for  $R^1 = R^2 = Ph$ ) with the planar tridentate ligand **63d** or the three-dimensional tetratendate ligand **63e**.

Lin et al. immobilized functionalized Ru–binap derivatives by self-assembly with one equivalent of soluble Zr( $OrBu$ )<sub>4</sub> to give chiral, porous zirconium phosphonates **66** (Figure 2, type b) for asymmetric hydrogenation (Scheme 43).<sup>[65,108]</sup> The two metals incorporated fulfill different functions. While zirconium is responsible for the immobilization, ruthenium is the catalytically active metal in the hydrogenation. Scanning tunneling microscope (STM) images of the catalyst have shown the catalysts to be amorphous and highly porous, with a large pore distribution. The BET surface of catalyst **66** was found to be 400 m<sup>2</sup> g<sup>−1</sup> and the microscopic surface 81 m<sup>2</sup> g<sup>−1</sup>. The pore volume of the material was 98 cm<sup>3</sup> g<sup>−1</sup>.

The performance of this self-supported catalyst **68** is convincing: Higher selectivities in the hydrogenation of aromatic ketones were obtained than with the corresponding



**Scheme 39.** Chiral metal-organic polymers for the enantioselective ene reaction or oxidation of sulfides (CMHP: cumene hydroperoxide).

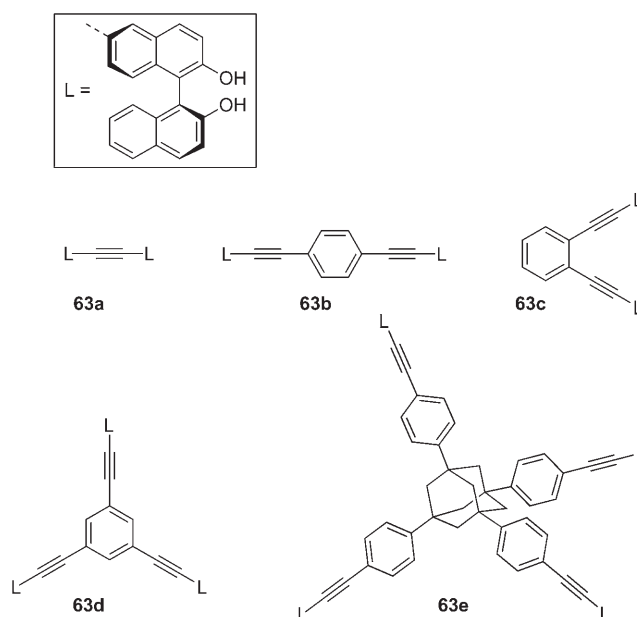


**Scheme 40.** Asymmetric hydrogenation with an immobilized, monodentate phosphoramidate ligand.

homogeneous ruthenium complex.<sup>[109]</sup> Moreover, as little as 0.005 mol % of the catalyst was sufficient for full conversion and high ee values of up to 98.6% ee (reaction time 40 h, TOF = 500 h<sup>-1</sup>). The heterogeneous catalyst **66** could be recycled and reused up to eight times without loss of enantioselectivity.

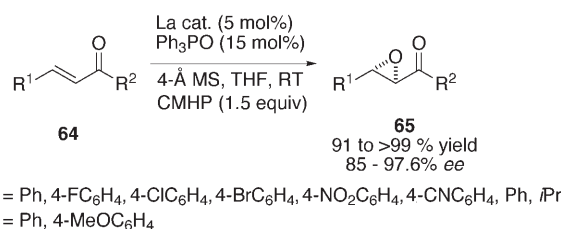
Recently, Lin and co-workers introduced another catalytically active, porous metal-organic network.<sup>[110]</sup> Treatment of

ligand **67** with CdCl<sub>2</sub> gives the crystalline solid **68**. X-ray analysis of **68** reveals that the cadmium(II) ions are surrounded octahedrally and are bridged by two chloride atoms, thus resulting in one-dimensional zigzag chains of the formula [Cd(μ-Cl)<sub>2</sub>]<sub>n</sub>. The metal center is also coordinated by two pyridine nitrogen atoms, thus leading to the formation of a three-dimensional network with large chiral channels (ca. 1.6 × 1.8 nm). While some hydroxy groups are shielded, two binol hydroxy groups are placed at regular distances in the channel. Reaction of the free binols with Ti-(O*i*Pr)<sub>4</sub> gives the active catalyst. The Lewis-acidic titanium complex

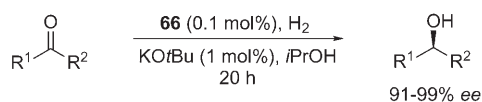
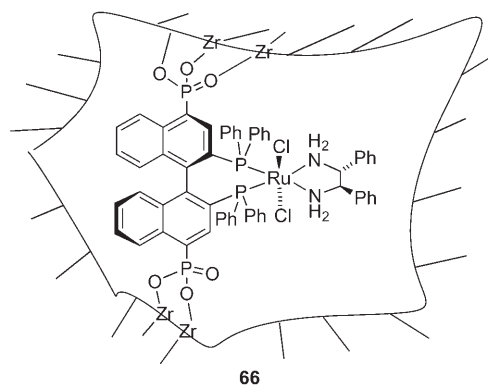


**Scheme 41.** One-, two-, and three-dimensional multidentate binol ligands.

catalyzes the addition of diethylzinc to aromatic aldehydes with comparable conversions and enantioselectivities as the homogeneous binol/Ti(O*i*Pr)<sub>4</sub> catalyst (Scheme 44). By using highly sterically demanding, dendritic aldehydes (up to 2 nm)

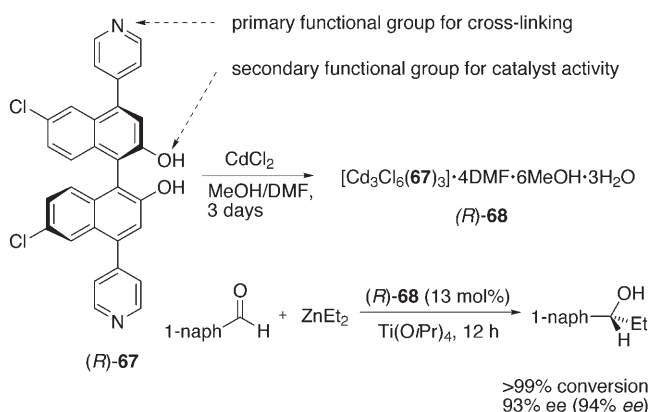


**Scheme 42.** Epoxidation of chalcones **64** catalyzed by La-**63**.



$R^1 = \text{Ph}, 1\text{-naphthyl}, 2\text{-naphthyl}, 4\text{-tBuC}_6\text{H}_4, 4\text{-MeO-C}_6\text{H}_4, 4\text{-Cl-C}_6\text{H}_4, 4\text{-Me-C}_6\text{H}_4$   
 $R^2 = \text{Me}, \text{Et}, \text{cyclopropyl}$

**Scheme 43.** Self-supported ruthenium-binap catalyst in enantioselective hydrogenation.



**Scheme 44.** Titanium(IV)-catalyzed  $\text{ZnEt}_2$  addition to aromatic aldehydes (*ee* values obtained with the corresponding homogeneous conditions are given in brackets).

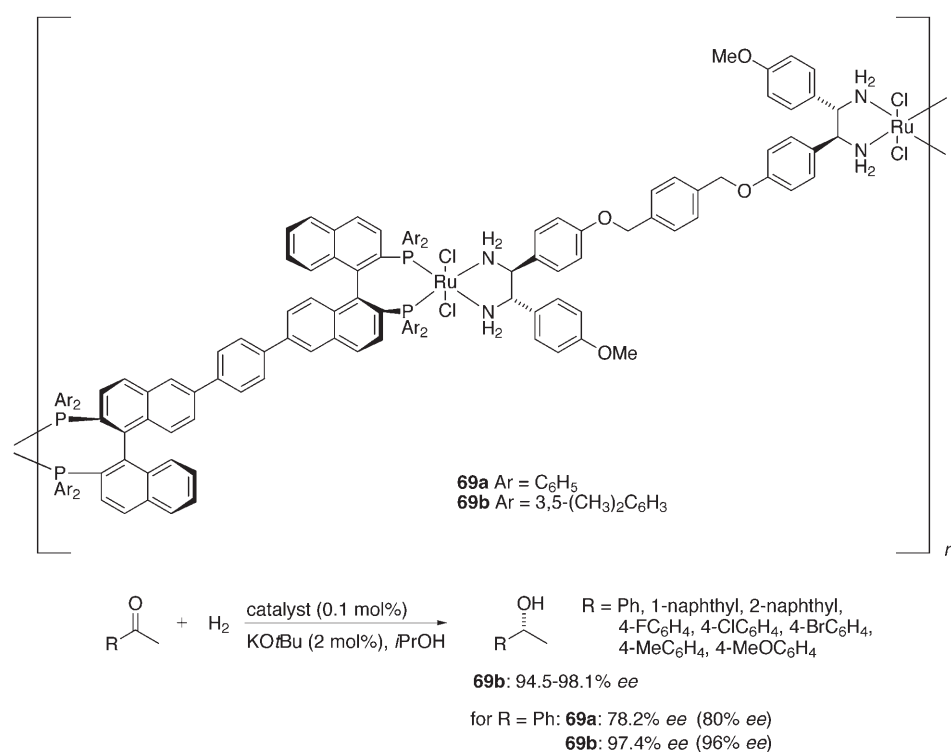
as starting materials, it was shown that the catalytically active sites are located in the channels. Whereas good conversions (>95%) were obtained for these bulky substrates under homogeneous conditions, the conversion decreased to zero when the heterogeneous catalyst was used.

The third type of a metal–organic polymer (Figure 2, type c) is formed by the alternating complexation of one metal *M* with two different ligands *L*<sup>1</sup> and *L*<sup>2</sup>, as recently exemplified by Ding and co-workers with the immobilization of Noyori's catalyst.<sup>[111]</sup> The synthesis of the metal–organic network proved to be facile: The reaction of binap and dpen dimers with the ruthenium complex  $[(\text{C}_6\text{H}_6)\text{RuCl}_2]_2$  selectively provided the desired heterocomplexes **69** (Scheme 45, Figure 4). High selectivities, comparable to those obtained under homogeneous conditions, were obtained with this catalyst in the hydrogenation of acetophenone (Scheme 45). Moreover, the heterogeneous catalyst **69b** could be recycled by simple filtration and was reused seven times without significant loss of enantioselectivity (95% *ee* in the seventh cycle). Furthermore, the catalyst's concentration could be reduced to 0.01 mol% in the hydrogenation of acetophenone (95% *ee*, 500 h<sup>−1</sup>). Several experiments convincingly demonstrated that catalyst **69b** is insoluble in isopropanol. No ruthenium was detected in solution by inductively coupled plasma (ICP) spectroscopy, the supernatant was shown not to be catalytically active, and the product obtained after filtration contained less than 0.1 ppm ruthenium. This type of catalyst prepared from two different ligands and one metal seems to be especially suited for the efficient synthesis of heterogeneous catalyst libraries.

The attractive properties of these metal–organic catalysts are their ready separation from the product and their reusability. Moreover, in contrast to homogeneous catalysts immobilized on an external support, they have the advantage of possessing an especially high density of catalytically active units. The enantioselectivities obtained are often comparable or better than those obtained with the corresponding homogeneous complexes. In some cases, the structure of these systems is highly ordered on the microscopic level. Therefore, in contrast to most other heterogeneous catalysts, their structure can be solved and the information used for a better mechanistic understanding. It is expected that further research will allow for a better predictability of the structures of the catalysts which will consequently lead to this research area becoming increasingly attractive.

#### 4. Chiral Modifiers

Catalysis at chiral surfaces is a fascinating research goal. In a few cases, enantiospecific adsorption<sup>[113]</sup> has been reported on chiral metal surfaces.<sup>[112]</sup> This effect was utilized in an enantioselective electrooxidation of D- and L-glucose;<sup>[114]</sup> however, these systems are no way near a synthetic application thus far. In a completely different and very successful approach, an achiral heterogeneous catalyst and small enantiomerically pure, organic molecules—chiral modifiers—work together as catalysts. This kind of “tandem catalysis” is one of the most fascinating areas of asymmetric catalysis, which lies at the boundary between homogeneous and heterogeneous catalysis.<sup>[115]</sup> Organic compounds such as cinchona alkaloids, chiral acids, and glucose were already utilized as modifiers in the heterogeneous hydrogenation of C=C, C=N, and C=O bonds in the middle of the last century,



**Scheme 45.** Enantioselective hydrogenation of aromatic ketones (results of the corresponding homogeneous catalyst are given in brackets).

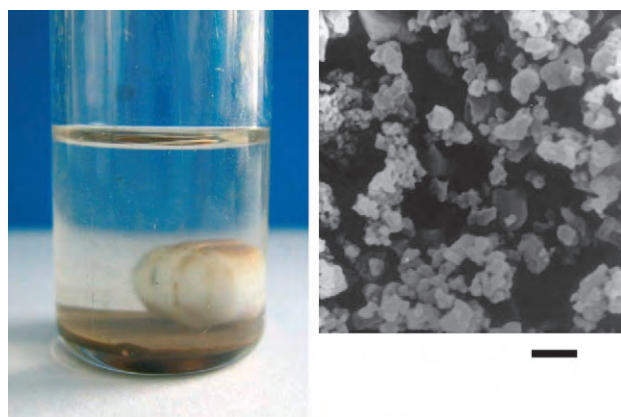
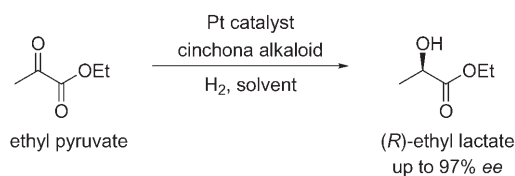


**Figure 4.** a) Self-supported ruthenium(II) catalyst **69b** (pale brown solid) in 2-propanol. b) SEM image of the self-supported ruthenium(II) catalyst **69b**. The scale bar corresponds to 2 μm. (Reproduced from Ref. [111].)

although the observed stereoselectivities were quite low. Investigation of the mechanisms remains limited because spectroscopic methods are difficult to apply and small variations in the reaction conditions often have a dramatic effect on the outcome.

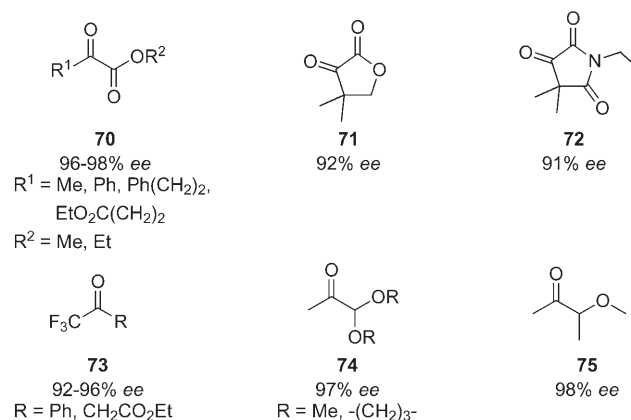
#### 4.1. The Platinum–Cinchona System<sup>[115,116]</sup>

In 1979 Orito et al. reported that methyl pyruvate can be enantioselectively hydrogenated to (*R*)-methyl lactate with a



**Scheme 46.** Enantioselective hydrogenation of pyruvate (97% ee); 5% Pt/Al<sub>2</sub>O<sub>3</sub>, *O*-methyl dihydroquinine (*O*-Methyl-**83**), AcOH, 10 bar H<sub>2</sub>, 25 °C, ultrasound.<sup>[118]</sup>

Heterogeneous platinum catalysts were found to give the best results in the hydrogenation of ketones, with different supports such as Al<sub>2</sub>O<sub>3</sub>, SiO<sub>2</sub>, TiO<sub>2</sub>, and zeolites being equally

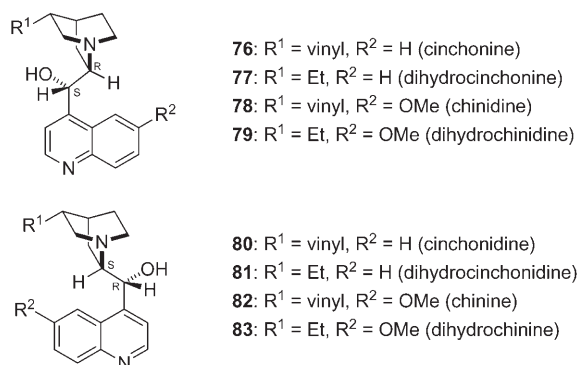


**Scheme 47.** Suitable substrates for ketone hydrogenation with platinum/cinchona alkaloids.



well suited. Platinum colloids have also proven to be successful.<sup>[125]</sup> The size of the platinum particles and their morphology plays an important role in obtaining optimum results; a flat shape of these particles is particularly favorable.<sup>[126]</sup>

The cinchona alkaloids cinchonine (**76**), chinidine (**78**), cinchonidine (**80**), and chinine (**82**; Scheme 48), isolated from

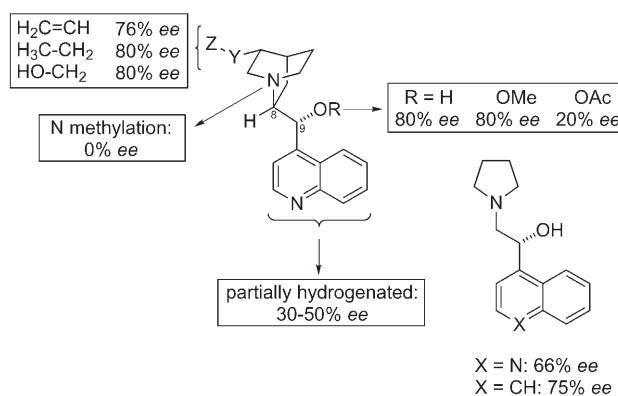


**Scheme 48.** Natural cinchona alkaloids and simple derivatives.

the bark of different cinchona trees, are inexpensive and available in high quantities. The corresponding dihydro derivatives **77**, **79**, **81**, and **83** have also been applied frequently with great success. Interestingly, the cinchona alkaloids promote the reaction rate of the ketone hydrogenation of pyruvates often to such an extent (10 to 100 times) that high substrate/modifier ratios of typically 300:1 to > 1000:1<sup>[119d]</sup> can be used.<sup>[127]</sup> The chiral auxiliary does not cover all the active sites of the catalyst during catalysis but rather activates the substrate for hydrogenation. Good results have been obtained when a ratio of 5 to 12 surface platinum atoms per modifier molecule is used, whereas much higher or lower loadings lead to significantly lower selectivities.<sup>[128]</sup>

The choice of solvent also has a great impact on the enantioselectivity of the hydrogenation. The best results were obtained with cinchonidine in acetic acid, but alcohols and nonpolar solvents such as toluene can also be used.<sup>[115]</sup>

What are the reasons for the surprisingly high enantioselectivities and which structural elements of the cinchona alkaloids are essential?<sup>[129]</sup> Variations of the structure of cinchonidine (**80**) and the resulting influence on the selectivity in the hydrogenation of ethyl pyruvate gives an important insight into the structure–activity relationship. (Scheme 49). While the hydrogenation of the vinyl moiety or the methylation of the alcohol function does not have a great influence, a partial hydrogenation of the quinoline system leads to a decrease and the N-alkylation to a total loss of enantioinduction. Besides the cinchona alkaloid derivatives,<sup>[131]</sup> epicinchona alkaloids,<sup>[132]</sup> chiral amino alcohols,<sup>[133]</sup> and amines,<sup>[134]</sup> as well as amino acids and amino acid derivatives have been employed.<sup>[135]</sup> Nevertheless, the selectivity and activity obtained with the natural cinchona alkaloids is still unrivaled. In conclusion, a successful chiral modifier has to have an expanded aromatic ring system, a basic N atom, and a properly located asymmetric center.<sup>[136]</sup> Three different



**Scheme 49.** Influence of the structure of the modifier on the enantioselectivity in the hydrogenation of ethyl pyruvate.<sup>[129,130]</sup>

models have been proposed for the mechanism of the platinum-catalyzed hydrogenation of pyruvates with cinchonidine (**80**): the adsorption model, the shielding model, and the zwitterion model (Figure 5).<sup>[137]</sup>

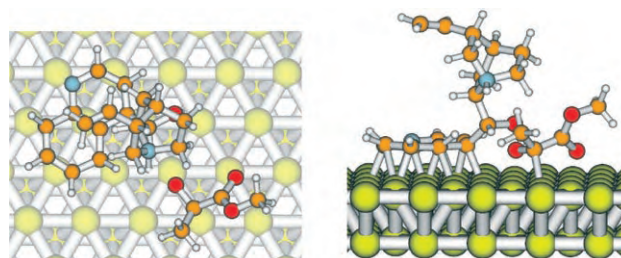


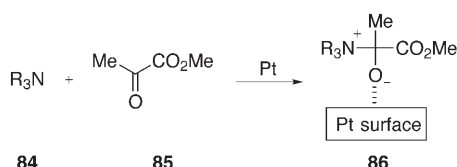
**Figure 5.** Adsorption model of the interaction between the platinum-adsorbed cinchonidine and methyl pyruvate on the basis of DFT calculations. (Reproduced from Ref. [138].)

Experiments and theoretical calculations suggest that the quinoline moiety of the cinchona alkaloid adsorbs on the metal surface. On the basis of the adsorption model, the stereoselectivity is attributed to the different stability of the diastereomeric 1:1 complexes formed between the surface-bound cinchonidine (**80**) and the pyruvate adsorbed through either of its two enantiotopic  $\pi$  faces. In protic solvents such as acetic acid, a protonation of the cinchonidine N atom occurs and a NH $\cdots$ O hydrogen bond with the ketone is formed. The formation of a N $\cdots$ HO hydrogen bond between the non-protonated N atom and a “partially” hydrogenated pyruvate was also proposed in aprotic solvents.<sup>[138]</sup> Such hydrogen bonding together with steric repulsion are responsible for the formation of a preferred conformation of the starting material on the surface of the catalyst. Consequently, hydrogenation takes place predominantly from one of the two enantiotopic faces.

Less popular is the shielding model, which proposes a complexation of the substrate and the modifier in solution. This complex is proposed to be selectively hydrogenated on the metal surface. The selectivity is attributed to the bulky aromatic substituents of the modifier shielding the opposite

face of the substrate.<sup>[139]</sup> However, some experimental evidence, such as the observed saturation effect that also occurs at low concentrations, contradict this model.<sup>[140]</sup>

Recently, more attention has been paid to the zwitterion model,<sup>[141]</sup> which has also been supported by theoretical calculations.<sup>[142]</sup> According to this model, the cinchonidine N atom of the cinchonidine attacks the ketone moiety of the pyruvate as a nucleophile to give the zwitterion **86** on the platinum surface (Scheme 50). The modifier (NR<sub>3</sub>) could then be substituted by platinum with subsequent hydrogenolysis of the Pt–C bond.

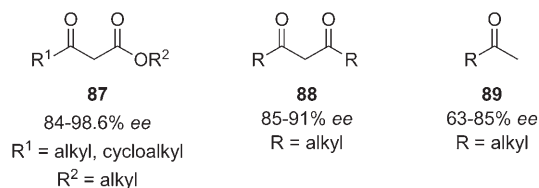


**Scheme 50.** Formation of zwitterionic adduct **86**.

It is still too early to come to a final decision in favor of one of these models. It is important to note that depending on the substrate and the reaction conditions employed, more than one mechanism could be involved. Changing the solvent from acetic acid to toluene in the hydrogenation of ethyl pyruvate over  $\beta$ -isocinchonine-modified Pt/Al<sub>2</sub>O<sub>3</sub> led to a reversal of the enantioselectivity, thus indicating a switch from one reaction mechanism to another.<sup>[132c]</sup>

#### 4.2. The Nickel Tartaric Acid/NaBr System

Tartaric acid modified nickel catalysts<sup>[143]</sup> are important catalysts, especially for the enantioselective hydrogenation of  $\beta$ -functionalized ketones **87**,<sup>[144]</sup>  $\beta$ -diketones **88**,<sup>[145]</sup> and sterically demanding methyl ketones **89**<sup>[146]</sup> (Scheme 51). The



**Scheme 51.** Substrates for ketone hydrogenation with modified nickel catalysts.

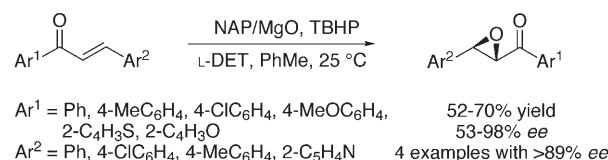
practicability of this catalyst was demonstrated by the industrial synthesis of tetrahydrolipstatine/orlistat (up to 92% *ee*, 100 kg), a potent inhibitor of pancreatic lipase.<sup>[147]</sup> Preferentially, freshly prepared Raney nickel is treated with tartaric acid, the modifier of choice, to give the active catalyst. To obtain high selectivities NaBr needs to be present as a co-catalyst. Once again, the mode of action of this catalysis is not well understood.<sup>[148]</sup> The nickel surface consists of highly ordered, crystalline and additional amorphous areas. Only the ordered, crystalline parts can successfully be modified by

tartaric acid and result in high enantioselectivities. The amorphous areas cannot be modified efficiently with the chiral modifier and therefore produce racemic product. Hence, it is thought that the co-catalyst NaBr, which is essential for the high selectivity, binds to the amorphous sections of the nickel surface thereby reducing their catalytic activity. In addition, tartaric acid is thought to be adsorbed on the nickel surface in the form of nickel sodium tartrate. The tartrate influences not only the preferred conformation of the substrate through hydrogen bonding and steric interactions but also by the way it approaches the heterogeneous catalyst.<sup>[115,143,149]</sup>

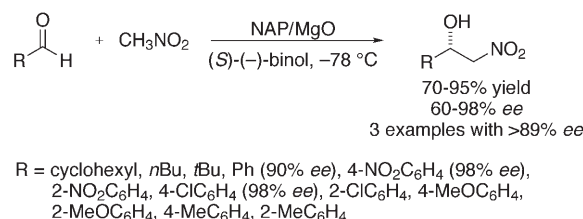
#### 4.3. Other Catalyst-Modifier Systems

The application of chiral modifiers is not limited to transition-metal catalysts. New catalyst-modifier systems have been developed successfully by Choudary et al. for numerous asymmetric reactions (Scheme 52).<sup>[150]</sup> They

##### a) Asymmetric epoxidation



##### b) Asymmetric Henry reaction



**Scheme 52.** NAP/MgO-catalyzed asymmetric reactions (DET: diethyl tartrate, TBHP: *tert*-butylhydroperoxide).

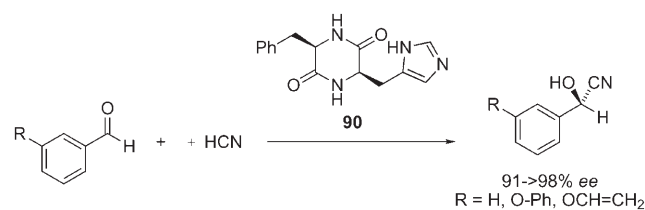
employed NAP/magnesium oxide (nanoactive MgO plus: magnesium oxide with 590 m<sup>2</sup> mg<sup>-1</sup> prepared by an aerogel process) as the heterogeneous catalyst, modified by small amounts of a bidentate ligand. L-Diethyl tartrate proved to be a good modifier in the asymmetric epoxidation of chalcone derivatives and gave good yields and enantioselectivities even after five recycles (Scheme 52a). The Henry reaction of aldehydes can be catalyzed with up to 98% *ee* by using binol as the modifier (Scheme 52b). The best results in the asymmetric Michael addition of chalcone derivatives were obtained using the basic (*R,R*)-1,2-diaminocyclohexane as a modifier.<sup>[150b]</sup> The authors attribute the stereoinduction of these catalyst systems to a hydrogen bonding of the modifier with a hydroxy group at the surface of the MgO and with the substrate. However, additional investigations are required to gain a better understanding of the mechanism.

#### 4.4. Conclusion

The examples shown above illustrate clearly that the cooperation between an achiral heterogeneous catalyst and a chiral modifier has enormous potential for asymmetric catalysis. It can be expected that the field of chiral modifiers (organocatalysts!) will benefit from the rapidly developing field of organocatalysis.<sup>[151]</sup> New mechanistic insights into the existing systems will hopefully lead to the rational design of these catalyst systems in the future.

### 5. Di- and Polypeptides as Chiral Macromolecular Catalysts

One of the first attempts to prepare asymmetric heterogeneous catalysts was by the treatment of chiral biopolymers such as silk fibroin with transition metals.<sup>[152]</sup> Cyclic dipeptides are suitable organocatalysts for the hydrocyanation of aromatic aldehydes.<sup>[153]</sup> High enantiomeric excess values of over 90 % were obtained using electron-rich aromatic aldehydes as substrates, especially with diketopiperazine **90** (Scheme 53).<sup>[153]</sup> These catalysts are readily synthesized



**Scheme 53.** Enantioselective hydrocyanation of aromatic aldehydes with cyclic dipeptides as catalysts.

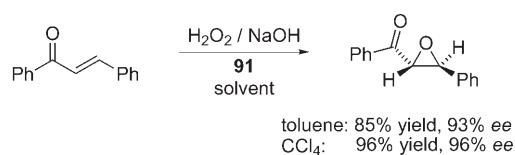
from the corresponding amino acids but need to be activated before use, and intriguingly the catalyst needs to be heterogeneous to be active. The best results in terms of activity and selectivity are obtained if the catalyst is precipitated in the form of an amorphous clear gel from a rapidly stirred methanol/diethyl ether solution.

The mechanism of this reaction remains unclear, although a few fascinating models<sup>[153d,g]</sup> have been suggested on the basis of numerous investigations. Kinetic results indicate a cooperation of two molecules of the catalyst.<sup>[153e]</sup> For a number of reasons, interest in this area has faded somewhat: on the one hand the development of new catalysts has proven to be difficult, while on the other hand only HCN can be employed as the cyanide source and the substrate spectrum is limited.

Larger synthetic polyamino acids have also been employed successfully as catalysts in different asymmetric reactions such as Michael additions, oxidations, and reductions.<sup>[154]</sup> The most important reaction catalyzed by polyamino acids is the epoxidation of  $\alpha,\beta$ -unsaturated ketones with hydrogen peroxide under basic conditions to give epoxy ketones (Julià-Colonna epoxidation).<sup>[155]</sup> The most commonly used polyamino acid catalysts poly-(*S*)-alanine (**91**) and poly-

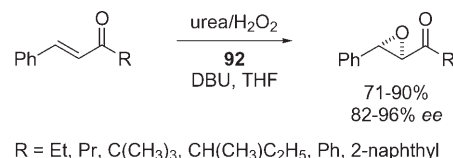
(*S*)-leucine (**92**; Scheme 54) can be prepared on a multi-kilogram scale, and are commercially available.<sup>[155a,156]</sup>

Julià and Colonna initially reported a highly enantioselective epoxidation of chalcone with polyamino acid catalysts, the best results being obtained with poly-(*S*)-alanine (**91**) with a degree of polymerization of  $n=30$  (Scheme 55).<sup>[157]</sup> Since the reaction takes place in a three-phase system (water, organic solvent, insoluble catalyst), vigorous stirring is important for the proper mixing of the reactants.



**Scheme 55.** Julià-Colonna epoxidation of chalcone.

The development of a biphasic system by Robert and co-workers was a great improvement for the practical application of the Julià-Colonna epoxidation.<sup>[158]</sup> The use of a solid urea/hydrogen peroxide complex as the oxidant allows for water-free reaction conditions and results in a significant enhancement in the reaction rate of up to a hundred times relative to the original three-phase system (Scheme 56).



R = Et, Pr, C(CH<sub>3</sub>)<sub>3</sub>, CH(CH<sub>3</sub>)C<sub>2</sub>H<sub>5</sub>, Ph, 2-naphthyl

**Scheme 56.** Water-free Julià-Colonna epoxidation. DBU = 1,8-diazabicyclo[5.4.0]undec-7-ene.

In contrast to most other heterogeneous catalysts, the separation of the polyamino acid catalyst after the reaction is often problematic, because it remains as a viscous “paste”. Therefore, filtration becomes laborious and time consuming on a large scale. A solution to this problem is the adsorption of the catalyst on polymeric<sup>[159]</sup> or silica gel supports.<sup>[160]</sup> As a consequence, the supported catalysts can be readily separated, and a rate enhancement as well as an increase in enantioselectivity has often also been observed.

The Julià-Colonna epoxidation is synthetically useful and has been applied in numerous total synthesis, such as for SK&F 104353 (an active ingredient for the treatment of asthma) and diltiazem (an antihypertensive drug).<sup>[161]</sup> However, the substrate spectrum is limited to  $\alpha,\beta$ -unsaturated ketones, especially *E*-configured, disubstituted ones, and a few cyclic enones.

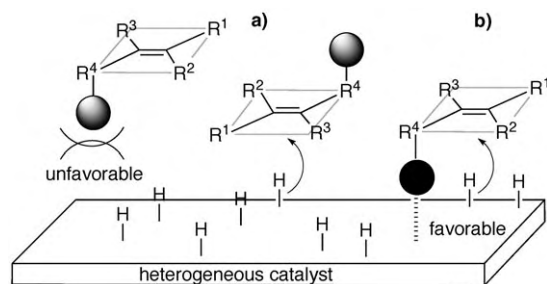
A detailed analysis of the mechanism in the enantioselective epoxidation reaction catalyzed by polyamino acids

would speed up the development of new, highly selective catalysts. The suggestion of the involvement of hydrogen bonding is supported by the fact that no enantioinduction is observed if the reaction is conducted in methanol. Moreover, poly-(*S*)-proline or N-terminal-protected polyamino acids that lack any amide protons are catalytically inactive.<sup>[155d,157b]</sup> Berkessel et al. reported an increase in the yield and enantioselectivity with an increasing degree of polymerization when they used supported poly-(*S*)-leucine.<sup>[162]</sup> More than 90% *ee* was obtained in the epoxidation of chalcone when the supported tetrapeptide, which can already form a helical structure, was employed. The maximum *ee* value obtained with the pentapeptide was 98%, but unfortunately this was accompanied by a low yield of 50%. These results together with additional calculations suggest that the enone is activated by binding to the N terminus of the polyamino acid through hydrogen bonding.<sup>[162]</sup> However, more investigations are needed to gain a deeper understanding of the underlying mechanistic principles. Hopefully, the application of polypeptides in catalysis will profit from the increased interest in organocatalysis.<sup>[151]</sup> Mechanistic insight will likely be the key to the development of new catalysts and expansion to other reactions.

## 6. Diastereoselective Heterogeneous Catalysis

Besides enantioselective catalysis, which was the focus of the previous chapters, heterogeneous catalysts can also be applied in the stereoselective conversion of compounds that bear one or more stereocenters. The interaction of the heterogeneous catalyst with the substrate can be sterically disfavored or electronically favored. In both cases the interaction determines which diastereotopic face of the substrate will preferentially bind to or react with the catalyst surface. (Scheme 57).<sup>[163]</sup> It is thus understandable that cyclic compounds with their limited degrees of freedom have been the preferred substrates for highly diastereoselective heterogeneous hydrogenation reactions.

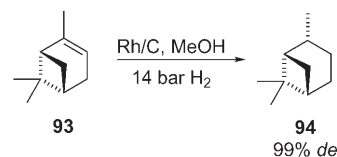
Besides a few reactions catalyzed by solid Lewis acids, such as Diels–Alder, ene reactions,<sup>[164]</sup> and epoxidations,<sup>[165]</sup> the research area of highly diastereoselective heterogeneously catalyzed reactions is clearly dominated by hydrogenations.<sup>[166,167c]</sup> Although, homogeneous asymmetric hydrogenation can be achieved with a very high level of selectivity for the conversion of numerous substrate classes,<sup>[5a,167]</sup> diaste-



**Scheme 57.** Schematic presentation of: a) steric and b) electronic influences on the facial selectivity.

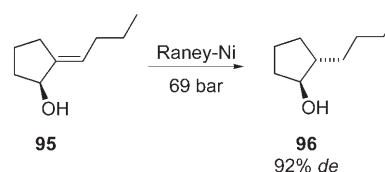
reoselective, heterogeneous hydrogenation can still offer more efficient solutions in some cases. Commonly employed catalysts are supported or unsupported transition metals or their derivatives, for example, PtO<sub>2</sub>, Pt/Al<sub>2</sub>O<sub>3</sub>, Pd/C, Pd(OH)<sub>2</sub>/C, Rh/C, Rh/Pd/C, and Raney Ni.

Of the plethora of highly selective reactions, the hydrogenation of (1*S*,5*S*)-2-pinene (**93**) to (1*S*,2*R*,5*S*)-pinane (**94**) is a representative example for the steric influence of the backbone of the substrate on the diastereoselectivity obtained (Scheme 58).<sup>[168]</sup> The rigid bicyclic ring system provides a strong shield to the bottom face of the double bond, thus resulting in a highly selective hydrogenation from the top face.



**Scheme 58.** Diastereoselective hydrogenation of pinene (**93**).

Functional groups such as amines or alcohols can influence the diastereoselectivity through an attractive interaction with the surface of the catalyst (see Scheme 57b).<sup>[169]</sup> Hydrogen transfer occurs from the site of the interacting OH group, and therefore the cyclopentanol derivative **95** is hydrogenated with good diastereoselectivity to product **96** (Scheme 59). As



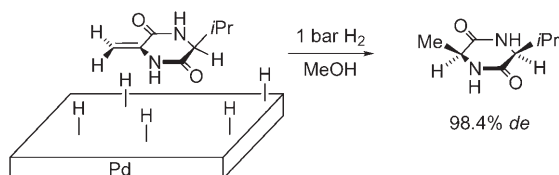
**Scheme 59.** Diastereoselective hydrogenation influenced by the adsorption of the alcohol moiety on to the surface of the catalyst.

the polarity of the solvent increases, alcohols lose their ability to bind to the surface of the catalyst; thus, the use of a highly polar solvent such as DMF or ethanol results in a reversal of the diastereoselectivity.<sup>[170]</sup>

Diastereoselective hydrogenations can also employ cleavable, chiral auxiliaries. In 1961, D-valine was already synthesized with a moderate *ee* value of 39% by hydrogenation using enantiomerically pure  $\alpha$ -methylbenzylamine as the chiral auxiliary.<sup>[171]</sup> The utilization of proline and proline derivatives as chiral auxiliaries in similar hydrogenations improved the *ee* value of the amino acid products significantly.<sup>[172]</sup> The hydrogenation of diketopiperazines or cyclic dehydrideptides allows the formation of enantiomerically pure amino acids (Scheme 60).<sup>[173]</sup>

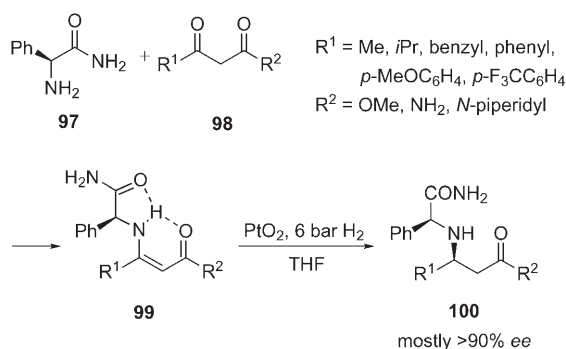
$\beta$ -Amino acid derivatives can be prepared with high efficiency by the heterogeneous hydrogenation of auxiliary-substituted *Z* enamines.<sup>[174]</sup> Treatment of the corresponding  $\beta$ -ketoester or -amide with the chiral auxiliary (*S*)-phenyl-





**Scheme 60.** Selective hydrogenation of a cyclic dipeptide on a palladium surface.

glycinamide provides the substituted *Z*-enamide **99**. Hydrogen bonding results in a rigid conformation of **99**, with the phenyl substituent on the auxiliary shielding the top face of the molecule, which results in stereoselectivities of up to 200:1 being obtained in the hydrogenation over  $\text{PtO}_2$  (Scheme 61).<sup>[174a]</sup> Pretreatment of the catalyst with acetic

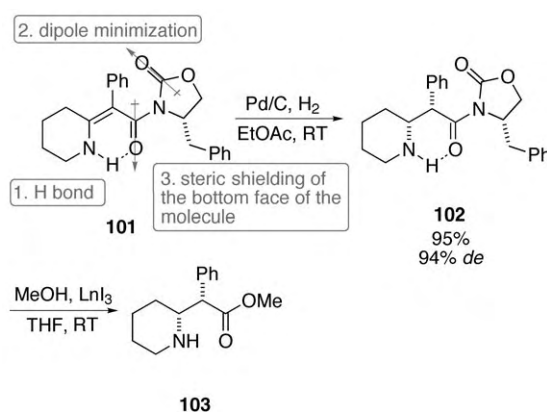


**Scheme 61.** Synthesis of  $\beta$ -amino acids with (*S*)-phenylglycinamide (**97**) as an auxiliary.

acid was found to be very important for good catalytic activity. Since acid would lead to an undesired *E/Z* isomerization, and hence, reduced selectivities, the catalyst was carefully dried after acid treatment and only used in conjunction with a small amount of  $\text{NEt}_3$ . The reaction products without an aromatic  $\text{R}^1$  group can undergo hydrogenolysis to give the free  $\beta$ -amino acid esters and amides.

Oxazolidinones were successfully employed as chiral auxiliaries for the diastereoselective hydrogenation of double bonds.<sup>[175]</sup> Prasad et al. developed a stereoselective synthesis of (2*S*,2'*R*)-*erythro*-methylphenidate (**103**) by using this approach. The key step—the diastereoselective hydrogenation of a tetrasubstituted double bond—is controlled by a chiral oxazolidinone. The excellent diastereoselectivity obtained was attributed to a number of effects (Scheme 62). First of all, the conformation of **101** is locked by hydrogen bonding. In addition, the minimization of the dipole moment results in a preferred antiparallel orientation of the carbonyl moieties in **101**. As a consequence, the benzyl group of the oxazolidinone selectively shields the bottom face of the molecule in the hydrogenation step.

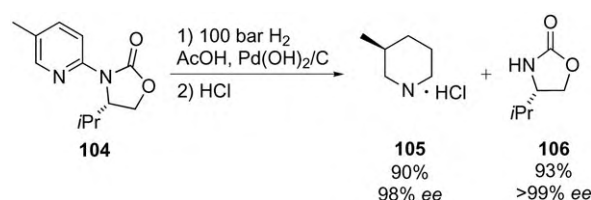
The stereoselective synthesis of substituted cyclohexanes, piperidines, or other saturated heterocycles is of high synthetic interest because they are common building blocks of numerous biologically active compounds. One approach towards an efficient synthesis of these rings is the asymmetric



**Scheme 62.** Asymmetric hydrogenation of a highly substituted double bond.

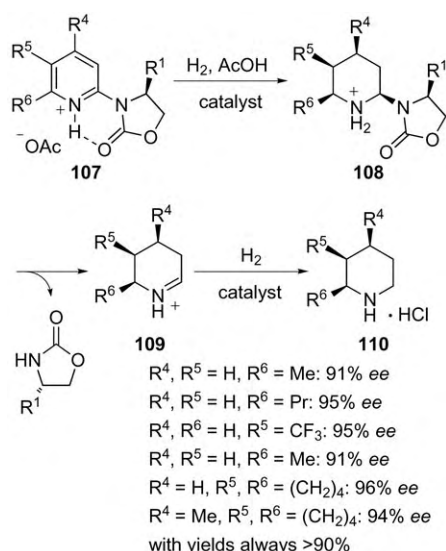
hydrogenation of the corresponding aromatic or heteroaromatic compounds. However, so far, only a few highly selective examples have been reported.<sup>[176]</sup>

Our research group obtained good results in the asymmetric hydrogenation of pyridines.<sup>[177]</sup> 2-Oxazolidinone-substituted pyridines that can be readily prepared from 2-halogen-substituted pyridines by copper catalysis, are the substrates of choice. Remarkably, the hydrogenation of 2-oxazolidinone-5-methylpyridine (**104**) provided (*S*)-3-methylpiperidine (**105**) in high enantiomeric excess (Scheme 63).



**Scheme 63.** Asymmetric hydrogenation of pyridine.

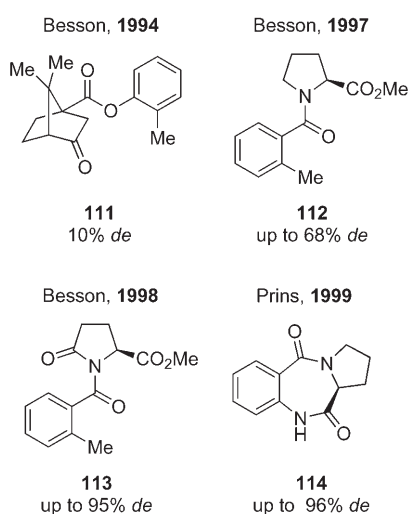
According to the proposed mechanism, a hydrogen bond rigidifies molecule **107** and results in a shielding of the top face of the substrate by the  $\text{R}^1$  substituent (Scheme 64). An efficient  $\text{H}_2$  transfer to the pyridine ring then provides aminal **108**. The auxiliary is subsequently cleaved under the same reaction conditions and results in the direct formation of the *N*-unsubstituted piperidine **110**, isolated in the form of a hydrochloride salt. An attractive feature of this method is that the auxiliary can be separated from the insoluble piperidine hydrochloride by simple extraction with organic solvents and recovered in high yield. This method can be applied to the highly selective hydrogenation of numerous differently substituted pyridines, except pyridines substituted in the 3-position (4% *ee* for 3-methylpiperidine). This limitation can be explained by an unfavorable steric interaction between the substituent in the 3-position and the chiral auxiliary. This method allows the synthesis of natural products and the generation of multiple stereocenters in the ring, as exempli-



**Scheme 64.** Postulated mechanism for the asymmetric hydrogenation of pyridines.

fied in the formation of **108** with four newly formed stereocenters in the ring.<sup>[177]</sup>

Benzene derivatives can also be hydrogenated heterogeneously with diastereoselectivities of up to 96%. However, the spectrum of substrates is very limited, and 2-methylbenzoic acid derivatives have almost always been used (Scheme 65).<sup>[166,178]</sup> The substrates have to adopt highly preferred conformations (minimization of the dipole moment) or have rigid cyclic structures to obtain high selectivities, such as in tricycle **114**.<sup>[178c,f]</sup> However, the hydrogenation of aromatic substrates remains a challenging problem. The implementation of new strategies such as the innovative utilization of readily accessible chiral auxiliaries might advance this field to the next level of sophistication.<sup>[179]</sup>



**Scheme 65.** Substituted benzenes as substrates for diastereoselective hydrogenation.

## 7. Conclusion

In this Review we have given an overview of the current important areas of asymmetric heterogeneous catalysis, which is a rapidly developing, highly interdisciplinary, and multifarious research area. The main topic is the immobilization of chiral homogeneous metal–ligand complexes (Section 2), an area which has grown rapidly in the last few years by profiting from the development and investigation of new innovative supports. This area has now reached a certain level of maturity, and thus these catalysts will find increasing application in industry. Furthermore, the young area of asymmetric metal–organic catalysts (Section 3) with their easily assembled, highly porous, and in a few cases even crystalline structures, is developing rapidly. Crystalline catalysts would be especially attractive, since they can easily be characterized by X-ray structural analysis which would greatly facilitate mechanistic investigations and a rational catalyst design. These asymmetric metal–organic catalysts deserve even more research interest and will most likely become a very important class of catalysts.

The use of chiral modifiers (Section 4) and peptides (Section 5) as heterogeneous asymmetric catalysts is fascinating since they involve new mechanisms that are unparalleled by any other reaction. A better mechanistical understanding would be required for a new rational design of catalyst systems of this kind. Hopefully, new developments and principles in the area of organocatalysis will have a positive impact on this area of heterogeneous, organocatalyzed reactions.

Finally, diastereoselective heterogeneous catalysis (Section 6) often enables remarkably selective transformations in cases where all other asymmetric methods fail.

Although some of the discussed methods give good results, most areas of heterogeneous asymmetric catalysis are probably just beginning to show their full potential. Newly developed analytical and preparative methods as well as the interaction of organic and inorganic structures during catalysis offer new opportunities for catalysis. In addition to the methods discussed in this Review, numerous other fascinating but less efficient methodologies exist, such as catalysis at inherently chiral metal surfaces<sup>[9f,112,113]</sup> and the application of artificial antibodies, derived from the imprinting<sup>[180]</sup> of organic or inorganic compounds as transition-state analogues.

The possibility to separate and recycle the catalyst as well as high activity and selectivity are the main criteria for the quality of a heterogeneous asymmetric catalyst. Thus, the following research trends are especially important for the advancement of the field of heterogeneous asymmetric catalysis:

- Investigation of the structure of heterogeneous catalysts and their reaction mechanisms;
- improvement of the catalyst performance;
- simplification of the catalyst system and their synthesis;
- taking advantage of the special properties of solid supports and the unique mechanisms of heterogeneous catalysis.

The ongoing research will no doubt increase the importance of catalysis as an essential technology for the future<sup>[1]</sup>

and eventually allow the rational design of heterogeneous asymmetric catalysts.

We thank the Deutsche Forschungsgemeinschaft and the Fonds der Chemischen Industrie (Dozentenstipendium to F.G., Chemiefondsstipendium to M.H.), Lilly Deutschland (Lilly Lecture Award), and BASF AG (BASF Catalysis Award) for generous financial support, and the referees for their very helpful comments, as well as A. Baiker, T. Bürgi, K. Ding, and K. Kim for their kind support.

Received: November 25, 2005

Published online: June 27, 2006

- [1] a) *Roadmap der deutschen Katalyseforschung*, brochure of CONNECAT, **2006**, <http://www.conneecat.de/content.php>; b) *Asymmetric Catalysis on Industrial Scale* (Eds.: H. U. Blaser, E. Schmidt), Wiley-VCH, Weinheim, **2004**.
- [2] S. C. Stinson, *Chem. Eng. News* **2001**, 79(40), 79.
- [3] *Principles and Practice of Heterogeneous Catalysis* (Eds.: J. M. Thomas, W. J. Thomas), Wiley-VCH, Weinheim, **1997**.
- [4] a) *Chiral Reactions in Heterogeneous Catalysis*, (Eds.: V. Dubois, G. Jannes), Plenum, New York, **1995**; b) D. C. Sherrington, *Catal. Today* **2000**, 57, 87; c) H.-U. Blaser, B. Pugin, M. Studer in *Chiral Catalyst Immobilization and Recycling* (Eds.: D. E. De Vos, I. F. J. Vankelecom, P. A. Jacobs), Wiley-VCH, Weinheim, **2000**, p. 1.
- [5] For excellent reviews on asymmetric catalysis, see: a) *Comprehensive Asymmetric Catalysis* (Eds.: E. N. Jacobsen, A. Pfaltz, H. Yamamoto), Springer, Berlin, **1999**; b) *Catalytic Asymmetric Synthesis*, 2nd ed. (Eds.: I. Ojima), Wiley, New York, **2000**; see also: c) T. P. Yoon, E. N. Jacobsen, *Science* **2003**, 299, 1691.
- [6] H. U. Blaser, F. Spindler, M. Studer, *Appl. Catal. A* **2001**, 221, 119.
- [7] A. Weissberg, B. Halak, M. Portnoy, *J. Org. Chem.* **2005**, 70, 4556.
- [8] B. Pugin, *J. Mol. Catal. A* **1996**, 107, 273.
- [9] For reviews on the immobilization of asymmetric homogeneous catalysts, see: a) H.-U. Blaser, B. Pugin in *Chiral Reactions in Heterogeneous Catalysis* (Eds.: V. Dubois, G. Jannes), Plenum, New York, **1995**, p. 33; b) *Chiral Catalyst Immobilization and Recycling* (Eds.: D. E. De Vos, I. F. J. Vankelecom, P. A. Jacobs), Wiley-VCH, Weinheim, **2000**; c) A. Baiker, *Chimia* **2001**, 55, 796; d) *Recoverable Catalysts and Reagents* (Ed.: J. A. Gladysz), *Chem. Rev.* **2002**, 102, 3215–3892; e) Q.-H. Fan, Y.-M. Li, A. S. C. Chan, *Chem. Rev.* **2002**, 102, 3385; f) M. Jacoby, *Chem. Eng. News* **2004**, 82(11), 37; g) J. Horn, F. Michalek, C. C. Tzschucke, W. Bannwarth, *Top. Curr. Chem.* **2004**, 242, 43; h) P. McMorn, G. Hutchings, *Chem. Soc. Rev.* **2004**, 33, 108.
- [10] Enzymes as biocatalysts: a) *Enzyme catalysis in organic synthesis: a comprehensive handbook* (Eds.: K. Drauz, H. Waldmann), Wiley-VCH, Weinheim, **2002**; b) P. Rasor in *Chiral Catalyst Immobilization and Recycling* (Eds.: D. E. De Vos, I. F. J. Vankelecom, P. A. Jacobs), Wiley-VCH, Weinheim, New York, **2000**, p. 97; c) M. T. Reetz, *Proc. Natl. Acad. Sci. USA* **2004**, 101, 5716, and references therein; attachment to supports: d) T. Honda, M. Miyazaki, H. Nakamura, H. Maeda, *Chem. Commun.* **2005**, 5062; e) B. P. Sharma, L. F. Bailey, R. A. Messing, *Angew. Chem.* **1982**, 94, 836; *Angew. Chem. Int. Ed. Engl.* **1982**, 21, 837; f) A. Corma, V. Fornés, J. L. Jordá, F. Rey, R. Fernandez-Lafuente, J. M. Guisán, C. Mateo, *Chem. Commun.* **2001**, 419; g) C. Lei, Y. Shin, J. Liu, E. J. Ackerman, *J. Am. Chem. Soc.* **2002**, 124, 11242; h) M. Tortajada, D. Ramón, D. Beltrán, P. Amorós, *J. Mater. Chem.* **2005**, 15, 3859; i) J. M. Palomo, R. L. Segura, G. Fernandez-Lorente, J. M. Guisán, R. Fernandez-Lafuente, *Tetrahedron: Asymmetry* **2004**, 15, 1157; j) J. Ceynowa, M. Rauchfleisz, *J. Mol. Catal. B* **2003**, 9, 43; k) A. M. Dessouki, K. S. Atia, *Biomacromolecules* **2002**, 3, 432; l) O. Yemul, T. Imae, *Biomacromolecules* **2005**, 6, 2809; for an example of the successful application of an immobilized enzyme in synthesis, see: m) I. R. Baxendale, M. Ernst, W.-R. Krahnert, S. V. Ley, *Synlett* **2002**, 1641; application of enzyme crystals: n) N. L. St. Clair, M. Navia, *J. Am. Chem. Soc.* **1992**, 114, 7314; o) R. A. Persichetti, N. L. St. Clair, J. P. Griffith, M. A. Navia, A. L. Margolin, *J. Am. Chem. Soc.* **1995**, 117, 2732; p) review: A. L. Margolin, M. A. Navia, *Angew. Chem.* **2001**, 113, 2262; *Angew. Chem. Int. Ed.* **2001**, 40, 2204.
- [11] a) For a recent review on the asymmetric synthesis using soluble polymers as supports, see: S. Chandrasekhar, J. S. Yadav, Jhilla, J.-C. Guillemin, P. Lakshmiipathi, R. Gree, *Indian J. Chem. Sect. B* **2002**, 41, 2116; for a review on asymmetric C–C and C–heteroatom bond formation, including the use of soluble polymers, see b) S. Bräse, F. Lauterwasser, R. E. Ziegert, *Adv. Synth. Catal.* **2003**, 345, 869; for a review on soluble polymers as supports for catalysts, see: c) D. E. Bergbreiter, *Chem. Rev.* **2002**, 102, 3345; d) T. J. Dickerson, N. N. Reed, K. D. Janda, *Chem. Rev.* **2002**, 102, 3325.
- [12] a) R. van Heerbeek, P. C. J. Kamer, P. W. N. M. van Leeuwen, J. N. H. Reek, *Chem. Rev.* **2002**, 102, 3717; b) G.-J. Deng, Q.-H. Fan, X.-M. Chen, G.-H. Liu, *J. Mol. Catal. A* **2003**, 193, 21.
- [13] R. B. Merrifield, *J. Am. Chem. Soc.* **1963**, 85, 2149.
- [14] a) R. Manzotti, T. S. Reger, K. D. Janda, *Tetrahedron Lett.* **2000**, 41, 8417; b) P. H. Toy, K. D. Janda, *Tetrahedron Lett.* **1999**, 40, 6329.
- [15] a) S. Lundgren, S. Lutsenko, C. Jönsson, C. Moberg, *Org. Lett.* **2003**, 5, 3663; b) H. Nakano, K. Takahashi, Y. Suzuki, R. Fujita, *Tetrahedron: Asymmetry* **2005**, 16, 609.
- [16] H. Hocke, Y. Uozumi, *Tetrahedron* **2004**, 60, 9297.
- [17] C. E. Song, J. W. Yang, E. J. Roh, S.-G. Lee, J. H. Ahn, H. Han, *Angew. Chem.* **2002**, 114, 4008; *Angew. Chem. Int. Ed.* **2002**, 41, 3852.
- [18] Q.-H. Fan, R. Wang, A. S. C. Chan, *Bioorg. Med. Chem. Lett.* **2002**, 12, 1867.
- [19] A. Cornejo, J. M. Fraile, J. I. García, M. J. Gil, S. V. Luis, V. Martínez-Merino, J. A. Mayoral, *J. Org. Chem.* **2005**, 70, 5536.
- [20] C. Saluzzo, T. Lamouille, D. Hérault, M. Lemaire, *Bioorg. Med. Chem. Lett.* **2002**, 12, 1841.
- [21] D. Hérault, C. Saluzzo, R. Duval, M. Lemaire, *J. Mol. Catal. A* **2002**, 182–183, 249.
- [22] C. E. Song, S.-G. Lee, *Chem. Rev.* **2002**, 102, 3495.
- [23] a) Y. Tao, H. Kanoh, L. Abrams, K. Kaneko, *Chem. Rev.* **2006**, 106, 896; b) J. Y. Ying, C. P. Mehnert, M. S. Wong, *Angew. Chem.* **1999**, 111, 58; *Angew. Chem. Int. Ed.* **1999**, 38, 56; c) P. Yang, D. Zhao, D. I. Margolese, B. F. Chmelka, G. D. Stucky, *Nature* **1998**, 396, 152; d) D. Zhao, J. Feng, Q. Huo, N. Melosh, G. H. Fredrickson, B. F. Chmelka, G. D. Stucky, *Science* **1998**, 279, 548; for the investigation of the mechanical stability of MCM-41, see: e) V. Y. Gusev, X. Feng, Z. Bu, G. L. Haller, J. A. O'Brien, *J. Phys. Chem.* **1996**, 100, 1985.
- [24] a) For a comparison of carbosil and MCM-41, see: B. F. G. Johnson, S. A. Raynor, D. S. Shepard, T. Mashmeyer, J. M. Thomas, G. Sankar, S. Bromley, R. Oldroyd, L. Gladden, M. D. Mantle, *Chem. Commun.* **1999**, 1167; b) an example using Grace332: B. Pugin, H. Landert, F. Spindler, H. U. Blaser, *Adv. Synth. Catal.* **2002**, 344, 974; c) an example using USY: M. J. Alcón, A. Corma, M. Iglesias, F. Sánchez, *J. Organomet. Chem.* **2002**, 655, 134.
- [25] a) P. N. Liu, P. M. Gu, F. Wang, Y. Q. Tu, *Org. Lett.* **2004**, 6, 169; b) P.-N. Liu, P.-M. Gu, J.-G. Deng, Y.-Q. Tu, Y.-P. Ma, *Eur. J. Org. Chem.* **2005**, 3221.
- [26] For an application in water, see: P. N. Liu, J. G. Deng, Y. Q. Tu, S. H. Wang, *Chem. Commun.* **2004**, 2070.



- [27] J. M. Thomas, T. Maschmeyer, B. F. G. Johnson, D. S. Shephard, *J. Mol. Catal. A* **1999**, *141*, 139.
- [28] a) J. M. Thomas, *Angew. Chem.* **1999**, *111*, 3881; *Angew. Chem. Int. Ed.* **1999**, *38*, 3588; b) K. Borszeky, T. Burgi, Z. Zhaohui, T. Mallet, A. Baiker, *J. Catal.* **1999**, *187*, 160.
- [29] M. D. Jones, R. Raja, J. M. Thomas, B. F. G. Johnson, D. W. Lewis, J. Rouzaud, K. D. M. Harris, *Angew. Chem.* **2003**, *115*, 4462; *Angew. Chem. Int. Ed.* **2003**, *42*, 4326.
- [30] R. Raja, J. M. Thomas, M. D. Jones, B. F. G. Johnson, D. E. W. Vaughan, *J. Am. Chem. Soc.* **2003**, *125*, 14982.
- [31] D. Rechavi, B. Albela, L. Bonnevot, M. Lemaire, *Tetrahedron* **2005**, *61*, 6976.
- [32] J. K. Park, S.-W. Kim, T. Hyeon, B. M. Kim, *Tetrahedron: Asymmetry* **2001**, *12*, 2931.
- [33] A. Vidal-Ferran, N. Bamps, A. Moyano, M. A. Pericàs, A. Riera, J. K. M. Sanders, *J. Org. Chem.* **1998**, *63*, 6309.
- [34] A. Hu, G. T. Yee, W. Lin, *J. Am. Chem. Soc.* **2005**, *127*, 12486.
- [35] T. Steiner, *Angew. Chem.* **2002**, *114*, 50; *Angew. Chem. Int. Ed.* **2002**, *41*, 48.
- [36] a) F. M. de Rege, D. K. Morita, K. C. Ott, W. Tumas, R. D. Broene, *Chem. Commun.* **2000**, 1797; b) J. Rouzaud, M. D. Jones, R. Raja, B. F. G. Johnson, J. M. Thomas, M. J. Duer, *Helv. Chim. Acta* **2003**, *86*, 1753; c) C. Bianchini, V. Dal Santo, A. Meli, S. Moneti, M. Moreno, W. Oberhauser, R. Psaro, L. Sordelli, F. Vizza, *J. Catal.* **2003**, *213*, 47.
- [37] a) J. P. Arhancet, M. E. Davis, J. S. Merola, B. E. Hanson, *Nature* **1989**, *339*, 454; b) A. J. Sandee, V. F. Slagt, J. N. H. Reek, P. C. J. Kamer, P. W. N. M. van Leeuwen, *Chem. Commun.* **1999**, 1633.
- [38] I. Tóth, I. Guo, B. E. Hanson, *J. Mol. Catal. A* **1997**, *116*, 217.
- [39] a) G. J. Hutchings, *Chem. Commun.* **1999**, 301; b) S. Taylor, J. Gullick, P. McMorn, D. Bethell, P. C. Bulman Page, F. E. Hancock, F. King, G. J. Hutchings, *Top. Catal.* **2003**, *24*, 43; c) S. Taylor, J. Gullick, N. Galea, P. McMorn, D. Bethell, P. C. Bulman Page, F. E. Hancock, F. King, D. J. Willock, G. J. Hutchings, *Top. Catal.* **2003**, *25*, 81; d) D. Ryan, P. McMorn, D. Bethell, G. Hutchings, *Org. Biomol. Chem.* **2004**, *2*, 3566.
- [40] S. Feast, P. C. Bethell, P. C. B. Pate, F. King, C. H. Rochester, M. R. H. Siddiqui, D. J. Willock, G. J. Hutchings, *J. Chem. Soc. Chem. Commun.* **1995**, 2499.
- [41] Y. Wang, P. McMorn, F. E. Hancock, G. J. Hutchings, *Catal. Lett.* **2003**, *3*, 145.
- [42] N. A. Caplan, F. E. Hancock, P. C. Bulman Page, G. J. Hutchings, *Angew. Chem.* **2004**, *116*, 1717; *Angew. Chem. Int. Ed.* **2004**, *43*, 1685.
- [43] For an overview on polymer-supported cinchona alkaloids in asymmetric dihydroxylation, see: P. Salvadori, D. Pini, A. Petri, *Synlett* **1999**, 1181.
- [44] B. M. Choudary, N. S. Chowdari, M. L. Kantam, V. R. Kondapuram, *J. Am. Chem. Soc.* **2001**, *123*, 9220.
- [45] F. Trifiro, A. Vaccari, *Comprehensive Supramolecular Chemistry*, Vol. 7, Pergamon/Elsevier Science, Oxford, **1996**, p. 251.
- [46] B. M. Choudary, N. S. Chowdari, K. Jyothi, M. L. Kantam, *J. Am. Chem. Soc.* **2002**, *124*, 5341.
- [47] B. M. Choudary, J. Karangula, S. Madhi, M. L. Kantam, *Adv. Synth. Catal.* **2003**, *345*, 1190.
- [48] M. L. Kantam, B. V. Prakash, B. Bharathi, C. V. Reddy, *J. Mol. Catal. A* **2005**, *226*, 119.
- [49] a) S. B. Ogunwumi, T. Bein, *Chem. Commun.* **1997**, 901; b) A. Zsigmond, K. Bögar, F. Notheisz, *J. Catal.* **2003**, *213*, 103.
- [50] For chiral Rh and Ru complexes encapsulated in a sol-gel, see: a) F. Gelman, D. Avnir, H. Schumann, J. Blum, *J. Mol. Catal. A* **1999**, *146*, 123; b) for an example of a membrane, see: R. F. Parton, I. F. J. Vankelecom, D. Tas, K. B. M. Janssen, P.-P. Knops-Gerrits, P. A. Jacobs, *J. Mol. Catal. A* **1996**, *113*, 283.
- [51] A. Wolfson, S. Janssens, I. Vankelecom, S. Geresh, M. Gottlieb, M. Herskowitz, *Chem. Commun.* **2002**, 388.
- [52] H. M. L. Davies, A. M. Walji, T. Nagashima, *J. Am. Chem. Soc.* **2004**, *126*, 4271.
- [53] H. M. L. Davies, A. M. Walji, *Org. Lett.* **2005**, *7*, 2941.
- [54] D. J. Bayston, J. L. Fraser, M. R. Ashton, A. D. Baxter, M. E. C. Polwka, E. Moses, *J. Org. Chem.* **1998**, *63*, 3137.
- [55] T. Ohkuma, H. Takeno, Y. Honda, R. Noyori, *Adv. Synth. Catal.* **2001**, *343*, 369.
- [56] A. Fujii, M. Sodeoka, *Tetrahedron Lett.* **1999**, *40*, 8011.
- [57] C. Chapuis, M. Barthe, J.-Y. de Saint Laumer, *Helv. Chim. Acta* **2001**, *84*, 230.
- [58] a) C. Saluzzo, T. Lamouille, F. Le Guyader, M. Lemaire, *Tetrahedron: Asymmetry* **2002**, *13*, 1141; b) R. Ter Halle, B. Colasson, E. Schulz, M. Spagnol, M. Lemaire, *Tetrahedron Lett.* **2000**, *41*, 643.
- [59] R. Ter Halle, E. Schulz, M. Spagnol, M. Lemaire, *Tetrahedron Lett.* **2000**, *41*, 3323.
- [60] H.-B. Yu, Q.-S. Hu, L. Pu, *Tetrahedron Lett.* **2000**, *41*, 1681.
- [61] A. Hu, H. L. Ngo, W. Lin, *Angew. Chem.* **2004**, *116*, 2555; *Angew. Chem. Int. Ed.* **2004**, *43*, 2501.
- [62] B. Kesali, W. Lin, *Chem. Commun.* **2004**, 2284.
- [63] A. Hu, H. L. Ngo, W. Lin, *J. Am. Chem. Soc.* **2003**, *125*, 11490.
- [64] I. F. J. Vankelecom, D. Tas, R. F. Parton, V. V. Vyver, P. A. Jacobs, *Angew. Chem.* **1996**, *108*, 1717; *Angew. Chem. Int. Ed. Engl.* **1996**, *35*, 1346.
- [65] F. Gelman, D. Avnir, H. Schumann, J. J. Blum, *J. Mol. Catal. A* **1999**, *146*, 123.
- [66] J. Jamis, J. R. Anderson, R. S. Dickson, E. M. Campi, W. R. Jackson, *J. Organomet. Chem.* **2001**, *627*, 37.
- [67] K. T. Wan, M. E. Davis, *Nature* **1994**, *370*, 449.
- [68] M. Tamura, H. Fujihara, *J. Am. Chem. Soc.* **2003**, *125*, 15742.
- [69] A. Crozman, W. F. Hoelderich, *J. Catal.* **2005**, *232*, 43.
- [70] a) R. Augustine, S. Tanielyan, S. Anderson, H. Yang, *Chem. Commun.* **1999**, 1257; b) R. L. Augustine, P. Goel, N. Mahata, C. Reyes, S. K. Tanielyan, *J. Mol. Catal. A* **2004**, *189*, 216; for a related immobilization of Rh(diphosphine) complexes on basic carbon (acticarbon) with very good enantioselectivities and activities, see: C. F. J. Barnard, J. Rouzaud, S. H. Stevenson, *Org. Process Res. Dev.* **2005**, *9*, 164.
- [71] Montmorillonite K is a smectic clay that resembles a sandwich structure consisting of two layers of silica and a layer of aluminum ions in between.
- [72] C. Simons, U. Hanefeld, I. W. C. E. Arend, R. A. Sheldon, T. Maschmeyer, *Chem. Eur. J.* **2004**, *10*, 5829.
- [73] This intrinsic instability was reported previously: a) S.-G. Lee, Y. J. Zhang, J. Y. Piao, H. Yoon, C. E. Song, J. H. Choi, J. Hong, *Chem. Commun.* **2003**, 2624; b) S. Guernik, A. Wolfson, M. Herskowitz, N. Greenspoon, S. Geresh, *Chem. Commun.* **2001**, 2314.
- [74] W. P. Hems, P. McMorn, S. Riddell, S. Watson, F. E. Hancock, G. J. Hutchings, *Org. Biomol. Chem.* **2005**, *3*, 1547.
- [75] H. H. Wagner, H. Hausmann, W. F. Hölderich, *J. Catal.* **2001**, *203*, 150.
- [76] Besides the purified unsymmetrical salen ligand, the crude mixture of symmetrical tetra-*tert*-butyl-substituted and the dihydroxy-substituted as well as the unsymmetrical salen ligand can also be employed, thus resulting in the immobilization of the unsymmetrical ligand on the functionalized resin. This saves an elaborate purification step.
- [77] For the asymmetric epoxidation using [Mn(salen)] complexes on MCM-41, see also: a) D.-W. Park, S.-D. Choi, C.-Y. Lee, G.-J. Kim, *Catal. Lett.* **2002**, *78*, 145; b) I. Domínguez, V. Fornés, M. J. Sabater, *J. Catal.* **2004**, *228*, 92.
- [78] D. A. Annis, E. N. Jacobsen, *J. Am. Chem. Soc.* **1999**, *121*, 4147, and references therein.
- [79] For related salen polymers and their application in the manganese-catalyzed epoxidation of alkenes, see: M. Nielsen,



- A. H. Thomsen, T. R. Jensen, H. J. Jakobsen, J. Skibsted, K. V. Gothelf, *Eur. J. Org. Chem.* **2005**, 342.
- [80] M.-a. Kwon, G.-J. Kim, *Catal. Today* **2003**, 87, 145.
- [81] S. Peukert, E. N. Jacobsen, *Org. Lett.* **1999**, 1, 1245.
- [82] L. Canali, E. Cowan, H. Deleuze, C. L. Gibson, D. C. Sherrington, *J. Chem. Soc. Perkin Trans. 1* **2000**, 2055.
- [83] a) H. Zhang, Y. Zhang, C. Li, *Tetrahedron: Asymmetry* **2005**, 16, 2417; b) H. Zhang, S. Xiang, C. Li, *Chem. Commun.* **2005**, 1209; for an analogous immobilization on silicates, see: c) H. Zhang, S. Xiang, J. Xiao, C. Li, *J. Mol. Catal. A* **2005**, 238, 175; d) S. Xiang, Y. Zhang, Q. Xin, C. Lin, *Chem. Commun.* **2002**, 2696.
- [84] H. Sellner, J. K. Karjalainen, D. Seebach, *Chem. Eur. J.* **2001**, 7, 2873.
- [85] H. Sellner, D. Seebach, *Angew. Chem.* **1999**, 111, 2039; *Angew. Chem. Int. Ed.* **1999**, 38, 1918.
- [86] a) C. Baleizao, B. Gigante, H. García, A. Corma, *Tetrahedron* **2004**, 60, 10461; b) C. Baleizao, B. Gigante, H. García, A. Corma, *J. Catal.* **2004**, 221, 77.
- [87] a) M. J. Sabatier, A. Corma, A. Domenech, V. Fornes, H. García, *Chem. Commun.* **1997**, 1285; b) C. Schuster, E. Mollmann, A. Thompos, W. F. Hölderich, *Catal. Lett.* **2001**, 74, 69.
- [88] B. M. L. Dooos, P. A. Jacobs, *Tetrahedron Lett.* **2003**, 44, 8815.
- [89] S.-D. Choi, G.-J. Kim, *Catal. Lett.* **2004**, 92, 35.
- [90] R. I. Kureshy, N. H. Khan, S. H. R. Abdi, I. Ahmad, S. Singh, R. V. Jasra, *J. Catal.* **2004**, 221, 234.
- [91] For a comprehensive review on immobilized bisoxazolines in asymmetric catalysis, see: D. Rechavi, M. Lemaire, *Chem. Rev.* **2002**, 102, 3467.
- [92] a) J. G. Knight, P. E. Belcher, *Tetrahedron: Asymmetry* **2005**, 16, 1415; b) M. I. Burguete, J. M. Fraile, J. I. García, E. García-Verdugo, S. V. Luis, J. A. Mayoral, *Org. Lett.* **2000**, 2, 3905; c) E. Díez-Barra, J. M. Fraile, J. I. García, E. García-Verdugo, C. I. Herrerías, S. V. Luis, J. A. Mayoral, P. Sánchez-Verdú, J. Tolosa, *Tetrahedron: Asymmetry* **2003**, 14, 773; d) M. I. Burguete, J. M. Fraile, J. I. García, E. García-Verdugo, C. I. Herrerías, S. V. Luis, J. A. Mayoral, *J. Org. Chem.* **2001**, 66, 8893; e) A. Mandoli, S. Orlandi, D. Pini, P. Salvadori, *Chem. Commun.* **2003**, 2466.
- [93] a) A. Mandoli, S. Orlandi, D. Pini, P. Salvadori, *Tetrahedron: Asymmetry* **2004**, 15, 3233; for comparison with the homogeneous reaction, see: b) D. A. Evans, C. S. Burgey, N. A. Paras, T. Vojkovsky, S. W. Tregay, *J. Am. Chem. Soc.* **1998**, 120, 5824; c) D. A. Evans, S. W. Tregay, C. S. Burgey, N. A. Paras, T. Vojkovsky, *J. Am. Chem. Soc.* **2000**, 122, 7936.
- [94] a) D. Rechavi, M. Lemaire, *Org. Lett.* **2001**, 3, 2493; b) D. Rechavi, M. Lemaire, *J. Mol. Catal. A* **2002**, 182–183, 239.
- [95] R. J. Clarke, I. J. Shannon, *Chem. Commun.* **2001**, 1936.
- [96] a) A. Corma, H. García, A. Moussaif, M. J. Sabater, R. Zniber, A. Redouane, *Chem. Commun.* **2002**, 1058; b) homogeneous Friedel–Crafts hydroalkylation: W. Zhuang, N. Gathergood, R. G. Hazell, K. A. Jørgensen, *J. Org. Chem.* **2001**, 66, 1009.
- [97] For an application in an asymmetric copper-catalyzed cyclopropanation, see: a) J. M. Fraile, J. I. García, M. A. Harmer, C. I. Herrerías, J. A. Mayoral, O. Reiser, H. Werner, *J. Mater. Chem.* **2002**, 12, 3290; b) J. M. Fraile, J. I. García, C. I. Herrerías, J. A. Mayoral, M. A. Harmer, *J. Catal.* **2004**, 221, 532.
- [98] a) S. Taylor, J. Gullick, P. McMorn, D. Bethell, P. C. Bulman Page, F. E. Hancock, F. King, G. J. Hutchings, *J. Chem. Soc. Perkin Trans. 2* **2001**, 1714; b) S. Taylor, J. Gullick, P. McMorn, D. Bethell, P. C. Bulman Page, F. E. Hancock, F. King, G. J. Hutchings, *J. Chem. Soc. Perkin Trans. 2* **2001**, 1724; c) D. Ryan, P. McMorn, D. Bethell, G. Hutchings, *Org. Biomol. Chem.* **2004**, 2, 3566.
- [99] Y. Wan, P. McMorn, F. E. Hancock, G. J. Hutchings, *Catal. Lett.* **2003**, 91, 145.
- [100] Y. Traa, D. M. Murphy, R. D. Farley, G. J. Hutchings, *Phys. Chem. Chem. Phys.* **2001**, 3, 1073.
- [101] W. J. Drury, D. Ferraris, C. Cox, B. Young, T. Lectka, *J. Am. Chem. Soc.* **1998**, 120, 11006.
- [102] a) H. Li, M. Eddaoudi, M. O'Keeffe, O. M. Yaghi, *Nature* **1999**, 402, 276; b) T. Sawaki, Y. Aoyama, *J. Am. Chem. Soc.* **1999**, 121, 4793; c) J. Heo, S.-Y. Kim, D. Whang, K. Kim, *Angew. Chem.* **1999**, 111, 675; *Angew. Chem. Int. Ed.* **1999**, 38, 641; d) X. Wang, K. Ding, *J. Am. Chem. Soc.* **2004**, 126, 10524; e) for a recent review, see: L.-X. Dai, *Angew. Chem.* **2004**, 116, 5846; *Angew. Chem. Int. Ed.* **2004**, 43, 5726.
- [103] M. Fujita, Y. J. Kwon, S. Washizu, K. Ogura, *J. Am. Chem. Soc.* **1994**, 116, 1151.
- [104] T. Sawaki, T. Dewa, Y. Aoyama, *J. Am. Chem. Soc.* **1998**, 120, 8539.
- [105] J. S. Seo, D. Whang, H. Lee, S. I. Jun, J. Oh, Y. J. Jeon, K. Kim, *Nature* **2000**, 404, 982.
- [106] a) S. Takizawa, H. Somei, D. Jayaprakash, H. Sasai, *Angew. Chem.* **2003**, 115, 5889; *Angew. Chem. Int. Ed.* **2003**, 42, 5711; b) H. Guo, X. Wang, K. Ding, *Tetrahedron Lett.* **2004**, 45, 2009; c) X. Wang, K. Ding, *Chem. Eur. J.* **2005**, 11, 4078.
- [107] X. Wang, L. Shi, M. Li, K. Ding, *Angew. Chem.* **2005**, 117, 6520; *Angew. Chem. Int. Ed.* **2005**, 44, 6362.
- [108] A. Hu, H. L. Ngo, W. Lin, *Angew. Chem.* **2003**, 115, 6182; *Angew. Chem. Int. Ed.* **2003**, 42, 6000.
- [109] a) T. Ohkuma, H. Ooka, T. Ikariya, R. Noyori, *J. Am. Chem. Soc.* **1995**, 117, 10417; b) H. Doucet, T. Ohkuma, K. Murata, T. Yokozawa, *Angew. Chem.* **1998**, 110, 1792; *Angew. Chem. Int. Ed.* **1998**, 37, 1703.
- [110] C.-D. Wu, A. Hu, L. Zhang, W. Lin, *J. Am. Chem. Soc.* **2005**, 127, 8940.
- [111] Y. Liang, Q. Jing, X. Li, L. Shi, K. Ding, *J. Am. Chem. Soc.* **2005**, 127, 7694.
- [112] a) M. Jacoby, *Chem. Eng. News* **2002**, 80(12), 43; b) A. Baiker, *Catal. Today* **2005**, 100, 159; c) C. F. McFadden, P. S. Cremer, A. J. Gellman, *Langmuir* **1996**, 12, 2483.
- [113] J. D. Horvath, A. J. Gellman, *J. Am. Chem. Soc.* **2001**, 123, 7953.
- [114] G. A. Attard, *J. Phys. Chem. B* **2001**, 105, 3158.
- [115] For an excellent review on the use of chiral modifiers in asymmetric hydrogenation reactions, see: M. Studer, H.-U. Blaser, C. Exner, *Adv. Synth. Catal.* **2003**, 345, 45.
- [116] General review: a) A. Baiker, H.-U. Blaser, in *Handbook of Heterogeneous Catalysis* (Eds.: G. Ertl, H. Knözinger, J. Weitkamp), VCH, Weinheim, **1997**; b) P. B. Wells, R. P. K. Wells in *Chiral Catalyst Immobilization and Recycling* (Eds.: D. E. De Vos, I. F. J. Vankelecom, P. A. Jacobs), Wiley-VCH, Weinheim, **2000**, p. 123; c) A. Baiker in *Chiral Catalyst Immobilization and Recycling* (Eds.: D. E. De Vos, I. F. J. Vankelecom, P. A. Jacobs), Wiley-VCH, Weinheim, **2000**, p. 155.
- [117] a) Y. Orito, S. Imai, S. Niwa, G. H. Nguyen, *J. Synth. Org. Chem. Jpn.* **1979**, 37, 173; b) Y. Orito, S. Imai, S. Niwa, *J. Chem. Soc. Jpn.* **1979**, 1118; c) Y. Orito, S. Imai, S. Niwa, *J. Chem. Soc. Jpn.* **1980**, 670; d) Y. Orito, S. Imai, S. Niwa, *J. Chem. Soc. Jpn.* **1982**, 137.
- [118] a) H.-U. Blaser, H. P. Jalett, J. Wiehl, *J. Mol. Catal.* **1991**, 68, 215; b) B. Török, K. Balazsik, M. Török, G. Szöllösi, M. Bartok, *Ultrason. Sonochem.* **2000**, 7, 151.
- [119] a) X. Zuo, H. Liu, D. Guo, X. Xang, *Tetrahedron* **1999**, 55, 7787; b) M. Sutyinski, K. Szöri, K. Felföldi, M. Bartok, *Catal. Commun.* **2002**, 3, 125; c) K. Balazsik, K. Szöri, K. Felföldi, B. Török, M. Bartok, *Chem. Commun.* **2000**, 555; for the hydrogenation of ketopantolactone with a spectacular substrate/modifier ratio of better 200000:1, see: d) M. Schürch, N. Künzle, T. Mallat, A. Baiker, *J. Catal.* **1998**, 176, 569; e) N. Künzle, A. Szabo, M. Schürch, G. Wang, T. Mallat, A. Baiker, *Chem. Commun.* **1998**, 1377.

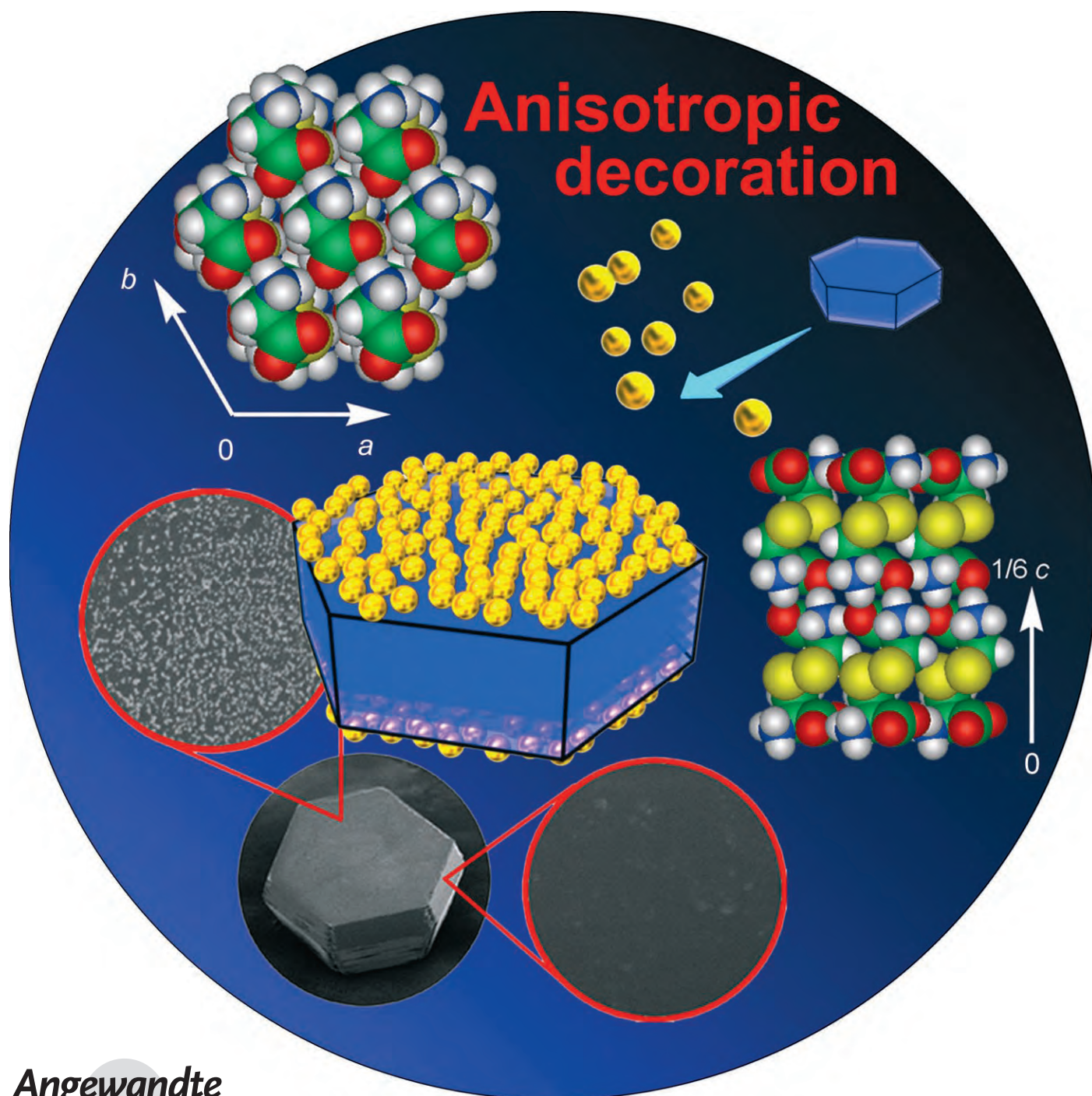
- [120] M. von Arx, T. Mallat, A. Baiker, *Chem. Eur. J.* **2002**, *8*, 1430, and references therein.
- [121] a) B. Török, K. Felföldi, K. Balazsik, M. Bartók, *Chem. Commun.* **1999**, 1275; b) M. Studer, S. Burkardt, H.-U. Blaser, *Chem. Commun.* **1999**, 1727.
- [122] M. Studer, H.-U. Blaser, S. Burkardt, *Adv. Synth. Catal.* **2002**, *344*, 511.
- [123] a) J. R. G. Perez, J. Malthete, J. Jacques, *C. R. Acad. Sci. Ser. II* **1985**, *300*, 169; b) K. Borszeky, T. Mallat, A. Baiker, *Tetrahedron: Asymmetry* **1997**, *8*, 3745; c) D. Ferri, T. Bürgi, A. Baiker, *J. Chem. Soc. Perkin Trans. 2* **2002**, 437.
- [124] Very recently, rhodium modifier systems giving high levels of enantioselectivity in the hydrogenation of C=O bonds were reported: a) W. Xiong, H. Ma, Y. Hong, H. Chen, X. Li, *Tetrahedron: Asymmetry* **2005**, *16*, 1449; b) R. Hess, F. Krummeich, T. Mallat, A. Baiker, *J. Mol. Catal. A* **2004**, *212*, 205; c) O. J. Sonderegger, G. M.-W. Ho, T. Bürgi, A. Baiker, *J. Catal.* **2005**, *230*, 499.
- [125] a) H. Bönemann, G. A. Braun, *Angew. Chem.* **1996**, *108*, 2120; *Angew. Chem. Int. Ed. Engl.* **1996**, *35*, 1992; b) H. Bönemann, G. A. Braun, *Chem. Eur. J.* **1997**, *3*, 1200.
- [126] a) H. U. Blaser, H. P. Jalett, D. M. Monti, J. T. Wehrli, *Appl. Catal.* **1989**, *52*, 19; b) J. T. Wehrli, A. Baiker, D. M. Monti, H. U. Blaser, *J. Mol. Catal.* **1989**, *49*, 195; c) J. T. Wehrli, A. Baiker, D. M. Monti, H. U. Blaser, *J. Mol. Catal.* **1990**, *61*, 207.
- [127] a) H. U. Blaser, H. P. Jalett, D. M. Monti, J. F. Reber, J. T. Wehrli in *Studies in Surface Science and Catalysis* (Eds.: M. Guisnet, J. Barrault, C. Bouchoule, D. Duprez, C. Monassier, G. Pérot), Elsevier, Amsterdam **1988**; b) M. Garland, H.-U. Blaser, *J. Am. Chem. Soc.* **1990**, *112*, 7048.
- [128] a) C. LeBlond, J. Wang, J. Liu, T. Andrews, Y.-K. Sun, *J. Am. Chem. Soc.* **1999**, *121*, 4920; b) J. Kubota, F. Zaera, *J. Am. Chem. Soc.* **2001**, *123*, 11115.
- [129] H.-U. Blaser, H. P. Jalett, D. M. Monti, A. Baiker, J. T. Wehrli, *Stud. Surf. Sci. Catal.* **1991**, *67*, 147.
- [130] A. Pfaltz, T. Heinz, *Top. Catal.* **1997**, *4*, 229.
- [131] a) E. Orglmeister, T. Mallat, A. Baiker, *J. Catal.* **2005**, *233*, 333; b) C. Exner, A. Pfaltz, M. Studer, H.-U. Blaser, *Adv. Catal.* **2003**, *345*, 1253; c) H.-U. Blaser, H. P. Jalett, W. Lottenbach, M. Studer, *J. Am. Chem. Soc.* **2000**, *122*, 12675; d) A. Lindholm, P. Mäki-Arvela, E. Toukonitty, T. A. Pakkanen, J. T. Hirvi, T. Salmi, D. Y. Murzin, R. Sjöholm, R. Leino, *J. Chem. Soc. Perkin Trans. 1* **2002**, 2605; e) I. Busygin, E. Toukonitty, R. Sillanpää, D. Yu. Murzin, R. Leiko, *Eur. J. Org. Chem.* **2005**, 2811.
- [132] a) M. Bartók, K. Felföldi, B. Török, T. Bartók, *Chem. Commun.* **1998**, 23, 2605; b) M. Bartók, K. Felföldi, G. Szöllösi, T. Bartók, *Catal. Lett.* **1999**, *61*, 1; c) M. Bartók, M. Sutyinszki, K. Felföldi, G. Szöllösi, *Chem. Commun.* **2002**, 1130; d) M. Bartók, M. Sutyinszki, K. Felföldi, *J. Catal.* **2003**, *220*, 207.
- [133] a) B. Minder, T. Mallat, A. Baiker, G. Wang, T. Heinz, A. Pfaltz, *J. Catal.* **1995**, *154*, 371; b) M. Schürch, T. Heinz, R. Aeschmann, T. Mallat, A. Pfaltz, A. Baiker, *J. Catal.* **1998**, *173*, 187; c) K. E. Simons, G. Wang, T. Heinz, T. Giger, T. Mallat, A. Pfaltz, A. Baiker, *Tetrahedron: Asymmetry* **1995**, *6*, 505; d) A. Solladié-Cavallo, C. Marsol, F. Garin, *Tetrahedron Lett.* **2002**, *43*, 4733; e) É. Sípós, A. Tungler, I. Bitter, M. Kubinyi, *J. Mol. Catal. A* **2002**, *186*, 187; f) C. Thorey, S. Bouquillon, A. Helimi, F. Henin, J. Muzart, *Eur. J. Org. Chem.* **2002**, *13*, 2151.
- [134] a) T. Heinz, G. Z. Wang, A. Pfaltz, B. Minder, M. Schürch, T. Mallat, A. Baiker, *J. Chem. Soc. Chem. Commun.* **1995**, 1421; b) B. Minder, M. Schürch, T. Mallat, A. Baiker, T. Heinz, A. Pfaltz, *J. Catal.* **1996**, *160*, 261; c) B. Minder, M. Schürch, T. Mallat, A. Baiker, *Catal. Lett.* **1995**, *31*, 143.
- [135] a) É. Sípós, A. Tungler, I. Bitter, *J. Mol. Catal. A* **2003**, *198*, 167; b) G. Szöllösi, C. Somlai, P. T. Szabó, M. Bartók, *J. Mol. Catal. A* **2001**, *170*, 165.
- [136] See, however: a) 1-naphthyl-1,2-ethandiol, a modifier without an amine function (30% ee): A. Marinas, T. Mallat, A. Baiker, *J. Catal.* **2004**, *221*, 666; b) an N-methylated cinchonidine derivative (45% ee) bearing no basic sp<sup>3</sup> nitrogen atom: E. Orglmeister, T. Mallat, A. Baiker, *J. Catal.* **2005**, *233*, 333.
- [137] a) O. Schwalm, B. Minder, J. Weber, A. Baiker, *Catal. Lett.* **1994**, *23*, 271; b) K. E. Simons, P. A. Meheux, S. P. Griffiths, I. M. Sutherland, P. Johnston, P. B. Wells, A. F. Carley, M. K. Rajumon, M. W. Roberts, A. Ibbotson, *Recl. Trav. Chim. Pays-Bas* **1994**, *113*, 465.
- [138] T. Bürgi, A. Baiker, *Acc. Chem. Res.* **2004**, *37*, 909.
- [139] J. L. Margitfalvi, M. Hegedus, E. Tfirst, *Tetrahedron: Asymmetry* **1996**, *7*, 571.
- [140] A. Baiker, *J. Mol. Catal. A* **2000**, *163*, 205.
- [141] R. L. Augustine, S. K. Tanielyan, L. K. Doyle, *Tetrahedron: Asymmetry* **1993**, *4*, 1803.
- [142] G. Vayner, K. N. Houk, Y.-K. Sun, *J. Am. Chem. Soc.* **2004**, *126*, 199.
- [143] a) Y. Izumi, M. Imaida, H. Fukawa, S. Akabori, *Bull. Chem. Soc. Jpn.* **1963**, *36*, 21; for reviews, see: b) A. Tai, T. Sagimura in *Chiral Catalyst Immobilization and Recycling* (Eds.: D. E. De Vos, I. F. J. Vankelecom, P. A. Jacobs), Wiley-VCH, Weinheim, **2000**, p. 173; c) T. Osawa, T. Harada, O. Takayasu, *Top. Catal.* **2000**, *13*, 155; see also: d) T. Heinz, PhD thesis, Universität Basel (Switzerland), **1997**, and references therein.
- [144] T. Sagimura, S. Nakagawa, A. Tai, *Bull. Chem. Soc. Jpn.* **2002**, *75*, 355.
- [145] A. Kai, K. Ito, T. Harada, *Bull. Chem. Soc. Jpn.* **1981**, *54*, 223.
- [146] T. Osawa, T. Harada, A. Tai, *J. Mol. Catal.* **1994**, *87*, 333.
- [147] R. Schmid, M. Scalone in *Comprehensive Asymmetric Catalysis* (Eds.: E. N. Jacobsen, H. Yamamoto, A. Pfaltz), Springer, Berlin, **1999**, p. 1439.
- [148] T. Harada, A. Tai, M. Yamamoto, H. Ozaki, Y. Izumi, *Stud. Surf. Sci. Catal.* **1981**, *7*, 364.
- [149] V. Humblot, S. Haq, C. Murny, W. A. Hofer, R. Raval, *J. Am. Chem. Soc.* **2002**, *124*, 503.
- [150] a) B. M. Choudary, M. L. Kantam, K. V. S. Ranganath, K. Mahendar, B. Sreedhar, *J. Am. Chem. Soc.* **2004**, *126*, 3396; b) B. M. Choudary, K. V. S. Ranganath, U. Pal, M. L. Kantam, B. Sreedhar, *J. Am. Chem. Soc.* **2005**, *127*, 13167.
- [151] a) B. List, *Org. Biomol. Chem.* **2005**, *3*, 719; b) P. I. Dalko, L. Moisan, *Angew. Chem.* **2004**, *116*, 5248; *Angew. Chem. Int. Ed.* **2004**, *43*, 5138; c) P. I. Dalko, L. Moisan, *Angew. Chem.* **2001**, *113*, 3840; *Angew. Chem. Int. Ed.* **2001**, *40*, 3726; d) A. Berkessel, H. Gröger, *Asymmetric Organocatalysis*, VCH, Weinheim, **2004**.
- [152] S. Akabori, S. Sakurai, Y. Izumi, Y. Fujii, *Nature* **1956**, *178*, 323. However, it is important to note that enantioselectivities were determined only after repeated crystallization of the products. Moreover, it was found that the results are not reproducible.<sup>[4c]</sup>
- [153] a) K. Tanaka, A. Mori, S. Inoue, *J. Org. Chem.* **1990**, *55*, 181; b) H. Danda, *Synlett* **1991**, 263; c) H. J. Kim, W. R. Jackson, *Tetrahedron: Asymmetry* **1994**, *5*, 1541; d) M. North, *Tetrahedron: Asymmetry* **2003**, *14*, 147; e) Y. Shvo, M. Gal, Y. Becker, A. Elgavi, *Tetrahedron: Asymmetry* **1996**, *7*, 911; f) E. F. Kogut, J. C. Thoen, M. A. Lipton, *J. Org. Chem.* **1998**, *63*, 4604; g) L. Xie, W. Hua, A. S. C. Chan, Y.-C. Leung, *Tetrahedron: Asymmetry* **1999**, *10*, 4715.
- [154] a) S. Inoue, *Adv. Polym. Sci.* **1976**, *21*, 78; b) K. Ueyanagi, S. Inoue, *Makromol. Chem.* **1977**, *178*, 235; c) T. Sugimoto, Y. Matsumura, S. Tanimoto, M. Okano, *J. Chem. Soc. Chem. Commun.* **1978**, 926; d) N. Baba, Y. Matsumura, S. Tanimoto, M. Okano, *Tetrahedron Lett.* **1978**, *19*, 4281.
- [155] For reviews on the Julia-Colonna epoxidation, see: a) C. Lauret, S. M. Roberts, *Aldrichimica Acta* **2002**, *35*, 47; b) M. J. Porter, J. Skidmore, *Chem. Commun.* **2000**, 1215; c) H. Gielen,

- Synlett* **1999**, 656; d) L. Pu, *Tetrahedron: Asymmetry* **1998**, 9, 1457.
- [156] S. Julià, J. Masana, J. C. Vega, *Angew. Chem.* **1980**, 92, 968; *Angew. Chem. Int. Ed. Engl.* **1980**, 19, 929, and references therein.
- [157] a) S. Julià, J. Guixer, J. Masana, J. Rocas, S. Colonna, R. Annuziata, H. Molinari, *J. Chem. Soc. Perkin Trans. 1* **1982**, 1317; b) S. Banfi, S. Colonna, H. Molinari, S. Julià, J. Guixer, *Tetrahedron* **1984**, 40, 5207.
- [158] a) P. A. Bentley, S. Bergeron, M. W. Cappi, D. E. Hibbs, M. B. Hursthouse, T. C. Nugent, R. Pulido, S. M. Roberts, L. E. Wu, *Chem. Commun.* **1997**, 739; b) M. W. Cappi, W.-P. Chen, R. W. Flood, Y.-W. Liao, S. M. Roberts, J. Skidmore, J. A. Smith, N. M. Williamson, *Chem. Commun.* **1998**, 1159.
- [159] S. Itsuno, M. Sakakura, K. Ito, *J. Org. Chem.* **1990**, 55, 6047.
- [160] a) H. Ihara, N. Nakonishi, T. Sagawa, C. Hirayama, T. Sakurai, T. Kinoshi, Y. Tsujita, *Chem. Lett.* **1998**, 963; b) T. Geller, S. M. Roberts, *J. Chem. Soc. Perkin Trans. 1* **1999**, 1397; c) A. Dhanda, K.-H. Drauz, T. P. Geller, S. M. Roberts, *Chirality* **2000**, 12, 313; d) H. Yi, G. Zou, Q. Li, Q. Chen, J. Tang, M. He, *Tetrahedron Lett.* **2005**, 46, 5665.
- [161] a) J. R. Flisak, K. J. Gombatz, M. M. Holmes, A. A. Jarmas, I. Lantos, W. L. Mendelson, V. J. Novack, J. J. Remich, L. Snyder, *J. Org. Chem.* **1993**, 58, 6247; b) B. M. Adger, J. V. Barkley, S. Bergeron, M. W. Cappi, B. E. Flowerdew, M. P. Jackson, R. McCague, T. C. Nugent, S. M. Roberts, *J. Chem. Soc. Perkin Trans. 1* **1997**, 3501.
- [162] a) A. Berkessel, N. Gasch, K. Glaubitz, C. Koch, *Org. Lett.* **2001**, 3, 3839; see also b) R. Takagi, T. Manabe, A. Shiraki, A. Yoneshige, Y. Hiraga, S. Kojima, K. Ohkata, *Bull. Chem. Soc. Jpn.* **2000**, 73, 2115.
- [163] For an insightful review on substrate-directable reactions, see: A. H. Hoveyda, D. A. Evans, G. C. Fu, *Chem. Rev.* **1993**, 93, 1307.
- [164] a) K. Kogami, J. Kumanotani, *Bull. Chem. Soc. Jpn.* **1968**, 41, 2530; b) N. Ravasio, M. Antenori, F. Babudri, M. Gargano, *Stud. Surf. Sci. Catal.* **1997**, 108, 625; c) P. Mäki-Arvela, N. Kumar, V. Nieminen, R. Sjöholm, T. Salmi, D. Y. Murzin, *J. Catal.* **2004**, 225, 155; d) J. Tateiwa, A. Kimura, M. Takasuka, S. Uemura, *J. Chem. Soc. Perkin Trans. 1* **1997**, 2169; e) K. Arata, C. Matsuura, *Chem. Lett.* **1989**, 1788; f) Z. Yongzhong, N. Yuntong, S. Jaenicke, G.-K. Chuah, *J. Catal.* **2005**, 229, 404.
- [165] a) L. Palombi, F. Bonadies, A. Scettri, *Tetrahedron* **1997**, 53, 11369; b) W. Adam, A. Corma, T. I. Reddy, M. Renz, *J. Org. Chem.* **1997**, 62, 3631; c) W. Adam, A. Corma, A. Martínez, C. M. Mitchell, T. I. Reddy, M. Renz, A. K. Smerz, *J. Mol. Catal. A* **1997**, 117, 357; d) M. Dusi, T. Mallat, A. Baiker, *J. Mol. Catal. A* **1999**, 138, 15; e) M. Guidotti, L. Conti, A. Fusi, N. Ravasio, R. Psaro, *J. Mol. Catal. A* **2002**, 182–183, 151; f) C.-P. Du, Z.-K. Li, X.-M. Wen, J. Wu, X.-Q. Yu, M. Yang, R.-G. Xie, *J. Mol. Catal. A* **2004**, 216, 7; g) A. Massa, A. Scettri, *Synlett* **2000**, 1348.
- [166] For recent reviews on diastereoselective heterogeneous hydrogenations, see: a) A. Tungler, G. Fogassy, *J. Mol. Catal. A* **2001**, 173, 231; b) A. Tungler, E. Sípós, V. Háda, *ARKIVOC* **2004**, 223; c) M. Besson, C. Pinel, *Top. Catal.* **1998**, 5, 25; d) P. Kukula, R. Prins, *Top. Catal.* **2003**, 25, 29; e) M. Besson, C. Pinel, *Top. Catal.* **2003**, 25, 43; f) D. E. De Vos, M. De Bruyn, V. I. Parvulesco, F. G. Cocu, P. A. Jacobs in *Chiral Catalyst Immobilization and Recycling* (Eds.: D. E. De Vos, I. F. J. Vankelecom, P. A. Jacobs), Wiley-VCH, Weinheim, **2000**, p. 283; for books on heterogeneous hydrogenation, see: g) S. Nishimura, *Handbook of Heterogeneous Catalytic Hydrogenation for Organic Synthesis*, Wiley, New York, **2001**; h) P. N. Rylander, *Hydrogenation Methods*, Academic Press, New York, **1990**.
- [167] a) R. Noyori, *Angew. Chem.* **2002**, 114, 2108; *Angew. Chem. Int. Ed.* **2002**, 41, 2008; b) T. Ohkuma, M. Kitama, R. Noyori in *Catalytic Asymmetric Synthesis* (Ed.: I. Ojima), VCH, Weinheim, **2000**, p. 1; c) H.-U. Blaser, C. Malan, B. Pugin, F. Spindler, H. Steiner, M. Studer, *Adv. Synth. Catal.* **2003**, 345, 103; d) W. S. Knowles, *Angew. Chem.* **2002**, 114, 2096; *Angew. Chem. Int. Ed.* **2002**, 41, 1998.
- [168] a) M. S. Pavlin, US patent 4310714, **1982**; b) L. A. Canova, US patent 4018842, **1977**.
- [169] R. K. Sehgal, R. U. Koenigsberger, T. J. Howard, *J. Org. Chem.* **1975**, 40, 3037.
- [170] H. Thompson, E. McPherson, B. Lences, *J. Org. Chem.* **1976**, 41, 2903.
- [171] J. Sheehan, R. Chandler, *J. Am. Chem. Soc.* **1961**, 83, 4795.
- [172] a) I. N. Lisichkina, A. I. Vinogradova, B. O. Tserevitinov, M. B. Saporovskaya, V. K. Latov, V. M. Belikov, *Tetrahedron: Asymmetry* **1990**, 1, 567; b) U. Schmidt, S. Kumpf, K. Neumann, *J. Chem. Soc. Chem. Commun.* **1994**, 1915.
- [173] a) B. Bycroft, G. Lee, *J. Chem. Soc. Chem. Commun.* **1977**, 988; b) H. Poisel, U. Schmidt, *Chem. Ber.* **1973**, 106, 3408; c) N. Izumiya, S. Lee, T. Kanmera, H. Aoyagi, *J. Am. Chem. Soc.* **1977**, 99, 8346; d) P. Leeming, F. R. Fronczek, D. J. Ager, S. A. Laneman, *Top. Catal.* **2000**, 13, 175.
- [174] a) N. Ikemoto, D. M. Tellers, S. D. Dreher, J. Liu, A. Huang, N. R. Rivera, E. Njolito, Y. Hsiao, J. C. McWilliams, J. M. Williams, J. D. Armstrong III, Y. Sun, D. J. Mathre, E. J. J. Grabowski, R. D. Tiller, *J. Am. Chem. Soc.* **2004**, 126, 3048; additional syntheses of  $\beta$ -amino acid derivatives by heterogeneous hydrogenation: b) J. H. Cohen, A. F. Abdel-Magid, H. R. Almond, C. A. Maryanoff, *Tetrahedron Lett.* **2002**, 43, 1977; c) M. Furukawa, T. Okawara, Y. Noguchi, Y. Terawaki, *Chem. Pharm. Bull.* **1979**, 27, 2223; d) S. Jolindon, T. Meul, U.S. patent 4585887, **1986**; e) D. G. Melillo, R. J. Cvetovich, K. M. Ryan, M. Slettinger, *J. Org. Chem.* **1986**, 51, 1498.
- [175] M. Prashad, Y. Liu, H.-Y. Kim, O. Repic, T. J. Blacklock, *Tetrahedron: Asymmetry* **1999**, 10, 3479.
- [176] For a short review on successful asymmetric hydrogenations of heteroaromatic substrates, see: F. Glorius, *Org. Biomol. Chem.* **2005**, 3, 4171.
- [177] a) F. Glorius, N. Spielkamp, S. Holle, R. Goddard, C. W. Lehmann, *Angew. Chem.* **2004**, 116, 2910; *Angew. Chem. Int. Ed.* **2004**, 43, 2850; b) for an application in the synthesis of natural products, see: B. Scheiper, F. Glorius, A. Leitner, A. Fürstner, *Proc. Natl. Acad. Sci. USA* **2004**, 101, 11960.
- [178] a) K. Nasar, F. Fache, M. Lemaire, J. C. Béziat, M. Besson, P. Gallezot, *J. Mol. Catal.* **1994**, 87, 107; b) M. Besson, B. Blanc, M. Champelet, P. Gallezot, K. Nasar, C. Pinel, *J. Catal.* **1997**, 170, 254; c) M. Besson, P. Gallezot, S. Neto, C. Pinel, *Chem. Commun.* **1998**, 1431; d) L. A. M. M. Barbosa, P. Sautet, *J. Catal.* **2003**, 217, 23; e) V. S. Ranade, G. Consiglio, R. Prins, *Catal. Lett.* **1999**, 58, 71; f) V. S. Ranade, R. Prins, *J. Catal.* **1999**, 185, 479.
- [179] For an up-to-date review on chiral auxiliaries, see Y. Gnás, F. Glorius, *Synthesis* **2006**, 1899.
- [180] Review: a) M. E. Davis, A. Katz, W. R. Ahmad, *Chem. Mater.* **1996**, 8, 1820; b) G. Wulff, *Angew. Chem.* **1995**, 107, 1958; *Angew. Chem. Int. Ed. Engl.* **1995**, 34, 1812; for a recent report on molecular imprinting resulting in the formation of a synthetic transaminase, see: c) J. Svenson, N. Zheng, I. A. Nicholls, *J. Am. Chem. Soc.* **2004**, 126, 8554, and references therein.



# Anisotropic Decoration of Gold Nanoparticles onto Specific Crystal Faces of Organic Single Crystals\*\*

Yuzo Fujiki, Nami Tokunaga, Seiji Shinkai, and Kazuki Sada\*





Anisotropy, various polyhedral shapes with well-defined faces, and a wide range of sizes from nano- to millimeter are characteristic features of organic single crystals. The anisotropy is attributed to the anisotropic packing of organic molecules in the crystalline state, and each face has different surface properties. Therefore, organic single crystals should play a key role in making multicomponent composites through their face-selective association with other materials. Anisotropic adhesion of organic single crystals by other organic molecules is the first step toward the preparation of such composites and has been studied mainly from the viewpoint of crystal growth and dissolution.<sup>[1]</sup> More recently, face-selective dyeing of inorganic single crystals by dye molecules in solution has been documented<sup>[2]</sup> and controlled aggregation of inorganic mesocrystals has been discussed for the formation of inorganic superstructures as models of biomineralization.<sup>[3–5]</sup>

Gold nanoparticles are a fascinating material as a result of their unique optical (plasmon band), electronic, catalytic, and supramolecular properties, as well as their wide applications for nanotechnology and biotechnology.<sup>[6]</sup> Composite materials with one- or two-dimensional arrays of gold nanoparticles have attracted considerable interest in a bottom-up approach for nanometer-sized devices. They are generally prepared by treatment of gold nanoparticles with inorganic substrates,<sup>[7]</sup> polymer surfaces,<sup>[8]</sup> and single atomic monolayers,<sup>[9]</sup> as examples. However, utility of organic single crystals remains in its infancy.<sup>[10]</sup> Only recently, Moore and co-workers reported inorganic microcrystals coated with gold nanoparticles developed by crystal-lattice-mediated self-assembly (CLAMS).<sup>[11]</sup> In this composite material, the whole surfaces were covered by gold nanoparticles as a result of the isotropic nature of the inorganic crystals. Therefore, anisotropic coating of gold nanoparticles onto the selective faces has not yet been reported. Here we demonstrate the first example of a composite crystalline material of organic single crystals with gold nanoparticles and anisotropic face-selective adhesion of gold nanoparticles onto the crystal faces of the organic crystals.

Single-crystal transparent hexagonal prisms of L-cystine (**1**; Figure 1) were immersed in a solution of gold nanoparticles at room temperature by both a batch method and a mounted method. After two hours, the crystals were stained

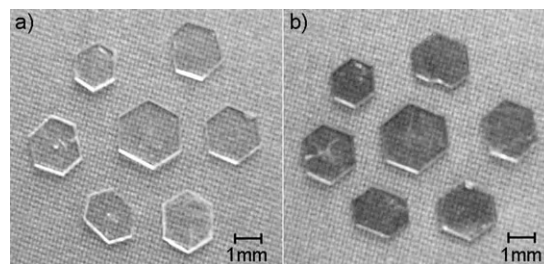


**Figure 1.** Hexagonal single crystals of L-cystine (**1**) before (a) and after (b) immersion in a solution of gold nanoparticles.

purple although their hexahedral shape remained unchanged. After washing with water, composite crystals of L-cystine decorated with gold nanoparticles were obtained by both methods. Under the microscope, all the surfaces of the crystals appeared slightly rough and a few small hexagonal crystals were deposited on the hexagonal faces. The two hexagonal faces of the hexagonal prism were stained purple and all the six rectangular side surfaces remained colorless. This result was confirmed by the absorption spectra, which were dependent on the crystal surfaces. As shown in Figure 2,

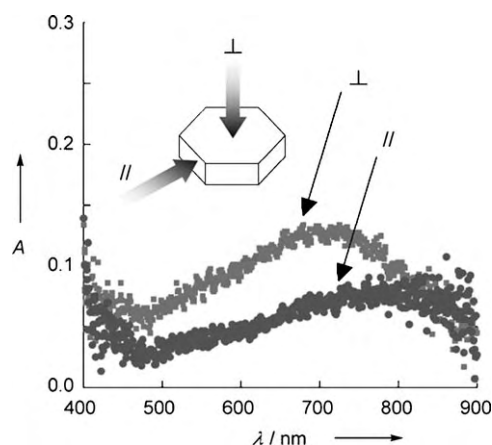


**Figure 2.** UV/Vis absorption spectra of a single crystal of **1** decorated with gold nanoparticles, showing the absorption perpendicular (⊥) and parallel (||) to the hexagonal face.

the absorption spectrum from the direction perpendicular to the hexagonal face revealed an absorption maximum around 700 nm assignable to the surface plasmon band of the aggregated gold nanoparticles,<sup>[12]</sup> whereas that from the parallel direction displayed no apparent absorption maximum. The anisotropy of the absorption spectra was attributed to the adhesion of the gold nanoparticles. This result indicates that the gold nanoparticles were deposited selectively on the hexagonal faces of **1**.

To investigate the face-selective decoration of the gold nanoparticles by electron microscopy, we carried out the decorating experiments on micrometer-sized crystals. The smaller crystals were prepared by a similar method and were analyzed by scanning electron microscopy (SEM) and atomic force microscopy (AFM). Figure 3 shows the SEM images of the hexagonal micrometer-sized single crystals, which

[\*] Y. Fujiki, N. Tokunaga, Prof. Dr. S. Shinkai, Dr. K. Sada  
Department of Chemistry and Biochemistry  
Graduate School of Engineering, Kyushu University  
744 Motoooka, Nishi-ku Fukuoka, 819-039 (Japan)  
Fax: (+81) 928-022-820  
E-mail: sadatcm@mbox.nc.kyushu-u.ac.jp

[\*\*] Financial support for this research was provided by the Ministry of Education, Culture, Sports, Science, and Technology, Japan (MEXT), and the 21st century COE program (to K.S. and S.S.). We thank Prof. M. Irie, Dr. K. Matsuda, and Mr. H. Muto for the measurement of UV/Vis absorption spectra of the single crystal, Prof. Y. Hisaeda, Dr. H. Shimakoshi, and Dr. I. Aritome for X-ray diffraction measurements, and Prof. N. Kimizuka, Dr. K. Kuroiwa, and Mr. H. Matsukizono for XPS measurements. K.S. is especially grateful to Keyence Corporation for use of a 3D real surface view microscope.

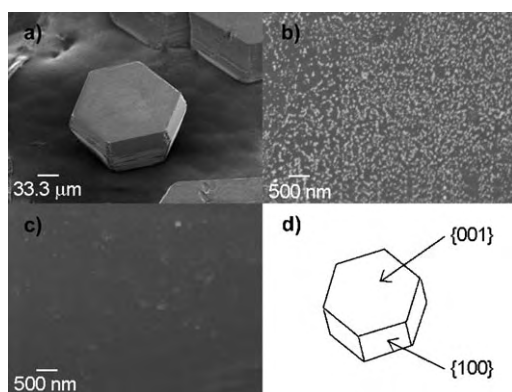


**Figure 3.** SEM images of a) the hexagonal crystals decorated by gold nanoparticles, b) the {001} face, and c) the {100} face. d) A drawing of the orientation of the crystallographic axes deduced from X-ray crystallographic studies.

revealed well-defined shapes with sharp edges. The crystal faces could be easily assigned by the similar shape of the micrometer-sized crystals to those of the millimeter-sized crystals. Interestingly, deposition of the nanoparticles was observed only on the hexagonal surfaces while the rectangular faces remained smooth. The diameters of the nanoparticles were the same magnitude as those of the added gold nanoparticles. Moreover, the AFM image (Figure 4) of the

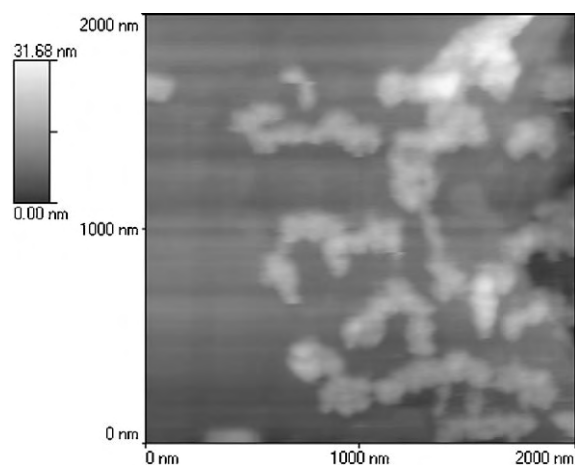


**Figure 4.** AFM image of the {001} face of the hexagonal crystal decorated by gold nanoparticles.

hexagonal faces illustrated aggregation of the smaller nanoparticles on the hexagonal surface. X-ray photoelectron spectroscopy (XPS) data of the single crystals indicated the presence of Au(4f) on the colored crystals of **1**. These results indicate that the hexagonal faces were selectively decorated with gold nanoparticles. The side rectangular faces were intact even in the solution of gold nanoparticles.

The cell parameters and the Miller indices of the crystal faces of the hexagonal single crystals were determined by X-ray diffraction studies. The hexagonal crystals revealed the same cell parameters as those of the previously reported example.<sup>[13]</sup> The hexagonal faces were assigned to the crystallographic {001} or {00 $\bar{1}$ } faces and the rectangular

faces were assigned to {100} and {010} faces, and so on. This result indicates that the gold nanoparticles selectively interacted with the {001} and {00 $\bar{1}$ } faces. The molecular packing diagrams of **1** are shown in Figure 5.<sup>[13]</sup> In the crystal structure,

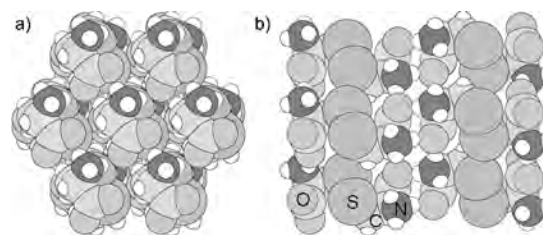


**Figure 5.** Crystal packing diagram<sup>[11]</sup> of the hexagonal form of **1**: a) the {001} face viewed from the crystallographic *c* axis and b) the {100} face viewed from the crystallographic *a* axis. H atoms are shown as small white spheres.

the molecules **1** are arranged in layered structures by the two-dimensional hydrogen-bonding network between primary ammonium cations and carboxylate anions. The hydrogen-bonding network runs parallel to the hexagonal faces, and the zwitterionic groups are exposed on the surface of the {001} or {00 $\bar{1}$ } hexagonal faces. They have the potential to interact with gold nanoparticles by an electrostatic interaction. On the other hand, the rectangular faces are constructed by the alternative stacking of the hydrophobic disulfide layers and the hydrophilic zwitterionic layers, with a periodic distance of about 9 Å. Therefore, the gold nanoparticles were attached selectively on the surfaces of the {001} and {00 $\bar{1}$ } faces as a result of the higher density of polar residues on the hexagonal faces than on the rectangular ones.

In conclusion, we prepared a composite crystalline material containing gold nanoparticles and organic crystals of L-cystine (**1**). The anisotropic decoration that arises as a result of different functional groups on the crystal faces should lead to further decoration of other materials by other intermolecular interactions, which might induce anisotropic aggregation of the single crystals by the attractive or repulsive interaction between the uncoated or coated faces.<sup>[3]</sup> As the surfaces of organic single crystals should be more varied than those of inorganic ones and partially controllable by recent advances in the crystal engineering of organic molecules,<sup>[14]</sup> a wide variety of composite materials may be prepared by organic crystals as a nucleus. Moreover, the wide variations in the shapes and sizes of the organic crystals should provide various polyhedral composite materials decorated by nanoparticles.<sup>[11]</sup> Details of the anisotropic adhesion onto the {001} or {00 $\bar{1}$ } faces and screening of multicomponent composite materials from organic crystals and nanoparticles are currently under investigation.

## Experimental Section

**Materials:** Single crystals of L-cystine (**1**) were prepared by recrystallization from 0.5% hydrochloric acid solution. Single-crystal transparent hexagonal prisms of **1** were deposited from the solution by

cooling to room temperature. The sizes of the single crystals were in the range of a few micrometers to 2 mm in length.

General procedure of the batch method: Several single crystals of **1** were immersed in a solution of gold nanoparticles (1.0 mL, diameter 20 Å; BB International) at room temperature. After immersion for two hours, the crystals were collected by filtration or isolated using forceps and washed with water.

General procedure of the mounted method: A single crystal of **1** was mounted in a glass capillary such that the hexagonal faces were parallel to the side walls of the capillary. Then the capillary containing the mounted crystal was placed in a solution of the gold nanoparticles such that the hexagonal faces were vertical, eliminating the effect of gravity, and immersed for two hours. The mounted crystal was then taken out from the solution and washed with water.

Received: April 13, 2006

Published online: June 23, 2006

**Keywords:** amino acids · crystal engineering · gold · nanostructures · organic–inorganic hybrid composites

Hensel, A. Godt, R. Popovitz-Biro, H. Cohen, T.-R. Jensen, K. Kjaer, I. Weissbuch, E. Lifshitz, M. Lahav, *Chem. Eur. J.* **2002**, *8*, 1413–1423; A. Samokhvalov, R. W. Gurney, M. Lahav, R. Naaman, *J. Phys. Chem. B* **2002**, *106*, 9070–9078; A. Samokhvalov, R. W. Gurney, M. Lahav, S. Cohen, H. Cohen, R. Naaman, *J. Phys. Chem. B* **2003**, *107*, 4245–4252.

[11] M. Murugesan, D. Cunningham, J.-L. Martinez-Albertos, R. M. Vrcelj, B. D. Moore, *Chem. Commun.* **2005**, 2677–2679.

[12] T. Okamoto, I. Yamaguchi *J. Phys. Chem. B* **2003**, *107*, 10321–10324.

[13] S. Dahaoui, V. Pichon-Pesme, J. A. K. Howard, C. Lecomte, *J. Phys. Chem. A* **1999**, *103*, 6240–6250.

[14] G. R. Desiraju, *Crystal Engineering: The Design of Organic Solids*, Elsevier, Amsterdam, **1989**; G. R. Desiraju, *Angew. Chem.* **1995**, *107*, 2541–2558; *Angew. Chem. Int. Ed. Engl.* **1995**, *34*, 2311–2327; M. W. Hosseini, *Acc. Chem. Res.* **2005**, *38*, 313–323; D. Braga, L. Brammer, N. R. Champness, *CrystEngComm* **2005**, *7*, 1–19.

- [1] L. Addadi, Z. Berkovitch-Yellin, I. Weissbuch, J.-v. Mil, L.-J. W. Shimon, M. Lahav, L. Leiserowitz, *Angew. Chem.* **1985**, *97*, 476–496; *Angew. Chem. Int. Ed. Engl.* **1985**, *24*, 466–485; I. Weissbuch, R. Popovitz-Biro, M. Lahav, L. Leiserowitz, *Acta Crystallogr. Sect. B* **1995**, *51*, 115–148; I. Weissbuch, M. Lahav, L. Leiserowitz, *Cryst. Growth Des.* **2003**, *3*, 125–150.
- [2] B. Kahr, R. W. Gurney, *Chem. Rev.* **2001**, *101*, 893–951.
- [3] H. Coelfen, M. Antonietti, *Angew. Chem.* **2005**, *117*, 5714–5730; *Angew. Chem. Int. Ed.* **2005**, *44*, 5576–5591.
- [4] For adhesion of dyes, see: J. B. Benedict, P. M. Wallace, P. J. Reid, S.-H. Jang, B. Kahr, *Adv. Mater.* **2003**, *15*, 1068–1070; A. Barbon, M. Bellinazzi, J. B. Benedict, M. Brustolon, S. D. Fleming, S.-H. Jang, B. Kahr, A. L. Rohl, *Angew. Chem.* **2004**, *116*, 5442–5445; *Angew. Chem. Int. Ed.* **2004**, *43*, 5328–5331.
- [5] For adhesion of proteins, see: L. Addadi, S. Weiner, *Proc. Natl. Acad. Sci. USA* **1985**, *82*, 4110–4114; R. Bromberg, N. Kessler, L. Addadi, *J. Cryst. Growth* **1998**, *193*, 656–664.
- [6] For recent reviews on gold nanoparticles, see: a) M.-C. Daniel, D. Astruc, *Chem. Rev.* **2004**, *104*, 293–346; b) T. Teranishi, *C. R. Chim.* **2003**, *6*, 979–987; c) S. Link, M. A. El-Sayed, *Int. Rev. Phys. Chem.* **2000**, *19*, 409–453.
- [7] K. Murakoshi, Y. Nakato, *Adv. Mater.* **2000**, *12*, 791–795; K. Mougin, H. Haidara, G. Castelein, *Colloids Surf. A* **2001**, *193*, 231–237; T. Teranishi, S. Hasegawa, T. Shimizu, M. Miyake, *Adv. Mater.* **2001**, *13*, 1699–1701; T. Teranishi, A. Sugawara, T. Shimizu, M. Miyake, *J. Am. Chem. Soc.* **2002**, *124*, 4210–4211; L. Bardotti, B. Prevel, P. Jensen, M. Treilleux, P. Melinon, A. Perez, J. Gierak, G. Faini, D. Mailly, *Appl. Surf. Sci.* **2002**, *191*, 205–210; T. Shimizu, T. Teranishi, S. Hasegawa, M. Miyake, *J. Phys. Chem. B* **2003**, *107*, 2719–2724.
- [8] R. S. Henhar, T. B. Norstern, V. M. Rotello, *Adv. Mater.* **2005**, *17*, 657–669.
- [9] T. Yonezawa, S.-y. Onoue, T. Kunitake, *Adv. Mater.* **1998**, *10*, 414–416; T. Yonezawa, H. Matsune, T. Kunitake, *Chem. Mater.* **1999**, *11*, 33–35; T. T. Taton, R. C. Mucic, C. A. Mirkin, R. R. Letsinger, *J. Am. Chem. Soc.* **2000**, *122*, 6305–6306; H. X. He, H. Zhang, Q. G. Li, T. Zhu, S. F. Y. Li, Z. F. Liu, *Langmuir* **2000**, *16*, 3846–3851; A. C. Templeton, F. P. Zamborini, W. P. Wuelfing, R. W. Murray, *Langmuir* **2000**, *16*, 6682; W. L. Chan, L. Yu, *Langmuir* **2002**, *18*, 311–313; L. Nagle, D. Ryan, S. Cobbe, D. Fitzmaurice, *Nano Lett.* **2003**, *3*, 51–53.
- [10] S. Guo, L. Konopny, R. Popovitz-Biro, H. Cohen, H. Porteanu, E. Lifshitz, M. Lahav, *J. Am. Chem. Soc.* **1999**, *121*, 9589–9598; L. Konopny, M. Berfeld, R. Popovitz-Biro, I. Weissbuch, L. Leiserowitz, M. Lahav, *Adv. Mater.* **2001**, *13*, 580–584; V.

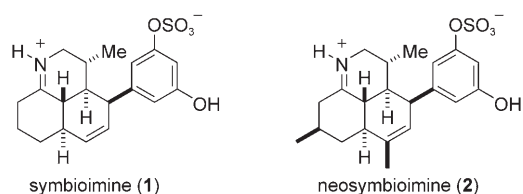
Cycloaddition

DOI: 10.1002/anie.200601418

Total Synthesis of (±)-Symbioimine\*\*

Georgy N. Varseev and Martin E. Maier\*

Symbioimine (**1**) is a novel tricyclic iminium alkaloid that was recently isolated from the symbiotic marine dinoflagellate *Symbiodinium* sp.<sup>[1]</sup> This rather unusual compound occurs in nature as an inner salt of an imine and an aryl sulphuric acid (Scheme 1). Such zwitterionic compounds are very rare,<sup>[2,3]</sup> and the total synthesis of **1** certainly poses a challenging task.



**Scheme 1.** Structures of the iminium alkaloids symbioimine (**1**) and neosymbioimine (**2**).

[\*] G. N. Varseev, Prof. Dr. M. E. Maier  
Institut für Organische Chemie  
Universität Tübingen  
Auf der Morgenstelle 18, 72076 Tübingen (Germany)  
Fax: (+49) 7071-295-137  
E-mail: martin.e.maier@uni-tuebingen.de

[\*\*] Financial support from the Deutsche Forschungsgemeinschaft and the Fonds der Chemischen Industrie is gratefully acknowledged. We thank Dr. Cäcilia Maichle-Mössmer for the X-ray structures and Graeme Nicholson for measuring the high-resolution mass spectra.

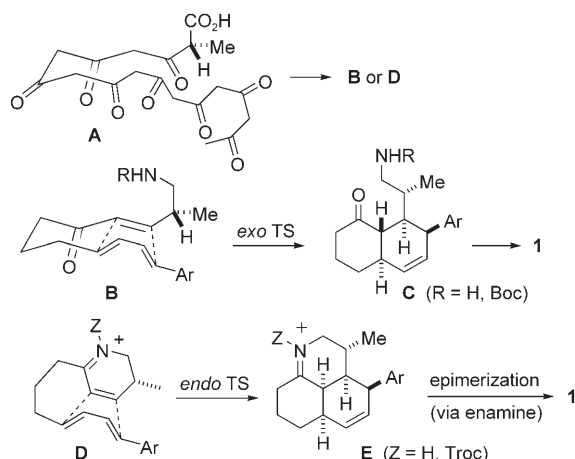


Supporting information for this article is available on the WWW under <http://www.angewandte.org> or from the author.



A related compound is the amphoteric neosymbioimine (**2**).<sup>[4]</sup> Besides its unique structural features, the biological activity of **1** is noteworthy as well: it inhibits the differentiation of progenitor cells (RAW264) into mature osteoclasts with  $EC_{50} = 44 \text{ mg mL}^{-1}$  ( $116 \text{ }\mu\text{M}$ ). Therefore, **1** might show the way to a new lead structure in the search for drugs directed at the treatment of osteoporosis. In addition, **1** significantly reduces cyclooxygenase-2 (COX-2) activity at  $10 \text{ }\mu\text{M}$ .<sup>[3]</sup>

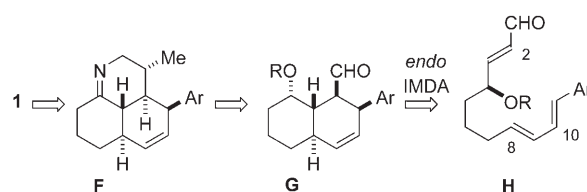
Most likely **1** is constructed through the polyketide pathway, as illustrated with structure **A**, which consists of eight acetate and one propionate groups. The key step in the biosynthesis of **1** might involve an intramolecular Diels–Alder (IMDA) reaction,<sup>[5]</sup> either of a trienone via an *exo* transition state of type **B** followed by cyclization to an imine (Scheme 2). Alternatively, an *endo* IMDA reaction of a



**Scheme 2.** Model reactions for biosynthetic key steps towards **1**. Boc = *tert*-butoxycarbonyl, Troc = trichloroethoxycarbonyl, TS = transition state.

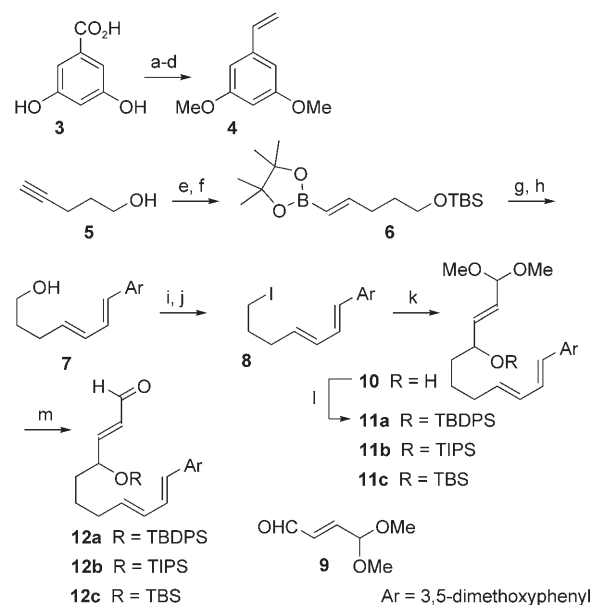
dihydropyridinium cation (compare with transition state **D**) followed by epimerization of the cycloadduct via an enamine might be operative.<sup>[4]</sup> There is support for the latter mode from a model study by Snider and Che,<sup>[6,7]</sup> who prepared desulfodeoxysymbioimine through an IMDA reaction of a 2,3-dihydropyridinium cation (Scheme 2; Z = Troc, Ar = Ph). While both routes seem attractive and possible, one should note that the orbital overlap is not ideal as large and small coefficients at the termini do not really match. In fact, we found in preliminary studies that trienone **A** (Scheme 2; R = Boc, Ar = 3,5-dimethoxyphenyl) did not undergo any Diels–Alder reaction, even after heating the substrate in a sealed tube (xylene,  $180^\circ\text{C}$ ) for 24 h. Under these conditions, slow decomposition of the substrate was observed.

We reasoned that positioning an electron-withdrawing group on the other side of the double bond should allow for a more facile IMDA reaction (Scheme 3).<sup>[8]</sup> Some literature precedence indicates that this approach should be feasible.<sup>[9]</sup> However, a solution for extension of the aldehyde function in the cycloadduct **G** combined with a diastereoselective introduction of the methyl group would have to be found. Herein, we present the realization of these goals.



**Scheme 3.** Retrosynthetic plan for the synthesis of **1**.

As an initial milestone, we targeted an efficient and large scale synthesis of (*E,E,E*)-undeca-2,8,10-trienals **12** (structure **H**). A key step of this synthesis is the preparation of the 1-aryl-1,3-*E,E*-diene moiety, which might be accessible through a palladium-catalyzed Stille or Suzuki coupling. *E*-Vinyl halide building blocks are required for both methods. However, all attempts to prepare suitable Stille or Suzuki precursors were more or less unsuccessful. Therefore, we turned to the palladium-catalyzed oxygen-promoted Heck-type coupling of alkenes with vinyl boronates.<sup>[10,11]</sup> Accordingly, the styrene<sup>[12–14]</sup> **4** and the vinyl boronate<sup>[15]</sup> **6** were prepared by standard procedures (Scheme 4). Under the reported reaction conditions (5 mol %  $\text{Pd}(\text{OAc})_2$ , dimethylamine (DMA),  $23^\circ\text{C}$ , slow addition of **6**), we got only 30% of the coupling product. We significantly improved the yield for

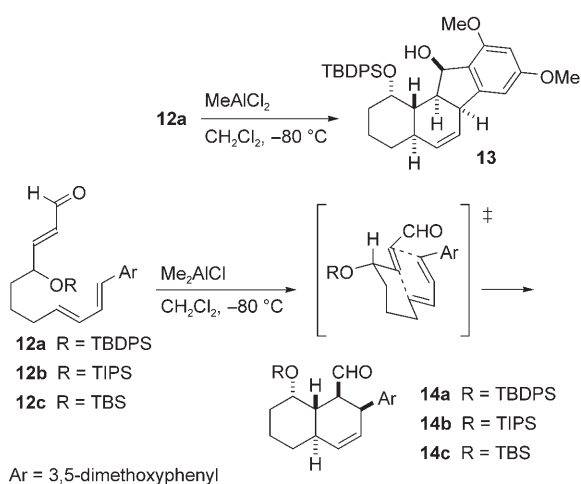


**Scheme 4.** Synthesis of the Diels–Alder substrates **12**. a)  $(\text{CH}_3\text{O})_2\text{SO}_2$  (3.5 equiv),  $\text{K}_2\text{CO}_3$ , acetone, reflux, 4 h (96%); b)  $\text{NaBH}_4$  (5 equiv), DME, MeOH, reflux, 1 h (99%); c)  $\text{CrO}_3/\text{pyridine}$  (1.2 equiv),  $\text{CH}_2\text{Cl}_2$ , RT, 24 h (81%); d)  $\text{Ph}_3\text{PCH}_3^+\text{Br}^-$  (1.2 equiv),  $\text{KOtBu}$  (1.4 equiv), THF,  $-65^\circ\text{C}$  to RT (96%); e) TBSCl, imidazole,  $\text{CH}_2\text{Cl}_2$ , RT, 24 h (99%); f) catechol borane (1.1 equiv),  $70^\circ\text{C}$ , 12 h, then pinacol (1.2 equiv),  $23^\circ\text{C}$ , 3 h (85%); g) **4** (2 equiv),  $\text{Pd}(\text{OAc})_2$  (0.1 equiv),  $\text{Na}_2\text{CO}_3$ , DMF,  $60^\circ\text{C}$ , **6** (1 equiv), 24 h; h) HCl, MeOH,  $23^\circ\text{C}$ , 0.5 h (68% from **6**); i)  $\text{MsCl}$  (1.3 equiv),  $\text{NEt}_3$ ,  $\text{CH}_2\text{Cl}_2$ ,  $-30^\circ$ , 1 h (98%), j)  $\text{NaI}$ , acetone,  $23^\circ\text{C}$ , 24 h (93%); k)  $t\text{BuLi}$  (2.5 equiv), then **9** (1.2 equiv),  $\text{Et}_2\text{O}$ ,  $-80^\circ\text{C}$ , 1 h (60%); l)  $\text{R}_3\text{SiCl}$  (2 equiv), imidazole,  $\text{CH}_2\text{Cl}_2$ , RT, 24 h; m) amberlyst 15, acetone, RT, 40 min (**12a**: 80%, 2 steps; **12b**: 75%; **12c**: 83%). TBS = *tert*-butyldimethylsilyl, TBDPS = *tert*-butyldiphenylsilyl, TIPS = triisopropylsilyl, DMF = dimethylformamide, DME = dimethoxyethane,  $\text{MsCl}$  = methanesulfonyl chloride.

this reaction by using 2 equivalents of **4** and 10 mol % of Pd(OAc)<sub>2</sub> in DMF at 60 °C. The starting styrene was readily recovered by flash chromatography after acidic cleavage of the TBS group to provide the dienol **7** in 68 % yield based on recovered **4** and 59 % based on **6**. This reaction is highly regio- and stereoselective, and only the *E,E* diene was found to be produced in more than 99 % diastereomeric purity.

Continuing with the synthesis, **7** was converted into the iodide **8** in two steps by mesylation (98 %) and S<sub>N</sub>2 substitution by using NaI in acetone (93 %). Transmetalation of **8** with *t*BuLi at –80 °C followed by trapping of the organolithium intermediate with the known (2*E*)-4,4-dimethoxybut-2-enal<sup>[16]</sup> **9**, successfully afforded aldehydes **12** after protection of the hydroxy group with a silicon protecting group followed by hydrolysis of the acetal. Thus, syntheses of all-*E*-undeca-2,8,10-trienals **12** with TBDPS, TIPS, and TBS protecting groups were possible. The synthesis of **12c** was performed on a gram-scale.

With substrates **12** in hand, the Lewis acid catalyzed IMDA reaction was investigated (Scheme 5).<sup>[17]</sup> A fast



**Scheme 5.** Lewis acid induced IMDA reaction of trienals **12**.

reaction of **12a** was observed with MeAlCl<sub>2</sub> (1 equiv) as the Lewis acid in CH<sub>2</sub>Cl<sub>2</sub> at –80 °C. However, the reaction did not stop at the stage of the Diels–Alder product. Rather, a subsequent intramolecular Friedel–Crafts reaction of the aldehyde function with the electron-rich aryl ring took place, thus leading to the tetracyclic compound **13** (50 % yield). The reaction of **12a** with one equivalent of the weaker Lewis acid Me<sub>2</sub>AlCl at –80 °C led to a conversion of approximately 60 % of **12a** within 24 h to give a 50 % yield of the isolated product **14a** as a single diastereomer, and no Friedel–Crafts adducts were observed.

The configuration of **14a** was determined by X-ray analysis (Figure 1). It is interesting to note that both bulky substituents (Ar and OSiR<sub>3</sub>) are axially oriented relative to the decalin ring. The silicon protecting groups do not significantly affect the outcome of the IMDA reaction. Also, the TIPS- and TBS-protected aldehydes **12b** and **12c** gave a conversion of approximately 50 % to the corresponding cycloadducts under these conditions. A higher yield could

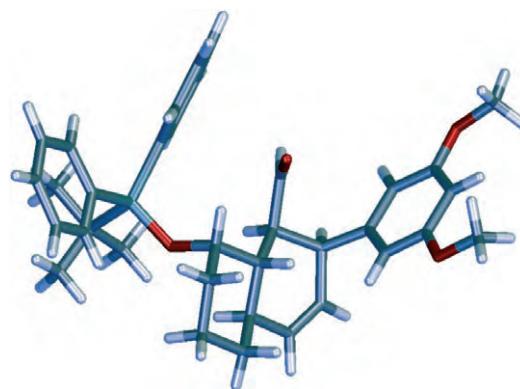
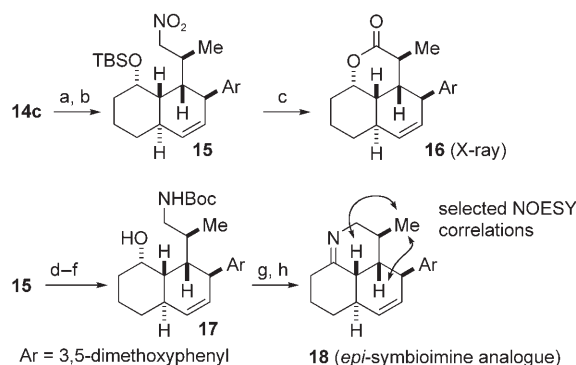


**Figure 1.** X-ray structure of cycloadduct **14a**.

be realized by using 1.6 equivalents of Me<sub>2</sub>AlCl, thus yielding, for example, **12c** in 85 % yield on a gram-scale. The cycloadducts already contain four of the five required stereocenters with the correct relative configuration.

For conversion of the aldehyde function into the amino-propyl appendage, several options were considered.<sup>[18]</sup> In a first attempt, **14c** was subjected to a Henry condensation<sup>[19]</sup> with nitromethane followed by a Michael addition of the resulting nitroalkene with MeMgBr at –80 °C. These transformations proceeded smoothly in good yields and were highly stereoselective and produced the nitro compound **15** (Scheme 6). Attempts to cleave the silyl ether of **15** with TBAF surprisingly gave the corresponding lactol, which was oxidized to lactone **16** with PDC in 65 % yield of the isolated product.

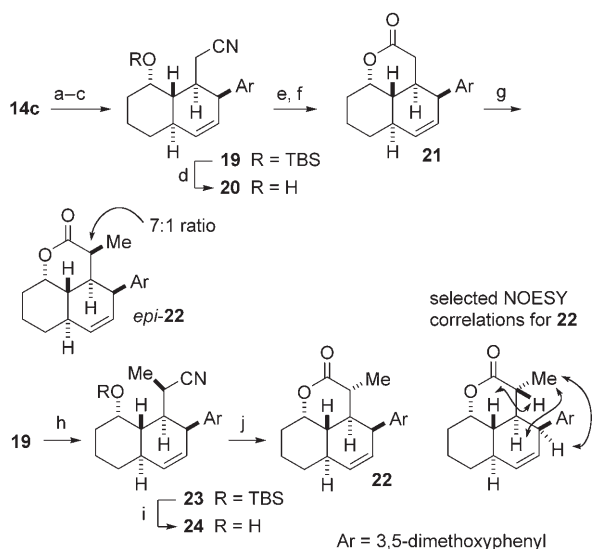


**Scheme 6.** Extension of cycloadduct **14c** through a tandem Henry Michael addition. a) CH<sub>3</sub>NO<sub>2</sub>, NH<sub>4</sub>OAc, 70 °C, 24 h (88 %), b) MeMgBr, Et<sub>2</sub>O, –80 °C, 3 h (70 %); c) 1. TBAF, THF, RT, 12 h; 2. PDC, CH<sub>2</sub>Cl<sub>2</sub>, RT, 24 h (65 %); d) LiAlH<sub>4</sub>, THF, –20 °C → RT, 24 h, then reflux, 1 h; e) Boc<sub>2</sub>O, NEt<sub>3</sub>, MeOH, RT, 0.5 h; f) TBAF, THF, 60 °C, 24 h (55 %, 3 steps); g) PDC, CH<sub>2</sub>Cl<sub>2</sub>, RT, 24 h; h) AcCl, MeOH, 50 °C, 30 min (80 %, 2 steps). TBAF = tetrabutylammonium fluoride, PDC = pyridinium dichromate.

The X-ray structure of lactone **16** showed that two stereocenters were not correct with respect to the natural product (see the Supporting Information). Most likely, the conditions of the Henry reaction caused a base-catalyzed epimerization at the γ-atom of the nitroalkene to give the

thermodynamically favored *trans*-1,2-substituted cyclohexane compound. The stereochemistry of **16** was also evident from NOESY data. To probe the formation of the tetrahydropyridine ring, the nitro group of **15** was reduced with  $\text{LiAlH}_4$ , the amino group protected with Boc anhydride, and the TBS-group cleaved with TBAF to give alcohol **17**. Oxidation of **17** followed by acid-induced Boc cleavage indeed gave imine **18**, an epimeric analogue of **1**.

Finally, a practical solution was found starting with a three-step sequence involving the reduction of aldehyde **14c** with  $\text{NaBH}_4$ , conversion of the alcohol into the corresponding mesylate, and nucleophilic substitution of the mesylate with cyanide in dimethyl sulfoxide (DMSO), thus leading to nitrile **19** in more than 90 % yield from **14c** (Scheme 7). Removal of

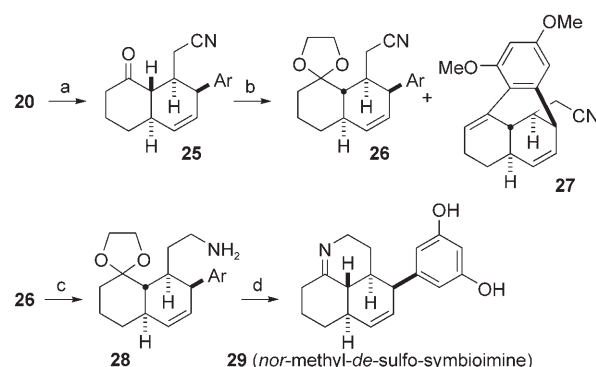


**Scheme 7.** Diastereoselective alkylation of lactone **21** and nitrile **19**. a)  $\text{NaBH}_4$ , EtOH, RT, 24 h (99%); b)  $\text{MsCl}$ ,  $\text{NEt}_3$ ,  $\text{CH}_2\text{Cl}_2$ ,  $-50^\circ\text{C}$  to RT, 1 h (96%); c)  $\text{NaCN}$ , DMSO,  $50^\circ\text{C}$ , 48 h (95%); d) TBAF, THF, RT, 2 h (98%); e)  $\text{KOH}$ , EtOH,  $80^\circ\text{C}$ , 24 h; f)  $p\text{-TsOH}$ , toluene,  $110^\circ\text{C}$ , 1 h (90% for 2 steps); g) LDA (2 equiv),  $-80^\circ\text{C}$ , 3 h, then MeI (4 equiv), 0.5 h (65%); h) LDA (2 equiv),  $-80^\circ\text{C}$ , 2 h, then MeI (2 equiv), 0.5 h (92%); i) TBAF, THF, RT, 24 h (92%); j)  $\text{TMSCl}$ , HCl, toluene, reflux, 48 h (75%). DMSO = dimethyl sulfoxide, LDA = lithium diisopropylamide

the TBS group with TBAF in THF followed by nitrile saponification allowed for the formation of lactone **21**. Although monomethylation of **21** was possible, careful NMR spectroscopic analysis of the major diastereomer showed that methylation had taken place from the wrong side of the enolate. Next, methylation of the nitrile group was investigated. Deprotonation of **19** with LDA (2 equiv) followed by addition of MeI gave a single isomer, tentatively assigned as structure **23**, in 92 % yield of the isolated product. Indeed, conversion of **23** into the corresponding lactone allowed for determination of the stereochemistry from the NOESY data (see the NOESY correlations indicated in Scheme 7).

After the diastereoselective introduction of the methyl group had been resolved, a method was sought that would avoid protection of the amino group en route to the

tetrahydropyridine. This approach was initially investigated by using hydroxy nitrile **20** (Scheme 8). Dess–Martin oxidation of **20** afforded ketone **25** quantitatively. Ketone **25** was protected with ethylene glycol in toluene to give 68 % yield of

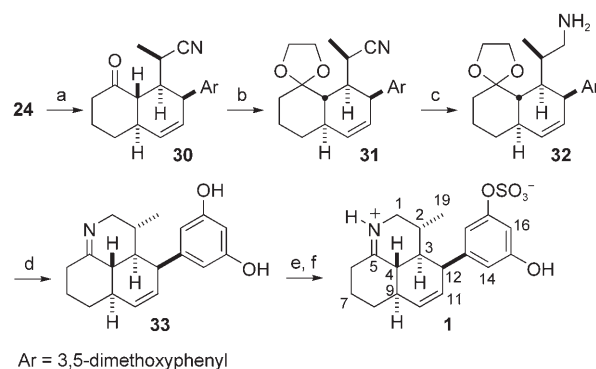


**Scheme 8.** Synthesis of *nor*-methyl-*de*-sulfo-symbioimine (**29**). a) Dess–Martin periodinane,  $\text{CH}_2\text{Cl}_2$ , RT, 8 h (99%); b)  $(\text{CH}_2\text{OH})_2$ , CSA, toluene, reflux, 12 h, (68% of **26**, 20% of **27**); c)  $\text{LiAlH}_4$ ,  $\text{Et}_2\text{O}$ ,  $0^\circ\text{C}$  to RT, 12 h (87%); d)  $\text{BBr}_3$ ,  $\text{CH}_2\text{Cl}_2$ ,  $-80^\circ\text{C}$  to RT, 24 h (55%). Ar = 3,5-dimethoxyphenyl, CSA = camphorsulfonic acid.

the expected dioxolane **26** and 20 % yield of the polycycle **27**, which resulted from attack of the aromatic ring to the keto function. The nitrile group of **26** was then reduced with  $\text{LiAlH}_4$  to the amine **28**. Cleavage of the aryl methyl ethers, the 1,3-dioxolane, and cyclization to the imine could be achieved in one step using  $\text{BBr}_3$  in  $\text{CH}_2\text{Cl}_2$ . Imine **29** is a close analogue of **1**.

Hydroxy nitrile **24** served as starting material for the synthesis of **1**. As before, oxidation to the ketone **30** and protection of the keto function as 1,3-dioxolane led to nitrile **31** (Scheme 9). After reduction of the nitrile to the primary amine, treatment of **32** with  $\text{BBr}_3$  generated imine **33**.

The sulfatation of the resorcinol posed a real challenge, as it was not known whether the imine or iminium function would be compatible with the reaction conditions. In addition,



**Scheme 9.** Completion of the total synthesis of symbioimine (**1**). a) Dess–Martin periodinane,  $\text{CH}_2\text{Cl}_2$ , RT, 8 h (99%); b)  $(\text{CH}_2\text{OH})_2$ , CSA, benzene, reflux, 6 h, (99%); c)  $\text{LiAlH}_4$ ,  $\text{Et}_2\text{O}$ ,  $0^\circ\text{C}$  to RT, 12 h; d)  $\text{BBr}_3$ ,  $\text{CH}_2\text{Cl}_2$ ,  $-80^\circ\text{C}$  to RT, 24 h (55% from **31**); e)  $\text{SO}_3/\text{Py}$ , pyridine,  $70^\circ\text{C}$ , 6 h; f)  $p\text{-TsOH}$ , dioxane,  $\text{H}_2\text{O}$ , RT, 3 h (74% from **33**). Py = pyridine.

sulfonation of the aryl ring might take place with  $\text{SO}_3$  or related agents. Although sulfate monoesters are less common in nature relative to phosphate monoesters, sulfated biomolecules do have a certain role in cellular events. Typical sulfated biomolecules are carbohydrates, proteins (tyrosines), and steroids.<sup>[20,21]</sup> The transfer of sulfate groups to hydroxy functions is catalyzed by sulfotransferases, which use 3'-phosphoadenosine 5'-phosphosulfate as the sulfate source. In a laboratory setting, the attachment of the sulfate is preferentially done at the end of the synthesis, as the resulting products are very polar and the sulfate group is somewhat acid labile. Common methods for the preparation of aryl sulfates include the use of  $\text{SO}_3$ /amine complexes<sup>[22]</sup> (amine = pyridine,  $\text{NEt}_3$ ) or tetrabutylammonium hydrogen sulfate ( $\text{Bu}_4\text{N}^+ \text{HSO}_4^-$ ) in presence of dicyclohexyl carbodiimide (DCC).<sup>[23]</sup> In the case at hand, the treatment of imine **33** with the  $\text{SO}_3$ /pyridine complex (10 equiv) in pyridine for 6 h at 70 °C afforded about 20 % of the inner salt of **1** and 70 % of a compound that was characterized as a bisulfate derivative of **33**. The bisulfate is a water soluble analogue of **1**, which might also be biologically active. We found that the bisulfate could readily be converted into **1** with *p*-toluenesulfonic acid (*p*-TsOH) in a water/dioxane system at room temperature. Under these conditions, one sulfate group is selectively hydrolyzed to give additional **1** (54 %) and about 10 % of **33**, which could be recovered. The NMR spectra of **1** were found to be identical to the spectra from the isolated natural product.

In summary, we developed an efficient synthesis of ( $\pm$ )-symbioimine (**1**), a novel tricyclic iminium alkaloid. The total synthesis of **1** was accomplished in 22 steps from 3,5-dihydroxy benzoic acid (**5**) in more than 5 % total yield, which corresponds to an average yield of 88 % per step. Our approach features a Lewis acid induced *endo*-IMDA reaction of 2,8,10-*E,E,E*-trienal **12** and a diastereoselective alkylation of nitrile **19** as key steps. This route opens the way to other symbioimine-type compounds. This study also emphasizes the high reactivity of the electron-rich aryl ring if it comes close to another electrophilic group that yields interesting polycyclic structures. This strategy might actually be of interest in the context of diversity oriented synthesis.<sup>[24]</sup>

Received: April 10, 2006

Published online: June 27, 2006

**Keywords:** alkaloids · cycloaddition · Diels–Alder reaction · imines

- [1] M. Kita, M. Kondo, T. Koyama, K. Yamada, T. Matsumoto, K.-H. Lee, J.-T. Woo, D. Uemura, *J. Am. Chem. Soc.* **2004**, *126*, 4794–4795.
- [2] M. Kita, D. Uemura, *Chem. Lett.* **2005**, *34*, 454–459.
- [3] Recently, a sulfated derivative of the alkaloid aaptamine, which contains a 1*H*-benzo[*d,e*][1,6]-naphthyridine core, was described: A. Herlt, L. Mander, W. Rombang, R. Rumampuk, S. Soemitro, W. Steglich, P. Tarigan, F. von Nussbaum, *Tetrahedron* **2004**, *60*, 6101–6104.
- [4] M. Kita, N. Ohishi, K. Washida, M. Kondo, T. Koyama, K. Yamada, D. Uemura, *Bioorg. Med. Chem.* **2005**, *13*, 5253–5258.
- [5] For a review about Diels–Alder reactions in nature, see: E. M. Stocking, R. M. Williams, *Angew. Chem.* **2003**, *115*, 3186–3223; *Angew. Chem. Int. Ed.* **2003**, *42*, 3078–3115.
- [6] B. B. Snider, Q. Che, *Angew. Chem.* **2006**, *118*, 946–949; *Angew. Chem. Int. Ed.* **2006**, *45*, 932–935.
- [7] See, also: Y. Kobayashi, E. E. Olson, Abstracts of Papers, 229th ACS National Meeting, San Diego, CA, United States, March 13–17, **2005**, ORGN-605.
- [8] For reviews about IMDA reactions, see: a) E. Ciganek, *Org. React.* **1984**, *32*, 1–374; b) D. Craig, *Chem. Soc. Rev.* **1987**, *16*, 187–238; c) W. R. Roush in *Comprehensive Organic Synthesis*, Vol. 5 (Ed.: L. A. Paquette), Pergamon, Oxford **1991**, pp. 513–550; d) A. G. Fallis, *Acc. Chem. Res.* **1999**, *32*, 464–474; e) K. C. Nicolaou, S. A. Snyder, T. Montagnon, G. Vassilikogiannakis, *Angew. Chem.* **2002**, *114*, 1742–1773; *Angew. Chem. Int. Ed.* **2002**, *41*, 1668–1698; f) K.-i. Takao, R. Munakata, K.-i. Tadano, *Chem. Rev.* **2005**, *105*, 4779–4807.
- [9] For some related examples (secondary alcohol next to dienophile): a) R. L. Funk, W. E. Zeller, *J. Org. Chem.* **1982**, *47*, 180–182; b) S. D. Burke, D. R. Magnin, J. A. Oplinger, J. P. Baker, A. Abdelmagid, *Tetrahedron Lett.* **1984**, *25*, 19–22; c) J. A. Marshall, J. E. Audia, J. Grote, *J. Org. Chem.* **1984**, *49*, 5277–5279; d) J. A. Marshall, J. E. Audia, J. Grote, B. G. Shearer, *Tetrahedron* **1986**, *42*, 2893–2902; e) B. M. Trost, R. C. Holcomb, *Tetrahedron Lett.* **1989**, *30*, 7157–7160.
- [10] C. H. Yoon, K. S. Yoo, S. W. Yi, R. K. Mishra, K. W. Jung, *Org. Lett.* **2004**, *6*, 4037–4039.
- [11] X. Du, M. Suguro, K. Hirabayashi, A. Mori, T. Nishikata, N. Hagiwara, K. Kawata, T. Okeda, H. F. Wang, K. Fugami, M. Kosugi, *Org. Lett.* **2001**, *3*, 3313–3316.
- [12] H. Ishii, T. Ishikawa, T. Deushi, K. Harada, T. Watanabe, E. Ueda, T. Ishida, M. Sakamoto, E. Kawanabe, T. Takahashi, Y.-I. Ichikawa, K. Takizawa, T. Masuda, I.-S. Chen, *Chem. Pharm. Bull.* **1983**, *31*, 3024–3038.
- [13] A. Zanka, H. Ohmori, T. Okamoto, *Synlett* **1999**, 1636–1638.
- [14] L. Gehringer, C. Bourgoigne, D. Guillon, B. Donnio, *J. Am. Chem. Soc.* **2004**, *126*, 3856–3867.
- [15] Vinyl boronate: a) prepared according to reference [10]; b) for a review, see: D. E. Kaufmann, N. Ocal, *Science of Synthesis*, Vol. 6, Thieme, Stuttgart, **2004**, pp. 635–658.
- [16] D. Frederico, P. M. Donato, M. G. Constantino, E. S. Bronze, M. I. Sairre, *J. Org. Chem.* **2003**, *68*, 9126–9128.
- [17] For some Lewis acid catalyzed IMDA reactions, see: a) J. A. Marshall, J. Grote, J. E. Audia, *J. Am. Chem. Soc.* **1987**, *109*, 1186–1194; b) D. A. Evans, J. S. Johnson, *J. Org. Chem.* **1997**, *62*, 786–787; c) T. A. Dineen, W. R. Roush, *Org. Lett.* **2005**, *7*, 1355–1358.
- [18] For another attempt at extending aldehyde **14c**, see the Supporting Information.
- [19] F. A. Luzzio, *Tetrahedron* **2001**, *57*, 915–945.
- [20] J. I. Armstrong, X. Ge, D. E. Verdugo, K. A. Winans, J. A. Leary, C. R. Bertozzi, *Org. Lett.* **2001**, *3*, 2657–2660.
- [21] L. S. Simpson, T. S. Widlanski, *J. Am. Chem. Soc.* **2006**, *128*, 1605–1610, and references therein.
- [22] O. Soidinsalo, K. Wahala, *Steroids* **2004**, *69*, 613–616.
- [23] D. Barron, R. K. Ibrahim, *Tetrahedron* **1987**, *43*, 5197–5202.
- [24] M. D. Burke, S. L. Schreiber, *Angew. Chem.* **2004**, *116*, 48–60; *Angew. Chem. Int. Ed.* **2004**, *43*, 46–58.



DOI: 10.1002/anie.200600989

**Enzymatically Derived Sugar-Containing Self-Assembled Organogels with Nanostructured Morphologies\*\***

George John, Guangyu Zhu, Jun Li, and Jonathan S. Dordick\*

Control of building-block assembly and phase behavior is crucial for the ultimate design of functional architectures ranging from the nano- to the macroscales, with organogels representing one important example of this functional architecture.<sup>[1]</sup> An ideal gelator is an amphiphile that induces gel formation through self-assembly into highly ordered structures in which the hydrophilic moieties interact through extensive hydrogen bonding and the hydrophobic moieties interact with the organic liquid. Among the growing list of low molecular weight compounds that induce gelation,<sup>[2]</sup> sugars appear to satisfy these requirements, and numerous alkyl- and aryl-based monosaccharide gelators have been generated.<sup>[3]</sup> As opposed to chemical synthesis, enzymatic catalysis is highly selective and has been used to generate low-molecular-weight compounds that can gel organic solvents,<sup>[4]</sup> generate a wide range of sugar-based esters,<sup>[5]</sup> and in particular, prepare highly regioselective symmetrical diesters.<sup>[6]</sup> We reasoned that such a biocatalytic approach would provide an alternative route to the synthesis of disaccharide-based diesters with physical and structural features appropriate for a low-molecular-weight gelator along with a controlled symmetry that may aid in self-assembly. Combining the principles of supramolecular chemistry with the selectivity of biocatalysis may represent a new and powerful strategy to develop new molecularly defined and functional materials.

To that end, we examined the synthesis of sugar-based diesters by using the lipase B from *Candida antarctica* (CALB). Transesterification reactions were performed in acetone that contained either vinyl stearate or vinyl butyrate as highly or moderately hydrophobic ester donors, respectively, and with several common disaccharides including sucrose, maltose, lactose, and trehalose. Interestingly, only the reactions with trehalose, a symmetrical disaccharide with an  $\alpha$ -1,1 glycosidic bond, resulted in gel formation during the course of the transesterification reactions (Table 1, gelators **2** and **5**), thereby confirming the importance of monomer structure in gel assembly. Trehalose-6,6'-distearate and trehalose-6,6'-dibutyrate were obtained as the sole products from the respective enzymatic reactions in yields of > 50%. Hence, CALB was highly regiospecific in its acylation of trehalose. The purified diesters were tested in a wide range of solvents for their gelation ability (see the Supporting Information). The trehalose distearate was insoluble in water and soluble in chloroform and 1,4-dioxane, whereas trehalose 6,6'-dibutyrate was insoluble in cyclohexane and olive oil and soluble in water. Gels were formed in all other solvents tested.

As a result of these studies, we generated a series of additional diesters with chain lengths of C2 to C14 (**1**, **3**, **4**, and **6**) and assessed their gelation capacity in several key solvents, ranging from the hydrophilic acetonitrile to the hydrophobic *p*-xylene (Table 1). The minimum gelator concentration ( $c_{\min}$ ) required to induce gelation is strongly dependent on the acyl-chain length. In most of the cases, a shorter chain length promotes gelation at lower gelator concentration, with the exception of gelation in acetonitrile and isopropanol. These results sharply contrast with typical sugar-based amphiphilic organogels, which require long-chain alkyl or aryl moieties to induce gelation.<sup>[3a-e]</sup> Surprisingly, the trehalose-6,6'-diacetate (**1**) was capable of inducing gelation at a  $c_{\min}$  of 0.04 % (w/v; 0.84 mM) in ethyl acetate and nearly this low in methyl methacrylate. This represents, to our knowledge, the lowest  $c_{\min}$  value reported for a sugar ester gelator.<sup>[7]</sup> For ethyl acetate, the  $c_{\min}$  represents over 12000 solvent molecules being associated per molecule of **1**. This can be translated into a swelling of the weight of the gelator approximately 2500-fold.

The trehalose diesters are excellent gelators over a broad range of organic solvents (see the Supporting Information) and in a mixture of solvents. For example, in the case of a 1:1 binary mixture of ethyl acetate and acetonitrile, the minimum gelation concentration was between the  $c_{\min}$  values in the pure solvents (see the Supporting Information), therefore showing no preference for a given solvent. Interestingly, the longer-ester-chain trehalose derivatives could form gels in olive oil (Table 1) with relatively low  $c_{\min}$  values. Addition of 5 % free oleic acid, which would be present in low-purity olive oil, did not affect the swelling capacity of the gel. Hence, complex, multicomponent solvent systems, such as that found in a natural oil and in the presence of a charged hydrolysis product, could be subject to gelation.

As described above, although regiospecificity was achieved to give the respective 6,6'-diesters for all disaccharides tested, gel formation only occurred with trehalose, suggesting that the unique symmetry of this molecule, which

[\*] Dr. G. Zhu, Prof. J. S. Dordick  
Department of Chemical and Biological Engineering and  
Rensselaer Nanotechnology Center  
Rensselaer Polytechnic Institute  
Troy, NY 12180 (USA)  
Fax: (+1) 518-276-2207  
E-mail: dordick@rpi.edu

Prof. G. John  
Department of Chemistry  
The City College of the City University of New York  
New York, NY 10031 (USA)

Dr. J. Li  
Department of Polymer Science  
The University of Southern Mississippi  
Hattiesburg, MS 39406 (USA)

[\*\*] We thank Dr. Maura Weathers of the Cornell Center for Material Research (CCMR) for small-angle X-ray scattering (SAXS) measurements and Dr. Praveen of CCNY, CUNY for calculations. This research was supported by an NSF-Nanoscale Science and Engineering Center at Rensselaer (DMR-0117792).

Supporting information for this article is available on the WWW under <http://www.angewandte.org> or from the author.

**Table 1:** Minimum gelation concentration (weight percent) of trehalose-based diesters in different solvents at 25 °C.<sup>[a]</sup>

Solvent (log P value)	R =	<b>1</b> -CH <sub>3</sub>	<b>2</b> -(CH <sub>2</sub> ) <sub>2</sub> CH	<b>3</b> -(CH <sub>2</sub> ) <sub>8</sub> CH <sub>3</sub>	<b>4</b> -(CH <sub>2</sub> ) <sub>12</sub> CH <sub>3</sub>	<b>5</b> -(CH <sub>2</sub> ) <sub>16</sub> CH <sub>3</sub>	<b>6</b> -CH=CH <sub>2</sub>
acetonitrile (-0.34)		G (0.36)	G (0.69)	G (0.18)	G (0.11)	G	G
Acetone (-0.24)		G (0.34)	G (1.0)	G (1.3)	G (1.4)	G	G
isopropanol (0.05)		G (0.54)	G (1.39)	G (2.21)	G (1.31)	G	G
ethyl acetate (0.73)		G (0.04)	G (0.13)	G (0.71)	G (1.1)	G (0.72)	G
methyl methacrylate (1.38)		G (0.05)	G (0.11)	G (0.82)	G (0.85)	G (0.40)	G
<i>p</i> -xylene (3.15)		I	G (0.14)	G (0.18)	G (0.25)	G (0.37)	G (0.72)
olive oil (N/A)		I	I	G (0.09)	G (0.13)	G (0.18)	I

[a] G indicates that the gel formed and I indicates that the gelator could not dissolve in the organic solvent at elevated temperatures.

was maintained by the regioselectivity of lipase-catalyzed acylation, may play the key role in its strong gelation ability. To test this hypothesis, we chemically acylated trehalose with stearoyl chloride to yield a mixture of trehalose esters. Following isolation of the diesters (a mixture of regioisomers among the eight free hydroxy groups, data not shown), gelation studies were performed in ethyl acetate. Gelation did not occur until a diester mixture concentration of approximately 10 % (w/v) was reached; well over 10-fold higher than that required by the 6,6'-distearate. When the 6,6'-distearate was purified from the diester mixture, identical gelation properties to those synthesized enzymatically were obtained. Similar results were obtained with the 6,6'-diacetate and 6,6'-dibutyrate derivatives. These results indicate that gelation is strongly favored with highly symmetrical disaccharide ester derivatives that can be synthesized through regioselective enzymatic catalysis.

Differential scanning calorimetry (DSC) of gels **1–4** was performed in ethyl acetate to yield a gel→sol transition temperature as a function of gelator mole fraction and therefore enable calculation of gel melting enthalpy ( $\Delta H_m$ ; see the Supporting Information). Values of  $\Delta H_m$  for gelators **1–4** were determined to be approximately 55, 44, 30, and 22 kJ mol<sup>-1</sup>, respectively. The high  $\Delta H_m$  of **1** indicates that this gelator is the most effective in forming highly stable gels in ethyl acetate, which is consistent with its low  $c_{min}$ . Longer acyl chains favor greater solvation of the diester in ethyl acetate and therefore reduce their ability to form strong gels.

The morphological properties of the trehalose-based organogels were obtained through scanning electron microscopy (SEM). Figure 1 depicts selected SEM images of the

xerogels of **1** in ethyl acetate (Figure 1 a,b) and in isopropanol (Figure 1 c,d), as well as **6** in ethyl acetate (Figure 1 e,f). These xerogels consist of 3D entangled fiber-like aggregates with diameters of 10–500 nm and lengths in the micron scale. The high aspect ratios of the gel fibers clearly indicate that the intergelator interactions are highly anisotropic. Most likely, the fibers observed in the electron micrographs consist of bundles of gelator aggregates, similar to the structures observed in other gel systems. The solvent clearly influences the gel structure, for example, the ethyl acetate gel of **1** is transparent and shows extended fibrous structures (Figure 1 a), whereas the isopropanol gel of **1** is opaque and consist of larger and more crystalline fibers (Figure 1 c). Furthermore, the fact that low gelator concentrations can yield gels with the weak hydrophobicity of the C2 acyl moiety suggests that H-bonding is the

predominant mechanism for gel assembly, although hydrophobic interactions may also contribute to gelation at longer acyl-chain lengths. The ability of H-bonding to dominate gel assembly is supported by the extremely high hydroxy-group density in a disaccharide like trehalose, as depicted in Figure 2 e (for more detail, see the Supporting Information).

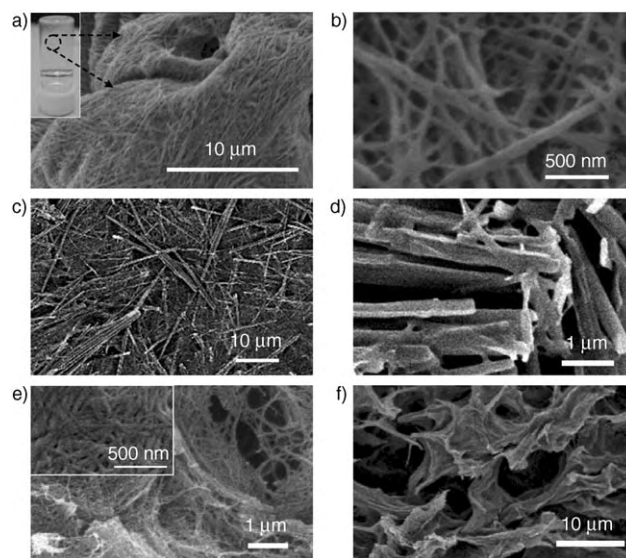


**Figure 1.** FE-SEM images of the organogels from a) **1** in ethyl acetate, b) **1** in ethyl acetate at a higher magnification, c) **1** in isopropanol, d) **1** in isopropanol at a higher magnification, e) **6** in ethyl acetate; inset shows higher magnification of **6** in ethyl acetate, f) **6** self-supporting and porous scaffold after UV polymerization in ethyl acetate.

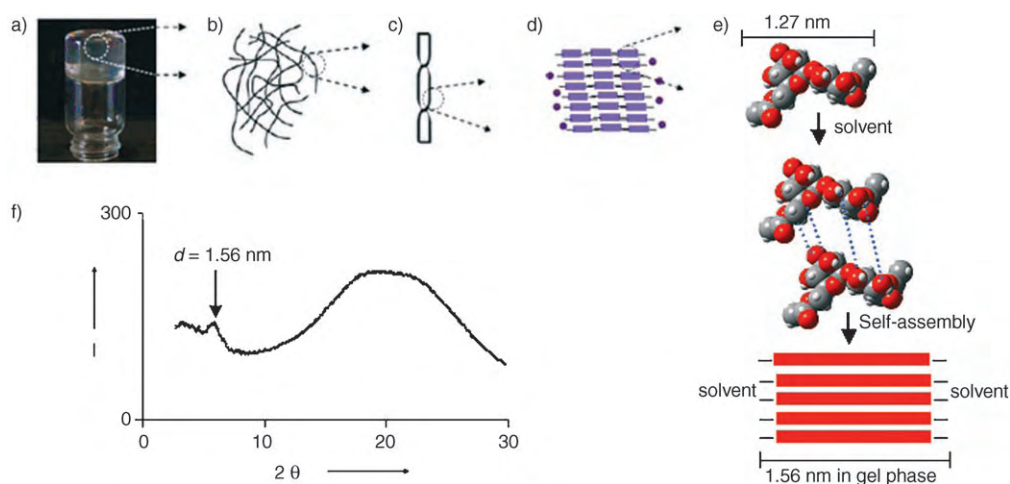


**Figure 2.** Proposed scheme of molecular packing. a) Gel formed by **1** in ethyl acetate, b) 3D network, c) fibers, d) multilayers, and e) modeled molecular packing. f) SAXS data for ethyl acetate gel of **1**.

To gain additional insight into the structures that comprise the gel formed from **1**, small-angle X-ray diffraction (XRD) was employed. XRD of the wet gel gave a weak Bragg reflection at 1.56 nm, indicating that the sugar diester assembled into a well-ordered structure (Figure 2f). This reflection is approximately the same as that of the molecular length of **1**, which was confirmed by crystalline-sample measurements (1.25 nm) and molecular modeling studies by using energy-minimized calculations.<sup>[8]</sup> XRD measurements of the gels from **2–6** also gave similar diffraction patterns showing that, in a suitable organic solvent, the trehalose diesters self-assemble into ordered structures. Based on these results, we propose a molecular arrangement of the trehalose diesters in the organic liquid (Figure 2e). Molecular stacking of the multilayers (Figure 2d) leads to the formation of gel fibers (Figure 2c) followed by further growth into fibrous 3D networks (Figure 2b) and finally formation of the gel (Figure 2a). The transparency of the resulting ethyl acetate gel of **1** attests to a low-gelator-volume fraction along with a nanoscale fiber size that does not interfere with light transmission. Additional information on the packing arrangement of the trehalose-6,6'-distearate (**5**) gelators through H-bonding was further obtained by temperature-dependent <sup>1</sup>H NMR spectroscopic measurements in isopropanol and acetone (see the Supporting Information). The gelators exhibit peaks in both the sol and gel states, and as expected, the peak width becomes sharper when the temperature increases above the  $T_{\text{gel}}$  (46 °C). The peak width at 2.17–2.21 ppm (COOCH<sub>2</sub> adjacent to the sugar) decreases below  $T_{\text{gel}}$  but remains constant at  $T > T_{\text{gel}}$ . This result is consistent with the loosening of H-bonds that occur at the gel→sol transition temperature. Interestingly, the organogels retain visible <sup>1</sup>H NMR spectroscopic peaks in the gel state, suggesting that the gelator molecules maintain sufficient thermal motion<sup>[3d,e,9]</sup> in contrast to other gelating systems.<sup>[10]</sup>

Although the gel structure can be dissociated in several ways, such as by adding a good solvent of the gelator, another route to degradation of these particular trehalose diester gels is through selective ester-bond hydrolysis catalyzed by lipase

in the presence of a small amount of added water. Indeed CALB (0.5 mg mL<sup>-1</sup>) in the presence of 2% (v/v) water caused the ethyl acetate gel of **1** to undergo disintegration with concomitant formation of free trehalose and some trehalose 6-acetate.

Gels containing acrylate esters (for example, **6**) can be further subjected to post-gelation cross-linking<sup>[11]</sup> in the presence of 2,2-dimethoxy-2-phenylacetophenone (5 mol %) as the photoinitiator and subsequent polymerization through UV irradiation. Following solvent evaporation, the cross-linked organogel from **6** was lyophilized to yield a highly porous material (Figure 1f). This material has a far-larger pore structure than the gel from **6**, which is not cross-linked (Figure 1e). This suggests that it is suitable as a porous scaffold. No gel shrinkage occurred during lyophilization. Following drying into the aerogel, the cross-linked material remained intact as a self-supporting scaffold (Figure 3a). This material was capable of behaving as a modest hydrogel; within 5 h the gel absorbed its weight 12-fold in water to give a self-supporting transparent material (Figure 3b). We believe that this is the first example of the generation of nanostructures from self-assembled precursors in organic solvents with hydrogel function.

In conclusion, we have used a biocatalytic strategy to design and synthesize a novel family of highly symmetrical trehalose diesters that self-assemble in a range of organic solvents and form gels at concentrations as low as 0.04% (w/v). The gel fibers, particularly those obtained from short acyl-chain length, are self-assembled and stabilized most likely through the extensive H-bonding networks that are available in the sugar; although both van der Waals packing and hydrophobic interactions are also expected to contribute to gel stability particularly as the acyl-chain length increases. Combining the principles of supramolecular chemistry and the selectivity of biocatalysis represents a powerful strategy to develop new molecularly defined and functional materials. The organogels reported herein may find potential applications in the food, pharmaceutical, and cosmetic industries in which trehalose is already used routinely.<sup>[12]</sup> In particular, the



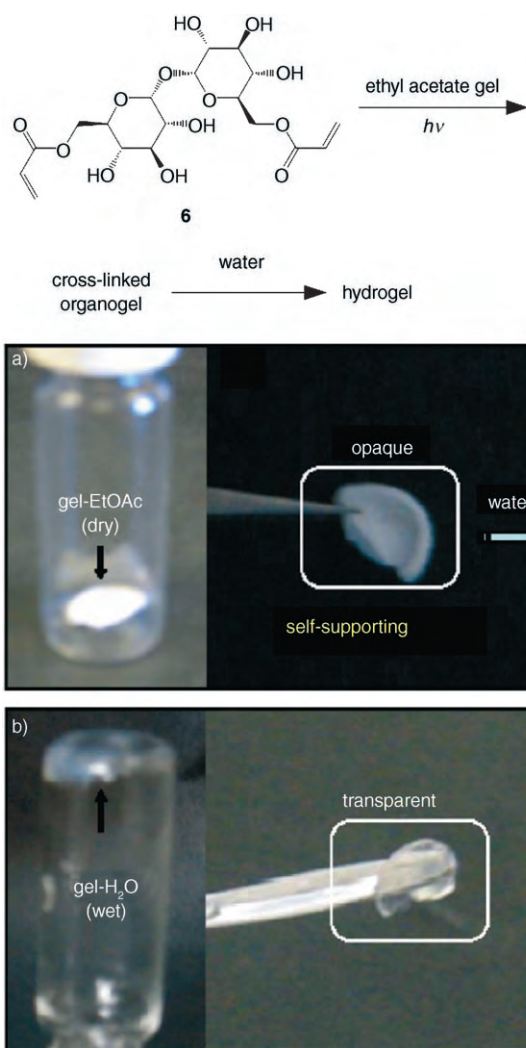


**Figure 3.** Self-supporting organo a) and hydrogel b) from trehalose 6,6'-diacrylate after polymerization.

ability of the longer-chain trehalose diesters to gel olive oil attests to its potential use as a food or cosmetic additive that can be prepared by using food-approved enzymatic synthesis approaches.<sup>[13]</sup> Finally, photopolymerization of diacrylate esters results in stable organo- and hydrogels. These porous, self-supporting structures may find use as a scaffold for tissue engineering, templated materials synthesis, nanoreactors for chemical and enzyme catalysis, and controlled-pore, hydrophilic membranes.

### Experimental Section

Trehalose diesters were synthesized as follows: Novozyme 435 (1.5 g) was added to acetone (100 mL) containing trehalose dihydrate (0.01 mol) and vinyl ester (0.03 mol). The reaction mixtures were then incubated at 45°C and agitated at approximately 200 rpm for 48 h. The reactions were terminated by filtering the reaction mixtures to remove the solid enzyme. The crude products were purified by flash chromatography by using an ethyl acetate/methanol/water (17:4:1 v/v) mixture as the eluent. The yields of the isolated products ranged from 50–80%. The trehalose diesters were analyzed by standard spectroscopic and elemental analysis procedures.

Gel→sol transition temperatures ( $T_m$ ) were determined by DSC with a Mettler DSC-822 differential scanning calorimeter equipped with a nitrogen-gas cooling system. Field emission (FE)-SEM measurements were carried out with a JEOL electron microscope. A piece of the gel was placed on a carbon-coated copper grid and dried for 3 h under vacuum before imaging. XRD measurements were conducted by using a Bruker axs-D8 Discover with GADDS diffractometer with graded  $d$ -space elliptical side-by-side multiplayer optics, monochromated  $\text{Cu K}\alpha$  radiation (40 kV, 40 mA), and imaging plate. The organogel was used as prepared in wet conditions for the analysis. The typical exposure time was 1 min for self-assembled structures with a 100 mm camera length.

Received: March 13, 2006

Published online: June 8, 2006

**Keywords:** enzyme catalysis · hydrogen bonds · organogels · self-assembly · trehalose

- a) P. Terech, R. G. Weiss, *Chem. Rev.* **1997**, *97*, 3133–3159; b) D. J. Abdallah, R. G. Weiss, *Adv. Mater.* **2000**, *12*, 1237–1247; c) J. H. Van Esch, B. L. Feringa, *Angew. Chem.* **2000**, *112*, 2351–2354; *Angew. Chem. Int. Ed.* **2000**, *39*, 2263–2266; d) L. A. Estroff, A. D. Hamilton, *Chem. Rev.* **2004**, *104*, 1201–1217.
- a) K. Hanabusa, M. Yamada, M. Kimura, H. Shirai, *Angew. Chem.* **1996**, *108*, 2086–2088; *Angew. Chem. Int. Ed. Engl.* **1996**, *35*, 1949–1951; b) K. Murata, M. Aoki, T. Suzuki, T. Harada, H. Kawabata, T. Komori, F. Ohseto, K. Ueda, S. Shinkai, *J. Am. Chem. Soc.* **1994**, *116*, 6664–6676; c) F. M. Menger, K. L. Caran, *J. Am. Chem. Soc.* **2000**, *122*, 11679–11691; d) L. A. Estroff, A. D. Hamilton, *Angew. Chem.* **2000**, *112*, 3589–3592; *Angew. Chem. Int. Ed.* **2000**, *39*, 3447–3450; e) R. Oda, I. Huc, S. J. Candau, *Angew. Chem.* **1998**, *110*, 2835–2838; *Angew. Chem. Int. Ed.* **1998**, *37*, 2689–2691.
- a) S. Bhattacharya, S. N. G. Acharya, *Chem. Mater.* **1999**, *11*, 3504–3511; b) K. Yoza, N. Amanokura, Y. Ono, T. Akao, H. Shinmori, M. Takeuchi, S. Shinkai, D. N. Reinhoudt, *Chem. Eur. J.* **1999**, *5*, 2722–2729; c) R. J. H. Hafkamp, M. C. Feiters, R. J. M. Nolte, *J. Org. Chem.* **1999**, *64*, 412–426; d) J. H. Jung, G. John, M. Masuda, K. Yoshida, S. Shinkai, T. Shimizu, *Langmuir* **2001**, *17*, 7229–7232; e) G. John, J. H. Jung, M. Masuda, T. Shimizu, *Langmuir* **2004**, *20*, 2060–2065.
- V. P. Vassilev, M. R. Wood, C.-H. Wong, *Chem. Commun.* **1998**, 1865–1866.
- a) J. O. Rich, B. A. Bedell, J. S. Dordick, *Biotechnol. Bioeng.* **1995**, *45*, 426–434; b) Y. Yan, U. T. Bornscheuer, R. D. Schmid, *Biotechnol. Lett.* **1999**, *21*, 1051–1054.
- O.-J. Park, D.-Y. Kim, J. S. Dordick, *Biotechnol. Bioeng.* **2000**, *70*, 208–216.
- R. Luboradzki, O. Gronwald, A. Ikeda, S. Shinkai, *Chem. Lett.* **2000**, 1148–1149.
- Gaussian 98 (Revision A.11.3), Gaussian, Inc., Pittsburgh, PA, **2003**.
- K. Sakurai, Y. Jeong, K. Koumoto, A. Friggeri, O. Gronwald, S. Sakurai, S. Okamoto, K. Inoue, S. Shinkai, *Langmuir* **2003**, *19*, 8211–8217.
- M. George, R. G. Weiss, *J. Am. Chem. Soc.* **2001**, *123*, 10393–10394.
- M. de Loos, J. van Esch, I. Stokroos, R. M. Kellogg, B. L. Feringa, *J. Am. Chem. Soc.* **1997**, *119*, 12675–12676.
- a) A. D. Elbein, Y. T. Pan, I. Pastuszak, D. Carroll, *Glycobiology* **2003**, *13*, 17R–27R; b) T. Higashiyama, *Pure Appl. Chem.* **2002**, *74*, 1263–1269.
- J. Kim, D. H. Altreuter, D. S. Clark, J. S. Dordick, *J. Am. Oil Chem. Soc.* **1998**, *75*, 1109–1113.



DOI: 10.1002/anie.200504359

# Highly Efficient Aerobic Oxidation of Alcohols Using a Recoverable Catalyst: The Role of Mesoporous Channels of SBA-15 in Stabilizing Palladium Nanoparticles\*\*

Babak Karimi,\* Sedigheh Abedi, James H. Clark, and Vitaly Budarin

Dedicated to Professor Dieter Enders  
on the occasion of his 60th birthday

Ever-increasing environmental concerns has resulted in much attention being recently directed toward the development of new protocols for the aerobic oxidation of alcohols using transition-metal catalysts.<sup>[1]</sup> Among them, palladium-based catalysts show very interesting and promising catalytic activity, and different types of palladium-based homogeneous<sup>[2]</sup> and heterogeneous<sup>[3]</sup> catalysts in the form of metal complexes or nanoparticles<sup>[4]</sup> have been developed for this purpose. Accordingly, the application of palladium-based catalysts has also been well documented for the asymmetric oxidation of alcohols.<sup>[5]</sup> Although, significant progress has been achieved in improving catalytic activity, selectivity, and substrate scope, there is still the major problem that palladium agglomeration and the formation of palladium black can cause catalyst deactivation in many cases. Recently, Tsuji and co-workers have shown that novel pyridine derivatives with 2,3,4,5-tetraphenylphenyl substituents and higher dendritic units at the 3-position significantly suppress the formation of palladium black and give the highest reported turnover numbers (TON) of 1480 in the homogeneous palladium-catalyzed oxidation of alcohols in air.<sup>[2o]</sup> Very recently, we explored a new silica-based palladium(II) interphase catalyst for the aerobic oxidation of alcohols.<sup>[3g]</sup> However, this method requires high catalyst concentrations (up to 5 mol%) and it suffers from the disadvantage of a significant reduction in its reactivity after three reaction cycles. Furthermore, this catalyst did not show good catalytic

activity in the aerobic oxidation of allylic alcohols. Quite recently, the use of palladium nanoparticles dispersed in an organic polymer has also been demonstrated in the aerobic oxidation of alcohols.<sup>[4a,b]</sup> However, these heterogeneous Pd systems also suffer from high catalyst loading (typically substrate/catalyst ratios are ca. 20:1) and also the organic polymers used in these systems are potentially susceptible to oxidative degradation under aerobic oxidation conditions, thus restricting catalyst recovery over a long period. Moreover, it is well known that the small particle size as well as the high surface area of nanoparticles means they are very mobile and thermodynamically susceptible to agglomeration and the formation of larger inactive particles.<sup>[6]</sup> Ordered mesoporous structures (such as MCM-41<sup>[7]</sup> and SBA-15<sup>[8]</sup>) with regular channel structures and pore diameters in the range of 2 to 30 nm, their easy separation from the reaction mixtures, and their relatively high surface area, would seem to be ideal for forming a scaffold in which three-dimensional dispersions of metal nanoparticles could be supported. Furthermore, because the majority of the nanoparticles are usually formed inside the channels of ordered porous materials, the support prevents agglomeration while providing the inherent advantages of a heterogeneous catalyst such as easy recovery and product separation. For these reasons, the preparation<sup>[9]</sup> and the use<sup>[10]</sup> of metal nanoparticles deposited on such porous materials have received much attention in recent years. However, despite these attractive features, to our knowledge there is no report on the use of metal nanoparticles supported on mesoporous materials for the aerobic oxidation of alcohols. We disclose herein a simple procedure for the preparation of a new type of palladium catalyst immobilized on functionalized SBA-15 and its application as a heterogeneous catalyst for the aerobic oxidation of alcohols. Transmission electron microscopy (TEM) before and after catalysis indicates the involvement of Pd nanoparticles confined inside the channels of SBA-15 as a reservoir of active species for catalysis. SBA-15 was obtained from pluronic P123 (EO<sub>20</sub>PO<sub>70</sub>EO<sub>20</sub> (EO = ethylene oxide, PO = propylene oxide),  $M_{Av}$  = 5800, Aldrich) and (EtO)<sub>4</sub>Si under acidic conditions following the reported procedure.<sup>[8]</sup> The resulting SBA-15 was functionalized with a bipyridylamide ligand followed by complexation with Pd(OAc)<sub>2</sub> to afford the corresponding immobilized palladium catalyst **1**.<sup>[11]</sup> The TEM

[\*] Prof. Dr. B. Karimi, S. Abedi  
Department of Chemistry  
Institute for Advanced Studies in Basic Sciences (IASBS)  
PO. Box 45195-1159, Gava Zang, Zanjan (Iran)  
Fax: (+98) 241-424-9023  
E-mail: karimi@iasbs.ac.ir  
Prof. Dr. J. H. Clark, Dr. V. Budarin  
Clean Technology Centre  
University of York  
York YO105DD (UK)

[\*\*] This work was supported by the IPM and IASBS Research Councils. We also acknowledge Dr. E. Shams for the atomic absorption analysis of the samples, and we thank the referees for their valuable comments.

Supporting information for this article is available on the WWW under <http://www.angewandte.org> or from the author.

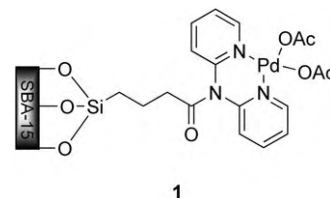
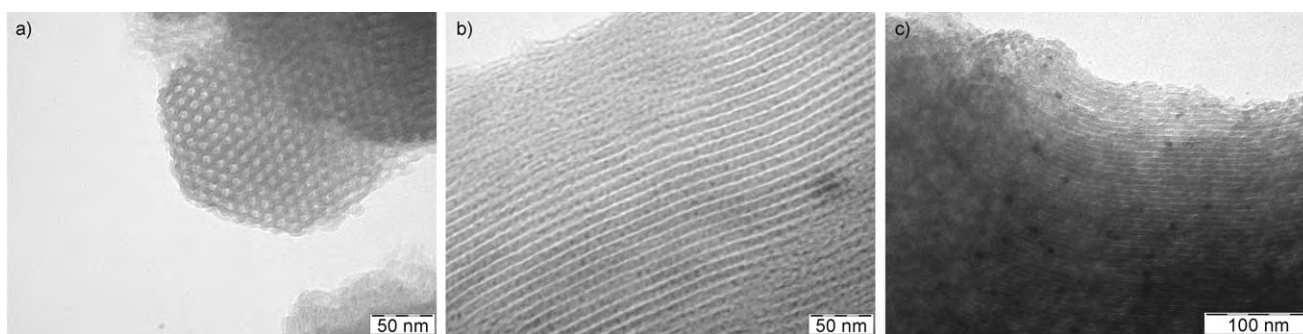


image of catalyst **1** is shown in Figure 1a and b, and reveals the absence of any palladium particles inside the channels. An interesting point is that the nanoarchitecture of the catalyst (SBA-15 channel) largely survived even after prolonged reflux at 150°C in concentrated sulfuric acid during the preparation procedure.<sup>[11]</sup> A typical nitrogen adsorption/



**Figure 1.** TEM images of **1**: a) perpendicular to the ordered channels, b) across the ordered mesoporous channels, and c) after the first recovery.

desorption type IV profile with a sharp hysteresis loop, which is characteristic of the highly ordered mesoporous materials, was obtained for **1** (see the Supporting Information).<sup>[11]</sup>

A BET surface area of 455 m<sup>2</sup> g<sup>-1</sup> and a total pore volume of 0.76 cm<sup>3</sup> g<sup>-1</sup> were measured for the material. These values are smaller than those for the starting SBA-15 (864 m<sup>2</sup> g<sup>-1</sup>). BJH calculations showed an average pore diameter of 7.6 nm for **1**, a value which is in good agreement with the pore diameter estimated from the TEM image (Figure 1 a,b).<sup>[11]</sup>

As summarized in Table 1, **1** (ca. 0.004 equiv) is an efficient heterogeneous catalyst for the aerobic oxidation of a wide range of alcohols. A number of different solvents for the oxidation reaction were investigated, and both toluene and trifluorotoluene (TFT) led to high yields of the products.

**Table 1:** Aerobic oxidation of alcohols using **1**.

Entry	R <sup>1</sup>	R <sup>2</sup>	t [h]		Yield [%] <sup>[a,b,c]</sup>	
			O <sub>2</sub>	air	O <sub>2</sub>	air
1	Ph	H	3.5	5.5	> 99 (83)	> 99
2	4-MeC <sub>6</sub> H <sub>4</sub>	H	3.5	5	> 99	> 99
3	2-MeC <sub>6</sub> H <sub>4</sub>	H	8	–	25	–
4	2-ClC <sub>6</sub> H <sub>4</sub>	H	12	–	35	–
5	4-MeOC <sub>6</sub> H <sub>4</sub>	H	2.5	2.5	> 99	> 99
6	4-ClC <sub>6</sub> H <sub>4</sub>	H	12	13	> 99	> 99
7	4-NO <sub>2</sub> C <sub>6</sub> H <sub>4</sub>	H	14	15	> 99	> 99
8	Ph	Me	15	17	> 99 (91)	96
9	Ph	Et	15	17	> 99	93
10	PhCO	Ph	12	12	> 99 (95)	94
11	Ph	Ph	20	20	> 99	> 99
12	PhCH=CH-	H	5	6	98	97
13	PhCH=CH-	Me	6	7	> 95	94
14	(CH <sub>3</sub> ) <sub>2</sub> C=CHCH-	H	6	6.5	> 99	> 99
15	CH <sub>3</sub> (CH <sub>2</sub> ) <sub>4</sub>	CH=CH <sub>2</sub>	6	6	93	93
16	cyclohexenol		7	8	> 95	92
17	CH <sub>3</sub> (CH <sub>2</sub> ) <sub>3</sub>	H	24	–	> 99 <sup>[d]</sup>	–
18	CH <sub>3</sub> (CH <sub>2</sub> ) <sub>5</sub>	H	24	–	> 99 <sup>[d]</sup>	–
19	PhCH <sub>2</sub> CH <sub>2</sub>	H	24	–	> 99 <sup>[d]</sup>	–
20	PhCH <sub>2</sub> CH <sub>2</sub> CH <sub>2</sub>	H	24	–	> 99 <sup>[d]</sup>	–
21	4-phenylcyclohexanol		16	–	53	–
22	4-tert-butylcyclohexanol		16	–	45	–

[a] GC yield based on an internal-standard method unless otherwise stated. [b] Yields in parentheses refer to isolated pure products. [c] The molar ratios of substrate/**1** are 1:0.004. [d] Conversions refer to the corresponding esters.

However, the high cost and toxicity of TFT resulted in us choosing toluene for the subsequent studies. High catalytic activity for both benzylic and allylic alcohols was observed and afforded the corresponding carbonyl compounds in excellent yields.

In particular, the catalyst showed excellent activity for the selective oxidation of various types of allylic alcohols to afford the corresponding  $\alpha,\beta$ -unsaturated carbonyl compounds in excellent yields (Table 1, entries 12–16). Interestingly, the oxidation of primary aliphatic alcohols under the same reaction conditions furnished the corresponding esters in excellent yields in all cases (Table 1, entries 17–20). However, the oxidation of secondary aliphatic alcohols only produced moderate yields of the corresponding ketones (Table 1, entries 21 and 22).

It is worth mentioning that the reaction in air proceeded at a rate comparable to that in pure oxygen, thus indicating that the reaction is not retarded by the concentration of oxygen dissolved in the solvent. However, the oxidation of 2-substituted benzylic alcohols gave the corresponding aldehydes in only low yields (Table 1, entries 3 and 4). A TEM image of the catalyst **1** after the oxidation reaction showed that Pd nanoparticles with a relatively regular size of about 7 nm were mostly formed inside the regular mesoporous channels (Figure 1c). The low conversion of 2-substituted benzylic alcohols can be ascribed to steric hindrance by the quasi-two-dimensional surface of the nanoparticles.<sup>[12]</sup>

Moreover, after the first use of catalyst **1** in the aerobic oxidation of benzyl alcohol (Table 1, entry 1) to give benzaldehyde in 83 % yield, the recovered catalyst was successfully used in 12 subsequent reactions and exhibited consistent catalytic activity (total TON  $\approx$  3000). All recycling runs gave a product purity of greater than 99 % by GC analysis (see the Supporting Information).<sup>[13]</sup> To rule out the contribution of homogeneous catalysis the reaction with benzyl alcohol was also conducted in the presence of catalyst **1** for one hour to obtain a conversion of 37 %. The solid was then hot-filtered off and transferred to another Schlenk flask containing K<sub>2</sub>CO<sub>3</sub> in toluene at 80 °C under O<sub>2</sub>. The catalyst-free solution was then left for 12 hours, but no further reaction took place. Furthermore, analysis of the solution by atomic absorption indicated that no Pd species had leached into the reaction. Nevertheless, it is difficult at this stage to attribute the actual catalytic activity solely to the ligand-bound Pd or to the Pd nanoparticles. It would also not be a surprise if the Pd

nanoparticles stabilized inside the channels of SBA-15 serve as a reservoir for a trace and nondetectable number of Pd particles to react through a homogeneous pathway.<sup>[13]</sup> Further studies on this particular area are currently underway and the results will be published in due course.

It is also noteworthy that the N<sub>2</sub> adsorption/desorption analysis of the recovered catalyst showed very similar isotherms to those of the fresh catalyst **1**, with relatively sharp adsorption and desorption branches in the  $P/P_0$  range of 0.5:1–0.8:1. This observation strongly indicates a relatively narrow size distribution of the mesopores, even in the recovered catalyst (see the Supporting Information), even though the total pore volume decreased from 0.76 to 0.57 cm<sup>3</sup> g<sup>−1</sup>. This observation accompanied by the TEM results suggests that most of the nanometer-scale void space and the channels of the host SBA-15 remain open, although a small portion of the channels may be blocked by Pd nanoparticles (see the Supporting Information).

To better clarify the role of the bipyridyl ligands in our protocol we set up two sets of control experiments. First, we prepared a new catalyst in which SBA-15 without any organic ligands was loaded with Pd(OAc)<sub>2</sub> at the same Pd loading as in **1**. The oxidation of benzyl alcohol was then conducted under the same reaction conditions as before, but using this catalyst. Interestingly, we found that the corresponding benzaldehyde was produced in greater than 99% conversion after 5 h in the first experiment. However, the catalyst activity decreased dramatically when it was used in two further oxidations of benzyl alcohol. The significant deactivation of the catalyst along with a color change to dark grayish is presumably a consequence of the formation of large palladium clusters (palladium black) on the outer surface of SBA-15. In the second experiment, SBA-15 modified with 3-cyanopropyl groups was loaded with Pd(OAc)<sub>2</sub> and the resulting pale yellow solid was tested for its catalytic activity in the same reaction as above. In this case, the solid catalyst showed a high degree of leaching and also the corresponding benzaldehyde was produced in low (less than 25%) conversion after 5 h as a result of the rapid formation of palladium black. Therefore, we believe that the bipyridyl ligands in catalyst **1** might indeed provide a means of uniformly distributing the mononuclear palladium species throughout the solid support to ensure the controlled formation of nanoparticles mostly inside the ordered mesoporous channels of SBA-15. It may also be concluded that the presence of the bipyridyl ligand in the size-restricted mesopores of the parent SBA-15 is effective for preventing both the leaching and the agglomeration of coordinated palladium nanoparticles to form huge particles of palladium black, and this results in the high durability and recycling characteristics of **1**.

In conclusion, we have described a new highly recoverable and efficient palladium-based catalyst for the aerobic oxidation of alcohols. We have also demonstrated that the combination of an organic ligand and ordered mesoporous channels resulted in an interesting synergistic effect that led to enhanced activity, the prevention of the agglomeration of the Pd nanoparticles, and the generation of a durable catalyst. This approach may find potential applications in other types

of nanocatalyzed reactions involving transition metals. Further applications of this new approach on other transition-metal-based nanoparticles are currently ongoing.

## Experimental Section

A mixture of K<sub>2</sub>CO<sub>3</sub> (1 mmol) and **1** (0.18 g, ca. 0.4 mol % of Pd) in toluene (5 mL) was prepared in a two-necked flask. The flask was then evacuated (water aspirator) and refilled with pure oxygen three times (balloon filled). A solution of the alcohol (1 mmol) in toluene (1 mL) was then injected into the solution and the resulting mixture was stirred at 80 °C under oxygen or air (for the time indicated in Table 1). After completion of the reaction, the mixture was filtered off and the catalyst rinsed twice with CH<sub>2</sub>Cl<sub>2</sub> (5 mL). The excess solvent was then removed under reduced pressure to give the corresponding carbonyl compounds (Table 1).

Received: December 8, 2005

Revised: May 4, 2006

Published online: June 23, 2006

**Keywords:** aerobic oxidation · alcohols · mesoporous materials · nanoparticles · palladium

- [1] a) R. A. Sheldon, I. W. C. E. Arend, A. Dijkman, *Catal. Today* **2000**, 57, 157; b) B. Z. Zhan, A. Thompson, *Tetrahedron* **2004**, 60, 2917; c) R. A. Sheldon, *Green Chem.* **2000**, 2, G1; d) P. T. Anastas, L. B. Bartlett, M. M. Kirchhoff, T. C. Williamson, *Catal. Today* **2000**, 55, 11.
- [2] a) K. Kaneda, Y. Fujii, K. Morioka, *J. Org. Chem.* **1996**, 61, 4502; b) K. Kaneda, Y. Fujii, K. Ebitani, *Tetrahedron Lett.* **1997**, 38, 9023; c) K. P. Peterson, R. C. Larock, *J. Org. Chem.* **1998**, 63, 3185; d) T. Nishimura, T. Onoue, K. Ohe, S. Uemura, *Tetrahedron Lett.* **1998**, 39, 6011; e) T. Nishimura, T. Onoue, K. Ohe, S. Uemura, *J. Org. Chem.* **1999**, 64, 6750; f) G.-J. T. Brink, I. W. C. E. Arends, R. A. Sheldon, *Science* **2000**, 287, 1636; g) K. Hallman, C. Moberg, *Adv. Synth. Catal.* **2001**, 343, 260; h) M. J. Schultz, C. C. Park, M. S. Sigman, *Chem. Commun.* **2002**, 3034; i) D. R. Jensen, M. J. Schultz, J. A. Mueller, M. S. Sigman, *Angew. Chem.* **2003**, 115, 3940; *Angew. Chem. Int. Ed.* **2003**, 42, 3810; j) G.-J. T. Brink, I. W. C. E. Arends, R. A. Sheldon, *Adv. Synth. Catal.* **2002**, 344, 355; k) T. Nishimura, S. Uemura, *Synlett* **2004**, 201; l) S. Paavola, K. Zetterberg, T. Privalov, I. Csöreg, C. Moberg, *Adv. Synth. Catal.* **2004**, 346, 237; m) T. Iwasawa, M. Tokunaga, T. Obora, Y. Tsuji, *J. Am. Chem. Soc.* **2004**, 126, 6554; n) M. J. Schultz, S. S. Hamilton, D. R. Jensen, M. S. Sigman, *J. Org. Chem.* **2005**, 70, 3343; o) T. Iwasawa, M. Tokunaga, Y. Obora, Y. Tsuji, *J. Am. Chem. Soc.* **2004**, 126, 6554; p) for a recent excellent review on the palladium-catalyzed oxidation of alcohols, see: J. Muzart, *Tetrahedron* **2003**, 59, 5789; for a recent excellent review on the palladium-catalyzed aerobic oxidation of organic chemicals, see: q) S. S. Stahl, *Angew. Chem.* **2004**, 116, 3400; *Angew. Chem. Int. Ed.* **2004**, 43, 3480; r) T. Nishimura, S. Uemura, *Catal. Surv. Jpn.* **2000**, 4, 135; s) B. A. Steinhoff, A. E. King, S. S. Stahl, *J. Org. Chem.* **2006**, 71, 1861.
- [3] a) T. Nishimura, N. Kakiuchi, M. Inoue, S. Uemura, *Chem. Commun.* **2000**, 1245; b) N. Kakiuchi, Y. Maeda, T. Nishimura, S. Uemura, *J. Org. Chem.* **2001**, 66, 6620; c) N. Kakiuchi, M. Nishimura, M. Inoue, S. Uemura, *Bull. Chem. Soc. Jpn.* **2001**, 74, 165; d) K. Moroi, K. Yamaguchi, T. Hara, T. Mizugaki, K. Ebitani, K. Kaneda, *J. Am. Chem. Soc.* **2002**, 124, 11572; e) K. Mori, T. Hara, T. Mizugaki, K. Ebitani, K. Kaneda, *J. Am. Chem. Soc.* **2004**, 126, 10657; f) U. R. Pillai, E. Sahle-Demessie, *Green*

- Chem.* **2004**, *6*, 161; g) B. Karimi, A. Zamani, J. H. Clark, *Organometallics* **2005**, *24*, 4695.
- [4] a) Y. Uozumi, R. Nakao, *Angew. Chem.* **2003**, *115*, 204; *Angew. Chem. Int. Ed.* **2003**, *42*, 194; b) Z. Hou, N. Theyssen, A. Brinkmann, W. Leitner, *Angew. Chem.* **2005**, *117*, 1370; *Angew. Chem. Int. Ed.* **2005**, *44*, 1346; c) M. S. Kwon, N. Kim, C. M. Park, J. S. Lee, K. Y. Kang, J. Park, *Org. Lett.* **2005**, *7*, 1077.
- [5] a) E. M. Ferreira, B. M. Stoltz, *J. Am. Chem. Soc.* **2001**, *123*, 7725; b) J. T. Bagdanoff, E. M. Ferreira, B. M. Stoltz, *Org. Lett.* **2003**, *5*, 835; c) S. K. Mandal, D. R. Jensen, J. S. Pugsley, M. S. Sigman, *J. Org. Chem.* **2003**, *68*, 4600; d) J. T. Bagdanoff, B. M. Stoltz, *Angew. Chem.* **2004**, *116*, 357; *Angew. Chem. Int. Ed.* **2004**, *43*, 353.
- [6] a) D. R. Rolison, *Science* **2003**, *299*, 1698; b) M. Moreno-Mañas, R. Pleixats, S. Villarroja, *Organometallics* **2001**, *20*, 4524.
- [7] a) C. T. Kresge, M. E. Leonowicz, W. J. Roth, J. C. Vartuli, J. S. Beck, *Nature* **1992**, *359*, 710; b) J. S. Beck, J. C. Vartuli, W. J. Roth, M. E. Leonowicz, C. T. Kresge, *J. Am. Chem. Soc.* **1992**, *114*, 10834.
- [8] a) D. Zhao, J. Feng, Q. Huo, N. Melosh, G. H. Fredrickson, B. F. Chmelka, G. D. Stucky, *Science* **1998**, *279*, 548; b) D. Zhao, Q. Huo, J. Feng, B. F. Chmelka, G. D. Stucky, *J. Am. Chem. Soc.* **1998**, *120*, 6024.
- [9] a) C. Yang, P. Liu, Y. Ho, C. Chiu, K. Chao, *Chem. Mater.* **2003**, *15*, 275; b) J. Zhu, Z. Konya, V. F. Puentes, I. Kiricsi, C. X. Miao, J. W. Ager, A. P. Alivisatos, G. A. Somorjai, *Langmuir* **2003**, *19*, 4396; c) J. He, T. Kunitake, A. Nakao, *Chem. Mater.* **2003**, *15*, 4401; d) T. F. Baumann, J. H. Satcher, *Chem. Mater.* **2003**, *15*, 3745.
- [10] a) S. D. Jackson, G. D. McLellan, G. Webb, L. Conyers, B. T. Keegan, S. Matter, S. Simpson, P. B. Wells, D. A. Whan, R. Whyman, *J. Catal.* **1996**, *162*, 10; b) G. Jacobs, F. Ghadiali, A. Pisanu, A. Borgna, W. Alvarez, D. E. Resasco, *Appl. Catal. A* **1999**, *188*, 79; c) S. Mandal, D. Roy, R. V. Chaudhari, M. Sastry, *Chem. Mater.* **2004**, *16*, 3714.
- [11] See the Supporting Information for details.
- [12] a) H. Tsunoyama, H. Sakurai, Y. Negishi, T. Tsukuda, *J. Am. Chem. Soc.* **2005**, *127*, 9374; b) H. Tsunoyama, H. Sakurai, N. Ichikuni, Y. Negishi, T. Tsukuda, *Langmuir* **2004**, *20*, 11 293.
- [13] For recent examples of metal colloids as reservoirs for homogeneous metal species, see: a) S. Tasler, B. H. Lipshutz, *J. Org. Chem.* **2002**, *67*, 1190; b) I. W. Davis, L. Matty, D. L. Hughes, P. J. Reider, *J. Am. Chem. Soc.* **2001**, *123*, 10 139.



# Multiple Length-Scale Patterning of DNA by Stamp-Assisted Deposition\*\*

Eva Bystrenova, Massimo Facchini,  
Massimiliano Cavallini, Marcello G. Cacace, and  
Fabio Biscarini\*

The adsorption of biopolymers on solid surfaces determines their functionality, thus affecting the response of biomedical devices based on hybrid biological/(in-)organic interfaces. In the case of DNA molecules, the control of their hierarchical organization at surfaces must be achieved. There is a gap in controlling the length scales in experiments with DNA molecules on surfaces. In experiments in which individual molecules are manipulated by local probes or optical tweezers<sup>[1]</sup> the molecules are randomly deposited, anchored, or passed in a flowing liquid in the proximity of a surface. Their precise position cannot be predefined, and the addressing of individual molecules relies on high-resolution microscopes. On the other hand, devices for diagnostics are based on specific oligonucleotide sequences patterned into arrays whose cells have a lateral size in the range of tens of micrometers. In order to hybridize with complementary target sequences, DNA single strands in the cells must retain their own degrees of freedom to as great an extent as possible. A major limitation to the quantitative application of bioarray diagnostics is the interference of steric hindrance in a solid monolayer with the kinetics of hybridization. Therefore devising techniques for patterning individual DNA molecules or oligonucleotide probes from solution onto planar surfaces is of great significance.<sup>[2]</sup> These techniques could also be used for patterning peptides, antibodies, and their aggregates for the fabrication of functional membranes, scaffolds for cell and tissue growth, biosensors with specific recognition, and rewritable memories.<sup>[3]</sup>

Several approaches have been used to control the organization of DNA molecules on a solid surface, mostly with the purpose to align individual molecules along the stretching direction. These include deposition of a DNA solution on polydimethylsiloxane (PDMS) stamp followed by transfer printing on mica,<sup>[4]</sup> molecular combing<sup>[5]</sup> by capillary flow, spin stretching,<sup>[6]</sup> and casting solutions on a surface prepatterned with PDMS.<sup>[7]</sup> Arrays of DNA have been patterned by dip-pen nanolithography,<sup>[8]</sup> deposition on pre-patterned templates by electron-beam lithography,<sup>[9]</sup> drop projection,<sup>[10]</sup> and microcontact printing ( $\mu$ CP).<sup>[11]</sup> All of these

[\*] E. Bystrenova, M. Facchini, M. Cavallini, M. G. Cacace, F. Biscarini  
CNR-Istituto per lo Studio dei Materiali Nanostrutturati  
Sez. di Bologna  
Via P. Gobetti 101, 40129 Bologna (Italy)  
Fax: (+39) 051-639-8539/40  
E-mail: f.biscarini@bo.ismn.cnr.it

[\*\*] This work was supported by MRTN-CT-2004-512161.

approaches yield micropatterned DNA surfaces. The only reports of ordered nanopatterns exploit deposition assisted by nanobeads<sup>[12]</sup> and templates made of anodic porous alumina.<sup>[13]</sup>

We report here on the multiple length-scale patterning of DNA on surfaces based on a printing technique coupled to dewetting. The results consist of nanodots on an area of a few mm<sup>2</sup>, where each dot consists of a few DNA molecules. Our method exploits the self-organization of the DNA molecules in a solution confined between a stamp and the surface. The stamp imposes the larger length scale, and the self-organization brings about the smaller characteristic length scale<sup>[14]</sup> The shape, size, and spacing of DNA nanostructures can be modulated by the choice of stamp features and the concentration of the DNA solution, the latter controlling the wetting regime. For the first time dewetting is demonstrated as a viable route to the patterning of arrays of biomolecules.

Mica was used as a prototype surface for this experiment. Normally a solution of DNA in dilute buffer, such as that employed in the present study, does not wet mica, and when a drop of DNA buffer solution is cast on the mica surface, it generates a random aggregation of biomolecules and their counterions (Figure 1a). This behavior is dictated by the electrostatic repulsion between the negatively charged DNA and the mica surface. The deposited DNA molecules are arranged randomly. This approach is not suitable for any application where localization of molecules at precise positions is required.

To overcome the problem of the placement of biomolecules, we applied micromolding in capillaries (MIMIC)<sup>[15]</sup> to confine the DNA solution within micrometric channels defined by the stamp protrusions in intimate contact with the surface. When the solution is placed at an open end of the cavity, the solution flows inside driven by capillary forces and surface tension with the boundary walls. Self-organization of the molecular solute occurs at the later stages of solvent evaporation. The process is depicted in Scheme 1, and an example of the resulting patterned DNA deposit is shown in Figure 1b.

The large length scale is imposed by the periodicity of the stamp protrusions, while the smaller length scales, specifically the size and separation of the DNA deposits, are controlled by the wetting phenomena that occur in the space between the

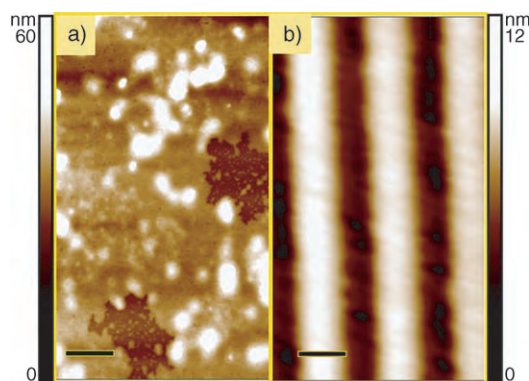
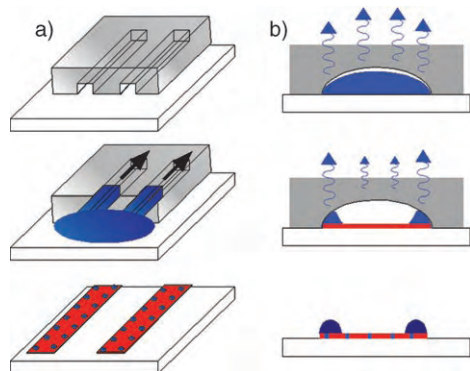


**Figure 1.** AFM images of 10  $\mu\text{L}$  of a solution of  $\lambda\text{DNA}$  on mica. Samples prepared by a) drop casting and b) patterning as shown in Scheme 1a. Scale bar is 1  $\mu\text{m}$ .

stamp and the surface. Depending on the concentration, the solute precipitates when the critical concentration is reached. If this occurs in when the channel is filled with a homogeneous layer of solution (Scheme 1a), the solute precipitates in the form of a thin film. As the solution is pinned to the edges of the channel, the fluid section profile results in an inhomogeneous rate of evaporation of the solvent (Scheme 1b). The convective flow of the solute towards the pinning sites results in the precipitation of split structures in the channel. The stamp was made of PDMS by replica molding.<sup>[15a]</sup> It consists of an array of parallel channels whose width and height are 1  $\mu\text{m}$  and  $230 \pm 15$  nm, respectively, and the pitch is 1.4  $\mu\text{m}$ . The dimensional control can be achieved by changing the stamp features (periodicity and volume of the channels), the DNA concentration, and the volume of the infilling solution. Atomic force microscopy (AFM) was performed with an NT-MDT microscope in semicontact mode in air.  $\lambda\text{DNA}$  solution (100–8000 bp, D9793 Sigma Aldrich) in 10 mM tris(hydroxymethyl)aminomethane hydrogen chloride (Tris-chloride, 93377 Sigma Aldrich) pH 7.4 buffer was used in our experiments. The stamp was placed onto freshly cleaved mica, and a 10- $\mu\text{L}$  droplet of solution was deposited next to it and allowed to dry over approximately 12 h under ambient conditions. The stamp was then gently removed and the sample imaged.

When the concentration of the DNA solution was  $1.25 \mu\text{g mL}^{-1}$ , the resulting pattern consisted of homogeneous lines (Figure 2a) whose full width at half maximum is approximately  $750 \pm 50$  nm, with a periodicity of 1.4  $\mu\text{m}$  and an average height of  $10 \pm 1$  nm. When a more concentrated solution was used, dots formed on top of a layer a few Å thick stretching along the length of the channels. For DNA concentrations between 2 and  $4 \mu\text{g mL}^{-1}$  the dots are roughly aligned but without well-defined spacing (Figure 2b,c). When the concentration exceeded  $5 \mu\text{g mL}^{-1}$  spatial correlations emerge among the dots, and the dot size increases. In this case, the dots are perfectly aligned along the edges of the channel (Figure 2d) as a result of the pinning of the solution and the convective flow from the center towards the edges. The height of the aligned hemispherically capped dots (full width at half maximum: 150 nm) is  $18 \pm 2$  nm on average, at a distance of  $600 \pm 30$  nm along and 1.4  $\mu\text{m}$  perpendicular to the



**Scheme 1.** a) Deposition of DNA from solution by micromolding in capillaries (MIMIC) as described in the text. b) Pinning occurs during the last stages of solvent evaporation.

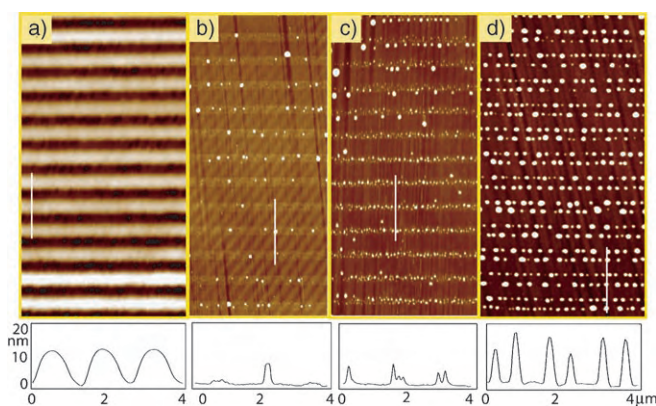


**Figure 2.** AFM images (above) and height profiles (below) of  $\lambda$ DNA (100–8000 bp) patterned on a mica surface at different concentrations: a)  $1.25 \mu\text{g mL}^{-1}$ , b)  $2.0 \mu\text{g mL}^{-1}$ , c)  $2.8 \mu\text{g mL}^{-1}$ , and d)  $5.0 \mu\text{g mL}^{-1}$ .

patterned line. Whereas the height can be measured accurately, the full width at half maximum of the dots may be overestimated by nearly a factor of two because the tip convolution for curvature radii of tips is 10–20 nm.

To verify the results, we performed a control experiment by patterning 10 mM TRIS buffer alone; in this case stripes approximately  $2 \text{ \AA}$  in height were observed. Moreover, we observed an ordered dot array also when the DNA concentration was kept constant at  $5 \mu\text{g mL}^{-1}$  and the buffer concentration was varied between 20 and 100 mM. DNA is known to adopt coiled conformations at high concentration of salts, provided that they are salting-out or “structuring” salts.<sup>[16]</sup> The Tris-chloride system behaves as a neutral or slightly stabilizing salt. We therefore conclude that the arrays consist of DNA dots. We estimate that a dot of average volume,  $3 \times 10^5 \text{ nm}^3$ , may contain up to 10000 base pairs, based on a density of  $1.3 \text{ g cm}^{-3}$  and considering DNA as the most abundant species in the dot.

Patterning occurs during the deposition of DNA molecules inside the channels. The DNA molecules, with a negatively charged shell, have a low affinity to the negatively charged mica surface, and the surface tension is a major driving force for the dot formation. In dilute DNA solutions the repulsive electrostatic interaction between the DNA molecules and the surface are shielded by the buffer, and a homogeneous continuous layer with salt and DNA is deposited. The transition from continuous lines to split strings of dots at higher DNA concentration arises from either dewetting of the initially continuous stripes,<sup>[17]</sup> or nucleation and growth in a partial wetting regime.<sup>[18]</sup> Both phenomena have been observed in thin films of molecular materials and are known to result in spontaneous spatial correlations in size and distance.<sup>[19]</sup> Dewetting is the rupture of an initially continuous film upon an external stimulation. It can develop by nucleation and growth of holes<sup>[20]</sup> or a spinodal mechanism,<sup>[21]</sup> which occurs by fluctuations of the film surface with the emergence of a characteristic wavelength. In the case of growth in partial wetting regime, correlations arise because of intertwined nucleation and ripening, the latter of which is a size- and distance-dependent phenomenon that stops when the nuclei have reached the same size at an equilibrium

distance. In both regimes, the smaller length scales, dot size and spacing, depend on the initial concentration of the solution.

At high concentration, the dots are attracted to the corner formed by the stamp and the surface as a result of both capillary forces and the need to minimize their surface energy. The effect of surface tension and viscosity<sup>[22]</sup> on the channel-filling rate at increasing DNA concentration, as well as the interplay between the flow profile and deposition, are currently under investigation.

In summary, the possibility to pattern ordered arrays of nanostructures made of DNA has been demonstrated using a featureless stamp with micrometer channels. Our results hint at the possibility of the patterning of DNA for many applications by stamp-assisted deposition from a solution onto a substrate in a regime of partial wetting or dewetting. Our method is suitable for upscaling the deposition onto large areas. The control of multiple length scales by exploiting confinement and competing interactions between the adsorbate and the substrate represents a remarkable example of integrated top-down/bottom-up processes.

Received: January 11, 2006

Published online: June 27, 2006

**Keywords:** biotechnology · DNA · nanotechnology · scanning probe microscopy · surface analysis

- [1] C. Bustamante, Z. Bryant, S. B. Smith, *Nature* **2003**, 424, 338–341.
- [2] A. A. Yu, T. Savas, S. Cabrini, E. diFabrizio, H. I. Smith, F. Stellacci, *J. Am. Chem. Soc.* **2005**, 127, 16774–16775.
- [3] J. S. Shin, N. A. Pierce, *Nano Lett.* **2004**, 4, 905–909.
- [4] H. Nakao, M. Gad, S. Sugiyama, K. Otobe, T. Ohtani, *J. Am. Chem. Soc.* **2003**, 125, 7162–7163.
- [5] a) Z. Gueroui, C. Place, E. Freyssingeas, B. P. Berge, *Proc. Natl. Acad. Sci. USA* **2002**, 99, 6005–6010; b) Y. Y. Liu, P. Y. Wang, S. X. Dou, W. C. Wang, P. Xie, H. W. Yin, X. D. Zhang, *J. Chem. Phys.* **2004**, 121, 4302–4309.
- [6] H. Yokota, J. Sunwoo, M. Sarikaya, G. van den Engh, R. Aebbersold, *Anal. Chem.* **1999**, 71, 4418–4422.
- [7] a) P. Bjork, A. Herland, I. G. Scheblykin, O. Inganas, *Nano Lett.* **2005**, 5, 1948–1953; b) D. Mijatovic, J. C. T. Eijkel, A. van den Berg, *Lab Chip* **2005**, 5, 492–500.
- [8] a) N. L. Rosi, C. A. Mirkin, *Chem. Rev.* **2005**, 105, 1547–1562; b) L. M. Demers, D. S. Ginger, S. J. Park, Z. Li, S. W. Chung, C. A. Mirkin, *Science* **2002**, 296, 1836–1838.
- [9] G. J. Zhang, T. Tani, T. Funatsu, I. Ohdomari, *Chem. Commun.* **2004**, 7, 786–787.
- [10] a) V. Dugas, J. Broutin, E. Souteyrand, *Langmuir* **2005**, 21, 9130–9136; b) M. Fujita, W. Mizutani, M. Gad, H. Shigekawa, H. Tokumoto, *Ultramicroscopy* **2002**, 91, 281–285.
- [11] S. A. Lange, V. Benes, D. P. Kern, J. K. Heinrich Horber, A. Bernard, *Anal. Chem.* **2004**, 76, 1641–1647.
- [12] P. Pammer, R. Schlapak, M. Sonnleitner, A. Ebner, R. Zhu, P. Hinterdorfer, O. Hoglinger, H. Schindler, S. I. Howorka, *ChemPhysChem* **2005**, 6, 900–903.
- [13] F. Matsumoto, M. Kamiyama, K. Nishio, H. Masuda, *Jpn. J. Appl. Phys.* **2005**, 44, L355–L358.
- [14] M. Cavallini, F. Biscarini, J. Gomez-Segura, D. Ruiz, J. Veciana, *Nano Lett.* **2003**, 3, 1527–1530.
- [15] a) Y. Xia, G. M. Whitesides, *Angew. Chem.* **1998**, 110, 568–594; *Angew. Chem. Int. Ed.* **1998**, 37, 550–575; b) D. Qin, Y. Xia,

- G. M. Whitesides, *Adv. Mater.* **1996**, 8, 917–919; c) M. Cavallini, P. Stoliar, J. F. Moulin, M. Surin, P. Leclère, R. Lazzaroni, D. W. Breiby, J. W. Andreasen, M. M. Nielsen, P. Sonar, A. C. Grimsdale, K. Müllen, F. Biscarini, *Nano Lett.* **2005**, 5, 2422–2425.
- [16] M. G. Cacace, E. M. Landau, J. J. Ramsden, *Q. Rev. Biophys.* **1997**, 30, 241–278.
- [17] G. Reiter, *Langmuir* **1993**, 9, 1344–1351.
- [18] D. Beysens, C. M. Knobler, *Phys. Rev. Lett.* **1986**, 57, 1433–1436.
- [19] a) M. Brinkmann, F. Biscarini, C. Taliani, I. Aiello, M. Ghedini, *Phys. Rev. B* **2000**, 61, R16339–R16342; b) M. Brinkmann, S. Graff, F. Biscarini, *Phys. Rev. B* **2002**, 66, 165430–165438; c) M. Cavallini, F. Biscarini, S. Léon, F. Zerbetto, G. Bottari, D. A. Leigh, *Science* **2003**, 299, 531.
- [20] R. Seemann, S. Herminghaus, K. Jacobs, *Phys. Rev. Lett.* **2001**, 86, 5534–5537.
- [21] R. Xie, A. Karim, J. F. Douglas, C. C. Han, R. A. Weiss, *Phys. Rev. Lett.* **1998**, 81, 1251–1254.
- [22] P. Doty, B. Bunce McGill, S. A. Rice, *Proc. Natl. Acad. Sci. USA* **1958**, 44, 432–438.



## Efficient Hydrogenation

DOI: 10.1002/anie.200600359

Single-Step Conversion of Dimethyl Terephthalate into Cyclohexanedimethanol with Ru<sub>5</sub>PtSn, a Trimetallic Nanoparticle Catalyst\*\*

Ana B. Hungria, Robert Raja, Richard D. Adams,\*  
 Burjor Captain, John Meurig Thomas,\*  
 Paul A. Midgley, Vladimir Golovko, and  
 Brian F. G. Johnson

As a linker molecule in the polymer industry, 1,4-cyclohexanedimethanol (CHDM) is a highly valued and extensively used reagent.<sup>[1]</sup> It is, for example, preferred<sup>[2]</sup> over

ethylene glycol as a stepping stone in the production of polyester fibers for applications involving polycarbonates and polyurethanes.<sup>[1,3]</sup> Industrially, CHDM is prepared by a two-step process using two reactors.<sup>[1,4]</sup> The first step is the highly exothermic conversion of dimethyl terephthalate (DMT) into dimethyl hexahydroterephthalate (DMHT) by using a supported Pd catalyst in the temperature range of 160–180 °C and an H<sub>2</sub> pressure of 30–48 MPa (300–480 bar). The intermediate DMHT is then converted into CHDM by using a copper–chromite catalyst at temperatures about 200 °C and an H<sub>2</sub> pressure of about 40 bar.<sup>[4]</sup> We have already shown that bimetallic nanoparticle catalysts,<sup>[5]</sup> such as (silica-supported) Ru<sub>5</sub>Pt, Ru<sub>10</sub>Pt<sub>2</sub>, Ru<sub>6</sub>Pd<sub>6</sub>, and Ru<sub>12</sub>Cu<sub>4</sub>, can promote the single-step conversion of DMT into CHDM and are more efficient than the Angelici-type catalyst,<sup>[6]</sup> which consists of a rhodium complex tethered on silica-supported palladium. Herein, we report that of the wide range of possible hydrogenation products of DMT (Scheme 1) mainly the desired products DMHT and CHDM are formed with supported nanoparticles of the trimetallic cluster Ru<sub>5</sub>PtSn. This catalyst shows both the highest activity and selectivity yet observed in any single-step conversion of DMT into CHDM under mild conditions (100 °C, 20 bar H<sub>2</sub>).

The parent material, [PtRu<sub>5</sub>(CO)<sub>15</sub>(μ-SnPh<sub>2</sub>)(μ<sub>6</sub>-C)] (**1**; Figure 1),<sup>[7]</sup> was obtained from the reaction of Ph<sub>3</sub>SnH with the hexanuclear bimetallic complex [PtRu<sub>5</sub>(CO)<sub>16</sub>(μ<sub>6</sub>-C)].<sup>[8]</sup> For comparison, we also carried out a few experiments (see below) using [PtRu<sub>5</sub>(CO)<sub>15</sub>(μ-GePh<sub>2</sub>)(μ<sub>6</sub>-C)] (**2**) prepared from the same hexanuclear complex and Ph<sub>3</sub>GeH. The heterotrinnuclear (Ru–Pt–Sn) complex was anchored onto a mesoporous silica (Davison 38 Å) through silanol groups, as described previously.<sup>[5a,9]</sup> The reaction conditions and the results for the hydrogenation of DMT are presented in Table 1. From these data and from Figure 2, the superior performance of the trimetallic nanoparticle catalyst is clear. This is not surprising in view of the well-known role of tin as a modifier in bimetallic petroleum-reforming catalysts.<sup>[10]</sup> It has also been shown that Pt enhances the activity of RuSn catalysts for the hydrogenation of 1,4-cyclohexanedicarboxylic acid to CHDM.<sup>[11]</sup>

The significant improvement in performance<sup>[9a]</sup> that tin effects to bimetallic catalysts is also relevant here. In previous studies, EXAFS measurements showed that the tin atom serves to anchor the metal clusters firmly to the siliceous supports.<sup>[12]</sup> Similar measurements (now underway) are needed to shed light on the dramatic difference in behavior between Ru<sub>5</sub>PtSn and Ru<sub>5</sub>PtGe, but we can say right away that it was extremely difficult to anchor the germanium parent **2** onto the silica under the same conditions for which **1** became firmly attached. Both Sn<sup>IV</sup> and Ge<sup>IV</sup> are well-known<sup>[13,14]</sup> to be able to replace tetrahedrally coordinated Si<sup>IV</sup> ions in open-framework solids. However, in this work, only infinitesimal quantities of Ge could be detected by electron-induced X-ray emission. We believe that it is more difficult to attach Ge to the siliceous surface because it is more difficult to cleave Ge–C bonds than Sn–C bonds in the Eph<sub>2</sub> ligands of the precursors **1** and **2**, respectively.

High-angle annular-dark-field (HAADF) examination<sup>[15]</sup> of the monodispersed trimetallic catalysts showed high

[\*] Prof. Dr. R. D. Adams, Dr. B. Captain  
 Department of Chemistry and Biochemistry  
 University of South Carolina  
 Columbia, SC 29208 (USA)  
 Fax: (+1) 803-777-6781  
 E-mail: adams@mail.chem.sc.edu

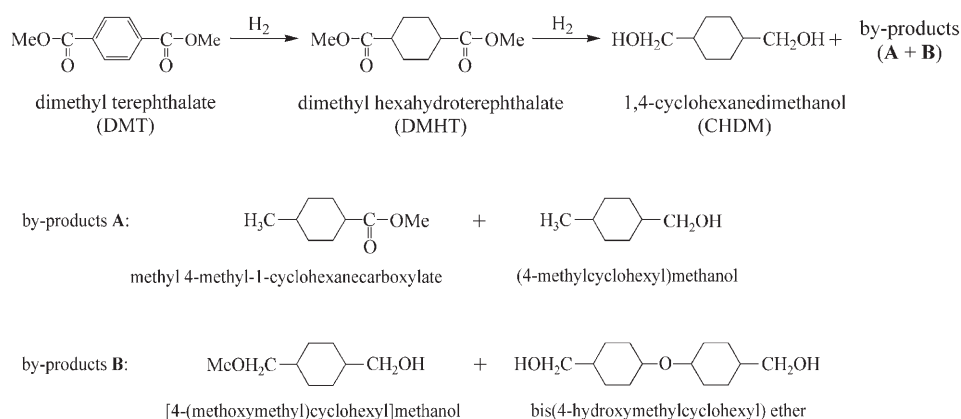
Dr. A. B. Hungria, Prof. J. M. Thomas, Dr. P. A. Midgley  
 Department of Materials Science  
 University of Cambridge  
 Cambridge, CB2 3QZ (UK)  
 Fax: (+44) 1223-334-563  
 E-mail: jmt2@cam.ac.uk

Dr. R. Raja, Dr. V. Golovko, Prof. B. F. G. Johnson  
 University Chemical Laboratory  
 University of Cambridge  
 Cambridge, CB2 1EW (UK)

[\*\*] This research was supported by the Office of Basic Energy Sciences of the US Department of Energy under Grant No. DE-FG02-00ER14980.



Supporting information for this article is available on the WWW under <http://www.angewandte.org> or from the author.



**Scheme 1.** Possible hydrogenation products of DMT.

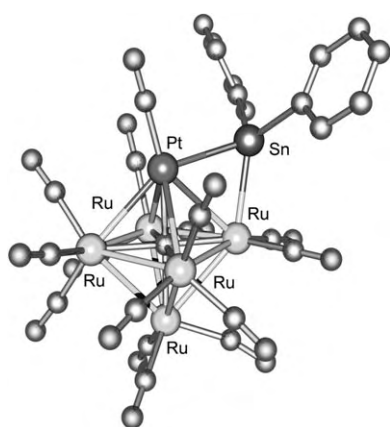


**Figure 1.** Molecular structure of complex 1.

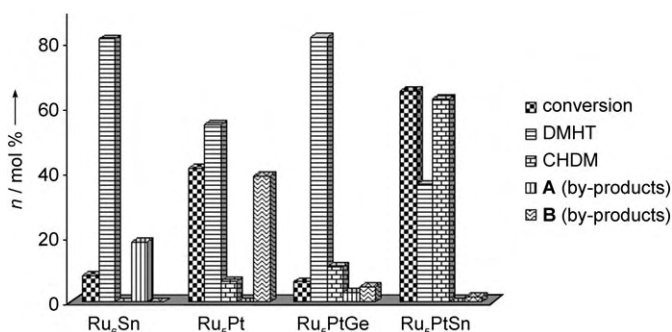


**Figure 2.** Bar chart comparing the activity and selectivity of the  $Ru_5PtSn$  catalyst with those of other bi- and trimetallic catalysts for the hydrogenation of DMT.  $H_2$  pressure: 20 bar;  $T = 373$  K;  $t = 24$  h. See Table 1 and Experimental Section for further details.

**Table 1:** Comparison of catalysts for the hydrogenation of DMT.<sup>[a]</sup>

Catalyst	<i>t</i> [h]	<i>T</i> [K]	Conv. [mol %]	TOF <sup>[b]</sup> [h <sup>−1</sup> ]	Product distribution [mol %]			
					DMHT	CHDM	A	B
$Ru_5PtSn/SiO_2$	4	373	16.8	247	54.7	45.2	—	—
	8	373	36.5	278	41.5	57.5	—	0.9
	24	373	64.9	242	36.2	62.5	—	1.5
$Ru_5PtSn/SiO_2$	8	393	45.4	339	34.9	60.0	—	5.0
	24	393	76.6	290	29.7	45.1	8.9	16.4
$Ru_5PtSn/SiO_2$	8	413	61.2	376	30.3	43.9	9.9	15.8
$Ru_5PtSn/SiO_2^{[c]}$	8	393	63.9	387	9.5	71.2	8.3	11.2
$Ru_5PtGe/SiO_2$	4	373	2.2	19	85.0	10.2	2.2	2.5
	8	373	4.1	35	83.3	10.5	2.5	3.7
	24	373	6.2	22	81.5	10.8	2.9	4.7
$Ru_5Pt/SiO_2$	4	373	6.8	148	55.3	31.9	—	12.7
	8	373	21.2	198	51.2	11.5	—	37.2
	24	373	41.3	145	54.6	6.5	—	38.8
$Ru_6Sn/SiO_2^{[d]}$	4	373	—	—	—	—	—	—
	8	373	5.3	54	77.2	—	22.6	—
	24	373	8.0	27	81.0	—	18.6	—

[a] Conditions, unless otherwise given:  $SiO_2$ : mesoporous Davison silica with a pore diameter of 38 Å;  $H_2$  pressure: 20 bar. [b]  $TOF = [(mol_{substr}) / (mol_{cluster})^{-1} h^{-1}]$ . [c]  $H_2$  pressure: 40 bar. [d] Mesoporous  $SiO_2$  of the MCM-41 type.

dispersion on the supports both before and after catalysis (Figure 3). There was clearly no sintering of the nanoparticles during the exothermic hydrogenation reaction. Moreover, extremely localized nanoanalysis—by electron-induced X-ray emission (Figure 4)—showed that the composition of individual particles (volumes of ca. 1 nm<sup>3</sup> analyzed) is very close to the stoichiometry  $Ru_5PtSn$  of the precursor 1.

HAADF tomography has been successfully applied before to explore the spatial distribution and morphology of supported nanoparticles.<sup>[5,16]</sup> With this purpose, a series of Z-

contrast ( $Z$  = atomic number) images of the  $Ru_5PtSn$  catalyst was acquired every 2° between −70° and 70°. Figure 5 shows the axial projection of a specimen tomogram together with a series of single slices through the tomogram, from which a tendency of the particles to be evenly distributed mainly close to the surface of the material can be observed. In certain slices (Figures 5b and c) there are some zones with a greater density of particles inside the volume of the material. (A movie showing the tomographic retrieval of the interior distribution of the trimetallic nanoparticle catalysts is provided in the Supporting Information.)

In summary, we have discovered the synergistic value of the

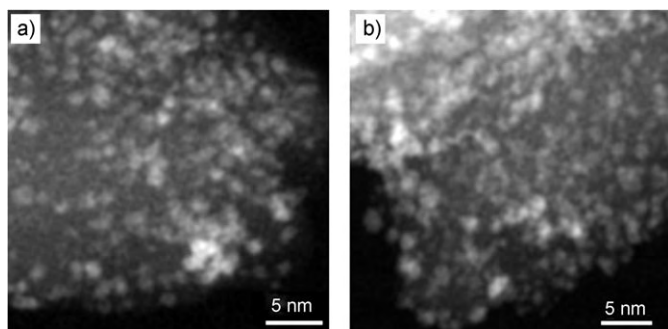


**Figure 3.** HAADF images of  $\text{Ru}_5\text{PtSn}$  nanoclusters on Davison 38 Å silica before (a) and after (b) catalysis.

trimetallic nanoparticle catalyst  $\text{Ru}_5\text{PtSn}$  as a highly efficient and selective means of effecting the catalytic single-step hydrogenation of DMT to CHDM under mild conditions. The presence of tin in the nanoparticle catalyst appears to play a key role in anchoring the particle owing to its oxophilicity for the support, which in turn diminishes the tendency for the nanoparticles to sinter.

### Experimental Section

The organometallic complexes **1** and **2** were prepared according to a published procedure.<sup>[7]</sup> The catalysts were prepared following standard procedures reported earlier.<sup>[5a,9]</sup> Rather than employing as porous support the popular (organic-template-derived) MCM-type (which have non-intersecting pores) and related silicas such as SBA-15, we used a commercially available (from Grace Davison) desiccant silica with a narrow pore-size distribution (designated Davison 923; pore diameter 38 Å). This support is made by reacting sodium silicate with a strong mineral acid (usually sulfuric acid); the pore size is controlled by gel time, final pH value, temperature, concentration of reactants, etc. Compared to MCM-41 type silica, the Davison silica is much lower in cost, thermally and mechanically more stable, and less susceptible to structural collapse. It also has some intersecting pores that facilitate the diffusion of the reactant species to the immobilized catalyst, and its surface area is close to  $700 \text{ m}^2 \text{ g}^{-1}$ .

A slurry of cluster **1** or **2** (100 mg) in dichloromethane (20 mL) and diethyl ether (20 mL) was added under inert atmosphere (Ar) to 400 mg of thoroughly degassed mesoporous silica Davison 923. The mixture was stirred for 12 h. The support with the adsorbed cluster was allowed to settle and the liquid (on top) was removed. The

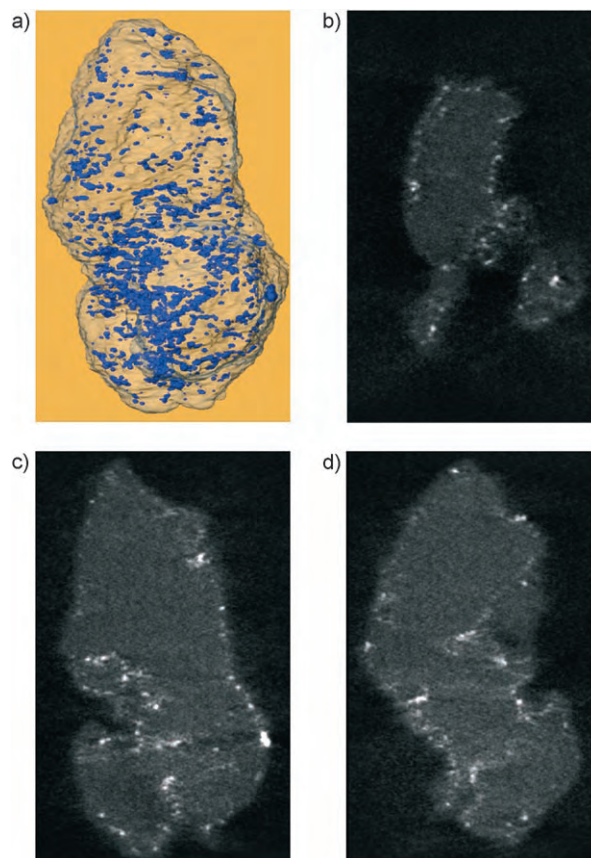


**Figure 5.** Axial projection of a specimen tomogram (a), with successive slices (b–d) through a scanning electron tomogram of  $\text{Ru}_5\text{PtSn}$  supported on Davison 38 Å silica. See Supporting Information for a video of the full dynamic tomogram.

support (with the anchored cluster) was washed twice with diethyl ether (20 mL) and dried in vacuum. The catalyst was activated (decarbonylated) by calcination in vacuum at ca.  $200^\circ\text{C}$  for 2 h. The loading of the clusters on the mesoporous support varied from sample to sample; it was accurately determined by inductively coupled plasma (ICP) analysis for each catalytic experiment. For the  $\text{Ru}_5\text{PtSn}$  cluster, the loadings on the support varied from 0.0015 to 0.0026 mmol, whereas for the  $\text{Ru}_5\text{PtGe}$  cluster the loadings were in the range of 0.00165 to 0.00372 mmol.

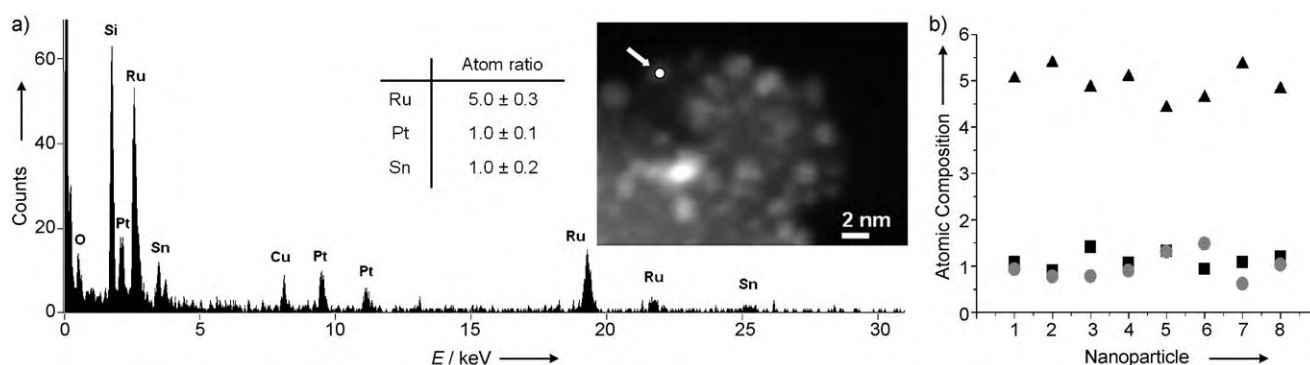


**Figure 4.** a) Electron-induced X-ray emission spectrum of nanoparticles of  $\text{Ru}_5\text{PtSn}$  nanoclusters on Davison 38 Å silica. The arrow in the inset points to the particle for which this emission spectrum was recorded. The peak for Cu in this spectrum originates from the sample holder. b) Plot showing the uniformity of the composition of several nanoparticles of the  $\text{Ru}_5\text{PtSn}$  catalyst: triangles Ru; circles Sn; squares Pt.



**Electron microscopy:** For the tomograms shown in Figure 5, 71 images were recorded with an acquisition time of 20 s every 2° from +70° to −70° using a Fischione ultrahigh-tilt tomography holder model 2020 and a FEI Tecnai F20 field emission gun transmission electron microscope operated at 200 kV in scanning transmission electron microscope (STEM) mode. The probe size was approximately 0.5 nm in diameter, and each HAADF image was recorded with a pixel size of 0.27 nm using a Fischione HAADF detector. The “missing wedge” of data (at high tilts) leads to anisotropic spatial resolution, with a degradation of resolution in the direction parallel to the optical axis of about 30%. Image acquisition was undertaken using the FEI software package Xplore3D. Images were then aligned sequentially using Inspect 3D. Reconstructions, again with Inspect 3D, were performed using either weighted back-projection (WBP) routines or an iterative routine (SIRT) that constrains the reconstructed volume to match the original images when re-projected back along the original tilt directions. This constraint has the effect of minimizing some of the unwanted effects of the limited data sampling and greatly reduces the “fan” artifact that can be evident in many WBP reconstructions. Voxel projections were constructed in Inspect 3D, and surface rendering (after a segmentation process) was undertaken using Amira software.

**Catalysis:** The liquid-phase hydrogenation of DMT was carried out in a high-pressure, teflon-lined, stainless steel catalytic reactor (150 mL). The catalyst (50 mg), which was stored under inert conditions (Ar), was transferred to the reactor (using a robotically controlled catalyst-delivery unit) containing about 2.5 g of DMT (Aldrich, ≥ 99% pure) dissolved in ethanol (75 mL) and 0.5 g of the internal standard (hexadecane). The reactor was sealed, and its contents were inertized (thrice) with dry N<sub>2</sub> prior to reaction. The contents of the reactor were stirred (1700 rpm) and heated to the desired temperature (from a low of 373 K to a high of 413 K). Dry hydrogen (dynamic pressure of 20 or 40 bar, see Table 1) was pressurized into the reaction vessel and, using mini-robot liquid- and gas-sampling valves, small aliquots (0.1 µL) of liquid and gas samples were removed to study the kinetics of the reaction without perturbing the pressure in the reactor.

The composition of the liquid and gaseous products was continuously monitored by using an online computer-controlled system linked to a GC and LC-MS system (Shimadzu QP 8000). The products were analyzed (using hexadecane as the internal standard) by gas chromatography (Varian, Model 3400 CX) employing an HP-1 capillary column (25 m × 0.32 mm) and a flame ionization detector. The identities of the products were first confirmed using authenticated standards, and their individual response factors were determined by using a suitable internal standard (calibration method). The conversions (Conv.) and selectivities (Sel.) were determined as defined by Equations (1) and (2), and the yields were normalized

$$\text{Conv. [\%]} = \frac{\text{mol}_{\text{substrate (initial)}} - \text{mol}_{\text{substrate (residual)}}}{\text{mol}_{\text{substrate (initial)}}} \times 100 \quad (1)$$

$$\text{Sel. [\%]} = \frac{\text{mol}_{\text{individual product}}}{\text{mol}_{\text{total products}}} \times 100 \quad (2)$$

with respect to the response factors obtained as described above. For the internal-standard GC method, the response factor (RF) and mol % of individual products were calculated using Equations (3) and (4). The identity of the products was further confirmed by GC-MS.

$$\text{RF} = \frac{\text{mol}_{\text{product}}}{\text{mol}_{\text{standard}}} \times \frac{\text{area}_{\text{standard}}}{\text{area}_{\text{product}}} \quad (3)$$

$$\text{mol \% product} = \text{RF} \times \text{mol}_{\text{standard}} \times \frac{\text{area}_{\text{product}}}{\text{area}_{\text{standard}}} \times \frac{100}{\text{mol}_{\text{sample}}} \quad (4)$$

The Ru<sub>3</sub>PtSn catalysts were reused three times without appreciable loss in catalytic activity or selectivity. Further experiments

analogous to those reported earlier<sup>[5a]</sup> were carried out to rule out the possibility of leaching, and analysis of the resulting filtrate at the end of reaction (24 h) by ICP and AAS revealed only trace amounts (< 5 ppb) of dissolved metal ions (Pt, Ru, Sn).

Received: January 27, 2006

Revised: April 24, 2006

Published online: June 23, 2006

**Keywords:** electron microscopy · heterogeneous catalysis · hydrogenation · nanoparticles · tomography

- [1] S. R. Turner, *Polym. Sci.* **2004**, *42*, 5847.
- [2] B. J. Sublett, G. W. Connell (Eastman Chemical), US-A 5559159, **1995** [*Chem. Abstr.* **1996**, *125*, 277914v].
- [3] R. R. Amborse, J. B. O'Dwyer, B. K. Johnston, D. P. Zielinski, S. Porter, W. H. Tyger (PPG Industries), US-A 4859743, **1988** [*Chem. Abstr.* **1990**, *112*, 38296v].
- [4] a) M. L. Schlossman (Tevco), US-A 4301046, **1981** [*Chem. Abstr.* **1982**, *96*, 24664c]; b) P. Appleton, M. A. Wood (Eastman Chemical), US 5414159, **1993** [*Chem. Abstr.* **1995**, *123*, 170535d].
- [5] a) R. Raja, T. Khimyak, J. M. Thomas, S. Hermans, B. F. G. Johnson, *Angew. Chem.* **2001**, *113*, 4774; *Angew. Chem. Int. Ed.* **2001**, *40*, 4638; b) J. M. Thomas, B. F. G. Johnson, R. Raja, G. Sankar, P. A. Midgley, *Acc. Chem. Res.* **2003**, *36*, 20.
- [6] H. Yang, H. R. Gao, R. J. Angelici, *Organometallics* **2000**, *19*, 622.
- [7] R. D. Adams, B. Captain, W. Fu, *J. Organomet. Chem.* **2003**, *671*, 158.
- [8] R. D. Adams, W. Wu, *J. Cluster Sci.* **1991**, *2*, 271.
- [9] a) S. Hermans, R. Raja, J. M. Thomas, B. F. G. Johnson, G. Sankar, D. Gleeson, *Angew. Chem.* **2001**, *113*, 1251; *Angew. Chem. Int. Ed.* **2001**, *40*, 1211; b) D. S. Shephard, T. Maschmeyer, G. Sankar, J. M. Thomas, D. Ozkaya, B. F. G. Johnson, R. Raja, R. D. Oldroyd, R. G. Bell, *Chem. Eur. J.* **1998**, *4*, 1214.
- [10] a) R. Burch, *J. Catal.* **1981**, *71*, 348; b) R. Burch, L. C. Garla, *J. Catal.* **1981**, *71*, 360; c) R. Srinivasan, B. H. Davis, *Platinum Met. Rev.* **1992**, *36*, 151; d) T. Fujikawa, F. H. Ribeiro, G. A. Somorjai, *J. Catal.* **1998**, *178*, 58.
- [11] Y. Hara, K. Endou, *Appl. Catal. A: General* **2003**, *239*, 181.
- [12] a) B. F. G. Johnson, S. A. Raynor, D. B. Brown, D. S. Shephard, T. Maschmeyer, J. M. Thomas, S. Hermans, R. Raja, G. Sankar, *J. Mol. Catal. A* **2002**, *182–183*, 89; b) J. M. Thomas, R. Raja, G. Sankar, B. F. G. Johnson, D. W. Lewis, *Chem. Eur. J.* **2001**, *7*, 2973.
- [13] R. M. Barrer in *Hydrothermal Chemistry of Zeolites*, Academic Press, London, **1982**.
- [14] a) R. D. Oldroyd, J. M. Thomas, G. Sankar, *Chem. Commun.* **1997**, 2025; b) R. D. Oldroyd, G. Sankar, J. M. Thomas, D. Ozkaya, *J. Phys. Chem. B* **1998**, *102*, 1849; c) J. M. Thomas, G. Sankar, M. C. Klunduk, M. P. Attfield, T. Maschmeyer, B. F. G. Johnson, R. G. Bell, *J. Phys. Chem. B* **1999**, *103*, 8809.
- [15] a) D. Ozkaya, W. Z. Zhou, J. M. Thomas, P. Midgley, V. J. Keast, S. Hermans, *Catal. Lett.* **1999**, *60*, 113; b) J. M. Thomas, P. A. Midgley, *Chem. Commun.* **2004**, 1253.
- [16] a) P. A. Midgley, M. Weyland, J. M. Thomas, P. L. Gai, E. D. Boyes, *Angew. Chem.* **2002**, *114*, 3958; *Angew. Chem. Int. Ed.* **2002**, *41*, 3804; b) J. M. Thomas, P. A. Midgley, T. J. Yates, J. S. Barnard, R. Raja, I. Arslan, M. Weyland, *Angew. Chem.* **2004**, *116*, 6913; *Angew. Chem. Int. Ed.* **2004**, *43*, 6745.



DOI: 10.1002/anie.200600837

**Formation of Monodisperse (WO<sub>3</sub>)<sub>3</sub> Clusters on TiO<sub>2</sub>(110)\*\****Oleksandr Bondarchuk, Xin Huang, Jooho Kim, Bruce D. Kay, Lai-Sheng Wang, J. M. White,\* and Zdenek Dohnálek\**

The preparation and characterization of small clusters on supporting surfaces remains a significant challenge for nanoscience in general and, in particular, for systems used in surface science as catalysis models.<sup>[1–4]</sup> In the case of metals, clusters of specific size can display dramatically different catalytic properties.<sup>[5–7]</sup> Owing to the high mobility of metals and their tendency to cluster, the preparation methods of mass-selected clusters have been restricted exclusively to soft-landing of gas-phase mass-selected charged species.<sup>[8]</sup> To date, no studies have been reported on mass-selected supported oxide clusters. The preparation techniques that lead to formation of supported oxides have been restricted to metal evaporation in an oxidizing environment and/or postoxidation of evaporated metals both on metal<sup>[9–14]</sup> and metal oxide

substrates.<sup>[15–18]</sup> In all cases, clusters with a distribution of sizes were reported.

Here, we focus our attention on tungsten trioxide, an early transition-metal oxide (TMO) that represents a particularly important class of catalytically active oxides. TMO clusters, and in particular vanadium oxide clusters, have received significant attention in model catalytic studies and have been prepared on such substrates as Pd(111),<sup>[12]</sup> Rh(111),<sup>[11,12]</sup> TiO<sub>2</sub>(110),<sup>[16]</sup> Al<sub>2</sub>O<sub>3</sub>/NiAl(110),<sup>[17,18]</sup> and SiO<sub>2</sub>/Mo(112).<sup>[17]</sup> On Rh(111), a disattachment and diffusion of cyclic V<sub>6</sub>O<sub>12</sub> clusters from two-dimensional vanadium oxide islands was observed, demonstrating that large, cyclic oxide cluster structures can be stable on surfaces.<sup>[11,12]</sup> In this study, we employed a qualitatively different deposition approach, which involved direct sublimation of tungsten trioxide, and prepared monodisperse WO<sub>3</sub> clusters on TiO<sub>2</sub>(110). On the basis of atomically resolved imaging, X-ray photoelectron spectroscopy (XPS), mass balance of deposited WO<sub>3</sub>, and supporting theoretical calculations, we conclude that the clusters are cyclic (WO<sub>3</sub>)<sub>3</sub>. To our knowledge, this is the first successful attempt to form monodisperse oxide clusters supported on another oxide. As such, this system shows great promise as an ideal platform for reactivity studies on well-defined supported model TMO catalysts.

The empty-state scanning tunneling microscopy (STM) image of a clean TiO<sub>2</sub>(110) (1×1) surface is shown in Figure 1a. The bright features along the [001] direction correspond to topographically low-lying pentacoordinated Ti<sup>IV</sup> ions, and the dark rows correspond to topographically high-lying bridge-bonded oxygen (BBO) ions.<sup>[19]</sup> The bright spots between Ti<sup>IV</sup> rows are BBO vacancies (typically 8–14 %) generated from thermally induced TiO<sub>2</sub> bulk reduction.

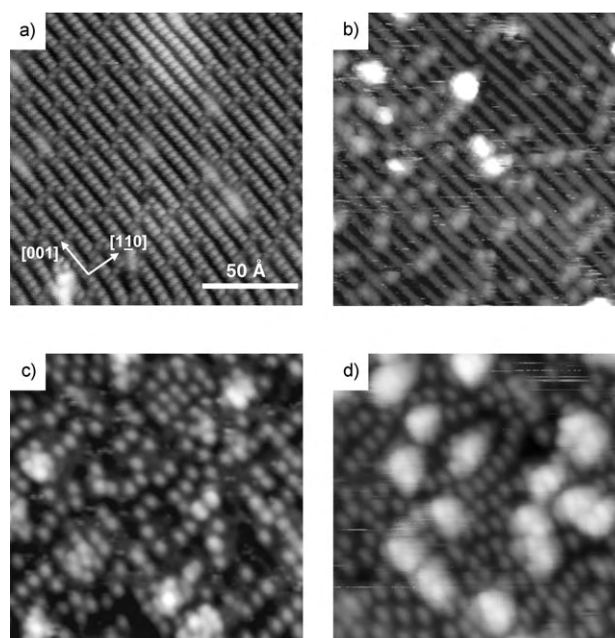


**Figure 1.** STM images (150×150 Å<sup>2</sup>) of a) clean TiO<sub>2</sub>(110) (1×1) and b–d) TiO<sub>2</sub>(110) with different coverages of WO<sub>3</sub>: b) 0.7×10<sup>14</sup>, c) 3.5×10<sup>14</sup>, and d) 5.0×10<sup>14</sup> WO<sub>3</sub> cm<sup>−2</sup>. All images (empty states) were taken with a sample bias of +1.5 V and a current of 0.1 nA.

[\*] Dr. O. Bondarchuk, Prof. J. M. White  
Center for Materials Chemistry  
Texas Materials Institute  
University of Texas  
Austin, TX 78712 (USA)  
Fax: (+1) 509-376-6066  
E-mail: jmwwhite@mail.utexas.edu

Dr. J. Kim, Dr. B. D. Kay, Dr. Z. Dohnálek  
Fundamental Sciences Directorate and  
Institute for Interfacial Catalysis  
Pacific Northwest National Laboratory  
P.O. Box 999, M/S K8-88, Richland, WA 99352 (USA)  
Fax: (+1) 509-376-6066  
E-mail: Zdenek.Dohnalek@pnl.gov

Dr. X. Huang, Prof. L.-S. Wang  
Department of Physics  
Washington State University  
and  
Fundamental Sciences Directorate and  
Institute for Interfacial Catalysis  
Pacific Northwest National Laboratory  
P.O. Box 999, M/S K8-88, Richland, WA 99352 (USA)

[\*\*] J.M.W. and L.S.W. acknowledge support by the US Department of Energy, Office of Basic Energy Sciences, Chemical Sciences Division, under grants DE-FG02-03ER15480 to the University of Texas (J.M.W.) and DE-FG02-03ER15481 to Washington State University (L.S.W.). J.M.W. also acknowledges support from the Robert A. Welch Foundation (Grant F-0032) and the Center for Materials Chemistry at the University of Texas. This work was supported by the US Department of Energy, Office of Basic Energy Sciences, Chemical Sciences, and it was performed at the W. R. Wiley Environmental Molecular Science Laboratory, a national scientific user facility sponsored by the DOE's Office of Biological and Environmental Research located at Pacific Northwest National Laboratory, operated for the US DOE by Battelle (contract DE-AC06-76RLO 1830).

Figure 1b–d show STM images after deposition of  $\text{WO}_3$  at 300 K followed by 10 min of annealing at 600 K. The images clearly exhibit bright features related to deposited  $\text{WO}_3$ . Our attempts to image the as-deposited  $\text{WO}_3$  yielded poorly defined, amorphous-like images (not shown). Clearly, the annealing at 600 K results in the formation of well-defined, monodisperse  $\text{WO}_3$  clusters. From XPS data (not shown), the oxidation state of W remains as +6 upon heating to 600 K.

At low coverage of  $\text{WO}_3$  ( $0.7 \times 10^{14} \text{ WO}_3 \text{ cm}^{-2}$  in Figure 1b), the images show only isolated clusters that are identical in size. While a small fraction ( $\approx 1/5$ ) are centered on the BBO rows, most clusters are centered on the  $\text{Ti}^{\text{IV}}$  rows. As a result of insufficient STM resolution, we were unable to determine whether the latter clusters are centered on top of the  $\text{Ti}^{\text{IV}}$  sites or bridged between them. We speculate that the clusters centered on the BBO rows are located at positions where there were BBO vacancies initially.

At intermediate coverage of  $\text{WO}_3$  ( $3.5 \times 10^{14} \text{ WO}_3 \text{ cm}^{-2}$  in Figure 1c), the majority of the clusters are centered on the  $\text{Ti}^{\text{IV}}$  rows, a small fraction are centered on BBO rows, and some larger three-dimensional aggregates appear. Line scans along the [001] direction over the cluster maxima (not shown) give an apparent cluster height of approximately 1.5 Å and diameter of about 6 Å. Additionally, spatial distribution analysis of the nanoclusters along the [001] direction shows that they never occupy two neighboring  $\text{Ti}^{\text{IV}}$  sites. This arrangement is most likely the result of steric repulsions due to the large cluster size. From this observation, we conclude that the maximum cluster density in the first layer is half the density of  $\text{Ti}^{\text{IV}}$  sites, that is,  $2.6 \times 10^{14} \text{ cm}^{-2}$ .

A further increase in the  $\text{WO}_3$  coverage (Figure 1d,  $5.0 \times 10^{14} \text{ WO}_3 \text{ cm}^{-2}$ ) results primarily in an increased number of larger 3D clusters. The smaller, monodisperse clusters directly in contact with  $\text{TiO}_2(110)$  are also resolved in the image.

Having established that for low doses the clusters are monodisperse (STM) and composed of  $\text{WO}_3$  (XPS), we could determine the number of  $\text{WO}_3$  units in each cluster by correlating (Figure 2) the number of clusters per unit area (from STM) with the areal mass density (from quartz crystal

microbalance, QCM). Within experimental error the slope is three, which is indicative of trimers,  $(\text{WO}_3)_3$ . Note that mass spectrometry studies of vacuum-sublimed  $\text{WO}_3$  reveal that the dominant gas-phase product of  $\text{WO}_3$  sublimation is  $(\text{WO}_3)_3$ .<sup>[20,21]</sup>

In this context, the structure of gas-phase  $(\text{WO}_3)_3$  is known from photoelectron spectroscopy (PES) and density functional theory (DFT) calculations.<sup>[20,21]</sup> The gas-phase  $(\text{WO}_3)_3$  trimer is cyclic with  $D_{3h}$  symmetry<sup>[20]</sup> (its structure is shown schematically in the inset of Figure 2). The calculated diameter of 5.3 Å<sup>[20]</sup> is consistent with STM data and indicates that two  $\text{Ti}^{\text{IV}}$  sites are required to accommodate one cluster. Additional STM data strengthen the evidence favoring the cyclic  $(\text{WO}_3)_3$  trimers on  $\text{TiO}_2(110)$ . In a number of cases, presumably when the STM tip was very sharp, we observed signal contrast within the  $(\text{WO}_3)_3$  clusters. An example is shown in Figure 3, in which clusters exhibit a dark triangular feature with one corner aligned with a  $\text{Ti}^{\text{IV}}$  row and the opposite side tilted with equal probability to the left or right away from the  $\text{Ti}^{\text{IV}}$  row where the cluster is centered. This observation confirms that this structure is not an STM artifact.



**Figure 3.** High-resolution STM image ( $70 \times 70 \text{ Å}^2$ ) exhibiting strong trigonal intensity contrast within each  $(\text{WO}_3)_3$  cluster. One of the corners aligns with a  $\text{Ti}^{\text{IV}}$  row and the opposite side is tilted with equal probability to the left or right away from this row.

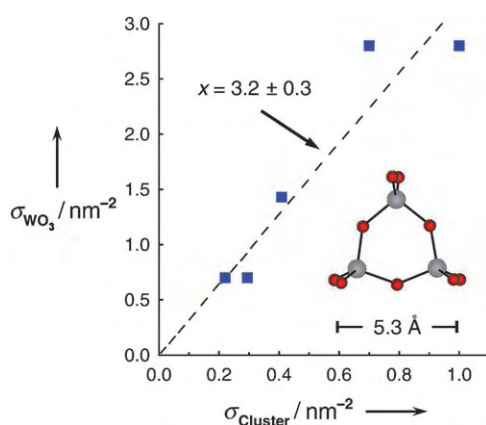


**Figure 2.** Areal mass density of deposited  $\text{WO}_3$  ( $\sigma_{\text{WO}_3}$ ) from QCM studies as a function of the number density of tungsten trioxide clusters ( $\sigma_{\text{Cluster}}$ ) from STM studies. The slope ( $x = 3.2 \pm 0.3$ ) confirms that the clusters are trimers  $(\text{WO}_3)_3$ . The inset indicates the cyclic structure and observed size of gas-phase  $(\text{WO}_3)_3$  trimers.

To explain the contrast within the clusters we turn to DFT calculations of isolated  $(\text{WO}_3)_3$ , as detailed in Reference [20]. A schematic view of the expected acceptor orbitals on the  $D_{3h}$   $(\text{WO}_3)_3$  cluster is shown in Figure 4a. All the empty states in  $(\text{WO}_3)_3$  are W 5d-based, in-plane or out-of-plane molecular orbitals. As the out-of-plane orbitals are expected to have better overlap with states from the STM tip, they should constitute primarily the accepting (imaged) orbitals. The orbital shown in Figure 4a represents one of such out-of-plane 5d orbitals. The bright features with a dark triangular center observed in the high-resolution STM image (Figure 3) resemble the symmetry of the accepting molecular orbitals of the  $(\text{WO}_3)_3$  trimer (Figure 4a).

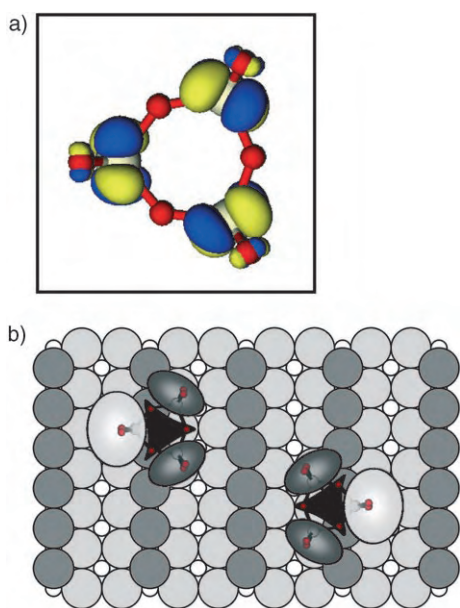


**Figure 4.** a) One of the empty low-lying out-of-plane molecular orbitals of  $(\text{WO}_3)_3$ <sup>[20]</sup> expected to be the accepting states in the high-resolution STM images of  $(\text{WO}_3)_3$ . b) Schematic view of the  $\text{TiO}_2(110)$  surface (small white circles:  $\text{Ti}^{\text{IV}}$ ; light gray circles: bridge-bonded oxygen; dark gray circles: second-layer oxygen) with two cyclic  $(\text{WO}_3)_3$  clusters. The orientation of the top cluster is identical with that shown in part (a). Both clusters have the plane of the rings tilted with two tungsten atoms pointing into the  $\text{Ti}^{\text{IV}}$  row and the third tungsten atom tilted up and pointing towards the neighboring BBO row (one to the left and the other to the right). This tilt results in a different brightness above the three tungsten atoms of the ring, with the top one being significantly brighter than the other two.

To further illustrate the qualitative agreement between the out-of-plane empty states of isolated  $(\text{WO}_3)_3$  clusters (Figure 4a) and the high-resolution empty-state STM image (Figure 3), we show a schematic view of the  $\text{TiO}_2(110)$  surface with two  $(\text{WO}_3)_3$  clusters bound along the  $\text{Ti}^{\text{IV}}$  row. The clusters have the plane of the rings tilted away from the surface normal with two tungsten atoms pointing into the  $\text{Ti}^{\text{IV}}$  row and the third tungsten atom tilted towards the neighboring BBO row (one to the left and the other to the right), as observed in the STM images (Figure 3). This tilt results in a different brightness above the three tungsten atoms of the ring, with the tungsten atom toward the BBO row being significantly brighter than the other two. The structure that emerges involves bonding between neighboring cationic  $\text{Ti}^{\text{IV}}$  and terminal oxygen atoms on adjacent W atoms of the trimer. The tilt to the left or right is likely due to an attractive interaction between the BBO row of the substrate with the third  $\text{W}^{\text{VI}}$  ion of the trimer.

In conclusion, we have synthesized monodisperse oxide clusters supported on  $\text{TiO}_2(110)$  by using direct thermal evaporation of  $\text{WO}_3$ . On the basis of results from STM, XPS, and mass balance of deposited  $\text{WO}_3$ , we conclude that the clusters are cyclic  $(\text{WO}_3)_3$ . This conclusion is further supported by prior mass spectrometric, photoelectron spectroscopy, and density functional theory studies of tungsten trioxide gas-phase species.<sup>[20–22]</sup> The apparent similarity

between the supported and free  $(\text{WO}_3)_3$  clusters suggests stability and robustness, which may prove important for their use as model catalysts.

## Experimental Section

STM experiments were carried out in an ultrahigh vacuum (UHV) chamber equipped with an Omicron variable-temperature scanning tunneling microscope as well as apparatus for Auger electron spectroscopy and quadrupole mass spectrometry. The  $\text{TiO}_2(110)$  rutile single crystal ( $10 \times 5 \times 1 \text{ mm}^3$ , Princeton Scientific) was mounted on a standard Omicron single-plate tantalum holder and heated radiatively with a tungsten filament heater located behind the sample plate. The temperature dependence of the sample on heater power was calibrated in a separate experiment by using a  $\text{TiO}_2(110)$  crystal with a chromel–alumel thermocouple glued directly to the crystal surface. Well-ordered  $\text{TiO}_2(110)$  surfaces were prepared by using repeated cycles of Ar ion sputtering and UHV annealing at 900 K. All STM images (empty states) were taken at room temperature under tunneling conditions typical for  $\text{TiO}_2(110)$  imaging (+1.0–1.7 V, 0.1–0.2 nA). Prior to use, commercial STM tips (Tungsten, Custom Probe Unlimited) were cleaned by means of Ar sputtering and UHV annealing.

$\text{WO}_3$  was deposited by direct sublimation of  $\text{WO}_3$  powder (99.95%, Aldrich) onto  $\text{TiO}_2(110)$  at 300 K using a high-temperature effusion cell (CreaTec). The deposition flux ( $0.2\text{--}1.4 \text{ ng s}^{-1} \text{ cm}^{-2}$ ) was monitored with a quartz crystal microbalance (Inficon). The composition and oxidation state of evaporated tungsten oxide were determined in separate experiments conducted in a second UHV system equipped with an identical deposition setup, XPS apparatus, and other surface analytical tools described previously.<sup>[23]</sup> The W 4f XPS spectra (not shown) demonstrate that the tungsten in the deposited tungsten oxide is exclusively in the +6 oxidation state. Additionally, the W/O ratio in the W 4f and O 1s XPS peaks from the thicker films ( $\approx 50$  monolayers) is 1:3. From these data, we conclude, in agreement with prior mass spectrometric studies,<sup>[22]</sup> that only  $(\text{WO}_3)_x$  is sublimed.<sup>[21]</sup>

Received: March 3, 2006

Published online: June 23, 2006

**Keywords:** heterogeneous catalysis · scanning probe microscopy · surface analysis · transition metals

- [1] C. R. Henry, *Surf. Sci. Rep.* **1998**, *31*, 235.
- [2] B. Kaiser, B. Stegemann, *ChemPhysChem* **2004**, *5*, 37.
- [3] C. T. Campbell, *Surf. Sci. Rep.* **1997**, *27*, 1.
- [4] H. Freund, *Surf. Sci.* **2002**, *500*, 271.
- [5] M. Valden, X. Lai, D. W. Goodman, *Science* **1998**, *281*, 1647.
- [6] B. Yoon, H. Hakkinen, U. Landman, A. S. Worz, J. M. Antonietti, S. Abbet, K. Judai, U. Heiz, *Science* **2005**, *307*, 403.
- [7] X. Tong, L. Benz, P. Kemper, H. Metiu, M. Bowers, S. Buratto, *J. Am. Chem. Soc.* **2005**, *127*, 13516.
- [8] U. Heiz, W. D. Schneider, *Crit. Rev. Solid State Mater. Sci.* **2001**, *26*, 251.
- [9] Z. Song, T. H. Cai, Z. P. Chang, G. Liu, J. A. Rodriguez, J. Hrbek, *J. Am. Chem. Soc.* **2003**, *125*, 8059.
- [10] J. Kim, J. Dohnalek, J. M. White, B. D. Kay, *J. Phys. Chem. B* **2004**, *108*, 11666.
- [11] J. Schoiswohl, G. Kresse, S. Surnev, M. Sock, M. G. Ramsey, F. P. Netzer, *Phys. Rev. Lett.* **2004**, *92*, 206103.
- [12] J. Schoiswohl, S. Surnev, F. P. Netzer, *Top. Catal.* **2005**, *36*, 91.
- [13] J. Biener, E. Farfan-Arribas, M. Biener, C. M. Friend, R. J. Madix, *J. Chem. Phys.* **2005**, *123*.
- [14] D. Song, J. Hrbek, R. Osgood, *Nano Lett.* **2005**, *5*, 1327.

- [15] J. Biener, M. Baumer, R. J. Madix, *Surf. Sci.* **1999**, 432, 178.
- [16] Q. G. Wang, R. J. Madix, *Surf. Sci.* **2001**, 474, L213.
- [17] N. Magg, B. Immaraporn, J. B. Giorgi, T. Schroeder, M. Baumer, J. Dobler, Z. L. Wu, E. Kondratenko, M. Cherian, M. Baerns, P. C. Stair, J. Sauer, H. J. Freund, *J. Catal.* **2004**, 226, 88.
- [18] N. Magg, J. B. Giorgi, T. Schroeder, M. Baumer, H. J. Freund, *J. Phys. Chem. B* **2002**, 106, 8756.
- [19] U. Diebold, *Surf. Sci. Rep.* **2003**, 48, 53.
- [20] X. Huang, H.-J. Zhai, B. Kiran, L.-S. Wang, *Angew. Chem.* **2005**, 117, 7417; *Angew. Chem. Int. Ed.* **2005**, 44, 7251.
- [21] Q. Sun, B. K. Rao, P. Jena, D. Stolcic, Y. D. Kim, G. Gantefor, A. W. Castleman, *J. Chem. Phys.* **2004**, 121, 9417.
- [22] S. Maleknia, J. Brodbelt, K. Pope, *J. Am. Soc. Mass Spectrom.* **1991**, 2, 212.
- [23] Z. Dohnálek, G. A. Kimmel, S. A. Joyce, P. Ayotte, R. S. Smith, B. D. Kay, *J. Phys. Chem. B* **2001**, 105, 3747.



## Nanoparticle Assemblies

DOI: 10.1002/anie.200504107

### Generalized Fabrication of Multifunctional Nanoparticle Assemblies on Silica Spheres\*\*

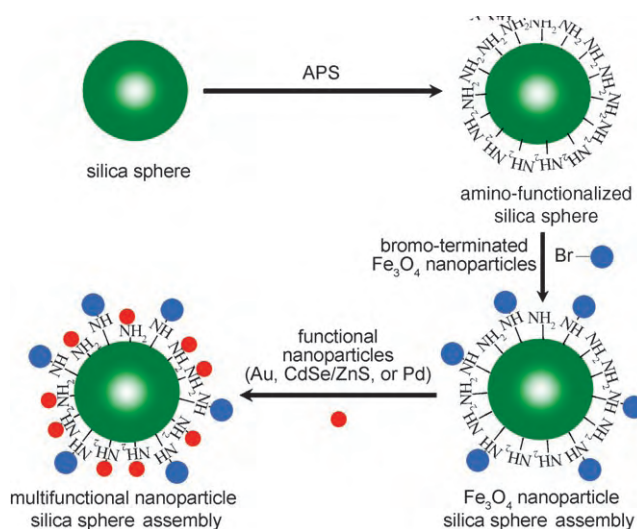
Jaeyun Kim, Ji Eun Lee, Jinwoo Lee, Youngjin Jang, Sang-Wook Kim, Kwangjin An, Jung Ho Yu, and Taeghwan Hyeon\*

Uniformly sized colloidal nanoparticles have attracted a great deal of attention, not only for their fundamental scientific interest, which is derived from their size-dependent properties, but also for their many technological applications, which include biomedical imaging and functional building blocks for nanoscale devices.<sup>[1]</sup> Many types of nanoparticles have been assembled on the surfaces of various spherical supports, such as Stöber silica and polymer latex spheres, by various methods including layer-by-layer (LbL) techniques using oppositely charged polyelectrolytes,<sup>[2]</sup> methods based on direct electrostatic interactions between nanoparticles and supports,<sup>[3]</sup> and techniques based on the coordination of the nanoparticles on amino- or thiol-functionalized silica spheres.<sup>[4]</sup> Magnetic nanoparticles<sup>[5]</sup> have been applied as magnetically separable

catalysts, contrast-enhancement agents for magnetic resonance imaging (MRI), magnetic carriers for drug-delivery systems, biosensors, and bioseparation.<sup>[6]</sup>

Controlled assembly of magnetic nanoparticles on the desired supports is important for these applications. There have been several reports on the assembly of magnetic nanoparticles on spherical templates by the LbL technique.<sup>[2d–g]</sup> For example, alternating layers of polyelectrolytes and magnetite nanoparticles, synthesized in an aqueous phase, were assembled on polystyrene latex spheres. Nanoparticles synthesized in an organic phase are generally more crystalline and uniform than those prepared in the aqueous phase. Recently, FePt alloy nanoparticles<sup>[7]</sup> and magnetite nanoparticles,<sup>[8]</sup> synthesized in an organic phase, were assembled on silica spheres by electrostatic interaction. However, it was necessary for these nanoparticles, initially synthesized in an organic phase, to be transformed into water-dispersible nanoparticles, because the assembly procedures were performed in the aqueous phase. Herein we report on a new procedure to assemble hydrophobic magnetite (Fe<sub>3</sub>O<sub>4</sub>) nanoparticles through covalent bonding on silica spheres by means of a nucleophilic substitution reaction in organic media. We also fabricated multifunctional nanoparticle/silica sphere assemblies by subsequent assembly of nanoparticles of Au, CdSe/ZnS, or Pd on the magnetite nanoparticle-bearing silica spheres. The synthesized multifunctional silica spheres exhibited a combination of magnetism and surface plasmon resonance (Au), luminescence (CdSe/ZnS), or catalysis (Pd).

The general synthetic procedure for multifunctional nanoparticle/silica sphere assemblies is shown in Scheme 1 (see also the Experimental Section). Uniformly sized silica spheres were prepared by the Stöber method.<sup>[9]</sup> For the assembly of the nanoparticles, the surfaces of the silica spheres were functionalized with amino groups by treatment with (3-aminopropyl)trimethoxysilane (APS). Monodisperse nanoparticles of Fe<sub>3</sub>O<sub>4</sub>,<sup>[5h]</sup> Au,<sup>[10]</sup> CdSe/ZnS,<sup>[11]</sup> and Pd<sup>[12]</sup> were synthesized by procedures described previously. To assemble Fe<sub>3</sub>O<sub>4</sub> nanoparticles on the silica spheres, the capping oleic



**Scheme 1.** Synthetic procedure to obtain multifunctional nanoparticle/silica sphere assemblies.

[\*] J. Kim, J. E. Lee, Dr. J. Lee, Y. Jang, K. An, J. H. Yu, Prof. Dr. T. Hyeon National Creative Research Initiative Center for Oxide Nanocrystalline Materials and School of Chemical and Biological Engineering Seoul National University Seoul 151-744 (Korea) Fax: (+82) 2-886-8457 E-mail: thyeon@snu.ac.kr Prof. Dr. S.-W. Kim Department of Molecular Science and Technology Ajou University, Suwon 443-749 (Korea)

[\*\*] T.H. is thankful for financial support by the Korean Ministry of Science and Technology through the National Creative Research Initiative Program.

acid ligands of the  $\text{Fe}_3\text{O}_4$  nanoparticles were exchanged with 2-bromo-2-methylpropionic acid (BMPA).<sup>[13]</sup> The BMPA-stabilized  $\text{Fe}_3\text{O}_4$  nanoparticles were assembled on the surfaces of the amino-functionalized silica spheres. The resulting  $\text{Fe}_3\text{O}_4$  nanoparticle/silica sphere assemblies were designated as Mag-SiO<sub>2</sub>. Subsequently, functional nanoparticles of Au, CdSe/ZnS, or Pd were additionally assembled on Mag-SiO<sub>2</sub> to give multifunctional assemblies designated as Mag-SiO<sub>2</sub>-Au, Mag-SiO<sub>2</sub>-CdSe/ZnS, and Mag-SiO<sub>2</sub>-Pd, respectively.

A field-emission scanning electron microscopy (FE-SEM) image of Mag-SiO<sub>2</sub> (Figure 1 a) shows that uniform 14-nm

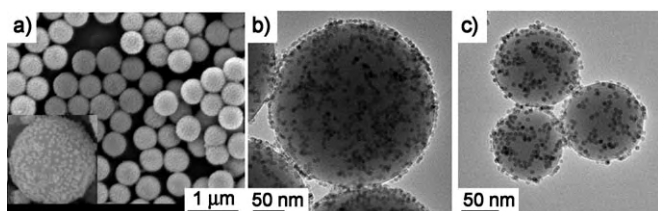


**Figure 1.** SEM and TEM images of Mag-SiO<sub>2</sub>. a) FE-SEM image of 500-nm silica spheres assembled with 14-nm  $\text{Fe}_3\text{O}_4$  nanoparticles (inset: high-magnification FE-SEM image). b) TEM image of 300-nm silica spheres assembled with 7-nm  $\text{Fe}_3\text{O}_4$  nanoparticles. c) TEM image of 100-nm silica spheres assembled with 7-nm  $\text{Fe}_3\text{O}_4$  nanoparticles.

$\text{Fe}_3\text{O}_4$  nanoparticles were well assembled on the surfaces of the 500-nm silica spheres. Figure 1 b and c shows transmission electron microscopy (TEM) images of 7-nm  $\text{Fe}_3\text{O}_4$  nanoparticles assembled on 300- and 100-nm silica spheres, respectively. The BMPA-stabilized  $\text{Fe}_3\text{O}_4$  nanoparticles were covalently bonded onto the surfaces of the amino-functionalized silica spheres by a direct nucleophilic substitution reaction between the terminal Br groups of the ligands and  $\text{NH}_2$  groups on the silica spheres in THF.<sup>[14]</sup> This constitutes a new and simple method of assembling magnetite nanoparticles synthesized in organic media on silica spheres by direct covalent bonding, as opposed to the more complicated LbL method, which is conducted in the aqueous phase by using the electrostatic interaction between magnetic nanoparticles and polyelectrolytes. When the original oleic acid stabilized  $\text{Fe}_3\text{O}_4$  nanoparticles were used instead of BMPA-stabilized ones in assembling  $\text{Fe}_3\text{O}_4$  nanoparticles on the silica spheres, the number of magnetite nanoparticles attached to the silica spheres was substantially reduced.

By using Mag-SiO<sub>2</sub> as support, various multifunctional composite nanoparticle assemblies were fabricated by coordinating functional nanoparticles of Au, CdSe/ZnS, or Pd to the residual surface amino groups. It is well known that alkyl amines such as hexadecylamine and oleylamine, which are often used as stabilizing ligands for nanoparticles of noble metals and semiconductors, bind to the metal atoms on the surfaces of the nanoparticles through the lone-pair electrons on the nitrogen atom.<sup>[11,12]</sup> Similarly, the lone-pair electrons in the amino groups of the amino-modified silica spheres seem to bind to the metal atoms (Au in Au nanoparticles, Zn in the case of CdSe/ZnS core/shell nanoparticles, and Pd in Pd nanoparticles). For example, when we assembled Pd nanoparticles on both amino-modified silica spheres and pristine

unmodified silica spheres, the number of Pd nanoparticles assembled on the former was much higher than that on the latter. Figure 2 a shows a TEM image of Mag-SiO<sub>2</sub>-Au, in which gold nanoparticles 1–3 nm in size and 7-nm  $\text{Fe}_3\text{O}_4$

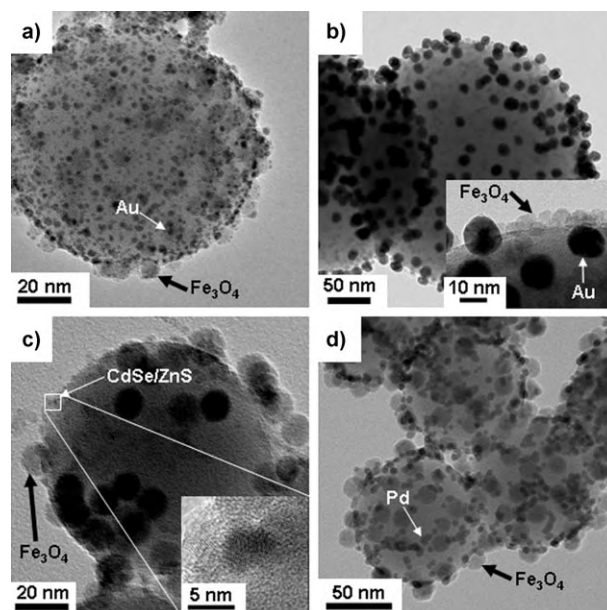


**Figure 2.** a) TEM image of Mag-SiO<sub>2</sub>-Au, in which gold nanoparticles 1–3 nm in size and 7-nm  $\text{Fe}_3\text{O}_4$  nanoparticles were assembled on 100-nm silica spheres. b) TEM image of Mag-SiO<sub>2</sub>-Au, in which 13-nm Au nanoparticles and 7-nm  $\text{Fe}_3\text{O}_4$  nanoparticles were assembled on 300-nm silica spheres. c) TEM image of Mag-SiO<sub>2</sub>-CdSe/ZnS, in which 4.5-nm CdSe/ZnS quantum dots and 14-nm  $\text{Fe}_3\text{O}_4$  nanoparticles were assembled on 100-nm silica spheres. d) TEM image of Mag-SiO<sub>2</sub>-Pd, in which 5-nm Pd nanoparticles and 14-nm  $\text{Fe}_3\text{O}_4$  nanoparticles were simultaneously assembled on 100-nm silica spheres.

nanoparticles were assembled on 100-nm silica spheres. Larger Au nanoparticles (13 nm) were also assembled on 300-nm silica spheres with 7-nm magnetite nanoparticles (Figure 2 b). The TEM and high-resolution TEM (HRTEM) images of Mag-SiO<sub>2</sub>-CdSe/ZnS showed that these composite nanoparticle assemblies consist of highly crystalline 4.5-nm CdSe/ZnS quantum dots coexisting with 14-nm  $\text{Fe}_3\text{O}_4$  nanoparticles on the surfaces of 100-nm silica spheres (Figure 2 c). Assembly of 14-nm  $\text{Fe}_3\text{O}_4$  nanoparticles and 5-nm Pd nanoparticles on 100-nm silica spheres produced Mag-SiO<sub>2</sub>-Pd (Figure 2 d).

The properties of these multifunctional nanoparticle assemblies are depicted in Figure 3. For applications involving magnetic delivery or separation, superparamagnetic properties are more desirable than ferromagnetism, because there should be no residual magnetism after the magnetic field is removed. The field-dependent magnetization curve of the Mag-SiO<sub>2</sub> sample of Figure 1 a at 300 K shows no hysteresis (Figure 3 a), that is, Mag-SiO<sub>2</sub> exhibits superparamagnetic behavior derived from the well-assembled magnetite nanoparticles on the silica spheres. The UV/Vis spectrum of the Mag-SiO<sub>2</sub>-Au of Figure 2 b shows the characteristic surface plasmon band at 530 nm (solid line in Figure 3 b). On the other hand, the supernatant solution after removal of Mag-

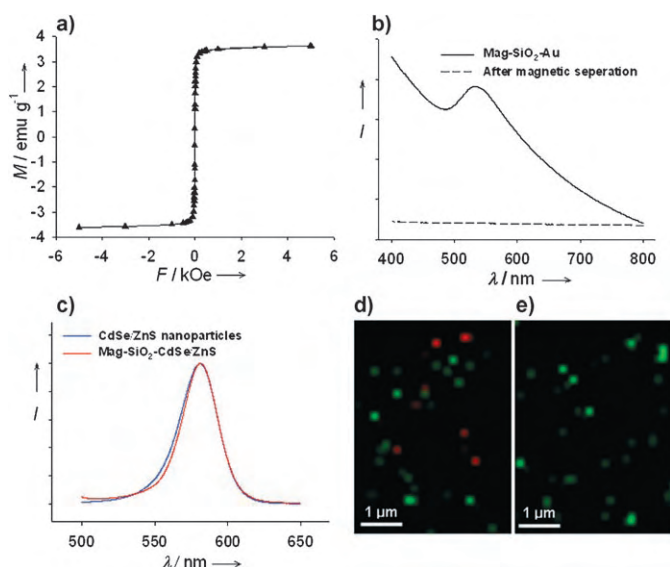


**Figure 3.** a) Field-dependent magnetization at 300 K of the Mag-SiO<sub>2</sub> sample of Figure 1 a. b) UV/Vis absorption spectra of a suspension of the Mag-SiO<sub>2</sub>-Au sample of Figure 2 b before (solid line) and after (dotted line) removal of Mag-SiO<sub>2</sub>-Au by magnetic separation. c) Photoluminescence spectra ( $\lambda_{\text{ex}} = 450$  nm) of pristine CdSe/ZnS nanoparticles (blue line) and the Mag-SiO<sub>2</sub>-CdSe/ZnS sample of Figure 2 c (red line). d, e) Confocal micrographs obtained from a mixed suspension of red-emitting Mag-SiO<sub>2</sub>-CdSe/ZnS and green-emitting SiO<sub>2</sub>-CdSe/ZnS before and after removal of red-emitting Mag-SiO<sub>2</sub>-CdSe/ZnS by using a magnet, respectively.

SiO<sub>2</sub>-Au with a magnet showed no absorption peak (dotted line in Figure 3b) and thus demonstrated the magnetic-separation characteristics of the silica spheres. The Mag-SiO<sub>2</sub>-CdSe/ZnS spheres of Figure 2c exhibited an emission peak at a position slightly red-shifted from that of the pristine CdSe/ZnS nanoparticles (Figure 3c).

To demonstrate the combined magnetic and luminescent properties of Mag-SiO<sub>2</sub>-CdSe/ZnS simultaneously, we prepared red-emitting Mag-SiO<sub>2</sub>-CdSe/ZnS (Fe<sub>3</sub>O<sub>4</sub> nanoparticles and red-emitting CdSe/ZnS nanoparticles assembled on silica spheres) and green-emitting SiO<sub>2</sub>-CdSe/ZnS (green-emitting CdSe/ZnS nanoparticles assembled on silica spheres without Fe<sub>3</sub>O<sub>4</sub> nanoparticles). Then, the two samples were mixed in chloroform and magnetic separation was performed. The confocal micrograph of the mixed solution (Figure 3d) showed that red and green dots were coexistent, whereas only green dots remained after magnetic separation (Figure 3e), that is, red-emitting Mag-SiO<sub>2</sub>-CdSe/ZnS was completely removed from the mixture. This combination of magnetic and optical properties should enable the Mag-SiO<sub>2</sub>-CdSe/ZnS nanoparticle assemblies to be used simultaneously for biolabeling and MRI.

To investigate the catalytic activity of Mag-SiO<sub>2</sub>-Pd, a Sonogashira coupling reaction was performed. After completion of the coupling reaction, Mag-SiO<sub>2</sub>-Pd could easily be separated from the reaction mixture by using a magnet. The reaction solution was dark before magnetic separation (Figure 4a), whereas black Mag-SiO<sub>2</sub>-Pd was attracted to the magnet and a yellowish solution remained after magnetic separation (Figure 4b). High catalytic activities for aryl

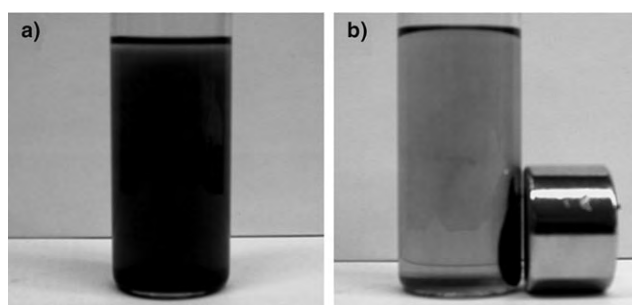
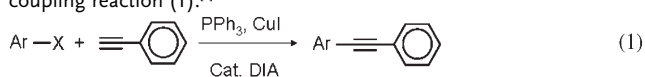


**Figure 4.** Photographs of reaction mixtures a) before and b) after magnetic separation of Mag-SiO<sub>2</sub>-Pd used in reaction (1).

iodides and aryl bromides were shown by Mag-SiO<sub>2</sub>-Pd (Table 1). To investigate the stability of the silica spheres during the catalytic reactions, we performed recycling experiments.

**Table 1:** Test of catalytic activity of Mag-SiO<sub>2</sub>-Pd in the Sonogashira coupling reaction (1).<sup>[a]</sup>



Entry	X	Ar	Catalyst (mol %) <sup>[b]</sup>	Yield [%] <sup>[c]</sup>
1	I	4-acetylphenyl	Mag-SiO <sub>2</sub> -Pd (3)	95.0
2	I	2-thienyl	Mag-SiO <sub>2</sub> -Pd (3)	99.3
3	I	2-thienyl	recovered from entry 2 (3)	98.1
4	I	phenyl	Mag-SiO <sub>2</sub> -Pd (3)	100
5	Br	2-thienyl	Mag-SiO <sub>2</sub> -Pd (5)	99.5
6	Br	2-thienyl	recovered from entry 5 (5)	98.2
7	Br	2-thienyl	recovered from entry 6 (5)	88.1
8	Br	2-thienyl	recovered from entry 7 (5)	75.7
9	Br	2-thienyl	recovered from entry 8 (5)	16.9

[a] DIA = diisopropylamine; reaction conditions: 85 °C, 18 h. [b] Catalyst concentration based on Pd. [c] Yield of isolated product.

As summarized in Table 1 (entries 5–9), Mag-SiO<sub>2</sub>-Pd was recycled four times for coupling 2-bromothiophene. Recently, Nacci et al. reported that the yield of Suzuki and Stille coupling reactions with Pd nanoparticles gradually decreased as recycling proceeded.<sup>[15]</sup> Our recycling experiments showed a similar trend. The catalytic activity of Mag-SiO<sub>2</sub>-Pd for the Sonogashira coupling was maintained above 75 % yield until the third recycling. However, the yield steeply decreased to 17 % in the fourth recycling reaction. The TEM image of the recovered Mag-SiO<sub>2</sub>-Pd after the first reaction showed that not only Fe<sub>3</sub>O<sub>4</sub> nanoparticles but also Pd nanoparticles were firmly attached to the silica spheres. In contrast, the TEM image after the fourth recycling experiment revealed that most of Pd nanoparticles were detached from the silica spheres, whereas many Fe<sub>3</sub>O<sub>4</sub> nanoparticles were still firmly attached to the silica spheres. These results demonstrate that the decrease in yield of the catalytic coupling reactions resulted from detachment of Pd nanoparticles from the silica spheres.

In summary, we have reported a simple, reproducible, and general method of preparing multifunctional nanoparticle assemblies on silica spheres. Magnetite nanoparticles synthe-



sized in an organic phase were covalently bonded on silica spheres, and subsequently nanoparticles of Au, CdSe/ZnS, or Pd were assembled. These multifunctional nanoparticle/silica sphere assemblies are likely to find many catalytic and biomedical applications derived from their combination of magnetic properties with surface plasmon resonance, luminescence, or catalysis.

## Experimental Section

**Synthesis of amino-functionalized Stöber silica spheres:** Uniform 100-, 300-, and 500-nm silica spheres were synthesized by the Stöber method.<sup>[9]</sup> The surfaces of the silica spheres were functionalized with amino groups by treatment with APS in refluxing ethanol.

**Ligand exchange of Fe<sub>3</sub>O<sub>4</sub> nanoparticles synthesized in an organic phase:** Monodisperse Fe<sub>3</sub>O<sub>4</sub> nanoparticles (14- and 7-nm) capped with oleic acid were synthesized in an organic phase by procedures described previously.<sup>[5b]</sup> 50 mg of the as-synthesized nanoparticles were dispersed in 3 mL of chloroform and the resulting solution was added to 30 mL of BMPA in chloroform (0.1 M solution).<sup>[13]</sup> After stirring the solution at room temperature for 48 h, the nanoparticles were precipitated by adding an excess of ethanol. The precipitated nanoparticles were retrieved by centrifugation.

**Synthesis of Mag-SiO<sub>2</sub>:** The BMPA-stabilized magnetite nanoparticles dispersed in 3 mL of THF were added to a solution containing 0.1 g of amino-functionalized silica spheres dispersed in 20 mL of THF, and the resulting dispersion was heated to reflux for 3 h. The magnetite nanoparticle/silica sphere assemblies were isolated by three cycles of centrifugation, redispersion in THF, and magnetic separation.

**Synthesis of Mag-SiO<sub>2</sub>-Au:** Citrate-stabilized gold nanoparticles with sizes of 1–3 and 13 nm were prepared by procedures described previously.<sup>[10]</sup> 10 mg of Mag-SiO<sub>2</sub> was dispersed in 30 mL of aqueous Au nanoparticle solution, and the resulting aqueous dispersion was stirred for 6 h at room temperature. The Mag-SiO<sub>2</sub>-Au spheres were isolated by three cycles of centrifugation, redispersion in water, and magnetic separation.

**Synthesis of Mag-SiO<sub>2</sub>-CdSe/ZnS:** CdSe/ZnS nanoparticles were prepared by a procedure described previously.<sup>[11]</sup> A dispersion of 20 mg of CdSe/ZnS nanoparticles in 3 mL of chloroform was mixed with 10 mg of Mag-SiO<sub>2</sub> in 10 mL of chloroform, and the resulting dispersion was stirred at room temperature for 6 h. The Mag-SiO<sub>2</sub>-CdSe/ZnS spheres were isolated by three cycles of centrifugation, redispersion in chloroform, and magnetic separation.

**Synthesis of Mag-SiO<sub>2</sub>-Pd:** 5-nm Pd nanoparticles were prepared by a procedure described previously.<sup>[12]</sup> A dispersion of 20 mg of Pd nanoparticles in 3 mL of chloroform was mixed with 10 mg of Mag-SiO<sub>2</sub> in 10 mL of chloroform, and the resulting dispersion was stirred at room temperature for 6 h. The Mag-SiO<sub>2</sub>-Pd spheres were isolated by three cycles of centrifugation, redispersion in chloroform, and magnetic separation.

Received: November 18, 2005

Revised: May 12, 2006

Published online: June 27, 2006

**Keywords:** colloids · materials science · nanostructures · self-assembly

- [1] a) G. Schmid, *Nanoparticles: From Theory to Application*, Wiley-VCH, Weinheim, **2004**; b) K. J. Klabunde, *Nanoscale Materials in Chemistry*, Wiley-Interscience, New York, **2001**; c) T. Hyeon, *Chem. Commun.* **2003**, 923; d) A. L. Rogach, D. V. Talapin, E. V. Shevchenko, A. Kornowski, M. Haase, H. Weller,

*Adv. Funct. Mater.* **2002**, *12*, 653; e) A. P. Alivisatos, *Science* **1996**, *271*, 933; f) C. B. Murray, C. R. Kagan, M. G. Bawendi, *Annu. Rev. Mater. Sci.* **2000**, *30*, 545.

- [2] a) F. Caruso, *Adv. Mater.* **2001**, *13*, 11; b) F. Caruso, R. A. Caruso, H. Möhwald, *Science* **1998**, *282*, 1111; c) F. Caruso, H. Lichtenfeld, H. Möhwald, M. Giersig, *J. Am. Chem. Soc.* **1998**, *120*, 8523; d) F. Caruso, A. S. Susha, M. Giersig, H. Möhwald, *Adv. Mater.* **1999**, *11*, 950; e) F. Caruso, M. Spasova, A. Susha, M. Giersig, R. A. Caruso, *Chem. Mater.* **2001**, *13*, 109; f) M. Spasova, V. Salgueiriño-Maceira, A. Schlachter, M. Hilgendorff, M. Giersig, L. M. Liz-Marzán, M. J. Farle, *J. Mater. Chem.* **2005**, *15*, 2095; g) V. Salgueiriño-Maceira, M. Spasova, M. Farle, *Adv. Funct. Mater.* **2005**, *15*, 1036; h) A. Rogach, A. Susha, F. Caruso, G. Sukhorukov, A. Kornowski, S. Kershaw, H. Möhwald, A. Eychmüller, H. Weller, *Adv. Mater.* **2000**, *12*, 333; i) F. Caruso, M. Spasova, V. Salgueiriño-Maceira, L. M. Liz-Marzán, *Adv. Mater.* **2001**, *13*, 1090; j) T. Cassagneau, F. Caruso, *Adv. Mater.* **2002**, *14*, 732.
- [3] a) A. G. Dong, Y. J. Wang, Y. Tang, N. Ren, W. L. Yang, Z. Gao, *Chem. Commun.* **2002**, 350; b) E. M. Claesson, A. P. Philipse, *Langmuir* **2005**, *21*, 9412.
- [4] a) S. J. Oldenburg, R. D. Averitt, S. L. Westcott, N. J. Halas, *Chem. Phys. Lett.* **1998**, *288*, 243; b) S.-W. Kim, M. Kim, W. Y. Lee, T. Hyeon, *J. Am. Chem. Soc.* **2002**, *124*, 7642.
- [5] a) C. B. Murray, D. J. Norris, M. G. Bawendi, *J. Am. Chem. Soc.* **1993**, *115*, 8706; b) S. Sun, C. B. Murray, D. Weller, L. Folks, A. Moser, *Science* **2000**, *287*, 1989; c) T. Hyeon, S. S. Lee, J. Park, Y. Chung, H. B. Na, *J. Am. Chem. Soc.* **2001**, *123*, 12798; d) S. Sun, H. Zeng, D. B. Robinson, S. Raoux, P. M. Rice, S. X. Wang, G. Li, *J. Am. Chem. Soc.* **2004**, *126*, 273; e) F. Dumestre, B. Chaudret, C. Amiens, M.-C. Fromen, M.-J. Casanove, M. Respaud, P. Zurcher, *Angew. Chem.* **2002**, *114*, 4462; *Angew. Chem. Int. Ed.* **2002**, *41*, 4286; f) F. Dumestre, B. Chaudret, C. Amiens, M. Respaud, P. Fejes, P. Renaud, P. Zurcher, *Angew. Chem.* **2003**, *115*, 5371; *Angew. Chem. Int. Ed.* **2003**, *42*, 5213; g) J. Park, E. Lee, N.-M. Hwang, M. Kang, S. C. Kim, Y. Hwang, J.-G. Park, H.-J. Noh, J.-Y. Kim, J.-H. Park, T. Hyeon, *Angew. Chem.* **2005**, *117*, 2932; *Angew. Chem. Int. Ed.* **2005**, *44*, 2873; h) J. Park, K. An, Y. Hwang, J.-G. Park, H.-J. Noh, J.-Y. Kim, J.-H. Park, N.-M. Hwang, T. Hyeon, *Nat. Mater.* **2004**, *3*, 891; i) F. Dumestre, B. Chaudret, C. Amiens, P. Renaud, P. Fejes, *Science* **2004**, *303*, 821; j) C. Desvieux, C. Amiens, P. Fejes, P. Renaud, M. Respaud, P. Lecante, E. Snoeck, B. Chaudret, *Nat. Mater.* **2005**, *4*, 750; k) E. V. Shevchenko, D. V. Talapin, A. L. Rogach, A. Kornowski, M. Hasse, H. Weller, *J. Am. Chem. Soc.* **2002**, *124*, 11480; l) E. V. Shevchenko, D. V. Talapin, H. Schnablegger, A. Kornowski, Ö. Festin, P. Svedlindh, M. Hasse, H. Weller, *J. Am. Chem. Soc.* **2003**, *125*, 9090.
- [6] a) A. Hu, G. T. Yee, W. Lin, *J. Am. Chem. Soc.* **2005**, *127*, 12486; b) R. Weissleder, K. Kelly, E. Y. Sun, T. Shtatland, L. Josephson, *Nat. Biotechnol.* **2005**, *23*, 1418; c) J. W. M. Bulte, S.-C. Zhang, P. van Gelderen, V. Herynek, E. K. Jordan, I. D. Duncan, J. A. Frank, *Proc. Natl. Acad. Sci. USA* **1999**, *96*, 15256; d) Y.-W. Jun, Y.-M. Huh, J.-S. Choi, J.-H. Lee, H.-T. Song, S. Kim, S. Yoon, K.-S. Kim, J.-S. Shin, J.-S. Suh, J. Cheon, *J. Am. Chem. Soc.* **2005**, *127*, 5732; e) H. Gu, P.-L. Ho, K. W. T. Tsang, L. Wang, B. Xu, *J. Am. Chem. Soc.* **2003**, *125*, 15702; f) C. Xu, K. Xu, H. Gu, R. Zheng, H. Liu, X. Zhang, Z. Guo, B. Xu, *J. Am. Chem. Soc.* **2004**, *126*, 9938; g) C. Xu, K. Xu, H. Gu, X. Zhong, Z. Guo, R. Zheng, X. Zhang, B. Xu, *J. Am. Chem. Soc.* **2004**, *126*, 3392; h) J. Won, M. Kim, Y.-W. Yi, Y. H. Kim, N. Jung, T. K. Kim, *Science* **2005**, *309*, 121.
- [7] V. Salgueiriño-Maceira, M. A. Correa-Duarte, M. Farle, *Small* **2005**, *1*, 1073.
- [8] S. I. Stoeva, F. Huo, J.-S. Lee, C. A. Mirkin, *J. Am. Chem. Soc.* **2005**, *127*, 15362.
- [9] W. Stöber, A. Fink, E. Bohn, *J. Colloid Interface Sci.* **1968**, *26*, 62.



- [10] a) D. G. Duff, A. Baiker, *Langmuir* **1993**, *9*, 2301; b) B. V. Enüstün, J. Turkevich, *J. Am. Chem. Soc.* **1963**, *85*, 3317.
- [11] D. V. Talapin, A. L. Rogach, A. Kornowski, M. Haase, H. Weller, *Nano Lett.* **2001**, *1*, 207.
- [12] S.-W. Kim, J. Park, Y. Jang, Y. Chung, S. Hwang, T. Hyeon, *Nano Lett.* **2003**, *3*, 1289.
- [13] Y. Wang, X. Teng, J.-S. Wang, H. Yang, *Nano Lett.* **2003**, *3*, 789.
- [14] a) K. Ha, Y.-J. Lee, H. J. Lee, K. B. Yoon, *Adv. Mater.* **2000**, *12*, 1114; b) S.-S. Bae, D. K. Lim, J.-I. Park, W.-R. Lee, J. Cheon, S. Kim, *J. Phys. Chem. B* **2004**, *108*, 2575.
- [15] V. Calò, A. Nacci, A. Monopoli, F. Montingelli, *J. Org. Chem.* **2005**, *70*, 6040.

# Ferrocene Derivatives

DOI: 10.1002/anie.200601067

## Visible-Light Photochromism of Bis(ferrocenylethynyl)ethenes Switches Electronic Communication between Ferrocene Sites\*\*

Ryota Sakamoto, Masaki Murata, and Hiroshi Nishihara\*

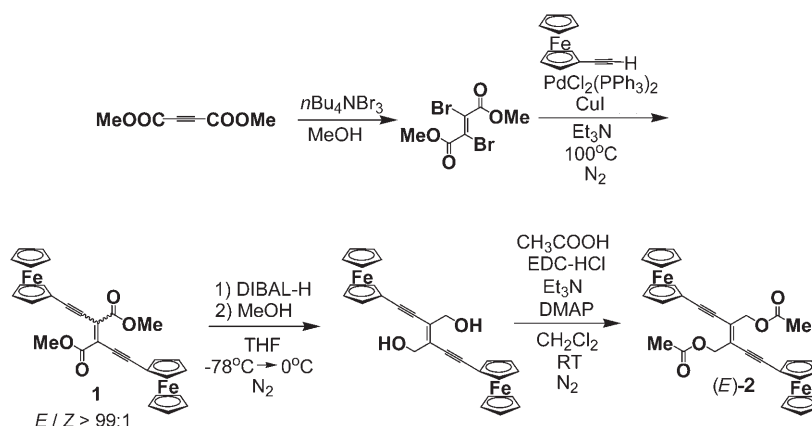
Ferrocene has many attractive features, such as excellent reversible redox properties, high solubility in organic media, and high modifiability with organic chemical methods,<sup>[1]</sup> and it remains a promising molecular fragment for molecular devices. Related to the redox properties, intramolecular mixed-valence interactions between multiple ferrocene sites have been regarded as a key to the realization of molecular electronics, such as molecular quantum cellular automata (QCA),<sup>[2]</sup> and the fundamental evaluation of their ability as molecular electronic wires.<sup>[3]</sup>

Ferrocene exhibits an excellent affinity for organic  $\pi$ -bridge systems, with strong electronic coupling between the Fe d orbitals and the  $\pi$  orbitals of the cyclopentadienyl ring and  $\pi$  bridges. This mutual interaction can yield an intramolecular mixed-valence interaction<sup>[4]</sup> and a charge-transfer (CT) band in the visible region.<sup>[5–7]</sup> This CT transition from ferrocene d orbitals to the LUMO of either the acceptor group<sup>[5]</sup>

or the  $\pi^*$  orbital of the bridge<sup>[6]</sup> is key to the excellent nonlinear optical properties of ferrocene(donor)–acceptor combinations<sup>[5]</sup> and, for example, the green-light-induced *trans*-to-*cis* isomerization of the azobenzene moiety in ferrocenylazobenzenes.<sup>[6]</sup>

To our knowledge, light-triggered electronic communication between ferrocenes has never been reported before. In the present study, we adopted an ethynylethene  $\pi$  framework<sup>[8]</sup> as a bridge fragment, which undergoes *Z*–*E* photoisomerization on the central C–C double bond. The greatest benefit of introducing this class of photochromic compounds is the thermal stability of the *Z* and *E* isomers,<sup>[8]</sup> which is important in terms of their applications as, for example, molecular switching devices. Additionally, the possibility of modifying substituents on the central C–C double bond is also likely to be important in terms of tuning the photoisomerization behavior and mixed-valence communication by the electronic perturbation of the  $\pi$  system. These properties of ethynylethene are superior to those of other photochromic species such as the azo group. Our attempts at quantitative analysis of the mixed-valence interaction in *cis*-azoferrocene have not been successful because of the low stability of the *cis* isomer.<sup>[9,10]</sup>

Herein, we report two types of ferrocene-conjugated ethynylethenes, (*E*)-**1** and (*E*)-**2** (Scheme 1), which differ in the presence of a  $\pi$  or  $\sigma$  substituent on the central double bond. Their photophysical properties also contrast with each other: (*E*)-**1** showed visible-light photochromism, whereas



**Scheme 1.** Syntheses of (*E*)-**1**, (*Z*)-**1**, and (*E*)-**2**. EDC-HCl = 1-ethyl-3-(dimethylaminopropyl)-carbodiimide hydrochloride; DIBAL-H = diisobutylaluminumlithium hydride; DMAP = 4-(*N,N*-dimethyl)aminopyridine.

[\*] R. Sakamoto, Dr. M. Murata, Prof. Dr. H. Nishihara  
Department of Chemistry  
School of Science  
The University of Tokyo  
7-3-1, Hongo, Bunkyo-ku, Tokyo, 113-0033 (Japan)  
Fax: (+81) 3-5841-8063  
E-mail: nishihara@chem.s.u-tokyo.ac.jp

[\*\*] This work was supported by Grants-in-Aid for Scientific Research (Nos. 16047204 (area 434) and 17205007) and by a grant from The 21st Century COE Program for Frontiers in Fundamental Chemistry from MEXT, Japan.

Supporting information for this article is available on the WWW under <http://www.angewandte.org> or from the author.

(*E*)-**2** did not show any photochromic behavior. Also discussed is the decrease in the strength of the mixed-valence interaction between the two ferrocene moieties accompanying *E*→*Z* isomerization in **1**. Compounds (*E*)-**1** and (*E*)-**2** were synthesized according to the procedure outlined in Scheme 1. The *Z* isomer of **1** was obtained as a minor by-product during the synthesis of (*E*)-**1**.<sup>[11]</sup> The absolute configurations of (*E*)-**1** and (*Z*)-**1** were confirmed by single-crystal X-ray analysis (Figure 1).<sup>[12]</sup> The configuration of **2** (*E*) was assigned with the aid of IR spectroscopy, by comparison of the absorptions derived from the carbonyl and C–C triple bonds of **2** with those of (*E*)-**1** and (*Z*)-**1**.

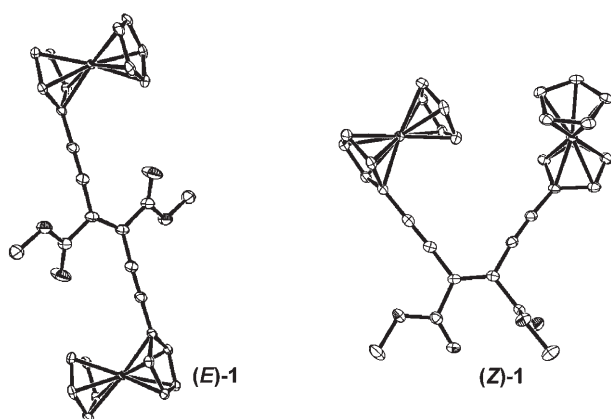


**Figure 1.** ORTEP drawings of (E)-1 and (Z)-1 with thermal ellipsoids set at the 50% probability level. Hydrogen atoms are omitted.

Both (E)-1 and (E)-2 displayed electronic absorption bands in the visible region, together with the  $\pi$ - $\pi^*$  band in the UV region (Figure 2). On the other hand, the analogues (E)-3 (*p*-tol-C $\equiv$ C-(COOMe)C=C(COOMe)-C $\equiv$ C-*p*-tol) and (E)-4

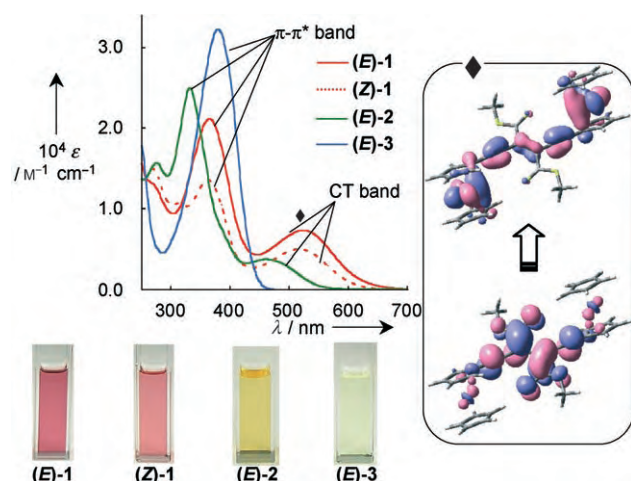


**Figure 2.** Electronic spectra of (E)-1, (Z)-1, (E)-2, and (E)-3 in dichloromethane, the main transition in the CT band of (E)-1 (marked with  $\blacklozenge$ ), and photos of each compound in dichloromethane.

(*p*-tol-C $\equiv$ C-(CH<sub>2</sub>OAc)C=C(CH<sub>2</sub>OAc)-C $\equiv$ C-*p*-tol), which lack the ferrocene moieties, showed only the  $\pi$ - $\pi^*$  band. Such dual absorptions were previously seen in ferrocene-containing pigments, which are excellent nonlinear optical materials,<sup>[5b]</sup> and in our azo precursors.<sup>[6,9,10]</sup> Time-dependent density functional theory (TD-DFT) calculations indicate that these bands in the visible region are assignable to CT-like transitions from the ferrocene d to the ethynylethene  $\pi^*$  orbitals (Figure 2), with some contribution by the enyne bridge, which again showed the same features as in two previous studies.<sup>[5b,6]</sup> Lower extinction coefficients ( $\epsilon$ ) were observed for both the  $\pi$ - $\pi^*$  and CT bands in (Z)-1 compared to those in (E)-1. With regards to (E)-2, a decrease in  $\epsilon$  and a blue shift in the CT band were found (Figure 2).

Irradiation of (E)-1 in dichloromethane with a mixture of green (546 nm) and yellow (578 nm) light from a superhigh-pressure Hg lamp<sup>[13]</sup> led to excitation of the CT band, with a

stepwise decrease observed in the  $\pi$ - $\pi^*$  band, as is typical in the *E*-to-*Z* transformation,<sup>[8]</sup> as well as in the CT band with time (Figure 3). In addition, one isosbestic point was observed which confirmed the absence of side reactions such as decomposition. A one-step reaction from the *E* to *Z* form was observed by <sup>1</sup>H NMR spectroscopy (Figure 3). The

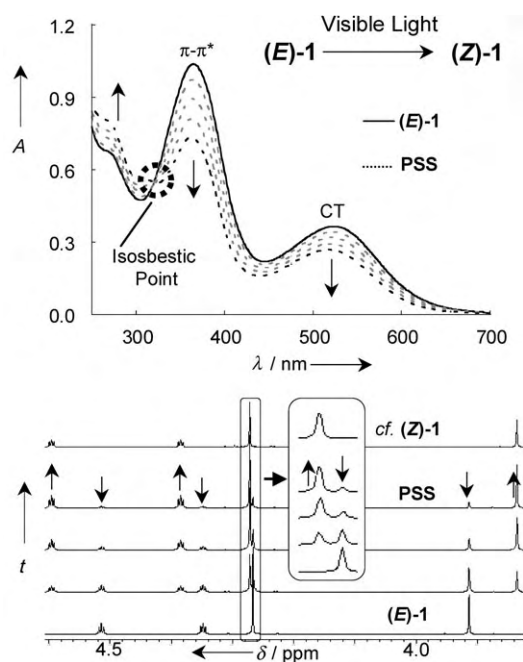


**Figure 3.** Time-course UV/Vis (upper) and <sup>1</sup>H NMR (lower) spectral changes of (E)-1 upon irradiation with light at 546 nm and 578 nm in dichloromethane and [D<sub>2</sub>]dichloromethane. PSS = photostationary state.

proportion of *Z* isomer in the photostationary state was calculated to be 89% based on the ratio of the integrals. This value is much higher than the percentage found for azo compounds<sup>[6,14]</sup> upon excitation of the CT transition from the metal moiety to the  $\pi^*$  orbital of the azo moiety. The quantum yields in toluene upon irradiation with green light at 546 nm<sup>[15]</sup> were found to be  $\Phi_{E \rightarrow Z} = 1.7 \times 10^{-5}$  and  $\Phi_{Z \rightarrow E} = 0.47 \times 10^{-5}$ .<sup>[16,17]</sup> Additionally,  $\pi$ - $\pi^*$  excitation with UV light at 365 nm also afforded *E*→*Z* isomerization, which is an intrinsic property in ethynylethenes.<sup>[8]</sup>

In contrast, (E)-2 showed no photochemical response to excitation of the CT band in the visible region or to excitation of the  $\pi$ - $\pi^*$  band in the UV region, as confirmed also by <sup>1</sup>H NMR spectroscopy. If we consider the photoisomerization behavior together with the differences in the electronic spectra, it can be concluded that the substituents attached directly to the central double bond contribute greatly to the photochemical properties in our ferrocene-conjugated ethynylethene system. This speculation is well supported by the photochemical responses of the analogues that lack the ferrocene moieties. For example, (E)-3 showed *E*→*Z* photoisomerization upon excitation of the  $\pi$ - $\pi^*$  band, just as (E)-1. On the contrary, (E)-4 revealed no photochromic behavior just as (E)-2, but instead it underwent photochemical degradation.

We evaluated the mixed-valence interaction by studying the splitting between the two redox potentials,  $\Delta E^0$ , as determined from cyclic voltammograms of (E)-**1** and (Z)-**1** measured in dichloromethane containing  $n\text{Bu}_4\text{NBF}_4$  ( $0.1 \text{ mol dm}^{-3}$ ). The result showed a larger  $\Delta E^0$  value in (E)-**1** (70 mV) than in (Z)-**1** (48 mV) (Figure 4).<sup>[18]</sup> This is

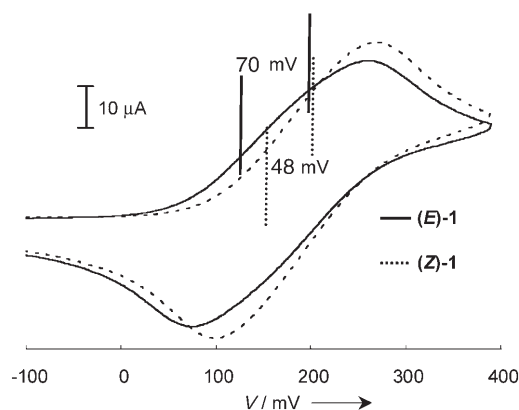


**Figure 4.** Cyclic voltammograms of (E)-**1** ( $1.2 \times 10^{-3} \text{ mol dm}^{-3}$ ) in dichloromethane containing  $n\text{Bu}_4\text{NBF}_4$  ( $0.1 \text{ mol dm}^{-3}$ ) at a sweep rate of  $100 \text{ mV s}^{-1}$ . The potential was measured relative to the ferrocenium/ferrocene couple.

consistent with the fact that  $\pi$  conjugation, namely through-bond interaction,<sup>[4]</sup> is stronger in the E form and spatial interaction<sup>[19]</sup> is negligible because the two redox sites are well separated even in (Z)-**1** (Fe–Fe 6.17 Å), as indicated by the single-crystal X-ray structural analysis (Figure 2).

In summary, the perturbation by the transition-metal complex (ferrocene) by the organic photochromic framework (ethynylethene) and vice versa in the system reported here were both sophisticatedly utilized to attain visible-light photochromism that causes a change in electronic communication between the ferrocene sites. This result is expected to contribute to the development of well-defined supramolecular devices.

Received: March 17, 2006

Revised: May 1, 2006

Published online: June 26, 2006

**Keywords:** electrochemistry · metallocenes · mixed-valent compounds · molecular devices · photochromism

- [1] *Ferrocenes* (Eds.: A. Togni, T. Hayashi), VCH Publishers, New York, **1995**.
- [2] a) J. Jiao, G. J. Long, F. Grandjean, A. M. Beatty, T. P. Fehlner, *J. Am. Chem. Soc.* **2003**, *125*, 7522–7523; b) J. Jiao, G. J. Long, L. Rebbouh, F. Grandjean, A. M. Beatty, T. P. Fehlner, *J. Am. Chem. Soc.* **2005**, *127*, 17819–17831; c) C. S. Lent, B. Isakaen, M. Lieberman, *J. Am. Chem. Soc.* **2003**, *125*, 1056–1063; d) C. S. Lent, *Science* **2000**, *288*, 1597–1599.
- [3] G.-L. Xu, R. J. Crutchley, M. C. DeRosa, Q.-J. Pan, H.-X. Zhang, X. Wang, T. Ren, *J. Am. Chem. Soc.* **2005**, *127*, 13354–13363.
- [4] a) D. Astruc, *Acc. Chem. Res.* **1997**, *30*, 383–391; b) A.-C. Ribou, J.-P. Launay, M. L. Sachtelben, H. Li, C. W. Spangler,

- Inorg. Chem.* **1996**, *35*, 3735–3740; c) M. Rosenblum, N. Brown, J. Papenmeier, M. Applebaum, *J. Organomet. Chem.* **1966**, *6*, 173–180; d) M. Kurosawa, T. Nankawa, T. Matsuda, K. Kubo, M. Kurihara, H. Nishihara, *Inorg. Chem.* **1999**, *38*, 5113–5123; e) T.-Y. Dong, T.-J. Ke, S.-M. Peng, S.-K. Yeh, *Inorg. Chem.* **1989**, *28*, 2103–2106; f) Y. J. Chen, D.-S. Pan, C.-F. Chiu, J.-X. Su, S.-J. Lin, K. S. Kwan, *Inorg. Chem.* **2000**, *39*, 953–958; g) A. Carella, G. Rapenne, J.-P. Launay, *New. J. Chem.* **2005**, *29*, 288–290.
- [5] a) M. L. H. Green, S. R. Marder, M. E. Thompson, J. A. Bandy, D. Bloor, P. V. Kolinsky, R. J. Jones, *Nature* **1987**, *330*, 360–362; b) S. Barlow, H. E. Bunting, C. Ringham, J. C. Green, G. U. Bublitz, S. G. Boxer, J. W. Perry, S. R. Marder, *J. Am. Chem. Soc.* **1999**, *121*, 3715–3723.
- [6] a) M. Kurihara, A. Hirooka, S. Kume, M. Sugimoto, H. Nishihara, *J. Am. Chem. Soc.* **2002**, *124*, 8800–8801; b) A. Sakamoto, A. Hirooka, K. Namiki, M. Kurihara, M. Murata, M. Sugimoto, H. Nishihara, *Inorg. Chem.* **2005**, *44*, 7547–7558.
- [7] W. Ding, C. T. Sanderson, R. C. Conover, M. K. Johnson, I. J. Amster, C. Kutal, *Inorg. Chem.* **2003**, *42*, 1532–1537.
- [8] a) L. Gobbi, P. Seiler, F. Diederich, *Angew. Chem.* **1999**, *111*, 737–740; *Angew. Chem. Int. Ed.* **1999**, *38*, 674–678; b) R. E. Martin, J. Bartek, F. Diederich, R. R. Tykwinski, E. C. Meister, A. Hilger, H. P. Lüthi, *J. Chem. Soc. Perkin Trans. 2* **1998**, 233–242; c) L. Gobbi, P. Seiler, F. Diederich, *Helv. Chim. Acta* **2000**, *83*, 1711–1723.
- [9] M. Kurihara, T. Matsuda, A. Hirooka, T. Yutaka, H. Nishihara, *J. Am. Chem. Soc.* **2000**, *122*, 12373–12374.
- [10] Y. Men, S. R. Korupolu, M. Kurihara, J. Mizutani, H. Nishihara, *Chem. Eur. J.* **2005**, *11*, 7322–7327.
- [11] This may be attributable to the fact that the central double bond rotated when the reactant was on a Pd atom. However, the possibility that stray light triggered the E→Z photoisomerization in the reaction pot or during purification cannot be excluded.
- [12] Intensity data were collected at 113(2) K on a RIGAKU Mercury CCD using monochromated MoK $\alpha$  radiation ( $\lambda = 0.71073 \text{ Å}$ ). (E)-**1**:  $\text{C}_{30}\text{H}_{24}\text{O}_4\text{Fe}_2$ ,  $M_r = 560.19$ ,  $P2_1/c$ ,  $a = 15.739(8) \text{ Å}$ ,  $b = 7.404(4) \text{ Å}$ ,  $c = 10.196(5) \text{ Å}$ ,  $\beta = 95.294(3)^\circ$ ,  $V = 1183(1) \text{ Å}^3$ ,  $Z = 2$ ,  $\mu = 1.263 \text{ mm}^{-1}$ , unique reflections = 2696 [ $R(\text{int}) = 0.0176$ ],  $R_1 = 0.0269$  [ $I > 2.00\sigma(I)$ ],  $wR_2 = 0.0646$  [ $I > 2.00\sigma(I)$ ]. (Z)-**1**:  $\text{C}_{30}\text{H}_{24}\text{O}_4\text{Fe}_2$ ,  $M_r = 560.19$ ,  $P\bar{1}$ ,  $a = 9.968(5) \text{ Å}$ ,  $b = 11.115(6) \text{ Å}$ ,  $c = 12.022(6) \text{ Å}$ ,  $\alpha = 111.838(7)^\circ$ ,  $\beta = 92.640(6)^\circ$ ,  $\gamma = 96.769(6)^\circ$ ,  $V = 1222(1) \text{ Å}^3$ ,  $Z = 2$ ,  $\mu = 1.223 \text{ mm}^{-1}$ , unique reflections = 5353 [ $R(\text{int}) = 0.0176$ ],  $R_1 = 0.0337$  [ $I > 2.00\sigma(I)$ ],  $wR_2 = 0.0935$  [ $I > 2.00\sigma(I)$ ]. CCDC 600138 ((E)-**1**) and 600139 ((Z)-**1**) contain the supplementary crystallographic data for this paper. These data can be obtained free of charge from The Cambridge Crystallographic Data Centre via [www.ccdc.cam.ac.uk/data\\_request/cif](http://www.ccdc.cam.ac.uk/data_request/cif).
- [13] Cut-off filter Y-47 and IR cut-off filter IRA-25S by Asahi Techno Glass Inc. were used to extract light with wavelengths of 546 nm and 578 nm.
- [14] R. Sakamoto, M. Murata, S. Kume, H. Sampei, M. Sugimoto, H. Nishihara, *Chem. Commun.* **2005**, 1215–1217.
- [15] Light with a wavelength of 546 nm was separated with a Jasco CT-10T monochromator.
- [16] G. Zimmerman, L.-Y. Chow, U.-J. Paik, *J. Am. Chem. Soc.* **1958**, *80*, 3528–3531.
- [17] Photon flux was measured with Q8230 and Q82311, a semiconductor photon counter, by ADVANTEST.
- [18] The CV simulation was implemented with Digisim 3.03b. See Supporting Information for the detailed parameters used in the simulation.
- [19] S. C. Jones, S. Barlow, D. O'Hare, *Chem. Eur. J.* **2005**, *11*, 4473–4481.

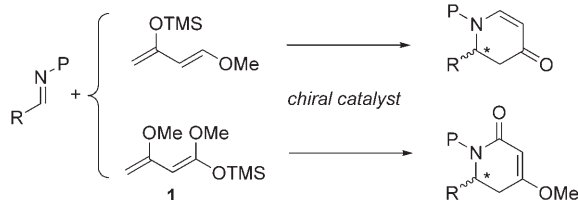


DOI: 10.1002/anie.200601345

# Chiral Brønsted Acid Catalyzed Enantioselective Aza-Diels–Alder Reaction of Brassard’s Diene with Imines\*\*

Junji Itoh, Kohei Fuchibe, and Takahiko Akiyama\*

Piperidine derivatives are precursors of the biologically important piperidine alkaloids,<sup>[1]</sup> peptides, and aza sugars, and are therefore important synthetic targets. Development of novel efficient methods for the synthesis of piperidine derivatives in optically pure form is important from the standpoint of the pharmaceutical sciences as well as synthetic organic chemistry. The enantioselective aza-Diels–Alder reaction of electron-rich dienes with aldimines provides an efficient protocol for the preparation of piperidine derivatives in scalemic form.<sup>[2]</sup> Thus, the aza-Diels–Alder reaction of an imine with 1-alkoxy-3-siloxy-1,3-butadienes and its derivatives (Danishefsky’s diene)<sup>[3]</sup> furnishes functionalized piperidinones. A catalytic asymmetric version of the aza-Diels–Alder reaction was investigated recently, and high enantioselectivity was attained.<sup>[4]</sup> Another potential candidate as an electron-rich diene is 1,3-dimethoxy-1-(trimethylsiloxy)butadiene **1** (Brassard’s diene),<sup>[5]</sup> the reaction of which provides piperidinone derivatives (Scheme 1).<sup>[6]</sup> In contrast to Danishefsky’s diene, Brassard’s diene has been less extensively studied. Although diastereoselective versions of aza-Diels–Alder reactions with chiral imines that lead to optically active piperidinone derivatives have been reported by Waldmann et al.,<sup>[7]</sup> Midland and Koops,<sup>[8]</sup> and Kawecky,<sup>[9]</sup> the catalytic



**Scheme 1.** The aza-Diels–Alder reaction. TMS = trimethylsilyl.

[\*] J. Itoh, Dr. K. Fuchibe, Prof. Dr. T. Akiyama  
Department of Chemistry  
Faculty of Science  
Gakushuin University  
Mejiro, Toshima-ku, Tokyo 171-8588 (Japan)  
Fax: (+81) 3-5992-1029  
E-mail: takahiko.akiyama@gakushuin.ac.jp

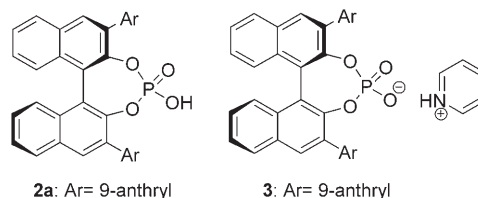
[\*\*] We thank Professor Youichi Ishii and Dr. Yoshiaki Tanabe (Chuo University, Tokyo, Japan) for the X-ray structural determination. This work was partially supported by a Grant-in-Aid for Scientific Research from the Ministry of Education, Science, Sports, Culture, and Technology, Japan. J.I. is grateful for a JSPS Research Fellowship for Young Scientists.



Supporting information for this article is available on the WWW under <http://www.angewandte.org> or from the author.

enantioselective reaction of Brassard’s diene with imines has, to the best of our knowledge, not been reported.<sup>[10]</sup> The high reactivity and lability of Brassard’s diene is associated with the paucity of its hetero-Diels–Alder reaction.

Recently, chiral Brønsted acid catalysis,<sup>[11,12]</sup> a variant of metal-free organocatalysis, has become a rapidly growing area.<sup>[13]</sup> We have already developed chiral phosphoric acid **2**,



derived from (*R*)-BINOL, as a chiral Brønsted acid catalyst.<sup>[14,15]</sup> One of the potential problems associated with **2** lies in its strong acidity,<sup>[16]</sup> in particular when applied to labile substrates. We have found that its pyridinium salt **3** also exhibits efficient catalytic activity as a chiral Brønsted acid catalyst but is more compatible than **2** with labile substrates such as Brassard’s diene. Herein, we report the chiral Brønsted acid catalyzed aza-Diels–Alder reaction of aldimines with Brassard’s diene **1** to afford piperidinone derivatives in high yields and with excellent enantioselectivities (up to 99% *ee*). To our knowledge, this is the first report of an enantioselective aza-Diels–Alder reaction of Brassard’s diene with aldimines.<sup>[17]</sup>

Screening of substituents at the 3,3’-positions of phosphoric acid **2** revealed that 9-anthryl groups as in **2a**<sup>[15c]</sup> were the most effective for the aza-Diels–Alder reaction. Thus, aldimine **4a** (*R* = Ph), derived from benzaldehyde and 2-amino-4-methylphenol, and Brassard’s diene **1** were treated with **2a** (3 mol %) in mesitylene at –40 °C for 24 h. Treatment of the reaction mixture with PhCO<sub>2</sub>H (1 equiv) with heating for 12 h afforded cycloadduct **5a** in 72% yield and with 92% *ee* (Table 1, entry 1). Note that as little as 3 mol % of the catalyst suffices for the reaction to proceed efficiently. Interestingly, use of the equivalent amount (3 mol %) of its pyridinium salt **3** improved the yield significantly with comparable enantioselectivity (Table 1, entry 2). A range of aldimines derived from aromatic and heteroaromatic aldehydes underwent the aza-Diels–Alder reaction to afford cyclization products with excellent enantioselectivities (Table 1, entries 3–14). Aliphatic aldimines, which were generated in situ, also gave corresponding cycloadducts with excellent *ee* values (Table 1, entries 15, 16). The absolute stereochemistry of **5** (*R* = *p*-BrC<sub>6</sub>H<sub>4</sub>; Table 1, entry 3) was unambiguously determined by X-ray crystallographic analysis,<sup>[18]</sup> and those of the other cycloadducts were assigned by analogy.

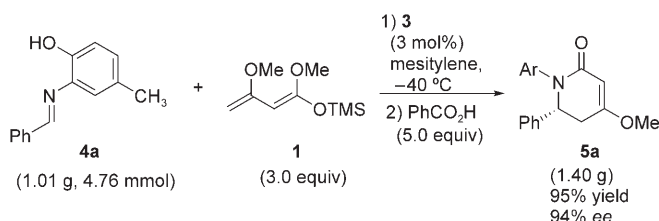
To demonstrate the utility of the present aza-Diels–Alder reaction, the experiment was performed on a gram scale. Thus, when 1.01 g of aldimine **4a** was treated with **3** (3 mol %), 1.40 g of the corresponding cyclization product **5a** was obtained without any loss in the enantioselectivity or yield (Scheme 2).

The methoxy group in **5a** could be transformed into other functionalities. As an example, acid hydrolysis of the methyl

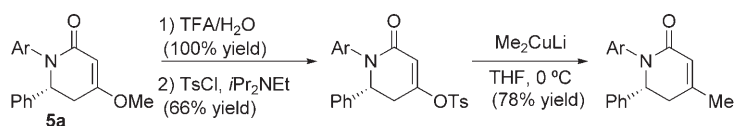
**Table 1:** Results of the aza-Diels–Alder reaction.<sup>[a]</sup>

$  \begin{array}{c}  \text{HO} \\    \\  \text{C}_6\text{H}_3\text{CH}_3 \\    \\  \text{N}=\text{C}-\text{R} \\  \text{4}  \end{array}  +  \begin{array}{c}  \text{OMe} \quad \text{OMe} \\    \quad   \\  \text{C}=\text{C} \\    \\  \text{OTMS} \\  \text{1}  \end{array}  \xrightarrow[2) \text{PhCO}_2\text{H} \quad (1.0 \text{ equiv})]{1) \text{cat.} \quad (3 \text{ mol\%}) \quad \text{mesitylene,} \quad -40^\circ\text{C}}  \begin{array}{c}  \text{O} \\     \\  \text{Ar}-\text{N} \\    \\  \text{C}=\text{C} \\    \\  \text{OMe} \\  \text{5}  \end{array}  $				
Entry	Catalyst	R	Yield [%]	ee [%]
1 <sup>[b]</sup>	<b>2a</b>	C <sub>6</sub> H <sub>5</sub>	72	92
2 <sup>[b]</sup>	<b>3</b>	C <sub>6</sub> H <sub>5</sub>	87	94
3	<b>3</b>	<i>p</i> -BrC <sub>6</sub> H <sub>4</sub>	86	96
4	<b>3</b>	<i>p</i> -ClC <sub>6</sub> H <sub>4</sub>	90	97
5 <sup>[b]</sup>	<b>3</b>	<i>p</i> -FC <sub>6</sub> H <sub>4</sub>	76	98
6	<b>3</b>	<i>p</i> -CH <sub>3</sub> C <sub>6</sub> H <sub>4</sub>	90	95
7	<b>3</b>	<i>p</i> -CH <sub>3</sub> OC <sub>6</sub> H <sub>4</sub>	84	99
8 <sup>[b]</sup>	<b>3</b>	<i>o</i> -BrC <sub>6</sub> H <sub>4</sub>	83	98
9 <sup>[b]</sup>	<b>3</b>	<i>o</i> -ClC <sub>6</sub> H <sub>4</sub>	86	98
10	<b>3</b>	<i>o</i> -CH <sub>3</sub> C <sub>6</sub> H <sub>4</sub>	76	96
11	<b>3</b>	1-naphthyl	79	98
12 <sup>[b]</sup>	<b>3</b>	2-naphthyl	91	97
13 <sup>[b,c,d]</sup>	<b>3</b>	2-furyl	63	97
14 <sup>[b,c]</sup>	<b>3</b>	PhCH=CH	76	98
15	<b>3</b>	cyclohexyl	69	99
16	<b>3</b>	<i>i</i> Pr	65	93

[a] 3.0 equiv of **1** was employed. [b] 5 equiv of PhCO<sub>2</sub>H was employed. [c] 4.0 equiv of **1** was employed. [d] **1** was added in one portion.


**Scheme 2.** Scaled-up version of the aza-Diels–Alder reaction.

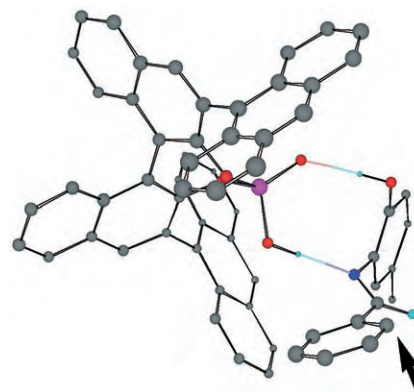
ether and a subsequent addition–elimination reaction of the tosylate with Me<sub>2</sub>CuLi introduced a methyl group (Scheme 3).


**Scheme 3.** Transformation of the cycloadduct **5a**. Ar = 2-hydroxy-5-methylphenyl; TFA = trifluoroacetic acid; Ts = *p*-toluenesulfonyl.

The stability of Brassard's diene **1** toward acid **2a** and toward **3** in the presence of phosphoric acid was studied in wet [D<sub>8</sub>]toluene at room temperature. The amount of **1** was monitored by <sup>1</sup>H NMR spectroscopy.<sup>[19]</sup> In the presence of **2a** only 12 % of Brassard's diene was detected after 1 h, whereas in the presence of **3** 75 % of the starting amount of diene was measured. This result clearly shows that the weaker acidity of **3** is responsible for the increased yields of the cycloadduct **5**, as compared to those with **2a**.

As the presence of the hydroxy moiety on the *N*-aryl group is essential for attaining high enantioselectivity,<sup>[20]</sup> we

surmised that the present aza-Diels–Alder reaction proceeds via a nine-membered cyclic transition state, wherein the phosphoryl oxygen atom forms a hydrogen bond with the hydrogen atom of the imine OH moiety, with the nucleophile attacking the *Re* face of the aldimine preferentially (Figure 1).<sup>[21,22]</sup>


**Figure 1.** Chem3D representation of a minimized structure of the complex derived from **2a** and **4a**. Most of the hydrogen atoms are omitted for clarity. Hydrogen bonds are shown. P pink, O red, N blue, C gray, H turquoise. The arrow indicates *Re* facial attack.

In summary, we have developed the aza-Diels–Alder reaction of Brassard's diene with imines, catalyzed by a chiral Brønsted acid derived from (*R*)-BINOL, to give dihydropyridone derivatives with excellent enantioselectivities. The application of the present chiral Brønsted acid catalysis system to other asymmetric reactions is underway.

Received: April 5, 2006

Published online: June 23, 2006

**Keywords:** asymmetric synthesis · aza-Diels–Alder reaction · Brønsted acids · enantioselectivity · organocatalysis

- [1] P. D. Bailey, P. A. Millwood, P. D. Smith, *Chem. Commun.* **1998**, 633.
- [2] a) H. Waldmann, *Synthesis* **1994**, 535; b) K. A. Jørgensen, *Angew. Chem.* **2000**, 112, 3702; *Angew. Chem. Int. Ed.* **2000**, 39, 3558; c) P. Buonora, J.-C. Olsen, T. Oh, *Tetrahedron* **2001**, 57, 6099; d) *Cycloaddition Reactions in Organic Synthesis* (Eds: S. Kobayashi, K. A. Jørgensen), Wiley-VCH, Weinheim, **2002**.
- [3] S. Danishefsky, T. Kitahara, *J. Am. Chem. Soc.* **1974**, 96, 7807.
- [4] a) S. Kobayashi, S. Komiyama, H. Ishitani, *Angew. Chem.* **1998**, 110, 1026; *Angew. Chem. Int. Ed.* **1998**, 37, 979; b) S. Yao, M. Johannsen, R. G. Hazell, K. A. Jørgensen, *Angew. Chem.* **1998**, 110, 3318; *Angew. Chem. Int. Ed.* **1998**, 37, 3121; c) S. Kobayashi, K. Kusakabe, S. Komiyama, H. Ishitani, *J. Org. Chem.* **1999**, 64, 4220; d) S. Kobayashi, K. Kusakabe, H. Ishitani, *Org. Lett.* **2000**, 2, 1225; e) N. S. Josephsohn, M. L. Snapper, A. H. Hoveyda, *J. Am. Chem. Soc.* **2003**, 125, 4018; f) O. G. Mancheno, R. G. Arrayas, J. C. Carretero, *J. Am. Chem. Soc.* **2004**, 126, 456; g) Y. Yamashita, Y. Mizuki, S. Kobayashi, *Tetrahedron Lett.* **2005**, 46, 1803.
- [5] J. Savard, P. Brassard, *Tetrahedron Lett.* **1979**, 20, 4911.

- [6] M. M. Midland, J. I. McLoughlin, *Tetrahedron Lett.* **1988**, 29, 4653.
- [7] a) H. Waldmann, M. Braun, M. Draeger, *Angew. Chem.* **1990**, 102, 1445; *Angew. Chem. Int. Ed. Engl.* **1990**, 29, 1468; b) H. Waldmann, M. Braun, M. Dräger, *Tetrahedron: Asymmetry* **1991**, 2, 1231.
- [8] M. M. Midland, R. W. Koops, *J. Org. Chem.* **1992**, 57, 1158.
- [9] R. Kaweck, *Tetrahedron* **2001**, 57, 8385.
- [10] For the enantioselective hetero-Diels–Alder reaction of Brassard’s diene with aldehydes, see: a) Q. Fan, L. Lin, J. Liu, Y. Huang, X. Feng, G. Zhang, *Org. Lett.* **2004**, 6, 2185; b) H. Du, D. Zhao, K. Ding, *Chem. Eur. J.* **2004**, 10, 5964.
- [11] For reviews on Brønsted acid catalysis, see: a) P. R. Schreiner, *Chem. Soc. Rev.* **2003**, 32, 289; b) P. M. Pihko, *Angew. Chem.* **2004**, 116, 2110; *Angew. Chem. Int. Ed.* **2004**, 43, 2062; c) C. Bolm, T. Rantanen, I. Schiffrers, L. Zani, *Angew. Chem.* **2005**, 117, 1778; *Angew. Chem. Int. Ed.* **2005**, 44, 1758; d) P. M. Pihko, *Lett. Org. Chem.* **2005**, 2, 398; e) M. S. Taylor, E. N. Jacobsen, *Angew. Chem.* **2006**, 118, 1550; *Angew. Chem. Int. Ed.* **2006**, 45, 1520; f) T. Akiyama, J. Itoh, K. Fuchibe, *Adv. Synth. Catal.* **2006** DOI: 10.1002/adsc.200606074.
- [12] For recent representative papers, see: a) A. G. Wenzel, E. N. Jacobsen, *J. Am. Chem. Soc.* **2002**, 124, 12964; b) N. T. McDougal, S. E. Schaus, *J. Am. Chem. Soc.* **2003**, 125, 12094; c) T. Okino, Y. Hoashi, Y. Takemoto, *J. Am. Chem. Soc.* **2003**, 125, 1267; d) B. M. Nugent, R. A. Yoder, J. N. Johnston, *J. Am. Chem. Soc.* **2004**, 126, 3418; e) N. T. McDougal, W. L. Trevellini, S. A. Rodgen, L. T. Kliman, S. E. Schaus, *Adv. Synth. Catal.* **2004**, 346, 1231; f) Y. Huang, A. K. Unni, A. N. Thadani, V. H. Rawal, *Nature* **2003**, 424, 146; g) A. N. Thadani, A. R. Stankovic, V. H. Rawal, *Proc. Natl. Acad. Sci. USA* **2004**, 101, 5846; h) T. Okino, Y. Hoashi, T. Furukawa, X. Xu, Y. Takemoto, *J. Am. Chem. Soc.* **2005**, 127, 119; i) N. Momiyama, H. Yamamoto, *J. Am. Chem. Soc.* **2005**, 127, 1080; j) A. K. Unni, N. Takenaka, H. Yamamoto, V. H. Rawal, *J. Am. Chem. Soc.* **2005**, 127, 1336; k) M. Shi, L.-H. Chen, C.-Q. Li, *J. Am. Chem. Soc.* **2005**, 127, 3790; l) E. Fuerst, E. N. Jacobsen, *J. Am. Chem. Soc.* **2005**, 127, 8964.
- [13] For reviews on organocatalysts, see: a) P. I. Dalko, L. Moisan, *Angew. Chem.* **2001**, 113, 3840; *Angew. Chem. Int. Ed.* **2001**, 40, 3726; b) P. I. Dalko, L. Moisan, *Angew. Chem.* **2004**, 116, 5248; *Angew. Chem. Int. Ed.* **2004**, 43, 5138; c) Special Issue on Organocatalysis (Eds.: K. N. Houk, B. List), *Acc. Chem. Res.* **2004**, 37, 487; d) Special Issue on Organocatalysis (Eds.: B. List, C. Bolm), *Adv. Synth. Catal.* **2004**, 346, 1021; e) J. Seayad, B. List, *Org. Biomol. Chem.* **2005**, 3, 719; f) *Asymmetric Organocatalysis* (Eds.: A. Berkessel, H. Gröger), Wiley-VCH, Weinheim, **2005**.
- [14] a) T. Akiyama, J. Itoh, K. Yokota, K. Fuchibe, *Angew. Chem.* **2004**, 116, 1592; *Angew. Chem. Int. Ed.* **2004**, 43, 1566; b) T. Akiyama, H. Morita, J. Itoh, K. Fuchibe, *Org. Lett.* **2005**, 7, 2583; c) T. Akiyama, Y. Saitoh, H. Morita, K. Fuchibe, *Adv. Synth. Catal.* **2005**, 347, 1523; d) T. Akiyama, Y. Tamura, J. Itoh, H. Morita, K. Fuchibe, *Synlett* **2006**, 141.
- [15] a) D. Uraguchi, M. Terada, *J. Am. Chem. Soc.* **2004**, 126, 5356; b) D. Uraguchi, K. Sorimachi, M. Terada, *J. Am. Chem. Soc.* **2004**, 126, 11804; c) D. Uraguchi, K. Sorimachi, M. Terada, *J. Am. Chem. Soc.* **2005**, 127, 9360; d) M. Terada, K. Sorimachi, D. Uraguchi, *Synlett* **2006**, 133; e) G. B. Rowland, H. Zhang, E. B. Rowland, S. Chennamadhavuni, Y. Wang, J. C. Antilla, *J. Am. Chem. Soc.* **2005**, 127, 15696; f) M. Rueping, E. Sugiono, C. Azap, T. Theissmann, M. Bolte, *Org. Lett.* **2005**, 7, 3781; g) S. Hoffmann, A. M. Seayad, B. List, *Angew. Chem.* **2005**, 117, 7590; *Angew. Chem. Int. Ed.* **2005**, 44, 7424; h) R. I. Storer, D. E. Carrera, Y. Ni, D. W. C. MacMillan, *J. Am. Chem. Soc.* **2006**, 128, 84; i) J. Seayad, A. M. Seayad, B. List, *J. Am. Chem. Soc.* **2006**, 128, 1086; j) M. Terada, K. Machioka, K. Sorimachi, *Angew. Chem.* **2006**, 118, 2312; *Angew. Chem. Int. Ed.* **2006**, 45, 2254.
- [16] The  $pK_a$  value of diethyl phosphate is 1.39; see: L. D. Quin, *A Guide to Organophosphorus Chemistry*, Wiley, New York, **2000**, chap. 5, pp. 133–165.
- [17] For organocatalyzed hetero-Diels–Alder reactions of aldehydes with Brassard’s diene, see ref. [10b].
- [18] CCDC-280243 contains the supplementary crystallographic data for this paper. These data can be obtained free of charge from The Cambridge Crystallographic Data Centre via [www.ccdc.cam.ac.uk/data\\_request/cif](http://www.ccdc.cam.ac.uk/data_request/cif).
- [19] See Supporting Information for details.
- [20] An aldimine derived from *p*-methoxyaniline exhibited lower enantioselectivity.
- [21] The nine-membered cyclic structure was observed as one of the energy minima of the complex derived from **2a** and **4a** by quantum chemical calculations (PM3, Spartan’02, Wavefunction, Inc.).
- [22] We suppose pyridine would not participate in the transition state but may stabilize Brassard’s diene in the reaction.

## Cluster Compounds

DOI: 10.1002/anie.200504600

**Discovery of a Family of Isopolyoxotungstates  $[\text{H}_4\text{W}_{19}\text{O}_{62}]^{6-}$  Encapsulating a  $\{\text{WO}_6\}$  Moiety within a  $\{\text{W}_{18}\}$  Dawson-like Cluster Cage\*\****De-Liang Long,\* Paul Kögerler, Alexis D. C. Parenty, John Fielden, and Leroy Cronin\**

Polyoxotungstates are continuing to attract attention because of their appealing electronic and molecular properties that give rise to many applications in, for example, catalysis<sup>[1]</sup> and materials science.<sup>[2]</sup> Since their materials properties are intricately linked to their structural features, the creation of novel polyoxotungstate structural types remains a pressing challenge. However, the development of new structures has thus far mostly involved the integration of heteroanions or heterometals that support the tungstate-based frameworks.<sup>[3]</sup> Only a few examples of basic types of isopolyoxotungstates are known, including  $[\text{HW}_5\text{O}_{19}]^{7-}$ ,<sup>[4]</sup>  $[\text{W}_6\text{O}_{19}]^{2-}$ ,<sup>[5]</sup>

[\*] Dr. D.-L. Long, Dr. A. D. C. Parenty, Prof. Dr. L. Cronin  
Department of Chemistry  
The University of Glasgow  
Glasgow, G12 8QQ (UK)  
Fax: (+44) 141-330-4888  
E-mail: longd@chem.gla.ac.uk  
l.cronin@chem.gla.ac.uk

Dr. P. Kögerler, Dr. J. Fielden  
Ames Laboratory and Department of Physics and Astronomy  
Iowa State University  
Ames, IA 50011 (USA)

[\*\*] This work was supported by the EPSRC and the University of Glasgow.



Supporting information for this article is available on the WWW under <http://www.angewandte.org> or from the author.



$[\text{H}_3\text{W}_6\text{O}_{22}]^{5-}$ ,<sup>[6]</sup>  $[\text{W}_7\text{O}_{24}]^{6-}$ ,<sup>[7]</sup>  $[\text{W}_{10}\text{O}_{32}]^{4-}$ ,<sup>[8]</sup>  $[\text{H}_4\text{W}_{11}\text{O}_{38}]^{6-}$ ,<sup>[9]</sup>  $[\text{H}_2\text{W}_{12}\text{O}_{40}]^{6-}$ ,  $[\text{H}_2\text{W}_{12}\text{O}_{42}]^{10-}$ , and  $[\text{W}_{24}\text{O}_{84}]^{24-}$ .<sup>[10]</sup> The synthesis of fundamentally new isopolyoxotungstates, which may subsequently be used as building blocks in constructing larger architectures or networks, therefore requires new strategies that exploit supramolecular interactions during the construction of the cluster architecture. In this context we recently explored the use of larger, flexible organic cations that allowed us to isolate new cluster structures, for example, the isopolyoxomolybdate  $[\text{H}_2\text{Mo}_{16}\text{O}_{52}]^{10-}$ <sup>[11]</sup> using protonated hexamethylenetetramine, which encapsulates this unit in solution, thereby limiting its reorganization to simpler structure types. We extended this strategy to tungstate-based systems by using protonated triethanolamine ( $\text{TEAH}^+$ ) as cations at around pH 2 and isolated the isopolyoxotungstate  $[\text{H}_{12}\text{W}_{36}\text{O}_{120}]^{12-}$ , which can be thought of as an inorganic “crown ether”.<sup>[12]</sup> Notably, the same reaction system at lower pH values (around 1) yields a fundamentally new type of isopolyoxotungstate  $[\text{H}_4\text{W}_{19}\text{O}_{62}]^{6-}$  (**1a**), which was isolated as its salt  $(\text{TEAH})_6[\text{H}_4\text{W}_{19}\text{O}_{62}]$  (**1**).

Compound **1** forms after refluxing a solution of sodium tungstate and  $\text{TEAH}^+$  at pH 0.8 for more than three days, during which time the solution gradually changes from colorless to pale green. In the absence of the bulky organic  $\text{TEAH}^+$  cations, under otherwise identical reaction conditions, only the well-known  $[\text{W}_{10}\text{O}_{32}]^{4-}$  cluster compound forms, which implies the existence of a crucial cation effect.<sup>[13]</sup> Although crystals of **1** were of poor quality, which meant that the cluster oxido positions and the  $\text{TEAH}^+$  cations could not be well resolved because of disorder,<sup>[14]</sup> the metal skeleton of 19 W centers is clearly resolved and resembles that of a Dawson-type  $\{\text{W}_{18}\}$  cage (realized for instance as  $[\text{W}_{18}\text{O}_{54}(\text{PO}_4)_2]^{6-}$ )<sup>[15]</sup> featuring an additional W center located in the center of the cluster and the absence of the two heteroatoms typically associated with Dawson-type clusters.

Analysis of **1** by  $^{183}\text{W}$  NMR spectroscopy in aqueous solution shows three groups of W centers, which correspond to a single tungsten center and two types of tungsten centers typically found in a Dawson-type cluster sphere (consisting of six “cap” and twelve “belt” W atoms). Furthermore, recrystallization of **1** in water yields a new crystal form **1'**,<sup>[14]</sup> which has cubic morphology and composition  $(\text{TEAH})_6[\text{H}_4\text{W}_{19}\text{O}_{62}] \cdot 6\text{H}_2\text{O}$ . The vastly improved crystal quality led to a better resolved structure with minimal disorder of the central  $\text{WO}_6$  environment and the positions of the capping W centers.<sup>[14]</sup> Thus,  $[\text{H}_4\text{W}_{19}\text{O}_{62}]^{6-}$  represents the first example of an isopolyanion adopting a Dawson-type heteropolyanion framework structure.<sup>[15,16]</sup>

The disorder pattern found in the structures of **1** (and **1'**) implies that different isomers of **1a** cocrystallize in **1** (and **1'**) which cannot be resolved in the presence of water as a solvent and  $\text{TEAH}^+$  cations. To explore the  $\{\text{W}_{19}\}$  cluster type fully, cation exchange and transformation of the clusters into organic solvent were performed by redissolving **1** in water and precipitating the  $\{\text{W}_{19}\}$  cluster with *n*-tetrapropylammonium ( $\text{Pr}_4\text{N}^+$ ) and recrystallizing the resulting precipitate from acetonitrile. Two isomers  $(\text{Pr}_4\text{N})_6[\text{H}_4\text{W}_{19}\text{O}_{62}] \cdot 6\text{CH}_3\text{CN}$  (**2**) and  $(\text{Pr}_4\text{N})_6[\text{H}_4\text{W}_{19}\text{O}_{62}] \cdot 3\text{CH}_3\text{CN}$  (**3**) were successfully

obtained as crystalline solids and were fully characterized by single-crystal X-ray diffraction.<sup>[14]</sup> Compound **2** crystallizes in a monoclinic system (space group  $C2$ ) with two crystallographically independent cluster halves in the asymmetric unit, where both complete clusters consist of a Dawson-type  $\{\text{W}_{18}\}$  cage and an additional central W site that lies on crystallographic  $C_2$  axes. Figure 1 shows one of the two complete

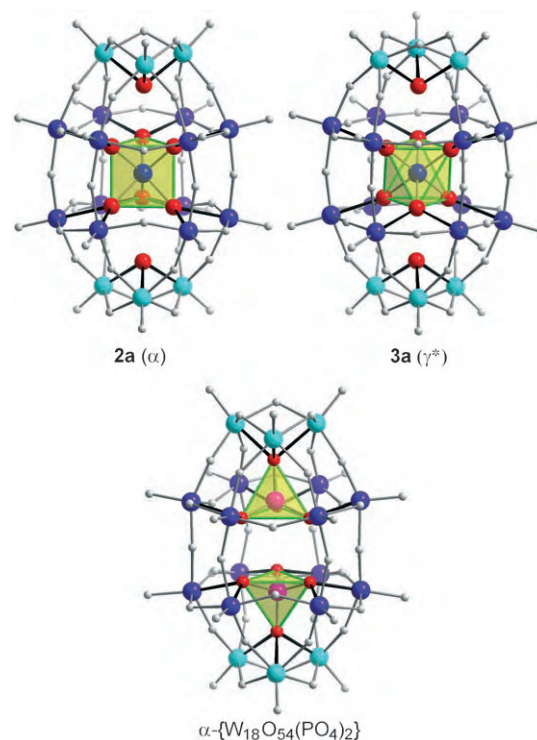


**Figure 1.** Structural representation of the  $\{\text{W}_{19}\}$  isopolyoxotungstate isomers **2a** and **3a** as well as the phosphate-based Dawson anion  $\alpha\text{-}[\text{W}_{18}\text{O}_{54}(\text{PO}_4)_2]^{6-}$ <sup>[15]</sup> for comparison. The central  $\text{XO}_n$  anion templates are emphasized as green/transparent yellow polyhedra (a trigonal  $\text{WO}_6$  prism in **2a**, a  $\text{WO}_6$  octahedron in **3a**, two  $\text{PO}_4$  tetrahedra in  $\alpha\text{-}[\text{W}_{18}\text{O}_{54}(\text{PO}_4)_2]^{6-}$ ). The eight oxido ligands in each cluster that span the two tetrahedral areas (empty in **2a** and **3a**, occupied by P in the phosphate Dawson structure) are shown in red; their bonds to W centers are emphasized in black. W: blue (“belt” positions and central position), light blue (“cap” positions), O: light gray, P: pink.

clusters (**2a**), defined as the  $D_{3h}$ -symmetric  $\alpha$  isomer of the new isopolyoxotungstate  $[\text{H}_4\text{W}_{19}\text{O}_{62}]^{6-}$  family. Cluster **2a** consists of the  $\{\text{W}_{18}\text{O}_{54}\}$  cage framework and interior oxido ligands of the conventional Dawson cluster anion  $\alpha\text{-}[\text{W}_{18}\text{O}_{54}(\text{XO}_4)_2]^{n-}$  ( $\text{X} = \text{P}, \text{S}$ )<sup>[15]</sup> but, in contrast to the classical Dawson structure, the two tetrahedral  $\text{XO}_4^{n-}$  heteroanions are replaced by a trigonal-prismatic  $\text{WO}_6^{6-}$  anion and two  $\mu_3$ -oxido ligands (partially protonated, see below), each of which bridges the capping  $\{\text{W}_3\}$  triangle from the inside of the cluster with an average W–O bond length of 2.23(3) Å. To the best of our knowledge, this is the first observation in polyoxotungstates of a  $\{\text{WO}_6\}$  unit in which the W center adopts a trigonal-prismatic coordination environment with all W–O bond lengths virtually identical (1.96(3) Å)—in all previous examples the  $\{\text{WO}_6\}$  units typically display octahedral geometries

with one or two short terminal W=O bonds and some longer W-(μ-O) bonds. Two tetrahedral “voids” exist in **2a** at the positions that are typically occupied by the heteroatoms in conventional Dawson cluster anions  $\alpha$ -[W<sub>18</sub>O<sub>54</sub>(XO<sub>4</sub>)<sub>2</sub>]<sup>n-</sup>. Two of the four oxido ions that define each tetrahedral “void” are protonated and form H-bonds with the other two ions, which is similar to the corresponding situations inside the Keggin cluster [H<sub>2</sub>W<sub>12</sub>O<sub>40</sub>]<sup>6-</sup>[17] and the semivacant Dawson polyoxotungstate [Ce{P(H<sub>4</sub>)W<sub>17</sub>O<sub>61</sub>}<sub>2</sub>]<sup>19-</sup>[18]. This protonation assignment is supported by <sup>1</sup>H NMR measurements, elemental analyses, bond valence sum analysis, and crystal structure determinations, which showed only six Pr<sub>4</sub>N<sup>+</sup> counteranions per cluster in **2**. Interestingly, **2a** bears some resemblance to the {W<sub>18</sub>}-type cluster  $\alpha$ -[H<sub>2</sub>W<sub>18</sub>NaO<sub>56</sub>F<sub>6</sub>]<sup>7-</sup> previously reported by Baker and co-workers[19] in which the central template [NaF<sub>6</sub>]<sup>5-</sup> also displays a trigonal prismatic configuration with six Na-F bond lengths in the range from 2.17 to 2.32 Å, which are significantly longer than those of the corresponding W-O bond lengths of the central {WO<sub>6</sub>}<sup>6-</sup> unit in **2a**. The F-W bonds (ca. 2.22 Å) are much shorter than the corresponding O-W bonds (ca. 2.42 Å) in **2a**. Bearing the geometric similarity of these two structures in mind, we have carefully checked the position of the central W atom in **2a**. However, all evidence from structure refinement, spectra, and chemical analyses unambiguously confirmed the central position as a tungsten center. In addition we have measured the cold-spray mass spectra of an acetonitrile solution of **2** and **3**, which clearly showed the intact cluster in the gas phase: {(Pr<sub>4</sub>N)<sub>5</sub>-**2a**}<sup>1+</sup> and {(Pr<sub>4</sub>N)<sub>5</sub>-**3a**}<sup>1+</sup> were observed at *m/z* 5420 and could be unambiguously assigned by comparison to the expected isotopic envelope.

Compound **3** crystallizes in an orthorhombic system (space group *Pccn*)[14] and contains the [H<sub>4</sub>W<sub>19</sub>O<sub>62</sub>]<sup>6-</sup> cluster **3a** as the centrosymmetric γ\* isomer with *D*<sub>3d</sub> symmetry (Figure 1). Cluster **3a** is based on the geometry of the {W<sub>18</sub>O<sub>54</sub>} cage framework and interior oxido ligands as found in the conventional Dawson cluster anion γ\*-[W<sub>18</sub>O<sub>54</sub>(SO<sub>4</sub>)<sub>2</sub>]<sup>4-</sup>[20]. Again, an additional W site is located at the center of the cluster and coordinates to six oxido ligands to form a central {WO<sub>6</sub>} centrosymmetric template of octahedral geometry. As in **2a**, two further μ<sub>3</sub>-oxido ligands inside the cluster each bridge one of the capping {W<sub>3</sub>} triangles with an average W-O bond length of 2.28(1) Å. All W-O bond lengths in the {WO<sub>6</sub>} central template of **3a** are nearly identical (1.95(3) Å), and such a {WO<sub>6</sub>} octahedral geometry is also the first observation of this kind in polyoxotungstates. Two tetrahedral “voids” similar to those in **2a** are occupied by two protons each and this is confirmed by <sup>1</sup>H NMR results. Unlike the chemical shift values found in the <sup>1</sup>H NMR spectrum of the Keggin cluster [H<sub>2</sub>W<sub>12</sub>O<sub>40</sub>]<sup>6-</sup>, which only shows one peak at around 6.0 ppm because of the inner regular tetrahedral O<sub>4</sub> environment (with O...O distances of approximately 2.90 Å), several peaks corresponding to the four protons present within the clusters **2** and **3** are found in the range 4.7–8.1 ppm (and all these peaks integrate to about 4 protons per cluster). This observation can be explained by the trigonal pyramidal (nontetrahedral) environment. In **2**, the average base length (O...O) of the pyramid is 2.61(5) Å, while the side length is 2.85(2) Å. In **3**, these two values are

2.73(3) and 2.96(2) Å. Strong hydrogen bonding (indicated by short O...O separations in **2** and **3**) means that the protons will be observed at lower chemical shifts (e.g. δ = 4.7 ppm), and, since the local symmetry is lowered, the four protons are not equivalent. In the <sup>1</sup>H NMR spectrum of **1** in D<sub>2</sub>O, only aliphatic protons (-CH<sub>2</sub>- in TEAH<sup>+</sup>) are resolved as the protons present in the clusters were not observed owing to rapid exchange with solvent, which is similar to the case in semivacant Dawson polyoxotungstate [Ce{P(H<sub>4</sub>)W<sub>17</sub>O<sub>61</sub>}<sub>2</sub>]<sup>19-</sup>[18]. However, we were able to measure a <sup>1</sup>H NMR spectrum of **1** in DMSO which shows several peaks at δ = 8.01, 7.23, 5.74, 5.27, 4.66, 4.45, and 4.0 ppm. As **1** is not soluble in CD<sub>3</sub>CN, any comparison of <sup>1</sup>H NMR spectra for **1**, **2**, and **3** is purely qualitative; this is because of the possibility of several protonation sites and uncertainty about the population at a given site. However, it is notable that the same types of proton environment associated with pure isomers **2** and **3** all have corresponding shifts found in **1**, which contains the isomers found in **2** and **3**.

The difference between the {W<sub>19</sub>} isomers **2a** and **3a** concerns the {W<sub>18</sub>O<sub>54</sub>} cage and central template {WO<sub>6</sub>} geometries. Topological analysis indicates that, besides **2a** and **3a**, other isomers are possible: the [H<sub>4</sub>W<sub>19</sub>O<sub>62</sub>]<sup>6-</sup> family consists of six isomers that are also observed for the conventional Dawson anions [W<sub>18</sub>O<sub>54</sub>(XO<sub>4</sub>)<sub>2</sub>]<sup>n-</sup> (X = P, S, etc.)[15,20] that is, the same {W<sub>18</sub>O<sub>54</sub>} cage variations and interior bridging oxido group orientations are present; we therefore adopt the same isomer designations (α, α\*, β, β\*, γ, γ\*)[21]. The α, β, and γ isomers all contain the trigonal prismatic {WO<sub>6</sub>} central unit (*D*<sub>3h</sub>), whereas the α\*, β\*, and γ\* isomers contain a centrosymmetric octahedral {WO<sub>6</sub>} central unit (*D*<sub>3d</sub>). α, β\*, and γ isomers all form a *D*<sub>3h</sub>-symmetric {W<sub>18</sub>} cage whereas the α\*, β, and γ\* isomers all form a *D*<sub>3d</sub>-symmetric {W<sub>18</sub>} cage. As the point groups of the {W<sub>18</sub>} cages and the {WO<sub>6</sub>} central units match, the complete α and γ cluster isomers adopt *D*<sub>3h</sub> symmetry, whereas the α\* and γ\* cluster isomers adopt *D*<sub>3d</sub> symmetry. The symmetry mismatch for the {W<sub>18</sub>} cages and central {WO<sub>6</sub>} units in both β and β\* isomers reduces their overall symmetry to *C*<sub>3v</sub>. Therefore, the comparison between the {W<sub>18</sub>} Dawson and the {W<sub>19</sub>} structure types is strengthened not only by their framework topology, but also by the fact that the 18 tungsten centers of the {W<sub>18</sub>} cages of the corresponding α and γ\* isomers occupy exactly the same positions in both structure types within an error margin of 0.2 Å.

Planar projections (Schlegel diagrams) were constructed to understand the connectivity of the Dawson-type {W<sub>18</sub>} and our {W<sub>19</sub>} frameworks better and to examine the similarity between the two.[22] Schlegel diagrams can be used for the Dawson-like clusters to describe the {W<sub>18</sub>} cage frameworks in which each link represents a bridging oxido ligand between W atoms. Therefore in the *D*<sub>3h</sub>-symmetric systems (Figure 2a), the edges of the outmost and innermost triangles (capping {W<sub>3</sub>} groups) are parallel, whereas in the *D*<sub>3d</sub>-symmetric systems (Figure 2b), these two triangles are inverted with respect to each other. These two configurations, combined with the orientations and geometries of the central {WO<sub>6</sub>} units as described above, produce planar projections of all six isomers. Figure 2 demonstrates the α isomer **2a** and γ\* isomer

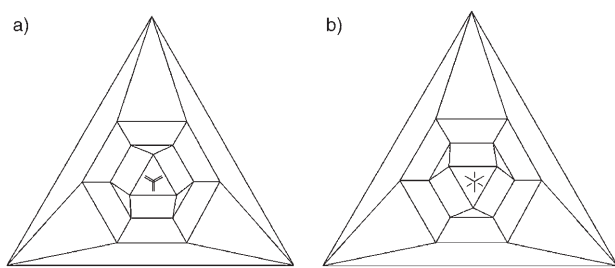
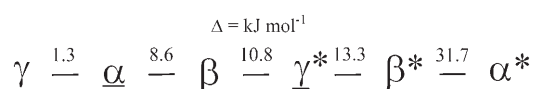


**Figure 2.** Schlegel diagrams of the  $\{W_{18}\}$  cage structures together with the central  $WO_6$  units shown as eclipsed (trigonal prismatic) and staggered lines (octahedral). a)  $\alpha$  isomer and b)  $\gamma^*$  isomer. Other isomers can be deduced in the following ways:  $\beta$  isomer: the  $\{W_{18}\}$  cage in (b) plus  $WO_6$  unit in (a);  $\gamma$  isomer:  $\alpha$  isomer in (a) with the  $WO_6$  unit turned by  $60^\circ$  along the main  $C_3$  axis;  $\alpha^*$  isomer:  $\gamma^*$  isomer in (b) with the  $WO_6$  unit turned by  $60^\circ$  along the main  $C_3$  axis;  $\beta^*$  isomer: the cage in (a) plus  $WO_6$  unit in (b).

**3a.** Other representations of the remaining four isomers can be derived from these projections.

To examine the principal relation of these isomers further, we scaled the stabilities of all six isomers by their relative energies from density functional theory calculations on the cluster anions (Scheme 1).<sup>[23]</sup> These calculations, performed



**Scheme 1.** Scheme of the relative energies of the cluster isomers as calculated by DFT. The experimentally characterized cluster isomers **2a** ( $\alpha$ ) and **3a** ( $\gamma^*$ ) are underlined.

on geometrically relaxed isolated cluster geometries in the gas phase, suggest that the  $D_{3h}$ -symmetric  $\alpha$  isomer is more stable than the  $D_{3d}$ -symmetric  $\gamma^*$  isomer. The  $\gamma$  and  $\gamma^*$  structures are only separated by  $21 \text{ kJ mol}^{-1}$ , whereas the  $\alpha$ -to- $\alpha^*$  energy difference is over three times larger ( $64 \text{ kJ mol}^{-1}$ ). It is important to note that these relative energies only reflect the differing connectivities of the idealized isomer geometries; the actual formation and interconversion of individual isomers is subject to a large set of bulk phase parameters. Having isolated pure  $\alpha$  and  $\gamma^*$  isomers, we investigated the stability of these compounds by using differential scanning calorimetry (DSC). The DSC trace for compound **2** shows a broad endothermic peak starting at  $315^\circ\text{C}$ , possibly resulting from the reduction of the cluster by the organic cations, as suggested by the color change to blue observed at this temperature. Compound **3** also shows this feature, as well as a small endothermic peak immediately followed by an exothermic peak ( $291$ – $298^\circ\text{C}$ ). These latter irreversible processes are possibly due to either a rearrangement/decomposition in the cluster shell or associated cations; however, solvent effects have been ruled out.<sup>[24]</sup>

In summary, we have demonstrated that it is possible to isolate isopolyoxotungstate clusters that are structural analogues of heteropolyacids, in this case, of the Dawson structural archetype. The isolation of two of the six isomers that make up this new family, along with the chemical,

thermogravimetric, and theoretical analysis, demonstrates interesting features related to the inclusion of the  $[WO_6]^{6-}$  anion template. Furthermore, the stabilization of the  $[WO_6]$  moiety in a trigonal prismatic coordination environment is unprecedented in polyoxotungstate chemistry. Future work will include exploring the potential redox chemistry, photochemistry, and acidic nature of the clusters to compare their physical properties directly with the classical Dawson clusters. In addition, the inclusion of the metal-based octahedra may allow control of the formation of clusters using other  $\{MO_6\}$  or  $\{MX_6\}$  units as templates.

## Experimental Section

**1:** Triethanolamine hydrochloride (14.0 g, 75.4 mmol) and  $Na_2WO_4 \cdot 2H_2O$  (13.0 g, 39.4 mmol) were dissolved in water (80 mL). Hydrochloric acid (6M) was added with stirring to adjust the pH to 1.2. The solution was then heated at reflux with stirring for 3 days. After the solution was cooled to room temperature, pale green needles crystallized over 2 days; these were then filtered, washed with ethanol, and dried in vacuum (3.8 g, 34% yield). IR (KBr):  $\tilde{\nu} = 3434, 1631, 1446, 1400, 1258, 1202, 1091, 1060, 1027, 961, 767, 614 \text{ cm}^{-1}$ ; elemental analysis (%) calcd for  $C_{36}H_{100}N_6O_{80}W_{19}$ : C 8.02, H 1.87, N 1.56, W 64.8; found: C 8.04, H 1.84, N 1.54, W 64.5.  $^1H$  NMR (400 MHz, DMSO): TEAH<sup>+</sup> was observed at  $\delta = 8.48$  NH (6H), 5.27 OH (18H), 3.79  $CH_2$  (36H), 3.4 ppm  $CH_2$  (36H);  $[H_4W_{19}O_{62}]^{6-}$  at  $\delta = 8.01, 7.23, 5.74, 5.27, 4.66, 4.45, 4.0$  ppm, integrated to ca. 3.2.  $^{183}W$  NMR (16.668 MHz,  $D_2O$ ,  $Na_2WO_4$ ): three sets of resonances reflecting the presence of multiple isomers centered at  $\delta = -115, -143, -165$  ppm which can be assigned to the central  $\{W_1\}$ ,  $\{W_{12}\}$  belt, and  $\{W_6\}$  caps on the basis of Löwdin charge analysis from the DFT calculations. Recrystallization of **1** in water give pale green cubic crystals of  $(TEAH)_6[H_4W_{19}O_{62}] \cdot 6H_2O$  (**1'**).

**2 and 3:** Freshly prepared compound **1** (2.0 g, 0.37 mmol) was dissolved in water (80 mL) with stirring.  $Pr_4NBr$  (2.2 g) in water (50 mL) was added and the mixture was stirred for a further 10 minutes. The light precipitate was centrifuged, washed with water, ethanol, and diethyl ether, and dried in vacuum. The dried sample was then extracted with acetonitrile (140 mL). Evaporation of the extract yielded colorless lath crystals of **2** (0.68 g, 33%) and very light cream yellow polyhedral crystals of **3** (0.45 g, 21%), along with some noncrystalline powder of other possible isomers on the glass wall with elemental analyses close to those calculated for the composition  $C_{72}H_{172}N_6O_{62}W_{19}$ . **2** and **3** were separated manually, and recrystallization of **2** and **3** helped to purify them further. **2** loses solvent and decays in minutes after being taken from the solution, whereas **3** is stable with included solvent molecules and is still suitable for X-ray structure determination several days after being taken from the solution. Analysis of **2**:  $^1H$  NMR (400 MHz,  $CD_3CN$ ):  $\delta = 1.00$  - $CH_3$  (72H), 1.7 - $CH_2$ - (48H), 3.1 - $CH_2$ - (48H), 4.5 H (0.8H), 7.6 H (0.7H), 8.1 ppm H (2.5H); IR (KBr):  $\tilde{\nu} = 3542, 2970, 2881, 1627, 1387, 1324, 1158, 1024, 961, 876, 799 \text{ cm}^{-1}$ ; elemental analysis (%) calcd for  $C_{72}H_{172}N_6O_{62}W_{19}$  (after losing solvated acetonitrile and vacuum drying): C 15.42, H 3.09, N 1.50, W 62.3; found: C 15.30, H 2.95, N 1.50, W 61.8. Analysis of **3**:  $^1H$  NMR (400 MHz,  $CD_3CN$ ):  $\delta = 1.00$  - $CH_3$  (72H), 1.7 - $CH_2$ - (48H), 3.1 - $CH_2$ - (48H), 4.7 H (2.2H), 6.7 H (0.5H), 7.6 H (0.8H), 8.1 H (0.5H); IR (KBr):  $\tilde{\nu} = 3410, 2975, 2881, 1484, 1385, 1013, 962, 815 \text{ cm}^{-1}$ ; elemental analysis (%) calcd for  $C_{78}H_{181}N_9O_{62}W_{19}$ : C 16.35, H 3.18, N 2.20; found: C 16.30, H 3.17, N 2.23.

$(Pr_4N)_4[W_{10}O_{32}] \cdot CH_3CN$  (in the absence of TEA):  $Na_2WO_4 \cdot 2H_2O$  (3.3 g, 10 mmol) was dissolved in water (50 mL). The pH of the solution was adjusted to 1.2 using hydrochloric acid (6M), and the solution was heated at reflux for 3 days. After the solution was cooled to room temperature, a solution of  $Pr_4NBr$  (1.7 g) in water (30 mL)



was added and the precipitated product was collected, washed with ethanol, dried in vacuum, and recrystallized from CH<sub>3</sub>CN (2.8 g, 89% yield, based on W). IR (KBr):  $\tilde{\nu}$  = 2976, 1681, 1629, 1474, 1380, 1325, 1105, 1041, 961, 894, 804, 589 cm<sup>-1</sup>; elemental analysis (%) calcd for C<sub>30</sub>H<sub>115</sub>N<sub>5</sub>O<sub>32</sub>W<sub>10</sub>: C 19.14, H 3.70, N 2.23, W 58.6; found: C 19.01, H 3.47, N 2.15, W 57.9.

Received: December 28, 2005

Revised: April 25, 2006

Published online: June 28, 2006

**Keywords:** cluster compounds · electronic structure · polyoxometalates · self-assembly · tungsten

- [1] V. M. Hultgren, B. P. Timko, A. M. Bond, W. R. Jackson, A. G. Wedd, *J. Am. Chem. Soc.* **2003**, *125*, 10133; W. B. Kim, T. Voitl, G. J. Rodriguez-Rivera, S. T. Evans, J. A. Dumesic, *Angew. Chem.* **2005**, *117*, 788; *Angew. Chem. Int. Ed.* **2005**, *44*, 778.
- [2] K. F. Aguey-Zinsou, P. V. Bernhardt, U. Kappler, A. G. McEwan, *J. Am. Chem. Soc.* **2003**, *125*, 530; D. A. Judd, J. H. Nettles, N. Nevins, J. P. Snyder, D. C. Liotta, J. Tang, J. Ermoloeff, R. F. Schinazi, C. L. Hill, *J. Am. Chem. Soc.* **2001**, *123*, 886; M. T. Pope, A. Müller, *Angew. Chem.* **1991**, *103*, 56; *Angew. Chem. Int. Ed. Engl.* **1991**, *30*, 34; F. Ogliaro, S. P. de Visser, S. Cohen, P. K. Sharma, S. Shaik, *J. Am. Chem. Soc.* **2002**, *124*, 2806; T.-R. Zhang, W. Feng, R. Lu, C.-Y. Bao, T.-J. Li, Y.-Y. Zhao, J. N. Yao, *J. Solid State Chem.* **2002**, *166*, 259; T. Yamase, *Chem. Rev.* **1998**, *98*, 307.
- [3] For recent examples of novel polyanion structures, see for example: a) Y. Jeannin, *C. R. Chim.* **2004**, *7*, 1235; b) W. Yang, C. Lu, H. Zhuang, *Inorg. Chem. Commun.* **2002**, *5*, 865; c) D. Drewes, G. Vollmer, B. Krebs, *Z. Anorg. Allg. Chem.* **2004**, *630*, 2573; d) U. Kortz, M. G. Savelieff, B. S. Bassil, M. H. Dickman, *Angew. Chem.* **2001**, *113*, 3488; *Angew. Chem. Int. Ed.* **2001**, *40*, 3384; e) B. S. Bassil, S. Nellutla, U. Kortz, A. C. Stowe, J. van Tol, N. S. Dalal, B. Keita, L. Nadjo, *Inorg. Chem.* **2005**, *44*, 2659.
- [4] J. Fuchs, R. Palm, H. Hartl, *Angew. Chem.* **1996**, *108*, 2820; *Angew. Chem. Int. Ed. Engl.* **1996**, *35*, 2651.
- [5] R. Bhattacharyya, S. Biswas, J. Armstrong, E. M. Holt, *Inorg. Chem.* **1989**, *28*, 4297.
- [6] H. Hartl, R. Palm, J. Fuchs, *Angew. Chem.* **1993**, *105*, 1545; *Angew. Chem. Int. Ed. Engl.* **1993**, *32*, 1492.
- [7] K. G. Burtseva, T. S. Chernaya, M. I. Sirota, *Dokl. Akad. Nauk* **1978**, *243*, 104; J. Fuchs, E. P. Flindt, *Z. Naturforsch. B* **1979**, *34*, 412.
- [8] Y. Sasaki, T. Yamase, Y. Ohashi, Y. Sasada, *Bull. Chem. Soc. Jpn.* **1987**, *60*, 4285.
- [9] T. Lehmann, J. Z. Fuchs, *Z. Naturforsch. B* **1988**, *43*, 89.
- [10] I. Brüdgam, J. Fuchs, H. Hartl, R. Palm, *Angew. Chem.* **1998**, *110*, 2814; *Angew. Chem. Int. Ed.* **1998**, *37*, 2668, and references therein.
- [11] D.-L. Long, P. Kögerler, L. J. Farrugia, L. Cronin, *Angew. Chem.* **2003**, *115*, 4312; *Angew. Chem. Int. Ed.* **2003**, *42*, 4180; D.-L. Long, P. Kögerler, L. J. Farrugia, L. Cronin, *Dalton Trans.* **2005**, 1372.
- [12] D.-L. Long, H. Abbas, P. Kögerler, L. Cronin, *J. Am. Chem. Soc.* **2004**, *126*, 13880; D.-L. Long, O. Brücher, C. Streb, L. Cronin, *Dalton Trans.* **2006**, 2852.
- [13] Crystal data and structure refinements for (Pr<sub>4</sub>N)<sub>4</sub>[W<sub>10</sub>O<sub>32</sub>]-CH<sub>3</sub>CN: C<sub>52</sub>H<sub>118</sub>N<sub>6</sub>O<sub>32</sub>W<sub>10</sub>,  $M_r$  = 3178.02 g mol<sup>-1</sup>; triclinic, space group  $P\bar{1}$ ,  $a$  = 12.0974(4),  $b$  = 13.9624(4),  $c$  = 14.2581(4) Å,  $\alpha$  = 70.213(2),  $\beta$  = 75.129(2),  $\gamma$  = 79.298(2)°,  $V$  = 2177.26(11) Å<sup>3</sup>,  $Z$  = 1,  $\rho$  = 2.424 g cm<sup>-3</sup>,  $\mu$ (MoK $\alpha$ ) = 13.22 mm<sup>-1</sup>,  $F(000)$  = 1468, 30461 reflections measured, 7663 unique ( $R_{int}$  = 0.052), 450 refined parameters,  $R1$  = 0.0372,  $wR2$  = 0.0911.
- [14] Crystal data and structure refinements for **1**: C<sub>36</sub>H<sub>100</sub>N<sub>6</sub>O<sub>80</sub>W<sub>19</sub>,  $M_r$  = 5390.13 g mol<sup>-1</sup>; triclinic, space group  $P\bar{1}$ ,  $a$  = 13.7245(10),  $b$  = 13.9719(10),  $c$  = 16.2396(9) Å,  $\alpha$  = 86.865(5),  $\beta$  = 74.245(4),  $\gamma$  = 61.093(2)°,  $V$  = 2612.8(3) Å<sup>3</sup>,  $Z$  = 1,  $\rho$  = 3.426 g cm<sup>-3</sup>,  $\mu$ (MoK $\alpha$ ) = 20.92 mm<sup>-1</sup>,  $F(000)$  = 2404, 28808 reflections measured, 7231 unique ( $R_{int}$  = 0.089), 415 refined parameters,  $R1$  = 0.0667,  $wR2$  = 0.2014. **1'**: C<sub>36</sub>H<sub>112</sub>N<sub>6</sub>O<sub>86</sub>W<sub>19</sub>,  $M_r$  = 5498.47 g mol<sup>-1</sup>; trigonal, space group  $R\bar{3}$ ,  $a$  = 21.471(2),  $c$  = 19.9668(12),  $V$  = 7971.6(12) Å<sup>3</sup>,  $Z$  = 3,  $\rho$  = 3.436 g cm<sup>-3</sup>,  $\mu$ (MoK $\alpha$ ) = 20.58 mm<sup>-1</sup>,  $F(000)$  = 7392, 7325 reflections measured, 2921 unique ( $R_{int}$  = 0.065), 239 refined parameters,  $R1$  = 0.0536,  $wR2$  = 0.1172. **2**: C<sub>84</sub>H<sub>190</sub>N<sub>12</sub>O<sub>62</sub>W<sub>19</sub>,  $M_r$  = 5853.63 g mol<sup>-1</sup>; monoclinic, space group  $C2$ ,  $a$  = 30.7860(4),  $b$  = 15.3098(2),  $c$  = 29.9306(4) Å,  $\beta$  = 94.515(1)°,  $V$  = 14063.3(3) Å<sup>3</sup>,  $Z$  = 4,  $\rho$  = 2.765 g cm<sup>-3</sup>,  $\mu$ (MoK $\alpha$ ) = 15.551 mm<sup>-1</sup>,  $F(000)$  = 10720, 56613 reflections measured, 24330 unique ( $R_{int}$  = 0.054), 1412 refined parameters,  $R1$  = 0.0441,  $wR2$  = 0.0709. **3**: C<sub>78</sub>H<sub>181</sub>N<sub>9</sub>O<sub>62</sub>W<sub>19</sub>,  $M_r$  = 5730.47 g mol<sup>-1</sup>; orthorhombic, space group  $Pccn$ ,  $a$  = 22.4058(7),  $b$  = 24.6486(9),  $c$  = 25.2268(8) Å,  $V$  = 13932.0(8) Å<sup>3</sup>,  $Z$  = 4,  $\rho$  = 2.732 g cm<sup>-3</sup>,  $\mu$ (MoK $\alpha$ ) = 15.693 mm<sup>-1</sup>,  $F(000)$  = 10456, 241605 reflections measured, 13703 unique ( $R_{int}$  = 0.068), 737 refined parameters,  $R1$  = 0.0269,  $wR2$  = 0.0671. Crystal data for **3** were measured on a Bruker ApexII CCD diffractometer by using MoK $\alpha$  radiation ( $\lambda$  = 0.71073 Å) at 100(2) K. For all other compounds, crystal data were measured on a Nonius Kappa CCD diffractometer by using MoK $\alpha$  radiation ( $\lambda$  = 0.71073 Å) at 150(2) K. CCDC 292393–292397 ((Pr<sub>4</sub>N)<sub>4</sub>[W<sub>10</sub>O<sub>32</sub>]-CH<sub>3</sub>CN, **1**, **1'**, **2**, and **3**, respectively) contain the supplementary crystallographic data for this paper. These data can be obtained free of charge from The Cambridge Crystallographic Data Centre via [www.ccdc.cam.ac.uk/data\\_request/cif](http://www.ccdc.cam.ac.uk/data_request/cif).
- [15] B. Dawson, *Acta Crystallogr.* **1953**, *6*, 113; M. Holscher, U. Englert, B. Zibrowius, W. F. Holderich, *Angew. Chem.* **1994**, *106*, 2552; *Angew. Chem. Int. Ed. Engl.* **1994**, *33*, 2491.
- [16] For nonconventional Dawson-like cluster compounds, see for examples: Y. Ozawa, Y. Sasaki, *Chem. Lett.* **1987**, 923; Y. Jeannin, J. Martin-Frere, *Inorg. Chem.* **1979**, *18*, 3010; U. Kortz, M. T. Pope, *Inorg. Chem.* **1994**, *33*, 5645. D.-L. Long, P. Kögerler, L. Cronin, *Angew. Chem.* **2004**, *116*, 1853; *Angew. Chem. Int. Ed.* **2004**, *43*, 1817; D.-L. Long, H. Abbas, P. Kögerler, L. Cronin, *Angew. Chem.* **2005**, *117*, 3481; *Angew. Chem. Int. Ed.* **2005**, *44*, 3415. All clusters contain heteroelements.
- [17] M. T. Pope, G. M. Varga, Jr., *Chem. Commun.* **1966**, 653; J. J. Hastings, O. W. Howarth, *J. Chem. Soc. Dalton Trans.* **1992**, 209.
- [18] N. Belai, M. H. Dickman, M. T. Pope, R. Constant, B. Keita, I.-M. Mbomekalle, L. Nadjo, *Inorg. Chem.* **2005**, *44*, 169.
- [19] T. L. Joriss, M. Kozik, L. C. W. Baker, *Inorg. Chem.* **1990**, *29*, 4584.
- [20] P. J. S. Richardt, R. W. Gable, A. M. Bond, A. G. Wedd, *Inorg. Chem.* **2001**, *40*, 703.
- [21] R. Contant, R. Thouvenot, *Inorg. Chim. Acta* **1993**, *212*, 41.
- [22] A. L. Loeb, *Space Structures—Their Harmony and Counterpoint*, Addison-Wesley, London, **1976**, p. 45.
- [23] Density functional theory calculations (including Löwdin and Mulliken population analysis) with the TURBOMOLE 5.7 package (O. Treutler, R. Ahlrichs, *J. Chem. Phys.* **1995**, *102*, 346) employed TZVP basis sets and hybrid B3-LYP exchange-correlation functionals. Equilibrated structures were obtained from free geometry optimizations starting with crystallographic data ( $\alpha$  and  $\gamma^*$ ) and with modeled geometries derived from these structures ( $\alpha^*$ ,  $\beta$ ,  $\beta^*$ ,  $\gamma$ ). In both cases, proton positions were added by modeling and allowed to vary without symmetry restrictions in the course of the geometry optimization. The resulting optimized structures were found to be slightly expanded (owing to coulomb repulsion in the absence of countercharges). Calculated dipole moments:  $\alpha$ : 0.538,  $\alpha^*$ :



1.1352,  $\beta$ : 0.438,  $\beta^*$ : 1.034,  $\gamma$ : 0.998,  $\gamma^*$ : 0.976 debye. For a review on ab initio calculations on polyoxotungstates, see also J. M. Poblet, X. López, C. Bo, *Chem. Soc. Rev.* **2003**, 32, 297.

- [24] The two inherently coupled processes have been reproduced for multiple samples on two different DSC instruments. Changes in the heating rate do not change the relative peak positions or integrated energies associated with each of the processes; the process at 291–298 °C cannot be due to solvent loss since a simultaneous DSC/TGA experiment demonstrates total solvent loss below 250 °C.

## Nanotechnology

DOI: 10.1002/anie.200503770

# From Single Molecules to Nanoscopically Structured Functional Materials: Au Nanocrystal Growth on TiO<sub>2</sub> Nanowires Controlled by Surface-Bound Silicatein\*\*

Muhammad Nawaz Tahir, Marc Eberhardt, Helen Annal Therese, Ute Kolb, Patrick Theato, Werner E. G. Müller, Heinz-Christoph Schröder, and Wolfgang Tremel\*

*Dedicated to Professor Hans-Georg von Schnering on the occasion of his 75th birthday*

The chemical construction of organized inorganic matter by using inorganic nanoparticles as building blocks offers a new and promising approach to functional materials with complex architectures and properties.<sup>[1]</sup> The multiscale ordering, interlinking, and interfacing of preformed nanoparticles

may be directed by using artificially structured synthetic templates or through a programmed assembly based on self-encoding elements such as streptavidin–biotin<sup>[2]</sup> and antibody–antigen complexes,<sup>[3]</sup> complementary DNA strands,<sup>[4]</sup> or electrostatic self-assembly.<sup>[5]</sup> Alternatively, artificial structuring can be achieved by using (meso)porous templates such as silica, synthetic opals,<sup>[6]</sup> foams,<sup>[7]</sup> emulsions,<sup>[8]</sup> or polymers.<sup>[9]</sup> The exploitation of these strategies remains a significant challenge as the properties and functions of materials are controlled not only by the nature of their building blocks, that is, atoms, molecules, and nanoparticles, but also through their organization into complex assemblies on various length scales.

Recently there has been much interest in the fabrication of ordered two- and three-dimensional devices by using nanotubes/wires as building blocks.<sup>[10]</sup> Nanotubes/wires with various electronic and mechanical properties can be synthesized by a variety of methods, depending on the nature of the constituent material. Nanotube/wire–nanoparticle hybrid materials, in which nanoparticles are attached to the walls of nanotubes/wires, may combine the unique structural and electronic properties of nanotubes/wires and the outstanding properties of nanoparticles which can tune their electronic structures through their size and morphology. In the past, most efforts towards such hybrid materials focused on carbon nanotubes, with prototype guest particles being Au<sup>[11]</sup> or Pt<sup>[11a,c]</sup> as well as semiconductors such as CdSe.<sup>[12]</sup> This observation is surprising, as carbon nanotubes are very inert and therefore difficult to functionalize. Nanotubes/wires from compounds other than carbon (e.g. TiO<sub>2</sub>,<sup>[13]</sup> V<sub>2</sub>O<sub>5</sub>,<sup>[14]</sup> or WS<sub>2</sub><sup>[15]</sup>) can be expected to exhibit unique properties depending on the constituent compounds and their morphologies. In particular, oxidic nanotubes/wires would combine the versatile physical and chemical properties of ceramic materials and the tube/wire morphology.

A straightforward procedure to attach colloids onto the surface of nanotubes/wires is to grow the nanoparticles stabilized with capping ligands in solution and to anchor them to the outer tube/wire surface by chemical interactions in the final step.<sup>[16]</sup> Whereas this synthetic approach has to rely on sophisticated stabilizing ligands to control nanoparticle size and binding to the surface,<sup>[17]</sup> biological systems are able to control nucleation processes highly precisely and reproducibly to produce an amazing diversity of nanostructured particle morphologies.<sup>[18]</sup> Therefore, it is a logical approach to use “biological surfaces”, for example, biofunctionalized nanowires, as templates for the growth of nanoparticles on the wire surface. Biological methods using bacteria or proteins for the synthesis of metal<sup>[19]</sup> and semiconductor<sup>[20]</sup> nanoparticles still represent a relatively unexplored and underexploited alternative. The use of polypeptides or proteins seems advantageous because some bacteria and peptides have been shown to form and bind metal or semiconductor nanocrystals. Recently we reported the immobilization of silicatein, an enzyme involved in the biosilicification processes in marine sponges, onto self-assembled monolayers, and we demonstrated the catalytic activity of surface-bound silicatein for the formation of SiO<sub>2</sub> from tetraethoxysilane (TEOS)<sup>[21]</sup> and ZrO<sub>2</sub> from ZrF<sub>6</sub><sup>2–</sup>.<sup>[22]</sup>

[\*] M. N. Tahir, Dr. H. A. Therese, Prof. Dr. W. Tremel  
Institut für Anorganische Chemie und Analytische Chemie  
Johannes Gutenberg-Universität  
Duesbergweg 10–14, 55099 Mainz (Germany)  
Fax: (+49) 6131-39-25605  
E-mail: tremel@uni-mainz.de

M. Eberhardt, Dr. P. Theato  
Institut für Organische Chemie  
Johannes Gutenberg-Universität  
Duesbergweg 10–14, 55099 Mainz (Germany)  
Prof. Dr. W. E. G. Müller, Prof. Dr. Dr. H.-C. Schröder  
Institut für Physiologische Chemie  
Johannes Gutenberg-Universität  
Duesbergweg 6, 55099 Mainz (Germany)  
Dr. U. Kolb  
Institut für Physikalische Chemie  
Johannes Gutenberg-Universität  
Welderweg 11, 55099 Mainz (Germany)

[\*\*] This work was supported by the Deutsche Forschungsgemeinschaft (DFG). We are grateful to S. Faiß for help with the CLSM studies.

Supporting information for this article is available on the WWW under <http://www.angewandte.org> or from the author.

Herein, we report a facile procedure for the surface functionalization of  $\text{TiO}_2$  nanowires by immobilization of a His-tagged enzyme and the fabrication of Au nanoparticles onto the  $\text{TiO}_2$  nanowires as a result of the bioreduction of  $\text{HAuCl}_4$  that is mediated by the immobilized enzyme. The enzyme under consideration is versatile in its catalytic functions, as reported by Morse and co-workers<sup>[23,24]</sup> and us.<sup>[22]</sup> The methodology can be further extended to make core-shell materials of metal and metal oxide.

Surface functionalization was achieved using a polymeric ligand which can be used for the in situ and postfunctionalization of  $\text{TiO}_2$ <sup>[25]</sup> as well as for other metal oxides such as  $\text{Fe}_2\text{O}_3$ .<sup>[26]</sup> The architecture of the polymeric ligand is of major importance, because it provides the basis of a comprehensive toolbox to construct supramolecular assemblies of organic-inorganic hybrid nanomaterials. Polymeric ligands offer an enhanced binding efficiency over low-molecular-weight ligands as a consequence of their multifunctional interaction with the surface, as demonstrated by Whitesides and co-workers.<sup>[27]</sup> The fact that active ester polymers react quickly and quantitatively with amines to form the corresponding poly(acrylamide)s opens up the possibility to obtain multifunctional polymeric materials.<sup>[28]</sup> Compared to the commonly used poly(*N*-hydroxysuccinimide acrylate)s, active ester polymers based on pentafluorophenyl acrylates exhibit better solubility and higher reactivity.<sup>[28b]</sup>

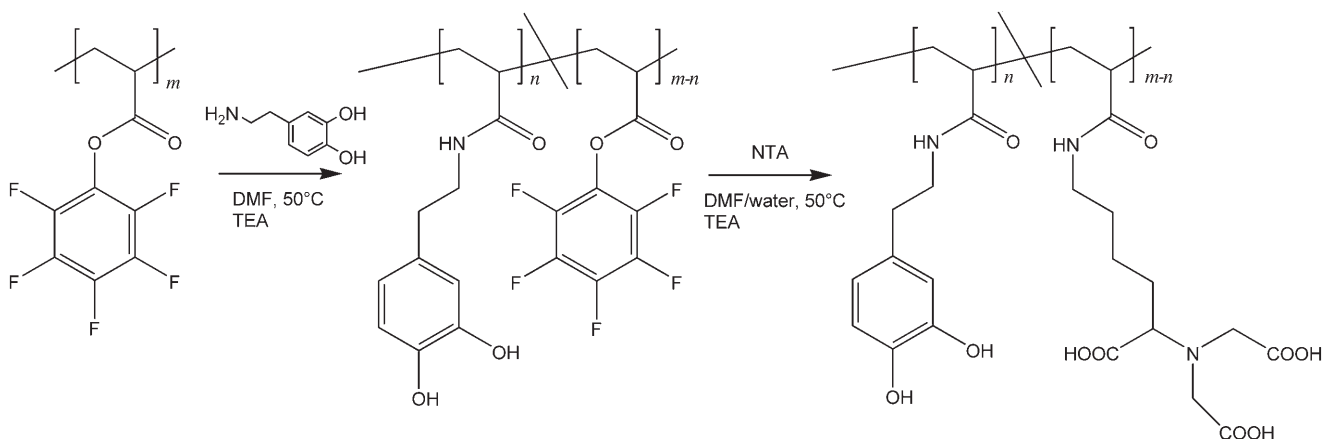
The synthesis of the multifunctional polymeric ligand starting from this precursor polymer is illustrated in Scheme 1. The active ester polymer was prepared by free-radical polymerization to yield a polymer with a molecular weight of  $M_n = 29.7 \text{ kg mol}^{-1}$  and  $M_w = 58.5 \text{ kg mol}^{-1}$  (PDI = 1.96). This precursor polymer was then transformed into the multifunctional polymeric ligand by substitution with amino-containing functionalities. The polymeric ligand was prepared by a stepwise substitution of the active ester groups: in the first step, 3-hydroxytyramine was added as an anchor group for the attachment onto  $\text{TiO}_2$  nanoparticles, and in the second step amino-functionalized nitrilotriacetic acid (NTA) in water and triethylamine were added and the resulting mixture was kept at  $50^\circ\text{C}$  for 6 h and then the solution was adjusted to pH 2 with  $\text{H}_2\text{SO}_4$ . Characterization of the polymeric ligand by  $^1\text{H}$  NMR and FTIR spectroscopy as well as GPC (see the

Supporting Information) showed the composition to be 80 mol % NTA and 20 mol % 3-hydroxytyramine. The resulting polymer exhibits two different features: 1) An NTA linker to immobilize the His-tagged protein<sup>[29]</sup> 2) 3-hydroxytyramine as an anchor group for attachment to the  $\text{TiO}_2$  nanoparticle surface.<sup>[30]</sup>

Functionalization of  $\text{TiO}_2$  nanowires was achieved by sealing a mixture of  $\text{TiO}_2$  nanowires and polymeric ligand in benzyl alcohol (10 mL) under inert conditions and stirring the mixture at  $60^\circ\text{C}$  for 4 h. The product was repeatedly washed with  $\text{CH}_2\text{Cl}_2$  to remove any remaining ligand. The functionalized  $\text{TiO}_2$  nanowires were characterized by TEM as well as FTIR,  $^1\text{H}$  NMR, and UV/Vis spectroscopy.

The binding of silicatein to the surface of the  $\text{TiO}_2$  nanowires functionalized with polymeric ligand incorporating NTA in the backbone of the polymer was confirmed by confocal laser scanning microscopy (CLSM, Leica TCS SL with an argon laser) using fluorophore-labeled antibodies against silicatein.<sup>[31]</sup>

The dye molecules were excited at 488 nm and the resulting fluorescence detected from 504–514 nm using a  $20\times$  dry objective. The advantages of CLSM are that: 1) the detection of protein using fluorophore-labeled antibodies is very specific, that is, this antibody does not bind to any other component, and 2) a large surface area can be seen. Figure 1 a illustrates the identification of surface-bound silicatein. Figure 1 b, c show the CLSM images of immobilized silicatein after exposing the surface to fluorophore-labeled antibodies. Monoclonal antibodies raised against the silicatein immobilized onto the functionalized  $\text{TiO}_2$  nanowires were used.<sup>[31]</sup> The functionalized nanowires with immobilized silicatein were treated with solutions containing the antibody (mAb-aSilic); the immunocomplexes were then stained with fluorophore-labeled (Cy2-label) secondary goat anti-rabbit antibodies. The surface-bound silicatein reacted strongly with the antibodies as illustrated in Figure 1 b, c. The presence of Cy2 resulted in the silicatein appearing green and fluorescing at 520 nm. The high magnification image in Figure 1 c indicates that several silicatein molecules are immobilized onto the backbone of functionalized  $\text{TiO}_2$  nanowires and shows the globular morphology of silicatein, as already reported using AFM and CLSM.<sup>[21,22,32]</sup> It is difficult to comment on the



**Scheme 1.** Synthesis of a functional polymeric ligand containing nitrilotriacetic acid (NTA) and dopamine units. TEA = triethylamine.

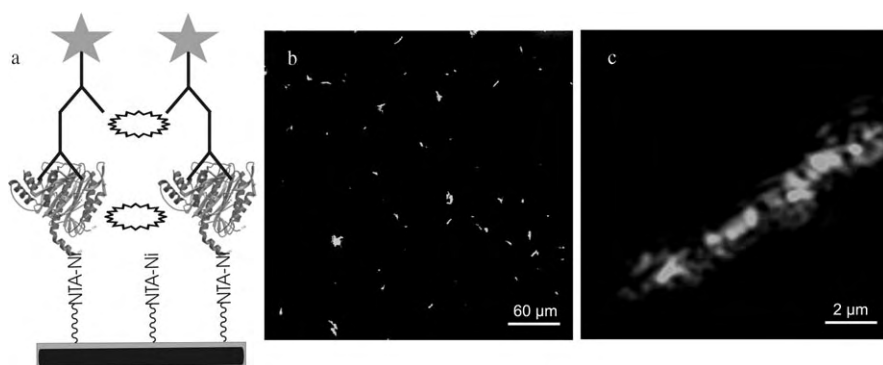


**Figure 1.** a) Antigen capture assay. a)  $\text{TiO}_2$ /silicatein complex (globular symbol = silicatein, oval dentate symbol = nonspecific bovine serum albumin (BSA), and Y symbol = specific monoclonal anti-silicatein of *Suberites domuncula*). The assay is visualized by recognition of the antigen/antibody by fluorophore Cy2 coupled to antibodies detecting the mouse  $F_{AB}$ . Upon immobilization of fluorophore-labeled antibodies (Ab) onto the  $\text{TiO}_2$ /polymer/silicatein surface, the surface-bound silicatein can be visualized by using confocal laser scanning microscopy (CLSM). b) Overview image showing many functionalized and immobilized silicatein  $\text{TiO}_2$  nanowires. c) HRCLSM image showing the presence of several adjacent fluorescence spots which indicates the binding of several silicatein molecules onto a  $\text{TiO}_2$  nanowire.

actual size of the silicatein because it is beyond the resolution limits of CLSM. In our control experiment where functionalized  $\text{TiO}_2$  nanowires were exposed to fluoro-labeled antibodies, no fluorescence was observed.

The fabrication of  $\text{TiO}_2$  nanowires decorated with Au nanocrystals is illustrated in Figure 2. In the first step the surface of the  $\text{TiO}_2$  nanowire (white) is functionalized with

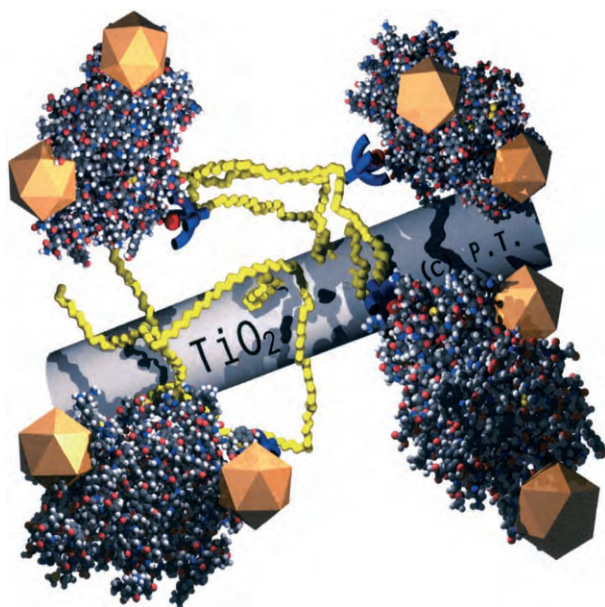


**Figure 2.** Schematic presentation of the fabrication of the  $\text{TiO}_2$  nanowire/Au nanocrystals. In the first step the  $\text{TiO}_2$  nanowire is functionalized with the multifunctional polymer ligand (gray) by complexation through the catechol groups. The NTA tripod ligand is bound to the side groups of the polymer. In the next step, the silicatein-containing His-tag is attached to the NTA ligand by complexation of  $\text{Ni}^{2+}$  ions through the His-tag. Finally, tetrachloroauric acid is reduced by the sulfhydryl groups of the immobilized silicatein. The Au nanocrystals are chemically bonded to the amino groups at the protein periphery.

the multifunctional polymer ligand (gray) by complexation through the hydroxy groups of dopamine, thus tailoring the surface of the  $\text{TiO}_2$  nanowires with the NTA tripod ligand attached to the polymer. In the second step, silicatein containing the His-tag was immobilized onto the NTA ligand by complexation with  $\text{Ni}^{2+}$  ions. Finally, tetrachloroauric acid was reduced by the surface-bound silicatein. The growing Au nanocrystals were thus chemically bonded to the protein through complexation/surface binding.

The addition of aqueous chloroauric acid to a solution of the silicatein-functionalized  $\text{TiO}_2$  nanowires resulted in the color of the solution changing from pale yellow to red, which indicates the formation of gold nanoparticles by the reductive

action of the protein. The UV/Vis spectrum (Figure 3) recorded 3 h after mixing the solutions at room temperature

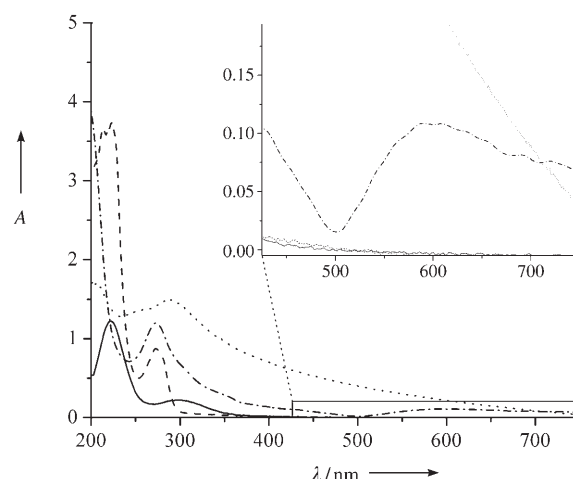


**Figure 3.** UV/Vis absorption spectrum of: synthesized  $\text{TiO}_2$  nanowires (.....), polymeric ligand (-----),  $\text{HAuCl}_4$  solution (—), and polymer-functionalized  $\text{TiO}_2$  nanowires with immobilized silicatein and bioreduced Au nanoparticles (—·—·).

showed the appearance of a surface-plasmon resonance band at about 570 nm which shifted to longer wavelength with time. This shift is accompanied by an increase in the near-infrared (NIR) region of the electromagnetic spectrum. Clearly, the absorption at 275 nm for the polymeric ligand (dashed line) shows the presence of aromatic catechol groups and the absorption at 220 nm shows the presence of carbonyl groups. The blue shift of 15 nm in the absorption of the carbonyl groups (dashed line) indicates the His-tagged binding of the protein through Ni complexation by the NTA groups. A broad plasmon absorption band ranging from 520–700 nm for the composite (see inset of Figure 3) indicates the aligned attach-



ment of Au nanoparticles in the  $\text{TiO}_2/\text{Au}$  nanocomposites. The UV/Vis absorption of the functionalized  $\text{TiO}_2$  nanowires carrying no protein and  $\text{AuCl}_4^-$  did not show any plasmon absorption band, which indicates that polymer-functionalized  $\text{TiO}_2$  nanowires alone cannot reduce tetrachloroauric acid. In contrast, the polymeric ligand reduces  $\text{AuCl}_4^-$  in solution at the expense of the free hydroxy groups of dopamine, whereas the surface-bound polymeric ligand exhibits no reducing properties because all the hydroxy groups are involved in surface binding. Moreover, free silicatein can reduce  $\text{AuCl}_4^-$  efficiently to Au nanoparticles (see the Supporting Information). These results indicate that Au reduction is restricted to protein-functionalized  $\text{TiO}_2$  nanowires only.

Our findings are compatible with the formation of anisotropic particles whose aspect ratio increases with time<sup>[19c,e]</sup> as a result of a uniaxial plasmon coupling or indicate the formation of spherical gold nanoparticles that aggregate with time (or a combination of both processes). Since recombinant silicatein does not contain any reducible saccharide groups, the SH groups of cysteine or OH groups of tyrosine within the protein mantle are considered to be involved in the reduction of  $\text{AuCl}_4^-$  to  $\text{Au}^0$  and the subsequent growth of Au nanoparticles. As electron transfer can occur easily over distances of 20 Å and more,<sup>[33]</sup> this reduction does not require the SH groups to be located at the periphery of the protein. The amino groups arranged at the outer surface of silicatein may be assumed to act as coordinating centers for the surface binding of the gold colloids.

The HRSEM image of  $\text{TiO}_2$  nanowires decorated with Au nanocrystals (Figure 4, inset top left) shows that the  $\text{TiO}_2/\text{Au}$  hybrid is composed of hierarchically templated assemblies of Au nanoparticles and  $\text{TiO}_2$  nanowires. The individual  $\text{TiO}_2/\text{Au}$  nanocomposites with a uniform  $\text{TiO}_2$  backbone are clearly seen with a high aspect ratio in Figure 4. A high-resolution view in the inset (bottom right) reveals a triangular or hexagonal morphology of the Au nanoparticles, with a uniform statistical distribution across the  $\text{TiO}_2$  nanowire.

The morphology of the  $\text{TiO}_2/\text{Au}$  composite was confirmed by TEM. Figure 5a shows a TEM image of the as-synthesized  $\text{TiO}_2$  nanowires. It reveals  $\text{TiO}_2$  nanowires with diameters of 25–50 nm and wire lengths of up to a few micrometers. Figure 5b shows an overview image of several  $\text{TiO}_2$  nanowires

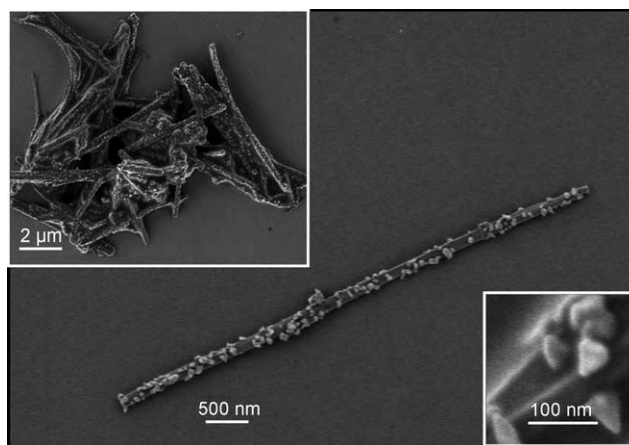


**Figure 4.** HRSEM image demonstrating the hierarchical structure of the  $\text{TiO}_2$  nanowire/Au nanoparticle composite. Overview images of the  $\text{TiO}_2/\text{Au}$  nanocomposites (top left) and a magnified view (right bottom) are given.

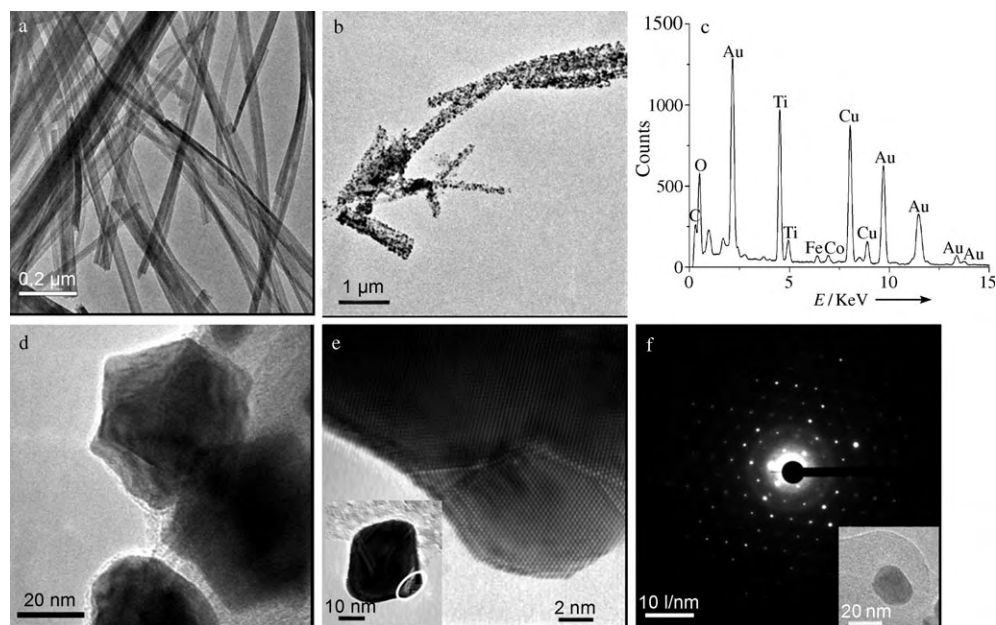


**Figure 5.** a) TEM image of  $\text{TiO}_2$  nanowires. b) Overview image of  $\text{TiO}_2$  nanowires decorated with Au nanocrystals, obtained by reduction with surface-bound silicatein. c) EDX spectrum of a  $\text{TiO}_2$  nanowire decorated with Au nanocrystals, thus indicating the presence of Ti, O, and Au. d) Magnified view of a single  $\text{TiO}_2$  nanowire with Au nanocrystals attached. e) HRTEM of a crystal edge, (marked by a circle in the inset) which shows the polycrystalline nature of the nanocrystal. f) Nano-electron diffraction (NED) spectrum of an Au nanocrystal shown in the inset.

decorated homogeneously over their entire length with Au nanoparticles. The corresponding EDX spectrum in Figure 5c clearly confirms the presence of Au, along with Ti and O. The TEM image of nanocrystals in Figure 5d, however, appears to be composed of triangular platelets inverted with respect to each other, which is in agreement with the results from the HRSEM image in Figure 4, where some of the nanocrystals grown in the presence of surface-bound silicatein exhibited triangular morphology of Au nanocrystals. The HRTEM image of one particle (see Figure 5e) exhibits the view down  $\langle 110 \rangle$  with grain boundaries clearly visible. A typical electron

diffraction pattern of a 20-nm-sized gold nanocrystal viewed along  $\langle 110 \rangle$  is given in Figure 5 f. This triangular crystal shape<sup>[19e,34]</sup> is very unusual; except for one case<sup>[19e]</sup> the limited number of examples reported so far have been obtained by chemical/photochemical methods. Shape control of inorganic materials in biological systems is achieved either by growth in constrained environments such as membrane vesicles,<sup>[35]</sup> or through functional molecules such as polypeptides that bind specifically to inorganic surfaces.<sup>[36]</sup> Specific polypeptide repeating sequences in proteins secreted by the bacterium *Escherichia coli* have been shown to induce the growth of flat, triangular gold nanocrystals in low yield relative to the total formation of nanoparticles.<sup>[36]</sup> Therefore, a possible explanation for the formation of the surface-bound nanotriangles is based on the chirality of the nucleation centers at the surface of the protein. Whereas hexagonal crystals are achiral, because they have an inversion center in the center of the Au hexagons, triangular crystals are chiral, because the inversion symmetry is lost during the formation of the triangular crystal. An  $S_6$  axis of the hexagon is maintained as the high symmetry element, that is, chiral information contained in the silicatein structure is transmitted to the nucleating gold nanocrystals during the  $\text{AuCl}_4^- \rightarrow \text{Au}$  reduction and the subsequent Au nucleation at the outer surface of the protein, and maintained during the growth of the nanocrystal. This scenario is compatible with the observation that triangular nanocrystals were also formed by reduction of  $\text{AuCl}_4^-$  in the presence of lemon grass extract,<sup>[19e]</sup> which presumably contains a multitude of as yet unidentified proteins. In contrast, no triangular (or even pronounced) Au nanocrystal morphologies were observed when Au precursor compounds were reduced chemically and attached to histidine-rich peptides on the surface of carbon nanotubes.<sup>[16,37]</sup> These findings suggest that the morphology of the Au nanocrystals is determined by the coordination and simultaneous reduction during the nucleation process in the presence of the protein rather than by the chemical reduction in solution and subsequent binding to the polypeptide chain.

In summary, we have fabricated a functional nanocomposite of immobilized silicatein—a hydrolytic protein involved in the biomineralization of  $\text{SiO}_2$ —on the surface of  $\text{TiO}_2$  nanowires with the aid of a reactive polymeric ligand, which simultaneously serves as an anchor to the oxide surface and as a chelating ligand for the binding of the protein. The strategy of using such polymeric multifunctional ligands offers at least two advantages over the use of small (low-molecular-weight) molecules as ligands: Our polymeric ligand can be prepared by a two-step synthesis, whereas a multistep synthesis is required for a low-molecular-weight ligand which is compatible in function to our polymeric ligand,<sup>[38]</sup> and polymeric ligands provide multidentate properties for binding, whose surface bonding is much stronger than that of monodentate low-molecular-weight ligands.

The surface-bound protein not only retains its original hydrolytic properties,<sup>[21,22]</sup> but also acts as a reductant for  $\text{AuCl}_4^-$  in the synthesis of hybrid  $\text{TiO}_2/\text{Au}$  nanocomposites. The fabrication of hybrid materials with functional nanobiocomposites is without precedence. The advantage of applying biological and chiral “recognition” to the synthesis

of metal nanoparticles on one-dimensional building blocks such as nanowires/nanotubes is not only the efficient and reproducible production of nanoparticles, it may be viewed also as an environmentally friendly alternative to chemical methods for the synthesis of nanoparticles.

We believe that this procedure can be generalized for various metals and semiconductors and other nanotube/nanowire materials such as  $\text{WS}_2$ . The biofunctionalization of the highly rigid oxide/chalcogenide wires/tubes also opens up possibilities for the programmed assembly of strictly one-dimensional building blocks based on self-encoding elements such as streptavidin–avidin and antibody–antigen complexes, complementary DNA strands, or electrostatic self organization.

## Experimental Section

PFA was prepared as reported earlier.<sup>[28b]</sup> GPC analysis of the obtained polymer (THF, light-scattering detection) gave the following values:  $M_n = 29.7 \text{ kg mol}^{-1}$ ;  $M_w = 58.5 \text{ kg mol}^{-1}$ , where the number of repeating units (246) is based on the  $M_w$  value.

For the synthesis of the multifunctional poly(acrylamides), PFA (110 mg, 0.46 mmol repeating units) was dissolved in dry DMF (3 mL). A solution of 3-hydroxytyramine hydrochloride (10.5 mg, 0.055 mmol) in DMF (1.5 mL) and triethylamine (0.1 mL) were added and the clear mixture stirred for 1 h at 50°C. A solution of amino-functionalized NTA (120 mg, 0.46 mmol) in MilliQ water (0.9 mL) and triethylamine (2.1 mL) were then added and the resulting mixture kept at 50°C for 6 h. The slight excess of NTA was used to ensure complete conversion of the remaining active ester groups. After removal of the DMF, the solution was adjusted to pH 3 and the crude viscous product was cleaned by dialysis in MilliQ water, isolated, and finally dried in a vacuum oven at 40°C for 1 h to give 64 mg of a white polymeric powder. Recombinant silicatein was prepared as described.<sup>[39]</sup>

The  $\text{TiO}_2$  nanowires were synthesized following a modified procedure reported by Bruce and co-workers.<sup>[40]</sup> In brief, titanium isopropoxide (1 g; ACROS) was placed in a teflon vessel and analytical grade ethanol (99.8%, 6 mL) was added. The teflon vessel was kept in a desiccator. The precipitation of  $\text{TiO}_2$  was initiated under a moist atmosphere induced by placing a petri dish filled with water at the bottom of the desiccator. The diffusion experiment was stopped after 12 h, and then a 10 M aqueous solution of NaOH (25 mL) added. The reaction vessel was then sealed in a stainless-steel hydrothermal bomb, which was placed in an oven maintained at 180°C for 20 h. The obtained sample was filtered and repeatedly washed with 0.1 M  $\text{HNO}_3$ , 1 N HCl, and de-ionized water. The product was dried under vacuum for 3 h.

$\text{TiO}_2$  nanowires (5 mg) were then dispersed in benzyl alcohol (10 mL) and sonicated for 15 min. In a separate vial, polymer ligand (10 mg) was dissolved in benzyl alcohol (10 mL). Both the suspension and solution were mixed under inert conditions and stirred at 60°C for 4 h. Then polymer-functionalized nanowires were isolated and purified by repeatedly washing them with  $\text{CH}_2\text{Cl}_2$  using centrifugation, followed by drying them under vacuum and dispersing under water. To immobilize the silicatein,  $\text{Ni}^{2+}$  ions were bound to NTA group, and the  $\text{TiO}_2$  nanowires functionalized with the polymeric ligand containing NTA in the backbone were treated with 1 mmol aqueous solution of NaOH for 10 min using continuous stirring. The mixture was then centrifuged, washed with  $18.2 \text{ M}\Omega \text{ cm}^{-1}$  MilliQ water, and the  $\text{TiO}_2$  nanowires rotated in a solution of  $\text{NiSO}_4$  (40 mmol) for 1 h. The  $\text{TiO}_2$  nanowires containing complexed  $\text{Ni}^{2+}$  ions were then removed, washed with a solution of NaCl and deionized water (150 mmol), and dried in a stream of  $\text{N}_2$ . A solution of silicatein (30 nmol) in 3-(*N*-morpholino)propane sulfonic acid

(MOPS) buffer was then added to the Ni<sup>2+</sup>-bound TiO<sub>2</sub> nanowires and the mixture left for 1 h. Then silicatein-immobilized TiO<sub>2</sub> nanowires were washed with MOPS buffer and deionized water to remove unbound protein. The immobilization of silicatein was monitored by CLSM. To monitor the specific immobilization or activity of the enzyme, silicatein-immobilized TiO<sub>2</sub> nanowires in water were added to an aqueous solution of H<sub>2</sub>AuCl<sub>4</sub> (10<sup>-3</sup> M, 1 mL) in a polyethylene vial (2 mL). The suspension of silicatein-coated TiO<sub>2</sub> nanowires and acidic gold solution was immediately placed on a rotator (biocentrifuge). The suspension of the protein-immobilized TiO<sub>2</sub> precursor was mixed on the rotator at a speed of 1000 rpm for 24 h under normal conditions. The "bioreduction" of tetrachloroauric acid was monitored by UV/Vis spectroscopy. The biomass was then centrifuged at 3000 rpm for 10 min and repeatedly washed with sterile distilled water before carrying out all subsequent characterization.

Received: October 24, 2005

Revised: March 1, 2006

Published online: June 23, 2006

**Keywords:** biofunctionalization · hybrid nanocomposites · nanotechnology · nanowires · titanium oxides

- [1] S. Mann, S. A. Davis, S. R. Hall, M. Li, K. H. Rhodes, W. Shenton, S. Vaucher, B. Zhang, *J. Chem. Soc. Dalton Trans.* **2000**, 3753–3753.
- [2] a) S. Connolly, D. Fitzmaurice, *Adv. Mater.* **1999**, *11*, 1202–1205.
- [3] W. Shenton, S. A. Davis, S. Mann, *Adv. Mater.* **1999**, *11*, 449–452.
- [4] a) C. A. Mirkin, R. L. Lesinger, R. C. Mucic, J. J. Storhoff, *Nature* **1996**, *382*, 607–609; b) P. Alivisatos, K. P. Johnsson, X. Peng, T. E. Wilson, C. J. Loweth, M. Bruchez, P. G. Schultz, *Nature* **1996**, *382*, 609–612; c) E. Dujardin, L.-B. Hsin, C. R. C. Wang, S. Mann, *Chem. Commun.* **2001**, 1264–1265; d) A. N. Shipway, I. Willner, *Chem. Commun.* **2001**, 2035–2045.
- [5] A. K. Boal, T. H. Galow, F. Alhan, V. M. Rotello, *Adv. Funct. Mater.* **2001**, *11*, 461–465.
- [6] a) Y. A. Vlasov, N. Yao, D. J. Morris, *Adv. Mater.* **1999**, *11*, 165–169; b) B. T. Holland, C. F. Blanford, T. Do, A. Stein, *Chem. Mater.* **1999**, *11*, 795–805; c) G. Subramania, V. N. Manoharan, J. D. Thorne, D. J. Pine, *Adv. Mater.* **1999**, *11*, 1261–1265; d) F. Fleischhaker, A. C. Arsenault, Z. Wang, V. Kitaev, F. C. Peiris, G. von Freymann, I. Manners, R. Zentel, G. Ozin, *Adv. Mater.* **2005**, *17*, 2455–2458.
- [7] a) F. Carn, F. A. Colin, M. F. Achrad, H. Deleuze, Z. Saadi, R. Backov, *Adv. Mater.* **2004**, *16*, 140; b) S. Mandal, S. K. Arumugam, S. D. Adyanthaya, R. Pasricha, M. Sastry, *J. Mater. Chem.* **2004**, *14*, 43–47.
- [8] B. zu Pulitz, K. Landfester, H. Fischer, M. Antonietti, *Adv. Mater.* **2001**, *13*, 500–503.
- [9] M. Breulmann, S. A. Davis, S. Mann, H. P. Hentze, M. Antonietti, *Adv. Mater.* **2000**, *12*, 502–507.
- [10] a) M. R. Diehl, S. N. Yaliraki, R. A. Beckman, M. Barahona, J. R. Heath, *Angew. Chem.* **2002**, *114*, 363–366; *Angew. Chem. Int. Ed.* **2002**, *41*, 353–356; b) A. Bachthold, P. Hadley, T. Nakanishi, C. Decker, *Science* **2001**, *294*, 1317–1320; c) Y. Cui, Q. Q. Wie, H. K. Park, C. M. Lieber, *Science* **2001**, *293*, 1289; d) W. U. Huynh, J. J. Dittmer, A. P. Alivisatos, *Science* **2002**, *295*, 2425–2427; e) P. G. Collins, M. S. Arnold, P. Avouris, *Science* **2001**, *292*, 706–708.
- [11] a) B. C. Satishkumar, M. G. Chapline, E. M. Vogl, A. Govindaraj, C. N. R. Rao, *J. Appl. Phys. D* **1996**, *29*, 3173–3176; b) S. Fullam, D. Cottell, H. Rensmo, D. Fitzmaurice, *Adv. Mater.* **2000**, *12*, 1430–1432; c) H. Shoi, M. Shim, S. Bangsaruntip, H. Dai, *J. Am. Chem. Soc.* **2002**, *124*, 9058; d) K. Jiang, A. Eitan, L. S. Schadler, P. M. Ajayan, R. W. Siegel, N. Grobert, M. Mayne, M. Reyes-Reyes, H. Terrones, M. Terrones, *Nano Lett.* **2003**, *3*, 275–278; e) A. V. Ellis, K. Vijayamohan, R. Goswami, N. Chakrapani, L. S. Ramanathan, P. M. Ajayan, G. Ramanath, *Nano Lett.* **2003**, *3*, 279–282.
- [12] a) S. Banerjee, S. S. Wong, *Nano Lett.* **2002**, *2*, 195–199; b) J. M. Haremza, M. A. Hahn, T. D. Krauss, S. Chen, J. Calcines, *Nano Lett.* **2002**, *2*, 1253–1256.
- [13] a) G. Armstrong, A. R. Armstrong, J. Canales, P. G. Bruce, *Chem. Commun.* **2005**, 2454–2456; b) Z. V. Saponjic, N. M. Dimitrijevic, D. M. Tiede, A. J. Goshee, Z. Zuo, L. X. Chen, A. S. Barnard, P. Zapol, L. Curtiss, T. Rajh, *Adv. Mater.* **2005**, *17*, 965–971.
- [14] a) M. E. Spahr, P. Bitterli, R. Nesper, M. Müller, F. Krumeich, H.-U. Nissen, *Angew. Chem.* **1998**, *110*, 1339–1342; *Angew. Chem. Int. Ed.* **1998**, *37*, 1263–1266; b) F. Krumeich, H.-J. Muhr, M. Niederberger, F. Bieri, B. Schnyder, R. Nesper, *J. Am. Chem. Soc.* **1999**, *121*, 8324–8331.
- [15] a) A. Rothschild, G. L. Frey, M. Homyonfer, R. Tenne, M. Rappaport, *Mater. Res. Innovations* **1999**, *3*, 145–149; b) A. Rothschild, J. Sloan, R. Tenne, *J. Am. Chem. Soc.* **2000**, *122*, 5169–5179; c) H. A. Therese, J. Li, U. Kolb, W. Tremel, *Solid State Sci.* **2005**, *7*, 67–72.
- [16] H. Matsui, S. Pan, G. E. Douberly, Jr., *J. Phys. Chem. B* **2001**, *105*, 1683–1686.
- [17] O. Masala, R. Seshadri, *Annu. Rev. Mater. Res.* **2004**, *34*, 41–81.
- [18] a) S. Mann, *Biomineralization*, Oxford University Press, New York, **2001**; b) E. Bäuerlein, *Biomineralization*, Wiley-VCH, Cambridge, **2004**.
- [19] a) M. Field, C. J. Smith, D. D. Awschalom, N. H. Mendelson, E. L. Mayes, S. A. Davis, D. Mann, *Appl. Phys. Lett.* **1998**, *73*, 1739–1741; b) T. Klaus, R. Joerger, E. Olsson, C.-G. Granqvist, *Proc. Natl. Acad. Sci. USA* **1999**, *96*, 13611–13614; c) E. Dujardin, L.-B. Hsin, C. R. C. Wang, S. Mann, *Chem. Commun.* **2001**, 1264–1265; d) R. R. Naik, S. J. Stringer, G. Agarwal, S. E. Jones, M. O. Stone, *Nat. Mater.* **2002**, *1*, 169–172; e) S. S. Shankari, A. Rai, B. Ankamwar, A. Singh, A. Ahmad, M. Sastry, *Nat. Mater.* **2004**, *3*, 482–488; f) S. Senapati, A. Ahmad, M. I. Khan, M. Sastry, R. Kumar, *Small* **2005**, *1*, 517–520.
- [20] a) W. Shenton, T. Doughlas, M. Young, G. Stubbs, S. Mann, *Adv. Mater.* **1999**, *11*, 253–256; b) J. D. Hartgering, E. Beniash, S. I. Stupp, *Science* **2001**, *294*, 1684–1688; c) S.-W. Lee, C. Mao, C. E. Flynn, A. M. Belcher, *Science* **2002**, *296*, 892–895; d) C. Mao, D. J. Solis, B. D. Reiss, S. T. Kottmann, R. Y. Sweeney, A. Hayhurst, G. Georgiou, B. Iverson, A. M. Belcher, *Science* **2004**, *303*, 213–217; e) D. Rautaray, A. Ahmad, M. Sastry, *J. Mater. Chem.* **2004**, *14*, 2333–2340; f) V. Bansal, D. Rautaray, A. Ahmad, M. Sastry, *J. Mater. Chem.* **2004**, *14*, 3303–3305.
- [21] M. N. Tahir, P. Théato, W. E. G. Müller, H. C. Schröder, A. Janshoff, J. Zhang, J. Huth, W. Tremel, *Chem. Commun.* **2004**, 2848–2849.
- [22] M. N. Tahir, P. Théato, W. E. G. Müller, H. C. Schröder, A. Borejko, S. Faiß, A. Janshoff, J. Huth, W. Tremel, *Chem. Commun.* **2005**, 5533–5535.
- [23] a) K. Shimizu, J. N. Cha, G. D. Stucky, D. E. Morse, *Proc. Natl. Acad. Sci. USA* **1998**, *95*, 6234–6238; b) J. N. Cha, K. Shimizu, Y. Zhou, S. C. Christianssen, B. F. Chmelka, G. D. Stucky, D. E. Morse, *Proc. Natl. Acad. Sci. USA* **1999**, *96*, 361–365.
- [24] a) J. N. Cha, K. Shimizu, Y. Zhou, S. C. Christianssen, B. F. Chmelka, G. D. Kisailus, J. H. Choi, J. C. Weaver, W. Yang, G. D. Stucky, D. E. Morse, *Adv. Mater.* **2005**, *17*, 314–318.
- [25] a) M. Niederberger, G. Garnweitner, F. Krumeich, R. Nesper, H. Cölfen, M. Antonietti, *Chem. Mater.* **2004**, *16*, 1202–1208; b) N. M. Dimitrijevic, Z. V. Saponjic, B. M. Rabatic, T. Rajh, *J. Am. Chem. Soc.* **2005**, *127*, 1344–1345.
- [26] M. Nawaz Tahir, M. Eberhardt, P. Theato, S. Faiß, A. Janshoff, T. Gorelik, U. Kolb, W. Tremel, *Angew. Chem.* **2006**, *118*, 922–926; *Angew. Chem. Int. Ed.* **2006**, *45*, 908–912.



- [27] a) J. L. Dalsin, L. Lin, S. Tosatti, J. Vörös, M. Textor, P. B. Messersmith, *Langmuir* **2005**, *21*, 640–646; b) M. Mammen, S.-H. Gu, Z. Yang, J. Gao, C. K. Choi, G. M. Whitesides, *Angew. Chem.* **1998**, *110*, 2908–2953; *Angew. Chem. Int. Ed.* **1998**, *37*, 2754–2794.
- [28] a) I. Potavova, R. Mruk, S. Prehl, R. Zentel, T. Basche, A. Mews, *J. Am. Chem. Soc.* **2003**, *125*, 320–321; b) M. Eberhardt, R. Mruk, P. Theato, R. Zentel, *Eur. Polym. J.* **2005**, *41*, 1569–1575.
- [29] a) G. B. Sigal, C. Bamdad, A. Barberis, J. Strominger, G. M. Whitesides, *Anal. Chem.*, 1996, **68**, 490–497; b) I. T. Dorn, K. R. Neumaier, R. Tampe, *J. Am. Chem. Soc.* **1998**, *120*, 2753–2763.
- [30] T. Rajh, L. X. Chen, K. Lukas, T. Liu, M. C. Thurnauer, D. M. Tiede, *J. Phys. Chem. B* **2002**, *106*, 10543–10552.
- [31] W. E. G. Müller, M. Rothenberger, A. Borejko, W. Tremel, A. Reiber, H. C. Schröder, *Cell Tissue Res.* **2005**, *321*, 285–297.
- [32] A. Pisera, *Microsc. Res. Tech.* **2003**, *62*, 312–326.
- [33] a) *Electron Transfer in Biology and the Solid State* (Eds.: M. K. Johnson, R. B. King, D. M. Kurtz, C. Kutal, M. L. Norton, R. A. Scott), *Adv. Chem. Ser.* 226, American Chemical Society, Washington, **1990**.
- [34] a) A. Ahmad, S. Senapati, M. I. Khan, R. Kumar, M. Sastry, *Langmuir* **2003**, *19*, 3550–3553; b) Y. Sun, Y. Xia, *Science* **2002**, *298*, 2176–2179; c) Y. Sun, B. Mayers, Y. Xia, *Nano Lett.* **2003**, *3*, 675–679; d) S. Chen, D. L. Carroll, *Nano Lett.* **2002**, *2*, 1003–1007; e) R. Jin, Y. W. Cao, C. A. Mirkin, K. L. Kelly, G. C. Schatz, J. G. Zheng, *Science* **2001**, *294*, 1901–1903; f) R. Jin, Y. C. Cao, E. Hao, G. S. Metraux, G. C. Schatz, C. A. Mirkin, *Nature* **2003**, *425*, 487–490.
- [35] N. Kröger, R. Deutzmann, M. Sumper, *Science* **1999**, *286*, 1129–1132.
- [36] S. Brown, M. Sarikaya, E. A. Johnson, *J. Mol. Biol.* **2000**, *299*, 725–735.
- [37] R. Djalali, Y.-F. Chen, H. Matsui, *J. Am. Chem. Soc.* **2002**, *124*, 13660–13661.
- [38] H. W. Gu, P.-L. Ho, K. W. Tsang, L. Wang, B. Xu, *J. Am. Chem. Soc.* **2003**, *125*, 15702–15703.
- [39] W. E. G. Müller, A. Krasko, G. Le Pennec, R. Steffen, M. S. A. Ammar, M. Wiens, I. M. Müller, H. C. Schröder, *Prog. Mol. Subcell. Biol.* **2003**, *33*, 195.
- [40] A. R. Armstrong, G. Armstrong, J. Canales, P. G. Bruce, *Angew. Chem.* **2004**, *116*, 2336–2338; *Angew. Chem. Int. Ed.* **2004**, *43*, 2286–2288.



DOI: 10.1002/anie.200504211

# Overcoming the Insolubility of Molybdenum Disulfide Nanoparticles through a High Degree of Sidewall Functionalization Using Polymeric Chelating Ligands\*\*

Muhammad Nawaz Tahir, Nicole Zink,  
Marc Eberhardt, Helen A. Therese, Ute Kolb,  
Patrick Theato, and Wolfgang Tremel\*

*Dedicated to Professor H. Schmöckel  
on the occasion of his 65th birthday*

The covalent attachment of functional ligands such as photo- or redox-active molecular compounds to inorganic nanoparticle surfaces is an important first step in the design of new materials. These applications, however, usually require designated molecules to be immobilized on the nanoparticle. A wide variety of chemical linkages to the molecular surface have been devised for oxide surfaces by utilizing siloxane,<sup>[1]</sup> carboxylic acid,<sup>[2]</sup> acetyl acetate,<sup>[3]</sup> phosphonate,<sup>[4]</sup> and catecholate functional groups.<sup>[5]</sup> Carbon nanotubes, which are chemically inert, can be surface-activated by oxidative treatment with anchor groups such as hydroxy (-OH), carboxy (-COOH), or carbonyl (>C=O),<sup>[6]</sup> which are necessary to tether metal ions to the tube. Besides metal oxides and carbon nanotubes,<sup>[7]</sup> metal chalcogenide nanoparticles<sup>[8]</sup> and nanotubes,<sup>[9]</sup> firstly reported by Tenne and co-workers in 1992, have opened up an exciting new area of research into nanomaterials with sheet structures, which—unlike single-layer graphite—are multiple layer structures. These MQ<sub>2</sub> (Q = S, Se, Te) species, termed inorganic fullerenes and inorganic nanotubes, are akin to carbon nanotubes in that they exhibit analogous mechanical<sup>[10]</sup> and electronic<sup>[11]</sup> properties. Their excellent lubrication properties<sup>[12]</sup> can be explained on the basis of their crystal structures, which are characterized by weak van der Waals forces between the individual MQ<sub>2</sub> slabs which contain metal atoms sandwiched between two inert chalcogen layers. It is the inertness of the

[\*] Dr. M. N. Tahir, N. Zink, Dr. H. A. Therese, Prof. Dr. W. Tremel  
Institut für Anorganische Chemie und Analytische Chemie  
Johannes Gutenberg-Universität  
Duesbergweg 10–14, 55099 Mainz (Germany)  
Fax: (+49) 6131-392-5605  
E-mail: tremel@mail.uni-mainz.de

M. Eberhardt, Dr. P. Theato  
Institut für Organische Chemie  
Johannes Gutenberg-Universität  
Duesbergweg 10–14, 55099 Mainz (Germany)  
Dr. U. Kolb  
Institut für Physikalische Chemie  
Johannes Gutenberg-Universität  
Welderweg 11, 55099 Mainz (Germany)

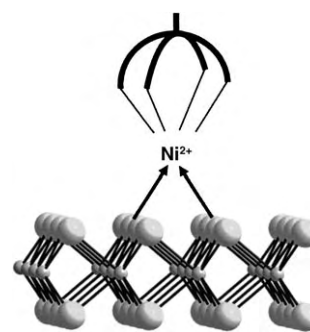
[\*\*] This work was supported by the Deutsche Forschungsgemeinschaft (DFG/SFB 625).

chalcogen surface layer and the associated shielding of the molybdenum atoms from nucleophilic attack by organic ligands which are the main obstacles for the functionalization of MoS<sub>2</sub> nanoparticles.<sup>[13]</sup>

In principle, a functional surface ligand consists of an anchor group that attaches to the nanocrystal, functional group, and a spacer in between. The purpose of the functional group is to render the particles soluble or to provide the proper reactivity when the inorganic fullerenes are to be used as chemical agents, for example, to disperse them in polymers or in oils. For example, aliphatic chains make the particles soluble in nonpolar solvents,<sup>[14]</sup> while deprotonated carboxylic functions will lead to charged particles that are soluble in water.<sup>[15]</sup> Some strategies employed for carbon nanotubes, but unsuccessful for metal chalcogenides, are polymer wrapping<sup>[16]</sup> or coating with surfactants.<sup>[17]</sup> A functionalization of chalcogenide nanoparticles and nanotubes can serve not only to improve their solubility, and therefore, dispersion, but also to create attractive van der Waals interactions between a nanotube and a polymer addend, or transfer the properties of functional ligands to the chalcogenide nanoparticle.

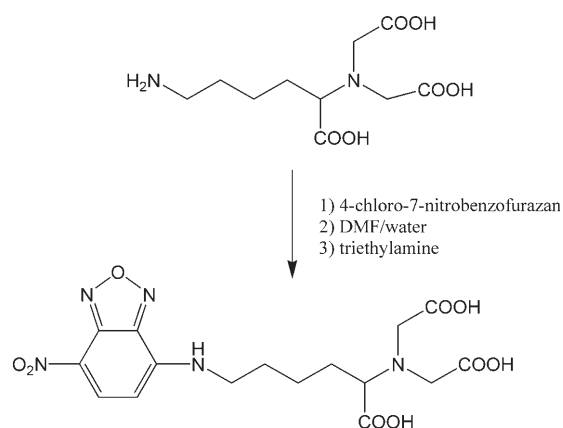
While thiolated organic molecules serve as excellent anchors to link the functional molecules on metallic nanoparticles such as Au, Pt, or Co,<sup>[18,19]</sup> amines and/or thiols are prototypical organic anchor groups for inorganic semiconductors such as CdSe, ZnS, or ZnO which have reasonable affinities to nanoparticle surfaces with vacant metal cation (M<sup>2+</sup>) sites.<sup>[19]</sup> Catechol-type chelating ligands<sup>[19,20]</sup> (for example, dopamine), on the other hand, are robust anchor groups for most early transition metal oxide particles such as TiO<sub>2</sub>,<sup>[21]</sup> ZrO<sub>2</sub>,<sup>[22]</sup> Al<sub>2</sub>O<sub>3</sub>,<sup>[23]</sup> Cr<sub>2</sub>O<sub>3</sub>,<sup>[24]</sup> or Fe<sub>2</sub>O<sub>3</sub>,<sup>[25]</sup> where the catechol group preferentially binds to the edges of the oxide nanocrystals where the surface energy is higher. These general principles of coordination chemistry are not new and have been used extensively for many years in the classic scheme of qualitative inorganic analysis with organic dyes.<sup>[19,20]</sup> The sandwich-type structure of the metal dichalcogenide particles, however, necessitates the use of a different strategy. As the established strategies proved unsuccessful to generate individually functionalized chalcogenide nanoparticles or nanotubes, we have employed functional surface ligands which can serve as linkers between the nanoparticles and an appropriate "metal docking site".

We report herein a facile method for the functionalization of inorganic fullerene/MoS<sub>2</sub> nanoparticles that employs nitrilotriacetic acid (NTA)<sup>[26]</sup> as a robust anchor to immobilize functional molecules on the outer sulfur layer. Since a direct anchoring of organic ligands to the sulfur surface is not possible, a transition-metal cation with a high sulfur affinity and octahedral coordination is used, whose coordination sphere is blocked completely on one side with an umbrella-type chelating ligand,<sup>[27]</sup> while the other part of the coordination sphere remains open for docking to the sulfur layer. Recently we have used a modified tetradentate NTA ligand for the immobilization of proteins to self-assembled monolayers.<sup>[28]</sup> In this approach two vacant coordination sites of the transition-metal ion (Ni<sup>2+</sup>) were used for binding to the "histidine tag" of the protein, whereas in the present case they bind to the sulfur layer of the inorganic fullerene/MoS<sub>2</sub>



nanoparticles. The resulting functionalized inorganic fullerene/MoS<sub>2</sub> particles can be dispersed in water and organic solvents, and they were characterized by high-resolution transmission electron microscopy (HRTEM), thermogravimetric analysis (TGA), FTIR and UV/Vis spectroscopy, and confocal laser scanning microscopy (CLSM).

The inorganic fullerene/MoS<sub>2</sub> particles were prepared as described previously by a metal organic chemical vapor deposition (MOCVD) method.<sup>[29]</sup> Surface functionalization was achieved using an NTA ligand functionalized with a fluorescent 7-nitrobenzofurazan unit (Scheme 1) and using a



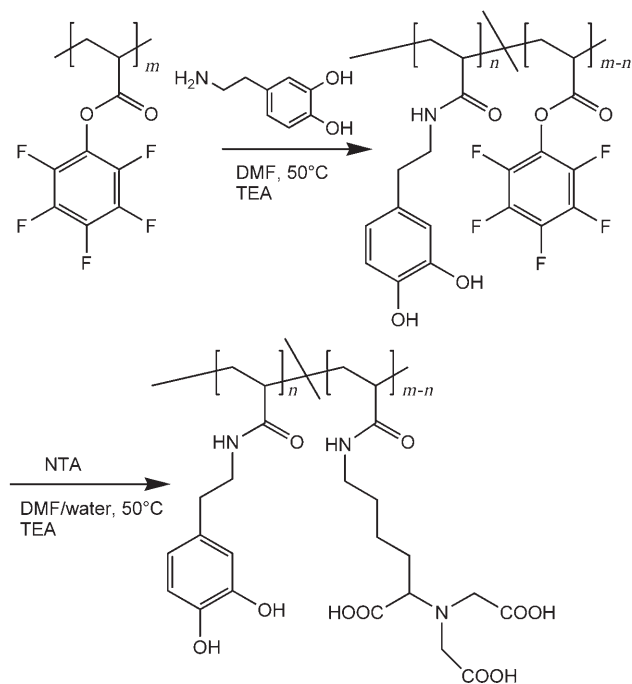
**Scheme 1.** Synthesis of the fluorescent ligand containing nitrilotriacetic acid (NTA) for binding to the MoS<sub>2</sub> surface.

polymeric ligand carrying an NTA group and a catechol type of ligand, which has been used as the anchor groups for the functionalization of metal oxides.<sup>[21]</sup> The architecture of the polymeric ligand is of special importance, because it provides the basis of a toolbox to construct supramolecular assemblies of organic–inorganic hybrid nanomaterials.

The multifunctional polymers that are necessary to realize such systems can be prepared by a flexible synthetic route starting from reactive precursor polymers. Active ester polyacrylates can be used as such reactive precursor polymers. The fact that active ester polymers react quickly and quantitatively with amines to form the corresponding poly(acrylamide)s opens up the possibility to obtain multifunctional polymeric materials.<sup>[30]</sup> Compared to the commonly used poly(*N*-hydroxysuccinimide acrylate)s, active ester polymers based on pentafluorophenyl acrylates exhibit

better solubility and higher reactivity, as described by Eberhardt et al. recently,<sup>[30b]</sup> thus opening up the possibility to work under mild conditions.

Free-radical polymerization of pentafluorophenyl acrylate yielded the polymeric active ester poly(pentafluorophenylacrylate) (PFA) with a molecular weight  $M_n = 29.7 \text{ kg mol}^{-1}$  and  $M_w = 58.5 \text{ kg mol}^{-1}$  (PDI = 1.96). This pre-polymer was then transformed into the multifunctional polymeric ligand by substitution with amino-functionalized molecules (Scheme 2). In the first step, 3-hydroxytyramine



**Scheme 2.** Synthesis of the block copolymer with catechol-type side groups for binding to metal oxides, and umbrella-type nitrilotriacetic acid ligands blocking the side of the coordination sphere of metals bonded to the S atoms of the MoS<sub>2</sub> surface layer, thereby preventing a precipitation of MoS<sub>2</sub> nanoparticles as a result of cross-linking.

(the anchor group for attachment onto TiO<sub>2</sub> nanowires) was covalently bound to the polymer backbone, and in the second step amino-functionalized nitrilotriacetic acid (NTA) was introduced. All the polymer-analogous reactions were carried out in a mixture of water, *N,N*-dimethylformamide (DMF), and triethylamine (TEA) at 50°C.

The resulting polymer exhibits two different features: 1) An NTA linker which can be used to coordinate to Ni<sup>2+</sup> ions which, in turn, can use their vacant coordination sites for binding to the surface S atoms of inorganic fullerene/MoS<sub>2</sub> nanoparticles, and 2) 3-hydroxytyramine as an anchor group for attachment onto the surface of metal oxides. Analysis

of the obtained multifunctional polymer by <sup>1</sup>H NMR and FTIR spectroscopy as well as by GPC showed it had an NTA content of 80 mol %, with the remaining 20 mol % being 3-hydroxytyramine.

A first indication concerning the surface functionalization of inorganic fullerene/MoS<sub>2</sub> and based on the solubility of the functionalized nanoparticles in water and chloroform. Inorganic fullerene/MoS<sub>2</sub> is completely insoluble in water, because of its hydrophobicity, but can be dispersed in nonpolar solvents such as chloroform. After surface functionalization using the polymeric ligand containing NTA/Ni<sup>2+</sup> (for surface binding) and polar (hydroxy, carbonyl) groups, the inorganic fullerene/MoS<sub>2</sub> nanoparticles could be transferred from apolar chloroform to the polar aqueous phase (Figure 1). The dark-brown color of the solution arises from

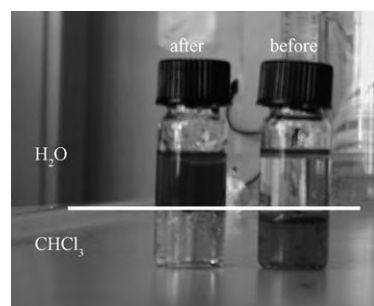


**Figure 1.** Photograph of a solution/dispersion of inorganic fullerene/MoS<sub>2</sub> before (right) and after (left) surface functionalization.

the ligand-to-metal charge-transfer interaction of the inorganic fullerene/MoS<sub>2</sub> nanoparticles and also between the ligand and surface-bound metal Ni<sup>2+</sup> ions. The solubility properties of the functionalized inorganic fullerene/MoS<sub>2</sub> nanoparticles are mainly determined by the functional groups on the surface ligand.

Figure 2a shows the HRTEM image of a large functionalized MoS<sub>2</sub> particle with a diameter of approximately 70 nm. The energy-dispersive X-ray (EDX) spectrum of the circled area in Figure 2a shows the presence of a significant nickel content, thus validating the surface binding of NTA. Further

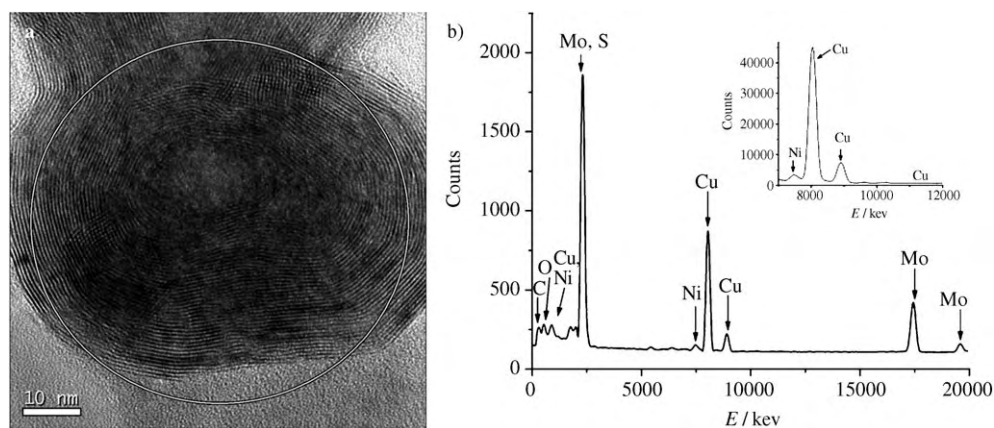


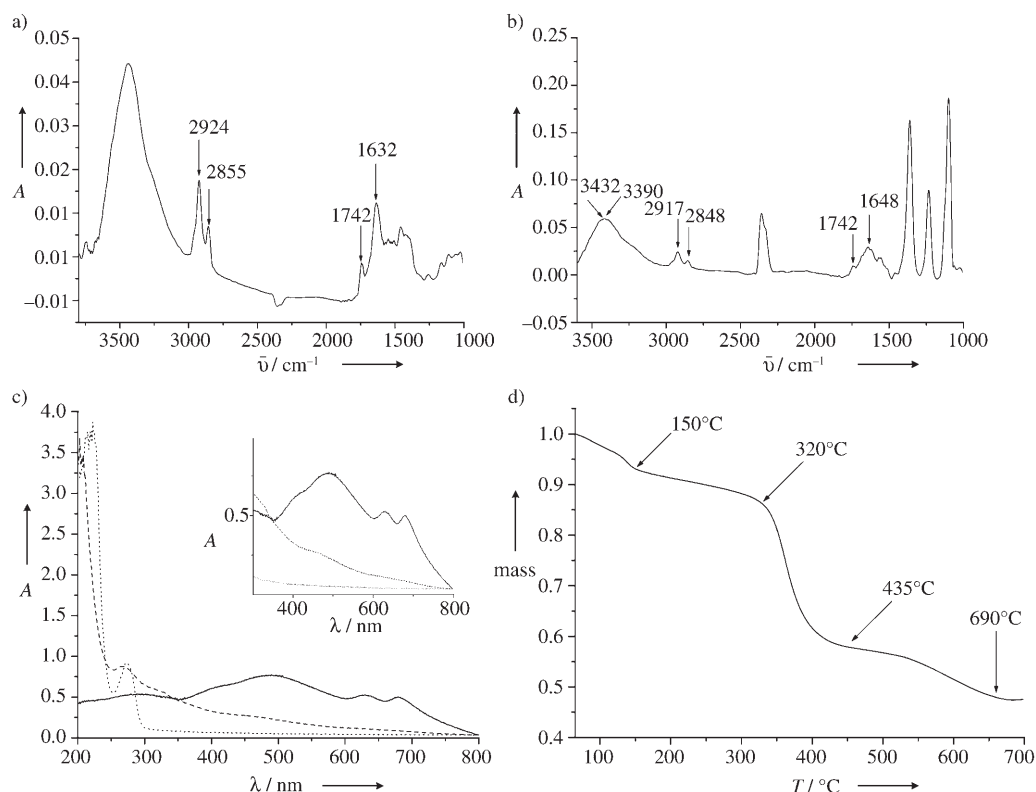
**Figure 2.** a) HRTEM image of a surface-functionalized inorganic fullerene/MoS<sub>2</sub> particle. b) EDX spectrum of the area marked by a circle in (a).

evidence of the sidewall functionalization was obtained by IR spectroscopy (Figure 3a,b) of polymer-functionalized inorganic fullerene/MoS<sub>2</sub> (Figure 3a) and inorganic fullerene/MoS<sub>2</sub> nanoparticles functionalized only with NTA ligands (Figure 3b). The most prominent bands in the 3500–3300 cm<sup>-1</sup> region arise from NH<sub>2</sub> stretching vibrations of the NTA ligand, the bands at 2920 (2917) and 2850 (2848) cm<sup>-1</sup> can be assigned to the stretching vibrations of the CH<sub>2</sub> groups, the absorption band at 1742 cm<sup>-1</sup> to the C=O stretches of the tricarboxylate anchor group, and the adsorption band at approximately 1632 cm<sup>-1</sup> to the aromatic ring of the 3-hydroxytyramine.

The UV/Vis spectrum of the functionalized MoS<sub>2</sub> particles (through catechol side groups attached to the polymer backbone) in water (Figure 3c) shows the characteristic broad absorption band of inorganic fullerene/MoS<sub>2</sub> at about 495 nm. The band at 280 nm for the polymer itself arises from the catechol side chains, while the strong absorption at 225 nm can be assigned to the C=O groups of the NTA moieties. The band corresponding to the inorganic fullerene/MoS<sub>2</sub> particles at 490 nm is still visible as a shoulder in the MoS<sub>2</sub> composite (inset in Figure 3c); the pronounced blue-shift of the C=O absorption from 225 nm to 205 nm in the inorganic fullerene/MoS<sub>2</sub>/polymer composite indicates the surface binding of the NTA groups through the Ni<sup>2+</sup> ions. A thermogravimetric (TG) analysis was performed to estimate the amount of polymer attached to the inorganic fullerene/MoS<sub>2</sub> surface. The inorganic fullerene/MoS<sub>2</sub>/polymer composite exhibits

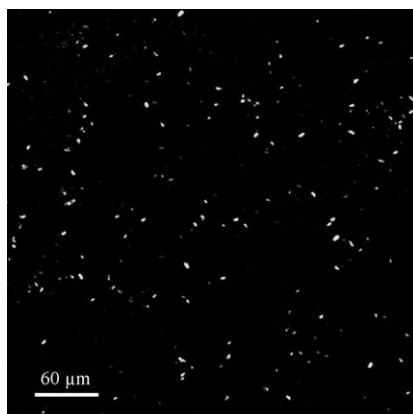
three thermal responses (Figure 3d): The thermal decomposition of the polymer begins at 150°C and is finished after 435°C, while the final step around 650°C may be related to a crystallization of the MoS<sub>2</sub> nanoparticles. The associated weight loss indicates that the amount of the polymeric ligand on the surface of MoS<sub>2</sub> is comparable to that of MoS<sub>2</sub> itself. An inorganic fullerene/MoS<sub>2</sub> particle, which has an average diameter of 30 nm and approximately 20 layers, has a mass of about  $23 \times 10^6$  g per particle, which is 400 times the molar mass of a polymer molecule ( $58.5 \times 10^3$  g mol<sup>-1</sup>). Therefore, each MoS<sub>2</sub> particle is covered by about 400 polymer molecules. We can assume that most of the NTA anchor groups are attached to the surface. From the approximate surface area of 5000 nm<sup>2</sup> for an inorganic fullerene/MoS<sub>2</sub> particle, we derive a surface area of approximately 13 nm<sup>2</sup> for a polymer molecule, if full surface coverage is assumed. For a polymer with about 250 monomer units, which carry an 80% NTA content, the surface volume covered by a single monomer unit can be estimated to be 6.5 Å<sup>2</sup>. However, as the polymer is not likely to be wrapped smoothly around the surface, a somewhat lower coverage may be possible. In summary, the small surface area value obtained for a single monomer unit indicates a full surface coverage by the polymer.

Figure 4 shows the confocal laser scanning microscopy (CLSM) image of inorganic fullerene/MoS<sub>2</sub> nanoparticles after surface-functionalization with a benzofurazene derivative (NBD, see Scheme 1) of NTA exhibiting strong fluores-



**Figure 3.** a) FTIR spectrum of polymer-functionalized inorganic fullerene/MoS<sub>2</sub> nanoparticles. b) FTIR spectrum of NTA-functionalized inorganic fullerene/MoS<sub>2</sub> nanoparticles. c) UV/Vis absorption spectrum of an inorganic fullerene/MoS<sub>2</sub> dispersion (solid line), the polymer (dotted line), and the functionalized inorganic fullerene/MoS<sub>2</sub> nanoparticles (dashed line). d) Determination of the mass ratio of inorganic fullerene/MoS<sub>2</sub> polymer by thermogravimetry.





**Figure 4.** Fluorescence spectrum of inorganic fullerene/MoS<sub>2</sub> nanoparticles coated with an NBD fluorophore coupled to the NH<sub>2</sub> group of the NTA ligand. MoS<sub>2</sub> nanoparticles coated with NTA-NBD were excited at 488 nm.

cence when bound to primary or secondary amines. A 10  $\mu\text{L}$  droplet of the sample was placed and dispersed carefully on a thin glass slide and the solvent was evaporated. The NBD dyes were excited at 488 nm and the fluorescence detected between 504 and 514 nm. A 40 $\times$  (NA 1.25) oil immersion objective was used for the imaging. It is reasonable to conclude from the fluorescence images that the nanoparticles are fully coated by NTA ligands covalently bound to the inorganic fullerene/MoS<sub>2</sub> particle surface. It is, however, difficult to comment on the actual size of the functionalized nanoparticles because they are beyond the resolution limits of CLSM.

It is unclear so far as to whether the Ni<sup>2+</sup>/NTA units are bound to the close-packed sulfur surface layer of the MoS<sub>2</sub> nanocrystals or to defects present on the surface. The chemical reactivity of MoS<sub>2</sub> is associated with the edges of the sandwich layer, with the basal planes being less reactive. Therefore, the edges form the sites where gases adsorb on MoS<sub>2</sub> in hydro-desulfurization catalysis,<sup>[31]</sup> and it seems logical to expect that the edges (because of their higher surface energy) are the seat of surface binding as well. Similarly, catechol is known to bind preferentially to the edges of the TiO<sub>2</sub> nanocrystals (which have a higher surface energy).<sup>[32]</sup> However, full surface coverage, protection, and concomitant functionalization may be envisioned using the novel copolymer ligand containing a large number of NTA anchor groups covalently linked to the polymer backbone, thus forming a sheath around the nanoparticles—partly by surface-bound anchor groups and partly by steric shielding through the polymer ligand.

A final clue concerning the surface functionalization of inorganic fullerene/MoS<sub>2</sub> is based on the decoration of TiO<sub>2</sub> nanorods with inorganic fullerene/MoS<sub>2</sub> particles using the catechol groups to bind to the TiO<sub>2</sub> nanorods. In the first reaction step both the polymer ligand immobilized on the inorganic fullerene/MoS<sub>2</sub> nanoparticles and free catecholate groups were used to bind to undercoordinated surface sites of the TiO<sub>2</sub> nanorods. Figure 5 shows TEM images of a TiO<sub>2</sub> nanorod with several inorganic fullerene/MoS<sub>2</sub> particles attached; no unbound inorganic fullerene/MoS<sub>2</sub> particles

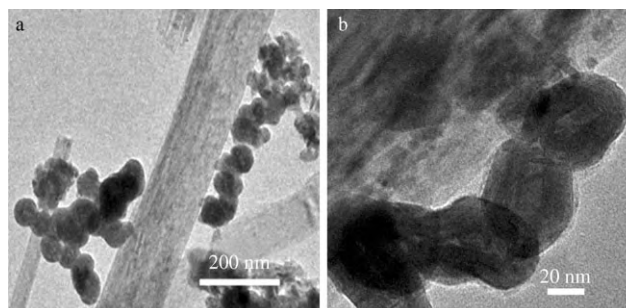


**Figure 5.** a) TEM image of inorganic fullerene/MoS<sub>2</sub> particles immobilized on a TiO<sub>2</sub> nanorod by functionalization of the surface wall. b) Magnified image of the rectangle marked in (a).

were detectable in the sample. Without the presence of reactive ligands, the wetting properties of TiO<sub>2</sub> and MoS<sub>2</sub> would preclude an aggregation of the hydrophobic MoS<sub>2</sub> particles on the hydrophilic TiO<sub>2</sub> surfaces. We note the aggregation behavior of inorganic fullerene/MoS<sub>2</sub> particles at the TiO<sub>2</sub> surface, which may be rationalized by the simultaneous binding of several MoS<sub>2</sub> particles to a single multifunctional polymer ligand (as a consequence of the high NTA content of 80%).

In summary, we have used the principles of coordination chemistry and multidentate ligand design to functionalize highly inert MoS<sub>2</sub> nanoparticles through a high degree of surface binding. For this purpose we have used the tetradentate NTA ligand which was coupled either to a fluorescent ligand for detection purposes or to a reactive polymer, which simultaneously serves as an anchor to the sulfide (through the NTA groups) and the oxide surfaces (through the catecholate groups) of inorganic fullerene/MoS<sub>2</sub> and TiO<sub>2</sub>. We believe that this functionalization protocol can be generalized for various layered chalcogenide nanoparticles.

The functionalization of fullerene-type chalcogenide nanoparticles allows access to several fields which have been pursued actively during the past few years for the related carbon nanotubes and various oxide materials: 1) the functionalization of chalcogenide nanotubes for the attachment of electronically active components (metal and semiconductor nanoparticles, light-harvesting ligands for solar-cell applications) to the sidewalls of the tubes; 2) dispersion of nanotubes, for example, for the integration in composites, which is of interest because of their exceptional mechanical properties; and 3) fabrication of thin films by surface-binding of chalcogenide particles to oxide surfaces, which might allow their use as lubricants on seemingly incompatible ceramic materials.

## Experimental Section

**Synthesis:** Inorganic fullerene/MoS<sub>2</sub> nanoparticles were synthesized according to the method recently reported by us.<sup>[29]</sup> The active ester polymer PFA was prepared by free-radical polymerization as reported earlier.<sup>[30b]</sup> The obtained polymer had a molecular weight of  $M_n = 29.7 \text{ kg mol}^{-1}$ ;  $M_w = 58.5 \text{ kg mol}^{-1}$ , where the number of repeating units (246) is based on the  $M_w$  value. These data were obtained by gel-permeation chromatography (GPC) analysis in THF (light-scattering detection). The functional polymeric ligand was

synthesized by stirring a mixture of PFA (110 mg, 0.46 mmol repeating units) in dry DMF (3 mL) and 3-hydroxytyramine hydrochloride (10.5 mg, 0.055 mmol) in DMF (1.5 mL) and triethylamine (0.1 mL) at 50 °C for 1 h. A solution of amino-functionalized NTA (120 mg, 0.46 mmol) in MilliQ water (0.9 mL) and triethylamine (2.1 mL) were introduced and the resulting mixture heated at 50 °C for an additional 6 h. NTA was added in a slight excess to ensure complete quenching of the polymeric active ester groups. DMF was removed and the obtained polymeric product cleaned by dialysis in MilliQ water. Finally the ligand was isolated and dried in a vacuum oven at 40 °C for 1 h and afforded 64 mg of a white polymeric powder.

<sup>1</sup>H NMR ([D<sub>6</sub>]DMSO):  $\delta$  = 7.50–6.50 ppm (3H, brm), 6.50–4.00 ppm (1H, brs), 3.96–3.19 (5H, brm), 3.17–2.66 (5H, brs), 1.87–0.34 ppm (8H, brm); <sup>19</sup>F NMR ([D<sub>6</sub>]DMSO): no signals found; FTIR (ATR mode): 3200–2400 cm<sup>-1</sup>: COOH (NTA), 3045 cm<sup>-1</sup>: arom. C–H (dopamine); 1639 cm<sup>-1</sup>: N–H (1° amide), 1199 cm<sup>-1</sup>: C–N (1° amide).

For the functionalization, inorganic fullerene/MoS<sub>2</sub> nanoparticles (3 mg) were dispersed in ethanol (2 mL) and sonicated for 15 min. In a separate vial, polymer ligand (20 mg) or lysine nitriloacetic acid (NTA; 20 mg) was dissolved in H<sub>2</sub>O (10 mL) and then 0.01 M NaOH (2 mL) and a 40 mmol aqueous solution of NiSO<sub>4</sub> (2 mL) added. Both the suspension and solution were mixed under inert conditions and stirred at 60 °C for 4 h. The polymer-functionalized inorganic fullerene/MoS<sub>2</sub> particles were isolated and purified by repeated washing with H<sub>2</sub>O, using centrifugation to remove the unbound polymer and water-soluble salt. To immobilize the inorganic fullerene/MoS<sub>2</sub> onto TiO<sub>2</sub> nanowires, a solution of inorganic fullerene/MoS<sub>2</sub> functionalized with polymer ligands in H<sub>2</sub>O (1 mL) were mixed under inert conditions in a glove box with presuspended TiO<sub>2</sub> nanorods (1 mg mL<sup>-1</sup>) in H<sub>2</sub>O. The TiO<sub>2</sub> nanowires coated with functionalized inorganic fullerene/MoS<sub>2</sub> nanoparticles were then centrifuged and dried under vacuum. The product was used as such for characterization.

Instrumental analyses: The products obtained after functionalization and binding onto nanowires were analyzed by IR and UV/Vis spectroscopy as well as CLSM and HRTEM. The morphology of the MoS<sub>2</sub> nanoparticles and onions was characterized by high-resolution transmission electron microscopy (FEI Tecnai F30 ST operated at an extraction voltage of 300 kV, equipped with an energy-dispersive X-ray spectrometer) and by selected area electron-diffraction techniques (SAED). For TEM studies, carbon-film-coated copper grids containing a drop of a suspension of the sample in ethanol was used. A laser scanning microscope (Leica TCS SL, Leica Microsystems, Bensheim, Germany) with inverted laser was used for recording fluorescence images. UV/Vis absorption spectra were recorded on an Omega-10 spectrometer (Bruins Instruments).

Received: November 25, 2005

Published online: June 23, 2006

Delayed at author's request

**Keywords:** chalcogens · fullerenes · nanocomposites · nanotubes · surface chemistry

- [1] a) P. Ghosh, T. G. Spiro, *J. Am. Chem. Soc.* **1980**, *102*, 5543–5549; b) D. C. Bookbinder, M. S. Wrighton, *J. Electrochem. Soc.* **1983**, *130*, 1080–1086; c) W. E. Ford, M. A. Rodgers, *J. Phys. Chem.* **1988**, *92*, 3822–3841.
- [2] S. Anderson, E. C. Constable, M.-P. Dare-Edwards, J. B. Goodenough, K. R. Seddon, R. D. Wright, *Nature* **1979**, *280*, 571–573.
- [3] T. A. Heimer, S. T. Darcangelis, F. Farzad, J. M. Stipkala, G. J. Meyer, *Inorg. Chem.* **1996**, *35*, 5319–5324.
- [4] a) P. Pechy, F. P. Rotzinger, M. K. Nazeeruddin, O. Kohle, S. M. Zakeeruddin, R. Humphry-Baker, M. Grätzel, *J. Chem. Soc. Chem. Commun.* **1995**, 65–66; b) G. Alberti, F. Marmottini, S. Murcia-Mascaros, R. Vivani, *Angew. Chem.* **1994**, *106*, 1655–1658; *Angew. Chem. Int. Ed. Engl.* **1994**, *33*, 1594–1597; c) A. Clearfield, C. Y. Ortiz-Avila, *ACS Symp. Ser.* **1992**, *499*, 178–193; d) M. Nagtegaal, J. K  t  her, J. Ensling, P. G  tlich, W. Tremel, *J. Mater. Chem.* **1999**, *9*, 1115–1120.
- [5] a) T. E. Wolff, J. M. Berg, R. H. Holm, *Inorg. Chem.* **1981**, *20*, 174–180; b) C. Bianchini, D. Masi, C. Mealli, A. Meli, G. Martini, F. Laschi, P. Zanello, *Inorg. Chem.* **1987**, *26*, 3683–3693.
- [6] Y. Li, C. Xu, B. Wei, X. Zhang, M. Zheng, D. Wu, P. M. Ajayan, *Chem. Mater.* **2002**, *14*, 483–485.
- [7] S. Iijima, *Nature* **1991**, *354*, 56–58.
- [8] R. Tenne, L. Margulis, M. Genut, G. Hodes, *Nature* **1992**, *360*, 444–446.
- [9] Y. Feldman, E. Wasserman, D. J. Srolovitz, R. Tenne, *Science* **1995**, *267*, 222–225.
- [10] R. Tenne, M. Homyonfer, Y. Feldman, *Chem. Mater.* **1998**, *10*, 3225–3238.
- [11] a) G. Seifert, H. Terrones, M. Terrones, G. Jungnickel, T. Frauenheim, *Phys. Rev. Lett.* **2000**, *85*, 146–149; b) G. Seifert, H. Terrones, M. Terrones, T. Frauenheim, *Solid State Commun.* **2000**, *115*, 635–638.
- [12] a) L. Rapoport, Yu. Bilik, Y. Feldman, M. Homyonfer, S. R. Cohen, R. Tenne, *Nature* **1997**, *387*, 791–793; b) M. Chhowalla, G. A. J. Amaratunga, *Nature* **2000**, *407*, 164–167.
- [13] In a recent paper, Coleman and co-workers (V. Nicolosi, D. Vrbancic, A. Mrzel, J. McCauley, S. O'Flaherty, C. McGuinness, G. Compagnini, D. Mihailovic, W. J. Blau, J. N. Coleman, *J. Phys. Chem. B* **2005**, *109*, 7124–7133) described the solubilization of Mo<sub>6</sub>S<sub>4.5</sub>I<sub>4.5</sub> nanowires in common solvents. The structure of Mo<sub>6</sub>S<sub>4.5</sub>I<sub>4.5</sub> nanowire does not seem comparable to that of inorganic fullerene/MoS<sub>2</sub> nanoparticles. Moreover, the presence of iodine (a good leaving group for nucleophilic substitutions) makes the system much more reactive and enhances its surface polarity, as a result Mo<sub>6</sub>S<sub>4.5</sub>I<sub>4.5</sub> is soluble in common solvents such as propanol. It is well known that the halide ligands in various metal chalcogenide halides can be substituted by inorganic and organic ligands (S. C. Lee, R. H. Holm, *Angew. Chem.* **1990**, *102*, 868–885; *Angew. Chem. Int. Ed. Engl.* **1990**, *29*, 840–856; G. Pilet, S. Cordier, S. Golden, C. Perrin, L. Ouahab, A. Perrin, *Solid State Sci.* **2003**, *5*, 1263–1270; D. Mery, C. Ornelas, M.-C. Daniel, J. Ruiz, J. Rodrigues, D. Astruc, S. Cordier, K. Kira, C. Perrin, *C. R. Chim.* **2006**, in press), and it is for that reason, that these compounds are generally moisture-sensitive.
- [14] C. B. Murray, D. J. Morris, M. G. Bawendi, *J. Am. Chem. Soc.* **1993**, *115*, 8706–8715.
- [15] W. C. H. Chan, S. Nie, *Science* **1998**, *281*, 2016–2019.
- [16] M. J. O'Connell, P. Boul, L. M. Ericson, C. B. Huffman, Y. H. Wang, E. Haroz, C. Kuper, J. M. Tour, K. D. Ausman, R. E. Smalley, *Chem. Phys. Lett.* **2001**, *342*, 265–271.
- [17] M. J. O'Connell, S. M. Bachilo, C. B. Huffman, V. C. Moore, M. S. Strano, E. H. Haroz, K. L. Rialon, P. J. Boul, W. H. Noon, C. Kittrell, J. Ma, R. H. Hauge, R. B. Weisman, R. E. Smalley, *Science* **2002**, *297*, 593–596.
- [18] M. Brust, M. Walker, D. Bethell, D. J. Schiffrin, R. Whyman, *Chem. Commun.* **1994**, 801–802.
- [19] G. Jander, E. Blasius, *Lehrbuch der analytischen und pr  parativen anorganischen Chemie*, Hirzel, Stuttgart, **1970**.
- [20] G. Ebner, D. Schelz, *Textilf  rberei und Farbstoffe*, Springer, Berlin, **1988**.
- [21] a) N. T. Lucas, J. M. Hook, A. M. McDonagh, S. B. Colbran, *Eur. J. Inorg. Chem.* **2005**, 496–503; b) C. R. Rice, M. D. Ward, M. K. Nazeeruddin, M. Gr  tzel, *New J. Chem.* **2000**, *24*, 651–652; c) M. N. Tahir, M. Eberhardt, P. Theato, S. Fai  , A. Janshoff, T. Gorelik, U. Kolb, W. Tremel, *Angew. Chem.* **2006**, *118*, 922–926; *Angew. Chem. Int. Ed.* **2006**, *45*, 908–912.
- [22] C. V. McNeff, Y. Bingwen, S. Dwight, US Pat. US 2005023613.

- [23] a) R. Laucournet, C. Pagnoux, T. Chartier, J. F. Baumard, *J. Eur. Ceram. Soc.* **2001**, *21*, 869–878; b) G. S. Tulevski, Q. Miao, M. Fukuto, R. Abram, B. Ocko, R. Pindak, M. L. Steigerwald, C. R. Kagan, C. Nuckolls, *J. Am. Chem. Soc.* **2004**, *126*, 15048–15050.
- [24] L. Vermeulen, D. De Baets, Eur. Pat. EP657297.
- [25] C. Xu, K. Xu, G. Gu, R. Zheng, H. Liu, X. Zhang, Z. Guo, B. Xu, *J. Am. Chem. Soc.* **2004**, *126*, 9938–9939.
- [26] a) D. Kröger, M. Liley, W. Schiweck, A. Skerra, H. Vogel, *Biosens. Bioelectron.* **1999**, *14*, 155–161; b) G. B. Sigal, C. Bamdad, A. Barberis, J. Strominger, G. M. Whitesides, *Anal. Chem.* **1996**, *68*, 490–497; c) I. T. Dorn, K. R. Neumaier, R. Tampe, *J. Am. Chem. Soc.* **1998**, *120*, 2753–2763; d) S. Hut-schenreiter, L. Neumann, U. Rädler, L. Schmitt, R. Tampe, *ChemBioChem* **2003**, *4*, 1340–1344.
- [27] a) C. Mealli, S. Midollini, L. Sacconi, *Chem. Commun.* **1975**, 765–766; b) C. Bianchini, C. Mealli, A. Orlandini, L. Sacconi, *Inorg. Chem.* **1980**, *19*, 2968–2975; c) R. Alsasser, S. Trofi-menko, A. Looney, G. Parkin, H. Vahrenkamp, *Inorg. Chem.* **1991**, *30*, 4098–4100; d) R. Alsasser, M. Ruf, S. Trofimenko, H. Vahrenkamp, *Chem. Ber.* **1993**, *126*, 703–710; e) M. A. Halcrow, B. Chaudret, S. Trofimenko, *J. Chem. Soc. Chem. Commun.* **1993**, 465–467; f) S. Trofimenko, *Chem. Rev.* **1993**, *93*, 943–980; g) S. Trofimenko, *Scorpionates: The Coordination Chemistry of Polypyrazolylborate Ligands*, Imperial College Press, London, **1999**.
- [28] a) M. N. Tahir, P. Théato, W. E. G. Müller, H. C. Schröder, A. Janshoff, J. Zhang, J. Huth, W. Tremel, *Chem. Commun.* **2004**, 2848–2849; b) M. N. Tahir, P. Théato, W. E. G. Müller, H. C. Schröder, A. Borejko, S. Faiß, A. Janshoff, J. Huth, W. Tremel, *Chem. Commun.* **2005**, 5533–5535.
- [29] J. Etzkorn, H. A. Therese, F. Rocker, N. Zink, U. Kolb, W. Tremel, *Adv. Mater.* **2005**, *17*, 2372–2375.
- [30] a) I. Potavova, R. Mruk, S. Prehl, R. Zentel, T. Basche, A. Mews, *J. Am. Chem. Soc.* **2003**, *125*, 320–321; b) M. Eberhardt, R. Mruk, P. Theato, R. Zentel, *Eur. Polym. J.* **2005**, *41*, 1569–1575.
- [31] K. Suzuki, M. Soma, T. Onishi, K. Tamaru, *J. Electron Spectrosc. Relat. Phenom.* **1981**, *24*, 283–286.
- [32] a) T. Lana-Villareal, A. Rodes, J. M. Perez, R. Gomez, *J. Am. Chem. Soc.* **2005**, *127*, 12601–12611; b) T. Rajh, L. X. Chen, K. Lukas, T. Liu, M. C. Thurnauer, D. M. Tiede, *J. Phys. Chem. B* **2002**, *106*, 10543–10552; c) H. Gu, Z. Yang, J. Gao, C. K. Chang, B. Xu, *J. Am. Chem. Soc.* **2005**, *127*, 34–35.

DOI: 10.1002/anie.200600073

# Biocatalytic Evolution of a Biocatalyst Marker: Towards the Ultrasensitive Detection of Immunocomplexes and DNA Analysis\*\*

Bella Shlyahovsky, Valeri Pavlov, Lubov Kaganovsky, and Itamar Willner\*

The amplification of biorecognition events is a fundamental topic in bioanalytical chemistry. The use of enzyme labels as catalysts that generate numerous readable product molecules as the result of a single recognition event is the basis of the enzyme-labeled immunosorbant assay (ELISA) technology.<sup>[1]</sup> Different enzyme-linked configurations of biosensors have been developed, in which color,<sup>[2]</sup> fluorescence,<sup>[3]</sup> or electroactive products<sup>[4]</sup> are used as readout signals. Also, enzyme labels have been used to catalyze the precipitation of insoluble products on electrode supports, and the resulting interfacial electron-transfer resistance,<sup>[5]</sup> or the microgravimetric changes on piezoelectric quartz-crystal microbalance crystals,<sup>[6]</sup> are used as readout signals of the precipitation processes. Different biosensing schemes that include enzyme labels as amplifying agents have been developed for different biorecognition events such as DNA hybridization,<sup>[7]</sup> antigen–antibody complexes,<sup>[8]</sup> and others.<sup>[9]</sup> Other amplifying labels that have been developed in recent years include nanoparticles,<sup>[10]</sup> beads that act as containers for redox-active units,<sup>[11]</sup> and liposomes.<sup>[12,13]</sup>

Herein, we describe a new concept to amplify biorecognition events based on the catalytic evolution of a biocatalytic label that leads to a readable signal of the biosensing process. Specifically, we applied ecarin (EC) conjugates that catalyze the transformation of prothrombin (PTh) to thrombin (Th).<sup>[14]</sup> The latter product acts as a biocatalyst for the hydrolysis of the nonfluorescent moiety bis(*p*-tosyl-Gly-Pro-Arg)rhodamine110 (**1**) to the fluorescent product **2** (Figure 1A). That is, the surface concentration of the catalytic EC conjugate is low due to the low coverage by the recognition sites of the analyte units. The EC-mediated conversion of PTh into Th evolves the catalyst for the hydrolysis of **1** and leads to the formation of numerous fluorescent molecules of **2**. We applied this amplification method for the detection of antigen–antibody and DNA recognition complexes and demonstrate the use of the analytical procedure for the detection of telomerase in cancer cells.

[\*] B. Shlyahovsky, Dr. V. Pavlov, L. Kaganovsky, Prof. I. Willner  
Institute of Chemistry  
Farkas Center for Light-Induced Processes  
The Hebrew University of Jerusalem  
Jerusalem 91904 (Israel)  
Fax: (+ 972) 2-652-7715  
E-mail: willnea@vms.huji.ac.il

[\*\*] This research was supported in part by the Prostate Cancer Research Foundation (PCRF) and by the Israel Ministry of Science as an Infrastructure Project.



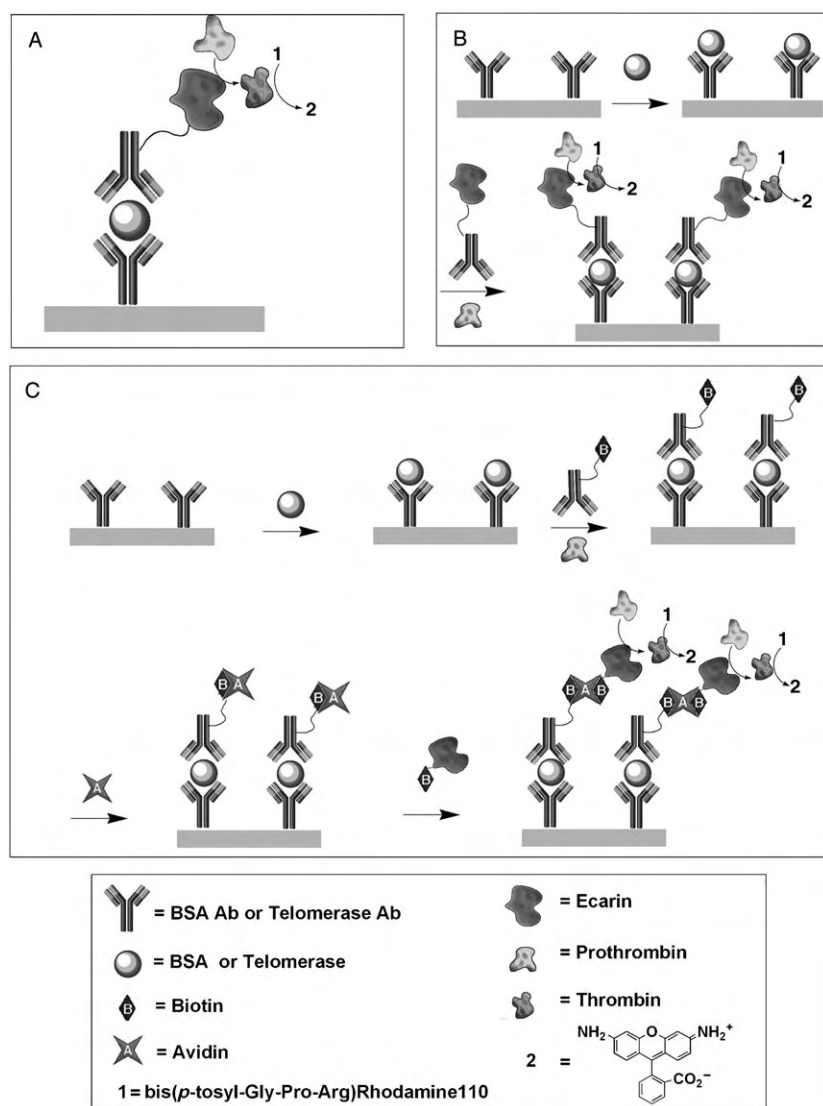


**Figure 1.** Amplified analysis of immunocomplexes by the ecarin-catalyzed evolution of the thrombin biocatalyst. A) Concept for ecarin-stimulated evolution of thrombin and the subsequent hydrolysis of nonfluorescent bis(*p*-tosyl-Gly-Pro-Arg)-R110 (**1**) to the fluorescent product **2** upon analysis of an antigen–antibody complex. B) Analysis of BSA. C) Analysis of telomerase originating from HeLa cancer cells.

Anti-bovine serum albumin (polyclonal BSA Ab) was immobilized on ELISA plates (Figure 1B). The resulting surfaces were blocked to minimize nonspecific adsorption and then interacted with different concentrations of bovine serum albumin (BSA). The rinsed surfaces were then treated with ecarin-labeled BSA Ab, then with PTh, and last with bis(*p*-tosyl-Gly-Pro-Arg)-R110 to yield the fluorescent product **2**.<sup>[15]</sup> Figure 2A shows the integrated fluorescence intensities generated in the solution of a single well upon analyzing different concentrations of the BSA antigen. The antibody was detected with a sensitivity limit that corresponds to  $2 \times 10^{-18}$  M, with a signal-to-background ratio of about 1.8, with respect to the background fluorescence originating from nonspecific adsorption. Figure 2B depicts the extracted calibration curve.

This amplification procedure was applied to detect telomerase, a ribonucleoprotein that catalyzes the elongation of telomere units on chromosomes. The shortening of telomers during the cell life cycle provides an intracellular trigger to terminate cell growth and proliferation.<sup>[16,17]</sup> The appearance of telomerase in malignant or cancer cells leads to the constant elongation of the telomers and to their transformation into immortal cells. Indeed, in over 95% of the different cancerous cells elevated amounts of telomerase were detected, thus providing a general marker for cancer cells.<sup>[18,19]</sup> The detection of telomerase is usually based on the analysis of the enzyme activity that originates from cell extracts. The TRAP test is based on the labeling of the resulting telomers with fluorescent dyes and their electrophoretic analysis.<sup>[20]</sup> Other methods to detect telomerase activity include electrochemiluminescent detection,<sup>[21]</sup> fluorescent analysis of the telomerase-generated telomers on semiconductor nanoparticles,<sup>[22]</sup> or optical detection of the telomerase-synthesized telomers.<sup>[23]</sup>

In contrast to previously reported procedures for the analysis of telomers, the telomerase itself was detected in the present study. The advantages are obvious, as we do not need to rely on the time-consuming telomerization process, the labeling of the telomers, or the secondary separation of the

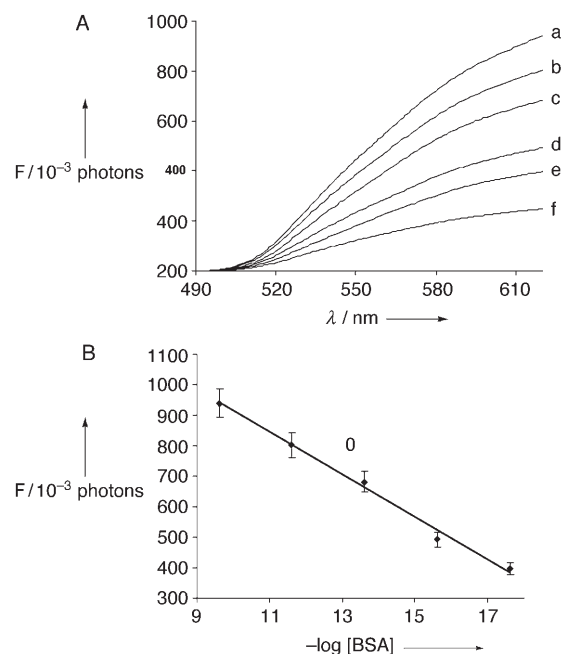


**Figure 2.** A) Integrated light intensities emitted upon the analysis of different concentrations of BSA according to Figure 1B: a)  $2.43 \times 10^{-10}$  M, b)  $2.43 \times 10^{-12}$  M, c)  $2.43 \times 10^{-14}$  M, d)  $2.43 \times 10^{-16}$  M, and e)  $2.43 \times 10^{-18}$  M; f) curve shows a control experiment in which the entire analytical protocol is applied in the absence of BSA (error bars were derived from five independent experiments). B) Calibration curve corresponding to the emitted light intensities at  $\lambda = 620$  nm upon analyzing different concentrations of BSA.

telomers. Figure 1C outlines the method for detecting telomerase. The polyclonal rabbit anti-telomerase antibody was immobilized on the ELISA plate and treated with telomerase that originated from different numbers of HeLa cancer cells. The association of the telomerase was followed by the binding of the biotinylated polyclonal anti-telomerase antibody. Subsequently, the association of avidin and biotinylated ecarin resulted in the biocatalytic structure for the evolution of the thrombin biocatalyst. The latter product biocatalyzes the hydrolysis of **1** to **2**. Figure 3A shows the integrated light intensity emitted upon analyzing the telomerase originating from extracts of different number of HeLa cells. Telomerase originating from 1000 cells can be analyzed.

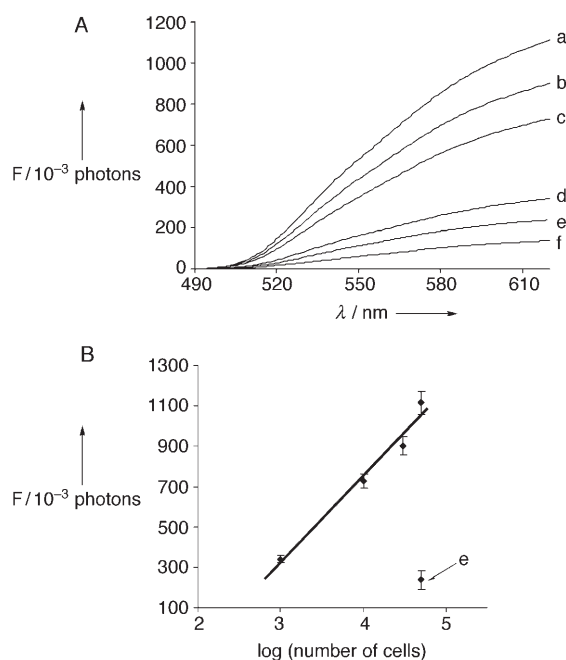


**Figure 3.** A) Integrated light intensities emitted upon the analysis of different numbers of HeLa cancer cells (or control system consisting of normal cells) according to Figure 1C: Curves a–d correspond to the analysis of 50 000, 30 000, 10 000, and 1000 HeLa cells, respectively. Curve e corresponds to the analysis of 50 000 HaCat normal cells. Curve f corresponds to a control experiment in which no HeLa cell extract (or telomerase) is added to the system. B) Calibration curve corresponding to the light intensity emitted by the system at  $\lambda = 620$  nm upon the analysis of telomerase originating from different numbers of HeLa cancer cells. For comparison, the point marked (e) corresponds to the normal HaCat cells.

Figure 3A, curve e, depicts the application of the analyzing protocol on an extract of the cells that does not include telomerase (HaCat, normal skin). The resulting light intensity may be considered as the background level, as a result of nonspecific adsorption of the biocatalytic labels onto the sensing interface. Thus, the telomerase originating from 1000 HeLa cells is detected with a signal-to-background ratio of 2. Figure 3B shows the derived calibration curve. Note that we failed to analyze telomerase activity originating from 1000 HeLa cells by using the commercial TRAP assay.

The amplification of the biorecognition events by the ecarin/prothrombin system was also applied to analyze DNA (Figure 4). The thiolated nucleic acid **4** was assembled on an Au surface and hybridized with the analyzed DNA **3**. The

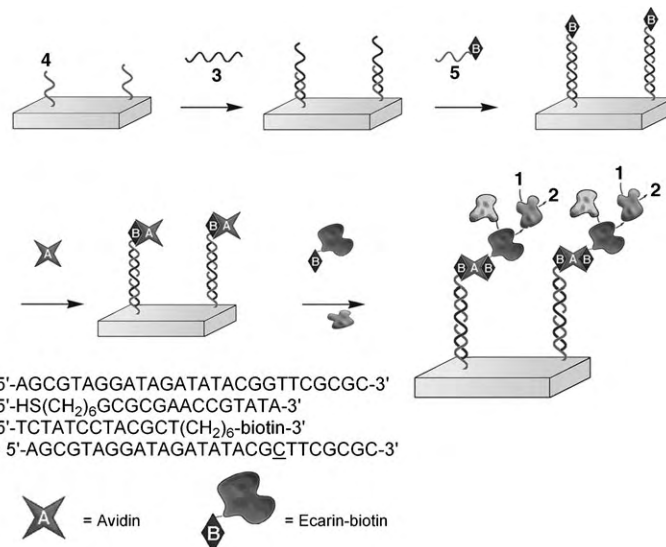


**Figure 4.** Amplified analysis of DNA by the ecarin-catalyzed evolution of the thrombin biocatalyst and generation of the fluorescent product **2**.

surface coverage of **4** was determined by Tarlov's method<sup>[24]</sup> and corresponded to approximately  $5 \times 10^{11}$  DNA strands per cm<sup>2</sup>. The subsequent hybridization of the biotinylated nucleic acid **5**, followed by the association of avidin and biotinylated ecarin, led to the formation of the catalytic label on the gold surface. Figure 5A shows the integrated light intensity emitted by the system upon analyzing different concentrations of DNA. For comparison, curve e in Figure 5A shows the integrated light emitted by the system upon analysis of the nucleic acid **3a**, which includes one base-mismatch relative to **3**. The results indicate that the analyzed DNA **3** can be detected by the method with a sensitivity limit corresponding to  $3 \times 10^{-12}$  M. We also note that the DNA analyzed at a concentration of  $3.4 \times 10^{-8}$  M (Figure 5A, curve a) yields an integrated light intensity that is about threefold higher than the light intensity emitted by the system in which the DNA with one base-mismatch was analyzed at a concentration of  $1 \times 10^{-8}$  M (Figure 5A, curve e). These results imply that the analysis of DNA is selective and that the analyte DNA can be detected with a sensitivity limit of  $3 \times 10^{-12}$  (signal/background > 1.5). Figure 5B shows the derived calibration curve.

To conclude, the present study has introduced the catalytic evolution of a biocatalyst as a new concept to amplify biorecognition events. We employed ecarin and prothrombin as a catalytic evolution system for the generation of thrombin. The advantage of the reported system rests on the fact that the content of the enzyme (thrombin) increases in the system with time, and thus a nonlinear enhancement in the intensities of the evolved fluorescence is observed. Accordingly, by prolonging the time intervals for evolution of the thrombin the sensitivity limits might be further improved. It is difficult to perform a fair comparison of the proposed method with

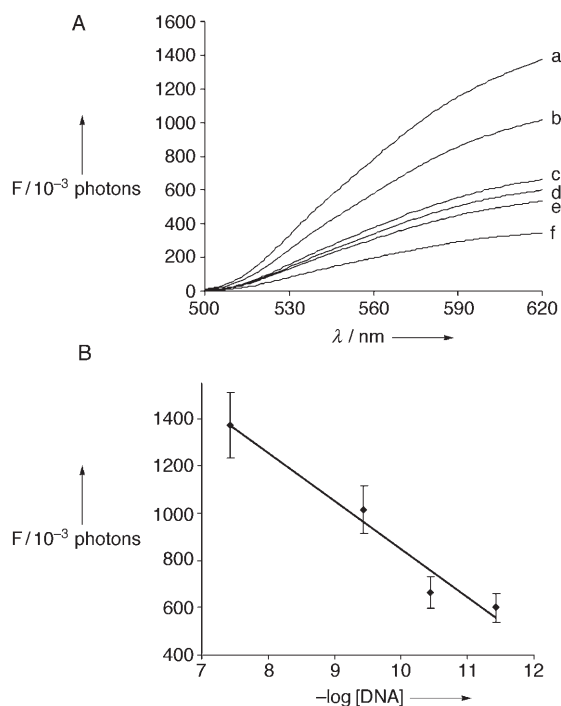


**Figure 5.** A) Integrated light intensities emitted by systems analyzing different concentrations of DNA **3** according to Figure 4. The concentrations of **3** correspond to a)  $3.4 \times 10^{-8}$  M, b)  $3.4 \times 10^{-10}$  M, c)  $3.4 \times 10^{-11}$  M, d)  $3.4 \times 10^{-12}$  M, and f) 0 M; curve e corresponds to the analysis of DNA **3a** with one base mismatch at a concentration of  $1 \times 10^{-8}$  M. B) Calibration curve corresponding to the emitted light intensity at  $\lambda = 620$  nm upon analysis of different concentrations of DNA **3** (error bars were derived from four independent experiments).

available enzyme-amplified bioanalytical procedures because thrombin exhibits a substantially lower specific activity relative to other enzymes (e.g. peroxidase). Nonetheless, we note that for the analysis of BSA we find a  $10^2$ – $10^3$ -fold higher sensitivity in the ecarin–prothrombin system as compared to a system that employed the horseradish peroxidase–BSA Ab conjugate. For the analysis of DNA using biocatalysts as amplifying labels, we note that our system reveals an approximate  $10^2$ -fold enhanced sensitivity as compared to a system that employed the horseradish peroxidase–nucleic acid label.<sup>[25]</sup> Also, our analytical procedure reveals comparable sensitivity to the reported bioelectrocatalytic detection of DNA using the polymerase-induced replication of redox-active DNA replica, which activates the electrocatalytic oxidation of glucose in the presence of glucose oxidase.<sup>[26]</sup> The simple and relatively rapid procedure described here for analyzing DNA is certainly an advantage. We thus anticipate that the method described here will find immense practical applications, as it can be adapted for any biorecognition process, and specifically, for systems that require high sensitivities.

## Experimental Section

**Preparation of ecarin–BSA Ab conjugate:** Rabbit anti-bovine serum albumin IgG (Bethyl Laboratories;  $1.64 \times 10^{-7}$  M) was reduced with 2-mercaptoethylamine ( $1.3 \times 10^{-5}$  M) in 500  $\mu$ L of phosphate buffer

(20 mM, pH 7.4, 0.15 M NaCl) at 37°C for 90 min, and the product was purified using centrifugal filter devices (Centricon, 30000 MWCO, Millipore). Ecarin from *Echis carinatus* venom (55 kDa, Sigma-Aldrich;  $6 \times 10^{-7}$  M) was treated with *N*-(maleimidobutyroxy)sulfo-succinimide ester ( $1.25 \times 10^{-4}$  M) in 450  $\mu$ L of phosphate buffer (20 mM, pH 7.4, 0.15 M NaCl) for 30 min at room temperature and was then purified again using the Centricon filter (30000 MWCO). The resulting functionalized ecarin was reacted with the reduced BSA Ab for 30 min at room temperature.

**Preparation of biotinylated anti-telomerase Ab:** Anti-telomerase Ab (rabbit polyclonal antiserum, Oncogene Research Products) was reduced by a similar procedure as that described above for the reduction of BSA. The product was reacted with biotin-maleimide (Sigma-Aldrich;  $3.3 \times 10^{-4}$  M) in 1 mL of phosphate-buffered saline (PBS; pH 7.2).

**Preparation of biotinylated ecarin:** Ecarin ( $2 \times 10^{-5}$  M) was treated with sulfo-NHS-LC-LC-biotin (Pierce Biotechnology;  $1.5 \times 10^{-5}$  M) in 1000  $\mu$ L of phosphate buffer (20 mM, pH 7.4, 0.15 M NaCl) for 30 min at room temperature.

**Analysis of BSA:** For the analysis of BSA, an ELISA Nunc-Immuno Plate MaxiSorp Surface was treated with polyclonal BSA Ab for 60 min at 37°C. The resulting plates were blocked with PBS solution that included 1 % goat serum. After rinsing, the plates were treated with different concentrations of BSA in borate saline buffer (BSB; pH 8.4) for 90 min at 37°C. The plates were then rinsed and treated with the ecarin–BSA Ab conjugate in BSB (pH 8.4) for 60 min at 37°C. The rinsed plates were then treated with a solution of prothrombin (Sigma-Aldrich;  $1 \times 10^{-8}$  M) in Tris buffer (20 mM, pH 8, 0.1 M NaCl) for 40 min, and then **1** ( $8 \times 10^{-6}$  M) was added during 20 min to allow the hydrolysis to **2**. The fluorescence of the resulting solutions was monitored by using a photon-counting spectrometer (Edinburgh Instruments, FLS 920) connected to a computer (F900 v. 6.3 software).

**Analysis of telomerase:** HeLa cells were cultivated in Dulbecco's Modified Eagle Medium (DMEM) solution that included 2.5 % foetal bovine serum (Biological Industries, Beit Haemek, Israel) during 4 days. Trypsin (3 mL) was added to the resulting suspension (50 mL), and the cells were centrifuged and washed with the DMEM solution. Lysis of the HeLa cells was performed by treatment of a pellet of about  $10^6$  HeLa cells with 200  $\mu$ L CHAPS (3,3-cholamidopropyl-dimethylammonio-1-propanesulfonate) buffer solution for 30 min at 4°C. The resulting suspension was then centrifuged to yield the cell extract. The anti-telomerase Ab was deposited on the ELISA plates and blocked against nonspecific adsorption in a similar manner to that described for BSA Ab. The plates were then treated with solutions containing the extracts of variable numbers of HeLa cells. The resulting rinsed plates were interacted with biotinylated anti-telomerase Ab and then treated with avidin and biotinylated ecarin (the plates were rinsed between the reaction steps). Finally, the resulting plates were treated with prothrombin and **1** as described for the analysis of BSA.

**Analysis of DNA:** For the analysis of DNA, a 100- $\mu$ L drop of solution of thiolated nucleic acid **4** (OD = 0.5) was placed on the plates and allowed to react overnight. Then, the surfaces were blocked with mercaptohexanol (1 mM) during 60 min. The modified plates were then hybridized with different concentrations of **3** in 100  $\mu$ L of phosphate buffer (10 mM, 0.3 M NaCl) for 3 h. The double-stranded assemblies were then hybridized to the biotinylated nucleic acid **5** ( $1 \times 10^{-6}$  M) at room temperature. Subsequently, the surface was treated with avidin and biotinylated ecarin (with rinsing between each of the steps). The resulting surfaces were then treated with prothrombin as described for the analysis of BSA, and the resulting fluorescence was monitored.

Received: January 8, 2006

Revised: February 26, 2006

Published online: June 26, 2006

**Keywords:** antibodies · antigens · DNA · fluorescence · immunochemistry

- 
- [1] J. R. Crowther, *ELISA: Theory and Practice*, Humana, Totowa, NJ, **1995**.
- [2] a) J. Y. Douillard, T. Hoffmann, *Methods Enzymol.* **1983**, 92, 168; b) C. Regalado, B. E. Garcia-Almendarez, M. Duarte-Vazquez, *Phytochem. Rev.* **2004**, 3, 243.
- [3] S. Fujita, M. Momiyama, Y. Kondo, *Anal. Chem.* **1994**, 66, 1347.
- [4] J. Rishpon, I. Rosen, *Biosensors* **1989**, 4, 61.
- [5] a) E. Katz, I. Willner, *Electroanalysis* **2003**, 15, 913; b) Y. J. Ding, H. Wang, G. L. Shen, R. Q. Yu, *Anal. Bioanal. Chem.* **2005**, 382, 1491.
- [6] Y. Weizmann, F. Patolsky, I. Willner, *Analyst* **2001**, 126, 1502.
- [7] F. Patolsky, A. Lichtenstein, M. Kotler, I. Willner, *Angew. Chem.* **2001**, 113, 2321; *Angew. Chem. Int. Ed.* **2001**, 40, 2261.
- [8] L. Alfonta, A. K. Singh, I. Willner, *Anal. Chem.* **2001**, 73, 91.
- [9] L. Alfonta, I. Blumenzweig, M. Zayats, L. Baraz, M. Kotler, I. Willner, *ChemBioChem* **2004**, 5, 949.
- [10] J. Wang, D. Xu, A.-N. Kawde, R. Polsky, *Anal. Chem.* **2001**, 22, 5576.
- [11] J. Wang, R. Polsky, A. Merkoçi, K. L. Turner, *Langmuir* **2003**, 19, 989.
- [12] F. Patolsky, A. Lichtenstein, I. Willner, *Angew. Chem.* **2000**, 112, 970; *Angew. Chem. Int. Ed.* **2000**, 39, 940.
- [13] F. Patolsky, A. Lichtenstein, I. Willner, *J. Am. Chem. Soc.* **2001**, 123, 5194.
- [14] M. F. Doyle, K. G. Mann, *J. Biol. Chem.* **1990**, 265, 10693.
- [15] S. E. Zweig, B. G. Meyer, S. Sharma, C. Min, J. M. Krakower, S. B. Shohet, *Biomed. Instrum. Technol.* **1996**, 30, 245.
- [16] C. B. Harley, B. Villeponteau, *Curr. Opin. Genet. Dev.* **1995**, 5, 249.
- [17] N. D. Hastie, M. Dempster, M. G. Dunlop, A. M. Thompson, D. K. Green, *Nature* **1990**, 346, 866.
- [18] W. E. Wright, M. A. Piatyszek, W. E. Rainey, W. Byrd, J. W. Shay, *Dev. Genet.* **1996**, 18, 173.
- [19] J. W. Shay, S. Bacchetti, *Eur. J. Cancer* **1997**, 33, 787.
- [20] N. W. Kim, M. A. Piatyszek, K. R. Prowse, C. B. Harley, M. D. West, P. L. C. Ho, G. M. Coviello, W. E. Wright, S. L. Weinrich, J. W. Shay, *Science* **1994**, 266, 2011.
- [21] T. Niazov, V. Pavlov, Y. Xiao, R. Gill, I. Willner, *Nano Lett.* **2004**, 4, 1683.
- [22] F. Patolsky, R. Gill, Y. Weizmann, T. Mokari, U. Banin, I. Willner, *J. Am. Chem. Soc.* **2003**, 125, 13918.
- [23] a) P. M. Schmidt, C. Lehmann, E. Matthes, F. F. Bier, *Biosens. Bioelectron.* **2002**, 17, 1081; b) P. M. Schmidt, E. Matthes, F. W. Scheller, M. Bienert, C. Lehmann, A. Ehrlich, F. F. Bier, *Biol. Chem.* **2002**, 383, 1659.
- [24] A. B. Steel, T. M. Herne, M. Tarlov, *Anal. Chem.* **1998**, 70, 4670.
- [25] D. J. Caruana, A. Heller, *J. Am. Chem. Soc.* **1999**, 121, 769.
- [26] F. Patolsky, Y. Weizmann, I. Willner, *J. Am. Chem. Soc.* **2002**, 124, 770.
-



DOI: 10.1002/anie.200600356

**Bioconjugated Ag Nanoparticles and CdTe Nanowires: Metamaterials with Field-Enhanced Light Absorption\*\****Jaebeom Lee, Tanveer Javed, Timur Skeini, Alexander O. Govorov, Garnett W. Bryant, and Nicholas A. Kotov\**

The hybrid assembly of inorganic and metallic nanomaterials by means of chemical and biological bonding to yield manifold optical and electromagnetic properties has received widespread attention.<sup>[2–11]</sup> Currently available highly mono-dispersed nanomaterials such as semiconductors and noble metals that can be conjugated by ligand–receptor, antigen–antibody reactions, polymer tethering, and DNA hybridization are used as building blocks for 2D or 3D superstructures in which new collective properties of these artificial assemblies have been obtained.<sup>[12–15]</sup> They represent a large class of new materials (i.e., metamaterials) in which the properties are determined not only by classical atomic composition, but also by nanoscale organization of structural components. Recently, metamaterials based on metallic composites have received special attention as these are expected to display negative values for permittivity and refractive index. This property should lead to a multitude of unique optical effects.<sup>[11,16,17]</sup> Many of these effects are related to surface plasmons on Au or Ag nanoparticles (NPs), which generate exceptionally high localized electromagnetic fields, and have been exploited in surface-enhanced Raman spectroscopy<sup>[18–21]</sup> and some optoelectronic devices.<sup>[12,22]</sup> Metamaterials from semiconductors and their combinations with metals can also produce optical effects that are useful for development of advanced sensing and imaging technologies.<sup>[23,24]</sup> Recently, we

[\*] Dr. J. Lee, Prof. Dr. N. A. Kotov  
Department of Chemical Engineering  
Department of Materials Science and Engineering and  
Department of Biomedical Engineering  
University of Michigan  
Ann Arbor, MI 48109 (USA)  
Fax: (+1) 734-764-7454  
E-mail: kotov@umich.edu  
T. Javed, T. Skeini, Prof. Dr. A. O. Govorov  
Department of Physics and Astronomy  
Ohio University  
Athens, OH 45701 (USA)  
Dr. G. W. Bryant  
Quantum Processes and Metrology Group  
National Institute of Standards and Technology  
Atomic Physics Division  
100 Bureau Drive, Stop 8423  
Gaithersburg, MD 20899-8423 (USA)

[\*\*] This work was supported in part by NSF Biophotonics and NSF CAREER at UM, and NIST and BNNT initiative at OU.



Supporting information for this article is available on the WWW under <http://www.angewandte.org> or from the author.

observed that the collective plasmon resonance in a specially designed assembly of Au NPs can stimulate radiative recombination of excitons in CdTe NPs and nanowires (NWs). For example, the bioconjugates of Au NPs and CdTe NWs assembled with streptavidin (SA) and D-biotin (B) exhibited fivefold enhancement of luminescence and blue shifts of emission bands. Modeling studies showed that the luminescence enhancement originates from amplification of electromagnetic fields induced by Au NPs in the vicinity of CdTe NWs.<sup>[1,25]</sup> Other experiments with Au and CdTe NPs in which polymer linkers were used to produce a dynamically conjugated system proved that the interaction between surface plasmons and excitons is a substantial factor in the different ratios of luminescence enhancements obtained. This interaction was dynamically modified by the reversible swelling and deswelling of the polymeric spacers inside the assembled nanoscale superstructures.<sup>[26]</sup>

Herein, we report new superstructures based on Ag NPs. Although collective interactions between NPs and NWs in the superstructures are also important for Au NPs, the mechanism for the enhancement of the emission of the Ag-NP conjugates is qualitatively different from that of Au-based NW-NP metamaterials.<sup>[1,25,26]</sup> In the latter, the emission enhancement comes mostly from the increase of the photon emission that is stimulated by resonance with plasmon oscillations in the NP. However, when Au is replaced with Ag, the emission enhancement comes from the increase in absorption. A theoretical model for the experiments describes collective plasmon excitations in the Ag-NP shell and provides an accurate explanation of the optical properties of Ag-based NP-NW superstructures. This paper investigates the mechanisms of interactions between NPs and develops the understanding of such hybrid materials, which could be used for a novel class of sensors and actuators with enhanced optical and thermal properties.<sup>[1,25]</sup>

Morphological characterization of each component of the superstructure was carried out by high-resolution transmission electron microscopy (HRTEM) and atomic force microscopy (AFM). From AFM images, the average diameters of Ag NPs and CdTe NWs were measured to be  $3.11 \pm 1.2$  nm and  $8.09 \pm 2.3$  nm, respectively (see the Supporting Informa-

tion). The NWs were assembled from 3.7-nm CdTe NPs according to a procedure described elsewhere ( $>98\%$  yield).<sup>[27]</sup> The NWs had an average length of  $1400 \pm 128$  nm (with an aspect ratio of 173) and luminesced at  $658 \pm 2$  nm. It is known that bulk Ag film has a (111) lattice spacing of 0.2359 nm. The Ag NPs have a lattice spacing of  $0.235 \pm 0.003$  nm, which corresponds to the spacing between (111) planes of Ag crystals.<sup>[28]</sup> The TEM image showed the Ag NPs attached to the surface or in the vicinity of a CdTe NW to form a fuzzy shell (Figure 1a). There was a noticeable red shift in UV/Vis absorption peak after attachment of proteins to the Ag NPs (Figure 1b, i–ii); this shift correlates very well with the change of dielectric constant.<sup>[29,30]</sup>

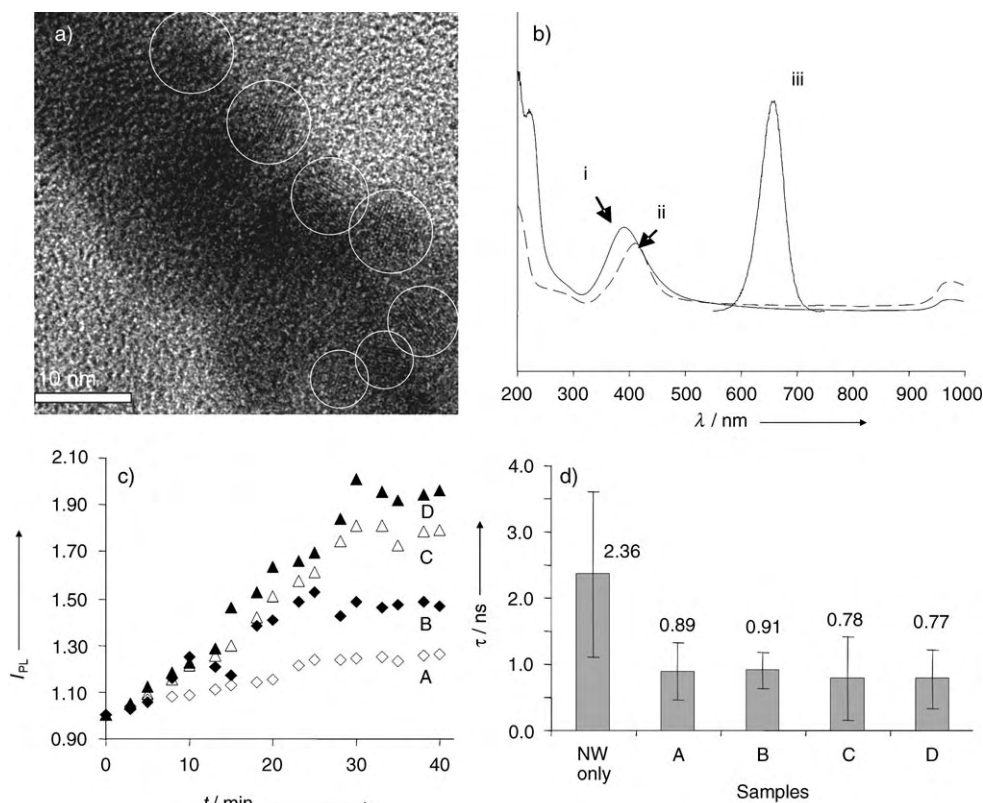


**Figure 1.** a) TEM image of bioconjugates of NPs and NWs, 300000 $\times$ , b) UV/Vis and luminescence spectra of Ag NPs and CdTe NWs; i: Ag NPs, ii: Ag NPs with SA, iii: PL of NWs; c) Time courses of the luminescence peak intensities for solutions A to D. d) PL lifetimes of the respective samples.

The superstructures of Ag NPs and CdTe NWs were obtained by combining appropriate volumes of two stock solutions (NP-SA and NW-B; SA: streptavidin, B: D-biotin). The approximate molarities of the Ag NP and CdTe NW stock solutions were  $2.7 \times 10^{-6}$  and  $2.95 \times 10^{-9}$  M, respectively. The formation reaction of the NP-NW assemblies took place in 3 mL of water at pH 9 (pH adjusted with 0.1 M NaOH) in a quartz optical cuvette. Solutions were prepared with different aliquots of Ag NP dispersion (20–100  $\mu$ L) and a constant volume of the CdTe NW dispersion (20  $\mu$ L). The NP/NW ratios for the different superstructures are given in Table 1.<sup>[1]</sup>

The intensity of the NW emission steadily increased up to twofold and the peak wavelengths were blue-shifted by up to

**Table 1:** Composition of different NW–NP assemblies prepared from different volume ratios of the stock NW-B and NP-SA dispersions. An averaged NW length of 1400 nm was used for calculation.

	Solution A	Solution B	Solution C	Solution D
volume ratio (CdTe NW/Au NP)	20:20	20:40	20:80	20:100
NP/NW ratio	4468	8936	17872	22340

10 nm during the bioconjugation process; these changes are smaller than those for the analogous reaction with Au NPs (see the Supporting Information).<sup>[1]</sup> The bioconjugation of ligand receptors with attached nanocolloids was completed in approximately 30 minutes for different molar ratios of CdTe NWs and Ag NPs (Figure 1 c). The photoluminescence (PL) lifetime was about 2.36 ns for the NWs alone, but decreased to around 0.84 ns for the Ag-conjugated NWs (Figure 1 d). The PL intensity after that period was considered the ultimate fluorescence intensity and the assembly process was considered to reach saturation. The kinetics of the luminescence intensity is well-correlated with the conjugation of SA and B involving nanocolloids.<sup>[1,31,32]</sup> Higher PL intensities at saturation were observed for higher NP/NW ratios (Figure 1 c). The spectra of the Ag NP–NW superstructures appear similar to those of Au NP–NW superstructures, and this was initially explained on the basis of exciton–plasmon interactions.<sup>[1]</sup> However, the underlying mechanism is essentially different. A strong indication of this is that the plasmon-resonance peak of the Ag particles does not overlap in any way with the emission peak of the NWs (Figure 1 b), which is required for resonance.

The answer to this apparent discrepancy between the expected mechanism and the experimental results was found in the excitation spectra (Figure 2). As the superstructure

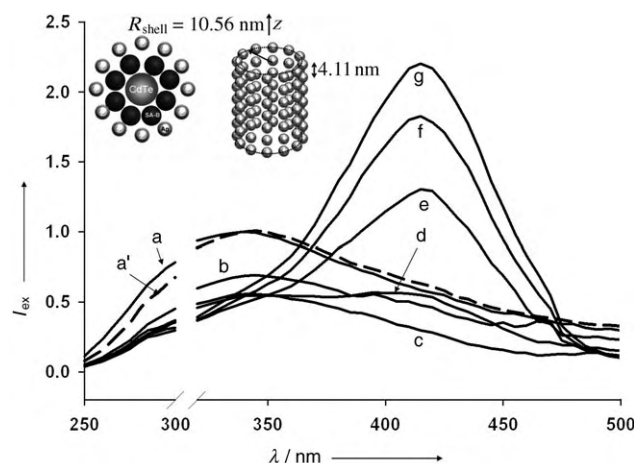


**Figure 2.** Photoluminescence excitation spectra of conjugated superstructures: spectra of Ag-conjugated NWs recorded every 10 minutes (a–g) for an emission wavelength of 660 nm (solution D); Au-conjugated NWs after 60 minutes (a', dashed line). The gap at 300 nm corresponds to the strong  $\lambda/2$  peak of the excitation light, removed from the spectra for clarity. Inset: Cross section of the superstructure of Ag NPs, SA–B linkers, and an NW (left). Theoretical model (right) of an Ag shell with periodicity along the cylinder axis. The electro-magnetic field is calculated at the center of the Ag-NP shell.

forms over a period of 20–30 min, a new feature develops in the vicinity of 420 nm. Importantly, no change is observed at this same wavelength over a period of 60 min in an experiment with the Au-conjugated NW superstructures under the same conditions (spectrum a'). Firstly, this correlates very well with the plasmon–exciton resonance mechanism suggested previously for Au NP–NW superstructures.<sup>[32]</sup> Secondly, the excitation peak that develops at 420 nm for Ag NP–NW superstructures indicates that absorption increases drastically at this wavelength, with the energy eventually channeled into the emission of the NW at 600 nm. Thus, the reason for increase in luminescence of the Ag NP–NW superstructures is stimulated light absorption rather than light emission. The absorption of the CdTe NWs is enhanced at the exciton wavelength as a result of the proximity of the Ag NPs, which have a plasmon band that can oscillate in resonance with the exciton in the semiconductor.

To confirm this hypothesis, we calculated the electric fields inside a superstructure. The theoretical model incorporates an NW, an Ag-NP shell, and SA–B biolinkers (Figure 2, left inset). The radii of the components are taken as follows:  $R_{\text{NW}} = 4$  nm,  $R_{\text{SA-B}} = 2.5$  nm, and  $R_{\text{AgNP}} = 1.56$  nm. The corresponding radius of the Ag-NP shell  $R_{\text{shell}}$  is 10.56 nm. The emission intensity of the superstructure is proportional to the factor  $P_{\text{emiss}}(\lambda_{\text{excitation}}, \lambda_{\text{emiss}})$  [Eq. (1)], whereby  $\lambda_{\text{excitation}}$  and  $\lambda_{\text{emiss}}$  are the excitation and exciton peak wavelengths and  $P_{\text{field}}(\lambda)$  is the electric-field enhancement factor at a particular wavelength [Eq. (2)]. In Equation (2),  $E_0$  is the amplitude of the external electric field, and  $E_{\text{tot}}$  is the resultant field in the center of the Ag-NP shell. The squared resultant electric field is averaged over all solid angles. Although the position of NPs with respect to the NW are assumed to be constant and unaffected by tumbling in solution, this assumption is necessary to account for the fact that the NWs in a solution may have variable orientation with respect to the electric field of incident light.

$$P_{\text{emiss}}(\lambda_{\text{excitation}}, \lambda_{\text{emiss}}) = P_{\text{field}}(\lambda_{\text{excitation}}) P_{\text{field}}(\lambda_{\text{emiss}}) \quad (1)$$

$$P_{\text{field}}(\lambda) = \frac{\langle E_{\text{tot}}^2 \rangle_{\Omega}}{E_0^2} \quad (2)$$

Figure 3 shows numerical simulations of the factors  $P_{\text{emiss}}(\lambda_{\text{excitation}}, \lambda)$  and  $P_{\text{field}}(\lambda)$  at the center of the Ag-NP superstructure (Figure 2, right inset) with Maxwell equations (see the Supporting Information). For the curves in Figure 3 b, we fixed the excitation wavelength ( $\lambda_{\text{excitation}} = 420$  nm) and varied the emission wavelength ( $\lambda$ ). The data were obtained for three superstructures with total numbers of NPs  $N_{\text{tot}} = 56$ , 84, and 112. Each superstructure has seven rings, and the inter-ring spacing was taken as 4.11 nm. The corresponding numbers of NPs per ring ( $N_{\text{ring}}$ ) were 8, 12, and 16. Note that the above numbers are less than the maximum possible number of Ag NPs per ring (i.e., 21). The corresponding linear densities of NPs were then calculated as  $N_{\text{ring}}/4.11$  nm  $\approx 1.95$ , 2.92, and 3.89 nm<sup>−1</sup>. If we now assume that total length of the NW is 1400 nm and calculate the total numbers of attached NPs using the above linear densities, we obtain 3610,

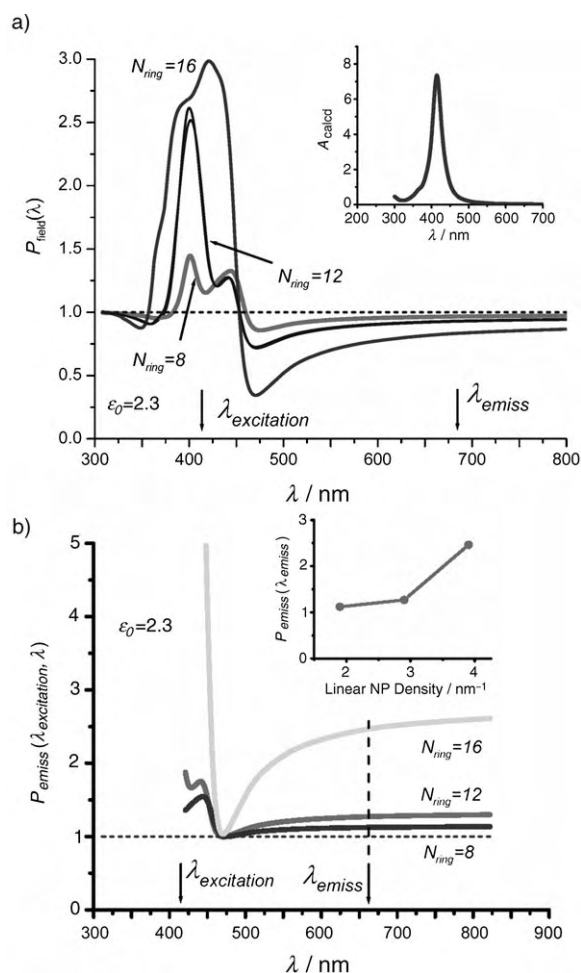


**Figure 3.** a) Field-enhancement factor for three superstructures with linear NP densities of 1.95, 2.92, and 3.89 nm<sup>-1</sup>. Inset: Calculated absorption by a single Ag NP. The position of the plasmon resonance corresponds well with the experimental data (Figure 1b). The two curves for the 12-NP rings correspond to  $l_{\max} = 1$  and 2 ( $l$  is the spherical harmonic index); the differences are minimal. b) Emission-enhancement factor as a function of the emission wavelength for three superstructures with linear NP densities of 1.95, 2.92, and 3.89 nm<sup>-1</sup>; the excitation wavelength is taken as 420 nm. Inset: Calculated emission-enhancement factor at an emission wavelength of 660 nm.

5510, and 7391. These numbers are comparable to the NP/NW ratios for solutions A and B (Table 1).

The calculations demonstrate (Figure 3a) that the strength of the collective plasmon field increases gradually with increasing density of metal NPs in the shell. The spectral characteristic (energy) of the collective plasmons resonating between many Ag particles in the NP shell of the superstructure becomes wider. The factor  $P_{\text{field}}(\lambda)$  is strongly enhanced for  $\lambda_{\text{excitation}}$  between 400 and 450 nm and slightly reduced for  $\lambda_{\text{emission}}$  at around 660 nm; thus the probability of photon emission at 660 nm in Ag-based structures is not increased but rather is even reduced slightly as a result of dynamic screening inside the shell (Figure 2, inset a). For higher density of NPs, the plasmon peak is located around 425 nm, which is red-shifted relative to the spectrum of

individual particles. This shift is illustrated by a comparison of the plasmon resonance in the Ag-NP shell (Figure 3a) with the plasmon peak of a single Ag NP (Figure 3a, inset). Again, this change results from the formation of collective plasmon resonance in the Ag-NP shell. This change is in exactly the same spectral region in which the new peak develops in the excitation spectrum (Figure 2). The nice match of the experimental results and calculations demonstrates the validity of the hypothesis of the enhanced absorption.

Some shortening of exciton lifetime of the Ag-based superstructures is observed, as was the case for Au-based superstructures (Figure 1d), although the difference is far less drastic. This effect is attributed mostly to exciton-energy dissipation in the metal. This difference between Au- and Ag-based structures is the position of the plasmon resonance with respect to the exciton energy in the CdTe NWs. In the Au-CdTe complex, the exciton energy is close to the Au plasmon peak. In the Ag-based system, the plasmon resonance is relatively far from the exciton peak. Moreover, the electric field from Ag NPs might activate some other decay mechanisms, such as nonradiative recombination pathways, which are likely to contribute to the reduced lifetime as well.

To evaluate the emission-enhancement effect qualitatively, we calculated the emission-enhancement factor  $P_{\text{emiss}}(\lambda_{\text{excitation}}, \lambda)$  for the emission wavelengths  $\lambda > \lambda_{\text{excitation}}$  (Figure 3b). In the experimentally important region around  $\lambda_{\text{emission}} = 660$  nm, the factor  $P_{\text{emiss}}(\lambda_{\text{excitation}}, \lambda)$  increases rapidly with the number of attached NPs (Figure 3b, inset). The theoretical factor  $P_{\text{emiss}}(\lambda_{\text{excitation}}, \lambda)$  for a linear NP density of 2.9 nm<sup>-1</sup> is more than 2, which is very similar to actual fluorescence enhancement in Figure 1c. The theoretical estimate from Figure 3b (2.5) also compares well with the experimental value of  $P_{\text{emiss}}(\lambda_{\text{excitation}}, \lambda) \approx 3.4$  (derived in the Supporting Information). Thus, the idealized model presented herein gives a very good description of the processes in NP-NW superstructures and metal-semiconductor metamaterials.

In conclusion, we observed a twofold enhancement of luminescence intensity in the nanoscale bioconjugated superstructures made from CdTe NWs and Ag NPs. Theoretical calculations of the electric field in the cylindrically organized NPs and experimental data suggest that the enhancement in emission originates from the increase in absorption of the Ag-NP shells in the regime of the collective plasmon resonance. This situation is qualitatively different from the PL enhancement in the Au-NP/NW system studied previously. The fundamental importance of these findings is twofold: 1) The results demonstrate metamaterials for which the spatial organization of metal particles has direct consequences on the optical properties as a result of the collective nature of interactions. 2) The described calculation method can be used to predict properties of nanoscale superstructures. From a practical point of view, the combination of Au and Ag NPs may lead to the enhancement of both absorption and emission in semiconductor nanostructures, which could be utilized in a variety of optoelectronic or energy-conversion devices, for example, in solar-energy devices.



## Experimental Section

CdTe NPs and NWs were prepared as described in detail elsewhere.<sup>[27,34]</sup> Ag NPs were synthesized in solution from AgNO<sub>3</sub> (Aldrich<sup>[35]</sup>), soluble starch (Aldrich<sup>[35]</sup>), and D-glucose (Aldrich<sup>[35]</sup>).<sup>[36]</sup> Ethylene dichloride (EDC) and sulfo-*N*-hydroxysuccinimide (NHS) were used as zero-length cross-links to bind the inorganic and biological materials covalently (Ag NPs with streptavidin (SA), CdTe NWs with D-biotin).<sup>[1,37]</sup> Ag NPs were bioconjugated with SA as follows: unbound starches in the Ag-NP solution were removed by repeated centrifugation and redispersion until a clear and transparent Ag-NP solution was obtained. An Ag-NP dispersion (1 mL) was mixed with thioglycolic acid (8.7  $\mu$ M) for 24 h. The EDC and NHS procedures were followed to activate the carboxylic acid groups. Spectra of the bioconjugates were measured with a UV/Vis spectrophotometer (Agilent, Model-8453<sup>[35]</sup>). The luminescence and excitation spectra of the NP–NW dispersions were measured on a Fluoromax-3 spectrofluorometer (Jobin Yvon/SPEX Horiba<sup>[35]</sup>) every 1–2 minutes for up to 40 minutes. Atomic force microscopy (AFM)<sup>[35]</sup> and JEOL 2010F TEM<sup>[35]</sup> (with an accelerator voltage of 200 kV) were used to observe the morphology of the bioconjugates of Ag NPs and CdTe NWs. The lifetimes of the respective nanomaterials were measured with a Fluorolog Tau-3 (Jobin Yvon/SPEX Horiba<sup>[35]</sup>).

Received: January 26, 2006

Published online: June 27, 2006

**Keywords:** bioconjugation · luminescence · metamaterials · nanotechnology · silver

- [1] J. Lee, A. O. Govorov, J. Dulka, N. A. Kotov, *Nano Lett.* **2004**, *4*, 2323–2330.
- [2] E. Prodan, C. Radloff, N. J. Halas, P. Nordlander, *Science* **2003**, *302*, 419–422.
- [3] X. Michalet, F. Pinaud, T. D. Lacoste, M. Dahan, M. P. Bruchez, A. P. Alivisatos, S. Weiss, *Single Mol.* **2001**, *2*, 261–276.
- [4] J. Zhang, N. Coombs, E. Kumacheva, Y. Lin, E. H. Sargent, *Adv. Mater.* **2002**, *14*, 1756–1759.
- [5] Z. Li, R. Jin, C. A. Mirkin, R. L. Letsinger, *Nucleic Acids Res.* **2002**, *30*, 1558–1562.
- [6] S. Westenhoff, N. A. Kotov, *J. Am. Chem. Soc.* **2002**, *124*, 2448–2449.
- [7] G. P. Goodrich, M. R. Helfrich, J. J. Overberg, C. D. Keating, *Langmuir* **2004**, *20*, 10246–10251.
- [8] J. Jiang, K. Bosnick, M. Maillard, L. Brus, *J. Phys. Chem. B* **2003**, *107*, 9964–9972.
- [9] K. Kneipp, Y. Wang, H. Kneipp, L. T. Perelman, I. Itzkan, R. R. Dasari, M. S. Feld, *Phys. Rev. Lett.* **1997**, *78*, 67–1670.
- [10] M. Maillard, P. Huang, L. Brus, *Nano Lett.* **2003**, *3*, 11–1615.
- [11] S. Riikonen, I. Romero, F. J. Garcia de Abajo, *Phys. Rev. B* **2005**, *71*, 5104.
- [12] I. Willner, B. Willner, *Pure Appl. Chem.* **2002**, *74*, 73–1783.
- [13] A. L. Rogach, *Angew. Chem.* **2003**, *115*, 150–151; *Angew. Chem. Int. Ed.* **2003**, *42*, 148–149.
- [14] Y. Lin, H. Skaff, T. Emrick, A. D. Dinsmore, T. P. Russell, *Science* **2003**, *299*, 226–229.
- [15] S. Chen, K. Kimura, *Chem. Lett.* **1999**, 233–234.
- [16] E. V. Shevchenko, D. V. Talapin, S. O'Brien, C. B. Murray, *J. Am. Chem. Soc.* **2005**, *127*, 8741–8747.
- [17] S. Zhang, W. Fan, N. C. Panou, K. J. Malloy, R. M. Osgood, S. R. J. Brueck, *Phys. Rev. Lett.* **2005**, *95*, 137404.
- [18] T. Vo-Dinh, *Trends Anal. Chem.* **1998**, *17*, 557–582.
- [19] K. G. Thomas, P. V. Kamat, *Acc. Chem. Res.* **2003**, *36*, 888–898.
- [20] Y. C. Cao, R. Jin, C. A. Mirkin, *Science* **2002**, *297*, 1536–1540.
- [21] S. Link, M. A. El Sayed, *Annu. Rev. Phys. Chem.* **2003**, *54*, 331–366.
- [22] A. N. Shipway, E. Katz, I. Willner, *ChemPhysChem* **2000**, *1*, 18–52.
- [23] J. D. Baena, R. Marques, F. Medina, J. Martel, *Phys. Rev. B* **2004**, *69*, 014402.
- [24] R. Marques, F. Medina, R. Rafii-El-Idrissi, *Phys. Rev. B* **2002**, *65*, 144440.
- [25] A. O. Govorov, W. Zhang, T. Skeini, H. Richardson, J. Lee, N. A. Kotov, *Nanoscale Res. Lett.* **2005**, *1*, 100101.
- [26] J. Lee, A. O. Govorov, N. A. Kotov, *Angew. Chem.* **2005**, *117*, 7605–7608; *Angew. Chem. Int. Ed.* **2005**, *44*, 7439–7442.
- [27] Z. Tang, N. A. Kotov, M. Giersig, *Science* **2002**, *297*, 237–240.
- [28] Z. Liu, H. Li, H. Wang, D. Shen, X. Wang, P. F. A. Alkemade, *J. Mater. Res.* **2000**, *15*, 1245–1247.
- [29] L. M. Liz-Marzan, P. Mulvaney, *J. Phys. Chem. B* **2003**, *107*, 7312–7326.
- [30] H. C. van de Hulst, *Light Scattering by Small Particles*, John Wiley & Sons, New York, **1957**, p. 470.
- [31] R. M. Penner, *J. Phys. Chem. B* **2002**, *106*, 3339–3353.
- [32] J. Lee, A. O. Govorov, N. A. Kotov, *Nano Lett.* **2005**, *5*, 2063–2069.
- [33] E. D. Palik, *Handbook of Optical Constants of Solids*, Academic Press, Orlando, **1985**, p. 804.
- [34] N. Gaponik, D. V. Talapin, A. L. Rogach, K. Hoppe, E. V. Shevchenko, A. Kornowski, A. Eychmueller, H. Weller, *J. Phys. Chem. B* **2002**, *106*, 7177–7185.
- [35] Certain commercial equipment, instruments, or materials are identified in this paper to specify the experimental procedure adequately. Such identification is not intended to imply recommendation or endorsement by the National Institute of Standards and Technology, nor is it intended to imply that the materials or equipment identified are necessarily the best available for the purpose.
- [36] P. Raveendran, J. Fu, S. L. Wallen, *J. Am. Chem. Soc.* **2003**, *125*, 13940–13941.
- [37] N. N. Mamedova, N. A. Kotov, A. L. Rogach, J. Studer, *Nano Lett.* **2001**, *1*, 281–286.

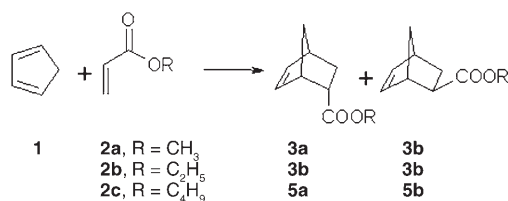
DOI: 10.1002/anie.200600426

## Diels–Alder Reactions Are Faster in Water than in Ionic Liquids at Room Temperature\*\*

Shraeddha Tiwari and Anil Kumar\*

Over the past few years, there has been an increasing concern over the environmental effects of the use of volatile organic compounds as solvents. The quest for “green” solvents has led to the study of water, room-temperature ionic liquids (RTILs), and supercritical CO<sub>2</sub>. Water, also known as nature’s solvent, has been in focus after the pioneering work of Rideout and Breslow.<sup>[1,2]</sup> Meanwhile, much attention has been paid to the synthesis and characterization of RTILs and their use as solvents for carrying out organic reactions that are usually performed in organic solvents.<sup>[3]</sup> The advantages of using RTILs have been discussed in several reports.<sup>[4]</sup> Based on the studies made so far, the conclusion has been drawn that RTILs are highly effective in accelerating organic reactions, including Diels–Alder reactions.<sup>[5]</sup>

We demonstrate here that RTILs are not as effective as water in promoting Diels–Alder reactions. For this purpose, we have carried out three simple Diels–Alder reactions involving cyclopentadiene (**1**) with methyl acrylate (**2a**), ethyl acrylate (**2b**), and butyl acrylate (**2c**) (Scheme 1) both in



Scheme 1. Diels–Alder reactions studied in water and RTILs.

water and RTILs (Figure 1) under identical conditions. In Table 1 are listed the second-order rate constants,  $k_2$ , for these reactions. The reaction of **1** with **2a** is ten times faster in water than in [BMIM]I. Similarly, rates of the reactions of **1** with **2b** and **2c** are at least three to four times higher in water than in [BMIM]I.

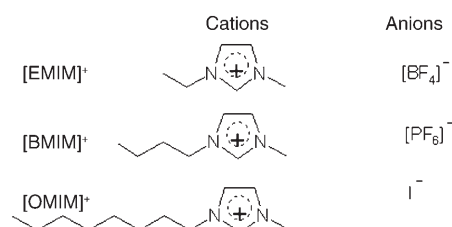


Figure 1. Structures of the RTILs used.

Table 1: Second-order rate constants ( $k_2$ ) for Diels–Alder reactions in water and RTILs.<sup>[a]</sup>

Solvent	$k_2 \cdot 10^5 \text{ [dm}^3 \text{ mol}^{-1} \text{ s}^{-1}]^{[b]}$		
	<b>1 + 2a</b>	<b>1 + 2b</b>	<b>1 + 2c</b>
water	24.1	7.9	5.7
[EMIM][BF <sub>4</sub> ]	5.9	5.7	5.2
[BMIM][BF <sub>4</sub> ]	4.5	3.9	3.4
[BMIM][PF <sub>6</sub> ]	3.9	3.3	3.1
[OMIM][PF <sub>6</sub> ]	3.1	2.4 <sup>[c]</sup>	2.4
[BMIM]I	2.5	2.5 <sup>[c]</sup>	2.1

[a] Reactions were carried out on a 1-mmol scale in 1 mL of solvent with a 1:1 ratio of the diene and dienophile at 298.15 K. The rate constants determined with 10 mm of **1** and 50 mm and 100 mm of **2a** agreed to within experimental error ( $\pm 6\%$ ). [b] An average of three runs. [c] Values equal to within experimental error ( $\pm 6\%$ ).

The experimental data present clear evidence that water can be a more powerful solvent than the ionic liquids, as far as Diels–Alder reactions are concerned. In the case of water, the rate enhancement has been ascribed to several factors, such as solvent polarity,<sup>[6a]</sup> hydrophobic packing,<sup>[1]</sup> hydrophobic hydration,<sup>[7]</sup> hydrogen bonding,<sup>[8]</sup> surface cohesive pressure,<sup>[2a,9]</sup> and surface tension.<sup>[2a,c]</sup> In general, the water-promoted Diels–Alder reactions can be better interpreted in terms of enforced hydrophobic hydration<sup>[7]</sup> and hydrogen bonding,<sup>[8]</sup> as discussed by Engberts and Jorgensen, respectively. The absence of hydrophobic interactions and weaker hydrogen bonding in RTILs may be important reasons for the observed difference in the rates between water and RTILs.

For the Diels–Alder reactions conducted in the RTILs, the rates drop by a factor of 2 on going from [EMIM][BF<sub>4</sub>] to [BMIM]I. The trend is consistent for all three dienophiles studied, irrespective of the change in cation or anion. Thus the observed rate deceleration has to originate from a property that varies in a nonspecific fashion for all the RTILs used. An extensive examination of a range of properties was undertaken. Surface tensions<sup>[10d]</sup> of RTILs do not show any correlation with the reaction rates, as evident from such a comparison. The solvophobicity,  $\delta_{11}(\text{H}^2)$ , is also a weak correlating property in the case of RTILs.<sup>[5d]</sup> However, the rate constants of a Diels–Alder reaction carried out in different RTILs have been correlated with the H-bonding ability, expressed in terms of the  $E_{\text{T}}^{30}$  parameter.<sup>[5d]</sup> Our results support this correlation: the  $k_2$  values of these reactions decrease with the decrease in  $E_{\text{T}}^{30}$  values of the RTILs.

The literature reports<sup>[10]</sup> suggest that the viscosities of different RTILs used in this investigation follow the order: water < [EMIM][BF<sub>4</sub>] < [BMIM][BF<sub>4</sub>] < [BMIM][PF<sub>6</sub>] <

[\*] S. Tiwari, Dr. A. Kumar  
Physical Chemistry Division  
National Chemical Laboratory  
Pune 411008 (India)  
Fax: (+91) 20-2590-2636  
E-mail: a.kumar@ncl.res.in

[\*\*] This research was supported DST Grant No. SR/S1/PC-13/2002. S.T. is grateful to CSIR New Delhi for a Junior Research Fellowship. We thank anonymous referees for valuable suggestions.

Supporting information for this article is available on the WWW under <http://www.angewandte.org> or from the author.

[OMIM][PF<sub>6</sub>] < [BMIM]I. Our preliminary investigation suggested that the  $k_2$  values for these reactions decrease with the increase in the viscosity of RTILs. To provide tentative support for this observation, the reaction of **1** with **2a** was carried out at 298.15 K in a mixture of [BMIM][BF<sub>4</sub>] with dichloromethane (DCM) (45 mol % of [BMIM][BF<sub>4</sub>] in 55 mol % of DCM). Here, DCM ( $\eta \approx 18$  cP)<sup>[11]</sup> was used as a “viscosity reducer” for [BMIM][BF<sub>4</sub>] ( $\eta = 233$  cP). The resulting rate constant,  $k_2 = 5.79 \times 10^{-5} \text{ dm}^3 \text{ mol}^{-1} \text{ s}^{-1}$ , is about 20 % higher than that measured in pure [BMIM][BF<sub>4</sub>]. It is, however, not possible to state at this stage with confidence that the viscosity of a RTIL is an important parameter to correlate kinetic data of Diels–Alder reactions. In a recent study with a series of RTILs, it was shown that the Diels–Alder reaction was fastest in the RTIL of highest viscosity.<sup>[5d]</sup> Inadequate experimental data do not allow us to draw any conclusion at this stage.

The results of preliminary temperature-dependent kinetic investigations are shown in Figure 2. The  $\Delta H^\ddagger$  values for the reaction of **1** with **2a**, obtained from the transition-state theory plots (Figure 2), are 55.3 kJ mol<sup>-1</sup> and 60.9 kJ mol<sup>-1</sup> for [EMIM][BF<sub>4</sub>] and [BMIM][PF<sub>6</sub>], respectively. Any change in temperature is bound to alter both the H-bonding ability and the viscosity of RTILs. The observed temperature effect may result from a change in either or both these parameters. A detailed study of the theories of condensed-phase kinetics to explain the results is being carried out in our laboratory and will be reported in the future.

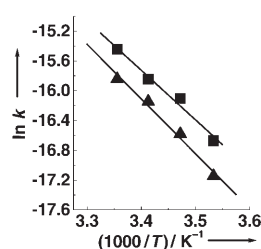


**Figure 2.** Eyring plots of Diels–Alder reaction of **1** + **2a** in [EMIM][BF<sub>4</sub>] (■) ( $r^2 = 0.991$ ) and [BMIM][PF<sub>6</sub>] (▲) ( $r^2 = 0.996$ ).

The present results indicate that water, and not a RTIL, is definitely the solvent of choice for carrying out Diels–Alder reactions. The results merit further investigation to correlate the rates of these reactions with other properties of RTILs. Also designing new RTILs or using RTIL mixtures with better properties is highly desirable in order to encourage their use as “green solvents”.

## Experimental Section

Cyclopentadiene (**1**) was freshly distilled from dicyclopentadiene prior to use. Acrylates **2a**, **2b** (low-pressure distillation), and **2c** were distilled prior to use. 1-Butyl-3-methylimidazolium tetrafluoroborate [BMIM][BF<sub>4</sub>], 1-butyl-3-methylimidazolium hexafluorophosphate [BMIM][PF<sub>6</sub>], 1-butyl-3-methylimidazolium iodide [BMIM]I, 1-octyl-3-methylimidazolium tetrafluoroborate [OMIM][BF<sub>4</sub>] and 1-ethyl-3-methylimidazolium tetrafluoroborate [EMIM][BF<sub>4</sub>] were synthesized by the reported procedure.<sup>[8a]</sup> The RTILs were thoroughly dried by heating at 70 °C under high vacuum for several hours before each kinetic run. All manipulations were carried out under an atmosphere of dry nitrogen to exclude moisture.

**Kinetic analysis:** In a standard kinetic run the dienophile was added to the ionic liquid (1 mmol in 1 mL of ionic liquid), and the reaction mixture was allowed to equilibrate at the desired temperature. The temperature was controlled using a Julabo constant-temperature bath with an accuracy of  $\pm 0.01$  K. The reaction was initiated by addition of **1** (1 mmol in 1 mL). The reaction progress was monitored at appropriate time intervals by extraction of aliquots with ether followed by appropriate dilution and GC analysis. (Varian CP-3800 gas chromatograph; for details, see the Supporting Information). The rate constants thus determined were reproducible to within 6 %.

Received: February 1, 2006

Revised: April 25, 2006

Published online: June 27, 2006

**Keywords:** Diels–Alder reaction · ionic liquids · kinetics · solvent effects · viscosity

- [1] D. C. Rideout, R. Breslow, *J. Am. Chem. Soc.* **1980**, *102*, 7816.
- [2] For examples of water-promoted Diels–Alder reactions, see: a) R. Breslow, *Acc. Chem. Res.* **1991**, *24*, 159; b) W. Blokzijl, M. J. Blandamer, J. B. F. N. Engberts, *J. Am. Chem. Soc.* **1991**, *113*, 4241; c) R. Breslow, T. Guo, *Proc. Natl. Acad. Sci. USA* **1990**, *87*, 167.
- [3] a) *Ionic Liquids in Synthesis* (Eds.: P. Wassercheid, T. Welton), Wiley-VCH, Weinheim, **2003**; b) R. D. Rogers, K. R. Seddon in *Ionic Liquids: Industrial Applications to Green Chemistry*, ACS Symposium Series 818, American Chemical Society, Washington, DC, **2002**; c) C. F. Poole, *J. Chromatogr. A* **2004**, *1037*, 49.
- [4] a) T. Welton, *Chem. Rev.* **1999**, *99*, 2071; b) M. J. Earle, K. R. Seddon, *Pure Appl. Chem.* **2000**, *72*, 1391; c) P. Wassercheid, M. Keim, *Angew. Chem. Int. Ed.* **2000**, *39*, 3772; d) R. Sheldon, *Chem. Commun.* **2001**, *23*, 2399; e) C. Chiappe, D. J. Pieraccini, *J. Phys. Org. Chem.* **2005**, *18*, 275.
- [5] For reports on Diels–Alder reactions in ionic liquids see: a) D. A. Jaeger, C. E. Tucker, *Tetrahedron Lett.* **1989**, *30*, 1785; b) M. J. Earle, P. B. McCormac, K. R. Seddon, *Green Chem.* **1999**, *1*, 23; c) C. Lee, *Tetrahedron Lett.* **1999**, *40*, 2461; d) A. Aggarwal, N. L. Lancaster, A. R. Sethi, T. Welton, *Green Chem.* **2002**, *4*, 517; e) A. Kumar, S. S. Pawar, *J. Org. Chem.* **2004**, *69*, 1419.
- [6] C. Reichardt, *Solvent Effects in Organic Chemistry*, Verlag Chemie, Weinheim, **1979**.
- [7] a) W. Blokzijl, J. B. F. N. Engberts, M. J. Blandamer, *J. Am. Chem. Soc.* **1990**, *112*, 1197; b) W. Blokzijl, J. B. F. N. Engberts, *J. Am. Chem. Soc.* **1991**, *113*, 5440; c) W. Blokzijl, J. B. F. N. Engberts, *Angew. Chem.* **1993**, *32*, 1610; *Angew. Chem. Int. Ed. Engl.* **1993**, *32*, 1545; d) T. Rispens, J. B. F. N. Engberts, *J. Org. Chem.* **2002**, *67*, 7369; e) S. Otto, J. B. F. N. Engberts, *Org. Biomol. Chem.* **2003**, *1*, 2809.
- [8] J. F. Blake, W. L. Jorgensen, *J. Am. Chem. Soc.* **1991**, *113*, 7430.
- [9] a) M. R. J. Dack, *Chem. Soc. Rev.* **1975**, *4*, 211; b) M. C. Pirrung, *Chem. Eur. J.* **2006**, *12*, 1312.
- [10] The  $\eta$  values of the RTILs were obtained from the following sources: a) P. Bonhote, A. P. Dias, K. Kalyansundaram, M. Gratzel, *Inorg. Chem.* **1996**, *35*, 1168; b) P. A. Z. Suarez, S. Einloft, J. E. Dudlis, R. F. deSouza, J. Dupont, *J. Chim. Phys.* **1998**, *95*, 1626; c) K. R. Seddon, A. Stark, J. Torres, *Pure Appl. Chem.* **2000**, *72*, 2275; d) J. G. Huddleston, A. E. Visser, W. M. Reichert, H. D. G. A. Brokers, R. D. Rogers, *Green Chem.* **2001**, *3*, 156; e) A. Noda, K. Hayamizu, M. Watanabe, *J. Phys. Chem. B* **2001**, *105*, 4603; f) S. N. Baker, G. A. Baker, M. A. Kane, F. V. Bright, *J. Phys. Chem. B* **2001**, *105*, 9663; g) L. C. Bronco, J. N. Rosa, C. A. M. Afonso, *Chem. Eur. J.* **2002**, *8*, 3671.
- [11] J. Wang, Y. Tian, Y. Zhao, K. Zhuo, *Green Chem.* **2003**, *5*, 618.

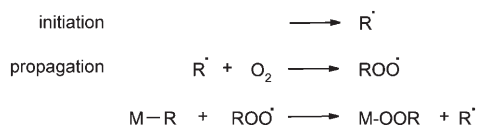
DOI: 10.1002/anie.200601001

Reactions of  $[ZnR_2(L)]$  Complexes with Dioxygen: A New Look at an Old Problem\*\*

Janusz Lewiński,\* Witold Śliwiński, Maciej Dranka, Iwona Justyniak, and Janusz Lipkowski

The interaction of zinc alkyls with dioxygen has received continuous interest for over 150 years, and common wisdom states that the oxygenation reactions of homoleptic zinc alkyls are uncontrollably fast. Moreover, significant uncertainties concerning both the composition of the products and mechanistic considerations have persisted. In pioneering studies, Frankland contended in 1849 that controlled oxygenation of  $ZnEt_2$  affords  $Zn(OEt)_2$ ,<sup>[1]</sup> and in 1864 Butlerov<sup>[2]</sup> and Lissenko<sup>[3]</sup> independently argued for the formation of the partly oxygenated species  $Zn(Et)OEt$ . In 1890 Demuth and Meyer postulated the formation of the alkylperoxide  $Zn(Et)OOEt$  from the insertion of an  $O_2$  molecule into the  $Zn-C$  bond.<sup>[4]</sup> These pioneering interpretations have since been the subject of considerable debate;<sup>[5]</sup> however, most of the later studies considered the oxygenation reaction as proceeding with oxidation of both  $Zn-C$  bonds and the formation of compounds formulated as  $Zn(OOR)_2$ ,  $Zn(OR)OOR$ , and  $Zn(OR)_2$ .<sup>[5c-f]</sup> Only very recently our group demonstrated convincingly that the controlled oxygenation of  $ZnMe_2$  leads to the formation of partially oxygenated species in high yields,<sup>[6]</sup> and we structurally characterized the first examples of zinc alkylperoxides that were derived from the reaction of  $O_2$  with monoalkylzinc chelate complexes.<sup>[6,7]</sup> The latter results have come in contradiction to the commonly accepted mechanism, which assumes a radical-chain process (Scheme 1).<sup>[8]</sup>

Apart from fundamental interest in the interaction of zinc alkyls with dioxygen, many practical applications have been found in both organic and materials chemistry which involve



Scheme 1.

[\*] Dr. J. Lewiński, W. Śliwiński, M. Dranka  
Department of Chemistry  
Warsaw University of Technology  
Noakowskiego 3, 00-664 Warsaw (Poland)  
Fax: (+48) 22-6607-279  
E-mail: lewin@ch.pw.edu.pl

Dr. I. Justyniak, Prof. Dr. J. Lipkowski  
Institute of Physical Chemistry  
Polish Academy of Sciences  
Kasprzaka 44/52, 01-224 Warsaw (Poland)

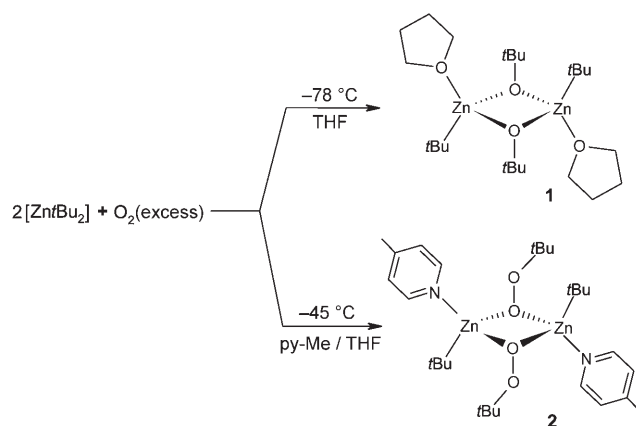
[\*\*] This work was supported by the State Committee for Scientific Research (Grant No. 3 T09B 037 28).

the oxygenation process. For example, the seminal studies of Chaudret and co-workers demonstrated that controlled oxygenation of the  $ZnR_2$  precursor in THF in the presence of an amine ligand and moisture affords in one step crystalline  $ZnO$  nanoparticles of controlled size and shape.<sup>[9,10]</sup> The importance of zinc alkylperoxide complexes is also readily apparent from their continued use as reagents in organic synthesis. For decades, the reaction of organozinc complexes (particularly  $Zn(R)X$  compounds in the presence of ether solvents) with  $O_2$  has been used to prepare hydroperoxides or alcohols, depending on the reaction conditions.<sup>[11]</sup> Furthermore, the alkylperoxide species  $Zn(R)OOR$ , prepared in situ by treating  $ZnR_2$  with molecular oxygen, was reported as an efficient epoxidizing reagent for enones,<sup>[12]</sup> and the modified systems that were supported by auxiliary ligands enabled to conduct the epoxidation stereoselectively<sup>[13]</sup> and regioselectively.<sup>[7,14]</sup> Contemporaneously, there has also been increased interest in various radical additions initiated by the  $ZnR_2/O_2$  system, in which an alkyl radical, as it has been commonly assumed, is generated through the reaction of dialkylzinc with dioxygen and acts as the chain carrier.<sup>[15]</sup> In spite of many contributions in this area, there is no answer to the question of how the oxygenated products participate in the radical reactions. Pertinent to the subject of our studies is also the fact that in the latter reactions, organic substrates usually bear electron-donor sites that are capable of forming Lewis acid–base adducts with  $ZnR_2$ , and essentially adducts of the type  $[ZnR_2(L)_n]$  are actually involved in the reaction with dioxygen.

To obtain a deeper understanding of the factors that control reactions involving the  $ZnR_2/O_2$  system, detailed information about the structure and properties of the organozinc intermediates is undoubtedly needed. However, it is perhaps astonishing that the reported systematic studies on the mechanistic aspects concerning the oxygenation of homoleptic zinc alkyls essentially end in the late 1960s.<sup>[5]</sup> As part of the ongoing exploration of the fundamental question as to whether well-defined zinc peroxides/alkoxides can be synthesized by the selective oxygenation of dialkylzinc complexes, we have conducted several control experiments to probe for factors that influence the reactivity and selectivity in the reaction of  $Zn/Bu_2$  with dioxygen in the presence of donor ligands.

In the first step of our studies, a solution of  $Zn/Bu_2$  in THF at  $-78^\circ\text{C}$  was treated with an excess of molecular oxygen, and the reaction mixture was stirred for approximately one minute. Then, the excess  $O_2$  was removed in vacuum, and a white crystalline solid deposited from the solution after several hours at  $-25^\circ\text{C}$ . The spectroscopic data indicated that the interaction of the putative Lewis acid–base adduct  $[Zn/Bu_2(thf)]$  with  $O_2$  led to the selective oxygenation of one  $Zn-C$  bond and the formation of the alkoxide compound  $\{[Zn/Bu(\mu-OiBu)(thf)]_2\}$  (**1**, Scheme 2). The IR spectrum of the resulting product did not show the characteristic O–O peroxidic stretching vibration for alkylperoxide moieties, and the  $^1\text{H}$  NMR spectrum consisted of single resonances for each group of protons. Thus, the oxidation of the first  $Zn-C$  bond in the presence of THF does not lead to an isolable alkylperoxide species. Nevertheless, this process offers a





**Scheme 2.** Synthesis of **1** and **2**.

route for the selective formation of alkylzinc alkoxides. Repetition of the reaction at room temperature resulted in the formation of a complex mixture of inseparable products. The crystals of **1** that were obtained directly by the procedure outlined above were found to be suitable for single-crystal X-ray diffraction analysis. The structure consists of a centrosymmetric dimer in which the two four-coordinate zinc centers are bridged by the *tert*-butoxide groups with the formation of a planar  $\text{Zn}_2\text{O}_2$  core ( $\text{Zn1}-\text{O1}$  1.982(1) Å,  $\text{Zn1}-\text{O1}'$  1.986(1) Å, Figure 1). The coordination environment of

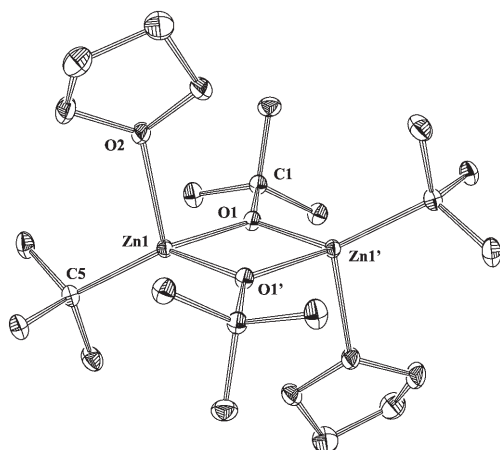


**Figure 1.** Molecular structure of **1** with thermal ellipsoids set at 30% probability; hydrogen atoms are omitted for clarity.

the zinc atoms is completed by one *tert*-butyl group ( $\text{Zn1}-\text{C5}$  2.016(2) Å) and one thf molecule ( $\text{Zn1}-\text{O2}$  2.239(1) Å).<sup>[16]</sup>

To determine the effect of the strength of donor ligands on the oxygenation reaction, we conducted the analogous studies in the presence of 4-methylpyridine (py-Me). We expected that the application of py-Me as a strong N-donor ligand should decrease the reactivity of the Lewis acid–base adduct  $[\text{Zn}(\text{tBu})_2(\text{py-Me})_n]$  as well as enhance the stability of the resulting oxygenated products. Indeed, when a solution of  $\text{Zn}(\text{tBu})_2$  in THF with one or two equivalents of py-Me was exposed to an excess of molecular oxygen (1 atm) at  $-78^\circ\text{C}$ , only traces of the oxygenation products were detected in the

$^1\text{H}$  NMR spectrum after two hours. However, when the reaction involving the 1:1 or 1:2  $\text{Zn}(\text{tBu})_2/\text{py-Me}$  system was conducted at about  $-45^\circ\text{C}$  for approximately 15 minutes, the *tert*-butylperoxide compound  $[\{\text{Zn}(\text{tBu})_2(\mu\text{-OOtBu})(\text{py-Me})\}_2]$  (**2**) was isolated in good yield as a colorless solid after work up. Apparently, the pyridine ligand stabilizes the *tert*-butylperoxide species that results from the insertion of  $\text{O}_2$  into one  $\text{Zn}-\text{C}$  bond. In the case of this  $\text{Zn}(\text{tBu})_2/\text{py-Me}$  system, the oxygenation reaction is easy to monitor as the reaction mixture is initially yellow and becomes colorless upon the formation of the *tert*-butylperoxide compound. Strikingly, we did not observe any induction period or inhibition of the oxygenation reaction in the presence of 0.1 mol % TEMPO (2,2,6,6-tetramethylpiperidine *N*-oxide).

The  $^1\text{H}$  NMR spectrum of **2** indicated two chemically inequivalent *tert*-butyl groups and one py-Me molecule. The presence of the  $\text{Zn}-\text{OOtBu}$  linkage was confirmed by the IR spectrum, which exhibited a band of weak intensity at  $868\text{ cm}^{-1}$  that is attributable to the O–O peroxidic stretching vibration. The alkylperoxide compound **2** is surprisingly stable in solution in a nitrogen atmosphere under ambient conditions. Prolonged exposure of the reaction mixture to dioxygen resulted in further oxygenation, albeit at a significantly slower rate than the first step. Presumably, the formation of relatively stable four-coordinate alkylzinc species inhibits the oxidation of the remaining  $\text{Zn}-\text{C}$  bonds.<sup>[6]</sup> Single crystals of **2** suitable for an X-ray crystal structure determination were grown from THF at  $-25^\circ\text{C}$ . As seen in Figure 2, the molecule adopts a dimeric aggregation in the solid state by bridging through the *tert*-butylperoxide groups and the two four-coordinate zinc centers. The coordination environment of the zinc atoms is completed by one *tert*-butyl group and one py-Me ligand. The *tert*-butylperoxide ligands are oriented in an eclipsed–staggered conformation. A similar *tert*-butylperoxide geometry was found in the related indium and gallium complexes  $[\{\text{M}(\text{tBu})_2(\mu\text{-OOtBu})\}_2]$ ,<sup>[17]</sup> and such a geometry presumably minimizes repulsion between the lone

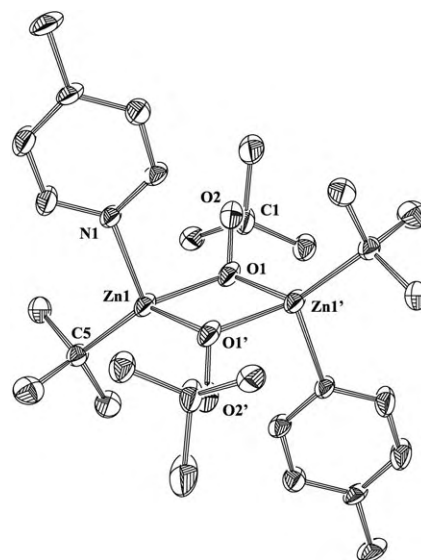
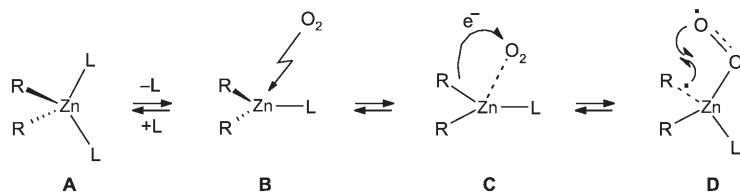


**Figure 2.** Molecular structure of **2** with thermal ellipsoids set at 30% probability; hydrogen atoms are omitted for clarity.

pairs of electrons on the oxygen atoms. The aromatic rings of the py-Me ligands are perpendicular with respect to the central  $\text{Zn}_2\text{O}_2$  ring. The corresponding bond lengths  $\text{Zn1-C5}$  (2.008(11) Å),  $\text{Zn1-O1}$  (1.990(8) Å), and  $\text{Zn1-O1'}$  (1.987(8) Å) and the  $\text{Zn1-O1-Zn1'}$  angle (101.88(27)°) are similar to those found for **1**. The  $\text{O1-O2}$  bond length of 1.4289(11) Å is close to that found in other zinc alkylperoxides.<sup>[6,7]</sup>

The results not only highlight the marked tendency of zinc dialkyls to undergo oxidation of only one alkyl group under controlled conditions but also demonstrate that the identity of the donor ligand has a significant influence on the oxygenation process. The relatively strong Lewis base py-Me essentially inhibited the oxygenation of  $\text{Zn}t\text{Bu}_2$  at  $-78^\circ\text{C}$ , whereas the reaction at slightly elevated temperature (ca.  $-45^\circ\text{C}$ ) resulted in the highly selective formation of the alkylzinc peroxide compound **2**. In contrast, the thf-solvated species  $[\text{Zn}t\text{Bu}_2(\text{thf})]$  reacted rapidly with dioxygen even at  $-78^\circ\text{C}$  to selectively form the alkylzinc alkoxide **1**. Our recent studies demonstrated that the attack of  $\text{O}_2$  on the three-coordinate metal center is the initial step in the oxygenation of the alkylzinc chelate complexes  $[\text{RZn}(\text{L}, \text{L}')_n]$  ( $\text{L}, \text{L}' = \text{deprotonated amino alcohol}$ ).<sup>[6]</sup> Thus, the lower reactivity of the methylpyridine adduct(s)  $[\text{Zn}t\text{Bu}_2(\text{py-Me})_n]$  toward  $\text{O}_2$  at  $-78^\circ\text{C}$  compared to that of the tetrahydrofuran adduct(s)  $[\text{Zn}t\text{Bu}_2(\text{thf})_n]$  may be understood in terms of the more hindered access of the oxygen molecule to the low-coordinate metal centers of the former species. Presumably, the dissociation of a ligand from the putative four-coordinate  $[\text{ZnR}_2(\text{L})_2]$  complex is required prior to the effective attack of dioxygen (see **A** and **B**, Scheme 3).<sup>[18]</sup>



**Scheme 3.** Proposed reaction pathways for dioxygen insertion into the Zn-C bond.

Furthermore, the selective formation of the partially oxygenated four-coordinate compounds **1** and **2** are perhaps unexpected in view of the high reactivity of previously reported zinc dialkyls toward dioxygen, though this result is fully consistent with our recent findings that four-coordinate alkylzinc species are inert toward further oxygenation.<sup>[6]</sup> Another key observation is the stabilization of the resulting alkylperoxide  $\text{Zn}(t\text{Bu})\text{OO}t\text{Bu}$  species by the nitrogen ligand.

The observed high selectivity is not consistent with the widely accepted mechanism involving a free-radical chain reaction that is initiated by an advantageous radical  $\text{R}^\cdot$  (Scheme 1). Moreover, our earlier studies demonstrated that the initial step in the oxygenation of the main-group-metal alkyls involves the attack of  $\text{O}_2$  on the metal center and that the approaching  $\text{O}_2$  molecule has strong geometric requirements.<sup>[19]</sup> These findings indicate that  $\text{O}_2$  must enter the first coordination sphere to oxidize alkylzinc complexes (**B**,

Scheme 3), and one may view the primary step as involving the noncovalent activation of  $\text{O}_2$  by the metal center (**C**). This weak interaction changes the electronic structure of the dioxygen molecule and induces low-energy pathways. Accordingly, the coordination of dioxygen to the metal center is followed by electron transfer from the Zn-C bond to  $\text{O}_2$  to afford a solvent-caged radical pair **D**. At low temperature the postulated caged radical pair rearranges to generate selectively the alkylperoxide **E** (triplet-to-singlet surface crossing is required in order to transform **D** into **E**). However, at higher temperature the alkyl radical may diffuse away from the cage, which potentially constitutes the source of alkyl radical. This view finds support in the mentioned observation that the thf solvate of  $\text{Zn}t\text{Bu}_2$  reacted with  $\text{O}_2$  with the formation of a complex mixture of products at ambient temperature.

In conclusion, the reported studies open the way for the preparative exploitation of reactions involving zinc dialkyls and dioxygen. Moreover, a plausible hypothesis concerning the mechanism of  $\text{O}_2$  activation by organometallic compounds has certainly been advanced. With more experimental results, it should then be possible to test and quantitatively improve the accuracy of the description of the proposed stepwise mechanism for the insertion of dioxygen into M-C bonds.

### Experimental Section

**1:** A stirred solution of  $\text{Zn}t\text{Bu}_2$  (0.403 g, 2.25 mmol) in THF (5 mL) was cooled to  $-78^\circ\text{C}$ . Under slightly reduced pressure an excess of dry dioxygen (1 atm) was introduced. After a minute the excess  $\text{O}_2$  was removed, and the system was purged with nitrogen by using a vacuum-nitrogen line. The reaction mixture was stored at  $-25^\circ\text{C}$ , and white crystalline product deposited. Yield: 76%;  $^1\text{H}$  NMR (400 MHz,  $[\text{D}_8]\text{THF}$ ,  $25^\circ\text{C}$ , TMS):  $\delta = 1.00$  (s, 9H,  $\text{C}(\text{CH}_3)_3$ ), 1.15 (s, 9H,  $\text{OC}(\text{CH}_3)_3$ ), 1.67 (m, 4H,  $\text{CH}_2$ ), 3.5 ppm (m, 4H,  $\text{OCH}_2$ ); IR (nujol):  $\tilde{\nu} = 1465(\text{s})$ ,  $1389(\text{s})$ ,  $1377(\text{s})$ ,  $1368(\text{s})$ ,  $1360(\text{s})$ ,  $1241(\text{s})$ ,  $1175(\text{s})$ ,  $1075(\text{m})$ ,  $1023(\text{m})$ ,  $1009(\text{m})$ ,  $940(\text{m})$ ,  $932(\text{m})$ ,  $895(\text{s})$ ,  $808(\text{m})$ ,  $756(\text{m})$ ,  $535\text{ cm}^{-1}$  (s). Elemental analysis (%) calcd for  $\text{C}_{24}\text{H}_{52}\text{O}_4\text{Zn}$ : C 53.93, H 9.74; found: C 53.82, H 9.78.

**2:** 4-Methylpyridine (0.209 g, 2.25 mmol) was added to a solution of  $\text{Zn}t\text{Bu}_2$  (0.403 g, 2.25 mmol) in THF (4 mL) at ambient temperature. The resulting yellow solution was then cooled to  $-45^\circ\text{C}$ , and an excess of dry dioxygen (1 atm) was introduced. The oxygenation was continued until the solution became colorless (ca. 15 min). The reaction mixture was cooled to  $-78^\circ\text{C}$ , and the system was purged with nitrogen by using a vacuum-nitrogen line. The mixture was stored at  $-25^\circ\text{C}$ , and white crystalline product deposited. Yield: 67%;  $^1\text{H}$  NMR (400 MHz,  $[\text{D}_8]\text{THF}$ ,  $25^\circ\text{C}$ , TMS):  $\delta = 0.95$  (s, 9H,  $\text{C}(\text{CH}_3)_3$ ), 1.00 (s, major, 9H,  $\text{C}(\text{CH}_3)_3$ ), 1.02 (s, major, 9H,  $\text{OOC}(\text{CH}_3)_3$ ), 1.10 (m, 9H,  $\text{OOC}(\text{CH}_3)_3$ ), 2.31 (s, 3H, py- $\text{CH}_3$ ), 7.20 (d,  $^3J(\text{H}, \text{H}) = 5.6\text{ Hz}$ , 2H, py), 8.52 ppm (d,  $^3J(\text{H}, \text{H}) = 5.6\text{ Hz}$ , 2H, py); the two observed inequivalent signals for the  $t\text{Bu}$  group and the  $\text{OO}t\text{Bu}$  group in the relative ratio 1:8 for each group indicates the presence of geometrical isomers of **2**; IR (nujol):  $\tilde{\nu} = 1670(\text{m})$ ,  $1622(\text{s})$ ,  $1607(\text{m})$ ,  $1584(\text{m})$ ,  $1562(\text{m})$ ,  $1504(\text{m})$ ,  $1463(\text{s})$ ,  $1377(\text{s})$ ,  $1355(\text{s})$ ,  $1251(\text{m})$ ,  $1238(\text{m})$ ,  $11228(\text{m})$ ,  $1218(\text{m})$ ,  $1195(\text{s})$ ,  $1162(\text{w})$ ,  $1117(\text{w})$ ,  $1099(\text{w})$ ,  $1070(\text{m})$ ,  $1024(\text{s})$ ,  $1010(\text{m})$ ,  $979(\text{w})$ ,  $958(\text{w})$ ,  $938(\text{w})$ ,

919(w), 895(w), 868(w), 840(m), 811(s), 804(s), 748(m), 722(m), 540 cm<sup>-1</sup> (s). Elemental analysis (%) calcd for C<sub>28</sub>H<sub>50</sub>N<sub>2</sub>O<sub>4</sub>Zn<sub>2</sub>: C 55.26, H 8.22, N 4.61; found: C 55.35, H 8.31, N 4.59.

Crystal data for **1**, C<sub>28</sub>H<sub>50</sub>N<sub>2</sub>O<sub>4</sub>: *M*<sub>r</sub> = 535.40, crystal dimensions 0.45 × 0.38 × 0.22 mm<sup>3</sup>, monoclinic, space group *P*2<sub>1</sub>/*c* (no. 14), *a* = 8.8503(2), *b* = 9.6881(2), *c* = 18.0968(3) Å, β = 117.2500(10)°, *V* = 1379.79(4) Å<sup>3</sup>, *Z* = 2, *F*(000) = 576, ρ<sub>calcd</sub> = 1.289 g cm<sup>-3</sup>, θ<sub>max</sub> = 27.49°, *R*<sub>1</sub> = 0.0335, *wR*<sub>2</sub> = 0.0845 for 2841 reflections with *I*<sub>o</sub> > 2σ(*I*<sub>o</sub>). The structure was solved by direct methods with the SHELXS-97<sup>[20]</sup> program and was refined by full matrix least squares on *F*<sup>2</sup> by using the program SHELXL-97.<sup>[21]</sup> H-atoms were included in idealized positions and refined isotropically. Crystal data for **2**, C<sub>28</sub>H<sub>50</sub>N<sub>2</sub>O<sub>4</sub>: *M*<sub>r</sub> = 609.44, crystal dimensions 0.50 × 0.45 × 0.25 mm<sup>3</sup>, triclinic, space group *P*1̄ (no. 2), *a* = 8.9759(9), *b* = 9.2799(8), *c* = 10.8850(12) Å, α = 113.108(4), β = 98.931(6), γ = 101.346(6)°, *V* = 790.18(15) Å<sup>3</sup>, *Z* = 1, *F*(000) = 324, ρ<sub>calcd</sub> = 1.281 g cm<sup>-3</sup>, θ<sub>max</sub> = 20.98°. The structure was solved by direct methods with the SHELXS-97<sup>[20]</sup> program and was refined by full matrix least-squares on *F*<sup>2</sup> by using the program SHELXL-97.<sup>[21]</sup> H-atoms were included in idealized positions and refined isotropically. Final *R* indices: *R*<sub>1</sub> = 0.0694, *wR*<sub>2</sub> = 0.1824 for 1359 reflections with *I*<sub>o</sub> > 2σ(*I*<sub>o</sub>). CCDC-297287 (**1**) and CCDC-297288 (**2**) contain the supplementary crystallographic data for this paper. These data can be obtained free of charge from The Cambridge Crystallographic Data Centre via www.ccdc.cam.ac.uk/data\_request/cif.

Received: March 14, 2006

Published online: June 23, 2006

**Keywords:** alkylperoxo ligands · dioxygen activation · reaction mechanisms · structure elucidation · zinc

- [1] E. Frankland, *Justus Liebigs Ann. Chem.* **1849**, 71, 171.
- [2] A. Butlerov, *Z. Pharm. Chem.* **1864**, 7, 402.
- [3] A. Lissenko, *Jahresber. Pharm.* **1864**, 470.
- [4] R. Demuth, V. Meyer, *Ber. Dtsch. Chem. Ges.* **1890**, 23, 394.
- [5] For selected examples, see: a) H. Thompson, N. S. Kelland, *J. Chem. Soc.* **1933**, 746; b) C. H. Bamford, D. M. Newitt, *J. Chem. Soc.* **1946**, 688; c) M. H. Abraham, *J. Chem. Soc.* **1960**, 4130; d) G. A. Razuvayev, *Zh. Obshch. Khim.* **1963**, 33, 3358; e) G. Sosnovsky, J. H. Brown, *Chem. Rev.* **1966**, 66, 529; f) A. G. Davies, B. P. Roberts, *J. Chem. Soc. B* **1968**, 1074.
- [6] J. Lewiński, W. Marciniak, I. Justyniak, J. Lipkowski, *J. Am. Chem. Soc.* **2003**, 125, 12698.
- [7] J. Lewiński, Z. Ochal, E. Bojarski, E. Tratkiewicz, I. Justyniak, J. Lipkowski, *Angew. Chem.* **2003**, 115, 4791; *Angew. Chem. Int. Ed.* **2003**, 42, 4643.
- [8] J. M. Grévy in *Encyclopedia of Inorganic Chemistry*, Vol. 9 (Ed.: R. B. King), Wiley, Chichester, **2005**, p. 5953.
- [9] a) M. Monge, M. L. Kahn, A. Maisonnat, B. Chaudret, *Angew. Chem.* **2003**, 115, 5479; *Angew. Chem. Int. Ed.* **2003**, 42, 5321; b) M. L. Kahn, M. Monge, V. Colliere, F. Senocq, A. Maisonnat, B. Chaudret, *Adv. Funct. Mater.* **2005**, 15, 458.
- [10] Alkylzinc alkoxides that are derived from dialkylzinc and the corresponding alcohol have also recently been employed as single-molecule precursors for the synthesis of ZnO by thermolytic methods: a) C. G. Kim, K. Sung, T. M. Chung, D. Y. Jung, Y. Kim, *Chem. Commun.* **2003**, 2068; b) J. Hambrock, S. Rabe, K. Merz, A. Birkner, A. Wohlfart, R. A. Fisher, M. Driess, *J. Mater. Chem.* **2003**, 13, 1731; c) T. J. Boyle, S. D. Bunge, N. L. Andrews, L. E. Matzen, K. Sieg, M. A. Rodriguez, T. J. Headley, *Chem. Mater.* **2004**, 16, 3279; d) S. Polarz, A. Roy, M. Merz, S. Halm, D. Schröder, L. Schneider, G. Bacher, F. K. Kruis, M. Driess, *Small* **2005**, 1, 540.
- [11] For selected examples, see: a) H. Hock, H. Kropf, F. Ernst, *Angew. Chem.* **1959**, 71, 541; b) H. Hock, F. Ernst, *Chem. Ber.* **1959**, 92, 2716; c) H. E. Seyfarth, J. Henkel, A. Rieche, *Angew. Chem.* **1965**, 77, 1078; *Angew. Chem. Int. Ed. Engl.* **1965**, 4, 1074; d) I. Klement, H. Lütjens, P. Knochel, *Tetrahedron Lett.* **1995**, 36, 3136; e) F. Chemla, J. Normant, *Tetrahedron Lett.* **1995**, 36, 3157; f) T. Harada, E. Kutsuwa, *J. Org. Chem.* **2003**, 68, 6716.
- [12] K. Yamamoto, N. Yamamoto, *Chem. Lett.* **1989**, 1149.
- [13] D. Enders, J. Zhu, G. Raabe, *Angew. Chem.* **1996**, 108, 1827; *Angew. Chem. Int. Ed. Engl.* **1996**, 35, 1725.
- [14] Very recently, ZnOOR species were also used for the stereoselective and chemoselective epoxidation of allylic olefins. a) A. R. Kelly, A. E. Lurain, P. J. Walsh, *J. Am. Chem. Soc.* **2005**, 127, 14668; b) P. J. Carroll, A. E. Lurain, P. J. Walsh, *J. Org. Chem.* **2005**, 70, 1262.
- [15] For selected recent examples, see: a) S. Bazin, L. Feray, N. Vanthuyne, M. P. Bertrand, *Tetrahedron* **2005**, 61, 4261; b) K. I. Yamada, Y. Yamamoto, M. Maekawa, K. Tomioka, *J. Org. Chem.* **2004**, 69, 1531; c) K. Yamada, Y. Yamamoto, M. Maekawa, J. B. Chen, K. Tomioka, *Tetrahedron Lett.* **2004**, 45, 6595; d) Y. Yamamoto, K. Yamada, K. Tomioka, *Tetrahedron Lett.* **2004**, 45, 795; e) H. Miyabe, A. Nishimura, Y. Fujishima, T. Naito, *Tetrahedron* **2003**, 59, 1901; f) K. Yamada, Y. Yamamoto, K. Tomioka, *Org. Lett.* **2003**, 5, 797.
- [16] We note that during the course of our studies a publication reporting the synthesis and molecular structure of [[ZnBu(μ-OrBu)(thf)]<sub>2</sub>], which was derived from the direct reaction between ZnBu<sub>2</sub> and *t*BuOH, appeared; see reference [10c].
- [17] a) W. C. Cleaver, A. R. Barron, *J. Am. Chem. Soc.* **1989**, 111, 8966; b) M. B. Power, J. W. Ziller, A. R. Barron, *Organometallics* **1993**, 12, 4908.
- [18] It is reasonable to assume that the four-coordinate adducts [ZnBu<sub>2</sub>(py-Me)<sub>2</sub>] and [ZnBu<sub>2</sub>(py-Me)(thf)] are relatively stable at low temperature in contrast to the [ZnBu<sub>2</sub>(thf)<sub>2</sub>] adduct, which likely easily dissociates to the three-coordinate species [ZnBu<sub>2</sub>(thf)] even at -78°C. For a discussion of the relative stability of zinc dialkyls with donor ligands, see: A. C. Jones, P. O'Brien, *CVD of Compound Semiconductors*, VCH, Weinheim, **1997**, chap. 2.
- [19] J. Lewiński, J. Zachara, P. Goś, E. Grabska, T. Kopeć, I. Madura, W. Marciniak, I. Prowotorow, *Chem. Eur. J.* **2000**, 6, 3215.
- [20] G. M. Sheldrick, *Acta Crystallogr. Sect. A* **1990**, 46, 467.
- [21] G. M. Sheldrick, University Göttingen, Germany, **1997**.

DOI: 10.1002/anie.200601060

**Experimental Evidence for Linear Metal–Azido Coordination: The Binary Group 5 Azides [Nb(N<sub>3</sub>)<sub>5</sub>], [Ta(N<sub>3</sub>)<sub>5</sub>], [Nb(N<sub>3</sub>)<sub>6</sub>]<sup>−</sup>, and [Ta(N<sub>3</sub>)<sub>6</sub>]<sup>−</sup>, and 1:1 Acetonitrile Adducts [Nb(N<sub>3</sub>)<sub>5</sub>(CH<sub>3</sub>CN)] and [Ta(N<sub>3</sub>)<sub>5</sub>(CH<sub>3</sub>CN)]\*\***

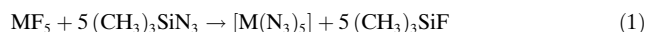
Ralf Haiges,\* Jerry A. Boatz, Thorsten Schroer, Muhammed Yousufuddin, and Karl O. Christe\*

*Dedicated to Professor Reint Eujen on the occasion of his 60th birthday*

Whereas the existence of numerous binary transition-metal–azido complexes has been reported,<sup>[1–3]</sup> no binary Group 5 azides are known. Only a limited number of partially azido-substituted compounds of vanadium, niobium, and tantalum have previously been reported.<sup>[4–21]</sup>

Herein, we communicate the synthesis and characterization of [Nb(N<sub>3</sub>)<sub>5</sub>], [Ta(N<sub>3</sub>)<sub>5</sub>], and their 1:1 adducts with CH<sub>3</sub>CN, as well as the anions [Nb(N<sub>3</sub>)<sub>6</sub>]<sup>−</sup> and [Ta(N<sub>3</sub>)<sub>6</sub>]<sup>−</sup>. The crystal structures of [Nb(N<sub>3</sub>)<sub>5</sub>(CH<sub>3</sub>CN)] and [PPh<sub>4</sub>][Nb(N<sub>3</sub>)<sub>6</sub>] and the first experimental evidence for the existence of azido compounds with linear M–N–N coordination are also reported.

The reactions of NbF<sub>5</sub> or TaF<sub>5</sub> with excess (CH<sub>3</sub>)<sub>3</sub>SiN<sub>3</sub> in SO<sub>2</sub> solution at −20 °C resulted in complete fluorido–azido exchange and yielded clear solutions of [Nb(N<sub>3</sub>)<sub>5</sub>] or [Ta(N<sub>3</sub>)<sub>5</sub>], respectively [Eq. (1) (M = Nb, Ta)].



When the volatile compounds (SO<sub>2</sub>, (CH<sub>3</sub>)<sub>3</sub>SiF, and excess (CH<sub>3</sub>)<sub>3</sub>SiN<sub>3</sub>) were removed in a vacuum at −20 °C, pure, yellow, solid, room-temperature-stable pentaazido complexes were produced in quantitative yield. As expected for covalently bonded polyazido complexes,<sup>[22]</sup> they are shock-sensitive and can explode violently when touched with a metal spatula or by heating in the flame of a Bunsen burner. Their identity was established by the observed mass balances, vibrational spectroscopy, and their conversions with N<sub>3</sub><sup>−</sup> into hexaazido metalates and with CH<sub>3</sub>CN into 1:1 acetonitrile donor–acceptor adducts, as shown by the crystal structures of [P(C<sub>6</sub>H<sub>5</sub>)<sub>4</sub>]<sup>+</sup>[Nb(N<sub>3</sub>)<sub>6</sub>]<sup>−</sup> and [Nb(N<sub>3</sub>)<sub>5</sub>(CH<sub>3</sub>CN)].

The observed IR and Raman spectra of [Nb(N<sub>3</sub>)<sub>5</sub>] and [Ta(N<sub>3</sub>)<sub>5</sub>] are shown in the Supporting Information, and the observed frequencies and intensities are listed in the Experimental Section. These data were assigned by comparison with those calculated at the B3LYP<sup>[23]</sup> and MP2<sup>[24]</sup> levels of theory by using SBKJ + (d) basis sets.<sup>[25]</sup> The agreement between the observed and calculated spectra is satisfactory and supports the existence of trigonal-bipyramidal structures (Table 1) for [Nb(N<sub>3</sub>)<sub>5</sub>] and [Ta(N<sub>3</sub>)<sub>5</sub>]. The internal vibrational modes of the azido ligands are split into clusters of five as a result of in-phase and out-of-phase coupling of the individual motions. There are always one in-phase and four out-of-phase vibrations, with the in-phase vibration readily identifiable from its higher Raman intensity. The MN<sub>5</sub> skeletal modes can be derived from D<sub>3h</sub> symmetry in which the double degeneracy of the E modes is lifted as a result of the presence of the azido ligands, which lowers the overall symmetry to C<sub>s</sub> and is likely to produce some distortion from D<sub>3h</sub> symmetry.

Whereas trigonal-bipyramidal arrangements of the azido ligands have previously also been found for [Fe(N<sub>3</sub>)<sub>5</sub>]<sup>2−</sup><sup>[26]</sup> and theoretically predicted for [Sb(N<sub>3</sub>)<sub>5</sub>] and [As(N<sub>3</sub>)<sub>5</sub>],<sup>[27,28]</sup> the details of these structures are very different. In [Fe(N<sub>3</sub>)<sub>5</sub>]<sup>2−</sup>, [As(N<sub>3</sub>)<sub>5</sub>], and [Sb(N<sub>3</sub>)<sub>5</sub>], all five M–N–N units are strongly bent, and the two axial M–N bonds are significantly longer than the equatorial ones, as expected from VSEPR arguments.<sup>[29]</sup> In contrast, the axial M–N–N arrangements in [Nb(N<sub>3</sub>)<sub>5</sub>] and [Ta(N<sub>3</sub>)<sub>5</sub>] are calculated to be almost linear, while the equatorial ones have calculated angles of about 137°. Furthermore, all five M–N bond lengths and the internal N–N bond lengths of the five azido ligands are essentially the same in each compound.

Linear M–N–N coordination had previously been predicted also for the tetraazido complexes of the d<sup>0</sup> centers Ti<sup>IV</sup>, Zr<sup>IV</sup>, and Hf<sup>IV</sup>,<sup>[30]</sup> as well as for the d<sup>6</sup> Fe<sup>II</sup> center,<sup>[31]</sup> but the hexaazido dianion of the d<sup>0</sup> Ti<sup>IV</sup> center was shown experimentally to possess strongly bent Ti–N–N units.<sup>[1]</sup> These findings show that the linearity of the M–N–N units cannot be caused by either a trigonal-bipyramidal structure, multiple M–N bonds, or a d<sup>0</sup> electronic configuration per se.

The occurrence of linear M–N–N groups can be predicted by theoretical calculations.<sup>[30,31]</sup> A plausible explanation for the linearity of these M–N–N groups has recently been given,<sup>[1]</sup> as based on an analogy with the known crystal structure of [Zr(BH<sub>4</sub>)<sub>4</sub>].<sup>[32]</sup> A tentative model was proposed in which the N<sub>α</sub> atoms of the azido ligands act as tridative<sup>[1]</sup> ligands.

[\*] Dr. R. Haiges, Dr. T. Schroer, Dr. M. Yousufuddin, Prof. Dr. K. O. Christe  
Loker Research Institute and Department of Chemistry  
University of Southern California  
Los Angeles, CA 90089-1661 (USA)  
Fax: (+1) 213-740-6679  
E-mail: haiges@usc.edu  
kchriste@usc.edu

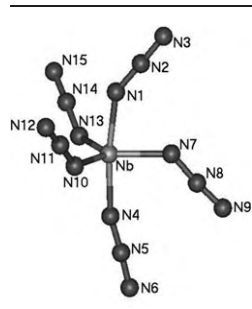
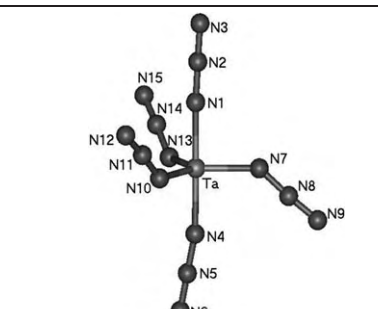
Dr. J. A. Boatz  
Space and Missile Propulsion Division  
Air Force Research Laboratory (AFRL/PRSP)  
10 East Saturn Boulevard, Bldg 8451  
Edwards Air Force Base, CA 93524 (USA)

[\*\*] This work was funded by the Air Force Office of Scientific Research and the National Science Foundation. We thank Prof. Dr. G. A. Olah and Dr. M. Berman for their steady support, and Prof. D. Dixon, Prof. Dr. R. Bau, Drs. R. Wagner and W. W. Wilson, and C. Bigler Jones for their help and stimulating discussions. We gratefully acknowledge grants of computer time at the Aeronautical Systems Center (Wright–Patterson Air Force Base, Dayton, OH), the Naval Oceanographic Office (Stennis Space Center, MS), the Engineer Research and Development Center (Vicksburg, MS), the Army Research Laboratory (Aberdeen Proving Ground, MD), and the Army High Performance Computing Research Center (Minneapolis, MN), under sponsorship of the Department of Defense High Performance Computing Modernization Program Office.

Supporting information for this article is available on the WWW under <http://www.angewandte.org> or from the author.

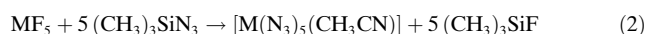


**Table 1:** Calculated structures of  $[\text{Nb}(\text{N}_3)_5]$  and  $[\text{Ta}(\text{N}_3)_5]$  at the B3LYP/SBKJ + (d) level of theory (MP2/SBKJ + (d) values in parentheses).

			
Bond lengths [Å]		Bond lengths [Å]	
Nb-N1	2.025 (2.013)	Ta-N1	1.997 (1.996)
Nb-N4	2.001 (2.002)	Ta-N4	1.991 (1.993)
Nb-N7	2.048 (2.060)	Ta-N7	2.003 (1.997)
Nb-N10	2.008 (2.014)	Ta-N10	2.008 (2.009)
Nb-N13	2.008 (2.014)	Ta-N13	2.008 (2.009)
N1-N2	1.234 (1.241)	N1-N2	1.226 (1.235)
N4-N5	1.230 (1.241)	N4-N5	1.225 (1.234)
N7-N8	1.243 (1.249)	N7-N8	1.240 (1.242)
N10-N11	1.240 (1.245)	N10-N11	1.240 (1.244)
N13-N14	1.240 (1.245)	N13-N14	1.240 (1.244)
N2-N3	1.162 (1.208)	N2-N3	1.163 (1.209)
N5-N6	1.163 (1.210)	N5-N6	1.163 (1.209)
N8-N9	1.162 (1.210)	N8-N9	1.160 (1.206)
N11-N12	1.160 (1.208)	N11-N12	1.160 (1.206)
N14-N15	1.160 (1.208)	N14-N15	1.160 (1.206)
Bond angles [°]		Bond angles [°]	
N1-Nb-N4	171.9 (169.0)	N1-Ta-N4	179.2 (177.9)
N1-Nb-N7	82.8 (81.4)	N1-Ta-N7	89.4 (90.2)
N1-Nb-N10	91.0 (92.1)	N1-Ta-N10	90.2 (89.8)
N1-Nb-N13	91.0 (92.1)	N1-Ta-N13	90.2 (89.8)
N4-Nb-N7	89.1 (87.6)	N4-Ta-N7	91.4 (91.8)
N4-Nb-N10	93.2 (93.6)	N4-Ta-N10	89.4 (89.2)
N4-Nb-N13	93.2 (93.6)	N4-Ta-N13	89.4 (89.2)
N7-Nb-N10	121.3 (121.3)	N7-Ta-N10	119.6 (119.1)
N7-Nb-N13	121.3 (121.3)	N7-Ta-N13	119.6 (119.1)
N10-Nb-N13	117.2 (117.1)	N10-Ta-N13	120.9 (121.7)
Nb-N1-N2	145.3 (147.2)	Ta-N1-N2	176.9 (178.5)
Nb-N4-N5	165.0 (157.3)	Ta-N4-N5	169.3 (173.8)
Nb-N7-N8	131.8 (130.8)	Ta-N7-N8	137.7 (143.0)
Nb-N10-N11	137.2 (138.8)	Ta-N10-N11	137.1 (138.9)
Nb-N13-N14	137.2 (138.8)	Ta-N13-N14	137.1 (138.9)

However, this explanation might be incorrect, and a detailed analysis of the occurrence of linear M-N-N configurations in the periodic system and of the nature of the bonds involved is presently being carried out by us and will be the subject of a future publication.

By using  $\text{CH}_3\text{CN}$  instead of  $\text{SO}_2$  as a solvent for the reactions of  $\text{NbF}_5$  and  $\text{TaF}_5$  with excess  $(\text{CH}_3)_3\text{SiN}_3$ , yellow solutions of  $[\text{Nb}(\text{N}_3)_5(\text{CH}_3\text{CN})]$  and  $[\text{Ta}(\text{N}_3)_5(\text{CH}_3\text{CN})]$ , respectively, were obtained [Eq. (2) ( $\text{M} = \text{Nb}, \text{Ta}$ )].



Removal of the volatile compounds ( $\text{CH}_3\text{CN}$ ,  $(\text{CH}_3)_3\text{SiF}$ , and excess  $(\text{CH}_3)_3\text{SiN}_3$ ) at  $-20^\circ\text{C}$  resulted in the isolation of the acetonitrile adducts of the pentaazido complexes.

Although still dangerous and explosive, both acetonitrile adducts are less shock-sensitive than the corresponding donor-free complexes.

Both acetonitrile adducts were isolated as yellow solids and were characterized by vibrational spectroscopy, their conversions with  $\text{N}_3^-$  into the hexaazido metalates, and, in the case of  $[\text{Nb}(\text{N}_3)_5(\text{CH}_3\text{CN})]$ , by its crystal structure.<sup>[33]</sup> The observed Raman spectra of  $[\text{Nb}(\text{N}_3)_5(\text{CH}_3\text{CN})]$  and  $[\text{Ta}(\text{N}_3)_5(\text{CH}_3\text{CN})]$  are shown in Figure 1 and in the Supporting

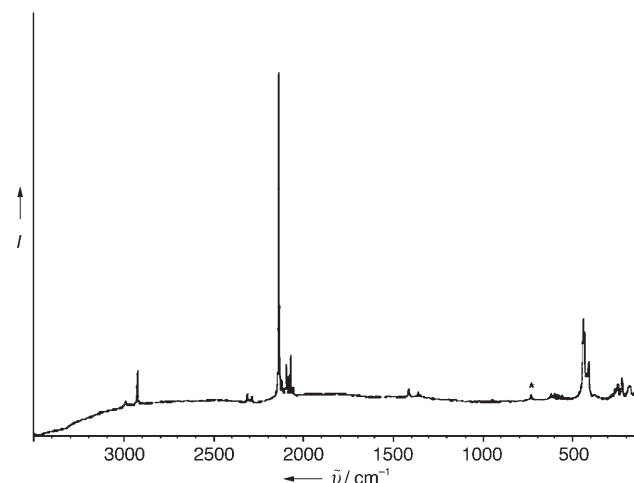


**Figure 1.** Raman spectrum of solid  $[\text{Nb}(\text{N}_3)_5(\text{CH}_3\text{CN})]$ . The band marked by an asterisk (\*) is from the teflon-FEP sample tube.

Information, respectively, and their frequencies and intensities are given in the Experimental Section. A comparison with the calculated spectra is given in the Supporting Information, and the given assignments are in accord with those previously reported<sup>[34,35]</sup> for the related  $[\text{SbF}_5(\text{CH}_3\text{CN})]$  adduct.

$[\text{Nb}(\text{N}_3)_5(\text{CH}_3\text{CN})]$  crystallizes in the monoclinic space group  $P2_1/c$ . The X-ray structure analysis<sup>[33]</sup> (Figure 2) reveals the presence of isolated  $[\text{Nb}(\text{N}_3)_5(\text{CH}_3\text{CN})]$  units. The closest intermolecular  $\text{Nb} \cdots \text{N}$  and  $\text{N} \cdots \text{N}$  contacts are 3.98 Å and 3.04 Å, respectively. The molecule consists of a pseudo-octahedral  $\text{NbN}_6$  skeleton with the  $\text{CH}_3\text{CN}$  ligand and one azido ligand in the axial positions. The equatorial positions are occupied by the remaining four azido ligands, which, interestingly, are all bent away from the axial azido ligand. The axial  $\text{Nb}-\text{N}_{\text{axial}}$  bond length is about 0.09 Å shorter than the four equatorial ones. The most interesting feature, however, is the fact that the axial azido ligand exhibits a large  $\text{Nb}-\text{N}-\text{N}$  bond angle of  $168.8(3)^\circ$ , compared to an average angle of  $137.8^\circ$  for the four equatorial ligands. The small deviation of the observed axial  $\text{Nb}-\text{N}-\text{N}$  bond angle from  $180^\circ$  is attributed to solid-state effects, as our theoretical calculations for the free gaseous molecule at the B3LYP and MP2 levels of theory with an SBKJ + (d) basis set resulted in  $\text{Nb}-\text{N}-\text{N}$  bond angles of  $179.6^\circ$  and  $178.3^\circ$ , respectively. For free  $[\text{Ta}(\text{N}_3)_5(\text{CH}_3\text{CN})]$ , analogous calculations gave  $\text{Ta}-\text{N}-\text{N}$  bond angles of  $179.6^\circ$  and  $180.0^\circ$ . The significant shortening of the axial  $\text{Nb}-\text{N}_{\text{axial}}$  bond length can be attributed to a *trans* effect that is caused by the long  $\text{Nb}-\text{NCCCH}_3$  bond.

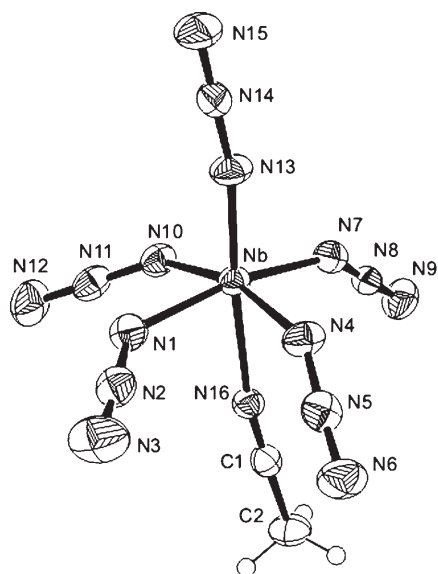
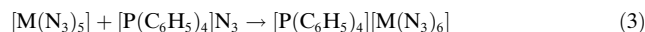


**Figure 2.** ORTEP plot of  $[\text{Nb}(\text{N}_3)_5(\text{CH}_3\text{CN})]$ . Thermal ellipsoids are shown at the 50% probability level. Selected bond lengths [Å] and angles [°]: Nb–N1 2.031(3), Nb–N4 1.998(3), Nb–N7 2.004(3), Nb–N10 2.017(3), Nb–N13 1.935(3), Nb–N16 2.259(3), N1–N2 1.217(4), N2–N3 1.139(4), N4–N5 1.212(4), N5–N6 1.133(4), N7–N8 1.212(4), N8–N9 1.129(4), N10–N11 1.211(4), N11–N12 1.132(4), N13–N14 1.205(4), N14–N15 1.137(4), N16–C1 1.139(4), C1–C2 1.447(5); N1–Nb–N4 87.55(12), N1–Nb–N7 165.51(11), N1–Nb–N10 82.89(12), N1–Nb–N13 99.16(12), N1–Nb–N16 84.59(10), N4–Nb–N7 93.90(12), N4–Nb–N10 162.91(12), N4–Nb–N13 96.38(12), N4–Nb–N16 81.15(10), N7–Nb–N10 91.93(11), N7–Nb–N13 95.01(12), N7–Nb–N16 81.40(11), N10–Nb–N13 99.11(12), N10–Nb–N16 83.86(10), N13–Nb–N16 175.45(11), Nb–N1–N2 132.7(2), Nb–N4–N5 141.9(2), Nb–N7–N8 144.1(2), Nb–N10–N11 132.3(2), Nb–N13–N14 168.8(3), Nb–N16–C1 170.6(3).

The average Nb–N<sub>azido</sub> bond length of 1.997 Å in  $[\text{Nb}(\text{N}_3)_5(\text{CH}_3\text{CN})]$  is significantly smaller than those found for the terminal azido ligands of two isomers of  $[\{\text{Cp}^*\text{NbCl}(\text{N}_3)(\mu\text{-N}_3)_2(\mu\text{-O})\}]^{16}$  (2.081 Å and 2.105 Å) and that found for the cluster  $[\text{Nb}_6\text{Br}_{12}(\text{N}_3)_6]^{4-}$ <sup>[18]</sup> (2.27 Å), but slightly longer than that found in  $[\text{NbCl}_5(\text{N}_3)]^{-}$ <sup>[19]</sup> (1.92 Å), and is attributed to varying degrees of ionicity of the azido ligands in these compounds.

The reactions of the pentaazido complexes with ionic azides, such as  $[\text{P}(\text{C}_6\text{H}_5)_4]^+\text{N}_3^-$ , in  $\text{CH}_3\text{CN}$  solution produced the corresponding  $[\text{Nb}(\text{N}_3)_6]^-$  and  $[\text{Ta}(\text{N}_3)_6]^-$  salts [Eq. (3) ( $\text{M} = \text{Nb}, \text{Ta}$ )].



The hexaazido niobates and tantalates were isolated as yellow-orange solids and are stable at room temperature. The compounds were characterized by the observed mass balances, vibrational spectroscopy, and, in the case of  $[\text{P}(\text{C}_6\text{H}_5)_4][\text{Nb}(\text{N}_3)_6]$ , by its crystal structure.<sup>[36]</sup> The observed vibrational spectra of  $[\text{P}(\text{C}_6\text{H}_5)_4][\text{Nb}(\text{N}_3)_6]$  and  $[\text{P}(\text{C}_6\text{H}_5)_4][\text{Ta}(\text{N}_3)_6]$  are shown in the Supporting Information, and their frequencies and intensities are given in Table 2 ( $[\text{Nb}(\text{N}_3)_6]^-$ ) and in the Experimental Section ( $[\text{Ta}(\text{N}_3)_6]^-$ ). The free  $[\text{Nb}(\text{N}_3)_6]^-$  anion is predicted to have perfect  $S_6$  ( $\equiv C_{3i}$ ) symmetry in the gas phase, which is quite rare,<sup>[37]</sup> and, therefore, a complete

vibrational analysis was carried out (Table 2).  $[\text{Ta}(\text{N}_3)_6]^-$  is slightly distorted from  $S_6$  to  $C_1$  symmetry, but its structure is almost identical to that of  $[\text{Nb}(\text{N}_3)_6]^-$ , and the splittings of its degenerate vibrational modes are extremely small (Supporting Information).

Because of the presence of a large counterion, which serves as an inert spacer and suppresses detonation propagation, these salts are much less shock-sensitive than  $[\text{Nb}(\text{N}_3)_5]$  and  $[\text{Ta}(\text{N}_3)_5]$ , and are thermally surprisingly stable. Single crystals of  $[\text{P}(\text{C}_6\text{H}_5)_4][\text{Nb}(\text{N}_3)_6]$  were obtained by recrystallization from  $\text{CH}_3\text{CN}$ . The salt crystallizes in the rare orthorhombic space group  $P2_12_12$ . The X-ray structure analysis<sup>[36]</sup> of  $[\text{P}(\text{C}_6\text{H}_5)_4][\text{Nb}(\text{N}_3)_6]$  (Figure 3) reveals no significant

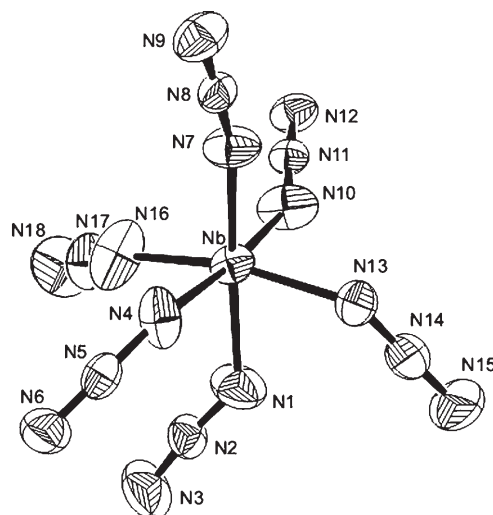


**Figure 3.** ORTEP plot of the anion in the crystal structure of  $[\text{P}(\text{C}_6\text{H}_5)_4][\text{Nb}(\text{N}_3)_6]$ . Thermal ellipsoids are shown at the 50% probability level. Selected bond lengths [Å] and angles [°]: Nb–N1 2.078(5), Nb–N4 2.035(4), Nb–N7 1.989(4), Nb–N10 2.008(4), Nb–N13 2.032(4), Nb–N16 2.026(5), N1–N2 1.164(5), N2–N3 1.126(6), N4–N5 1.198(5), N5–N6 1.128(5), N7–N8 1.192(5), N8–N9 1.133(5), N10–N11 1.196(5), N11–N12 1.118(5), N13–N14 1.203(6), N14–N15 1.137(6), N16–N17 1.173(6), N17–N18 1.137(6); N1–Nb–N4 89.54(19), N1–Nb–N7 173.25(18), N1–Nb–N10 94.23(18), N1–Nb–N13 80.45(18), N1–Nb–N16 85.2(2), N4–Nb–N7 86.30(18), N4–Nb–N10 174.15(18), N4–Nb–N13 95.40(15), N4–Nb–N16 86.78(17), N7–Nb–N10 90.34(17), N7–Nb–N13 94.63(17), N7–Nb–N16 99.86(19), N10–Nb–N13 89.63(18), N10–Nb–N16 89.1(2), N13–Nb–N16 165.46(18), Nb–N1–N2 134.4(4), Nb–N4–N5 141.2(4), Nb–N7–N8 156.2(4), Nb–N10–N11 152.3(4), Nb–N13–N14 131.7(4), Nb–N16–N17 142.3(4).

cation–anion and anion–anion interactions. The closest intermolecular Nb⋯N and N⋯N contacts are 4.20 Å and 3.15 Å, respectively. The structure of the  $[\text{Nb}(\text{N}_3)_6]^-$  anion in the solid state is distorted from the perfect  $S_6$  symmetry that was predicted by our theoretical calculations for the free anion in the gas phase, and has a structure similar to those of  $[\text{As}(\text{N}_3)_6]^-$ ,<sup>[28]</sup>  $[\text{Sb}(\text{N}_3)_6]^-$ ,<sup>[27]</sup>  $[\text{Si}(\text{N}_3)_6]^-$ ,<sup>[38]</sup>  $[\text{Ge}(\text{N}_3)_6]^-$ ,<sup>[39]</sup> and  $[\text{Ti}(\text{N}_3)_6]^{2-}$ ,<sup>[1]</sup> but contrary to that of  $[\text{Te}(\text{N}_3)_6]^{2-}$ <sup>[40]</sup> which contains a sterically active free valence electron pair on its central atom. The average Nb–N bond length in  $[\text{Nb}(\text{N}_3)_6]^-$  (2.027 Å) is larger than that found for  $[\text{Nb}(\text{N}_3)_5(\text{CH}_3\text{CN})]$  (1.997 Å), as expected from the formal negative charge in the

**Table 2:** Comparison of observed and unscaled calculated vibrational frequencies [ $\text{cm}^{-1}$ ] and intensities for  $[\text{Nb}(\text{N}_3)_6]^{-}$  in point group  $S_6$ .

Description			Observed	Calculated <sup>[b]</sup> (IR) [Raman]	
			IR	B3LYP/SBKJ + (d)	MP2/SBKJ + (d)
$A_g$	$\nu_1$	$\nu_{as}\text{N}_3$		2131 (10.0)	2129 (0) [1388]
				2112 (5.6)	
	$\nu_2$	$\nu_s\text{N}_3$		1342 (2.0)	1283 (0) [60]
	$\nu_3$	$\delta\text{N}_3$		616 (2.8)	565 (0) [39]
	$\nu_4$	$\delta\text{N}_3$			524 (0) [2.3]
	$\nu_5$	$\nu_s\text{NbN}_6$		433 (5.3)	402 (0) [367]
				414 (4.8)	
	$\nu_6$	$\delta_s\text{NbN}_6$		225 (3.5)	242 (0) [51]
	$\nu_7$	$\tau$		74 (0) [14]	72 (0) [31]
	$\nu_8$	$\tau$		34 (0) [37]	32 (0) [39]
$E_g$	$\nu_9$	$\nu_{as}\text{N}_3$		2080 (2.1)	2146 (0) [110]
				2060 (2.3)	
	$\nu_{10}$	$\nu_s\text{N}_3$		1413 (0) [50]	1279 (0) [154]
	$\nu_{11}$	$\delta\text{N}_3$		582 (0) [8.4]	550 (0) [73]
	$\nu_{12}$	$\delta\text{N}_3$		580 (0) [0.63]	521 (0) [4.2]
	$\nu_{13}$	$\nu_s\text{NbN}_6$		334 (0) [12]	350 (0) [38]
	$\nu_{14}$	$\delta_s\text{NbN}_6$		238 (0) [34]	234 (0) [31]
	$\nu_{15}$	$\tau$		87 (0) [36]	89 (0) [92]
	$\nu_{16}$	$\tau$		36 (0) [69]	38 (0) [80]
	$\nu_{17}$	$\nu_{as}\text{N}_3$	2121 s	2185 (4084) [0]	2152 (2577) [0]
$A_u$			2080 vs		
	$\nu_{18}$	$\nu_s\text{N}_3$	1336 ms	1406 (677) [0]	1271 (338) [0]
	$\nu_{19}$	$\delta\text{N}_3$	640 vw	580 (0.91) [0]	549 (100) [0]
	$\nu_{20}$	$\delta\text{N}_3$	624 w	574 (49) [0]	505 (8.0) [0]
	$\nu_{21}$	$\nu_{as}\text{NbN}_6$	409 mw	400 (536) [0]	418 (629) [0]
	$\nu_{22}$	$\delta_{as}\text{NbN}_6$		276 (15) [0]	262 (31) [0]
	$\nu_{23}$	$\tau\text{NbN}_6$		140 (2.8) [0]	114 (0.48) [0]
	$\nu_{24}$	$\tau$		27 (0.006) [0]	29 (0.022) [0]
	$\nu_{25}$	$\tau$		24 (1.6) [0]	14 (0.37) [0]
	$\nu_{26}$	$\nu_{as}\text{N}_3$	2069 vs	2170 (4366) [0]	2141 (2681) [0]
$E_u$			2060 vs		
	$\nu_{27}$	$\nu_s\text{N}_3$	1361 m	1409 (739) [0]	1278 (314) [0]
			1351 m		
	$\nu_{28}$	$\delta\text{N}_3$	600 w	577 (126) [0]	544 (94) [0]
	$\nu_{29}$	$\delta\text{N}_3$	583 vw	570 (38) [0]	502 (8.2) [0]
	$\nu_{30}$	$\nu_{as}\text{NbN}_6$	409 mw	391 (874) [0]	404 (1045) [0]
	$\nu_{31}$	$\delta_{as}\text{NbN}_6$		233 (26) [0]	223 (30) [0]
	$\nu_{32}$	$\delta_{\text{wag/rock}}\text{NbN}_6$		154 (13) [0]	128 (31) [0]
	$\nu_{33}$	$\tau$		36 (4.8) [0]	38 (3.1) [0]
	$\nu_{34}$	$\tau$		15 (1.6) [0]	6 (1.9) [0]

[a] Calculated IR and Raman intensities are given in  $\text{kmol}^{-1}$  and  $\text{\AA}^4\text{amu}^{-1}$ , respectively; observed spectra are for the solid  $[\text{P}(\text{C}_6\text{H}_5)_4]^+$  salt. [b] Values shown in parentheses and square brackets are the respective IR and Raman intensities. [c] Intensities shown in parentheses.

former, which increases the ionic character of the azido ligands. The relatively large variation in the Nb-N-N bond angles in  $[\text{Nb}(\text{N}_3)_6]^{-}$ , which range from 131.7 to 156.2°, is attributed to intramolecular repulsion effects among the ligands.

In summary, this paper reports the synthesis and characterization of the first examples of binary Group 5 azides and provides the first experimental proof for the existence of linear M-N-N coordination for azido ligands.

## Experimental Section

**Caution!** Covalent azido compounds are potentially hazardous and can decompose explosively under various conditions! The polyazido

compounds of this work are extremely shock-sensitive and can explode violently upon the slightest provocation. They should be handled only on a scale of less than 1 mmol. Because of the high energy content and high detonation velocities of these azides, their explosions are particularly violent and can cause, even on a 1-mmol scale, significant damage. The use of appropriate safety precautions (safety shields, face shields, leather gloves, protective clothing, such as heavy leather welding suits, and ear plugs) is mandatory. Teflon containers should be used, whenever possible, to avoid hazardous shrapnel formation. The manipulation of these materials is facilitated by handling them, whenever possible, in solution to avoid detonation propagation, by the use of large inert counterions as spacers, and by anion formation, which increases the partial negative charge on the terminal  $\text{N}_\gamma$  atoms and thereby reduces the  $\text{N}_\beta\text{--N}_\gamma$  triple-bond character and strengthens the weak  $\text{N}_\alpha\text{--N}_\beta$  single bond. **Ignoring safety precautions can lead to serious injuries!**

**Materials and Apparatus:** All reactions were carried out in teflon-FEP ampoules that were closed by stainless steel valves. Volatile materials were handled in a Pyrex glass or stainless steel/teflon-FEP vacuum line.<sup>[41]</sup> All reaction vessels were passivated with  $\text{ClF}_3$  prior to use. Nonvolatile materials were handled in the dry argon atmosphere of a glovebox.

Raman spectra were recorded directly in the teflon reactors in the range 3600–80  $\text{cm}^{-1}$  on a Bruker Equinox 55 FT-RA spectrophotometer by using a Nd-YAG laser at 1064 nm with power levels less than 50 mW. Infrared spectra were recorded in the range 4000–400  $\text{cm}^{-1}$  on a Midac M Series FT-IR spectrometer by using KBr pellets. The pellets were prepared inside the glovebox with an Econo minipress (Barnes Engineering Co.) and transferred in a closed container to the

spectrometer before placing them quickly into the sample compartment, which was purged with dry nitrogen to minimize exposure to atmospheric moisture and potential hydrolysis of the sample.

The starting materials  $\text{NbF}_5$ ,  $\text{TaF}_5$  (both Ozark Mahoning), and  $[\text{P}(\text{C}_6\text{H}_5)_4]\text{I}$  (Aldrich) were used without further purification.  $(\text{CH}_3)_3\text{SiN}_3$  (Aldrich) was purified by fractional condensation prior to use. Solvents were dried by standard methods and freshly distilled prior to use.  $[\text{P}(\text{C}_6\text{H}_5)_4]\text{N}_3$  and  $[\text{P}(\text{C}_6\text{H}_5)_4]\text{F}$  were prepared from  $[\text{P}(\text{C}_6\text{H}_5)_4]\text{I}$  and stoichiometric amounts of  $\text{AgN}_3$  and  $\text{AgF}$ , respectively, in aqueous solution and separated from the precipitated  $\text{AgI}$  by filtration.

$[\text{M}(\text{N}_3)_5]$  ( $\text{M} = \text{Nb}, \text{Ta}$ ): A sample of  $\text{NbF}_5$  (0.55 mmol) or  $\text{TaF}_5$  (0.59 mmol) was loaded into a teflon-FEP ampoule, and  $\text{SO}_2$  (1 g) and  $(\text{CH}_3)_3\text{SiN}_3$  (5.5 mmol) were added in vacuo at  $-196^\circ\text{C}$ . The mixture was warmed to  $-30^\circ\text{C}$ . After 2 h, the temperature was raised to

–20°C, and all volatile material was removed in vacuum, leaving behind solid  $[\text{M}(\text{N}_3)_5]$ .

$[\text{Nb}(\text{N}_3)_5]$ : Mass of isolated material: 0.175 g; calcd for 0.55 mmol: 0.166 g. Raman (–80°C):  $\tilde{\nu}$  [intensity in  $\text{\AA}^4\text{amu}^{-1}$ ]: 2155 [10.0], 2106 [5.5] ( $\nu_{\text{as}} \text{N}_3$ ), 1385 [1.6] ( $\nu_{\text{s}} \text{N}_3$ ), 628 [0.7], 590 sh ( $\delta \text{N}_3$ ), 427 sh ( $\nu_{\text{as}} \text{NbN}_3$  eq), 413 [3.2] ( $\nu_{\text{s}} \text{NbN}_3$  eq), 360 sh ( $\nu_{\text{s}} \text{NbN}_2$  ax), 288 [0.7] ( $\delta_{\text{sciss}} \text{NbN}_3$  eq), 234  $\text{cm}^{-1}$  [0.7], ( $\rho \text{NbN}_2$  ax); IR (KBr):  $\tilde{\nu}$  = 2124 vs, 2088 vs ( $\nu_{\text{as}} \text{N}_3$ ), 1374 m, 1347 s ( $\nu_{\text{s}} \text{N}_3$ ), 591 mw, 569 w ( $\delta \text{N}_3$ ), 450 sh ( $\nu_{\text{as}} \text{NbN}_3$  eq), 440 mw ( $\nu_{\text{as}} \text{NbN}_2$  ax), 422  $\text{cm}^{-1}$  w ( $\nu_{\text{s}} \text{NbN}_3$  eq); ax = axial, eq = equatorial.

$[\text{Ta}(\text{N}_3)_5]$ : Mass of isolated material: 0.247 g; calcd for 0.59 mmol: 0.231 g. Raman (–80°C):  $\tilde{\nu}$  [intensity in  $\text{\AA}^4\text{amu}^{-1}$ ]: 2182 [10.0], 2129 [3.3] ( $\nu_{\text{as}} \text{N}_3$ ), 623 [1.1], 590 sh ( $\delta \text{N}_3$ ), 450 sh ( $\nu_{\text{as}} \text{Ta}(\text{N}_3)_5$  eq), 426 [2.5] ( $\nu_{\text{s}} \text{Ta}(\text{N}_3)_5$  eq), 390 sh ( $\nu_{\text{s}} \text{Ta}(\text{N}_2)$  ax), 256 [1.7] ( $\delta_{\text{sciss}} \text{Ta}(\text{N}_3)_5$  eq), 221  $\text{cm}^{-1}$  [2.0] ( $\rho \text{Ta}(\text{N}_2)$  ax); IR (KBr):  $\tilde{\nu}$  = 2141 vs, 2103 vs ( $\nu_{\text{as}} \text{N}_3$ ), 1403 ms, 1364 m ( $\nu_{\text{s}} \text{N}_3$ ), 613 mw, 578 w ( $\delta \text{N}_3$ ), 410  $\text{cm}^{-1}$  mw ( $\nu_{\text{as}} \text{Ta}(\text{N}_2)$  ax).

In addition to the bands listed above, the following weak IR bands were observed which are attributed to overtones or combination bands:  $[\text{Nb}(\text{N}_3)_5]$ : 1667 w, 1263 w, 1195 sh, 1176 w, 1037 vw, 696 w, 660  $\text{cm}^{-1}$  w;  $[\text{Ta}(\text{N}_3)_5]$ : 1669 w, 1508 vw, 1274 sh, 1252 w, 1203 w, 1180 sh, 1036 vw, 850 w, 712 w, 683  $\text{cm}^{-1}$  w.

$[\text{M}(\text{N}_3)_5(\text{CH}_3\text{CN})]$  (M = Nb, Ta):  $\text{NbF}_5$  (0.39 mmol) or  $\text{TaF}_5$  (0.37 mmol) was loaded into a teflon-FEP ampoule, and  $\text{CH}_3\text{CN}$  (2 mL) and  $(\text{CH}_3)_3\text{SiN}_3$  (3.7 mmol) were added in vacuo at –196°C. The mixture was warmed to –20°C. After 2 h, all volatile material was removed in a vacuum at this temperature, leaving behind solid  $[\text{M}(\text{N}_3)_5(\text{CH}_3\text{CN})]$ .

$[\text{Nb}(\text{N}_3)_5(\text{CH}_3\text{CN})]$ : Mass of isolated material: 0.129 g; calcd for 0.39 mmol: 0.136 g. Raman (–80°C):  $\tilde{\nu}$  [intensity in  $\text{\AA}^4\text{amu}^{-1}$ ]: 2928 [1.8] ( $\nu_{\text{s}} \text{CH}_3$ ), 2315 [1.2], 2289 [1.1] ( $\nu \text{CN}$ ), 2140 [10.0], 2121 [1.5], 2097 [1.9], 2090 [1.6], 2074 [2.2], 2058 [1.4] ( $\nu_{\text{as}} \text{N}_3$ ), 1415 [1.3], 1363 [1.2], 1351 [1.1], 1331 [1.1] ( $\delta \text{CH}_3$ ) and ( $\nu_{\text{s}} \text{N}_3$ ), 947 [1.0] ( $\nu \text{CC}$ ), 620 [1.2], 610 [1.0], 599 [1.2], 580 [1.1], 566 [1.0], 557 [1.1] ( $\delta \text{N}_3$ ), 441 [3.1], 435 [2.8], 423 [1.7], 419 [1.7], 411 [2.0] ( $\nu \text{NbN}_x$ ), 281 [1.1], 266 [1.3], 256 [1.3], 248 [1.3], 226 [1.6] ( $\delta \text{NbN}_x$ ), 189 [1.3], 180 [1.3], 139 [1.6], 96 [2.9] (torsional modes).

$[\text{Ta}(\text{N}_3)_5(\text{CH}_3\text{CN})]$ : Mass of isolated material: 0.175 g; calcd for 0.37 mmol: 0.161 g. Raman (–80°C):  $\tilde{\nu}$  [intensity in  $\text{\AA}^4\text{amu}^{-1}$ ]: 2933 [1.7] ( $\nu_{\text{s}} \text{CH}_3$ ), 2319 [0.5], 2291 [0.5] ( $\nu \text{CN}$ ), 2172 [10.0], 2162 [1.2], 2123 [1.2], 2103 [1.1] ( $\nu_{\text{as}} \text{N}_3$ ), 1389 [0.4], 1361 [0.4] ( $\delta \text{CH}_3$ ) and ( $\nu_{\text{s}} \text{N}_3$ ), 948 [1.0] ( $\nu \text{CC}$ ), 592 [0.3] ( $\delta \text{N}_3$ ), 438 [2.1], 417 [0.6] ( $\nu \text{NbN}_x$ ), 250 [0.7], 266 [1.3], 226 [0.6] ( $\delta \text{NbN}_x$ ), 192 [0.9] (torsional mode).

$[\text{P}(\text{C}_6\text{H}_5)_4][\text{M}(\text{N}_3)_6]$  (M = Nb, Ta): Neat  $[\text{P}(\text{C}_6\text{H}_5)_4\text{N}_3]$  (0.25 mmol) was added to a frozen solution of  $[\text{M}(\text{N}_3)_5]$  (0.25 mmol) in  $\text{CH}_3\text{CN}$  (15 mmol) at –78°C. The reaction mixture was warmed to –25°C and occasionally agitated. After 2 h, all volatiles were removed at ambient temperature in a dynamic vacuum, leaving behind solid  $[\text{P}(\text{C}_6\text{H}_5)_4][\text{M}(\text{N}_3)_6]$ .

$[\text{P}(\text{C}_6\text{H}_5)_4][\text{Nb}(\text{N}_3)_6]$ : Orange solid. Mass of isolated material: 0.160 g; calcd for 0.25 mmol: 0.171 g. The IR and Raman bands of  $[\text{Nb}(\text{N}_3)_6]^-$  are given in Table 2.

$[\text{P}(\text{C}_6\text{H}_5)_4][\text{Ta}(\text{N}_3)_6]$ : Pale yellow solid. Mass of isolated material 0.207 g; calcd for 0.25 mmol: 0.193 g. Raman bands from  $[\text{Ta}(\text{N}_3)_6]^-$  (–80°C):  $\tilde{\nu}$  [intensity in  $\text{\AA}^4\text{amu}^{-1}$ ]: 2159 [10.0], 2111 [1.0], 2103 [1.0], 2091 [0.8], 2081 [0.7] ( $\nu_{\text{as}} \text{N}_3$ ), 1355 [0.8] ( $\nu_{\text{s}} \text{N}_3$ ), 609 [0.6], 582 [0.4] ( $\delta \text{N}_3$ ), 437 [2.8], 372 [0.7], 364 [0.8], 353 [0.8] ( $\nu \text{Ta}(\text{N}_6)$ ), 225 [1.8], 215 [1.8] ( $\delta \text{Ta}(\text{N}_6)$ ), 168 [2.6], 160  $\text{cm}^{-1}$  [2.6] (torsions); IR bands from  $[\text{Ta}(\text{N}_3)_6]^-$  (KBr):  $\tilde{\nu}$  = 2124 vs, 2113 vs, 2096 vs, 2087 vs ( $\nu_{\text{as}} \text{N}_3$ ), 1383 m, 1372 m, 1360 ms, 1348 s ( $\nu_{\text{s}} \text{N}_3$ ), 648 vw, 615 m, 600 mw, 585 mw, 576 w ( $\delta \text{N}_3$ ), 433 w, 418 mw, 414  $\text{cm}^{-1}$  mw ( $\nu \text{Ta}(\text{N}_6)$ ).

Theoretical Methods: The molecular structures, harmonic vibrational frequencies, and IR and Raman vibrational intensities were calculated by using second-order perturbation theory (MP2, also known as MBPT(2)<sup>[24]</sup>) and also at the DFT level by using the B3LYP hybrid functional,<sup>[23a]</sup> which included the VWN5 correlation functional.<sup>[23b]</sup> The Stevens, Basch, Krauss, and Jasien (SBKJ) effective core potentials and the corresponding valence-only basis sets were

used.<sup>[25a]</sup> The SBKJ valence basis set for nitrogen was augmented with a d-polarization function<sup>[25b]</sup> and a diffuse s + p shell,<sup>[25c]</sup> denoted as SBKJ + (d). Hessians (energy second derivatives) were calculated for the final equilibrium structures to verify them as local minima, that is, having a positive definite Hessian. All calculations were performed by using the electronic structure code GAMESS.<sup>[42]</sup>

Received: March 17, 2006

Published online: June 23, 2006

**Keywords:** azides · density functional calculations · niobium · tantalum · vibrational spectroscopy

- [1] R. Haiges, J. A. Boatz, S. Schneider, T. Schroer, K. O. Christe, *Angew. Chem.* **2004**, *116*, 3210; *Angew. Chem. Int. Ed.* **2004**, *43*, 3148.
- [2] R. Haiges, J. A. Boatz, R. Bau, S. Schneider, T. Schroer, M. Yousufuddin, K. O. Christe, *Angew. Chem.* **2005**, *117*, 1894; *Angew. Chem. Int. Ed.* **2005**, *44*, 1860.
- [3] A. Kornath, *Angew. Chem.* **2001**, *113*, 3231; *Angew. Chem. Int. Ed.* **2001**, *40*, 3135, and references therein.
- [4] K. Dehnicke, J. Strähle, *Z. Anorg. Allg. Chem.* **1965**, *338*, 287.
- [5] K. Dehnicke, *J. Inorg. Nucl. Chem.* **1965**, *27*, 809.
- [6] J. Strähle, *Z. Anorg. Allg. Chem.* **1974**, *405*, 139.
- [7] R. Choukroun, D. Gervais, *J. Chem. Soc. Dalton Trans.* **1980**, 1800.
- [8] U. Müller, R. Dübgen, K. Dehnicke, *Z. Anorg. Allg. Chem.* **1981**, *473*, 115.
- [9] a) W. Beck, E. Schuierer, P. Poellmann, W. P. Fehlhammer, *Z. Naturforsch. B* **1966**, *21*, 811; b) W. Beck, W. P. Fehlhammer, P. Poellmann, E. Schuierer, K. Feldt, *Chem. Ber.* **1967**, *100*, 2335.
- [10] D. B. Sable, W. H. Armstrong, *Inorg. Chem.* **1992**, *31*, 161.
- [11] J. H. Espenson, J. R. Pladziewicz, *Inorg. Chem.* **1970**, *9*, 1380.
- [12] M. Kasper, R. Bereman, *Inorg. Nucl. Chem. Lett.* **1974**, *10*, 443.
- [13] M. Herberhold, A.-M. Dietel, W. Milius, *Z. Anorg. Allg. Chem.* **1999**, *625*, 1885.
- [14] J. H. Osborne, A. L. Rheingold, W. C. Troglor, *J. Am. Chem. Soc.* **1985**, *107*, 7945.
- [15] M. Herberhold, A. Goller, W. Milius, *Z. Anorg. Allg. Chem.* **2003**, *629*, 1162.
- [16] M. Herberhold, A. Goller, W. Milius, *Z. Anorg. Allg. Chem.* **2003**, *629*, 1557.
- [17] M. Herberhold, A. Goller, W. Milius, *Z. Anorg. Allg. Chem.* **2001**, *627*, 891.
- [18] J. H. Meyer, *Z. Anorg. Allg. Chem.* **1995**, *621*, 921.
- [19] O. Reckeweg, H.-J. Meyer, A. Simon, *Z. Anorg. Allg. Chem.* **2002**, *628*, 920.
- [20] H.-J. Meyer, *Z. Anorg. Allg. Chem.* **1995**, *621*, 921.
- [21] R. Dübgen, U. Müller, F. Weller, K. Dehnicke, *Z. Anorg. Allg. Chem.* **1980**, *471*, 89.
- [22] A. M. Golub, H. Köhler, V. V. Stopenko, *Chemistry of Pseudo-halides*, Elsevier, Amsterdam, **1986**.
- [23] a) A. D. Becke, *J. Chem. Phys.* **1993**, *98*, 5648; P. J. Stephens, F. J. Devlin, C. F. Chabrowski, M. J. Frisch, *J. Phys. Chem.* **1994**, *98*, 11623; R. H. Hertwig, W. Koch, *Chem. Phys. Lett.* **1997**, *268*, 345; b) S. H. Vosko, L. Wilk, M. Nusair, *Can. J. Phys.* **1980**, *58*, 1200.
- [24] C. Moller, M. S. Plesset, *Phys. Rev.* **1934**, *46*, 618; J. A. Pople, J. S. Binkley, R. Seeger, *Int. J. Quantum Chem. Symp.* **1976**, *10*, 1; M. J. Frisch, M. Head-Gordon, J. A. Pople, *Chem. Phys. Lett.* **1990**, *166*, 275; R. J. Bartlett, D. M. Silver, *Int. J. Quantum Chem. Symp.* **1975**, *9*, 1927.
- [25] a) W. J. Stevens, H. Basch, M. Krauss, *J. Chem. Phys.* **1984**, *81*, 6026; W. J. Stevens, M. Krauss, H. Basch, P. G. Jasien, *Can. J. Chem.* **1992**, *70*, 612; b) P. C. Hariharan, J. A. Pople, *Theor.*



- Chim. Acta* **1973**, 28, 213; c) T. Clark, J. Chandrasekhar, G. W. Spitznagel, P. von R. Schleyer, *J. Comput. Chem.* **1983**, 4, 294.
- [26] J. Drummond, J. S. Wood, *Chem. Commun.* **1969**, 1373.
- [27] R. Haiges, J. A. Boatz, A. Vij, V. Vij, M. Gerken, S. Schneider, T. Schroer, M. Yousufuddin, K. O. Christe, *Angew. Chem.* **2004**, 116, 6844; *Angew. Chem. Int. Ed.* **2004**, 43, 6676.
- [28] a) K. Karaghiosoff, T. M. Klapötke, B. Krumm, H. Nöth, T. Schütt, M. Suter, *Inorg. Chem.* **2002**, 41, 170; b) T. M. Klapötke, H. Nöth, T. Schütt, M. Warchhold, *Angew. Chem.* **2000**, 112, 2197; *Angew. Chem. Int. Ed.* **2000**, 39, 2108.
- [29] a) R. J. Gillespie, I. Hargittai, *The VSEPR Model of Molecular Geometry*, Allyn and Bacon, Needham Heights, MA, **1991**; b) R. J. Gillespie, P. L. A. Popelier, *Chemical Bonding and Molecular Geometry: from Lewis to Electron Densities*, Oxford University Press, Oxford, **2001**.
- [30] L. Gagliardi, P. Pyykkö, *Inorg. Chem.* **2003**, 42, 3074.
- [31] M. Teichert, J. A. Boatz, personal communication.
- [32] P. H. Bird, M. R. Churchill, *J. Chem. Soc. Chem. Commun.* **1967**, 403.
- [33] Crystal data for  $C_2H_3N_{16}Nb$ :  $M_r = 344.11$ , monoclinic, space group  $P2_1/c$ ,  $a = 7.9805(12)$ ,  $b = 10.4913(16)$ ,  $c = 14.695(2)$  Å,  $\alpha = 90$ ,  $\beta = 96.353(2)$ ,  $\gamma = 90^\circ$ ,  $V = 1222.8(3)$  Å<sup>3</sup>,  $F(000) = 672$ ,  $\rho_{\text{calcd}} = 1.869$  g cm<sup>-3</sup>,  $Z = 4$ ,  $\mu = 1.004$  mm<sup>-1</sup>, approximate crystal dimensions  $0.25 \times 0.08 \times 0.02$  mm<sup>3</sup>,  $\theta = 2.39$  to  $27.48^\circ$ ,  $Mo_{K\alpha}$  ( $\lambda = 0.71073$  Å),  $T = 163(2)$  K, 3392 measured data (Bruker 3-circle, SMART APEX CCD with  $\chi$ -axis fixed at  $54.74^\circ$  using the SMART V 5.625 program, Bruker AXS: Madison, WI, 2001), of which 839 ( $R_{\text{int}} = 0.0204$ ) were unique. Lorentz and polarization correction (SAINT V 6.22 program, Bruker AXS: Madison, WI, **2001**), absorption correction (SADABS program, Bruker AXS: Madison, WI, **2001**). Structure solution by direct methods (SHELXTL 5.10, Bruker AXS: Madison, WI, **2000**), full-matrix least-squares refinement on  $F^2$ , data-to-parameters ratio: 15.9:1, final  $R$  indices [ $I > 2\sigma(I)$ ]:  $R1 = 0.0341$ ,  $wR2 = 0.0692$ ,  $R$  indices (all data):  $R1 = 0.0546$ ,  $wR2 = 0.0746$ , GOF on  $F^2 = 1.003$ . CCDC-246594 contains the supplementary crystallographic data for  $[Nb(N_3)_5(CH_3CN)]$ . These data can be obtained free of charge from The Cambridge Crystallographic Data Centre via [www.ccdc.cam.ac.uk/data\\_request/cif](http://www.ccdc.cam.ac.uk/data_request/cif).
- [34] B. v. Ahlsen, B. Bley, S. Proemmel, R. Wartchow, H. Willner, F. Aubke, *Z. Anorg. Allg. Chem.* **1998**, 624, 1225.
- [35] a) D. M. Byler, D. F. Shriver, *Inorg. Chem.* **1973**, 12, 1412; b) D. M. Byler, D. F. Shriver **1974**, 13, 2697.
- [36] Crystal data for  $C_{24}H_{20}N_{18}NbP$ :  $M_r = 684.46$ , orthorhombic, space group  $P2_12_12$ ,  $a = 18.480(3)$ ,  $b = 23.153(4)$ ,  $c = 6.7831(13)$  Å,  $\alpha = 90$ ,  $\beta = 90$ ,  $\gamma = 90^\circ$ ,  $V = 2902.3(9)$  Å<sup>3</sup>,  $F(000) = 1384$ ,  $\rho_{\text{calcd}} = 1.566$  g cm<sup>-3</sup>,  $Z = 4$ ,  $\mu = 0.521$  mm<sup>-1</sup>, approximate crystal dimensions  $0.33 \times 0.05 \times 0.04$  mm<sup>3</sup>,  $\theta = 1.41$  to  $27.51^\circ$ ,  $Mo_{K\alpha}$  ( $\lambda = 0.71073$  Å),  $T = 133(2)$  K, 17936 measured data (Bruker 3-circle, SMART APEX CCD with  $\chi$ -axis fixed at  $54.74^\circ$  using the SMART V 5.625 program, Bruker AXS: Madison, WI, **2001**), of which 6575 ( $R_{\text{int}} = 0.0597$ ) were unique. Lorentz and polarization correction (SAINT V 6.22 program, Bruker AXS: Madison, WI, **2001**), absorption correction (SADABS program, Bruker AXS: Madison, WI, **2001**). Structure solution by direct methods (SHELXTL 5.10, Bruker AXS: Madison, WI, **2000**), full-matrix least-squares refinement on  $F^2$ , data-to-parameters ratio: 16.5:1, final  $R$  indices [ $I > 2\sigma(I)$ ]:  $R1 = 0.0518$ ,  $wR2 = 0.0936$ ,  $R$  indices (all data):  $R1 = 0.0858$ ,  $wR2 = 0.1049$ , GOF on  $F^2 = 1.028$ . CCDC-251934 contains the supplementary crystallographic data for  $[P(C_6H_5)_4][Nb(N_3)_6]$ . These data can be obtained free of charge from The Cambridge Crystallographic Data Centre via [www.ccdc.cam.ac.uk/data\\_request/cif](http://www.ccdc.cam.ac.uk/data_request/cif).
- [37] J. Weidlein, U. Mueller, K. Dehnicke, *Schwingungsspektroskopie*, Georg Thieme, Stuttgart, **1982**, p. 102.
- [38] A. C. Filippou, P. Portius, G. Schnakenburg, *J. Am. Chem. Soc.* **2002**, 124, 12396.
- [39] A. C. Filippou, P. Portius, D. U. Neumann, K.-D. Wehrstedt, *Angew. Chem.* **2000**, 112, 4524; *Angew. Chem. Int. Ed.* **2000**, 39, 4333.
- [40] T. M. Klapötke, H. Nöth, T. Schuett, M. Warchhold, *Angew. Chem.* **2000**, 112, 2197; *Angew. Chem. Int. Ed.* **2000**, 39, 2108.
- [41] K. O. Christe, W. W. Wilson, C. J. Schack, R. D. Wilson, *Inorg. Synth.* **1986**, 24, 39.
- [42] M. W. Schmidt, K. K. Baldrige, J. A. Boatz, S. T. Elbert, M. S. Gordon, J. H. Jensen, S. Koseki, N. Matsunaga, K. A. Nguyen, S. J. Su, T. L. Windus, M. Dupuis, J. A. Montgomery, *J. Comput. Chem.* **1993**, 14, 1347.

Synthetic Methods

DOI: 10.1002/anie.200601181

**Ruthenium-Catalyzed Propargylic Reduction of Propargylic Alcohols with Silanes\*\***

Yoshiaki Nishibayashi,\* Akira Shinoda,  
Yoshihiro Miyake, Hiroshi Matsuzawa, and  
Mitsunobu Sato

*Dedicated to Professor Sakae Uemura  
on the occasion of his 65th birthday*

A number of transition-metal complexes are known to promote the hydrosilylation of alkynes with silanes to give the corresponding vinyl silanes, which are versatile building blocks in organic synthesis.<sup>[1]</sup> The development of highly stereo- and regioselective hydrosilylation reactions of alkynes with silanes is an important subject in organic synthesis.<sup>[1]</sup> The selectivity in transition-metal-catalyzed hydrosilylation depends on the nature of catalysts, substrates, silanes, and solvents.<sup>[2,3]</sup> Recently, Trost and co-workers reported a highly selective preparation of  $\alpha$ -vinyl silanes from a wide range of

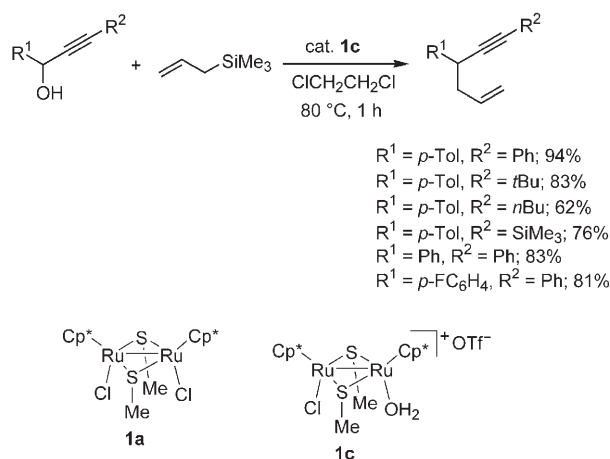
[\*] Prof. Dr. Y. Nishibayashi, Dr. Y. Miyake, Dr. H. Matsuzawa  
Institute of Engineering Innovation  
The University of Tokyo  
Yayoi, Bunkyo-ku, Tokyo, 113-8656 (Japan)  
Fax: (+ 81) 3-5841-1175  
E-mail: ynishiba@sogo.t.u-tokyo.ac.jp

A. Shinoda, Prof. Dr. M. Sato  
Department of Material Science and Technology  
Faculty of Engineering  
Kogakuin University  
Hachioji, Tokyo, 192-0015 (Japan)

[\*\*] This work was supported by a Grant-in-Aid for Scientific Research for Young Scientists (A, No. 15685006) and Grant-in-Aid for Scientific Research on Priority Areas (No. 18037012) to Y.N. from the Ministry of Education, Culture, Sports, Science and Technology, Japan.

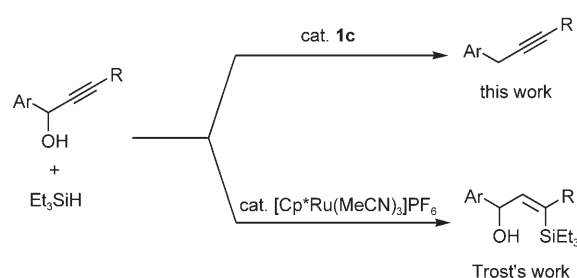
alkynes by catalysis with the cationic ruthenium complex  $[\text{Cp}^*\text{Ru}(\text{MeCN})_3]\text{PF}_6$  ( $\text{Cp}^* = \eta^5\text{-C}_5\text{Me}_5$ ).<sup>[2a,d,f]</sup>

We have recently disclosed a novel catalytic activity of thiolate-bridged diruthenium complexes<sup>[4]</sup> such as  $[\{\text{Cp}^*\text{RuCl}(\mu_2\text{-SR})\}_2]$  ( $\text{R} = \text{Me}$  (**1a**),  $n\text{Pr}$ ,  $i\text{Pr}$  (**1b**)) and  $[\text{Cp}^*\text{RuCl}(\mu_2\text{-SMe})_2\text{RuCp}^*(\text{OH}_2)]\text{OTf}$  (**1c**;  $\text{OTf} = \text{OSO}_2\text{CF}_3$ ). These complexes were shown to be suitable catalysts for the propargylic substitution reactions of propargylic alcohols with a variety of heteroatom- and carbon-centered nucleophiles to give the corresponding propargylic-substituted compounds in high yields with complete selectivity.<sup>[5]</sup> Some other groups reported the transition-metal-catalyzed propargylic allylation of propargylic alcohols with allyltrimethylsilane to give the corresponding allylated products in good to high yields with high selectivity.<sup>[6]</sup> These results first prompted us to investigate the ruthenium-catalyzed allylation of propargylic alcohols with allylsilane. As a result, we confirmed that only cationic thiolate-bridged diruthenium complexes promote the substitution by an allyl group of the hydroxy moiety of propargylic alcohols that bear an internal alkyne, as was expected (Scheme 1).



**Scheme 1.** Ruthenium-catalyzed propargylic substitution reactions of propargylic alcohols with allyltrimethylsilane.

As an extension of our study on the catalytic reactions with other organosilicon compounds, we have now observed the unexpected and completely chemoselective reduction at the propargylic position of propargylic alcohols that bear an internal alkyne with a variety of silanes to give the corresponding reduction products (substitution of the OH moiety by hydride, referred to herein as propargylic reduction) in good to high yields. This result is in sharp contrast to the recently reported selective formation of (*E*)-vinyl silanes by the hydrosilylation of propargylic alcohols with silanes which was catalyzed by the cationic ruthenium complex  $[\text{Cp}^*\text{Ru}(\text{MeCN})_3]\text{PF}_6$  (Scheme 2).<sup>[2c,e]</sup> Although some transition-metal complexes other than ruthenium are also known to promote the propargylic substitution reactions of propargylic alcohol derivatives with a variety of heteroatom- and carbon-centered nucleophiles to afford the corresponding functionalized propargylic compounds,<sup>[6–10]</sup> the catalytic propargylic reduction with a hydride has not yet been reported to the best



**Scheme 2.** Diverging pathways in ruthenium-catalyzed transformations of propargylic alcohols with triethylsilane.

of our knowledge. Preliminary results of the ruthenium-catalyzed propargylic reduction of propargylic alcohols with triethylsilane are presented herein. It is noteworthy that the reactions of propargylic alcohols with pinacolborane in the presence of a catalytic amount of **1a** unexpectedly gave the reductive homocoupling products of the propargylic alcohols in good yields with high selectivity.<sup>[11]</sup>

Treatment of 1-(4-methylphenyl)-3-phenyl-2-propyn-1-ol (**2a**) with triethylsilane in the presence of the cationic diruthenium complex **1c** (5 mol %) in  $\text{ClCH}_2\text{CH}_2\text{Cl}$  at  $80^\circ\text{C}$  for one hour afforded the propargylic reduction product 1-phenyl-3-(4-methylphenyl)-1-propyne (**3a**) in 77 % yield after isolation (Table 1, entry 1). The reaction also proceeded quite

**Table 1:** Propargylic reduction of propargylic alcohol **2a** with various silanes in the presence of **1c**.<sup>[a]</sup>

Entry	Silane (equiv)	<i>t</i> [h]	Yield of <b>3a</b> [%] <sup>[b]</sup>
1	$\text{Et}_3\text{SiH}$ (10)	1	77
2	$\text{Et}_3\text{SiH}$ (5)	1	59
3	$t\text{BuMe}_2\text{SiH}$ (10)	1	67
4	$\text{PhMe}_2\text{SiH}$ (10)	1	50
5	$i\text{Pr}_3\text{SiH}$ (10)	3	15
6	$\text{Ph}_3\text{SiH}$ (10)	3	0
7	$\text{Ph}_2\text{SiH}_2$ (10)	1	0
8	$\text{PhMeSiH}_2$ (10)	1	0
9	$\text{PhSiH}_3$ (10)	1	0
10	$[\text{MeSi}(\text{H})\text{O}]_n$ (10) <sup>[c]</sup>	1	0

[a] All reactions of **2a** (0.30 mmol) with silane were carried out at  $80^\circ\text{C}$  in the presence of **1c** (0.015 mmol) in  $\text{ClCH}_2\text{CH}_2\text{Cl}$  (10 mL). [b] Yield of isolated product. [c] Poly(methylhydrosiloxane) was used.

smoothly at room temperature with a slight decrease of the product yield. This reductive reaction did not proceed at all when either neutral thiolate-bridged diruthenium complexes **1a** and **1b** or mono- and polynuclear ruthenium complexes such as  $[(\eta^5\text{-C}_9\text{H}_7)\text{RuCl}(\text{PPh}_3)_2]$ ,  $[\{\text{Cp}^*\text{RuCl}_2\}_2]$ , and  $[\{\text{Cp}^*\text{RuCl}\}_4]$ , were employed as catalysts. Although gold-catalyzed propargylic substitution reactions of propargylic alcohols with nucleophiles were reported by Campagne and co-workers,<sup>[6b]</sup> the present reductive reaction hardly proceeded when  $\text{AuCl}_3$  was used as a catalyst in place of **1c** under similar conditions. Other silanes such as *tert*-butyldimethylsi-

lane, dimethylphenylsilane, and triisopropylsilane also worked as reducing agents (Table 1, entries 3–5), but triphenylsilane, diphenylsilane, methylphenylsilane, phenylsilane, and poly(methylhydrosiloxane) were not effective (Table 1, entries 6–10).

Reactions of a variety of propargylic alcohols **2** with triethylsilane were subsequently investigated. Typical results are shown in Table 2. The presence of an electron-donating

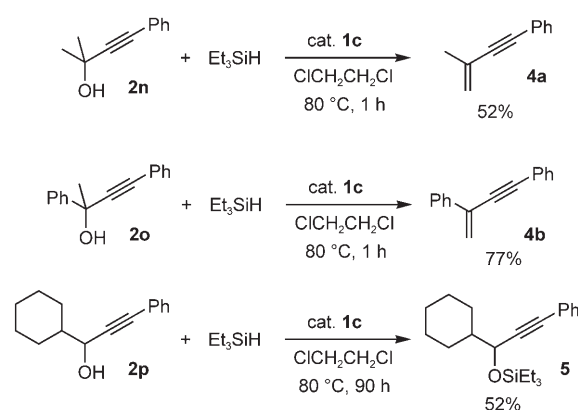
**Table 2:** Propargylic reduction of propargylic alcohols **2** with triethylsilane in the presence of **1c**.<sup>[a]</sup>

$\text{R}-\text{CH}(\text{OH})-\text{C}\equiv\text{C}-\text{R}' + \text{Et}_3\text{SiH} \xrightarrow[\text{ClCH}_2\text{CH}_2\text{Cl}, 80^\circ\text{C}]{\text{cat. 1c}} \text{R}-\text{CH}_2-\text{C}\equiv\text{C}-\text{R}'$					
Entry	R	R'	t [h]	Yield of <b>3</b> [%] <sup>[b]</sup>	
1	<i>p</i> -MeOC <sub>6</sub> H <sub>4</sub>	Ph	( <b>2b</b> )	1	97
2	<i>p</i> -MeC <sub>6</sub> H <sub>4</sub>	Ph	( <b>2a</b> )	1	77
3	Ph	Ph	( <b>2c</b> )	1	43
4	<i>p</i> -ClC <sub>6</sub> H <sub>4</sub>	Ph	( <b>2d</b> )	5	42
5	<i>p</i> -FC <sub>6</sub> H <sub>4</sub>	Ph	( <b>2e</b> )	5	46
6	<i>p</i> -CF <sub>3</sub> C <sub>6</sub> H <sub>4</sub>	Ph	( <b>2f</b> )	23	0
7	<i>p</i> -MeOC <sub>6</sub> H <sub>4</sub>	<i>n</i> Bu	( <b>2g</b> )	1	94
8	<i>p</i> -MeOC <sub>6</sub> H <sub>4</sub>	<i>t</i> Bu	( <b>2h</b> )	1	93
9	<i>p</i> -MeOC <sub>6</sub> H <sub>4</sub>	SiMe <sub>3</sub>	( <b>2i</b> )	1	99
10	1-naphthyl	Ph	( <b>2j</b> )	3	66
11	2-naphthyl	Ph	( <b>2k</b> )	3	55
12	Ph <sub>2</sub> C=CH	Ph	( <b>2l</b> )	1	51 <sup>[c]</sup>

[a] All reactions of **2** (0.30 mmol) with triethylsilane (3.00 mmol) were carried out at 80 °C in the presence of **1c** (0.015 mmol) in ClCH<sub>2</sub>CH<sub>2</sub>Cl (10 mL). [b] Yield of isolated product. [c] 10 mol % of **1c** was used.

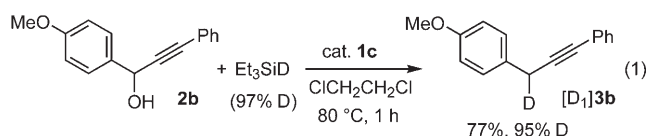
group such as methoxy and methyl on the propargylic benzene ring (**2b** and **2a**) increased the yield of the propargylic reduction product (Table 2, entries 1 and 2; compare with entry 3). In contrast, no improvement of the yield of the reduced products was observed when an electron-withdrawing group such as chloro or fluoro was introduced onto the propargylic benzene ring (**2d** and **2e**; Table 2, entries 4 and 5), and no reduction proceeded at 80 °C even for 23 hours when a trifluoromethyl moiety (**2f**) was introduced (Table 2, entry 6). These results suggest that propargylic cations might be involved as reactive intermediates. In the case of reactions of propargylic alcohols that bear a naphthyl moiety (**2j** and **2k**), the corresponding reduced products were formed in good yields (Table 2, entries 10 and 11). From an alkenyl-substituted propargylic alcohol (**2l**), the corresponding 1,4-enyne compound was obtained in moderate yield (Table 2, entry 12). However, when 1,1,3-triphenyl-2-propyn-1-ol (**2m**), 2-methyl-4-phenyl-3-buten-2-ol (**2n**), 2,4-diphenyl-3-buten-2-ol (**2o**), 1-cyclohexyl-3-phenyl-2-propyn-1-ol (**2p**), 1-phenyl-2-propyn-1-ol (**2q**), and 3-phenyl-2-propyn-1-ol (**2r**) were used as substrates, the propargylic reduction did not proceed under the same reaction conditions, and some unexpected reactions occurred (Scheme 3).<sup>[12]</sup>

To elucidate the mechanism of the propargylic reduction, the following reactions were investigated. When **2b** was treated with [D<sub>1</sub>]triethylsilane (97 % D) in the presence of a catalytic amount of **1c**, deuterated 1-phenyl-3-(4-methoxy-



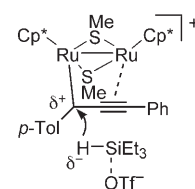
**Scheme 3.** Ruthenium-catalyzed reactions of propargylic alcohols with triethylsilane.

phenyl)-1-propyne ([D<sub>1</sub>]**3b**) was produced with a high deuterium incorporation at the propargylic position (95 % D) [Eq. (1)]. This result indicates that triethylsilane



works as a reducing agent for the reduction at the propargylic position. The pronounced electronic effect of the substituent at the *para* position of the benzene ring in the propargylic alcohol substrate (see above) leads us to propose the presence of a propargylic cation as a reactive intermediate, in which the alkyne moiety may interact with the ruthenium centers of the thiolate-bridged diruthenium complex, although direct evidence of such a reactive intermediate has not yet been obtained. A nucleophilic attack of hydride from the triflate-activated silane on this ruthenium-coordinated propargylic cation might give the corresponding reduction product. A proposed reactive intermediate in the propargylic reduction is shown in Scheme 4. This proposal may be supported by the observation that no reduction occurred in the reactions of allylic alcohols and secondary alcohols such as cinnamyl alcohol and phenylethyl alcohol with triethylsilane under the same reaction conditions.

Nicholas and Siegel have reported the propargylic reduction of [Co<sub>2</sub>(CO)<sub>6</sub>]-complexed propargylic cations, which were prepared by reactions of propargylic alcohols with a stoichiometric amount of [Co<sub>2</sub>(CO)<sub>8</sub>], with sodium borohydride.<sup>[13]</sup> In this stoichiometric reaction, several steps were necessary to obtain the corresponding reduction products. However, catalytic and direct reduction of secondary or tertiary alcohols and primary alcohols with silanes to give the corresponding alkanes in high to excellent yields has been reported by Baba and co-workers<sup>[14]</sup> and by Yamamoto and

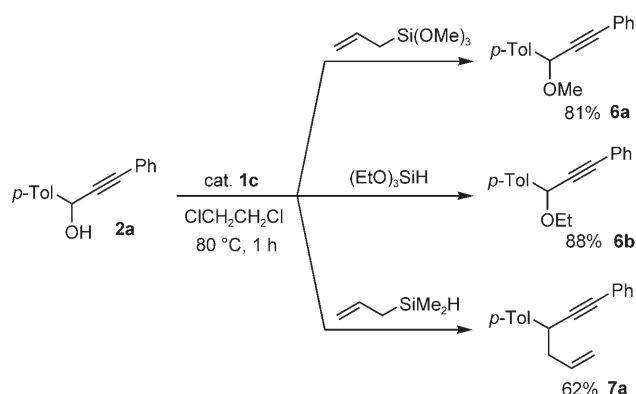


**Scheme 4.** A proposed reactive intermediate.



co-workers<sup>[15]</sup> by using indium trichloride and tris(pentafluorophenyl)borane, respectively, as catalysts. During our work, the propargylic reduction of propargylic acetates with triethylsilane by use of a catalytic amount of indium tribromide<sup>[16]</sup> was reported, in which the propargylic reduction of propargylic alcohols did not proceed smoothly. The reaction described herein provides the first example of the catalytic and direct propargylic reduction of propargylic alcohols to form the corresponding reduced products in good to high yields, although the scope of the reaction is still limited.

Furthermore, we have investigated the ruthenium-catalyzed reactions of propargylic alcohols with organosilicon compounds other than trialkylsilanes under the same reaction conditions. Interestingly, the reactions of **2a** with allyltrimethoxysilane and triethoxysilane at 80 °C for one hour afforded the corresponding ethers **6a** and **6b** in 81 % and 88 % yields, respectively, after isolation (Scheme 5). The reaction of **2a**



**Scheme 5.** Ruthenium-catalyzed propargylic substitution reactions of propargylic alcohol with organosilicon compounds.

with allyldimethylsilane under the same reaction conditions led to the formation of the allylated compound **7a** in 62 % yield after isolation (Scheme 5).<sup>[17]</sup> These results indicate that the ability of substituent transfer from a silicon center to the propargylic position has the following trend in these catalytic reactions: alkoxy > allyl > hydride ≫ alkyl, aryl.

In summary, we have observed novel ruthenium-catalyzed propargylic reduction of propargylic alcohols with triethylsilane to give the corresponding alkynes in good to high yields with complete selectivity. The transition-metal-catalyzed propargylic reduction of propargylic alcohols has until now been an unknown reaction system, in contrast to the recently reported transition-metal-catalyzed propargylic substitution reactions of propargylic alcohol derivatives with nucleophiles. Further investigations for elucidating the reaction mechanism in detail and for broadening the synthetic application of this propargylic reduction are currently in progress.

## Experimental Section

Typical procedure for the propargylic reduction of propargylic alcohol (**2a**) with triethylsilane, catalyzed by **1c**: Compound **1c** (11.5 mg, 0.015 mmol) was placed in a 20-mL flask under N<sub>2</sub>. Distilled and degassed 1,2-dichloroethane (10 mL) was then added to the flask,

and **2a** (66.7 mg, 0.30 mmol) and triethylsilane (0.48 mL, 3.00 mmol) were added. The flask was kept at 80 °C for 1 h with magnetic stirring. After the flask had cooled, the solvent was concentrated in vacuo, and the residue was purified by column chromatography on SiO<sub>2</sub> with EtOAc/*n*-hexane (5:95) to give **3a**<sup>[16]</sup> as a yellow oil (47.6 mg, 0.231 mmol, 77 % yield). <sup>1</sup>H NMR: δ = 2.33 (s, 3H), 3.78 (s, 2H), 7.12–7.44 ppm (m, 9H); <sup>13</sup>C NMR: δ = 21.0, 25.3, 82.4, 87.8, 123.7, 127.7, 127.8, 128.2, 129.2, 131.6, 133.7, 136.1 ppm.

**3l**: Brown oil. Yield: 51 %. <sup>1</sup>H NMR: δ = 3.22 (d, *J* = 7.3 Hz, 2H), 6.18 (t, *J* = 7.3 Hz, 1H), 7.29–7.36 ppm (m, 15H); <sup>13</sup>C NMR: δ = 20.6, 80.9, 88.1, 123.4, 127.3, 127.4, 127.7, 128.1, 128.2, 128.4, 128.6, 128.7, 129.8, 131.6, 139.2, 142.0, 143.3 ppm. HRMS: calcd for C<sub>23</sub>H<sub>18</sub>: 294.1409; found: 294.1404.

Received: March 24, 2006

Revised: April 30, 2006

Published online: June 27, 2006

**Keywords:** homogeneous catalysis · reduction · ruthenium · silanes · synthetic methods

- [1] a) I. Ojima, *The Chemistry of Organic Silicon Compounds* (Eds.: S. Patai, Z. Rappaport), Wiley, Chichester, **1989**, p. 1479; b) T. Hiyama, T. Kusumoto, *Comprehensive Organic Synthesis*, Vol. 8 (Eds.: B. M. Trost, I. Fleming), Pergamon, Oxford, UK, **1991**, p. 763; c) B. Marciniec, *Comprehensive Handbook on Hydro-silylation*, Pergamon, Oxford, UK, **1992**, p. 130; d) J. A. Reiche, D. H. Bery, *Adv. Organomet. Chem.* **1998**, *43*, 197; e) For a recent example, see: B. M. Trost, Z. T. Ball, *Synthesis* **2005**, 853.
- [2] a) B. M. Trost, Z. T. Ball, *J. Am. Chem. Soc.* **2001**, *123*, 12726; b) B. M. Trost, Z. T. Ball, *J. Am. Chem. Soc.* **2003**, *125*, 30; c) B. M. Trost, Z. T. Ball, T. Jöge, *Angew. Chem.* **2003**, *115*, 3537; *Angew. Chem. Int. Ed.* **2003**, *42*, 3415; d) L. W. Chung, Y.-D. Wu, B. M. Trost, Z. T. Ball, *J. Am. Chem. Soc.* **2003**, *125*, 11578; e) B. M. Trost, Z. T. Ball, K. M. Laemmerhold, *J. Am. Chem. Soc.* **2005**, *127*, 10028; f) B. M. Trost, Z. T. Ball, *J. Am. Chem. Soc.* **2005**, *127*, 17644.
- [3] a) K. Itami, K. Mitsudo, A. Nishino, J. Yoshida, *J. Org. Chem.* **2002**, *67*, 2645; b) Y. Kawanami, Y. Sonoda, T. Mori, K. Yamamoto, *Org. Lett.* **2002**, *4*, 2825; c) A. Mori, E. Takahisa, Y. Yamamura, T. Kato, A. P. Mudalige, H. Kajiro, K. Hirabayashi, Y. Nishihara, T. Hiyama, *Organometallics* **2004**, *23*, 1755; d) H. Aneetha, W. Wu, J. G. Verkade, *Organometallics* **2005**, *24*, 2590; e) H. Katayama, M. Nagao, T. Nishimura, Y. Matsui, K. Umeda, K. Akamatsu, T. Tsuruoka, H. Nawafune, F. Ozawa, *J. Am. Chem. Soc.* **2005**, *127*, 4350; f) M. Nagao, K. Asano, K. Umeda, H. Katayama, F. Ozawa, *J. Org. Chem.* **2005**, *70*, 10511; g) C. Menozzi, P. I. Dalko, J. Cossy, *J. Org. Chem.* **2005**, *70*, 10717; h) G. D. Bo, G. Berthon-Gelloz, B. Tinant, I. E. Markó, *Organometallics* **2006**, *25*, 1881.
- [4] a) Y. Nishibayashi, H. Imajima, G. Onodera, M. Hidai, S. Uemura, *Organometallics* **2004**, *23*, 26; b) Y. Nishibayashi, H. Imajima, G. Onodera, Y. Inada, M. Hidai, S. Uemura, *Organometallics* **2004**, *23*, 5100.
- [5] a) S. C. Ammal, N. Yoshikai, Y. Inada, Y. Nishibayashi, E. Nakamura, *J. Am. Chem. Soc.* **2005**, *127*, 9428; b) Y. Inada, Y. Nishibayashi, S. Uemura, *Angew. Chem.* **2005**, *117*, 7893; *Angew. Chem. Int. Ed.* **2005**, *44*, 7715; c) Y. Inada, M. Yoshikawa, M. D. Milton, Y. Nishibayashi, S. Uemura, *Eur. J. Org. Chem.* **2006**, 881.
- [6] Re: a) B. D. Sherry, A. T. Radosevich, F. D. Toste, *J. Am. Chem. Soc.* **2003**, *125*, 6076; Au: b) M. Georgy, V. Boucard, J.-M. Campagne, *J. Am. Chem. Soc.* **2005**, *127*, 14180.
- [7] Cu: Y. Imada, M. Yuasa, I. Nakamura, S.-I. Murahashi, *J. Org. Chem.* **1994**, *59*, 2282.
- [8] Ti: R. Mahrwald, S. Quint, *Tetrahedron* **2000**, *56*, 7463.

- [9] Ir: I. Matsuda, K. Komori, K. Itoh, *J. Am. Chem. Soc.* **2002**, *124*, 9072.
- [10] Re: a) M. R. Luzung, F. D. Toste, *J. Am. Chem. Soc.* **2003**, *125*, 15760; b) J. J. Kennedy-Smith, L. A. Young, F. D. Toste, *Org. Lett.* **2004**, *6*, 1325; c) R. V. Ohri, A. T. Radosevich, K. J. Hrovat, C. Musich, D. Huang, T. R. Holman, F. D. Toste, *Org. Lett.* **2005**, *7*, 2501.
- [11] G. Onodera, Y. Nishibayashi, S. Uemura, *Organometallics* **2006**, *25*, 35.
- [12] No reaction occurred when **2m**, **2q**, or **2r** was used as a substrate.
- [13] a) K. M. Nicholas, J. Siegel, *J. Am. Chem. Soc.* **1985**, *107*, 4999; b) K. M. Nicholas, *Acc. Chem. Res.* **1987**, *20*, 207.
- [14] M. Yasuda, Y. Onishi, M. Ueba, T. Miyai, A. Baba, *J. Org. Chem.* **2001**, *66*, 7741.
- [15] a) V. Gevorgyan, J.-X. Liu, M. Rubin, S. Benson, Y. Yamamoto, *Tetrahedron Lett.* **1999**, *40*, 8919; b) V. Gevorgyan, M. Rubin, S. Benson, J.-X. Liu, Y. Yamamoto, *J. Org. Chem.* **2000**, *65*, 6179.
- [16] N. Sakai, M. Hirasawa, T. Konakahara, *Tetrahedron Lett.* **2005**, *46*, 6407.
- [17] Separately, we investigated the reaction of **2a** with a mixture of allyltrimethylsilane and triethylsilane in the presence of 5 mol % of **1c** at 80 °C for 1 h; only **7a** was isolated in 81 % yield.

## Helical Structures

DOI: 10.1002/anie.200601351

### Dinuclear Double-Stranded Metallosupramolecular Ruthenium Complexes: Potential Anticancer Drugs\*\*

Anna C. G. Hotze, Benson M. Kariuki, and  
Michael J. Hannon\*

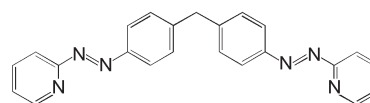
Platinum metallodrugs are among the most effective clinical agents for the treatment of cancer, and three such agents (cisplatin, carboplatin, and oxaliplatin) are in widespread use. These agents are believed to act by binding to DNA and to have similar molecular-level actions.<sup>[1]</sup> Clinical problems include acquired cisplatin resistance the limited spectrum of cancers that can be treated. To address these issues, alternative metallodrug designs that are distinct from cisplatin and have different molecular-level interactions are being explored. Recently, some ruthenium compounds have been shown to have antitumor<sup>[2–4]</sup> and antimetastatic<sup>[5]</sup> actions; two

such compounds are currently in clinical trials and have a different spectrum of activity to the platinum drugs.<sup>[2,5]</sup> Polynuclear drugs in which the metal centers are linked by an alkyl chain have also been designed.<sup>[6–8]</sup> Some of these show very high activity and overcome both acquired and intrinsic cisplatin resistance as a result of their ability to form long-range inter- and intrastrand DNA cross-links.<sup>[6]</sup>

Rather than using a flexible alkyl chain to link the metal centers, we were interested in exploring whether activity could be obtained by positioning the metal centers within a more-rigid metallosupramolecular architecture. The architecture would impose the relative spatial positions of the two metal centers and the ligands, and their structural conformations might afford additional effects. Our reasoning was informed by our observations that the external surfaces of metallosupramolecular helicates can impart unprecedented noncovalent DNA-binding properties, such as the recognition of unusual DNA junction structures and remarkable intramolecular DNA coiling effects.<sup>[9,10]</sup>

In most helicates (such as those used in our previous DNA-binding studies<sup>[9,10]</sup>), the metal centers are fully coordinated by the helical ligands; these are termed “saturated”<sup>[11]</sup> helicates. The focus of our design herein is on “unsaturated”<sup>[12]</sup> helicates, in which there are vacant coordination sites that offer the additional possibility of the metal center interacting directly with DNA. We selected ruthenium, rather than platinum, as our metal center of choice for its higher coordination number and because mononuclear azopyridine ruthenium(II) complexes with two vacant coordination sites have been shown to exhibit cytotoxic activity.<sup>[3]</sup> There are only a few previous reports of helicates based on ruthenium, and their properties have not been explored.<sup>[13]</sup> We describe herein three isomeric dinuclear unsaturated ruthenium(II) complexes each with a different double-stranded supramolecular architecture and report their activity in cell lines, thus presenting the first direct biomedical application of metallosupramolecular helical arrays.

The investigated complexes  $[\text{Ru}_2\text{Cl}_4\text{L}_2]$  are based on a dinucleating bisazopyridine ligand with a di(4-phenyl)methane spacer (Scheme 1), which is the azo analogue of the



**Scheme 1.** The bisazopyridine ligand (L).

bispyridylimine ligand systems<sup>[9]</sup> whose DNA binding we have previously described. The related mononuclear complexes  $[\text{RuCl}_2(\text{azpy})_2]$  (azpy = 2-phenylazopyridine) have five possible geometric isomers (three *cis* and two *trans*).<sup>[3]</sup> Of these, two of the isomers (*cis*- $\alpha$  and *trans*- $\gamma$ ) show the highest cytotoxicities. As shown below, the steric constraints inherent in our bisazopyridine-ligand design are such that these configurations at the metal center are favored in a dinuclear double-stranded array.

The dinuclear double-stranded ruthenium complexes were synthesized from  $[\text{RuCl}_2(\text{dmsO})_4]$  (dmsO = dimethyl

[\*] Dr. A. C. G. Hotze, Dr. B. M. Kariuki, Prof. M. J. Hannon  
School of Chemistry  
University of Birmingham  
Edgbaston, Birmingham, B15 2TT (UK)  
Fax: (+44) 121-414-7871  
E-mail: m.j.hannon@bham.ac.uk

[\*\*] We thank the EU for funding (MARCY RTN HPRN-CT-2002-00175; Marie Curie fellowship MEIF-CT-2005-024818) and Professor Kevin Chipman (Birmingham) for access to cell-line testing facilities.



Supporting information for this article is available on the WWW under <http://www.angewandte.org> or from the author.

sulfoxide) and the bisazopyridine ligand (L) in acetone (see the Experimental Section). The crude product that precipitated from the reaction was purified using column chromatography. NMR spectroscopic analysis of the green main product confirmed a single species of high symmetry (a single set of pyridinyl and phenyl resonances), and ESI-mass-spectrometric analysis indicated the desired dinuclear double-stranded formulation. The compound was recrystallized by slow diffusion of diethyl ether into a solution of the product in  $\text{CHCl}_3$ , thus resulting in needle-shaped crystals that proved suitable for X-ray diffraction studies.<sup>[14]</sup> The molecular structure reveals the compound to be the isomer in which the chlorine ligands at both ruthenium centers are in a *trans* configuration (Figure 1). The constraints of the ligand

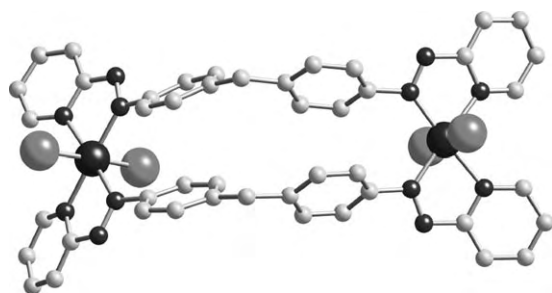


**Figure 1.** Structure of the metallocyclophane *trans/trans* isomer **1**. Hydrogen atoms are omitted for clarity.

structure and the dinuclear double-stranded formulation mean that the pyridine nitrogen atoms and the azo nitrogen atoms are both in *cis* configurations. In accordance with literature nomenclature,<sup>[3]</sup> this structure is the  $\gamma\gamma$  isomer. The double-stranded compound is not helical, but rather a metallocyclophane. However, this structure is very different from the metallocyclophane box-type architecture seen when this type of ligand system interacts with tetrahedral metal ions.<sup>[15]</sup> In that system, the ligands are disposed on opposite sides of the metal–metal axis, whereas the ligands are placed side-by-side in this structure. Therefore, the phenyl rings of one strand are located above the rings of the other strand at a distance (centroid–centroid distance: 3.6 Å) and orientation (offset coplanar) consistent with face–face  $\pi$ -stacking interactions. The side-by-side ligand arrangement gives the structure an overall arc shape (see the Supporting Information). The intramolecular Ru–Ru separation is 12.2 Å, which is similar, though slightly longer, than in the related triple-stranded helical dinickel(II) complex (11.6 Å)<sup>[16]</sup> and the double-stranded helical copper(I) complex (11.1 Å).<sup>[15]</sup>

Careful column chromatography allowed the isolation of a second green–blue isomer from the reaction mixture. The NMR spectroscopic analysis showed lower symmetry (two sets of pyridinyl and phenyl resonances), and the ESI-mass-spectrometric analysis indicated the desired dinuclear double-stranded formulation. This isomer was recrystallized by slow diffusion of diethyl ether into a solution of the product in  $\text{CHCl}_3$ . An X-ray diffraction study<sup>[14]</sup> revealed this species to be the *trans/cis*-[Ru<sub>2</sub>Cl<sub>4</sub>L<sub>2</sub>] (**2**) compound (Figure 2). The *trans* metal center is in the  $\gamma$  conformation, as in **1**, whereas

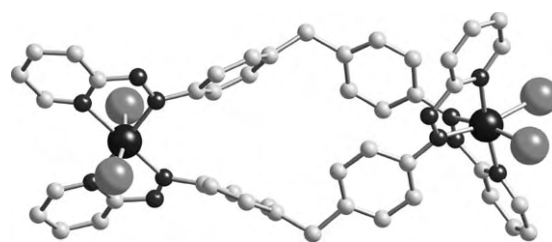


**Figure 2.** Structure of the double-helical *trans/cis* isomer **2**. Hydrogen atoms are omitted for clarity.

the other ruthenium center has the chlorine ligands in a *cis* configuration, the pyridine nitrogen atoms *trans*, and the azo nitrogen atoms *cis*, which corresponds to the  $\alpha$  configuration. The two ligand strands are wrapped about the metal–metal axis in a helical fashion. This compound is in fact a completely new class of helical complex, in that it has a dinuclear double-helical structure, but the chiral twist is induced by just one of the two metal centers (the *cis*- $\alpha$  center). Proton–proton interactions between the pyridine units do lead to a small chiral twist at the *trans* center (similar to the distortions observed in palladium bipyridine complexes),<sup>[17]</sup> but to a first approximation the ligands are coplanar at the *trans* center.<sup>[18]</sup> The intramolecular Ru–Ru distance of 12.5 Å is similar to that in the *trans/trans* isomer.

We have, on one occasion, observed conversion of a sample of **2** into a third isomer **3** on standing in a solution of  $\text{CHCl}_3$ . The conversion was revealed by a dramatic color change from green–blue to blue. NMR spectroscopic analysis confirmed a single species of high symmetry (a single set of pyridinyl and phenyl resonances), and the ESI-mass-spectrometric analysis again indicated a dinuclear double-stranded formulation. This sample was recrystallized by diffusion of diethyl ether into a solution of the product in  $\text{CHCl}_3$ , and a few crystals were isolated and an X-ray structural determination undertaken.<sup>[14]</sup>

The molecular structure of **3** shows the two chlorine ligands on both ruthenium centers to be in a *cis* configuration (Figure 3). These *cis* ruthenium(II) centers have the same  $\alpha$  configuration as that seen for the *cis* center in **2**. The two ligand strands are again wrapped about each other in a double-helical fashion. This structure thus has a more conventional unsaturated double-helical structure with both

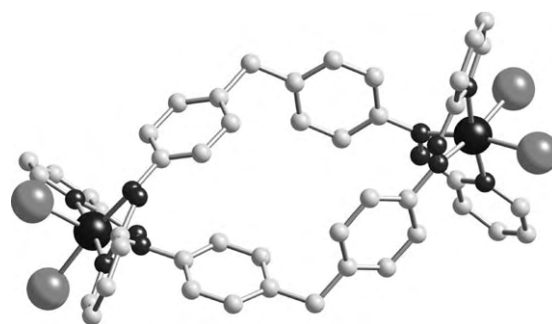


**Figure 3.** Structure of the double-helical *cis/cis* isomer **3**. Hydrogen atoms are omitted for clarity.



metal centers of the same chirality. As would be expected, the two centers cause more extensive ligand wrapping in **3** than **2**. The intramolecular Ru–Ru separation of 12.1 Å is again similar to that in the other isomers.

In these three isomers, only the *cis*- $\alpha$  and *trans*- $\gamma$  configurations of the metal centers are observed. The azo nitrogen atoms must lie *cis* to create a dinuclear double-stranded array, and this requirement decreases the number of potential configurations to *cis*- $\alpha$ , *cis*- $\beta$ , or *trans*- $\gamma$ . Although dinuclear double-stranded species are likely to be intermediates in the assembly of triple-stranded helicates, the addition of a third ligand strand to the three isomers characterized herein would require considerable rearrangement (at the metal center and of ligands) to generate *cis*- $\beta$  configurations. The diphenylmethane spacer units of the two ligand strands would be forced closer in space by the *cis*- $\beta$  configuration: previous unsaturated helicates also contain *cis*- $\alpha$  configurations.<sup>[12]</sup>

In view of the cytotoxicity of the mononuclear counterparts, these dinuclear compounds have been tested on human-breast-tumor HBL100 and T47D cell lines. Two isomers have been tested (the third isomer was not available in suitable quantities), and the IC<sub>50</sub> data are shown in Table 1. Both

**Table 1:** IC<sub>50</sub> values ( $\mu$ M) in breast-cancer cell lines.

	HBL100	T47D
cisplatin	4.9	28.3
<b>1</b>	0.16	0.29
<b>2</b>	5.1	6.7

compounds are very active against these cell lines: The *cis/trans* isomer **2** has similar activity to cisplatin in the HBL100 cell lines and better activity in the T47D cell lines, whereas the *trans/trans* isomer **1** shows extremely high activity, with approximately 30 times more potency than cisplatin in the HBL100 cell lines and 100 times more in the T47D cell lines. The activity is in the same range as the mononuclear counterparts tested on other cell lines. Interestingly, mononuclear [RuCl<sub>2</sub>(azpy)<sub>2</sub>] shows higher activity for the  $\gamma$  isomer (0.02–0.2  $\mu$ M in a panel of cell lines, but different from those herein) than the  $\alpha$  isomer (0.06–0.5  $\mu$ M).<sup>[3]</sup> The same trend is seen herein as the *trans/trans* species being more active than the *cis/trans* isomer.

The isomeric dinuclear [Ru<sub>2</sub>Cl<sub>4</sub>L<sub>2</sub>] complexes reported herein are among the first, and to date the most promising, dinuclear ruthenium anticancer agents. The IC<sub>50</sub> values compare very favorably with those of previously reported dinuclear ruthenium complexes. The dinuclear complexes derived from the new antitumor metastasis inhibitor A (NAMI-A) do not show direct cytotoxicity<sup>[19]</sup> (just as NAMI-A does not). Compounds in which two [Ru(phen)<sub>2</sub>dppz]<sup>2+</sup> (dppz = dipyridophenazine, phen = phenyl) moieties are joined through long alkane linkers show IC<sub>50</sub> values that range from 8 to 45  $\mu$ M,<sup>[7]</sup> whereas a bisruthenium organometallic compound has a reported IC<sub>50</sub> value of 5  $\mu$ M.<sup>[8]</sup>

In summary, the three compounds reported herein represent a new set of dinuclear coordination isomers, each

of which have quite different supramolecular architectures. The three isomers comprise an arc-shaped nonhelical metal-lacyclophane, an unsaturated conventional double helicate, and a new type of double helicate, in which just one of the two metal centers is responsible for imparting helicity to the ligand strands. The ability to isolate a range of different architectures of the same nuclearity from a single metal–ligand combination makes this a particularly remarkable system. Moreover, these compounds are the first compounds to bridge the fields of metallosupramolecular architecture and anticancer drug design. The initial cell-line experiments indicate that the compounds show very good activity. Further biological studies are in progress to fully understand the activity and DNA binding of this new class of complex.

## Experimental Section

*trans/trans*-[Ru<sub>2</sub>Cl<sub>4</sub>L<sub>2</sub>] (**1**): A mixture of [RuCl<sub>2</sub>(dmsO)<sub>4</sub>] (0.150 g, 0.31 mmol) and the bispyridylazo ligand L (0.117 g, 0.31 mmol) in acetone (75 mL) was heated under reflux for 16 h. The green precipitate that formed was isolated by filtration and washed with a little acetone and diethyl ether to afford 110 mg of the crude product, which consisted of the desired product and insoluble polymeric material. The filtrate was reduced to half volume and treated with diethyl ether to afford a second precipitate, which was isolated, washed with diethyl ether, and purified as below to afford **2**. The first precipitate was purified by column chromatography on alumina with dichloromethane/acetonitrile (1:1) as the eluent. The first fraction was collected, and NMR spectroscopy showed a single compound **1** (yield = 10 mg). (3 %) ESI MS: *m/z* 1097 [Ru<sub>2</sub>Cl<sub>3</sub>L<sub>2</sub>(MeOH)]<sup>+</sup>, 1143 [Ru<sub>2</sub>Cl<sub>3</sub>L<sub>2</sub>(dmsO)]<sup>+</sup>, 1065 [Ru<sub>2</sub>Cl<sub>3</sub>L<sub>2</sub>]<sup>+</sup>; <sup>1</sup>H NMR (500 MHz, [D<sub>6</sub>]DMSO):  $\delta$  = 9.07 (1H, d, *J* = 5.6 Hz, 6py), 8.76 (1H, d, *J* = 7.7 Hz, 3py), 8.43 (1H, t, *J* = 7.7 Hz, 4py), 8.04 (1H, br t, *J* = 6.0 Hz, 5py), 7.24 (2H, d, *J* = 8.2 Hz, Ph<sup>a</sup>), (2H, d, *J* = 8.4 Hz, Ph<sup>b</sup>), 4.32 ppm (2H, s, CH<sub>2</sub>); UV/Vis (CHCl<sub>3</sub>)  $\lambda_{\text{max}}$ : 642, 430, 304 nm.

*trans/cis*-[Ru<sub>2</sub>Cl<sub>4</sub>L<sub>2</sub>] (**2**): The second precipitate (18 mg), obtained from the filtrate of **1**, was purified by column chromatography on alumina with acetonitrile/dichloromethane (1:3) as the eluent. The second fraction was collected, and NMR spectroscopy showed a single compound **2** (yield = 3 mg). (1 % with respect to starting materials) ESI MS: *m/z* 1097 [Ru<sub>2</sub>Cl<sub>3</sub>L<sub>2</sub>(MeOH)]<sup>+</sup>, 1143 [Ru<sub>2</sub>Cl<sub>3</sub>L<sub>2</sub>(dmsO)]<sup>+</sup>, 1065 [Ru<sub>2</sub>Cl<sub>3</sub>L<sub>2</sub>]<sup>+</sup>; <sup>1</sup>H NMR (500 MHz, [D<sub>6</sub>]DMSO; prime numbering is used for the *cis*- $\alpha$  segment):  $\delta$  = 9.59 (1H, d, *J* = 5.6 Hz, 6py'), 9.15 (1H, d, *J* = 5.6 Hz, 6py), 8.76 (1H, d, *J* = 7.8 Hz, 3py'), 8.67 (1H, d, *J* = 7.6 Hz, 3py), 8.40 (1H, t, *J* = 7.7 Hz, 4py), 8.36 (1H, t, *J* = 7.8 Hz, 4py'), 8.0 (2H, m, 5py + 5py'), 7.95 (2H, d, *J* = 8.5 Hz, Ph<sup>a</sup>), 7.12 (2H, d, *J* = 8.5 Hz, Ph<sup>b</sup>), 6.43 (2H, d, *J* = 8.5 Hz, Ph<sup>b</sup>), 6.25 (2H, d, *J* = 8.5 Hz, Ph<sup>a</sup>), 3.84 (1H, d, *J* = 16.0 Hz, CH<sub>2</sub>), 3.79 ppm (1H, d, *J* = 16.0 Hz, CH<sub>2</sub>); UV/Vis (CHCl<sub>3</sub>)  $\lambda_{\text{max}}$ : 601, 389, 349 nm.

*cis/cis*-[Ru<sub>2</sub>Cl<sub>4</sub>L<sub>2</sub>] (**3**): An sample of **2** in CDCl<sub>3</sub> in an NMR tube changed color from green–blue to blue on standing. ESI MS: *m/z* 1125 [Ru<sub>2</sub>L<sub>2</sub>Cl<sub>4</sub> + Na]<sup>+</sup>, 1148 [Ru<sub>2</sub>L<sub>2</sub>Cl<sub>4</sub> + 2Na]<sup>+</sup>, 1099 [Ru<sub>2</sub>L<sub>2</sub>Cl<sub>3</sub>(MeOH)]<sup>+</sup>; <sup>1</sup>H NMR (500 MHz, [D<sub>6</sub>]DMSO):  $\delta$  = 9.35 (1H, d, *J* = 5.9 Hz, 6py), 8.76 (1H, d, *J* = 8.4 Hz, 3py), 8.30 (1H, t, *J* = 7.7 Hz, 4py), 7.85 (1H, br t, *J* = 7.0 Hz, 5py), 6.68 (2H, d, *J* = 8.4 Hz, Ph<sup>b</sup>), 6.46 (2H, d, *J* = 8.6 Hz, Ph<sup>a</sup>), 3.72 ppm (2H, s, CH<sub>2</sub>).

Received: April 5, 2006

Published online: June 27, 2006

**Keywords:** antitumor agents · bioinorganic chemistry · helical structures · ruthenium · supramolecular chemistry

- [1] B. Lippert, *Cisplatin, Chemistry and Biochemistry of a Leading Anticancer Drug*, Wiley-VCH, Weinheim, **1999**; J. Reedijk, *Chem. Commun.* **1996**, 801–806; Z. J. Guo, P. J. Sadler, *Adv. Inorg. Chem.* **2000**, 49, 183–306; J. D. Roberts, J. Peroutka, N. Farrell, *J. Inorg. Biochem.* **1999**, 77, 51–57; S. J. Lippard, J. M. Berg, *Principles of Bioinorganic Chemistry*, University Science Books, Mill Valley, CA, **1994**.
- [2] C. G. Hartinger, S. Zorbas-Selfried, M. A. Jakupce, B. Kynast, H. Zorbas, B. K. Keppler, *J. Inorg. Biochem.* **2006**, 100, 891–904.
- [3] A. C. G. Hotze, S. E. Caspers, D. de Vos, H. Kooijman, A. L. Spek, A. Flamigni, M. Bacac, G. Sava, J. G. Haasnoot, J. Reedijk, *J. Biol. Inorg. Chem.* **2004**, 9, 354–364; A. H. Velders, K. van der Schilden, A. C. G. Hotze, J. Reedijk, H. Kooijman, A. L. Spek, *Dalton Trans.* **2004**, 448–455.
- [4] Y. K. Yan, M. Melchart, A. Habtemariam, P. J. Sadler, *Chem. Commun.* **2005**, 4764–4776.
- [5] E. Alessio, G. Mestroni, A. Bergamo, G. Sava, *Curr. Top. Med. Chem.* **2004**, 4, 1525–1535; E. Alessio, G. Mestroni, A. Bergamo, G. Sava, *Met. Ions Biol. Syst.* **2004**, 42, 323–351.
- [6] N. Farrell, *Met. Ions Biol. Syst.* **2004**, 42, 251–296; T. D. McGregor, A. Hegmans, J. Kasparkova, K. Neplechova, O. Novakova, H. Penazova, O. Vrana, V. Brabec, N. Farrell, *J. Biol. Inorg. Chem.* **2002**, 7, 397–404.
- [7] P. Lincoln, B. Nordén, PCT/SE98/01655, **1998**.
- [8] R. E. Morris, P. J. Sadler, H. Chen, D. Jodrell, US 6,750,251 B2, **2004**; see also: H. C. Chen, J. A. Parkinson, O. Nováková, J. Bella, F. Wang, A. Dawson, R. Gould, S. Parsons, V. Brabec, P. J. Sadler, *Proc. Natl. Acad. Sci. USA* **2003**, 100, 14623–14628.
- [9] M. J. Hannon, V. Moreno, M. J. Prieto, E. Molderheim, E. Sletten, I. Meistermann, C. J. Isaac, K. J. Sanders, A. Rodger, *Angew. Chem.* **2001**, 113, 903–908; *Angew. Chem. Int. Ed.* **2001**, 40, 880–884; I. Meistermann, V. Moreno, M. J. Prieto, E. Molderheim, E. Sletten, S. Khalid, P. M. Rodger, J. Peberdy, C. J. Isaac, A. Rodger, M. J. Hannon, *Proc. Natl. Acad. Sci. USA* **2002**, 99, 5069–5074; A. Oleski, A. G. Blanco, R. Boer, I. Usón, J. Aymami, A. Rodger, M. J. Hannon, M. Coll, *Angew. Chem.* **2006**, 118, 1249–1253; *Angew. Chem. Intl. Ed.* **2006**, 45, 1227–1231; C. Uerpmann, J. Malina, M. Pascu, G. J. Clarkson, V. Moreno, A. Rodger, A. Grandas, M. J. Hannon, *Chem. Eur. J.* **2005**, 11, 1750–1756.
- [10] L. J. Childs, J. Malina, B. E. Rolfsnes, M. Pascu, M. J. Prieto, M. J. Broome, P. M. Rodger, E. Sletten, V. Moreno, A. Rodger, M. J. Hannon, *Chem. Eur. J.* **2006**, 12, 4919–4927.
- [11] C. Piguat, G. Bernardinelli, G. Hopfgartner, *Chem. Rev.* **1997**, 97, 2005–2062; M. Albrecht, *Chem. Rev.* **2001**, 101, 3457–3497; M. J. Hannon, L. J. Childs, *Supramol. Chem.* **2004**, 16, 7–22; A. F. Williams, *Pure Appl. Chem.* **1996**, 68, 1285–1289.
- [12] For example, see: E. C. Constable, M. J. Hannon, A. J. Edwards, P. R. Raithby, *J. Chem. Soc. Dalton Trans.* **1994**, 2669–2677; E. C. Constable, M. J. Hannon, D. A. Tocher, *J. Chem. Soc. Dalton Trans.* **1993**, 1883–1890; S. G. Telfer, T. Sato, R. Kuroda, *Angew. Chem.* **2004**, 116, 591–594; *Angew. Chem. Int. Ed.* **2004**, 43, 581–584 and Refs [11b] and [11c].
- [13] a) J. D. Crane, J.-P. Sauvage, *New. J. Chem.* **1992**, 16, 649–650; b) E. C. Constable, J. V. Walker, *Polyhedron* **1997**, 28, 3089–3100; c) P. K.-K. Ho, K.-K. Cheung, C.-M. Che, *Chem. Commun.* **1996**, 1197–1198; d) M. H. W. Lam, S. T. C. Cheung, K.-M. Fung, W.-T. Wong, *Inorg. Chem.* **1997**, 36, 4618–4619; e) S. Torelli, S. Delahaye, A. Hauser, G. Bernardinelli, C. Piquet, *Chem. Eur. J.* **2004**, 10, 3503–3516.
- [14] a) Crystal data for **1** (*trans/trans*):  $C_{46}H_{36}Cl_4N_{12}Ru_2 \cdot 2CHCl_3 \cdot 2H_2O$ ;  $M_r = 1375.58$ ;  $T = 296(2)$  K,  $\lambda = 1.54178$  Å; monoclinic; space group  $C2/c$ ,  $a = 34.6167(11)$ ,  $b = 11.2147(4)$ ,  $c = 15.9881(5)$  Å,  $\beta = 91.166(2)^\circ$ ;  $V = 6205.5(4)$  Å<sup>3</sup>;  $Z = 4$ ;  $D_c = 1.472$  Mg m<sup>-3</sup>;  $\mu = 8.278$  mm<sup>-1</sup>; crystal size =  $0.50 \times 0.04 \times 0.04$  mm<sup>3</sup>;  $\theta$  range for data collection:  $4.97$ – $70.64^\circ$ ; 19343 reflections collected; 5638 reflections unique ( $R_{int} = 0.077$ ); absorption correction: semiempirical from equivalents; max. and min. transmission: 0.733 and 0.104; 337 parameters; final  $R$  indices: ( $I > 2\sigma(I)$ ):  $R1 = 0.0580$ ,  $wR2 = 0.1530$ ; largest diff. peak and hole: 0.968 and  $-0.771$  e Å<sup>-3</sup>; riding model for hydrogen atoms except those for disordered water positions, which are not included. b) Crystal data for **2** (*trans/cis*):  $C_{46}H_{36}Cl_4N_{12}Ru_2 \cdot 4.5CHCl_3$ ;  $M_r = 1637.9$ ;  $T = 200(2)$  K;  $\lambda = 1.54178$  Å; triclinic; space group  $P\bar{1}$ ,  $a = 13.5414(5)$ ,  $b = 20.8960(6)$ ,  $c = 24.5813(9)$  Å,  $\alpha = 94.338(2)$ ,  $\beta = 94.386(2)$ ,  $\gamma = 95.160(2)^\circ$ ;  $V = 6883.2(4)$  Å<sup>3</sup>;  $Z = 4$ ;  $D_c = 1.581$  Mg m<sup>-3</sup>;  $\mu = 10.161$  mm<sup>-1</sup>; crystal size =  $0.24 \times 0.24 \times 0.06$  mm<sup>3</sup>;  $\theta$  range for data collection:  $2.68$ – $60.88^\circ$ ; 35195 reflections collected; 16611 reflections unique ( $R_{int} = 0.121$ ); absorption correction: semiempirical from equivalents; max. and min. transmission: 0.958 and 0.069; 1428 parameters; final  $R$  indices: ( $I > 2\sigma(I)$ ):  $R1 = 0.0795$ ,  $wR2 = 0.1985$ ; largest diff. peak and hole: 1.77 and  $-1.20$  e Å<sup>-3</sup>; riding model for hydrogen atoms. Solvent positions are disordered, ADPs and geometry were restrained (366 restraints). c) Crystal data for **3** (*cis-cis*):  $C_{46}H_{36}Cl_4N_{12}Ru_2 \cdot 2.5CHCl_3 \cdot 5H_2O$ ;  $M_r = 1481.75$ ;  $T = 200(2)$  K,  $\lambda = 1.54178$  Å; monoclinic; space group  $C2/c$ ,  $a = 16.5258(5)$ ,  $b = 17.4447(5)$ ,  $c = 25.3085(8)$  Å,  $\beta = 105.3280(10)^\circ$ ;  $V = 7036.6(4)$  Å<sup>3</sup>;  $Z = 4$ ;  $D_c = 1.399$  Mg m<sup>-3</sup>;  $\mu = 7.887$  mm<sup>-1</sup>; crystal size =  $0.30 \times 0.28 \times 0.14$  mm<sup>3</sup>;  $\theta$  range for data collection:  $3.62$ – $70.59^\circ$ ; 22137 reflections collected; 6099 reflections unique ( $R_{int} = 0.071$ ); absorption correction: semiempirical from equivalents; max. and min. transmission: 0.8798 and 0.1027; 438 parameters; final  $R$  indices: ( $I > 2\sigma(I)$ ):  $R1 = 0.0773$ ,  $wR2 = 0.2362$ ; largest diff. peak and hole: 1.65 and  $-1.44$  e Å<sup>-3</sup>; riding model for hydrogen atoms. Solvent/water positions are disordered, ADPs and geometry were restrained (60 restraints), water hydrogen atoms for disordered water positions were not included in the refinement. d) Data were recorded on a Bruker Smart 6000 CCD diffractometer using  $Cu_{K\alpha}$  radiation. Structure solution was by direct methods using SIR92 (A. Altomare, G. Cascarano, C. Giacovazzo, A. Guagliardi, *J. Appl. Crystallogr.* **1993**, 26, 343–350) and refinement was by full-matrix least-squares on  $F^2$  using SHELXL97 (G. M. Sheldrick, SHELXL97, Program for Crystal Structure refinement, University of Göttingen, Germany, **1997**). CCDC-603390–603392 contain the supplementary crystallographic data for this paper. These data can be obtained free of charge from The Cambridge Crystallographic Data Center via [www.ccdc.cam.ac.uk/data\\_request/cif](http://www.ccdc.cam.ac.uk/data_request/cif).
- [15] L. J. Childs, M. Pascu, A. J. Clarke, N. W. Alcock, M. J. Hannon, *Chem. Eur. J.* **2004**, 10, 4291–4300.
- [16] M. J. Hannon, C. L. Painting, J. Hamblin, A. Jackson, W. Errington, *Chem. Commun.* **1997**, 1807–1808.
- [17] P. C. Chieh, *J. Chem. Soc. Dalton Trans.* **1972**, 1643; S. Maeda, Y. Nishida, H. Okawa, S. Kida, *Bull. Chem. Soc. Jpn.* **1986**, 59, 2013.
- [18] In fact, in the crystal structure, the twist at the *trans* center is of the opposite helicity to that of the *cis* center, but the twist is so small that it does not affect the double-helical wrapping of the two ligands; the same effect is seen in the *trans/trans* isomer, in which the two *trans* centers have the same helicity but do not induce ligand-strand helical wrapping.
- [19] A. Bergamo, G. Stocco, B. Gava, M. Cocchietto, E. Alessio, B. Serli, E. Iengo, G. Sava, *J. Pharmacol. Exp. Ther.* **2003**, 305, 725–732.

DOI: 10.1002/anie.200601358

# Asymmetric Total Synthesis of (–)-Merrilactone A: Use of a Bulky Protecting Group as Long-Range Stereocontrolling Element\*\*

Masayuki Inoue,\* Takaaki Sato, and Masahiro Hirama

(–)-Merrilactone A ((–)-**1**, Figure 1), a sesquiterpenoid isolated from *Illicium merrillianum* in 2000 by Fukuyama and co-workers,<sup>[1,2]</sup> has been shown to possess neuroprotective and

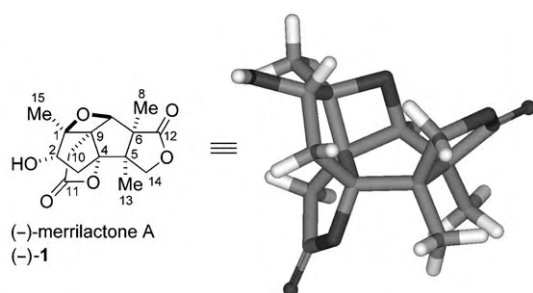


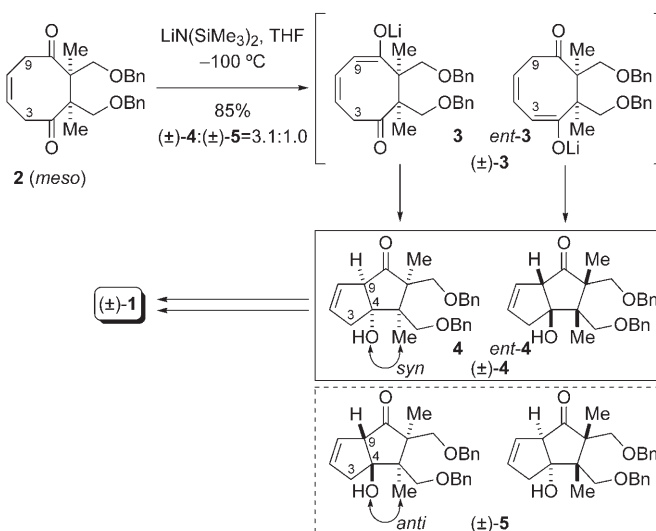
Figure 1. Structure of (–)-merrilactone A.

neurotogenic activity in cultures of fetal rat cortical neurons. Small molecules with these neurotrophic effects are expected to be useful as metabolically stable alternatives to endogenous neurotrophic factors, and thus as therapeutic agents for the neurodegeneration associated with Alzheimer's and Parkinson's diseases.<sup>[3]</sup> By X-ray crystallographic analysis together with extensive NMR spectroscopic studies, **1** was determined to possess a unique pentacyclic cage structure comprising a central bicyclo[3.3.0]octane framework, two  $\delta$ -lactone rings, and an oxetane ring. The absolute configuration

of **1** was established on the basis of the modified Mosher method<sup>[4]</sup> by using MTPA derivatives at C2–OH.<sup>[1]</sup> In addition to its evident architectural complexity, **1** is also very complex from a stereochemical point of view: Five of its seven asymmetrically substituted carbon atoms are contiguous and carry only non-hydrogen substituents (C6, C5, C4, C9, C1). The molecular architecture of **1** is a daunting challenge for chemical synthesis.

Motivated by the important biological activity and unusual structure of **1**, we began a synthetic study, which resulted in the total synthesis of racemic merrilactone A (( $\pm$ )-**1**) in 2003.<sup>[5]</sup> To date, two other chemical routes to ( $\pm$ )-**1** have been developed by the Danishefsky and Mehta research groups,<sup>[6,7]</sup> and Danishefsky and co-workers have reported an elegant asymmetric synthesis of a key intermediate en route to **1**.<sup>[8]</sup> Herein, we report an asymmetric total synthesis of the natural enantiomer (–)-**1** in which a remote bulky protecting group is used to control the stereochemistry. This study also confirmed the assigned absolute configuration for the first time.

In our total synthesis of ( $\pm$ )-**1**, the bicyclo[3.3.0]octane framework was constructed in the form of ( $\pm$ )-**4** through an intramolecular aldol reaction of the benzyl-protected *meso* diketone **2** (Scheme 1).<sup>[9,10]</sup> Importantly, by controlling the



Scheme 1. Diastereoselective transannular aldol reaction of the *meso* diketone **2** in the total synthesis of ( $\pm$ )-**1**.<sup>[5]</sup> Bn = benzyl.

reaction conditions (using LiN(SiMe<sub>3</sub>)<sub>2</sub> in THF) it was possible to favor the selective formation of the desired *syn* isomer ( $\pm$ )-**4** over that of the *anti* isomer ( $\pm$ )-**5**. The key intermediate ( $\pm$ )-**4** was then converted into ( $\pm$ )-**1** through a series of functional-group transformations.

Our plan for preparing enantiomerically pure merrilactone A (–)-**1** was based on the transannular aldol chemistry described above. Theoretically, exclusive deprotonation of C9 of diketone **2** would lead to the bicyclo[3.3.0]octane system **4** with the absolute configuration found in the natural product (**2**→**3**→**4** versus **2**→*ent*-**3**→*ent*-**4**, Scheme 1). We were intrigued by the possibility of differentiating the deprotona-

[\*] Prof. M. Inoue, Dr. T. Sato, Prof. M. Hirama  
Department of Chemistry  
Graduate School of Science, Tohoku University  
Sendai 980-8578 (Japan)  
Fax: (+81) 22-795-6566  
E-mail: inoue@ykbsc.chem.tohoku.ac.jp

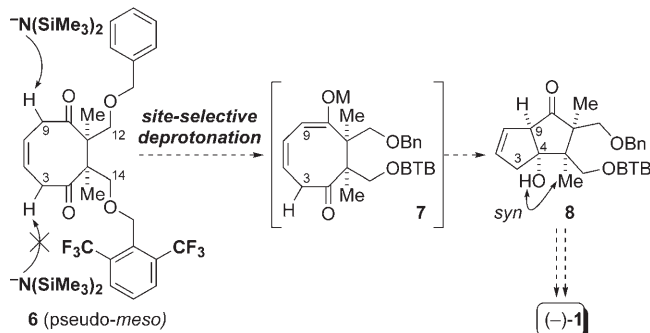
Prof. M. Inoue  
Research and Analytical Center for Giant Molecules  
Graduate School of Science, Tohoku University  
and  
PRESTO  
Japan Science and Technology Agency  
Sendai 980-8578 (Japan)

[\*\*] This research was supported by a Grant-in-Aid for Young Scientists (A) from the Japan Society for the Promotion of Science (JSPS) and a SUNBOR Grant awarded to M.I. A fellowship awarded to T.S. by the JSPS is gratefully acknowledged. We thank Professor Yoshiyasu Fukuyama (Tokushima Bunri University) for providing NMR spectra of merrilactone A and its MTPA derivatives, and Dr. Chizuko Kabuto for crystallographic analyses.

Supporting information for this article is available on the WWW under <http://www.angewandte.org> or from the author.



tion rates at C9 and C3 by utilizing a pseudo-*meso* substrate: The attachment of a bulky protecting group at C14–OH would effectively shield C3–H through a long-range steric interaction (Scheme 2).<sup>[11]</sup> To apply the reaction sequence

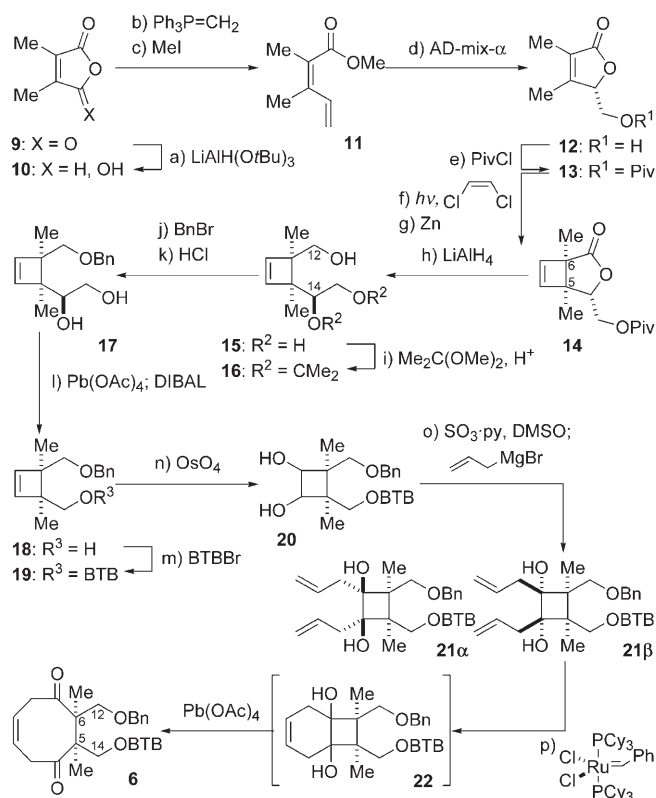


**Scheme 2.** Strategy for the asymmetric synthesis of the core bicyclo[3.3.0]octane framework of (-)-merrillactone A from a pseudo-*meso* diketone.

developed from ( $\pm$ )-4 to ( $\pm$ )-1, this bulky protecting group needed to be as stable as Bn in a variety of reactions and to be removed simultaneously with Bn in the final stage of the total synthesis. Since no existing alcohol protecting group met these requirements, we designed a new benzyl ether, 2,6-bis(trifluoromethyl)benzyl (BTB) ether, which has chemically inert CF<sub>3</sub> groups at the two *ortho* positions to impose a large steric effect.<sup>[12]</sup> Thus, our subsidiary goals in the asymmetric total synthesis were to prepare the differentially protected diketone 6 and to evaluate the BTB group as a remote stereocontrolling element for the selective generation of 7 and 8.

To establish the absolute configuration of the two quaternary carbon atoms (C5, C6) of diketone 6, we planned a [2+2] photocycloaddition of the chiral tetrasubstituted olefin 13 (Scheme 3).<sup>[13,14]</sup> The reduction of 2,3-dimethylmaleinic anhydride (9) to 10,<sup>[15]</sup> followed by Wittig olefination and esterification, afforded methyl ester 11 in 68% yield (three steps). Chemo- and enantioselective dihydroxylation of dienone 11 under Sharpless asymmetric dihydroxylation conditions with the catalyst (DHQD)<sub>2</sub>PHAL led to enantiomerically pure 12 (>99% *ee*) in 65% yield after one recrystallization.<sup>[16]</sup> This hydroxy- $\gamma$ -lactone was protected as its pivalate ester 13.<sup>[17]</sup> The irradiation of 13 in the presence of *cis*-1,2-dichloroethylene with a high-pressure mercury lamp, followed by Zn-promoted dechlorination then afforded 14, the LiAlH<sub>4</sub> reduction of which gave cyclobutene 15 (75%) along with its facial diastereomer (8%). Thus, furanone 13 showed excellent facial discrimination (9.8:1) in the photocycloaddition and acted as a template for the stereoselective introduction of the two quaternary carbon atoms C5 and C6.<sup>[18]</sup> The structure of triol 15 was determined unambiguously by single-crystal X-ray analysis of 23 (Figure 2), the product of mono-*p*-bromobenzoylation of 15.

The additional hydroxymethyl group attached to C14 of 15 made it possible to introduce the two benzyl-type protecting groups at the C12 and C14 alcohol groups in a stepwise fashion (Scheme 3). After triol 15 had been protected as its



**Scheme 3.** Synthesis of the pseudo-*meso* diketone 6; (the principal reagents are also shown in the Scheme): a) LiAlH(OtBu)<sub>3</sub>, DME, -15 °C  $\rightarrow$  RT, 85%; b) Ph<sub>3</sub>PCH<sub>3</sub><sup>+</sup>Br<sup>-</sup>, tBuOK, 0 °C  $\rightarrow$  RT, 87%; c) MeI, K<sub>2</sub>CO<sub>3</sub>, THF, 50 °C, 92%; d) AD-mix- $\alpha$ , tBuOH/H<sub>2</sub>O (1:1), 0 °C, 90%, 90% *ee*; then recrystallization: 65%, > 99% *ee*; e) PivCl, py, DMAP, CH<sub>2</sub>Cl<sub>2</sub>, room temperature, 99%; f) *cis*-dichloroethylene, CH<sub>3</sub>CN, -20 °C; g) Zn, Ac<sub>2</sub>O, toluene, 120 °C; h) LiAlH<sub>4</sub>, Et<sub>2</sub>O, room temperature, 75% (15, 3 steps), 8% (the facial diastereomer, 3 steps); i) Me<sub>2</sub>C(OMe)<sub>2</sub>, TsOH·H<sub>2</sub>O, CH<sub>2</sub>Cl<sub>2</sub>, room temperature, 81%; j) BnBr, NaH, THF/DMF (10:1), room temperature; k) THF/3 M HCl (5:1), room temperature, 91% (2 steps); l) Pb(OAc)<sub>4</sub>, py, CH<sub>2</sub>Cl<sub>2</sub>, -50 °C; then DIBAL, -78 °C  $\rightarrow$  -50 °C, 93% (90% conversion); m) BTBBr, KH, [18]crown-6, DMF, room temperature; n) OsO<sub>4</sub>, NMO, tBuOMe/tBuOH/H<sub>2</sub>O (2:1:1), room temperature, 94% (89% conversion; 2 steps); o) SO<sub>3</sub>·Py, iPr<sub>2</sub>NEt, DMSO, CH<sub>2</sub>Cl<sub>2</sub>, -15 °C; then allylmagnesium bromide, -78 °C, 78% (21 $\alpha$ /21 $\beta$  2.7:1); p) [(PCy<sub>3</sub>)<sub>2</sub>Cl<sub>2</sub>Ru=CHPh], CH<sub>2</sub>Cl<sub>2</sub>, reflux; then Pb(OAc)<sub>4</sub>, room temperature, 97%. Cy = cyclohexyl, DMAP = 4-dimethylaminopyridine, DME = dimethoxyethane, DIBAL = dibutylaluminum hydride, DMF = *N,N*-dimethylformamide, DMSO = dimethyl sulfoxide, NMO = *N*-methylmorpholine *N*-oxide, Piv = pivaloyl, py = pyridine, Ts = *p*-toluenesulfonyl.

isopropylidene acetal 16, Bn protection of the C12–OH group of 16 and subsequent removal of the acetonide under acidic conditions delivered the 1,2-diol 17 (91%, two steps). One-carbon-atom truncation from 17 to liberate the masked primary C14–OH functionality was carried out in a single-flask reaction involving Pb(OAc)<sub>4</sub>-induced oxidative cleavage and DIBAL reduction, and led to 18 in 93% yield.<sup>[19]</sup> The BTB group was then introduced at C14–OH in 18 to afford differentially protected 19.

By exploiting the pseudo-*meso* symmetry of 19, diketone 6 was prepared in only three steps through pairwise functionalization.<sup>[20]</sup> Olefin 19 was subjected to dihydroxylation to afford diol 20, the one-pot treatment of which with SO<sub>3</sub>·py<sup>[21]</sup>



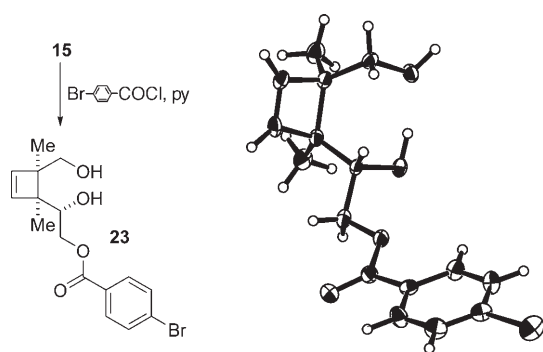
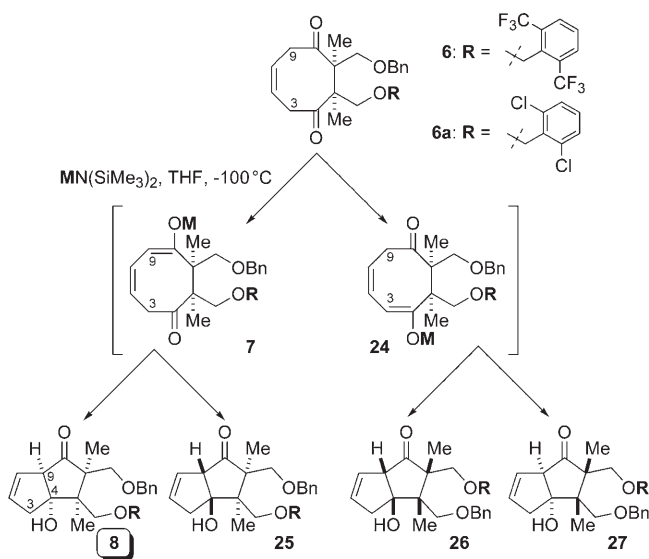


**Figure 2.** X-ray crystallographic analysis of compound **23** to confirm the structure of triol **15**.<sup>[41]</sup>

and an allyl Grignard reagent provided adducts **21a** and **21b** in 78 % yield.<sup>[22]</sup> The *cis* relationship of the olefinic side chains of **21a** and **21b** facilitated the subsequent ring-closing metathesis reaction to produce the bicyclo[4.2.0]octyl system **22**,<sup>[23]</sup> which was subjected in situ to Pb(OAc)<sub>4</sub>-promoted oxidative ring expansion<sup>[24]</sup> to yield the substituted eight-membered ring **6**.

Having established a route to the differentially protected diketone **6**, we undertook the crucial transannular aldol reaction. To our gratification, the reaction of **6** with LiN(SiMe<sub>3</sub>)<sub>2</sub> (Scheme 4, entry 1) exhibited both site-selective deprotonation (**7/24**) and diastereoselective C–C bond for-

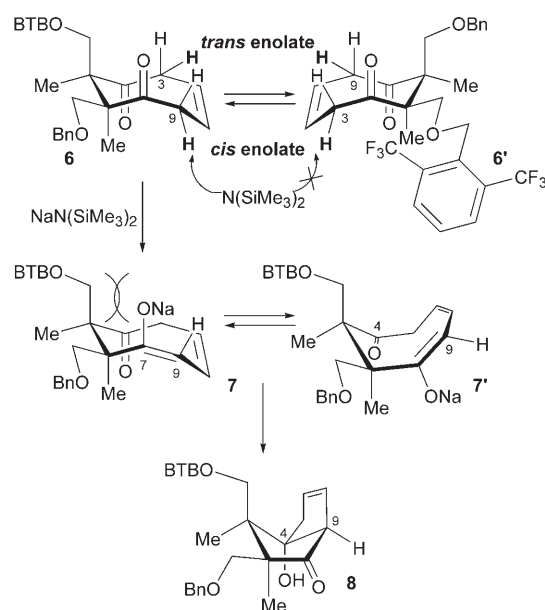


Entry	R	M <sup>+</sup>	7/24	8/25	Yield	
					combined	8
1	BTB	Li <sup>+</sup>	3.5 : 1	9.2 : 1	91%*	65%*
2	BTB	Na <sup>+</sup>	4.5 : 1	17.0 : 1	97%	75%
3	BTB	K <sup>+</sup>	2.5 : 1	9.5 : 1	78%	51%
4	DCB	Na <sup>+</sup>	2.8 : 1	7.9 : 1	89%	58%

**Scheme 4.** Diastereoselective transannular aldol reaction of pseudo-meso diketones **6** and **6a**. The yields of entry 1 are based on recovered starting material (82% conversion).

mation (**8/25**) to give the desired bicyclo[3.3.0]octane system **8**<sup>[25]</sup> along with smaller amounts of the other three diastereomers **25–27**. To enhance the formation of **8**, the effect of the counter cation of the amide base was examined (entries 2, 3): When **6** was treated with NaN(SiMe<sub>3</sub>)<sub>2</sub>, enantiomerically pure **8** was isolated in 75 % yield after purification by column chromatography with SiO<sub>2</sub>. Interestingly, the selectivity of the same base treatment of **6a**, which possesses the less sterically demanding protecting group 2,6-dichlorobenzyl (DCB; effective radii: 2.2 Å (CF<sub>3</sub>) versus 1.7 Å (Cl)),<sup>[26]</sup> was lower in both the deprotonation and the C–C bond-forming steps (entry 4). This result clearly suggests that the steric bulk of the *ortho* substituents of the phenyl ring has a significant effect on the selectivity of the reaction. As expected, our BTB group functioned as a long-range stereocontrolling element for the aldol reaction.

A plausible mechanism for the reaction is shown in Scheme 5. Molecular modeling (MM2\*, MacroModel Ver-



**Scheme 5.** Plausible mechanism for the diastereoselective transannular aldol reaction of **6**.

sion 8.5)<sup>[27]</sup> indicated that the eight-membered ring exists as a mixture of two pseudoenantiomeric conformers **6** and **6'**.<sup>[28]</sup> Since *cis*-enolate formation from the eight-membered ring is energetically more favorable than *trans*-enolate formation, in each conformer only one of the two protons (indicated in bold face in Scheme 5) orthogonal to the C=O bonds is thought to be abstracted by the base. The selective deprotonation of **6** to generate the *cis* enolate **7** can be explained by effective insulation of C9 of **6'** by the remote bulky BTB group. After enolate formation, the severe 1,3-diaxial-like steric interaction between the large BTB-protected oxymethylene group and the C7–O bond in **7**<sup>[29]</sup> would enforce a conformational flip of the C7–C9 olefin to form **7'**, from which the enolate can react with the ketone at C4 to generate the desired *cis*-fused 5,5 ring system **8**. The proposed mechanism agrees well with the observation that the bulkier protecting group is more

selective in both the deprotonation and C–C bond-forming steps (Scheme 4, entries 2 and 4).

With the enantiomerically pure bicyclo[3.3.0]octane framework **8** in hand, we proceeded to synthesize the entire carboskeleton of (–)-**1** by introduction of the C9 quaternary center and the C15 methylene group (Scheme 6).  $\alpha$ -Epoxidation of **8** and subsequent florasil treatment produced allylic alcohol **28**, which was converted into enedione **29**.<sup>[30]</sup> An  $\alpha$ -bromoacetal unit was then introduced to afford **30** as a mixture of diastereomers.<sup>[31]</sup>

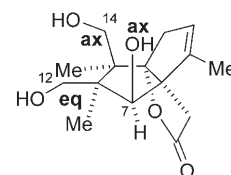
Despite the steric congestion induced around C9 by the three proximal tetrasubstituted carbon atoms (C4, C5, C6), radical cyclization of **30** smoothly delivered the 5-*exo* cyclized product **31** along with its C11 epimer **32** in 90% combined yield. Upon treatment with EtOSiMe<sub>3</sub> in the presence of BF<sub>3</sub>·Et<sub>2</sub>O, the minor isomer **32** was transformed into the major isomer **31** in 72% yield. NOESY data obtained for **31** allowed the assignment of configuration and conformation (Scheme 6): The CH<sub>2</sub> group at position 3 was found to be in spatial proximity to the ethoxy and BTB-protected oxy-methylene groups. Presumably because of low base accessibility to the sterically crowded C3 center, in the next step the reaction of **31** with Me<sub>3</sub>SiOTf and Et<sub>3</sub>N produced predominantly silyl enol ether **33** through site-selective deprotonation at the less-shielded C1 center. The C15 methylene group was introduced by the treatment of **33** with the Eschenmoser reagent<sup>[32]</sup> and then with *m*CPBA to give **34**.

To complete the total synthesis, the remaining functional-group manipulations needed to be orchestrated judiciously. First, acetal **34** was converted quantitatively into  $\gamma$ -lactone **35**.<sup>[33]</sup> Hydride addition to the *exo* alkene of the unsaturated ketone **35**, followed by in situ triflation, afforded the enol

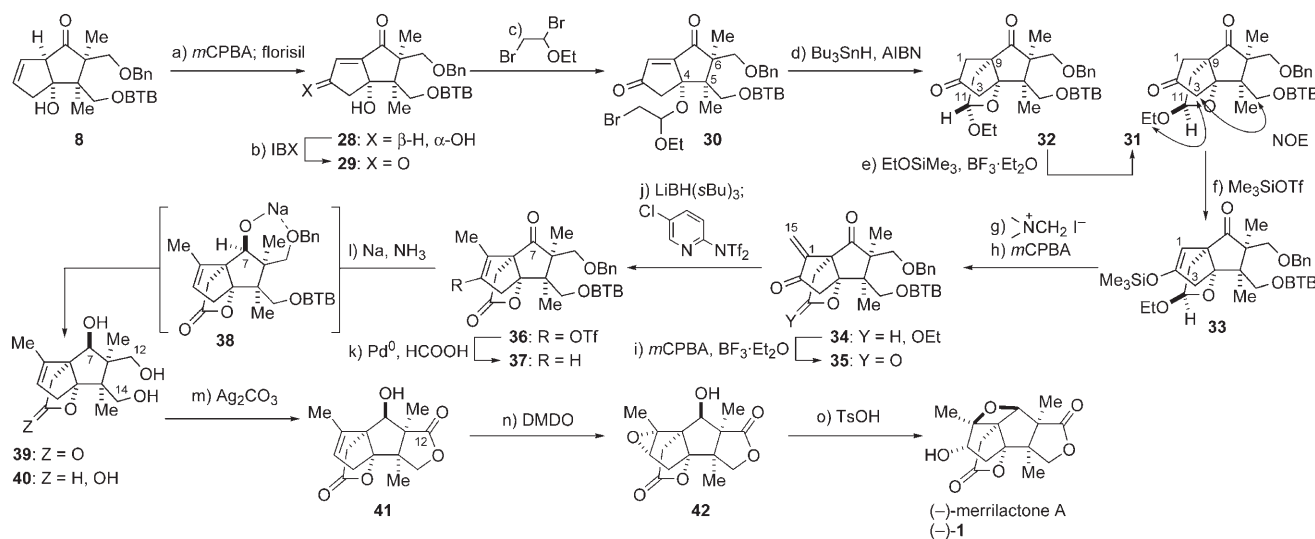
triflate **36**,<sup>[34,35]</sup> which was converted into the trisubstituted alkene **37** through palladium-mediated reduction.<sup>[36]</sup> The exposure of **37** to Na in NH<sub>3</sub><sup>[37]</sup> effected both the stereoselective reduction of the hindered ketone at C7 to the  $\beta$ -hydroxy group, presumably via **38** through a six-membered chelate ring, and the removal of both benzyl-type protecting groups (Bn and BTB) to give lactol **40** along with lactone **39**.

The mixture of **39** and **40** was in turn subjected to Fetizon oxidation<sup>[38]</sup> to produce the desired bis- $\gamma$ -lactone **41** as a single isomer. It appears that the reactivity of the hydroxy group at C12 in **39/40** towards oxidation is higher than that of the hydroxy groups at C7 and C14 as a result of its more exposed nature: Molecular modeling of **40** suggested that only the C12 hydroxymethyl group adopts a pseudoequatorial position, as depicted in Scheme 7. Thus, the remarkable selectivities of the reduction (**37**→**40**) and oxidation (**40**→**41**) steps are governed by the intrinsic three-dimensional orientation of the reacting substituents. Moreover, the stereochemical controlling factor for the aldol reaction, the BTB ether, was shown to be robust under a variety of reaction conditions up to those for the synthesis of **39**, yet was removed smoothly through Birch reduction.

Finally, stereoselective  $\alpha$  epoxidation of **41** with dimethyldioxirane<sup>[39]</sup> to give **42** and subsequent acid-mediated epoxide opening–oxetane formation delivered (–)-merrilactone A ((–)-**1**).<sup>[1]</sup> Synthetic (–)-**1** exhibited <sup>1</sup>H NMR, <sup>13</sup>C NMR, IR, and HRMS spectra that were indistinguishable



**Scheme 7.** Conformation of **40** according to molecular modeling.



**Scheme 6.** Asymmetric total synthesis of (–)-merrilactone A; (the principal reagents are also shown in the Scheme): a) *m*CPBA, CH<sub>2</sub>Cl<sub>2</sub>; then florasil, CH<sub>2</sub>Cl<sub>2</sub>, room temperature, 75%; b) IBX, DMSO, room temperature, 91%; c) BrCH<sub>2</sub>Br(OEt), PhNMe<sub>2</sub>, CH<sub>2</sub>Cl<sub>2</sub>, –78 °C → RT, 92% (d.r. 4.4:1, 79% conversion); d) Bu<sub>3</sub>SnH, AIBN, toluene, 85 °C, 73% (**31**), 17% (**32**); e) EtOSiMe<sub>3</sub>, BF<sub>3</sub>·Et<sub>2</sub>O, CH<sub>2</sub>Cl<sub>2</sub>, room temperature, 72%; f) Me<sub>3</sub>SiOTf, Et<sub>3</sub>N, CH<sub>2</sub>Cl<sub>2</sub>, –20 °C; g) Me<sub>2</sub>NCH<sub>2</sub><sup>+</sup>I<sup>–</sup>, CH<sub>3</sub>CN, room temperature; h) *m*CPBA, CH<sub>2</sub>Cl<sub>2</sub>, room temperature, 64% (3 steps); i) *m*CPBA, BF<sub>3</sub>·Et<sub>2</sub>O, CH<sub>2</sub>Cl<sub>2</sub>, room temperature, 100%; j) LiBH(sBu)<sub>3</sub>, 2-Tf<sub>2</sub>N-5-chloropyridine, THF, –78 °C, 73%; k) Pd(OAc)<sub>2</sub>, PPh<sub>3</sub>, NBu<sub>3</sub>, HCOOH, DMF, 40 °C, 92%; l) Na, NH<sub>3</sub>, THF/EtOH (5:1), –78 °C (**39/40** 1:1.4); m) Ag<sub>2</sub>CO<sub>3</sub> on celite, toluene, 130 °C, 41% (2 steps); n) DMDO, CH<sub>2</sub>Cl<sub>2</sub>, room temperature, 91%; o) TsOH·H<sub>2</sub>O, CH<sub>2</sub>Cl<sub>2</sub>, room temperature, 96%. AIBN = *N,N*-azobisisobutyronitrile, DMDO = dimethyldioxirane, IBX = *o*-iodoxybenzoic acid, *m*CPBA = *m*-chloroperbenzoic acid, Tf = trifluoromethanesulfonyl, Ts = *p*-toluenesulfonyl.

from those of the natural compound. The measured optical rotation of synthetic (–)-**1** confirmed the absolute configuration of the natural product ( $[\alpha]_{\text{D}}^{27} = -15.7$  ( $c = 0.19$ ,  $\text{CHCl}_3$ ); natural (–)-**1**:  $[\alpha]_{\text{D}}^{18} = -16.7$  ( $c = 1.10$ ,  $\text{CHCl}_3$ )).<sup>[2, 40]</sup>

In summary, we have completed the asymmetric total synthesis of (–)-merrillactone A (1.1% overall yield, 31 steps). The defining step in our synthesis is the diastereoselective transannular aldol reaction of **6** to construct the bicyclo[3.3.0]octane core **8**. The selectivity observed in the construction of the two new stereocenters in **8** is a long-range effect of the bulky protecting group BTB. Other remarkable features of our total synthesis include 1) a [2+2] cycloaddition to install the two contiguous quaternary carbon atoms of **14**, 2) efficient pairwise symmetrical functionalization to synthesize **6** by taking advantage of the pseudo-*meso* symmetry, 3) radical cyclization to form the sterically congested C9 quaternary carbon atom of **31**, and 4) highly selective substrate-controlled reactions to introduce three functional groups: the C15 methylene group of **34**, the  $\beta$ -hydroxy group at C7 of **40**, and the C12-containing  $\gamma$ -lactone in **41**.

Received: April 6, 2006

Published online: June 23, 2006

**Keywords:** aldol reaction · asymmetric synthesis · medium-ring compounds · protecting groups · terpenoids

- [1] a) J.-M. Huang, R. Yokoyama, C.-S. Yang, Y. Fukuyama, *Tetrahedron Lett.* **2000**, *41*, 6111; b) J.-M. Huang, C.-S. Yang, M. Tanaka, Y. Fukuyama, *Tetrahedron* **2001**, *57*, 4691.
- [2] The reported optical rotation of merrillactone A ( $[\alpha]_{\text{D}}^{21} = +11.8$  ( $c = 1.20$ ,  $\text{CH}_3\text{OH}$ ), reference [1a]) was found to be an error. The correct value for the natural product is:  $[\alpha]_{\text{D}}^{18} = -16.7$  ( $c = 1.10$ ,  $\text{CH}_3\text{OH}$ ): private communication from Prof. Y. Fukuyama (Tokushima Bunri University).
- [3] For reviews on neurotrophic activity, see: a) F. Hefti, *J. Neurobiol.* **1994**, *25*, 1418; b) F. Hefti, *Annu. Rev. Pharmacol. Toxicol.* **1997**, *37*, 239; c) M. V. Sofroniew, C. L. Howe, W. C. Mobley, *Annu. Rev. Neurosci.* **2001**, *24*, 1217.
- [4] I. Ohtani, T. Kusumi, Y. Kashman, H. Kakisawa, *J. Am. Chem. Soc.* **1991**, *113*, 4092.
- [5] M. Inoue, T. Sato, M. Hiram, *J. Am. Chem. Soc.* **2003**, *125*, 10772.
- [6] a) V. B. Birman, S. J. Danishefsky, *J. Am. Chem. Soc.* **2002**, *124*, 2080; b) G. Mehta, S. R. Singh, *Angew. Chem.* **2006**, *118*, 967; *Angew. Chem. Int. Ed.* **2006**, *45*, 953.
- [7] For synthetic studies on merrillactone A, see: a) B.-C. Hong, Y.-J. Shr, J.-L. Wu, A. K. Gupta, K.-J. Lin, *Org. Lett.* **2002**, *4*, 2249; b) G. Mehta, S. R. Singh, *Tetrahedron Lett.* **2005**, *46*, 2079; c) J. Iriondo-Alberdi, J. E. Perea-Buceta, M. F. Greaney, *Org. Lett.* **2005**, *7*, 3969; d) K. Harada, H. Kato, Y. Fukuyama, *Tetrahedron Lett.* **2005**, *46*, 7407.
- [8] a) Z. Meng, S. J. Danishefsky, *Angew. Chem.* **2005**, *117*, 1535; *Angew. Chem. Int. Ed.* **2005**, *44*, 1511; b) H. Yun, Z. Meng, S. J. Danishefsky, *Heterocycles* **2005**, *66*, 711.
- [9] For reviews on the construction of eight-membered rings, see: a) N. A. Petasis, M. A. Patane, *Tetrahedron* **1992**, *48*, 5757; b) G. Mehta, V. Singh, *Chem. Rev.* **1999**, *99*, 881; c) M. E. Maier, *Angew. Chem.* **2000**, *112*, 2153; *Angew. Chem. Int. Ed.* **2000**, *39*, 2073; d) L. Yet, *Chem. Rev.* **2000**, *100*, 2963.
- [10] For selected examples of the synthesis of bicyclo[3.3.0]octane systems from eight-membered rings, see: a) J. T. Negri, T. Morwick, J. Doyon, P. D. Wilson, E. R. Hickey, L. A. Paquette, *J. Am. Chem. Soc.* **1993**, *115*, 12189; b) L. A. Paquette, F. Geng, *J. Am. Chem. Soc.* **2002**, *124*, 9199; c) L. A. Paquette, *Eur. J. Org. Chem.* **1998**, 1709; d) P. A. Wender, C. R. D. Correia, *J. Am. Chem. Soc.* **1987**, *109*, 2523; e) P. A. Wender, G. G. Gamber, R. D. Hubbard, L. Zhang, *J. Am. Chem. Soc.* **2002**, *124*, 2876; f) M. Zora, I. Koyuncu, B. Yucel, *Tetrahedron Lett.* **2000**, *41*, 7111; g) S. K. Verma, E. B. Fleischer, H. W. Moore, *J. Org. Chem.* **2000**, *65*, 8564; h) D. M. Hodgson, I. D. Cameron, *Org. Lett.* **2001**, *3*, 441; i) K. G. Dongol, R. Wartchow, H. Butenschön, *Eur. J. Org. Chem.* **2002**, 1972; j) T. Hamura, S. Tsuji, T. Matsumoto, K. Suzuki, *Chem. Lett.* **2002**, 280.
- [11] For recent applications of O-protecting groups as long-range stereocontrolling elements, see: a) G. Guanti, S. Perrozzi, R. Riva, *Tetrahedron: Asymmetry* **2002**, *13*, 2703; b) I. A. I. Ali, E. S. H. El Ashry, R. R. Schmidt, *Eur. J. Org. Chem.* **2003**, 4121; c) M. Inoue, T. Sasaki, S. Hatano, M. Hiram, *Angew. Chem.* **2004**, *116*, 6662; *Angew. Chem. Int. Ed.* **2004**, *43*, 6500; d) H. Tokimoto, Y. Fujimoto, K. Fukase, S. Kusumoto, *Tetrahedron: Asymmetry* **2005**, *16*, 441.
- [12] It is important from a practical viewpoint that the requisite bulky benzyl bromide BTBB (Scheme 3) was prepared in two steps from commercially available 1,3-bis(trifluoromethyl)benzene (see the Supporting information).
- [13] For reviews on the construction of quaternary stereocenters, see: a) E. J. Corey, A. Guzman-Perez, *Angew. Chem.* **1998**, *110*, 402; *Angew. Chem. Int. Ed.* **1998**, *37*, 388; b) J. Christoffers, A. Mann, *Angew. Chem.* **2001**, *113*, 4725; *Angew. Chem. Int. Ed.* **2001**, *40*, 4591; c) I. Denisova, L. Barriault, *Tetrahedron* **2003**, *59*, 10105; d) C. J. Douglas, L. E. Overman, *Proc. Natl. Acad. Sci. USA* **2004**, *101*, 5363.
- [14] a) R. Alibés, P. D. March, M. Figueredo, J. Font, M. Racamonde, A. Rustullet, A. Alvarez-Larena, J. F. Piniella, T. Parella, *Tetrahedron Lett.* **2003**, *44*, 69; b) R. Alibés, P. D. March, M. Figueredo, J. Font, M. Racamonde, T. Parella, *Org. Lett.* **2004**, *6*, 1449.
- [15] T. Harrison, P. L. Myers, G. Pattenden, *Tetrahedron* **1989**, *45*, 5247.
- [16] a) H. Becker, M. A. Soler, K. B. Sharpless, *Tetrahedron* **1995**, *51*, 1345; b) H. C. Kolb, M. S. VanNieuwenhze, K. B. Sharpless, *Chem. Rev.* **1994**, *94*, 2483.
- [17] For an alternative synthetic route to a related compound, see: S. Hanessian, P. J. Murray, *J. Org. Chem.* **1987**, *52*, 1170.
- [18] For recent reviews on cyclobutane derivatives, see: a) E. Lee-Ruff, G. Mladenova, *Chem. Rev.* **2003**, *103*, 1449; b) J. C. Namyslo, D. E. Kaufmann, *Chem. Rev.* **2003**, *103*, 1485.
- [19] The yield of this reaction was highly dependent on the reaction temperature. When the oxidative cleavage of **17** was performed at room temperature, the resulting aldehyde underwent facile electrocyclic ring opening to generate a 2Z,4E dienal as the sole product. For related reactions, see: F. Binns, R. Hayes, S. Ingham, S. T. Saengchantara, R. W. Turner, T. W. Wallace, *Tetrahedron* **1992**, *48*, 515.
- [20] For reviews on related approaches, including two-directional synthesis, see: a) C. S. Poss, S. L. Schreiber, *Acc. Chem. Res.* **1994**, *27*, 9; b) S. R. Magnuson, *Tetrahedron* **1995**, *51*, 2167.
- [21] J. R. Parikh, W. E. Doering, *J. Am. Chem. Soc.* **1967**, *89*, 5505.
- [22] R. E. Ireland, D. W. Norbeck, *J. Org. Chem.* **1985**, *50*, 2198.
- [23] a) G. C. Fu, S. T. Nguyen, R. H. Grubbs, *J. Am. Chem. Soc.* **1993**, *115*, 9856; b) P. Schwab, R. H. Grubbs, J. W. Ziller, *J. Am. Chem. Soc.* **1996**, *118*, 100; c) A. Fürstner, *Angew. Chem.* **2000**, *112*, 3140; *Angew. Chem. Int. Ed.* **2000**, *39*, 3012; d) T. M. Trnka, R. H. Grubbs, *Acc. Chem. Res.* **2001**, *34*, 18; e) K. C. Nicolaou, P. G. Bulger, D. Sarlah, *Angew. Chem.* **2005**, *117*, 4564; *Angew. Chem. Int. Ed.* **2005**, *44*, 4490.
- [24] E. P. Balskus, J. Méndez-Andino, R. M. Arbit, L. A. Paquette, *J. Org. Chem.* **2001**, *66*, 6695.

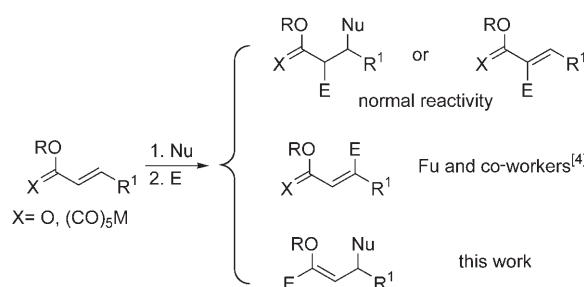
- [25] The structure of **8** was determined by NMR spectroscopy on the basis of HMBC and NOE data, and was later confirmed through the X-ray crystallographic analysis of **29** (see the Supporting information).<sup>[41]</sup>
- [26] G. Bott, L. D. Field, S. Sternhell, *J. Am. Chem. Soc.* **1980**, *102*, 5618.
- [27] F. Mohamadi, N. G. J. Richards, W. C. Guida, R. Liskamp, M. Lipton, C. Caufield, G. Chang, T. Hendrickson, W. C. Still, *J. Comput. Chem.* **1990**, *11*, 440.
- [28] When the temperature was lowered to  $-100^{\circ}\text{C}$  in  $[\text{D}_8]\text{THF}$ , the  $^1\text{H}$  NMR signals separated into two sets of peaks corresponding to two interconverting conformers (2.5:1). The structures of the conformers could not be determined because of signal overlap.
- [29] The formation of a highly strained *trans*-fused 5,5 ring system from conformer **7** is unlikely; see: a) S. Chang, D. McNally, S. Shary-Tehrany, S. M. J. Hickey, R. H. Boyd, *J. Am. Chem. Soc.* **1970**, *92*, 3109; b) N. L. Allinger, M. T. Tribble, M. A. Miller, D. H. Wertz, *J. Am. Chem. Soc.* **1971**, *93*, 1637.
- [30] M. Frigerio, M. Santagostino, S. Sputore, G. Palmisano, *J. Org. Chem.* **1995**, *60*, 7272.
- [31] a) Y. Ueno, K. Chino, M. Watanabe, O. Moriya, M. Okawara, *J. Am. Chem. Soc.* **1982**, *104*, 5564; b) G. Stork, R. Mook, Jr., S. A. Biller, S. D. Rychnovsky, *J. Am. Chem. Soc.* **1983**, *105*, 3741; c) W. Zhang, *Tetrahedron* **2001**, *57*, 7237; d) X. J. Salom-Roig, F. Dénès, P. Renaud, *Synthesis* **2004**, 1903; e) G. S. C. Srikanth, S. L. Castle, *Tetrahedron* **2005**, *61*, 10377.
- [32] S. Danishefsky, T. Kitahara, R. McKee, P. F. Schuda, *J. Am. Chem. Soc.* **1976**, *98*, 6715.
- [33] P. A. Grieco, T. Oguri, Y. Yokoyama, *Tetrahedron Lett.* **1978**, 419.
- [34] G. T. Crisp, W. J. Scott, *Synthesis* **1985**, 335.
- [35] D. L. Comins, A. Dehghani, *Tetrahedron Lett.* **1992**, *33*, 6299.
- [36] S. Cacchi, E. Morera, G. Ortar, *Tetrahedron Lett.* **1984**, *25*, 4821.
- [37] J. W. Huffman, J. T. Charles, *J. Am. Chem. Soc.* **1968**, *90*, 6486.
- [38] a) M. Fetizon, M. Golfier, *C. R. Hebd. Seances Acad. Sci.* **1968**, *267*, 900; b) A. McKillop, D. W. Young, *Synthesis* **1979**, 401.
- [39] a) R. W. Murray, *Chem. Rev.* **1989**, *89*, 1187; b) W. Adam, R. Curci, J. O. Edwards, *Acc. Chem. Res.* **1989**, *22*, 205.
- [40] The absolute structure of (–)-**1** was further supported by  $^1\text{H}$  NMR spectroscopic data of MTPA ester derivatives of synthetic and natural (–)-**1** (see the Supporting Information).
- [41] CCDC-603839 (**23**) and CDCC-603840 (**29**) contain the supplementary crystallographic data for this paper. These data can be obtained free of charge from The Cambridge Crystallographic Data Centre via [www.ccdc.cam.ac.uk/data\\_request/cif](http://www.ccdc.cam.ac.uk/data_request/cif).



# Umpolung Reactivity of Alkenyl Fischer Carbene Complexes, Copper Enolates, and Electrophiles\*\*

José Barluenga,\* Abraham Mendoza,  
Alejandro Diéguez, Félix Rodríguez, and  
Francisco J. Fañanás

The umpolung of the “normal” reactivity of a functional group stands as a very interesting objective in synthetic organic chemistry.<sup>[1]</sup> For example, in general,  $\alpha,\beta$ -unsaturated esters react with nucleophiles at the  $\beta$ -position through a conjugate addition to generate an enolate that further reacts with electrophiles at the  $\alpha$ -position (Scheme 1).<sup>[2], [3]</sup> Fu and



**Scheme 1.** Comparison of conjugate normal and umpolung reactivity of Michael acceptors. E = electrophile, Nu = nucleophile, M = metal.

co-workers very recently reported an umpolung reactivity of  $\alpha,\beta$ -unsaturated esters (Scheme 1).<sup>[4]</sup> In this interesting work, the normally electrophilic  $\beta$ -carbon atom is transformed into a nucleophilic site through an addition–tautomerization sequence.<sup>[5]</sup> Herein, we wish to report a new conjugate umpolung reactivity of Michael acceptors (Scheme 1).

Fischer carbene complexes,<sup>[6]</sup> and in particular  $\alpha,\beta$ -unsaturated carbene complexes, have become very interesting tools in organic synthesis.<sup>[7]</sup> It is well known that these compounds, which may be considered as  $\alpha,\beta$ -unsaturated ester equivalents, behave as Michael acceptors. Thus, in this context we recently reported the 1,4-addition of enolates to

[\*] Prof. Dr. J. Barluenga, A. Mendoza, Dr. A. Diéguez, Dr. F. Rodríguez, Dr. F. J. Fañanás  
Instituto Universitario de Química Organometálica “Enrique Moles”  
Unidad Asociada al C.S.I.C., Universidad de Oviedo  
Julián Clavería, 8, 33006 Oviedo (Spain)  
Fax: (+ 34) 985-103-450  
E-mail: barluenga@uniovi.es

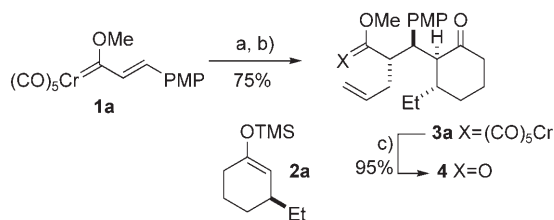
[\*\*] This research was supported by the DGICYT (BQU-2001-3853). The authors thank the MEC (FPU predoctoral grant to A.M.), FICYT (predoctoral grant to A.D.), and the MEC and Fondo Social Europeo (“Ramón y Cajal” contract to F.R.).



Supporting information for this article is available on the WWW under <http://www.angewandte.org> or from the author.

alkenyl carbene complexes.<sup>[8]</sup> Moreover, the  $\alpha$ -position of Fischer carbene complexes is also known to become a nucleophilic position when these complexes are treated with bases.<sup>[9]</sup>

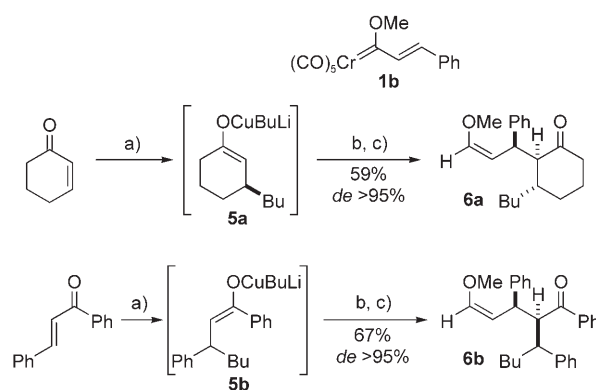
Taking all these facts into account, it is supposed that treatment of an alkenyl carbene complex with a ketone enolate would generate a new anionic species that would further react with an electrophile at the  $\alpha$ -position (see Scheme 1, path 1). To test this hypothesis, carbene complex **1a** was sequentially treated with the lithium enolate derived from silyl enol ether **2a** and then with allyl bromide to obtain, as expected, the new carbene complex **3a** (Scheme 2). It is



**Scheme 2.** Normal reactivity of alkenyl carbene complexes, lithium enolates, and allyl bromide. Reagents and conditions: a) **2a**, BuLi, THF, 0°C, 30 min, then **1a**, THF,  $-78 \rightarrow -30^\circ\text{C}$ ; b) allyl bromide,  $-78^\circ\text{C} \rightarrow \text{RT}$ ; c) pyridine-*N*-oxide, THF, RT. PMP = 4-MeOC<sub>6</sub>H<sub>4</sub>, TMS = trimethylsilyl.

interesting to note that the reaction occurs with complete selectivity, and we only observed the formation of a single diastereoisomer of the final product **3a**.<sup>[10]</sup> Moreover, this carbene complex **3a** is readily transformed into the corresponding ester **4** by simple oxidation of the metal fragment.

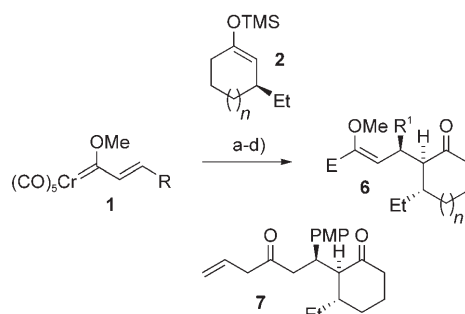
In an attempt to find the optimal conditions to perform the sequence mentioned above, we decided to check the reaction by using copper enolates instead of lithium enolates. In an initial experiment, we generated the necessary copper enolate by simple 1,4-addition of lithium dibutylcuprate to cyclohexenone (Scheme 3). This reaction leads to the corresponding enolate **5a**, which was added to the carbene complex **1b**. The resulting solution was hydrolyzed with an aqueous saturated solution of ammonium chloride. To our surprise, this reaction did not produce the expected carbene complex from the 1,4-addition of the enolate to **1b** and protonation at the  $\alpha$ -position of the carbene complex; instead, the enol ether **6a** was obtained in a totally regio- and diastereoselective manner.<sup>[10]</sup> This result indicates that the anionic species generated after the 1,4-addition of the copper enolate to the carbene complex **1b** did not react with electrophiles at the  $\alpha$ -position, as could be anticipated (and as shown in Scheme 2), but at the initial carbene carbon atom.<sup>[11]</sup> This unexpected mode of reactivity of alkenyl Fischer carbene complexes can be considered to be a new umpolung of Michael acceptors. As shown in Scheme 3, the reaction could also be performed with open-



**Scheme 3.** Umpolung reactivity of alkenyl carbene complexes, copper enolates, and a proton as the electrophile. Reagents and conditions: a) Bu<sub>2</sub>CuLi, Et<sub>2</sub>O,  $-78^\circ\text{C}$ ; b) **1b**, THF,  $-78^\circ\text{C} \rightarrow \text{RT}$ ; c) NH<sub>4</sub>Cl (aq).

chain copper enolates. Thus, enol ether **6b** could readily be obtained by reaction of the enolate **5b**, derived from chalcone, and carbene complex **1b**.

The scope of this new umpolung reaction of alkenyl Fischer carbene complexes has been investigated. We found that several carbene complexes, enolates, and electrophiles can be used (Scheme 4 and Table 1). Also, we found that the



**Scheme 4.** Synthesis of enol ethers **6** (or diketone **7**). Reagents and conditions: a) **2**, BuLi, THF, 0°C, 30 min, then CuI, 0°C and 15 min, RT; b) **1**, THF,  $-78 \rightarrow -30^\circ\text{C}$ ; c) E<sup>+</sup>,  $-30^\circ\text{C} \rightarrow \text{RT}$ ; d) NH<sub>4</sub>Cl (aq).

**Table 1:** Enol ethers **6** (or diketone **7**) from alkenyl carbene complexes **1**, enolates **2**, and electrophiles.

<b>1</b>	R <sup>1</sup>	<b>2</b> <sup>[a]</sup>	<i>n</i>	E <sup>+</sup>	<b>6</b>	E	Yield [%] <sup>[b]</sup>	<i>de</i> [%] <sup>[c]</sup>	<i>ee</i> [%] <sup>[d]</sup>
<b>1a</b>	PMP <sup>[e]</sup>	<b>2a</b>	1	PhCOCl	<b>6c</b>	PhCO	82	> 95	–
<b>1a</b>	PMP <sup>[e]</sup>	<b>2a</b>	1	H <sub>2</sub> C=CHCH <sub>2</sub> Br	<b>7</b> <sup>[f]</sup>	HC=CHCH <sub>2</sub>	63	> 95	–
<b>1c</b>	2-Fu <sup>[e]</sup>	<b>2a</b>	1	PhCOCl	<b>6d</b>	PhCO	80	> 95	–
<b>1b</b>	Ph	<b>2a</b> <sup>[g]</sup>	1	H <sub>2</sub> O	<b>6e</b>	H	70	> 95	> 95
<b>1c</b>	2-Fu <sup>[e]</sup>	<b>2a</b>	1	D <sub>2</sub> O	<b>6f</b>	D	73	> 95	–
<b>1a</b>	PMP <sup>[e]</sup>	<b>2a</b> <sup>[g]</sup>	1	H <sub>2</sub> O	<b>6g</b>	H	74	> 95	> 95
<b>1a</b>	PMP <sup>[e]</sup>	<b>2a</b> <sup>[g]</sup>	1	MeCOCl	<b>6h</b>	MeCO	68	> 95	> 95
<b>1c</b>	2-Fu <sup>[e]</sup>	<b>2a</b> <sup>[g]</sup>	1	HC≡CCH <sub>2</sub> Br	<b>6i</b>	HC≡CCH <sub>2</sub>	53	> 95	> 95
<b>1d</b>	Fc <sup>[e]</sup>	<b>2a</b> <sup>[g]</sup>	1	H <sub>2</sub> O	<b>6j</b>	H	76	> 95	> 95
<b>1e</b>	( <i>E</i> )-styryl	<b>2a</b> <sup>[g]</sup>	1	H <sub>2</sub> O	<b>6k</b>	H	78	> 95	95
<b>1a</b>	PMP <sup>[e]</sup>	<b>2b</b> <sup>[g]</sup>	2	H <sub>2</sub> O	<b>6l</b>	H	72	> 95	> 95
<b>1b</b>	Ph	<b>2b</b> <sup>[g]</sup>	2	<i>t</i> BuCOCl	<b>6m</b>	<i>t</i> BuCO	76	> 95	> 95

[a] Unless noted, racemic silyl enol ether **2** was used. [b] Yield of the isolated product based on starting carbene complex **1**. [c] Determined by <sup>1</sup>H NMR spectroscopic analysis of the crude reaction product. [d] Determined by HPLC analysis on a chiral support. [e] PMP = 4-MeOC<sub>6</sub>H<sub>4</sub>, 2-Fu = 2-furyl; Fc = ferrocenyl. [f] The corresponding enol ether could not be isolated. [g] Enantiopure (> 95% *ee*) silyl enol ether was used (see Ref. [12]).

reaction can be performed in a very simple way that starts from the readily available silyl enol ether **2**. Thus, **2** was treated with butyllithium to generate the corresponding lithium enolate. Treatment of these intermediates with solid CuI and addition to the corresponding carbene complex **1** generated the final enol ether **6**, after reaction with the corresponding electrophile, as a single regio- and diastereoisomer.<sup>[10]</sup> With allyl bromide as the electrophile, **6** could not be isolated and the diketone **7** was directly obtained. As exemplified by this result, this methodology allows the simple synthesis of chiral 1,5-diketone derivatives by simple hydrolysis of the enol ether functionality of **6**. The straightforward procedure described herein allowed us to synthesize enantiomerically pure products **6** when the reaction was carried out using readily available enantiopure silyl enol ethers **2**.<sup>[12]</sup> Interestingly,  $\alpha,\beta,\gamma,\delta$ -unsaturated carbene complex **1e** could also be used. Although a 1,6-addition of the copper enolate to **1e** could be expected, we only observed the corresponding 1,4-addition and further reaction with the electrophile at the initial carbene carbon atom. Finally, it is important to remark that similar results were obtained when carbene complexes **1** were initially treated with the lithium enolates derived from **2** and CuI was added just before the reaction with the corresponding electrophile.

In summary, we have developed a new regio- and diastereoselective one-pot three-component coupling reaction of alkenyl carbene complexes, copper enolates, and several electrophiles. Highly functionalized enol ethers or 1,5-diketone derivatives are readily available from very simple starting materials in a straightforward manner. The process is amenable to the synthesis of enantiomerically pure compounds. As the process described herein is very simple, it could be easily adapted for diversity-oriented synthesis (DOS). Thus, a large range of structurally diverse compounds that are not readily available from traditional organic transformations could be obtained by following this straightforward multicomponent coupling reaction. Our study has shown for the first time a differential behavior between ketone lithium and copper enolates when they are treated with alkenyl carbene complexes. A conceptually new mode of reactivity of Michael acceptors and a clear example of umpolung reactivity is reflected.

Received: April 6, 2006  
Published online: June 23, 2006

**Keywords:** C–C coupling · carbenes · multicomponent reactions · synthetic methods · umpolung

- [1] a) D. Seebach, *Angew. Chem.* **1979**, *91*, 259; *Angew. Chem. Int. Ed. Engl.* **1979**, *18*, 239; b) *Umpoled Synthons* (Ed.: T. A. Hase), Wiley, New York, **1987**.
- [2] For some representative leading examples, see: a) D. J. Dixon, S. V. Ley, F. Rodríguez, *Angew. Chem.* **2001**, *113*, 4899; *Angew. Chem. Int. Ed.* **2001**, *40*, 4763; b) G. H. Posner, K. S. Webb, E. Asirvatham, S. Jew, A. Del'Innocenti, *J. Am. Chem. Soc.* **1988**, *110*, 4754.
- [3] Also, a clear example of this kind of reactivity is the Morita-Baylis-Hillman reaction; for leading references, see: D. Basavaiah, A. J. Rao, T. Satyanarayana, *Chem. Rev.* **2003**, *103*, 811.
- [4] C. Fischer, S. W. Smith, D. A. Powell, G. C. Fu, *J. Am. Chem. Soc.* **2006**, *128*, 1472.
- [5] For interesting recent examples of the conjugate umpolung of  $\alpha,\beta$ -unsaturated aldehydes, see: a) S. S. Sohn, E. L. Rosen, J. W. Bode, *J. Am. Chem. Soc.* **2004**, *126*, 14370; b) C. Burstein, F. Glorius, *Angew. Chem.* **2004**, *116*, 6331; *Angew. Chem. Int. Ed.* **2004**, *43*, 6205.
- [6] For selected recent reviews on Fischer carbene complexes, see: a) J. Barluenga, J. Santamaría, M. Tomás, *Chem. Rev.* **2004**, *104*, 2259; b) J. W. Herndon, *Coord. Chem. Rev.* **2004**, *248*, 3; c) M. A. Sierra, *Chem. Rev.* **2000**, *100*, 3591; d) F. Zaragoza-Dörwald, *Metal Carbenes in Organic Synthesis*, Wiley-VCH, New York, **1999**; e) K. H. Dötz, P. Tomuschat, *Chem. Soc. Rev.* **1999**, *28*, 187.
- [7] A. de Meijere, H. Schirmer, H. Duetsch, *Angew. Chem.* **2000**, *112*, 4124; *Angew. Chem. Int. Ed.* **2000**, *39*, 3964.
- [8] a) J. Barluenga, A. Diéguez, F. Rodríguez, F. J. Fañanás, *J. Am. Chem. Soc.* **2002**, *124*, 9056; b) J. Barluenga, J. M. Montserrat, J. Flórez, S. García-Granda, E. Martín, *Chem. Eur. J.* **1995**, *1*, 236.
- [9] For example, see: a) Y.-C. Xu, W. D. Wulff, *J. Org. Chem.* **1987**, *52*, 3263; b) R. Aumann, H. Heinen, *Chem. Ber.* **1987**, *120*, 537; c) W. D. Wulff, S. R. Gilbertson, *J. Am. Chem. Soc.* **1985**, *107*, 503.
- [10] The relative configuration of all new stereocenters was assigned according to our previous studies in this field;<sup>[8]</sup> see also: a) E. Nakamura, K. Tanaka, T. Fujimura, S. Aoki, P. G. Williard, *J. Am. Chem. Soc.* **1993**, *115*, 9015; b) S. Aoki, T. Fujimura, E. Nakamura, *J. Am. Chem. Soc.* **1992**, *114*, 2985.
- [11] Anions generated from  $\alpha,\beta$ -unsaturated carbene complexes have been found to act as alkenyl metallic species on oxidation with iodine; see, K. Fuchibe, N. Iwasawa, *Tetrahedron* **2000**, *56*, 4907; for a related cyclisation process, see: J. Barluenga, M. Tomás, A. Ballesteros, J. Santamaría, C. Brillet, S. García-Granda, A. Piñera-Nicolás, J. T. Vázquez, *J. Am. Chem. Soc.* **1999**, *121*, 4516; also, the acylation of carbene complex copper anions occurs in very low yield at the initial carbene carbon atom; see: C. A. Merlic, F. Wu, *J. Organomet. Chem.* **1998**, *553*, 183.
- [12] Enantiopure (> 95 % ee) silyl enol ethers **2** were obtained from the following procedure: B. L. Feringa, M. Pineschi, L. A. Arnold, R. Imbos, A. H. M. de Vries, *Angew. Chem.* **1997**, *109*, 2733; *Angew. Chem. Int. Ed. Engl.* **1997**, *36*, 2620.

**Selective Excision of C5 from D-Ribose in the Gas Phase by Low-Energy Electrons (0–1 eV): Implications for the Mechanism of DNA Damage\*\***

Ilko Bald, Janina Kopyra, and Eugen Illenberger\*

Sugar is the central unit within a nucleotide connecting the DNA base with the phosphate group, which itself couples to the neighboring nucleotides within single-stranded DNA. The study of the excitation, ionization, and fragmentation of biomolecular systems is essential for the understanding of many problems in the area of life sciences such as the mechanism of radiation damage in cellular systems or the action of radiosensitisers used in tumor therapy.

The passage of high-energy radiation through dense media such as water or a living cell leaves a trace of free electrons. These secondary electrons are created in numbers ( $5 \times 10^4$  per MeV of deposited energy<sup>[1]</sup>) that makes them the most abundant radiolytic species. In the course of thermalization they can induce further ionization or excitation processes, but they can also efficiently attach at specific energies (resonances) and sites to DNA, forming transient negative ions that subsequently dissociate (dissociative electron attachment, DEA).<sup>[2]</sup>

Ample evidence exists that DEA with its unique features plays an important role in the nascent states of cellular DNA radiolysis.<sup>[2]</sup> To date, these phenomena have been investigated at two extremes of DNA complexity, namely, plasmid DNA and isolated nucleobases in the gas phase. Experiments on plasmid DNA have demonstrated that low-energy electrons can efficiently induce single-strand breaks (SSBs), as well as double-strand breaks (DSBs).<sup>[3]</sup> In the very low-energy domain (0–3 eV), below the threshold of electronic excitation, only SSBs are observed.<sup>[4]</sup> In these experiments it became apparent that the efficiency of both DSBs and SSBs as a function of the primary electron energy exhibits a resonant behavior, indicating that the formation of negative-ion resonances is the initial step.

Studies on isolate nucleobases (NBs) in the gas phase<sup>[5–11]</sup> have demonstrated that they undergo DEA in the range of roughly 6–9 eV and also at much lower energies ( $< 3$  eV) where SSBs are observed.<sup>[5]</sup> While the high-energy feature leads to loss of  $H^-$  and further fragment ions associated with the rupture of the NB ring structure,<sup>[5–7]</sup> the low-energy resonance exclusively leads to the loss of neutral hydrogen with the excess charge remaining on the nucleobase.

In a recent theoretical study<sup>[12]</sup> modeling a section of DNA composed of cytosine, sugar, and the phosphate group, an interesting mechanism for electron-initiated strand breaks was proposed. The calculations predict a low-lying anionic potential energy surface that connects the initial  $\pi^*$  anion state of the base to a  $\sigma^*$  state in the backbone. An electron captured by a DNA base may thereby be transferred to the backbone, leading to rupture of the C–O bond between the phosphate and the sugar. On the other hand, very recent experiments on thymidine (thymine coupled to sugar)<sup>[13]</sup> indicate that such an electron transfer is not operative; instead it appears that sugar moiety itself has a pronounced ability to capture low-energy electrons with subsequent fragmentation. For the detailed investigation of the response of sugar following electron attachment we use D-ribose ( $C_5H_{10}O_5$ ) and some isotopically labeled analogues ( $1-^{13}C$ ,  $5-^{13}C$ ,  $C,1-D$ ). For simplicity we will use the term ribose for D-ribose throughout this manuscript.

A previous study by the Innsbruck Laboratory on deoxyribose ( $C_5H_{10}O_4$ ) revealed that electron capture at energies already close to 0 eV induces a variety of fragmentation reactions.<sup>[14]</sup> As we shall demonstrate, isotopic labeling enables us to identify the underlying decomposition process and to specify the site of the target molecule involved. This provides essential information for the molecular process of DNA damage by low-energy electrons.

The experiments were carried out in a crossed electron molecular beam arrangement consisting of an electron source, an oven, and a quadrupole mass analyzer (QMA).<sup>[15]</sup> The components were housed in a ultrahigh-vacuum chamber at a base pressure of  $10^{-8}$  mbar. A well-defined electron beam generated from a trochoidal electron monochromator<sup>[16]</sup> (resolution 90–120 meV fwhm) intersected orthogonally with an effusive molecular beam consisting of ribose molecules. They emanated from a resistively heated oven directly connected to the reaction chamber by a capillary. At a temperature of about 370 K (measured by a platinum resistance) the density of intact ribose molecules was high enough to yield a reasonable negative-ion signal. The generated anions were extracted by a small electric field towards the entrance of the QMA where they were analyzed and detected by a single-pulse counting technique. The energy scale was calibrated using the well-known resonance in  $SF_6^-$  near 0 eV generating metastable  $SF_6^-$ . To prevent ion-molecule reactions involving  $SF_6^-$  ions, the flow of the calibration gas was switched off prior to each measurement. Ribose and the  $5-^{13}C$  analogue were obtained from Sigma Aldrich (stated purity 98 and 99%, respectively),  $[1-^{13}C]$ ribose and  $[C,1-D]$ ribose were obtained from Cambridge Isotope Laboratories, Inc. (stated purity 99 and 98%, respectively). All samples were used as delivered.

[\*] Dipl.-Chem. I. Bald, Dr. J. Kopyra,<sup>[†]</sup> Prof. Dr. E. Illenberger  
Institut für Chemie und Biochemie  
Physikalische und Theoretische Chemie  
Freie Universität Berlin  
Takustrasse 3, 14195 Berlin (Germany)  
Fax: (+49) 30-838-55378  
E-mail: iln@chemie.fu-berlin.de

[†] Permanent address:  
Chemistry Department, University of Podlasie  
08-110 Siedlce (Poland)

[\*\*] This research was supported by the Deutsche Forschungsgemeinschaft, the EU via the Network EPIC, and the Freie Universität Berlin. I.B. is a fellow of the Studienstiftung des Deutschen Volkes, and J.K. acknowledges support from the EIPAM program of the European Science Foundation.



Before considering the present results, we note that in DNA the deoxyribose unit is present as a furanose five-membered-ring structure with the C1 position connected to the DNA base through the glycosidic C–N bond and the C5 position to the phosphate group through the C–O bond. The nucleotide is then formed from its building blocks (base–sugar–phosphate) by a condensation reaction releasing two H<sub>2</sub>O molecules. In gas-phase experiments it was demonstrated that ribose and deoxyribose exist in the six-membered ring form (pyranose form).<sup>[17]</sup> It was shown that the crystalline structure of pentose sugars (the pyranose form) is in fact preserved in the course of thermal evaporation, and we hence assume that in the present experiments the ribose molecule is present as a six-membered ring. Owing to the availability of isotopic labeling we use ribose instead of deoxyribose. This should not affect the general conclusions since ribose, deoxyribose,<sup>[14]</sup> and fructose<sup>[18]</sup> all show a rather similar fragmentation behavior in the way that electrons at very low energies decompose the respective molecule by the loss of one or more water molecules as well as C-containing neutral units.

From the selected DEA spectra shown in Figure 1, Figure 2, and Figure 3 it is immediately obvious that ribose

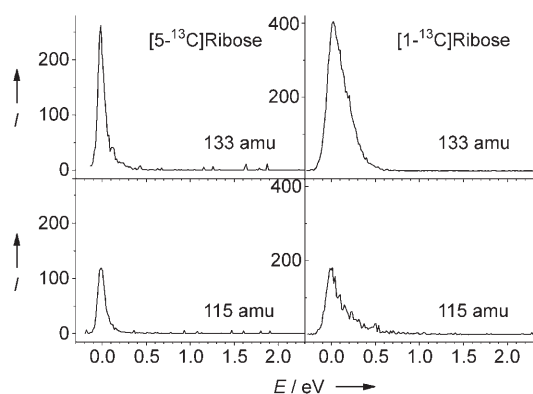


**Figure 1.** Ion yields obtained from [5-<sup>13</sup>C]ribose and [1-<sup>13</sup>C]ribose at 133 amu (C<sub>5</sub>H<sub>8</sub>O<sub>4</sub><sup>−</sup>) and 115 amu (C<sub>5</sub>H<sub>6</sub>O<sub>3</sub><sup>−</sup>) due to the loss of one and two water molecules, respectively.

(C<sub>5</sub>H<sub>10</sub>O<sub>5</sub><sup>−</sup>, 150 amu) and its isotopically labeled analogues show a unique and surprisingly rich fragmentation behavior in the course of electron interaction at very low energies (<1 eV). In a tentative reaction scheme [Eqs. (1)–(6)] we list the dominant negative fragment ions as observed from nonlabeled ribose in the order of decreasing mass numbers.

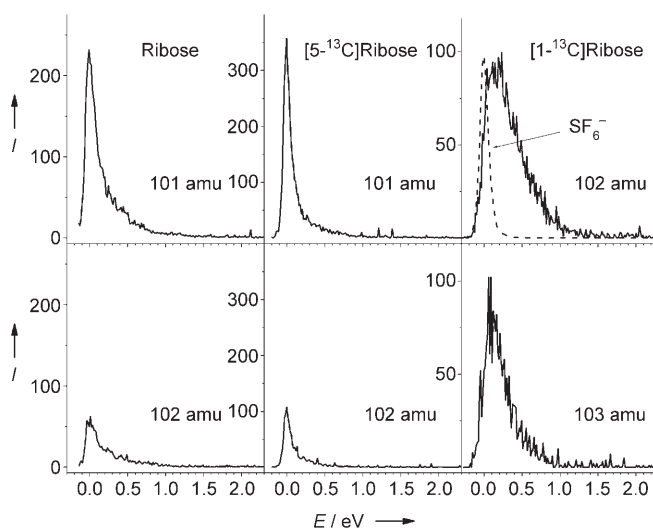
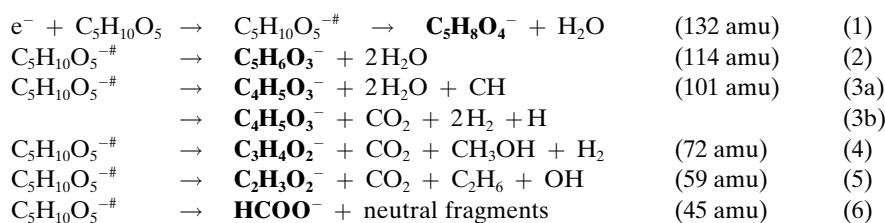


**Figure 2.** Ion yields from ribose (left) at 101 amu (C<sub>4</sub>H<sub>5</sub>O<sub>3</sub><sup>−</sup>) and 102 amu (C<sub>4</sub>H<sub>6</sub>O<sub>3</sub><sup>−</sup>) arising from the excision of a carbon-containing unit. In [1-<sup>13</sup>C]ribose (right) the signal is shifted by one mass unit, while in [5-<sup>13</sup>C]ribose (middle) this is not the case.

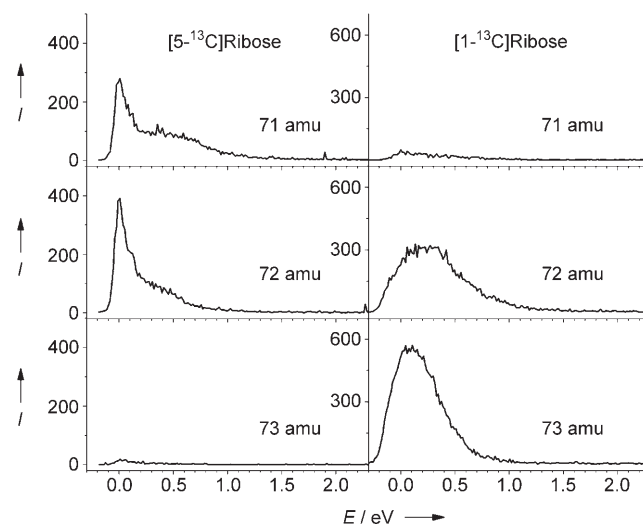


**Figure 3.** Ion yields at 71 amu (C<sub>3</sub>H<sub>3</sub>O<sub>2</sub><sup>−</sup>) and 72 amu (C<sub>3</sub>H<sub>4</sub>O<sub>2</sub><sup>−</sup>) arising from the excision of two C atoms. In [5-<sup>13</sup>C]ribose (left) the situation corresponds to that in nonlabeled ribose (not shown), while in [1-<sup>13</sup>C]ribose (right) and [C,1-D]ribose (not shown) the signal is shifted by one mass unit.

C<sub>5</sub>H<sub>10</sub>O<sub>5</sub><sup>−#</sup> corresponds to the transient anion formed upon electron capture. The reactions result from the loss of one or more neutral water units as well as the excision of one and more C-containing units from the target molecule. Since we do not observe a measurable change of the relative intensity between light and heavy fragment anions when the temperature is increased to 410 K we can assume that the gaseous sample consists completely of intact ribose molecules.

Since the present experiment yields only information on the ionic products, the neutral decomposition channels assigned in reactions (3)–(5) are tentative and refer to reasonable and energetically favorable dissociation limits. Also, the stoichiometric assignment of the ions can be ambiguous; for example, the 101-amu anion ( $\text{C}_4\text{H}_5\text{O}_3^-$ ) could also be assigned as  $\text{C}_5\text{H}_9\text{O}_2^-$ . As we shall substantiate below, however, experiments using the isotopically labeled analogues immediately show that only  $\text{C}_4\text{H}_5\text{O}_3^-$  is generated. More importantly, isotopic labeling enables us to specify the site of the target molecule involved in the reaction under consideration.

The observation that free electrons with essentially no (or little) energy can trigger such reactions is a remarkable result. Water loss, for example, is associated with multiple bond cleavages and formation of new bonds. On the other hand, from the energetic point of view it has to be remembered that sugar molecules are (thermodynamically) rather unstable species with respect to the loss of water units; this can be rationalized easily by considering the corresponding thermodynamic values<sup>[19]</sup> (Table 1). Of course in the neutral system

**Table 1:** Heats of formation ( $\Delta H_f^\circ$ ) for some compounds relevant to the present reactions.<sup>[a]</sup>

Compound	$\Delta H_f^\circ$ [kJ mol <sup>-1</sup> ]
$\text{C}_5\text{H}_{10}\text{O}_5$ (D-ribose, solid)	-1050
$\text{C}_5\text{H}_8\text{O}_4$ (pentanedioic acid, solid)	-960
$\text{H}_2\text{O}$ (liquid)	-242
$\text{H}_2\text{O}$ (gas)	-286
C (gas)	717
CH (gas)	594
$\text{CO}_2$ (gas)	-394
$\text{CH}_3\text{OH}$ (liquid)	-239
$\text{CH}_3\text{OH}$ (gas)	-201
H	218

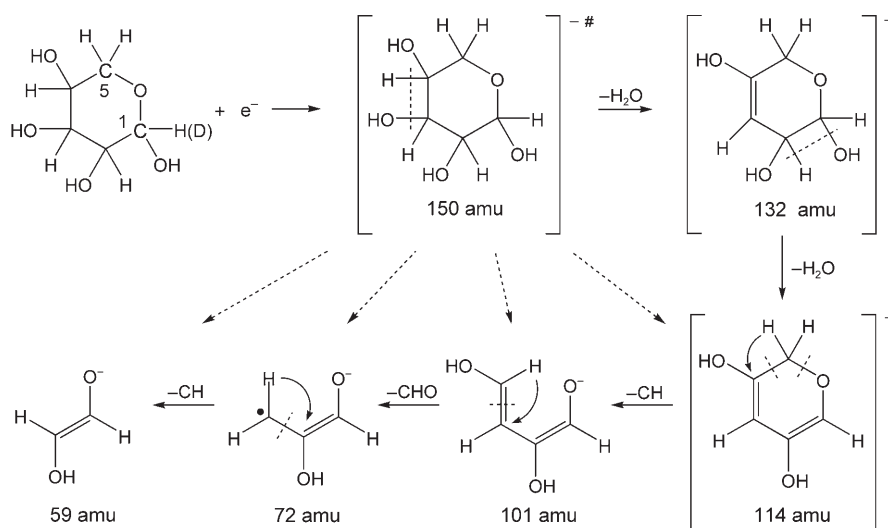
[a] Taken from reference [19].

such a reaction possesses large activation barriers, and hence sugar molecules can be considered as stable compounds also on a macroscopic time scale. Obviously, the presence of an excess electron changes the situation completely, as the transient anion decomposes into all the negatively charged fragments indicated above on a microscopic time scale. In this case, the electron affinity (which is not known for the larger of the observed anions) will further energetically drive the reaction. It must be emphasized that all the anionic fragments are simultaneously detected within the time window of the present experiment extending from 0 (formation of the transient ion) to 8–20  $\mu\text{s}$  corresponding to the (mass-dependent) traveling time of an ion from the reaction zone to the entrance of the mass spectrometer.<sup>[15]</sup> Ions decomposing within the quadrupole will strike the rods and will not be detected.

We do not have direct information on the neutral products or the question to what degree the underlying reactions are sequential or concerted. A further point concerns the mechanism of electron attachment. In the usual picture of resonances, electron attachment is pictured as accommodation of the extra electron into virtual MOs. In ribose these are  $\sigma^*$  MOs which, however, are expected to be located at considerably higher energies within the Franck–Condon region. It is therefore likely that a description by the usual resonance mechanism may no longer apply for the present system (see below).

In ribose the loss of one and two neutral water units is observed on the ion signals appearing at 132 and 114 amu, respectively (not shown here). With  $[5-^{13}\text{C}]$ ribose and  $[1-^{13}\text{C}]$ ribose (Figure 1) the ion signals are completely shifted to 133 and 115 amu as expected. Figure 1 shows, however, a noticeable difference in the width of the corresponding ion yield curve between the two isotopes which is probably related to the mechanism of anion formation (see below). More interestingly, by taking the C,1-D isotope (not shown here) the signals are also shifted to 133 and 115 amu, respectively, indicating that the C,1-D site is not involved in the abstraction of the neutral water units. We hence propose a sequential and/or concerted abstraction of the two water units according to Scheme 1 with the excess electron finally residing in a  $\pi^*$ -type orbital of the corresponding cyclic structure.

Figure 2 shows the ion yields in the vicinity of 101 amu [Eq. (3)] for ribose and the  $^{13}\text{C}$ -labeled isotopes. Obviously the nonlabeled molecule (left) also generates a comparatively smaller signal ( $\approx 25\%$ ) at 102 amu which is to some extent due to the natural  $^{13}\text{C}$  isotopes (4%) of  $\text{C}_4\text{H}_5\text{O}_3^-$ . The majority of the intensity, however, has to be assigned to the ion  $\text{C}_4\text{H}_6\text{O}_3^-$  associated either with the neutral channel  $2\text{H}_2\text{O} + \text{C}$  or  $\text{CO}_2 + 2\text{H}_2$ . With the  $[5-^{13}\text{C}]$ ribose (middle) the relative intensity between 101 and 102 amu remains



**Scheme 1.** Sequential decomposition of the ribose transient negative ion (and its labeled analogues) formed by low-energy electron attachment. Alternate concerted reaction pathways are indicated by the dotted arrows (see text).

unchanged. This shows that 1) the reaction exclusively proceeds by the loss of  $5\text{-}^{13}\text{C}$  and 2) the alternate stoichiometric composition mentioned above ( $\text{C}_5\text{H}_9\text{O}_2^-$ ) can be excluded. Accordingly, by using  $[1\text{-}^{13}\text{C}]\text{ribose}$  (right), the signal at 101 amu completely disappears (within the detection limit) in favor of the signal at 102 amu (and 103 amu) which complements the above conclusion that only the C5 atom is excised while the  $1\text{-}^{13}\text{C}$  atom remains on the negative-ion fragment. There are two more noticeable effects, namely, 1) the considerably broader resonance feature in the signal from the  $1\text{-}^{13}\text{C}$  isotopomer (similar to Figure 1) and 2) the different relative intensities between the neighboring masses. The broader ion yield cannot be attributed to the slightly different energy resolution (120 meV in  $[1\text{-}^{13}\text{C}]\text{ribose}$  compared to 90 meV in  $[5\text{-}^{13}\text{C}]\text{ribose}$ , see also the  $\text{SF}_6^-$  calibration curve) and its origin is not yet clear. With  $[\text{C},1\text{-D}]\text{ribose}$  the signals appear at 102 and 103 amu (at essentially the same intensity ratio as the nonlabeled compound and the  $5\text{-}^{13}\text{C}$ -labeled ribose) while there is no detectable signal at 101 amu.

We can hence conclude that the ion  $\text{C}_4\text{H}_5\text{O}_3^-$  appears from a reaction in which the C5 atom of the original molecule is excised while the C1 atom and the hydrogen (deuterium) at the C1 position remain on the negative ion. Within the detection limit of the present experiment, this decomposition is completely selective. For the deuterated compound this selectivity is remarkable as one could expect some kind of hydrogen scrambling as often observed in mass spectrometry. On the other hand, it has to be noted that the transient anion of formic acid generated at low energy is not subject to hydrogen scrambling as previously shown in DEA to the isotopomers  $\text{HCOOD}$  and  $\text{DCOOH}$ .<sup>[20]</sup>

From the thermodynamic point of view a sequential reaction creating the  $\text{C}_4\text{H}_5\text{O}_3^-$  fragment at 101 amu (with the tentative structure shown in Scheme 1) and with the neutral channel consisting of  $2\text{H}_2\text{O} + \text{CH}$  is rather unfavourable, while a concerted reaction associated with  $\text{CO}_2 + 2\text{H}_2 + \text{H}$  is appreciably lower in energy (Table 1). For the fragment at 102 amu, the neutral channel becomes  $\text{CO}_2 + 2\text{H}_2$ , which is several hundred kJ below the alternate channel  $2\text{H}_2\text{O} + \text{C}$ . It remains to be explored what kind of isotope effect is responsible for intensity ratio between 102 and 103 amu arising from the decomposition of the  $1\text{-}^{13}\text{C}$  isotopomer.

Figure 3 shows a selection of ion yields around 71 and 72 amu [Eq. (4)], which arise from the excision of two carbon atoms. The  $[5\text{-}^{13}\text{C}]\text{ribose}$  (left) shows the same behavior as nonlabeled ribose (not shown here), namely signals at 71 and 72 amu at approximately the same level of intensity, while in  $[1\text{-}^{13}\text{C}]\text{ribose}$  (Figure 3 right) and also in  $[\text{C},1\text{-D}]\text{ribose}$  (not shown here) the signals are nearly completely shifted to 72 and 73 amu. We can therefore conclude that the final fragments  $\text{C}_3\text{H}_3\text{O}_2^-$  and  $\text{C}_3\text{H}_4\text{O}_2^-$  must contain the initial  $1\text{-}^{13}\text{C}$  atom or the D atom from the original C1 position, respectively. In addition, the particular behavior concerning the broadening of the resonance curve when it originates from the ribose  $1\text{-}^{13}\text{C}$  isotope is also preserved on this ion signal. As can be seen from Figure 3 there is now a small signal at 71 amu from the  $1\text{-}^{13}\text{C}$  isotopomer. This indicates that the selectivity is no longer complete, but a small percentage of the reaction also proceeds by excision of the  $1\text{-}^{13}\text{C}$  atom.

If one continues the line along decreasing masses we always find analogous behavior, namely, a remarkable selectivity in the way that both the  $1\text{-}^{13}\text{C}$  isotope and the D atom originally attached to the C1 site are found on the final ionic product. The initial complete selectivity, however, is slightly degraded towards lower mass units.

Scheme 1 presents a reaction scheme (ending at the 59-amu ion) based on a sequential reaction mechanism. As considered above, the decomposition processes yielding the lighter fragments may rather proceed along energetically more favorable concerted reaction pathways. Apart from the structure of the 59-amu fragment indicated in Scheme 1, the acetate anion  $\text{CH}_3\text{COO}^-$  is also known as a stable negative ion.<sup>[21]</sup>

We finally note that low-energy electron attachment to ribose generates a number of more ionic fragments at low electron energies, namely at 107 amu ( $\text{C}_3\text{H}_7\text{O}_4^-/\text{C}_2\text{H}_3\text{O}_5^-$ ), 46 amu ( $\text{CH}_3\text{CH}_2\text{OH}^-/\text{CH}_2\text{O}_2^-$ ), and 17 amu ( $\text{OH}^-$ ).  $\text{O}^-$  (16 amu) is also observed but only via resonant structures in the energy range above 6.5 eV. Ions at 46 amu were also observed in acetic acid<sup>[21]</sup> and propanoic acid,<sup>[22]</sup> but the geometrical and electronic structure of this compound has not been identified so far. It is interesting to note that ribose exhibits an additional resonance in the energy range around 7 eV which (apart from  $\text{O}^-$ ) also decomposes into some of the larger fragment ions. It appears, however, that the decomposition of this excited transient anion is not as selective as that observed for the transient anion generated below 1 eV, as will be described and discussed in a forthcoming publication.<sup>[23]</sup>

The low-energy process discussed here must be associated with shape resonances, that is, accommodation of the extra electron into a virtual MO, leaving the initial electronic configuration unchanged. The energy of the relevant  $\sigma^*$  MOs, on the other hand, are expected at higher energies and may thus not directly be accessed by Franck–Condon transitions. It is not known whether vibrational Feshbach resonances (VFR), acting as doorways for DEA or other mechanisms, are responsible for the mechanism of electron attachment to sugars. For the DNA/RNA bases thymine and uracil a VFR (supported by the large dipole of the molecule) that couples to  $\sigma^*$  valence states was proposed as the mechanism for DEA at 1 eV.<sup>[11]</sup> In any case, the electronic structure of the precursor ion seems to have a strong tendency to localize the excess charge in the initial molecule towards the site around the C1 atom.

In conclusion from the data presented here it can be seen that ribose is appreciably sensitive towards the attack of very low energy electrons as it decomposes by the loss of water molecules and also by the excision of C5 (and more C-containing units) associated with the degradation of the cyclic structure. The decomposition is remarkably site selective in the way that C5 is excised while the excess charge is localized on the C1 site. Under the assumption that the gas pressure measured at the ionization gauge at one of the flanges behaves similarly for  $\text{SF}_6$  and the gas-phase ribose molecules (with respect to the pressure in the reaction zone), we can estimate the absolute cross section for a particular DEA reaction by taking the known absolute electron attachment

cross section for thermal electron attachment to  $\text{SF}_6$  generating  $\text{SF}_6^-$  ( $2.5 \times 10^{-18} \text{ m}^2$ <sup>[24,25]</sup>). This procedure results in absolute DEA cross sections for the above processes in the range of  $10^{-21}$ – $10^{-20} \text{ m}^2$ , which is close to the geometrical cross section of a ribose molecule.

For the problem of the molecular mechanism of DNA damage by electrons it appears that the sugar itself presumably plays the most active role as a scavenger for low-energy electrons. Both the isolated DNA bases and also the phosphate group<sup>[23]</sup> are active electron scavengers, however, at energies appreciably above 0 eV. It remains to be investigated to what degree the presently studied DEA reactions are preserved when sugar is coupled to the phosphate group and to what degree the C5–O bond is involved. Rupture of the C5–O sugar–phosphate bond would represent a single-strand break, and as demonstrated here the C5 atom is selectively excised from isolated ribose.

Received: January 24, 2006

**Keywords:** bioorganic chemistry · dissociative electron attachment · DNA damage · gas-phase reactions · negative ion mass spectrometry

- [21] W. Sailer, A. Pelc, M. Probst, J. Limtrakul, P. Scheier, E. Illenberger, T. D. Märk, *Chem. Phys. Lett.* **2003**, 378, 250.
- [22] A. Pelc, W. Sailer, P. Scheier, T. D. Märk, E. Illenberger, *Chem. Phys. Lett.* **2004**, 392, 465.
- [23] C. König, J. Kopyra, I. Bald, E. Illenberger, *Phys. Rev. Lett.*, accepted.
- [24] L. G. Christophorou, J. K. Olthoff, *J. Phys. Chem. Ref. Data* **2000**, 29, 267.
- [25] L. G. Christophorou, J. K. Olthoff, *Fundamental Electron Interactions with Plasma Processing Gases*, Kluwer Academic/Plenum Publishers, New York, **2004**.

- [1] V. Cobut, Y. Fongillo, J. P. Patau, T. Goulet, M.-J. Fraser, J.-P. Jay-Gerin, *Radiat. Phys. Chem.* **1998**, 51, 229.
- [2] L. Sanche, *Eur. Phys. J. D* **2005**, 35, 367 (Review).
- [3] B. Boudaiffa, P. Cloutier, D. Hunting, M. A. Huels, L. Sanche, *Science* **2000**, 287, 1658.
- [4] F. Martin, P. D. Burrow, Z. Cai, P. Cloutier, D. J. Hunting, L. Sanche, *Phys. Rev. Lett.* **2004**, 93, 068101.
- [5] G. Hanel, B. Gstir, P. S. Denifl, P. Scheier, B. Farizon, M. Farizon, E. Illenberger, T. D. Märk, *Phys. Rev. Lett.* **2003**, 90, 188104.
- [6] S. Ptasinska, S. Denifl, V. Grill, P. Scheier, T. D. Märk, S. Gohlke, M. A. Huels, E. Illenberger, *Angew. Chem.* **2005**, 117, 1673; *Angew. Chem. Int. Ed.* **2005**, 44, 1647.
- [7] S. Ptasinska, S. Denifl, E. Illenberger, P. Scheier, T. D. Märk, *Phys. Rev. Lett.* **2005**, 95, 093201.
- [8] H. Abdoul-Carime, S. Gohlke, E. Illenberger, *Phys. Rev. Lett.* **2004**, 92, 168103.
- [9] S. Ptasinska, S. Denifl, P. Scheier, E. Illenberger, T. D. Märk, *Angew. Chem.* **2005**, 117, 7101; *Angew. Chem. Int. Ed.* **2005**, 44, 6941.
- [10] R. Abouaf, H. Dunet, *Eur. Phys. J. D* **2005**, 35, 405.
- [11] A. M. Scheer, K. Aflatoon, G. A. Gallup, P. D. Burrow, *Phys. Rev. Lett.* **2004**, 92, 068102.
- [12] J. Berdys, I. Anusiewicz, P. Skurski, J. Simons, *J. Am. Chem. Soc.* **2004**, 126, 6441.
- [13] S. Ptasinska, S. Denifl, P. Scheier, T. D. Märk, S. Gohlke, E. Illenberger, *Angew. Chem.* **2006**, 118, 1926; *Angew. Chem. Int. Ed.* **2006**, 45, 1893.
- [14] S. Ptasinska, S. Denifl, P. Scheier, T. D. Märk, *J. Chem. Phys.* **2004**, 120, 8505.
- [15] R. Balog, J. Langer, S. Gohlke, M. Stano, H. Abdoul-Carime, E. Illenberger, *Int. J. Mass Spectrom.* **2004**, 233, 267.
- [16] A. Stamatovic, G. J. Schulz, *Rev. Sci. Instrum.* **1970**, 41, 423.
- [17] L.-P. Guler, Y.-Q. Yu, H. I. Kenttämä, *J. Phys. Chem. A* **2002**, 106, 6754.
- [18] P. Sulzer et al., *J. Chem. Phys.*, submitted.
- [19] NIST Chemistry webbook: <http://webbook.nist.gov/chemistry>.
- [20] I. Martin, T. Skalicky, J. Langer, H. Abdoul-Carime, G. Karwasz, E. Illenberger, M. Stano, S. Matejcik, *Phys. Chem. Chem. Phys.* **2005**, 7, 2212.



## Allylation

DOI: 10.1002/anie.200600509

**Highly Stereoselective Allylic Alkylations of Peptides\*\****Uli Kazmaier,\* Jan Deska, and Anja Watzke**Dedicated to Professor Barry M. Trost  
on the occasion of his 65th birthday*

Cell proteins and peptides in eukaryotes are generally produced by means of ribosomal peptide synthesis. In contrast, prokaryotes employ a completely different mechanism comparable to polyketide synthesis.<sup>[1]</sup> This nonribosomal peptide synthesis enables the lower organisms to generate a high diversity of peptide structures. Therefore, their metabolites often contain rather exotic amino acids, such as D- and N-methylated amino acids, which are often incorporated into cyclic peptides.<sup>[2]</sup> A typical example is cyclosporin C, an immunosuppressant used after organ transplants (Figure 1).<sup>[3]</sup>

In general, these secondary metabolites show interesting biological properties, and because of that, flexible synthetic protocols for structure–activity investigations are highly desirable. Besides the classical peptide syntheses, the modification of peptides is an interesting, alternative approach. While the modification of a functionalized side chain is not really that difficult,<sup>[4]</sup> the direct introduction of a side chain into a given peptide is far from trivial, especially with respect to the stereochemical outcome of the reaction. In principle, peptide-incorporated glycine cations,<sup>[5]</sup> radicals,<sup>[6]</sup> and anions

[\*] Prof. Dr. U. Kazmaier, Dipl.-Chem. J. Deska, Dr. A. Watzke  
Universität des Saarlandes  
Institut für organische Chemie  
Im Stadtwald, Geb. 23.2, 66123 Saarbrücken (Germany)  
Fax: (+ 49) 681-302-2409  
E-mail: u.kazmaier@mx.uni-saarland.de

[\*\*] This work was supported by the Deutsche Forschungsgemeinschaft (Ka880/6) and the Fonds der Chemischen Industrie.

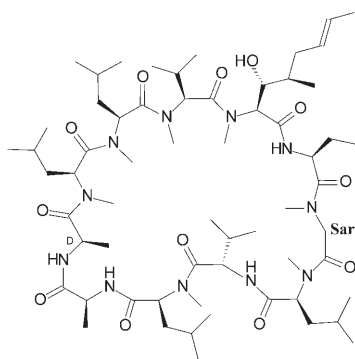
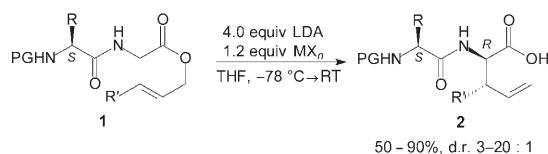


Figure 1. Cyclosporin C; Sar = sarcosine subunit.

can be generated as reactive intermediates for further modifications. Especially the last approach was investigated intensively by Seebach et al.<sup>[7]</sup> Probably the most spectacular success was the regio- and stereoselective alkylation of the sarcosine (Sar) subunit in cyclosporin.<sup>[8]</sup> In this case, one face of the enolate is shielded by the deprotonated peptide ring, and therefore the attack of the electrophile occurs preferentially from the opposite face. In comparison, modifications of linear peptides proceed unselectively, giving rise to diastereomeric mixtures.

Our group has also been investigating stereoselective peptide modifications for some time. Our goal is to transfer the chiral information of a given peptide chain via metal-peptide complexes to the newly formed stereogenic center.<sup>[9]</sup> A first successful example was the Claisen rearrangement of a peptide enolate which provided allylated peptides in high yields. Depending on the protecting group (PG) and chelating metal salt (MX<sub>n</sub>) used, the diastereoselectivity was good to excellent and the *S,R* diastereomer was always formed preferentially (Scheme 1).<sup>[10]</sup> The diastereoselectivity may be explained by a highly ordered chair-like transition state and the likely multiple coordination of the chelating metal to the peptide chain,<sup>[11]</sup> resulting in a one-sided shielding of the peptide enolate.



Scheme 1. Chelatenolate Claisen rearrangement of peptides. R = alkyl; R' = alkyl, aryl. LDA = lithium diisopropylamide, PG = protecting group.

As we were interested to see whether this concept can also be applied to intermolecular modifications, we investigated the alkylation of tosyl- and *tert*-butoxycarbonyl (Boc)-protected leucine peptides **3** with several alkylating agents (Table 1). To determine the configuration of the new stereogenic center, we introduced preferentially alkyl groups corresponding to the natural proteinogenic amino acids, or those which can be interconverted easily into these. We found that both protecting groups are suitable. In general, the Boc protecting group gave the best yields, the tosyl group the best

Table 1. Stereoselective modifications of dipeptides **3**.

Entry	Substr.	PG	RX	Prod.	Yield [%]	d.r. <sup>[a]</sup>
1	<b>3a</b>	Boc	Mel	<b>4a</b>	92	50:50
2	<b>3b</b>	Ts	Mel	<b>4b</b>	70	85:15
3	<b>3a</b>	Boc	BnBr	<b>5a</b>	50	60:40
4	<b>3b</b>	Ts	BnBr	<b>5b</b>	53	85:15
5	<b>3a</b>	Boc		<b>6a</b>	73	50:50
6	<b>3b</b>	Ts		<b>6b</b>	63	90:10
7	<b>3b</b>	Ts		<b>7b</b>	60	88:12
8	<b>3a</b>	Boc		<b>8a</b>	61	85:15
9	<b>3b</b>	Ts		<b>8b</b>	75	76:24
10	<b>3c</b>	TFA		<b>8c</b>	82	73:27

[a] *S,R/S,S*. [b] The catalyst was 1 mol % [(allyl)PdCl]<sub>2</sub>; E = COOEt, Ts = tosyl, TFA = trifluoroacetate.

selectivities. With respect to the chelating metal salt, many different salts (MgCl<sub>2</sub>, CoCl<sub>2</sub>, NiCl<sub>2</sub>, MnCl<sub>2</sub>) can be used, but ZnCl<sub>2</sub> gave the most reproducible results. Like to the Claisen rearrangement, the *S,R* products were formed preferentially. Besides alkyl and allyl halides also carbonyl compounds could be used with comparable results (Table 1, entry 7). In this case diastereomeric ratios (d.r.) up to 9:1 could be obtained.

Since some time we have also been investigating palladium-catalyzed allylic alkylations of chelated enolates,<sup>[12]</sup> and therefore it was obvious to investigate this reaction also with deprotonated peptides of type **3** as nucleophiles. This is not a trivial issue, because peptides are known to form relatively stable complexes with palladium,<sup>[11]</sup> which might result in complexation and deactivation of the catalyst. But we hoped that in the case of the metal peptide complexes this might not be a major problem. Therefore, we also investigated the reaction of our model peptides **3a/b** with methylallyl carbonate **9** in the presence of Pd<sup>0</sup> and found that in this case the Boc derivative **3a** gave the best selectivity (Table 1, entry 8) and the tosyl derivative **3b** the best yield (Table 1, entry 9).

After our good experience with *N*-trifluoroacetylated amino acid esters, we also used this protecting group on our model peptide. Indeed, the best yield was achieved with **3c** (Table 1, entry 10). In principle, the yields obtained in the allylic alkylation were comparable to those using allyl bromide (Table 1, entries 5 and 6), although in the Pd-catalyzed version a side product formed: the corresponding ethyl ester resulting from a nucleophilic attack of the liberated EtOH (from the allylic carbonate) onto the terminal ester functionality.

To suppress this side reaction and to increase the yield we switched to the more stable *tert*-butyl ester **10a** (Table 2). For complete conversion of the peptide we used an excess of **9**. At least 3 equiv of base were required for peptide enolate formation (two for the acidic NH groups, one for the enolate).

**Table 2:** Palladium-catalyzed allylic alkylation of dipeptides **10**.

$  \begin{array}{c}  \text{3.5 equiv LHMDS} \\  \text{1.2 equiv ZnCl}_2 \\  \text{x equiv 9, cat.} \\  \text{THF, } -78 \rightarrow -50^\circ\text{C} \\  \text{catalyst} \\  \text{2 mol\% } [(allyl)PdCl]_2 \\  \text{9 mol\% PPh}_3  \end{array}  $						
Entry	Substr.	AA	Equiv <b>9</b>	Prod.	Yield [%] <sup>[a]</sup>	d.r. <sup>[b]</sup>
1	<b>10a</b>	Leu	2	<b>11a</b>	76	84:16
2	<b>10b</b>	Phe	2	<b>11b</b>	82	90:10
3	<b>10c</b>	Tle	2	<b>11c</b>	59	92:8
4	<b>10a</b>	Leu	0.85	<b>11a</b>	77	90:10
5	<b>10a</b>	Leu	0.7	<b>11a</b>	89	90:10
6	<b>10a</b>	Leu	0.5	<b>11a</b>	91	90:10
7	<b>10b</b>	Phe	0.7	<b>11b</b>	92	93:7
8	<b>10c</b>	Tle	0.7	<b>11c</b>	73	93:7
9	<b>10d</b>	Tyr-OMe	0.7	<b>11d</b>	93	92:8
10	<b>10e</b>	Ala	0.7	<b>11e</b>	85	83:17
11	<b>10f</b>	Met	0.7	<b>11f</b>	60	90:10
12	<b>10g</b>	Ser-OBOM <sup>[c]</sup>	0.7	<b>11g</b>	71	81:19
13	<b>10h</b>	Ser-OTBDPS <sup>[c]</sup>	0.7	<b>11h</b>	98	92:8

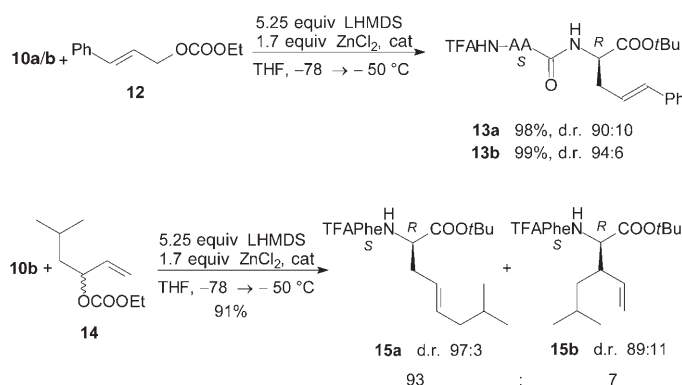
[a] Yield determined relative to the minor component. [b] *S,R/S,S*. [c] Tle = *tert*-leucine, BOM = benzyloxymethyl, TBDPS = *tert*-butyldiphenylsilyl.

Variation of the amount of base used indicated that a slight excess of base increases the yield, while a large excess is counterproductive. Therefore, we carried out all reactions in the presence of 3.5 equiv of base. Interestingly, with the *tert*-butyl ester **10a** the selectivity was superior to that of the corresponding methyl ester **3c** (Table 1, entry 1). For example, with the phenylalanine derivative **10b** a diastereomeric ratio of 9:1 could be obtained, and this in a very high yield (Table 2, entry 2). Owing to the high reactivity of the chelated enolates, the reactions started at temperatures as low as  $-78^\circ\text{C}$  and were complete after warming up to  $-50^\circ\text{C}$ . One might expect that the selectivity should increase with growing steric bulk of the inducing amino acid. Therefore, we also investigated the *tert*-leucine (Tle) derivative **10c**, and indeed, the highest selectivity was obtained in this case, although the yield was a little lower (Table 2, entry 3).

The last parameter of optimization that we varied was the ratio of peptide enolates to allylic carbonate **9**. When the peptide enolate was used in excess, not only the yield but also the selectivity increased significantly (Table 2, entries 1 and 4–6). The optimal peptide enolate/allyl carbonate ratio was found to be 1.5:1. Under these optimized conditions both yields and the selectivities were about 90% (Table 2, entry 5). To illustrate the broad applicability of this protocol we allylated a wide range of other dipeptides. And indeed, under the new, optimized conditions excellent yields were achieved with the phenylalanine peptide **10b** (Table 2, entry 7), and even the *tert*-leucine derivative **11c** was obtained in good yield (Table 2, entry 8). The results with the protected tyrosine derivative **10d** were similar (Table 2, entry 9). While the diastereoselectivity obviously depends on the steric bulk of the inducing amino acid, it was interesting to see how much the selectivity drops when only “small” amino acids were incorporated into the peptide. But even with the alanine derivative **10c** the diastereoselectivity still reached

83% (Table 2, entry 11). Other amino acids with linear side chains, such as methionine, gave better results (Table 2, entry 12). The lowest selectivity so far was obtained with the serine derivative **10g**, but in this case both the yield and the selectivity could be increased without any problem by using a sterically more demanding protecting group (Table 2, entry 13).

In reactions of peptides with functionalized side chains, such as **10f** and **10g**, coordination of the catalyst to the side chain might be an option theoretically and would result in the opposite *S,S* diastereomer as the favored product. In all examples investigated so far, however, the *S,R* diastereomer was the major isomer, as determined by HPLC of the hydrogenated allylation products.<sup>[13]</sup> To illustrate that this concept is suitable for the introduction of several types of side chains, we also varied the allylic carbonates used (Scheme 2).



**Scheme 2.** Stereoselective allylations of peptides. LHMDS = lithium hexamethyldisilazane.

In all examples investigated the yields and the selectivities were excellent. For example, with the cinnamyl carbonate **12** the linear substitution product **13** was formed exclusively. In contrast, the reaction of the alkyl-substituted carbonate **14** can be expected to give the regioisomeric products **15a** and **15b**, but also in this case the linear product was **15a** formed preferentially.

In conclusion, we could show that palladium-catalyzed allylic alkylation is an excellent tool for the stereoselective modification of peptides. The selectivities obtained are in the range of 80–90%. Reactions using chiral  $\pi$ -allyl palladium complexes and those in the presence of chiral ligands as well as applications to natural product synthesis are currently under investigation.

## Experimental Section

**11b:** In a Schlenk tube hexamethyldisilazane (233 mg, 1.44 mmol) was dissolved in abs. THF (2.0 mL) under argon. After the solution had been cooled to  $-78^\circ\text{C}$ , a 1.6M solution of *n*BuLi (0.82 mL, 1.31 mmol) was added slowly. The solution was stirred for 10 min before the cooling bath was removed and the solution was stirred for a further 10 min. In a second Schlenk flask  $\text{ZnCl}_2$  (57 mg, 0.42 mmol) was dried with a heat gun under vacuum. After the solution had been cooled to room temperature, a solution of (*S*)-Tfa-Phe-Gly-OrBu (140 mg, 0.375 mmol) in THF (2 mL) was added. The freshly

prepared LHMDS solution was cooled again to  $-78^{\circ}\text{C}$  before the peptide/ $\text{ZnCl}_2$  solution was slowly added. A solution of  $[\text{[(allyl)PdCl]}_2]$  (1.8 mg, 5.0  $\mu\text{mol}$ ),  $\text{PPh}_3$  (5.9 mg, 22.5  $\mu\text{mol}$ ), and methallyl ethylcarbonate (36 mg, 0.25 mmol) was prepared in THF (0.5 mL). This solution was added to the enolate at  $-78^{\circ}\text{C}$ . The dry ice was removed from the cooling bath, and the reaction mixture was allowed to warm to  $-50^{\circ}\text{C}$  over 2 h before it was diluted with ether and hydrolyzed with 1 M HCl. After the reaction mixture was allowed to warm to room temperature, the layers were separated and the aqueous layer was extracted twice with ether. The combined organic layers were dried ( $\text{Na}_2\text{SO}_4$ ), the solvent was evaporated in vacuo, and the crude product was purified by flash chromatography (silica gel, hexanes/ $\text{EtOAc}$  92:8). Yield: 99 mg (0.231 mmol, 92%) **11b** as a white solid, m.p. 113–114  $^{\circ}\text{C}$ .  $^1\text{H}$  NMR (500 MHz,  $\text{CDCl}_3$ ):  $\delta$  = 1.35 (s, 9H) 1.63 (s, 3H), 2.20 (dd,  $J$  = 7.9, 6.3 Hz, 2H), 2.27 (dd,  $J$  = 7.6, 6.3 Hz, 2H), 3.03 (d,  $J$  = 6.9 Hz, 2H), 4.41 (dt,  $J$  = 7.9, 6.3 Hz, 1H), 4.56 (s, 1H), 4.64 (dt,  $J$  = 7.6, 6.7 Hz, 1H), 4.71 (s, 1H), 6.33 (d,  $J$  = 7.9 Hz, 1H), 7.22–7.11 (m, 5H), 7.56 ppm (d,  $J$  = 7.6 Hz, 1H).  $^{13}\text{C}$  NMR (125 MHz,  $\text{CDCl}_3$ ):  $\delta$  = 21.71, 27.88, 38.56, 40.61, 51.13, 54.69, 82.62, 114.63, 116.33 (q, 106 Hz), 127.42, 128.77, 129.25, 135.30, 140.29, 156.62 (q, 37.2 Hz), 168.78, 170.46 ppm. HRMS (CI): calcd for  $\text{C}_{23}\text{H}_{30}\text{N}_2\text{F}_3\text{O}_4$   $[M+H]^+$ : 429.1992; found: 429.2041; HPLC (Reprosil 100 Chiral-NR 8  $\mu\text{m}$ , hexane/*i*PrOH 99.5:0.5, 1.5 mL min $^{-1}$ ,  $\lambda$  = 209 nm):  $t_{(S,S)}$  = 16.65 min,  $t_{(S,R)}$  = 22.07 min; d.r. 93:7.

Received: February 7, 2006

**Keywords:** allylation · asymmetric synthesis · chelates · palladium · peptides

- Kazmaier, S. Maier, F. L. Zumpe, *Synlett* **2000**, 1523–1535; e) S. Maier, U. Kazmaier, *Eur. J. Org. Chem.* **2000**, 1241–1251.
- [10] U. Kazmaier, S. Maier, *J. Org. Chem.* **1999**, 64, 4574–4575.
- [11] Review on peptide–metal complexes: K. Severin, R. Bergs, W. Beck, *Angew. Chem.* **1998**, 110, 1722–1743; *Angew. Chem. Int. Ed.* **1998**, 37, 1634–1654.
- [12] a) U. Kazmaier, F. L. Zumpe, *Angew. Chem.* **1999**, 111, 1572–1574; *Angew. Chem. Int. Ed.* **1999**, 38, 1468–1470; b) U. Kazmaier, F. L. Zumpe, *Angew. Chem.* **2000**, 112, 805–807; *Angew. Chem. Int. Ed.* **2000**, 39, 802–804; c) T. D. Weiß, G. Helmchen, U. Kazmaier, *Chem. Commun.* **2002**, 1270–1271; d) U. Kazmaier, *Curr. Org. Chem.* **2003**, 317–328; e) U. Kazmaier, M. Pohlman, *Synlett* **2004**, 623–626; f) U. Kazmaier, T. Lindner, *Angew. Chem.* **2005**, 117, 3368–3371; *Angew. Chem. Int. Ed.* **2005**, 44, 3303–3306.
- [13] Determination of the configuration for dipeptide **11b**: An analytical sample of allylated dipeptide **11b** was dissolved in MeOH und subjected to hydrogenation (10% Pd/C) under normal pressure. The resulting dipeptide, TFA-Phe-Leu-OrBu, was compared with a *S,S* reference sample: HPLC (Reprosil 100 Chiral-NR 8  $\mu\text{m}$ , hexane/*i*PrOH 99.5:0.5, 1.5 mL min $^{-1}$ ,  $\lambda$  = 209 nm): *S,S* Reference:  $t_R$  = 13.94 min; **H<sub>2</sub>-11b**:  $t_{\text{minor}}$  = 13.97 min,  $t_{\text{major}}$  = 19.62 min.

- [1] Reviews: a) M. A. Marahiel, T. Stachelhaus, H. D. Moetz, *Chem. Rev.* **1997**, 97, 2651–2673; b) H. v. Döhren, U. Keller, J. Vater, R. Zocher, *Chem. Rev.* **1997**, 97, 2675–2705.
- [2] Reviews: a) D. R. W. Hogson, J. M. Sanderson, *Chem. Soc. Rev.* **2004**, 33, 422–430; b) N. Fusetani, S. Matsunaga, *Chem. Rev.* **1993**, 93, 1793–1806.
- [3] a) A. D. Hess, A. Esa, P. M. Colombani, *Transplant. Proc.* **1988**, 20, 29–40; b) H. Fliri, in *Antibiotics and Antiviral Compounds* (Eds.: K. Krohn, H. A. Kirst, H. Maag), VCH, Weinheim, **1993**, pp. 229–240.
- [4] a) J.-C. Gfeller, A. K. Beck, D. Seebach, *Helv. Chim. Acta* **1980**, 63, 728–732; b) M. J. Dunn, S. Gomez, R. F. W. Jackson, *J. Chem. Soc. Perkin Trans. 1* **1995**, 1639–1640; c) J. Barluenga, M. A. García-Martín, J. M. González, P. Clapés, G. Valencia, *Chem. Commun.* **1996**, 1505–1506.
- [5] a) C. J. Easton, I. M. Scharfbillig, E. W. Tan, *Tetrahedron Lett.* **1988**, 29, 1565–1568; b) G. Apitz, W. Steglich, *Tetrahedron Lett.* **1991**, 32, 3163–3166; c) W. Steglich, M. Jäger, S. Jaroch, P. Zistler, *Pure Appl. Chem.* **1994**, 66, 2167–2170.
- [6] a) M. Ricci, P. Blakskjaer, T. Skrydstrup, *J. Am. Chem. Soc.* **200**, 122, 12413–12421; b) M. Ricci, L. Madariaga, T. Skrydstrup, *Angew. Chem.* **2000**, 112, 248–252; *Angew. Chem. Int. Ed.* **2000**, 39, 2242–2246; c) C. J. Easton, *Chem. Rev.* **1997**, 97, 53–82.
- [7] Reviews: a) D. Seebach, *Angew. Chem.* **1988**, 100, 1685–1715; *Angew. Chem. Int. Ed. Engl.* **1988**, 27, 1624–1654; b) D. Seebach, *Aldrichimica Acta* **1992**, 25, 59–66; c) D. Seebach, A. K. Beck, A. Studer in *Modern Synthetic Methods, Vol. 7* (Eds.: B. Ernst, C. Leumann), Helvetica Chimica Acta/VCH, Basel/Weinheim, **1995**, pp. 1–178.
- [8] a) D. Seebach, A. K. Beck, H. G. Bossler, C. Gerber, S. Y. Ko, C. W. Murtiashaw, R. Naef, S.-I. Shoda, A. Thaler, M. Krieger, R. Wenger, *Helv. Chim. Acta* **1993**, 76, 1564–1590; b) S. A. Miller, S. L. Griffiths, D. Seebach, *Helv. Chim. Acta* **1993**, 76, 563–595.
- [9] a) U. Kazmaier, *J. Org. Chem.* **1994**, 59, 6667–6670; b) U. Kazmaier, S. Maier, *Chem. Commun.* **1998**, 2535–2536; c) U. Kazmaier, S. Maier, *Org. Lett.* **1999**, 1, 1763–1766; d) U.



DOI: 10.1002/anie.200600905

**Heterobimetallic Half-Lanthanidocene Clusters:  
Novel Mixed Tetramethylaluminato/Chloro  
Coordination\*\***

*H. Martin Dietrich, Oliver Schuster, Karl W. Törnroos,  
and Reiner Anwander\**

The beauty of symmetry has been a stimulus and driving force for ligand-based cluster research.<sup>[1]</sup> By spanning the border-line between molecular and solid-state chemistry, large nanosized inorganic clusters not only emulate intermediates of sol-gel chemistry<sup>[2]</sup> but also contribute to a better understanding of the intriguing quantum-confinement phenom-

[\*] H. M. Dietrich, Prof. K. W. Törnroos, Prof. R. Anwander  
Department of Chemistry  
University of Bergen  
Allégaten 41, 5007 Bergen (Norway)  
Fax: (+ 47)-5558-9490  
E-mail: reiner.anwander@kj.uib.no  
Dr. O. Schuster  
Anorganisch-chemisches Institut  
Technische Universität München  
Lichtenbergstrasse 4, 85747 Garching (Germany)

[\*\*] Financial support from the Norwegian Research Council (Project No. 171245/V30), the program Nanoscience@UiB, and the Fonds der Chemischen Industrie is gratefully acknowledged.



Supporting information for this article is available on the WWW under <http://www.angewandte.org> or from the author.

enon of semiconductors.<sup>[3–5]</sup> Moreover, cluster molecules can act as model systems for addressing delicate questions in catalysis science by giving insight into unique coordination modes and reactivities.<sup>[6,7]</sup> In organometallic cluster chemistry, trailblazing structural reports such as those of the inorganic fullerene-like molecule  $[(\text{Cp}^*\text{Fe}(\eta^5\text{-}\eta^1\text{-}\eta^1\text{-}\eta^1\text{-}\eta^1\text{-}\text{P}_5))_{12}\{\text{CuCl}\}_{10}\{\text{Cu}_2\text{Cl}_3\}_5\{\text{Cu}(\text{CH}_3\text{CN})_2\}_5]$ <sup>[8]</sup> and low-valent aluminum complexes  $[\text{Al}_{50}\text{Cp}^*_{12}]$ <sup>[9a]</sup> or  $[\text{SiAl}_{14}\text{Cp}^*_6]$ <sup>[9b]</sup> bear witness to the uniqueness of the ubiquitous cyclopentadienyl ancillary ligand environment in d-transition-metal and main-group-metal chemistry ( $\text{Cp}^* = \text{C}_5\text{Me}_5$ ).<sup>[10]</sup> Because of its steric bulk, rigidity, and thermal and chemical stability, the Cp ligand and its substituted variants are also ideal for cluster design/stabilization involving the large oxophilic rare-earth metal ions, which participate predominantly in ionic bonding.<sup>[11]</sup> While hydrolysis- or oxophilicity-driven cluster formation meanwhile includes numerous structurally characterized examples—Ln nuclearities as high as 15, as in  $[\text{Eu}_{15}(\text{Cl})(\mu_3\text{-Tyr})_{10}(\mu_3\text{-OH})_{20}(\mu_2\text{-H}_2\text{O})_5(\text{OH})_{12}(\text{H}_2\text{O})_8][\text{ClO}_4]_2 \cdot 56\text{H}_2\text{O}$  (Tyr = tyrosine), were identified<sup>[12,13]</sup>—the feasibility of Cp-derived organolanthanide clusters is directed by the ratio  $\text{Cp}/\text{Ln} < 2$ .<sup>[11]</sup> Accordingly, half-lanthanidocene complexes should exhibit prolific cluster chemistry.<sup>[14]</sup> Table 1 summarizes such half-sandwich clusters, which are highlighted by  $[(\text{Cp})_{12}\text{Sm}_{12}(\mu_3\text{-Cl})_{24}]$  and  $[(\text{Me}_4\text{CpSiMe}_3)_n\text{Ln}(\mu\text{-H})_2]_4$  ( $\text{Ln} = \text{Y}, \text{Lu}$ ).<sup>[15–36]</sup> The latter hydrido clusters are rare examples of organolanthanide clusters which feature highly reactive ligands.<sup>[35]</sup>

Recently we described a convenient method for the synthesis of half-sandwich complexes  $[\text{Cp}^*\text{Ln}(\text{AlMe}_4)_2]$  (**1**), which comprise small and large rare-earth-metal centers.<sup>[37]</sup> The study herein shows that such well-defined, thermally stable, and highly soluble bis(aluminate) complexes offer access to unprecedented heteroleptic organolanthanide cluster chemistry. Compared to the lanthanidocene-based  $[\text{Cp}^*_2\text{Sm}(\text{thf})_x]/\text{R}_2\text{AlCl}$  and  $[\text{Cp}^*_2\text{LnCl}]/\text{R}_3\text{Al}$  ( $\text{Ln} = \text{Y}, \text{Sm}$ ;  $\text{R} = \text{Me}, \text{Et}, i\text{Bu}$ ) reaction mixtures, which produce homo- (“ $\text{Ln}(\mu\text{-Cl})_2\text{AlR}_2$ ”) and heterobridged (“ $\text{Ln}(\mu\text{-R})(\mu\text{-Cl})\text{AlR}_2$ ”) moieties,<sup>[38]</sup> the half-lanthanidocene system **1**/Me<sub>2</sub>AlCl leads to intrinsic AlMe<sub>4</sub>/Cl ligand exchange and variable Ln nuclearity, depending on the size of the Ln<sup>III</sup> metal. Furthermore, the “open” coordination sphere of monocyclopentadienyl complexes facilitates novel coordination modes of the AlMe<sub>4</sub> ligand.

Treatment of  $[\text{Cp}^*\text{Ln}(\text{AlMe}_4)_2]$  (**1a**: Ln = Y, **1b**: Ln = La, **1c**: Ln = Nd) with varying amounts of Me<sub>2</sub>AlCl in hexane led to crystalline materials of net composition  $[\text{Cp}^*\text{Ln}(\text{AlMe}_4)_x(\text{Cl})_y]$  (**2**: Ln = Y,  $x = y$ ; **3**: Ln = La,  $y = 2x$ ; **4**: Ln = Nd,  $y = 9x$ ) as indicated by elemental analysis (Scheme 1). Though the white and bluish materials obtained for the larger rare-earth-metal centers are completely insoluble in benzene and toluene, the colorless yttrium derivative **2** slightly dissolves in aromatic solvents. The <sup>1</sup>H NMR spectrum of **2** in C<sub>6</sub>D<sub>6</sub> revealed Cp\* ( $\delta = 1.91$  ppm) and AlMe<sub>4</sub> signals ( $\delta = -0.15$  ppm) which were slightly shifted to higher field relative to the precursor compound **1a** ( $\delta = 1.76$  and  $-0.34$  ppm), albeit with the same <sup>2</sup>J<sub>YH</sub> coupling constant of 2.4 Hz as for **1a**. The sharp doublet of the aluminate group is indicative of a highly fluxional behavior with fast exchange of bridging and

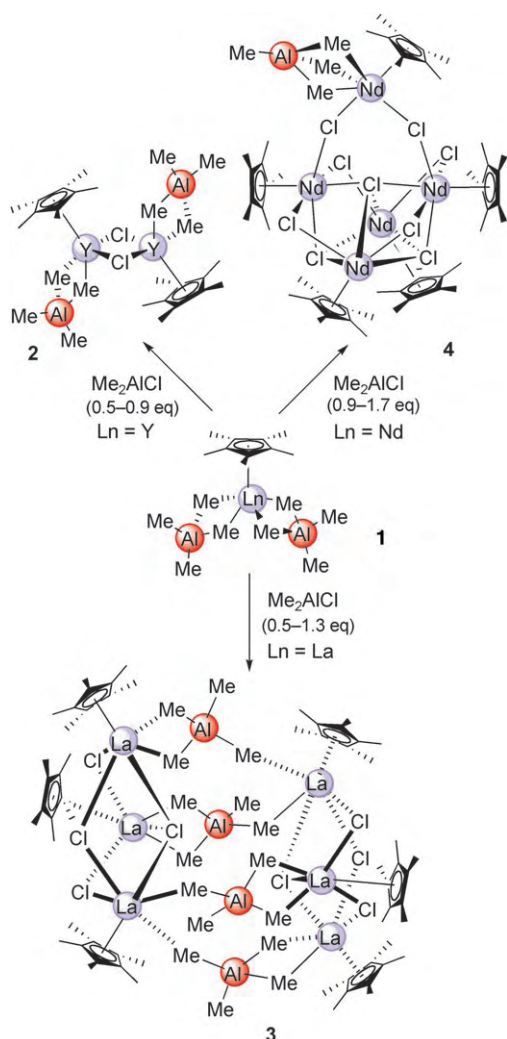
**Table 1:** Structurally characterized half-sandwich organolanthanide clusters.

Formula	Ref.
oxide/chalcogenide/hydroxide	
$[\text{Pr}_4\text{Cp}_2(\text{acacen})_4(\mu\text{-OH})_2]$ <sup>[a]</sup>	[15]
$[\text{Nd}_4\text{Cp}_2(\text{saltn})_4(\mu\text{-OH})_2]$ <sup>[a]</sup>	[15]
$[\text{Yb}_4\text{Cp}^*_5(\mu_4\text{-O})(\mu_3\text{-Cl})(\mu\text{-Cl})_6(\text{Et}_2\text{O})_2]$	[16]
$[\text{Nd}_4\text{Cp}_4(\mu_4\text{-O})(\mu\text{-CH}_3)_2(\mu\text{-Cl})_6][\text{Li}(\text{dme})_3]_2$	[17]
$[\text{Yb}_5\text{Cp}^*_5(\mu_3\text{-O})(\mu_3\text{-Cl})(\mu\text{-Cl})_7]$	[18]
$[\text{Yb}_5\text{Cp}_5(\mu_5\text{-O})(\mu_3\text{-OCH}_3)_4(\mu\text{-OCH}_3)_4]$ (Ln = Yb, Gd)	[19]
$[\text{Sm}_6\text{Cp}^*_6\text{O}_3(\text{OH})_6]$	[20]
$[\text{Sm}_6\text{Cp}^*_6\text{Se}_{11}]$	[21]
(pseudo)halide	
$[\text{K}\{(\text{C}_5\text{Me}_5\text{Yb})_3\text{Cl}_8\text{K}(\text{dme})_2\}_2][\text{K}(\text{dme})_3]$	[22]
$[\text{Yb}_5\text{Cp}^*_6(\mu_4\text{-F})(\mu_3\text{-F})_2(\mu\text{-F})_6]$	[23]
$[\text{Nd}_6(2,4\text{-C}_7\text{H}_{11})_6\text{Cl}_{12}(\text{thf})_2]$ <sup>[b]</sup>	[24]
$[\text{Yb}_6(\text{C}_5\text{Me}_5\text{SiMe}_2\text{tBu})_6(\mu_3\text{-I})_8][\text{Li}(\text{thf})_4]$ <sup>[c]</sup>	[25]
$[\text{Yb}_6(\text{C}_5\text{H}_4\text{Pr}_4)_6(\mu_{1,1'}\text{-N}_3)_2(\mu_{1,3'}\text{-N}_3)_{10}(\mu_{1,1',3'}\text{-N}_3)_2][\text{Na}(\text{dme})_3]_2$	[26]
$[\text{Yb}_3\text{Cp}_3(\mu_3\text{-Cl})_2(\mu\text{-Cl})_3(\text{thf})_3][\text{Yb}_6\text{Cp}_6(\mu_6\text{-Cl})(\mu\text{-Cl})_{12}]$	[27]
$[\text{Sm}_{12}\text{Cp}_{12}(\mu_3\text{-Cl})_{24}]$	[27]
(boro)hydride	
$[\text{Lu}_4(\text{C}_5\text{H}_3\text{tBu-1,3})_4\text{H}_4][\text{AlH}_4(\text{OEt}_2)]_2[\text{AlH}_4]_2$	[28]
$[\text{Ln}_6(\text{C}_5\text{Me}_4\text{nPr})_6(\text{BH}_4)_{(12-x)}\text{Cl}_x(\text{thf})_n]$ (Ln = Sm, Nd; $x = 0, 5, 10$ )	[29]
$[\text{Y}_4(\text{C}_5\text{Me}_4\text{SiMe}_2\text{PC}_6\text{H}_{11})_4(\mu\text{-H})_4]$	[30]
$[\text{Ln}_4(\text{C}_5\text{Me}_4\text{SiMe}_3)_4(\mu\text{-H})_8](\text{thf})_n$ (Ln = Lu, Y) <sup>[d]</sup>	[31]
$[\text{Sm}_6\text{Cp}^*_5(\mu\text{-H})_{12}][(\mu\text{-H})\text{K}(\text{thf})_2]_3$	[32]
alkyl(aluminate)	
$[\text{La}_3\text{Cp}^*_3(\mu\text{-}\eta^2\text{-}\eta^6\text{-}\eta^6\text{-C}_{16}\text{H}_{10})(\mu\text{-Cl})_3(\text{thf})]^{[e,f]}$	[33]
$[\text{Y}_3\text{Cp}^*_3(\mu\text{-Me})_6]^{[f]}$	[34]
$[\text{Cp}^*_4\text{Y}_4(\mu_2\text{-CH}_3)_2\{(\text{CH}_3)\text{Al}(\mu_2\text{-CH}_3)_2\}_4(\mu_4\text{-CH})_2]^{[f]}$	[34]
$[\text{Nd}_5\text{Cp}^*_5\{(\mu\text{-Me})_3\text{AlMe}\}(\mu_4\text{-Cl})(\mu_3\text{-Cl})_2(\mu\text{-Cl})_6]$ ( <b>4</b> )	[g]
$[\text{La}_6\text{Cp}^*_6\{(\mu\text{-Me})_3\text{AlMe}\}_4(\mu_3\text{-Cl})_2(\mu_2\text{-Cl})_6]$ ( <b>3</b> )	[g]

[a] H<sub>2</sub>acacen = bis(acetone)ethylenediamine, H<sub>2</sub>saltn = bis(salicylidene)trimethylenediamine. [b] 2,4-C<sub>7</sub>H<sub>11</sub> = 2,4-dimethylpentadienyl. [c] Yb<sup>II</sup> center. [d] Subsequent reactions gave imido clusters  $[\text{Lu}_4(\text{C}_5\text{Me}_4\text{SiMe}_3)_4(\mu\text{-NCH}_2\text{C}_6\text{H}_5)_4]$  and  $[\text{Y}_4(\text{C}_5\text{Me}_4\text{SiMe}_3)_4(\mu\text{-NCH}_3)_4(\mu\text{-NCC}_6\text{H}_5)_4]$  as well as partially exchanged hydrido clusters  $[\text{Y}_4(\text{C}_5\text{Me}_4\text{SiMe}_3)_4(\mu\text{-H})_7(\text{C}_7\text{H}_7)]$ ,  $[\text{Y}_4(\text{C}_5\text{Me}_4\text{SiMe}_3)_4(\mu\text{-H})_4(\text{Me}_3\text{SiCCHCHCSiMe}_3)]$ ,  $[\text{Y}_4(\text{C}_5\text{Me}_4\text{SiMe}_3)_4(\mu\text{-H})_2(\mu_3\text{-O})(\text{Me}_3\text{SiCCHCHCSiMe}_3)]$ ,  $[\text{Lu}_4(\text{C}_5\text{Me}_4\text{SiMe}_3)_4(\mu\text{-H})_2(\text{O}(\text{CH}_2)_4\text{O})]$  and completely exchanged clusters  $[\text{Y}_4(\text{C}_5\text{Me}_4\text{SiMe}_3)_4(\mu_3\text{-O})_2(\text{Me}_3\text{SiCCHCHCSiMe}_3)]$ ,  $[\text{Y}_4(\text{C}_5\text{Me}_4\text{SiMe}_3)_4(\mu\text{-CH}_2\text{O})_2(\text{Me}_3\text{SiCCHCHCSiMe}_3)]$ ,  $[\text{Y}_4(\text{C}_5\text{Me}_4\text{SiMe}_3)_4(\mu\text{-CH}_2\text{O}_2)(\mu\text{-CO}_2)(\text{Me}_3\text{SiCCHCHCSiMe}_3)]$ , and  $[\text{Y}_4(\text{C}_5\text{Me}_4\text{SiMe}_3)_4(\mu\text{-CO}_3)_2(\text{Me}_3\text{SiCCHCHCSiMe}_3)]$ .<sup>[35]</sup> [e] Deprotonated pyrene ligand. [f] Metal-ring arrangement. [g] This work.

terminal methyl groups. Molar ratios of **1a**/Me<sub>2</sub>AlCl < 0.9 in the reactions gave increasing amounts of amorphous white solid, which was not further characterized. Examination of the hexane-soluble fractions by NMR spectroscopy only revealed AlMe<sub>3</sub> as a coproduct as well as unreacted **1** and Me<sub>2</sub>AlCl. Complexes **2–4** were further characterized by the signal patterns of their IR spectra, which featured few bands and weak signal intensities, and their solid-state structures.

X-ray structure analysis of complex **2** revealed the dimeric complex  $[(\text{Cp}^*\text{Y}[(\mu\text{-Me})_2\text{AlMe}_2](\mu\text{-Cl}))_2]$  (Figure 1) with formally heptacoordinate yttrium centers and a rare combination of homometal-bridging chloride ligands and  $\eta^2$ -coordinated aluminate ligands (Al1 lies  $-0.207(3)$  Å out of the



**Scheme 1.** Reaction pathways of  $[\text{Cp}^*\text{Ln}(\text{AlMe}_4)_2]$  (**1a**:  $\text{Ln} = \text{Y}$ , **1b**:  $\text{Ln} = \text{La}$ , **1c**:  $\text{Ln} = \text{Nd}$ ) with  $\text{Me}_2\text{AlCl}$ .

least-squares C3–Y1–C4 plane).<sup>[39]</sup> The average  $\text{Y}–\text{C}(\mu\text{-Me})$  bond length (2.573 Å) is slightly larger than that in hexacoordinate  $[\text{Y}(\text{AlMe}_4)_3]$  (2.508 Å).<sup>[40]</sup> The  $\text{Y}–\text{Cl}$  bond lengths (2.6326(9), 2.7177(9) Å) are comparable to the corresponding bond lengths for the bridging chloro ligand in hepta-/octacoordinate  $[\text{Cp}^*_2\text{Y}(\mu\text{-Cl})\text{YCp}^*_2\text{Cl}]$  (2.640(5), 2.776(6) Å).<sup>[41]</sup>

Lanthanum complex **3** was reproducibly obtained as colorless crystals for a relatively wide range of  $\text{La}/\text{Al}$  ratios, and the reaction with 0.9 equivalents of  $\text{Me}_2\text{AlCl}$  gave an almost quantitative yield (Scheme 1). Three independent X-ray crystallographic studies<sup>[39]</sup> proved the formation of the hexalanthanum cluster  $[\text{Cp}^*_6\text{La}_6(\mu\text{-Me})_3\text{AlMe}_4(\mu_3\text{-Cl})_2(\mu_2\text{-Cl})_6]$  (Figure 1) and, hence, an “over-exchange” of aluminate ligands. The  $\text{La}_6\text{Al}_4$  hetero-bimetallic cluster is composed of two  $\{\text{Cp}^*_3\text{La}_3\text{Cl}_4\}$  subunits which are connected by a strand of four  $\text{AlMe}_4$  ligands and can thus be described by the formula  $[\text{Cp}^*_3\text{La}_3\text{Cl}_4]_2(\mu\text{-AlMe}_4)_4$ . Each lanthanum center is octacoordinate and bound by one  $\text{Cp}^*$  ligand, three chloro ligands, and

two methyl groups of the aluminate strand. The bridging chloro ligands are arranged in the form of a distorted tetrahedron. The average  $\text{La}–\text{Cl}$  bond lengths of 2.8280 Å ( $\mu_2\text{-Cl}$ ) and 3.0444 Å ( $\mu_3\text{-Cl}$ ) are in the range of those in  $[\text{La}_3\text{Cp}^*_3(\mu\text{-}\eta^2\text{:}\eta^6\text{-C}_{16}\text{H}_{10})(\mu\text{-Cl})_3(\text{thf})]$  (2.810(3)–2.894(2) Å).<sup>[33]</sup> Two lanthanum centers of each equilateral  $\text{La}_3$  triangle are coordinated by an  $\text{AlMe}_4$  group in  $\eta^2$  mode. The same two aluminate groups interact with the third lanthanum center of the other  $\text{La}_3$  subunit in  $\eta^1$  fashion. The planar  $\text{LaMe}_2\text{Al}$  ( $\text{Al1}$  lies 0.088(4) Å out of the least-squares C31–La1–C32 plane and Al2 0.045(4) Å out of the least-squares C37–La3–C38 plane) and almost linear  $\text{La}–\text{Me}–\text{Al}$  (av. 170.0°) hetero-bimetallic units combine to give an unprecedented  $\{\text{La}(\mu\text{-Me}_2)\text{Al}(\text{Me})(\mu\text{-Me})\text{La}\}$  hetero-trinuclear arrangement. The  $\text{La}–\text{C}(\mu\text{-Me})[\eta^1]$  bonds (2.950(3) Å) are significantly longer than the  $\text{La}–\text{C}(\mu\text{-Me})[\eta^2]$  bonds (av. 2.795 Å). For comparison, the  $\text{La}–\text{C}(\mu\text{-Me})$  bond lengths in  $[\text{Cp}^*\text{La}\{(\mu\text{-Me})_2\text{AlMe}_2\}_2]$  range from 2.694(3) to 2.802(4) Å.<sup>[37b]</sup> The  $\text{Al}–\text{C}$  bond lengths decrease gradually in the order  $\mu\text{-Me}[\eta^2]$  (2.042 Å) >  $\mu\text{-Me}[\eta^1]$  (2.013 Å) > terminal (1.967 Å). Similar hexalanthanide ( $\text{CpLn}$ )<sub>6</sub> cluster arrangements have been isolated in the presence of borohydrido coligands (Table 1).<sup>[29]</sup>

Blue-green single crystals of neodymium complex **4** were obtained within one day from unstirred reaction mixtures. Two independent X-ray crystallographic studies showed that the pentanuclear neodymium cluster  $[\text{Cp}^*_5\text{Nd}_5\{(\mu\text{-Me})_3\text{AlMe}\}(\mu_4\text{-Cl})(\mu_3\text{-Cl})_2(\mu_2\text{-Cl})_6]$  was formed with a low  $\text{Nd}/\text{Cl}$  ratio of 1:1.7 (Figure 1).<sup>[39]</sup> Each neodymium center is octacoordinate; however, three different neodymium environments are observed. Four of the Nd atoms adopt a butterfly arrangement with two different “ $\text{Cp}^*\text{NdCl}_5$ ” coordination polyhedra. The Nd<sub>4</sub> unit is connected to the fifth Nd atom through two  $\mu_2$ -bridging chloro ligands, and the pseudotetrahedral coordination geometry of this atom is completed by a  $\text{Cp}^*$  ligand and an  $\text{AlMe}_4$  ligand. A similar cluster geometry was previously found in  $[\text{Yb}_5\text{Cp}^*_6(\mu_4\text{-F})(\mu_3\text{-F})_2(\mu\text{-F})_6]$ , in which fluoro instead of chloro ligands are involved and the tetramethylaluminate ligand is replaced by a second  $\text{Cp}^*$  ligand.<sup>[23]</sup> The most striking feature of the  $\text{Nd}_5\text{Al}$  cluster is the  $\eta^3$ -coordinated tetramethylaluminate group, which has three similar  $\text{Nd}–\text{C}(\mu\text{-Me})$  bond lengths (2.878(18), 2.875(16), 2.779(16) Å) and a short  $\text{Nd}\cdots\text{Al}$  separation of 2.920(5) Å. These  $\text{Nd}–\text{C}$  bonds are significantly longer than the  $\eta^2$ -coordinated  $\text{Nd}–\text{C}(\mu\text{-Me})$  bonds in hexacoordinate  $[\text{Nd}(\text{AlMe}_4)_3]$  (av.  $\text{Nd}–\text{C}$  bond length: 2.592 Å).<sup>[40]</sup> To our knowledge, no structural evidence of a true  $\eta^3$  coordination of an  $\text{AlMe}_4$  group to a lanthanide center has been reported so far.<sup>[42]</sup> The average  $\text{Nd}–\text{Cl}$  bond lengths increase with the degree of metal bridging in the order 2.775 ( $\mu_2\text{-Cl}$ ), 2.921 ( $\mu_3\text{-Cl}$ ), and 2.980 Å ( $\mu_4\text{-Cl}$ ) and are comparable to the range of  $[(\mu_2\text{-Cl});(\mu_3\text{-Cl})]$  bond lengths in  $[\text{Nd}_6(2,4\text{-C}_7\text{H}_{11})_6\text{Cl}_{12}(\text{thf})_2]$  (2.759(2)–2.934(1) Å).<sup>[24]</sup>

In conclusion, complexes **2–4** feature rare examples of alkali-metal-free organolanthanide complexes which contain both alkyl and chloro ligands.<sup>[43]</sup> The open half-lanthanido-cene coordination sphere facilitates new coordination modes **C** and **E** of the tetramethylaluminate ligand (Figure 2), which exhibit extremely long  $\text{Ln}–\text{C}$  bond lengths.

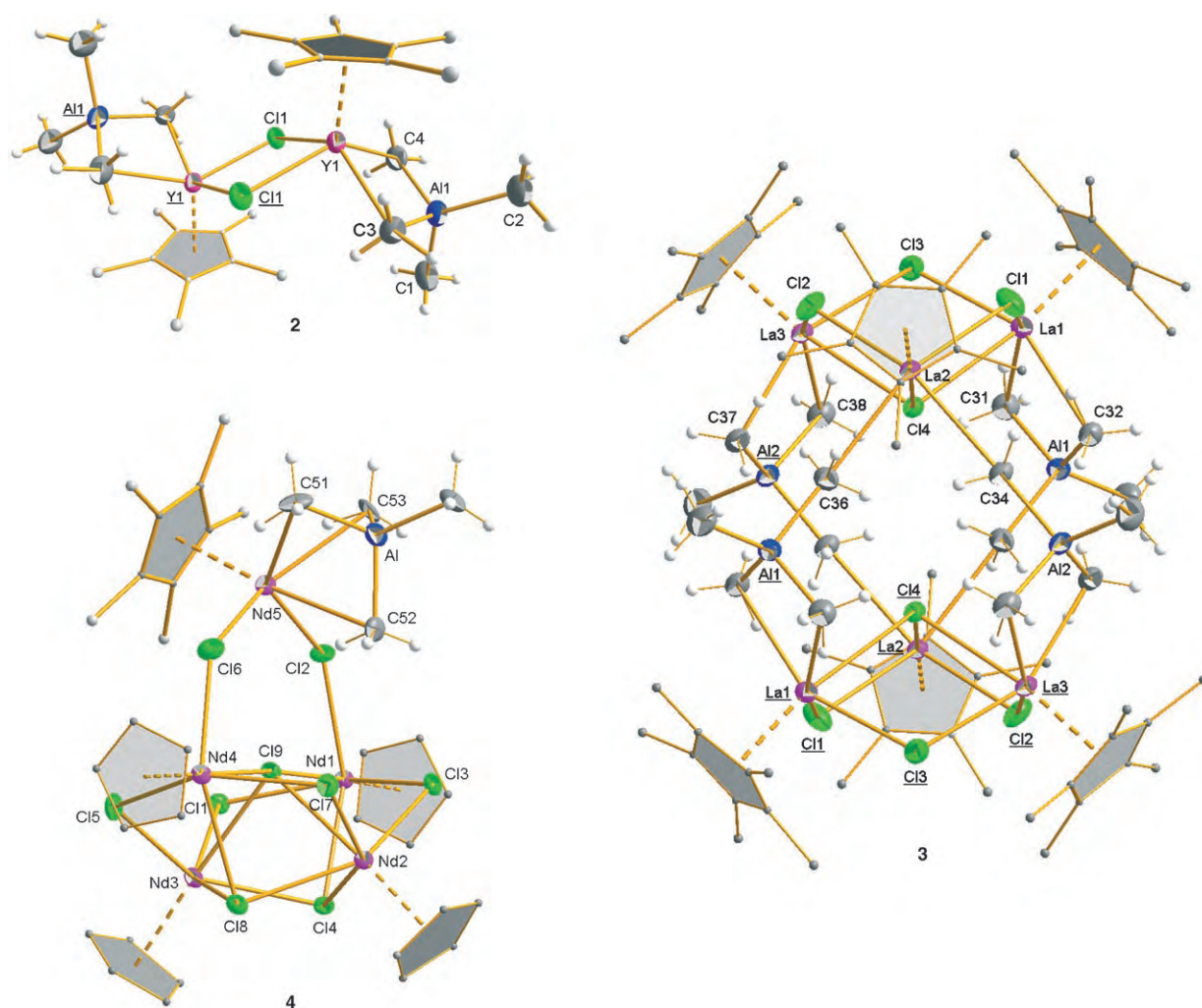


**Figure 1.** Molecular structures of **2–4** (atomic displacement parameters set at the 50% level). Atoms of the Cp\* groups are shown isotropically with an arbitrary radius and without H atoms. Underlined atom labels indicate symmetry-related atoms. For **3** only the first of the two unique half molecules is shown. For **4** the methyl groups of the cyclopentadienyl ligands at Nd1–Nd4 were omitted for clarity. Selected bond distances [Å] and angles [°]: **2**: Y1–Al1 3.0584(12), Y1–Cl1 2.6326(9), Y1–Cl1' 2.7177(9), Y1–C3 2.554(3), Y1–C4 2.592(3), Y1–C(Cp\*) 2.567(4)–2.610(4), Al1–C1 1.954(5), Al1–C2 1.897(4), Al1–C3 2.138(3), Al1–C4 2.106(4); Cl1–Y1–Cl1' 82.14(3), Y1–Cl1–Y1' 97.86(3), C3–Y1–C4 86.14(10), Y1–C3–Al1 80.83(9), C3–Al1–C4 111.79(12). **3**: La1/4–Al1/3 3.3531/3.3534(11), La3/6–Al2/Al4 3.3186/3.3150(11), La1/4–Cl1/5 2.8355/2.8263(9), La1/4–Cl3/7 2.8170/2.8179(10), La1/4–Cl4/8 3.0565/3.0504(8), La2/5–Cl1/5 2.8232/2.8049(9), La2/5–Cl2/6 2.8197/2.8153(9), La2/5–Cl4/8 3.0060/3.0067(7), La3/6–Cl2/6 2.8439/2.8373(9), La2/6–Cl3/7 2.8284/2.8339(10), La3/6–Cl4/8 3.0708/3.0652(8), La1/4–C31/69 2.819/2.826(4), La1/4–C32/70 2.799/2.783(4), La2/5–C34/72 2.950/2.955(3), La2/5–C36/74 2.950/2.938(3), La3/6–C37/76 2.790/2.774(4), La3/6–C38/75 2.771/2.784(4), La–C(Cp\*) 2.728(3)–2.819(4), Al1/3–C31/69 2.044/2.040(4), Al1/3–C32/70 2.042/2.040(4), Al1/3–C36/74 2.010/2.015(4), Al1/3–C33/71 1.969/1.976(4), Al2/4–C37/76 2.041/2.045(4), Al2/4–C38/75 2.042/2.044(4), Al2/4–C34/72 2.016/2.014(3), Al2/4–C35/73 1.965/1.963(4); La1/4–Cl1/5–La2/5 110.96/110.94(3), La2/5–Cl2/6–La3/6 111.85/111.72(3), La1/4–Cl3/7–La3/6 113.19/113.07(3), La1/4–Cl4/8–La2/5 100.53/99.97(2), La1/4–Cl4/8–La3/6 100.55/100.88(2), La2/5–Cl4/8–La3/6 101.05/100.80(2), La1/4–C31/69–Al1/3 85.61/85.52(1), C31/69–La1/4–C32/70 74.78/74.65(1), La2/5–C36/74–Al1/3 168.77/168.84(2), La2/5–C34/72–Al2/4 170.70/171.63(2). **4**: Nd5–Al 2.920(5), Nd5–C51 2.878(18), Nd5–C52 2.875(16), Nd–C53 2.779(16), Nd–Cl( $\mu_2$ ) 2.731(4)–2.809(4), Nd–Cl( $\mu_3$ ) 2.866(4)–3.000(4), Nd–Cl( $\mu_4$ ) 2.961(4)–3.005(4), Nd–C(Cp\*) 2.650(15)–2.728(17); Nd5–C51–Al 70.7(5), C51–Nd5–C52 69.4(6), Nd5–Cl2–Nd1 132.48(15), Nd5–Cl6–Nd4 131.71(16), Cl2–Nd5–Cl6 119.44(12), Nd1–Cl9–Nd4 175.17(14), Nd2–Cl9–Nd3 91.00(10), Nd2–Cl4–Nd3 94.89(11), Nd1–Cl3–Nd2 96.40(12), Cl1–Nd1–Cl3 143.54(12).

We recently reported that the binary system  $[\text{Ln}(\text{AlMe}_4)_3]/\text{Me}_2\text{AlCl}$  acts as a highly efficient initiator for isoprene polymerization.<sup>[44]</sup> Those findings were in accordance with a) chloro transfer to an alkylated rare-earth-metal center as the crucial activation step and b) the fact that neodymium is the most active rare-earth-metal center (“neodymium effect”).<sup>[45]</sup> Our findings that subtle changes in rare-earth-metal size considerably affect the  $\text{AlMe}_4/\text{Cl}$  exchange

and coordination behavior of the  $\text{AlMe}_4$  ligand, might provide more insight into the obscure neodymium effect. Both binary  $[\text{Ln}(\text{AlMe}_4)_3]/\text{Me}_2\text{AlCl}$  and commercially employed ternary  $[\text{Ln}(\text{carboxylate})_3]/\text{HALiBu}_2/\text{Et}_3\text{Al}_2\text{Cl}_3$  “Ziegler mixed catalysts” initially produce a fine precipitate upon addition of the chloro-ligand source which redissolves upon addition of diene monomer.<sup>[44,46]</sup> Clearly, such an activation scenario suggests that cluster formation is part of the initiating steps.



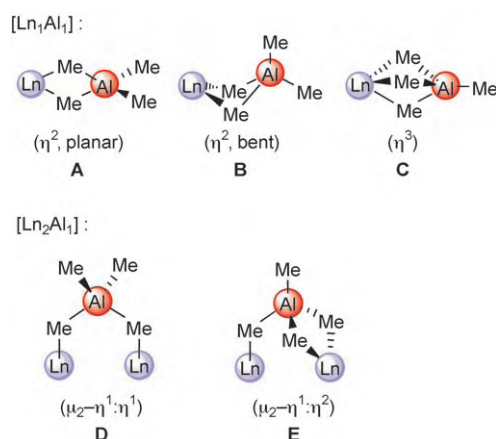


Figure 2. Structurally characterized Ln-AlMe<sub>4</sub> coordination modes.

## Experimental Section

**2:** In a glovebox, [Cp\*Y(AlMe<sub>4</sub>)<sub>2</sub>] (**1a**, 200 mg, 0.50 mmol) was dissolved in hexane (5 mL). Without stirring, a solution of Me<sub>2</sub>AlCl (452 μL, 1 M in hexane, 0.9 equiv) was added at -35 °C. Within 5 h at ambient temperature the product was obtained as colorless crystals (77 mg, 49% based on Me<sub>2</sub>AlCl). After 7 days, an additional crop (45 mg) was isolated from the solution, thus resulting in an overall yield of 78%. The product was slightly soluble in toluene and benzene. Impurities of [Cp\*Y(AlMe<sub>4</sub>)<sub>3</sub>] were best separated from the product by washing with small amounts of toluene. According to <sup>1</sup>H NMR spectroscopic analysis, this transformation gave pure products for 0.5–0.9 equiv of Me<sub>2</sub>AlCl. The product was also obtained from a stirred reaction mixture as a white solid in good yield. IR (nujol):  $\tilde{\nu}$  = 1211 (m), 1189 (m), 1169 (m), 1021 (w), 965 (w), 769 (w), 578 (w), 477 cm<sup>-1</sup> (w); <sup>1</sup>H NMR (400 MHz, [D<sub>8</sub>]toluene, 25 °C):  $\delta$  = 1.91 (s, 15H, Cp\*), -0.16 ppm (d, 12H, AlMe<sub>4</sub>); <sup>13</sup>C{<sup>1</sup>H} NMR (100 MHz, [D<sub>8</sub>]toluene, 25 °C):  $\delta$  = 122.2 (C<sub>5</sub>Me<sub>5</sub>), 11.3 ppm (C<sub>5</sub>Me<sub>5</sub>). Elemental analysis (%) calcd for C<sub>28</sub>H<sub>54</sub>Al<sub>2</sub>Cl<sub>2</sub>Y<sub>2</sub> (693.416 g mol<sup>-1</sup>): C 48.50, H 7.85; found: C 47.79, H 7.60.

**3:** In a glovebox, [Cp\*La(AlMe<sub>4</sub>)<sub>3</sub>] (**1b**, 200 mg, 0.45 mmol) was dissolved in hexane (5 mL). Without stirring, a solution of Me<sub>2</sub>AlCl (446 μL, 1 M in hexane, 1 equiv) was added at -35 °C. The formation of single crystals was observed within 30 min at ambient temperature. Within 2 days the product was obtained as colorless crystals (130 mg, > 95% based on Me<sub>2</sub>AlCl). According to elemental analysis and X-ray analysis, the reaction resulted in the pure product for 0.5–1.3 equiv of Me<sub>2</sub>AlCl. The product was also obtained from a stirred mixture as a white solid in quantitative yield. IR (nujol):  $\tilde{\nu}$  = 1305 (m), 1190 (m), 1042 (m), 1027 (m), 967 (w), 769 (w), 722 (m), 702 (m), 623 (m), 585 (w), 532 cm<sup>-1</sup> (w). Elemental analysis (%) calcd for C<sub>76</sub>H<sub>138</sub>Al<sub>4</sub>Cl<sub>8</sub>La<sub>6</sub>·C<sub>6</sub>H<sub>14</sub> (2363.119 g mol<sup>-1</sup>): C 41.68, H 6.48; found: C 42.11, H 6.64.

**4:** Following the above procedure, blue-green crystals (36 mg, 21% based on **1c**) were obtained within 24 h from **1c** (200 mg, 0.46 mmol) and Me<sub>2</sub>AlCl (528 μL, 1 M in hexane, 1.2 equiv). According to the elemental analysis, the product was formed also by addition of 1.2–1.7 equiv of Me<sub>2</sub>AlCl. IR (nujol):  $\tilde{\nu}$  = 1305 (m), 1190 (m), 1042 (m), 1027 (m), 967 (w), 769 (w), 722 (m), 702 (m), 623 (m), 585 (w), 532 cm<sup>-1</sup> (w). Elemental analysis (%) calcd for C<sub>54</sub>H<sub>87</sub>AlCl<sub>9</sub>Nd<sub>5</sub>·C<sub>6</sub>H<sub>14</sub> (1889.721 g mol<sup>-1</sup>): C 38.14, H 5.39; found: C 37.61, H 5.21.

Full experimental and physicochemical details for complexes **2–4** are available in the Supporting Information.

**Keywords:** alkyl aluminates · cluster compounds · rare earths · structure elucidation

- [1] a) A. Müller, *Science* **2003**, *300*, 749; b) A. Müller, E. Beckmann, H. Bögge, M. Schmidtman, A. Dress, *Angew. Chem.* **2002**, *114*, 1210; *Angew. Chem. Int. Ed.* **2002**, *41*, 1162; Na<sub>48</sub>[H<sub>4</sub>Mo<sub>368</sub>O<sub>1032</sub>·(H<sub>2</sub>O)<sub>240</sub>(SO<sub>4</sub>)<sub>48</sub>], ca. 1000 H<sub>2</sub>O.
- [2] a) C. D. Chandler, C. Roger, M. J. Hampden-Smith, *Chem. Rev.* **1993**, *93*, 1205; b) D. C. Bradley, R. C. Mehrotra, I. P. Rothwell, A. Singh, *Alkoxo and Aryloxo Derivatives of Metals*, Academic Press, London, **2001**; C. Sanchez, G. J. de A. A. Soler-Illia, F. Ribot, T. Lalot, C. R. Mayer, V. Cabuil, *Chem. Mater.* **2001**, *13*, 3061; c) H. Schubert, *J. Mater. Chem.* **2005**, *15*, 3701.
- [3] D. Fenske, C. E. Anson, A. Eichhöfer, O. Fuhr, A. Ingendoh, C. Persau, C. Richert, *Angew. Chem.* **2005**, *117*, 5376; *Angew. Chem. Int. Ed.* **2005**, *44*, 5242; [Ag<sub>344</sub>S<sub>124</sub>(*StBu*)<sub>96</sub>], and references therein.
- [4] A. Kornienko, T. J. Emge, G. A. Kumar, R. E. Riman, J. G. Brennan, *J. Am. Chem. Soc.* **2005**, *127*, 3501; [(thf)<sub>14</sub>Er<sub>10</sub>S<sub>6</sub>(Se<sub>2</sub>)<sub>6</sub>I<sub>6</sub>].
- [5] a) Y. Yin, R. M. Rioux, C. K. Erdonmez, S. Hughes, G. A. Somorjai, A. P. Alivisatos, *Science* **2004**, *304*, 711; b) J. Liu, T. Tanaka, K. Sivula, A. P. Alivisatos, J. M. Frechet, *J. Am. Chem. Soc.* **2004**, *126*, 6550.
- [6] a) F. Bottomley, L. Sutin, *Adv. Organomet. Chem.* **1988**, *28*, 339; b) C. Limberg, *Angew. Chem.* **2005**, *117*, 6256; *Angew. Chem. Int. Ed.* **2005**, *44*, 524.
- [7] C. Shan, Y. Lin, J. Quyang, Y. Fan, G. Yang, *Macromol. Chem.* **1987**, *188*, 629–635.
- [8] J. Bai, A. V. Virovets, M. Scheer, *Science* **2003**, *300*, 781.
- [9] a) J. Vollet, J. R. Hartig, H. Schnöckel, *Angew. Chem.* **2004**, *116*, 3248; *Angew. Chem. Int. Ed.* **2004**, *43*, 3186; b) A. Purath, C. Dohmeier, A. Ecker, R. Köppe, H. Krautscheid, H. Schnöckel, R. Ahlrichs, C. Stoermer, J. Friedrich, P. Jutzi, *J. Am. Chem. Soc.* **2000**, *122*, 6955.
- [10] For an example from late-transition-metal chemistry, see: M. Ohashi, K. Matsubara, T. Iizuka, H. Suzuki, *Angew. Chem.* **2003**, *115*, 967; *Angew. Chem. Int. Ed.* **2003**, *42*, 937; [Ru<sub>3</sub>Cp\*(μ<sub>3</sub>-AlEt)(μ-H)]<sub>3</sub>.
- [11] R. Anwander, *Angew. Chem.* **1998**, *110*, 619; *Angew. Chem. Int. Ed.* **1998**, *37*, 599.
- [12] R. Wang, Z. Zheng, T. Jin, R. Staples, *Angew. Chem.* **1999**, *111*, 1929; *Angew. Chem. Int. Ed.* **1999**, *38*, 1813.
- [13] For further examples, see: a) M. R. Bürgstein, P. W. Roesky, *Angew. Chem.* **2000**, *112*, 559; *Angew. Chem. Int. Ed.* **2000**, *39*, 549; [Ln<sub>14</sub>(μ<sub>3</sub>-O)<sub>2</sub>(μ<sub>3</sub>-NC<sub>6</sub>H<sub>4</sub>O)<sub>24</sub>(μ<sub>3</sub>-OH)<sub>2</sub>(μ<sub>3</sub>-OH)<sub>16</sub>] (Ln = Er, Yb); b) W. J. Evans, M. S. Sollberger, *Inorg. Chem.* **1988**, *27*, 4417; [Y<sub>14</sub>(μ<sub>3</sub>-O)<sub>2</sub>(μ<sub>3</sub>-Cl)<sub>2</sub>(μ<sub>3</sub>-OrBu)<sub>4</sub>(μ<sub>3</sub>-OrBu)<sub>14</sub>(μ<sub>3</sub>-Cl)<sub>8</sub>(OrBu)<sub>10</sub>(thf)<sub>4</sub>].
- [14] a) S. Arndt, J. Okuda, *Chem. Rev.* **2002**, *102*, 1953; b) Z. Hou, *Bull. Chem. Soc. Jpn.* **2003**, *76*, 2253.
- [15] Y.-P. Cai, H.-Z. Ma, B.-S. Kang, C.-Y. Su, W. Zhang, J. Sun, Y.-L. Xiong, *J. Organomet. Chem.* **2001**, *628*, 99.
- [16] A. Zalkin, D. J. Berg, *Acta Crystallogr. Sect. C* **1989**, *45*, 1630.
- [17] Z.-S. Jin, J. -W. Guan, G.-C. Wei, J.-Y. Hu, Q. Shen, *Jiegou Huaxue* **1990**, *9*, 140.
- [18] X. Zhou, H. Ma, Z. Wu, X. You, Z. Xu, X. Huang, *J. Organomet. Chem.* **1995**, *503*, 11.
- [19] a) W. J. Evans, M. S. Sollberger, *J. Am. Chem. Soc.* **1986**, *108*, 6095; b) H. Schumann, G. Kociok-Köhn, J. Loebel, *Z. Anorg. Allg. Chem.* **1990**, *581*, 69.
- [20] W. J. Evans, N. T. Allen, M. A. Greci, J. W. Ziller, *Organometallics* **2001**, *20*, 2936.
- [21] W. J. Evans, G. W. Rabe, M. A. Ansari, J. W. Ziller, *Angew. Chem.* **1994**, *106*, 2200; *Angew. Chem. Int. Ed. Engl.* **1994**, *33*, 2110.

Received: March 8, 2006

- [22] H. Schumann, I. Albrecht, M. Gallagher, E. Hahn, C. Janiak, C. Kolax, J. Loebel, S. Nickel, E. Palamidis, *Polyhedron* **1988**, *7*, 2307.
- [23] P. L. Watson, T. H. Tulip, I. Williams, *Organometallics* **1990**, *9*, 1999.
- [24] J. Sieler, A. Simon, K. Peters, R. Taube, M. Geitner, *J. Organomet. Chem.* **1989**, *362*, 297.
- [25] S. P. Constantine, G. M. De Lima, P. B. Hitchcock, J. M. Keates, G. A. Lawless, *Chem. Commun.* **1996**, 2421.
- [26] M. D. Walter, F. Weber, G. Wolmershäuser, H. Sitzmann, *Angew. Chem.* **2006**, *118*, 1937; *Angew. Chem. Int. Ed.* **2006**, *45*, 1903.
- [27] W. P. Kretschmer, J. H. Teuben, S. I. Troyanov, *Angew. Chem.* **1998**, *110*, 92; *Angew. Chem. Int. Ed.* **1998**, *37*, 88.
- [28] S. Ya. Knjazhanskij, E. B. Lobkovsky, B. M. Bulychev, V. K. Belsky, G. L. Soloveichik, *J. Organomet. Chem.* **1991**, *419*, 311.
- [29] F. Bonnet, M. Visseaux, D. Barbier-Baudry, A. Hafid, E. Vigier, M. Kubicki, *Inorg. Chem.* **2004**, *43*, 3682.
- [30] O. Tardif, M. Nishiura, Z. Hou, *Tetrahedron* **2003**, *59*, 10525.
- [31] a) O. Tardif, M. Nishiura, Z. Hou, *Organometallics* **2003**, *22*, 1171; b) K. C. Hultsch, P. Voth, T. P. Spaniol, J. Okuda, *Z. Anorg. Allg. Chem.* **2003**, *629*, 1272.
- [32] Z. Hou, Y. Zhang, O. Tardif, Y. Wakatsuki, *J. Am. Chem. Soc.* **2001**, *123*, 9216.
- [33] K.-H. Thiele, S. Bambirra, J. Sieler, S. Yelonek, *Angew. Chem.* **1998**, *110*, 3016; *Angew. Chem. Int. Ed.* **1998**, *37*, 2886.
- [34] H. M. Dietrich, H. Grove, K. W. Törnroos, R. Anwender, *J. Am. Chem. Soc.* **2006**, *128*, 1458.
- [35] a) D. Cui, O. Tardif, Z. Hou, *J. Am. Chem. Soc.* **2004**, *126*, 1312; b) O. Tardif, D. Hashizume, Z. Hou, *J. Am. Chem. Soc.* **2004**, *126*, 8080; c) D. Cui, M. Nishiura, Z. Hou, *Angew. Chem.* **2005**, *117*, 981; *Angew. Chem. Int. Ed.* **2005**, *44*, 959; d) Y. Luo, J. Baldamus, O. Tardif, Z. Hou, *Organometallics* **2005**, *24*, 4362.
- [36] For examples of half-neodymocene network structures, see: W. J. Evans, D. G. Giarikos, P. S. Workman, J. W. Ziller, *Inorg. Chem.* **2004**, *43*, 5754.
- [37] a) R. Anwender, M. G. Klimpel, H. M. Dietrich, D. J. Shorokhov, W. Scherer, *Chem. Commun.* **2003**, *8*, 1008; b) H. M. Dietrich, C. Zapilko, E. Herdtweck, R. Anwender, *Organometallics* **2005**, *24*, 5767.
- [38] W. J. Evans, T. M. Champagne, D. G. Giarikos, J. W. Ziller, *Organometallics* **2005**, *24*, 570.
- [39] Compound **2** ( $C_{28}H_{54}Al_2Cl_2Y$ ,  $M_r = 693.39$ ) crystallized from hexane in the triclinic space group  $P\bar{1}$ ,  $a = 8.6804(6)$ ,  $b = 10.2662(8)$ ,  $c = 10.3573(6)$  Å,  $\alpha = 69.501(3)^\circ$ ,  $\beta = 86.674(7)^\circ$ ,  $\gamma = 84.192(3)^\circ$ ,  $V = 859.85(10)$  Å<sup>3</sup>,  $\rho_{\text{calcd}} = 1.331$  g cm<sup>-3</sup>,  $Z = 1$ . Data were collected at 143 K on a Nonius DIP 2020 system. The structure was solved by Patterson methods, and least-square refinement of the model based on 2966 (all data) and 2653 reflections ( $I > 2.0\sigma(I)$ ) converged to the final values  $wR2 = 0.1108$  and  $R1 = 0.0417$ . Compound **3** ( $C_{82}H_{152}Al_4Cl_8La_6$ ·hexane,  $M_r = 2363.02$ ) crystallized from hexane in the triclinic space group  $P\bar{1}$ ,  $a = 14.5831(6)$ ,  $b = 15.8066(7)$ ,  $c = 24.8320(10)$  Å,  $\alpha = 80.097(1)^\circ$ ,  $\beta = 85.614(1)^\circ$ ,  $\gamma = 65.919(1)^\circ$ ,  $V = 5147.9(4)$  Å<sup>3</sup>,  $\rho_{\text{calcd}} = 1.524$  g cm<sup>-3</sup>,  $Z = 2$ . Data were collected at 153 K on a BRUKER-AXS 2 K CCD system. The structure was solved by direct methods, and least-square refinement of the model based on 24553 (all data) and 21252 reflections ( $I > 2.0\sigma(I)$ ) converged to the final values  $wR2 = 0.0795$  and  $R1 = 0.0309$ . The asymmetric unit contains two independent half molecules (La1–La3 etc. and La4–La6 etc.) that are related by inversion centers into two full complexes (symmetry operations  $2-x$ ,  $-y$ ,  $2-z$  and  $-x$ ,  $1-y$ ,  $3-z$ ) and one hexane solvate molecule. Compound **4** ( $C_{60}H_{101}AlCl_9Nd_5$ ·hexane,  $M_r = 1889.64$ ) crystallized from hexane in the triclinic space group  $P\bar{1}$ ,  $a = 12.3712(15)$ ,  $b = 13.7414(17)$ ,  $c = 24.038(3)$  Å,  $\alpha = 75.839(2)^\circ$ ,  $\beta = 84.498(2)^\circ$ ,  $\gamma = 66.827(2)^\circ$ ,  $V = 3642.5(8)$  Å<sup>3</sup>,  $\rho_{\text{calcd}} = 1.723$  g cm<sup>-3</sup>,  $Z = 2$ . Data were collected at 123 K on a BRUKER-AXS 2K CCD system.
- The structure was solved by direct methods, and least-square refinement of the model based on 14871 (all data) and 11427 reflections ( $I > 2.0\sigma(I)$ ) converged to the final values  $wR2 = 0.2232$  and  $R1 = 0.0886$ . Compounds **3** and **4** each cocrystallized with a molecule of hexane which could not be removed in high vacuum. All hydrogen atoms of the methyl groups that are bonded to aluminum centers were found in the difference Fourier maps but were thereafter placed in calculated positions (SHELXL riding models AFIX 33 and 137) for structures **3** and **4**. For compound **2** the hydrogen atoms of the coordinating methyl groups were refined. CCDC-600834–600836 contain the supplementary crystallographic data for this paper. These data can be obtained free of charge from The Cambridge Crystallographic Data Centre via [www.ccdc.cam.ac.uk/data\\_request/cif](http://www.ccdc.cam.ac.uk/data_request/cif).
- [40] W. J. Evans, R. Anwender, J. W. Ziller, *Organometallics* **1995**, *14*, 1107.
- [41] W. J. Evans, T. T. Peterson, M. D. Rausch, W. E. Hunter, H. Zang, J. L. Atwood, *Organometallics* **1985**, *3*, 554.
- [42]  $\eta^3$ -Coordinated  $AlEt_4$  groups were found in  $[ \{ Al_3Nd_6(\mu-Cl)_6(\mu_3-Cl)_6(\mu-C_2H_5)_9(C_2H_5)_5(OiPr)_2 \} ]^{[7]}$  and  $[ \{ Yb(AlEt_4)_2 \}_n ]$ : M. G. Klimpel, R. Anwender, M. Tafipolsky, W. Scherer, *Organometallics* **2001**, *20*, 3983.
- [43] a) For a half-lutetocene complex with mixed chloro/donor-functionalized alkyl ligands, see: H. Schumann, J. A. Meese-Marktscheffel, A. Dietrich, J. Pickardt, *J. Organomet. Chem.* **1992**, *433*, 241; b) for a  $\beta$ -diketiminato samarium complex with mixed chloro/tetramethylaluminate ligands, see: C. Cui, A. Shafir, J. A. R. Schmidt, A. G. Oliver, J. Arnold, *Dalton Trans.* **2005**, 1387.
- [44] A. Fischbach, M. G. Klimpel, M. Widenmeyer, E. Herdtweck, W. Scherer, R. Anwender, *Angew. Chem.* **2004**, *116*, 2284; *Angew. Chem. Int. Ed.* **2004**, *43*, 2234.
- [45] R. Taube, G. Sylvester in *Applied Homogeneous Catalysis with Organometallic Compounds* (Eds.: B. Cornils, W. A. Herrmann), Wiley-VCH, Weinheim, **2000**.
- [46] W. J. Evans, D. G. Giarikos, J. W. Ziller, *Organometallics* **2001**, *20*, 5751.

DOI: 10.1002/anie.200600244

**Microwave-Assisted Synthesis of Luminescent  $\text{LaPO}_4\text{:Ce,Tb}$  Nanocrystals in Ionic Liquids\*\***

Gunnar Bühler and Claus Feldmann\*

*Dedicated to Professor Hansgeorg Schnöckel on the occasion of his 65th birthday*

Nanoscale luminescent materials are of increasing importance for established technologies (for example, displays, lamps, and X-ray detectors),<sup>[1]</sup> and are essential for upcoming applications. New applications of nanoscale phosphors include transparent luminescent layers or markers (for example, on metal, ceramics, plastics, or paper), luminescent fillers in transparent matrices (for example, glass or plastics), as well as biomedical applications such as fluorescence resonance energy transfer (FRET) assays, biolabelling, optical imaging, or phototherapy.<sup>[2]</sup>

With quantum yields exceeding 50 %, quantum dots of II–VI or III–V semiconductors, and nanoparticles of rare-earth-doped metal phosphates are the state-of-the-art luminescent materials.<sup>[3]</sup> Core-shell structures have proven to be particularly favorable.<sup>[4]</sup> To obtain top-quality luminescent nanocrystals, the synthesis must be performed at elevated temperatures (typically 150–250 °C) to minimize lattice defects. Coordinating solvents or stabilizers (for example, trioctylphosphine, octylphosphate, octylamine, thioglycerol, diethylene glycol, oleic acid, or polyvinyl pyrrolidone) are necessary to control the particle size and the degree of agglomeration, and to protect the particle surfaces. A modification of the resulting “synthesis-determined” surface conditioning requires additional process steps and bears the risks of colloidal collapse, agglomeration, and surface damage. All things considered, the synthesis of luminescent nanocrystals is often complicated and time-consuming. Toxic solids, solvents, or stabilizers are frequently used. All of these issues can be major limitations for potential technical applications.

Herein, we present a novel and facile synthesis of highly luminescent  $\text{LaPO}_4\text{:Ce,Tb}$  nanocrystals based on the use of ionic liquids (ILs) as reaction media. In recent years, ILs have attracted considerable interest, owing to their exceptional features (for example, wide liquid range, thermal stability, noncoordinating properties, electrochemical stability, and

adjustable solvent polarity).<sup>[5]</sup> ILs have also had a significant impact on organic synthesis.<sup>[6]</sup> In contrast, an exploration of their potential in the synthesis of nanocrystals has just begun.<sup>[7]</sup>

Owing to the noncoordinating properties of ILs,<sup>[5,8]</sup> their complete removal after the synthesis should, in principal, be much easier than that of standard coordinating solvents. However, it is expected that surface stabilization at elevated temperatures, which is a prerequisite for non-agglomerated and highly luminescent nanoscale phosphors, will be significantly reduced. Our strategy to avoid agglomeration is a rapid heating over a short time interval, which can be accomplished by microwave irradiation in the case of highly polar ILs.

In the first step of the synthesis, a solution of the rare-earth chlorides in the IL tributylmethylammonium triflylimide and a cosolvent (for example, ethanol, dimethylformamide (DMF), dimethyl sulfoxide (DMSO), or pyridine) was added to the phosphate precursor (for example, phosphoric acid, or ammonium or pyridinium phosphate), likewise dissolved in the IL and a cosolvent, at 70 °C. The IL was selected from a variety of candidates for its extraordinary thermal and chemical stability.<sup>[9]</sup> Precipitation of  $\text{LaPO}_4\text{:Ce,Tb}$  occurs immediately, as indicated by the appearance of a slight opalescence. Thereafter, all volatiles were removed under reduced pressure. In the second step, the crystallinity of the preformed nanoparticles was enhanced by heating the dispersion to 300 °C within 10 s in a microwave oven. After centrifugation and washing, the nanocrystals were collected in yields of 90 %. The white powder obtained can be easily redispersed in ethanol by sonification. The resulting transparent dispersions show an intense green emission upon excitation with UV light (Figure 1).

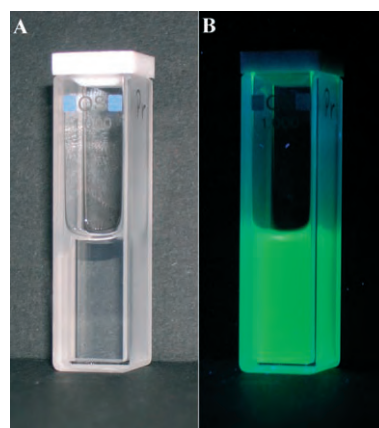


**Figure 1.** Transparent dispersion of  $\text{LaPO}_4\text{:Ce,Tb}$  nanocrystals redispersed in ethanol: A) in daylight and B) with UV excitation.

The size and morphology of the  $\text{LaPO}_4\text{:Ce,Tb}$  nanocrystals were investigated by electron microscopy. Transmission electron microscopy (TEM) images reveal spherical to slightly ellipsoidal particles with sizes of 9–12 nm (Figure 2A). Their electron diffraction pattern (Figure 2B), and the lattice fringes observed in high-resolution images (Figure 2A) indicate that the particles are crystalline. TEM and

[\*] Dr. G. Bühler, Prof. Dr. C. Feldmann  
Institut für Anorganische Chemie  
Universität Karlsruhe  
Engesserstrasse 15, 76131 Karlsruhe (Germany)  
Fax: (+49) 721-608-4892  
E-mail: feldmann@aoe1.uni-karlsruhe.de

[\*\*] We thank Dr. S. Lebedkin and Prof. Dr. M. M. Kappes for the photoluminescence measurements, and W. Send and Prof. Dr. D. Gerthsen for the TEM analyses. We are also grateful to the DFG Center for Functional Nanostructures (CFN) at the Universität Karlsruhe for financial support.



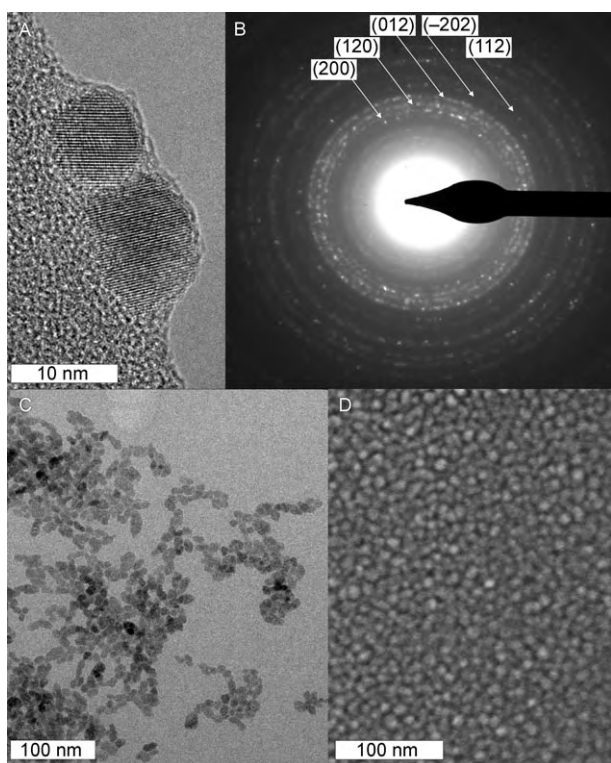


**Figure 2.** TEM and SEM images of the as-prepared  $\text{LaPO}_4\text{:Ce,Tb}$  nanocrystals: A) high-resolution TEM image showing lattice fringes; B) electron diffraction pattern of a bundle of particles with Miller indices indicated; C) TEM and D) SEM images showing the uniformity of the particles.

scanning electron microscopy (SEM) images of samples isolated from ethanol dispersions reveal a large amount of nearly spherical and monodispersed particles (Figure 2 C,D). A particle diameter of 10(1) nm was determined by the statistical evaluation of 170 particles.

According to its electron diffraction (Figure 2 B) and powder X-ray diffraction (PXRD; Figure 3) patterns, the

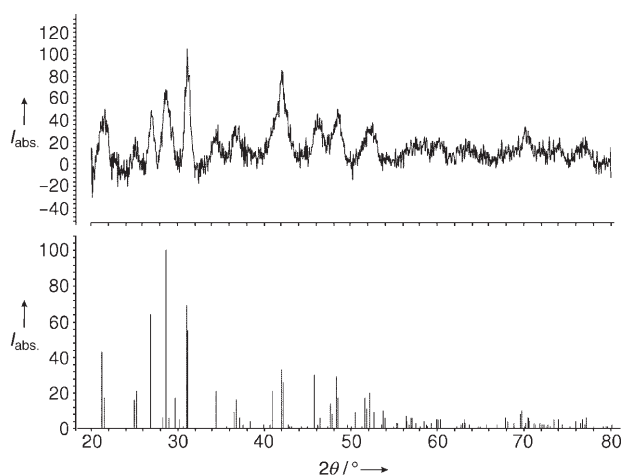


**Figure 3.** PXRD pattern of the as-prepared  $\text{LaPO}_4\text{:Ce,Tb}$  nanocrystals (top) and the reference pattern for  $\text{LaPO}_4$  (bottom; JCPDS file no. 84-600).

nanocrystalline material adopts a monoclinic structure of the monazite type.<sup>[10]</sup> With the assumption of spherical particles, a mean particle diameter of 8–10 nm is calculated using Scherrer's equation. This value agrees with that determined by electron microscopy.

To verify the particle diameter and size distribution, dynamic light scattering (DLS) experiments were performed. First, as-prepared  $\text{LaPO}_4\text{:Ce,Tb}$  was investigated after washing and redispersion in ethanol (Figure 4 A). Considering the

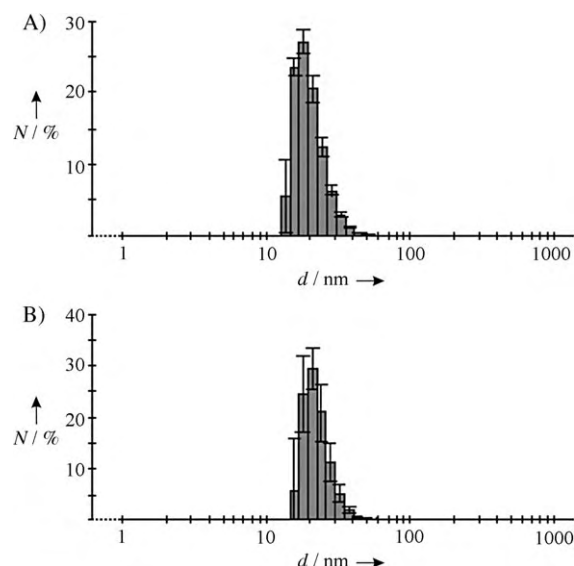


**Figure 4.** Particle size distribution of the  $\text{LaPO}_4\text{:Ce,Tb}$  nanocrystals: A) after synthesis, washing, and redispersion in ethanol; B) after subsequent treatment with a dilute NaCl solution, centrifugation, and redispersion in ethanol.

slight mismatch between the viscosity of the pure solvent and that of the real dispersion, the measured hydrodynamic diameter of 18 nm corresponds well with the results from electron microscopy. By comparing the IR spectrum of the pure IL with that of the as-prepared and washed  $\text{LaPO}_4\text{:Ce,Tb}$  nanocrystals, the surface conditioning of the particles can be verified (Figure 5 A,B). In addition to vibrational bands assigned to phosphate groups ( $\tilde{\nu} = 1100\text{--}900$ ,  $650\text{--}500\text{ cm}^{-1}$ ) and water ( $\tilde{\nu} = 3500\text{--}3300$ ,  $1630\text{ cm}^{-1}$ ), weak absorption bands ( $\tilde{\nu}(\text{C-H}) = 2970\text{--}2880\text{ cm}^{-1}$ ;  $\tilde{\nu}(\text{S-O}) =$

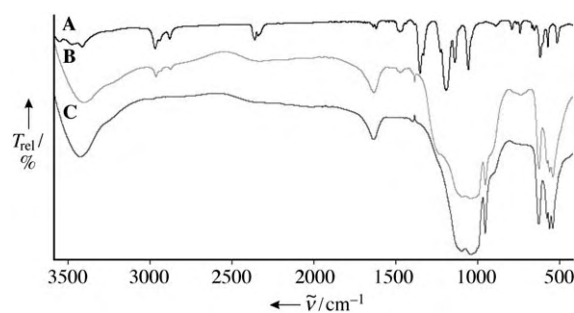


**Figure 5.** IR spectra of: A) the IL  $[\text{MeBu}_3\text{N}][(\text{SO}_2\text{CF}_3)_2\text{N}]$ ; B) the as-prepared  $\text{LaPO}_4\text{:Ce,Tb}$  nanocrystals; C) the  $\text{LaPO}_4\text{:Ce,Tb}$  nanocrystals after treatment with a dilute NaCl solution.



1470–1060  $\text{cm}^{-1}$ ) arising from components of the IL appear in the spectrum of the as-prepared  $\text{LaPO}_4\text{:Ce,Tb}$  nanocrystals.<sup>[11]</sup> As the IL is noncoordinating, the effective prevention of agglomeration can be attributed to a charge stabilization of the particles.

The IL can be removed completely by adding a dilute NaCl solution to a dispersion of  $\text{LaPO}_4\text{:Ce,Tb}$  in ethanol. Indeed, the IR spectra of the powder samples isolated by centrifugation after this treatment do not exhibit any vibrational bands arising from the IL (Figure 5C). After the NaCl treatment and centrifugation, redispersion of the  $\text{LaPO}_4\text{:Ce,Tb}$  nanocrystals in ethanol, for example, is still possible by prolonged sonification. The average particle diameter of 21 nm in this dispersion is nearly identical to that of the original dispersion (Figure 4B), indicating that significant agglomeration does not occur in the absence of the IL. This observation is remarkable, because no coordinating solvents or modifiers are present. Moreover, the straightforward removal of the IL enables synthesis-independent surface conditioning that can be adjusted to the specific needs of a particular application.

The luminescence properties of  $\text{LaPO}_4\text{:Ce,Tb}$  have been extensively investigated for both the macroscopic solid, as well as the nanoscale material.<sup>[3,12]</sup> A UV excitation of  $\text{Ce}^{3+}$  occurs through a  $4f^1 \rightarrow 4f^0 5d^1$  transition. After an energy transfer from  $\text{Ce}^{3+}$  to  $\text{Tb}^{3+}$ , a  $\text{Tb}^{3+}$  emission of green light resulting from a  $^5\text{D}_4 \rightarrow ^7\text{F}_j$  relaxation takes place. The emission spectrum of the as-prepared  $\text{LaPO}_4\text{:Ce,Tb}$  (45, 15 mol %) nanocrystals dispersed in ethanol corresponds with expectations (Figure 6). The quantum yield is 0.70(2), if only the

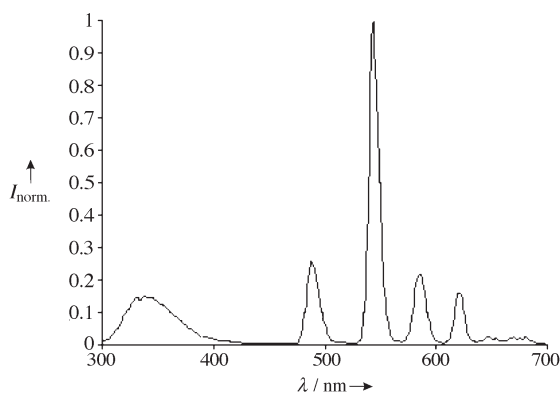


**Figure 6.** PL spectrum of the as-prepared  $\text{LaPO}_4\text{:Ce,Tb}$  (45, 15 mol %) nanocrystals redispersed in ethanol ( $\lambda_{\text{exc}} = 273 \text{ nm}$ ).

$\text{Tb}^{3+}$  emission is considered, and 0.90(2), if the  $\text{Ce}^{3+}$  emission is also taken into account. The fact that neither an inorganic shell nor coordinating surface modifiers are required for the protection of the nanocrystals makes these values even more remarkable. In fact, the quantum yield is of the same magnitude as that of the bulk material (0.86 for  $\text{Tb}^{3+}$  emission, 0.93 for the sum of  $\text{Ce}^{3+}$  and  $\text{Tb}^{3+}$  emissions).<sup>[13]</sup>

To our knowledge, the concept of a microwave-assisted synthesis of luminescent nanocrystals in IL media is presented for the first time herein.<sup>[14]</sup> Because of the high quantum yields and the possibility of synthesis-independent surface

conditioning, this strategy could have a large impact on technical applications. The absence of harmful solids, surface modifiers, and solvents could be particularly beneficial for biomedical applications.

## Experimental Section

All procedures were performed using standard Schlenk equipment. All chemicals were used as received from the supplier. The IL  $[\text{MeBu}_3\text{N}][(\text{SO}_2\text{CF}_3)_2\text{N}]$  was synthesized according to a literature method.<sup>[15]</sup>

$\text{LaCl}_3 \cdot 6\text{H}_2\text{O}$  (124 mg, 0.334 mmol),  $\text{CeCl}_3 \cdot 7\text{H}_2\text{O}$  (140 mg, 0.367 mmol), and  $\text{TbCl}_3 \cdot 6\text{H}_2\text{O}$  (47 mg, 0.126 mmol) were dissolved in a mixture of ethanol (5 mL) and the IL (10 mL). A solution of crystalline  $\text{H}_3\text{PO}_4$  (163 mg, 1.66 mmol) in ethanol (2 mL) and the IL (5 mL) was added dropwise with vigorous stirring over 30 min at 70 °C. Thereafter, the transparent dispersion was heated to 100 °C under reduced pressure ( $10^{-2}$  mbar), and kept at this temperature until the gas evolution stopped. The vessel was kept under reduced pressure and placed in a standard laboratory microwave oven (MLS rotaprep). The mixture was heated to 300 °C (pyrometric control) through irradiation with 800 W for approximately 10 s. After cooling, the transparent dispersion was diluted with ethanol (20 mL), and the reaction container was placed in an ultrasound bath. The nanocrystals were collected by centrifugation, and then redispersed in ethanol. This washing procedure was performed three times. After drying under reduced pressure, a colorless solid was obtained in a yield of 86–92 %. For further analytical characterization, the nanocrystals were used as prepared or after redispersion in ethanol. To remove the IL, a NaCl solution (0.08 M, 15 mL) was added to a dispersion of  $\text{LaPO}_4\text{:Ce,Tb}$  in ethanol (15 mL). The resulting dispersion was centrifuged, and the isolated solid was redispersed in ethanol.

DLS was performed in polystyrene or quartz cuvettes with a Nanosizer ZS from Malvern Instruments. Prior to the investigation, highly viscous dispersions in the IL were diluted with diethylene glycol. The ethanol dispersions were diluted with ethanol only.

SEM was carried out with a Zeiss Supra 40 VP microscope. The nanocrystals were deposited on silicon wafers and sputtered with platinum, and characterized at room temperature at an acceleration voltage of 10 kV and a working distance of 3 mm.

TEM and electron diffraction were performed with a Philips CM200 FEG/ST microscope at an acceleration voltage of 200 kV. Samples were prepared by the ultrasonic nebulization of ethanol dispersions on a lacey-film copper grid.

PXRD was carried out with a Stoe STADI-P diffractometer operating with Ge-monochromatized  $\text{Cu}_{\text{K}\alpha}$  radiation.

IR spectra were measured with a Bruker Vertex 70 FT-IR spectrometer. The samples were measured as KBr pellets to a resolution of 4  $\text{cm}^{-1}$ .

PL spectra were recorded with a Jobin Yvon Spex Fluorlog 3 spectrometer equipped with a 450 nm xenon lamp and double-grating excitation and emission monochromators. Dispersions of  $\text{LaPO}_4\text{:Ce,Tb}$  nanocrystals in ethanol were measured in standard quartz cuvettes at room temperature. Emission spectra were corrected for the wavelength-dependent response of the spectrometer. The quantum yield of the dispersion ( $\phi_{\text{PL-LaPO}_4}$ ,  $\lambda_{\text{exc}} = 273 \text{ nm}$ ) was determined relative to the quantum yield of Coumarin 307 in methanol ( $\phi_{\text{PL-Coumarin}} = 0.95(2)$ ,  $\lambda_{\text{exc}} = 273 \text{ nm}$ ) with a similar optical density.<sup>[16]</sup>

Received: January 19, 2006

Revised: April 6, 2006

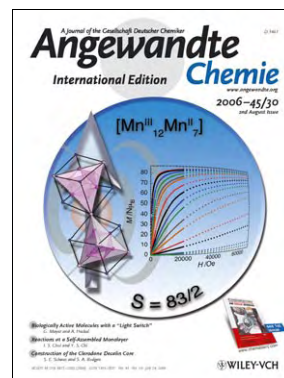
**Keywords:** colloids · ionic liquids · luminescence · microwaves · synthetic methods

- [1] *Phosphor Handbook* (Eds.: S. Shionoya, W. M. Yen), CRC, Boca Raton, **1999**.
- [2] a) T. Pellegrino, S. Kudera, T. Liedl, A. M. Javier, L. Manna, W. Parak, *Small* **2005**, *1*, 48; b) C. Y. Zhang, H. C. Yeh, M. T. Kuroki, T. H. Wang, *Nat. Mater.* **2005**, *4*, 826; c) S. Kim, Y. T. Lim, E. G. Soltesz, A. M. DeGrand, J. Lee, A. Nakayama, J. A. Parker, T. Mihaljevic, R. G. Laurence, D. M. Dor, L. H. Cohn, M. G. Bawendi, J. V. Frangioni, *Nat. Biotechnol.* **2003**, *22*, 93; d) B. Dubertret, P. Skourides, D. J. Norris, V. Noireaux, A. H. Brivanlou, A. Libchaber, *Science* **2002**, *298*, 1759; e) A. N. Shipway, E. Katz, I. Willner, *ChemPhysChem* **2000**, *1*, 19.
- [3] a) C. Feldmann, *Adv. Funct. Mater.* **2003**, *13*, 101; b) S. T. Selvan, C. Bullen, M. Ashokkumar, P. Mulvaney, *Adv. Mater.* **2001**, *13*, 985; c) K. Riwozki, H. Meyssamy, H. Schnablegger, A. Kornowski, M. Haase, *Angew. Chem.* **2001**, *113*, 574; *Angew. Chem. Int. Ed.* **2001**, *40*, 573; d) X. Peng, L. Manna, W. Yang, J. Wickham, E. Scher, A. Kadavanich, A. P. Alivisatos, *Nature* **2000**, *404*, 59; e) T. Vossmeier, L. Katsikas, M. Giersig, I. G. Popov, K. Diesner, A. Chemseddine, A. Eychmüller, H. Weller, *J. Phys. Chem.* **1994**, *98*, 7665; f) C. B. Murray, D. J. Norris, M. G. Bawendi, *J. Am. Chem. Soc.* **1993**, *115*, 8706.
- [4] a) J. S. Steckel, J. P. Zimmer, S. Coe-Sullivan, N. E. Scott, V. Bulovic, M. G. Bawendi, *Angew. Chem.* **2004**, *116*, 2206; *Angew. Chem. Int. Ed.* **2004**, *43*, 2154; b) J. W. Stouwdam, F. C. J. M. van Veggel, *Langmuir* **2004**, *20*, 11763; c) K. Kömpe, H. Borchert, J. Storz, A. Lobo, S. Adam, T. Möller, M. Haase, *Angew. Chem.* **2003**, *115*, 5672; *Angew. Chem. Int. Ed.* **2003**, *42*, 5513; d) M. T. Harrison, S. V. Kershaw, A. L. Rogach, A. Kornowski, A. Eychmüller, H. Weller, *Adv. Mater.* **2000**, *12*, 123.
- [5] a) *Ionic Liquids in Synthesis* (Eds.: P. Wasserscheid, T. Welton), Wiley-VCH, Weinheim, **2002**; b) W. Xu, C. A. Angeli, *Science* **2003**, *302*, 422; c) P. Bonhôte, A. P. Dias, N. Papageorgiou, K. Kalyanasundaram, M. Grätzel, *Inorg. Chem.* **1996**, *35*, 1168.
- [6] a) T. J. S. Schubert, *Nachr. Chem.* **2005**, *53*, 1222; b) J. Dupont, R. F. de Souza, P. A. Z. Suarez, *Chem. Rev.* **2002**, *102*, 3667; c) P. Wasserscheid, W. Keim, *Angew. Chem.* **2000**, *112*, 3926; *Angew. Chem. Int. Ed.* **2000**, *39*, 3772.
- [7] a) B. Smarsly, H. Kaper, *Angew. Chem.* **2005**, *117*, 3876; *Angew. Chem. Int. Ed.* **2005**, *44*, 3809; b) M. Antonietti, D. Kuang, B. Smarsly, Y. Zhou, *Angew. Chem.* **2004**, *116*, 5096; *Angew. Chem. Int. Ed.* **2004**, *43*, 4989; c) H. Itoh, K. Naka, Y. Chujo, *J. Am. Chem. Soc.* **2004**, *126*, 3026; d) T. Nakashima, N. Kimizuka, *J. Am. Chem. Soc.* **2003**, *125*, 6386; e) G. S. Fonseca, A. P. Umpierre, P. F. P. Fichtner, S. R. Teixeira, J. Dupont, *Chem. Eur. J.* **2003**, *9*, 3263.
- [8] I. Krossing, I. Raabe, *Angew. Chem.* **2004**, *116*, 2116; *Angew. Chem. Int. Ed.* **2004**, *43*, 2066.
- [9] A. Tellenbach, C. Feldmann, unpublished results.
- [10] D. F. Mullica, W. D. Milligan, D. A. Grossie, G. W. Beall, L. A. Boatner, *Inorg. Chim. Acta* **1984**, *95*, 231.
- [11] J. Weidlein, U. Müller, K. Dehnike, *Schwingungsspektroskopie*, Thieme, Stuttgart, **1988**.
- [12] G. Blasse, B. C. Grabmaier, *Luminescent Materials*, Springer, Berlin, **1994**.
- [13] B. M. J. Smets, *Mater. Chem. Phys.* **1987**, *16*, 283.
- [14] G. Bühler, C. Feldmann, patent application DE 10 2006 001 414.6.
- [15] T. Welton, *Chem. Rev.* **1999**, *99*, 2071.
- [16] S. Lebedkin, T. Langetepe, P. Sevilano, D. Fenske, M. M. Kappes, *J. Phys. Chem. B* **2002**, *106*, 9019.

## Cover Picture

**Ayuk M. Ako, Ian J. Hewitt, Valeriu Mereacre, Rodolphe Clérac, Wolfgang Wernsdorfer, Christopher E. Anson, and Annie K. Powell\***

King of the spins is provided by the mixed-valent  $\text{Mn}_{19}$  aggregate as reported by A. K. Powell et al. in their Communication on page 4926 ff. The use of bridging azido ligands leads to a completely ferromagnetically coupled system with a record ground spin state of  $S = 83/2$ . This remarkable molecule has been investigated and characterized by scientists from three laboratories working together in the European Network of Excellence “MAGMANet”, the logo of which provides the background to the cover picture.



### **Photoresponsive Compounds**

Photoactivatable proteins, nucleic acids, and small-molecule compounds offer numerous possibilities for investigating biological processes, even in cells. In their Review on page 4900 ff, G. Mayer and A. Heckel summarize recent developments in this field.



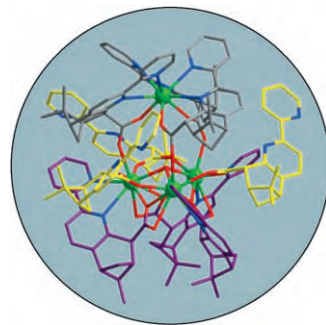
### **Nanotubes**

In their Communication on page 4922 ff., C. Ye et al. report the preparation of  $\text{SrAl}_2\text{O}_4$  nanoscrolls through a roll-up process under hydrothermal conditions. Post-annealing transforms the nanoscrolls into crystalline nanotubes.



### **Self-assembly**

$\text{Pr}^{\text{III}}$  ions and chiral ligands can diastereoselectively build two different superstructures, in which the ligands form helical domains and are attached to trigonal  $\text{Pr}_3$  or pyramidal  $\text{Pr}_4$  metallic scaffolds. Details of this solvent-induced self-assembly process can be found in the Communication by O. Mamula et al. on page 4940 ff.





The following Communications have been judged by at least two referees to be "very important papers" and will be published online at [www.angewandte.org](http://www.angewandte.org) soon:

H. Niu, M. Gao\*

**Synthesis of Diameter-Tunable CdTe Nanotubes Templated by One-Dimensional Nanowires of Cadmium Thiolate Polymer**

Y. Li, B. S. Lokitz, C. L. McCormick\*

**Thermally Responsive Vesicles and their Structural "Locking" through Polyelectrolyte Complex Formation**

A. Fürstner,\* C. Nevado, M. Tremblay, C. Chevrier, F. Teplý, C. Aïssa, M. Waser

**Total Synthesis of Iejimalide B**

C. P. Gros, J.-M. Barbe,\* E. Espinosa, R. Guillard\*

**Room-Temperature Autoconversion of Free-Base Corrole to Free-Base Porphyrin**

S. Cobo, G. Molnár, J. A. Real, A. Bousseksou\*

**Multilayer Sequential Assembly of Thin Films Displaying Room-Temperature Spin Crossover with Hysteresis**

R. J. Wright, M. Brynda, P. P. Power\*

**Synthesis and Structure of "Dialuminyne"  $\text{Na}_2\text{Ar}'\text{AlAlAr}'$  and "Cyclotrialuminene"  $\text{Na}_2(\text{Ar}''\text{Al})_3$ : Al–Al Bonding in  $\text{Al}_2\text{Na}_2$  and  $\text{Al}_3\text{Na}_2$  Clusters**

## News

Supramolecular Chemistry:

Echegoyen appointed \_\_\_\_\_ **4890**

Organic Chemistry:

Curran honored \_\_\_\_\_ **4890**

Organic Chemistry:

Huisgen honored \_\_\_\_\_ **4890**

## Books

Drug Discovery Handbook

Shayne C. Gad

reviewed by G. Hölzemann \_\_\_\_\_ **4891**

Nitric Oxide Donors

Peng G. Wang, Tingwei B. Cai, Naoyuki Taniguchi

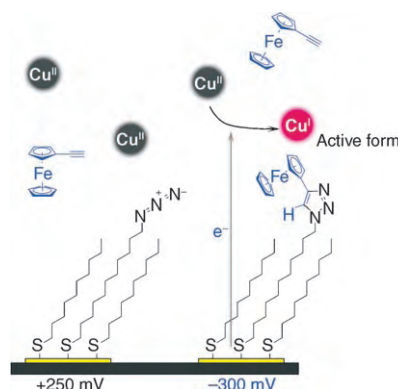
reviewed by J. Lehmann \_\_\_\_\_ **4892**

## Highlights

### Tailor-Made Surfaces

I. S. Choi,\* Y. S. Chi \_\_\_\_\_ **4894–4897**

Surface Reactions On Demand:  
Electrochemical Control of SAM-Based  
Reactions



**Controlled exterior:** Electrochemically induced, SAM-based reactions have a potential in the site-selective functionalization of surfaces. A recent study shows that a reaction, Sharpless click chemistry, can be site-selectively performed at microelectrodes by electrochemically controlling the activity of a catalyst for the reaction.

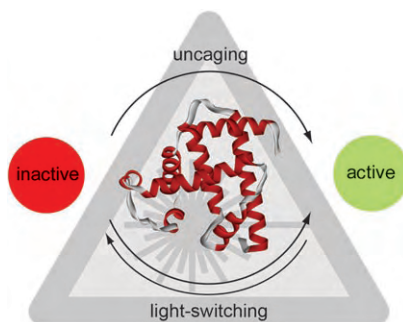


## Reviews

### Photoresponsive Compounds

G. Mayer,\* A. Heckel\* — 4900 – 4921

Biologically Active Molecules with a “Light Switch”

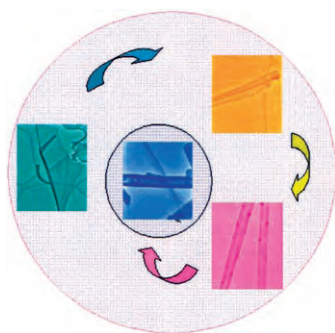


**A trick of the light:** Photolabile protecting groups, attached to a defined position of a molecule, can be used to gain spatio-temporal control over the concentration of the active form of a molecule. Such “caged compounds” can be applied for the analysis of biological phenomena. Together with synthesis strategies of biomolecules the caging strategy enables the characterization of single molecules in cells.

## Communications

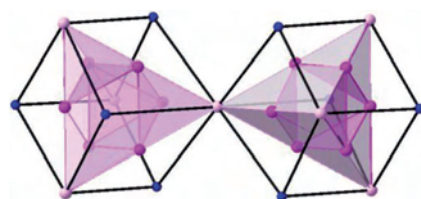
### Nanotube Growth

C. Ye,\* Y. Bando, G. Shen,  
D. Golberg — 4922 – 4926

Formation of Crystalline  $\text{SrAl}_2\text{O}_4$  Nanotubes by a Roll-Up and Post-Annealing Approach


**On a roll:** Nanotubes of  $\text{SrAl}_2\text{O}_4$ , an important phosphorescent host material, are prepared. Nanoscrolls are first formed through the roll-up of an artificial lamellar precursor in solution. The layer interfaces are then removed by high-temperature annealing, resulting in single-crystalline nanotubes.

**Mixing it up:** A ground spin state of  $S=83/2$  is found in the mixed-valent manganese aggregate  $[\text{Mn}^{\text{III}}_{12}\text{Mn}^{\text{II}}_7(\mu_4\text{-O})_8(\mu_3, \eta^1\text{-N}_3)_8(\text{HL})_{12}(\text{MeCN})_6]^{2+}$  ( $\text{H}_3\text{L}=2,6\text{-bis}(\text{hydroxymethyl})\text{-4-methylphenol}$ ; see polyhedral representation of the core) and arises through ferromagnetic coupling of all the metal centers.



### Molecular Magnets

A. M. Ako, I. J. Hewitt, V. Mereacre,  
R. Clérac, W. Wernsdorfer, C. E. Anson,  
A. K. Powell\* — 4926 – 4929

A Ferromagnetically Coupled  $\text{Mn}_{19}$  Aggregate with a Record  $S=83/2$  Ground Spin State

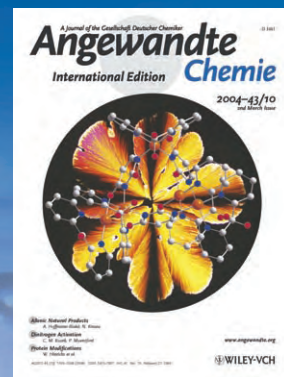
#### For the USA and Canada:

ANGEWANDTE CHEMIE International Edition (ISSN 1433-7851) is published weekly by Wiley-VCH PO Box 191161, D 69451 Weinheim, Germany. Air freight and mailing in the USA by Publications Expediting Inc. 200

Meacham Ave., Elmont, NY 11003. Periodicals postage paid at Jamaica NY 11431. US POSTMASTER: send address changes to *Angewandte Chemie*, Wiley-VCH, 111 River Street, Hoboken, NJ 07030. Annual subscription price for institutions: US\$ 5685/5168 (valid for print and

electronic / print or electronic delivery); for individuals who are personal members of a national chemical society prices are available on request. Postage and handling charges included. All prices are subject to local VAT/sales tax.

# The best in chemistry – for more than a hundred years



A Journal of the Gesellschaft Deutscher Chemiker  
**Angewandte Chemie**  
International Edition

[www.angewandte.org](http://www.angewandte.org)

**1888:** The beginning  
of a success story

## Constant Innovations

- 1962:** First issue of the International Edition
- 1976:** Graphical abstracts
- 1979:** Cover pictures
- 1988:** Centenary of Angewandte
- 1989:** Routine use of color
- 1991:** New section: Highlights
- 1992:** Computerized editorial tracking system
- 1995:** Internet service for readers
- 1998:** Regular press service; full-text online
- 2000:** New section: Essays; EarlyView: Communications available online ahead of the printed version
- 2001:** New section: Minireviews
- 2002:** Online submission of manuscripts
- 2003:** Weekly publication; new section: News; new layout
- 2004:** Backfiles (1962-1997); ManuscriptXpress: Online system for authors and referees



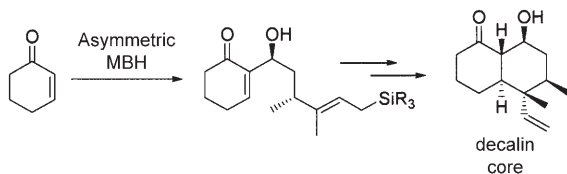
**Angewandte's  
advisors...**

**Richard N. Zare**  
Stanford University

» Size does matter, as well as shape, motion, composition, and chemical complexity. I read **Angewandte Chemie** each week to learn about the latest, most exciting developments in the world of chemistry. «

Angewandte Chemie International Edition is  
a journal of the German Chemical Society (GDCh)





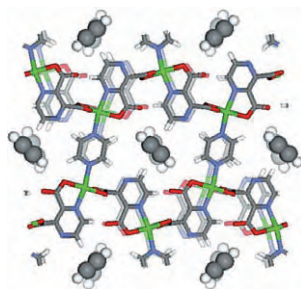
**Linking rings:** A general route toward the clerodane diterpene core using an asymmetric Morita-Baylis-Hillman (MBH)/Lewis acid mediated ring-annulation process has been developed. The scope of the

asymmetric Brønsted acid catalyzed MBH reaction has been expanded to include silane-containing aldehydes, which are elaborated into the *trans* decalin core in high diastereo- and enantioselectivities.

## Asymmetric Catalysis

S. A. Rodgen, S. E. Schaus\* 4929–4932

Efficient Construction of the Clerodane Decalin Core by an Asymmetric Morita-Baylis-Hillman Reaction/Lewis Acid Promoted Annulation Strategy



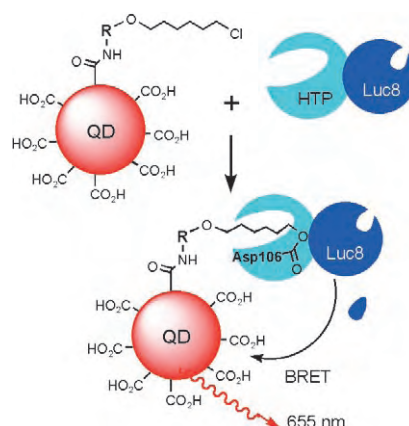
**Guest-responsive framework:** Gas adsorption into a metal-organic porous material was studied in situ. Structure analysis of empty phase I, intermediate phase M as a metastable state of gas adsorption, and saturated phase S showed rearrangement of guest molecules and framework transformation in response to guest size, shape, and amount. The picture shows these changes for the superimposed phases M and S.

## Metal-Organic Frameworks

Y. Kubota,\* M. Takata, R. Matsuda, R. Kitaura, S. Kitagawa, T. C. Kobayashi 4932–4936

Metastable Sorption State of a Metal-Organic Porous Material Determined by In Situ Synchrotron Powder Diffraction

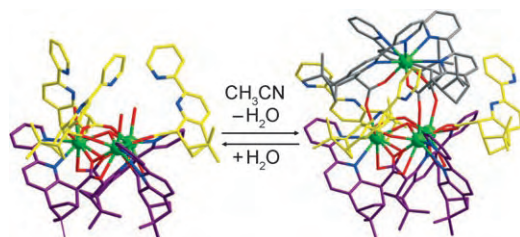
**On the dot:** A genetically engineered haloalkane dehalogenase was used to conjugate *Renilla* luciferase to quantum dots (see picture). The quantum dots can emit light through bioluminescence resonance energy transfer (BRET). This specific conjugation occurs upon simple mixing under mild conditions, and may be applied for specific in vivo labeling of proteins with quantum dots for imaging.



## Luminescence Marker

Y. Zhang, M.-K. So, A. M. Loening, H. Yao, S. S. Gambhir, J. Rao\* 4936–4940

HaloTag Protein-Mediated Site-Specific Conjugation of Bioluminescent Proteins to Quantum Dots



**Triangular or pyramidal?** Solvent-induced divergent self-assembly of a chiral ligand and  $\text{Pr}^{\text{III}}$  ions leads diastereoselectively to two distinct but related superstructures, in which the ligands form helical domains

attached to triangular ( $\text{Pr}_3$ ) or pyramidal ( $\text{Pr}_4$ ) metallic scaffolds (Pr green). The two structures are reversibly interconverted simply by varying the amount of water present in the solvent ( $\text{CH}_3\text{CN}$ ).

## Supramolecular Chemistry

O. Mamula,\* M. Lama, H. Stoeckli-Evans, S. Shova 4940–4944

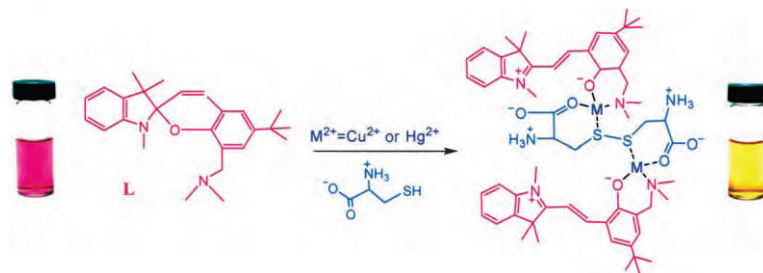
Switchable Chiral Architectures Containing  $\text{Pr}^{\text{III}}$  Ions: An Example of Solvent-Induced Adaptive Behavior



## Amino Acid Assay

N. Shao, J. Y. Jin, S. M. Cheung,  
R. H. Yang,\* W. H. Chan,\*  
T. Mo \_\_\_\_\_ 4944–4948

A Spiropyran-Based Ensemble for Visual Recognition and Quantification of Cysteine and Homocysteine at Physiological Levels



**Isomerization of the ligand**, followed by cooperative metal–ligand interactions leads to the ternary ensemble shown on the right, which has potential for the recognition and quantification of cysteine

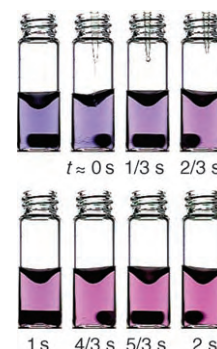
and homocysteine. The free ligand (left) is red-violet in solution, but when metal ions and cysteine or homocysteine are simultaneously introduced, the solution turns yellow.

## Visual Sensing

S.-Y. Lin, S.-H. Wu,  
C.-h. Chen\* \_\_\_\_\_ 4948–4951

A Simple Strategy for Prompt Visual Sensing by Gold Nanoparticles: General Applications of Interparticle Hydrogen Bonds

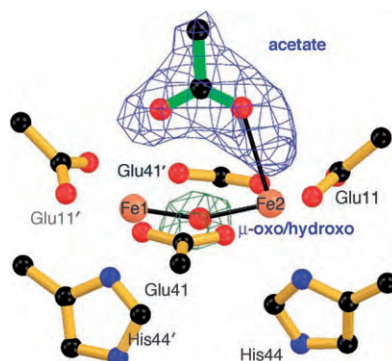
**Local color:** Gold nanoparticles (GNPs) bifunctionalized with a crown ether and thioctic acid can be used for the rapid sensing of a target analyte with the naked eye. A color transformation occurs when the interparticle hydrogen bonds of aggregated GNPs are broken forming a dispersion. For example, the detection of Pb<sup>II</sup> takes only 1 s (see picture).



## Model Diiron Protein

H. Wade, S. E. Stayrook,  
W. F. DeGrado\* \_\_\_\_\_ 4951–4954

The Structure of a Designed Diiron(III) Protein: Implications for Cofactor Stabilization and Catalysis



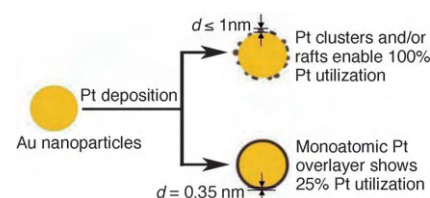
**A closer look** into the function of diiron proteins, such as methane monooxygenase and ribonucleotide reductase, is provided by the crystal structure of a designed diiron protein (the picture shows the Fe environment). Cofactor rigidity may be a factor in O<sub>2</sub> reactivity and a possible role of HisC<sup>α</sup>H...O hydrogen bonds in cofactor stabilization is implicated.

## Heterogeneous Catalysis

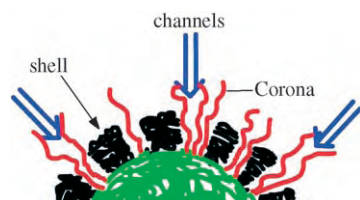
D. Zhao, B.-Q. Xu\* \_\_\_\_\_ 4955–4959

Enhancement of Pt Utilization in Electrocatalysts by Using Gold Nanoparticles

**Full employment** of a Pt catalyst is reached by depositing very small ( $\leq 1.0$  nm) Pt particles onto Au nanoparticles of about 10 nm in diameter (see picture) then loading the Pt/Au particles onto a conventional carbon support. Data obtained from the electrooxidation of methanol demonstrate that every Pt atom assumes the function of an active site for electrocatalysis.





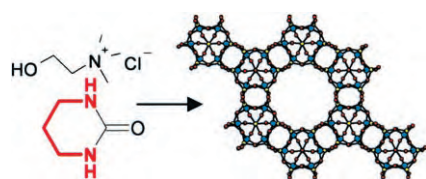


**Getting to the core of the micelle:** Phase separation between the hydrophobic shell and the hydrophilic corona leads to channels in the shells of complex micelles (see picture), through which ions and other small molecules could pass. The size of the channels can be regulated by changing the environmental conditions or by manipulating the composition of the two diblock copolymers that form the micelles.

### Channels in Micelles

G. Li, L. Shi,\* R. Ma, Y. An,  
N. Huang ————— 4959 – 4962

Formation of Complex Micelles with  
Double-Responsive Channels from Self-  
Assembly of Two Diblock Copolymers



**It came from the deep:** Deep-eutectic solvents based on mixtures of derivatized ureas and choline chloride can be used as the reaction media and the source of the organic template in the synthesis of aluminum phosphonate and organophosphonate materials. The template (red in structural formula) is formed by the decomposition of the derivatized urea.

### Template Synthesis

E. R. Parnham, E. A. Drylie, P. S. Wheatley,  
A. M. Z. Slawin,  
R. E. Morris\* ————— 4962 – 4966

Ionothermal Materials Synthesis Using  
Unstable Deep-Eutectic Solvents as  
Template-Delivery Agents



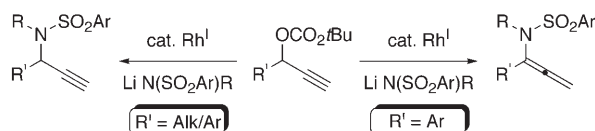
**Nature, our teacher!** The natural alkaloids quinine (Q) and quinidine (QD) serve as efficient bifunctional organocatalysts in the asymmetric conjugate addition of 1,3-dicarbonyl compounds to maleimides (see scheme). Very high selectivity is

observed in this one-step construction of highly functionalized compounds with two adjacent stereogenic centers from commercially available precursors.  $R^1, R^3$  = alkyl, aryl, O-alkyl;  $R^2$  = alkyl, Bn;  $R^4$  = Bn.

### Asymmetric Synthesis

G. Bartoli,\* M. Bosco, A. Carlone,  
A. Cavalli, M. Locatelli, A. Mazzanti,  
P. Ricci, L. Sambri,  
P. Melchiorre\* ————— 4966 – 4970

Organocatalytic Asymmetric Conjugate  
Addition of 1,3-Dicarbonyl Compounds to  
Maleimides



**Construction work:** Rh-catalyzed propargylic amination provides an efficient, versatile method for the preparation of aliphatic propargylic sulfonamides. This Rh-catalyzed variant has a divergent nature, from which aryl-substituted pro-

pargylic and allenyl sulfonamides can be constructed. A one-pot two-component Rh-catalyzed propargylic amination/isomerization followed by a [4+2] carbocycloaddition demonstrates the synthetic utility of this divergent behavior.

### Cyclization

P. A. Evans,\* M. J. Lawler — 4970 – 4972

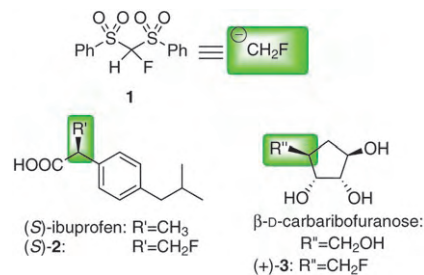
Rhodium-Catalyzed Propargylic  
Substitution: A Divergent Approach to  
Propargylic and Allenyl Sulfonamides

## Monofluoromethylation

T. Fukuzumi, N. Shibata,\* M. Sugiura,  
H. Yasui, S. Nakamura,  
T. Toru\* — 4973 – 4977

Fluorobis(phenylsulfonyl)methane: A Fluoromethide Equivalent and Palladium-Catalyzed Enantioselective Allylic Monofluoromethylation

**Selective introduction of fluorine:** Mono-fluoromethylation with the fluoromethide equivalent fluorobis(phenylsulfonyl)methane (**1**) was crucial in the syntheses of the pharmacologically important compounds monofluorinated (*S*)-ibuprofen (**2**) and 5-deoxy-5-fluoro- $\beta$ -D-carbarylbofuranose (**3**). The key step was a palladium-catalyzed allylic monofluoromethylation reaction.

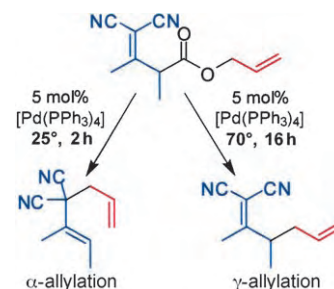


## Allylation

S. R. Waetzig, D. K. Rayabarapu,  
J. D. Weaver, J. A. Tunge\* — 4977 – 4980

A Versatile Hexadiene Synthesis by Decarboxylative  $sp^3$ - $sp^3$  Coupling/Cope Rearrangement

**Have it both ways:** The palladium-catalyzed decarboxylative coupling of esters with two allyl groups results in kinetic allylation at a position  $\alpha$  to electron-withdrawing groups. Tandem allylation/Cope rearrangement provides access to  $\gamma$ -coupling products (see scheme). Thus, the desired regioisomer is obtained simply by controlling the temperature of the reaction mixture.

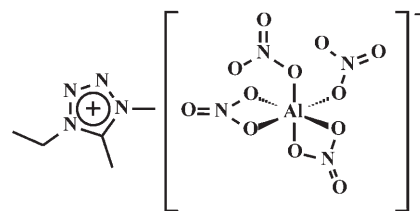


## Propellants

C. B. Jones, R. Haiges, T. Schroer,  
K. O. Christe\* — 4981 – 4984

Oxygen-Balanced Energetic Ionic Liquid

**On the way to the perfect propellant:** The energetic oxidizer-balanced ionic liquid 1-ethyl-4,5-dimethyltetrazolium tetranitratoluminate (see scheme) has been prepared and characterized. Oxidizer-balanced ionic liquids are promising propellants with good performance and no vapor toxicity.

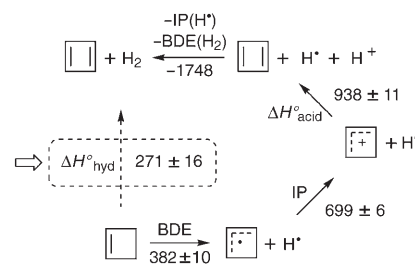


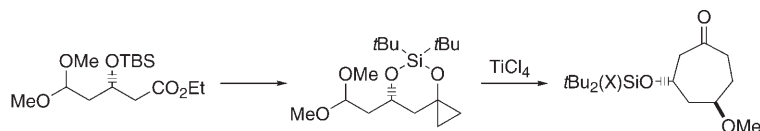
## Thermodynamics

A. Fattahi, L. Lis, Z. Tian,  
S. R. Kass\* — 4984 – 4988

The Heat of Formation of Cyclobutadiene

**How unstable can it be?** Gas-phase measurements on the 3-cyclobutenyl cation were combined in a thermodynamic cycle to provide the first experimental determination of the heat of formation of cyclobutadiene (see scheme, IP = ionization potential, BDE = bond-dissociation energy). The resulting value of  $428 \pm 16$  kJ mol $^{-1}$  is in good accord with previous predictions based upon similar energetic determinations of benzo- and phenylcyclobutadiene.





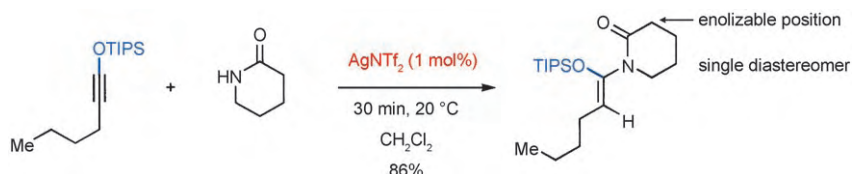
**Straightforward ring-closure:** An expedient entry to seven-membered carbocycles is achieved by the Kulinkovich cyclopropanation of acetal-tethered esters and the subsequent addition of the resulting

cyclopropyl silyl ethers to the oxocarbenium ion intermediates. Of particular note is the effective use of a *tert*-butylsilylene group for diastereoselective cyclization.

## Carbocycles

O. L. Epstein, S. Lee,  
J. K. Cha\* 4988–4991

Formation of Seven-Membered Carbocycles by the Use of Cyclopropyl Silyl Ethers as Homoenols



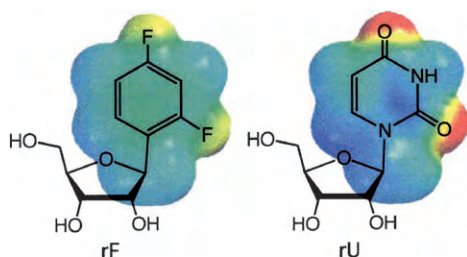
**New catalytic process:** The silver-catalyzed hydroamination of siloxy alkynes with secondary amides furnishes silyl ketene aminals with high efficiency and excellent diastereoselectivity (see scheme), including some that are una-

vailable by conventional silylation methods. The reaction comprises a fast and reversible silver–alkyne complexation, followed by a rate-determining C–N bond-forming step.

## Hydroamination

J. Sun, S. A. Kozmin\* 4991–4993

Silver-Catalyzed Hydroamination of Siloxy Alkynes



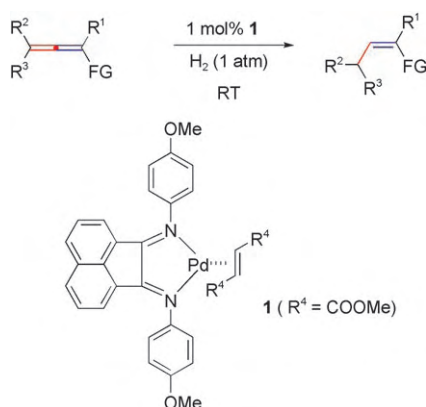
**Better than normal:** RNA-interference studies with mismatched target RNA have demonstrated sequence selectivity (at the single-nucleotide level) at many different

positions of the RNA strand. The use of rF in place of rU at position 7 appears to enhance sequence selectivity beyond that of the natural base.

## RNA Structures

A. Somoza, J. Chelliserrykattil,  
E. T. Kool\* 4994–4997

The Roles of Hydrogen Bonding and Sterics in RNA Interference



**Often elusive,** trisubstituted (Z)-1-alkenyl phosphonates can be prepared by the semihydrogenation of allenyl phosphonates in the presence of Pd complex **1**. This reaction, which occurs in high yield with high chemo-, regio-, and stereoselectivity, can be extended to related functionalized allenes and the corresponding Z alkene products (see scheme). R<sup>1</sup> = H, alkyl, aryl, benzyl; R<sup>2</sup>, R<sup>3</sup> = H, alkyl; FG = P(O)(OR)<sub>2</sub>, P(O)Ph<sub>2</sub>, SO<sub>2</sub>Ph, COOEt.

## Catalytic Hydrogenation

H. Guo, Z. Zheng, F. Yu, S. Ma,\*  
A. Holuigue, D. S. Tromp, C. J. Elsevier,\*  
Y. Yu 4997–5000

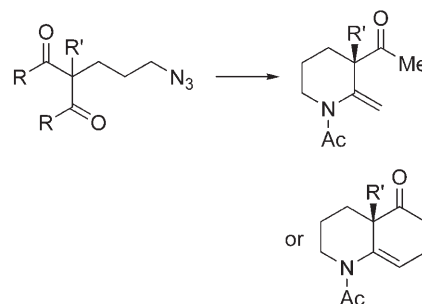
[Pd(Ar-BIAN)(alkene)]-Catalyzed Highly Chemo-, Regio-, and Stereoselective Semihydrogenation of 1,2-Allenyl Phosphonates and Related Compounds

## Asymmetric Synthesis

D. Lertpibulpanya, S. P. Marsden,\*  
I. Rodriguez-Garcia,  
C. A. Kilner \_\_\_\_\_ **5000–5002**

Asymmetric Aza-Wittig Reactions:  
Enantioselective Synthesis of  $\beta$ -  
Quaternary Azacycles

**A hindrance no more:** The direct asymmetric synthesis of nitrogen heterocycles containing  $\beta$ -quaternary stereocenters, widely found for example in alkaloids, is highly challenging. The novel approach shown exploits the desymmetrization of prochiral diketo azides to unmask the asymmetric quaternary center, and represents the first reported examples of the asymmetric aza-Wittig reaction.



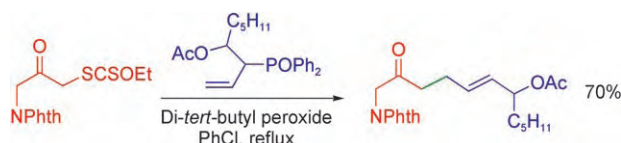
## Allylation

G. Ouvry, B. Quiclet-Sire,  
S. Z. Zard\* \_\_\_\_\_ **5002–5006**

Substituted Allyl Diphenylphosphine  
Oxides as Radical Allylating Agents

**Radically useful:** The radical addition of dithiocarbonates to branched allyl diphenylphosphine oxides can be followed by elimination of a diphenylphosphinoyl radical, thereby giving rise to allylated

products (see scheme; Phth = phthalimido). Highly functionalized structures can thus be rapidly assembled under mild conditions and from cheap and readily available substrates and reagents.

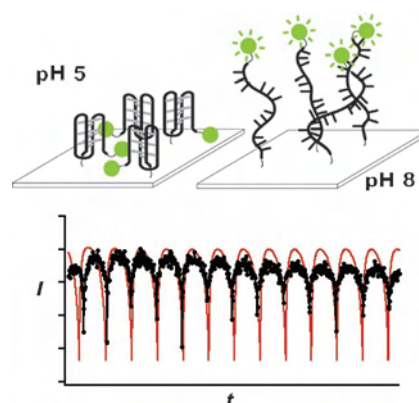


## DNA Nanoswitch

T. Liedl, M. Olapinski,  
F. C. Simmel\* \_\_\_\_\_ **5007–5010**

A Surface-Bound DNA Switch Driven by a  
Chemical Oscillator

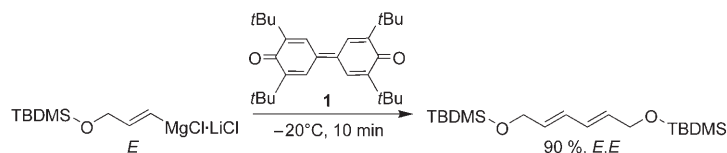
**Proton control:** Chemical oscillations produced in a continuously stirred tank reactor can be used to drive the conformational changes of DNA nanoswitches immobilized on a thin gold film (see scheme). The autonomous switching events of these substrate-bound actuators are characterized in fluorescence measurements by utilizing energy transfer between the fluorophores and gold substrate.



## C–C Coupling

A. Krasovskiy, A. Tishkov, V. del Amo,  
H. Mayr,\* P. Knochel\* \_\_\_\_\_ **5010–5014**

Transition-Metal-Free Homocoupling of  
Organomagnesium Compounds

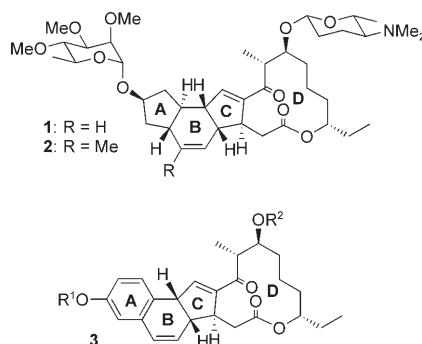


**Without palladium or copper:** A wide range of functionalized Grignard compounds were coupled by using diphenylquinone **1** as an electron acceptor. The oxidative dimerization of alkenylmagne-

sium reagents proceeds with complete retention of the stereochemistry (see scheme; TBDMS = *tert*-butyldimethylsilyl).



**Resistance is useless?** The increasing resistance towards (–)-spinosyns A (**1**) and D (**2**) used as plant-protection agents makes new derivatives of these natural products necessary. On the basis of investigations into the structure–activity relationships a convergent approach to the synthesis of novel spinosyn A analogues (**3**) is developed. A double Heck reaction is the key step in the construction of the basic carbocyclic framework.



## Plant Protection Agents

L. F. Tietze,\* G. Brasche, C. Stadler,  
A. Grube, N. Böhnke — 5015–5018

Multiple Palladium-Catalyzed Reactions  
for the Synthesis of Analogues of the  
Highly Potent Insecticide Spinosyn A

## Sources

### Product and Company Directory

You can start the entry for your company in “Sources” in any issue of *Angewandte Chemie*.

If you would like more information, please do not hesitate to contact us.

Wiley-VCH Verlag – Advertising Department

Tel.: 0 62 01 - 60 65 65

Fax: 0 62 01 - 60 65 50

E-Mail: MSchulz@wiley-vch.de

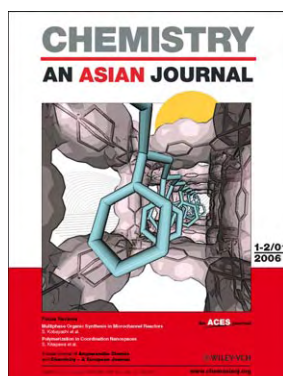
## Service

Keywords — 5020

Authors — 5021

Angewandte's  
Sister Journals — 5022–5023

Preview — 5025



For more information on  
Chemistry—An Asian Journal see  
[www.chemasianj.org](http://www.chemasianj.org)



## Awarded...

### L. Echegoyen To Head NSF Chemistry

From August 2006, Luis Echegoyen (Clemson University, SC, USA) will head the Chemistry Division of the US National Science Foundation (NSF). He has previously served as a Program Officer and on an Advisory Committee at the NSF. Echegoyen completed his



L. Echegoyen

PhD on the stability of radical anions in solution in 1974 with G. R. Stevenson at the University of Puerto Rico. He then carried out postdoctoral research with S. F. Nielsen at the University of Wisconsin in Madison before joining Union Carbide in New Jersey as an NMR specialist (1975–77). Echegoyen held faculty positions at the University of Puerto Rico (1977–83), the University of Maryland (1982–83), and the University of Miami (1983–2001), before joining Clemson University in 2002.

Echegoyen and his research group are interested in the chemistry of fullerenes as well as electrochemistry and supramolecular chemistry. They synthesize new fullerene derivatives by electrochemical methods and use electrocrystallization techniques to prepare new conducting materials derived from

transition metal complexes with bipyridine-like ligands. His recent publication on the retro-cycloaddition of pyrrolidinofullerenes in collaboration with N. Martín (Madrid) featured on the cover of issue 1/2006 of *Angewandte Chemie*,<sup>[1a]</sup> while his work on multilayer fullerenes (“nano-onions”) was illustrated recently on the cover picture of *Chemistry – A European Journal*.<sup>[1b]</sup>

### D. Curran in Paris

Dennis P. Curran (University of Pittsburgh, PA, USA) was recently honored with a “Chaire Blaise Pascal”, which will allow him to spend a year as a visiting scientist in the group of M. Malacria at the Université Pierre et Marie Curie in Paris. Curran studied at Boston College and completed his PhD in 1979 at the University of Rochester



D. P. Curran

(NY, USA) with A. S. Kende. Following a two-year postdoctoral stay in the group of B. M. Trost at the University of Wisconsin, Curran joined the University of Pittsburgh in 1981 as Assistant Professor. His research interests cover radical chemistry, organic synthesis, and fluorine chemistry, which capitalizes on the ready separation of highly fluorinated reaction components from standard organic and inorganic molecules. Such “strategy-level separations” were discussed some time ago in a Review in *Angewandte Chemie*.<sup>[2a]</sup> More recently, he reported the total synthesis of eight stereoisomers of passifloricins in *Angewandte Chemie*.<sup>[2b]</sup>

### Japanese honor R. Huisgen

Rolf Huisgen (Ludwig-Maximilians-Universität München, LMU) obtained

his PhD in 1943 under the guidance of Nobel Laureate H. O. Wieland. He completed his habilitation in 1947 and joined the Eberhard-Karls-Universität Tübingen in 1949. Huisgen joined the LMU as Professor in 1952 and remained there until his retirement in 1988. His research interests lay with 1,3-dipolar cycloadditions,<sup>[3a]</sup> which have undergone a renaissance recently with the development of “click chemistry” by K. B. Sharpless. Huisgen is still active: a computational study on cycloadditions and methylene transfer in substituted thiocarbonyl S-methylides with thiobenzenes appeared in issue 8/2005 of the *European Journal of Organic Chemistry* and featured on the cover.<sup>[3b]</sup> Following appointment as an honorary member of the German Chemical Society (GDCh) in 1991, he has now been named an honorary member of the Japanese Chemical Society.



R. Huisgen

- [1] a) N. Martín, M. Altable, S. Filippone, A. Martín-Domenech, L. Echegoyen, C. M. Cardona, *Angew. Chem.* **2006**, *118*, 116; *Angew. Chem. Int. Ed.* **2006**, *45*, 110; b) A. S. Rettenbacher, B. Elliott, J. S. Hudson, A. Amirkhanyan, L. Echegoyen, *Chem. Eur. J.* **2006**, *12*, 376.
- [2] a) D. P. Curran, *Angew. Chem.* **1998**, *110*, 1230; *Angew. Chem. Int. Ed.* **1998**, *37*, 1174; b) D. P. Curran, G. Moura-Letts, M. Pohlman, *Angew. Chem.* **2006**, *118*, 2483; *Angew. Chem. Int. Ed.* **2006**, *45*, 2423.
- [3] a) R. Huisgen, *Angew. Chem.* **1963**, *75*, 604; *Angew. Chem. Int. Ed. Engl.* **1963**, *2*, 565; b) R. Sustmann, W. Sicking, R. Huisgen, *Eur. J. Org. Chem.* **2005**, 1505.

DOI: 10.1002/anie.200602363

# Surface Reactions On Demand: Electrochemical Control of SAM-Based Reactions\*\*

Insung S. Choi\* and Young Shik Chi

## Keywords:

electrochemistry · microelectrodes · monolayers · self-assembly · surface chemistry

**S**elf-assembled monolayers (SAMs) are well-ordered, single-molecule-thick structures in two dimensions, which form spontaneously at interfaces (usually at solid surfaces).<sup>[1]</sup> SAMs have been used for controlling physical properties of interfaces, such as wetting, adhesion, lubrication, and corrosion, as well as understanding fundamental aspects of interfacial phenomena. In addition, SAMs comprise an excellent platform for generating two-dimensional micro- and nanostructures. For example, SAMs are widely utilized for the spatially resolved immobilization of biomolecules (i.e., DNAs, peptides, and polysaccharides) and cells onto surfaces. Although useful in these various domains, these applications are based on the “static” property of SAMs. In other words, SAMs (especially the head groups of SAMs) are designed to meet the criteria of the applications because the head groups intimately, but “statically”, interact with the outside environment. SAMs execute their predetermined roles once they are formed on surfaces, these roles are exemplified by corrosion barriers, etching masks, and recognition of biological entities.

One of the next challenges in the study of SAMs was how to induce surface reactions only when needed (“surface reactions on demand”). These surface reactions on demand have sev-

eral implications in surface science: 1) we can generate dynamic surfaces (in other words, stimuli-responsive surfaces) in which the physical, chemical, and biological properties of surfaces are reversibly tuned at our disposal as we dynamically tailor the functional groups that interact with the environments, and 2) we can site-selectively localize chemical reactions at surfaces, leading to independent addressability of surface reactions. Two reaction methods would be obvious candidates for surface reactions on demand: photochemically induced and electrochemically induced reactions. Photochemical induction can be combined with photolithographic techniques. The “static” property of the SAMs manifests in the fabrication of well-known DNA microarrays in which photolabile protecting groups are site-selectively removed by photolithography. Recently, a light-induced Wolff rearrangement of diazomethylcarbonyl groups was combined with photolithography to generate micropatterns.<sup>[2]</sup> In addition to the static surface, dynamic

changes in the water wettability of surfaces were demonstrated by the use of a light-induced, reversible *cis-trans* transition of azo groups.<sup>[3]</sup>

On the other hand, electrochemical induction has some advantages over other methods for surface reactions on demand. It is easily incorporated into electronic devices because the electrochemically induced surface reaction involves an electron transfer between a surface (e.g., gold and silicon) and a reaction site. The electrochemical control of surface reactions at electrodes could generate independently addressable electrodes because a reaction can be induced electrochemically on a designated electrode. Furthermore, dynamic control of surface properties could be achieved easily by electrical potentials and reversible oxidation–reduction reactions.

Initial attempts to use electrochemistry for SAM-based reactions were at the early stage in the development of surface reactions on demand. These attempts were based on simple desorp-

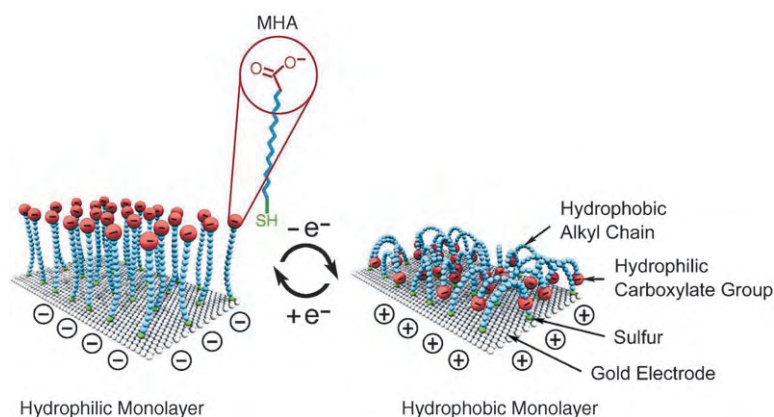


**Figure 1.** Electrochemically controlled transition between straight (hydrophilic) and bent (hydrophobic) molecular conformations on gold. MHA: 16-mercaptohexadecanoic acid.

[\*] Prof. Dr. I. S. Choi, Y. S. Chi  
Department of Chemistry  
KAIST  
Daejeon 305-701 (Korea)  
Fax: (+82) 42-869-2810  
E-mail: ischoi@kaist.ac.kr

[\*\*] Figure 1 and Scheme 2b were kindly provided by Prof. Langer and Prof. Kwak.

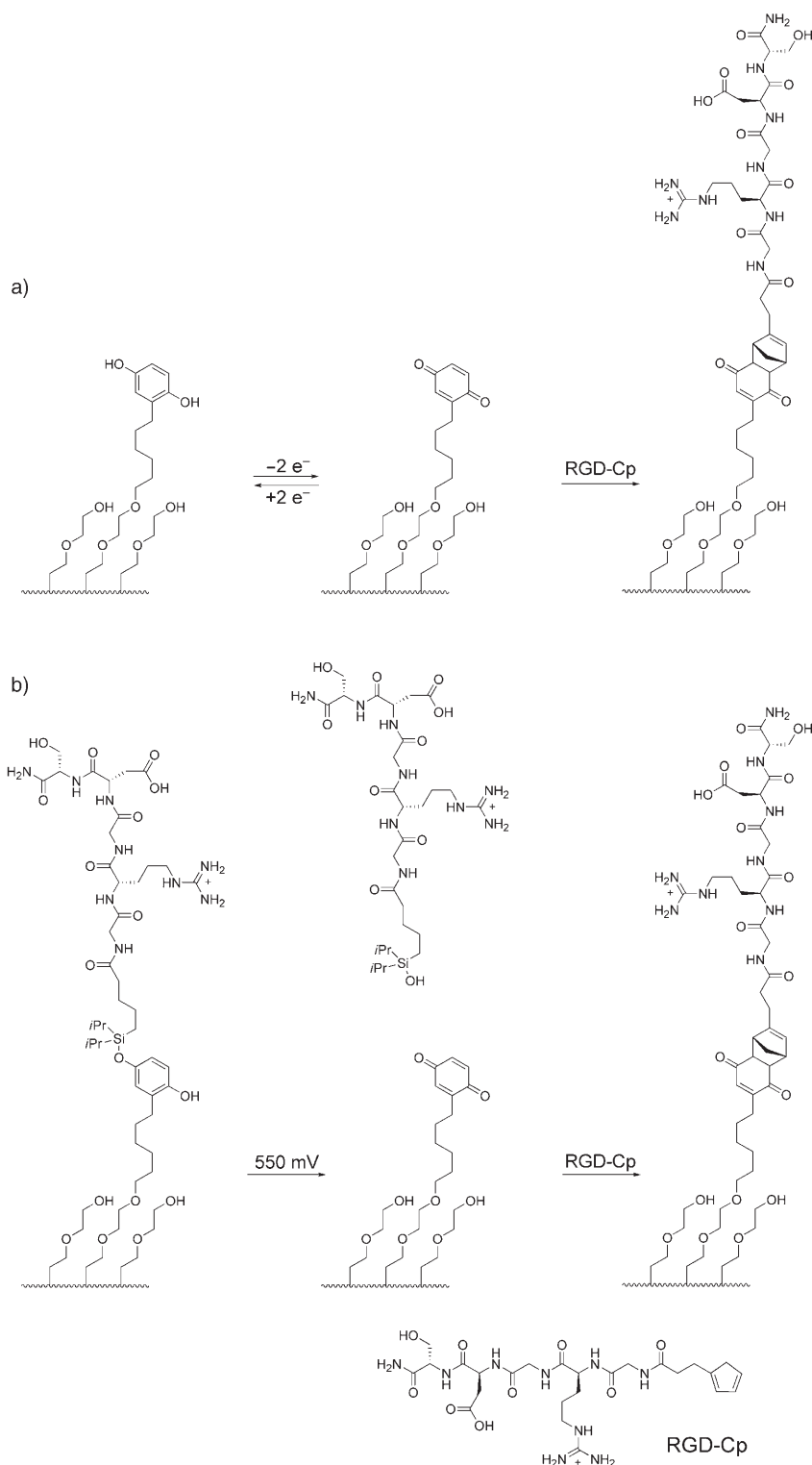
tion/adsorption of alkanethiols on gold. However, the methods were applied to the construction of individually addressed electrodes.<sup>[4]</sup> For example, hexadecanethiol was electrochemically desorbed from a gold microelectrode and a second thiol was adsorbed onto the electrode.<sup>[4a]</sup> Electrochemically directed formation of self-assembled monolayers (SAMs) is another interesting approach. Freund, Ferguson, and co-workers selectively modified one electrode in the close proximity of another by electrochemical oxidation of alkyl thiosulfates to gold-reacting species, such as alkyl-sulfide radicals and disulfides.<sup>[4b]</sup> In addition, the accelerated formation of SAMs of alkanethiols was achieved by using a cathodic polarization.<sup>[4c]</sup> The property of SAM-coated surfaces was also dynamically tuned by electrochemical control. Langer and co-workers demonstrated that electrical potential could be used for dynamically controlling conformational transitions of surface-confined alkanethiols. To establish sufficient spatial freedom for each alkanethiol at the surface, they elegantly designed a low-density SAM of 16-mercaptohexadecanoic acid. They reported that electrochemically controlled conformational reorientations of single-layered alkanethiols at the surface were amplified into a macroscopically detectable change in wettability (Figure 1).<sup>[5]</sup>

The concepts above are limited to simple alkanethiols. Although SAMs of more complicated, but technologically useful alkanethiols (and other self-assembling molecules) could also be generated, this approach requires a separate solution-based synthesis of the required molecules. In principle, the separate synthesis of self-assembling molecules in solution gives an opportunity to introduce virtually any functional group, but in practice, this approach requires cumbersome syntheses and shows a limited compatibility with functional groups. In other words, practically, it is not simple to introduce the large, complex molecules and ligands needed for wider applications. In this respect, it is preferable to perform surface reactions after the formation of SAMs, which would be one of the solid approaches to surface reactions on demand.

The first demonstration of electrochemically induced, surface reactions on

demand was Mrksich and co-worker's quinone chemistry (Scheme 1).<sup>[6]</sup> They formed a SAM that presented hydroquinone (HQ) and studied electrochem-

ical characteristics of the SAM. Cyclic voltammetry showed that HQ underwent oxidation at 220 mV to give quinone (Q) and reduction at -150 mV,



**Scheme 1.** a) Electrochemical oxidation of hydroquinone to quinone, and introduction of the RGD peptide by a Diels–Alder reaction. b) Selective release of the RGD ligand from the monolayer presenting the O-silyl-hydroquinone by electrochemical oxidation and introduction of a second ligand by a Diels–Alder reaction.

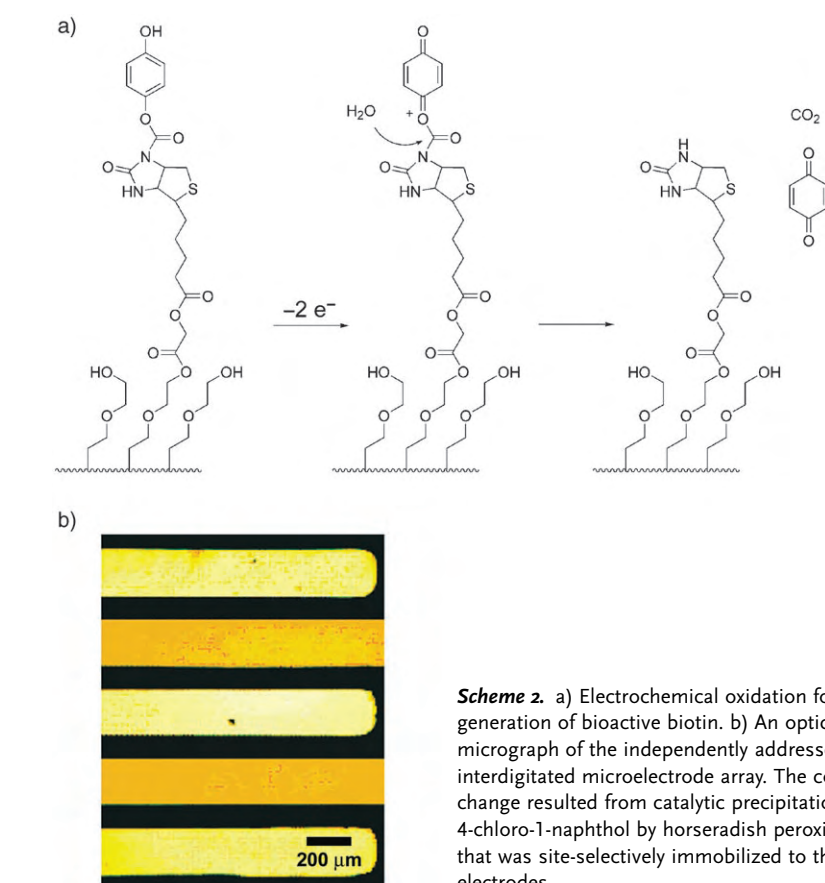


and the oxidation–reduction was reversibly controlled by voltages.<sup>[6a]</sup> The electrochemically generated quinone has been utilized for immobilizing various functional molecules, such as small molecules, peptides, and polysaccharides, through Diels–Alder reactions with cyclopentadiene (Cp)-containing molecules. A salient demonstration would entail electrochemically controlled “turning-on” of cell migration at surfaces by a surface reaction on demand for the attachment of a cell-adhering tripeptide, Arg-Gly-Asp (RGD) (Scheme 1a).<sup>[6b]</sup> This report was the first example of an electroactive substrate that uses electrical stimulation to modulate the activity of ligands. The same reaction was subsequently applied to the pattern generation of two different cell types.<sup>[6c]</sup> Mrksich and co-workers also reported the release of one ligand and the subsequent immobilization of a second ligand by surface reactions on demand (Scheme 1b).<sup>[6d]</sup> RGD-containing *O*-silyl-HQ was oxidized at the surface. Upon the oxidation of HQ to Q, the silyl ether was hydrolyzed and the RGD ligand was selectively released. After the release of the RGD ligand, the electrochemically generated Q was coupled with another Cp-containing ligand.

The electrochemical oxidation of HQ to Q was also used for site-selective conjugation of biotin onto silicon micro- and nanoelectrodes.<sup>[7]</sup> Heath and co-workers demonstrated that the surface reaction on demand could be used for differentiating 100-nm wide Si nanowire electrodes (separated by 300 nm). They, for the first time, applied the surface reaction on demand to individual electrodes. Similarly, the array of indium oxide nanowires was selectively functionalized by the oxidation of HQ to Q and subsequent bioconjugation.<sup>[8]</sup>

Kwak and co-workers elegantly utilized the HQ-based, surface reaction on demand to selectively functionalize individual electrodes (Scheme 2).<sup>[9]</sup> They oxidized the HQ group, which was used as a protecting group for biologically active biotin, to a hydrolysis-labile Q group. Through this process, a biologically inactive surface was controllably transformed to a biologically active surface.

Recently, another ingenious approach to surface reactions on demand



**Scheme 2.** a) Electrochemical oxidation for the generation of bioactive biotin. b) An optical micrograph of the independently addressed, interdigitated microelectrode array. The color change resulted from catalytic precipitation of 4-chloro-1-naphthol by horseradish peroxidase that was site-selectively immobilized to the electrodes.

was reported. Instead of activating surface-bound reactants, such as HQ, Chidsey, Collman, and co-workers electrochemically activated a catalyst for copper(I)-catalyzed Huisgen 1,3-dipolar cycloaddition (Sharpless “click” chemistry) (Figure 2).<sup>[10]</sup> The click chemistry between azido and acetylenyl groups, leading to the formation of 1,2,3-triazoles,<sup>[11]</sup> has been applied to SAM-based reactions<sup>[12]</sup> because the reaction is fast and proceeds under mild aqueous conditions. To demonstrate individual addressability, they brought an electrode in contact with a solution containing copper(II) species, and biased the electrode at  $-300$  mV versus a Ag/AgCl/saturated NaCl reference electrode (roughly 300 mV negative of the copper(II/I) standard potential). This potential ensured that copper(I) was formed at the electrode surface. The electrode was coated with a SAM terminating in azido groups. Therefore, upon the selective electrochemical induction of copper(I), acetylenyl-containing compounds could be coupled with the azido groups at the electrode through the use of click

chemistry. The electrical potential of  $+250$  mV was applied to the other electrodes for deactivating the catalyst near the electrodes. By using electroactive ethynylferrocene, they confirmed a selective coupling at the designated electrode. This approach is rather simple and advantageously differentiated from the activation of reactants in some aspects. The stoichiometric amount of electroactive reactants is not necessary because a catalyst is activated. In the system designed by Chidsey, Collman, and co-workers, a single catalyst amplifies the response due to a single electron. In addition, because surface-bound reactants need not be electroactive, design flexibility in immobilizing molecules is increased. It is worth noting that this work is the first report on the catalytic version of SAM-based, surface reactions on demand.<sup>[13]</sup>

In summary, recent advances in the study of SAMs promise wider applications of SAMs to many areas in science and technology. Especially SAM-based surface reactions on demand would find applications in the construction of dy-

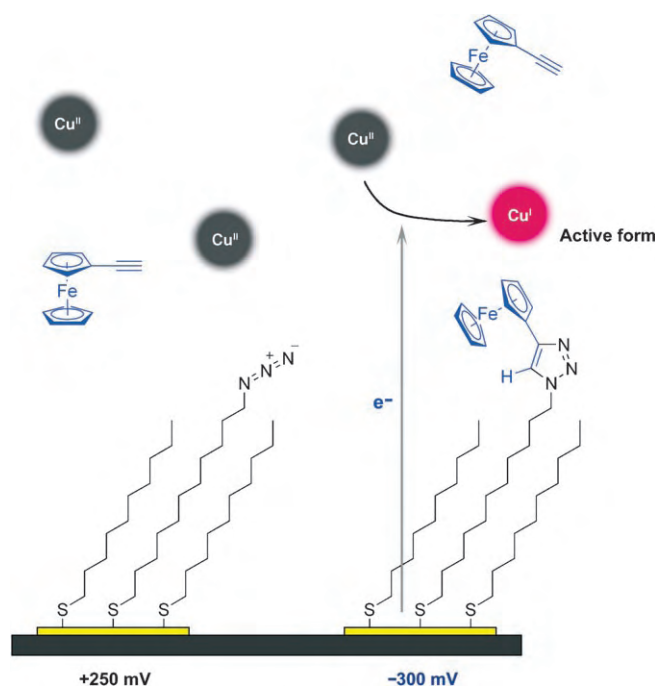


**Figure 2.** Selective functionalization of independently addressed microelectrodes. Copper(II) was electrochemically reduced to copper(I), and copper(I) catalyzed the click chemistry between surface-bound azido groups and acetylenyl-containing compounds (ethynylferrocene in the figure).

namic surfaces and multianalyte-sensor arrays for multiplexing. In addition to the applications to electrode- and nano-wire-based sensors, surface reactions on demand can also be applied to other technologically important areas, such as cantilever-based sensors.<sup>[14]</sup> Electrochemically induced, surface reactions on demand are one of the strong candidates for the above-mentioned applications. They are largely insensitive to the shape and spatial extent of surfaces to be differentiated. All manner of three-dimensional structures should be differentiable as long as they have contact with a fluid electrolyte. Therefore, individual addressability of surface reactions could be achieved by electrochemical control. One problem that remains to be solved is how one performs parallel surface reactions on demand because the serial processing might be time-consuming and produce non-negligible wastes.

- [1] a) J. C. Love, L. A. Estroff, J. K. Kriebel, R. G. Nuzzo, G. M. Whitesides, *Chem. Rev.* **2005**, *105*, 1103; b) Y. S. Chi, J. K. Lee, K.-B. Lee, D. J. Kim, I. S. Choi, *Bull. Korean Chem. Soc.* **2005**, *26*, 361.
- [2] J. Hu, Y. Liu, C. Khemtong, J. M. El Khoury, T. J. McAfoos, I. S. Taschner, *Langmuir* **2004**, *20*, 4933.
- [3] a) K. Ichimura, S.-K. Oh, M. Nakagawa, *Science* **2000**, *288*, 1624; b) N. Delorme, J.-F. Bardeau, A. Bulou, F. Poncin-Epaillard, *Langmuir* **2005**, *21*, 12278.
- [4] a) M. G. Sullivan, H. Utomo, P. J. Fagan, M. D. Ward, *Anal. Chem.* **1999**, *71*, 4369; b) C.-C. Hsueh, M.-T. Lee, M. S. Freund, G. S. Ferguson, *Angew. Chem.* **2000**, *112*, 1281; *Angew. Chem. Int. Ed.* **2000**, *39*, 1227; c) J. Wang, M. Jiang, A. M. Kawde, R. Polsky, *Langmuir* **2000**, *16*, 9687; d) L. M. Tender, R. L. Worley, H. Fan, G. P. Lopez, *Langmuir* **1996**, *12*, 5515.
- [5] J. Lahann, S. Mitragotri, T.-N. Tran, H. Kaido, J. Sundaram, I. S. Choi, S. Hoffer, G. A. Somorjai, R. Langer, *Science* **2003**, *299*, 371.

- [6] a) M. N. Yousaf, M. Mrksich, *J. Am. Chem. Soc.* **1999**, *121*, 4286; b) M. N. Yousaf, B. T. Houseman, M. Mrksich, *Angew. Chem.* **2001**, *113*, 1127; *Angew. Chem. Int. Ed.* **2001**, *40*, 1093; c) M. N. Yousaf, B. T. Houseman, M. Mrksich, *Proc. Natl. Acad. Sci. USA* **2001**, *98*, 5992; d) W.-S. Yeo, M. N. Yousaf, M. Mrksich, *J. Am. Chem. Soc.* **2003**, *125*, 14994; e) M. Mrksich, *Curr. Opin. Chem. Biol.* **2002**, *6*, 794, and references therein.
- [7] Y. L. Bunimovich, G. Ge, K. C. Beverly, R. S. Ries, L. Hood, J. R. Heath, *Langmuir* **2004**, *20*, 10630.
- [8] M. Curreli, C. Li, Y. Sun, B. Lei, M. A. Gundersen, M. E. Thompson, C. Zhou, *J. Am. Chem. Soc.* **2005**, *127*, 6922.
- [9] K. Kim, H. Yang, S. Jon, E. Kim, J. Kwak, *J. Am. Chem. Soc.* **2004**, *126*, 15368.
- [10] N. K. Devaraj, P. H. Dinolfo, C. E. D. Chidsey, J. P. Collman, *J. Am. Chem. Soc.* **2006**, *128*, 1794.
- [11] V. V. Rostovtsev, L. G. Green, V. V. Fokin, K. B. Sharpless, *Angew. Chem.* **2002**, *114*, 2708; *Angew. Chem. Int. Ed.* **2002**, *41*, 2596.
- [12] a) Y. Zhang, S. Luo, Y. Tang, L. Yu, K.-Y. Hou, J.-P. Cheng, X. Zeng, P. G. Wang, *Anal. Chem.* **2006**, *78*, 2001; b) X.-L. Sun, C. L. Stabler, C. S. Cazalis, E. L. Chaikof, *Bioconjugate Chem.* **2006**, *17*, 52; c) N. K. Devaraj, G. P. Miller, W. Ebina, B. Kakaradov, J. P. Collman, E. T. Kool, C. E. D. Chidsey, *J. Am. Chem. Soc.* **2005**, *127*, 8600; d) T. Lummerstorfer, H. Hoffman, *J. Phys. Chem. B* **2004**, *108*, 3963; e) J. K. Lee, Y. S. Chi, I. S. Choi, *Langmuir* **2004**, *20*, 3844; f) J. P. Collman, N. K. Devaraj, C. E. D. Chidsey, *Langmuir* **2004**, *20*, 1051.
- [13] As a related work, Moeller and co-workers reported the electrochemical activation of catalysts for chemical reactions on polymeric films. Independent addressability of the reactions on electrodes was also demonstrated: a) E. Tesfu, K. Maurer, S. R. Ragsdale, K. D. Moeller, *J. Am. Chem. Soc.* **2004**, *126*, 6212; b) J. Tian, K. Maurer, E. Tesfu, K. D. Moeller, *J. Am. Chem. Soc.* **2005**, *127*, 1392.
- [14] G. Shekhawat, S.-H. Tark, V. P. Dravid, *Science* **2006**, *311*, 1592, and references therein.



# Biologically Active Molecules with a “Light Switch”

Günter Mayer\* and Alexander Heckel\*

**Keywords:**

bioorganic chemistry · caged compounds · photochemistry · photoswitches · protecting groups

*Dedicated to Peter Dervan  
on the occasion of his 60th birthday*



**B**Biologically active compounds which are light-responsive offer experimental possibilities which are otherwise very difficult to achieve. Since light can be manipulated very precisely, for example, with lasers and microscopes rapid jumps in concentration of the active form of molecules are possible with exact control of the area, time, and dosage. The development of such strategies started in the 1970s. This review summarizes new developments of the last five years and deals with “small molecules”, proteins, and nucleic acids which can either be irreversibly activated with light (these compounds are referred to as “caged compounds”) or reversibly switched between an active and an inactive state.

## 1. Introduction

A prerequisite for a continuing improvement in the models of the processes in single cells and in organisms is a constant improvement in the repertoire of available tools for the design of experiments. An important general criterion is, for example, how selectively a particular aspect in a cell or organism can be manipulated. To achieve a spatiotemporal control or to enhance the selectivity of a certain effect which is caused by a biologically active compound one strategy is to put the compound under the control of a conditional trigger signal which can be either internal or external. Light is an ideal external trigger signal: In many cases it is an orthogonal trigger because the cells do not react to light unless highly specialized cells, such as the photoreceptors of the eye or certain plant cells, are used. Also, provided the wavelengths used are not too short the cells are not harmed by light. In addition, most of the cells which are commonly studied in laboratories are transparent and the same is true for many small model organisms, such as the nematode *C. elegans* or the zebrafish *D. rerio*, which are transparent throughout their lifetime, while others have at least some stages in their development in which the interior of the organism is still light-accessible (for example the embryos of *D. melanogaster*). Under certain conditions, an application in animals and humans is also possible. For example, 20 years ago cutaneous T-cell lymphoma was treated with 8-methoxypsoralen (8-MOP) in combination with UV-A irradiation, either directly of the skin, or of blood samples which had temporarily been removed from the body of the patient and treated with 8-MOP.<sup>[1]</sup> Psoralens had even been used in ancient Egypt to treat the skin disorder vitiligo.<sup>[1]</sup> Finally, the technology for the highly spatiotemporally controlled application of light is well-established: (Confocal) microscopes can be used both to irradiate samples and to analyze changes. Applying two-photon technology it is possible to restrict the region in a sample which is irradiated with light even further, down to cellular resolution.<sup>[2]</sup>

This Review will focus on two strategies for making a biologically active molecule light-responsive: the first one is nowadays usually referred to as “caging” and involves the modification of a biologically active substance with a photolabile “protecting” group to make it temporarily inactive. The

second strategy makes use of bistable photoswitches. Thus, this Review will not deal with naturally occurring light-dependent (macro)molecules, such as phototropins<sup>[3]</sup> (from flavin mononucleotide (FMN)-dependent light-activated kinases) and photolyases,<sup>[4]</sup> or phenomena such as the light-regulation of photosynthetic genes,<sup>[5]</sup> or other light-dependent technologies, like for example photoaffinity labeling<sup>[6]</sup> (even though some examples of this have been included where it seemed appropriate). Also, because of the biological focus of this Review, materials like light-sensitive polymers<sup>[7]</sup> will not be discussed.

The term “caging” was coined in 1978 by J. F. Hoffman.<sup>[8]</sup> Unfortunately this choice of word is not unproblematic for several reasons: Unless somebody is already knowledgeable in the field they will inevitably think that the molecules in question are in fact inside of a cage in the topological sense—for example inside of a C<sub>60</sub> molecule. Also, they might be erroneously reminded of the “cage effect” observed in the recombination of radicals. Furthermore, since the term “cage” is used very liberally in the biochemical literature it is very difficult to conduct literature searches, especially since we are dealing with a concept which can be realized with many different chemical structures. Other authors choose not to use this term at all and use “light-activated” or something along these lines instead even though this can refer to much more than just caged molecules in the sense of the above definition.<sup>[9]</sup> However, after over 30 years it is too late to propose a new technical term.<sup>[10]</sup>

Caged molecules can be irreversibly activated by irradiation with light whereby the photolabile group is removed.

## From the Contents

1. Introduction	4901
2. Caging Groups and Reversible Photoswitches	4903
3. Caged and Light-Switchable Small Molecules	4904
4. Caged and Light-Switchable Proteins	4908
5. Caged and Light-Switchable Nucleic Acids	4913
6. Summary and Outlook	4917

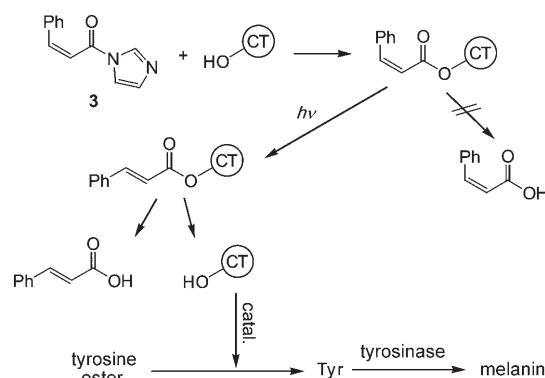
[\*] Dr. G. Mayer, Dr. A. Heckel  
Kekulé-Institut für Organische Chemie und Biochemie  
Rheinische Friedrich-Wilhelms-Universität Bonn  
Gerhard-Domagk-Strasse 1, 53121 Bonn (Germany)  
Fax: (+49) 228-73-4809  
E-mail: gmayer@uni-bonn.de  
heckel@uni-bonn.de



Ideally, caged molecules are water soluble, the “cage” is stable to hydrolysis, the photodeprotection occurs with high quantum yield and at wavelengths which are not too short ( $> 300$  nm), and the byproducts are nontoxic.<sup>[11]</sup> For studying light-induced kinetic events the photodeprotection must be faster than the reaction to study.<sup>[12]</sup>

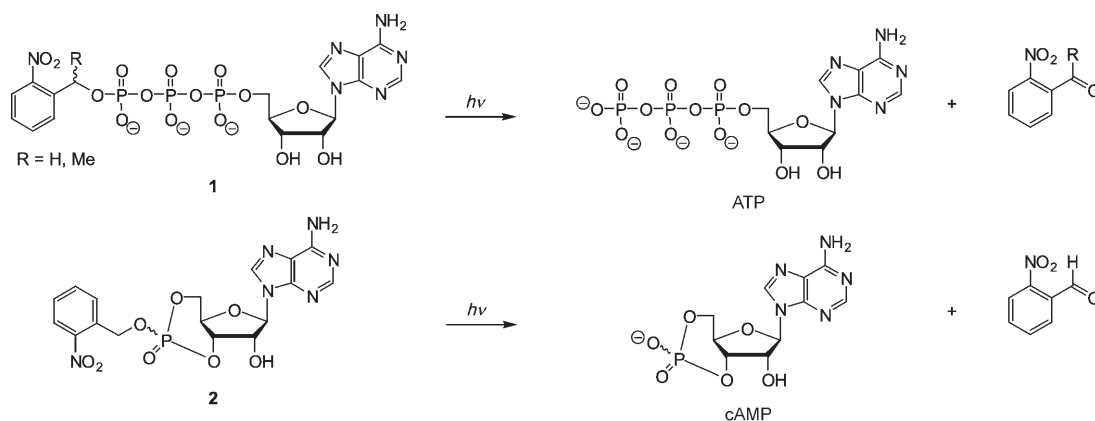
The first “caged molecule” was the adenosine triphosphate (ATP) derivative **1**<sup>[8]</sup> (Scheme 1)—synthesized by Hoffman et al. at Yale—even though a year earlier Engels et al. at the University of Constance had synthesized the cyclic adenosine monophosphate (AMP) derivative **2**<sup>[13]</sup> but did not use the word “caged” and the potential for light-activation was not the main focus of the paper.<sup>[14]</sup> Of course, by that time, photolabile protecting groups for synthetic purposes were already known<sup>[15]</sup> but the new idea was to use them for biochemical experiments with spatiotemporal control. Early studies with caged ATP included experiments in which single turnovers of the  $\text{Na}^+$ -pump could be observed.<sup>[16]</sup> Caged ATP is commercially available today<sup>[17]</sup> and has been used in a vast number of studies which cannot be discussed in detail herein.

Even earlier than the studies by Hoffman or Engels another very interesting series of studies took place in which the peptidase  $\alpha$ -chymotrypsin (CT) was incubated with *cis*-cinnamoyl imidazole (**3**),<sup>[18]</sup> resulting in an acylation of the active site of CT (Scheme 2). However, only the *trans*-



**Scheme 2.** Before the term “caging” was coined  $\alpha$ -chymotrypsin (CT) had already been temporarily deactivated by *cis*-cinnamoylation.<sup>[18]</sup> Only upon isomerization to the *trans*-form is the cinnamoyl group cleaved, regenerating the active enzyme which can then, for example, cleave a tyrosine ester. The resulting tyrosine can then be converted into the pigment melanin by tyrosinase. This setup can be used to amplify weak light signals.<sup>[20]</sup>

cinnamoylated adduct can be cleaved by the enzyme to regenerate the active site for another turnover. Strictly speaking, *cis*-cinnamoylated CT could also have been called “caged” since upon irradiation the cinnamoyl-group undergoes *cis-trans* isomerization and the active enzyme is



**Scheme 1.** Top: The first light-activatable molecule **1** to be called “caged”.<sup>[8]</sup> Bottom: The very similar light-activatable cAMP derivative **2** had in fact been published one year before.<sup>[13]</sup> For mechanistic details of the photoreaction see for example Ref. [12].



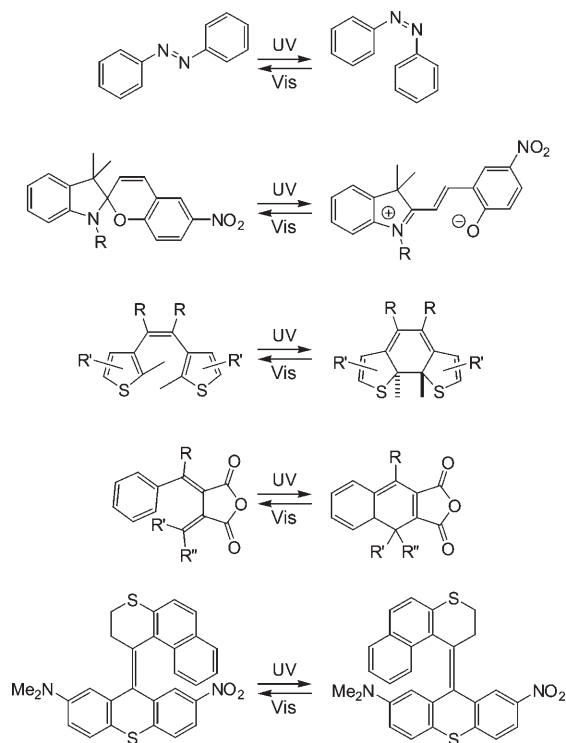
Alexander Heckel, born in Lindau, studied chemistry at the University of Constance and did his diploma thesis in the field of oligosaccharide solid phase synthesis with R. R. Schmidt. Then he joined the group of D. Seebach at the ETH Zurich for a PhD on enantioselective heterogeneous catalysis with taddol and salen on silica gel. During his postdoctorate at Caltech with P. B. Dervan he worked on the recognition of DNA with “Dervan-polyamides”. In 2003 he has joined the University of Bonn where he is currently working on his “Habilitation” under the mentorship of M. Famulok. In his spare time he is a volunteer paramedic and search and rescue diver for the Red Cross.



Günter Mayer, born in Munich, studied chemistry at the Ludwig Maximilian University in Munich and after his diploma thesis (M. Famulok; selection of RNA aptamers) he obtained his PhD from the University of Bonn on the functional analysis of cytohesin-1 in T-cells with RNA intramers. In 2001 he joined the biotech company NascaCell, which he co-founded, where he headed the combinatorial biotechnology department. He rejoined the Famulok group at the University of Bonn in 2004 where he is currently working on his “Habilitation”. His research interests are the spatiotemporal control of aptamer activity and the discovery of new proteins based on aptamer selections.

liberated. *Cis*-cinnamoylated CT had no remaining peptidase activity and was stable for several hours in the dark. Lee et al. realized that this light-activated catalyst could be used to amplify a light signal<sup>[19]</sup> by coupling to another enzymatic reaction in which tyrosine, which was liberated upon activation of the CT, was converted by a tyrosinase to produce the pigment melanin (Scheme 2).<sup>[20]</sup>

Also in the seventies the first experiments to reversibly switch the activity of enzymes with light were carried out.<sup>[21]</sup> Compounds of the spiropyran-type can be switched between two states (see Section 2 and Scheme 3). In the case of normal



**Scheme 3.** Overview of some bistable photoswitches based on (from top to bottom) azobenzene,<sup>[49]</sup> spiropyrans,<sup>[50]</sup> diarylethenes,<sup>[51]</sup> fulgides<sup>[52]</sup> and overcrowded alkenes<sup>[53]</sup>. Some of these systems have already been used to create biologically active compounds which can be reversibly activated and deactivated.

photochromism the ring opens upon irradiation with UV light and it closes again in the dark or upon irradiation with visible light. Enzymes such as  $\alpha$ -amylase have been modified (through their amine groups) with spiropyran substituents.<sup>[22]</sup> Upon irradiation the activity of the enzyme, after modification, decreased by one third. In the dark the full enzymatic activity was recovered within one hour.

While the examples above show the first ideas to control biological activity with light the aim of this Review is not to give a full account of the beginnings of the field but rather to illustrate the more recent developments of the last five years (though publication date has not been used as a strict cutoff criterion where it seemed inappropriate). Of course, since the beginnings over 30 years ago the field has been reviewed several times.<sup>[12, 23–25]</sup>

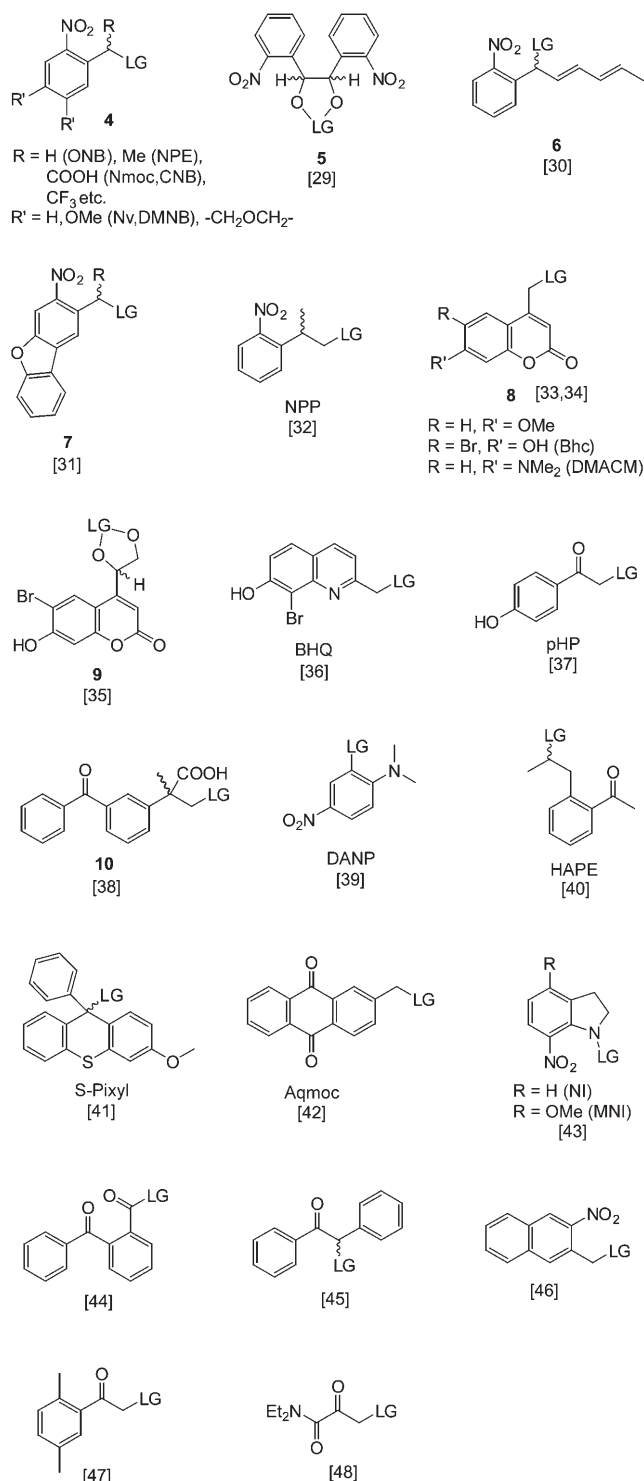
## 2. Caging Groups and Reversible Photoswitches

A comprehensive account of all known caging groups and reversible photoswitches including synthetic access and mechanisms of the light-dependent reaction would be beyond the scope of this application-based Review. Thus, only a brief overview of the respective systems is given herein.<sup>[26]</sup>

The terms “caging group” and photolabile protecting group are for all practical purposes synonyms because the main difference is the intention behind the photorelease. Thus, the most commonly used caging group—the *ortho*-nitrobenzyl group with all its derivatives (**4**, R=H, Scheme 4)—had already been widely used as protecting group for synthetic purposes and as photolabile linker in solid-phase applications.<sup>[15]</sup> One disadvantage of the *ortho*-nitrobenzyl group is that upon photolysis a nitrosoaldehyde is formed which can be harmful in a biological context.<sup>[12, 27]</sup> The nitrophenylethyl (NPE) group (**4**, R=Me) can be deprotected faster and results in the formation of a nitrosoketone. However, a new stereogenic center is introduced into the molecule. The wavelength of the absorption can be fine-tuned, for example, by dimethoxy substituents.<sup>[28]</sup> Variants exist for the protection of carbonyl groups (compound **5**)<sup>[29]</sup> as well as modifications which trap the resulting nitroso species in a hetero Diels–Alder reaction (compound **6**).<sup>[30]</sup> Very recently the nitrodibenzofurane chromophore **7** has been introduced which has very promising properties: Not only is its extinction coefficient significantly higher in the near UV region, which is commonly used for uncaging, but it has also a very high quantum yield for the deprotection reaction and it is suitable for two-photon activation.<sup>[31]</sup> An interesting alternative was also introduced by Pfeleiderer et al.: the NPP group (scheme 4) which upon irradiation yields a less harmful nitrostyryl species.<sup>[32]</sup>

Other very versatile and commonly used caging groups are based on the coumarin system **8**.<sup>[33]</sup> For example, the DMACM group releases its attached active compound in nanoseconds.<sup>[34]</sup> Again variants for the caging of aldehydes and ketones are available (compound **9**)<sup>[35]</sup> as well as closely related analogues (such as BHQ; Scheme 4).<sup>[36]</sup> Another well-studied caging group is the PHP group.<sup>[37]</sup> The ketoprofen-derived caging group **10** is a newcomer in the field which could have great potential.<sup>[38]</sup> Scheme 4 also shows some newer photolabile groups, not all of which have been used for biological applications yet.

The advantage of the caging technology is the possibility of a clean switching behavior: If the caging group is placed in the correct position, completely inactive molecules can be obtained. Upon uncaging the unmodified active molecule is formed. However, this is an irreversible reaction affording stoichiometric amounts of byproducts in the process. Therefore a competing strategy is to put molecules under the control of bistable photoswitches. In this case the price for the apparent advantage of reversible switching is the difficulty of finding the right location for the switching moiety. Since both the “active” and the “inactive” form are derivatives of the parent molecule it becomes difficult to obtain a binary on/off behavior even if an ideally switchable system is used.



**Scheme 4.** Non-comprehensive overview of photolabile groups. Not all of them have actually been used for caging of biologically active compounds. (LG = leaving group, in some cases this includes a carbonate or carbamate linker)

Scheme 3 gives an overview of some known bistable photo-switches. Not all of these systems have been used in biological applications.

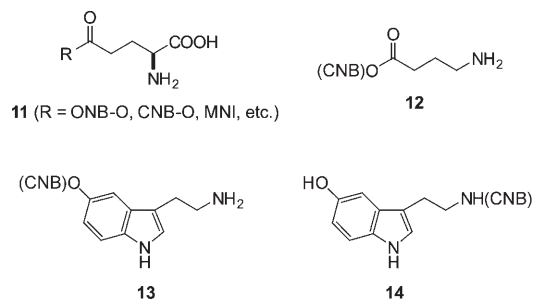
### 3. Caged and Light-Switchable “Small Molecules”

As mentioned in Section 1, the first molecules to be caged were what would nowadays be called “small molecules”. Many different classes of small molecules have been caged to date. Among them caged ATP remains the most often used compound of all. Its applications are so numerous that herein we can only refer to other reviews.<sup>[23,24]</sup> Besides amino acids also steroids, second messengers, sugars, and lipids have been caged and used for the analysis of biological phenomena.<sup>[54,55]</sup>

#### 3.1. Caged Compounds for the Analysis of Neurological Processes

The spatially well-defined and rapid change in the concentration of caged agonists or antagonists of neuronal receptors induced by flash photolysis is of great value, for example, for the investigation of kinetic and mechanistic aspects of receptors, transporters, and ion channels at a resolution down to the single cellular level.<sup>[56,57]</sup> Therefore, caging technology was applied to various neurotransmitters, including glutamate, dopamine, carbamoylcholine, and other neuroactive amino acids.<sup>[54,56]</sup>

One of the most intensively studied compounds in this regard is the amino acid glutamate. A significant body of literature exists in this field already. Caged glutamate variants have been synthesized carrying different photolabile groups (**11**, Scheme 5) and CNB-caged glutamate is already com-



**Scheme 5.** Caged glutamate and serotonin derivatives which have been used in neurological studies.

mercially available.<sup>[17]</sup> Caged glutamate has been applied to address different questions regarding the kinetics of neuronal signaling and highly regulated spatiotemporal events. In addition, with the CNB group glutamate has also been caged with ONB, MNI (Scheme 4), and other groups<sup>[58]</sup> and the resulting compounds have been used for the analysis of receptor kinetics of ion channels gated by glutamate in different neuronal cell lines.<sup>[56]</sup>

In this way Shao and Dudek analyzed the localization of the excitatory synaptic input in CA1 pyramidal cells.<sup>[59]</sup> They selectively stimulated different regions of subicular neurons by focal flash photolysis thereby triggering the local release of glutamate and thus the cellular stimulation. With a resolution of approximately 100  $\mu\text{m}$  they could assign the generation of postsynaptic currents after CA1 pyramidal cell stimulation to the somatodendritic region.

In another study, the agonistic effects of caged compounds on *N*-methyl-D-aspartate (NMDA) receptors were investigated.<sup>[58]</sup> In this case, the authors compared the effects and results obtained by different caging strategies: They used MNI-caged glutamate<sup>[60]</sup> and CNB-caged variants. They provide evidence for the usefulness of the MNI-caged agonists and their results indicate that CNB derivatives of caged glutamate were not as effective in this system. In addition, they observed inhibitory effects of CNB-caged glutamate on NMDA receptors which were not observed with the MNI-caged glutamate variants. This result indicates that the choice of the photolabile group is critical and depends on the system under investigation and has to be adjusted carefully with respect to the analyzed biological function and receptor. However, the CNB-caged glutamate has a fast deprotection rate ( $t_{1/2} = 21 \mu\text{s}$ ), which makes it very practical for kinetic studies.<sup>[61]</sup> The CNB-glutamate compounds were used to analyze channel-opening kinetics of several glutamate induced ion-channel receptor types such as the AMPA-type ( $\alpha$ -amino-3-hydroxy-5-methyl-4-isoxazole-propionate) ionotropic glutamate receptor.<sup>[62]</sup>

The NI (Scheme 4) and MNI photolabile groups were also used to study the kinetics of metabotropic and ionotropic receptors, for example (*N*-methyl-D-aspartate) NMDA, and AMPA receptors, with respect to glutamate.<sup>[60,63]</sup> In another study Lowe used NI-caged glutamate to investigate the pharmacology and kinetics of mitral cell glutamate receptors.<sup>[64]</sup> Ellis-Davies et al. used the MNI-caged glutamate to stimulate the increase of the expression of postsynaptic AMPA receptors after uncaging of the glutamate in isolated dendritic spines.<sup>[65]</sup> In an interesting photoaffinity labeling approach England et al.<sup>[66]</sup> used a cell permeable AMPA receptor antagonist (instead of a receptor agonists), and its photosensitive variant (6-azido-7-nitro-1,4-dihydroquinoline-2,3-dione) for the analysis of AMPA trafficking in synaptic plasticity with high temporal (minute time scale) and spatial resolution.

Brasnjó and Otis used a caged glutamate derivative for the analysis of excitatory amino acid transporter (EAATs)-dependent Purkinje-cell glutamate uptake in response to single climbing fiber action potentials.<sup>[67]</sup> An earlier study by Grever and Rauen shows that glutamate translocation mediated by the neuronal EAAC1 amino acid transporter takes place on the millisecond timescale.<sup>[68]</sup>

Shimamoto et al. synthesized coumarin-based caged derivatives of glutamate and demonstrated their use to investigate glutamate transport upon light activation.<sup>[69]</sup> Jayaraman et al. demonstrated that Fourier transform infrared (FTIR) spectroscopy can be used to monitor the structural changes induced upon release of glutamate from caged inactive glutamate precursors.<sup>[70]</sup>

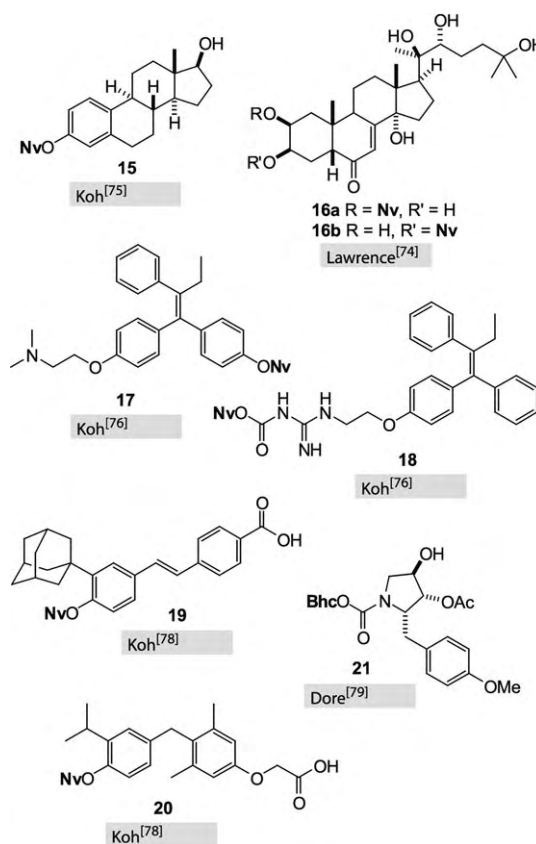
Molnár and Nadler chose a different approach to investigate processes at the synaptic area of neurons.<sup>[71]</sup> They used the caged GABA ( $\gamma$ -aminobutyrate) derivative (**12**; Scheme 5) to analyze GABA receptors. The caged GABA inhibited the polysynaptic inhibitory postsynaptic currents (IPSCs) induced in dentate granule cells by antidromic stimulation of the mossy fibres. In turn, no effect could be

observed on the excitatory postsynaptic currents (EPSCs) induced through perforant path stimulation.

Hess et al. described the synthesis of caged serotonin. They compared the deprotection kinetics of the O-derivative **13** with the N-derivative **14** (Scheme 5).<sup>[72]</sup> The O-derivative **13** could be deprotected in only 16  $\mu\text{s}$  whereas the N-derivative **14** showed rather slow kinetics (1.2 ms). Owing to its high solubility (2 mM) in aqueous solutions and the fast deprotection kinetics the caged serotonin was used for effector storage. The quick release of the active compound upon laser irradiation allows the analysis of receptor kinetics of the serotonin 5-HT<sub>3</sub> receptors in mouse neuroblastoma cells (NIE-115). Lee et al. synthesized a caged dopamine for the analysis of the influence of the dopamine concentration on the endogenous dopamine release and they showed that the endogenous dopamine release could be repressed by photoinduced dopamine concentration jumps.<sup>[73]</sup>

### 3.2. Steroid Hormones, Lipids, and Membranes

Hormones and hormone analogues can regulate gene expression upon binding to their cognate receptors, such as the estrogen receptor. Hence, these molecules can be used for the construction of gene expression systems.<sup>[74]</sup> Upon binding to estradiol the receptor undergoes conformational changes and then binds to promoter elements of distinct genes and thus initiates gene expression. Koh and co-workers synthesized a caged estradiol variant (**15**, Scheme 6) and showed



Scheme 6. Caged effectors for the regulation of gene expression.



that with this compound it is possible to trigger hormone-dependent gene expression by light.<sup>[75]</sup> This strategy allows the spatiotemporal analysis of gene expression and seems to be superior to other methods that are either unspecific with respect to the locality or initiation of gene expression. Caged  $\beta$ -ecdysone-4 (**16a,b**; Scheme 6) was synthesized by Lawrence et al. and used (similar to the approach by Koh) to gain control over the expression of genes by light.<sup>[74]</sup>

Selective estrogen receptor (ER) antagonists were used by Shi and Koh to trigger ER-mediated gene expression.<sup>[76]</sup> They synthesized caged 4-hydroxytamoxifen (**17**) and caged guanidine tamoxifen (**18**; Scheme 6) that both selectively antagonize ER $\alpha$ - and ER $\beta$ -mediated transcription triggered by estrogen response elements (EREs). In a very recent study they adopted the system for controlling the recombination of genes by targeting the ligand controlled Cre-ER<sup>T</sup> (a tamoxifen sensitive recombinase variant) recombinase activity with the caged 4-hydroxytamoxifen **17**.<sup>[77]</sup> Inside cells and upon addition of 4-hydroxytamoxifen, the Cre-ER<sup>T</sup> recombinase becomes active, and after recombination, the expression of a reporter gene can be monitored. Koh et al. showed that with compound **17** this system can be controlled by light, however in an irreversible manner.

In another study Koh et al. used the retinoic acid receptor (RAR) and the thyroid receptor (TR) system to analyze the duration of gene response after uncaging of an agonist, derivatized with a photolabile group.<sup>[78]</sup> They synthesized caged analogues of synthetic agonists of RAR and TR (**19** and **20**; Scheme 6) and used them to investigate the stability of the cages under cellular conditions, as well as photoactivated gene expression, mediated by TR and RAR after time-dependent irradiation with light. They observed almost no unintended uncaging under physiological conditions, whereas the duration of the gene expression response could be detected up to 35 h after irradiation in the TR system but the duration of the RAR system was as short as 5 h. This result demonstrates that the spatiotemporal control of gene expression and its duration after photolysis of caged nuclear hormone-receptor agonists depends on the system that is under investigation.

The control of gene expression can also be obtained by the regulation of translation. By this means Dore et al. synthesized a caged variant of anisomycin (**21**), a compound that interferes with the peptide-bond-forming step during eukaryotic translation. They could show that with Bhc-anisomycin the spatiotemporal inhibition of protein synthesis is possible and these compounds might be useful for the analysis of locally strongly regulated neuronal processes.<sup>[79]</sup>

Furuta et al. reported the synthesis of caged bile acids. Bile acids are end products of cholesterol metabolism.<sup>[80]</sup> These variants might be of importance for the analysis of biological processes that depend on bile acid interactions. In other studies the caging approach was applied to induce conformational changes and structural reorganization of lipid micelles or self-assembled structures.<sup>[81]</sup> Photoactivatable analogues of cholesterol have been used for several applications,<sup>[82]</sup> however, their use in affinity labeling applications predominates: A diazirine-containing cholesterol derivative was used to identify cholesterol binding proteins in neuro-

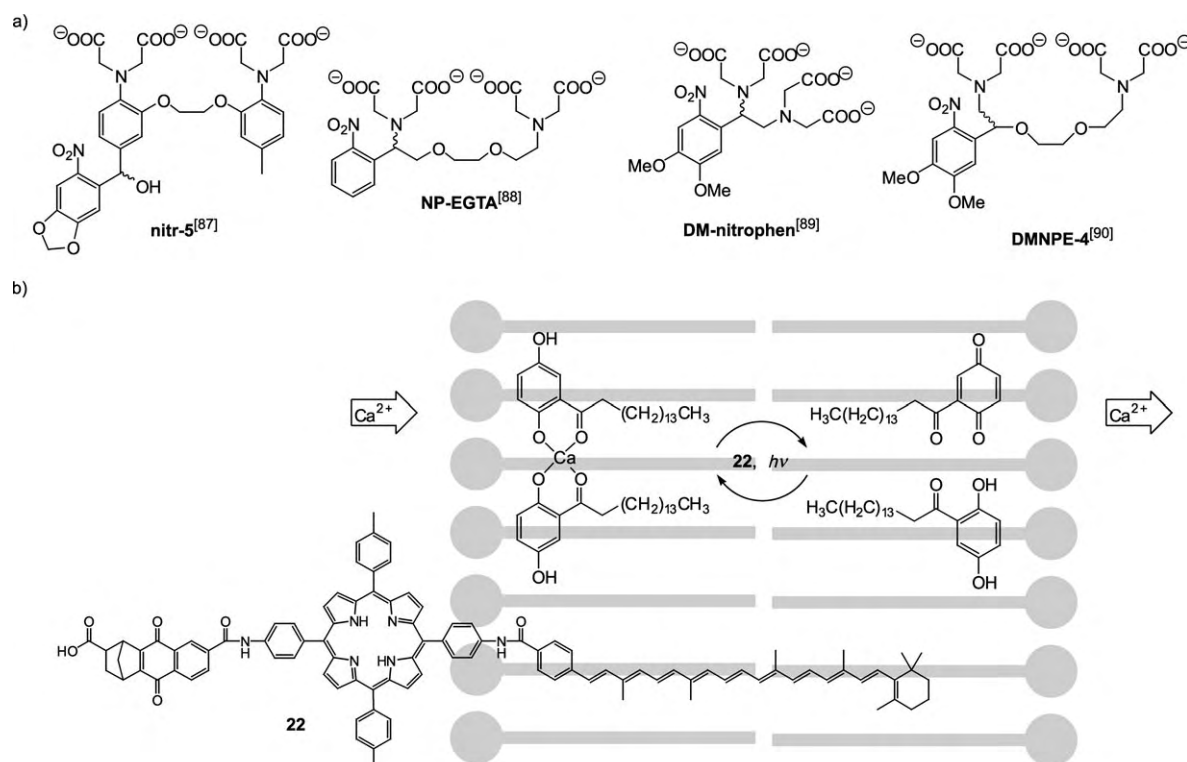
endocrine cells and in living organisms such as *C. elegans*.<sup>[83]</sup> In combination with UV-based cross-linking, the vitellogenin protein family could be identified as the major interaction partner of cholesterol in *C. elegans*. These proteins are also responsible for the correct distribution of cholesterol, this was determined by tracking the distribution and accumulation of cholesterol with the fluorescent analogue of cholesterol, dehydroergosterol. Simons et al. used the UV cross-linking method to link proteins with the photoactivatable cholesterol analogue. These compounds were used to pinpoint the cholesterol-based association of proteolipid protein with a low-density CHAPS-insoluble membrane fraction (CIMF) which is enriched in the myelin lipids of oligodendrocytes.<sup>[84]</sup> They identified the proteolipid protein as a major myelin component. In contrast, no interaction (UV induced cross-link) of proteolipid protein with phosphatidylcholin could be detected.

### 3.3. Secondary Messengers and Cellular Signaling Molecules

Quite a significant number of studies deal with the application of the light-induced release of Ca<sup>2+</sup> ions. Typical compounds are shown in Scheme 7. They are chelating ligands which either change their complex-forming abilities (nitr-5) or are cleaved upon irradiation.<sup>[12,23,24]</sup> Again, a comprehensive account of the many applications could be the subject of a specialized review. Herein though, just one study will be reported about photoreversible calcium binding even though it might not exactly fall into the definition of reversibly light-switchable systems as given in the Introduction: Gust et al. introduced a synthetic quinone-based Ca<sup>2+</sup>-ion shuttle system that is able to establish light-driven ion gradients across bilayer vesicles.<sup>[85,86]</sup> This system is uncharged and membrane soluble in the Ca<sup>2+</sup>-bound state. After complex formation at the outer membrane surface it diffuses through the membrane. The complex formation is disrupted by carotenoid radical cations (produced by the membrane-embedded photoexcited carotenoid-porphyrin-naphthoquinone **22**), by oxidation of the complex to quinone. Thus Ca<sup>2+</sup> ions are released at the inner membrane. These molecules are useful for the analysis of Ca<sup>2+</sup>-ion-dependent biological processes. The shuttle molecule is subsequently regenerated.

The control of NO levels has been identified as a possible strategy to combat several diseases. One such approach makes use of inhibitors that target nitric oxide synthases (NOS) with inhibitory molecules such as 1400W. In a recent study, caged derivatives of this inhibitor were synthesized and used as photosensitive drugs (Bhc-1400W, Scheme 8).<sup>[91,92]</sup> The group of Guillemette showed that the inhibitor molecule can be efficiently released by illumination with light from the caged 1400W and that the NOS inhibition can be restored. This result indicates that photolabile groups might serve as spatiotemporal drug-precursor molecules.

Another strategy is to directly liberate NO upon irradiation ("caged" NO). Organic compounds from which NO can be released have been known for quite some time<sup>[93]</sup> and have already been reviewed.<sup>[12]</sup> In a recent study Yip used caged



**Scheme 7.** a) Typical compounds used for the light-triggered release of calcium ions which either change their ligand properties (nitr-5<sup>[87]</sup>) or are cleaved upon irradiation (NP-EGTA,<sup>[88]</sup> DM-nitrophen,<sup>[89]</sup> DMNPE-4<sup>[90]</sup>). b) A reversible system for  $\text{Ca}^{2+}$  ion binding which can be photoswitched between two states. Through asymmetric insertion of compound **22** this system can transport  $\text{Ca}^{2+}$  ions across lipid bilayers.<sup>[85]</sup>

nitric oxide (potassium nitrosylpentachlororuthenate) to analyze NO-dependent effects on proximal tubular fluid reabsorption. He could demonstrate that the inhibition of the proximal tubular reabsorption is NO-dose dependent and can be triggered by flash photolysis of luminal caged NO.<sup>[94]</sup>

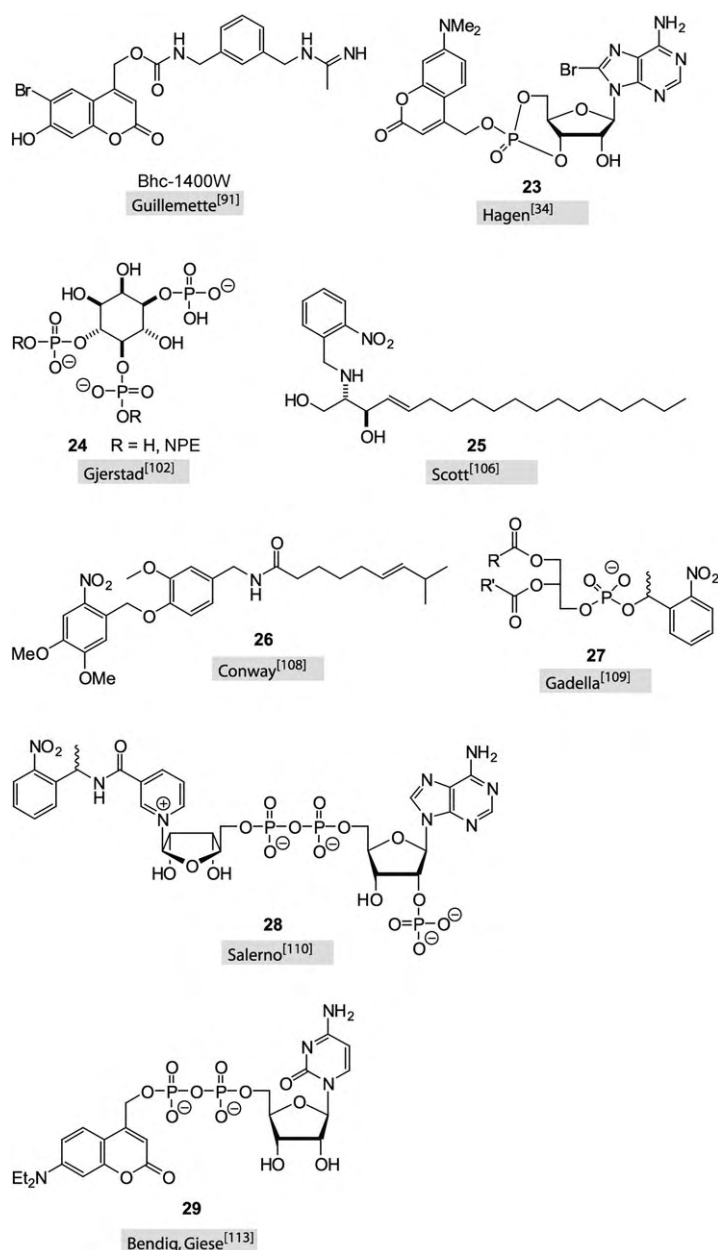
Cyclic nucleotides have been extensively studied<sup>[23, 95, 96]</sup> and caged derivatives can be purchased from commercial suppliers.<sup>[17]</sup> We focus herein on recent application of caged cyclic nucleotidemonophosphates (NMPs) and on the use of novel photolabile protecting groups: A recent study by Harz et al. demonstrated the spatiotemporal effects of cyclic AMP (cAMP) applied to neuronal growth cones, the terminal structures of elongating neurites.<sup>[96]</sup> Since the growth-cone turning is regulated by cAMP, Harz et al. generated an intracellular concentration gradient of cAMP by irradiating the growth cones of chicken sensory neurons with UV light at distinct positions, for example, the cone ends. Using this experimental setup they could show that only certain patterns of cAMP release are able to induce turning of the growth cones. This result indicates that the spatiotemporal pattern of cAMP gradients is critical for the growth-cone turning.

Yoshimura and Kato used a caged cAMP derivative in neurons to analyze effects of increasing cellular concentrations of cAMP. Using this technology they were able to pinpoint the synaptic up- or down-regulation of afterpotentials after an increase of cAMP in neurons. The synaptic up-regulation was detected in AHP-generating neurons and a down-regulation could be observed in ADP-generating neurons (ADP = after depolarization, AHP = after hyperpo-

larization).<sup>[97]</sup> Scott et al. compared the inward currents activated in rat neurons by the cellular increase in cGMP levels, maintained by the flash photolysis of caged cyclic guanine monophosphate (cGMP) precursors.<sup>[95]</sup> They used cultured dorsal root ganglion (DRG) neurons and investigated the effect of cGMP on inward currents by comparison of two differently caged cGMP molecules. Using this approach they detected in 52 % of DRG neurons an activated delayed  $\text{Ca}^{2+}$  inward current through the generation of cyclic ADP-ribose and mobilization of calcium from intracellular stores. But rapidly activating inward currents only occurred in a subpopulation of 12.5 % of neurons, a result of cGMP gated channels. These data indicate that the inward currents might be induced by diverse mechanisms in DRG neurons.

In another study Takeuchi and Kurahashi investigated secondary-messenger-based signal-transduction pathways in the olfactory receptor system using caged cNMP molecules.<sup>[98]</sup> They showed that the caged molecule was beneficial for the observation that the olfactory response is modulated by a uniform mechanism for many odorants. In a different study Lagostena and Menini also used caged compounds to investigate the olfactory system in neurons from mouse.<sup>[99]</sup> They used the patch-clamp method to measure inward currents induced by increasing concentrations of cGMP and cAMP. The concentration increase was obtained through flash photolysis of caged cNMP either in the soma or localized at the cilia of neurons.

Besides the commercially available caged cAMP,<sup>[17]</sup> efforts have been made to develop new caged derivatives of



**Scheme 8.** Caged derivatives of a NO synthase inhibitor, secondary messengers, and nucleotide cofactors.

cNMPs. The groups of Hagen, Tsien, and Corrie investigated other photolabile protecting groups, such as coumarin-based ones and water-soluble derivatives of nitrobenzyl-derived caging groups, that allow the fast and efficient photodeprotection and release of cNMPs (for example, compound **23**, Scheme 8).<sup>[34,100]</sup>

Gjerstad et al. used caged variants of inositol 1,4,5-triphosphate (**24**; Scheme 8)<sup>[101]</sup> to study the effects of IP<sub>3</sub> in frog vomeronasal microvillar receptor neurons. They performed whole cell recordings and observed that local IP<sub>3</sub> molecules can trigger transient depolarization and induce action potentials in neurons.<sup>[102]</sup> Advantageously and owing to the spatially localized activation of IP<sub>3</sub> in the terminal vesicle of the dendrite, the effector region could be localized. Dinkel

and Schultz reported the synthesis of caged myo-inositol 1,3,4,5-tetrakisphosphate.<sup>[103]</sup> Prestwich et al. synthesized caged inositol hexakisphosphate<sup>[104]</sup> which was used by Brearley et al. for studying intracellular signaling in plants.<sup>[105]</sup>

Caged sphingosine (**25**, Scheme 8) and dihydrosphingosine have been synthesized and reported for elucidating neuronal inward currents.<sup>[106]</sup> For affinity labeling experiments the group of Bittman now synthesized a photoactivatable analogue of the lipid mediator and secondary messenger sphingosine 1-phosphate in which they used two different photolabile groups, benzophenone and diazirinyl.<sup>[107]</sup> Using these molecules, different interaction patterns with proteins could be demonstrated indicating the suitability of these compounds for the identification of binding sites of different proteins on the pharmacophore of the sphingosines.

### 3.4. Other Small Molecules

Several other small molecules have also been caged and used for the analysis of signaling pathways or protein function. Conway et al. synthesized a caged capsaicin analogue (**26**; Scheme 8) and showed that upon irradiation, the analogue is capable of activating the capsaicin receptor TRPV1.<sup>[108]</sup>

Goedhart and Gadella reported the usefulness of caged phosphatidic acid (**27**; Scheme 8) to control the flagellar excision in *Chlamydomonas*.<sup>[109]</sup> Addition of caged phosphatidic acid showed no effect and only after UV irradiation does the *Chlamydomonas* deflagellate. This approach opens a controlled way for the investigation of phosphatidic acid dependent signaling pathways.

Salerno et al. used a combination of a synthetic and an enzymatic synthesis strategy to obtain caged NAD cofactors (**28**; Scheme 8).<sup>[110,111]</sup> The synthetic caged nicotinamides were able to act as substrates for the solubilized NAD glycohydrolase transglycosidase activity. By this means the generation of caged NAD cofactors was demonstrated.

Gerwert et al. analyzed the mechanism of Ras GTPase using caged guanine triphosphate (GTP).<sup>[112]</sup>

In combination with time-resolved FTIR difference spectroscopy they could monitor the reaction pathway, from GTP to GDP, in millisecond resolution.

Bendig and Giese et al. synthesized a caged variant of cytidine-5'-diphosphate (**29**, CDP).<sup>[113]</sup> They applied the coumarin-type photolabile protecting group and coupled this to the  $\beta$ -phosphate group of CDP; upon irradiation CDP can be efficiently released.

## 4. Caged and Light-Switchable Proteins

The irreversible photoactivation of proteins has been described for several protein classes including hydrolases,

proteases, kinases, nucleases, toxins, cell-matrix proteins, receptors, serum proteins, galactosidase, and antibodies.<sup>[114]</sup> Herein we focus on recent developments in this area. Cages and light-activatable photoswitches can be introduced into proteins by different methods. In the simplest way caging can be achieved by statistically modifying a protein through the reactivity of functional groups of amino acid side chains with caging agents. One such approach makes use of cysteine residues of proteins and the sulfhydryl groups of caging agents. In another approach, the multimeric properties of proteins can be used to generate a caged variant, if one subunit is synthetically accessible. Hence, the synthetic peptide can be generated bearing a caged moiety at a desired position. These peptides can then be used by replacing the wild-type counterpart to form heterodimeric proteins, which are caged. An elegant approach was introduced by Schultz et al.<sup>[115]</sup> They used a nonsense-codon and a corresponding tRNA, loaded with the desired caged amino acid. Slightly earlier an artificial four-base codon approach had been used by Endo et al.<sup>[116,117]</sup> By both these methods it is possible to introduce caged amino acids into larger proteins in a site-directed manner.

#### 4.1. Kinases

The cAMP-dependent protein kinase A (PKA) is necessary for several signaling pathways including developmental, neuronal plasticity, and hormone signaling. The catalytic subunit of the tetrameric holoenzyme (consisting of two catalytic and two regulatory domains) has been used to develop caged variants.<sup>[118,119]</sup> Therefore two crucial amino acid residues of the PKA catalytic domain, Cys199 and phosphothio-Thr197, were derivatized with ONB groups. The caged variants can be efficiently reactivated by the irradiation with UV light, whereas the non-irradiated proteins were almost inactive, showing a residual activity of only 5%. Bayley et al. further reported that the choice of the protecting group is critical for both the residual activity of the caged protein and efficient reactivation by photolysis. In their study the ONB group performed best whereas the CNB- and the Nv-derivatives showed significant background activity. In a step further, the same group expanded the caging principle of kinases by aiming at the modification of phosphothreonine 197 and thereby they generated a phosphothio-modified kinase appropriate for modification with a PHP group.<sup>[119]</sup> This caged kinase resulted in an inactive PKA protein and upon irradiation the activity could be efficiently restored.

#### 4.2. Ribonucleases

The group of Hamachi developed strategies for the caging of ribonucleases. They used a synthetic approach for the site-specific incorporation of *ortho*-nitrobenzyl-type groups. The ribonuclease S consists of two domains, the S-peptide (1–20) and the S-protein (21–124). By solid-phase synthesis several positions of the S-peptide were replaced with amino acids that bear caging groups. Subsequently they analyzed the activity of

the caged and irradiated peptides. By this means they identified the positions Q11 and D14 to be suitable for effective caging (**30**, Scheme 9) and suppression of RNase activity. After irradiation the RNA-cleaving activity could be restored.<sup>[120]</sup> In an other study, Hamachi et al. incorporated phenylazophenylalanine at specific sites of the same S-peptide (**31**, Scheme 9), resulting in on/off photoswitchable ribonuclease S variants. One ribonuclease variant, carrying the azophenyl moiety located in close proximity to a crucial His12 of the S peptide, showed a clear on/off behavior after alternating irradiation with UV and visible light.<sup>[121]</sup>

In a similar study Woolley et al. also used the phenylazophenylalanine photoisomerizable group for the synthesis of S-peptide variants. In accordance with the study by Hamachi et al. they identified the position 13 of the S peptide as being addressable for efficient introduction of a photo-switchable azobenzene group.<sup>[122]</sup>

#### 4.3. Caged Receptors and Receptor Agonists

Lestee et al. incorporated an ONB group by derivatizing the tyrosine residue 242 (Y242) of the Kir2.1 potassium channel of *Mus musculus*.<sup>[123]</sup> They took advantage of the fact that a cage at the critical position Y242 would provide both a mode to investigate the direct phosphorylation of the receptor at this position and the control of the activity of the receptor by light. Interestingly, it was shown that the tyrosine residue 242 is in fact involved in protein–protein interactions and is not phosphorylated by tyrosine-kinases.

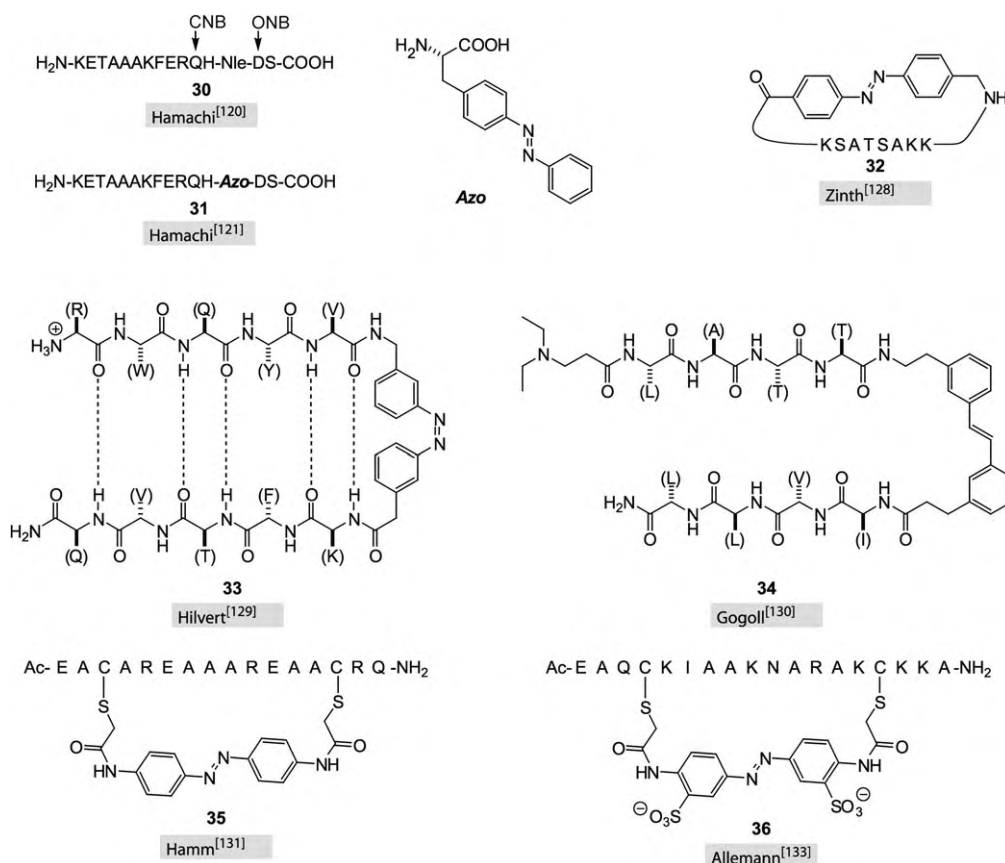
The ligand-gated ion channel nicotinic acetylcholin receptor (nAChR) is composed of five homologous subunits arranged in a pentameric fashion with a central pore. The group of Lester used the nonsense suppression method to introduce caged tyrosine and caged cysteine residues into transmembrane segments of the nAChR.<sup>[124]</sup> The study provided evidence that the caged tyrosine is more efficiently deprotected than caged cysteine by light irradiation and with the caged nACh receptors it was possible to analyze the kinetics of acetylcholine-induced currents before and after photolysis.

A different approach was followed by Trauner and Kramer et al. They synthesized a thiol-reactive azobenzene derivative that contains a tertiary amide and thus generated a switchable K<sup>+</sup>-ion channel.<sup>[125]</sup> This approach allows a precise spatiotemporal control for the analysis of neuronal firing over neuronal circuits in a reversible manner.

#### 4.4. Control of Conformation and Function of Peptides

The strategy of caging peptides and proteins can be used to analyze the folding and unfolding processes of peptide conformations in a time-resolved manner.<sup>[126]</sup> For example, Chan et al. used the 3',5'-dimethoxybenzoin group to cage a mutant of the GCN4-1p protein that causes the disruption of the coiled-coil structure of the wild-type protein.<sup>[127]</sup> In the presence of the cage, the coiled-coil structure can be built, since the mutation is masked and thus silent, whereas upon





**Scheme 9.** Caged peptides used for the analysis of ribonuclease function and peptide folding. For clarity, in some of the peptides the side chains have been abbreviated with the respective one letter code for the amino acid in parentheses. Nle = Norleucine.

photolysis the  $\alpha$ -helices, responsible for coiled-coil formation, are disrupted.

Zinth et al. used a different strategy to obtain switchable cyclic peptides. They used an azobenzene moiety and introduced them into cyclic bioactive peptides consisting of eight amino acids (**32**; Scheme 9).<sup>[128]</sup> The folding kinetics of the peptides by the photoinduced isomerization were monitored by femtosecond transient absorption spectroscopy.

The group of Hilvert employed *meta*-substituted azobenzene-containing peptides **33** (Scheme 9) for the construction of photoinducible  $\beta$ -hairpins.<sup>[129]</sup> When the azobenzene derivative was in its thermodynamically stable *trans* form no distinct structure could be determined, but after photoisomerization a well defined  $\beta$ -hairpin was observed. They claimed that this approach might be useful for the photocontrol of peptide hormone activity. A similar approach was described by Gogoll et al. Instead of azobenzene they used stilbene as a photoswitchable chromophore incorporated in a  $\beta$ -hairpin peptide **34** and with circular dichroism (CD) spectroscopy they visualized the *cis* and *trans* conformation of the peptide.<sup>[130]</sup>

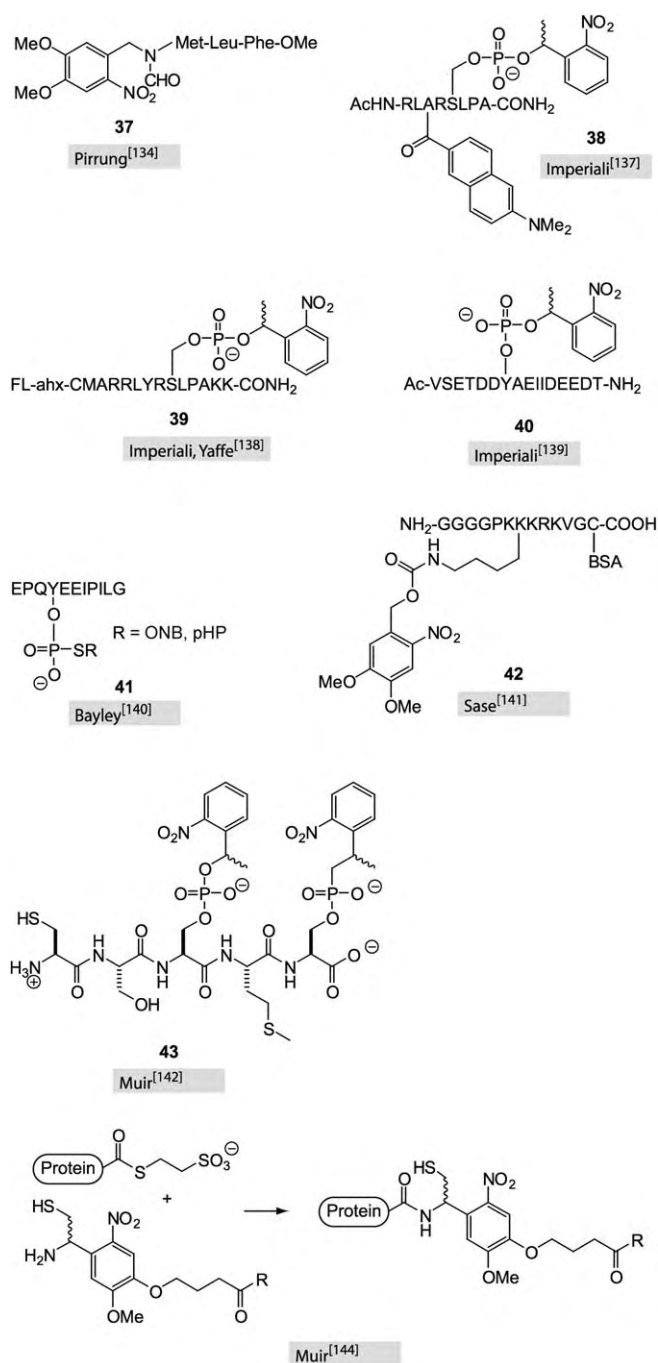
The studies of Woolley and Hamm made use of a 16 mer peptide that binds to DNA, in combination with an intramolecular azobenzene photoswitch, to analyze the formation of an  $\alpha$ -helix.<sup>[131–133]</sup> They attached the azobenzene group between two cysteine residues (**35**, **36**; Scheme 9), thus mimicking a disulfide bridge. The presence of the *cis*-isomer

of the photoswitchable group disrupts the  $\alpha$ -helix, upon photoinduced formation of the *trans*-isomer the  $\alpha$ -helix is reformed and thus DNA binding initiated.

The studies described above show that photoactivatable molecules together with controlled photolysis, can be used to investigate the folding of peptide secondary structures, such as  $\beta$ -hairpins and  $\alpha$ -helices and moreover, the control of the formation of super structures, such as coiled coils. Since the structures of peptides and proteins correlate with function, the caging technique can be also used to modulate the function of amino acid polymers.<sup>[114]</sup>

For this purpose, Pirrung et al. synthesized caged peptides that are part of the chemotactic process.<sup>[134]</sup> They derivatized a chemotactic trimer peptide at the *N*-formyl position with a nitroveratryl group (**37**, Scheme 10). This peptide can be useful to study lymphocyte movement, induced by a photo-activated increase in the concentration of an active molecule.

A different approach was followed by the group of Imperiali. They introduced NPE groups to the phosphoserine moiety of a peptide (**38**; Scheme 10).<sup>[114, 135–137]</sup> Upon flash hydrolysis the caged peptide variants were capable of releasing phosphopeptides that then mimic the phosphorylation state of a protein and thus can be used to modulate kinase signaling. In combination with fluorescent dyes, attached to proximal peptide side chains, the reported principle can be further used to monitor the binding state of phosphopeptides to the targeted protein.<sup>[137]</sup> In a step further Yaffe and



**Scheme 10.** Caged peptides and phosphopeptides used for functional characterization and for activation of signaling cascades. Ahx = amino-hexanoic acid, FL = fluorescein tag.

Imperiali used this approach for the assignment of the temporal role of 14-3-3 in G1 arrest and S-phase checkpoint function.<sup>[138]</sup> They introduced the caged peptide **39** (Scheme 10) in cells as an inactive precursor which, after uncaging, were able to sequester phosphoserine/phosphothreonine binding proteins, in a temporally controlled manner.

In an ongoing study Imperiali et al. demonstrated the feasibility of tRNA derivatized with caged serine, threonine,

or tyrosine to be useful for the incorporation of the caged amino acids into large proteins. This approach will open the door to further investigations and spatiotemporal control of large proteins.<sup>[135]</sup> Recently, they also applied the caged phosphotyrosine peptide **40** (Scheme 10) for the local analysis of focal adhesion kinase (FAK) and leading edge migration of tumor cells.<sup>[139]</sup> The uncaged peptides are able to compete with autophosphorylated FAK for its interaction with the SH2 domain of Src and phosphoinositide 3-kinase and thus interfere with downstream signaling thereby causing the arrest of cellular migration. A similar approach was reported by Bayley et al. They used thiophosphotyrosine residues in peptide sequences (**41**; Scheme 10) and derivatized them with two different thiol-reactive photolabile groups.<sup>[140]</sup> Using these peptides they explored the binding behavior to SH2 domains (which were coupled to solid resins) before and after irradiation.

Sase et al. caged a peptidic nuclear localization signal that was attached to the BSA protein (**42**; Scheme 10), and thus obtaining light-induced nuclear delocalization.<sup>[141]</sup> As expected, the caged peptide was found exclusively in the cytoplasm of HeLa cells whereas upon irradiation the translocation to the nucleus was observed. Similarly, but for the multimerization of proteins, Hahn and Muir constructed a caged Smad2-MH2/SARA-SBD protein by chemical ligation using the peptide **43** (Scheme 10).<sup>[142]</sup> After irradiation the caged protein releases the SARA-SBD moiety and thus the formation of a homotrimer is induced which then translocates into the nucleus. This approach opens an elegant way for the kinetic characterization of protein import and/or export processes of the nucleus. In an earlier study, by incorporation of both a fluorescent dye in proximity to a quenching molecule and a photoreactive release site, Muir et al. constructed Smad2 derivatives whose photoreactivity can be monitored by increasing fluorescence signals.<sup>[143]</sup> This method enables a direct correlation between fluorescence signaling and deprotection efficiency.

#### 4.5. Various Caged Proteins and Their Applications

The group of Muir used a native chemical ligation strategy to obtain photosensitive proteins hence allowing the spatiotemporal control of protein function (Scheme 10, bottom).<sup>[144]</sup> They constructed a chimeric protein, consisting of EGFP-NLS and a dipeptide containing a palmitoyl residue. Their design strategy aimed at the light-induced separation of the two components. As expected, after introduction of this chimera into living cells, fluorescence signals can be detected close to the membrane before and distributed intracellularly after irradiation. This approach allows the induced separation of two components in a spatiotemporal manner by light and the controlled localization of proteins inside cells.

The groups of Endo and Majima recently applied an artificial four-base codon to site-selectively incorporate photoreactive moieties in restriction enzymes and caspases.<sup>[116,117]</sup> By this means an inactive procaspase-3 was obtained that, similar to the endogenous activation by caspase-8, could be activated by irradiation with light.

The restriction endonuclease BamHI was derivatized in a way that allows the control of dimer formation of the protein. Therefore, a nitroveratryl or azobenzene group was attached to amino acids that reside in the dimerization region of BamHI. It was observed that the positioning of the photo-reactive moiety is important and most effective when amino acids were caged that are involved in the formation of salt bridges between the monomers. By this means it was possible to gain photocontrol over the activity of the restriction enzyme.<sup>[117]</sup>

Fournier et al. used a caged urotensin II peptide for the generation of photoswitchable vasoconstrictors. Photolysis of a caged urotensin II peptide was fast and photodependent contraction of the thoracic aorta rings could be obtained.<sup>[145]</sup> Advantageously, and as a requirement for in vivo application of the caged peptide, the cage was very stable under pharmacological conditions.

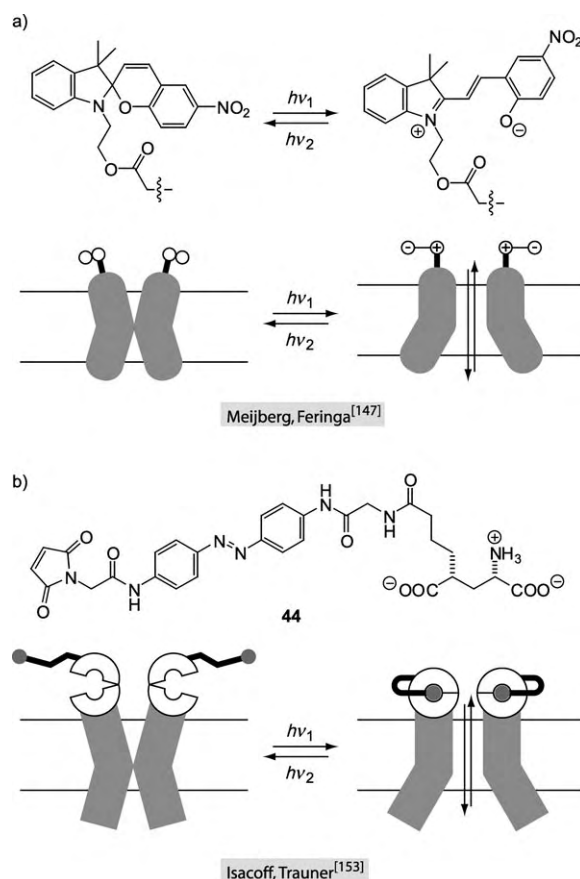
Cofilin induces the formation of protruding ends in actin filaments and cofilin activity can be regulated by the LIM-kinase. The phosphorylated cofilin is inactive and upon dephosphorylation activity can be induced. Condeelis and Lawrence et al. used a caged variant of a constitutively active mutant of cofilin, bearing a cysteine instead of a serine residue, which is inactive in the presence of the cage (CNB) and can be activated by light.<sup>[146]</sup>

A very recent study nicely demonstrated the feasibility of the light-activation approach for the analysis of channel proteins. A spiropyran-merocyanine photoswitchable mechanosensitive channel from *E. coli* was constructed and imbedded in liposomes (Scheme 11 a).<sup>[147]</sup> Upon irradiation with UV light (366 nm) the channel could be opened and closure, if desired, was obtained by repeated irradiation with visible light at wavelengths above 460 nm. This system might be useful for the light-gated delivery of bioactive molecules.

In another study the caging of an antibody (mAb), known to bind to the brain-derived neurotrophic factor (BDNF), was reported. In the study, the question addressed was whether neurotrophins are cofactors in, or the real mediators of, synaptic strengthening.<sup>[148]</sup> By applying the caging technique they were able to activate the inhibition properties of a mAb in a time-resolved manner. Activation of the mAb during induction of synaptic enhancement leads to the inhibition of endogenous BDNF and to a decrease of synaptic potential after stimulation in the CA1 region of acute hippocampal slices. This clearly indicates the role of BDNF in the manifestation of early induction of synaptic plasticity.

Jacobson et al. studied cell locomotion by using caged thymosin  $\beta$ 4 (T $\beta$ 4). T $\beta$ 4 was caged by the treatment with (*N*-nitroveratryloxy)chlorocarbamate. In vitro it could be demonstrated that the photoactivated T $\beta$ 4 inhibited actin polymerization but the caged variant did not.<sup>[149]</sup> Next, Jacobson et al. investigated the effects of locally activated T $\beta$ 4 in wing regions of locomoting keratinocytes and could observe a specific turning at the sites of photolysis. Based on these results they were able to propose a mechanistic model for the turning behavior of keratinocytes in response to T $\beta$ 4.

Bedel-Cloutour et al. investigated caged bovine haemoglobin in enzymatic assays by analyzing 2,2-azinobis(3-ethylbenzothiazoline-6-sulfonic acid) (ABTS) oxidation.<sup>[150]</sup> They



**Scheme 11.** a), b) Reversible light-controlled opening and closure of channels across lipid bilayers.

used unspecific caging with NPE groups to deactivate haemoglobin. In part, they were able to specifically recover enzymatic activity by time-dependent photolysis. However, this method led only to the reactivation of a portion of the enzyme and seems to be less efficient compared to approaches that aim at the strategic caging of distinct amino acid residues, for example, by nonsense codon-based techniques.

By using site-specific incorporation of phenylazophenylalanine the group of Sisido constructed variants of the horseradish peroxidase.<sup>[151]</sup> They constructed an on/off switchable protein derivative and as a result of their strategy they could define critical positions best suited to the caging approach.

In a different manner, Goeldner et al. used *N*-methyl-*N*-(2-nitrophenyl)carbamoyl chloride to obtain derivatized and inactivated butyrylcholinesterase (BChE).<sup>[152]</sup> This reagent was shown to be reactive towards alcohols and the corresponding caging group could be efficiently cleaved by photolysis. Subsequently, the structure of the caged BChE was solved and allowed a detailed insight into the coordination of the cage molecule and hence its structural basis for BChE inactivation.

In a very nice example Isacoff and Trauner et al. used the compound **44** (Scheme 11 b) to modify a cysteine residue in the ionotropic glutamate receptor (iGluR) and covalently

attach the receptor's cognate substrate glutamate to it. However, the *cis*- or *trans* conformation of the linker—which can be controlled by light—determines whether the triggering glutamate is actually binding to the active site or not.<sup>[153]</sup> By this means they constructed a reversibly light-gated iGluR and gained control over its activity in a time-resolved manner. The regulatory control over channel activity obtained can be useful for the study of biological phenomena and for application as a biosensor.

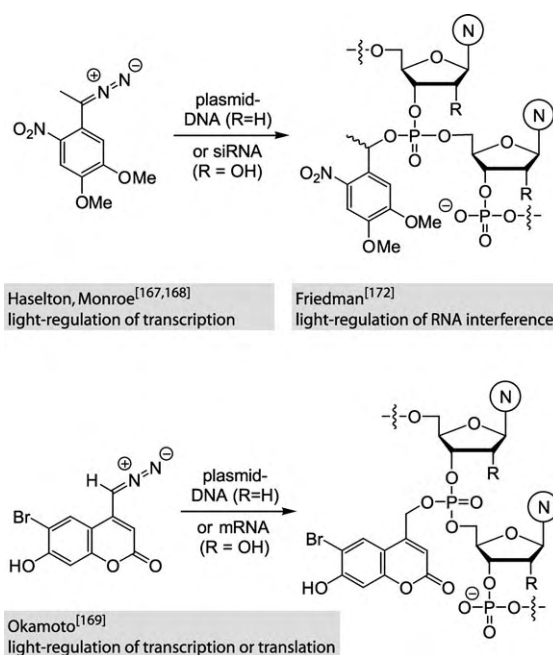
## 5. Caged and Light-Switchable Nucleic Acids

Compared to the other categories of compounds discussed so far the field of caged and light-switchable nucleic acids is a relatively new one. Apart from being a cellular information-storage device, nucleic acids offer a richness of applications, including, gene regulation (RNA interference,<sup>[154]</sup> micro-RNAs,<sup>[155]</sup> riboswitches,<sup>[156]</sup> antisense approach,<sup>[157]</sup> DNAzymes<sup>[158]</sup>), the modulation of protein function (aptamers,<sup>[159]</sup> DNA/RNA decoys<sup>[160]</sup>), molecular diagnostics (microarrays<sup>[161]</sup> or the use as catalysts<sup>[162]</sup> or structural or functional nanoscale materials.<sup>[163]</sup> To make the above-mentioned effects light-responsive, a modification of the nucleic acid components involved is not the only approach. Thus, to regulate gene expression with light, caged hormones could also be used (see Section 3). Other alternatives are the use of light-regulated plant promoter systems<sup>[164]</sup> or caging of GAL4 VP16 (a protein-based transcription activator),<sup>[165]</sup> or the use of light-dependent delivery strategies, such as the “photochemical internalization”<sup>[166]</sup> in which photosensitisers are used to facilitate endosomal release of endocytosed molecules.

One of the existing strategies for the preparation of caged nucleic acids relies on what could be called “statistical backbone caging”: In a pioneering investigation by Haselton et al. plasmid DNAs coding for luciferase or GFP were modified with Nv-groups (Scheme 12).<sup>[167]</sup> The plasmid DNA was allowed to react under benzylating conditions. Owing to the unselective nature of these conditions the plasmids were modified with caging groups with a statistical distribution of modified positions—presumably mainly backbone phosphate groups. For example, the plasmid coding for GFP was modified with approximately 270 Nv groups. The modified plasmids were introduced into either rat skin cells or HeLa cells and were transcriptionally inactive prior to activation with light. Irradiation with a laser at 355 nm induced transcription in a dose-dependent fashion. However, the full transcriptional activity could not be restored.

In a more recent publication Haselton and Monroe have studied the influence of DNA modified in this way on hybridization.<sup>[168]</sup> Using a caged 20-mer probe DNA with 14–16 Nv groups and a 30-mer molecular beacon they found out that hybridization of both partners was significantly reduced when the probe DNA was caged and that upon irradiation two to four caging groups remain, accounting for the incomplete restoration of hybridization compared to unmodified control DNA.

The same strategy of backbone caging was pursued in the group of Okamoto using Bhc-caged GFP-mRNA (ca. 30 sites



**Scheme 12.** One strategy to achieve light-dependent gene regulation is the statistical caging of backbone phosphate groups of plasmid DNA, mRNA, or siRNA. N = any nucleobase.

in a 1 kb RNA; Scheme 12).<sup>[169]</sup> Bhc-caged mRNA was injected in the one-cell stage of zebrafish embryos and turned out to be remarkably stable. The modified mRNA was almost translationally inactive prior to uncaging. Again, upon irradiation, the translational activity could be partly recovered in the irradiated part of the embryo despite the fact that mRNA injected in the one cell stage is distributed ubiquitously in the whole embryonic body. Plasmid DNA was also Bhc-caged and injected in the one-cell stage in this study and it turned out that in contrast to caged mRNA the caged DNA was not distributed evenly in all cells but rather in a mosaic fashion—but again expression was almost only observed after activation with light. Follow-up studies by the same group deal with the perfection of the preparation and handling procedures.<sup>[170]</sup> First attempts to use this method to study the brain development in zebrafish embryos have already been made.<sup>[169,171]</sup>

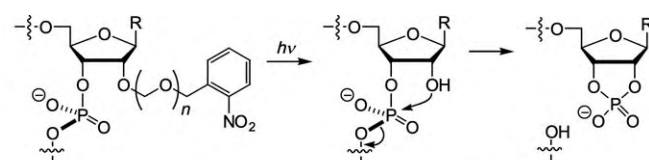
Friedman et al. have recently applied the strategy of statistical backbone phosphate caging to small interfering RNA (siRNA) (Scheme 12).<sup>[172]</sup> siRNA molecules are the key players in “RNA interference”—a very powerful and broadly applicable gene regulatory technique.<sup>[154]</sup> The double-stranded siRNA interacts with the RNA induced silencing complex (RISC) which will then degrade cellular mRNA with the same sequence as one of the siRNA strands. The rationale behind Friedman's approach is to prevent the interaction between the caged siRNA and the RISC complex. The caged siRNA in this study contained an average of 1.4 caging groups per duplex. As a model system, the silencing of GFP expression in HeLa cells was used. It turned out that the caged siRNA was not completely inactive but could be fully activated upon irradiation. An increase in the number of



caging groups made the siRNA inactive but then the full activity could no longer be restored by irradiation.

The elegance of this approach of statistical backbone caging clearly lies in its simplicity of preparation. However—at least with the modifying reactions and the caging groups used to date—a clean on/off behavior is not yet possible.

An alternative to circumvent these disadvantages is the introduction of caging groups on well-defined positions in nucleic acids, and indeed, even one year before the above-mentioned experiments by Haselton et al. MacMillan et al. used 2'-modified RNA to control the reaction of a ribozyme with light (Scheme 13).<sup>[173]</sup> Ribozymes are RNA sequences



MacMillan<sup>[173,175]</sup> ( $n = 0$ , R = adenine), Pitsch<sup>[177]</sup> ( $n = 1$ , R = cytosine)  
light-regulation of a ribozyme reaction via caged substrate

**Scheme 13.** RNA cleavage by a ribozyme has been made light-dependent by caging of the substrate RNA in the two similar approaches shown.<sup>[173,177]</sup> MacMillan et al. have used this approach to study the assembly of the spliceosome complex.<sup>[175]</sup>

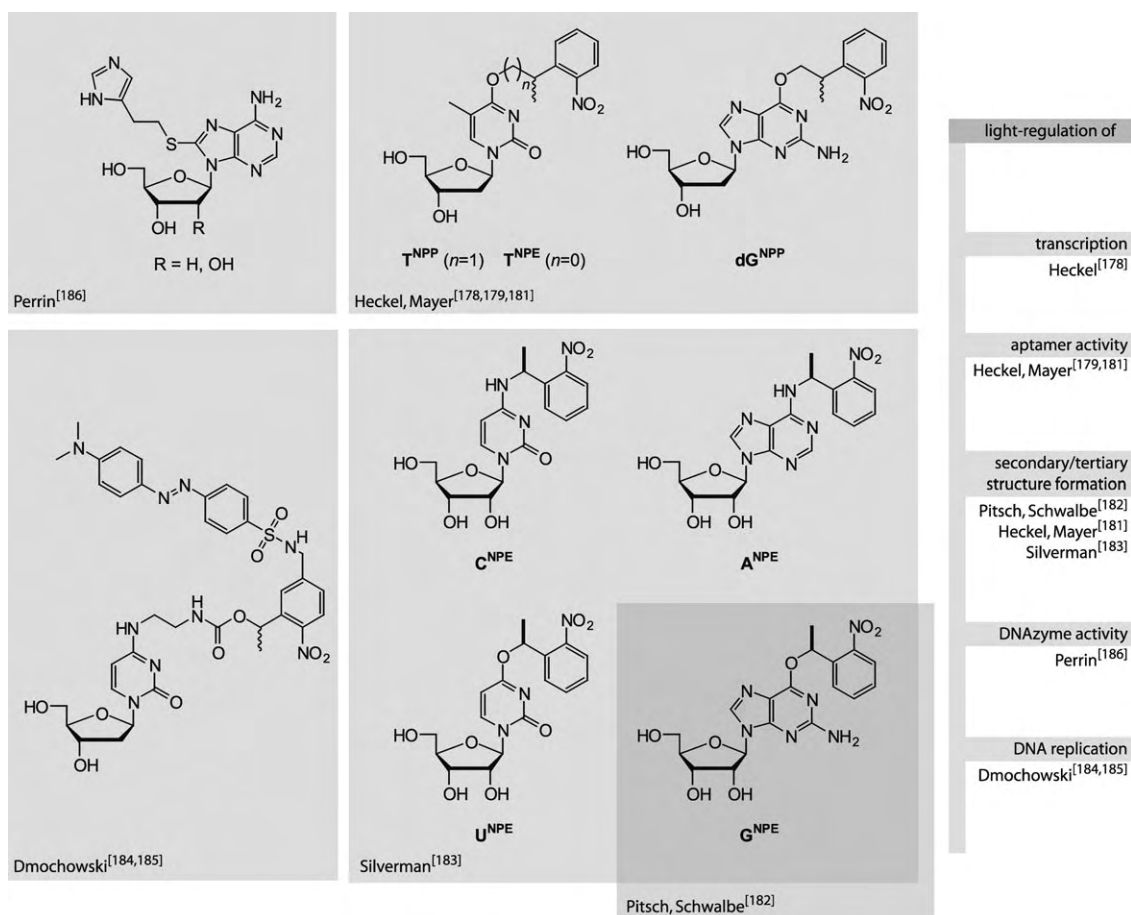
with catalytic activity.<sup>[162]</sup> In this case the so called hammer-head ribozyme was used which is able to cleave RNA.<sup>[174]</sup> To do this, it arranges the substrate RNA through base pairing in such a way that the attack of one of the 2'-OH groups in the substrate to the adjacent 3'-phosphate diester becomes favorable. Via the generation of a cyclic phosphate species, the substrate RNA strand is cleaved. Since the nucleophilic quality of this particular 2'-OH group in the substrate is important, MacMillan et al. decided to temporarily block it with a nitrobenzyl group, and indeed, the caged substrate was no longer processed by the ribozyme. Upon photolysis the caged substrate was cleaved to the same extent as unmodified substrate. In a later study MacMillan et al. used this technique for a stepwise study of the spliceosome in action.<sup>[175]</sup> The spliceosome is responsible for processing the so called pre-mRNA which is formed immediately after transcription. In doing so it removes the introns—parts of the pre-mRNA which will not leave the nucleus. However, since the spliceosome, which consists of several proteinogenic and RNA subunits, assembles only around the pre-mRNA to be processed (in an ATP-dependent stepwise fashion) its assembly can normally not be studied independently of its catalytic reaction. By caging a 2'-OH group in the substrate pre-mRNA, which is again the key nucleophile in the reaction, it was possible to introduce a breakpoint in this otherwise concerted reaction and study the assembly of the spliceosome independently.

The group of Pitsch has been studying different protecting groups for the 2'-OH group in RNA for synthetic reasons. Thus, they could demonstrate the superiority of their 2'-O-[(triisopropylsilyl)oxy]methyl (tom) protecting group strategy over the older (*tert*-butyl)dimethylsilyl (TBDMS) strategy.<sup>[176]</sup>

As one alternative to silyl protecting groups for the 2'-OH groups they also evaluated photolabile protecting groups, such as the NPEOM group<sup>[177]</sup> ([1-(2-nitrophenyl)ethoxy]-methyl; Scheme 13) and they did not fail to recognize that apart from being of synthetic interest these derivatives can also be used to make RNA light responsive. Again the test system was a ribozyme reaction, and with the caging group attached no reaction took place. After photolysis the ribozyme was fully active. In the 2'-position of RNA, the NPEOM group is a superior protecting group to the nitrobenzyl group because it is orthogonal to the silyl protecting groups for the 2'-positions of the other nucleobases. These groups are deprotected with fluoride after RNA solid-phase synthesis, and the nitrobenzyl group is also partly cleaved under these conditions.

The examples by MacMillan and Pitsch already show very nicely that by site-specific incorporation of caging groups it is possible to have a “binary” off/on-behavior before and after irradiation—albeit at the price of a somewhat higher synthetic effort—but they still leave the very nature of the nucleic acids intact: the Watson–Crick interaction capabilities. In our opinion, the nucleobases play the central role in the majority of the DNA- and RNA-based applications, simply because they carry the information which comes along with the nucleic acid. Thus, we have started our own projects to prepare caged nucleic acids. In a first study a thymidine has been modified at the O<sup>4</sup>-position with a photolabile NPP group (T<sup>NPP</sup>) and introduced in a DNA oligonucleotide (Scheme 14; top right).<sup>[178]</sup> The modified position can be seen as a temporary mismatch. It could be shown that with only one such local perturbation it was possible to prevent the T7 RNA polymerase from recognizing its cognate promoter region in duplex DNA and thus fully prevent transcription of the DNA. Upon photolysis the same amount of transcript RNA was formed as was the case for unmodified DNA. The same caged residue T<sup>NPP</sup> was then introduced in a DNA aptamer which selectively binds and inhibits thrombin, one of the key players in the blood clotting cascade.<sup>[179]</sup> DNA or RNA aptamers are single-stranded nucleic acids which are obtained by evolutionary methods and can have tailor-made properties, such as selective binding and inhibition of proteins.<sup>[180]</sup> In the aptamer the caged thymidine was no longer available for specific interaction with the thrombin even though the secondary structure, a G-quadruplex, was unharmed. The choice of the position to modify was possible because it was well-known which positions are responsible for the interaction with the target thrombin. In another study we used the caged residue dG<sup>NPP</sup> (Scheme 14, top right) to modify DNA oligonucleotides which are able to form a G-quadruplex structure.<sup>[181]</sup> With this approach it is far simpler to temporarily block otherwise active nucleic acids because, while for the determination of the exact location of the active site elaborate structural studies are necessary, it is most often easier to determine elements of secondary structure and to introduce a few cages at key locations to prevent the nucleic acid from forming its active conformation.

In a similar study, and at about the same time, Schwalbe and Pitsch used the similar G<sup>NPE</sup> residue (Scheme 14, bottom right) to determine the tertiary folding kinetics of a bistable



**Scheme 14.** Residues for the generation of nucleobase-caged nucleic acids. The resulting modified DNA or RNA has been used in the applications listed on the right side.

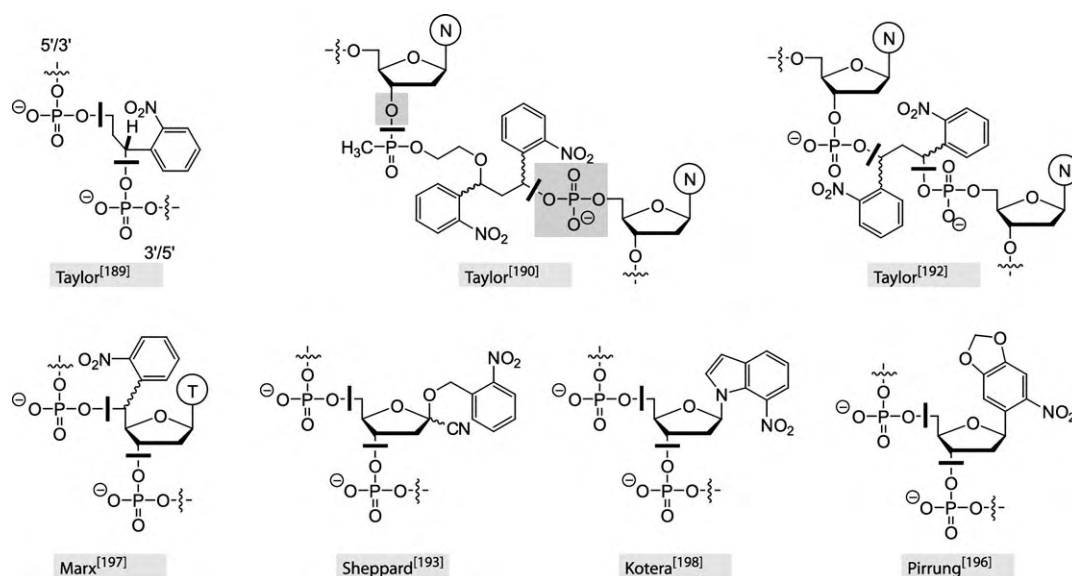
20 mer RNA sequence by NMR spectroscopy in real time.<sup>[182]</sup> This method has been further developed by Silverman et al. who were the first to come up with a complete set of caged RNA residues in which the nucleobases were each modified with NPE groups at their Watson–Crick hydrogen-bond interaction surface (Scheme 14, bottom right).<sup>[183]</sup> Again the caged residues were used to study tertiary folding in RNA.

The group of Dmochowski is also interested in nucleobase-caged nucleic acids.<sup>[184]</sup> In their approach, a cytidine residue is modified with a fluorescence quencher (DABSYL) through a photolabile, NPE-derived residue (Scheme 14, bottom left). In this case, the caging group is not only responsible for the modulation of the interaction capability of the nucleic acid but also triggers the fluorescence of an adjacent base-modified cytidine carrying a fluorescein moiety. The advantage of this system is that the result of uncaging can immediately be seen, for example, under a confocal microscope. It could be shown that this system can be used to photomodulate a primer extension reaction.<sup>[185]</sup>

The group of Perrin et al. finally used a very unconventional caged adenosine residue to photomodulate the activity of a DNase (Scheme 14, top left).<sup>[186]</sup> This study is one of the rare cases where a “traceless” cage has been used—leaving only a C–H bond after cleavage.

Interestingly, Rebek et al. had long ago prepared a caged adenosine derivative and used it for light-modulation of self-replication but they did not introduce this derivative in nucleic acids.<sup>[187]</sup>

Whereas the aim of the above-mentioned studies was to temporarily mask the activity of nucleic acids, there is quite a significant body of literature available on what was called “caged strand breaks”. The idea of introducing nicks in DNA by irradiation is not new<sup>[188]</sup> but the technique has been improved significantly, for example by the work of Taylor et al. In a very early study the *ortho*-nitrobenzene-containing residue (Scheme 15, top left) was introduced and used in phototriggered DNA hybridization.<sup>[189]</sup> Later they presented another residue (Scheme 15, top middle) which is capable of generating 3'-hydroxy- and 5'-phosphate-terminated strands after light-induced breakage which are, after a possible regrouping, available for a subsequent ligation strategy.<sup>[190]</sup> Other residues (for example Scheme 15 top left and right) give, after irradiation, phosphate groups on both the 3'- and the 5'- end.<sup>[191, 192]</sup> In the meantime, quite a number of different approaches to realize caged strand breaks have been developed (Scheme 15 gives an overview). For example, in the system introduced by Sheppard et al., after photoactivation a 2'-deoxyribonolactone is generated which can further



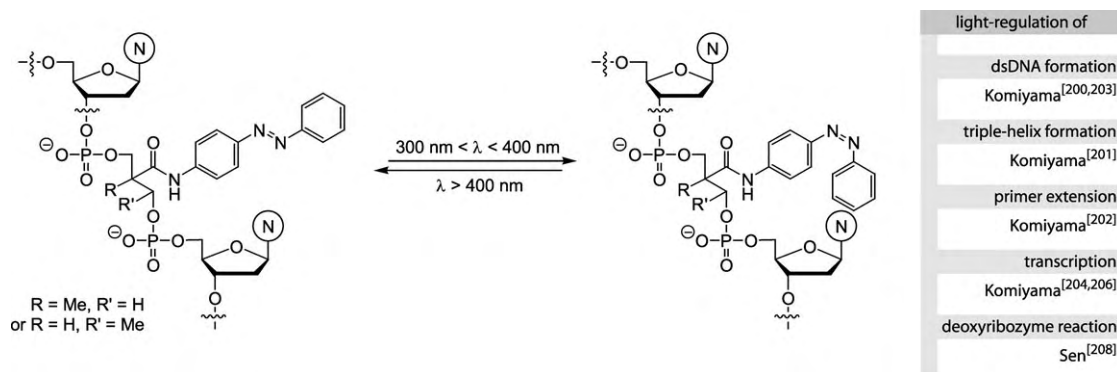
**Scheme 15.** Overview of different approaches to generate DNA strand breaks upon irradiation. Black bars indicate which bonds are finally broken (sometimes after additional treatment). The top middle strategy yields ligatable 3'-hydroxy-terminated and 5'-phosphorylated ends. N = any nucleobase.

undergo elimination.<sup>[193,194]</sup> A similar system is available for RNA abasic site generation.<sup>[195]</sup> While some systems require (partly) additional treatment after photoactivation,<sup>[196–198]</sup> others do not.

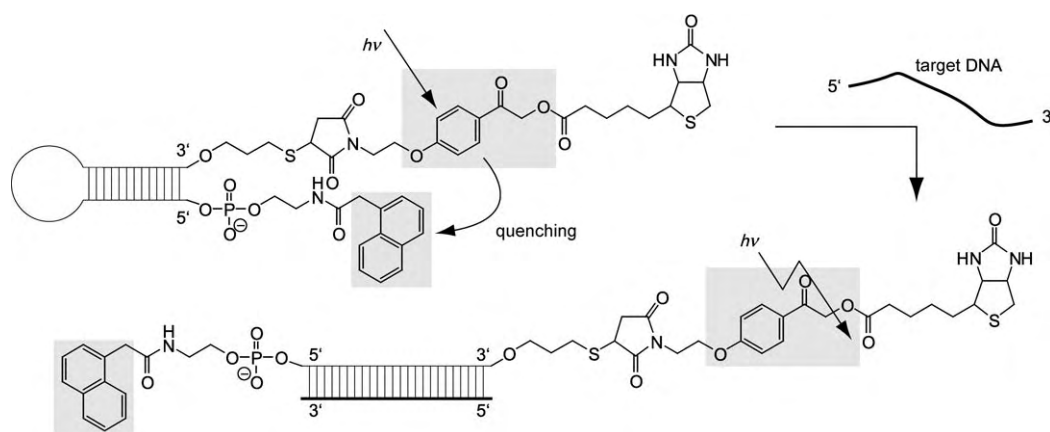
Light-induced DNA strand breakage at specific sites was also possible in a totally different approach in which caged  $\text{Mg}^{2+}$  ions (in the form of a DM-nitrophen complex, see Section 3 and Scheme 7) was used together with the restriction enzyme Sma1 (which needs  $\text{Mg}^{2+}$  ions for its cutting activity) and free ethylene diaminetetraacetate (EDTA).<sup>[199]</sup> Under a microscope, stretched-out DNA double strands were then locally irradiated, liberating a short “flash” of  $\text{Mg}^{2+}$  ions which were then again sequestered by EDTA. During this time the restriction enzyme was able to cut the DNA—but only in the irradiated area. The radius of that active region could be determined by adjustment of the EDTA concentration.

The concept of reversible photoswitches has also already been applied to nucleic acids—mostly by Komiyama et al. In a series of studies they used the azobenzene-containing replace-

ment nucleoside shown in Scheme 16.<sup>[200–206]</sup> By irradiating the *trans*-configured form of an octamer poly-dA, the melting temperature to a  $T_8$  counter strand could be reduced by 8.9 °C. By irradiation with visible light the effect was fully reversed.<sup>[200]</sup> This technique makes it possible to reversibly interfere with duplex or even triplex<sup>[201]</sup> DNA formation. Such a modified oligodeoxynucleotide can, for example, be used as a light-dependent modulator of a DNA polymerase reaction: By binding a modified oligodeoxynucleotide in the primer extension region, it was possible to stop the primer extension at its 5'-end (the T7 DNA polymerase which was used has no 5'→3' exonuclease activity).<sup>[202]</sup> Whereas the flat *trans*-azobenzene moiety is able to stack comfortably within a DNA double helix, the *cis* isomer, which is formed upon irradiation, has a helical shape and weakens the base pairing at the 5'-end of the modulator oligodeoxynucleotide so that the polymerase is able to knock off the modulator. Thus, depending on the conformational state of the modulator, either full-length or a shortened product strand was formed. Similarly, it was possible to regulate the transcription with T7 RNA



**Scheme 16.** A reversibly photoswitchable nucleotide replacement based on an azobenzene moiety. N = any nucleobase



**Scheme 17.** Example for conditional uncaging. In the absence of the modulating target DNA the quencher is close to the photolabile linker and blocks the bond-cleavage pathway.<sup>[209]</sup>

polymerase<sup>[204]</sup> or SP6 RNA polymerase<sup>[206]</sup> with light by including the azobenzene-containing residue in the double stranded promoter or TATA box region.

About at the same time as the first study by Komiyama et al. was published, Lewis et al. showed that they could trigger DNA hairpin formation with a stilbenediether-linked bisoligonucleotide conjugate.<sup>[207]</sup> More recently Sen et al. used the Komiyama method to build a light-regulatable RNA-cleaving deoxyribozyme<sup>[208]</sup> and obtained a five- to sixfold difference in the catalytic rate by irradiating with light of different wave lengths.

Two more applications are discussed in this Section even though they do not strictly deal with caged nucleic acids but rather with nucleic acids which are modified with a caging group, but it is not the nucleic acid which is released upon irradiation: Saito et al. have used the molecular beacon technique for conditional photorelease (Scheme 17).<sup>[209]</sup> For this approach, a single-stranded DNA which forms a stem-loop structure was used which was modified with a naphthalene quencher on the 5'-end and on the 3'-end with a photocleavable PHP group to which biotin, as a model for a drug, was attached. In this stem-loop state no bond cleavage takes place upon irradiation owing to the vicinity of the quencher. In the presence of a complementary DNA strand however, the stem-loop structure is opened and the quencher is moved away from the *p*-hydroxyphenacyl moiety which will now decay as usually upon irradiation—liberating the attached “drug”. In a similar study Tanabe and Nishimoto used the combination of a photocleavable *o*-nitrobenzyl linker and a naphthylamine quencher which works with light of a longer and hence less harmful wavelength.<sup>[210]</sup>

## 6. Summary and Outlook

Starting as an organic synthesis strategy the use of photolabile groups has become a valuable tool for the investigation of biological phenomena. Though the caging technique was reported 30 years ago it has gained significant impetus during the last five years. A number of recent publications describe the functional investigation of caged

biomolecules, based on peptides, proteins, and nucleic acids. Quite a few studies investigated neuronal signaling with caged effector molecules and this approach already “illuminates” the biology of receptors, ion channels, and the spatiotemporal assignment of neuronal activation sites and the following of synaptic currents. The commercial availability of caged effectors further underlines the applicability of light-activatable molecules. It will be very exciting to see how caging approach can help in the discovery of novel principles and functions of biomolecules during the next years.

Further developments of synthesis strategies, for example, the synthesis of novel caging moieties that are perfectly suited for cellular environments, and the availability of highly sophisticated analytical instrumentation enables the precise analysis of biological functions in respect to time and location. We believe that whenever synthetically and biologically motivated scientists work hand in hand rapid progress can be achieved within the field. The caging technique might develop as an invaluable approach for the elucidation of signaling cascades in a spatiotemporal manner.

Received: January 30, 2006

Published online: July 7, 2006

- [1] R. L. Edelson, *Sci. Am.* **1988**, 259, 50–57.
- [2] T. M. Dore in *Dynamic Studies in Biology* (Eds.: M. Goeldner, R. Givens), Wiley-VCH, Weinheim, **2005**, pp. 435–459.
- [3] S. M. Harper, L. C. Neil, K. H. Gardner, *Science* **2003**, 301, 1541–1544.
- [4] T. Carell, L. T. Burgdorf, L. M. Kundu, M. Cichon, *Curr. Opin. Chem. Biol.* **2001**, 5, 491–498.
- [5] K. Kloppstech, *Physiol. Plant.* **1997**, 100, 739–747.
- [6] D. A. Fancy, *Curr. Opin. Chem. Biol.* **2000**, 4, 28–33.
- [7] a) T. J. Trout, J. J. Schmieg, W. J. Gambogi, A. M. Weber, *Adv. Mater.* **1998**, 10, 1219–1224; b) A. Lendlein, H. Jiang, O. Jünger, R. Langer, *Nature* **2005**, 434, 879–882; c) Y. Yu, M. Nakano, T. Ikeda, *Nature* **2003**, 425, 145.
- [8] J. H. Kaplan, B. Forbush III, J. F. Hoffman, *Biochemistry* **1978**, 17, 1929–1935.
- [9] For this review several keyword searches had to be made resulting in over 20000 hits which had to be manually sorted according to certain criteria. Even though great care has been



taken in doing this, we cannot guarantee that we did not miss certain papers.

- [10] Furthermore, the term “caged” can only be very poorly translated to German. However, this will probably—if at all—only bother German scientists.
- [11] R. S. Givens, J. F. W. Weber, A. H. Jung, C.-H. Park, *Methods Enzymol.* **1998**, *291*, 1–29.
- [12] A. P. Pelliccioli, J. Wirz, *Photochem. Photobiol. Sci.* **2002**, *1*, 441–458.
- [13] J. Engels, E.-J. Schlaeger, *J. Med. Chem.* **1977**, *20*, 907–911.
- [14] It shall not remain unnoted that the paper by Engels et al.<sup>[13]</sup> has been correctly quoted in the paper by Hoffman et al.<sup>[12]</sup>
- [15] See for example the following review article: V. N. R. Pillai, *Synthesis* **1980**, 1–26.
- [16] B. Forbush III, *Proc. Natl. Acad. Sci. USA* **1984**, *81*, 5310–5314.
- [17] See for example <http://www.molecularprobes.com>.
- [18] K. Martinek, S. D. Varfolomeyev, I. V. Berezin, *Eur. J. Biochem.* **1971**, *19*, 242–249.
- [19] See, for example, the following review article: K. Martinek, I. V. Berezin, *Photochem. Photobiol.* **1979**, *29*, 637–649.
- [20] K. Kuan, Y. Y. Lee, L. Tebbetts, P. Melius, *Biotechnol. Bioeng.* **1979**, *21*, 443–459.
- [21] D. H. Hug, P. S. O'Donnell, J. K. Hunter, *Photochem. Photobiol.* **1980**, *32*, 841–848.
- [22] M. Aizawa, K. Namba, S. Suzuki, *Arch. Biochem. Biophys.* **1977**, *180*, 41–48.
- [23] M. Goeldner, R. Givens, *Dynamic Studies in Biology*, Wiley-VCH, Weinheim, **2005**.
- [24] G. Marriott, *Methods in Enzymology*, Vol. 291, Academic Press, San Diego, **1998**.
- [25] H. Morrison, *Bioorganic Photochemistry*, Vol. 2, Wiley, New York, **1993**; S. R. Adams, R. Y. Tsien, *Annu. Rev. Physiol.* **1993**, *55*, 755–784.
- [26] For reviews about photolabile groups see also the review articles mentioned above.<sup>[12,23–25]</sup>
- [27] J. E. T. Corrie, A. Barth, V. R. N. Munasinghe, D. R. Trentham, M. C. Hutter, *J. Am. Chem. Soc.* **2003**, *125*, 8546–8554.
- [28] S. R. Adams, J. P. Y. J. Kao, R. Y. Tsien, *J. Am. Chem. Soc.* **1989**, *111*, 7957–7968.
- [29] A. Blanc, C. G. Bochet, *J. Org. Chem.* **2003**, *68*, 1138–1141.
- [30] M. C. Pirrung, Y. R. Lee, K. Park, J. B. Springer, *J. Org. Chem.* **1999**, *64*, 5042–5047.
- [31] A. Momotake, N. Lindegger, E. Niggli, R. J. Barsotti, G. C. R. Ellis-Davies, *Nat. Methods* **2006**, *3*, 35–40.
- [32] S. Walbert, W. Pfleiderer, U. E. Steiner, *Helv. Chim. Acta* **2001**, *84*, 1601–1611.
- [33] a) T. Furuta, M. Iwamura, *Methods Enzymol.* **1998**, *291*, 50–63; b) T. Furuta, S. S. H. Wang, J. L. Dantzker, T. M. Dore, W. J. Bybee, E. M. Callaway, W. Denk, R. Y. Tsien, *Proc. Natl. Acad. Sci. USA* **1999**, *96*, 1193–1200; c) A. Z. Suzuki, T. Watanabe, M. Kawamoto, K. Nishiyama, H. Yamashita, M. Ishii, M. Iwamura, T. Furuta, *Org. Lett.* **2003**, *5*, 4867–4870.
- [34] V. Hagen, S. Frings, B. Wiesner, S. Helm, U. B. Kaupp, J. Bendig, *ChemBioChem* **2003**, *4*, 434–442.
- [35] M. Lu, O. D. Fedoryak, B. R. Moister, T. M. Dore, *Org. Lett.* **2003**, *5*, 2119–2122.
- [36] O. D. Fedoryak, T. M. Dore, *Org. Lett.* **2002**, *4*, 3419–3422.
- [37] a) C.-H. Park, R. S. Givens, *J. Am. Chem. Soc.* **1997**, *119*, 2453–2463; b) K. Zhang, J. E. T. Corrie, V. R. N. Munasinghe, P. Wan, *J. Am. Chem. Soc.* **1999**, *121*, 5625–5632; c) P. G. Conrad II, R. S. Givens, J. F. Weber, K. Kandler, *Org. Lett.* **2000**, *2*, 1545–1547.
- [38] M. Lukeman, J. C. Scaiano, *J. Am. Chem. Soc.* **2005**, *127*, 7698–7699.
- [39] A. Banerjee, C. Grever, L. Ramakrishnan, J. Jäger, A. Gameiro, H.-G. A. Breitingner, K. R. Gee, B. K. Carpenter, G. P. Hess, *J. Org. Chem.* **2003**, *68*, 8361–8367.
- [40] W. N. Atemnkeng, L. D. Louisiana II, P. K. Yong, B. Vottero, A. Banerjee, *Org. Lett.* **2003**, *5*, 4469–4471.
- [41] M. P. Coleman, M. K. Boyd, *J. Org. Chem.* **2002**, *67*, 7641–7648.
- [42] T. Furuta, Y. Hirayama, M. Iwamura, *Org. Lett.* **2001**, *3*, 1809–1812.
- [43] G. Papageorgiou, A. Barth, J. E. T. Corrie, *Photochem. Photobiol. Sci.* **2005**, *4*, 216–220.
- [44] J. Pika, A. Konosonoks, R. M. Robinson, P. N. D. Singh, A. D. Gudmundsdottir, *J. Org. Chem.* **2003**, *68*, 1964–1972.
- [45] T. Furuta, H. Torigai, M. Sugimoto, M. Iwamura, *J. Org. Chem.* **1995**, *60*, 3953–3956.
- [46] A. K. Singh, P. K. Khade, *Bioconjugate Chem.* **2002**, *13*, 1286–1291.
- [47] a) P. Klán, A. P. Pelliccioli, T. Pospíšil, J. Wirz, *Photochem. Photobiol. Sci.* **2002**, *1*, 920–923; b) P. Klán, M. Zabadal, D. Heger, *Org. Lett.* **2000**, *2*, 1569–1571.
- [48] C. C. Ma, M. G. Steinmetz, Q. Cheng, V. Jayaraman, *Org. Lett.* **2003**, *5*, 71–74.
- [49] J. A. Delaire, K. Nakatani, *Chem. Rev.* **2000**, *100*, 1817–1846.
- [50] G. Berkovic, V. Krongauz, V. Weiss, *Chem. Rev.* **2000**, *100*, 1741–1753.
- [51] M. Irie, *Chem. Rev.* **2000**, *100*, 1685–1716.
- [52] Y. Yokoyama, *Chem. Rev.* **2000**, *100*, 1717–1739.
- [53] B. L. Feringa, R. A. van Delden, N. Koumura, E. M. Geertsema, *Chem. Rev.* **2000**, *100*, 1789–1816.
- [54] G. Dormán, G. D. Prestwich, *Trends Biotechnol.* **2000**, *18*, 64–77.
- [55] a) O. Srinivas, N. Mitra, A. Surolia, N. Jayaraman, *Glycobiology* **2005**, *15*, 861–873; b) O. Srinivas, N. Mitra, A. Surolia, N. Jayaraman, *J. Am. Chem. Soc.* **2002**, *124*, 2124–2125; c) T. A. Kale, C. Raab, N. Yu, D. C. Dean, M. D. Distefano, *J. Am. Chem. Soc.* **2001**, *123*, 4373–4381; d) J. Juodaityte, N. Sewald, *J. Biotechnol.* **2004**, *112*, 127–138.
- [56] E. M. Callaway, R. Yuste, *Curr. Opin. Neurobiol.* **2002**, *12*, 587–592.
- [57] E. Korkotian, D. Oron, Y. Silberberg, M. Segal, *J. Neurosci. Methods* **2004**, *133*, 153–159.
- [58] W. Maier, J. E. T. Corrie, G. Papageorgiou, B. Laube, C. Grever, *J. Neurosci. Methods* **2005**, *142*, 1–9.
- [59] L.-R. Shao, F. E. Dudek, *J. Neurophysiol.* **2004**, *93*, 3007–3011.
- [60] M. Canepari, L. Nelson, G. Papageorgiou, J. E. T. Corrie, D. Ogden, *J. Neurosci. Methods* **2001**, *112*, 29–42.
- [61] a) Q. Cheng, M. G. Steinmetz, V. Jayaraman, *J. Am. Chem. Soc.* **2002**, *124*, 7676–7677; b) R. Wieboldt, K. R. Gee, L. Niu, D. Ramesh, B. K. Carpenter, G. P. Hess, *Proc. Natl. Acad. Sci. USA* **1994**, *91*, 8752–8756.
- [62] a) G. Li, L. Niu, *J. Biol. Chem.* **2004**, *279*, 3990–3997; b) G. Li, Z. Y. Sheng, Z. Huang, L. Niu, *Biochemistry* **2005**, *44*, 5835–5841; c) G. Li, W. M. Pei, L. Niu, *Biochemistry* **2003**, *42*, 12358–12366; d) G. Li, R. E. Oswald, L. Niu, *Biochemistry* **2003**, *42*, 12367–12375.
- [63] a) G. Papageorgiou, D. C. Ogden, A. Barth, J. E. T. Corrie, *J. Am. Chem. Soc.* **1999**, *121*, 6503–6504; b) G. Papageorgiou, J. E. T. Corrie, *Synth. Commun.* **2002**, *32*, 1571–1577; c) G. Papageorgiou, M. Lukeman, P. Wan, J. E. T. Corrie, *Photochem. Photobiol. Sci.* **2004**, *3*, 366–373; d) G. Papageorgiou, D. Ogden, J. E. T. Corrie, *J. Org. Chem.* **2004**, *69*, 7228–7233; e) M. Canepari, G. Papageorgiou, J. E. T. Corrie, C. Watkins, D. Ogden, *J. Physiol.* **2001**, *533*, 765–772.
- [64] G. Lowe, *J. Neurophysiol.* **2003**, *90*, 1737–1746.
- [65] M. A. Smith, G. C. R. Ellis-Davies, J. C. Magee, *J. Physiol.* **2003**, *548*, 245–258.
- [66] J. J. Chambers, H. Gouda, D. M. Young, I. D. Kuntz, P. M. England, *J. Am. Chem. Soc.* **2004**, *126*, 13886–13887.
- [67] G. Brasnjo, T. S. Otis, *Proc. Natl. Acad. Sci. USA* **2004**, *101*, 6273–6278.

- [68] C. Grewer, N. Watzke, M. Wiessner, T. Rauen, *Proc. Natl. Acad. Sci. USA* **2000**, 97, 9706–9711.
- [69] a) K. Takaoka, Y. Tatsu, N. Yumoto, T. Nakajima, K. Shimamoto, *Bioorg. Med. Chem. Lett.* **2003**, 13, 965–970; b) K. Takaoka, Y. Tatsu, N. Yumoto, T. Nakajima, K. Shimamoto, *Bioorg. Med. Chem.* **2004**, 12, 3687–3694.
- [70] V. Jayaraman, S. Thiran, D. R. Madden, *FEBS Lett.* **2000**, 475, 278–282.
- [71] P. Molnár, J. V. Nadler, *Eur. J. Pharmacol.* **2000**, 391, 255–262.
- [72] H.-G. A. Breiting, R. Wieboldt, D. Ramesh, B. K. Carpenter, G. P. Hess, *Biochemistry* **2000**, 39, 5500–5508.
- [73] T. H. Lee, K. R. Gee, C. Davidson, E. H. Ellinwood, *Neuroscience* **2002**, 112, 647–654.
- [74] W. Y. Lin, C. Albanese, R. G. Pestell, D. S. Lawrence, *Chem. Biol.* **2002**, 9, 1347–1353.
- [75] F. G. Cruz, J. T. Koh, K. H. Link, *J. Am. Chem. Soc.* **2000**, 122, 8777–8778.
- [76] Y. H. Shi, J. T. Koh, *ChemBioChem* **2004**, 5, 788–796.
- [77] K. H. Link, Y. H. Shi, J. T. Koh, *J. Am. Chem. Soc.* **2005**, 127, 13088–13089.
- [78] K. H. Link, F. G. Cruz, H.-F. Ye, K. E. O'Reilly, S. Dowdell, J. T. Koh, *Bioorg. Med. Chem.* **2004**, 12, 5949–5959.
- [79] M. Goard, G. Aakalu, O. D. Fedoryak, C. Quinonez, J. St. Julien, S. J. Poteet, E. M. Schuman, T. M. Dore, *Chem. Biol.* **2005**, 12, 685–693.
- [80] Y. Hirayama, M. Iwamura, T. Furuta, *Bioorg. Med. Chem. Lett.* **2003**, 13, 905–908.
- [81] a) S. Yagai, T. Karatsu, A. Kitamura, *Chem. Eur. J.* **2005**, 11, 4054–4063; b) J. Q. Jiang, X. Tong, Y. Zhao, *J. Am. Chem. Soc.* **2005**, 127, 8290–8291; c) D. F. O'Brien, D. A. Tirrell in *Bioorganic Photochemistry*, Vol. 2 (Ed.: H. Morrison), Wiley, New York, **1993**, pp. 111–167; d) S. Watanabe, R. Hiratsuka, Y. Kasai, K. Munakata, Y. Takahashi, M. Iwamura, *Tetrahedron* **2002**, 58, 1685–1691; e) P. Shum, J.-M. Kim, D. H. Thompson, *Adv. Drug Delivery Rev.* **2001**, 53, 273–284; f) R. H. Bisby, C. Mead, C. C. Morgan, *Biochem. Biophys. Res. Commun.* **2000**, 276, 169–173.
- [82] a) J. C. Cruz, M. Thomas, E. Wong, N. Ohgami, S. Sugii, T. Curphey, C. C. Y. Chang, T.-Y. Chang, *J. Lipid Res.* **2002**, 43, 1341–1347; b) A. Specht, M. Goeldner, J. Wirz, L. Peng, *Synlett* **1999**, 981–983; c) E. A. Mintzer, B.-L. Waarts, J. Wilschut, R. Bittman, *FEBS Lett.* **2002**, 510, 181–184.
- [83] a) C. Thiele, M. J. Hannah, F. Fahrenholz, W. B. Huttner, *Nat. Cell Biol.* **2000**, 2, 42–49; b) V. Matyash, C. Geier, A. Henske, S. Mukherjee, D. Hirsh, C. Thiele, B. Grant, F. R. Maxfield, T. V. Kurzchalia, *Mol. Biol. Cell* **2001**, 12, 1725–1736.
- [84] M. Simons, E.-M. Krämer, C. Thiele, W. Stoffel, J. Trotter, *J. Cell Biol.* **2000**, 151, 143–153.
- [85] I. M. Bennett, H. M. V. Farfano, F. Bogani, A. Primak, P. A. Liddell, L. Otero, L. Sereno, J. J. Silber, A. L. Moore, T. A. Moore, D. Gust, *Nature* **2002**, 420, 398–401.
- [86] D. H. Thompson, *Nat. Mater.* **2002**, 1, 214–215.
- [87] S. R. Adams, J. P. Y. Kao, G. Gryniewicz, A. Minta, R. Y. Tsien, *J. Am. Chem. Soc.* **1988**, 110, 3212–3220.
- [88] F. DelPrincipe, M. Egger, G. C. Ellis-Davies, E. Niggli, *Cell Calcium* **1999**, 25, 85–91.
- [89] J. H. Kaplan, G. C. Ellis-Davies, *Proc. Natl. Acad. Sci. USA* **1988**, 85, 6571–6575.
- [90] G. C. Ellis-Davies, J. H. Kaplan, *Proc. Natl. Acad. Sci. USA* **1994**, 91, 187–191.
- [91] H. J. Montgomery, B. Perdicakis, D. Fishlock, G. A. Lajoie, E. Jervis, J. G. Guillemette, *Bioorg. Med. Chem.* **2002**, 10, 1919–1927.
- [92] B. Perdicakis, H. J. Montgomery, G. L. Abbott, D. Fishlock, G. A. Lajoie, J. G. Guillemette, E. Jervis, *Bioorg. Med. Chem.* **2005**, 13, 47–57.
- [93] L. R. Makings, R. Y. Tsien, *J. Biol. Chem.* **1994**, 269, 6282–6285.
- [94] K. P. Yip, *Am. J. Physiol. Regul. Integr. Comp. Physiol.* **2005**, 289, R620–R626.
- [95] J. Pollock, J. H. Crawford, J. F. Wootton, J. E. T. Corrie, R. H. Scott, *Neurosci. Lett.* **2003**, 338, 143–146.
- [96] S. Munck, P. Bedner, T. Bottaro, H. Harz, *Eur. J. Neurosci.* **2004**, 19, 791–797.
- [97] H. Yoshimura, N. Kato, *J. Physiol.* **2000**, 522, 417–426.
- [98] H. Takeuchi, T. Kurahashi, *J. Gen. Physiol.* **2003**, 122, 557–567.
- [99] L. Lagostena, A. Menini, *Chem. Senses* **2003**, 28, 705–716.
- [100] a) V. Hagen, C. Dzeja, S. Frings, J. Bendig, E. Krause, U. B. Kaupp, *Biochemistry* **1996**, 35, 7762–7771; b) V. Hagen, S. Frings, J. Bendig, D. Lorenz, B. Wiesner, U. B. Kaupp, *Angew. Chem.* **2002**, 114, 3775–3777; *Angew. Chem. Int. Ed.* **2002**, 41, 3625–3628; c) V. Hagen, J. Bendig, S. Frings, T. Eckardt, S. Helm, D. Reuter, U. B. Kaupp, *Angew. Chem.* **2001**, 113, 1077–1080; *Angew. Chem. Int. Ed.* **2001**, 40, 1045–1048; d) V. Hagen, J. Bendig, S. Frings, B. Wiesner, B. Schade, S. Helm, D. Lorenz, U. B. Kaupp, *J. Photochem. Photobiol. B* **1999**, 53, 91–102; e) L. J. Wang, J. E. T. Corrie, J. F. Wootton, *J. Org. Chem.* **2002**, 67, 3474–3478; f) T. Furuta, H. Takeuchi, M. Isozaki, Y. Takahashi, M. Kanehara, M. Sugimoto, T. Watanabe, K. Noguchi, T. M. Dore, T. Kurahashi, M. Iwamura, R. Y. Tsien, *ChemBioChem* **2004**, 5, 1119–1128.
- [101] J. W. Walker, A. V. Somlyo, Y. E. Goldman, A. P. Somlyo, D. R. Trentham, *Nature* **1987**, 327, 249–252.
- [102] J. Gjerstad, E. C. Valen, D. Trotter, K. Døving, *Neuroscience* **2003**, 119, 193–200.
- [103] C. Dinkel, C. Schultz, *Tetrahedron Lett.* **2003**, 44, 1157–1159.
- [104] J. A. Chen, G. D. Prestwich, *Tetrahedron Lett.* **1997**, 38, 969–972.
- [105] F. Lemtiri-Chlieh, E. A. C. MacRobbie, A. A. R. Webb, N. F. Manison, C. Brownlee, J. N. Skepper, J. Chen, G. D. Prestwich, C. A. Brearley, *Proc. Natl. Acad. Sci. USA* **2003**, 100, 10091–10095.
- [106] R. H. Scott, J. Pollock, A. Ayar, N. M. Thatcher, U. Zehavi, *Methods Enzymol.* **2000**, 312, 387–400.
- [107] X. Q. Lu, S. Cseh, H.-S. Byun, G. Tigyi, R. Bittman, *J. Org. Chem.* **2003**, 68, 7046–7050.
- [108] J. L. Carr, K. N. Wease, M. P. Van Ryssen, S. Paterson, B. Agate, K. A. Gallagher, C. T. A. Brown, R. H. Scott, S. J. Conway, *Bioorg. Med. Chem. Lett.* **2006**, 16, 208–212.
- [109] J. Goedhart, T. W. J. Gadella, Jr., *Biochemistry* **2004**, 43, 4263–4271.
- [110] C. P. Salerno, D. Magde, A. P. Patron, *J. Org. Chem.* **2000**, 65, 3971–3981.
- [111] C. P. Salerno, M. Resat, D. Magde, J. Kraut, *J. Am. Chem. Soc.* **1997**, 119, 3403–3404.
- [112] a) C. Allin, M. R. Ahmadian, A. Wittinghofer, K. Gerwert, *Proc. Natl. Acad. Sci. USA* **2001**, 98, 7754–7759; b) C. Allin, K. Gerwert, *Biochemistry* **2001**, 40, 3037–3046.
- [113] R. O. Schönleber, J. Bendig, V. Hagen, B. Giese, *Bioorg. Med. Chem.* **2002**, 10, 97–101.
- [114] D. M. Rothman, M. D. Shults, B. Imperiali, *Trends Cell Biol.* **2005**, 15, 502–510.
- [115] a) N. Wu, A. Deiters, T. A. Cropp, D. King, P. G. Schultz, *J. Am. Chem. Soc.* **2004**, 126, 14306–14307; b) L. Wang, P. G. Schultz, *Angew. Chem.* **2005**, 117, 34–68; *Angew. Chem. Int. Ed.* **2005**, 44, 34–66.
- [116] M. Endo, K. Nakayama, Y. Kaida, T. Majima, *Angew. Chem.* **2004**, 116, 5761–5763; *Angew. Chem. Int. Ed.* **2004**, 43, 5643–5645.
- [117] a) M. Endo, K. Nakayama, T. Majima, *J. Org. Chem.* **2004**, 69, 4292–4298; b) K. Nakayama, M. Endo, T. Majima, *Chem. Commun.* **2004**, 2386–2387.

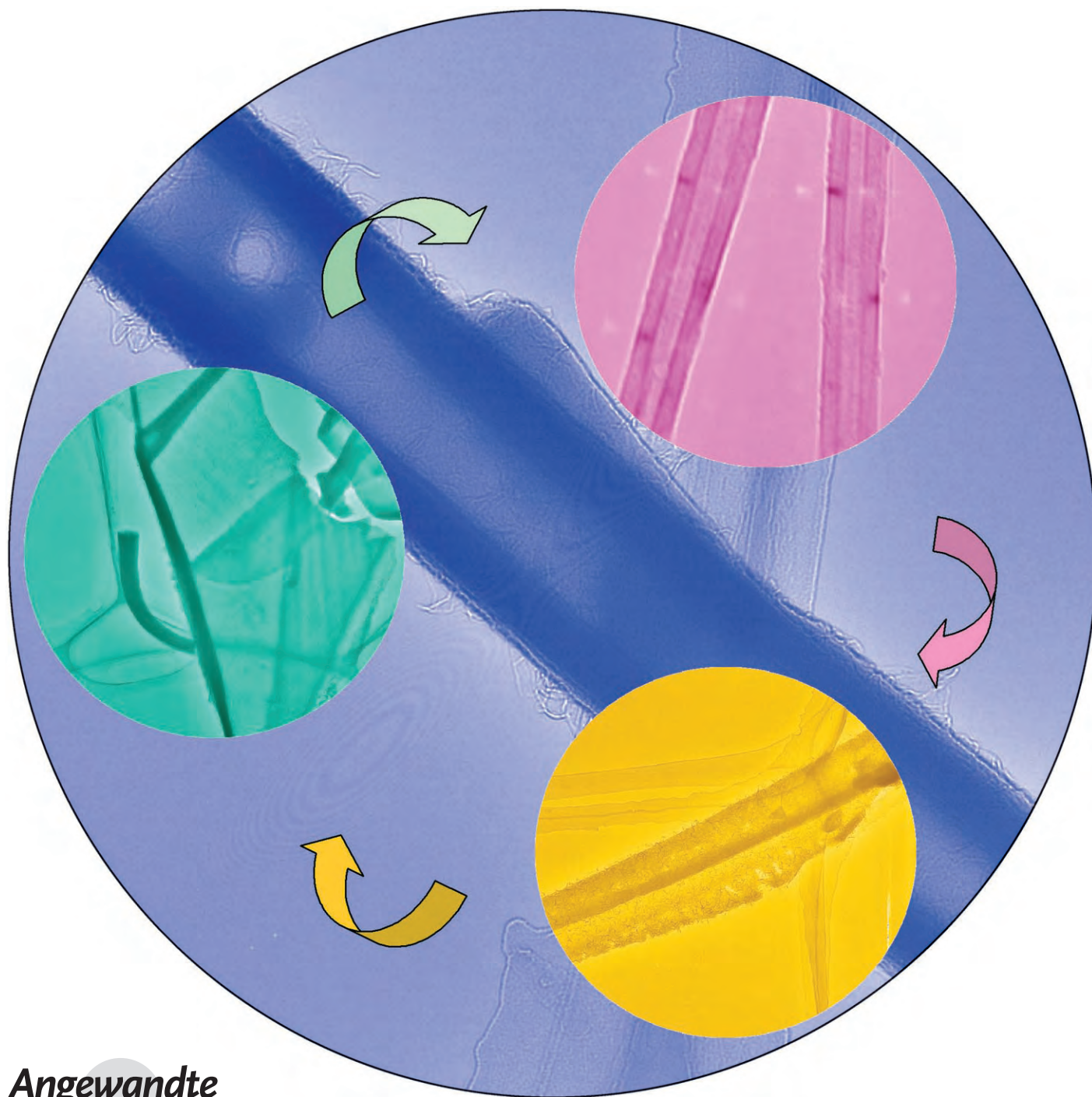
- [118] C.-Y. Chang, T. Fernandez, R. Panchal, H. Bayley, *J. Am. Chem. Soc.* **1998**, *120*, 7661–7662.
- [119] K. Y. Zou, S. Cheley, R. S. Givens, H. Bayley, *J. Am. Chem. Soc.* **2002**, *124*, 8220–8229.
- [120] T. Hiraoka, I. Hamachi, *Bioorg. Med. Chem. Lett.* **2003**, *13*, 13–15.
- [121] I. Hamachi, T. Hiraoka, Y. Yamada, S. Shinkai, *Chem. Lett.* **1998**, 537–538.
- [122] D. A. James, D. C. Burns, G. A. Woolley, *Protein Eng.* **2001**, *14*, 983–991.
- [123] Y. Tong, G. S. Brandt, M. Li, G. Shapovalov, E. Slimko, A. Karschin, D. A. Dougherty, H. A. Lester, *J. Gen. Physiol.* **2001**, *117*, 103–118.
- [124] a) J. C. Miller, S. K. Silverman, P. M. England, D. A. Dougherty, H. A. Lester, *Neuron* **1998**, *20*, 619–624; b) K. D. Phillips, J. P. Gallivan, G. S. Brandt, D. A. Dougherty, H. A. Lester, *Am. J. Physiol. Cell Physiol.* **2001**, *281*, C195–206.
- [125] M. Banghart, K. Borges, E. Isacoff, D. Trauner, R. H. Kramer, *Nat. Neurosci.* **2004**, *7*, 1381–1386.
- [126] a) G. A. Woolley, *Acc. Chem. Res.* **2005**, *38*, 486–493; b) C. Renner, U. Kusebauch, M. Lowenack, A. G. Milbradt, L. Moroder, *J. Pept. Res.* **2005**, *65*, 4–14.
- [127] R. S. Rock, K. C. Hansen, R. W. Larsen, S. I. Chan, *Chem. Phys.* **2004**, *307*, 201–208.
- [128] H. Satzger, C. Root, C. Renner, R. Behrendt, L. Moroder, J. Wachtveitl, W. Zinth, *Chem. Phys. Lett.* **2004**, *396*, 191–197.
- [129] A. Aemissegger, V. Kräutler, W. F. van Gunsteren, D. Hilvert, *J. Am. Chem. Soc.* **2005**, *127*, 2929–2936.
- [130] M. Erdélyi, A. Karlén, A. Gogoll, *Chem. Eur. J.* **2006**, *12*, 403–412.
- [131] J. Bredenbeck, J. Helbing, J. R. Kumita, G. A. Woolley, P. Hamm, *Proc. Natl. Acad. Sci. USA* **2005**, *102*, 2379–2384.
- [132] V. Borisenko, G. A. Woolley, *J. Photochem. Photobiol. A* **2005**, *173*, 21–28.
- [133] L. Guerrero, O. S. Smart, G. A. Woolley, R. K. Allemann, *J. Am. Chem. Soc.* **2005**, *127*, 15624–15629.
- [134] M. C. Pirrung, S. J. Drabik, J. Ahamed, H. Ali, *Bioconjugate Chem.* **2000**, *11*, 679–681.
- [135] D. M. Rothman, E. J. Petersson, M. E. Vázquez, G. S. Brandt, D. A. Dougherty, B. Imperiali, *J. Am. Chem. Soc.* **2005**, *127*, 846–847.
- [136] a) D. M. Rothman, E. M. Vázquez, E. M. Vogel, B. Imperiali, *Org. Lett.* **2002**, *4*, 2865–2868; b) D. M. Rothman, M. E. Vázquez, E. M. Vogel, B. Imperiali, *J. Org. Chem.* **2003**, *68*, 6795–6798.
- [137] M. E. Vázquez, M. Nitz, J. Stehn, M. B. Yaffe, B. Imperiali, *J. Am. Chem. Soc.* **2003**, *125*, 10150–10151.
- [138] A. Nguyen, D. M. Rothman, J. Stehn, B. Imperiali, M. B. Yaffe, *Nat. Biotechnol.* **2004**, *22*, 993–1000.
- [139] D. Humphrey, Z. Rajfur, M. E. Vázquez, D. Scheswohl, M. D. Schaller, K. Jacobson, B. Imperiali, *J. Biol. Chem.* **2005**, *280*, 22091–22101.
- [140] K. Y. Zou, W. T. Miller, R. S. Givens, H. Bayley, *Angew. Chem.* **2001**, *113*, 3139–3141; *Angew. Chem. Int. Ed.* **2001**, *40*, 3049–3051.
- [141] Y. Watai, I. Sase, H. Shiono, Y. Nakano, *FEBS Lett.* **2001**, *488*, 39–44.
- [142] M. E. Hahn, T. W. Muir, *Angew. Chem.* **2004**, *116*, 5924–5927; *Angew. Chem. Int. Ed.* **2004**, *43*, 5800–5803.
- [143] J.-P. Pellois, M. E. Hahn, T. W. Muir, *J. Am. Chem. Soc.* **2004**, *126*, 7170–7171.
- [144] J. P. Pellois, T. W. Muir, *Angew. Chem.* **2005**, *117*, 5859–5863; *Angew. Chem. Int. Ed.* **2005**, *44*, 5713–5717.
- [145] S. Bourgault, M. Létourneau, A. Fournier, *Peptides* **2005**, *26*, 1475–1480.
- [146] M. Ghosh, I. Ichetovkin, X. Song, J. S. Condeelis, D. S. Lawrence, *J. Am. Chem. Soc.* **2002**, *124*, 2440–2441.
- [147] A. Koçer, M. Walko, W. Meijberg, B. L. Feringa, *Science* **2005**, *309*, 755–758.
- [148] A. H. Kossel, S. B. Cambridge, U. Wagner, T. Bonhoeffer, *Proc. Natl. Acad. Sci. USA* **2001**, *98*, 14702–14707.
- [149] P. Roy, Z. Rajfur, D. Jones, G. Marriott, L. Loew, K. Jacobson, *J. Cell Biol.* **2001**, *153*, 1035–1048.
- [150] L. Bédouet, H. Adenier, S. Pulvin, C. Bedel-Cloutour, D. Thomas, *Biochem. Biophys. Res. Commun.* **2004**, *320*, 939–944.
- [151] N. Muranaka, T. Hoshida, M. Sisido, *FEBS Lett.* **2002**, *510*, 10–12.
- [152] S. Loudwig, Y. Nicolet, P. Masson, J. C. Fontecilla-Camps, S. Bon, F. Nachon, M. Goeldner, *ChemBioChem* **2003**, *4*, 762–767.
- [153] M. Volgraf, P. Gorostiza, R. Numano, R. H. Kramer, E. Y. Isacoff, D. Trauner, *Nat. Chem. Biol.* **2006**, *2*, 47–52.
- [154] Y. Dorsett, T. Tuschl, *Nat. Rev. Drug Discovery* **2004**, *3*, 318–329.
- [155] D. P. Bartel, *Cell* **2004**, *116*, 281–297.
- [156] M. Mandal, R. R. Breaker, *Nat. Rev. Mol. Cell Biol.* **2004**, *5*, 451–463.
- [157] S. T. Crooke, *Curr. Mol. Med.* **2004**, *4*, 465–487.
- [158] C. R. Dass, *Trends Pharmacol. Sci.* **2004**, *25*, 395–397.
- [159] M. Famulok, S. Verma, *Trends Biotechnol.* **2002**, *20*, 462–466; D. S. Wilson, J. W. Szostak, *Annu. Rev. Biochem.* **1999**, *68*, 611–647.
- [160] Y. S. Cho-Chung, Y. G. Park, Y. N. Lee, *Curr. Opin. Mol. Ther.* **1999**, *1*, 386–392.
- [161] M. C. Pirrung, *Angew. Chem.* **2002**, *114*, 1326–1341; *Angew. Chem. Int. Ed.* **2002**, *41*, 1276–1989.
- [162] J. A. Doudna, T. R. Cech, *Nature* **2002**, *418*, 222–228.
- [163] N. C. Seeman, *Nature* **2003**, *421*, 427–431.
- [164] a) S. Shimizu-Sato, E. Huq, J. M. Tepperman, P. H. Quail, *Nat. Biotechnol.* **2002**, *20*, 1041–1044; b) M. Chen, J. Chory, C. Fankhauser, *Annu. Rev. Genet.* **2004**, *38*, 87–117; c) G. Argüello-Astorga, L. Herrera-Estrella, *Annu. Rev. Plant Physiol. Plant Mol. Biol.* **1998**, *49*, 525–555; d) W. B. Terzaghi, A. R. Cashmore, *Annu. Rev. Plant Physiol. Plant Mol. Biol.* **1995**, *46*, 445–474; e) H.-M. Li, T. Washburn, J. Chory, *Curr. Opin. Cell Biol.* **1993**, *5*, 455–460.
- [165] J. Minden, R. Namba, J. Mergliano, S. Cambridge, *Sci. STKE* **2000**, *2000*, PL1.
- [166] A. Høgset, L. Prasmickaite, P. K. Selbo, M. Hellum, B. O. Engesæter, A. Bonsted, K. Berg, *Adv. Drug Delivery Rev.* **2004**, *56*, 95–115.
- [167] W. T. Monroe, M. M. McQuain, M. S. Chang, J. S. Alexander, F. R. Haselton, *J. Biol. Chem.* **1999**, *274*, 20895–20900.
- [168] B. Ghosn, F. R. Haselton, K. R. Gee, W. T. Monroe, *Photochem. Photobiol.* **2005**, *81*, 953–959.
- [169] H. Ando, T. Furuta, R. Y. Tsien, H. Okamoto, *Nat. Genet.* **2001**, *28*, 317–325.
- [170] a) H. Ando, H. Okamoto, *Methods Cell Sci.* **2003**, *25*, 25–31; b) H. Ando, T. Furuta, H. Okamoto, *Methods Cell Biol.* **2004**, *77*, 159–171.
- [171] a) H. Okamoto, Y. Hirate, H. Ando, *Front. Biosci.* **2004**, *9*, 93–99; b) H. Ando, M. Kobayashi, T. Tsubokawa, K. Uyemura, T. Furuta, H. Okamoto, *Dev. Biol.* **2005**, *287*, 456–468.
- [172] S. Shah, S. Rangarajan, S. H. Friedman, *Angew. Chem.* **2005**, *117*, 1352–1356; *Angew. Chem. Int. Ed.* **2005**, *44*, 1328–1332.
- [173] S. G. Chaulk, A. M. MacMillan, *Nucleic Acids Res.* **1998**, *26*, 3173–3178.
- [174] O. C. Uhlenbeck, *Nature* **1987**, *328*, 596–600.
- [175] S. G. Chaulk, A. M. MacMillan, *Angew. Chem.* **2001**, *113*, 2207–2210; *Angew. Chem. Int. Ed.* **2001**, *40*, 2149–2152.
- [176] S. Pitsch, P. A. Weiss, L. Jenny, A. Stutz, X. L. Wu, *Helv. Chim. Acta* **2001**, *84*, 3773–3795.
- [177] S. Pitsch, P. A. Weiss, X. L. Xu, D. Ackermann, T. Honegger, *Helv. Chim. Acta* **1999**, *82*, 1753–1761.

- [178] L. Kröck, A. Heckel, *Angew. Chem.* **2005**, *117*, 475–477; *Angew. Chem. Int. Ed.* **2005**, *44*, 471–473.
- [179] A. Heckel, G. Mayer, *J. Am. Chem. Soc.* **2005**, *127*, 822–823.
- [180] M. Famulok, G. Mayer, *ChemBioChem* **2005**, *6*, 19–26.
- [181] G. Mayer, L. Kröck, V. Mikat, M. Engeser, A. Heckel, *ChemBioChem* **2005**, *6*, 1966–1970.
- [182] P. Wenter, B. Furtig, A. Hainard, H. Schwalbe, S. Pitsch, *Angew. Chem.* **2005**, *117*, 2656–2659; *Angew. Chem. Int. Ed.* **2005**, *44*, 2600–2603.
- [183] C. Höbartner, S. K. Silverman, *Angew. Chem.* **2005**, *117*, 7471–7475; *Angew. Chem. Int. Ed.* **2005**, *44*, 7305–7309.
- [184] X. J. Tang, I. J. Dmochowski, *Org. Lett.* **2005**, *7*, 279–282.
- [185] X. J. Tang, J. L. Richards, A. E. Peritz, I. J. Dmochowski, *Bioorg. Med. Chem. Lett.* **2005**, *15*, 5303–5306.
- [186] R. Ting, L. Lermer, D. M. Perrin, *J. Am. Chem. Soc.* **2004**, *126*, 12720–12721.
- [187] J.-I. Hong, Q. Feng, V. Rotello, J. Rebek, Jr., *Science* **1992**, *255*, 848–850.
- [188] M. L. Dodson Jr., R. Hewitt, M. Mandel, *Photochem. Photobiol.* **1972**, *16*, 15–25.
- [189] P. Ordoukhanian, J.-S. Taylor, *J. Am. Chem. Soc.* **1995**, *117*, 9570–9571.
- [190] K. J. Zhang, J.-S. Taylor, *J. Am. Chem. Soc.* **1999**, *121*, 11579–11580.
- [191] P. Ordoukhanian, J.-S. Taylor, *Bioconjugate Chem.* **2000**, *11*, 94–103.
- [192] K. Zhang, J.-S. Taylor, *Biochemistry* **2001**, *40*, 153–159.
- [193] H. J. Lenox, C. P. McCoy, T. L. Sheppard, *Org. Lett.* **2001**, *3*, 2415–2418.
- [194] Y. Zheng, T. L. Sheppard, *Chem. Res. Toxicol.* **2004**, *17*, 197–207.
- [195] J. D. Trzuppek, T. L. Sheppard, *Org. Lett.* **2005**, *7*, 1493–1496.
- [196] M. C. Pirrung, X. D. Zhao, S. V. Harris, *J. Org. Chem.* **2001**, *66*, 2067–2071.
- [197] A. Dussy, C. Meyer, E. Quennet, T. A. Bickle, B. Giese, A. Marx, *ChemBioChem* **2002**, *3*, 54–60.
- [198] C. Crey-Desbiolles, J. Lhomme, P. Dumy, M. Kotera, *J. Am. Chem. Soc.* **2004**, *126*, 9532–9533.
- [199] V. Namasivayam, R. G. Larson, D. T. Burke, M. A. Burns, *Anal. Chem.* **2003**, *75*, 4188–4194.
- [200] H. Asanuma, T. Ito, T. Yoshida, X. G. Liang, M. Komiyama, *Angew. Chem.* **1999**, *111*, 2547–2549; *Angew. Chem. Int. Ed.* **1999**, *38*, 2393–2395.
- [201] H. Asanuma, X. G. Liang, T. Yoshida, A. Yamazawa, M. Komiyama, *Angew. Chem.* **2000**, *112*, 1372–1374; *Angew. Chem. Int. Ed.* **2000**, *39*, 1316–1318.
- [202] A. Yamazawa, X. G. Liang, H. Asanuma, M. Komiyama, *Angew. Chem.* **2000**, *112*, 2446–2447; *Angew. Chem. Int. Ed.* **2000**, *39*, 2356–2357.
- [203] H. Asanuma, T. Takarada, T. Yoshida, D. Tamaru, X. G. Liang, M. Komiyama, *Angew. Chem.* **2001**, *113*, 2743–2745; *Angew. Chem. Int. Ed.* **2001**, *40*, 2671–2673.
- [204] H. Asanuma, D. Tamaru, A. Yamazawa, M. Z. Liu, M. Komiyama, *ChemBioChem* **2002**, *3*, 786–789.
- [205] X. G. Liang, H. Asanuma, H. Kashida, A. Takasu, T. Sakamoto, G. Kawai, M. Komiyama, *J. Am. Chem. Soc.* **2003**, *125*, 16408–16415.
- [206] M. Z. Liu, D. Tamaru, H. Asanuma, M. Komiyama, *Chem. Lett.* **2003**, *32*, 1174–1175.
- [207] F. D. Lewis, X. Y. Liu, *J. Am. Chem. Soc.* **1999**, *121*, 11928–11929.
- [208] Y. Liu, D. Sen, *J. Mol. Biol.* **2004**, *341*, 887–892.
- [209] A. Okamoto, K. Tanabe, T. Inasaki, I. Saito, *Angew. Chem.* **2003**, *115*, 2606–2608; *Angew. Chem. Int. Ed.* **2003**, *42*, 2502–2504.
- [210] K. Tanabe, H. Nakata, S. Mukai, S. Nishimoto, *Org. Biomol. Chem.* **2005**, *3*, 3893–3897.



# Formation of Crystalline $\text{SrAl}_2\text{O}_4$ Nanotubes by a Roll-Up and Post-Annealing Approach\*\*

Changhui Ye,\* Yoshio Bando, Guozhen Shen, and Dmitri Golberg



Soon after the identification of carbon nanotubes,<sup>[1]</sup> it was demonstrated that many layered inorganic compounds could be prepared in tubular morphologies.<sup>[2]</sup> The formation of inorganic nanotubes was suggested to occur by a curving and seaming process. Later, artificial lamellar structures were prepared in solution, from which nanotubes (or nanoscrolls) could be formed after heat treatment.<sup>[3]</sup> The thermally driven roll-up of thin layers into scrolls as a result of lattice expansion mismatch was also reported.<sup>[4]</sup> Such a process occurs when a two-layer thin film of Si/SiGe is heated: the film rolls up to form nanoscrolls, owing to the asymmetric strain on its two sides.<sup>[4b,d]</sup>

The bending and roll-up of a thin layer to form tubular nanoscrolls is a thermally driven process. A layer with dangling bonds at its periphery is unstable. The decrease in the number of dangling bonds and reduction in the area of the active solid–vapor or solid–liquid interface that occur upon bending compensate the energy barrier associated with the strain of bending.<sup>[5]</sup> Thus, the formation of seamless nanotubes or nanoscrolls can be energetically favorable. As a result of bending, defects are commonly generated within a structure to allow strain release, which is beneficial for the overall stabilization of the tubular structure.

From a kinetic point of view, the rolling of the lamellar structure may be initiated by a stress of either a structural or an electrical nature caused by the asymmetry of the layer. Recently, Mallouk and co-workers demonstrated that the free-energy difference between the coiled and uncoiled forms of an exfoliated colloid was rather small; therefore, the occurrence of rolled-up nanoscrolls or unrolled layers depends on the chemical environment (such as the ionic strength and pH).<sup>[3d,e]</sup>

To date, there has been much theoretical and experimental work relating to the synthesis of inorganic nanotubes from layered or artificial lamellar structures and their mechanisms of formation. However, direct evidence of the bending, seaming, and roll-up processes is still lacking.<sup>[1–5]</sup> In addition, controversial arguments have recently arisen; for example, Kukovec et al. have questioned the roll-up mechanism for the formation of nanotubes from lamellar structures.<sup>[6]</sup> In fact, these authors found nanoloop intermediates and proposed an oriented-attachment mechanism for the formation of nanotubes. This hypothesis accounts for the fact that a smaller driving force is involved in the formation of nanotubes than that theoretically predicted for the roll-up of a layer. In contrast, our present results explicitly demonstrate that the

roll-up of a whole layer has indeed taken place and has contributed to nanoscroll formation.

Strontium aluminate ( $\text{SrAl}_2\text{O}_4$ ) is one of the most studied and most efficient host materials for long-lasting phosphorescence.<sup>[7]</sup> The low-temperature phase of  $\text{SrAl}_2\text{O}_4$  adopts a monoclinic structure (space group  $P2_1$ ,  $a = 8.447$ ,  $b = 8.816$ ,  $c = 5.163$  Å, and  $\beta = 93.42^\circ$ ) that consists of a three-dimensional network of corner-sharing  $\{\text{AlO}_4\}$  tetrahedra containing connected open channels, in which the  $\text{Sr}^{2+}$  ions are located.<sup>[7b]</sup> Rare-earth ions with the same valence and a similar radius to  $\text{Sr}^{2+}$  (1.21 Å), such as  $\text{Eu}^{2+}$  (1.20 Å), can be readily substituted for  $\text{Sr}^{2+}$  with minor (if any) local distortion of the crystal lattice.<sup>[7b]</sup> This property makes  $\text{SrAl}_2\text{O}_4$  an ideal host material for long-lasting phosphorescence. The synthesis and optical properties of  $\text{SrAl}_2\text{O}_4$ , in bulk form, or as films or nanoparticles, have been extensively explored during the past decades.<sup>[8]</sup> However, the production of one-dimensional aluminate nanomaterials has lingered far behind. To date, only one paper on the synthesis of  $\text{SrAl}_2\text{O}_4$  nanorods has been published; however, neither the details of the synthesis nor a complete structural characterization of the nanorods were provided.<sup>[9]</sup> Nanotubes of alkaline-earth-metal aluminates have not yet been observed.

Herein, we report the rational synthesis of crystalline  $\text{SrAl}_2\text{O}_4$  nanotubes by a roll-up and post-annealing route under hydrothermal conditions. In contrast to the synthesis of  $\text{BaAl}_2\text{O}_4$ , a mixture of cetyltrimethylammonium bromide (CTAB)/*n*-butanol/water, rather than CTAB/water, was used as the reaction medium, allowing a high loading of ionic reactants and a more efficient modulation of morphology.<sup>[10]</sup> Urea was used as a slow-release pH-adjusting agent. The products obtained after heating at 120 °C for 16 h possessed a whisker-like morphology, as shown in a scanning electron microscopy (SEM) image (Figure 1a).

To further investigate the product morphology and structure, transmission electron microscopy (TEM) and high-resolution (HR) TEM were employed. As shown in the TEM image of Figure 1b, the products have a tubular morphology. The selected area electron diffraction (SAED) pattern shown in the inset reveals that the nanotubes are amorphous. It is apparent that the nanotube diameter is not uniform throughout the whole length, which will be discussed below.

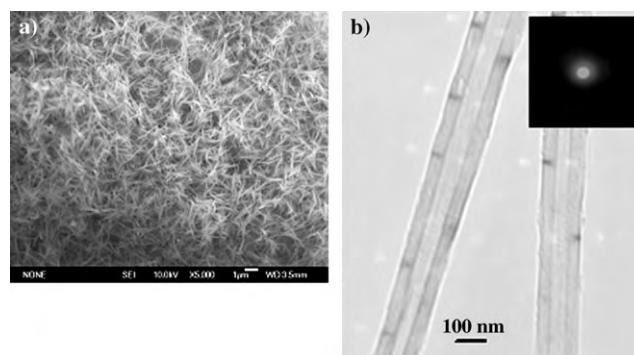


**Figure 1.** a) SEM image of the  $\text{SrAl}_2\text{O}_4$  product synthesized at 120 °C; scale bar = 1 μm. b) TEM image of two as-synthesized  $\text{SrAl}_2\text{O}_4$  nanotubes; corresponding SAED pattern in inset.

[\*] Dr. C. Ye, Prof. Y. Bando, Dr. G. Shen, Prof. D. Golberg  
Nanoscale Materials Center  
National Institute for Materials Science  
Namiki 1-1, Tsukuba, Ibaraki 305-0044 (Japan)  
Fax: (+81) 29-851-6280  
E-mail: Ye.Changhui@nims.go.jp

[\*\*] This work was supported by the Japan Society for the Promotion of Science (JSPS), in the form of a fellowship tenable at the National Institute for Materials Science, Tsukuba, Japan (C.Y.).

Supporting information for this article is available on the WWW under <http://www.angewandte.org> or from the author.

Note that the nanotubes were not induced by the sonication during the preparation of the TEM samples, because nanotubes were observed in the as-synthesized products (see Supporting Information).

In order to obtain well-crystallized  $\text{SrAl}_2\text{O}_4$  nanotubes, we annealed the product at  $1300^\circ\text{C}$  for 4 h. From the TEM image of an annealed nanotube shown in Figure 2a, it is clear that

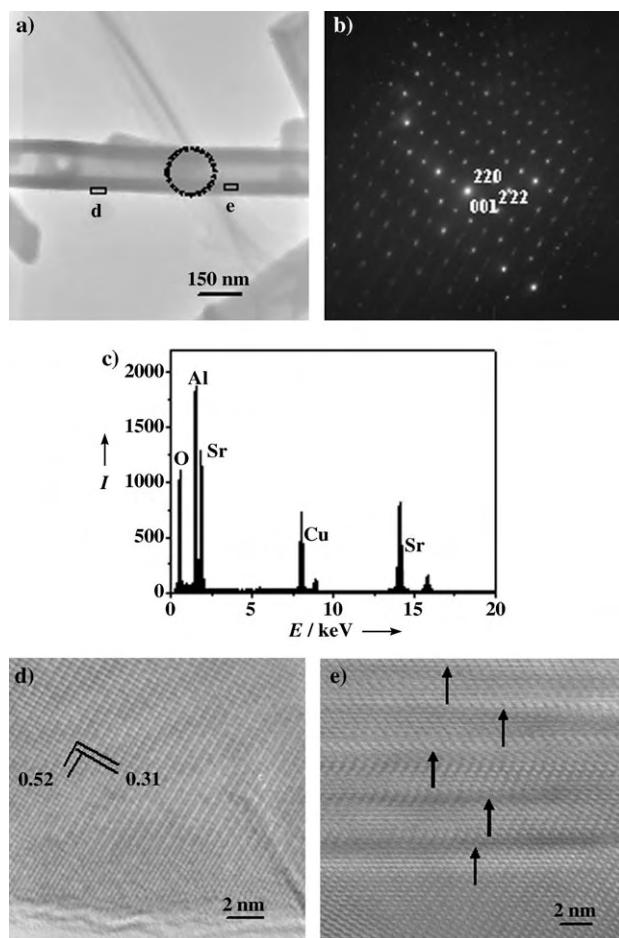


**Figure 2.** a) TEM image of a post-annealed  $\text{SrAl}_2\text{O}_4$  nanotube. b) SAED pattern of the area circled in (a), recorded along the  $[1\bar{1}0]$  zone axis. c) EDX spectrum of the nanotube. d) and e) HRTEM images corresponding to the marked regions in (a); in (d), lattice spacings discussed in text are indicated; the arrows in (e) point out stacking faults and antiphase boundaries.

the tubular morphology is preserved upon high-temperature annealing. An SAED pattern taken along the  $[1\bar{1}0]$  zone axis demonstrates the single-crystalline nature of the nanotube (Figure 2b). The slight streaking of the diffraction spots indicates that planar defects are present within the nanotube. Energy dispersive X-ray (EDX) spectroscopy indicates that the nanotube is composed of strontium, aluminum, and oxygen in an atomic ratio that agrees with the stoichiometric formula  $\text{SrAl}_2\text{O}_4$  (Figure 2c; the copper signal is due to the carbon-coated copper grid used as a sample holder). An HRTEM image shows the lattice fringes corresponding to the  $\{001\}$  and  $\{220\}$  planes, which have spacings of approximately

0.52 and 0.31 nm, respectively (Figure 2d). The nanotube walls are not perfect single crystals; as indicated by the arrows in Figure 2e, stacking faults and antiphase boundaries are present, consistent with the streaking observed in the SAED pattern. Note that antiphase boundary defects are common in  $\text{SrAl}_2\text{O}_4$  and related materials.<sup>[11]</sup>

The nanotube growth mechanism was investigated by systematically studying the evolution of the product morphology during the hydrothermal process. When the heating time is shorter than 2 h at  $120^\circ\text{C}$ , no solid product is produced, because an incubation period is necessary prior to nucleation. When the heating time is extended to 4–8 h, nanoparticles and nanoplatelets appear (see Supporting Information). A further extension of the heating time to 10 h results in the appearance of nanoscrolls. In Figure 3, both

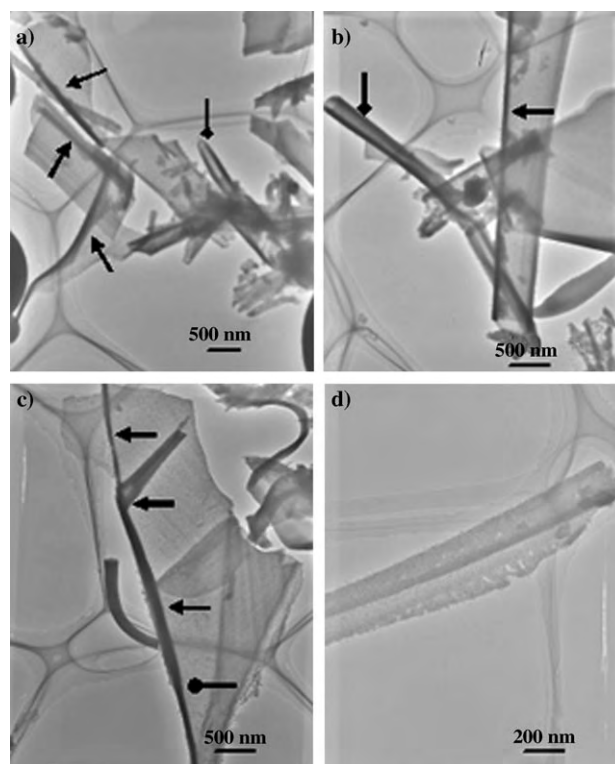


**Figure 3.** TEM images of the roll-up of  $\text{SrAl}_2\text{O}_4$  layers to form nanoscrolls during hydrothermal synthesis at  $120^\circ\text{C}$ ; the arrows in (a)–(c) point out structural features described in text.

nanoscrolls and nanoplatelets can be seen; the triangle arrowheads indicate the roll-up of nanoplatelets, and the diamond arrowheads indicate the roll-up of nanoscrolls. Note that the nanoplatelets are flexible enough to bend, but are rigid enough to bear the bending stress. It is rare to find a broken platelet, such as the one indicated by the triangle arrowhead with the thick tail in Figure 3c. From the TEM images, it is clear that the nanoplatelets are not uniform in shape; therefore, the diameter of the rolled-up nanoscrolls is not axially uniform, as indicated by the round arrowhead in Figure 3c. In Figure 3d, a nanoscroll near the end of the roll-up process is shown; it is again apparent that the diameter of the nanoscroll is not uniform throughout its length.



As discussed above, the as-synthesized nanoscrolls are amorphous prior to high-temperature annealing, as is characteristic for alkaline-earth-metal aluminates. After annealing at 1300 °C for 4 h, the nanoscrolls are fully transformed into crystalline nanotubes of monoclinic  $\text{SrAl}_2\text{O}_4$ . Nanoscrolls and nanotubes can be clearly differentiated: nanoscrolls are rolled up from a single sheet, whereas the original layered structure is lost in nanotubes, as a result of an atomic rearrangement. When the amorphous samples are annealed,  $\{\text{AlO}_4\}$  tetrahedra are formed through a dehydration process. During the rearrangement of the atoms within the layers, the  $\{\text{AlO}_4\}$  units may change their original positions and orientations to fit the resultant crystal symmetry of the monoclinic phase. Long-range ordering is an energy-consuming process; therefore, by virtue of the strain present in the nanoscrolls, crystals exhibiting stacking faults and antiphase boundaries are formed.

As stated above, the bending and roll-up of layers are thermally driven processes; that is, thermal energy is needed to overcome the potential-energy barrier associated with the induced strain. According to Yada et al.,<sup>[3c]</sup> Sun and Li,<sup>[3j]</sup> and Xiong et al.,<sup>[3i]</sup> hydrothermal reaction at higher temperatures favors the formation of solid rods. Because of the larger thermal energy input, the roll-up process begins at a smaller starting diameter, leaving a smaller hollow space in the nanoscroll. A small hollow space could be easily annealed out to form solid rods, whereas a large hollow space would be preserved to form hollow tubes upon annealing, as observed.<sup>[3c,i,j]</sup>

We carried out hydrothermal reactions at 180 °C for 10–48 h (without post-annealing) and invariably obtained solid nanorods. As shown in Figure 4, the nanorods are generally smaller than 50 nm in diameter, much thinner than the nanotubes. Some nanorods are bundled. Our results agree well with those reported previously.<sup>[3c,i,j]</sup>

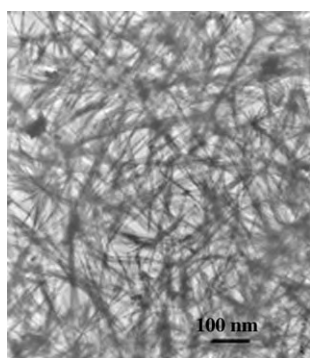


**Figure 4.** TEM image of  $\text{SrAl}_2\text{O}_4$  nanorods synthesized at 180 °C.

In conclusion, single-crystalline  $\text{SrAl}_2\text{O}_4$  nanotubes have been synthesized by a roll-up and post-annealing approach. We have found evidence for a roll-up mechanism driven by thermal energy, which compensates the surface energy. We have also found that the use of higher temperatures and pressures during the hydrothermal treatment favors the formation of solid nanorods over nanotubes. This facile preparation method could be extended to other materials,

such as titanates and zirconates. The single-crystalline  $\text{SrAl}_2\text{O}_4$  nanotubes may find important applications in after-glow and luminescence.

## Experimental Section

All chemicals were used as received without further purification.

Growth of  $\text{SrAl}_2\text{O}_4$  nanotubes:  $\text{Al}(\text{NO}_3)_3 \cdot 9\text{H}_2\text{O}$  (4 mmol),  $\text{Sr}(\text{NO}_3)_2$  (2 mmol), urea (0.01 mol), *n*-butanol (0.1 mol), and CTAB (2 mmol) were dissolved in deionized water (50 mL) and stirred magnetically for 2 h. Then, the solution was poured into two teflon-lined autoclaves of 40-mL capacity. The two solutions were treated under different experimental conditions, and were heated at temperatures in the range 100–180 °C for 30 min to 48 h. Post-annealing was carried out at 1200–1350 °C for 4 h in air.

Characterization: SEM images were recorded for as-synthesized samples on a JEOL JSM-6700F microscope. TEM and HRTEM images, and EDX spectra were recorded on a JEOL JEM-3000F microscope at an acceleration voltage of 300 kV. Samples were sonicated for several minutes in ethanol, and then several drops of the sample solutions were dripped onto carbon-coated copper grids.

Received: April 4, 2006

Published online: July 3, 2006

**Keywords:** aluminum · hydrothermal synthesis · nanostructures · nanotubes · strontium

- [1] S. Iijima, *Nature* **1991**, 354, 56.
- [2] a) R. Tenne, L. Margulis, M. Genut, G. Hodes, *Nature* **1992**, 360, 444; b) Y. Feldman, E. Wasserman, D. J. Srolovitz, R. Tenne, *Science* **1995**, 267, 222; c) N. G. Chopra, R. J. Luyken, K. Cherrey, V. H. Crespi, M. L. Cohen, S. G. Louie, A. Zettl, *Science* **1995**, 269, 966; d) P. M. Ajayan, O. Stephan, P. Redlich, C. Colliex, *Nature* **1995**, 375, 564; e) Y. R. Hachohen, E. Grunbaum, R. Tenne, J. Sloan, J. L. Hutchison, *Nature* **1998**, 395, 336; f) J. A. Hollingsworth, D. M. Poojary, A. Clearfield, W. E. Buhro, *J. Am. Chem. Soc.* **2000**, 122, 3562; g) M. Nath, C. N. R. Rao, *J. Am. Chem. Soc.* **2001**, 123, 4841; h) Y. Li, J. Wang, Z. Deng, Y. Wu, X. Sun, D. Yu, P. Yang, *J. Am. Chem. Soc.* **2001**, 123, 9904; i) C. Ye, G. Meng, Z. Jiang, Y. Wang, G. Wang, L. Zhang, *J. Am. Chem. Soc.* **2002**, 124, 15180; j) M. Brorson, T. W. Hansen, C. J. H. Jacobsen, *J. Am. Chem. Soc.* **2002**, 124, 11582; k) M. Nath, C. N. R. Rao, *Angew. Chem.* **2002**, 114, 3601; *Angew. Chem. Int. Ed.* **2002**, 41, 3451; l) Y. R. Hachohen, R. Popovitz-Biro, E. Grunbaum, Y. Prior, R. Tenne, *Adv. Mater.* **2002**, 14, 1075; m) J. Chen, Z. Tao, S. Li, *Angew. Chem.* **2003**, 115, 2197; *Angew. Chem. Int. Ed.* **2003**, 42, 2147; n) J. Chen, Z. Tao, S. Li, X. Fan, S. Chou, *Adv. Mater.* **2003**, 15, 1379; o) S. Y. Hong, R. Popovitz-Biro, Y. Prior, R. Tenne, *J. Am. Chem. Soc.* **2003**, 125, 10470; p) U. K. Gautam, S. R. C. Vivekchand, A. Govindaraj, G. U. Kulkarni, N. R. Selvi, C. N. R. Rao, *J. Am. Chem. Soc.* **2005**, 127, 3658.
- [3] a) M. Remskar, Z. Skrabar, F. Cleton, R. Sanjines, F. Levy, *Appl. Phys. Lett.* **1996**, 69, 351; b) R. Abe, K. Shinohara, A. Tanaka, M. Hara, J. N. Kondo, K. Domen, *Chem. Mater.* **1997**, 9, 2179; c) M. Yada, H. Hiyoshi, K. Ohe, M. Machida, T. Kijima, *Inorg. Chem.* **1997**, 36, 5565; d) G. B. Saupe, C. C. Waraksa, H. N. Kim, Y. Han, D. M. Kaschak, D. M. Skinner, T. E. Mallouk, *Chem. Mater.* **2000**, 12, 1556; e) R. E. Schaak, T. E. Mallouk, *Chem. Mater.* **2000**, 12, 3427; f) G. Du, Q. Chen, R. Che, Z. Yuan, L. Peng, *Appl. Phys. Lett.* **2001**, 79, 3702; g) Y. Li, X. Li, R. He, J. Zhu, Z. Deng, *J. Am. Chem. Soc.* **2002**, 124, 1411; h) M. Mo, J. Zeng, X. Liu, W. Yu, S. Zhang, Y. Qian, *Adv. Mater.* **2002**, 14, 1658; i) X. Sun, Y. Li, *Chem. Eur. J.* **2003**, 9, 2229; j) Y. Xiong, Y.



- Xie, Z. Li, X. Li, S. Gao, *Chem. Eur. J.* **2004**, *10*, 654; k) S. V. Krivovichev, V. Kahlenberg, R. Kaindl, E. Mersdorf, I. G. Tananaev, B. F. Myasoedov, *Angew. Chem.* **2005**, *117*, 1158; *Angew. Chem. Int. Ed.* **2005**, *44*, 1134; l) J. Hu, Y. Bando, J. Zhan, Z. Liu, D. Golberg, *Appl. Phys. Lett.* **2005**, *87*, 153112.
- [4] a) V. Y. Prinz, V. A. Seleznev, A. K. Gutakovsky, A. V. Chehofskiy, V. V. Preobrazhenskii, M. A. Putyato, T. A. Gavrilova, *Phys. E* **2000**, *6*, 828; b) Q. G. Schmidt, K. Eberl, *Nature* **2001**, *410*, 168; c) V. Y. Prinz, D. Grutzmacher, A. Beyer, C. David, B. Ketterer, E. Deckardt, *Nanotechnology* **2001**, *12*, 399; d) S. V. Golod, V. Y. Prinz, V. I. Mashanov, A. K. Gutakovsky, *Semicond. Sci. Technol.* **2001**, *16*, 181; e) Y. V. Nastaushv, V. Y. Prinz, S. N. Svitashva, *Nanotechnology* **2005**, *16*, 908.
- [5] a) D. J. Srolovitz, S. A. Safran, M. Homyonfer, R. Tenne, *Phys. Rev. Lett.* **1995**, *74*, 1779; b) G. Seifert, T. Kohler, R. Tenne, *J. Phys. Chem. B* **2002**, *106*, 2497; c) S. Zhang, L. Peng, Q. Chen, G. Du, G. Dawson, W. Zhou, *Phys. Rev. Lett.* **2003**, *91*, 256103; d) F. Xu, J. Hu, Y. Bando, *J. Am. Chem. Soc.* **2005**, *127*, 16860.
- [6] A. Kukovecz, N. Hodos, E. Horvath, G. Radnoci, Z. Konya, I. Kiricsi, *J. Phys. Chem. B* **2005**, *109*, 17781.
- [7] a) T. Katsumata, S. Toyomane, A. Tonegawa, Y. Kanai, U. Kaneyama, K. Shakuno, R. Sakai, S. Komuro, T. Morikawa, *J. Cryst. Growth* **2002**, *237*, 361; b) F. Clabau, X. Rocquefelte, S. Jobic, P. Deniard, M. H. Whangbo, A. Garcia, T. Le Mercier, *Chem. Mater.* **2005**, *17*, 3904; c) Y. Liu, C. Xu, *J. Phys. Chem. B* **2003**, *107*, 3991; d) J. Holsa, T. Aitasalo, H. Jungner, M. Lastusaari, J. Niittikoski, G. Spano, *J. Alloys Compd.* **2004**, *374*, 56.
- [8] a) Z. Fu, S. Zhou, S. Zhang, *J. Phys. Chem. B* **2005**, *109*, 14396; b) P. Escibano, M. Marchal, M. L. Sanjuán, P. A. Gutiérrez, B. Julián, E. Cordocillo, *J. Solid State Chem.* **2005**, *178*, 1978; c) L. Wang, Y. Zhu, *J. Alloys Compd.* **2004**, *370*, 276; d) N. Honda, T. Suzuki, T. Yunogami, H. Suematsu, W. Jiang, K. Yatsui, *Jpn. J. Appl. Phys.* **2005**, *44*, 695.
- [9] Y. Lin, Z. Zhang, F. Zhang, Z. Tang, Q. Chen, *Mater. Chem. Phys.* **2000**, *65*, 103.
- [10] a) M. Husein, E. Rodil, J. Vera, *Langmuir* **2003**, *19*, 8467; b) M. Husein, E. Rodil, J. Vera, *Langmuir* **2006**, *22*, 2264.
- [11] M. L. Ruiz-González, J. M. González-Calbet, M. Vallet-Regí, E. Cordocillo, P. Escibano, J. B. Carda, M. Marchal, *J. Mater. Chem.* **2002**, *12*, 1128.

DOI: 10.1002/anie.200601467

**A Ferromagnetically Coupled Mn<sub>19</sub> Aggregate with a Record  $S = 83/2$  Ground Spin State\*\***

Ayuk M. Ako, Ian J. Hewitt, Valeriu Mereacre, Rodolphe Clérac, Wolfgang Wernsdorfer, Christopher E. Anson, and Annie K. Powell\*

*Dedicated to Professor Hansgeorg Schnöckel on the occasion of his 65th birthday.*

The first evidence of single molecule magnet (SMM) behavior was discovered in the mixed-valence compounds  $[\text{Mn}^{\text{III}}_8\text{Mn}^{\text{IV}}_4\text{O}_{12}(\text{O}_2\text{CR})_{16}(\text{H}_2\text{O})_4]$  ( $\text{R} = \text{Ph}, \text{Me}$ ), which possess the structural motif originally reported by Lis for  $\text{R} = \text{Me}$  in 1980.<sup>[1]</sup> In the quest to synthesize SMMs that show hysteresis at higher temperatures, it has been recognized that large ground-state spins and a uniaxial anisotropy (large negative  $D$  and small  $E$  considering the following Hamiltonian anisotropy term:  $H = DS_z^2 + E(S_x^2 - S_y^2)$ ) are required.<sup>[1e,2,3]</sup> It is thus of interest to discover how to obtain the largest-spin ground state possible for a given size of aggregate. As well as having four unpaired electrons in its high-spin state, the  $\text{Mn}^{\text{III}}$  ion is particularly useful for introducing large anisotropies through the presence of Jahn–Teller distortions in this configuration and has been the most thoroughly studied candidate for synthesizing new SMMs. Amongst the large number of aggregates containing manganese(III) in the literature, a  $\text{Mn}_{25}$  cluster has been reported as having a ground spin state of  $51/2$ .<sup>[4]</sup> Herein we report on the realization of the maximum-spin ground state of  $83/2$  for the aggregate  $[\text{Mn}^{\text{III}}_{12}\text{Mn}^{\text{II}}_7(\mu_4\text{-O})_8(\mu_3\eta^1\text{-N}_3)_8(\text{HL})_{12}(\text{MeCN})_6]\text{Cl}_2 \cdot 10\text{MeOH} \cdot \text{MeCN}$  (**1**;  $\text{H}_3\text{L} = 2,6\text{-bis}(\text{hydroxymethyl})\text{-4-methylphenol}$ ).

[\*] Dr. A. M. Ako, Dr. I. J. Hewitt, Dr. V. Mereacre, Dr. C. E. Anson, Prof. A. K. Powell

Institut für Anorganische Chemie der Universität Karlsruhe  
Engesserstrasse Geb. 30.45, 76128 Karlsruhe (Germany)

Fax: (+49) 721-608-8142

E-mail: powell@chemie.uni-karlsruhe.de

Dr. R. Clérac

Centre de Recherche Paul Pascal

CNRS–UPR 8641

115 Avenue Dr. A. Schweitzer, 33600 Pessac (France)

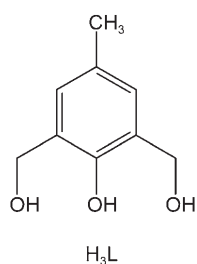
Dr. W. Wernsdorfer

Laboratoire Louis Néel–CNRS, BP 166

25 Avenue des Martyrs, 38042 Grenoble Cedex 9 (France)

[\*\*] This work was supported by Bordeaux 1 University, the CNRS, the Region Aquitaine, the DFG (SPP 1137 and the Center for Functional Nanostructures), QuEMolNa (MRTN-CT2003-504880), MAGMA-Net (NMP3-CT-2005-515767), and the Alexander von Humboldt Foundation.

Supporting information for this article is available on the WWW under <http://www.angewandte.org> or from the author.



The crystal structure of compound **1** (Figure 1) reveals that the aggregate is mixed-valent and contains seven  $\text{Mn}^{\text{II}}$  centers and twelve  $\text{Mn}^{\text{III}}$  centers, as derived from the metric parameters and BVS (bond valence sum) calculations.<sup>[5]</sup> The core of compound **1** (Figure 2a) can be described as being based on two  $\text{Mn}_9$  fragments that are linked through a central  $\text{Mn}^{\text{II}}$  center,  $\text{Mn1}$ ,

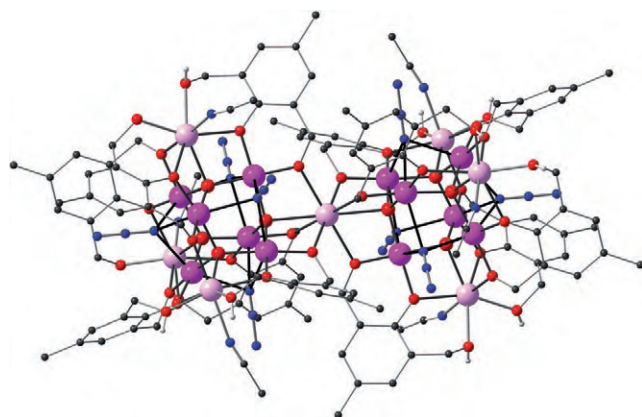


**Figure 1.** Molecular structure of **1** in the crystal ( $\text{Mn}^{\text{III}}$  dark pink,  $\text{Mn}^{\text{II}}$  pale pink, O red, N blue, C gray, H white). Carbon-bound hydrogen atoms and noncoordinated solvent molecules have been omitted for clarity.

which is coordinated to six  $\mu\text{-O}$  and two  $\mu_4\text{-O}$  donor atoms. Each half of the molecule is derived from an almost perfect cube in which the vertices consist alternately of  $\text{Mn}^{\text{II}}$  centers and central N atoms of the terminally coordinating  $\mu_3\text{-N}_3$  units. Thus, the  $\text{Mn}^{\text{II}}$  centers define a tetrahedron in each half. At the center of each of the faces of the cube there is a  $\text{Mn}^{\text{III}}$  center defining an octahedron such that the faces of the octahedron are capped alternately by  $\mu_3\text{-N}_3$  and  $\mu_4\text{-O}$  ligands, the latter of which is linked to the  $\text{Mn}^{\text{II}}$  centers. Closer inspection of the  $\text{Mn}^{\text{III}}$  geometries reveals that the Jahn–Teller elongation axes are those involving the two azido ligands (Figure 2b,c) which result in a trigonal arrangement for each  $\text{Mn}^{\text{III}}$  octahedron. The resulting nanosized particle has a structural arrangement corresponding to that found in Chevrel phases.<sup>[6]</sup>

The magnetic properties were measured on a polycrystalline sample of **1**. At room temperature, the  $\chi'T$  product (Figure 3a) is  $93\text{ cm}^3\text{ K mol}^{-1}$ , which is higher than the expected value ( $66.625\text{ cm}^3\text{ K mol}^{-1}$  taking  $g_{\text{av}} = 2$ ) for twelve  $\text{Mn}^{\text{III}}$  centers ( $S = 2$ ) and seven  $\text{Mn}^{\text{II}}$  centers ( $S = 5/2$ ). Owing to the large magnetic susceptibility of the molecule and in order to stay below the upper limit of detection of our SQUID magnetometer, the mass of the sample had to be decreased from 17.79 mg to 6.38 mg, and the temperature dependence of susceptibility had to be measured in zero field by using the ac technique. On decreasing the temperature, the  $\chi'T$  product continuously increases to reach  $894\text{ cm}^3\text{ K mol}^{-1}$  at 1.8 K, thus indicating dominant ferromagnetic interactions in the poly-

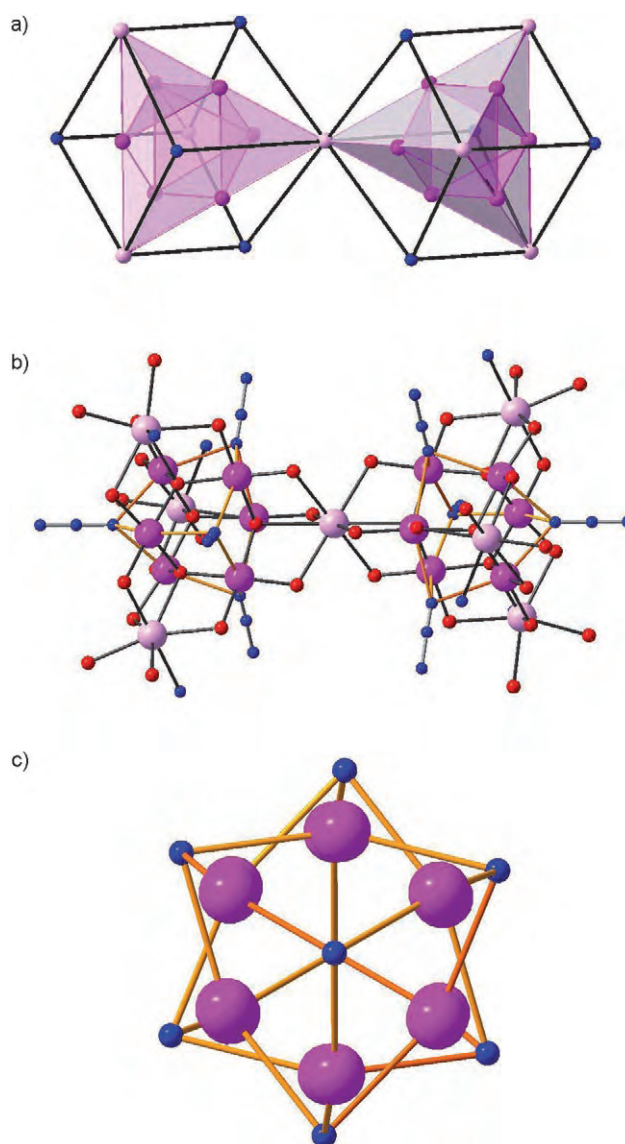


**Figure 2.** a) Polyhedral representation of the core of **1** with emphasis on the cubic-derived symmetry (same color scheme as above). b) Highlighted Jahn–Teller axes (yellow) on the  $\text{Mn}^{\text{III}}$  centers within the core. c) The trigonal arrangement of the Jahn–Teller axes as viewed along the crystallographic  $c$  axis.

nuclear complex. This value is close to the one expected when all the spins composing the Mn aggregate are parallel, thus for a ground spin state of  $S_T = 83/2$  ( $881.875\text{ cm}^3\text{ K mol}^{-1}$  taking  $g_{\text{av}} = 2$ ). The presence of strong ferromagnetic interactions easily explains the high  $\chi'T$  product at room temperature. Indeed, this unusually large magnetic susceptibility allows crystals of **1** to be moved easily at room temperature by using only a simple permanent magnet of 0.35 T. At 1.8 K, the field dependence of the magnetization saturates very fast above 1.5 T to reach about  $84.5\text{ }\mu_{\text{B}}$  (inset of Figure 3a), a value in good agreement with the expected value of  $83\text{ }\mu_{\text{B}}$  (with  $g_{\text{av}} = 2$ ) for a ground spin state of  $S_T = 83/2$ . At this temperature, the linear part of the plot of  $M$  versus  $H$  does not exceed 300 Oe, thus justifying the use of the ac technique.

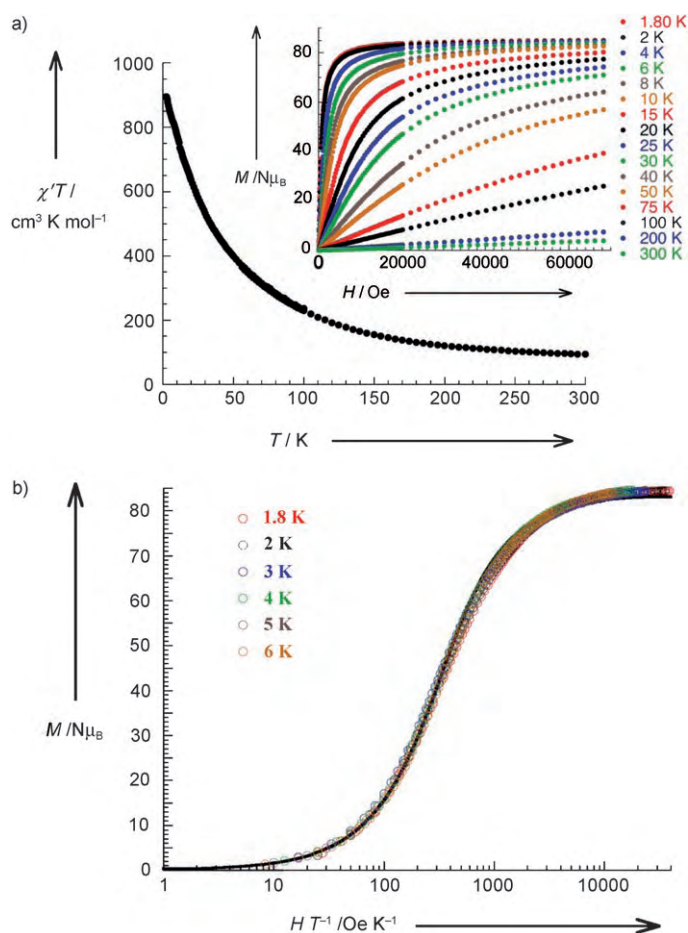


**Figure 3.** a) Temperature dependence of the  $\chi'T$  product (where  $\chi' = dM/dH$ ) measured in  $H_{ac} = 0$  Oe,  $H_{dc} = 3$  Oe, and  $\nu = 100$  Hz (inset: field dependence of the magnetization from 1.8 K to 300 K). b) Semilogarithmic  $M$  versus  $H/T$  plot with data between 1.8 and 6 K; the solid line is the best fit obtained with an  $S = 83/2$  Brillouin function.

At high field, the magnetization is fully saturated and no slope is observed, which proves the absence of significant anisotropy in the material. The ferromagnetic exchange energies thus seem to be much higher than the local anisotropic energies, forcing the spins to be parallel. Moreover, the presence of isotropic  $\text{Mn}^{\text{II}}$  metal ions and the triangular geometrical arrangement of the  $\text{Mn}^{\text{III}}$  centers probably make a significant contribution to the minimization of the magnetic anisotropy. In agreement with this conclusion, the data below 6 K which are presented as a plot of  $M$  versus  $H/T$  (Figure 3b) are all superposed on one single master curve. This result indicates that the ground state is essentially the only one populated below this temperature. This interpretation is further confirmed qualitatively by the plot of  $\chi'T$  versus  $T$ , which is weakly temperature-dependent below 6 K (see the Supporting Information).

In order to prove definitively the unprecedented  $S_T = 83/2$  ground spin state, the  $M$  versus  $H/T$  data below 6 K have been fitted to a Brillouin function. The agreement with the theoretical curve is close to perfect and represents a textbook example of a paramagnetic  $S = 83/2$  unit with an average

$g$  value of 2.00(6). Additional field dependences of the magnetization were measured below 1.8 K by using the micro-SQUID technique on single crystals. Below 0.5 K, the magnetization, which is independent of the field orientation, shows hysteresis effects with a coercive field that reaches 300 Oe at 0.04 K (Supporting Information). The two obvious possible sources of the hysteresis are the anisotropy of the  $\text{Mn}^{\text{III}}$  centers which is not completely compensated and the anisotropy of the dipolar interactions that is induced by the nonspherical shape of the molecule. This finding together with the fact that the system also shows relaxation (Supporting Information) suggests that the molecule is, indeed, an SMM but is dramatically influenced by the intermolecular dipolar interactions which are always present in SMM-based materials. However, in conventional SMMs the dipolar coupling energy is much smaller than the anisotropy energy while in compound **1** both energies are probably of the same order of magnitude. The situation is further complicated by the fact that all large molecules have small disorders which give a distribution of easy-axis directions, thus making it impossible to locate the easy axis by using the micro-SQUID technique.

Azido ligands in the terminal  $\mu_3$ -bridging mode as in compound **1** are known to favor ferromagnetic interactions,<sup>[7]</sup> and the  $\mu_4$ -O bridges are likely to mediate weaker interactions.<sup>[8]</sup> Thus, the combination of using an organic ligand which can bridge to multiple metal centers and using azido ligands has resulted in a  $\text{Mn}_{19}$  aggregate that exhibits dominant ferromagnetic interactions with the maximum-spin ground state possible, here 83/2. Achieving such a high ground spin state is clearly one of the elusive goals in the search for obtaining superior SMMs. However, although the  $\text{Mn}^{\text{III}}$  centers in **1** show a high degree of Jahn–Teller distortion, their geometrical arrangement and the strong ferromagnetic interactions between spin carriers lead to a system with a very low anisotropy. The challenge now is to find a means of introducing not only maximum spin but also greater anisotropy. Nevertheless, **1** represents a remarkable milestone in the quest for high-temperature SMMs.

## Experimental Section

A solution of  $\text{NaN}_3$  (0.2 g, 3 mmol) in MeOH (5 mL) was added with stirring to a slurry of 2,6-dihydroxymethyl-4-methylphenol (1 g, 6 mmol),  $\text{MnCl}_2 \cdot 4\text{H}_2\text{O}$  (0.4 g, 2 mmol), and  $\text{NaO}_2\text{CMe}$  (0.14 g, 1 mmol) in MeCN (20 mL). After the mixture had been stirred for 1 h at room temperature, the mixture was heated at reflux for 2 h. The resulting dark brown solution was allowed to cool and was filtered. After the solution had been left to stand in a sealed vessel for one week, well-formed black crystals of **1** were obtained. Yield: 350 mg, 40%. Selected IR data (KBr disk):  $\tilde{\nu} = 3352$  (b), 2922 (w), 2847 (w), 2062 (s), 1610 (w), 1469 (s), 1251 (m), 1224 (m), 1160 (m), 1026 (m), 989 (m), 863 (m), 810 (m), 634 (b,s), 556 (m), 475  $\text{cm}^{-1}$  (w). Compound **1** can also be synthesized by heating the reaction mixture directly after adding  $\text{NaN}_3$ , but this procedure results in a lower yield and microcrystalline product. The compound can also be obtained without the addition of  $\text{NaO}_2\text{CMe}$ , but analysis of the resulting crystals showed heavily disordered  $\text{Cl}^-$  and  $\text{N}_3^-$  ions, thus making a satisfactory refinement not possible. The two compounds were otherwise isostructural.



Crystal data for **1**:  $C_{132}H_{181}Cl_2Mn_{19}N_{31}O_{54}$ ,  $M_r = 4180.84$ , rhombohedral, space group  $R\bar{3}$ ,  $a = 20.9989(6)$ ,  $c = 34.7489(14)$  Å,  $V = 13269.8(8)$  Å<sup>3</sup>,  $T = 100$  K,  $Z = 3$ ,  $\mu = 1.418$  mm<sup>-1</sup>,  $F(000) = 6393$ ,  $\rho_{\text{calcd}} = 1.570$  Mg m<sup>-3</sup>, 22436 data measured, 6751 unique ( $R_{\text{int}} = 0.0253$ ), final  $wR_2(F^2, \text{all data}) = 0.1283$ ,  $S = 1.036$ ,  $R_1(4991 \text{ with } I > 2\sigma(I)) = 0.0414$ . The structure was solved by direct methods and refined by using the SHELXTL program suite.<sup>[9]</sup> The two chloride counteranions were refined as disordered over the twelve lattice solvent sites per Mn<sub>19</sub> cluster to which the ligand OH groups form hydrogen bonds through O5 and O8. CCDC-604216 contains the supplementary crystallographic data for this paper. These data can be obtained free of charge from The Cambridge Crystallographic Data Centre via [www.ccdc.cam.ac.uk/data\\_request/cif](http://www.ccdc.cam.ac.uk/data_request/cif).

The measurements of magnetic susceptibility were obtained with a Quantum Design SQUID magnetometer MPMS-XL. This magnetometer works between 1.8 and 400 K for dc applied fields ranging from -7 to 7 T. Measurements were performed on two finely ground crystalline samples of 6.38 and 17.79 mg. Measurements of  $M$  versus  $H$  were performed at 100 K to check for the presence of ferromagnetic impurities, which were found to be systematically absent. Measurements of ac susceptibility were made with an oscillating ac field of 3 Oe and ac frequencies ranging from 1 to 1500 Hz without applied dc fields. It is worth noting that the ac susceptibility shows no out-of-phase signal above 1.85 K and no frequency dependence of the in-phase component. The magnetic data were corrected for the sample holder and the diamagnetic contribution which was calculated from Pascal's constants.<sup>[10]</sup> Magnetization measurements on single crystals were performed with an array of micro-SQUIDS.<sup>[11]</sup> This magnetometer works in the temperature range of 0.04 to ca. 7 K and in fields of up to 0.8 T with sweeping rates as high as 0.28 T s<sup>-1</sup>, and exhibits field stability of better than  $\mu$ T. The time resolution is approximately 1 ms. The field can be applied in any direction of the micro-SQUID plane with precision much better than 0.1° by separately driving three orthogonal coils. In order to ensure good thermalization, a single crystal was fixed with apiezon grease.

Received: April 13, 2006

Published online: July 4, 2006

**Keywords:** cluster compounds · magnetic properties · manganese · molecular magnets · structure elucidation

Vicente, M. Font-Bardia, X. Solans, S. P. Perlepes, *Chem. Commun.* **2001**, 2414; c) G. S. Papaefstathiou, S. P. Perlepes, A. Escuer, R. Vicente, M. Font-Bardia, X. Solans, *Angew. Chem.* **2001**, *113*, 908; *Angew. Chem. Int. Ed.* **2001**, *40*, 894.

- [8] See, for example: C. Dendrinou-Samara, M. Alexiou, C. M. Zaleski, J. W. Kampf, M. L. Kirk, D. P. Kessissoglou, V. L. Pecoraro, *Angew. Chem.* **2003**, *115*, 3893; *Angew. Chem. Int. Ed.* **2003**, *42*, 3763.
- [9] G. M. Sheldrick, SHELXTL 5.1, Bruker AXS, Inc., 6300 Enterprise Lane, Madison, WI 53719-1173, USA, **1997**.
- [10] *Theory and Applications of Molecular Paramagnetism*, (Eds.: E. A. Boudreaux, L. N. Mulay), Wiley, New York, **1976**.
- [11] W. Wernsdorfer, *Adv. Chem. Phys.* **2001**, *118*, 99.

- [1] a) T. Lis, *Acta Crystallogr. Sect. B* **1980**, *36*, 2042; b) P. D. W. Boyd, Q. Li, J. B. Vincent, K. Folting, H.-R. Chang, W. E. Streib, J. C. Huffman, G. Christou, D. N. Hendrickson, *J. Am. Chem. Soc.* **1988**, *110*, 8537; c) A. Caneschi, D. Gatteschi, R. Sessoli, *J. Am. Chem. Soc.* **1991**, *113*, 5873; d) R. Sessoli, H.-L. Tsai, A. R. Schake, S. Wang, J. B. Vincent, K. Folting, D. Gatteschi, G. Christou, D. N. Hendrickson, *J. Am. Chem. Soc.* **1993**, *115*, 1804; e) R. Sessoli, D. Gatteschi, A. Caneschi, M. A. Novak, *Nature* **1993**, *365*, 141.
- [2] a) G. Christou, D. Gatteschi, D. N. Hendrickson, R. Sessoli, *MRS Bull.* **2000**, *25*, 66; b) D. Gatteschi, R. Sessoli, *Angew. Chem.* **2003**, *115*, 278; *Angew. Chem. Int. Ed.* **2003**, *42*, 268; c) M. N. Leuenberger, D. Loss, *Nature* **2001**, *410*, 789.
- [3] G. Aromí, E. K. Brechin, *Struct. Bonding (Berlin)* **2006**, *122*, 1.
- [4] M. Murugesu, M. Habrych, W. Wernsdorfer, K. A. Abboud, G. Christou, *J. Am. Chem. Soc.* **2004**, *126*, 4766.
- [5] W. Liu, H. H. Thorp, *Inorg. Chem.* **1993**, *32*, 4102 and see supplementary data.
- [6] a) R. Chevrel, M. Sergent, J. Prigent, *J. Solid State Chem.* **1971**, *3*, 315; b) T. Hughbanks, R. Hoffman, *J. Am. Chem. Soc.* **1983**, *105*, 1150.
- [7] See, for example: a) G. S. Papaefstathiou, A. Escuer, C. P. Raptopoulou, A. Terzis, S. P. Perlepes, R. Vicente, *Eur. J. Inorg. Chem.* **2001**, 1567; b) G. S. Papaefstathiou, A. Escuer, R.

## Asymmetric Catalysis

DOI: 10.1002/anie.200601076

**Efficient Construction of the Clerodane Decalin Core by an Asymmetric Morita–Baylis–Hillman Reaction/Lewis Acid Promoted Annulation Strategy\*\***

Stacy A. Rodgen and Scott E. Schaus\*

Dedicated to Professor James S. Panek  
on the occasion of his 50th birthday.

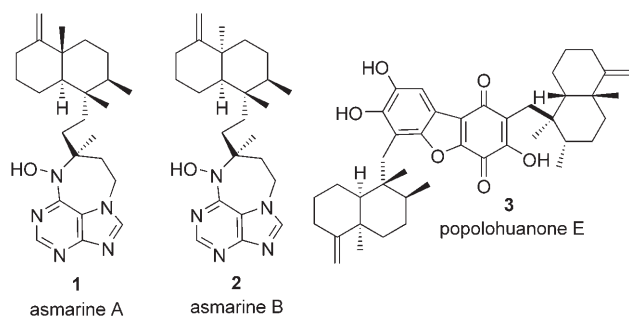
The clerodane class of natural products are diterpenes that exhibit wide-ranging structural diversity.<sup>[1]</sup> Over 150 new bioactive clerodanes have been reported since 2002.<sup>[2]</sup> Of particular interest are asmarines A (**1**) and B (**2**)<sup>[3]</sup> and popolohuanone E (**3**),<sup>[4]</sup> members of this class of natural products that exhibit potent antiproliferative activity against several types of human-cancer-cell lines (Scheme 1).<sup>[5]</sup> Popolohuanone E is a topoisomerase II inhibitor,<sup>[4]</sup> whereas the biological target of asmarine A or B is not known. Given their biological activity and the prevalence of the structural motif they display, a general and efficient strategy towards the core structure of the clerodane would be attractive.

[\*] S. A. Rodgen, Prof. Dr. S. E. Schaus  
Department of Chemistry  
Metcalf Center for Science and Engineering  
Boston University, 590 Commonwealth Avenue  
Boston, Massachusetts, 02215 (USA)  
Fax: (+1) 617-353-6466  
E-mail: seschaus@bu.edu

[\*\*] The authors acknowledge Dr. J. P. Lee (Boston University) for assistance with key NMR experiments and Dr. E. B. Lobkovsky (Cornell University) for X-ray crystallographic analysis. This research was supported by a NSF CAREER grant (CHE-0349206) and Amgen, Inc.

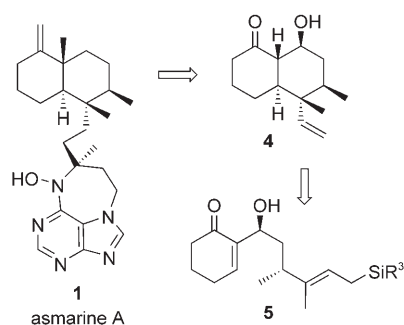


Supporting information for this article is available on the WWW under <http://www.angewandte.org> or from the author.



**Scheme 1.** Biologically active clerodane natural products.

Synthesis of the diterpene core structure has focused on elaboration of the Wieland–Miescher ketone.<sup>[6]</sup> Complementary approaches have elegantly utilized diastereoselective ring-annulation strategies towards substituted decalin structures; however, these approaches have mainly been racemic.<sup>[7]</sup> Recently, we reported the asymmetric Morita–Baylis–Hillman (MBH) reaction of cyclohexenone with aldehydes promoted by trialkyl phosphines and catalyzed by binaphthol-derived Brønsted acids.<sup>[8]</sup> We envisioned an asymmetric synthetic strategy toward the clerodane decalin core through a two-step ring-annulation procedure (Scheme 2).<sup>[9]</sup> The first



**Scheme 2.** Retrosynthetic analysis of asmarine A (**1**), thus illustrating the key MBH building block **5**.

step would be an asymmetric MBH reaction of cyclohexenone with an aldehyde functionalized with an appropriate nucleophile<sup>[10]</sup> followed by a Lewis acid promoted ring formation.<sup>[11]</sup> The ring-annulation strategy we chose was an intramolecular Hosomi–Sakurai reaction<sup>[12]</sup> that required the synthesis and use of aldehydes containing allyl silanes in the asymmetric MBH reaction. Herein, we report the construction of the clerodane decalin core through an asymmetric MBH reaction/Lewis acid promoted annulation strategy.

The strategy relies on two key experimental observations. First, the allyl silyl containing aldehyde must afford the MBH product with high enantioselectivity. Second, the enantiomeric excess of the product must be maintained during the ring-annulation process. We initially evaluated the scope of the MBH reaction of cyclohexenone with unsaturated silane containing aldehydes (Table 1). We found the Brønsted acid catalyzed phosphine-promoted MBH reaction conditions were mild enough to tolerate a variety of silane-containing aldehydes.<sup>[13]</sup>

**Table 1.** Brønsted acid catalyzed asymmetric MBH reactions.<sup>[a]</sup>

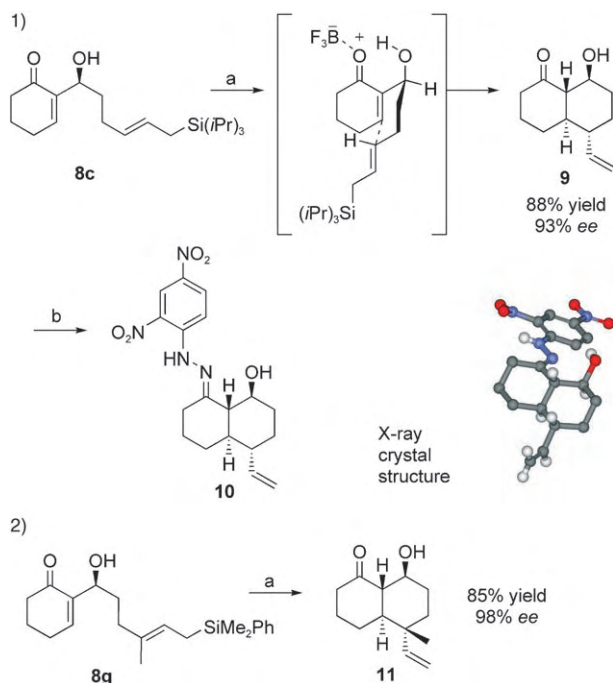
Entry	Aldehyde	Yield [%] <sup>[b]</sup>	<i>ee</i> <sup>[c]</sup> [%]
1		<b>8 a</b> (75)	86
2		<b>8 b</b> (94)	98
3		<b>8 c</b> (96)	93 <sup>[d]</sup>
4		<b>8 d</b> (80)	90
5		<b>8 e</b> (75)	91 <sup>[d]</sup>
6		<b>8 f</b> (94)	93
7		<b>8 g</b> (97)	98

[a] Reactions were run with **6** (1 mmol), cyclohexenone (2 mmol),  $\text{PEt}_3$  (2 mmol), and (*R*)-**7** (0.1 mmol) in THF (1 M) at  $-10^\circ\text{C}$  for 48 h under argon followed by flash chromatography on silica gel. [b] Yield of the isolated product. [c] Determined by chiral HPLC analysis. [d] Enantiomeric excess of the major olefin isomer. TBS = tributyltrimethylsilyl, TMS = trimethylsilyl.

We first considered alkynyl and vinyl silanes in the reaction (Table 1, entries 1 and 2). Although the general reaction conditions afforded the alkyne-containing product **8 a** in only 86% *ee*, the vinyl silane containing aldehyde underwent a more selective reaction (98% *ee*). The MBH reaction conditions proved general for allyl silane containing aldehydes **6 c–g** (Table 1, entries 3–7). The reaction of these aldehydes with cyclohexenone promoted by  $\text{PEt}_3$  and 10 mol% of catalyst **7** in THF at  $-10^\circ\text{C}$  afforded the corresponding MBH products **8 c–8 g** in good yields (75–97%) and with high enantioselectivities (90–99% *ee*). The successful MBH reactions of this substrate class illustrated that acid-sensitive, multifunctional aldehydes of this type could be tolerated in the reaction. With the successful production of these MBH products, we began our investigation of the Lewis acid promoted ring annulation as a way to access the desired decalin ring system.

Experiments were carried out to determine the feasibility of a diastereoselective ring annulation of **8 c**. A selection of Lewis acids ( $\text{BF}_3\cdot\text{OEt}_2$ ,  $[\text{TiCl}_4]$ ,  $[\text{Yb}(\text{OTf})_3]$ ,  $[\text{Sc}(\text{OTf})_3]$ , and  $\text{MgBr}_2\cdot\text{OTf}$  = triflate) were evaluated in the reaction for their ability to affect the intramolecular ring formation diastereo-

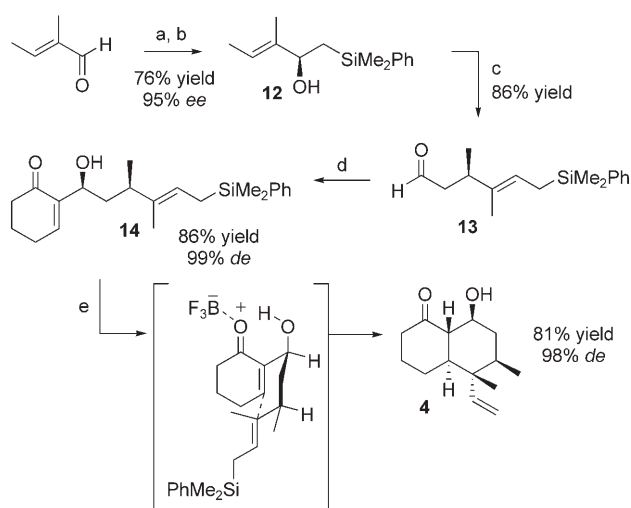
selectively and result in high yields while maintaining the enantiomeric excess during the reaction.<sup>[7a]</sup> Although many of these Lewis acids were capable of affecting ring formation,  $\text{BF}_3 \cdot \text{OEt}_2$  was found to be optimal for yield and chemo-selectivity. Treatment of allyl silane **8c** with  $\text{BF}_3 \cdot \text{OEt}_2$  at  $-78$  to  $-10^\circ\text{C}$  resulted in efficient ring formation to afford decalin **9** in 88 % yield of the isolated product as a single diastereomer (Scheme 3). The enantiomeric excess of the product was



**Scheme 3.** Ring-annulation reactions of allyl silane containing MBH products 1) **8c** and 2) **8g**. a)  $\text{BF}_3 \cdot \text{OEt}_2$ ,  $\text{CH}_2\text{Cl}_2$ ,  $-78 \rightarrow -10^\circ\text{C}$ ; b) dinitrophenylhydrazine, EtOH, RT. X-ray structure of **10**.

determined to be 93 % *ee* by chiral HPLC chromatography. The formation of the *trans* decalin bicyclic ring structure was confirmed by X-ray crystallographic analysis of the corresponding dinitrophenyl hydrazone **10**. The observed selectivity can be rationalized by a chairlike transition state that places the secondary alcohol in an equatorial position. Protonation of the resulting enolate after the conjugate addition affords the thermodynamically favored *trans* decalin system. The reaction conditions using  $\text{BF}_3 \cdot \text{OEt}_2$  proved equally effective at promoting the ring annulation of allyl silane **8g**. The bicyclic product was formed in 85 % yield without a significant change in the enantiomeric excess. The formation of *trans* decalin was confirmed by an observed NOE interaction between the axial  $-\text{CH}_3$  group and the axial methine hydrogen atom.

We next set out to construct the chiral aldehyde required for the synthesis of the clerodane core structure through the two-step asymmetric MBH reaction/Lewis acid promoted ring-annulation strategy. Our strategy for the synthesis of **13** relied on an asymmetric reduction followed by a stereoselective [3,3] sigmatropic rearrangement of the corresponding vinyl ether (Scheme 4).<sup>[14]</sup> The Grignard reaction of tiglic aldehyde with  $\text{ClMgCH}_2\text{SiMe}_2\text{Ph}$  followed by oxidation of



**Scheme 4.** Synthesis of clerodane core **4**. a) 1.  $\text{ClMgCH}_2\text{SiMe}_2\text{Ph}$ ,  $\text{Et}_2\text{O}$ ,  $0^\circ\text{C}$ ; 2. IBX, EtOAc,  $76^\circ\text{C}$ ; b) (*R*)-Me-CBS (0.4 equiv),  $\text{BH}_3$ , THF,  $-50^\circ\text{C}$ ; c) 1.  $\text{Hg}(\text{OAc})_2$  (0.028 equiv),  $\text{EtOCH}=\text{CH}_2$ ,  $35^\circ\text{C}$ ; 2. chromatography on silica gel; d) cyclohexenone,  $\text{PEt}_3$ , (*R*)-**7** (0.1 equiv), THF,  $-10^\circ\text{C}$ , 48 h; e)  $\text{BF}_3 \cdot \text{OEt}_2$ ,  $\text{CH}_2\text{Cl}_2$ ,  $-78 \rightarrow -10^\circ\text{C}$ . IBX = *o*-iodoxybenzoic acid. (*R*)-Me-CBS = (*R*)-methyl oxazaborolidine.

the resulting alcohol with IBX<sup>[15]</sup> in ethyl acetate afforded the ketone in 90 % yield. Asymmetric reduction of the unsaturated ketone with  $\text{BH}_3$  catalyzed by the Corey (*R*)-Me-CBS catalyst<sup>[16]</sup> provided the requisite chiral allylic alcohol **12** in 95 % *ee*. Formation of the vinyl ether was carried out in refluxing ethyl vinyl ether and catalyzed by  $\text{Hg}(\text{OAc})_2$ .<sup>[17]</sup> A stereoselective [3,3] sigmatropic rearrangement was found to proceed upon chromatography on silica gel to give the aldehyde in 85 % yield.<sup>[17]</sup> The asymmetric MBH reaction of aldehyde **13** with cyclohexenone using the Brønsted acid catalyst (*R*)-**7** afforded alcohol **14** in 86 % yield of the isolated product and 99 % *de*. The intramolecular Hosomi–Sakurai reaction using  $\text{BF}_3 \cdot \text{OEt}_2$  resulted in the clean formation of the desired clerodane core structure **4** in 81 % yield of isolated product and 98 % *de*. Based on our originally proposed transition state, the new methyl substituent in the six-membered transition state adopted an equatorial position that reinforced the chairlike transition state to yield *trans* decalin **4**. The substituents on the allyl silane work synergistically to produce high levels of diastereoselectivity; an approach that has previously been met with mixed success.<sup>[7c–d]</sup>

In summary, we have developed a general route to the clerodane diterpene core by using an asymmetric MBH/Lewis acid mediated ring-annulation process. We have expanded the scope of the asymmetric MBH reaction to include silane-containing aldehydes that can be utilized in synthesis. We have elaborated these MBH products into the *trans* decalin core by using an intramolecular Lewis acid promoted ring annulation. Utilization of this synthetic methodology in the synthesis of bioactive clerodanes is underway and will be reported in due course.

Received: March 19, 2006

Published online: June 27, 2006



**Keywords:** asymmetric catalysis · Brønsted acids · Morita–Baylis–Hillman reaction · organocatalysis · phosphanes · synthetic methods

- [1] a) A. T. Merritt, S. V. Ley, *Nat. Prod. Rep.* **1992**, 9, 243; b) T. J. Tokoroyama, *Synth. Org. Chem. Jpn.* **1993**, 51; c) J. R. Hanson, *Nat. Prod. Rep.* **2002**, 19, 125.
- [2] a) B. R. Copp, *Nat. Prod. Rep.* **2003**, 20, 535; b) J. R. Hanson, *Nat. Prod. Rep.* **2005**, 22, 594.
- [3] a) Y. Tesfamariam, A. Rudi, S. Zafra, I. Goldberg, G. Gravalos, M. Chleyer, Y. Kashman *Tetrahedron Lett.* **1998**, 39, 3323; b) T. Yosief, A. Rudi, Y. Kashman, *J. Nat. Prod.* **2000**, 63, 299.
- [4] J. R. Carney, P. J. Scheuer, *Tetrahedron Lett.* **1993**, 34, 3727.
- [5] D. Pappo, S. Shimony, Y. Kashman, *J. Org. Chem.* **2005**, 70, 199.
- [6] a) H. Kawano, M. Itoh, T. Katoh, S. Terashima, *Tetrahedron Lett.* **1997**, 38, 7769; b) A. X. Xiang, D. A. Watson, T. Ling, E. A. Theodorakis, *J. Org. Chem.* **1998**, 63, 6774; c) I. E. Marko, M. Wiaux, S. M. Warriner, P. R. Giles, P. Eustace, D. Dean, M. Bailey, *Tetrahedron Lett.* **1999**, 40, 5629; d) A. S. Kende, J. J. Rustenhoven, K. Zimmermann, *Tetrahedron Lett.* **2000**, 41, 843; e) T. T. Ling, F. Rivas, E. A. Theodorakis, *Tetrahedron Lett.* **2002**, 43, 9019.
- [7] a) T. Tokoroyama, M. Asada, H. Iio, *Tetrahedron Lett.* **1984**, 25, 5070; b) M. Tsukamoto, T. Asada, H. Iio, T. Tokoroyama, *Tetrahedron Lett.* **1987**, 28, 6645; c) T. Tokoroyama, H. Iio, K. Okada, *J. Chem. Soc. Chem. Commun.* **1989**, 1572; d) T. Aoto, T. Tokoroyama, *J. Org. Chem.* **1998**, 63, 4151; e) P. Wasnaire, M. Wiaux, M. R. Touillaux, I. E. Markó, *Tetrahedron Lett.* **2006**, 47, 985.
- [8] a) N. T. McDougal, S. E. Schaus, *J. Am. Chem. Soc.* **2003**, 125, 12024; b) N. T. McDougal, W. L. Trevellini, S. A. Rodgen, L. T. Kliman, S. E. Schaus, *Adv. Synth. Catal.* **2004**, 346, 1231.
- [9] M. Tsukamoto, H. Iio, T. Tokoroyama, *Tetrahedron Lett.* **1984**, 25, 5067.
- [10] For reviews on the synthetic utility of the MBH reaction, see: a) D. Basavaiah, A. J. Rao, T. Satyanarayana, *Chem. Rev.* **2003**, 103, 811; b) E. Ciganek, *Org. React.* **1997**, 51, 201; c) D. Basavaiah, P. D. Rao, R. S. Hyma, *Tetrahedron* **1996**, 52, 8001; d) S. E. Drewes, G. H. P. Roos, *Tetrahedron* **1988**, 44, 4653.
- [11] Reviews: a) E. Langkopf, D. Schinzer, *Chem. Rev.* **1995**, 95, 1375; b) M. A. Varner, R. B. Grossman, *Tetrahedron* **1999**, 55, 13867; examples: c) J. M. Luteijn, A. de Groot, *J. Org. Chem.* **1981**, 46, 3448; d) G. Majetich, R. Desmond, A. M. Casares, *Tetrahedron Lett.* **1983**, 24, 1913; e) P. S. Jones, S. V. Ley, N. S. Simpkins, A. J. Whittle, *Tetrahedron* **1986**, 42, 6519; f) G. Majetich, R. W. Desmond, Jr., J. J. Soria, *J. Org. Chem.* **1986**, 51, 1753; g) T. Tokoroyama, K. Okada, H. Iio, *J. Chem. Soc. Chem. Commun.* **1989**, 1572; h) H. Boushard, J. Y. Lallemand, *Tetrahedron Lett.* **1990**, 31, 5151; i) C. Dufresne, D. Cretney, C. K. Lau, V. Mascitti, N. Tsou, *Tetrahedron: Asymmetry* **2002**, 13, 1965.
- [12] a) A. Hosomi, H. Sakurai, *Tetrahedron Lett.* **1976**, 1295; b) E. W. Colvin, *Chem. Soc. Rev.* **1978**, 7, 15.
- [13] a) S. R. Wilson, M. F. Price, *J. Am. Chem. Soc.* **1982**, 104, 1124; b) K. Nonoshita, H. Banno, K. Maruoka, H. Yamamoto, *J. Am. Chem. Soc.* **1990**, 112, 316; c) R. T. Beres, J. S. Solomon, M. G. Yang, N. F. Jain, J. S. Panek, *Org. Synth.* **1997**, 75, 78.
- [14] J. D. More, N. S. Finney, *Org. Lett.* **2002**, 4, 3001.
- [15] a) E. J. Corey, R. K. Bakshi, S. Shibata, *J. Am. Chem. Soc.* **1987**, 109, 5551; b) E. J. Corey, C. J. Helal, *Angew. Chem.* **1998**, 110, 2092; *Angew. Chem. Int. Ed.* **1998**, 37, 1986.
- [16] J. C. Anderson, D. J. Pearson, *J. Chem. Soc. Perkin Trans. 1* **1998**, 2023.
- [17] For Brønsted acid catalyzed [3,3] sigmatropic rearrangements, see: a) L. H. Kuo, D. P. Curran, *Tetrahedron Lett.* **1995**, 36, 6647; b) G. Nordmann, S. L. Buchwald, *J. Am. Chem. Soc.* **2003**, 125, 4978.

DOI: 10.1002/anie.200600976

**Metastable Sorption State of a Metal–Organic Porous Material Determined by In Situ Synchrotron Powder Diffraction\*\****Yoshiki Kubota,\* Masaki Takata, Ryotaro Matsuda, Ryo Kitaura, Susumu Kitagawa, and Tatsuo C. Kobayashi*

Metal–organic microporous materials (MOMMs)<sup>[1]</sup> have attracted the attention of scientists for a number of reasons including the creation of nanometer-sized spaces, discovery of novel phenomena, and commercial interests such as their application in gas separation,<sup>[2]</sup> gas storage,<sup>[2,3]</sup> and heterogeneous catalysis.<sup>[4]</sup> Recent activity in crystal engineering has provided several examples of MOMMs which have rigid open frameworks and therefore the potential to be functionally related to zeolites. In fact, MOMMs often have a much more dynamic framework than is generally believed, and this is

[\*] Dr. Y. Kubota

Department of Physical Science  
Graduate School of Science  
Osaka Prefecture University  
Sakai, Osaka 590-0035 (Japan)  
Fax: (+81) 72-222-4791  
E-mail: kubotay@p.s.osakafu-u.ac.jp

Dr. M. Takata<sup>[†]</sup>

Japan Synchrotron Radiation Research Institute/SPRING-8  
Sayo-gun, Hyogo, 679-5198 (Japan)  
and

CREST, Japan Science and Technology Agency (Japan)

Dr. R. Matsuda, Dr. R. Kitaura,<sup>[††]</sup> Prof. Dr. S. Kitagawa  
Department of Synthetic Chemistry and Biological Chemistry  
Graduate School of Engineering, Kyoto University  
Katsura, Kyoto 615-8510 (Japan)

Prof. Dr. T. C. Kobayashi

Department of Physics  
Okayama University  
Okayama 700-8530 (Japan)

[†] Present address: Structural Materials Science Laboratory

Harima Institute, RIKEN SPRING-8 Center  
Sayo-gun, Hyogo, 679-5148 (Japan)

[††] Present address: Department of Chemistry

Graduate School of Sciences  
Nagoya University  
Nagoya 464-8603 (Japan)

[\*\*] This study was supported by CREST/JST and JASRI/SPRING-8 Nanotechnology Support Project of the Ministry of Education, Culture, Sports, Science and Technology of Japan. This study was also supported by a Grant-In-Aid for Science Research in a Priority Area "Chemistry of Coordination Space" from the Ministry of Education, Culture, Sports, Science and Technology of Japan. The authors thank Dr. K. Kato for the kind advice and support in data collection and Dr. H. Tanaka for the computer program ENIGMA for the MEM analysis.



Supporting information for this article is available on the WWW under <http://www.angewandte.org> or from the author.

characteristic of metal–organic species.<sup>[5]</sup> Dynamic pores could come from a sort of “soft” framework with multistability, whose states go back and forth between two counterparts; or a system could exist in one or two states for the same values of external field parameters. The structural rearrangement of the host framework in response to guest molecules proceeds from the “open” phase to the “closed” phase. The MOMMs could also be a unique class of materials with characteristics unlike those of rigid porous materials. While sorption profiles of MOMMs with saturated amounts of guests have been well characterized so far,<sup>[6]</sup> their intermediate profiles are still unknown. It is important to determine how guest molecules are recognized and finally confined by nanopores. An in-depth understanding of the intermediate state provides us with a feasible design for a porous framework which changes its structure into one well suited to a desired guest molecules and results in an efficient accommodation system. Therefore, fundamental structural information on not only the host framework but also the guest molecules is required throughout adsorption phenomena. X-ray diffraction is one of the most powerful methods that can directly provide structural information on the adsorbed molecules. Herein we report the structure analysis of an intermediate phase in the process of gas adsorption in the nanochannels of an MOMM by in situ synchrotron powder diffraction.

Previously,<sup>[2]</sup> we reported adsorption of acetylene gas on CPL-1 (coordination polymer 1 with pillared-layer structure:  $\text{Cu}_2(\text{pzdc})_2(\text{pyz})$  where pzdc is pyrazine-2,3-dicarboxylate and pyz is pyrazine).<sup>[7]</sup> From accurate structural analysis, acetylene molecules were found to be trapped by forming double hydrogen bonds with uncoordinated carboxylate oxygen atoms. In situ powder diffraction patterns for gas adsorption between the anhydrous hollow phase (phase I) and the saturated adsorbed phase (phase S) revealed another phase mixed with phase S. It was also observed in the desorption process. The acetylene gas adsorption isotherm for CPL-1 at 270 K shows a steep rise in the very low pressure region and reaches saturation. During the rise, a step is evident at about 0.7 molecules per unit pore. These data suggest the existence of an intermediate phase of adsorption, which we call intermediate phase M. In the diffraction patterns for an acetylene gas pressure of 10 kPa reported previously,<sup>[2]</sup> phases S and M are mixed. By careful adjustment of both temperature and gas pressure, we succeeded in obtaining phase M as a single phase. Figure 1 shows the temperature dependence of the diffraction patterns of CPL-1 with acetylene under a constant gas pressure of 150 kPa. The sample was cooled from 390 K. The change in diffraction pattern at 360 K indicates that acetylene adsorption has started. Subsequently, another phase, assigned as phase S, appeared below 360 K. The peak intensities of phase M gradually decreased and those of phase S increased. The diffraction pattern at 360 K for single phase M was analyzed.

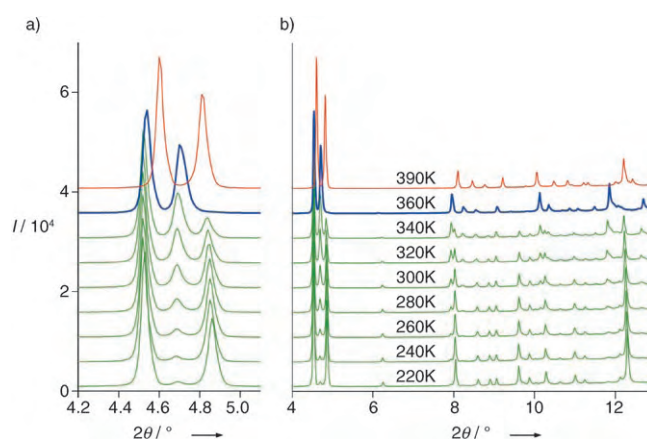


**Figure 1.** In situ synchrotron powder diffraction patterns of CPL-1 with adsorption of acetylene at 150 kPa. The  $2\theta$  ranges were a) from 4.2 to 5.1° and b) from 4.0 to 13.0°.

All the reflections were indexed with a monoclinic cell by the indexing program DICVOL91.<sup>[8]</sup> The lattice parameters were estimated to be  $a = 11.3050$ ,  $b = 20.2747$ ,  $c = 4.7272$  Å, and  $\beta = 98.669^\circ$ . The calculated figures of merit<sup>[9]</sup> were  $M(20) = 12.7$ ,  $F(20) = 57.4(0.0094, 37)$ . These lattice parameters are very similar to those reported for CPL-1.<sup>[7]</sup> The structure was analyzed by the maximum entropy method (MEM)/Rietveld technique.<sup>[10]</sup> The MEM calculation was performed with the computer program ENIGMA.<sup>[11]</sup> The Rietveld refinement with soft constraints on bond lengths and angles was carried out by using  $\sin \theta/\lambda = 0.45 \text{ \AA}^{-1}$ . The final Rietveld fitting of phase M of CPL-1 with acetylene molecules at 150 kPa and 360 K shows a satisfactory fitting. The reliability ( $R$ ) factors based on the powder profiles  $R_{\text{wp}}$  and the Bragg integrated intensities  $R_i$  were 3.27 and 4.70 %, respectively. The fundamental structures of the CPL-1 frameworks of phases I, M, and S are all identical. The space group of these phases is  $P2_1/c$ . The effect of acetylene adsorption on the lattice parameters, unit cell volumes, and pore volumes of CPL-1 is shown in Table 1. Lattice parameters  $b$ ,  $c$ , and  $\beta$  notably changed on acetylene adsorption. The unit cell of

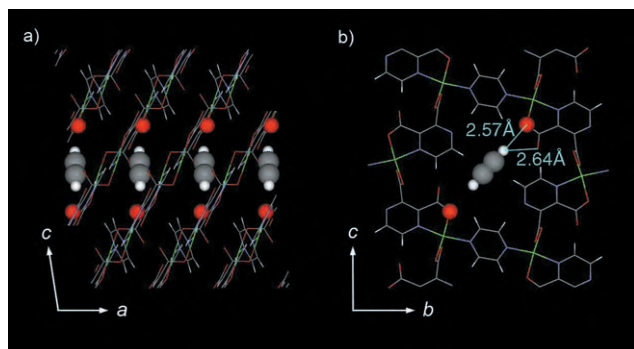
**Table 1:** Lattice parameters, unit cell volumes, and pore volumes of CPL-1.  $P$  is acetylene gas pressure,  $V_c$  is the unit cell volume, and  $V_p$  the pore volume.

Phase	$P$ [kPa]	$T$ [K]	$a$ [Å]	$b$ [Å]	$c$ [Å]	$\beta$ [°]	$V_c$ [Å <sup>3</sup> ]	$V_p$ [cm <sup>3</sup> g <sup>−1</sup> ]
Phase I <sup>[a]</sup>	0	390	4.7331(2)	19.9244(4)	10.8678(3)	96.009(4)	1019.25(5)	0.0876
Phase M	150	360	4.7094(1)	20.2467(5)	11.2824(4)	98.827(4)	1063.03(6)	0.104
Phase S <sup>[a]</sup>	10	170	4.81352(4)	20.2355(2)	10.7165(1)	96.937(1)	1036.18(3)	0.109
Phase I <sup>[b]</sup>	0	120	4.71534(6)	19.8280(2)	10.7184(1)	95.1031(10)	998.15(2)	0.0790

[a] From ref. [2]. [b] From ref. [6a].

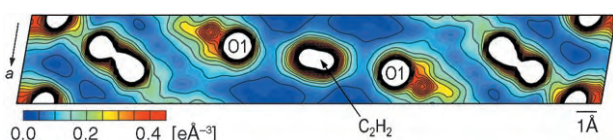
CPL-1 was found to expand once in phase M and contract to reach phase S, in which the acetylene molecules are trapped by forming double hydrogen bonds with oxygen atoms in the pore wall. On the other hand, the pore volume increased from phase I to M and was almost constant on going to phase S.

Figure 2 shows the determined crystal structure of phase M of CPL-1 with adsorbed acetylene. Acetylene



**Figure 2.** Determined crystal structure of phase M of CPL-1 with adsorbed acetylene. Views from a) side and b) front of the nanochannel directions. These figures show around one unit pore. Acetylene molecules (C gray, H white) and oxygen atoms (red; O1) of carboxylate bonded to the Cu ion are shown as spheres. Other atoms are connected by lines. Acetylene molecules occupy the sites with a probability of 0.7.

molecules are located in the center of the nanochannel with one molecular site per unit pore. The refined occupancy factor of the acetylene molecule was 0.70(2) and shows very good agreement with the step position in the adsorption isotherm. The isotropic thermal factor  $B$  of the acetylene molecule was refined to 17(3) Å<sup>2</sup>. This large  $B$  value means that the adsorbed acetylene molecules have pronounced thermal motion. The molecular axis of acetylene is perpendicular to the nanochannel direction and is on the line connecting the two oxygen atoms O1 of carboxylate bonded to a Cu ion. This orientation is different from that in phase S, in which the molecular axis is on the line connecting the uncoordinated oxygen atoms O2 of carboxylate. The interatomic distance between the hydrogen atom of acetylene and the neighboring O1 atom is 2.57 Å, while the distance to the O2 atom is 2.64 Å. These values are approximately equal to the sum of the van der Waals radii of hydrogen (1.2 Å) and oxygen (1.4 Å), that is 2.6 Å. Figure 3 shows a section through



**Figure 3.** Section through the MEM charge density of phase M of CPL-1 with adsorbed acetylene. The section contains the molecular axis of acetylene and the  $a$  axis. Contour lines are drawn from 0.00 to 1.00 eÅ<sup>-3</sup> with intervals of 0.05 eÅ<sup>-3</sup>. Higher density regions are omitted.

the MEM charge density containing the molecular axis of acetylene. Little electron density was observed between the adsorbed acetylene molecules and O1 atoms. From these results, the interaction of acetylene molecules with the oxygen sites is much weaker in phase M than in phase S.

The assembled structures of rod-shaped molecules confined in CPL-1 indicate that the dimers align approximately parallel to the nanochannel direction.<sup>[6a,12]</sup> However, in the most stable arrangement in acetylene adsorption, the molec-

ular axis of acetylene is perpendicular to the nanochannel direction in phase S. Since the size of an acetylene molecule is 5.5 × 3 Å and that of the rectangular nanochannel of CPL-1 is 4 × 6 Å, there is not enough space to permit acetylene molecules to adopt an orientation such as that allowed in phase S in the initial stage of adsorption. First, acetylene molecules are thought to be introduced into the nanochannels with their molecular axis along the nanochannel direction. Since the molecular size of 5.5 Å is larger than the lattice parameter  $a$ , which corresponds to the nanochannel direction in CPL-1, the adsorbed amount of molecules does not reach one molecule per unit pore and shows about 70% loading. After the introduction of acetylene molecules, they can easily rotate with thermal motion in the  $ac$  plane within the nanochannels. By this motion, they can align with the O1 atom for the first time within the restricted space of the nanochannel to form metastable phase M. Figure 4 shows

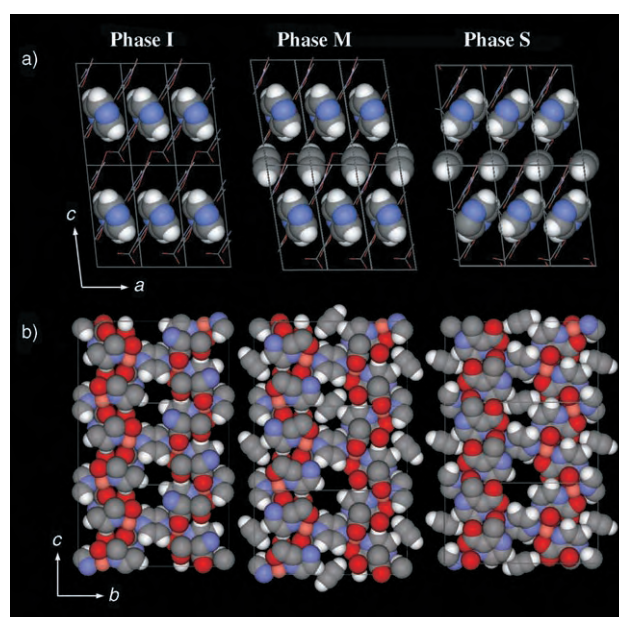


**Figure 4.** Crystal structures of CPL-1 with adsorbed acetylene. a) Side views of the nanochannels. Pillar molecules (pyrazine) and adsorbed acetylene molecules are shown as CPK models. Otherwise, they are connected by lines. b) Views from the nanochannel direction as CPK model. Adsorbed acetylene molecules are omitted from lower central pore in phases M and S (C gray, H white, N blue, O red).

crystal structures of phases I, M, and S of CPL-1 with adsorption of acetylene. Slight rotation of the pillar ligands, that is, the pyrazine rings, and shearing of the crystal lattice in the  $a$  direction indicate flexible transformation for efficient guest accommodation. Subsequently, phase M changes to phase S with a slight rotation of acetylene molecules, and then hydrogen bonds are formed with the two uncoordinated oxygen atoms. With this change, there is now sufficient space for the pyrazine ring to rotate. The hydrogen bond between the hydrogen atom of pyrazine and the neighboring O1 atom is associated with rotation of the pyrazine rings. Their interatomic distance is 2.3 Å in phase S. This results in rather a different orientation of pyrazine in phase S from



that in phases I and M. Shearing of the lattice also occurs again to permit more efficient guest accommodation. In the phase change from phase M to S, the unit cell volume decreases, whereby the lattice parameter  $c$  contracts due to the change in orientation of the acetylene molecule forming double hydrogen bonds with two oxygen atoms on the pore wall. However, rotation of the pillar ligand makes space without changing the pore volume significantly. At the same time, the change in size and shape of the nanochannel causes more acetylene loading to reach saturation of adsorption. This process is schematically shown in Figure 5.

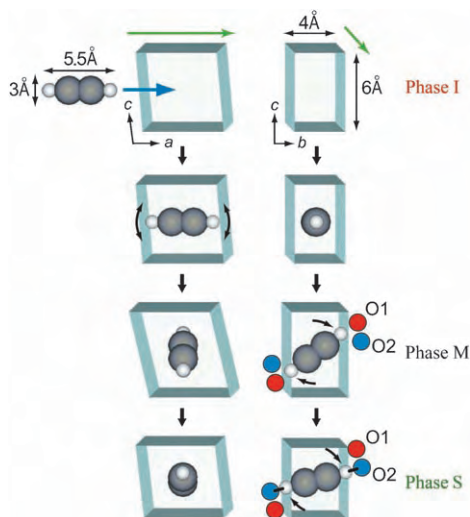


**Figure 5.** Schematic illustration of the adsorption process of acetylene in the nanochannel of CPL-1. Views from the side (left) and front (right) of the nanochannel directions. Boxes show the rectangular nanochannels. Green arrows show the nanochannel direction. Blue and red filled circles indicate the oxygen atoms of carboxylate. C gray, H white.

Phase M is the metastable state in the process. The molecular orientation changes within the restricted space in the nanochannel to reach the saturated adsorbed phase S. The CPL-1 framework expands once in phase M and contracts to reach phase S. Then rotation of the pillar ligands and lattice shearing occur to permit efficient guest accommodation. Using X-ray structure analysis, we have succeeded in visualizing the rearrangement of guest molecules and the transformation of the framework in the process of adsorption. We also found that the flexible framework of MOMMs can vary not only with guest size and/or shape but also with the amount of guest molecules to form optimum structures for guest accommodation. These findings will contribute to the development of novel functional MOMMs responsive to guest molecules. More structural studies on the gas adsorption process should be performed to attain an in-depth understanding of the adsorption phenomena.

## Experimental Section

The synthesis and fundamental crystal structure of CPL-1 were reported previously.<sup>[7]</sup> The in situ synchrotron powder diffraction

experiment was carried out at BL02B2 SPring-8 with a large Debye-Scherrer type diffractometer<sup>[13]</sup> equipped with a gas handling system. The wavelength of the incident X rays was 0.801 Å. The powder sample was loaded into a soda glass capillary with 0.4-mm inner diameter. The temperature was controlled by a low-temperature nitrogen gas blower. Before the measurements, the sample was heated to 390 K for 15 min in vacuum to remove water molecules present in the nanochannels. The diffraction pattern at 390 K was confirmed to be that of the anhydrous hollow phase of CPL-1. After that, acetylene gas was dosed into the capillary sample through a stainless steel tube. The amount of gas adsorption was controlled by changing the sample temperature under constant gas pressure. The exposure time of each temperature point was 5 min, and 10 min intervals were maintained before measurements so as to reach the equilibrium adsorption state. CCDC 294513 contains the supplementary crystallographic data for this paper. These data can be obtained free of charge from The Cambridge Crystallographic Data Centre via [www.ccdc.cam.ac.uk/data\\_request/cif](http://www.ccdc.cam.ac.uk/data_request/cif).

Received: March 13, 2006

Revised: April 28, 2006

Published online: June 29, 2006

**Keywords:** adsorption · metal–organic frameworks · microporous materials · structure elucidation · X-ray diffraction

- a) O. M. Yaghi, M. O'Keeffe, N. W. Ockwig, H. K. Chae, M. Eddaoudi, J. Kim, *Nature* **2003**, 423, 705–714; b) S. Kitagawa, R. Kitaura, S. Noro, *Angew. Chem.* **2004**, 116, 2388–2430; *Angew. Chem. Int. Ed.* **2004**, 43, 2334–2375.
- R. Matsuda, R. Kitaura, S. Kitagawa, Y. Kubota, R. V. Belosludov, T. C. Kobayashi, H. Sakamoto, T. Chiba, M. Takata, Y. Kawazoe, Y. Mita, *Nature* **2005**, 436, 238–241.
- a) S. Noro, S. Kitagawa, M. Kondo, K. Seki, *Angew. Chem.* **2000**, 112, 2161–2164; *Angew. Chem. Int. Ed.* **2000**, 39, 2082–2084; b) K. Seki, W. Mori, *J. Phys. Chem. B* **2002**, 106, 1380–1385; c) G. Férey, M. Latroche, C. Serre, F. Millange, T. Loiseau, A. Percheron-Guégan, *Chem. Commun.* **2003**, 24, 2976–2977; d) D. N. Dybtsev, H. Chun, S. H. Yoon, D. Kim, K. Kim, *J. Am. Chem. Soc.* **2004**, 126, 32–33; e) J. L. C. Rowsell, A. R. Millward, K. S. Park, O. M. Yaghi, *J. Am. Chem. Soc.* **2004**, 126, 5666–5667.
- a) O. Ohmori, M. Fujita, *Chem. Commun.* **2004**, 1586–1587; b) J. S. Seo, D. Whang, H. Lee, S. I. Jun, J. Oh, Y. J. Jeon, K. Kim, *Nature* **2000**, 404, 982–986.
- a) R. Matsuda, R. Kitaura, S. Kitagawa, Y. Kubota, T. C. Kobayashi, S. Horike, M. Takata, *J. Am. Chem. Soc.* **2004**, 126, 14063–14070; b) D. N. Dybtsev, H. Chun, K. Kim, *Angew. Chem.* **2004**, 116, 5143–5146; *Angew. Chem. Int. Ed.* **2004**, 43, 5033–5036.
- a) R. Kitaura, S. Kitagawa, Y. Kubota, T. C. Kobayashi, K. Kondo, Y. Mita, A. Matsuo, M. Kobayashi, H. Chang, T. C. Ozawa, M. Suzuki, M. Sakata, M. Takata, *Science* **2002**, 298, 2358–2361; b) Y. Kubota, M. Takata, R. Matsuda, R. Kitaura, S. Kitagawa, K. Kato, M. Sakata, T. C. Kobayashi, *Angew. Chem.* **2005**, 117, 942–945; *Angew. Chem. Int. Ed.* **2005**, 44, 920–923; c) S. Takamizawa, E. Nakata, *CrystEngComm* **2005**, 7, 476–479; d) G. J. Halder, C. J. Kepert, *J. Am. Chem. Soc.* **2005**, 127, 7891–7900; e) J. L. C. Rowsell, E. C. Spencer, J. Eckert, J. A. Howard, O. M. Yaghi, *Science* **2005**, 309, 1350–1354.
- M. Kondo, T. Okubo, A. Asami, S. Noro, T. Yoshitomi, S. Kitagawa, T. Ishii, H. Matsuzaka, K. Seki, *Angew. Chem.* **1999**, 111, 190–193; *Angew. Chem. Int. Ed.* **1999**, 38, 140–143.
- A. Boulton, D. Louer, *J. Appl. Crystallogr.* **1991**, 24, 987–993.
- a) P. M. de Wolff, *J. Appl. Crystallogr.* **1968**, 1, 108–113; b) G. S. Smith, R. L. Snyder, *J. Appl. Crystallogr.* **1979**, 12, 60–65.

- [10] a) M. Takata, B. Umeda, E. Nishibori, M. Sakata, Y. Saito, M. Ohno, H. Shinohara, *Nature* **1995**, 377, 46–49; b) M. Takata, E. Nishibori, M. Sakata, *Z. Kristallogr.* **2001**, 216, 71–86.
- [11] H. Tanaka, M. Takata, E. Nishibori, K. Kato, T. Iishi, M. Sakata, *J. Appl. Crystallogr.* **2002**, 35, 282–286.
- [12] R. Kitaura, R. Matsuda, Y. Kubota, S. Kitagawa, M. Takata, T. C. Kobayashi, M. Suzuki, *J. Phys. Chem. B* **2005**, 109, 23378–23385.
- [13] M. Takata, E. Nishibori, K. Kato, Y. Kubota, Y. Kuroiwa, M. Sakata, *Adv. X-ray Anal.* **2002**, 45, 377–384.

## Luminescence Marker

DOI: 10.1002/anie.200601197

**HaloTag Protein-Mediated Site-Specific Conjugation of Bioluminescent Proteins to Quantum Dots\*\***

Yan Zhang, Min-kyung So, Andreas M. Loening, Hequan Yao, Sanjiv S. Gambhir, and Jianghong Rao\*

Quantum dots are fluorescent semiconductor nanocrystals that have attracted much attention as fluorescence imaging probes owing to their unique optical properties such as high quantum yield, high molar extinction coefficients, narrow emission spectra, size-dependent tunable emission, and high photostability.<sup>[1–8]</sup> To apply quantum dots to biological detection and imaging applications, quantum dots have to be conjugated to molecules (e.g. peptide ligands, carbohydrate, antibodies, small molecule ligands) that can specifically recognize the biological target under study. Numerous examples have been reported on the use of quantum dots for both in vitro assays and in vivo imaging, but these

quantum dot conjugates are either assembled through non-specific interactions or prepared through site-nonspecific coupling reactions.<sup>[9–18]</sup> For example, for proteins, the conjugation typically involves random amide coupling with either amino- or carboxylate-presenting quantum dots.<sup>[9,15,16]</sup> Non-specific conjugation chemistry leads to chemical heterogeneity of synthesized conjugates, may compromise the protein activity and even induce aggregations, and is not applicable to specific labeling of target proteins in vivo.<sup>[19]</sup> Specific non-covalent interactions between receptors and ligands, such as carbohydrate–lectin and streptavidin–biotin, have been applied to assemble quantum-dot complexes.<sup>[1,20–21]</sup> Herein, we report a specific conjugation method that utilizes a genetically engineered hydrolase to covalently immobilize a bioluminescent protein at the quantum-dot surface. This immobilized bioluminescent protein can efficiently produce chemical energy to excite quantum dots through resonance energy transfer.

Our method employs a commercially available, engineered haloalkane dehalogenase, the HaloTag protein (HTP).<sup>[22]</sup> The native enzyme is a monomeric protein (MW  $\approx$  33 KDa) that cleaves carbon halogen bonds in aliphatic halogenated compounds.<sup>[22]</sup> Upon nucleophilic attack by the chloroalkane to Asp106 in the enzyme, an ester bond is formed between the HaloTag ligand and the protein (Scheme 1). HTP contains a critical mutation in the catalytic triad (His272 to Phe) so that the ester bond formed between HTP and HaloTag ligand cannot be further hydrolyzed (Scheme 1).<sup>[22]</sup> HaloTag ligands labeled with small organic dyes, such as coumarin and fluorescein, have been developed for in vivo labeling of target proteins.<sup>[22]</sup> Herein we apply this technology for the specific conjugation of proteins to quantum dots.

To take advantage of this specific protein–ligand interaction, quantum dots can be functionalized with HaloTag ligands. A protein target can in turn be genetically fused to HTP at either its N- or C- terminus. The resulting fusion protein can then be conjugated to quantum dots through the reaction between HaloTag ligands and HTP (Scheme 1).

To demonstrate the utility of this method for quantum dot conjugation, we chose a bioluminescent protein, *Renilla* luciferase, as our target. We have recently demonstrated that when *Renilla* luciferase is conjugated to quantum dots, bioluminescence resonance energy transfer (BRET) can take place.<sup>[23]</sup> Such quantum dot conjugates can emit light without light excitation and offer greatly improved sensitivity for in vivo imaging. With *Renilla* luciferase as the target protein for the conjugation, the conjugation reaction can be conveniently evaluated from the BRET emission of the quantum dots—a measure of both the conjugation chemistry and the function of the conjugated luciferase.

A stabilized mutant of *Renilla* luciferase (Luc8) was genetically fused to the N terminus of the HTP and expressed to obtain the fusion protein HTP–Luc8. The C terminus of HTP–Luc8 contained a 6  $\times$  His tag to facilitate its purification. Gel electrophoresis analysis indicated that the molecular weight of the fusion protein was consistent with the expected value, approximately 70 kDa (Figure 1a). The bioluminescence activity of the fusion protein was estimated to be 1.2  $\times$

[\*] Dr. Y. Zhang,<sup>[a]</sup> M.-K. So,<sup>[a]</sup> Dr. H. Yao, Prof. S. S. Gambhir, Prof. J. Rao  
Molecular Imaging Program at Stanford  
Department of Radiology  
Stanford University School of Medicine  
1201 Welch Road, Stanford, CA 94305-5484 (USA)  
Fax: (+1) 650-736-7925  
E-mail: jr Rao@stanford.edu

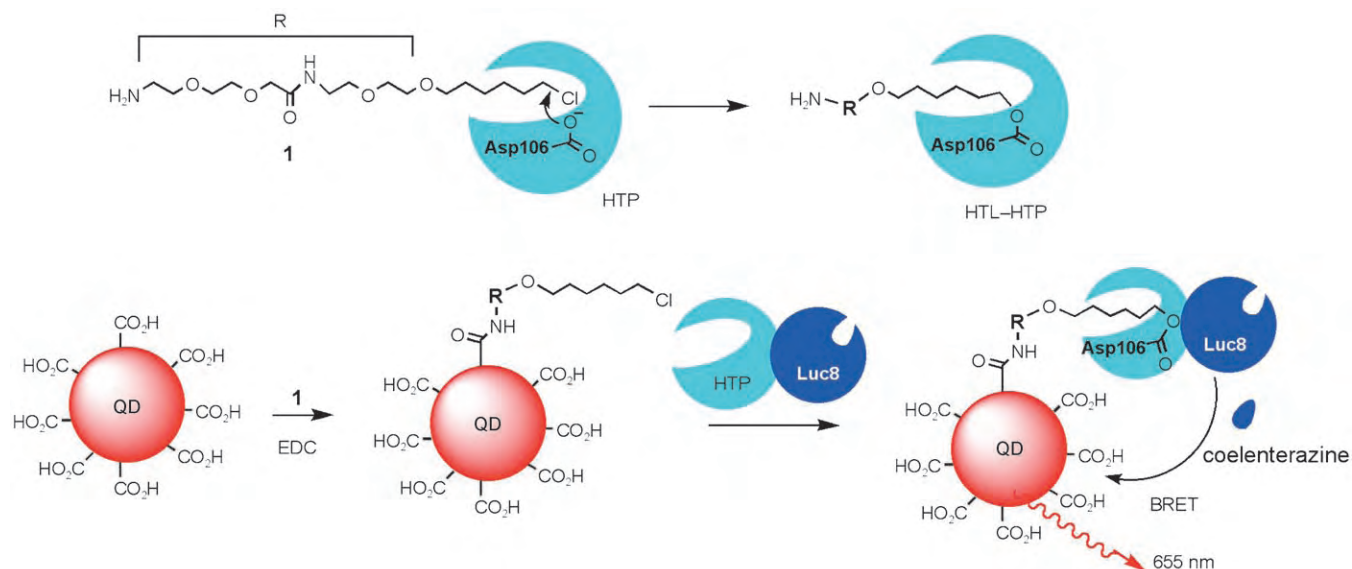
A. M. Loening, Prof. S. S. Gambhir  
Department of Bioengineering  
Stanford University  
Stanford, CA 94305 (USA)

[\*] Y. Zhang and M.-K. So equally contributed to this work.

[\*\*] This work was supported by the Burroughs Wellcome Fund (to J.R.), a Stanford School of Medicine Dean's Fellowship (to Y.Z.), the Korea Research Foundation Grant M07-2004-000-10234-0 (to M.K.S.), a Stanford Bio-X Graduate Fellowship (to A.M.L.), and the National Cancer Institute Centers of Cancer Nanotechnology Excellence (CCNE) U54.



Supporting information for this article is available on the WWW under <http://www.angewandte.org> or from the author.



**Scheme 1.** Schematic of the specific conjugation of proteins to quantum dots mediated by the HaloTag protein and its ligand. HTL = HaloTag ligand.

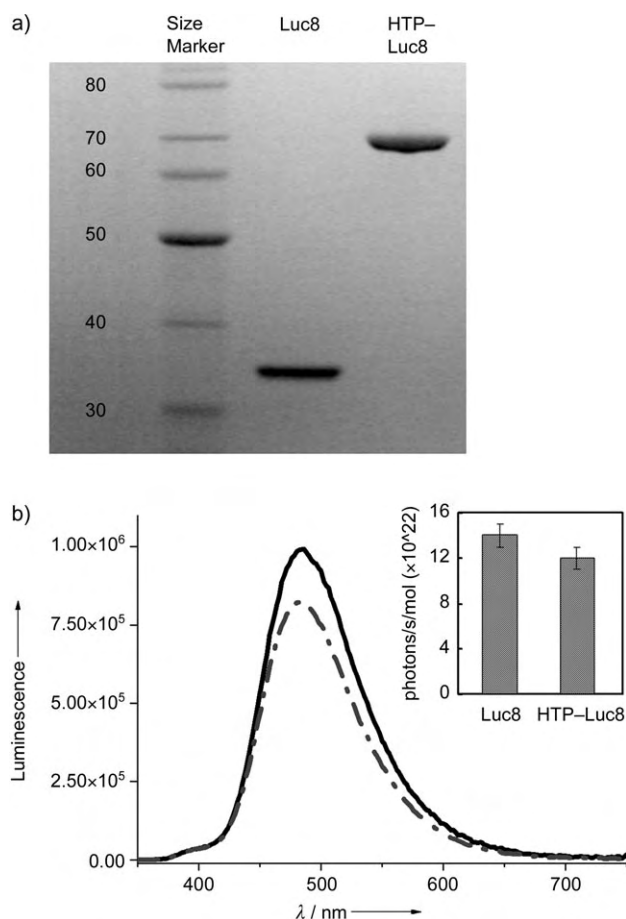


**Figure 1.** Characterization of the size and function of the fusion protein. a) Gel electrophoresis analysis confirmed the size of HTP-Luc8. Both proteins (0.5  $\mu$ g each) were run on a 4–12% Bis-Tris (bis(2-hydroxyethyl)amino-tris(hydroxymethyl)methane) gradient denaturing gel and stained with Coomassie Blue. The expected sizes for Luc8 and HTP-Luc8 were 37.1 and 70.3 kDa, respectively. b) Bioluminescence emission spectra of Luc8 (solid line) and HTP-Luc8 (dashed line). The inset shows the total photon production of Luc8 and HTP-Luc8.

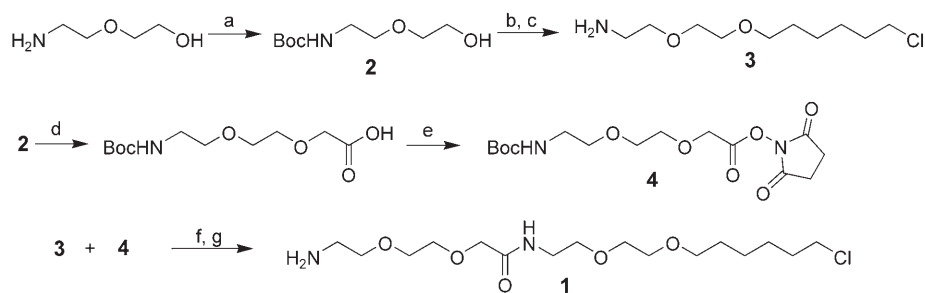
$10^{23}$  photons  $s^{-1}$  mol $^{-1}$ , which is approximately 86% of Luc8 (Figure 1b).

To minimize potential steric hindrance between the quantum dots and HaloTag proteins during conjugation, we designed a HaloTag ligand containing an amino ethylene glycol group that would help orient the ligand away from the quantum-dot surface (Scheme 1). The HaloTag ligand **1** was prepared from 6-chloro-1-iodohexane and 2-(2-aminoethoxy)ethanol by the synthetic route outlined in Scheme 2, and was then immobilized through its amino group to the carboxylate-presenting quantum dots (QD@COOH). The resulting quantum dots coated with the HaloTag ligand **1** (QD@1) showed good solubility in neutral pH buffer solution. The conjugation of the fusion protein HTP-Luc8 to QD@1 was carried out by a simple mixing of both at 37°C, resulting in the formation of an irreversible covalent bond between ligand **1** on quantum dots and HTP-Luc8.

As successful immobilization of HTP-Luc8 to quantum dots should allow BRET to occur, we measured the BRET emission from the quantum dots to follow the conjugation reaction. Addition of coelenterazine, the substrate for *Renilla* luciferase, to the purified conjugate QD@1-HTP-Luc8 resulted in a dual-peak bioluminescence emission spectrum (Figure 2). In addition to the Luc8 peak at 480 nm, there was an emission maximum at 655 nm that overlapped well with the fluorescence emission of the quantum-dot conjugates excited at 480 nm.

To evaluate whether the observed BRET emission was owing to specific conjugation between the quantum dots and fusion proteins, we examined the dependence of the BRET emission on the HaloTag ligand **1** that was used in the conjugation. QD@COOH was first functionalized with various concentrations of **1**. These modified quantum dots were subsequently conjugated with 20 equivalents of HTP-Luc8. Figure 3 shows that with increasing amounts of ligand **1** used in the conjugation, the bioluminescence emissions from both the immobilized HTP-Luc8 and the quantum dots through





**Scheme 2.** Synthesis of HaloTag ligand **1**. Reagent and conditions: a)  $\text{Boc}_2\text{O}/\text{EtOH}$ ,  $0^\circ\text{C}$ , 2 h; b)  $\text{NaH}/\text{DMF-THF}$  and 6-chloro-1-iodohexane; c)  $\text{TFA}/\text{anisole}$  in  $\text{DCM}$ ;  $\text{K}_2\text{CO}_3/\text{MeOH}$ ; d)  $\text{NaH}/\text{DMF-THF}$  and iodoacetic acid sodium salt; e)  $N$ -Hydroxysuccinimide and  $\text{DCC}$  in  $\text{DCM}$ ; f)  $\text{DIPEA}/\text{THF}$ ; g)  $\text{TFA}/\text{anisole}$  in  $\text{DCM}$ ;  $\text{K}_2\text{CO}_3/\text{MeOH}$ . Boc = *tert*-butoxycarbonyl, DMF = *N,N*-dimethylformamide, TFA = trifluoroacetic acid, DCM = dichloromethane, DCC = 1,3-dicyclohexylcarbodiimide, DIPEA = diisopropylethylamine.

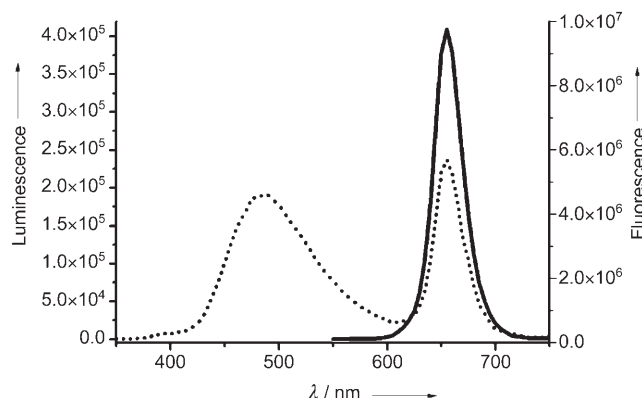


**Figure 2.** Bioluminescence (dashed line) and fluorescence (black solid line) spectra of conjugate QD@1-HTP-Luc8 in borate buffer solution. The fluorescence emission was collected with excitation at 480 nm.

BRET increased. When quantum dots (without a HaloTag ligand **1** attached) were similarly mixed with the fusion protein, there was only a small emission from HTP-Luc8 at 480 nm and a small BRET emission from the quantum dots. The small BRET emission probably arises from an electrostatic interaction between the  $6 \times \text{His}$  tag on HTP-Luc8 and the negative carboxylate groups on the quantum dots. These results confirm that the BRET emission reflects specific conjugation occurring between the quantum dots and the fusion protein HTP-Luc8, and that the fusion protein HTP-Luc8 retains its enzymatic activity after conjugation.

The efficiency of the resonance energy transfer process can be quantitatively estimated from the BRET ratio. The BRET ratio is defined by the acceptor emission relative to the donor emission.<sup>[23,24]</sup> In the quantum dot and HTP-Luc8 conjugate, the donor is Luc8 and the acceptor is the quantum dot. We calculated the BRET ratio by dividing the total emission from quantum dots by the total emission from HTP-Luc8, shown in Figure 3b. With the increase in the number of HaloTag ligand **1** and in turn the increase in immobilized fusion protein, the BRET ratio decreased gradually from 0.6 to 0.4. In principle, the BRET ratio should not depend on the

number of immobilized proteins if the BRET distance remains unchanged.<sup>[23]</sup> This small decrease in the BRET ratio may be due to a shift in the orientation of the conjugated fusion proteins on the quantum dot surface.<sup>[25]</sup>

Finally, we examined the dependence of the conjugation reaction on the amount of fusion-protein present. Quantum dots were reacted with 1000 equivalents of HaloTag ligand **1**, and then reacted with increasing concentrations of HTP-Luc8. As expected, the resulting conjugates showed increasing bioluminescence emissions both from HTP-Luc8 and from the quantum dots (Figure 4). As a control, Luc8 (without HTP fusion) was incubated with the QD@**1**. The control reaction showed no biolu-

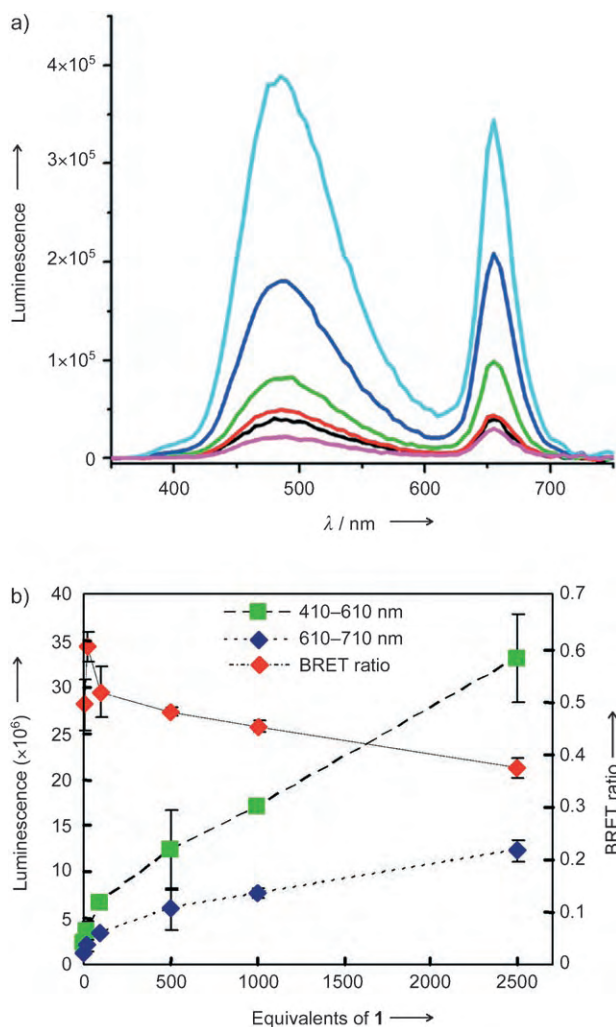


**Figure 3.** Dependence of the conjugation on the ligand **1**. a) Representative bioluminescence emission spectra of the conjugates synthesized at different concentrations of **1** (from bottom to top: 0, 20, 100, 500, 1000, and 2500 equivalents). b) Total bioluminescence emissions from HTP-Luc8 and from quantum dots, and the calculated BRET ratios of conjugates prepared in (a; in duplicate).

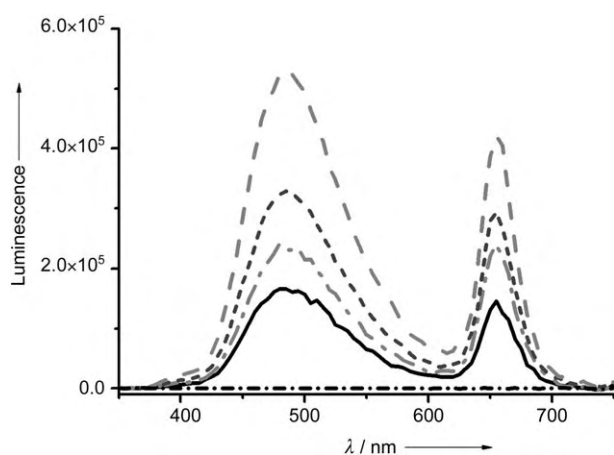


**Figure 4.** Bioluminescence emission spectra of quantum dots conjugated with HTP-Luc8 (going down from the top line: 100, 50, 20, and 10 equivalents) or 20 equivalents of Luc8 (bottom dash-dot line). The quantum dots were reacted with 1000 equivalents of HaloTag ligand **1** before the conjugation with HTP-Luc8. Unconjugated proteins were removed by filtration before measurement.

miniscence emission, therefore indicating no immobilization of Luc8 on the quantum dots and further confirming that the conjugation between quantum dots and HTP-Luc8 was specific.

In our previous demonstration of self-illuminating quantum dots for in vivo imaging, the quantum dots were conjugated with Luc8 in vitro before their introduction into living cells and animals. An important further step will be to specifically conjugate luciferases with quantum dots for functional imaging in vivo. The mild conjugation conditions used to immobilize proteins to quantum dots, mediated by the HaloTag protein and its ligand, may allow this method to be applied to specific labeling of target proteins with quantum dots in vivo. This method also offers an advantage in comparison to a widely used conjugation method based on biotin and streptavidin in that the HaloTag protein is monomeric and relatively small.

In summary, this communication reports a new method, based on the specific interaction between the HaloTag protein and its ligand, to functionalize quantum dots for biological imaging. By using this method, we successfully conjugated a bioluminescent protein to quantum dots and produced self-illuminating quantum dot conjugates. This specific conjugation under mild physiological conditions offers promises for specific in vivo labeling of proteins or cells with quantum dots for imaging.

## Experimental Section

Chemicals for HaloTag ligand synthesis were from Sigma-Aldrich. The coupling reagent 1-ethyl-3-(3-dimethylaminopropyl)carbodiimide hydrochloride (EDC) was from Fluka. Quantum dots were from Invitrogen and have typical CdSe/ZnS core-shell structures with the quantum yield (determined in 50 mM pH 9 borate buffer solution) of 83%. Coelenterazine was from Prolume. The plasmid pHT2 (HaloTag) was from Promega. NanoSep 100 K filters for quantum dot purification were from Pall, Life Science.

**Synthesis of **1**:** the compound was synthesized from 6-chloro-1-iodohexane and 2-(2-aminoethoxy)ethanol according to Scheme 2.  $^1\text{H}$  NMR (400 MHz,  $\text{CDCl}_3$ ):  $\delta$  = 3.92 (s, 2H), 3.70–3.20 (m, 18H), 2.09 (m, 2H), 2.64 (m, 2H), 2.50 (m, 2H), 1.40–1.20 ppm (s, 4H); LC-MS:  $m/z$  369.2 [ $M+1$ ] $^+$ ; calcd  $M^+$ : 368.2.

**Conjugation of **1** to quantum dots:** Quantum dots, HaloTag ligand **1**, and EDC (400 equiv) were mixed together in borate buffer solution (10 mM, pH 7.4) and incubated at room temperature for 1 h. QD@**1** was separated from free HaloTag ligand and excess EDC by filtration through a 100 K NanoSep filter. The quantum dot conjugates were washed three times with pH 8.5 borate buffer solution for 1 h before being recovered with pH 7.4 borate buffer solution. The concentration of QD@**1** was determined from the fluorescence intensity.

**Preparation and purification of HTP-Luc8:** the plasmid pBAD-Luc8-HaloTag encoded for the fusion protein was constructed from plasmid pBAD-RLuc8 and plasmid pHT2 by PCR and ligation. *E. coli* LMG194 cells transformed with this plasmid were induced with 0.2% arabinose and grown at 32°C to an optical density at a wavelength of 600 nm ( $\text{OD}_{600}$ ) of 0.7. Cells were lysed by thawing in wash buffer solution (WB; NaCl (300 mM), 2-[4-(2-hydroxyethyl)-1-piperazinyl]ethanesulfonic acid (HEPES; 20 mM), imidazole (20 mM), pH 8) containing lysozyme (1  $\text{mg mL}^{-1}$ ), RNase A (10  $\mu\text{g mL}^{-1}$ ), and DNase I (5  $\mu\text{g mL}^{-1}$ ). Lysates were clarified by centrifugation and allowed to bind to nickel affinity resin (Ni-NTA Superflow, Qiagen) for 1 h at 4°C with gentle mixing. After washing with WB, the protein was eluted with elution buffer solution (NaCl (300 mM), HEPES (20 mM), imidazole (250 mM), pH 8) and further purified by anion-exchange chromatography (Source 15Q resin, GE/Amersham) followed by gel-filtration chromatography with borate buffer solution.

**Conjugation of QD@**1** with HTP-Luc8:** Typically QD@**1** (5 pmol) was incubated with HTP-Luc8 (20 equiv) in borate buffer solution (10 mM, pH 7.4) at 37°C for 30 min. Free HTP-Luc8 was removed from the incubation mixture by filtration through a 100 K NanoSep filter at 4°C. The filtered conjugates were washed efficiently with pH 7.4 borate buffer solution at 4°C. The final quantum dot conjugates were recovered with ice-cold pH 7.4 borate buffer solution.

Fluorescence and bioluminescence spectra were collected with a Fluoro Max-3 (Jobin Yvon Inc.). Bioluminescence spectra were acquired with the excitation light blocked.

Received: March 26, 2006

Revised: May 19, 2006

Published online: June 29, 2006

**Keywords:** bioluminescence resonance energy transfer · conjugation · luciferase · protein structures · quantum dots

- [1] M. Bruchez, M. Moronne, P. Gin, S. Weiss, A. P. Alivisatos, *Science* **1998**, *281*, 2013–2016.
- [2] W. C. W. Chan, S. Nie, *Science* **1998**, *281*, 2016–2018.
- [3] I. L. Medintz, H. T. Uyeda, E. R. Goldman, H. Mattoussi, *Nat. Mater.* **2005**, *4*, 435–446.
- [4] X. Michalet, F. F. Pinaud, L. A. Bentolila, J. M. Tsay, S. Doose, J. J. Li, G. Sundaresan, A. M. Wu, S. S. Gambhir, S. Weiss, *Science* **2005**, *307*, 538–544.
- [5] C. M. Niemeyer, *Angew. Chem.* **2001**, *113*, 4254–4287; *Angew. Chem. Int. Ed.* **2001**, *40*, 4128–4158.
- [6] J. K. Jaiswal, S. M. Simon, *Trends Cell Biol.* **2004**, *14*, 497–504.
- [7] B. O. Dabbousi, J. Rodriguez-Viejo, F. V. Mikulec, J. R. Heine, H. Mattoussi, R. Ober, K. F. Jensen, M. G. Bawendi, *J. Phys. Chem. B* **1997**, *101*, 9463–9475.
- [8] C. A. Leatherdale, W. K. Woo, F. V. Mikulec, M. G. Bawendi, *J. Phys. Chem. B* **2002**, *106*, 7619–7622.

- [9] S. Kim, Y. T. Lim, E. G. Soltesz, A. M. De Grand, J. Lee, A. Nakayama, J. A. Parker, T. Mihaljevic, R. G. Laurence, D. M. Dor, L. H. Cohn, M. G. Bawendi, J. V. Frangioni, *Nat. Biotechnol.* **2004**, 22, 93–97.
- [10] R. Chakrabarti, A. M. Klibanov, *J. Am. Chem. Soc.* **2003**, 125, 12531–12540.
- [11] M. E. Akerman, W. C. W. Chan, P. Laakkonen, S. N. Bhatia, E. Ruoslahti, *Proc. Natl. Acad. Sci. USA* **2002**, 99, 12617–12621.
- [12] H. Mattoussi, J. M. Mauro, E. R. Goldman, G. P. Anderson, V. C. Sundar, F. V. Mikulec, M. G. Bawendi, *J. Am. Chem. Soc.* **2000**, 122, 12142–12150.
- [13] S. J. Rosenthal, I. Tomlinson, E. M. Adkins, S. Schroeter, S. Adams, L. Swafford, J. McBride, Y. Wang, L. J. DeFelice, R. D. Blakely, *J. Am. Chem. Soc.* **2002**, 124, 4586–4594.
- [14] X. Gao, Y. Cui, R. M. Levenson, L. W. K. Chung, S. Nie, *Nat. Biotechnol.* **2004**, 22, 969–976.
- [15] F. Pinaud, D. King, H.-P. Moore, S. Weiss, *J. Am. Chem. Soc.* **2004**, 126, 6115–6123.
- [16] X. Wu, H. Liu, J. Liu, K. N. Haley, J. A. Treadway, J. P. Larson, N. Ge, F. Peale, M. P. Bruchez, *Nat. Biotechnol.* **2003**, 21, 41–46.
- [17] I. L. Medinitz, A. R. Clapp, H. Mattoussi, E. R. Goldman, B. Fisher, J. M. Mauro, *Nat. Mater.* **2003**, 2, 630–638.
- [18] H. Mattoussi, J. M. Mauro, E. R. Goldman, T. M. Green, G. P. Anderson, V. C. Sundar, M. G. Bawendi, *Phys. Status Solidi B* **2001**, 224, 277–283.
- [19] For example, conjugation of biotin to firefly luciferase via non-specific N-hydroxysuccinimide ester coupling significantly decreases luciferase activity. See H. Arakawa, M. Maeda, A. Tsuji, *Anal. Lett.* **1992**, 25, 1055–1063.
- [20] X.-L. Sun, W. Cui, C. Haller, E. L. Chaikof, *ChemBioChem* **2004**, 5, 1593–1596.
- [21] M. Howarth, K. Takao, Y. Hayashi, A. Y. Ting, *Proc. Natl. Acad. Sci. USA* **2005**, 102, 7583–7588.
- [22] Technical Manual, Promega, “HaloTag Interchangeable Labeling Technology”; <http://www.promega.com>, **2006**.
- [23] M.-K. So, C. Xu, A. M. Loening, S. S. Gambhir, J. Rao, *Nat. Biotechnol.* **2006**, 24, 339–343.
- [24] K. D. G. Pflieger, K. A. Eidne, *Nat. Methods* **2006**, 3, 165–174.
- [25] A larger number of immobilized proteins would lead to denser packing at the surface, resulting in the Luc8 domain of the fusion proteins pushed further away from the quantum dot surface and consequently a larger average BRET distance.

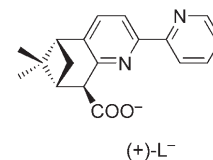
---

DOI: 10.1002/anie.200601939

**Switchable Chiral Architectures Containing Pr<sup>III</sup> Ions: An Example of Solvent-Induced Adaptive Behavior\*\****Olimpia Mamula,\* Marco Lama, Helen Stoeckli-Evans, and Sergiu Shova*

Discrete metallosupramolecular architectures are attractive synthetic targets and have found applications recently in catalysis, cavity-directed synthesis, and chemical sensing.<sup>[1]</sup> Some of these entities are the result of self-assembly processes that respond to environmental changes (solvent,<sup>[2]</sup> concentration,<sup>[3]</sup> template effect,<sup>[4]</sup> etc.) and represent interesting examples of dynamic combinatorial libraries<sup>[5]</sup> of interconverting self-assembled structures. As the lability of the metal–ligand coordination bonds is a prerequisite for such behavior, superstructures that contain arrays of lanthanide (Ln<sup>III</sup>) ions are expected to be relevant toward this end.<sup>[6]</sup> On the other hand, the complexation of f metal ions with chiral ligands opens new, little-explored, perspectives in the lanthanide series for a) the synthesis of configurationally stable, polynuclear, enantiopure species by using enantiopure ligands<sup>[7]</sup> and b) the study of chiral recognition phenomena when enantiomeric mixtures of ligands are employed.<sup>[8]</sup>

Recently, we demonstrated that a chiral bipyridine-carboxylate ligand (+)-L<sup>−</sup> self-assembles in the presence of Eu<sup>III</sup> cations to form a trinuclear helix, which displays an interesting version of supramolecular helical chirality.<sup>[9]</sup> Herein, we describe a solvent-dependent process in which a mixture of Pr<sup>III</sup> ions and the (+)-L<sup>−</sup> ligand with the same metal-to-ligand ratio (1:2.25) can follow two distinct self-assembly pathways that lead dia-



[\*] Dr. O. Mamula, M. Lama

Institut des sciences et ingénierie chimiques  
Ecole Polytechnique Fédérale de Lausanne, BCH 1403  
1015 Lausanne (Switzerland)  
Fax: (+41) 21-693-9815  
E-mail: olimpia.mamula@epfl.ch

Prof. H. Stoeckli-Evans  
Institut de microtechnologie  
Université de Neuchâtel  
Rue Emile-Argand 11, 2009 Neuchâtel (Switzerland)

Dr. S. Shova  
Department of Chemistry  
Moldova State University  
A. Mateevici 60, 2009 Chisinau (Moldova)

[\*\*] This work was supported by the Swiss National Science Foundation (grant no. 200020-105320). We thank Dr. R. Scopelliti for collecting the X-ray data for the compound *rac*-1, as well as S. Canarelli and F. Nydegger for the ES-MS measurements.



Supporting information for this article is available on the WWW under <http://www.angewandte.org> or from the author.



stereoselectively to two enantiopure architectures: a two-dimensional trinuclear array (in methanol) and a three-dimensional tetranuclear pyramidal polyhedron (in acetonitrile). Furthermore, the two polynuclear structures can be reversibly interconverted in acetonitrile simply by varying the amount of water that is present in the solvent.

In acetonitrile, the reaction between  $\text{Pr}(\text{ClO}_4)_3$  and the ligand (+)-HL·HCl (2.25 equiv) in the presence of triethylamine (5.2 equiv) did not give a precipitate, as was the case when the reaction was performed in methanol (see below), but gave a clear solution. This solution was homogeneous according to analysis by electrospray ionization mass spectrometry (ESI-MS), and the sole peak detected corresponded to the formula  $[\text{Pr}_4\text{L}_9(\text{OH})]^{2+}$  (see Supporting Information). Slow evaporation of the acetonitrile under anhydrous conditions (dessicator) led to the formation of crystals that were suitable for X-ray diffraction studies.<sup>[10]</sup> The crystal structure revealed a tetranuclear self-assembled compound,  $[\text{Pr}_4\{(+)\text{-L}\}_9(\mu_3\text{-OH})](\text{ClO}_4)_2$  (**1**), in which nine bridging ligands form three distinct helical domains with predetermined configuration (Figure 1).

The four metal ions, each displaying a coordination number of nine, form a pseudo-trigonal-pyramidal polyhedron. The basis of this metallic framework is a pseudo-equilateral triangle (metal–metal distances: 4.045(1), 4.076(1), and 4.070(1) Å), which is held together by a) a six bridging ligands that are divided into two sets of three and b) a  $\mu_3$ -hydroxy group, whose oxygen atom is situated on the pyramidal pseudo- $C_3$  axis and lies slightly above (0.96 Å) the triangular base. The fourth metal cation, which is situated 5.5 Å above the triangular base on the pseudo- $C_3$  axis on the same side as the  $\mu_3$ -OH group, represents the top vertex of the pyramidal metallic framework (averaged edge 6.0 Å). Three tridentate ligands (in gray), coordinated through the two nitrogen atoms from the bipyridine and one oxygen atom

from the carboxylate, are wrapped helically around this stereogenic metal center and induce a  $\Lambda$  configuration. Every second carboxylate oxygen atom from these three ligands is coordinated to one metal center from the triangular base to create a small cavity (see Figure 1b). The other six ligands included in this suprastructure are arranged in two distinct sets (yellow and violet) and are coordinated solely to the three basal  $\text{Pr}^{\text{III}}$  cations. In one set (yellow), the three ligands bridge symmetrically ( $\mu^2\text{-}\eta^1\text{:}\eta^1$ ) two adjacent metal ions through the two oxygen atoms from the carboxylate groups. Their uncoordinated bipyridine moieties adopt a *trans* conformation (dihedral angles vary from 2.05 to 16.43°) and form a supramolecular *M* helix. The term *supramolecular* as used here refers to the chirality and indicates the propeller-like arrangement of the ligands around a metallic core and not just one metal center as seen in classical mononuclear helical complexes. The three ligands of the other set (violet) are coordinated not only through the carboxylate oxygen atoms (one oxygen atom bridges asymmetrically two metal centers:  $\mu^2\text{-}\eta^2\text{:}\eta^1$ ; the second is monocoordinated) but also through the aromatic nitrogen centers. This set adopts a supramolecular *P*-helical arrangement.

The  $^1\text{H}$  NMR spectra of the crystals and the powder recovered from the reaction mixture displayed identical patterns, that is, 39 distinct signals spread over a large field (about 40 ppm in  $\text{CH}_3\text{CN}$  or  $\text{CH}_2\text{Cl}_2$ ) owing to the paramagnetism of the  $\text{Pr}^{\text{III}}$  ions (see Supporting Information). Different 2D NMR techniques (COSY, ROESY) allowed the grouping of these signals into three sets of 13 peaks (1:1:1). This result is not only an indication that the polyhedral structure is maintained in solution but also that the reaction occurs with high diastereoselectivity (> 95%). To further demonstrate this, we synthesized the complex by using an isotopically marked ligand, with a  $^{13}\text{C}$  label at the carboxylate carbon center. Indeed, the  $^{13}\text{C}$  NMR spectrum showed three

distinct signals that confirmed the presence of three distinct magnetic sites (Figure 2).

When the reaction between  $\text{Pr}(\text{ClO}_4)_3$  and the ligand (+)-HL·HCl (2.25 equiv) in the presence of triethylamine (5.2 equiv) was conducted in methanol, a precipitate was obtained quantitatively. All the data collected in solution (NMR, ESI-MS) and in the solid state (X-ray,<sup>[10]</sup> elemental analysis, IR) are in agreement with the formation of a helical trinuclear array with the formula  $[\text{Pr}_3\{(+)\text{-L}\}_6(\mu_3\text{-OH})(\text{H}_2\text{O})_3](\text{ClO}_4)_2$  (**2**; see Figure 3a and Supporting Information)). This  $C_3$ -symmetrical compound is isostructural with the  $\text{Eu}^{\text{III}}$  analogue<sup>[9]</sup> obtained under the same experimental

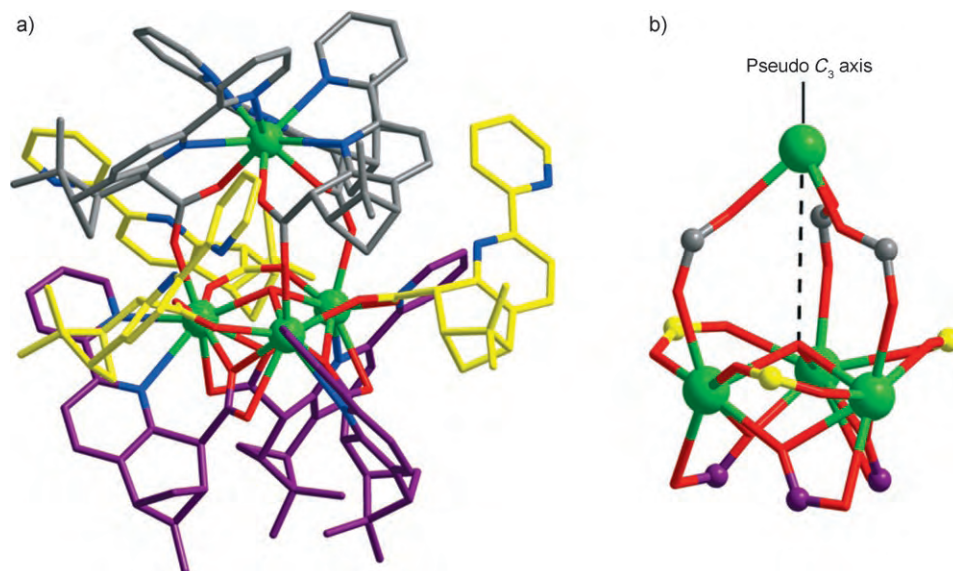


**Figure 1.** a) Crystal structure of  $[\text{Pr}_4\{(+)\text{-L}\}_9(\mu_3\text{-OH})](\text{ClO}_4)_2$  (**1**). Hydrogen atoms, perchlorate counterions, and acetonitrile molecules of crystallization have been omitted for clarity. b) Pyramidal metallic framework with the nine bridging carboxylic groups. Pr green, O red, N blue; the three sets of L ligands are colored gray, yellow, and violet.

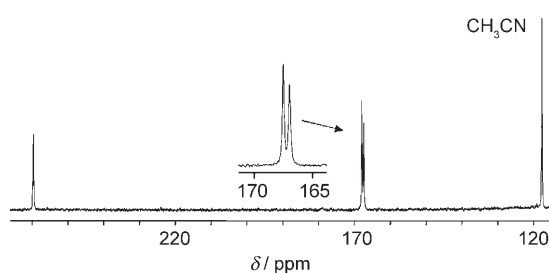


**Figure 2.**  $^{13}\text{C}$  NMR spectrum ( $\text{CD}_3\text{CN}$ ,  $c = 1 \cdot 10^{-2} \text{ M}$ ) of a labeled sample ( $^{13}\text{COOH}$ ) of **1**.

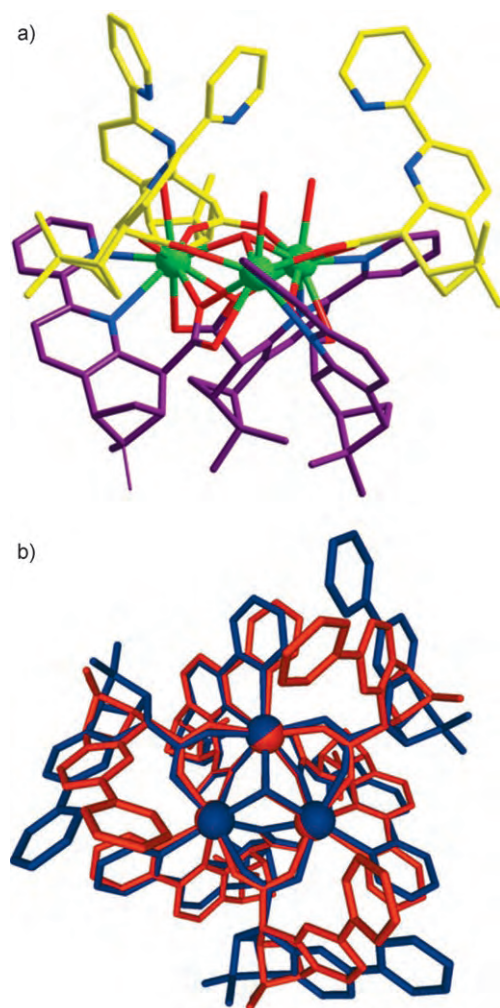


**Figure 3.** a) Crystal structure of  $[\text{Pr}_3\{(+)\text{-L}\}_6(\mu_3\text{-OH})(\text{H}_2\text{O})_3](\text{ClO}_4)_2$  (**2**) viewed perpendicular to the  $C_3$  crystallographic axis. Hydrogen atoms, perchlorate counterions, water, and acetonitrile molecules of crystallization have been omitted for clarity. Pr green, O red, N blue; L ligands are shown in yellow and violet. b) Superposition of the trinuclear bases of **1** (blue) and **2** (red) viewed down the  $C_3$  axis.

conditions. Moreover the discrete trinuclear structure of **2** is structurally very similar to the triangular base of the pyramidal array **1**. The main differences lie with the uncoordinated bipyridine moieties: a) To accommodate the new mononuclear unit  $\text{PrL}_3$ , they adopt a more “flattened” orientation in **1** as compared with **2** (Figure 3b). b) The

pseudo-*cis* conformation of the bipyridine, which is stabilized in **2** by a hydrogen-bonded network that involves six water molecules (three coordinated and three uncoordinated), is replaced by the energetically more favored *trans* conformation in the anhydrous compound **1**.

Compound **2** is stable in low-polar solvents, namely  $\text{CH}_2\text{Cl}_2$ .  $^1\text{H}$  NMR spectroscopy of a solution of **2** in  $\text{CD}_2\text{Cl}_2$  revealed 26 signals, which were attributed to the two magnetically distinct sets of ligands and remained unchanged with time. However, the spectrum recorded on a solution of **2** in dry  $\text{CD}_3\text{CN}$  was time-dependent. After about three hours, the initial 26 signals were completely replaced by 39 major peaks accompanied by some minor signals. The similarities in terms of chemical shifts and integration ratios between these dominant signals and those recorded for the pure tetranuclear species **1** (see Supporting Information) indicate the conversion  $2(\text{trinuclear}) \rightarrow 1(\text{tetranuclear}) + \text{minor species}$ .

This conversion was also confirmed by ESI-MS (see Supporting Information) and  $^{13}\text{C}$  NMR spectroscopy on a sample obtained from an isotopically marked ligand (see above). In the  $^{13}\text{C}$  NMR spectrum of the  $^{13}\text{C}$ -labeled sample (Figure 4), the two signals that correspond to the trinuclear structure are replaced by three other signals that originate from the three sets of ligands in compound **1**. Four small peaks are also visible therein and confirm that a part of the ligands make up the composition of the minor species. Detailed investigations by NMR and circular dichroism (CD) spectroscopy aimed to gain insights into the nature of the minor species as well as the reaction stoichiometry and mechanism are in progress.

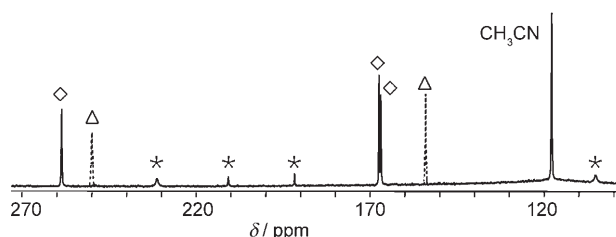


**Figure 4.** Superposed  $^{13}\text{C}$  NMR spectra (in  $\text{CD}_3\text{CN}$ ) of the labeled ( $^{13}\text{COOH}$ ) sample of **2** before the conversion (dashed peaks,  $\Delta$ ) and after the conversion  $2 \rightarrow 1 + \text{minor species}$  ( $\diamond$  signals from **1**;  $*$  signals from minor species).

Interestingly, the mixture containing **1** and the minor species in  $\text{CD}_3\text{CN}$  could be reconverted into **2** in the presence of water. After the addition of 40 equivalents of  $\text{H}_2\text{O}$  per equivalent of metal ion, the initial peaks in the  $^1\text{H}$  NMR spectrum were replaced by those of the trinuclear species **2** together with a few minor sharp signals that are associated to the decarboxylated ligand (see Supporting Information). In fact, during the regeneration of **2**, a small proportion of the anionic ligand (less than 10%) is neutralized by the water molecules and then decarboxylated according to a well-known mechanism.<sup>[11]</sup> Thus, the trinuclear array is stabilized in hydrated acetonitrile. A possible explanation is that the removal of water from the first coordination sphere in **2**, which is a necessary step in building up the water-free compound **1**, is unlikely due to the presence of solvated water

molecules. This hypothesis is supported by another experiment in which the water was removed from the acetonitrile solution by using molecular sieves, again leading to the conversion  $2 \rightarrow 1$  + minor species. The trinuclear cluster without water molecules in the first coordination sphere is unstable and generates a mixture that contains mainly the tetranuclear compound **1**. Consequently, such successive reversible cycles can be carried out simply by addition/removal of the water from the medium (acetonitrile). The number of interconversion cycles is limited only by the decarboxylation of the ligand which leads to its “consumption”.

Another interesting feature of the self-assembly processes presented here is their aptitude for chiral self-recognition. The reaction between the racemic ligand ( $\pm$ )-HL and  $\text{Pr}^{\text{III}}$  ions in methanol led to a racemate of **2** (*rac*-**2**). Its  $^1\text{H}$  NMR spectrum, which is identical in every respect with that for the enantiopure complex **2**, as well as its CD spectrum, which is devoid of any signal, denotes a high degree of chiral self-recognition (homorecognition) between the ligands. The same phenomenon takes place when *rac*-**2** is converted into *rac*-**1** upon dissolution in acetonitrile. As expected and furthermore demonstrated by X-ray analysis,<sup>[10]</sup> in *rac*-**1** each of the two enantiomeric structures is made up from one single enantiomer of the ligand to show opposite helical orientations (Figure 5). In contrast to the observations made above, the self-assembly of the racemic ligand ( $\pm$ )-HL and  $\text{Pr}^{\text{III}}$  ions in acetonitrile is highly perturbed. The tetranuclear species, which is obtained quantitatively when the enantiopure ligand is used, are in this case a minor part of a complicated mixture. This result shows the limits in terms of chiral recognition capabilities of the system; these limits are reached when a higher number of fundamental components (metal ions and ligands; 13 in the case of tetranuclear complexes and 9 in the case of trinuclear complexes) have to recognize and self-assemble.

In summary, we have described the first example in the lanthanide series of a solvent-adaptive system that can follow two distinct reaction pathways that lead diastereoselectively to discrete enantiopure polynuclear architectures **1** and **2**,

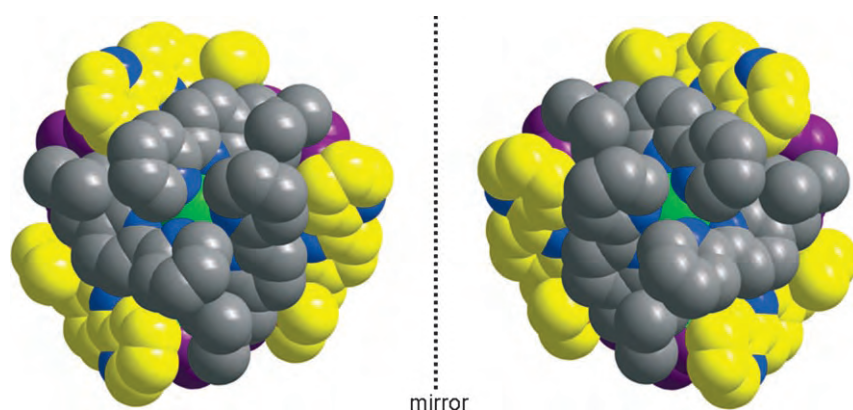


**Figure 5.** Space-filling representation of the two enantiomers present in *rac*-**1** viewed along the pseudo- $C_3$  axis. Ligands  $\text{L}^-$  coordinated around the metal center situated at the top of the pyramidal metallic framework are shown in gray; the other two sets of ligands are shown in yellow (coordination solely through carboxylate groups) and violet (coordination through carboxylate and nitrogen groups).  $\text{Pr}$  green, N blue.

respectively. In the pyramidal polyhedron **1**, an original combination of two types of helical arrangement of the ligands was revealed: one classical—around one metal center—and the other supramolecular—around a metallic triangular core. Their helical sense is predetermined by the ligand chirality. Facile reversible interconversion between the two structures **1** and **2** can be carried out in acetonitrile by the removal or addition of water, although no obvious templating effects or intra-/intermolecular interactions are involved in this process. If the racemic ligand is used instead of the enantiopure ligand, either chiral recognition processes are observed or the self-assembly is drastically affected.

Received: May 16, 2006

Published online: July 4, 2006

**Keywords:** chirality · helical structures · lanthanides · self-assembly · solvent effects

- [1] C. H. M. Amijs, G. P. M. van Klink, G. van Koten, *Dalton Trans.* **2006**, 308; A. Lützen, *Angew. Chem.* **2005**, *117*, 1022; *Angew. Chem. Int. Ed.* **2005**, *44*, 1000; F. Würthner, C.-C. You, Saha-Möller, *Chem. Soc. Rev.* **2004**, *33*, 133; M. J. Hannon, L. J. Childs, *Supramol. Chem.* **2004**, *16*, 7; A. V. Davis, R. M. Yeh, K. N. Raymond, *Proc. Nat. Acad. Sci. USA* **2002**, *99*, 4793.
- [2] P. N. W. Baxter, R. G. Khoury, J.-M. Lehn, G. Baum, D. Fenske, *Chem. Eur. J.* **2000**, *6*, 4140; S. J. Park, D. M. Shin, S. Sakamoto, K. Yamaguchi, Y. K. Chung, M. S. Lah, J.-I. Hong, *Chem. Eur. J.* **2005**, *11*, 235; M. Rodriguez, A. Llobet, M. Corbella, P. Müller, M. A. Usón, A. E. Martell, J. Reibenspeis, *J. Chem. Soc. Dalton Trans.* **2002**, 2900; S. A. Schuetz, V. W. Day, A. L. Rheingold, J. A. Belot, *Dalton Trans.* **2003**, 4303; L. Pirondini, A. G. Stendardo, S. Geremia, M. Campagnolo, P. Samori, J. P. Rabe, R. Fokkens, E. Dalacanal, *Angew. Chem.* **2003**, *115*, 1422; *Angew. Chem. Int. Ed.* **2003**, *42*, 1384; G. Baum, E. C. Constable, D. Fenske, C. E. Housecroft, T. Kulke, *Chem. Commun.* **1998**, 2659.
- [3] J.-M. Senegas, S. Koeller, G. Bernardinelli, C. Piguet, *Chem. Commun.* **2005**, 2235; T. Yamamoto, A. M. Arif, P. J. Stang, *J. Am. Chem. Soc.* **2003**, *125*, 12309; C. Provent, E. Rivara-Minten, S. Hewage, G. Brunner, A. F. Williams, *Chem. Eur. J.* **1999**, *5*, 3487; O. Mamula, F. Monlien, A. Porquet, G. Hopfgartner, A. E. Merbach, A. von Zelewsky, *Chem. Eur. J.* **2001**, *7*, 533.
- [4] C. S. Campos-Fernandez, B. L. Schottel, H. T. Chifotides, J. K. Bera, J. Bacsá, J. M. Koomen, D. H. Russell, K. R. Dunbar, *J. Am. Chem. Soc.* **2005**, *127*, 12909; M. Albrecht, J. Janser, J. Runsink, G. Raabe, P. Weis, R. Fröhlich, *Angew. Chem.* **2004**, *116*, 6832; *Angew. Chem. Int. Ed.* **2004**, *43*, 6662; M. Scherer, D. L. Caulder, D. W. Johnson, K. N. Raymond, *Angew. Chem.* **1999**, *111*, 1689; *Angew. Chem. Int. Ed.* **1999**, *38*, 1588; B. Hasenknopf, J.-M. Lehn, N. Boumediene, E. Leize, A. Van Dorsse-laer, B. Kneisel, D. Fenske, *J. Am. Chem. Soc.* **1997**, *119*, 10956.
- [5] Z. Grote, R. Scopelliti, K. Severin, *Angew. Chem.* **2003**, *115*, 3951; *Angew. Chem. Int. Ed.* **2003**, *42*, 3821; M. Ziegler, J. J. Miranda, U. N. Andersen, D. W. Johnson, J. A. Leary, K. N. Raymond, *Angew. Chem.* **2001**, *113*, 755; *Angew. Chem. Int. Ed.* **2001**, *40*, 733.



- [6] G. R. Choppin, in *Lanthanide Probes in Life, Chemical and Earth Sciences* (Eds.: J.-C. G. Bünzli, G. R. Choppin), Elsevier, Amsterdam, **1989**.
- [7] O. Mamula, A. von Zelewsky, *J. Chem. Soc. Dalton Trans.* **2000**, 219; J. J. Lessmann, W. D. Horrocks, *Inorg. Chem.* **2000**, 39, 3114.
- [8] O. Mamula, A. von Zelewsky, P. Brodard, C. W. Schlaepfer, G. Bernardinelli, H. Stoeckli-Evans, *Chem. Eur. J.* **2005**, 11, 3049.
- [9] O. Mamula, M. Lama, S. G. Telfer, A. Nakamura, R. Kuroda, H. Stoeckli-Evans, R. Scopelliti, *Angew. Chem.* **2005**, 117, 2583; *Angew. Chem. Int. Ed.* **2005**, 44, 2527.
- [10] Details regarding the X-ray crystal structure determinations for  $[\text{Pr}_4\{(+)\text{-L}\}_9(\mu_3\text{-OH})](\text{ClO}_4)_2 \cdot 10\text{CH}_3\text{CN}$  (**1**),  $[\text{Pr}_3\{(+)\text{-L}\}_6(\mu_3\text{-OH})(\text{H}_2\text{O})_3](\text{ClO}_4)_2 \cdot 4\text{CH}_3\text{CN} \cdot 3\text{H}_2\text{O}$  (**2**), and  $[\text{Pr}_4\{(\pm)\text{-L}\}_9(\mu_3\text{-OH})](\text{ClO}_4)_2 \cdot 4\text{CH}_3\text{CN}$  (*rac*-**1**) are given in the Supporting Information. CCDC 607510 (**1**), 607511 (**2**), and 607512 (*rac*-**1**) contain the supplementary crystallographic data for this paper. These data can be obtained free of charge from The Cambridge Crystallographic Data Centre via [www.ccdc.cam.ac.uk/data\\_request/cif](http://www.ccdc.cam.ac.uk/data_request/cif).
- [11] W. von E. Doering, V. Z. Pasternak, *J. Am. Chem. Soc.* **1950**, 72, 143.



## Amino Acid Assay

DOI: 10.1002/anie.200600112

**A Spiropyran-Based Ensemble for Visual Recognition and Quantification of Cysteine and Homocysteine at Physiological Levels\*\****Na Shao, Jian Yu Jin, Sin Man Cheung, Rong Hua Yang,\* Wing Hong Chan,\* and Tian Mo*

Spiroprans and spirooxazines belong to one of the most fascinating families of photochromic compounds; they undergo reversible structural isomerization between a colorless spiro form and a colored merocyanine upon either light, heat, or chemical stimulus.<sup>[1]</sup> In organic solvents the con-

version of spiropyran into merocyanine can be induced by complexation of a metal ion with cooperative ligation of another chelating functionality attached at the 8'-position.<sup>[2]</sup> Up to now, a number of such spiropyran receptors have been designed and widely applied for the optical detection of transition-metal and alkali-metal ions.<sup>[3]</sup> It should be pointed out, however, that despite the large number of reports, spiropyran structures have rarely been used to recognize anions or small organic molecules such as biologically important amino acids. Sunamoto et al. demonstrated early on that the zwitterionic feature of the opened merocyanine should enable it to bind with a polar amino acid molecule through electrostatic interactions; this approach was utilized for the photocontrolled transfer of amino acids across bilayers and membranes.<sup>[4]</sup> Later, Inouye et al. designed a spiropyridopyran capable of binding guanosine derivatives in non-hydroxylic organic solvents by forming triple hydrogen bonds.<sup>[5]</sup> And yet, development of new spiropyrans and spirooxazines probes capable of efficient recognition and quantification of amino acids in aqueous solution remains a challenge.<sup>[1b]</sup>

Of the twenty amino acids used as building blocks for proteins, the thiol-containing amino acids play crucial roles in biological systems. For example, cysteine (Cys), homocysteine (Hcy), and glutathione (GSH) have been proven to be linked to various human diseases.<sup>[6]</sup> At present, a wide variety of colorimetric and fluorescent probes for thiol-containing amino acids and peptides are valuable. The majority of the reported methods are based on redox chemistry or labeling with chromophores or fluorophores and a combination of separation techniques.<sup>[7]</sup> Recently, Strongin et al. as well as several others have made pioneering advances in developing highly selective probes for Cys and Hcy, as well as a thiol-quantification enzyme assay based on the covalent interaction between the probe molecule and the analyte,<sup>[8,9]</sup> which could be used for the direct assay of the amino acid content and the enzyme activity in body fluids. In addition, a sensing ensemble for Cys was also recently developed by Kim et al. based on the analyte competing for a metal receptor with a chromogenic indicator.<sup>[10]</sup> The approach showed excellent selectivity for Cys over other amino acids including Hcy. Although many reactions and various techniques have been developed for assaying Cys and Hcy,<sup>[7–10]</sup> there is still plenty of room for improvement in term of selectivity, sensitivity, and performance with a new interaction mechanism.

Here we present a new strategy for the efficient recognition and determination of Cys and Hcy in neutral aqueous solution using a spiropyran. In our proposed approach the interaction of the free spiropyran with an amino acid is comparatively weak, but the spiropyran molecule can bind a metal ion, which can interact with an amino acid ligand. The metal ion is thus expected to bind with both the spiropyran and the amino acid molecule through cooperative metal–ligand interactions. If the three components exist together, the selectivity of the approach is essentially determined by the binding affinity between the metal center and the amino acid, as well as the relative size of the analyte. In this context, we have shown that in the presence of Cu<sup>2+</sup> or Hg<sup>2+</sup> ions the interaction of the spiropyran with Cys or Hcy is remarkably

[\*] Dr. N. Shao, J. Y. Jin, Prof. R. H. Yang  
Beijing National Laboratory for Molecular Sciences  
College of Chemistry and Molecular Engineering  
Peking University  
Beijing, 100871 (P.R. China)  
Fax: (+86) 10-6275-1708  
E-mail: yangrh@pku.edu.cn

S. M. Cheung, Prof. W. H. Chan, T. Mo  
Department of Chemistry  
Hong Kong Baptist University  
Kowloon Tong, Hong Kong (P.R. China)  
Fax: (+852) 2339-7408  
E-mail: whchan@hkbu.edu.hk

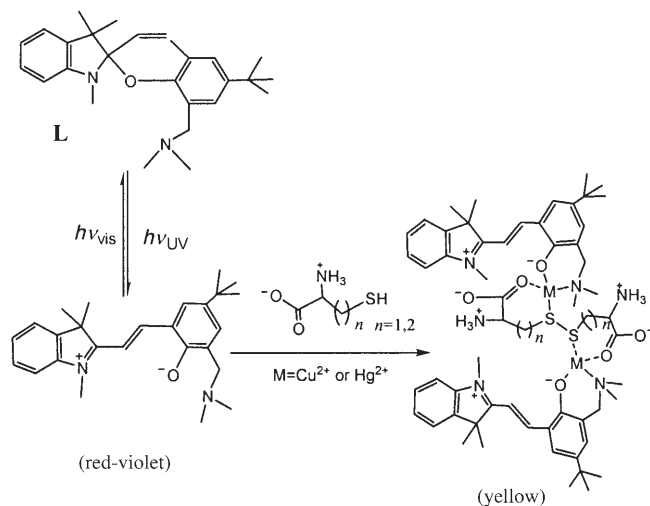
[\*\*] This research was supported by the National Outstanding Youth Science Foundation of China (grant no. 20525518) and the National Natural Foundation of China (grant no. 20475005).



Experimental procedures, titration curves for the amino acids and anions, pH effects, fitting curves, and association constants, and mass, <sup>1</sup>H NMR, and IR spectra are available in the supporting information for this article on the WWW under <http://www.angewandte.org> or from the author.

selective and sensitive, resulting in appreciable changes in color and absorption properties.

We designed the free ligand (**L**) based on a 1,3,3'-trimethylindolino-6'-*tert*-butylbenzopyran derivative with a *N,N*-dimethylaminomethyl moiety in the 8'-position (Scheme 1), which was employed previously for optical



**Scheme 1.** The free spiropyran ligand **L**, its isomerization on irradiation, and the proposed structure of the ternary complex containing **L**, Cys or Hcy, and metal ions.

recognition of  $\text{Cu}^{2+}$  ions in ethanol.<sup>[11]</sup> Figure 1 shows the changes in the absorption spectrum of **L** ( $1.0 \times 10^{-4} \text{ M}$ ) in 10% aqueous ethanol at pH 7.0 in the presence of metal ions and amino acids. The absorption spectrum of the free **L** in ethanol/water is characterized by an intense absorption band centered at 532 nm ( $\lg \epsilon = 4.06 \text{ M}^{-1} \text{ cm}^{-1}$ ) and a second band at approximately 378 nm. The UV/Vis spectrum of **L** hardly changes upon addition of 10 equiv of Cys (Figure 1, curves a and b), indicating there is little interaction between **L** and the amino acid. In contrast, when the same amount of Cys was added to the ethanol/water solution containing **L** and  $\text{Cu}^{2+}$ , or **L** and  $\text{Hg}^{2+}$ , the absorbance at 532 nm greatly decreased, while the

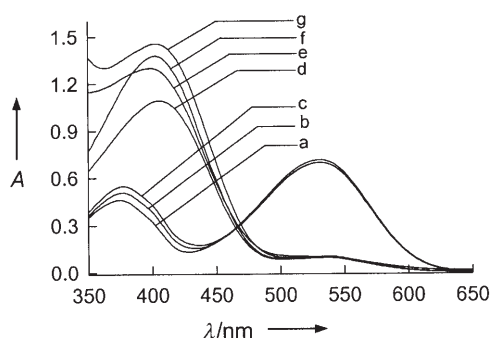


**Figure 1.** Effects of metal ions and amino acids on the absorption spectra of **L** in 10% aqueous ethanol solution at pH 7.0. The spectra correspond to: a) **L**, b) **L** + Cys, c) **L** +  $\text{Zn}^{2+}$  + Cys, d) **L** +  $\text{Hg}^{2+}$  + Hcy, e) **L** +  $\text{Cu}^{2+}$  + Cys, f) **L** +  $\text{Hg}^{2+}$  + Cys, and g) **L** +  $\text{Cu}^{2+}$  + Hcy.  $[\text{L}] = 1.0 \times 10^{-4} \text{ M}$ ,  $[\text{Cys}] = [\text{Hcy}] = 1.0 \times 10^{-3} \text{ M}$ ,  $[\text{metal ion}] = 2.5 \times 10^{-4} \text{ M}$ .

378-nm absorption band shifted to 405 nm concomitant with an increase in intensity (Figure 1, curves e and f). In contrast, in the presence of  $\text{Zn}^{2+}$  ions and Cys, the absorption spectrum of **L** changes only slightly (Figure 1, curve c). For Hcy, similar spectroscopic behavior was observed with both  $\text{Hg}^{2+}$  and  $\text{Cu}^{2+}$  ions (Figure 1, curves d and g), whereas the response sensitivity of **L** in the presence of  $\text{Cu}^{2+}$  ions is higher than that in the presence of  $\text{Hg}^{2+}$  ions. These results demonstrate that the interaction of **L** with Cys and Hcy is highly metal-ion-dependent.  $\text{Cu}^{2+}$  and  $\text{Hg}^{2+}$  ions can promote the binding of **L** to two different amino acids, which constitutes the basis for effective recognition of the amino acids with the proposed approach.

The selectivity of **L** in binding amino acids was studied by examining the amino acid induced changes in the color and UV/Vis spectra of ethanol/water solutions of **L** in the presence of  $\text{Hg}^{2+}$  or  $\text{Cu}^{2+}$  ions. The two metal ions show quite different effects on the color and absorption spectra of **L** in the presence of an amino acid; the most selective and distinctive binding was observed with  $\text{Hg}^{2+}$  ions. Addition of each amino acid, except glycine, to the ethanol/water solution of **L** and  $\text{Cu}^{2+}$  resulted in the shift of the absorption band of **L** and thus the color change.<sup>[12]</sup> Figure 2 shows a photograph of a



**Figure 2.** Color changes of the ethanol/water solution of **L**- $\text{Hg}^{2+}$  in the presence of different amino acids. Labeled vials: 1) no amino acid, 2) Gly, 3) Leu, 4) His, 5) Glu, 6) Asp, 7) Met, 8) Cys, 9) Hcy, and 10) GSH.  $[\text{L}] = 1.0 \times 10^{-4} \text{ M}$ ,  $[\text{Hg}^{2+}] = 2.5 \times 10^{-4} \text{ M}$ ,  $[\text{amino acid}] = 1.0 \times 10^{-3} \text{ M}$ .

series of solutions of amino acids in buffered ethanol/water solution containing  $1.0 \times 10^{-4} \text{ M}$  **L** and  $2.5 \times 10^{-4} \text{ M}$   $\text{Hg}^{2+}$ . Only Cys and Hcy induce a distinct color change from red-violet to yellow, which corresponds to the shift of the maximum absorption band from 532 nm to 405 nm. To quantify the spectral changes of **L** at 405 nm and 532 nm, the absorbance ratio of **L** at the two wavelengths ( $R = A_{405}/A_{532}$ ) in the presence of  $1.0 \times 10^{-3} \text{ M}$  of the amino acids and anions was determined.<sup>[12]</sup> Here  $R_0$  is the value of  $R$  without the analyte. In the absence of metal ions, the values of  $(R - R_0)$  are negligible except for solutions with Glu and GSH; in the presence of  $\text{Cu}^{2+}$  ions, obvious enhancements of the  $(R - R_0)$  value are observed for each amino acid. The only selective enhancement of the  $(R - R_0)$  value for Cys or Hcy was realized with  $\text{Hg}^{2+}$  ions. The results indicate that the **L**- $\text{Hg}^{2+}$  system is appropriate for selective recognition of Cys and Hcy.

The dynamic response range of **L** to Cys and Hcy strongly depends on the amount of the metal ion present in the solution. For the best response to the amino acids, we optimized the metal ion concentration by holding the concentration of **L** constant ( $1.0 \times 10^{-4} \text{ M}$ ) and varying the amount of  $\text{Hg}^{2+}$ . At a molar ratio of metal ions to **L** under 3.0,

both the sensitivity (response slope) and response range increase with increasing concentration of  $\text{Hg}^{2+}$ . At higher  $\text{Hg}^{2+}$  concentrations, the best response shifts from the lower concentration range to higher concentration range. Figure 3

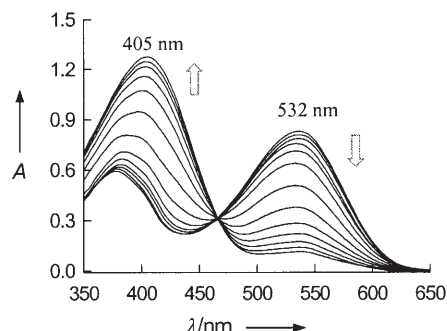


**Figure 3.** UV/Vis absorption spectra of  $\text{L-Hg}^{2+}$  in ethanol/water solution at pH 7.0 upon addition of Cys at varying concentrations. The arrows indicate the signal changes with increasing Cys concentration ( $0, 2.5 \times 10^{-8}, 2.5 \times 10^{-7}, 1.0 \times 10^{-6}, 2.5 \times 10^{-6}, 5.0 \times 10^{-6}, 1.0 \times 10^{-5}, 2.5 \times 10^{-5}, 5.0 \times 10^{-5}, 1.0 \times 10^{-4}, 2.5 \times 10^{-4}, 5.0 \times 10^{-4},$  and  $1.0 \times 10^{-3} \text{ M}$ ).  $[\text{L}] = 1.0 \times 10^{-4} \text{ M}$ ,  $[\text{Hg}^{2+}] = 2.5 \times 10^{-4} \text{ M}$ .

shows the typical UV/Vis spectroscopic response of a buffered ethanol/water solution containing  $1.0 \times 10^{-4} \text{ M}$  **L** and  $2.5 \times 10^{-4} \text{ M}$   $\text{Hg}^{2+}$  to increasing concentrations of Cys. At this metal ion concentration, a dramatic increase of the absorbance at 405 nm and a decrease of the absorbance at 532 nm are observed for the Cys concentration range of  $5.0 \times 10^{-6} \text{ M}$  to  $2.5 \times 10^{-4} \text{ M}$ . The detection limit, defined as  $3\sigma$  in blank solution, is  $4.0 \times 10^{-8} \text{ M}$ . The results suggest that our approach may be appropriate for quantification of Cys in physiological settings.<sup>[7a,8c]</sup> A similar response curve was obtained for Hcy.<sup>[12]</sup> By following the absorption change at 405 nm and a curve-fitting analysis, we estimate the stoichiometry of **L** with Cys or Hcy to be 2:2; the corresponding association constants in ethanol/water at pH 7.0 are  $2.04 \times 10^4 \text{ M}^{-2}$  and  $8.37 \times 10^3 \text{ M}^{-2}$ ,<sup>[12]</sup> respectively.

An important prerequisite for an amino acid probe is its ability to recognize a specific amino acid molecule in the presence of other biologically relevant substrates under physiological conditions. To further test the amino acid specificity of our system, complexation experiments with a range of other amino acids and anions were performed with  $\text{L-Hg}^{2+}$  ( $[\text{L}] = 1.0 \times 10^{-4} \text{ M}$ ,  $[\text{Hg}^{2+}] = 2.5 \times 10^{-4} \text{ M}$ ). The change of the absorbance ratio ( $R - R_0$ ) was plotted against the concentration of different amino acids and anions (Figure 4). The ( $R - R_0$ ) values increase linearly with the concentration of Hcy ( $(0.1\text{--}1.0) \times 10^{-3} \text{ M}$ ,  $R^2 = 0.9903$ ) and the concentration of Cys ( $(0.025\text{--}1.0) \times 10^{-3} \text{ M}$ ,  $R^2 = 0.9881$ ), which covers the upper limit of Cys concentration in normal organisms.<sup>[13]</sup> Although the system also responds to Glu as well at a concentration of  $5.0 \times 10^{-5} \text{ M}$ , the value of ( $R - R_0$ ) is substantially smaller than that caused by Cys or Hcy under the same conditions. The association constant of **L** with Glu in the presence of  $\text{Hg}^{2+}$  ions was  $6.81 \times 10^2 \text{ M}^{-1}$ . The amino acid selectivity factor for binding Cys over Glu, which was evaluated by comparing the association constants and the

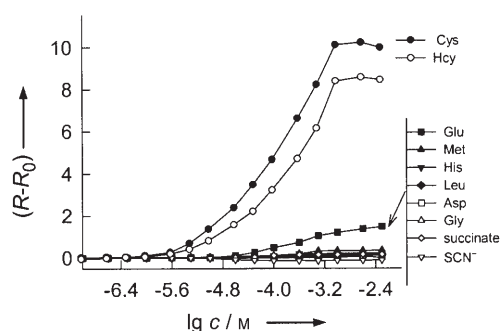


**Figure 4.** The dependence of the absorbance ratio of  $\text{L-Hg}^{2+}$  at 405 nm and 532 nm ( $R = A_{405}/A_{532}$ ) on the increasing concentration of different amino acids and anions.  $R_0$  is the value of  $R$  in the absence of amino acids or anions.

absorption signal changes at 405 nm with the relation  $[K\Delta\epsilon]$ ,<sup>[14]</sup> is approximately 206. Here  $K$  is the association constant and  $\epsilon$  is the extinction coefficient of the amino acid complex at 405 nm. The selectivity factors of  $\text{L-Hg}^{2+}$  for the amino acids and anions studied here are in the order  $\text{Cys} > \text{Hcy} > \text{GSH} \gg \text{Glu} > \text{Asp} \approx \text{His} \approx \text{Met} > \text{Leu} \approx \text{Gly} > \text{succinate} \approx \text{SCN}^-$ . Additionally, titrating Cys in the presence of the potential biologically interfering ions  $\text{Li}^+$ ,  $\text{K}^+$ ,  $\text{Ca}^{2+}$ ,  $\text{Zn}^{2+}$ , and  $\text{SCN}^-$  and amino acids such as Met and His<sup>-</sup> gave a curve almost superimposable with that obtained in the presence of Cys alone (Figure 5). These results clearly indicate that our

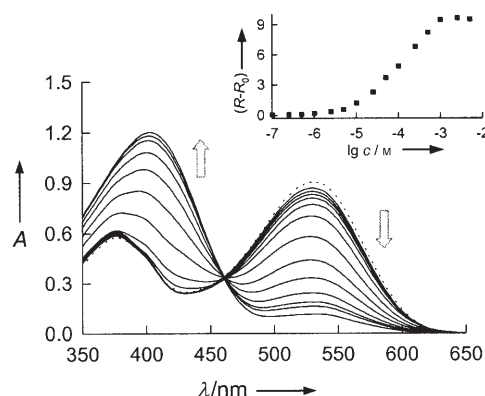


**Figure 5.** UV/Vis spectra of  $\text{L-Hg}^{2+}$  in ethanol/water solution in the presence of  $1.0 \times 10^{-3} \text{ M}$   $\text{Li}^+$ ,  $\text{Na}^+$ ,  $\text{K}^+$ , and  $\text{Ca}^{2+}$ ,  $1.0 \times 10^{-4} \text{ M}$   $\text{Zn}^{2+}$ , and  $1.0 \times 10^{-5} \text{ M}$  Met, His, and  $\text{SCN}^-$  with increasing amounts of Cys ( $1.0 \times 10^{-7} \text{ M}$  to  $1.0 \times 10^{-3} \text{ M}$ ). (The dashed line corresponds to the absorption spectrum of  $\text{L-Hg}^{2+}$  with only Cys). Inset: Absorbance ratio plotted against the logarithm of Cys concentration.

approach is not only insensitive to other cations, amino acids, and anions but also selective towards Cys and Hcy when they are present. Furthermore, it is possible to assay for Cys alone without interference from Hcy under physiological conditions. Although the response to Hcy is linear in the concentration range of  $1.0 \times 10^{-4} \text{ M}$  to  $1.0 \times 10^{-3} \text{ M}$ , the total concentration of Hcy in human blood plasma is much lower than that of Cys.<sup>[13]</sup> In reality, Hcy would not significantly interfere with the measurement of Cys, which is important

and helpful in validation of the method to meet the selectivity requirements of a Cys assay.

The interactions of **L**, metal ion, and amino acid are pH dependent. To observe the effect of pH on the amino acid complexation, we conducted a more detailed study using an acidic solution (0.001 M HNO<sub>3</sub>, *I* = 0.1) containing  $1.0 \times 10^{-4}$  M **L**,  $2.5 \times 10^{-4}$  M Hg<sup>2+</sup>, and  $1.0 \times 10^{-4}$  M Cys in 10 % aqueous ethanol solution, and subsequently the pH was adjusted by addition of 0.001 M NaOH. The pH values at which the complex formation and color change take place are in the range of 4.5–8.5 and thus a function of the pH of the medium. The  $A_{405}/A_{532}$  value reaches a maximum and remains constant between pH 4.5 and 8.5.<sup>[12]</sup> To further determine the complex equilibrium constant of **L** and Cys at various pH values, we performed potentiometric pH titrations of **L** with Cys in the absence and presence of Hg<sup>2+</sup> ions using commercially available glass electrodes.<sup>[12]</sup> The titration data were analyzed with the “BEST” program,<sup>[15]</sup> and the resulting complex formation constants are  $2.03 \times 10^2 \text{ M}^{-2}$  (without Hg<sup>2+</sup>) and  $1.52 \times 10^4 \text{ M}^{-2}$  ( $2.5 \times 10^{-4}$  M Hg<sup>2+</sup>), respectively. The value in the presence of Hg<sup>2+</sup> ions shows little deviation from that obtained by spectrophotometric titration at pH 7.0. In the present work, we deemed pH 7.0 to be ideal.

The exact stoichiometry and mechanism of the interaction between the metal ion, the ligand **L**, and the amino acid were key aspects that were not clearly understood. We thus first studied the effect of varying the concentration of the metal ion on the absorption spectra of **L** in the ethanol/water solution with and without Cys. In the absence of Cys, the absorption spectrum of **L** in 10 % aqueous ethanol solution is hardly affected upon addition of Hg<sup>2+</sup> or Cu<sup>2+</sup> ions. In the presence of Cys and with increasing metal ion concentration, the absorbance of **L** at 532 nm decreases significantly and that at 405 nm increases. In contrast, the effect of Zn<sup>2+</sup> or Cd<sup>2+</sup> ions on the absorbance of **L** at either 532 or 405 nm is negligible even in the presence of excess of Cys or Hcy. By following a curve-fitting analysis, we estimate the stoichiometry of the complex of **L** with either Cu<sup>2+</sup> or Hg<sup>2+</sup> ions to be 2:2. In addition, in the ESI mass spectrum of an ethanol solution containing  $1.0 \times 10^{-5}$  M **L**,  $2.5 \times 10^{-5}$  M Cu(NO<sub>3</sub>)<sub>2</sub>, and  $1.0 \times 10^{-5}$  M Cys, a peak at *m/z* 1269.4, which is assigned to  $[2\text{L} + 2\text{Cu} + 2\text{Cys} + 2\text{NO}_3 - 2\text{H}]^+$ , is clearly observed,<sup>[12]</sup> indicating that in aqueous ethanol solution, the sulfhydryl group of Cys may be deprotonated to form a S–S-linked dimer (cystine) through a two-electron oxidation process.<sup>[16,17]</sup> To clarify whether this oxidation process is the result of dioxygen or Cu<sup>2+</sup> (or Hg<sup>2+</sup>) interactions, we measured the optical response of **L** to Cys under both aerobic and anaerobic conditions with and without the metal ion.<sup>[12]</sup> In the absence of Cu<sup>2+</sup> or Hg<sup>2+</sup> ions **L** exhibits minimal spectral changes at increasing Cys concentrations even though the analyte solution was saturated with dioxygen. On the other hand, the response curves of **L**–Cu<sup>2+</sup> or **L**–Hg<sup>2+</sup> to Cys under anaerobic conditions were almost the same as those obtained under aerobic conditions.<sup>[12]</sup> This results suggest that the oxidation of Cys in the present system is indeed promoted by the redox-active Cu<sup>2+</sup> and Hg<sup>2+</sup> ions.<sup>[16,17]</sup> Additional evidence for the formation of the S–S bridge (cystine) in the complexation process can be obtained from the spectroscopic

responses of **L**–Cu<sup>2+</sup> to cystine and Met (it could not form the S–S linked dimer). The response of **L**–Cu<sup>2+</sup> with cystine is similar to that with Cys, whereas that with Met is considerable weaker under analogous conditions. Based on these results, we thus could presume that in the present system Cys is deprotonated at the sulfhydryl group to form a bridged dimer (cystine) through the redox-active Cu<sup>2+</sup> or Hg<sup>2+</sup> ions, then the metal center complexes with one cystine molecule and two **L** molecules to form a 2:1:2 (Cu<sup>2+</sup>/cystine/**L**) ternary assembly. Disappearance of the carboxyl and sulfhydryl absorptions of Cys in the IR spectra, and the pronounced downfield shifts of the methylene protons as well as the upfield shifts of the *N,N*-dimethylamino protons of **L** in the <sup>1</sup>H NMR spectra indicate that the binding interactions among the metal center, **L**, and cystine occur through the phenolate hydroxy group and the dimethylamino group of **L** and the sulfhydryl groups of the amino acid.

To further elucidate the roles of the binding sites of **L** in the complex formation, a reference compound, 2-dimethylaminomethylphenol (DAMP) was examined. Under comparable conditions, DAMP exhibits a absorption maximum at 274 nm, the intensity of which is enhanced ( $\approx 12\%$ ) upon addition of 0.5–10 equiv of Cys.<sup>[12]</sup> However, in the presence of Cu<sup>2+</sup>, a great enhancement of the DAMP absorption at 274 nm was observed upon addition of 0.5–10 equiv of Cys (3.29 times the initial value). The results clearly indicate that involvement of the phenolate hydroxy group and the dimethylamino group of **L** is reasonable in complex formation. A proposed structure of the assembled complex of **L**, metal ion, and Cys is shown in Scheme 1. The formation of the copper complex would lead to the disappearance of the **L** charge-transfer band and the appearance of blue-shifted band that probably arises from a new charge-transfer involving the orbitals of the metal center, which causes the color change of **L** from red-violet to yellow ( $\lg \epsilon_{405\text{nm}} = 3.712 \text{ M}^{-1} \text{ cm}^{-1}$ ).

In conclusion, we have proposed a new method that allows simple and efficient recognition and quantification of an amino acid in aqueous solution by a spiropyran derivative. The molecular recognition process has been proven to be sensitive to the presence of Cys and Hcy. To the best of our knowledge, this is the first spiropyran–metal receptor for amino acids, which might open up new opportunities for the application of spiropyran and spirooxazines. Current studies in our laboratory along these lines include developing more sophisticated systems based on the same mechanism for recognition of amino acids or anions of various types and complexities.

Received: January 11, 2006

Revised: April 9, 2006

Published online: June 29, 2006

**Keywords:** amino acids · molecular recognition · spiropyran · UV/Vis spectroscopy

- [1] a) R. Guglielmetti in *Photochromism: Molecules and Systems, Studies in Organic Chemistry* (Eds.: H. Dürr, H. Bouas-Laurent), Elsevier, Amsterdam, 1990, chap. 8 and 23, and references



- therein; b) G. Berkovic, V. Krongauz, V. Weiss, *Chem. Rev.* **2000**, *100*, 1741–1753.
- [2] a) J. Phillips, A. Mueller, F. Przystal, *J. Am. Chem. Soc.* **1965**, *87*, 4020; b) L. D. Taylor, J. Nicholson, R. B. Davis, *Tetrahedron Lett.* **1967**, *8*, 1585–1588.
- [3] Selected examples: a) M. Inouye, Y. Noguchi, K. Isagawa, *Angew. Chem.* **1994**, *106*, 1226–1228; *Angew. Chem. Int. Ed. Engl.* **1994**, *33*, 1163–1166; b) J. D. Winkler, C. M. Bowen, V. Michelet, *J. Am. Chem. Soc.* **1998**, *120*, 3237–3242; c) A. M. A. Salhin, M. Tanaka, K. Kamada, H. Ando, T. Ikeda, Y. Shibutani, S. Yajima, M. Nakamura, K. Kimura, *Eur. J. Org. Chem.* **2002**, 655–662; d) R. A. Kopelman, S. M. Snyder, N. L. Frank, *J. Am. Chem. Soc.* **2003**, *125*, 13684–13685; e) H. Sakamoto, H. Takagaki, M. Nakamura, K. Kimura, *Anal. Chem.* **2005**, *77*, 1999–2006.
- [4] a) J. Sunamoto, K. Iwamoto, Y. Mohri, T. Kominato, *J. Am. Chem. Soc.* **1982**, *104*, 5502–5504; b) S. Marx-Tibbon, I. Willner, *J. Chem. Soc. Chem. Commun.* **1994**, 1261–1262.
- [5] M. Inouye, K. Kim, T. Kitao, *J. Am. Chem. Soc.* **1992**, *114*, 778–780.
- [6] a) F. J. T. Staal, S. W. Ela, M. Roederer, M. T. Anderson, L. A. Herzenberg, *Lancet* **1992**, *339*, 909–913; b) K. S. McCully, *Nat. Med.* **1996**, *2*, 386–389.
- [7] For recent reviews, see: a) O. Nekrassova, N. S. Lawrence, R. G. Compton, *Talanta* **2003**, *60*, 1085–1095; b) R. P. Haugland, *Handbook of Fluorescent Probes and Research Products*, 9th ed., Molecular Probes, Eugene, OR, **2002**, pp. 79–98.
- [8] a) O. Rusin, N. N. St. Luce, R. A. Agbaria, J. O. Escobedo, S. Jiang, I. M. Warner, F. B. Dawan, K. Lian, R. M. Strongin, *J. Am. Chem. Soc.* **2004**, *126*, 438–439; b) W. H. Wang, J. O. Escobedo, C. M. Lawrence, R. M. Strongin, *J. Am. Chem. Soc.* **2004**, *126*, 3400–3401; c) W. Wang, O. Rusin, X. Xu, K. K. Kim, J. O. Escobedo, S. O. Fakayode, K. A. Fletcher, M. Lowry, C. M. Schowalter, C. M. Lawrence, F. R. Fronczek, I. M. Warner, R. M. Strongin, *J. Am. Chem. Soc.* **2005**, *127*, 15949–15958, and references therein.
- [9] H. Maeda, H. Matsuno, M. Ushida, K. Katayama, K. Saeki, N. Itoh, *Angew. Chem.* **2005**, *117*, 2982–2985; *Angew. Chem. Int. Ed.* **2005**, *44*, 2922–2925.
- [10] M. S. Han, D. H. Kim, *Tetrahedron* **2004**, *60*, 11251–11257.
- [11] N. Shao, Y. Zhang, S. M. Cheung, R. H. Yang, W. H. Chan, T. Mo, K. A. Li, F. Liu, *Anal. Chem.* **2005**, *77*, 7294–7303.
- [12] See the Supporting Information.
- [13] The total concentration of homocysteines in healthy plasma is 5–15  $\mu\text{M}$ . Cysteine concentrations are typically 20–30 times that of homocysteine (see Refs. [7a], [8c]).
- [14] J. Z. Zhao, T. M. Fyles, T. D. James, *Angew. Chem.* **2004**, *116*, 3543–3546; *Angew. Chem. Int. Ed.* **2004**, *43*, 3461–3464.
- [15] A. E. Martell, R. J. Motekaitis, *Determination and Use of Stability Constants*, 2nd ed, VCH, New York, **1992**.
- [16] M. Belcastro, T. Marino, N. Russo, M. Toscano, *J. Mass Spectrom.* **2005**, *40*, 300–306.
- [17] F. Jalilehvand, B. O. Leung, M. Izadifard, E. Damian, *Inorg. Chem.* **2006**, *45*, 66–73.

DOI: 10.1002/anie.200600771

**A Simple Strategy for Prompt Visual Sensing by Gold Nanoparticles: General Applications of Interparticle Hydrogen Bonds\*\****Shu-Yi Lin, Sung-Hsun Wu, and Chun-hsien Chen\**

Visual sensing based on gold nanoparticles (GNPs) is important and attractive because the intense red color arising from surface plasmon (SP) absorption<sup>[1]</sup> allows the outcome of analytical measurements to be read with the naked eye. The typical mechanism for such colorimetric sensing involves a color change from red to blue through the analyte-triggered aggregation of GNPs.<sup>[2–5]</sup> Herein, we report an opposite transformation in which the GNPs are initially aggregated and promptly become dispersive in response to an analyte. To achieve the goal of rapid sensing, the interparticle attraction for the initial aggregation should be easily weakened by the analyte–GNP interactions. Scheme 1 illustrates the proposed concept. The GNPs are bifunctionalized by ([15]crown-5)CH<sub>2</sub>O(CH<sub>2</sub>)<sub>4</sub>SH (denoted 15c5-C<sub>4</sub>-SH) and thiocetic acid (TA), which are responsible for recognition and GNP aggregation, respectively. Pb<sup>II</sup>, a common environmental contaminant that is detrimental to human health, is selected as the target ion for this model system because its association constants with 15c5 and acetic acid are 3630<sup>[6]</sup> and 500,<sup>[7]</sup> respectively, which are considerably higher than those of most metal ions. The affinity of Pb<sup>II</sup> toward the functionalities imposes positive electrostatics on the GNPs and leads to a very fast aggregation-to-dispersion transformation. Herein, we show that this methodology offers a rapid, highly selective, and sensitive Pb<sup>II</sup> sensor.

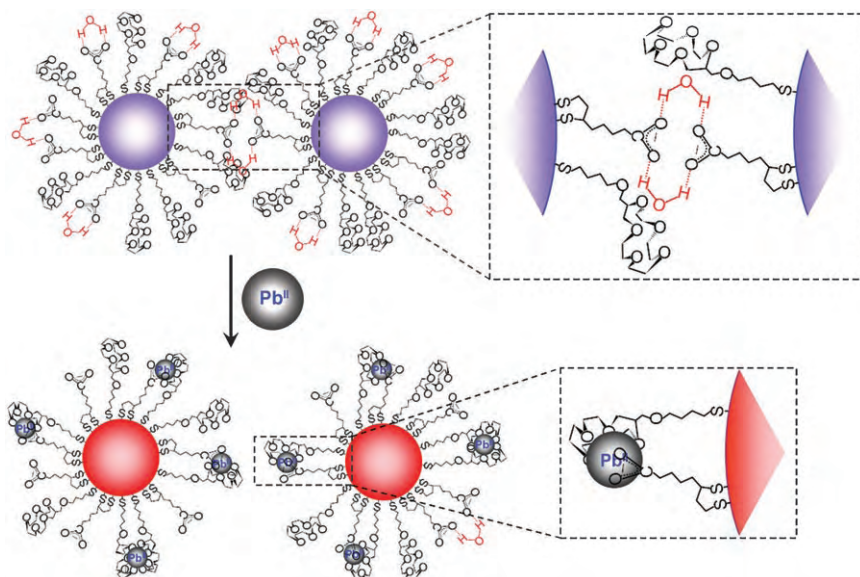
Chemical reduction of HAuCl<sub>4</sub> by sodium citrate was employed to synthesize water-soluble and spherical gold sols.<sup>[8]</sup> The GNPs were then bifunctionalized by a two-step method<sup>[9]</sup> in which the physisorbed anions are first displaced by TA, which is subsequently exchanged by crown ether thiols.<sup>[9,10]</sup> This approach typically yields GNPs with a diameter of (18 ± 3) nm and ligated by nominally 14500 thiol legs, one third of which are crown ether thiols.<sup>[10]</sup> The solvent system for immediate sensing of Pb<sup>II</sup> ions was prepared by mixing an aqueous solution of the GNPs with methanol. An aliquot (1.80 mL) of the GNPs in the solvent

[\*] Dr. S.-Y. Lin, S.-H. Wu, Prof. C.-h. Chen

Department of Chemistry  
National Tsing Hua University  
Hsinchu, Taiwan 30013 (China)  
Fax: (+ 886) 3-571-1082  
E-mail: chhchen@mx.nthu.edu.tw

[\*\*] We thank Dr. M.-S. Huang and Ms. S.-F. A. Chan at ITRI (Chutung, Hsinchu) for access to the zeta potential analyzer. The authors acknowledge the National Science Council and National Tsing Hua University for financial and research support.

Supporting information for this article is available on the WWW under <http://www.angewandte.org> or from the author.



**Scheme 1.** Proposed methodology for the recognition of metal cations by GNPs in methanol/water. The GNPs initially aggregate as a result of hydrogen bonds between carboxylic acid residues. The crown ether moiety selectively hosts metal ions whose positive charge produces electrostatic repulsion and results in dispersive GNPs.

mixture was subjected to a trial assay. Figure 1 shows that, one second after exposure to  $\text{Pb}^{\text{II}}$ , the solution transformed from blue to red, which is opposite to most sensing events of GNPs. The Supporting Information includes a video clip that demonstrates the promptness of the distinct color change.

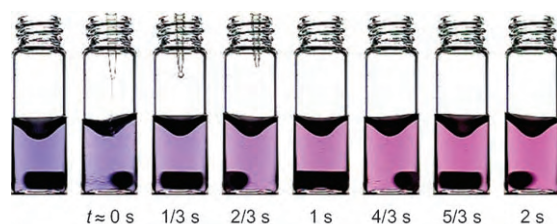


**Figure 1.** Photographs in chronological order that show the rapidity of  $\text{Pb}^{\text{II}}$  sensing. The snapshot on the far left was taken prior to the introduction of an aliquot (0.10 mL) of  $\text{Pb}^{\text{II}}$  (2.50 nmol) by micro-pipette. The approximate time for each frame is noted under the photographs. The concentration of the 15c5- $\text{C}_4$ /TA-GNPs in the vial is 0.22  $\text{mg mL}^{-1}$ . The solvent system is methanol/water (90%, v/v; 1.80 mL) buffered to pH 8.00 by 10 mM sodium Tris-HCl. Tris = tris(hydroxymethyl)aminomethane.

The change in color signifies that the presence of  $\text{Pb}^{\text{II}}$  triggers the events associated with a blue-shift of the SP absorption, indicative of the transformation of GNPs from aggregation to dispersion.<sup>[11–14]</sup> This scenario is supported by the shift of the SP band from 700 to 525 nm (Figure 2a), and confirmed by the size distribution of the GNPs whose average hydrodynamic diameter is reduced from  $(700 \pm 70)$  to  $(47 \pm 17)$  nm (Figure 2b). To show the selectivity and sensitivity of the bifunctionalized GNPs toward  $\text{Pb}^{\text{II}}$  ions, the extinction ratios at 530 and 660 nm are plotted against the concentrations of a variety of metal ions in Figure 3. The extinction

coefficients at the two wavelengths indicate the relative amounts of dispersive and aggregated GNPs.<sup>[11,12]</sup> The extinction ratio climbs sharply for  $\text{Pb}^{\text{II}}$  within a narrow range between 0.25 and 2.50  $\mu\text{M}$ , whereas they are unaffected by other metals at a 100-fold or higher concentration level. The narrow concentration range may offer a pass-or-fail diagnostic test by visual determination. The results demonstrate the selectivity of this sensing scheme toward  $\text{Pb}^{\text{II}}$  ions.

The effect of the amount of water in the methanol/water solutions of the GNPs was examined. The GNPs appear slightly purplish when the water content is more than 20% and become dispersive at 30% (see the Supporting Information). For solutions of GNPs containing less than 20% water, ten recipes with water contents

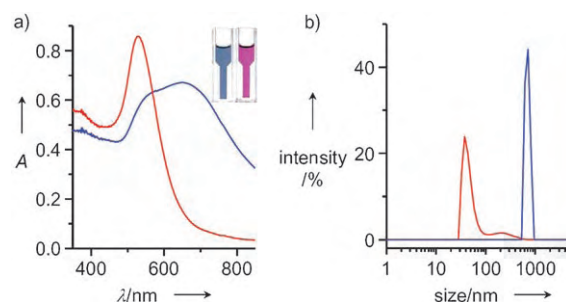


**Figure 2.** a) UV/Vis spectra and b) size distribution of the 15c5- $\text{C}_4$ /TA-GNPs before (blue traces) and after (red traces) addition of  $\text{Pb}^{\text{II}}$  (2.50 nmol). All experimental conditions, including the volume and the concentrations of  $\text{Pb}^{\text{II}}$  and GNPs, are identical to those in Figure 1.

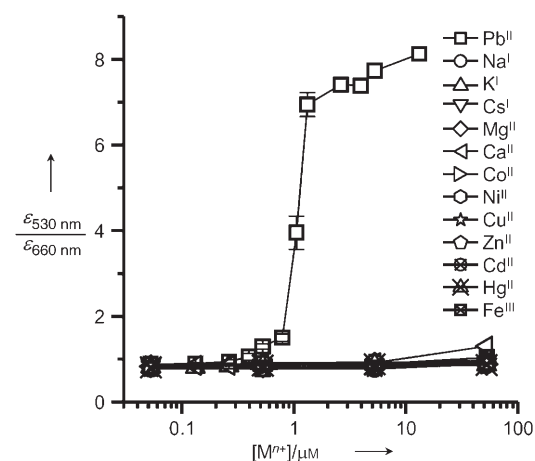


**Figure 3.** Selectivity and sensitivity of 15c5- $\text{C}_4$ /TA-GNPs toward  $\text{Pb}^{\text{II}}$  ions. UV/Vis spectra for extinction ratios (530 over 660 nm) were obtained about 3 min after the GNPs (1.80 mL) were exposed to the metal cations. The x axis represents the concentration of the metal cations in the solution (1.90 mL).

ranging from 2% to 18% were studied to optimize the sensing performance. However, to the naked eye they exhibit almost identical color and the responsive range of  $\text{Pb}^{\text{II}}$  concentrations, although a plot of extinction ratio ( $\epsilon_{530\text{ nm}}/\epsilon_{660\text{ nm}}$ ) against concentration differentiates their sensitivity by UV/Vis spectrometry. A water content of 10% is employed in this study because with this quantity (that is, 1.0 mL aqueous GNPs mixed with 9.0 mL methanol) it is easy to prepare the assay with accuracy and thus minimize the experimental deviation.

To clarify the effect of the crown ether and carboxylic moieties on the sensing mechanism, control experiments using GNPs with tailored surface functionality were carried out. To limit the presence of carboxylic acid at the GNP/solution interface, a crown ether thiol with a long spacer ( $[(15\text{c}5)\text{crown-5}]\text{CH}_2\text{O}(\text{CH}_2)_{12}\text{SH}$ ) was synthesized and used to modify the GNPs such that the carboxylic moieties were buried within the organic shell. In 90% methanol, this 15c5- $\text{C}_{12}$ /TA-GNP solution appears red, which demonstrates that hydrogen bonding between interparticle carboxylic moieties is responsible for the initial aggregation of 15c5- $\text{C}_4$ /TA-GNPs. The role of the carboxylic moieties in  $\text{Pb}^{\text{II}}$  sensing was further investigated by using TA-GNPs that contained no crown ether thiol. The color of these GNPs is blue, and shows no discernible difference from that of 15c5- $\text{C}_4$ /TA-GNPs. However, the TA-GNP solution does not respond to  $\text{Pb}^{\text{II}}$  ions even at a concentration 20-fold higher than that of Figure 1. Therefore, the sensing activity of the 15c5 moiety, rather than the carboxylic moieties alone, is indispensable to the signaling of an aggregation-to-dispersion transformation.

It is well-documented that aggregation of carboxylic acid-terminated GNPs takes place in organic solvents as a result of the formation of interparticle hydrogen bonds.<sup>[15–18]</sup> How does this attractive force become repulsive and why is this transition selective for  $\text{Pb}^{\text{II}}$  over other common metal ions? The key factors are electrostatic interactions between the GNPs and the relative size of the crown ether cavity to the diameter of the metal ion. The electrical potential at the hydrodynamic shear plane around a particle, namely the zeta potential, has been applied to predict the stability of nanosuspensions.<sup>[19,20]</sup>

For example, the criterion for nanoparticles being stable exclusively by electrostatic repulsion is a zeta potential larger than +30 mV or more negative than –30 mV.<sup>[19,20]</sup> In the 90% methanol solvent, the zeta potential of 15c5- $\text{C}_4$ /TA-GNPs increases with the amount of metal ion (Figure 4), which suggests some level of affinity of the ions toward either the carboxylic acid or crown ether moiety. Among the metal ions, only  $\text{Pb}^{\text{II}}$  can rapidly lift the zeta potential value higher than +30 mV, an apparent driving force that impairs the interparticle hydrogen bonding and triggers dispersive GNPs. Although other ions might also be caged in the crown ether cavity, the electrostatic repulsion appears insufficient to break the hydrogen bonds between the GNPs. Alternatively, GNPs may develop aggregates on account of a 2:1 15c5-to-cation sandwich complex when the crown ether cavity (1.70–2.20 Å)<sup>[21]</sup> is too small to accommodate the metal cations, for example,  $\text{K}^+$  (2.76 Å).<sup>[22]</sup> In either pathway the blue color of the GNP solution remains unchanged.

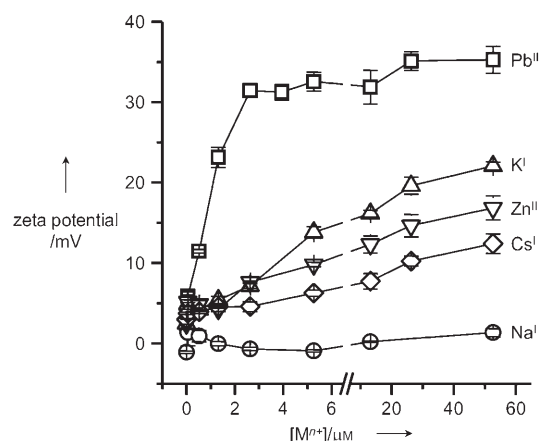


**Figure 4.** Zeta potential of 15c5- $\text{C}_4$ /TA-GNPs in response to metal ions. The measurements were performed 3 min after the metal ions were added to the 90% methanol solvent system.

The diameter of  $\text{Pb}^{\text{II}}$  is 2.38 Å,<sup>[23]</sup> only slightly larger than that of the 15c5 cavity (1.70–2.20 Å),<sup>[21]</sup> and the structures of 1:1<sup>[7,24]</sup> and 2:1<sup>[7,25]</sup> 15c5- $\text{Pb}^{\text{II}}$  complexes have both been found in the literature. To further elaborate the sensing mechanism, zeta potential measurements were carried out for the aforementioned 15c5- $\text{C}_{12}$ /TA-GNPs. After exposure to  $\text{Pb}^{\text{II}}$  (2.50 nmol) in 90% methanol, the zeta potential of the GNPs jumps from less than 10 mV and instantly reaches a plateau of +30 mV, indicative of the formation of a 15c5- $\text{Pb}^{\text{II}}$  complex. The color is red throughout the concentration examined (0.0–1.0 mM), and thus the possibility of interparticle sandwich complexation is ruled out. On the contrary, 2:1 sandwich complexation takes place in aqueous medium, where the same 15c5- $\text{C}_{12}$ /TA-GNPs (3.0 mL, 0.40 mg mL<sup>–1</sup>) are also sensitive to  $\text{Pb}^{\text{II}}$  (2.50 nmol) and the solution turns from red to blue.

The intriguing solvent-dependent response is consistent with how the solvent polarity may shape the microstructures of the highly flexible ethylene glycol moiety. The polar water molecules attract and exteriorize oxygen atoms of the crown ether, and thus expedite a 2:1 sandwich complexation of 15c5-functionalized nanoparticles to metal ions.<sup>[10,22,26]</sup> In methanol, the hydrophobic ethylene units become the exterior of the crown ether cavity.<sup>[27]</sup> The  $\text{Pb}^{\text{II}}$  ion is hosted by one crown ether or sandwiched by neighboring crown ether moieties at the same 15c5- $\text{C}_{12}$ /TA-GNP. Therefore, the value of the zeta potential increases and the GNPs do not aggregate.

In addition to the above 15c5- $\text{Pb}^{\text{II}}$  complexation schemes, there is an alternative for 15c5- $\text{C}_4$ /TA-GNPs. Note that the crown ether thiol has a short methylene spacer. The relative chain length of crown ether thiol and TA configures a cooperative sensing scheme (the enlarged frame of Scheme 1), in which the electrostatic attraction of  $\text{Pb}^{\text{II}}$  and carboxylate is facilitated by the chelation of a proximal crown ether moiety. The  $\text{Pb}^{\text{II}}$  takes over the hydrogen-bonding sites, and therefore the driving force for the initial aggregation is weakened and is displaced by electrostatic repulsion, which leads to dispersive GNPs.

In summary, we have demonstrated a novel and simple signaling scheme that promptly activates the color trans-



formation of GNPs by breaking the interparticle hydrogen bonds. By taking advantage of the favorable diameter ratio of  $\text{Pb}^{\text{II}}$  to the crown ether cavity of the 15c5 moiety, the bifunctionalized GNPs are shown to be highly selective to  $\text{Pb}^{\text{II}}$  ions. The high extinction coefficient of GNPs allows the determination of  $\text{Pb}^{\text{II}}$  down to  $1\ \mu\text{M}$  using the naked eye. This methodology can be generalized for other analytes of interest by using moieties such as assorted macrocycles, cyclodextrins, and many host functionalities.

Received: February 28, 2006

Revised: April 3, 2006

Published online: July 4, 2006

**Keywords:** crown compounds · hydrogen bonds · lead · nanoparticles · sensors

- 
- [1] P. Mulvaney, *Langmuir* **1996**, *12*, 788–800.
  - [2] C. M. Niemeyer, *Angew. Chem.* **2001**, *113*, 4254–4287; *Angew. Chem. Int. Ed.* **2001**, *40*, 4128–4158.
  - [3] R. Shenhar, V. M. Rotello, *Acc. Chem. Res.* **2003**, *36*, 549–561.
  - [4] M.-C. Daniel, D. Astruc, *Chem. Rev.* **2004**, *104*, 293–346.
  - [5] N. L. Rosi, C. A. Mirkin, *Chem. Rev.* **2005**, *105*, 1547–1562.
  - [6] R. M. Izatt, K. Pawlak, J. S. Bradshaw, *Chem. Rev.* **1991**, *91*, 1721–2085.
  - [7] D. A. Skoog, D. M. West, F. J. Holler, *Fundamentals of Analytical Chemistry*, 7th ed., Harcourt Brace, Orlando, **1996**.
  - [8] K. C. Grabar, R. G. Freeman, M. B. Hommer, M. J. Natan, *Anal. Chem.* **1995**, *67*, 735–743.
  - [9] S.-Y. Lin, Y.-T. Tsai, C.-C. Chen, C.-M. Lin, C.-h. Chen, *J. Phys. Chem. B* **2004**, *108*, 2134–2139.
  - [10] S.-Y. Lin, C.-h. Chen, M.-C. Lin, H.-F. Hsu, *Anal. Chem.* **2005**, *77*, 4821–4828.
  - [11] J. Liu, Y. Lu, *J. Am. Chem. Soc.* **2003**, *125*, 6642–6643.
  - [12] J. Liu, Y. Lu, *J. Am. Chem. Soc.* **2004**, *126*, 12298–12305.
  - [13] J. Liu, Y. Lu, *Chem. Mater.* **2004**, *16*, 3231–3238.
  - [14] J. Liu, Y. Lu, *J. Am. Chem. Soc.* **2005**, *127*, 12677–12683.
  - [15] H. Schmitt, A. Badia, L. Dickinson, L. Reven, R. B. Lennox, *Adv. Mater.* **1998**, *10*, 475–480.
  - [16] S. Chen, K. Kimura, *Langmuir* **1999**, *15*, 1075–1082.
  - [17] J. Simard, C. Briggs, A. K. Boal, V. M. Rotello, *Chem. Commun.* **2000**, 1943–1944.
  - [18] L. Han, J. Luo, N. N. Kariuki, M. M. Maye, V. W. Jones, C. J. Zhong, *Chem. Mater.* **2003**, *15*, 29–37.
  - [19] P. A. Webb, C. Orr, R. W. Camp, J. P. Olivier, *Analytical Methods in Fine Particle Technology*, Micromeritics Instrument Corporation, Norcross, GA, **1997**, p. 279.
  - [20] R. H. Muller, C. Jacobs, O. Kayser, *Adv. Drug Delivery Rev.* **2001**, *47*, 3–19, and references therein.
  - [21] J. W. Steed, J. L. Atwood, *Supramolecular Chemistry*, Wiley, New York, **2000**, p. 116.
  - [22] S.-Y. Lin, S.-W. Liu, C.-M. Lin, C.-h. Chen, *Anal. Chem.* **2002**, *74*, 330–335.
  - [23] R. D. Shannon, *Acta Crystallogr. Sect. A* **1976**, *32*, 751–767.
  - [24] R. M. Izatt, R. E. Terry, D. P. Nelson, Y. Chan, D. J. Eatough, J. S. Bradshaw, L. D. Hansen, J. J. Christensen, *J. Am. Chem. Soc.* **1976**, *98*, 7626–7630.
  - [25] J. Massaux, J. F. Desreux, *J. Am. Chem. Soc.* **1982**, *104*, 2967–2972.
  - [26] R. D. Rogers, A. H. Bond, *Inorg. Chim. Acta* **1992**, *192*, 163–171.
  - [27] J. W. Steed, J. L. Atwood, *Supramolecular Chemistry*, Wiley, New York, **2000**, pp. 107–109.

DOI: 10.1002/anie.200600042

# The Structure of a Designed Diiron(III) Protein: Implications for Cofactor Stabilization and Catalysis\*\*

Herschel Wade, Steven E. Stayrook, and William F. DeGrado\*

The de novo design of model metalloproteins provides a powerful approach to examine the functional consequences of metal cofactor–protein interactions.<sup>[1,2]</sup> Despite extensive work in this area, to date the structures of designed non-heme Fe proteins with bound cofactors have not been determined, rendering it difficult to fully develop structure–function relationships. Here we investigate structural properties of diiron(III) DF2t.<sup>[3]</sup> DF2t is a dimeric member of the due-ferri (DF) family of highly simplified models<sup>[3]</sup> of the more complex natural diiron enzymes. These systems, which include methane monooxygenase (MMOH),<sup>[4]</sup> ribonucleotide reductase (RNRR2),<sup>[5]</sup> and stearoyl ACP  $\Delta^9$ -desaturase ( $\Delta 9D$ )<sup>[6]</sup> show highly similar ligand sets (almost invariably, 4-Glu,2-His) and encapsulate the diiron cofactors within four-helix bundles (Table 1).<sup>[7]</sup> As shown for the natural enzymes, DF2t binds two iron(II) ions using a 4-Glu,2-His ensemble to generate an O<sub>2</sub>-reactive binuclear cluster. The spectroscopic properties of the diiron(III) DF2t product implicate an oxo-bridged cofactor, structurally akin to those presented by the diiron(III) enzymes.<sup>[8]</sup> The crystallographic structure of the diiron(III) DF2t cofactor is presented here, providing a simplified model of diiron enzymes.

DF2t idealizes the otherwise inexact symmetrical four-helix bundle motifs and arrangements of the Glu and His

**Table 1:** Diiron enzymes.

Enzyme	Abbreviation	Ligand set
methane monooxygenase	MMOH	4-Glu, 2-His
ribonucleotide R2	RNRR2	3-Glu, 1-Asp, 2-His
rubrerythrin	Rbr	4-Glu, 2-His
bacterioferritin	BFR	4-Glu, 2-His
stearoyl ACP	$\Delta 9D$	4-Glu, 2-His
$\Delta^9$ -desaturase		

[\*] H. Wade, S. E. Stayrook, W. F. DeGrado  
Department of Biochemistry and Biophysics  
University of Pennsylvania  
Philadelphia, PA 19104 (USA)  
E-mail: wdegrado@mail.med.upenn.edu  
W. F. DeGrado  
Department of Chemistry  
University of Pennsylvania  
Philadelphia, PA 19104 (USA)  
Fax: (+1) 215-573-7229

[\*\*] We thank the National Institutes of Health (GM65416) and the NSF (DMR-05 20020 and 0425780).



Supporting information for this article is available on the WWW under <http://www.angewandte.org> or from the author.

ligands found in more complex diiron enzymes.<sup>[10]</sup> In aggregate, the structures of di-Mn<sup>II</sup>-, di-Co<sup>II</sup>-, di-Zn<sup>II</sup>-, and di-Cd<sup>II</sup>-bound DF variants<sup>[3b]</sup> show variations about a “canonical bis-divalent” cluster consisting of two  $\mu$ -1,3-bridging Glu carboxylates, two chelating Glu carboxylates, and two  $\delta$ N-bound His ligands (Figure 1). Each metal ion has a labile coordination

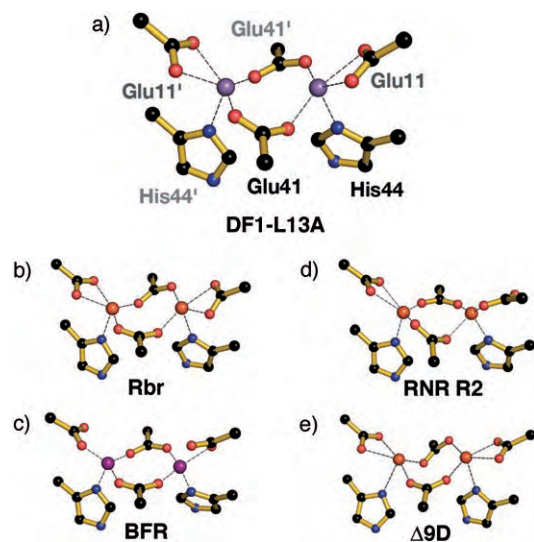


**Figure 1.** “Canonical bis-divalent” views of a) di-Mn<sup>II</sup>-DF1L13A (1OVR), b) di-Fe<sup>II</sup> Rbr (1LKO), c) di-Mn<sup>II</sup> BFR (1BCF), d) di-Fe<sup>II</sup> RNRR2 (1KIX), and e) di-Fe<sup>II</sup> Δ9D (1AFR). The structures were generated with Pymol.<sup>[9]</sup>

position *trans* to the Fe- $\delta$ NHis bonds. These sites are either vacant or they can accommodate exogenous ligands in either bridging or terminal geometries. Computational studies on RNRR2 and DF2t<sup>[11]</sup> suggest that the adjacent sites are configured optimally for facile two-electron reductions of Fe-bound O<sub>2</sub> to peroxide. The divalent metal-bound enzyme clusters are consonant with the “canonical” view, despite showing deviations resembling “carboxylate shifts”,<sup>[12]</sup> which are particularly accentuated in the diiron(III) proteins.<sup>[7,13]</sup> Smaller departures from the “canonical” view are observed in metal-bound DF proteins; the structure of diiron(III) DF2t permits the analysis of analogous deviations in a trivalent metal-bound DF complex. The structural simplicity and well-defined chemical properties of DF2t should facilitate an understanding of the minimal requirements for oxygen reactivity.

The structure of diiron(III) DF2t was solved to 2.1 Å using diffraction data collected at wavelengths shown to disfavor the photoreduction of diiron(III) enzyme centers.<sup>[15]</sup> The Fe environments (Figure 2a and Figure S1 in the Supporting Information) are consistent with those observed in diiron(III) enzymes and small-molecule models.<sup>[13,16]</sup> However, the DF2t center is more symmetric and displays fewer deviations from the “canonical” view than the diiron(III) enzyme clusters (Figure 3).<sup>[7]</sup> The close similarity between the divalent metal-bound and diiron(III) DF cofactors contrasts with the natural systems, which show more asymmetric diiron(III) centers featuring larger shifts of the Glu ligands.<sup>[17]</sup> The largest DF2t changes include minor perturbations of

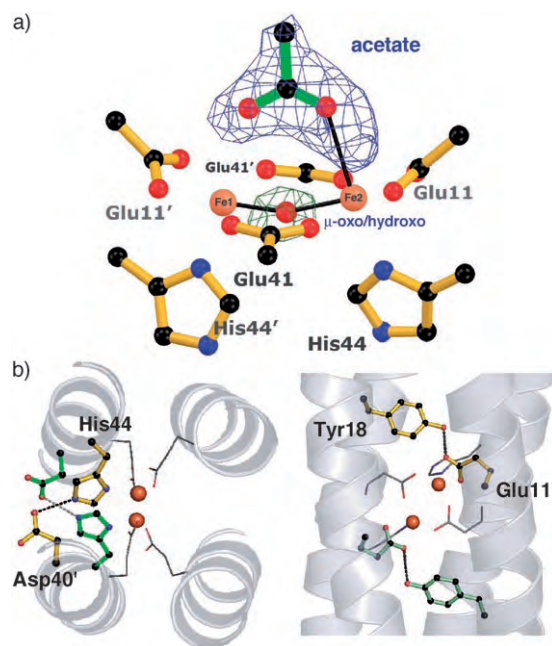


**Figure 2.** DF2t-cofactor interactions. a) The diiron(III) cluster ligands and  $\sigma_A$ -weighted  $F_o - F_c$  omit map peaks modeled by acetate and  $\mu$ -oxo ligands (4.0 $\sigma$ ). b) Second-shell hydrogen bonds (dashed lines). Symmetry-related His-Asp (right) and Tyr-Glu (left) acceptor-donor pairs are shown as ball-and-stick representations (yellow and green, respectively). Noninteracting ligands are represented by lines. The structures in part (a) were generated with Molscript and Raster3D;<sup>[14]</sup> those in part (b) with Pymol.<sup>[9]</sup>

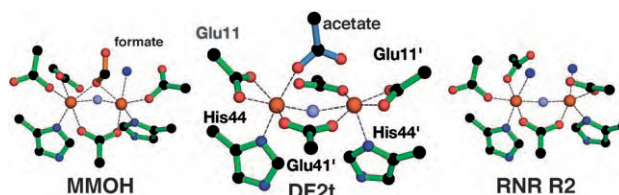


**Figure 3.** The Fe environments in diiron(III) DF2t, MMOH (1FZ1), and RNRR2 (1MXR). The  $\mu$ -oxo/ $\mu$ -hydroxo and solvent-derived ligands are depicted by light-blue and dark-blue spheres, respectively. The structures were generated with Pymol.<sup>[9]</sup>

Glu41 torsion angles, which afford Glu41 as a monodentate ligand that interacts strongly with only one iron center ( $d(\text{Fe}^1\text{-O}) = 2.1$  Å;  $d(\text{Fe}^2\text{-O}) = 2.4$  Å).

Two exogenous ligands were apparent from positive peaks in the electron density maps (Figure 2a). An oxo ligand was modeled at the  $\mu$ -bridging position, *cis* to both Fe- $\delta$ NHis bonds. This assignment is consistent with the UV/Vis absorption spectrum of diiron(III) DF2t<sup>[8]</sup> and similarly bound  $\mu$ -oxo/ $\mu$ -hydroxo ligands observed in the diiron(III) enzymes.<sup>[16,18]</sup> As compared to natural systems, we observe an atypically wide Fe<sup>1</sup>-O-Fe<sup>2</sup> angle of  $\approx 146^\circ$  and Fe<sup>1</sup>-Fe<sup>2</sup> distance of  $\approx 3.6$  Å (vs.  $\approx 120^\circ$  and  $\approx 3.2$  Å). The Fe<sup>1</sup>-O and Fe<sup>2</sup>-O distances of 1.8 and 2.0 Å, respectively, are within the range typically reported for Fe<sup>III</sup>-bound  $\mu$ -oxo/hydroxo ligands.<sup>[7]</sup>

An acetate ion from the crystallization buffer was modeled as the other non-protein ligand (Figure 2a); acetate

is also known to bind weakly to diiron(III) DF2 in solution. The acetate coordinates to  $\text{Fe}^2$  ( $d(\text{Fe}^2\text{--O})=2.2\text{ \AA}$ ) and interacts more weakly with  $\text{Fe}^1$  ( $d(\text{Fe}^1\text{--O})=2.4\text{ \AA}$ ). Comparable lengthening of the Fe–Fe distance was observed in an acetate-bound diiron(III) MMOH,<sup>[19]</sup> which also showed a widened Fe–O–Fe angle and comparable Fe–O<sub>oxo</sub> distances. The net  $-1$  charge on diiron(III) DF2t cluster raises the possibility of a protonated  $\mu$ -oxo bridge; this is deemed less likely as the  $\mu$ -oxo absorption features are only slightly diminished upon acetate binding.<sup>[20]</sup>

Significantly, acetate interacts with the Fe coordination positions occupied by peroxide in structures of DF2t and RNRR2 peroxodiiron(III) intermediates optimized by DFT.<sup>[11]</sup> Excluding the  $\mu$ -oxo ligand, the acetate-bound diiron(III) DF2t cluster may recapitulate interactions implicated in catalytically relevant peroxodiiron(III) species.<sup>[21]</sup>

An extensive series of second-shell hydrogen bonds (Figure 2b) restrain the protein Glu ligands to nearly the same positions as those observed in divalent metal-bound DF proteins despite the accommodation of exogenous  $\mu$ -oxo and acetate ligands. The observed rigidity does not appear to affect the reactivity of the cofactor. Stopped-flow kinetic experiments show that diiron(II) DF2t reacts rapidly with  $\text{O}_2$ , suggesting that cofactor flexibility does not influence largely the initial  $\text{O}_2$ -binding steps.<sup>[11]</sup> Although relatively rigid compared to natural systems, DF2t is able to react with  $\text{O}_2$  and rapidly funnel the reaction towards the diiron(III) product, apparently without large nuclear motions. The larger rearrangements observed in natural systems may not be required for the initial  $\text{O}_2$ -binding steps, but instead for modulating the reactivity of enzyme–peroxo intermediates, facilitating the formation of high-valent species and promoting the oxidation of substrates.

Furthermore, the simplified DF2t cluster displays a feature that might be of structural and mechanistic relevance to natural diiron proteins. The  $\mu$ -oxo ligand appears to be stabilized by second-shell  $\text{CH}\cdots\text{O}$  hydrogen bonds<sup>[22]</sup> between the  $\mu$ -oxo ligand and two His<sup>C</sup>H groups (Figure 4). The His<sup>C</sup>H proton is among the most acidic of the C–H groups in amino acid side chains and is potentially capable of participating in hydrogen bonds that are energetically on par with  $\text{C}^{\alpha}\text{H}\cdots\text{O}$  interactions<sup>[23]</sup> proposed to play a significant role in protein stabilization.<sup>[24]</sup> Hydrogen bonds involving His<sup>C</sup>H groups are also conserved in serine proteases, where they are believed to play an important role in catalysis.<sup>[25]</sup>

In DF2t, two His<sup>C</sup>H groups clamp the  $\mu$  ligand in pincerlike interactions. The distances and angles are restrained somewhat by the five-membered ring but lie

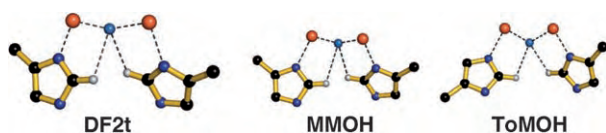


**Figure 4.** Second-shell interactions (dashed lines) involving His<sup>C</sup>H atoms and  $\mu$ -oxo/ $\mu$ -hydroxo ligands in diiron(III) DF2t, MMOH (1FZ1), and toluene monooxygenase hydroxylase (ToMOH, 1TOS). See Table S2 in the Supporting Information for geometric details. The  $\mu$ -oxo/ $\mu$ -hydroxo ligands and Fe atoms are depicted by blue and orange spheres, respectively. The structures were generated with Pymol.<sup>[9]</sup>

within the ranges observed for analogous systems (Table S2 in the Supporting Information).<sup>[22]</sup> Geometrically similar interactions are present in  $\mu$ -oxo/hydroxo-bridged diiron(III) and dimanganese(III) clusters of all structurally characterized  $\text{O}_2$ -activating enzymes, including dimanganese catalase<sup>[27]</sup> and toluene monooxygenase hydroxylase,<sup>[26]</sup> which displays an atypical combination of Fe– $\epsilon$ N and Fe– $\delta$ NHis bonds. The His<sup>C</sup>H pocket appears to be primed to stabilize negatively charged species; enzyme clusters that lack  $\mu$ -oxo/hydroxo bridges show comparable interactions with other anionic ligands. In divalent metal-substituted enzymes, the pocket is partially filled by  $\mu$ -1,1 oxygen bridges donated by coordinatively flexible Glu residues.<sup>[19,28]</sup> Moreover, an azide ion participates in two short His<sup>C</sup>H $\cdots$ N bonds in the diiron(II) E238A RNRR2 cluster, where the side chain of the Glu238 ligand is replaced by a methyl group.<sup>[29]</sup> Significantly, the His<sup>C</sup>H $\cdots$ O interactions display geometric variability among numerous diiron(III) and diiron(II) enzyme systems (Tables S2 and S3 in the Supporting Information), underscoring the flexibility to form one or two  $\text{CH}\cdots\text{O}$  hydrogen bonds with the His<sup>C</sup>H pair.

Possible mechanistic implications of the second-shell His<sup>C</sup>H $\cdots$ O interactions are shown in Scheme 1. As the



**Scheme 1.** The stabilization of metal-bound catalytic intermediates through His<sup>C</sup>H $\cdots$ O hydrogen bonds.

metal-bound oxygen atoms are reduced to  $\text{O}^{2-}$ , the His<sup>C</sup>H groups are positioned to stabilize the developing anionic character of oxygen atoms. Thus, His<sup>C</sup>H $\cdots$ O bonds resembling those found in diiron(III) enzymes structures may serve to stabilize catalytic transition states and reactive cofactor-bound intermediates, including the Q and X species.<sup>[5,30]</sup> Although  $\text{CH}\cdots\text{O}$  hydrogen bonds are considered weak (on the order of  $1\text{ kcal mol}^{-1}$ ), they may serve to tune more energetically dominant primary interactions to specify a given reaction mechanism or product, particularly in systems such as diiron enzymes where different pathways can have comparable energetics.<sup>[4]</sup> The structural and mechanistic roles of these interactions may now be examined through theoretical and biochemical studies.

In conclusion, the structure of diiron(III) DF2t provides the framework for further elaboration of designed diiron model proteins. The oxidized diiron DF2t cluster shows the hallmarks of natural diiron(III) enzymes and inorganic models. The center also displays unusual rigidity and is able to accommodate two additional non-protein ligands, while preserving the “canonical” appearance. Furthermore, the  $\mu$ -oxo bridge has access to functionally important DF2t Fe coordination sites *cis* to both Fe– $\delta$ NHis bonds, while the metal-bound acetate supports the binding capabilities of binuclear cofactors.



## Experimental Section

**Protein purification and crystallization:** Crystals of diiron(III) DF2t ( $50\ \mu\text{m} \times 75\ \mu\text{m} \times 80\ \mu\text{m}$ ) grown by vapor diffusion using the sitting-drop method were used in the diffraction experiments. DF2t was expressed in *E. coli* and purified as previously described.<sup>[3a]</sup> Diiron(III) DF2t was reconstituted from apo-DF2t and  $\text{Fe}(\text{NH}_4)_2(\text{SO}_4)_2$  in 0.1%  $\text{H}_2\text{SO}_4$  in 50 mM 3-(*N*-morpholine)propanesulfonic acid (MOPS), 150 mM NaCl, pH 7.0. Following the oxidation of diiron(II) DF2t, the sample was centrifuged to remove iron oxide precipitates. The sample was gel-filtered to remove nonspecifically bound Fe and dialyzed in 50 mM MOPS, 50 mM NaCl, pH 7.0. The dialysis buffer was exchanged into a salt-free 10 mM HEPES, pH 7.0 buffer by gel filtration. The final sample consisted of 1.5–2.0 mM diiron(III) DF2t. Crystals were obtained from 8.25 mM  $\text{Mg}(\text{OAc})_2$ , 24–28% PEG 1500, and 100 mM HEPES, pH 7.5 at 19.0°C. The crystals were cryoprotected by soaking in 8.25 mM  $\text{Mg}(\text{OAc})_2$ , 32–36% PEG 1500, and 100 mM HEPES, pH 7.5. Crystals were obtained over four to seven days.

**Diffraction data collection and refinement:** The diffraction data were collected at  $-160^\circ$  at the Advanced Light Source (beamline, 8.3.1), Lawrence Livermore Laboratories, Berkeley, CA. Data collected at 0.96 and 0.98 Å produced nearly identical models, whereas data collection at 1.08 Å produced features consistent with photoreduction (this will be reported separately). The data were integrated using DENZO and scaled with SCALEPACK. The initial phases were obtained by molecular replacement (di- $\text{Zn}^{\text{II}}$ -DF2turn-1Y47, search model).<sup>[8]</sup> All water molecules, metal ions, and exogenous ligands were removed as the Glu ligands from the coordinate file of the search model. The initial round of refinement using the CNS suite included a rigid-body refinement, simulated annealing, conjugate gradient minimizations, and an overall B-factor refinement against maximum likelihood targets.<sup>[31]</sup> Anomalous and  $\sigma_A$ -weighted  $F_o - F_c$  omit difference maps were used to determine positions of the metal ions. Positional and B-factor refinements of the ions were performed using the Lennard–Jones potential for  $\text{Fe}^{\text{III}}$ . Geometrical, thermal parameter, and strict noncrystallographic symmetry (NCS) restraints were imposed during early stages of refinement and relaxed as judged by  $R_{\text{free}}$  at later stages. Well-defined electron density for all ligands was observed in maps generated with Fourier coefficients  $2F_o - F_c$  and  $F_o - F_c$  and phases calculated from in-progress models built using coot and O. During later stages of refinement,  $\sigma_A$ -weighted  $3F_o - 2F_c$ ,  $2F_o - F_c$ ,  $F_o - F_c$ , and composite omit maps were used to guide model building. Water picking was guided by  $\sigma_A$ -weighted  $F_o - F_c$  difference maps; geometric considerations and B-values served as additional validation criteria. Final rounds of refinements were performed with REFMAC5, maximum likelihood residual, anisotropic scaling, bulk-solvent correction, and the “translation, libration, and screw rotation” (TLS) method.<sup>[31]</sup> Each DF2t monomer was treated as a rigid group, while all water molecules, metal ions, and exogenous ligands were excluded.

The final  $R_{\text{work}}$  and  $R_{\text{free}}$  values are provided in Table S1 in the Supporting Information along with rmsd values from ideal bond lengths and angles. Table S1 also lists estimated coordinate errors derived from Luzzati plots ( $R_{\text{free}}$  values) and final maximum-likelihood functions. Ramachandran plots (CCP4), WHATIF, and PROCHECK were used for validation and conformational analyses of the final models. The models exhibit good geometry with 100% of the residues in the most favored or additionally favored regions. The Fe–N<sub>HIS</sub> and Fe–O<sub>GLU</sub> bonds in the metal cluster are within the range expected based on data from high-resolution structures of small-molecule and protein–metal ion complexes extracted from the Cambridge Structural Database.<sup>[32]</sup>

**Keywords:** diiron enzymes · metalloproteins · protein models · protein structures

- [1] P. D. Barker, *Curr. Opin. Struct. Biol.* **2003**, *13*, 490.
- [2] M. L. Kennedy, B. R. Gibney, *Curr. Opin. Struct. Biol.* **2001**, *11*, 485.
- [3] a) S. J. Lahr, D. E. Engel, S. E. Stayrook, O. Maglio, B. North, S. Geremia, A. Lombardi, W. F. DeGrado, *J. Mol. Biol.* **2005**, *346*, 1441; b) J. R. Calhoun, F. Natri, O. Maglio, V. Pavone, A. Lombardi, W. F. DeGrado, *Biopolymers* **2005**, *80*, 264.
- [4] Y. Lindqvist, W. Huang, G. Schneider, J. Shanklin, *EMBO J.* **1996**, *15*, 4081.
- [5] B. F. Gherman, S. J. Lippard, R. A. Friesner, *J. Am. Chem. Soc.* **2005**, *127*, 1025.
- [6] J. Stubbe, P. Riggs-Gelasco, *Trends Biochem. Sci.* **1998**, *23*, 438.
- [7] P. Nordlund, H. Eklund, *Curr. Opin. Struct. Biol.* **1995**, *5*, 758.
- [8] O. Maglio, F. Natri, J. R. Calhoun, S. Lahr, H. Wade, V. Pavone, W. F. DeGrado, A. Lombardi, *J. Biol. Inorg. Chem.* **2005**, *10*, 539.
- [9] W. L. DeLano, Pymol, DeLano Scientific, San Carlos, CA, **2002**.
- [10] A. Lombardi, C. Summa, W. F. DeGrado, *Proc. Natl. Acad. Sci. USA* **2000**, *97*, 6298.
- [11] P.-P. Wei, A. J. Skulan, H. Wade, W. F. DeGrado, E. I. Solomon, *J. Am. Chem. Soc.* **2005**, *127*, 16098.
- [12] R. L. Rardin, W. B. Tolman, S. J. Lippard, *New J. Chem.* **1991**, *15*, 417.
- [13] D. Kurtz, *J. Biol. Inorg. Chem.* **1997**, *2*, 159.
- [14] P. Kraulis, *J. Appl. Crystallogr.* **1991**, *24*, 946.
- [15] A. Ericson, B. Hedman, K. O. Hodgson, J. Green, H. Dalton, J. G. Bentsen, R. H. Beer, S. J. Lippard, *J. Am. Chem. Soc.* **1988**, *110*, 2330.
- [16] E. Y. Tshuva, S. J. Lippard, *Chem. Rev.* **2004**, *104*, 987.
- [17] D. Whittington, S. J. Lippard, *J. Am. Chem. Soc.* **2001**, *123*, 872.
- [18] B. J. Waller, J. D. Lipscomb, *Chem. Rev.* **1996**, *96*, 2625.
- [19] A. C. Rosenzweig, P. Nordlund, P. M. Takahara, C. A. Frederick, S. J. Lippard, *Chem. Biol.* **1995**, *2*, 409.
- [20] L. DiConstanza, H. Wade, S. Geremia, L. Randaccio, V. Pavone, W. F. DeGrado, A. Lombardi, *J. Am. Chem. Soc.* **2001**, *123*, 12749.
- [21] M. Moche, J. Shanklin, A. Ghoshal, Y. Lindqvist, *J. Biol. Chem.* **2003**, *278*, 25072.
- [22] T. Steiner, *Cryst. Rev.* **2003**, *9*, 177.
- [23] S. Scheiner, *J. Phys. Chem. B* **2005**, *109*, 16132.
- [24] A. Senes, M. Gerstein, D. M. Engelman, *J. Mol. Biol.* **2000**, *296*, 921.
- [25] Z. S. Derewenda, U. Derewenda, P. M. Kobos, *J. Mol. Biol.* **1994**, *241*, 83.
- [26] M. H. Sazinsky, J. Bard, A. Di Donato, S. J. Lippard, *J. Biol. Chem.* **2004**, *279*, 30600.
- [27] V. V. Barynin, M. M. Whittaker, S. V. Antonyuk, V. S. Lamzin, P. M. Harrison, P. J. Artymiuk, J. W. Whittaker, *Structure* **2001**, *9*, 725.
- [28] W. C. Voegtli, M. Sommerhalter, L. Saleh, J. Baldwin, J. M. Bollinger, A. C. Rosenzweig, *J. Am. Chem. Soc.* **2003**, *125*, 15822.
- [29] M. Assarsson, M. E. Andersson, M. Hogbom, B. O. Persson, M. Sahlin, A. L. Barra, B. M. Sjöberg, P. Nordlund, A. Graslund, *J. Biol. Chem.* **2001**, *276*, 26852.
- [30] R. A. Friesner, M. H. Baik, B. F. Gherman, V. Guallar, M. Wirstam, R. B. Murphy, S. J. Lippard, *Coord. Chem. Rev.* **2003**, *238–239*, 267.
- [31] CCP4, The CCP4 Suite: Programs for Protein Crystallography, *Acta Crystallogr. Sect. D* **1994**, *50*, 760.
- [32] M. M. Harding, *Acta Crystallogr. Sect. D* **1999**, *55*, 1432.

Received: January 4, 2006

Revised: February 24, 2006

Published online: July 3, 2006

# Enhancement of Pt Utilization in Electrocatalysts by Using Gold Nanoparticles\*\*

Dan Zhao and Bo-Qing Xu\*

Many important reactions are strongly dependent on noble-metal catalysts, such as electrochemical reactions on the Pt electrode in proton-exchange membrane fuel cells (PEMFC).<sup>[1]</sup> The development of this promising application has been hampered because of the high cost of the catalyst.<sup>[2,3]</sup> One way to lower costs is to make the most efficient use of the noble metals so that every metal atom is used in the catalytic process. Because catalysis at the electrode of a fuel cell is a surface phenomenon, the utilization of Pt in electrocatalysts can be defined as the dispersion or exposed percentage of Pt atoms in the catalyst, which is approximately equal to the reciprocal of the Pt particle size in nanometers.<sup>[4,5]</sup> According to a number of recent reports, the most favorable particle size for Pt-based electrocatalysts is in the range of 2–4 nm.<sup>[6–9]</sup> Therefore, the utilization or exposed percentage of Pt atoms in these state-of-the-art electrocatalysts is in the range of 25–50%, far below a 100% utilization or dispersion of the ideal model. To enhance Pt utilization, it would be necessary to further decrease the particle size of Pt-based electrocatalysts.

A reasonable expectation would be that for Pt particle sizes of about 1 nm or smaller a 100% Pt utilization in electrocatalysts could be theoretically possible. In practice, however, metal particles smaller than 2 nm are readily pocketed by the micropores ( $\leq 2.0$  nm) of the conductive carbon supporting material and consequently become inaccessible for electrochemical reactions,<sup>[10–12]</sup> which leads to a significant lowering of the overall Pt utilization. Furthermore, the behavior of very small metal particles (ca. 1.0 nm or smaller) would deviate significantly from that of metallic particles owing to their strong interaction with the surface of the supporting material.<sup>[13–15]</sup> Therefore, it is important to seek alternative approaches for enhancing Pt utilization in carbon-supported electrocatalysts.

Herein, we present a method to enhance Pt utilization in Pt/C-based electrocatalysts by using Au nanoparticles to support the Pt. Gold is chosen because it is inert in the acid

electrolytes<sup>[16]</sup> and its surface favors the reductive deposition of Pt.<sup>[17–19]</sup> By depositing very small Pt particles or clusters onto Au nanoparticles of about 10 nm and by loading the Pt<sup>0</sup>Au particles onto a conventional carbon support, we have discovered a synthetic approach that prevents finely dispersed Pt particles from being pocketed in the micropores of the supporting carbon materials. By adjusting the Pt loading on the Au nanoparticles, we demonstrate that the exposed percentage of Pt atoms in such a model electrocatalyst can be enhanced to nearly 100%, that is, virtually every Pt atom in the electrode becomes available and catalytically active for the electrochemical reactions. This method makes the most efficient use of Pt in electrocatalysis and may also be exploited to improve the utilization of precious metals in other catalysts.

The deposition of Pt onto Au nanoparticles was carried out by reducing  $K_2[PtCl_6]$  with hydrogen in a solution that contained Au particles with a narrow size distribution ( $10.0 \pm 1.2$  nm) and polyvinylpyrrolidone (PVP). The prepared samples were coded as Pt<sub>m</sub>^Au, in which *m* denotes the atomic Pt/Au ratio within the nanoparticles. Figure 1 shows

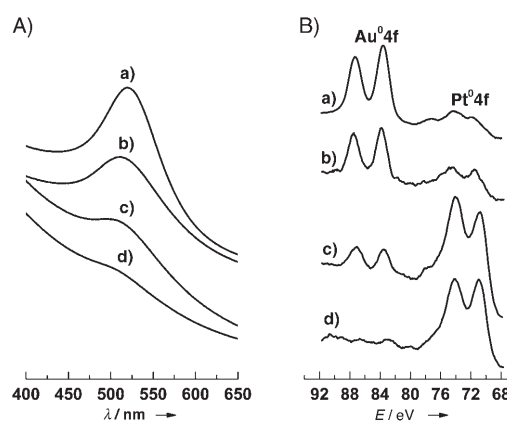


**Figure 1.** UV/Vis (A) and XPS (B) spectra of: a) Pt<sub>0.05</sub>^Au; b) Pt<sub>0.2</sub>^Au; c) Pt<sub>1.0</sub>^Au; d) Pt<sub>2.0</sub>^Au.

the UV/Vis and X-ray photoelectron spectroscopy (XPS) spectra of Au particles with varying amounts of deposited Pt. In the UV/Vis spectra (Figure 1A), the deposition of Pt onto the Au surface is characterized by a continued weakening of the gold plasmon absorption at around 520 nm.<sup>[17,20]</sup> At about *m* = 2.0, the plasmon absorption becomes almost invisible. In the XPS spectra (Figure 1B), continued weakening of the Au<sup>0</sup>4f signals at 83.9 and 87.8 eV<sup>[21,22]</sup> is accompanied by the appearance and strengthening of the Pt<sup>0</sup>4f signals at 70.8 and 74.3 eV with increasing Pt content. These results suggest that the surface of the Au nanoparticles becomes completely covered with Pt overlayers that shield the underlying Au surface from the XPS detection when the number of deposited Pt atoms reaches twice the number of Au atoms of the supporting Au nanoparticles (that is, *m* = 2.0).

Using the atomic Pt/Au ratios measured by XPS, we estimated the number density of Pt atoms (*N*<sub>Pt</sub>; number of Pt atoms per nm<sup>2</sup> of Au surface) at the Au surface by considering the initial Au particles as spheres and by assuming that the

[\*] D. Zhao, Prof. B.-Q. Xu  
Innovative Catalysis Program  
Key Lab of Organic Optoelectronics and Molecular Engineering  
Department of Chemistry, Tsinghua University  
Beijing 100084 (China)  
Fax: (+86) 10-6279-2122  
E-mail: bqxu@mail.tsinghua.edu.cn

[\*\*] The authors wish to thank Dr. Gang Wu for his help with the electrochemical measurements. This work was supported financially by the National Natural Science Foundation of China (20573062, 20590362 and 20125310).

Supporting information for this article is available on the WWW under <http://www.angewandte.org> or from the author.

area for a single Au atom is  $7.87 \times 10^{-2} \text{ nm}^2$ .<sup>[23–25]</sup> For example, the  $N_{\text{Pt}}$  values are 3, 12, and 62, respectively, for  $\text{Pt}_{0.05}/\text{Au}$ ,  $\text{Pt}_{0.2}/\text{Au}$ , and  $\text{Pt}_{1.0}/\text{Au}$  particles (see the Supporting Information). As the size of a Pt atom is basically the same as that of an Au atom, the atomic density of the metallic platinum surface is  $1.3 \times 10^{15}$  per  $\text{cm}^2$  (that is, 13 Pt atoms per  $\text{nm}^2$ ),<sup>[26]</sup> so the data clearly indicate that the deposited Pt atoms in the samples with  $m \leq 0.2$  are highly dispersed. In particular, the deposited Pt atoms at  $m = 0.2$  may form a complete monoatomic layer (about 12 Pt atoms per  $\text{nm}^2$  of Au surface) that covers the Au particles. When  $m$  is sufficiently small, for example  $m \leq 0.05$ , the density of the deposited Pt atoms is less than 3 Pt atoms per  $\text{nm}^2$  of the Au surface, which suggests that the deposited Pt would exist as very small cluster islands or two-dimensional rafts.

Figure 2 shows transmission electron microscopy (TEM) images of the as-prepared and carbon-supported  $\text{Pt}_m/\text{Au}$  particles, which assume an approximately spherical shape. Although the size of  $\text{Pt}_m/\text{Au}$  particles generally tends to increase with an increase in  $m$ , the sizes of  $\text{Pt}_{0.05}/\text{Au}$  (Figure 2b) and  $\text{Pt}_{0.03}/\text{Au}$  (not shown) particles are apparently very close to that of the original Au particles (Figure 2a). According to Henglein,<sup>[17]</sup> the size of the spheric  $\text{Pt}_m/\text{Au}$  particles ( $d_{\text{Pt}_m/\text{Au}}$ ) can be estimated by using Equation (1) in which  $n_{\text{Pt}}/n_{\text{Au}}$  is the number ratio of Pt and Au

$$d_{\text{Pt}_m/\text{Au}} = [(n_{\text{Pt}}/n_{\text{Au}})(V_{\text{Pt}}/V_{\text{Au}}) + 1]^{1/3} d_{\text{Au}} \quad (1)$$

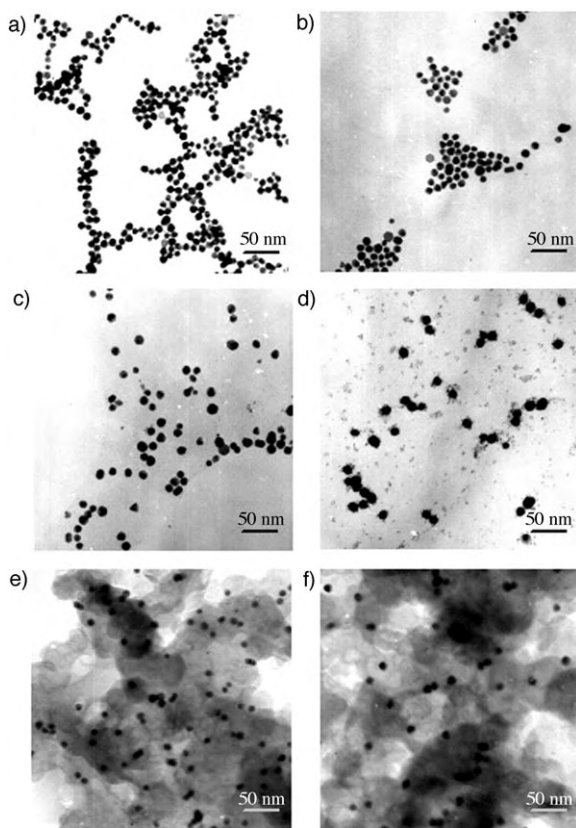


**Figure 2.** TEM images of: a) Au; b)  $\text{Pt}_{0.05}/\text{Au}$ ; c)  $\text{Pt}_{0.2}/\text{Au}$ ; d)  $\text{Pt}_{1.0}/\text{Au}$ ; e)  $\text{Pt}_{0.05}/\text{Au}/\text{C}$ ; f)  $\text{Pt}_{1.0}/\text{Au}/\text{C}$ .

atoms in the particles ( $n_{\text{Pt}}/n_{\text{Au}} = m$ );  $V_{\text{Pt}}/V_{\text{Au}}$  is the volume ratio of Pt and Au atoms, which is 0.89;<sup>[25]</sup>  $d_{\text{Au}}$  in our case is 10 nm; and the calculated  $d_{\text{Pt}_m/\text{Au}}$  sizes are 14.1, 12.4, 11.3, and 10.7 nm at  $m = 2.0, 1.0, 0.5$ , and  $0.2$ , respectively. These sizes agree well with the TEM sizes of the  $\text{Pt}_m/\text{Au}$  particles (see Figure 2 and the Supporting Information). In particular, the particle size of  $\text{Pt}_{0.2}/\text{Au}$  (that is,  $d_{\text{Pt}_m/\text{Au}} = 10.7 \text{ nm}$ ) suggests a thickness for the deposited Pt layer in this sample of 0.35 nm. This value also agrees well with the calculation based on the atomic Pt/Au ratio measured with XPS when the Au particles are completely covered with a monoatomic layer of Pt, as the thickness is equivalent to the diameter of a Pt atom (0.36 nm).<sup>[25]</sup>

In reference to the sample of  $m = 0.2$ , the deposited Pt in samples of  $m = 0.1, 0.05$ , and  $0.03$  would correspond up to 1/2, 1/4, and 1/6 monoatomic Pt layers, respectively, and thus would be insufficient to fully cover the Au surface. The indistinguishable particle sizes between Au and  $\text{Pt}_{0.05}/\text{Au}$  samples in the TEM images (Figure 2a and b) also support that the deposited Pt exists as very small cluster islands or 2D Pt rafts.

To study the potential of  $\text{Pt}_m/\text{Au}$  nanoparticles in the enhancement of Pt utilization in Pt-based electrocatalysts, the as-prepared  $\text{Pt}_m/\text{Au}$  particles were supported with the Vulcan XC-72 carbon blacks to make  $\text{Pt}_m/\text{Au}/\text{C}$  catalysts for electrochemical characterization. TEM images of the  $\text{Pt}_m/\text{Au}/\text{C}$  samples (Figure 2e and f) show that the  $\text{Pt}_m/\text{Au}$  particles in the catalysts are isolated from each other and maintain their original high dispersion.

An important parameter for Pt-based electrocatalysts is the electrochemically active surface (EAS,  $\text{m}^2$  per g Pt) of Pt in the electrode catalyst. As in most electrochemical studies,<sup>[27,28]</sup> we measured the EAS of  $\text{Pt}_m/\text{Au}$  catalysts by using the hydrogen-desorption or hydrogen-electrooxidation peaks on the cyclic voltammetry (CV) curves in acidic media (0.5 M  $\text{H}_2\text{SO}_4$ ; see the Supporting Information). Any hydrogen electrooxidation peak in the CV curves should arise from the presence of Pt in the  $\text{Pt}_m/\text{Au}/\text{C}$  electrocatalyst as carbon-supported gold nanoparticles (Au/C) without Pt are inactive for the adsorption and electrooxidation of hydrogen.<sup>[16]</sup> Thus, the EAS of  $\text{Pt}_m/\text{Au}/\text{C}$  catalysts can be obtained according to Equation (2),<sup>[29]</sup> in which  $Q_{\text{H}}$  is the charge consumed for the

$$\text{EAS} = (Q_{\text{H}}/Q_{\text{e}}) A_{\text{Pt}}/W_{\text{Pt}} = (A_{\text{Pt}}/Q_{\text{e}}) Q_{\text{H}}/W_{\text{Pt}} \quad (2)$$

electrooxidation of adsorbed hydrogen on the Pt surface (i.e., the electrode catalyst), which is equivalent to the calibrated area of the hydrogen-electrooxidation peak;  $Q_{\text{e}}$  is the elementary charge or charge of an electron ( $Q_{\text{e}} = 1.602 \times 10^{-19} \text{ C}$ );  $A_{\text{Pt}}$  is the averaged atomic area of surface Pt atoms, which is  $7.69 \times 10^{-2} \text{ nm}^2$  according to the atomic density of a Pt surface which is  $1.3 \times 10^{15}$  per  $\text{m}^2$ ,<sup>[26]</sup> and  $W_{\text{Pt}}$  is the Pt loading at the working electrode. This equation is based on the well-established hydrogen-adsorption stoichiometry at a Pt surface ( $\text{H}:\text{Pt} = 1:1$ ).<sup>[4,30]</sup>

Therefore, the data of CV measurements allow us to count the number of exposed Pt atoms ( $N_{\text{s}}$ ) as the number of adsorbed H atoms ( $N_{\text{H}}$ ) on the electrode catalyst, that is,  $N_{\text{s}} = N_{\text{H}} = Q_{\text{H}}/Q_{\text{e}}$ . Thus, the ratio of  $N_{\text{s}}$  or  $N_{\text{H}}$  to the total number of

Pt atoms ( $N_t$ ) in the electrode catalyst gives the utilization percentage of Pt [Eq. (3)].

$$U_{\text{Pt}} = N_s/N_t = N_H/N_t \quad (3)$$

Listed in Table 1 are the Pt utilization data from the CV measurements. It is apparent that the EAS and  $U_{\text{Pt}}$  data for the  $\text{Pt}_m^{\wedge}\text{Au/C}$  samples are close to those of a Pt/C catalyst at  $m \geq 0.5$ . Prominent enhancement in EAS and  $U_{\text{Pt}}$  emerges when  $m$  becomes lower than 0.2. In particular, when  $m$  is further decreased to 0.05 or less, the EAS and  $U_{\text{Pt}}$  increase to approach 234  $\text{m}^2$  per g Pt and 100 %, respectively, which are at least twice those of the Pt-based electrocatalysts documented in most reports.<sup>[28,31]</sup>

The  $\text{Pt}_m^{\wedge}\text{Au/C}$  catalysts were used for the electrooxidation of methanol. Figure 3 shows half curves of the normal-

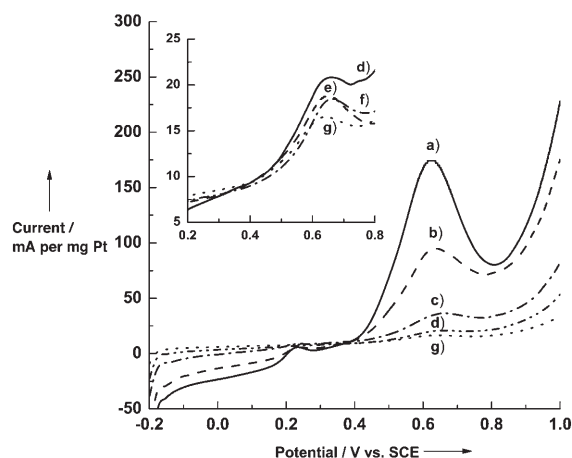


**Figure 3.** Cyclic voltammograms for the electrooxidation of methanol (scan rate: 20  $\text{mV s}^{-1}$ , 0.5 M  $\text{H}_2\text{SO}_4$ , 2 M  $\text{CH}_3\text{OH}$ , 298 K) with the following electrocatalysts: a)  $\text{Pt}_{0.05}^{\wedge}\text{Au/C}$ ; b)  $\text{Pt}_{0.1}^{\wedge}\text{Au/C}$ ; c)  $\text{Pt}_{0.2}^{\wedge}\text{Au/C}$ ; d)  $\text{Pt}_{0.5}^{\wedge}\text{Au/C}$ ; e)  $\text{Pt}_{1.0}^{\wedge}\text{Au/C}$ ; f)  $\text{Pt}_{2.0}^{\wedge}\text{Au/C}$ ; g) Pt/C.

ized cyclic voltammetry of this electrooxidation. It is evident that the normalized current increases remarkably with decreasing value of  $m$ , and that the current varies little from the normal Pt/C electrode when  $m \geq 0.5$ . The current variation over the  $\text{Pt}_m^{\wedge}\text{Au/C}$  catalysts mimics the change of  $U_{\text{Pt}}$  in these catalysts. The last column of Table 1 shows the quantitative mass activity of Pt in the  $\text{Pt}_m^{\wedge}\text{Au/C}$  catalysts, which is defined as the current of methanol electrooxidation

over a milligram of Pt in the electrode. The mass-activity data follow the same trend as the EAS and  $U_{\text{Pt}}$  results, thus proving that the electrocatalytic activity of Pt is directly associated with the utilization or dispersion of Pt in the electrode catalyst. It is not surprising that Pt in  $\text{Pt}_{0.03}^{\wedge}\text{Au/C}$  and  $\text{Pt}_{0.05}^{\wedge}\text{Au/C}$  catalysts exhibit virtually the same mass activity for the electrooxidation of methanol as the Pt utilization in these two catalysts already approaches 100 %.

To understand the electrocatalytic stability of the  $\text{Pt}_m^{\wedge}\text{Au/C}$  catalysts, the  $\text{Pt}_{0.05}^{\wedge}\text{Au/C}$  electrode catalyst was subjected to long-term repeated scanning by cyclic voltammetry in 0.5 M  $\text{H}_2\text{SO}_4$  with 2 M  $\text{CH}_3\text{OH}$  at 298 K, as described previously by Lebedeva and Janssen.<sup>[32]</sup> The change in peak current density (0.65 V vs. SCE) of the electrooxidation of methanol is shown in Figure 4 for 240 cycles. The working period of the electrocatalyst in this specific type of measurement is propor-

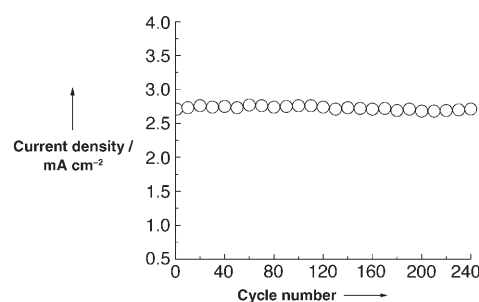


**Figure 4.** Stability of the  $\text{Pt}_{0.05}^{\wedge}\text{Au/C}$  electrocatalyst over 240 cycles of methanol electrooxidation.

tional to the number of scan cycles; each scan cycle lasted for 2 min, and the total working period was about 8 h. The data in Figure 4 show stable electrocatalytic activity of the catalyst electrode; variation in the current density was less than 5 %. Therefore, the finely dispersed Pt cluster islands prepared for this study are suitable electrode catalysts for the electrooxidation of methanol.

It is not known at present whether the Pt in  $\text{Pt}_m^{\wedge}\text{Au/C}$  exists as 3D clusters of about 1 nm or smaller in diameter or as 2D atomic rafts at the gold surface. Although small particles of transition metals have a long history in heterogeneous catalysis, supported metal particles with sizes smaller than 1 nm have rarely been investigated even in the field of heterogeneous catalysis. A few reports show that metal clusters of smaller than 1 nm would have significantly differ-

**Table 1:** Loading, surface concentration, and utilization of Pt and the electrochemical properties of the Pt electrocatalysts.

Catalyst	[Pt] [ $\text{mg cm}^{-2}$ ]	$N_t$ [ $\times 10^{17} \text{ cm}^{-2}$ ]	$Q_H$ [ $\text{mC cm}^{-2}$ ]	$N_s$ [ $\times 10^{16} \text{ cm}^{-2}$ ]	EAS [ $\text{m}^2 \text{ g}^{-1}$ ]	$U_{\text{Pt}}$ [%]	Catalytic activity <sup>[a]</sup> [ $\text{mA mg}^{-1}$ ]
Pt/C	0.22	6.79	11.2	7.00	24.2	10.3	7.3
$\text{Pt}_{2.0}^{\wedge}\text{Au/C}$	0.29	8.95	12.9	8.06	21.2	9.0	9.5
$\text{Pt}_{1.0}^{\wedge}\text{Au/C}$	0.19	5.86	10.6	6.63	26.6	11.3	8.5
$\text{Pt}_{0.5}^{\wedge}\text{Au/C}$	0.11	3.39	6.5	4.06	28.1	12.0	11.6
$\text{Pt}_{0.2}^{\wedge}\text{Au/C}$	0.05	1.54	6.1	3.81	58.1	24.7	26.2
$\text{Pt}_{0.1}^{\wedge}\text{Au/C}$	0.03	0.93	8.2	5.13	130.2	55.4	83.1
$\text{Pt}_{0.05}^{\wedge}\text{Au/C}$	0.02	0.62	9.9	6.15	233.3	99.2	162.5
$\text{Pt}_{0.03}^{\wedge}\text{Au/C}$	0.012	0.37	5.9	3.68	234.1	99.5	161.6

[a] For methanol oxidation, at 0.65 V.



ent chemical properties than larger metallic particles as a result of their strong interaction with the supporting material.<sup>[13–15]</sup> Nevertheless, very small Pt entities ( $\leq 1.0$  nm) supported on Au nanoparticles are still very effective for the electrooxidation of methanol. This activity may be related to the inert nature of the supporting gold surface. Surface-enhanced Raman spectroscopic studies of chemisorptions on ultrathin Pt-group metal films of 2–3 monolayer thickness deposited on Au substrates show that surface chemical properties of the Pt-group metals were not significantly affected by the presence of an underlying Au substrate.<sup>[33,34]</sup> It is also interesting that the very small noble-metal clusters on the Au particles did not react with each other, which may have important implications in understanding the role of the metal in conventional chemical catalysis of particles smaller than 1–2 nm in diameter.

In conclusion, we have demonstrated an approach to enable the most efficient use of Pt in electrocatalysts and to allow every Pt atom to assume the function of a catalytic site for an electrochemical reaction. The approach makes use of Au nanoparticles of about 10 nm in diameter as an immediate support for very small Pt entities with 100 % dispersion. Although the highest dispersion of Pt is realized only with low Pt loadings ( $m \leq 0.05$ ), loadings could be significantly increased by decreasing the size of the supporting Au particles (e.g., 2–5 nm). The effect of changing the size of the Au particles is being investigated and progress will be reported in the near future.

### Experimental Section

The deposition of Pt onto Au nanoparticles was carried out by reducing  $K_2[PtCl_6]$  with hydrogen in a solution containing Au particles (ca. 10.0 nm in diameter) and PVP. Au nanoparticles were prepared according to the methods of Enustun and Turkevich.<sup>[35]</sup> The gold concentration was kept constant at  $1.25 \times 10^{-4}$  mol L<sup>-1</sup> for each preparation, whereas the amount of  $K_2[PtCl_6]$  in the solution was varied to change the overall atomic Pt/Au ratios from 0.02 to 2.0. For comparison, Pt-only nanoparticles were also prepared under the same conditions in the absence of Au nanoparticles, as described in our earlier work.<sup>[36]</sup>

Colloids (Au, Pt, Pt<sub>m</sub>/Au) were supported on high-surface-area Vulcan XC-72 carbon (ca. 250 m<sup>2</sup> g<sup>-1</sup>) by combining a dispersion of the colloids with a suspension of the carbon support in ethanol. The mixture was vigorously stirred for 48 h after sonication (30 min). The powdered product was isolated by filtration, washed extensively with deionized water, and dried at 110 °C for 2 h. Inductively coupled plasma–atomic emission spectroscopy (ICP–AES) showed that the atomic Pt/Au ratios in the final catalysts agreed well with those in the preparation mixtures, thus indicating that Pt deposition from the mixture was complete.

Cyclic voltammetry was performed in 0.5 M H<sub>2</sub>SO<sub>4</sub> with a thermostated three-electrode glass cell at room temperature. The working electrode was prepared by using ultrasound to disperse the catalyst powders in 5 % Nafion solution (Aldrich). The resulting dispersion was spread over PTFE-treated carbon paper (DuPont) and then dried in air. The catalyst loading at the working electrode was 4 mg cm<sup>-2</sup>. A saturated calomel electrode was used as the reference electrode and a Pt foil of 1 × 1 cm<sup>2</sup> was used as the counter electrode.

Before CV measurements were recorded, the electrolyte was purged with nitrogen (99.9 %) for 30 min, and several tens of CV cycles (sweeping rate: 50 mV s<sup>-1</sup>) were performed between –0.24 and 1.0 V to stabilize the electrode surface. Methanol was electrooxidized

in an electrolyte containing 0.5 M H<sub>2</sub>SO<sub>4</sub> and 2 M CH<sub>3</sub>OH in a potential range from –0.20 to 1.0 V at a sweeping rate of 20 mV s<sup>-1</sup>.

Received: January 14, 2006

Revised: April 25, 2006

Published online: June 28, 2006

**Keywords:** cyclic voltammetry · electrochemistry · heterogeneous catalysis · nanostructures · platinum

- [1] R. J. Spiegel, *Transportation Res. Part D* **2004**, *9*, 357.
- [2] L. Carrette, K. A. Friedrich, U. Stimming, *ChemPhysChem* **2000**, *1*, 162.
- [3] R. Dillon, S. Srinivasan, A. S. Aricò, V. Antonucci, *J. Power Sources* **2004**, *127*, 112.
- [4] M. Boudart, G. Djéga-Mariadassou, *Kinetics of Heterogeneous Catalytic Reactions*, Princeton University Press, Princeton, **1984**, chap. 1.
- [5] G. A. Somorjai, *Introduction to Surface Chemistry and Catalysis*, Wiley-Interscience, New York, **1994**, chap. 1.
- [6] H. Bönemann, R. M. Richards, *Eur. J. Inorg. Chem.* **2001**, 2455.
- [7] Z. H. Zhou, S. Wang, W. J. Zhou, G. X. Wang, L. H. Jiang, W. Z. Li, S. Q. Song, J. G. Liu, G. Q. Sun, Q. Xin, *Chem. Commun.* **2003**, 394.
- [8] M. Arenz, J. Karl, K. J. J. Mayrhofer, V. Stamenkovic, B. B. Bliznac, T. Tomoyuki, P. N. Ross, N. M. Markovic, *J. Am. Chem. Soc.* **2005**, *127*, 6819.
- [9] Z. C. Tang, D. S. Geng, G. X. Lu, *J. Colloid Interface Sci.* **2005**, *287*, 159.
- [10] M. L. Anderson, C. A. Morris, R. M. Stroud, C. I. Merzbacher, D. R. Rolison, *Langmuir* **1999**, *15*, 674.
- [11] M. L. Anderson, R. M. Stroud, D. R. Rolison, *Nano Lett.* **2002**, *2*, 235.
- [12] G. Wu, B. Q. Xu, *Electrochem. Commun.* **2005**, *7*, 1237.
- [13] K. Kinoshita, P. Stonehart, *Mod. Aspects Electrochem.* **1977**, *12*, 191.
- [14] Z. Xu, F. S. Xiao, S. K. Purnoll, O. Alexeev, S. Kawl, S. E. Doutsch, B. C. Gates, *Nature*, **1994**, *372*, 346.
- [15] C. R. Henry, *Surf. Sci. Rep.* **1998**, *31*, 235.
- [16] D. B. Laurence, *Gold Bull.* **2004**, *37*, 125.
- [17] A. Henglein, *J. Phys. Chem. B* **2000**, *104*, 2201.
- [18] C. Damle, K. Biswas, M. Sastry, *Langmuir* **2001**, *17*, 7156.
- [19] L. Y. Cao, L. M. Tong, P. Diao, T. Zhu, Z. F. Liu, *Chem. Mater.* **2004**, *16*, 3239.
- [20] G. Schmid in *Nanoscale Materials in Chemistry* (Ed.: K. J. Klabunde), Wiley-Interscience, New York, **2001**, p. 30.
- [21] S. Mandal, A. B. Mandale, M. Sastry, *J. Mater. Chem.* **2004**, *14*, 2868.
- [22] Y. D. Jin, Y. Shen, S. Dong, *J. Phys. Chem. B* **2004**, *108*, 8142.
- [23] This area number was calculated by using the atomic density of a metallic gold surface, which is about 12.7 Au atoms per nm<sup>2</sup>.<sup>[24,25]</sup>
- [24] G. C. Bond, *Catal. Rev. Sci. Eng.* **1999**, *41*, 319.
- [25] D. R. Lide, *CRC Handbook of Chemistry and Physics*, 84th ed., CRC, Boca Raton, **2003**.
- [26] P. Stonehart in *Power Sources: Research and Development in Non-Mechanical Electrical Power Sources*, the 5th International Symposium (Ed.: D. H. Collins), **1966**, p. 514.
- [27] T. R. Ralph, G. A. Hards, J. E. Keating, *J. Electrochem. Soc.* **1997**, *144*, 3845.
- [28] A. Pozio, M. de Francesco, A. Cemmi, F. Cardellini, L. Giorgi, *J. Power Sources* **2002**, *105*, 13.
- [29] This equation is equivalent to the equation frequently used in the electrochemical evaluation of metal catalysts:  $EAS = Q_H / ([Pt]0.21)$ ,<sup>[28]</sup> as  $A_{Pt}/Q_c$  represents the contribution to the EAS associated with a unit charge consumption in electrooxidation of the adsorbed hydrogen atoms.  $Q_c/A_{Pt} = 2.1$  when the units of

charge and surface area are C and m<sup>2</sup>, respectively. The value becomes 0.21 when  $\mu\text{C}$  and cm<sup>2</sup> are used.

- [30] J. Bett, K. Kinoshita, K. Routsis, P. Stonehart, *J. Catal.* **1973**, *29*, 160.
- [31] F. Gloaguen, F. Andolfatto, R. Durand, P. Ozil, *J. Appl. Electrochem.* **1994**, *24*, 861.
- [32] N. P. Lebedeva, G. J. M. Janssen, *Electrochim. Acta* **2005**, *51*, 29.
- [33] S. Z. Zou, C. T. Williams, E. K.-Y. Chen, M. J. Weaver, *J. Phys. Chem. B* **1998**, *102*, 9039.
- [34] M. J. Weaver, *Top. Catal.* **1999**, *8*, 65.
- [35] B. V. Enustun, J. Turkevich, *J. Am. Chem. Soc.* **1963**, *85*, 3318.
- [36] D. Zhao, G. Wu, B. Q. Xu, *Chin. Sci. Bull.* **2005**, *50*, 1846.

## Channels in Micelles

DOI: 10.1002/anie.200600172

### Formation of Complex Micelles with Double-Responsive Channels from Self-Assembly of Two Diblock Copolymers\*\*

Guiying Li, Linqi Shi,\* Rujiang Ma, Yingli An, and Nan Huang

The establishment of an effective method to prepare desirable nanostructures and to eventually convert them into designed architectures is of increasing interest in nanotechnology, chemistry, and biology. Proteins that are located in the phospholipid bilayer of cell membranes are important in forming transient pores or channels to achieve ion transport, ion regulation, energy transduction, signal recognition, and other biological processes. Numerous functional materials, including nanoporous membranes and synthetic transmembrane channels, have been designed based on these important gating structures in order to mimic biological processes.<sup>[1–4]</sup>

It is now well established that amphiphilic block copolymers can self-assemble into lipid-like membranes with tunable channels, which considerably expand on the properties of natural biomembranes.<sup>[5–8]</sup> However, few studies have involved block copolymer micelles with channels. Typical polymeric micelles consist of a compact core formed by the

insoluble blocks of the polymer and a stretched shell formed by the soluble blocks so that the inner core can serve as a nanocontainer for various substances.<sup>[9,10]</sup> Many efforts have been made to broaden the range of potential applications by altering the properties of the core and the shell and to fabricate novel types of micelles with special and controllable structures.<sup>[11–15]</sup> For example, Jiang and co-workers reported core-stabilized polymeric micelles with a mixed shell made from two incompatible copolymers.<sup>[13]</sup> Liu and co-workers prepared water-soluble porous nanospheres from block copolymer micelles and nano- or microspheres bearing small hemispherical bumps with surface-segregated chains.<sup>[14,15]</sup> If the multifunctionality of channels is considered, more advantages would be offered if we combined the properties of polymeric micelles with tunable channels.

Environmental stimuli-responsive polymers are an interesting class of materials since their physical and chemical properties can be adjusted by external stimuli, such as temperature, pH value, and ionic strength; the design of these polymers has been based on lipid-like bilayer membranes.<sup>[16–19]</sup> We present herein a simple and effective method to prepare complex micelles with tunable channels from the self-assembly of two diblock copolymers, namely, poly(*tert*-butyl acrylate)-*b*-poly(*N*-isopropylacrylamide) (PtBA-*b*-PNIPAM) and poly(*tert*-butyl acrylate)-*b*-poly(4-vinylpyridine) (PtBA-*b*-P4VP).

The diblock copolymers PtBA<sub>45</sub>-*b*-PNIPAM<sub>91</sub> (polydispersity index (PDI) = 1.25) and PtBA<sub>60</sub>-*b*-P4VP<sub>80</sub> (PDI = 1.23) were synthesized by atom-transfer radical polymerization (ATRP). Both are molecularly dispersed in *N,N*-dimethylformamide (DMF). With the addition of acidic water (pH 2.5), opalescence appeared, which indicates the occurrence of micellization in the solutions. Since P4VP is protonated and soluble in aqueous solution at low pH values and PNIPAM is soluble at room temperature, the hydrophobic PtBA blocks of the two polymers associate together to form a dense core, protected by the mixed soluble P4VP/PNIPAM blocks acting as a shell. With an increase in temperature or pH value, the core-shell micelles convert into a new type of micelle, where soluble chains stretch out from the core through the now collapsed shell. The formation of the complex micelles is shown in Figure 1.

Dynamic light scattering (DLS) and static light scattering (SLS) are used to measure the scattered light intensity, which can indicate the aggregation of polymers in solution. The

[\*] G. Li, Prof. L. Shi, R. Ma, Y. An, N. Huang  
Key Laboratory of Functional Polymer Materials  
Ministry of Education  
Institute of Polymer Chemistry  
Nankai University  
Tianjin 300071 (P.R. China)  
Fax: (+86) 222-350-3510  
E-mail: shilingqi@nankai.edu.cn

[\*\*] This work is supported by the National Natural Science Foundation of China (grant nos.: 50273015, 20474032, and 23030407) and the Program for New Century Talents in Universities.

Supporting information for this article is available on the WWW under <http://www.angewandte.org> or from the author.

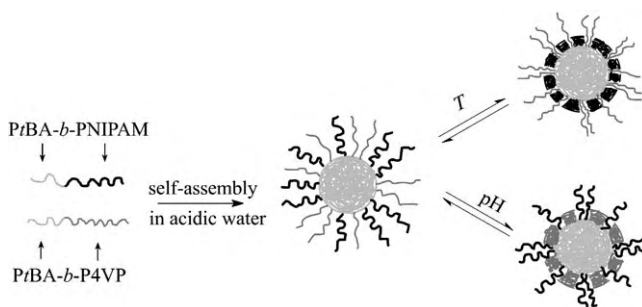


**Figure 1.** Formation of the complex micelles from self-assembly of PtBA<sub>45</sub>-*b*-PNIPAM<sub>91</sub> and PtBA<sub>60</sub>-*b*-P4VP<sub>80</sub>.

diameter distributions of  $\text{PtBA}_{45}\text{-}b\text{-PNIPAM}_{91}$  micelles,  $\text{PtBA}_{60}\text{-}b\text{-P4VP}_{80}$  micelles, and the complex micelles are shown in Figure 2. The average hydrodynamic diameters ( $D_h$ ) of these micelles are 79, 60, and 84 nm, respectively.

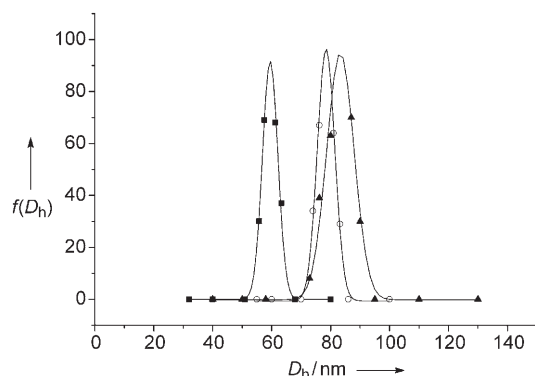


**Figure 2.** The hydrodynamic diameter distribution,  $f(D_h)$ , for  $\text{PtBA}_{45}\text{-}b\text{-PNIPAM}_{91}$  micelles ( $\circ$ ),  $\text{PtBA}_{60}\text{-}b\text{-P4VP}_{80}$  micelles ( $\blacksquare$ ), and the complex micelles ( $\blacktriangle$ ) at pH 2.5 and 25 °C.

Clearly, each of the micelles shows a narrow diameter distribution, while the average diameter of the complex micelles is somewhat larger than either of the two individual micelles.

From the fitted lines of the Berry plots for  $\text{PtBA}_{45}\text{-}b\text{-PNIPAM}_{91}$  micelles,  $\text{PtBA}_{60}\text{-}b\text{-P4VP}_{80}$  micelles, and the complex micelles at pH 2.5 and 25 °C (see the Supporting Information), the radii of gyration ( $R_g$ ) of these micelles are calculated to be 36, 26, and 31 nm, respectively. The  $R_g/R_h$  ( $R_h = 0.5D_h$ ) value can reveal the morphology of particles dispersed in solutions.<sup>[19]</sup> The values of  $R_g/R_h$  for these micelles are 0.91, 0.87, and 0.74, respectively, results suggesting that the micelles are spherical. Moreover, the  $R_g/R_h$  value of the complex micelles is much lower than that of either individual micelle, which indicates that the structure of the complex micelles is more compact.

With increasing temperatures, water progressively becomes a poor solvent for PNIPAM blocks, so the stretched chains collapse from an extended-coil conformation to a shrunken conformation. Figure 3 shows the temperature dependence of the  $R_g$  value during one cycle of the heating-

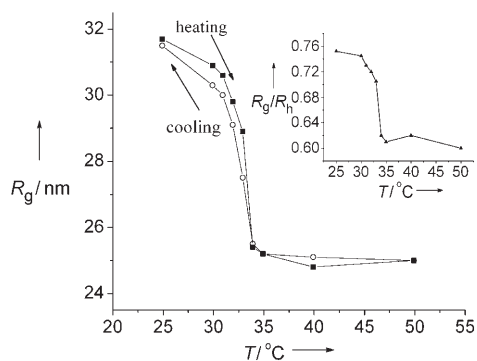


**Figure 3.** Temperature dependence of  $R_g$  (and of  $R_g/R_h$ , inset) for the complex micelles.

and-cooling process when the polymer solution was equilibrated for about two hours at each temperature. The values of  $R_g/R_h$  at different temperatures were also calculated, with results shown in the insert of Figure 3. The decrease of the  $R_g/R_h$  value from 0.74 to 0.60 indicates that the structure of the micelles has changed to a more compact state. The values of  $R_g$  in the cooling process reveal the reversible globule-to-coil transition of the PNIPAM chains, although there is a slight hysteresis as compared to the results of the heating process.

For individual  $\text{PtBA}_{45}\text{-}b\text{-PNIPAM}_{91}$  micelles, large aggregates form when the temperature rises above 33 °C due to the insolubility of both PtBA and PNIPAM. However, the  $D_h$  value for the complex micelles remains nearly constant with increasing temperatures because the hydrophilic P4VP chains can stabilize the micelles at pH 2.5. This result further confirms the formation of complex micelles between  $\text{PtBA}_{45}\text{-}b\text{-PNIPAM}_{91}$  and  $\text{PtBA}_{60}\text{-}b\text{-P4VP}_{80}$ . The values of  $D_h$ ,  $R_g$ , and  $R_g/R_h$  for the complex micelles measured under different temperature conditions are listed in Table 1.

**Table 1:** DLS and SLS data for the complex micelles under different conditions.

Conditions	$D_h$ [nm]	$R_g$ [nm]	$R_g/R_h$
pH 2.5, 25 °C	84	31	0.74
pH 2.5, 50 °C	84	25	0.60
pH 7.8, 25 °C	86	27	0.63

In addition, the stretched P4VP chains collapse due to their deprotonation when the pH value is increased from 2.5 to 7.8 at 25 °C. Individual  $\text{PtBA}_{60}\text{-}b\text{-P4VP}_{80}$  micelles would precipitate at pH 7.8, but the complex micelles remain stable and suspended because the PNIPAM block is still soluble. The values of  $D_h$ ,  $R_g$ , and  $R_g/R_h$  for the complex micelles at pH 7.8 and 25 °C are also listed in Table 1. The remarkable decrease in the  $R_g$  and  $R_g/R_h$  values for the complex micelles at higher pH values reveals the collapse of the P4VP chains.

$^1\text{H}$  NMR spectra recorded in  $\text{D}_2\text{O}$  at different temperatures and pH values were used to further study the thermo- and pH-responsive behavior of the complex micelles. In Figure 4a, peaks a and b, due to the PNIPAM blocks, and peaks c and d, due to the P4VP blocks, are all evident, which means that the two blocks are completely water soluble at pH 2.5 and 25 °C. The proton signals from the PtBA blocks are invisible, which suggests that they form the immobile and nonsolvated micellar core. The disappearance of the PNIPAM signals at 50 °C and the P4VP signals at pH 7.8 indicates the much lower mobility and decreased solubility of PNIPAM chains at 50 °C and P4VP chains at pH 7.8.

The fact that the complex micelles remain stable at high temperatures or pH values makes us believe that the PNIPAM chains and P4VP chains are mixed in the shell. If PNIPAM and P4VP were separately attached to different regions of the core to form Janus micelles, the complex micelles would further associate into much larger aggregates, as shown in Scheme S2 in the Supporting Information.<sup>[20]</sup>

From the above discussion, we conclude that core-shell complex micelles self-assembled from mixtures of  $\text{PtBA}_{45}\text{-}b\text{-}$



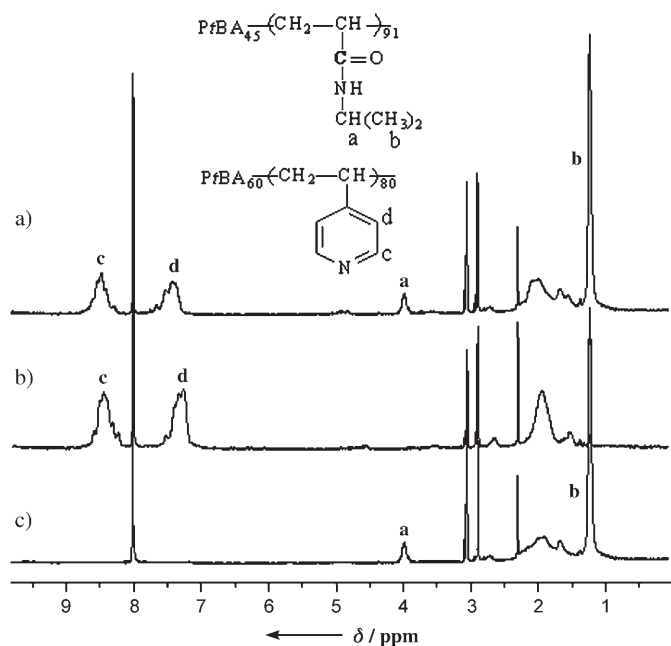


**Figure 4.**  $^1\text{H}$  NMR spectra of the complex micelles at a) pH 2.5 and 25 °C, b) pH 2.5 and 50 °C, and c) pH 7.8 and 25 °C. The peak labels are explained in the text.

PNIPAM<sub>91</sub> and PtBA<sub>60</sub>-*b*-P4VP<sub>80</sub> convert into a new type of micelles with increasing temperature or pH value. The resultant micelles are expected to have a structure with the hydrophobic PtBA blocks as a dense core surrounded by collapsed PNIPAM or P4VP blocks as the shell with soluble P4VP or PNIPAM chains stretching outside as the corona to protect the micelles (see Figure 1).

It should be noted that P4VP and PNIPAM are attached to a common core, which means that hydrophilic P4VP chains or PNIPAM chains are stretching outside from the core through the collapsed shell. Phase separation between the hydrophobic shell and the hydrophilic corona leads to channels in the shell, as shown in Figure 5a. The hydrophilic

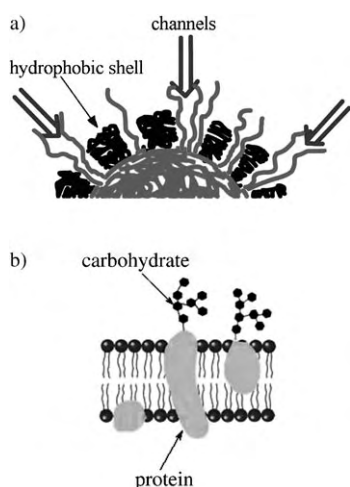


**Figure 5.** Illustration of double-responsive channels self-assembled from a) a complex micelle and b) a typical lipid-like bilayer membrane.

chains are embedded in the hydrophobic shell, just as the channel proteins through which ions and other small molecules can pass are embedded in a lipid-like membrane (Figure 5b). The solubility of the hydrophilic P4VP or PNIPAM chains depends on the pH value, ionic strength, and temperature of the solutions and, as a result, the size of the channels can be regulated by changing the environmental conditions or by manipulating the composition of the two diblock copolymers. Although the functions of the channels in this case are not as perfect as those of the protein channels in cellular membranes, these novel nanostructures may prove to be useful and versatile in applications such as controlled-release devices. A preliminary study on the release of bilirubin from the micelles has been performed, as discussed in the Supporting Information.

In summary, a new type of complex micelles with tunable channels is formed through the self-assembly of a binary mixture of PtBA<sub>45</sub>-*b*-PNIPAM<sub>91</sub> and PtBA<sub>60</sub>-*b*-P4VP<sub>80</sub> diblock copolymers upon increasing the temperature or pH value of the solution. The size and permeability of the channels may be regulated by manipulating the composition of the diblock copolymers or by changing the environmental conditions. These new complex micelles with controllable channels may be promising candidates for use in controlled-uptake/release processes. Detailed studies on the selective permeation of substances into these micelles is in progress.

## Experimental Section

**Preparation of block copolymers:** The macroinitiator PtBA-Cl was prepared by ATRP by using 1-chlorophenylethane (1-PECl) as the initiator and CuCl/*N,N,N',N',N''*-pentamethyl diethylenetriamine (PMDETA) as the catalyst in a solvent mixture of butanone and 2-propanol (7:3 v/v).

Block copolymers of PtBA-*b*-PNIPAM and PtBA-*b*-P4VP were obtained by using PtBA-Cl to initialize the polymerization of NIPAM or 4VP with CuCl/tris[2-(dimethylamino)ethyl]amine (Me<sub>6</sub>TREN) as the catalyst. A typical polymerization procedure for obtaining PtBA-*b*-PNIPAM is as follows: PtBA-Cl (5.0 g) was added to a reaction flask and then the solvent mixture of butanone and 2-propanol (6:4 v/v; 6 mL) was added. Subsequently, CuCl (0.15 g), Me<sub>6</sub>TREN (0.35 g), and NIPAM (10.0 g) were introduced into the flask and degassed with a nitrogen purge. Polymerization was performed at 40 °C for 48 h. The product was purified by passing the mixture through an Al<sub>2</sub>O<sub>3</sub> column and was then deposited in a methanol/water mixture.

The molecular weights and PDI values of PtBA-*b*-PNIPAM and PtBA-*b*-P4VP were determined by a Waters 600E gel permeation chromatography (GPC) analysis system with tetrahydrofuran or CHCl<sub>3</sub> as the eluent and polystyrene as the calibration standard. The composition of the block copolymers was determined in CDCl<sub>3</sub> by use of  $^1\text{H}$  NMR spectroscopy on a Varian UNITYplus 400 MHz NMR spectrometer.

**Preparation of the complex micelles:** PtBA-*b*-PNIPAM and PtBA-*b*-P4VP with a weight ratio of 1:1 were first dissolved in DMF to make a polymer concentration of 0.1 mg mL<sup>-1</sup>. Subsequently, a given volume of acidic water (pH 2.5) was added into the polymer solution with stirring. The formation of micelles occurred, as indicated by the appearance of opalescence in the solution, and then the solution was dialyzed in acidic water for four days to remove the DMF.

DLS and SLS measurements were performed on a laser light scattering spectrometer (BI-200SM) equipped with a digital correla-

tor (BI-10000AT) at 514 nm. All samples were first prepared by filtering solutions (about 1 mL) through a 0.45- $\mu$ m Millipore filter into a clean scintillation vial and were then characterized at the given temperatures.

Received: January 16, 2006

Revised: April 27, 2006

Published online: June 29, 2006

**Keywords:** channels · copolymerization · micelles · self-assembly

- [1] Y. Cheng, R. J. Bushby, S. D. Evans, P. F. Knowles, R. E. Miles, S. D. Ogier, *Langmuir* **2001**, *17*, 1240.
- [2] J. Gao, D. Lee, Y. Yang, S. Holdcroft, B. J. Frisken, *Macromolecules* **2005**, *38*, 5854.
- [3] J. Sánchez-Quesada, M. P. Isler, M. R. Ghadiri, *J. Am. Chem. Soc.* **2002**, *124*, 10004.
- [4] J. Thundimadathil, R. W. Roeske, H.-Y. Jiang, L. Guo, *Biochemistry* **2005**, *44*, 10259.
- [5] J. Grumelard, A. Taubert, W. Meier, *Chem. Commun.* **2004**, 1462.
- [6] G. Srinivas, D. E. Discher, M. L. Klein, *Nano Lett.* **2005**, *5*, 2343.
- [7] J. L. MacCallum, D. P. Tieleman, *J. Am. Chem. Soc.* **2006**, *128*, 125.
- [8] A. M. Brozell, M. A. Muha, B. Sanii, A. N. Parikh, *J. Am. Chem. Soc.* **2006**, *128*, 62.
- [9] a) G. Yu, A. Eisenberg, *Macromolecules* **1998**, *31*, 5546; b) F. Liu, A. Eisenberg, *J. Am. Chem. Soc.* **2003**, *125*, 15059.
- [10] a) J.-F. Gohy, N. Willet, S. Varshney, J.-X. Zhang, R. Jerome, *Angew. Chem.* **2001**, *113*, 3314; *Angew. Chem. Int. Ed.* **2001**, *40*, 3214; b) L. Lei, J.-F. Gohy, N. Willet, S. Varshney, J.-X. Zhang, S. Varshney, R. Jerome, *Macromolecules* **2004**, *37*, 1089.
- [11] S. Kubowicz, J.-F. Baussard, J.-F. Lutz, A. F. Thünemann, H. Berlepsch, A. Laschewsky, *Angew. Chem.* **2005**, *117*, 5397; *Angew. Chem. Int. Ed.* **2005**, *44*, 5262.
- [12] S. Liu, J. V. M. Weaver, Y. Tang, N. C. Billingham, S. P. Armes, *Macromolecules* **2002**, *35*, 6121.
- [13] T. Hui, D. Chen, M. Jiang, *Macromolecules* **2005**, *38*, 5834.
- [14] a) F. Henselwood, G. Liu, *Macromolecules* **1998**, *31*, 4213; b) J. Zhou, Z. Li, G. Liu, *Macromolecules* **2002**, *35*, 3690.
- [15] a) R. Zheng, G. Liu, X. Yan, *J. Am. Chem. Soc.* **2005**, *127*, 15358; b) J. Hu, G. Liu, *Macromolecules* **2005**, *38*, 8058.
- [16] a) C. M. Schilli, M. Zhang, E. Rizzardo, S. H. Thang, Y. K. Chong, K. Edwards, G. Karlsson, A. H. E. Müller, *Macromolecules* **2004**, *37*, 7861; b) X. Andre, M. Zhang, A. H. E. Müller, *Macromol. Rapid Commun.* **2005**, *26*, 558.
- [17] S. Liu, N. C. Billingham, S. P. Armes, *Angew. Chem.* **2001**, *113*, 2390; *Angew. Chem. Int. Ed.* **2001**, *40*, 2328.
- [18] Y. S. Park, Y. Ito, Y. Imanishi, *Langmuir* **1998**, *14*, 910.
- [19] Y. Tu, X. Wan, D. Zhang, Q. Zhou, C. Wu, *J. Am. Chem. Soc.* **2000**, *122*, 10201.
- [20] a) R. Erhardt, A. Böker, H. Zettl, H. Kaya, W. Pyckhout-Hintzen, G. Krausch, V. Abetz, A. H. E. Müller, *Macromolecules* **2001**, *34*, 1069; b) R. Erhardt, M. F. Zhang, A. Böker, H. Zettl, C. Abetz, P. Frederik, G. Krausch, V. Abetz, A. H. E. Müller, *J. Am. Chem. Soc.* **2003**, *125*, 3260.

DOI: 10.1002/anie.200600290

**Ionothermal Materials Synthesis Using Unstable Deep-Eutectic Solvents as Template-Delivery Agents\*\****Emily R. Parnham, Ewan A. Drylie, Paul S. Wheatley, Alexandra M. Z. Slawin, and Russell E. Morris\**

The use of organic templates (also called structure-directing agents) remains one of the most successful methods of preparing new inorganic materials.<sup>[1,2]</sup> Many of the most important recent advances in porous solids in particular depend on the clever use of organic species as templates to produce new zeolites,<sup>[3–5]</sup> transition-metal phosphates<sup>[6]</sup> or oxides,<sup>[7]</sup> and to make synthetic methods more efficient.<sup>[8]</sup> Ionothermal synthesis, where an ionic liquid is both the solvent and source of the template, provides opportunities to develop new synthetic routes that are based on different chemistry to traditional hydrothermal approaches.<sup>[9–12]</sup> Herein we describe the controlled use of deep-eutectic solvents (DESs) that are unstable at high temperatures as the media for ionothermal reactions. The organic template is not added to the reaction mixture in the normal way, but is delivered to the reaction by the breakdown of one of the components of the DES itself, demonstrating how the unique solvent properties of these ionic liquids can be harnessed to produce new types of solid.

A DES is a mixture of two compounds where there is a depression in the freezing point of the mixture compared with that of the separate components. One class of DES comprises mixtures of organic halide salts with hydrogen-bond donors, such as amides, amines, alcohols, and carboxylic acids.<sup>[13,14]</sup> The freezing-point depression in the mixture results from the formation of halide ion–hydrogen-bond-donor supramolecular complexes that alter the free energy of the solid phase compared to the liquid. DESs are therefore predominantly ionic liquids, with properties that differ markedly from those of molecular liquids and salts dissolved in molecular solvents. Such DESs have features that make them excellent choices

[\*] E. R. Parnham, E. A. Drylie, P. S. Wheatley, Prof. A. M. Z. Slawin, Prof. R. E. Morris  
EaStChem School of Chemistry  
University of St Andrews  
Purdie Building, St Andrews KY169ST (UK)  
Fax: (+44) 1334-463808  
E-mail: rem1@st-and.ac.uk

[\*\*] The authors thank Prof. George Ferguson and Dr. Philip Wormald of the University of St Andrews for interesting discussions and R.E.M. thanks the Royal Society for the provision of a University Research Fellowship. We thank the CCLRC and John Warren for access to the Synchrotron Radiation Source (Daresbury) and the EPSRC and David Apperley for access to solid-state NMR spectroscopy.



Supporting information for this article (full experimental details) is available on the WWW under <http://www.angewandte.org> or from the author.

for use in the preparation of materials of different kinds. Their ionic nature and relatively high polarity mean that many ionic species, such as metal salts, show high solubility. They also have some significant advantages over other types of ionic liquid, particularly their ease of preparation as pure phases from easily available (and toxicologically well characterized) components and their relative unreactivity towards atmospheric moisture.<sup>[14]</sup> Our previous report on zeolite synthesis used a urea/choline chloride eutectic to prepare a new zeolitic material<sup>[9]</sup> and Liao and co-workers have used the same method to prepare a new organophosphate material.<sup>[15]</sup> Herein we report how thermal decomposition of various urea derivatives as components in DES can be used to deliver particular organic templates to the reaction mixture in a controlled manner, leading to new types of structure and providing some insight into potential synthesis mechanisms of such materials.

Several urea derivatives (structural formula in Figure 1 and 2), including 1,3-dimethyl urea (DMU), 2-imidazolidone (IMI, ethylene urea) and tetrahydro-2-pyrimidione (THP, *N,N*-trimethylene urea) were investigated as eutectic mixtures with quaternary ammonium halides (choline chloride or tetraethylammonium bromide). IMI and THP are, we believe, used for the first time in deep-eutectic solvents. The expected decomposition products, and thus the expected templates delivered to the synthesis, of DMU, IMI, and THP are methylamine, ethylene diamine, and propylene diamine, respectively.

Aluminum phosphate materials can be prepared using all three urea derivatives, (Figure 1 and 2). Single-crystal X-ray diffraction, magic-angle spinning (MAS) NMR spectroscopy and elemental analysis indicate that the expected templates were occluded in the final solids (see Supporting Information). The materials vary from one-dimensional chains through to three-dimensional zeolitic-type structures and can be altered by adding suitable mineralizers, such as water or fluoride, to the systems. The dependence of final structure on mineralizer content mirrors the behavior seen in other ionothermal systems<sup>[9]</sup> and illustrates the rich potential of this system to produce different materials in a controlled manner. However, one difference between this system and other ionothermal methods is that templated materials are formed right across the range of water content from very low to very high. We have not seen any evidence for templating being stopped by intermediate water content, as is the case for imidazolium-based ionic liquids.<sup>[9]</sup>

A DMU/tetraethylammonium bromide DES can be used to prepare three different aluminophosphate solids, **1**, **2**, and **3** (Figure 1). A DMU/choline chloride DES can also be used to prepare **2**. In each case the template is the methylammonium cation as expected.

A DES containing the cyclic urea derivative IMI yields ethylene diammonium cations as the template at moderate temperatures, plus some ammonium cations above 200 °C. This approach produces two closely related aluminophosphate solids **4** and **5** (Figure 2). Using a DES with one extra carbon center in the cyclic urea component (TMP, Figure 2) leads to the crystallization of four different solids. Three of these materials, **6–8** have the expected propylene diammo-

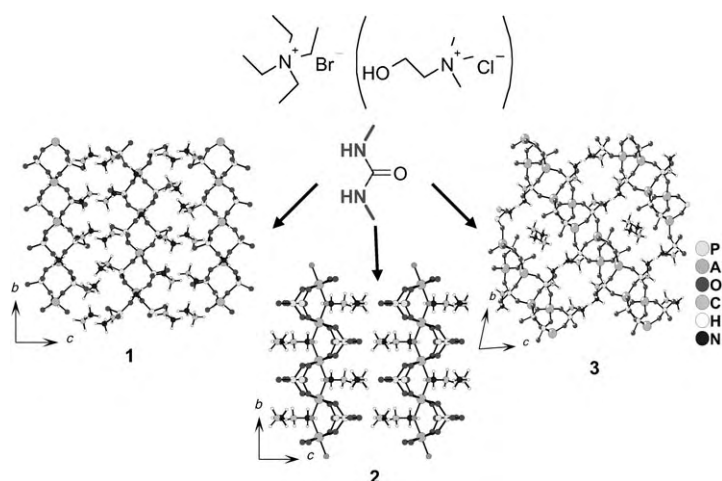


**Figure 1.** The synthesis of materials using dimethyl urea based eutectic mixtures. Dimethyl urea based eutectic mixtures with tetraethylammonium bromide or choline chloride decompose to give methylammonium cations as the templates for the preparation of three aluminophosphate materials, **1–3**. The portion of the urea derivative that delivers the template on decomposition is shown in bold in the structural formula. The conditions for the reactions are given in the Supporting Information.

nium template. However, if a large excess of water is added to the system, breakdown of the urea derivative proceeds further at temperatures of 200 °C to produce a material **9** that has only ammonium as the templating cation.

The nine aluminophosphate materials prepared in this way include five previously unknown compounds, although some related topologies are known, and four known materials, **3**, **4**, **7**, and **9**. Full details of the synthesis and crystallography of these materials can be found in the Supporting Information.

Interestingly, the different structures fit rather well with some proposed mechanistic pathways postulated in previous work. Oliver et al.<sup>[16]</sup> proposed that the crystallization of aluminophosphates proceeds through the initial formation of chains. Vidal and co-workers postulated exactly such a mechanism for the synthesis of Mu-7<sup>[17]</sup> by the hydrolytic condensation of so called parent chains. However, there was no evidence for the existence of the parent chain in any experiments Vidal and co-workers carried out. In our work, compound **3** (Figure 1) has the same structure as Mu-7 and compound **1** has the structure of the parent chain, which is isolated at lower temperatures. The reason given for the non-detection of the parent chain by Vidal was that the parent chain was “probably very labile”.<sup>[17]</sup> That the parent compound can be isolated using the eutectic mixture indicates rather milder hydrolysis conditions than in the hydrothermal or solvothermal synthesis. This situation suggests that synthesis in DES may be more controllable than other synthetic methods and perhaps more compounds that are not isolable under normal conditions can be recovered. Other workers have postulated different mechanisms of framework synthesis, in particular those based on crystal growth by condensation of small clusters rather than by condensation of chains or layers as proposed by Oliver et al. Indeed, Férey, Taulelle, and co-workers have shown from very elegant in situ



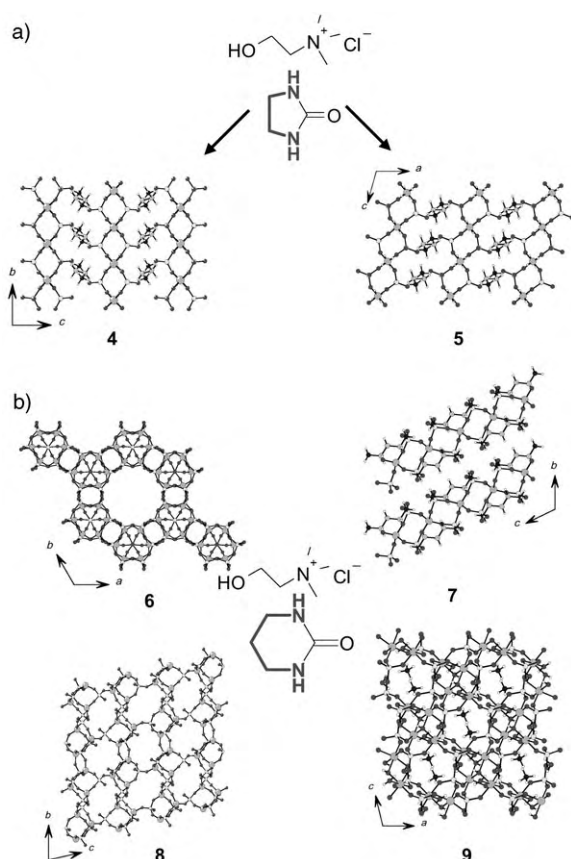


**Figure 2.** The synthesis of aluminophosphate materials from cyclic urea-based eutectic mixtures. a) Materials prepared from 2-imidazolin-dione-based eutectics templated by ethylene diammonium cations b) Four materials prepared from tetrahydro-2-pyrimidone. In compounds **6–8** the template is a propylene diammonium cation while in compound **9**, prepared at higher temperature, the template is ammonium. For clarity the location of the templates in **6** and **8** are not shown. The key is as for Figure 1 The portion of the urea derivative that delivers the template on decomposition is shown in bold in the structural formula. The Conditions for the reactions are given in the Supporting Information.

NMR spectroscopy in real time that the mechanism proposed by Oliver et al. is certainly not possible in all cases.<sup>[18]</sup> The isolation of the parent chain in our work is not evidence of the mechanistic pathway (since we only characterize the final products) but does raise some interesting points that may require further work.

Time studies using X-ray diffraction indicate that the crystallinity of the products reaches its maximum between 12 and 48 h after the reactions started, with overall yields of 50–70% after 48 h (see Supporting Information). Interestingly, <sup>1</sup>H NMR spectra of the DESs recovered after the reactions show that at 12 h the breakdown products are only just visible above background. However, after six days the DESs show quite complex <sup>1</sup>H NMR spectra indicating extensive degradation of the solvent systems. Clearly the nucleation and crystallization of the materials takes place at relatively low levels of solvent degradation under conditions where the concentration of the template species is slowly increasing as more of the DES decomposes.

While aluminophosphates are of special interest because of their close relationship to zeolites, other materials are also attractive targets for various reasons. Using a DES we have successfully synthesized **10**, the gallium phosphate version of the zeolite-A framework (Figure 3). Zeolite-A is an impor-

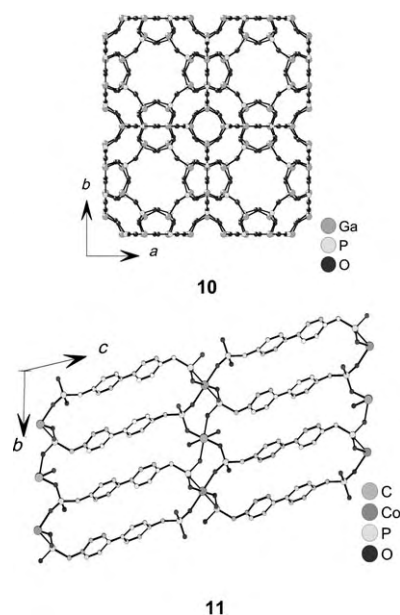


**Figure 3.** Phosphate and phosphonate and metal-organic solids prepared from eutectic mixture or related systems. Compound **10** is a gallium phosphate with the zeolite-A framework, and **11** is a cobalt organophosphonate material prepared from a chlorine chloride/succinic acid DES.

tant industrially used framework with emerging applications in, for example, gas storage for medical applications.<sup>[19]</sup> This material was prepared using a fluoride-free synthetic route, and is unusual in that it is, we believe, the first time this material has been prepared without fluoride at the center of the double four-ring secondary building units (SBUs) present in the structure.<sup>[20,21]</sup> We believe the only previous double four-ring unit occluding an atom other than fluorine are not linked into three-dimensional structures but are isolated anions.<sup>[22,23]</sup>

Carboxylic acid/quaternary ammonium eutectic mixtures seem to be more stable and do not contribute decomposition products as templates to the reactions. Using this approach a succinic acid/choline chloride DES can be used simply as a solvent to prepare the new transition-metal dibenzylidiphosphonate solid **11** (Figure 3) that contains no template. Such inorganic hybrid materials are of particular interest for their structural architectures<sup>[24–28]</sup> and potentially useful gas-adsorption characteristics.<sup>[29]</sup> Liao et al.<sup>[15]</sup> have recently shown that a choline chloride/urea mixture can be used to prepare a zinc organophosphate where ammonium acts as the template. Our work herein shows that we can control whether or not templating takes place by judicious choice of the eutectic solvent.

The use of deep-eutectic mixtures reported herein allows the ionic nature of the liquid, with the advantages this brings

in terms of solvent chemistry and control of mineralizer concentration to be retained while also providing a new mechanism by which the template is delivered to the reaction mixture. The synthesis technique has proved to be very versatile, delivering a number of different templates to aid in the preparation of a number of types of material. Several hundred functionalized ureas are commercially available and many of these will be suitable for this type of work, illustrating the scope of this method. The ease of preparation of eutectic mixtures and the different chemistry involved, as evidenced by, for example the non-fluoride preparation of gallium phosphate zeolite-A, indicate that this route may be useful for targeting materials that are difficult to prepare in traditional hydrothermal synthesis. This work also shows beyond doubt that the template comes from the urea part of the DES, as this is the only way in which the chemical structure of the templates can be explained. In work based on urea/choline chloride mixture there was the possibility that the ammonium ions could originate from the urea or the choline chloride. Thus this issue is now resolved. Further work aimed at preparing other types of material are currently underway to explore more fully the potential of this synthesis method.

## Experimental Section

**Synthesis of DESs:** The required amount of as bought amide and quaternary ammonium salt was measured out in a 2:1 ratio (or 1:1 in the case of the succinic acid based DES) and ground in a mortar. Melting points of the different DES are given in Table 1.

**Table 1:** Melting points of the deep-eutectic solvents and their constituent compounds.

H-bond donor (m.p. [°C])	Ammonium salt (m.p. [°C])	DES m.p. [°C]
1,3-dimethyl urea (101–105)	tetraethylammonium bromide (285–290)	20–25
1,3-dimethyl urea (101–105)	choline chloride (298–305)	69–71
tetrahydro-2-pyrimidione (264–266)	choline chloride (298–305)	150–155
2-imidazolidone (129–132)	choline chloride (298–305)	69–73
urea (134)	choline chloride (298–305)	12
succinic acid (183–187)	choline chloride (298–305)	73–77

**Aluminophosphates 1–9:** A Teflon-lined autoclave (volume 23 mL) was charged with eutectic mixture,  $\text{Al}[\text{OCH}(\text{CH}_3)_2]_3$  (Aldrich), and  $\text{H}_3\text{PO}_4$  (85 wt % in  $\text{H}_2\text{O}$ , Aldrich). HF (48 wt % in  $\text{H}_2\text{O}$ , Aldrich) and distilled water were added if required. The stainless steel autoclave was then heated in an oven to the required temperature. The reagent masses, temperatures, and length of time left in oven are as detailed in the Supporting Information. After cooling the autoclave to room temperature the product was suspended in distilled water, sonicated, filtered by suction, and washed with acetone. The products were white, crystalline solids.

**Gallium phosphate zeolite-A 10:** The method was followed as for the aluminophosphates but the  $\text{Al}[\text{OCH}(\text{CH}_3)_2]_3$  was replaced by  $\text{Ga}_2(\text{SO}_4)_3$  (0.105 g, Aldrich). Tetrahydro-2-pyrimidione (2.0 g, 0.020 mol, Fluka)/Choline Chloride (1.4 g, 0.010 mol, Avocado)

constituted the DES.  $\text{H}_3\text{PO}_4$  (0.173 g, 85 wt % in  $\text{H}_2\text{O}$ ), molar ratio of  $\text{Ga}_2(\text{SO}_4)_3\text{:H}_3\text{PO}_4$  was 1:6.1. The reaction was heated at 170 °C for 72 h.

**11:** A Teflon-lined autoclave (23 mL) was charged with the urea/choline chloride eutectic mixture (4 g), (4,4'-biphenylenedimethylene)diphosphonic acid (0.12 g,  $3.51 \times 10^{-4}$  mol) and cobalt acetate tetrahydrate (0.22 g,  $8.83 \times 10^{-4}$  mol). The autoclave was heated at 150 °C for three days. After cooling to room temperature the eutectic mixture was dissolved in distilled water and the resultant powder recovered by filtration, washed with distilled water and acetone then air dried. An isostructural material using nickel as the metal salt (nickel acetate tetrahydrate (0.23 g,  $9.24 \times 10^{-4}$  mol) can be prepared in a similar way using a 1:1 molar DES of succinic acid and choline chloride.

Single-crystal X-ray diffraction data for all materials except **3** were collected using  $\text{MoK}_\alpha$  radiation using a Rigaku rotating anode single-crystal X-ray diffractometer at the university of St Andrews or using a wavelength of  $\approx 0.7 \text{ \AA}$  station 9.8 at the Synchrotron Radiation Source (SRS), Daresbury Laboratories, Cheshire, UK. The structures were solved using standard direct methods and refined using least-squares minimization techniques against  $F^2$ . When ordered template molecules could not be refined the program SQUEEZE was used to remove the scattering from the channels/voids in the structures before the final cycle of least-squares refinement. Framework phase identification for **3** (which has the Mu-7 structure) was accomplished from the unit cell given by single crystal X-ray diffraction. Further details on the crystal structure investigation may be obtained from the Fachinformationszentrum Karlsruhe, 76344 Eggenstein-Leopoldshafen, Germany (fax: (+49) 7247-808-666; e-mail: crysdata@fiz-karlsruhe.de), on quoting the depository numbers CSD-416132 (**10**), CSD-416133 (**1**), CSD-416134 (**2**), CSD-416135 (**6**), and CSD-416132 (**9**). CCDC-295436, CCDC-295437, CCDC-295438, CCDC-295439 and CCDC-295440 contain the supplementary crystallographic data for this paper. These data can be obtained free of charge from The Cambridge Crystallographic Data Centre via [www.ccdc.cam.ac.uk/data\\_request/cif](http://www.ccdc.cam.ac.uk/data_request/cif).

Received: January 23, 2006  
Published online: July 3, 2006

**Keywords:** eutectic mixtures · ionic liquids · ionothermal synthesis · synthetic methods · zeolite analogues

- [1] M. E. Davis, *Nature* **2002**, *417*, 813.
- [2] C. S. Cundy, P. A. Cox, *Chem. Rev.* **2003**, *103*, 663.
- [3] A. Corma, M. Díaz-Cabañas, J. Martínez-Triguero, F. Rey, J. Rius, *Nature* **2002**, *418*, 514.
- [4] C. C. Freyhardt, M. Tsapatsis, R. F. Lobo, K. J. Balkus, M. E. Davis, *Nature* **1996**, *381*, 295.
- [5] A. Corma, F. Rey, J. A. Rius, M. J. Sabater, S. Valencia, *Nature* **2004**, *431*, 287.
- [6] P. Feng, X. Bu, G. D. Stucky, *Nature* **1997**, *388*, 735.
- [7] T. Sun, J. Y. Ying, *Nature* **1997**, *389*, 704.
- [8] H. Lee, S. I. Zones, M. E. Davis, *Nature* **2003**, *425*, 385.
- [9] E. R. Cooper, C. D. Andrews, P. S. Wheatley, P. B. Webb, P. Wormald, R. E. Morris, *Nature* **2004**, *430*, 1012.
- [10] E. R. Parnham, P. S. Wheatley, R. E. Morris, *Chem. Commun.* **2006**, 380.

- [11] E. R. Parnham, R. E. Morris, *J. Am. Chem. Soc.* **2006**, *128*, 2204.
- [12] Z. Lin, D. S. Wragg, R. E. Morris, *Chem. Commun.* **2006**, 2021.
- [13] A. P. Abbott, G. Capper, D. L. Davies, R. K. Rasheed, V. Tambyrajah, *Chem. Commun.* **2003**, 70.
- [14] A. P. Abbott, D. Boothby, G. Capper, D. L. Davies, R. K. Rasheed, *J. Am. Chem. Soc.* **2004**, *126*, 9142.
- [15] J. H. Liao, P. C. Wu, Y. H. Bai, *Inorg. Chem. Commun.* **2005**, *8*, 390.
- [16] S. Oliver, A. Kuperman, G. A. Ozin, *Angew. Chem.* **1998**, *110*, 48; *Angew. Chem. Int. Ed.* **1998**, *37*, 46.
- [17] L. Vidal, C. Marichal, V. Gramlich, J. Patarin, Z. Gabelica, *Chem. Mater.* **1999**, *11*, 2728.
- [18] F. Taulelle, M. Pruski, J. P. Amoureux, D. Lang, A. Bailly, C. Huguenard, M. Haouas, C. Gerardin, T. Loiseau, G. Férey, *J. Am. Chem. Soc.* **1999**, *121*, 12148.
- [19] P. S. Wheatley, A. R. Butler, M. S. Crane, S. Fox, B. Xiao, A. G. Rossi, I. L. Megson, R. E. Morris, *J. Am. Chem. Soc.* **2006**, *128*, 502.
- [20] A. Simmen, J. Patarin, C. H. Baerlocher, *Proc. 9th Int. Zeolite Conf.* **1993**, p. 433.
- [21] A. Matijasic, J. L. Paillaud, J. Patarin, *J. Mater. Chem.* **2000**, *10*, 1345.
- [22] D. S. Wragg, R. E. Morris, *J. Am. Chem. Soc.* **2000**, *122*, 11246.
- [23] D. S. Wragg, A. M. Z. Slawin, R. E. Morris, *J. Mater. Chem.* **2001**, *11*, 1850.
- [24] G. B. Hix, V. J. Carter, D. S. Wragg, R. E. Morris, P. A. Wright, *J. Mater. Chem.* **1999**, *9*, 179.
- [25] G. B. Hix, D. S. Wragg, P. A. Wright, R. E. Morris, *J. Chem. Soc. Dalton Trans.* **1998**, 3359.
- [26] V. J. Carter, P. A. Wright, J. D. Gale, R. E. Morris, E. Sastre, J. Perez-Pariente, *J. Mater. Chem.* **1997**, *7*, 2287.
- [27] K. Maeda, Y. Kiyozumi, F. Mizukami, *Angew. Chem.* **1994**, *106*, 2427; *Angew. Chem. Int. Ed. Engl.* **1994**, *33*, 2335.
- [28] K. Maeda, J. Akimoto, Y. Kiyozumi, F. Mizukami, *Angew. Chem.* **1995**, *107*, 1313; *Angew. Chem. Int. Ed. Engl.* **1995**, *34*, 1199.
- [29] K. Maeda, *Microporous Mesoporous Mater.* **2004**, *73*, 47.

---

DOI: 10.1002/anie.200600370

**Organocatalytic Asymmetric Conjugate Addition of 1,3-Dicarbonyl Compounds to Maleimides\*\***

Giuseppe Bartoli,\* Marcella Bosco, Armando Carlone, Andrea Cavalli, Manuela Locatelli, Andrea Mazzanti, Paolo Ricci, Letizia Sambri, and Paolo Melchiorre\*

*Dedicated to Professor Achille Umani-Ronchi on the occasion of his 70th birthday*

The enantioselective construction of quaternary stereogenic centers bonded to four carbon atoms by efficient asymmetric methods is a great synthetic challenge, as the creation of such complex fragments is complicated by steric factors.<sup>[1]</sup> Currently, despite the substantial progress that has been made in the last few years, only a few catalytic asymmetric C–C bond-forming strategies have proven to be useful for forming quaternary carbon centers.<sup>[2]</sup> Among them, the catalytic conjugate addition<sup>[3]</sup> of compounds with a prochiral trisubstituted nucleophilic carbon atom to  $\beta$ -substituted Michael acceptors constitutes an effective approach for the asymmetric construction of highly functionalized products with adjacent quaternary and tertiary carbon centers. The stereocontrolled, one-step synthesis of such important congested motifs from simple precursors is a formidable synthetic challenge, as the catalyst must provide high levels of stereoselectivity in a sterically demanding C–C bond-forming process.<sup>[4]</sup> To date, the acceptors employed in this powerful type of strategy have been enones,<sup>[5]</sup> nitroalkenes,<sup>[6]</sup> and unsaturated imides.<sup>[7]</sup> Expansion of the scope of such an efficient strategy to other classes of Michael acceptors is a useful and challenging objective.

Herein, we report the development of the first asymmetric direct conjugate addition of 1,3-dicarbonyl compounds to

[\*] Prof. G. Bartoli, Prof. M. Bosco, Dr. A. Carlone, Dr. M. Locatelli, Dr. A. Mazzanti, P. Ricci, Dr. L. Sambri, Dr. P. Melchiorre  
Dipartimento di Chimica Organica "A. Mangini"  
Alma Mater Studiorum-Università di Bologna  
Viale Risorgimento, 4, 40136 Bologna (Italy)  
Fax: (+39) 051-209-3654  
E-mail: giuseppe.bartoli@unibo.it  
pm@ms.fci.unibo.it

Dr. A. Cavalli  
Dipartimento di Scienze Farmaceutiche  
Alma Mater Studiorum-Università di Bologna  
Via Belmeloro, 6, 40126 Bologna (Italy)

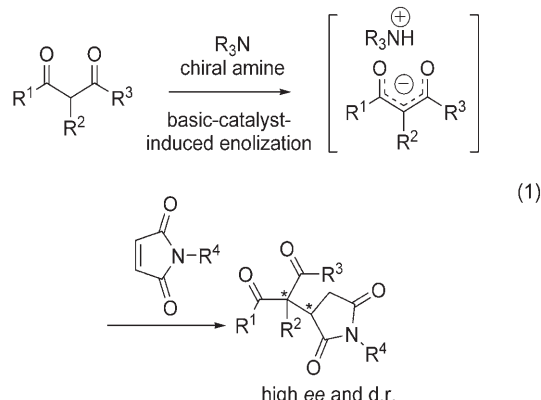
[\*\*] This research was carried out within the framework of the National Project "Stereoselezione in Sintesi Organica. Metodologie e Applicazioni" with the financial support of the MIUR (Rome) and the FIRB National Project "Progettazione, preparazione e valutazione biologica e farmacologica di nuove molecole organiche quali potenziali farmaci innovativi".



Supporting information for this article is available on the WWW under <http://www.angewandte.org> or from the author.



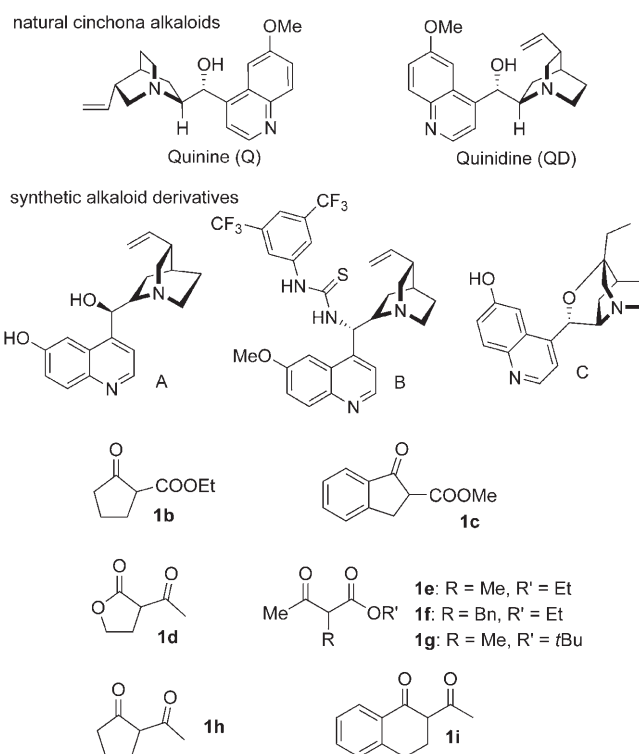
maleimides promoted by natural cinchona alkaloids as chiral-base catalysts.<sup>[8]</sup> The reaction affords highly functionalized products with two adjacent stereogenic carbon atoms, one of which is quaternary with only carbon-centered substituents [Eq. (1)]. This organocatalytic<sup>[9]</sup> approach affords high levels



of both enantio- (up to 98% *ee*) and diastereoselectivity (d.r. = up to > 98:2) with both cyclic and acyclic  $\beta$ -ketoesters and with cyclic  $\beta$ -diketones. Furthermore, the strategy is based on an operationally simple procedure in which unmodified cheap and commercially available starting materials and catalysts are used.

The asymmetric conjugate addition of carbon-centered nucleophiles to maleimides should provide a practical route to synthetically and biologically important chiral  $\alpha$ -substituted succinimides.<sup>[10]</sup> Therefore, it is surprising that, to our knowledge, just one effective asymmetric strategy has been described to date.<sup>[11]</sup> The feasibility of our organocatalytic asymmetric approach was first tested by mixing methyl-2-oxo-1-indanecarboxylate (**1a**) and maleimide (**2a**) in dichloromethane (0.5 M) in the presence of a catalytic amount of a cinchona alkaloid derivative (10 mol %); representative results of the extensive screen of reaction conditions using the alkaloids shown in Scheme 1 are listed in Table 1. The natural cinchona alkaloid quinine (Q) proved to be the most promising catalyst and afforded the 1,4-adduct with relatively good diastereo- and enantioselectivity (Table 1, entry 2). The synthetic cinchona alkaloid derivatives A and B, which are broadly effective bifunctional organocatalysts for several asymmetric C–C bond-forming reactions,<sup>[12]</sup> gave poor results (Table 1, entries 3 and 4). The rigid phenolic quinidine derivative  $\beta$ -isocupreidine (C; Scheme 1)<sup>[13]</sup> promoted the conjugate addition with satisfactory selectivity (Table 1, entry 5), but the results obtained when the reaction was performed at  $-20^{\circ}\text{C}$  indicated a significant difference between Q and C in terms of catalytic activity (Table 1, entries 6/7 and 8/9).

Next, we identified the nature of the substituent on the N atom of the maleimide as a critical parameter for the stereochemical outcome of the process (Table 1, entries 8, 10, and 11). The presence of a benzyl substituent had a dramatic impact on the enantioselectivity and, more importantly, on the diastereoselectivity: When the quinine-catalyzed reaction



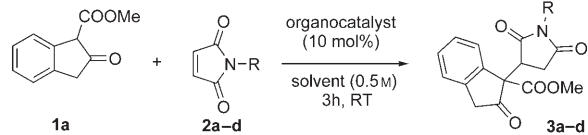
**Scheme 1.** Alkaloid catalysts and 1,3-dicarbonyl compounds **1b–1i** used in this study.

was performed at  $-20^{\circ}\text{C}$  in  $\text{CH}_2\text{Cl}_2$ , the product was isolated after 24 h in quantitative yield, with considerable preference shown for one of the two possible diastereomers (d.r. = 94:6) and with high enantioselectivity (92% *ee*; Table 1, entry 11). Importantly, the use of “pseudoenantiomeric” quinidine (QD) allowed access to the opposite enantiomer of the 1,4-adduct with similar selectivity (Table 1, entry 12). Further optimization of the reaction conditions revealed that apolar solvents favored optimal stereoselectivity (Table 1, entries 11–14);  $\text{CH}_2\text{Cl}_2$  was selected as the solvent of choice for its ability to increase reactivity. The use of hydrogen-bond-accepting solvents led to a drastic decrease in stereoselectivity (Table 1, entries 15 and 16).

The result obtained by using benzoylquinine (BQ) as the catalyst (Table 1, entry 17) clearly demonstrated that the presence of the free hydroxy group on Q is essential for high levels of reactivity and selectivity. This experimental evidence, together with preliminary kinetic studies, which established a first-order rate dependence on the catalyst, nucleophile, and electrophile for the conjugate addition (see the Supporting Information for details), is consistent with an acid–base bifunctional mode of catalysis by quinine. Importantly, although the double-activation ability of natural cinchona alkaloids was established 25 years ago by the seminal studies of Hiemstra and Wynberg,<sup>[14]</sup> there have been no previous reports of a very stereoselective (> 90% *ee*) conjugate addition reaction catalyzed by these compounds.<sup>[15]</sup>

We then examined the generality of this new organocatalytic asymmetric strategy under the optimized reaction conditions. Experiments that probe the range of possible 1,3-

**Table 1:** Screening of reaction conditions for the organocatalytic asymmetric conjugate addition of **1a** to maleimides **2**.<sup>[a]</sup>



Entry	Catalyst	R	Solvent	Conversion [%] <sup>[b]</sup>	<b>3</b>	d.r. <sup>[b]</sup>	ee [%] <sup>[c]</sup>
1	–	H ( <b>2a</b> )	CH <sub>2</sub> Cl <sub>2</sub>	0	<b>a</b>	–	–
2	Q	H ( <b>2a</b> )	CH <sub>2</sub> Cl <sub>2</sub>	> 95	<b>a</b>	74:26	69/28
3	A	H ( <b>2a</b> )	CH <sub>2</sub> Cl <sub>2</sub>	30	<b>a</b>	77:23	14/17
4	B	H ( <b>2a</b> )	CH <sub>2</sub> Cl <sub>2</sub>	65	<b>a</b>	75:25	33/34 <sup>[d]</sup>
5	C	H ( <b>2a</b> )	CH <sub>2</sub> Cl <sub>2</sub>	75	<b>a</b>	65:35	62/45
6 <sup>[e]</sup>	Q	H ( <b>2a</b> )	CH <sub>2</sub> Cl <sub>2</sub>	75	<b>a</b>	82:18	81/70
7 <sup>[e]</sup>	C	H ( <b>2a</b> )	CH <sub>2</sub> Cl <sub>2</sub>	25	<b>a</b>	75:25	74/–
8 <sup>[e]</sup>	Q	Ph ( <b>2b</b> )	CH <sub>2</sub> Cl <sub>2</sub>	> 95	<b>b</b>	87:13	63/40
9 <sup>[e]</sup>	C	Ph ( <b>2b</b> )	CH <sub>2</sub> Cl <sub>2</sub>	13	<b>b</b>	70:30	–/–
10 <sup>[e]</sup>	Q	<i>t</i> Bu ( <b>2c</b> )	CH <sub>2</sub> Cl <sub>2</sub>	15	<b>c</b>	95:5	–/–
11 <sup>[e]</sup>	Q	Bn ( <b>2d</b> )	CH <sub>2</sub> Cl <sub>2</sub>	> 95 (97) <sup>[f]</sup>	<b>d</b>	94:6	92/5
12 <sup>[e]</sup>	QD	Bn ( <b>2d</b> )	CH <sub>2</sub> Cl <sub>2</sub>	> 95 (95) <sup>[f]</sup>	<b>d</b>	94:6	87/4 <sup>[d]</sup>
13 <sup>[e]</sup>	Q	Bn ( <b>2d</b> )	toluene	80	<b>d</b>	95:5	92/6
14 <sup>[e]</sup>	Q	Bn ( <b>2d</b> )	THF	56	<b>d</b>	95:5	90/5
15 <sup>[g]</sup>	Q	Bn ( <b>2d</b> )	CH <sub>3</sub> CN	> 95	<b>d</b>	85:15	66/0
16 <sup>[g]</sup>	Q	Bn ( <b>2d</b> )	MeOH	> 95	<b>d</b>	44:56	24/0
17	BQ	Bn ( <b>2d</b> )	CH <sub>2</sub> Cl <sub>2</sub>	45	<b>d</b>	81:19	5/12

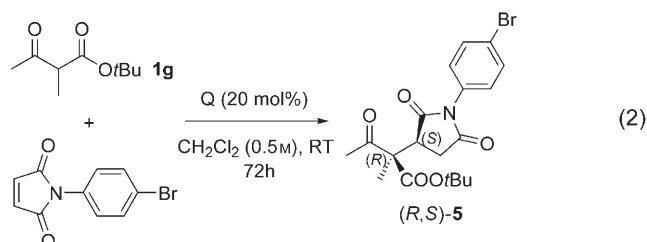
[a] The formulae of the catalysts can be found in Scheme 1. Experimental conditions (0.2-mmol scale): The reactions were carried out open to the air in undistilled solvent with a 1:1.2 ratio of **1a** to **2**. [b] Conversion and d.r. were determined by <sup>1</sup>H NMR spectroscopic analysis of the crude-product mixture. [c] Determined by HPLC analysis on commercially available chiral stationary phases; values for both diastereomers are given. [d] The opposite enantiomer was obtained. [e] Reaction time: 24 h, reaction temperature: –20 °C. [f] Number in parenthesis indicates the yield of the isolated product **3d**. [g] Reaction time: 16 h, reaction temperature: –20 °C.

dicarbonyl substrates are summarized in Table 2. Both enantiomers of the 1,4-adducts were synthesized efficiently with high selectivity by appropriate selection of the catalyst (Q or QD). The cyclic β-ketoesters **1b–d** were all converted into the corresponding 1,4-adducts in good yields and with very high levels of both diastereo- and enantioselectivity (Table 2, entries 1–6). The protocol also proved to be effective for acyclic β-ketoesters; the expected products were formed with high selectivity, although decreased reactivity was observed (Table 2, entries 7 and 8). Interestingly, we found that the size of the ester group had a significant effect on the stereoselectivity: the reaction of the acyclic *tert*-butyl ketoester **1g** occurred in a highly enantio- and diastereoselective fashion even at room temperature (92% ee, d.r. = 92:8; Table 2,

entry 9).<sup>[16]</sup> Outstanding results were obtained with β-diketones (Table 2, entries 10–13), a particularly challenging class of substrates, for which, to our knowledge, just two examples of effective asymmetric organocatalytic conjugate addition have been reported.<sup>[17]</sup>

As the conjugate addition products **4** are generally solid substances, it is possible to obtain a single stereoisomer in essentially enantiomerically pure form after a single crystallization, as demonstrated for adducts **4c** and **4d** (Table 2, entries 4 and 6).

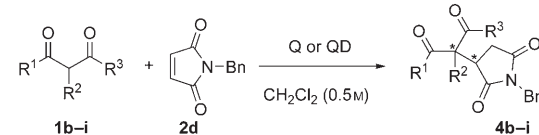
The absolute configuration of compound **5**, generated by the quinine-catalyzed addition of **1g** to *N*-(4-bromophenyl)-maleimide [Eq. (2)], was assigned by X-ray crystallographic



analysis.<sup>[18]</sup> The relative configuration of **4d** was determined unequivocally by X-ray crystallographic analysis,<sup>[18]</sup> whereas the relative configurations of **4b** and **4h** were assigned by NMR spectroscopic analysis with extensive NOE interaction studies (see the Supporting Information for details).

The synthetic utility of our organocatalytic approach was evaluated by a gram-scale experiment (10 mmol), which gave

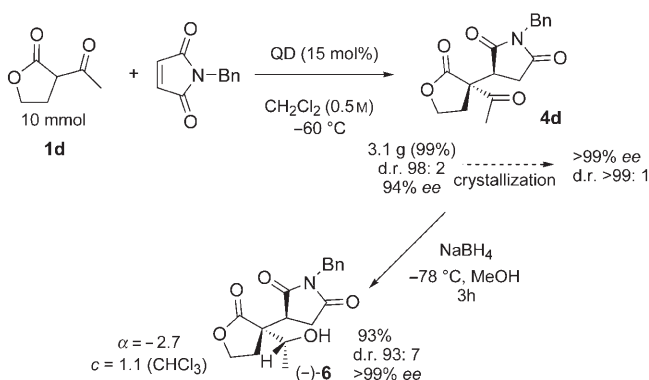
**Table 2:** Highly stereoselective conjugate addition of 1,3-dicarbonyl compounds **1** to **2d** catalyzed by natural cinchona alkaloids.<sup>[a]</sup>



Entry	<b>1/4</b>	Cat.	(mol %) <sup>[b]</sup>	T [°C]	t [h]	Yield [%] <sup>[c]</sup>	d.r. <sup>[d]</sup>	ee [%] <sup>[e]</sup>
1	<b>b</b>	Q	(10)	–30	24	99	84:16	94
2	<b>b</b>	QD	(10)	–60	40	99	87:13	98
3	<b>c</b>	Q	(10)	–60	38	98	91:9	94
4	<b>c</b>	QD	(10)	–60	38	99	90:10	95 (> 99 <sup>[f]</sup> )
5	<b>d</b>	Q	(15)	–60	40	99	> 98:2	89
6	<b>d</b>	QD	(15)	–60	40	91	> 98:2	93 (> 99 <sup>[f]</sup> )
7	<b>e</b>	QD	(20)	–15	50	52 (55)	93:7	85
8	<b>f</b>	QD	(20)	–15	88	63 (65)	77:23	85
9	<b>g</b>	Q	(20)	RT	72	75 (78)	92:8	92
10	<b>h</b>	Q	(15)	–30	24	72 (80)	92:8	82
11	<b>h</b>	QD	(15)	–60	40	99	92:8	91
12	<b>i</b>	Q	(20)	–15	48	55 (58)	95:5	82
13	<b>i</b>	QD (20)	–30	66	72 (75)	95:5	84	

[a] The formulae of **1b–1i** can be found in Scheme 1. Experimental conditions (0.2-mmol scale): The reactions were carried out open to the air in undistilled dichloromethane with a 1:1.2 ratio of **1** to **2d**. [b] The catalysts Q and QD gave opposite enantiomers of the product diastereomer. [c] Yield of the isolated products **4**. Numbers in parenthesis indicates reaction conversion, as determined by <sup>1</sup>H NMR spectroscopic analysis. [d] Determined by <sup>1</sup>H NMR spectroscopic analysis of the crude-product mixture. [e] Determined by HPLC analysis on commercially available chiral stationary phases; values for the major diastereomer are given. For the ee values of minor diastereomers, see the Supporting Information. [f] After a single crystallization.

**4d** in quantitative yield (Scheme 2). A single crystallization from an EtOH/Et<sub>2</sub>O mixture afforded the optically pure product. Subsequent highly stereo- and chemoselective reduction of the keto group allowed access to compound (–)-**6**, which has three consecutive stereogenic centers of defined absolute configuration.<sup>[19]</sup>



**Scheme 2.** Stereo- and chemoselective synthesis and reduction of **4d**.

In summary, we have developed an operationally simple protocol that employs unmodified and commercially available materials and catalysts for the first asymmetric organocatalytic conjugate addition of 1,3-dicarbonyl compounds to maleimides. The enantioselectivity of the reaction is the highest reported to date for this class of Michael acceptors. Natural cinchona alkaloids proved to be highly efficient catalysts. They promoted the one-step construction of functionalized products with two adjacent stereogenic carbon atoms with very high diastereo- and enantioselectivity. Investigations are currently underway toward a mechanistic understanding of the process and fully defining its utility as a synthetic tool in asymmetric synthesis.

Received: January 27, 2006

Revised: May 2, 2006

Published online: July 3, 2006

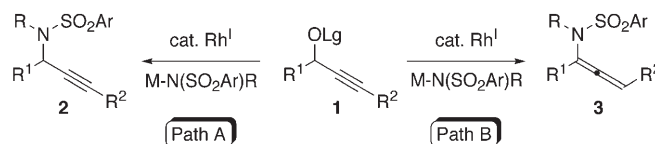
**Keywords:** asymmetric catalysis · cinchona alkaloids · conjugate addition · maleimides · organocatalysis

- [1] For reviews on the asymmetric construction of quaternary carbon centers, see: a) C. J. Douglas, L. E. Overman, *Proc. Natl. Acad. Sci. USA* **2004**, *101*, 5363, and references therein; b) J. Christoffers, A. Baro, *Angew. Chem.* **2003**, *115*, 1726; *Angew. Chem. Int. Ed.* **2003**, *42*, 1688; c) E. J. Corey, A. Guzman-Perez, *Angew. Chem.* **1998**, *110*, 402; *Angew. Chem. Int. Ed.* **1998**, *37*, 388.
- [2] For some leading examples that rely on different strategies, see: a) F. Wu, H. Li, R. Hong, L. Deng, *Angew. Chem.* **2006**, *118*, 961; *Angew. Chem. Int. Ed.* **2006**, *45*, 947; b) B. K. Corkey, F. D. Toste, *J. Am. Chem. Soc.* **2005**, *127*, 17168; c) P. Mauleon, J. C. Carretero, *Chem. Commun.* **2005**, 4961; d) M. D. Augustin, L. Palais, A. Alexakis, *Angew. Chem.* **2005**, *117*, 1400; *Angew. Chem. Int. Ed.* **2005**, *44*, 1376; e) A. W. Hird, A. H. Hoveyda, *J. Am. Chem. Soc.* **2005**, *127*, 14988.
- [3] For recent reviews on catalytic asymmetric conjugate additions, see: a) T. Hayashi, K. Yamasaki, *Chem. Rev.* **2003**, *103*, 2829; b) N. Krause, A. Hoffmann-Röder, *Synthesis* **2001**, 171.
- [4] For the catalytic asymmetric construction of adjacent tertiary and quaternary centers, see: a) T. B. Poulsen, C. Alemparte, S. Saaby, M. Bella, K. A. Jørgensen, *Angew. Chem.* **2005**, *117*, 2956; *Angew. Chem. Int. Ed.* **2005**, *44*, 2896; b) J. F. Austin, S.-G. Kim, C. J. Sinz, W.-J. Xiao, D. W. C. MacMillan, *Proc. Natl. Acad. Sci. USA* **2004**, *101*, 5482.
- [5] a) M. S. Taylor, D. N. Zalatan, A. M. Lerchner, E. N. Jacobsen, *J. Am. Chem. Soc.* **2005**, *127*, 1313; b) Y. Hamashima, D. Hotta, M. Sodeoka, *J. Am. Chem. Soc.* **2002**, *124*, 11240; see also reference [2a].
- [6] H. Li, Y. Wang, L. Tang, F. Wu, X. Liu, C. Guo, B. M. Foxman, L. Deng, *Angew. Chem.* **2005**, *117*, 107; *Angew. Chem. Int. Ed.* **2005**, *44*, 105.
- [7] M. S. Taylor, E. N. Jacobsen, *J. Am. Chem. Soc.* **2003**, *125*, 11204.
- [8] For recent examples of the use of cinchona alkaloid derivatives as efficient chiral-base catalysts, see: a) S. Sobhani, D. Fielenbach, M. Marigo, T. C. Wabnitz, K. A. Jørgensen, *Chem. Eur. J.* **2005**, *11*, 5689; b) G. Bartoli, M. Bosco, A. Carlone, M. Locatelli, P. Melchiorre, L. Sambri, *Angew. Chem.* **2005**, *117*, 6375; *Angew. Chem. Int. Ed.* **2005**, *44*, 6219; for a recent review, see: c) S.-K. Tian, Y. Chen, J. Hang, L. Tang, P. McDaid, L. Deng, *Acc. Chem. Res.* **2004**, *37*, 621.
- [9] For general reviews on organocatalysis, see: a) *Asymmetric Organocatalysis* (Eds.: A. Berkessel, H. Gröger), Wiley-VCH, Weinheim, **2004**; b) *Acc. Chem. Res.* **2004**, *37*(8), special issue (Eds.: K. N. Houk, B. List); c) P. I. Dalko, L. Moisan, *Angew. Chem.* **2004**, *116*, 5248; *Angew. Chem. Int. Ed.* **2004**, *43*, 5138.
- [10] For some biological studies on enantioenriched  $\alpha$ -substituted succinimides, see: a) S. Ahmed, *Drug Des. Discovery* **1996**, *14*, 77; b) M. L. Curtin, R. B. Garland, H. R. Heyman, R. R. Frey, M. R. Michaelides, J. Li, L. J. Pease, K. B. Glaser, P. A. Marcotte, S. K. Davidsen, *Bioorg. Med. Chem. Lett.* **2002**, *12*, 2919; for the synthetic derivatization of this useful scaffold to afford functionalized open-chain derivatives and substituted pyrrolidines, see: c) A. R. Katritzky, J. Yao, M. Qi, Y. Chou, D. J. Sikora, S. Davis, *Heterocycles* **1998**, *48*, 2677; d) R. Ballini, G. Bosica, G. Cioci, D. Fiorini, M. Petrini, *Tetrahedron* **2003**, *59*, 3603.
- [11] a) R. Shintani, W.-L. Duan, T. Nagano, A. Okada, T. Hayashi, *Angew. Chem.* **2005**, *117*, 4687; *Angew. Chem. Int. Ed.* **2005**, *44*, 4611; b) R. Shintani, K. Ueyama, I. Yamada, T. Hayashi, *Org. Lett.* **2004**, *6*, 3425. After our manuscript had been submitted, the use of the same strategy for asymmetric addition to substituted maleimides to afford quaternary stereocenters was reported: c) R. Shintani, W.-L. Duan, T. Hayashi, *J. Am. Chem. Soc.* **2006**, *128*, 5628.
- [12] For selected examples, see: a) B. Vakulya, Sz. Varga, A. Csámpai, T. Soos, *Org. Lett.* **2005**, *7*, 1967; b) S. H. McCooley, S. J. Connon, *Angew. Chem.* **2005**, *117*, 6525; *Angew. Chem. Int. Ed.* **2005**, *44*, 6367; c) Y. Wang, X. Liu, L. Deng, *J. Am. Chem. Soc.* **2006**, *128*, 3928.
- [13] a) Y. Iwabuchi, M. Nakatani, N. Yokoyama, S. Hatakeyama, *J. Am. Chem. Soc.* **1999**, *121*, 10219; b) S. Kawahara, A. Nakano, T. Esumi, Y. Iwabuchi, S. Hatakeyama, *Org. Lett.* **2003**, *5*, 3103.
- [14] a) H. Hiemstra, H. Wynberg, *J. Am. Chem. Soc.* **1981**, *103*, 417; b) H. Wynberg, *Top. Stereochem.* **1986**, *16*, 87.
- [15] For quinine-catalyzed conjugate additions of carbon-centered nucleophiles with low selectivity, see: a) H. Wynberg, R. Helder, *Tetrahedron Lett.* **1975**, *16*, 4057; b) G. Szöllösi, M. Bartók, *Chirality* **2001**, *13*, 614; for a review, see: c) K. Kacprzak, J. Gawroński, *Synthesis* **2001**, 961; during our studies, two highly selective reactions catalyzed by natural cinchona alkaloids were reported: d) B. Török, M. Abid, G. London, J. Esquibel, M. Török, S. C. Mhadgut, P. Yan, G. K. S. Prakash, *Angew. Chem.* **2005**, *117*, 3146; *Angew. Chem. Int. Ed.* **2005**, *44*, 3086; e) S. Lou,

- B. M. Taoka, A. Ting, S. E. Schaus, *J. Am. Chem. Soc.* **2005**, *127*, 11 256.
- [16] For similar effects of the size of the ester group on the selectivity of organocatalytic asymmetric transformations, see references [2a] and [8a].
- [17] M. Bella, K. A. Jørgensen, *J. Am. Chem. Soc.* **2004**, *126*, 5672; see also reference [6].
- [18] Compound **5**, obtained in 65 % yield, 85 % *ee*, and d.r. = 96:4, was crystallized slowly from a mixture of hexane/Et<sub>2</sub>O to give fine colorless needles of a single diastereomer with the configuration shown in Equation (2). The same crystal used for X-ray crystallography was analyzed by chiral HPLC, which confirmed the presence of the major enantiomer. CCDC-296418 (**5**) and -605040 (**4d**) contain the supplementary crystallographic data for this paper. These data can be obtained free of charge from The Cambridge Crystallographic Data Centre via [www.ccdc.cam.ac.uk/data\\_request/cif](http://www.ccdc.cam.ac.uk/data_request/cif).
- [19] The relative configuration of **6** was assigned by using NMR spectroscopic analysis with extensive NOE interaction studies; see the Supporting Information for details.



with this particular transition metal for related transformations.<sup>[4,5]</sup> Herein, we describe the first rhodium-catalyzed propargylic amination of secondary propargylic alcohol derivatives **1**, which provides a divergent approach for the preparation of propargylic sulfonamides **2** (path A: R<sup>1</sup> = alkyl/aryl, R<sup>2</sup> = H; Scheme 1) and 1,1-disubstituted allenyl sulfonamides **3** (path B: R<sup>1</sup> = aryl, R<sup>2</sup> = H).<sup>[6]</sup>



**Scheme 1.** General approach for the divergent construction of propargylic and allenyl sulfonamides.

Preliminary studies examined the feasibility of the rhodium-catalyzed propargylic amination of **1a** (R<sup>1</sup> = Ph-(CH<sub>2</sub>)<sub>2</sub>; R<sup>2</sup> = H) using *N*-benzyl toluenesulfonamide (Table 1). Although the attempted amination of propargylic

## Cyclization

DOI: 10.1002/anie.200600615

### Rhodium-Catalyzed Propargylic Substitution: A Divergent Approach to Propargylic and Allenyl Sulfonamides\*\*

P. Andrew Evans\* and Michael J. Lawler

The transition-metal-mediated substitution of propargylic alcohol derivatives using a stoichiometric cobalt–alkyne complex, represents a fundamentally important synthetic transformation that is often referred to as the Nicholas reaction.<sup>[1]</sup> The catalytic version of this process, in which a number of late-transition-metal complexes have been shown to be effective catalysts, has also been described.<sup>[2,3]</sup> Nonetheless, a key and striking feature with many of the catalytic variants is the preponderance of aryl-substituted propargylic alcohols, which presumably circumvents the problem of  $\beta$ -hydride elimination with alkyl derivatives.

We envisioned that the rhodium-catalyzed version would prove interesting, given the unique reactivity often observed

**Table 1:** Optimization of the rhodium-catalyzed propargylic amination reaction.<sup>[a]</sup>

Entry	R <sup>2</sup>	Additive (mol %)	Lg	Yield of <b>2a</b> [%] <sup>[b]</sup>
1	H	–	H	0
2	H	–	COMe	trace
3	H	P(OMe) <sub>3</sub> (40)	COMe	27
4	H	P(OMe) <sub>3</sub> (40)	CO <sub>2</sub> Me	66
5	H	P(OMe) <sub>3</sub> (40)	CO <sub>2</sub> <i>t</i> Bu	82
6	Me <sub>3</sub> Si	P(OMe) <sub>3</sub> (40)	CO <sub>2</sub> <i>t</i> Bu	20
7	Me	P(OMe) <sub>3</sub> (40)	CO <sub>2</sub> <i>t</i> Bu	0
8	Ph	P(OMe) <sub>3</sub> (40)	CO <sub>2</sub> <i>t</i> Bu	0

[a] See Scheme 1; **1a** R<sup>1</sup> = Ph(CH<sub>2</sub>)<sub>2</sub>; R = PhCH<sub>2</sub>, Ar = *p*-CH<sub>3</sub>C<sub>6</sub>H<sub>4</sub>. All reactions were carried out on a 0.25-mmol scale with 10 mol % [RhCl(PPh<sub>3</sub>)<sub>3</sub>] and 2.0 equivalents of the lithium anion of *N*-benzyl toluenesulfonamide (LiN(Ts)Bn; Ts = *p*-toluenemethanesulfonyl) at 30 °C. [b] Yield of the isolated product.

alcohol **1a** (Lg = H; entry 1) with the Wilkinson catalyst was completely unsuccessful, the acetate **1a** (Lg = Ac; entry 2) furnished a trace amount of the desired propargylic sulfonamide **2a**. Despite the fact that the yield was not particularly encouraging, we envisioned that additional improvement would be achieved through the modification of the catalyst with trimethyl phosphite in an analogous manner to the related allylic substitution reaction.<sup>[4,5]</sup> Indeed, the trimethyl phosphite modified Wilkinson catalyst afforded **2a** with an improved yield of 27% (entry 3), albeit with significant quantities of the propargylic alcohol derived from transacylation. This result prompted the examination of alternative leaving groups (see entries 3–5). Gratifyingly, treatment of the propargylic carbonate **1a** (Lg = *t*BuOCO) with the modified Wilkinson catalyst and the lithium anion of *N*-benzyl toluenesulfonamide, furnished the propargylic sulfonamide **2a** in 82% yield (entry 5). Additional studies focused on the effect of the terminal alkyne substituent R<sup>2</sup>. Interestingly, although a trimethylsilyl group provides the propargylic

[\*] Dr. P. A. Evans, M. J. Lawler  
Department of Chemistry  
Indiana University  
Bloomington, IN 47405 (USA)  
Fax: (+1) 812-855-8300  
E-mail: paevans@indiana.edu

[\*\*] We sincerely thank the National Science Foundation (CHE-0316689) for generous financial support. We also thank Johnson and Johnson for a Focused Giving Award.

Supporting information for this article is available on the WWW under <http://www.angewandte.org> or from the author.

sulfonamide **2a** (entry 6), albeit in low yield, the aryl- and alkyl-substituted derivatives are completely unreactive under the analogous reaction conditions (entries 7 and 8).

Table 2 summarizes the application of the optimized reaction conditions (Table 1, entry 5) to a variety of nucleophiles and aliphatic propargylic carbonates (see below). This

**Table 2:** Scope of the rhodium-catalyzed propargylic amination reaction.<sup>[a]</sup>

Entry	R <sup>1</sup>	1	MN(SO <sub>2</sub> Ar)R <sup>[b]</sup>	2	Yield [%] <sup>[c]</sup>
1	Ph(CH <sub>2</sub> ) <sub>2</sub>	<b>a</b>	LiN(Ts)Bn	<b>a</b>	82
2	Ph(CH <sub>2</sub> ) <sub>2</sub>	<b>a</b>	LiN(Ts)PMP	<b>ab</b>	74
3	Ph(CH <sub>2</sub> ) <sub>2</sub>	<b>a</b>	LiN(Ns)Allyl	<b>ac</b>	72
4	Ph(CH <sub>2</sub> ) <sub>2</sub>	<b>a</b>	LiN(Ts)N=C(Me)Ph	<b>ad</b>	83
5	Ph(CH <sub>2</sub> ) <sub>2</sub>	<b>a</b>	KPhth	<b>ae</b>	71
6	Ph(CH <sub>2</sub> ) <sub>2</sub>	<b>a</b>	NaCH(CO <sub>2</sub> Me) <sub>2</sub>	<b>af</b>	83
7	PhCH <sub>2</sub>	<b>b</b>	LiN(Ts)Bn	<b>b</b>	85
8	CH <sub>3</sub>	<b>c</b>	LiN(Ts)Bn	<b>c</b>	76
9	CH <sub>3</sub> (CH <sub>2</sub> ) <sub>2</sub>	<b>d</b>	LiN(Ts)Bn	<b>d</b>	74
10	CH <sub>2</sub> =CH(CH <sub>2</sub> ) <sub>3</sub>	<b>e</b>	LiN(Ts)Bn	<b>e</b>	78
11	(CH <sub>3</sub> ) <sub>2</sub> CHCH <sub>2</sub>	<b>f</b>	LiN(Ts)Bn	<b>f</b>	86
12	(CH <sub>3</sub> ) <sub>2</sub> CH	<b>g</b>	LiN(Ts)Bn	<b>g</b>	70
13	<i>c</i> -C <sub>6</sub> H <sub>11</sub>	<b>h</b>	LiN(Ts)Bn	<b>h</b>	74
14	(CH <sub>3</sub> ) <sub>3</sub> C	<b>i</b>	LiN(Ts)Bn	<b>i</b>	83
15	BnOCH <sub>2</sub>	<b>j</b>	LiN(Ts)Bn	<b>j</b>	72

[a] See Scheme 1; **1** Lg=CO<sub>2</sub>tBu, R<sup>2</sup>=H. All reactions were carried out on a 0.25-mmol reaction scale using 10 mol % [RhCl(PPh<sub>3</sub>)<sub>3</sub>] modified with 40 mol % P(OMe)<sub>3</sub> in THF at 30 °C. [b] 2.0 equivalents of the lithium anion of the *N*-substituted sulfonamide. [c] Yields of the isolated product. Phth=phthalimide.

transformation proved tolerant of both *N*-alkyl and aryl sulfonamides (entries 1 and 2), in which the *p*-toluenesulfonamide could be substituted for the more readily removed *p*-nitrobenzenesulfonyl group to improve the synthetic utility of this protocol (entry 3).<sup>[7,8]</sup> The *N*-sulfonyl hydrazone, phthalimide, and dimethyl malonate also provided suitable nucleophiles, thus clearly illustrating the scope of this process (entry 4–6).<sup>[9]</sup> Another impressive feature of this transformation is the range of aliphatic propargylic substituents that can be utilized. For example, linear (entries 7–10) and branched (entries 11–13) aliphatic substituents, including the *tert*-butyl (entry 14) and benzyloxymethyl (entry 15) substituents, afford the corresponding propargylic sulfonamides **2** in good yield.<sup>[10,11]</sup> Hence, the ability to accomplish the rhodium-catalyzed propargylic amination of a wide range of aliphatic propargylic alcohol derivatives represents an important addition to the area of metal-mediated propargylic substitution.

Although the propargylic substitution of alkyl-substituted propargylic carbonates was straightforward, the aryl derivative **1m** (R<sup>1</sup>=Ph) furnished the 1,1-disubstituted allenyl sulfonamide **3m** as the major product under analogous conditions (Table 3, entry 5). The origin of the divergent reactivity was attributed to a base-induced isomerization of the initially formed propargylic sulfonamides **2m** to the corresponding allene **3m**.<sup>[12]</sup> We reasoned that the isomerization could be suppressed with a weaker base. Gratifyingly, the propargylic amination of **1m** with potassium carbonate as

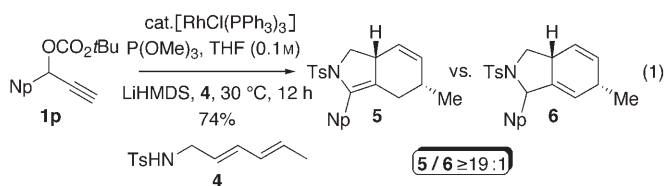
**Table 3:** Divergent approach to propargyl and allenyl sulfonamides through rhodium-catalyzed propargylic substitution.<sup>[a]</sup>

Entry	R <sup>1</sup>	1	Base	2/3 <sup>[b]</sup>	Yield [%] <sup>[c]</sup>
1	<i>p</i> -MeOC <sub>6</sub> H <sub>4</sub>	<b>k</b>	LiHMDS	≥ 19:1	51
2	<i>p</i> -MeOC <sub>6</sub> H <sub>4</sub>	<b>k</b>	K <sub>2</sub> CO <sub>3</sub>	≥ 19:1	78
3	<i>p</i> -MeC <sub>6</sub> H <sub>4</sub>	<b>l</b>	LiHMDS	1:1	63
4	<i>p</i> -MeC <sub>6</sub> H <sub>4</sub>	<b>l</b>	K <sub>2</sub> CO <sub>3</sub>	≥ 19:1	72
5	Ph	<b>m</b>	LiHMDS	≤ 1:19	77
6	Ph	<b>m</b>	K <sub>2</sub> CO <sub>3</sub>	≥ 19:1	74
7	<i>p</i> -BrC <sub>6</sub> H <sub>4</sub>	<b>n</b>	LiHMDS	≤ 1:19	70
8	<i>p</i> -BrC <sub>6</sub> H <sub>4</sub>	<b>n</b>	K <sub>2</sub> CO <sub>3</sub>	≥ 19:1	69
9	<i>p</i> -CF <sub>3</sub> C <sub>6</sub> H <sub>4</sub>	<b>o</b>	LiHMDS	≤ 1:19	48
10	<i>p</i> -CF <sub>3</sub> C <sub>6</sub> H <sub>4</sub>	<b>o</b>	K <sub>2</sub> CO <sub>3</sub>	2:1	61
11	Np	<b>p</b>	LiHMDS	≤ 1:19	82
12	Np	<b>p</b>	K <sub>2</sub> CO <sub>3</sub>	≥ 19:1	83
13	1-furyl	<b>q</b>	LiHMDS	≤ 1:19	63
14	1-furyl	<b>q</b>	K <sub>2</sub> CO <sub>3</sub>	≥ 19:1	55

[a] See Scheme 1; **1** Lg=CO<sub>2</sub>tBu, R<sup>2</sup>=H. All reactions were carried out on a 0.25-mmol reaction scale with 10 mol % [RhCl(PPh<sub>3</sub>)<sub>3</sub>] modified with 40 mol % P(OMe)<sub>3</sub> in THF at 30 °C with TsNHBN (2 equiv) and the requisite base (2 equiv). [b] Ratio of amination products was determined by NMR (400 MHz) spectroscopic analysis on the crude reaction mixture. [c] Yield of the isolated products. HMDS=hexamethyldisilazane.

the base furnished the propargylic sulfonamide **2m** in 74 % yield (entry 6). A series of *para*-substituted aryl propargyl alcohol derivatives **1k–o** were examined to determine the scope of this divergent behavior. This study indicates that the isomerization may be directly related to the relative acidity of the  $\alpha$ -proton in the propargylic sulfonamide **2**. For example, strongly electron-donating substituents suppress the isomerization (entries 1–4), whereas the strongly electron-withdrawing groups are prone to isomerization to the allene with even a weak base, albeit to a much lesser extent (entries 7 and 8 versus 9 and 10). The naphthyl (Np) **1p** and furyl **1q** derivatives demonstrate analogous behavior to the phenyl and *p*-bromophenyl derivatives **1m** and **1n** and facilitate the selective formation of either derivative (entries 11–14).

We developed a sequential one-pot two-component rhodium-catalyzed propargylic amination/isomerization followed by a [4+2] carbocyclization [Eq. (1)]<sup>[12–15]</sup> to highlight



the synthetic utility of the base-induced isomerization of aryl-substituted propargylic sulfonamides to the corresponding 1,1-disubstituted allenes in situ. Treatment of the aryl-substituted propargylic carbonate **1p** under the standard reaction conditions and with the lithium anion of sulfonamide derivative **4** afforded the bicyclohexadienes **5/6** in 74 % yield with 19:1 selectivity for **5** (d.r. ≥ 19:1, as determined by <sup>1</sup>H NMR spectroscopy). The relative configuration of **5** was determined by X-ray crystallography. Although allenes have

been utilized in an array of metal-catalyzed carbocyclization reactions, the ability to utilize 1,1-disubstituted derivatives in this manner represents a novel process.<sup>[15,16]</sup>

In conclusion, we have demonstrated that rhodium-catalyzed propargylic amination provides an efficient and versatile method for the construction of aliphatic-substituted propargylic sulfonamides. This study also demonstrates that the divergent behavior in the rhodium-catalyzed variant of the propargylic substitution, in which either aryl-substituted propargylic or allenyl sulfonamides can be prepared is dependent upon the acidity of the propargylic proton. Finally, the synthetic utility of the isomerization of aryl-substituted propargylic sulfonamides in situ was demonstrated in a one-pot two-component rhodium-catalyzed propargylic amination/isomerization followed by a [4+2] carbocyclization. We anticipate the ability to prepare functionalized bicyclohexadienes in this manner will have significant synthetic utility for target-directed synthesis.

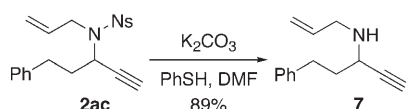
Received: February 15, 2006

Revised: April 13, 2006

Published online: July 3, 2006

**Keywords:** allenes · carbocyclization · isomerization · rhodium · sulfonamides

- [1] For a recent review on the Nicholas reaction, see: B. J. Teobald, *Tetrahedron* **2002**, 58, 4133–4170.
- [2] For a review on the palladium-catalyzed reactions of propargylic derivatives, see: J. Tsuji, T. Mandai, *Angew. Chem.* **1995**, 107, 2830–2854; *Angew. Chem. Int. Ed. Engl.* **1995**, 34, 2589–2612.
- [3] For leading references on the metal-catalyzed propargylic substitution reaction, see: a) Ir: I. Matsuda, K. Komori, K. Itoh, *J. Am. Chem. Soc.* **2002**, 124, 9072–9073; b) Ru: Y. Nishibayashi, Y. Inada, M. Hidai, S. Uemura, *J. Am. Chem. Soc.* **2003**, 125, 6060–6061; c) Re: M. R. Luzung, F. D. Toste, *J. Am. Chem. Soc.* **2003**, 125, 15760–15761; d) Au: M. Georgy, V. Boucard, J. M. Campagne, *J. Am. Chem. Soc.* **2005**, 127, 14180–14181, and pertinent references therein.
- [4] D. K. Leahy, P. A. Evans in *Modern Rhodium-Catalyzed Organic Reactions* (Ed.: P. A. Evans), Wiley-VCH, Weinheim, **2005**, chap. 10, p. 201.
- [5] a) P. A. Evans, J. E. Robinson, J. D. Nelson, *J. Am. Chem. Soc.* **1999**, 121, 6761–6762; b) P. A. Evans, J. E. Robinson, *Org. Lett.* **1999**, 1, 1929–1931; c) P. A. Evans, J. E. Robinson, K. K. Moffett, *Org. Lett.* **2001**, 3, 3269–3271.
- [6] For examples of metal-catalyzed propargylic amination reactions, see: a) Cu: Y. Imada, M. Yuasa, I. Nakuamura, S.-I. Murahashi, *J. Org. Chem.* **1994**, 59, 2282–2284; b) Pd: J. A. Marshall, M. A. Wolf, *J. Org. Chem.* **1996**, 61, 3238–3239; c) Ru: Y. Nishibayashi, I. Wakiji, M. Hidai, *J. Am. Chem. Soc.* **2000**, 122, 11019–11020; d) Re: R. V. Ohri, A. T. Radosevich, K. J. Hrovat, C. Musich, D. Huang, T. R. Holman, F. D. Toste, *Org. Lett.* **2005**, 7, 2501–2504.
- [7] Deprotection of the *p*-nitrobenzenesulfonyl group in **2ac** using the Fukuyama protocol furnished the *N*-allyl propargyl amine **7** in dimethylformamide (DMF) in 89% yield.<sup>[8]</sup>
- [8] T. Fukuyama, C.-K. Jow, M. Cheung, *Tetrahedron Lett.* **1995**, 36, 6373–6374.
- [9] R. Matunas, A. J. Lai, C. Lee, *Tetrahedron* **2005**, 61, 6298–6308.
- [10] LiHMDS (0.5 mL, 0.5 mmol, 1.0 M in THF) was added dropwise to *N*-benzyl *p*-toluenesulfonamide (0.132 g, 0.5 mmol) in anhydrous THF (1.5 mL). The anion was allowed to form over approximately 5 min. In a separate flask, trimethyl phosphite (12  $\mu$ L, 0.10 mmol) was added directly to a red solution of the Wilkinson catalyst (23.1 mg, 0.025 mmol) in anhydrous THF (1.0 mL) under an atmosphere of argon. The catalyst was allowed to form over approximately 5 min, thus resulting in a light-yellow homogeneous solution. The propargylic carbonate **1a** (65.6 mg, 0.25 mmol) was then added dropwise through a tared 250- $\mu$ L syringe, and the reaction mixture was heated to 30°C for approximately 15 h (tlc control). The reaction mixture was quenched with saturated aqueous NH<sub>4</sub>Cl solution (2 mL) and partitioned between diethyl ether and saturated NH<sub>4</sub>Cl solution. The aqueous phase was washed with diethyl ether, and the organic layers were combined, dried (Na<sub>2</sub>SO<sub>4</sub>), filtered, and concentrated in vacuo to afford a crude oil. Purification by flash chromatography (ethyl acetate/hexanes 5:95) furnished the propargylic sulfonamide **2a** (86.4 mg, 82%) as a colorless oil.
- [11] Interestingly, this transformation does not allow the chirality transfer observed with the analogous allylic substitution; for example, treatment of the enantiomerically enriched propargylic carbonate (*S*)-**1a** (85% *ee*) under the optimized reaction conditions, furnished propargylic sulfonamide **2a** in 75% yield as the racemate (0% *ee*).
- [12] Treatment of the propargylic sulfonamide **2m** with the lithium anion of the *N*-benzyl *p*-toluenesulfonamide furnished the 1,1-disubstituted allene **3m** in 99% yield, thus clearly demonstrating that the rhodium catalyst is not involved in the isomerization. For a similar process that involves a mixed catalyst, see: M. D. Milton, Y. Inada, Y. Nishibayashi, S. Uemura, *Chem. Commun.* **2004**, 2712–2713.
- [13] For a recent review on single-pot catalysis with the same metal-complex, see: A. Ajamian, J. L. Gleason, *Angew. Chem.* **2004**, 116, 3842–3848; *Angew. Chem. Int. Ed.* **2004**, 43, 3754–3760.
- [14] For recent examples of sequential rhodium-catalyzed allylic substitution/carbocyclization, see: a) P. A. Evans, J. E. Robinson, *J. Am. Chem. Soc.* **2001**, 123, 4609–4610; b) B. L. Ashfeld, K. A. Miller, A. J. Smith, K. Tran, S. F. Martin, *Org. Lett.* **2005**, 7, 1661–1663.
- [15] The excellent selectivity for the rhodium-catalyzed [4+2] cycloaddition with the allene versus the alkyne moiety to afford **5** rather than **6**, respectively, is feasible as the alkyne carbocyclization requires higher temperature (60°C).
- [16] For an example of a metal-catalyzed [4+2] carbocyclization reaction with an unactivated allene, see: P. A. Wender, T. E. Jenkins, *J. Am. Chem. Soc.* **1989**, 111, 6432–6434.



# Monofluoromethylation

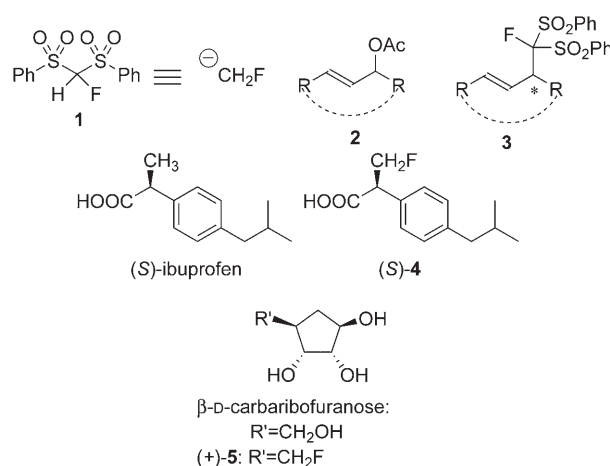
DOI: 10.1002/anie.200600625

## Fluorobis(phenylsulfonyl)methane: A Fluoromethide Equivalent and Palladium-Catalyzed Enantioselective Allylic Monofluoromethylation\*\*

Takeo Fukuzumi, Norio Shibata,\* Masayoshi Sugiura, Hiroyuki Yasui, Shuichi Nakamura, and Takeshi Toru\*

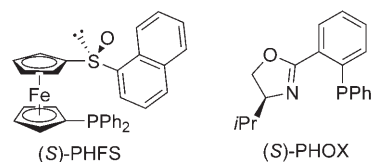
The development of efficient methodology for the synthesis of fluoroorganic compounds has attracted considerable attention particularly in the field of medicinal chemistry.<sup>[1]</sup> Owing to their unique and significant biological properties, fluorinated drugs have been commonly used in the treatment of a variety of diseases. Fluorination and fluoroalkylation reactions are two straightforward operations for the construction of fluorine-containing molecules, and their asymmetric versions are particularly useful.<sup>[2]</sup> Enantioselective electrophilic fluorination and enantioselective nucleophilic trifluoromethylation reactions probably represent the most versatile methodologies available for this purpose;<sup>[3]</sup> however, we are not aware of any reports of successful enantioselective monofluoromethylation reactions.<sup>[3d]</sup> Compounds with a monofluoromethyl unit are of great importance with regards to isostere-based drug design.<sup>[4]</sup> Indeed, monofluoroacetic acid is responsible for “lethal synthesis”, and it blocks the tricarboxylic acid cycle (Krebs cycle).<sup>[5]</sup> Monofluoromethylated amino acids such as D-fluoroalanine are well known to act as “suicide substrates” causing inactivation of the enzyme by alkylative capture of the aminoacylate-pyridoxal-P species.<sup>[6]</sup> In connection with our work on the asymmetric syntheses of fluorine-containing organic compounds,<sup>[7]</sup> we required a novel methodology for an enantioselective monofluoromethylation reaction. Herein we disclose our first step toward achieving this goal by demonstrating that 1-fluorobis-

(phenylsulfonyl)methane (**1**) acts as a synthetic equivalent for the monofluoromethide species. We found that the palladium-



catalyzed asymmetric allylic fluorobis(phenylsulfonyl)methylation reaction of allyl acetates **2** utilizing **1** smoothly proceed to afford the fluorobis(phenylsulfonyl)methylated compounds **3** with very high enantioselectivity up to 97% *ee*. We also show how this methodology can be applied to the synthesis of monofluoromethylated compounds, enantiopure methyl-fluorinated ibuprofens (*S*)- and (*R*)-**4** by reductive desulfonylation and oxidation of **3a**. An efficient access to fluorinated  $\beta$ -D-carbaribofuranose **5** from **3f** is also described.

Inspired by the reports on difluoromethylation by the groups led by Prakash,<sup>[8a]</sup> Olah,<sup>[8a]</sup> and Hu,<sup>[8a,b]</sup> with difluorophenylsulfonylmethane,<sup>[8]</sup> we envisaged that 1-fluorobis(phenylsulfonyl)methane (**1**) would be a useful reagent for enantioselective monofluoromethylation in the palladium-catalyzed allylic substitution reaction, which has been studied in detail by us<sup>[9]</sup> and others.<sup>[10]</sup> The previously unknown compound **1** was easily prepared in good yield from bis(phenylsulfonyl)methane,  $\text{CH}_2(\text{SO}_2\text{Ph})_2$ , by monofluorination with Selectfluor or molecular fluorine.<sup>[11a]</sup> Palladium-catalyzed fluorobis(phenylsulfonyl)methylation of (*E*)-1,3-bis(4-isobutylphenyl)-2-propenyl acetate (**2a**) with **1** was carried out in the presence of catalytic amounts of  $[\text{Pd}(\text{C}_3\text{H}_5\text{Cl})_2]$  and (*S*)-1-(1'-diphenylphosphino)ferrocenyl-1''-naphthyl sulfoxide ((*S*)-PHFS)<sup>[9]</sup> or (*S*)-2-(2-diphenylphosphinophenyl)-4-isopropyl-1,3-oxazoline ((*S*)-PHOX)<sup>[10c-e]</sup> at 0°C (Table 1).



First, the allylic substitution was examined under our previously optimized conditions using (*S*)-PHFS in the presence of cesium carbonate; however, the result was disappointing (Table 1, run 1). Next, (*S*)-PHOX was used as

[\*] Prof. Dr. N. Shibata, Prof. Dr. T. Toru  
Department of Applied Chemistry  
Graduate School of Engineering, Nagoya Institute of Technology  
Gokiso, Showa, Nagoya 466-8555 (Japan)  
Fax: (+81) 52-735-5442  
E-mail: nozshiba@nitech.ac.jp  
toru@nitech.ac.jp

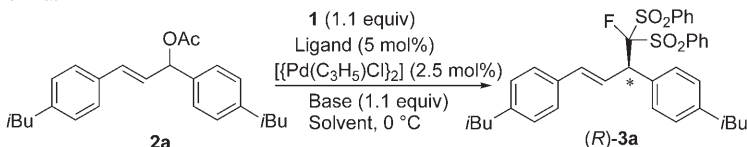
T. Fukuzumi, M. Sugiura, H. Yasui, Dr. S. Nakamura  
Department of Applied Chemistry  
Graduate School of Engineering, Nagoya Institute of Technology  
Gokiso, Showa, Nagoya 466-8555 (Japan)

[\*\*] This research was supported in part by a Grant-in-Aid for Scientific Research from the Ministry of Education, Culture, Sports, Science and Technology, Japan (17350047, 17590087) and by Japan Science & Technology (JST) Agency, Innovation Plaza Tokai. T.F. is grateful for research fellowships from JSPS. We thank Dr. Jon Bordner, Shin-ichi Sakemi, and Dr. Masami Nakane, Pfizer Inc., for X-ray crystallographic analysis.

Supporting information for this article is available on the WWW under <http://www.angewandte.org> or from the author.



**Table 1:** Optimization of the palladium-catalyzed enantioselective allylic fluorobis(phenylsulfonyl)methylation of **2a**.



Run	Ligand	Base	Solvent <sup>[a]</sup>	t [h]	Yield [%]/ <i>ee</i> <sup>[b]</sup> [%]
1	(S)-PHFS	Cs <sub>2</sub> CO <sub>3</sub>	CH <sub>2</sub> Cl <sub>2</sub> (0.1 M)	6	30/9 <sup>[c]</sup>
2	(S)-PHOX	BSA <sup>[d]</sup>	CH <sub>2</sub> Cl <sub>2</sub> (0.1 M)	17	14/90
3	(S)-PHOX	K <sub>2</sub> CO <sub>3</sub>	CH <sub>2</sub> Cl <sub>2</sub> (0.1 M)	14	31/94
4	(S)-PHOX	NaH <sup>[e]</sup>	THF (0.1 M)	9	39/96
5	(S)-PHOX	Cs <sub>2</sub> CO <sub>3</sub>	THF (0.1 M)	9	16/94
6	(S)-PHOX	Cs <sub>2</sub> CO <sub>3</sub>	CH <sub>2</sub> Cl <sub>2</sub> (0.1 M)	6	12/97
7	(S)-PHOX	Cs <sub>2</sub> CO <sub>3</sub>	CH <sub>2</sub> Cl <sub>2</sub> (0.1 M)	12 <sup>[f]</sup>	50/94
8	(S)-PHOX	Cs <sub>2</sub> CO <sub>3</sub>	CH <sub>2</sub> Cl <sub>2</sub> (0.5 M)	6	33/95
9	(S)-PHOX	Cs <sub>2</sub> CO <sub>3</sub>	CH <sub>2</sub> Cl <sub>2</sub> (1.0 M)	6	83/94
10 <sup>[g]</sup>	(S)-PHOX	Cs <sub>2</sub> CO <sub>3</sub>	CH <sub>2</sub> Cl <sub>2</sub> (1.0 M)	24 <sup>[f]</sup>	trace/65 <sup>[h]</sup>
11 <sup>[i]</sup>	(S)-PHOX	NaH <sup>[e]</sup>	dioxane (0.3 M)	48	23/89

[a] The concentration refers to **2a**. [b] The *ee* value was determined by HPLC analysis using CHIRALPAK AD-H. The absolute stereochemistry was tentatively assigned by comparing the optical rotation of **3a** with that of a non-fluorinated derivative of **3a**.<sup>[10a, 13b]</sup> [c] (S)-**3a** was obtained. [d] The reaction was carried out in the presence of CsOAc (0.1 equiv). [e] Preformed NaCF(SO<sub>2</sub>Ph)<sub>2</sub> was used. [f] The reaction was carried out at room temperature. [g] CH<sub>2</sub>(SO<sub>2</sub>Ph)<sub>2</sub> was used as a nucleophile instead of **1**. [h] A non-fluorinated analogue of (R)-**3a** was obtained. [i] The reaction was carried out at 73 °C.

a chiral ligand. Bis(trimethylsilyl)acetamide (BSA) and a catalytic amount of cesium acetate were examined as promoters for the reaction according to the procedure established for palladium-catalyzed allylic substitution using bis(phenylsulfonyl)methane.<sup>[10a]</sup> After overnight stirring at 0 °C, the desired 1-fluorobis(phenylsulfonyl)methylated product (R)-**3a** was obtained with 90 % *ee*, while the conversion was only 14 % (Table 1, run 2). With potassium carbonate or sodium hydride as a base, the enantioselectivities increased to 96 % *ee*, but the conversion was still low (Table 1, runs 3 and 4). Then the reaction was examined using cesium carbonate as a base in the concentration range 0.1–1.0 M (Table 1, runs 5–9). The adduct (R)-**3a** was produced in satisfactory yield with very high enantioselectivity when the reaction was carried out with Cs<sub>2</sub>CO<sub>3</sub> at a concentration of 1.0 M (Table 1, run 9).<sup>[11b]</sup> It should be noted that fluorine substitution has a striking effect on the reactivity and enantioselectivity of **1** (Table 1, cf. runs 9 and 10). As mentioned above, the allylic substitution reaction with **1** proceeds smoothly at temperatures below 0 °C within several hours and with very high enantioselectivity. In contrast, the non-fluorinated bis(phenylsulfonyl)methane, CH<sub>2</sub>(SO<sub>2</sub>Ph)<sub>2</sub>, has rather poor reactivity in allylic substitution reaction even at room temperature over 24 h, and therefore, the corresponding addition requires heating at, for example, 73 °C for 48 h.<sup>[10a]</sup> Only trace amount of the non-fluorinated analogue of **3a** was obtained with lower enantioselectivity (65 % *ee*) (Table 1, cf. runs 9 and 10). On the other hand, when the reaction of **2a** with **1** was carried out at elevated temperatures<sup>[10a]</sup> (i.e. the optimal conditions for CH<sub>2</sub>(SO<sub>2</sub>Ph)<sub>2</sub>), the yield and enantioselectivity decreased (Table 1, run 11). It may be possible to explain the difference in reactivity between **1** and CH<sub>2</sub>(SO<sub>2</sub>Ph)<sub>2</sub> in terms of the acidity of **1** relative to CH<sub>2</sub>(SO<sub>2</sub>Ph)<sub>2</sub> and the stability of its

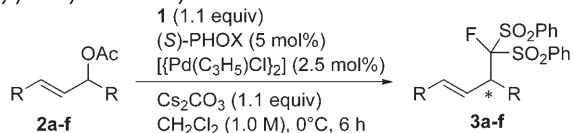
conjugate base. The high reactivity of **1** even at low temperatures might arise from the increased acidity of **1** as a result of the electron-withdrawing ability of fluorine. However, the effect of α-fluorine substitution on the stability of an anion generally arises from a compromise between its inductive electron-withdrawing ability and the repulsion between its electron pair and that on the carbanionic center.<sup>[12]</sup> The low stability of the conjugate base of **1** at higher temperatures could be the reason for the poor yield in run 11.

The 1-fluorobis(phenylsulfonyl)methylation reaction was also applied to a variety of allylic acetates (Table 2). Allylic acetates **2b–f** having methoxyphenyl, bromophenyl, and naphthyl groups were smoothly mono-fluoromethylated to furnish the desired fluorobis(phenylsulfonyl)methylated products **3b–f** in acceptable to high yields with high enantioselectivities (Table 2, entries 1–8).<sup>[13a]</sup> The reason for the loss in chemical yield for **3c,d** (Table 2, entries 2 and 5) is the partial decomposition of **2c,d**. The yield was improved when the reaction was carried out

under slightly modified conditions (amounts of reagents, reaction temperature; Table 2, entries 2–6). The opposite enantiomer, (S)-**3a**, is accessible from **2a** when (R)-PHOX is used as a catalyst ligand (Table 2, entry 9).<sup>[13b]</sup>

After testing acyclic electrophiles in our enantioselective allylic 1-fluorobis(phenylsulfonyl)methylation reaction with **1**, we next examined a similar process with cyclic electrophiles. Those with five- or six-membered rings are especially interesting since the products should be useful for the synthesis of fluorinated analogues of biologically important

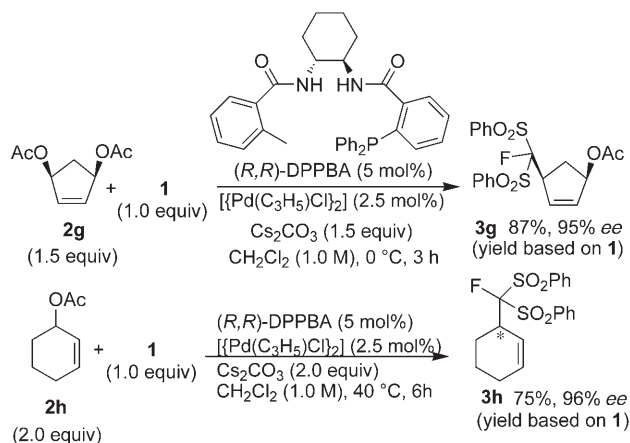
**Table 2:** Palladium-catalyzed enantioselective allylic fluorobis(phenylsulfonyl)methylation of allylic acetates **2a–f**.



Entry	2	Ar	3	Yield [%]	<i>ee</i> [%] <sup>[a]</sup>
1	<b>2b</b>	Ph	<b>3b</b>	92	96 (R) <sup>[e]</sup>
2	<b>2c</b>	4-MeOC <sub>6</sub> H <sub>4</sub>	<b>3c</b>	58	94
3 <sup>[b]</sup>	<b>2c</b>	4-MeOC <sub>6</sub> H <sub>4</sub>	<b>3c</b>	22 <sup>[b]</sup>	97
4 <sup>[c]</sup>	<b>2c</b>	4-MeOC <sub>6</sub> H <sub>4</sub>	<b>3c</b>	74	91
5	<b>2d</b>	4-BrC <sub>6</sub> H <sub>4</sub>	<b>3d</b>	54	95 (R) <sup>[e]</sup>
6 <sup>[b]</sup>	<b>2d</b>	4-BrC <sub>6</sub> H <sub>4</sub>	<b>3d</b>	69 <sup>[b]</sup>	94 (R) <sup>[e]</sup>
7	<b>2e</b>	2-naphthyl	<b>3e</b>	89	92
8	<b>2f</b>	2-(6-methoxynaphthyl)	<b>3f</b>	72	91
9 <sup>[d]</sup>	<b>2a</b>	<i>i</i> BuC <sub>6</sub> H <sub>4</sub>	<b>3a</b>	89	91 (S) <sup>[e]</sup>

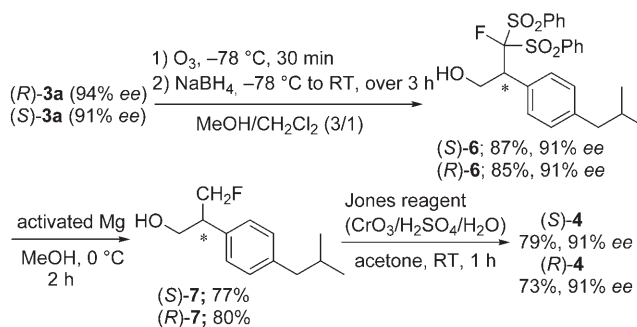
[a] Determined by HPLC analysis using CHIRALPAK AD-H or OD-H. [b] Reaction conditions: **1** (1.0 equiv), **2** (2.0 equiv), Cs<sub>2</sub>CO<sub>3</sub> (2.0 equiv), 2.5 mol % [Pd(C<sub>3</sub>H<sub>5</sub>)Cl]<sub>2</sub>, and 5 mol % (S)-PHOX at room temperature for 6 h. Yield is based on **1**. [c] The reaction was carried out at room temperature for 6 h. [d] (R)-PHOX (5 mol %) was used instead of (S)-PHOX. [e] See reference [13b].

molecules.<sup>[10b]</sup> A series of chiral ligands commonly employed were examined under conditions similar to those described above. We found that (+)-1,2-bis-*N*-(2'-(diphenylphosphino)-benzoyl)-(1*R*,2*R*)-diaminocyclohexane ((*R,R*)-DPPBA)<sup>[10f]</sup> was effective for the desymmetrization of the meso diester **2g** with **1** in the presence of  $[\text{Pd}(\text{C}_3\text{H}_5\text{Cl})_2]$  and  $\text{Cs}_2\text{CO}_3$  to afford the 1-fluorobis(phenylsulfonyl)methylated adduct **3g** in 87% yield with 95% *ee* (Scheme 1). Similarly, racemic acetate **2h** underwent efficient enantioselective reaction with **1** under the same conditions to provide enantioenriched **3h** in 75% with 96% *ee*.<sup>[13c]</sup>



**Scheme 1.** Palladium-catalyzed enantioselective allylic fluorobis(phenylsulfonyl)methylation of cyclic acetates **2g,h**.

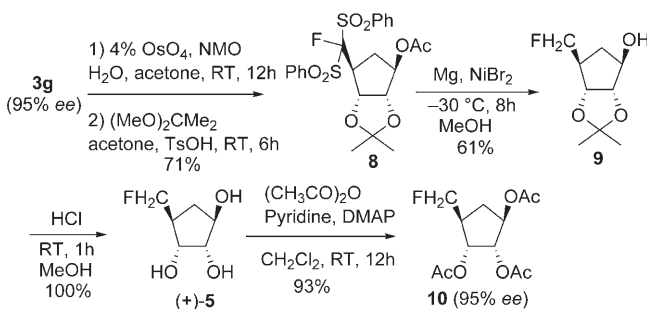
With facile access to this range of enantioenriched monofluorinated organic compounds, we next considered synthetic applications. Ibuprofen, a widely marketed non-steroidal anti-inflammatory drug (NSAID), is an interesting compound in terms of the pharmacokinetics of its enantiomers.<sup>[14]</sup> Ibuprofen exists as both *R* and *S* enantiomers, and it was revealed the metabolic chiral inversion of (*R*)-ibuprofen to the pharmacologically active *S* enantiomer occurs in humans. Racemic ibuprofen has been prescribed worldwide, and the *S* isomer, called dexibuprofen, is marketed in Austria and Switzerland. The physico-chemical and pharmacological properties and metabolic profiles of racemic ibuprofen and dexibuprofen are quite different, and a better understanding may be possible from studies of chiral derivatives of ibuprofen. A variety of ibuprofen derivatives have been prepared for this purpose including fluorinated ibuprofens;<sup>[15]</sup> we are interested in the previously unknown ibuprofen derivative **4**, which bears a fluoromethyl group.<sup>[16]</sup> Only the *R* enantiomer of **4** could potentially act as a suicide substrate by  $\beta$  elimination of HF by the enzyme during the chiral-inversion step, and it might consequently shed new light on the study of the pharmacokinetics of the enantiomers. To show the utility of our palladium-catalyzed enantioselective fluorobis(phenylsulfonyl)methylation reaction, we next applied the method for the synthesis of the ibuprofen analogues (*S*)- and (*R*)-**4** (Scheme 2). Similar to the conventional synthesis of ibuprofen,<sup>[10a]</sup> ozonolysis of (*R*)- and (*S*)-**3a** in  $\text{MeOH}/\text{CH}_2\text{Cl}_2$  (3:1) at  $-78^\circ\text{C}$  followed by reduction with



**Scheme 2.** Enantioselective synthesis of methylfluorinated ibuprofen **4**.

$\text{NaBH}_4$  gave the monofluoromethylated alcohols (*S*)- and (*R*)-**6** in yields of 87% and 85%, respectively, without major loss of enantiopurity (91% *ee*). The removal of the sulfonyl group at the fluorinated carbon by reaction with activated Mg in methanol afforded the chiral monofluoromethylated compounds (*S*)- and (*R*)-**7**, and subsequent oxidation with the Jones reagent gave the *S* and *R* enantiomers of **4**,<sup>[17]</sup> which were previously unknown.<sup>[16]</sup>

Carbafuranose is a synthetic target attracting much recent interest in view of both its enzyme inhibitor activities and antiviral properties.<sup>[18]</sup> Fluorinated carbohydrates have also recently received attention for their important role in the study of enzyme–carbohydrate interactions as well as their biological activities.<sup>[19]</sup> Therefore, fluoro sugars with a carbocyclic framework have emerged as important tools in this area. We examined the synthesis of 5-deoxy-5-fluoro- $\beta$ -D-carbarylbofuranose (**5**). The 1-fluorobis(phenylsulfonyl)methylated adduct **3g** (Scheme 1) underwent an osmium-catalyzed diastereoselective dihydroxylation; subsequent treatment with 2,2-dimethoxypropane furnished acetonide **8** in 71% yield (Scheme 3). Reductive double-desulfonylation of **8**



**Scheme 3.** Enantioselective synthesis of 5-deoxy-5-fluoro- $\beta$ -D-carbarylbofuranose (**5**).

using  $\text{Mg}/\text{NiBr}_2/\text{MeOH}$ <sup>[20]</sup> gave monofluoromethylated **9** in 61% yield. Finally, the acetonide moiety on **9** was removed by acid treatment to afford (+)-**5**, a previously unknown fluoro isostere of  $\beta$ -D-carbarylbofuranose, quantitatively.<sup>[21]</sup> The enantiopurity of (+)-**5** was determined to be 95% by chiral HPLC analysis of triacetate **10**.

In conclusion, 1-fluorobis(phenylsulfonyl)methane (**1**), a newly designed synthetic equivalent for the fluoromethide species, affords the enantiopure fluoromethylated products **3**

in a palladium-catalyzed allylic fluorobis(phenylsulfonyl)methylation reaction. The effect of fluorine substitution on the reactivity and enantioselectivity of the reagent **1** is remarkable. The products **3a** were readily converted to chiral methylfluorinated ibuprofens (*S*)- and (*R*)-**4** by reductive desulfonylation and oxidation. The biologically important fluoro- $\beta$ -D-carbaribofuranose **5** was also synthesized from **3g** by dihydroxylation and reductive desulfonylation. The present methodology can be applicable for a wider variety of monofluoromethylated derivatives of NSAIDs and fluoro sugars. The biological activities of (*S*)- and (*R*)-**4** as NSAIDs and the pharmacokinetics of the enantiomers of **4** will be evaluated and reported in due course.

Received: February 16, 2006

Revised: May 15, 2006

Published online: July 4, 2006

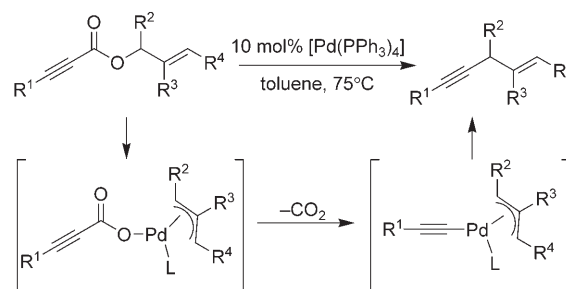
**Keywords:** asymmetric synthesis · drug design · fluorine · fluoromethylation · palladium

- [1] a) *Biomedical Aspects of Fluorine Chemistry* (Eds.: R. Filler, Y. Kobayashi), Elsevier Biomedical Press and Kodansha Ltd, New York, **1982**; b) "Biomedical Frontiers of Fluorine Chemistry": *ACS Symp. Ser.* **1996**, 639; c) *Organofluorine Compounds in Medicinal Chemistry and Biomedical Applications* (Eds.: R. Filler, Y. Kobayashi, L. M. Yagupolskii), Elsevier, Amsterdam, **1993**.
- [2] a) *Enantiocontrolled Synthesis of Fluoro-Organic Compounds: Stereochemical Challenges and Biomedical Targets* (Ed.: V. A. Soloshonok), Wiley, Chichester, **1999**; b) "Asymmetric Fluoroorganic Chemistry. Synthesis, Applications, and Future Directions": *ACS Symp. Ser.* **2000**, 746; c) R. D. Chambers, *Fluorine in Organic Chemistry*, Blackwell Publishing, Oxford, UK, **2004**; d) P. Kitsch, *Modern Fluoroorganic Chemistry*, Wiley-VCH, Weinheim, **2004**.
- [3] a) H. Ibrahim, A. Togni, *Chem. Commun.* **2004**, 1147–1155; b) J.-A. Ma, D. Cahard, *Chem. Rev.* **2004**, 104, 6119–6146; c) G. K. S. Prakash, A. K. Yudin, *Chem. Rev.* **1997**, 97, 757–786; d) After submission of this manuscript, the diastereoselective nucleophilic monofluoromethylation of imines with fluoro-methyl phenyl sulfone was described: Y. Li, C. Ni, J. Liu, L. Zhang, J. Zheng, L. Zhu, J. Hu, *Org. Lett.* **2006**, 8, 1693–1696.
- [4] a) *Fusso Yakugaku* (Eds.: Y. Kobayashi, I. Kumadaki, T. Taguchi), Hirokawa, Tokyo, **1992**; b) *Organofluorine Chemistry: Principles and Commercial Applications* (Eds.: R. E. Banks, B. E. Smart, J. C. Tatlow), Plenum, New York, **1994**, chap. 3; c) B. E. Smart, *J. Fluorine Chem.* **2001**, 109, 3–11.
- [5] a) G. W. Gribble, *J. Chem. Educ.* **1973**, 50, 460–462; b) R. Peters, R. W. Wakelin, *Proc. R. Soc. London Ser. B* **1953**, 140, 497–507; c) E. Kun, R. J. Dummel, *Methods Enzymol.* **1969**, 13, 623–672.
- [6] a) D. O'Hagan, H. S. Rzepa, *Chem. Commun.* **1997**, 645–652; b) J. Kollonitsch in *Biomedical Aspects of Fluorine Chemistry*, (Eds.: R. Filler, Y. Kobayashi), Elsevier Biomedical Press and Kodansha Ltd, New York, Tokyo, **1982**, pp. 93–122; c) R. H. Abeles, A. L. Maycock, *Acc. Chem. Res.* **1976**, 9, 313–319; d) R. B. Silverman, S. M. Nanavati, *J. Med. Chem.* **1990**, 33, 931–936; e) J. Kollonitsch, A. A. Patchett, S. Marburg, A. L. Maycock, L. M. Perkins, G. A. Doldouras, D. E. Duggan, S. D. Aster, *Nature* **1978**, 274, 906–908.
- [7] a) N. Shibata, J. Kohno, K. Takai, T. Ishimaru, S. Nakamura, T. Toru, S. Kanemasa, *Angew. Chem.* **2005**, 117, 4276–4279; *Angew. Chem. Int. Ed.* **2005**, 44, 4204–4207; b) N. Shibata, E. Suzuki, Y. Takeuchi, *J. Am. Chem. Soc.* **2000**, 122, 10728–10729; c) N. Shibata, E. Suzuki, T. Asahi, M. Shiro, *J. Am. Chem. Soc.* **2001**, 123, 7001–7009; d) N. Shibata, T. Ishimaru, E. Suzuki, K. L. Kirk, *J. Org. Chem.* **2003**, 68, 2494–2497; e) N. Shibata, T. Ishimaru, T. Nagai, J. Kohno, T. Toru, *Synlett* **2004**, 1703–1706; f) N. Shibata, T. Ishimaru, M. Nakamura, T. Toru, *Synlett* **2004**, 2509–2512; g) N. Shibata, T. Tarui, Y. Doi, K. L. Kirk, *Angew. Chem.* **2001**, 113, 4593–4595; *Angew. Chem. Int. Ed.* **2001**, 40, 4461–4463; .
- [8] a) G. K. S. Prakash, J. Hu, G. A. Olah, *J. Org. Chem.* **2003**, 68, 4457–4463; b) Y. Li, J. Hu, *Angew. Chem.* **2005**, 117, 6032–6036; *Angew. Chem. Int. Ed.* **2005**, 44, 5882–5886.
- [9] S. Nakamura, T. Fukuzumi, T. Toru, *Chirality* **2004**, 16, 10–12.
- [10] a) L. Acemoglu, J. M. J. Williams, *J. Mol. Catal. A* **2003**, 196, 3–11; b) B. M. Trost, M. L. Crawley, *Chem. Rev.* **2003**, 103, 2921–2944; c) P. V. Matt, A. Pfaltz, *Angew. Chem.* **1993**, 105, 614–615; *Angew. Chem. Int. Ed. Engl.* **1993**, 32, 566–568; d) J. Sprinz, G. Helmchen, *Tetrahedron Lett.* **1993**, 34, 1769–1772; e) G. J. Dawson, C. G. Frost, J. M. J. Williams, S. J. Coote, *Tetrahedron Lett.* **1993**, 34, 3149–3150; f) B. M. Trost, D. L. V. Vranken, C. Bingel, *J. Am. Chem. Soc.* **1992**, 114, 9327–9343.
- [11] a) See the Supporting Information. b) A typical experimental procedure is given in the Supporting Information.
- [12] H. J. Castejon, K. B. Wiberg, *J. Org. Chem.* **1998**, 63, 3937–3942.
- [13] a) The reaction mechanism is discussed in the Supporting Information. b) Absolute stereochemistries were assigned by X-ray crystallographic analysis (for **3d**, see the Supporting Information) or tentatively determined by comparing the optical rotations of **3a** and **3b** with those of their non-fluorinated derivatives (see the Supporting Information); c) Enantiomeric excesses of **3g,h** were determined by HPLC analysis using CHIRALCEL OD-H. The absolute stereochemistry of **3g** was assigned based on the proposed reaction mechanism (see reference [10b, f] and the Supporting Information) and tentatively determined by comparing the optical rotation with that of  $\beta$ -D-carbaribofuranose after chemical derivatization of **3g** to 5-deoxy-5-fluoro- $\beta$ -D-carbaribofuranose (**5**) (see Scheme 3).
- [14] H. Hao, G. Wang, J. Sun, *Drug Metab. Rev.* **2005**, 37, 215–234.
- [15] a) O. Goj, S. Kotila, G. Haufe, *Tetrahedron* **1996**, 52, 12761–12774; b) W. J. Middleton, E. M. Bingham, *J. Fluorine Chem.* **1983**, 22, 561–574; c) Y. Yamazaki, S. Yusa, Y. Kageyama, H. Tsue, K. Hirao, H. Okuno, *J. Fluorine Chem.* **1996**, 79, 167–171; d) M. Schlosser, D. Michel, Z. Guo, C. J. Sih, *Tetrahedron* **1996**, 52, 8257–8262; e) M. Villa, N. J. Smeyers, M. -L. Senent, Y. G. Smeyers, *THEOCHEM* **2001**, 537, 265–269; f) Y. Takeuchi, H. Fujisawa, T. Fujiwara, M. Matsuura, H. Komatsu, S. Ueno, T. Matsuzaki, *Chem. Pharm. Bull.* **2005**, 53, 1062–1064.
- [16] Other monofluoromethylarylpropionic acid derivatives besides **4** have been reported: a) D. Haigh, L. J. Jefcott, K. Magee, H. McNab, *J. Chem. Soc. Perkin Trans. 1* **1996**, 2895–2900; b) M. C. Lu, L. B. Shih, H. S. Jae, J. E. Gearien, E. B. Thompson, *J. Med. Chem.* **1987**, 30, 424–427; c) S. Hamman, C. G. Beguin, *Tetrahedron Lett.* **1983**, 24, 57–60; d) J. Barker, R. Keck, J. Rétey, *Tetrahedron Lett.* **1982**, 23, 1549–1552; e) F. Faustini, S. D. Munari, A. Panzeri, V. Villa, C. A. Gandolfi, *Tetrahedron Lett.* **1981**, 22, 4533–4536; f) G. A. Olah, G. K. S. Prakash, Y. L. Chao, *Helv. Chim. Acta* **1981**, 64, 2528–2530; g) R. Keck, J. Rétey, *Helv. Chim. Acta* **1980**, 63, 769–772; h) Y. Yamazaki, S. Yusa, Y. Kageyama, H. Tsue, K. Hirao, H. Okuno, *J. Fluorine Chem.* **1996**, 79, 167–171.
- [17] Absolute stereochemistries were determined by comparing the optical rotations of **4** with those of ibuprofen. (*S*)-**4** (91% ee):  $[\alpha]_D^{30} = +50.1$  ( $c = 0.57$  in EtOH); (*R*)-**4** (91% ee):  $[\alpha]_D^{30} = -50.1$  ( $c = 0.68$ , EtOH); (*S*)-ibuprofen (91% ee):  $[\alpha]_D^{30} = +60$  ( $c = 2$  in EtOH), see D. G. Kaiser, G. J. Vangiessen, R. J. Reischer, W. J. Weckter, *J. Pharm. Sci.* **1976**, 65, 269–273.

- [18] For example: a) M. T. Crimmins, *Tetrahedron* **1998**, *54*, 9229–9272; b) E. De Clercq, *Nucleosides Nucleotides* **1998**, *17*, 625–634; c) V. E. Marquez, *Adv. Antiviral Drug Des.* **1996**, *2*, 89–146; d) T. S. Mansour, R. Storer, *Curr. Pharm. Des.* **1997**, *3*, 227–264; e) G. Rassu, L. Auzzas, L. Pinna, V. Zambrano, L. Battistini, F. Zanardi, L. Marzocchi, D. Acquotti, G. Casiraghi, *J. Org. Chem.* **2001**, *66*, 8070–8075.
- [19] For example: a) P. Hadwiger, P. Mayr, B. Nidetzky, A. E. Stütz, A. Tauss, *Tetrahedron: Asymmetry* **2000**, *11*, 607–620; b) C. Schaffrath, S. L. Cobb, D. O'Hagan, *Angew. Chem.* **2002**, *114*, 4069–4071; *Angew. Chem. Int. Ed.* **2002**, *41*, 3913–3915; c) E. P. J. Boot, G. A. Koning, G. Storm, J. P. A. Wagenaar-Hilbers, W. van Eden, L. A. Everse, M. H. M. Wauben, *Arthritis Res. Ther.* **2005**, *7*, R604–R615.
- [20] I. Das, T. Pathak, *Org. Lett.* **2006**, *8*, 1303–1306.
- [21] (+)-**5** (95 % *ee*):  $[\alpha]_{\text{D}}^{30} = +10.6$  ( $c = 0.98$  in MeOH).  $\beta$ -D-carba-ribofuranose:  $[\alpha]_{\text{D}}^{20} = +10.0$  ( $c = 1.1$  in MeOH). See reference [18e].



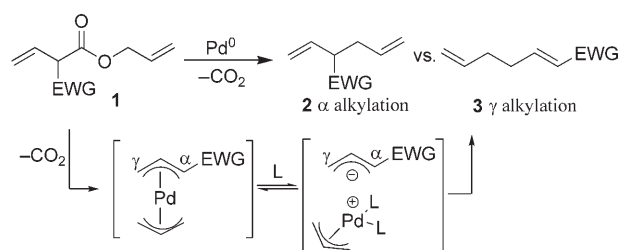
Recently, our group developed an  $sp^3$ – $sp^3$  coupling of allyl electrophiles with acetylide nucleophiles (Scheme 1).<sup>[6]</sup> In doing so, it was demonstrated that decarboxylative metalation can be used to access organometallic intermediates, and is



**Scheme 1.** Decarboxylative  $sp^3$ – $sp^3$  coupling of allyl electrophiles with acetylide nucleophiles.

thus an alternative to transmetalation. Such decarboxylative coupling reactions are advantageous because they allow the use of readily available carboxylic acids or esters (as opposed to organometallic reagents), occur under neutral conditions, and produce  $CO_2$  as the only by-product.<sup>[7,8]</sup>

As decarboxylative metalation can potentially be used to circumvent transmetalation, it is desirable to determine what other types of organometallic intermediates can be accessed by decarboxylation. With the goal of developing an alternative to the Stille-type allyl–allyl coupling, we became curious as to whether the loss of  $CO_2$  from 3-butenates could be used to produce bis(allyl) palladium complexes, thus allowing the coupling of two allyl species (Scheme 2).



**Scheme 2.** Decarboxylative  $sp^3$ – $sp^3$  coupling. EWG = electron-withdrawing group.

The  $sp^3$ – $sp^3$  coupling of two allyl fragments is a potentially powerful way of generating 1,5-dienes, which are found in a host of biologically active natural products.<sup>[1]</sup> However, there are surprisingly few catalytic transformations that couple two different allyl groups with high selectivity.<sup>[2–4]</sup> Seminal studies by Schwartz showed that electrophilic  $\pi$ -allyl palladium complexes, which are conveniently accessed by oxidative addition of allylic acetates, underwent stoichiometric coupling with nucleophilic magnesium allyl reagents.<sup>[4]</sup> Presumably this reaction proceeds by transmetalation from Mg to give bis(allyl) palladium complexes which reductively eliminate the hexadiene.<sup>[5]</sup> Transmetalation from tin was also possible, and allowed the catalytic Stille-type coupling of allylic bromides with allyl stannanes.<sup>[4]</sup> However, this method is clearly nonideal because it suffers from poor yields and requires the synthesis and use of stoichiometric quantities of toxic allyl stannanes.

Our research in this area has led us to believe that the rate of decarboxylation correlates with the  $pK_b$  of the anion generated following loss of  $CO_2$ .<sup>[7]</sup> Therefore, the development of a decarboxylative  $sp^3$ – $sp^3$  coupling was initiated using substrates **1**, where the allyl anion generated by decarboxylation is potentially stabilized by an electron-withdrawing carbonyl group such as a ketone.<sup>[9]</sup> Such substrates are readily prepared by the  $In(OTf)_3$ -catalyzed vinylation ( $TfO$  = trifluoromethanesulfonate) of  $\beta$ -keto esters with acetylenes.<sup>[10]</sup> Decarboxylation of these substrates could lead to two possible unsaturated ketones: one derived from alkylation of the  $\alpha$  position of the dienolate generated upon decarboxylation (**2**), and the other generated from  $\gamma$  alkylation of the

## Allylation

DOI: 10.1002/anie.200600721

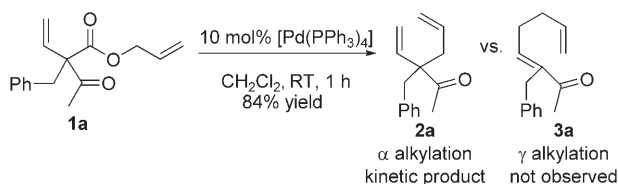
### A Versatile Hexadiene Synthesis by Decarboxylative $sp^3$ – $sp^3$ Coupling/Cope Rearrangement

Shelli R. Waetzig, Dinesh K. Rayabarapu, Jimmie D. Weaver, and Jon A. Tunge\*

[\*] S. R. Waetzig, D. K. Rayabarapu, J. D. Weaver, Prof. J. A. Tunge  
Department of Chemistry  
University of Kansas  
1251 Wescoe Hall Drive, Lawrence, KS 66045-7582 (USA)  
Fax: (+1) 785-864-5396  
E-mail: tunge@ku.edu

Supporting information for this article is available on the WWW under <http://www.angewandte.org> or from the author.

dienolate (**3**, Scheme 2).<sup>[11]</sup> It was gratifying to find that treatment of **1a** with 10 mol % [Pd(PPh<sub>3</sub>)<sub>4</sub>] in CH<sub>2</sub>Cl<sub>2</sub> resulted in the formation of  $\alpha$ -allylated product **2a** in 84% yield of isolated product (Scheme 3).

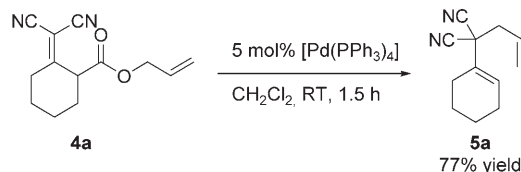


**Scheme 3.** Decarboxylative dienolate allylation.

A variety of vinyl-substituted  $\beta$ -keto esters likewise provided the  $\alpha$ -alkylation product as the only isolated product. As shown in Table 1, the reaction allows coupling of a variety of substituted allyl fragments with an unsubstituted allyl group. In fact, the chemistry was only limited by the variety of substrates that could be prepared by the vinylation of  $\beta$ -keto esters.<sup>[10]</sup>

As a consequence of the success of the catalytic decarboxylation of vinylic  $\beta$ -keto esters, our focus shifted to other compounds that incorporate electron-withdrawing groups

capable of facilitating decarboxylative metalation. Additionally, we were curious as to whether electron-withdrawing groups could initially be integrated at the olefinic position of the nucleophilic allyl fragment rather than at the position  $\alpha$  to the ester group. As nitrile groups are expected to stabilize the incipient charge during decarboxylation and can be further manipulated by reduction or hydrolysis, alkylidene malononitriles **4** were chosen as promising substrates. Moreover, the starting materials are easily prepared by a simple Knoevenagel condensation of malononitrile<sup>[12]</sup> with readily available allylic  $\beta$ -keto esters.<sup>[13]</sup> To test the feasibility of the proposed reaction, **4a** was allowed to react with 5 mol % [Pd(PPh<sub>3</sub>)<sub>4</sub>] in CH<sub>2</sub>Cl<sub>2</sub> (Scheme 4). After 1.5 h at ambient temperature, the



**Scheme 4.** Decarboxylative dicyanoallyl allylation.

reaction was complete and the product was isolated as a single regioisomer in good yield. Importantly, the analogous control reaction of **4a**, which was run in the absence of catalyst at 150°C for 30 min, showed no degradation or product formation. Thus, the reaction is palladium-catalyzed, and the predominance of  $\alpha$  alkylation indicates that the regioselectivity is the result of kinetic control.

We further examined the reactivity of other alkylidene malononitriles in the presence of a catalytic amount of [Pd(PPh<sub>3</sub>)<sub>4</sub>] and found that the reaction was tolerant of a variety of electrophilic allyl fragments (Table 2). Primary, substituted, cyclic, and acyclic allylic esters were all used, and the substitution pattern had no substantial effect on yields or reaction rates. Esters of disubstituted allylic alcohols exhibit excellent regioselectivity in favor of  $\alpha$  alkylation, while those of terminally unsubstituted allylic alcohols give rise to mixtures of  $\alpha$ - and  $\gamma$ -alkylated products.<sup>[14]</sup> These results suggest that the  $\alpha$  position is sterically less hindered and  $\gamma$  alkylation can be avoided if one employs a sufficiently large allylic alcohol fragment. Additionally, as might be expected for a reaction involving  $\pi$ -allyl palladium intermediates, ester **4i** of a monosubstituted allylic alcohol undergoes highly regioselective alkylation at the less substituted allyl terminus. Thus, decarboxylative coupling results in regioselective  $\alpha$  coupling at the cyanoallyl fragment and coupling at the electrophilic allyl fragment occurs at the less hindered site.

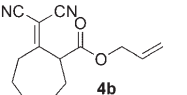
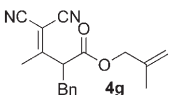
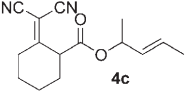
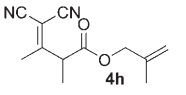
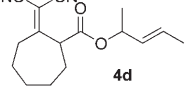
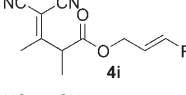
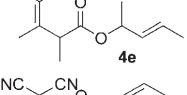
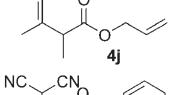
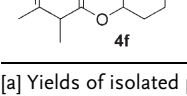
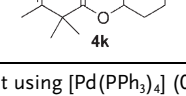
In addition to the regioselectivity of C–C bond formation, the utility of decarboxylative coupling lies in the ability to kinetically and *regiospecifically* generate allyl anion equivalents (Scheme 5). In contrast, generation of the equivalent anions by metalation with a strong base would produce mixtures of regioisomers (Scheme 5).<sup>[2a]</sup> By utilizing decarboxylative metalation, a variety of cyclic and acyclic dicyanoallyl anion equivalents are generated regiospecifically at the site that carries the carboxy group. One current limitation of this chemistry is that substitution at the  $\alpha$  position of the

**Table 1:** Decarboxylative allyl–dienolate coupling.<sup>[a]</sup>

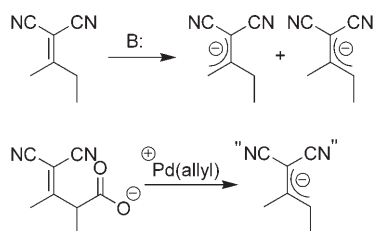
Substrate	Product	Yield [%]
		65
		77
		86
		61
		79
		80
		69
		82

[a] Yields of isolated products for reactions carried out using [Pd(PPh<sub>3</sub>)<sub>4</sub>] (0.05 mmol) and allyl  $\beta$ -keto esters (0.50 mmol) in CH<sub>2</sub>Cl<sub>2</sub> (3.0 mL) at room temperature under N<sub>2</sub> for 0.5–1 h.

**Table 2:** Decarboxylative coupling of alkylidene malononitriles.<sup>[a]</sup>

Substrate	$\alpha/\gamma$	Yield [%]	Substrate	$\alpha/\gamma$	Yield [%]
	78:22	80 <sup>[d]</sup>		79:21	58 <sup>[d]</sup>
	> 97:3	97		62:38	76 <sup>[d]</sup>
	93:7	84		86:14	97 <sup>[d]</sup>
	> 95:5 <sup>[b]</sup>	84		84:16	91 <sup>[d]</sup>
	> 95:5 <sup>[c]</sup>	92		> 95:5	93

[a] Yields of isolated products for reactions carried out using  $[\text{Pd}(\text{PPh}_3)_4]$  (0.05 mmol) and  $\beta$ -alkylidene malononitrile (1.0 mmol) in  $\text{CH}_2\text{Cl}_2$  (5 mL) at room temperature under  $\text{N}_2$  for 1–2 h. [b]  $E/Z = 15:1$ . [c]  $E/Z = 8.3:1$ . [d] Combined yield of two isomers.

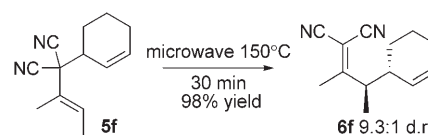

**Scheme 5.** Regiospecific generation of allyl anion equivalents. B = base.

substrates is necessary to prevent decomposition of the starting materials. However, Table 2 shows that compounds that are  $\alpha$ -substituted undergo coupling in good to excellent yields. Furthermore, NOE measurements indicate that the resulting olefinic products are preferentially formed as the *E* isomers.

The  $\alpha$ -selective decarboxylative allyl–allyl coupling is an efficient route to 1,5-dienes, whereas the development of an analogous  $\gamma$ -selective transformation would provide a versatile synthetic method for the synthesis of 1,5-hexadienes. In this regard, it was expected that Cope rearrangements could be used to access the thermodynamically favored  $\gamma$ -allylation products directly from the  $\alpha$ -allylation products. The resulting  $\alpha,\beta$ -unsaturated nitriles and ketones are expected to be versatile synthetic intermediates as a result of the electronic differentiation of the two olefinic double bonds. With this in mind, the optimal conditions for Cope rearrangement of the  $\alpha$ -allylation products to produce  $\gamma$ -allylation products were briefly investigated. Specifically, a number of the products were treated to either thermal conditions in a microwave reactor or conditions for  $\text{Pd}^{\text{II}}$  catalysis as described by Overman and Renaldo,<sup>[15]</sup> to afford the  $\alpha,\beta$ -unsaturated 1,5-dienes.<sup>[16]</sup>

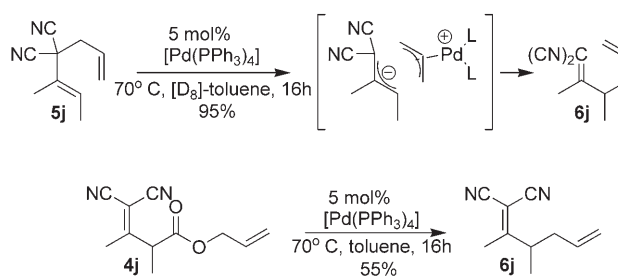
The  $\text{Pd}^{\text{II}}$ -catalyzed Cope rearrangement occurs under mild conditions with substrates such as **2i**, but the rearrangement is limited to substrates that are substituted at the 2- or 5-position as outlined by Overman and Renaldo.<sup>[17]</sup> For substrates that do not meet the criteria necessary for  $\text{Pd}^{\text{II}}$ -catalyzed rearrangement (that is, **2a**), the Cope rearrangement was effected in excellent yield by heating at 180°C in a microwave reactor.<sup>[18]</sup>

The  $\alpha$ -alkylated isomers of alkylidene malononitriles likewise underwent thermal Cope rearrangement to give the  $\gamma$ -alkylated isomers in a microwave reactor at 150°C in essentially quantitative yields (Scheme 6). Moreover, the Cope rearrangements occurred


**Scheme 6.** Microwave-assisted Cope rearrangement.

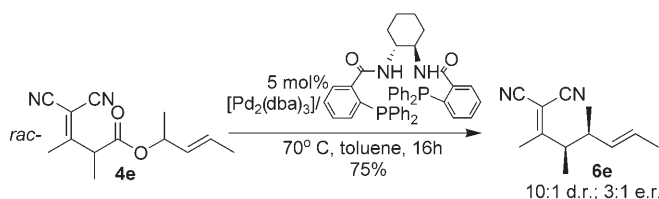
with the expected stereochemical control to provide substrates with contiguous stereocenters in good diastereoselectivity.

In addition to more standard thermal and  $\text{Pd}^{\text{II}}$ -catalyzed Cope rearrangements, Yamamoto and co-workers have demonstrated that it is possible to catalyze a Cope-like rearrangement of  $\alpha$ -allylation products resembling **5** by using  $\text{Pd}^0$ .<sup>[2a]</sup> As our decarboxylative coupling method allows the synthesis of a wide variety of  $\alpha$ -allylated products, we are able to subject these substrates to modified conditions for  $\text{Pd}^0$ -catalyzed Cope rearrangements. For example, the  $\alpha$ -allylation product **5j** underwent rearrangement to the  $\gamma$ -allylation product **6j** upon treatment with  $[\text{Pd}(\text{PPh}_3)_4]$  in toluene at 70°C (Scheme 7).


**Scheme 7.**  $\text{Pd}^0$ -catalyzed tandem allylation/Cope rearrangement.

The control reaction without  $[\text{Pd}(\text{PPh}_3)_4]$  resulted in <5% rearrangement under identical conditions. The fact that the decarboxylative coupling and the Cope-like rearrangement are both  $\text{Pd}^0$ -catalyzed suggested that a one-pot tandem decarboxylative allylation/Cope rearrangement was feasible. Indeed, reaction of the alkylidene malononitrile **4j** with  $[\text{Pd}(\text{PPh}_3)_4]$  in toluene at 70 °C provided the  $\gamma$ -allylation product **6j** as the exclusive regioisomer (Scheme 7).

Finally, the ability to perform a tandem decarboxylative coupling/Cope rearrangement suggested that an asymmetric rearrangement might be possible through appropriate choice of a chiral ligand. To test the feasibility of this approach, the rearrangement of *rac*-**4e** was performed using  $\text{Pd}^0$  modified with the Trost ligand, which led to product formation in good yield with high diastereoselectivity and modest enantioselectivity (Scheme 8). While the enantioselectivity is not optimal,



**Scheme 8.** Asymmetric tandem allylation/Cope rearrangement. dba = *trans,trans*-dibenzylideneacetone.

this reaction represents the first asymmetric rearrangement of this type. Moreover, the ability to set contiguous stereocenters by  $\text{Pd}^0$ -catalyzed allylation is rare, and thus tandem allylation/Cope rearrangements will potentially allow extension of allylation strategies to new substrates. Current efforts are directed toward maximizing the enantioselectivity of the allyl–allyl coupling while maintaining high diastereoselectivities.

In summary, we have shown that  $\text{Pd}^0$ -catalyzed decarboxylation is a simple and convenient way to trigger the formation of nucleophilic allyl species in the presence of electrophilic  $\pi$ -allyl palladium complexes. The resulting  $\text{sp}^3$ – $\text{sp}^3$  coupling reaction favors kinetic allylation at a position  $\alpha$  to electron-withdrawing groups, and the analogous  $\gamma$ -allylation products can be obtained by conversion to the thermodynamic product under conditions of microwave irradiation or  $\text{Pd}^{\text{II}}$  catalysis. With sufficiently stabilized allyl nucleophiles, the Cope rearrangement can be catalyzed by  $\text{Pd}^0$ , which leads to the development of a tandem allylation/Cope rearrangement. Thus, either  $\alpha$ - or  $\gamma$ -coupling products are available in high yield from methylene malononitrile nucleophiles, and the desired regioisomer is obtained simply by controlling the temperature of the reaction mixture.

## Experimental Section

General procedure for the palladium-catalyzed decarboxylation of vinylic  $\beta$ -keto esters: A round-bottom side-arm flask (25 mL) containing  $[\text{Pd}(\text{PPh}_3)_4]$  (0.050 mmol, 10.0 mol %) was evacuated and purged with argon gas. An allylic  $\beta$ -keto ester (0.50 mmol) and dichloromethane were added to the system and the reaction mixture was stirred at room temperature for 0.5–1.5 h. Next, the mixture was diluted with dichloromethane and filtered through a short Celite and

silica gel pad. The filtrate was concentrated and the residue was purified on a column of silica gel using hexane/dichloromethane (85:15) as eluent to afford the decarboxylative coupling products **2**.

General procedure for the palladium-catalyzed decarboxylation of alkylidene malononitriles: In a dried Schlenk flask under argon,  $[\text{Pd}(\text{PPh}_3)_4]$  (0.025 mmol) was added to substrates **4** (0.5 mmol) dissolved in dichloromethane (5 mL). The reaction mixture was stirred at room temperature for 1–2 h, then concentrated and directly purified by flash chromatography ( $\text{SiO}_2$ , 5% EtOAc/hexane).

Received: February 23, 2006

Revised: April 9, 2006

Published online: July 3, 2006

**Keywords:** allylation · decarboxylation · hexadienes · palladium · rearrangement

- [1] a) W. Boland, G. Pohnert, I. Maier, *Angew. Chem.* **1995**, *107*, 1717; *Angew. Chem. Int. Ed. Engl.* **1995**, *34*, 1602; b) M. J. Calvert, P. R. Ashton, R. K. Allemann, *J. Am. Chem. Soc.* **2002**, *124*, 11 636; c) A. Quintana, J. Reinhard, R. Faure, P. Uva, A.-G. Bagnères, G. Massiot, J.-L. Clément, *J. Chem. Ecol.* **2003**, *29*, 639.
- [2] a) H. Nakamura, H. Iwama, M. Ito, Y. Yamamoto, *J. Am. Chem. Soc.* **1999**, *121*, 10850; b) M. Mendez, J. M. Cuerva, E. Gomez-Bengoa, D. J. Cardenas, A. M. Echavarren, *Chem. Eur. J.* **2002**, *8*, 3620.
- [3] *Metal-Catalyzed Cross-Coupling Reactions* (Eds.: A. deMeijere, F. Diederich), 2nd ed., Wiley-VCH, New York, **2004**.
- [4] A. Goliaszewski, J. Schwartz, *Tetrahedron* **1985**, *41*, 5779.
- [5] a) K. J. Szabó, *Chem. Eur. J.* **2004**, *10*, 5268; b) D. J. Cardenas, E. M. Echavarren, *New J. Chem.* **2004**, *28*, 338.
- [6] D. K. Rayabarapu, J. A. Tunge, *J. Am. Chem. Soc.* **2005**, *127*, 13510.
- [7] a) E. C. Burger, J. A. Tunge, *Org. Lett.* **2004**, *6*, 4113; b) J. A. Tunge, E. C. Burger, *Eur. J. Org. Chem.* **2005**, 1715; c) S. R. Mellegaard-Waetzig, D. K. Rayabarapu, J. A. Tunge, *Synlett* **2005**, 2759.
- [8] For other recent decarboxylative allylations, see: a) M. Nakamura, A. Hajra, K. Endo, E. Nakamura, *Angew. Chem.* **2005**, *117*, 7414; *Angew. Chem. Int. Ed.* **2005**, *44*, 7248; b) B. M. Trost, J. Xu, *J. Am. Chem. Soc.* **2005**, *127*, 17180; c) J. T. Mohr, D. C. Behenna, A. M. Harned, B. M. Stoltz, *Angew. Chem.* **2005**, *117*, 7084; *Angew. Chem. Int. Ed.* **2005**, *44*, 6924.
- [9] Simple 3-butenic acid derivatives do not undergo metal-catalyzed decarboxylation under mild conditions.
- [10] a) M. Nakamura, K. Endo, E. Nakamura, *J. Am. Chem. Soc.* **2003**, *125*, 13002; b) M. Nakamura, K. Endo, E. Nakamura, *Org. Lett.* **2005**, *7*, 3279.
- [11] a) Y. Sato, Y. Oonishi, M. Mori, *J. Org. Chem.* **2003**, *68*, 9858; b) M. Sugiura, Y. Yagi, S.-Y. Wei, T. Nakai, *Tetrahedron Lett.* **1998**, *39*, 4351; c) P. M. Savu, J. A. Katzenellenbogen, *J. Org. Chem.* **1981**, *46*, 239.
- [12] T. R. Kasturi, V. K. Sharma, A. Srinivasan, *Tetrahedron* **1973**, *29*, 4103.
- [13] a) I. Collado, C. Pedregal, A. Mazon, J. F. Espinosa, J. Blanco-Urgoiti, D. D. Schoepp, R. A. Wright, B. G. Johnson, A. E. Kingston, *J. Med. Chem.* **2002**, *45*, 3619; b) A. Wilson, C. Augelli, *Org. Synth.* **1990**, *68*, 210.
- [14] The isomers were readily separated by column chromatography.
- [15] L. E. Overman, A. F. Renaldo, *Tetrahedron Lett.* **1982**, *23*, 3757.
- [16] See the Supporting Information for details of the Cope rearrangements.
- [17] L. E. Overman, A. F. Renaldo, *J. Am. Chem. Soc.* **1990**, *112*, 3945.
- [18] C. O. Kappe, *Angew. Chem.* **2004**, *116*, 6408; *Angew. Chem. Int. Ed.* **2004**, *43*, 6250.



# Oxygen-Balanced Energetic Ionic Liquid\*\*

C. Bigler Jones, Ralf Haiges, Thorsten Schroer, and Karl O. Christe\*

Energetic ionic liquids (EILs) are of great interest.<sup>[1–3]</sup> They offer enhanced stability, higher densities, no vapor pressure, and, hence, no vapor toxicity. As a general principle, the stability of energetic ionic compounds can be greatly enhanced by making the cation the fuel and the anion the oxidizer. The formal positive charge increases the ionization potential of the fuel cation, and the formal negative charge decreases the electron affinity of the anion. In this manner, the fuel cation becomes more oxidizer-resistant, and the oxidizer anion is protected against premature reduction by the cation. For environmental reasons, it is also desirable to avoid halogen-containing ingredients, such as perchlorates.

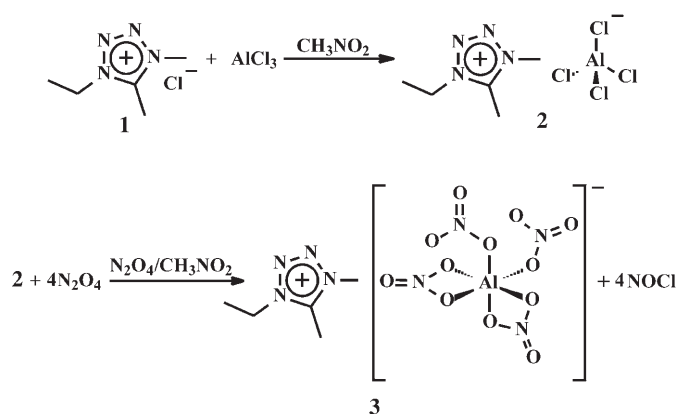
The previously known EILs consist of small oxidizing anions, such as  $\text{ClO}_4^-$ ,  $\text{NO}_3^-$ , or  $\text{N}(\text{NO}_2)_2^-$ , and large fuel cations containing quaternary nitrogen heterocycles with long, asymmetric, poorly packing side chains. The most serious drawback of these EILs is that they are under-oxidized. The small anions do not carry sufficient oxygen for complete oxidation of the large fuel cations to carbon monoxide, resulting in poor performance. In rocket propulsion, a low molecular weight of the exhaust products is very important.<sup>[4,5]</sup> Furthermore, at high flame temperatures  $\text{CO}_2$  is dissociated almost completely to  $\text{CO}$  and  $\text{O}_2$  (Boudouard equilibrium).<sup>[6]</sup> Therefore, it is often sufficient to oxidize the carbon content only to  $\text{CO}$  and not to  $\text{CO}_2$  to achieve near-maximum performance.<sup>[5]</sup> The aim of this study was the preparation of halogen-free, CO-balanced, EILs.

In 1998, the concept of oxidizer-balanced EILs was proposed, and in 2002, its practicability was shown by the preparation of 1-ethyl-3-methylimidazolium tetranitratoborate,<sup>[7]</sup> a compound that turned out to be indeed an ionic liquid with a freezing point of  $-25^\circ\text{C}$ . However, its energy content and thermal stability were marginal. Herein, we report on a significantly improved compound using the tetranitratooaluminate anion as a thermally more stable high-

oxygen carrier and the 1-ethyl-4,5-dimethyltetrazolium cation as a more energetic counterion (imidazole,  $\Delta H_f^\circ = +49.8 \text{ kJ mol}^{-1}$ ;<sup>[8]</sup> tetrazole,  $\Delta H_f^\circ = +237.1 \text{ kJ mol}^{-1}$ <sup>[9]</sup>). These are the first CO-balanced EILs. Although an oxygen-balanced tetrazolium salt, 5-aminotetrazolium nitrate, was recently reported,<sup>[10]</sup> its melting point of  $173^\circ\text{C}$  does not classify it as an ionic liquid.

Polynitratooaluminates were first studied in the 1960s in the USA<sup>[11]</sup> and, subsequently, during the 1970s in the USSR.<sup>[12–23]</sup> Several examples of alkali metal,<sup>[12–21]</sup>  $\text{NO}_2^+$ ,<sup>[22,23]</sup> and ethylammonium salts<sup>[24]</sup> of tetra-, penta-, and hexanitratooaluminate anions are known. The tetranitratooaluminate anion contains 12 oxygen atoms; of these, 10.5 are available to oxidize a fuel cation.

Alkylated tetrazolium cations were used in this work because of their large positive heats of formation and their potential to form ionic liquids. Ionic salts of the tetranitratooaluminate anion can be prepared in essentially quantitative yields in one-pot reactions in nitromethane solution. The starting materials are the chloride salt of the cation, aluminum trichloride, and dinitrogen tetroxide. The synthesis of 1-ethyl-4,5-dimethyltetrazolium tetranitratooaluminate (**3**) is shown in Scheme 1. The starting material 1-ethyl-4,5-dimethyltetra-



**Scheme 1.** Synthesis of 1-ethyl-4,5-dimethyltetrazolium tetranitratooaluminate (**3**).

lium chloride (**1**) was prepared by alkylation of 1,5-dimethyltetrazole with ethyl iodide, followed by anion exchange of iodide for chloride using an anion-exchange resin. The alkylation places the ethyl group primarily into the 1 position, but 16% is also found at the 2 position of the tetrazolium cation. The percentage of the minor isomer was reduced to 6% by recrystallization from ethanol and might be reduced further by additional recrystallizations. This relatively small isomeric impurity was not removed from the product. It offers the benefit of lowering the melting point of the salt without drastically altering its energetic or chemical properties.

The reaction of the tetrazolium chloride in nitromethane with one equivalent of anhydrous aluminum trichloride gives the tetrachloroaluminate salt **2**, which is a viscous ionic liquid. This intermediate can then be reacted directly with an excess of  $\text{N}_2\text{O}_4$  in nitromethane. Compound **3** is obtained as a clear, nearly colorless, viscous liquid by pumping off the volatile

[\*] C. B. Jones, Dr. R. Haiges, Dr. T. Schroer, Prof. Dr. K. O. Christe  
Loker Research Institute and Department of Chemistry  
University of Southern California  
Los Angeles, CA 90089-1661 (USA)  
Fax: (+1) 213-740-6679  
E-mail: kchriste@usc.edu

[\*\*] This work was funded by the Office of Naval Research, the Lawrence Livermore National Laboratory, and the National Science Foundation. We thank Dr. J. A. Boatz and Dr. J. Mills for the theoretical calculations, and Prof. G. A. Olah and Dr. J. Goldwasser, Dr. C. Bedford, Dr. M. Berman, Dr. J. Gilje, and Dr. J. Satcher for their steady support, and Prof. Dr. R. Bau and Dr. S. Schneider, Dr. W. W. Wilson, and Dr. R. Wagner for their help and stimulating discussions.

compounds, NOCl, CH<sub>3</sub>NO<sub>2</sub>, and excess N<sub>2</sub>O<sub>4</sub>, at ambient temperature. It is stable in dry air, hydrolyzes in water, and is soluble in CH<sub>3</sub>NO<sub>2</sub> and moderately soluble in CH<sub>2</sub>Cl<sub>2</sub>. The identity and purity of the product were established by Raman, infrared, <sup>1</sup>H, <sup>14</sup>N, <sup>15</sup>N, and <sup>13</sup>C NMR spectroscopy, and the observed material balance.

The <sup>14</sup>N NMR spectrum of **3** shows a strong signal at  $\delta = -25$  ppm, which is attributed to the four nitrogen atoms of the tetranitratoaluminate anion. The signals at  $\delta = -134$  and  $-144$  ppm, assigned to N1 and N4, respectively, of the tetrazolium cation, are much broader. Additional signals from N2 and N3 of the tetrazolium cation are obscured by the strong broad signal at  $\delta = -25$  ppm.

The <sup>15</sup>N NMR spectrum of the neat liquid shows the expected five signals, at  $\delta = -15.6$  (N2),  $-18.2$  (N3),  $-25.3$  (Al(NO<sub>3</sub>)<sub>4</sub><sup>-</sup>),  $-134.2$  (N1), and  $-145.8$  (N4) ppm. The tetranitratoaluminate anion contains two monodentate and two bidentate nitrato ligands, as shown by us by a crystal structure analysis of [N(CH<sub>3</sub>)<sub>4</sub>][Al(NO<sub>3</sub>)<sub>4</sub>].<sup>[25]</sup> In this pseudo-octahedral structure, the two monodentate ligands are *cis* to each other. The observation of a single nitrogen resonance for the monodentate and bidentate nitrato groups is attributed to fast intramolecular exchange. Even at  $-30^\circ\text{C}$  in CH<sub>3</sub>NO<sub>2</sub>, this exchange could not be slowed sufficiently to observe line broadening or separate signals for the nitrato groups. The assignments for the <sup>1</sup>H and <sup>13</sup>C NMR signals are given in the Experimental Section.

The presence of the tetranitratoaluminate anion was also confirmed by vibrational spectroscopy. The observed infrared and Raman spectra are shown in Figure 1, and the frequencies are listed in the Experimental Section. The anion part of the infrared spectrum is in good agreement with those previously reported for Rb[Al(NO<sub>3</sub>)<sub>4</sub>]<sup>[15]</sup> and Cs[Al(NO<sub>3</sub>)<sub>4</sub>].<sup>[12]</sup> Additional support came from calculations at the MP2/6-311 + G(d) level of theory. Two minimum-energy structures were obtained with C<sub>2</sub> and C<sub>1</sub> symmetry, respectively. Contrary to the tetranitratoborate anion, which possesses four monoden-

tate nitrato ligands,<sup>[26]</sup> both tetranitratoaluminate isomers are hexacoordinated with two monodentate and two bidentate ligands in *cis* configuration. These isomers differ only in the orientation of the NO<sub>2</sub> groups of the monodentate ligands with respect to each other and, at the MP2 level, differ only by 2.5 kJ mol<sup>-1</sup>. The energetically favored C<sub>2</sub> structure agrees with the crystal structure of [N(CH<sub>3</sub>)<sub>4</sub>][Al(NO<sub>3</sub>)<sub>4</sub>],<sup>[25]</sup> and its calculated spectra are in better agreement with the observed ones.

Individual modes are difficult to assign because of the size of the anion and strong vibrational coupling. In the region of the N–O stretching modes, three clusters are observed at about 1650–1500, 1350–1290, and 1030–990 cm<sup>-1</sup>, with each cluster containing four fundamental vibrations. These clusters are characteristic for covalently bound mono- and bidentate nitrato ligands and distinguish them from ionic nitrates.<sup>[27]</sup> The highest-frequency cluster contains the N=O stretching vibration of the bidentate ligands and the antisymmetric stretching vibration of the terminal NO<sub>2</sub> part of the monodentate ligands. The medium-frequency cluster contains the O–N–O antisymmetric stretching vibration of the bidentate ligands and the symmetric stretching vibration of the terminal NO<sub>2</sub> part of the monodentate ligands, while the lowest-frequency cluster is composed of the O–N–O symmetric stretching vibration of the bidentate ligands and the stretching vibration of the coordinating N–O part of the monodentate ligands. Although the spectra of the mono- and bidentate ligands exhibit different intensity patterns and the frequency separation between the first and the second cluster is somewhat larger for the bidentate nitrates, distinction between monodentate and bidentate nitrato ligands becomes difficult when dealing with molecules that contain both types of ligands at the same time.

For energetic materials, stability and physical properties are very important. The thermal stability of **3** was investigated with thermogravimetric analysis (TGA) and differential scanning calorimetry (DSC). The DSC trace showed a glass transition temperature (*T<sub>g</sub>*) at  $-46^\circ\text{C}$  and a strongly exothermic decomposition with a maximum at  $217^\circ\text{C}$  and an onset at  $183^\circ\text{C}$ . In accord with the DSC data, the TGA showed catastrophic weight loss to start at  $183^\circ\text{C}$ ; however, very slow weight loss also occurred at much lower temperatures, but the exact onset was difficult to ascertain. When a sample of **3** was held isothermally in the TGA apparatus at  $75^\circ\text{C}$  for 4 h, a 10.4% weight loss was observed. This slow weight loss is attributed to the loss of NO<sub>2</sub> and oxygen, accompanied by the formation of Al–O–Al bridges. Similar observations were previously reported by Shirokova and Rosolovskii for the cesium polynitratoaluminates.<sup>[13]</sup>

Ignition of EILs often presents major problems. The ignition of compound **3** and self-sustained burning were readily achieved by either thermal heating of **3** to about  $200^\circ\text{C}$  or by the use of a hot 40-gauge Ni/Cr wire wrapped around the sample container, a glass melting-point capillary. The capillary was filled to the top with the sample, and a direct current passed through the wire. After a few seconds, compound **3** ignited quite spectacularly, giving off flames and light, fluffy alumina, in accord with the predicted idealized combustion process [Eq. (1)]. Obviously, the composition of

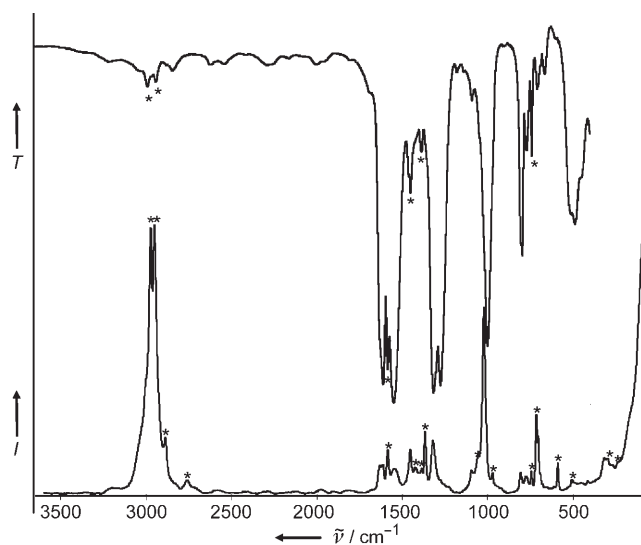
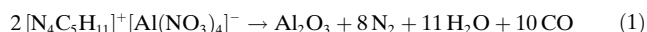


**Figure 1.** IR (upper trace) and Raman (lower trace) spectra of liquid **3**. The stars indicate bands assigned to the cation.

the combustion products at a given flame temperature would significantly deviate from those given in Equation (1).



When samples were heated in the TGA apparatus to their decomposition temperature, a false small mass increase was observed right before the catastrophic mass loss, due to the thrust of the burning liquid pushing down the TGA pan.

The theoretical performance of **3** as a propellant can be estimated from the calculated heats of formation of the free gaseous cation (836 kJ mol<sup>-1</sup>) and anion (−1486 kJ mol<sup>-1</sup>), calculated at the MP2/6-311+G(d) level of theory, an estimate<sup>[28]</sup> of the Coulomb energy of the ions in the liquid of about 419 kJ mol<sup>-1</sup>, using publicly available performance calculation codes.<sup>[29]</sup> Based on these estimates, the performance of this system significantly exceeds those of state-of-the-art materials, such as hydrazine.<sup>[30]</sup>

## Experimental Section

**Caution!** Although no difficulties were encountered when handling these materials, they are highly energetic and potentially explosive! They should be handled on a small scale while using appropriate safety precautions (safety shields, face shields, leather gloves, protective clothing, such as heavy leather welding suits and ear plugs).

**Materials and apparatus:** All reactions were carried out in Pyrex glass ampoules that were closed by Teflon/glass high-vacuum valves. Volatile materials were handled in a Pyrex glass vacuum line. Nonvolatile materials were handled in the dry argon atmosphere of a glove box.

Raman spectra were recorded directly in the glass reactors in the range 3600–80 cm<sup>-1</sup> on a Bruker Equinox 55 FRA 106/S FT-RA spectrometer, using a Nd-YAG laser at 1064 nm with power levels of 400 mW. Infrared spectra were recorded in the range 4000–400 cm<sup>-1</sup> on a Midac, M Series, FT-IR spectrometer. For liquid samples, a Wilks minicell with AgCl windows was used. Solids were recorded as AgCl or KBr pellets. The cells were filled inside the glove box using an Econo minipress (Barnes Engineering Co.) and transferred in a closed container to the spectrometer before placing them quickly into the sample compartment which was purged with dry nitrogen to minimize exposure to atmospheric moisture and potential hydrolysis of the sample. <sup>14</sup>N and <sup>15</sup>N NMR spectra were recorded at 36.13 and 50.68 MHz, respectively, on a Bruker AMX 500 spectrometer. Samples were either externally referenced to CH<sub>3</sub>NO<sub>2</sub> or dissolved in CH<sub>3</sub>NO<sub>2</sub>. TGA thermograms were measured on a Shimadzu TGA-50 instrument using a flow rate of 20 mL min<sup>-1</sup> of nitrogen. DSC measurements were recorded on a Shimadzu DSC-50(SH); the temperature was ramped at a rate of 10 K min<sup>-1</sup>. Densities were measured with a pycnometer.

The starting materials, N<sub>2</sub>O<sub>4</sub> (Matheson), ethyl iodide, AlCl<sub>3</sub>, and 5-methyltetrazole (Aldrich), were used without further purification. Deuterated solvents (Cambridge Isotopes) were dried using standard methods. Nitromethane (Fisher) was dried over CaCl<sub>2</sub>, vacuum-distilled and stored over 4-Å molecular sieves before use. All volatile materials were handled using standard high-vacuum techniques. 1,5-dimethyltetrazole was prepared by a literature method;<sup>[31]</sup> its identity and purity were confirmed by IR, Raman, and <sup>1</sup>H NMR spectroscopy.

1-Ethyl-4,5-dimethyltetrazolium chloride (**1**): 1,5-dimethyltetrazole (28 mmol) and ethyl iodide (15 mL) were placed into a 250-mL glass ampoule equipped with a high-vacuum valve and degassed by three freeze-pump-thaw cycles. The ampoule was immersed into a hot water bath at 100 °C for 10 h. The volatile material was removed under vacuum at room temperature, to give a yellow solid (5.466 g).

The solid was dissolved in a minimum amount of methanol, and passed through a column containing 15 g (55.5 meq) AMBER-JET 4200 (Cl) ion-exchange resin, using methanol as eluent. The bulk of the methanol was removed under vacuum, and the anion exchange was repeated until the effluent was free of iodide, as shown by the absence of an NH<sub>3</sub>-insoluble precipitate with AgNO<sub>3</sub>. All volatile material was pumped off, and the residue was recrystallized from ethanol. Yield: 1.412 g (31 %); <sup>1</sup>H NMR (CD<sub>3</sub>CN): δ = 1.56 (t, <sup>3</sup>J = 7.4 Hz, 3 H, CH<sub>3</sub>), 2.95 (s, 3 H, CH<sub>3</sub>), 4.23 (s, 3 H, CH<sub>3</sub>), 4.61 ppm (q, <sup>3</sup>J = 7.4 Hz, 2 H, CH<sub>2</sub>); minor isomer, 2-ethyl-4,5-dimethyltetrazolium chloride: <sup>1</sup>H NMR (CD<sub>3</sub>CN): δ = 1.60 (t, <sup>3</sup>J = 7.4 Hz, 3 H, CH<sub>3</sub>), 3.00 (s, 3 H, CH<sub>3</sub>), 4.27 (s, 3 H, CH<sub>3</sub>), 4.86 ppm (q, <sup>3</sup>J = 7.4 Hz, 2 H, CH<sub>2</sub>). Raman (400 mW): ν̄ = 2986 (7.4), 2953 (10.0), 2887 (2.5), 2814 (1.0), 2763 (0.4), 1589 (1.8), 1530 (1.0), 1474 (sh), 1456 (1.8), 1416 (1.0), 1396 (0.8), 1363 (2.9), 1324 (0.5), 1307 (0.5), 1287 (0.7), 1229 (0.2), 1116 (0.3), 1088 (0.3), 1065 (0.8), 1041 (0.5), 980 (0.8), 808 (0.3), 788 (0.2), 747 (1.0), 724 (3.9), 699 (0.6), 655 (0.6), 594 (1.1), 503 (0.7), 388 (0.6), 296 (1.5), 246 (0.8), 229 (0.8), 153 (sh) cm<sup>-1</sup>. IR (KBr): ν̄ = 2997 (m), 2946 (w), 2888 (w), 1629 (br), 1587 (s), 1526 (m), 1467 (sh), 1453 (m), 1409 (w), 1388 (w), 1360 (m), 1323 (w), 1287 (w), 1229 (w), 1181 (w), 1151 (w), 1113 (w), 1084 (vw), 1058 (sh), 1034 (s), 975 (m), 805 (w), 745 (s), 720 (w), 696 (vw), 648 (w) cm<sup>-1</sup>.

1-Ethyl-4,5-dimethyltetrazolium tetrachloroaluminate (**2**): In the glove box, compound **1** (3.25 mmol) and AlCl<sub>3</sub> (3.25 mmol) were placed into a 9-mm (outer diameter) glass ampoule. The ampoule was connected to the vacuum line, and evacuated at −196 °C. Nitromethane (≈ 1 mL) was added at −196 °C, and the ampoule was allowed to warm slowly to room temperature, which led to an orange solution. The nitromethane was removed under a dynamic vacuum overnight at ambient temperature, giving a quantitative yield of **2** as an amber viscous liquid.

1-Ethyl-4,5-dimethyltetrazolium tetranitratooaluminate (**3**): In the glove box, compound **2** (1.68 mmol) was loaded into a 9-mm glass ampoule. The ampoule was connected to the glass vacuum line and evacuated. After cooling to −196 °C, N<sub>2</sub>O<sub>4</sub> (39.92 mmol) was condensed in, followed by CH<sub>3</sub>NO<sub>2</sub> (27.06 mmol). The mixture was allowed to slowly warm to room temperature and stirred for 1.5 h. The volatile material was removed under a dynamic vacuum for 24 h, giving an almost colorless clear viscous oil. Expected mass 0.674 g, found mass 0.651 g. <sup>1</sup>H NMR (CD<sub>3</sub>NO<sub>2</sub>): δ = 1.62 (t, <sup>3</sup>J = 7.4 Hz, 3 H, CH<sub>3</sub>), 2.95 (s, 3 H, CH<sub>3</sub>), 4.90 (s, 3 H, CH<sub>3</sub>), 4.67 ppm (q, <sup>3</sup>J = 7.4 Hz, 2 H, CH<sub>2</sub>); minor isomer, 2-ethyl-4,5-dimethyltetrazolium tetranitratooaluminate: <sup>1</sup>H NMR (CD<sub>3</sub>NO<sub>2</sub>): δ = 1.70 (t, <sup>3</sup>J = 7.4 Hz, 3 H, CH<sub>3</sub>), 2.82 (s, 3 H, CH<sub>3</sub>), 4.33 (s, 3 H, CH<sub>3</sub>), 4.91 ppm (q, <sup>3</sup>J = 7.4 Hz, 2 H, CH<sub>2</sub>); <sup>13</sup>C NMR: δ = 8.77, 13.95, 37.53, 47.84, 153.87 ppm; <sup>14</sup>N NMR (CD<sub>3</sub>NO<sub>2</sub>): δ = −144, −134, −25 ppm; <sup>14</sup>N NMR (CD<sub>2</sub>Cl<sub>2</sub>): −141, −26 ppm; <sup>15</sup>N NMR (neat liquid): δ = −145.8 (s, 1 N, N<sub>4</sub>), −134.2 (s, 1 N, N<sub>1</sub>), −25.3 (s, 4 N, Al(NO<sub>3</sub>)<sub>4</sub>), −18.2 (s, 1 N, N<sub>3</sub>), −15.6 ppm (s, 1 N, N<sub>2</sub>). Raman (400 mW): ν̄ = 2973 (9.9), 2951 (10.0), 2887 (1.0), 2761 (0.5), 1630 (1.0), 1611 (1.0), 1585 (1.6), 1547 (0.9), 1453 (1.6), 1422 (1.0), 1387 (1.0), 1367 (2.3), 1321 (2.0), 1092 (0.9), 1057 (sh), 1021 (7.0), 970 (0.8), 808 (0.8), 775 (0.7), 743 (0.9), 715 (3.0), 703 (2.0), 703 (2.0), 589 (1.2), 508 (0.5), 317 (1.3), 300 (1.2), 271 (0.9), 237 (1.1) cm<sup>-1</sup>. IR (AgCl plates): ν̄ = 3032 (sh), 2995 (w), 2944 (w), 2850 (w,br), 2627 (w,br), 2547 (w,br), 2282 (w,br), 2004 (w,br), 1945 (sh), 1694 (sh), 1630 (sh), 1611 (s), 1583 (s), 1550 (s), 1466 (w), 1451 (m), 1388 (w), 1320 (s), 1275 (s), 1182 (w), 1142 (w), 1093 (w), 1047 (sh), 1021 (sh), 1001 (s), 806 (sh), 796 (m), 773 (w), 739 (m), 711 (w), 664 (w), 516 (sh), 489 (m), 450 (sh) cm<sup>-1</sup>.

Received: February 25, 2006

Published online: July 3, 2006

**Keywords:** energetic ionic liquids · propellants · tetranitratooaluminate · tetrazoles · tetrazolium ions

- [1] M. W. Schmidt, M. S. Gordon, J. A. Boatz, *J. Phys. Chem. A* **2005**, *109*, 7285.
- [2] K. E. Gutowski, J. D. Holbrey, R. D. Rogers, D. A. Dixon, *J. Phys. Chem. B* **2005**, *109*, 23196.
- [3] L. Courtheoux, D. Amariei, S. Rossignol, C. Kappenstein, *Eur. J. Inorg. Chem.* **2005**, 2293; L. Courtheoux, E. Gautron, S. Rossignol, C. Kappenstein, *J. Catal.* **2005**, 232, 10.
- [4] a) G. P. Sutton, *Rocket Propulsion Elements*, Wiley, New York, 2nd ed., **1956**; b) *An Introduction to Rocket Missile Propulsion*, A Technical Training Publication, prepared by the Rocketdyne Training Department, Rocketdyne, A Division of North American Aviation, Canoga Park, CA, **1958**.
- [5] A. Daddieu, R. Damm, E. W. Schmidt, *Raketentreibstoffe*, Springer, Wien, **1968**.
- [6] N. Wiberg, *Hollemann-Wiberg, Inorganic Chemistry*, Academic Press, New York, **2001**.
- [7] K. O. Christe, G. Drake, Provisional US Pat. Appl. 60/416,418, filed October 7, **2002** through the US Air Force.
- [8] P. Jimenez, M. V. Roux, C. Turron, *J. Chem. Thermodyn.* **1987**, *19*, 985.
- [9] W. S. McEwan, M. W. Rigg, *J. Am. Chem. Soc.* **1951**, *73*, 4725.
- [10] M. Denffer, T. M. Klapötke, G. Kramer, G. Spieß, J. M. Welch, *Propellants Explos. Pyrotech.* **2005**, *30*, 191.
- [11] Work done by Callery Chemical Company, from 1961 to 1966, for the US Air Force and Office of Naval Research.
- [12] G. N. Shirokova, V. Ya. Rosolovskii, *Russ. J. Inorg. Chem.* **1971**, *16*, 808.
- [13] G. N. Shirokova, V. Ya. Rosolovskii, *Russ. J. Inorg. Chem.* **1971**, *16*, 1106.
- [14] N. V. Krivtsov, G. N. Shirokova, V. Ya. Rosolovskii, *Russ. J. Inorg. Chem.* **1973**, *18*, 503.
- [15] G. N. Shirokova, S. Ya. Zhuk, V. Ya. Rosolovskii, *Russ. J. Inorg. Chem.* **1975**, *12*, 1868.
- [16] G. N. Shirokova, S. Ya. Zhuk, V. Ya. Rosolovskii, *Russ. J. Inorg. Chem.* **1975**, *20*, 856.
- [17] O. A. D'yachenko, L. O. Atovmyan, *Zh. Strukt. Khim.* **1975**, *16*, 85.
- [18] G. N. Shirokova, S. Ya. Zhuk, V. Ya. Rosolovskii, *Russ. J. Inorg. Chem.* **1976**, *21*, 527.
- [19] N. V. Krivtsov, G. N. Shirokova, S. Ya. Zhuk, V. Ya. Rosolovskii, *Russ. J. Inorg. Chem.* **1976**, *21*, 1409.
- [20] G. N. Shirokova, S. Ya. Zhuk, V. Ya. Rosolovskii, *Russ. J. Inorg. Chem.* **1976**, *21*, 1459.
- [21] G. N. Shirokova, S. Ya. Zhuk, V. Ya. Rosolovskii, *Russ. J. Inorg. Chem.* **1976**, *21*, 1557.
- [22] N. V. Krivtsov, V. Ya. Rosolovskii, G. N. Shirokova, *Russ. J. Inorg. Chem.* **1971**, *16*, 1402.
- [23] G. N. Shirokova, V. Ya. Rosolovskii, *Russ. J. Inorg. Chem.* **1971**, *16*, 1699.
- [24] C. C. Addison, P. M. Boorman, N. Logan, *J. Chem. Soc. A* **1966**, *10*, 1434.
- [25] C. Bigler Jones, R. Haiges, K. O. Christe, still unpublished.
- [26] O. A. D'yachenko, L. O. Atovmyan, S. M. Aldoshin, K. V. Titova, V. Ya. Rosolovskii, *Dokl. Akad. Nauk SSSR* **1978**, 238, 1132.
- [27] C. C. Addison, D. W. Amos, D. Sutton, *J. Chem. Soc. A* **1967**, 808.
- [28] The method used for the estimation of the Coulomb energy from molecular-volume-based lattice energy estimates by the Glasser and Jenkins method and sublimation enthalpy estimates has been described in a recent paper by K. E. Gutowski, J. D. Holbrey, R. D. Rogers, D. A. Dixon, *J. Phys. Chem. B* **2005**, *109*, 23196.
- [29] S. Gordon, B. J. McBride, *Computer Program for Calculation of Complex Chemical Equilibrium Compositions and Applications. I. Analysis and II. User's Manual and Program Description*, Reference Publication No. NASA/RP-1311, Lewis Research Center, Cleveland OH, June **1996**.
- [30] E. W. Schmidt, *Hydrazine and its Derivatives*, Wiley, New York, **1984**.
- [31] R. Spear, *Aust. J. Chem.* **1984**, *37*, 2453.



## Thermodynamics

DOI: 10.1002/anie.200600839

## The Heat of Formation of Cyclobutadiene\*\*

Alireza Fattahi, Lev Lis, Zhixin Tian, and  
Steven R. Kass\*

Cyclobutadiene (**1**) and its derivatives have beckoned to chemists ever since Kekule's deduction of the structure of benzene and his attempt to synthesize **1** in 1872.<sup>[1]</sup> Pioneering efforts by Willstätter and Finkelstein were followed by a century of studies which produced many remarkable findings. Room temperature stable derivatives such as tri-*tert*-butylcyclobutadiene<sup>[2]</sup> and tetra-*tert*-butylcyclobutadiene<sup>[3]</sup> were successfully prepared and spectroscopically characterized, whereas the parent compound was found to be more elusive. It dimerizes in solid matrices at  $\geq 35$  K, is a transient reactive intermediate in solution, and has a lifetime of only 2 ms at 0.1 Torr in the gas phase.<sup>[1a]</sup> Nevertheless, trapping<sup>[4]</sup> and spectroscopic results have revealed that cyclobutadiene has a ground-state singlet configuration and adopts a rectangular  $D_{2h}$  structure which rapidly undergoes automerization. An isolable and room temperature stable complex consisting of **1** in the cavity of a spherical crown ether (that is, a hemicarceplex) has even been prepared,<sup>[5]</sup> but the thermodynamic stability of cyclobutadiene remains experimentally unknown.

Conventional calorimetric methods are precluded when it comes to cyclobutadiene and its simple derivatives because of their high reactivity. Electrochemical,<sup>[6]</sup>  $pK_a$ ,<sup>[7]</sup> and kinetic<sup>[8]</sup> measurements of model compounds have been carried out and interpreted as indicating that **1** has a negative resonance energy of at least 50–67 kJ mol<sup>-1</sup>. This conclusion is in accord with many of the early computational findings and a

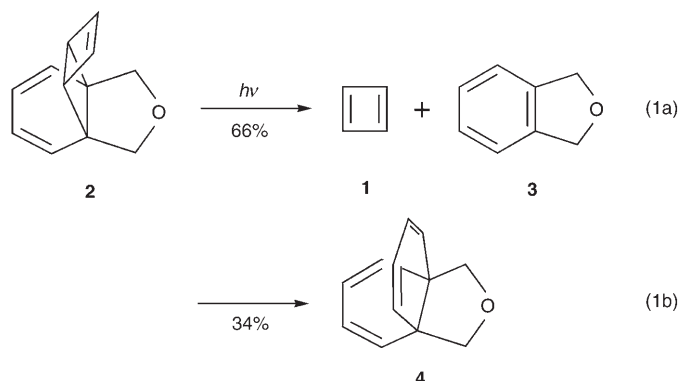
[\*] A. Fattahi, L. Lis, Z. Tian, Prof. S. R. Kass  
Department Chemistry  
University of Minnesota  
Minneapolis, MN 55455 (USA)  
Fax: (+1) 612-626-7541  
E-mail: kass@chem.umn.edu

[\*\*] We are grateful to the National Science Foundation, the donors of the Petroleum Research Foundation, as administered by the American Chemical Society, and the Minnesota Supercomputer Institute for support of this research. Fruitful discussions with Professor Thomas Bally also are acknowledged.



Supporting information for this article is available on the WWW under <http://www.angewandte.org> or from the author.

preliminary derivation of  $\Delta H_f^\circ(\mathbf{1}) = 377 \text{ kJ mol}^{-1}$  based on tentative mass spectrometry data.<sup>[1a]</sup> However, this proposal has been questioned and a small positive resonance energy has been suggested.<sup>[9]</sup> More recently, a photoacoustic calorimetry study was reported in which the heat liberated in the photochemical generation of cyclobutadiene was measured [Eq. (1)].<sup>[10]</sup> The resulting reaction enthalpy can be directly

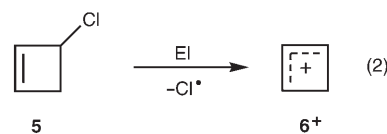


converted into the heat of formation of **1** if the energies of **2–4** are known. Unfortunately, these quantities are unavailable, and there is not enough information in the literature to estimate them by using additivity approaches such as the Benson's group equivalents method.<sup>[11]</sup> To solve this problem, Deniz et al.<sup>[10]</sup> computed the geometries and energies of **2–4** by using molecular mechanics (namely, the MM3 force field) and semiempirical AM1 calculations, respectively. These data enabled  $\Delta H_f^\circ(\mathbf{1}) = (477 \pm 46) \text{ kJ mol}^{-1}$  to be derived. This value has an unusually large uncertainty and does not represent an experimental determination, despite the claim to the contrary.

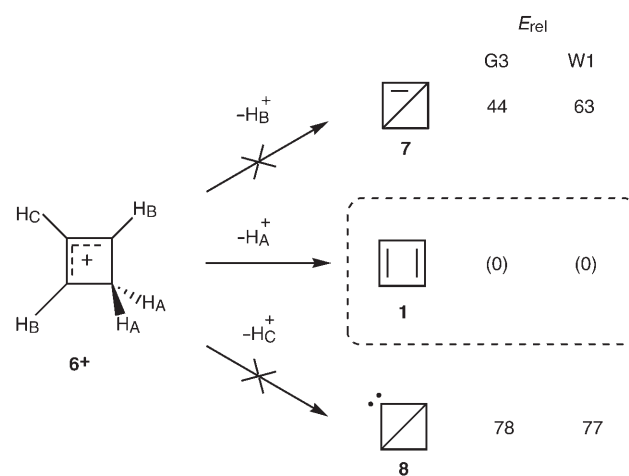
Gas-phase measurements in which thermodynamic cycles were employed to provide the heats of hydrogenation of benzocyclobutadiene<sup>[12]</sup> and phenylcyclobutadiene<sup>[13]</sup> have also been reported. By comparing these results to **1** by ab initio (MP2) and density functional theory (the Becke 3-parameter hybrid exchange and Lee–Yang–Parr correlation density functional, that is, B3LYP)<sup>[14]</sup> calculations,  $\Delta H_f^\circ(\mathbf{1}) = 427$  and  $(402 \pm 21) \text{ kJ mol}^{-1}$  were predicted. Thus, a range of values for the heat of formation of cyclobutadiene spanning from 377 to 477  $\text{kJ mol}^{-1}$  can be found in the literature.

The experimental uncertainty revolving around the energetics of cyclobutadiene is mirrored by computational data which span an even larger range from 364 (BLYP/6-311G-(2d,2p)) to 519  $\text{kJ mol}^{-1}$  (HF/4-31G).<sup>[15]</sup> More sophisticated methodologies (CCSD(T), CBS-Q, and G2)<sup>[15e,j,k,r]</sup> lead to predictions of 414–435  $\text{kJ mol}^{-1}$ , but a recent detailed analysis dealing with the factors responsible for the destabilization of cyclobutadiene ( $\sigma$  versus  $\pi$  electrons) is compatible with a heat of formation of 477  $\text{kJ mol}^{-1}$ .<sup>[15n]</sup> To resolve and settle this issue, we now report the first experimental determination of the heat of formation of cyclobutadiene as well as high level G3<sup>[16]</sup> and W1<sup>[17]</sup> computations, which typically are accurate to within 4–8  $\text{kJ mol}^{-1}$ .

Electron ionization (EI) of a static pressure of 3-chlorocyclobutene (**5**) leads to a signal at  $m/z$  53, which was assigned as the cyclobuten-3-yl cation (**6<sup>+</sup>**) [Eq. (2)]. This allylic ion is



stabilized by delocalization and has no apparent low-energy isomerization pathways available to it that would give more-stable species. To establish the identity of this ion hydrogen–deuterium exchange experiments were carried out. Isopropylamine-ND (*i*PrND<sub>2</sub>) was found to induce up to five hydrogen–deuterium exchanges in **6<sup>+</sup>**, as expected for the proposed structure. This result also confirms that the deprotonation of the cyclobuten-3-yl cation affords cyclobutadiene, otherwise five H/D exchanges would not be observed. This finding was anticipated because a  $\pi$  bond is formed on converting **6<sup>+</sup>** into cyclobutadiene, and its energetic benefit (ca. 272  $\text{kJ mol}^{-1}$ ) should outweigh the additional strain energy and antiaromaticity of **1** (ca. 167  $\text{kJ mol}^{-1}$ , see below). High level G3 and W1 computations are in agreement with this result in that they indicate that deprotonation of **6<sup>+</sup>** to afford the corresponding carbene (**7**,  $-\text{H}_\text{B}$ ) or allene (**8**,  $-\text{H}_\text{C}$ ) is much less favorable (Scheme 1).



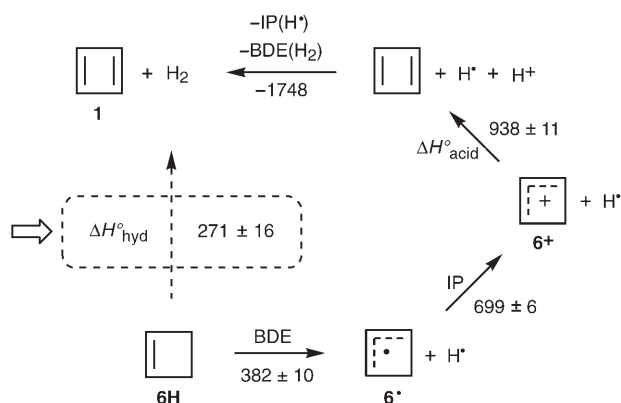
**Scheme 1.** Computed deprotonation energies of the cyclobuten-3-yl cation [ $\text{kJ mol}^{-1}$ ].

The acidity of the cyclobuten-3-yl cation corresponds to the proton affinity of cyclobutadiene, and this quantity was measured by treating **6<sup>+</sup>** with standard reference bases and observing the occurrence or absence of proton transfer. Strong bases such as ammonia (proton affinity (PA) =  $(854 \pm 8) \text{ kJ mol}^{-1}$ ) and isopropylamine (PA =  $(924 \pm 8) \text{ kJ mol}^{-1}$ )<sup>[18]</sup> do not abstract a proton from the cyclobuten-3-yl cation, whereas more basic reagents such as pyrrolidine (PA =  $(948 \pm 8) \text{ kJ mol}^{-1}$ ,  $k = 5.9 \times 10^{-10} \text{ cm}^3 \text{ molecule}^{-1} \text{ s}^{-1}$ ) and diisopropylamine (PA =  $(972 \pm 8) \text{ kJ mol}^{-1}$ ) are rapidly protonated.

Pyridine ( $PA = (929 \pm 8) \text{ kJ mol}^{-1}$ ) is also observed to abstract a proton, but the rate is modest ( $k = 1.3 \times 10^{-10} \text{ cm}^3 \text{ molecule}^{-1} \text{ s}^{-1}$  or about 7 in 100 collisions lead to reaction),<sup>[19]</sup> which indicates that this is a slightly ( $4\text{--}8 \text{ kJ mol}^{-1}$ ) endothermic process. In bracketing experiments, such a result is taken as a “no” and thus isopropylamine and pyrrolidine are the limiting reagents and  $PA(\mathbf{1}) = (938 \pm 11) \text{ kJ mol}^{-1}$  is assigned. This value is much larger than for other olefins (for example,  $PA((Z)\text{-}2\text{-butene}) = 753 \text{ kJ mol}^{-1}$ ,  $PA(1,3\text{-butadiene}) = 783 \text{ kJ mol}^{-1}$ , and  $PA(\text{isobutene}) = 802 \text{ kJ mol}^{-1}$ ), which is not surprising because of the antiaromaticity of cyclobutadiene. It is also in nearly perfect accord with computed results of 937 (G3) and 938 (W1)  $\text{kJ mol}^{-1}$ .

The ionization potential of the cyclobuten-3-yl radical ( $\mathbf{6}^\bullet$ ) was also measured by bracketing. In particular,  $\mathbf{6}^+$  does not abstract an electron from  $N,N,N',N'$ -tetramethylethylenediamine (ionization potential (IP) =  $(7.59 \pm 0.04) \text{ eV}$ ) or 1,1-dimethylhydrazine (IP =  $(7.29 \pm 0.05) \text{ eV}$ ), but rapidly does so from diphenylamine (IP =  $(7.19 \pm 0.05) \text{ eV}$ ,  $k = 9.9 \times 10^{-10} \text{ cm}^3 \text{ molecule}^{-1} \text{ s}^{-1}$ ),  $N,N$ -dimethylaniline (IP =  $(7.12 \pm 0.02) \text{ eV}$ ,  $k = 1.2 \times 10^{-9} \text{ cm}^3 \text{ molecule}^{-1} \text{ s}^{-1}$ ), and reagents with smaller ionization potentials. This finding leads to  $IP(\mathbf{6}^\bullet) = (7.24 \pm 0.06) \text{ eV}$ , which is in excellent agreement with computed values of 7.29 (G3) and 7.24 eV (W1).

By combining the measured proton affinity of cyclobutadiene and the ionization potential of the cyclobuten-3-yl radical with the recently determined allylic C–H bond dissociation energy (BDE) of cyclobutene ( $\mathbf{6H}$ ,  $(382 \pm 10) \text{ kJ mol}^{-1}$ )<sup>[20]</sup> and well-known ancillary data ( $IP(H^\bullet) = 1312 \text{ kJ mol}^{-1}$  and  $BDE(H_2) = 436 \text{ kJ mol}^{-1}$ ), one can obtain an experimentally determined heat of hydrogenation for  $\mathbf{1}$  of  $(271 \pm 16) \text{ kJ mol}^{-1}$  (Scheme 2). This value compares favor-

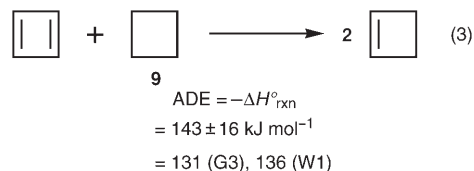


**Scheme 2.** Thermodynamic cycle for the heat of hydrogenation of  $\mathbf{1}$  [ $\text{kJ mol}^{-1}$ ].

ably with predicted values of 266 (G3) and 271 (W1)  $\text{kJ mol}^{-1}$ . It also leads to an experimentally determined heat of formation for cyclobutadiene of  $(428 \pm 16) \text{ kJ mol}^{-1}$ , since the enthalpy of formation of cyclobutene ( $\Delta H_f^\circ = (157 \pm 2) \text{ kJ mol}^{-1}$ )<sup>[21]</sup> has been determined by combustion calorimetry. The heat of formation of  $\mathbf{1}$  was also computed from its atomization energy, and the G3 and W1 results (435 and 427  $\text{kJ mol}^{-1}$ , respectively) are within the experimental uncertainty and the expected accuracy of these methods. This

observation provides a high level of confidence both in the experimental and computational results, and should serve to establish the energetics provided herein.

From the data above, the antiaromatic destabilization energy (ADE) of cyclobutadiene can be derived from the definition illustrated in Equation (3). A value of  $(143 \pm 16) \text{ kJ mol}^{-1}$  is obtained, which is in good accord with G3



and W1 predictions of 131 and 136  $\text{kJ mol}^{-1}$ , respectively. In the latter case, all but 1.7  $\text{kJ mol}^{-1}$  of the 7.1  $\text{kJ mol}^{-1}$  difference can be attributed to the discrepancy between the experimental and computed heat of formation of cyclobutane ( $\mathbf{9}$ ); that is,  $\Delta H_f^\circ = (28.4 \pm 0.6) \text{ (expt)}$  versus 19.6  $\text{kJ mol}^{-1}$  (W1)).<sup>[22,23]</sup>

It is important to add that the definition of the ADE used here is arbitrary, and that there is no model-free way of obtaining this quantity. Moreover, the implicit assumption made in Equation (3) is that the strain energy (SE) is the same in the reactants and products. This assumption seems reasonable since each species in the comparison is a four-membered ring and the difference in strain between cyclobutene ( $SE = 125 \text{ kJ mol}^{-1}$ ) and cyclobutane ( $SE = 112 \text{ kJ mol}^{-1}$ ) is only 13  $\text{kJ mol}^{-1}$ .<sup>[11]</sup> Of course, there is no reason why the strain energy of  $\mathbf{1}$  need be additive (that is,  $SE(\mathbf{1}) = SE(\mathbf{6H}) + SE(\mathbf{6H-9})$ ) and the addition of two formal  $sp^2$  centers to cyclobutene might lead to more than 13  $\text{kJ mol}^{-1}$  of additional strain. This would make 137  $\text{kJ mol}^{-1}$  a lower limit for the strain energy of cyclobutadiene. Alternatively, one could equate the measured strain energy of 3,4-bismethylenecyclobutene ( $\mathbf{10}$ , 160  $\text{kJ mol}^{-1}$ )<sup>[24]</sup> to that of  $\mathbf{1}$  since each ring carbon atom is formally  $sp^2$  hybridized in both compounds. In this case, a 23  $\text{kJ mol}^{-1}$  correction would need to be applied to the ADE, but this presumably is an upper limit because of the built in 1,4 hydrogen–hydrogen repulsion in  $\mathbf{10}$ . Consequently, an average value of  $(149 \pm 12) \text{ kJ mol}^{-1}$  is adopted for the strain energy of  $\mathbf{1}$ , which leads to a 12  $\text{kJ mol}^{-1}$  correction to the ADE derived by way of Equation (3) and a destabilization or delocalization energy of  $(131 \pm 20) \text{ kJ mol}^{-1}$ .

An alternative approach to obtaining the ADE of  $\mathbf{1}$  is to compute its heat of formation by an additivity method. Benson's group equivalents were used for this purpose and lead to  $\Delta H_f^\circ = 113.5 + x \text{ kJ mol}^{-1}$ , where  $x$  is the sum of the strain energy of cyclobutadiene and its antiaromatic destabilization energy.<sup>[11]</sup> By substituting the measured heat of formation into this equation one obtains  $x = (314 \pm 16) \text{ kJ mol}^{-1}$ , which cannot be separated into its two components in a model-independent way. If  $SE = (149 \pm 12) \text{ kJ mol}^{-1}$  is adopted as above, than an ADE or Dewar resonance energy of  $(165 \pm 20) \text{ kJ mol}^{-1}$  is obtained. This value is larger than the one derived from Equation (3), but

this is expected since conjugation is built into this model. If a nonconjugated reference is used (that is,  $C_d-(C)(H)$  (the energy equivalent for a double-bonded C atom attached to an  $sp^3$ -hybridized C atom and an H atom) rather than  $C_d-(C_d)(H)$ ) than  $ADE = (136 \pm 20) \text{ kJ mol}^{-1}$ , which is in excellent accord with the previous determination.

The gas-phase heat of hydrogenation for cyclobutadiene has been determined experimentally by making measurements on the cyclobuten-3-yl cation and applying the results in a thermodynamic cycle. Since the heat of formation of cyclobutene is well established by combustion calorimetry, this provides the first experimental determination of the heat of formation of cyclobutadiene. The resulting value,  $(428 \pm 16) \text{ kJ mol}^{-1}$ , is in good accord with previous predictions of 427 and  $(402 \pm 21) \text{ kJ mol}^{-1}$  based upon similar energetic determinations of benzocyclobutadiene and phenylcyclobutadiene.<sup>[12,13]</sup> In contrast, an early estimate of  $377 \text{ kJ mol}^{-1}$  is significantly too low and a recent photoacoustic calorimetry determination of  $(477 \pm 46) \text{ kJ mol}^{-1}$  is too large.<sup>[11a,10]</sup> The former value is incorrect presumably because the structure of the  $C_4H_4^+$  ion formed by the photoionization of pyridine is not ionized cyclobutadiene whereas the latter result is sensitive to the computational approach used to determine the energetics of **2–4**. The results reported herein are also in excellent agreement with G3, W1, and other very high level ab initio calculations, and were inspired in part by the G2-computed acidity of **6**<sup>+</sup> reported by Maksic et al.<sup>[25]</sup> A very recent detailed analysis of the  $\sigma$ - $\pi$  separability problem in **1**,<sup>[15n]</sup> however, leads to energetics ( $\Delta H_f^\circ$  and ADE) which are too large because electron correlation was thought to be unimportant and was omitted. Finally, a strain energy of  $(149 \pm 12) \text{ kJ mol}^{-1}$  is suggested for **1**, and this leads to an ADE value of  $131\text{--}136 \text{ kJ mol}^{-1}$  when a nonconjugated reference model is employed and  $165 \text{ kJ mol}^{-1}$  when conjugation is included. These findings indicate that the SE is similar in size to the ADE and that the latter is larger but in accord with the electrochemical, pK<sub>a</sub>, and kinetic measurements carried out on complex model systems.<sup>[6–8]</sup>

## Experimental Section

Gas-phase experiments: A dual cell model 2001 Finnigan Fourier transform mass spectrometer (FTMS) equipped with a 3 T superconducting magnet and operated with a Sun workstation running Odyssey 4.2 software or a similar instrument controlled by an IonSpec data system running IonSpec99 Ver. 7.0 software were used for these studies. 3-Chlorocyclobutene<sup>[26]</sup> was added into the first (analyzer) cell at a static pressure of approximately  $4 \times 10^{-8}$  Torr and ionized with 50 eV electrons for 20 ms. All of the resulting ions were transferred to the second (source) cell and translationally and vibrationally cooled with two pulses of argon, each leading to a pressure of about  $1 \times 10^{-5}$  Torr. The desired  $[M-Cl]^+$  ion at  $m/z$  53 was subsequently isolated with a stored-waveform inverse Fourier transform (SWIFT) excitation.<sup>[27]</sup> Neutral reagents were added into the source cell through a solid probe inlet or slow leak valves, and the resulting reactions were monitored as a function of time. To confirm the results of bracketing experiments, the reactions were monitored by continually ejecting the  $m/z$  53 ion and observing the effect on the product ions (that is, double resonance experiments) and by not transferring the reactant ion to the second cell. Rate constants reported in this work are estimated to have an uncertainty of  $\pm 50\%$ ,

largely because of the uncertainty in measuring reagent gas pressures with an ionization gauge.

Computations: G3<sup>[16]</sup> and W1<sup>[17]</sup> calculations were carried out as previously described in the literature using Gaussian 2003<sup>[28]</sup> on IBM and SGI workstations at the Minnesota Supercomputer Institute. All of the resulting energies are reported as enthalpies at 298 K, and were obtained by using scaled Hartree-Fock (0.8929, G3) and B3LYP (0.985, W1) vibrational frequencies. In both cases, small vibrational frequencies which contribute more than  $\frac{1}{2}(RT)$  to the thermal energy were replaced by  $\frac{1}{2}(RT)$ .

Received: March 4, 2006

Revised: April 26, 2006

Published online: July 3, 2006

**Keywords:** ab initio calculations · antiaromaticity · cyclobutadiene · mass spectrometry · thermodynamics

- a) T. Bally, S. Masamune, *Tetrahedron* **1980**, 36, 343–370; b) G. Maier, *Angew. Chem.* **1974**, 86, 491–505; *Angew. Chem. Int. Ed. Engl.* **1974**, 13, 425–490; c) G. Maier, *Angew. Chem.* **1988**, 100, 317–341; *Angew. Chem. Int. Ed. Engl.* **1988**, 27, 309–332; d) M. P. Cava, M. J. Mitchell, *Cyclobutadiene and Related Compounds*, Academic Press, New York, **1967**.
- a) G. Maier, A. Alzerreca, *Angew. Chem.* **1973**, 85, 1057–1058; *Angew. Chem. Int. Ed. Engl.* **1973**, 12, 1015–1016; b) S. Masamune, N. Nakamura, M. Suda, H. Ona, *J. Am. Chem. Soc.* **1973**, 95, 8481–8483.
- a) G. Maier, S. Pfriem, U. Schaefer, K. D. Malsch, R. Matusch, *Chem. Ber.* **1981**, 114, 3965–3987; b) G. Maier, S. Pfriem, U. Schaefer, R. Matusch, *Angew. Chem.* **1978**, 90, 552–553; *Angew. Chem. Int. Ed. Engl.* **1978**, 17, 519–520.
- a) D. W. Whitman, B. K. Carpenter, *J. Am. Chem. Soc.* **1980**, 102, 4272–4274; b) D. W. Whitman, B. K. Carpenter, *J. Am. Chem. Soc.* **1982**, 104, 6473–6474.
- D. J. Cram, M. E. Tanner, R. Thomas, *Angew. Chem.* **1991**, 103, 1048–1051; *Angew. Chem. Int. Ed. Engl.* **1991**, 30, 1024–1027.
- a) R. Breslow, R. Grubbs, S. Murahashi, *J. Am. Chem. Soc.* **1970**, 92, 4139–4140; b) R. Breslow, D. R. Murayama, S. Murahashi, R. Grubbs, *J. Am. Chem. Soc.* **1973**, 95, 6688–6699; c) M. Horner, S. Huenig, *Angew. Chem.* **1977**, 89, 424–425; *Angew. Chem. Int. Ed. Engl.* **1977**, 16, 410–411.
- R. Breslow, W. Washburn, *J. Am. Chem. Soc.* **1970**, 92, 427–428.
- F. G. Klaerner, E. K. G. Schmidt, M. A. Abdel Rahman, H. Kollmar, *Angew. Chem.* **1982**, 94, 136–137; *Angew. Chem. Int. Ed. Engl.* **1982**, 21, 139.
- N. L. Bauld, T. L. Welscher, J. Cessac, R. L. Holloway, *J. Am. Chem. Soc.* **1978**, 100, 6920–6924.
- A. A. Deniz, K. S. Peters, G. J. Snyder, *Science* **1999**, 286, 1119–1122.
- N. Cohen, S. Benson, *Chem. Rev.* **1993**, 93, 2419–2438.
- K. M. Broadus, S. R. Kass, *J. Am. Chem. Soc.* **2000**, 122, 10697–10703.
- A. Fattahi, L. Lis, S. R. Kass, *J. Am. Chem. Soc.* **2005**, 127, 13065–13069.
- a) A. D. Becke, *J. Chem. Phys.* **1993**, 98, 5648–5652; b) C. T. Lee, W. T. Yang, R. G. Parr, *Phys. Rev. B* **1988**, 37, 785–789.
- a) M. J. S. Dewar, H. W. Kollmar, *J. Am. Chem. Soc.* **1975**, 97, 2933–2934; b) R. L. Disch, J. M. Schulman, M. L. Sabio, *J. Am. Chem. Soc.* **1985**, 107, 1904–1906; c) Y. Feng, L. Liu, J.-T. Wang, S.-W. Zhao, Q.-X. Guo, *J. Org. Chem.* **2004**, 69, 3129–3138; d) M. N. Glukhovtsev, R. D. Bach, S. Laiter, *J. Mol. Struct. J. Mol. Struct. (Theorchem.)* **1997**, 417, 123–129; e) M. N. Glukhovtsev, S. Laiter, A. Pross, *J. Phys. Chem.* **1995**, 99, 6828–6831; f) M. N. Glukhovtsev, S. Laiter, A. Pross, *J. Phys. Chem.* **1996**, 100, 17801–17806; g) R. C. Haddon, *Pure Appl. Chem. Pure*



- App. Chem.* **1982**, *54*, 1129–1142; h) W. J. Hehre, J. A. Pople, *J. Am. Chem. Soc.* **1975**, *97*, 6941–6955; i) B. A. Hess, Jr., W. D. Allen, D. Michalska, L. J. Schaad, H. F. Schaefer, III, *J. Am. Chem. Soc.* **1987**, *109*, 1615–1621; j) V. Hrouda, M. Roeselova, T. Bally, *J. Phys. Chem. A* **1997**, *101*, 3925–3935; k) B. S. Jursic, *Theochem* **2000**, *507*, 185–192; l) H. Kollmar, *J. Am. Chem. Soc.* **1980**, *102*, 2617–2621; m) H. Kollmar, F. Carrion, M. J. S. Dewar, R. C. Bingham, *J. Am. Chem. Soc.* **1981**, *103*, 5292–5303; n) B. Kovacevic, D. Baric, Z. B. Maksic, T. Muller, *J. Phys. Chem. A* **2004**, *108*, 9126–9133; o) J. S. Murray, J. M. Seminario, P. Politzer, *Int. J. Quantum Chem.* **1994**, *49*, 575–579; p) J.-W. Pan, D. W. Rogers, F. J. McLafferty, *Theochem* **1999**, *468*, 59–66; q) P. Politzer, M. E. Grice, J. S. Murray, J. M. Seminario, *Can. J. Chem.* **1993**, *71*, 1123–1127; r) D. W. Rogers, F. J. McLafferty, A. V. Podosenin, *J. Phys. Chem. A* **1996**, *100*, 17148–17151; s) S. W. Staley, T. D. Norden, *J. Am. Chem. Soc.* **1989**, *111*, 445–449; t) K. B. Wiberg, *Chem. Rev.* **2001**, *101*, 1317–1331.
- [16] L. A. Curtiss, K. Raghavachari, P. C. Redfern, V. Rassolov, J. A. Pople, *J. Chem. Phys.* **1998**, *109*, 7764–7776.
- [17] a) J. M. L. Martin, G. de Oliveria, *J. Chem. Phys.* **1999**, *111*, 1843–1856; b) S. Parthiban, J. M. L. Martin, *J. Chem. Phys.* **2001**, *114*, 6014–6029.
- [18] All the thermochemical data come from the following sources unless noted otherwise: E. P. L. Hunter, S. G. Lias “Proton Affinity Evaluation” and “Ionization Energy Evaluation” in *NIST Chemistry WebBook, NIST Standard Reference Database Number 69* (Eds.: P. J. Linstrom, W. G. Mallard), June 2005, National Institute of Standards and Technology, Gaithersburg MD, 20899 (<http://webbook.nist.gov>).
- [19] T. Su, M. T. Bowers, *Int. J. Mass Spectrom. Ion Phys.* **1973**, *12*, 347–356.
- [20] Z. Tian, A. Fattahi, L. Lis, S. R. Kass, unpublished results.
- [21] K. B. Wiberg, R. A. Fenoglio, *J. Am. Chem. Soc.* **1968**, *90*, 3395–3397.
- [22] S. J. Kaarsemaker, J. Coops, *Recl. Trav. Chim. Pays-Bas* **1952**, *71*, 261–276.
- [23] G3 theory does a good job reproducing  $\Delta H_f^\circ(9)$  (30 kJ mol<sup>−1</sup>) and the error in the W1 value can be attributed to a poor zero-point energy (that is,  $\Delta zpe(W1-G3) = 7$  kJ mol<sup>−1</sup>).
- [24] W. R. Roth, H. W. Lennartz, E. Vogel, M. Leiendecker, M. Oda, *Chem. Ber.* **1986**, *119*, 837–843.
- [25] Z. B. Maksic, B. Kovacevic, A. Lesar, *Chem. Phys.* **2000**, *253*, 59–71.
- [26] The preparation of this compound is given in the Supporting Information.
- [27] T. C. L. Wang, T. L. Ricca, A. G. Marshall, *Anal. Chem.* **1986**, *58*, 2935–2938.
- [28] Gaussian03 (Revision A.1), M. J. Frisch et al., see the Supporting Information.

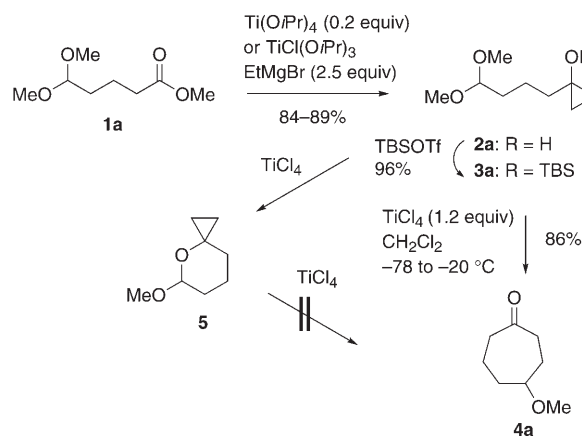
DOI: 10.1002/anie.200601011

# Formation of Seven-Membered Carbocycles by the Use of Cyclopropyl Silyl Ethers as Homoenols\*\*

Oleg L. Epstein, Sejin Lee, and Jin Kun Cha\*

The presence of heteroatom substituents on cyclopropanes enhances their reactivity toward electrophiles. Ring-opening reactions of cyclopropanols and siloxy derivatives have been extensively investigated.<sup>[1]</sup> An interesting variation involves the addition of other functionalities (e.g., vinyl or ethynyl) to cyclopropanols, which offers unique composite groups for the formation of C–C bonds.<sup>[2,3]</sup> The use of a cyclopropanol, which could be viewed as a “homoenol” or “homoenolate” equivalent, in the nucleophilic addition to a carbonyl compound or an acetal, has been limited primarily to 1-alkoxy-1-siloxycyclopropanes.<sup>[4]</sup> Little was known about the cognate homologous aldol or Mukaiyama reaction of parent cyclopropanols or siloxycyclopropanes.<sup>[5,6]</sup> We report herein an expedient entry to seven-membered carbocycles by the Kulinkovich cyclopropanation of acetal-tethered esters and a subsequent Lewis acid mediated ring expansion of the resulting cyclopropyl silyl ethers.

In an initial experiment, cyclopropanol **2a** was first prepared in 84–89% yield by the Kulinkovich cyclopropanation<sup>[7,8]</sup> of commercially available methyl 5,5-dimethoxyvalerate (**1**) with ethylmagnesium bromide (Scheme 1). Following silylation (96%), treatment of the resulting siloxycyclo-



**Scheme 1.** Annulation of seven-membered carbocycles. TBS = *tert*-butyldimethylsilyl, OTf = trifluoromethanesulfonate.

[\*] Dr. O. L. Epstein, Dr. S. Lee, Prof. J. K. Cha  
Department of Chemistry  
Wayne State University  
Detroit, MI 48202 (USA)  
Fax: (+1) 313-577-8822  
E-mail: jcha@chem.wayne.edu

[\*\*] This work was supported by NSF (CHE02-09321) and NIH (GM 35956).

propane **3a** with  $\text{TiCl}_4$  afforded 4-methoxycycloheptanone (**4a**) in 86% yield. The yield (63%) was lower when the corresponding trimethylsilyl (TMS) ether was employed. The use of a silyl ether proved to be necessary: cyclopropanol **2a** was quickly converted into **5** and its hemiacetal at  $-78^\circ\text{C}$  upon exposure to  $\text{TiCl}_4$ , but **5** gave only trace amounts of **4a** under several different conditions. This observation is in contrast to the interesting synthesis developed by Minbirole and co-workers of oxepanes from the respective endocyclic acetals.<sup>[6]</sup> These results suggest that the siloxycyclopropane is indeed the actual nucleophile that adds to the oxocarbenium ion intermediate.

Diastereoselectivity by a resident stereocenter was next examined with **3b–e** under two different conditions (Table 1). Both yields and stereoselectivity were improved by main-

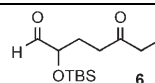
taining the reaction mixture at low temperature ( $-78^\circ\text{C}$ ; condition B). Unfortunately, 1,2- and 1,3-diastereoselectivity was surprisingly low (entries 1–4).<sup>[9]</sup> Enantioselective synthesis was achieved, albeit in modest selectivity, by means of a nonracemic  $\text{C}_2$ -symmetric acetal (entry 5). The stereochemistry of the major product **4f** was secured by X-ray analysis.<sup>[10]</sup> (*R,R*)-(+)-Hydrobenzoin was chosen as a chiral auxiliary primarily because of its commercial availability and ease of removal. At present, the origin for the observed 1,3-diastereofacial selectivity is unclear.<sup>[11]</sup>

Regioselectivity was also examined: it is the less-substituted C–C bond of the three-membered ring that reacts with the oxocarbenium ion (entries 6–8).<sup>[12]</sup> It is interesting to note that the major products **4h** and **4i**, obtained from **3h**<sup>[13a]</sup> and **3i**,<sup>[13b]</sup> are diastereomeric (Table 1).

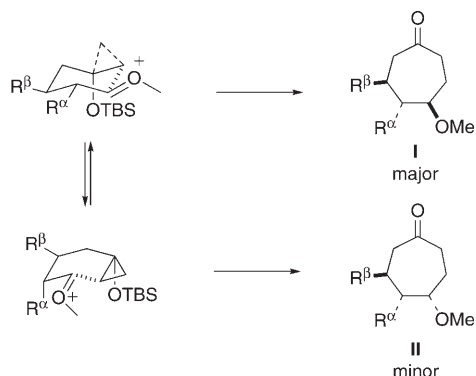
**Table 1:** Diastereo- and regioselectivity of seven-membered-ring formation.

Entry	Substrate	Conditions <sup>[a]</sup>	Major product	Yield [%]	Diastereoselectivity
		$\xrightarrow[\text{Condition A or B}]{\text{TiCl}_4, \text{CH}_2\text{Cl}_2}$			
1	<b>3b</b> : R = Me	A	<b>4b</b>	77	1:0.9
		B	<b>4b</b>	91	1.7:1
2	<b>3c</b> : R = OTBS	A	<b>4c</b> + <b>6</b> <sup>[b]</sup>	45 22	1:0.9
		$\xrightarrow[\text{CH}_2\text{Cl}_2]{\text{TiCl}_4}$			
3	<b>3d</b> : R <sup>1</sup> = TBS	A	<b>4d</b>	58	1.3:1
		B	<b>4d</b>	65	1.5:1
4	<b>3e</b> : R <sup>1</sup> = TIPS	A	<b>4e</b>	67	2:1
		$\xrightarrow[\text{CH}_2\text{Cl}_2]{\text{TiCl}_4}$			
5	<b>3f</b>	A	<b>4f</b>	72	3:1
		B	<b>4f</b>	84	3.5:1
		$\xrightarrow[\text{CH}_2\text{Cl}_2]{\text{TiCl}_4}$			
6	<b>3g</b> : R <sup>2</sup> = Me	A	<b>4g</b>	82	2.5:1
7	<b>3h</b> : R <sup>2</sup> = $(\text{CH}_2)_2\text{OTIPS}$	A	<b>4h</b>	76	2.5:1
		$\xrightarrow[\text{CH}_2\text{Cl}_2]{\text{TiCl}_4}$			
8	<b>3i</b> : R <sup>2</sup> = $(\text{CH}_2)_2\text{OTIPS}$	A	<b>4i</b>	68	3:1

[a] Condition A:  $\text{TiCl}_4$  (1.2 equiv),  $-78 \rightarrow -20^\circ\text{C}$ ; condition B:  $\text{TiCl}_4$  (2.0 equiv),  $-78^\circ\text{C}$ . [b]



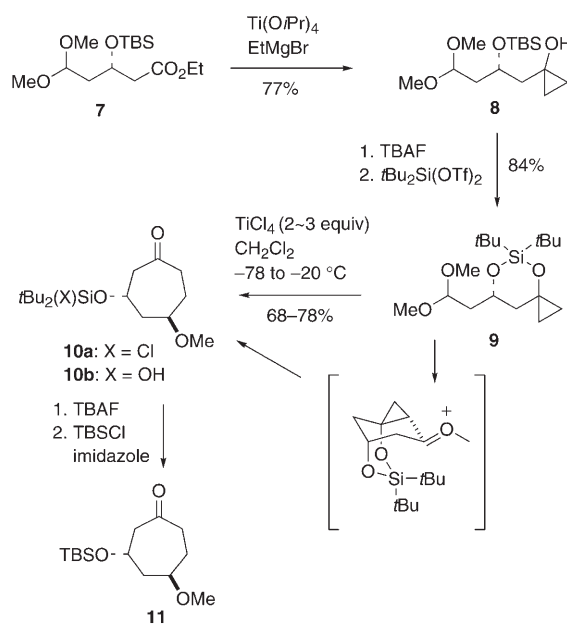
The surprisingly modest diastereoselectivity in the cyclization might be attributed to competing stereochemical pathways that involve chair, boat, and/or twist-boat (not shown) conformations (Scheme 2).<sup>[14]</sup> Assuming that a chair-



**Scheme 2.** Stereochemical rationale.

like transition state is of lower energy, the configuration of the major isomers **I** is tentatively assigned as shown in Table 1. The minor isomers **II** could arise from a boatlike transition state; for example, when  $R^a = H$  (e.g., **3d** and **3e**), the indicated boat conformation might become competing. At present, one cannot discount the involvement of a gauche conformation of the oxocarbenium ion in a chairlike transition state in the formation of the minor isomers. Elucidation of important factors that influence diastereocontrol might be possible by judicious placement of multiple substituents but must await further investigations.

Toward eventual applications in natural product synthesis, such as the stereoselective syntheses of skipped polyols, we developed an effective strategy for diastereoselective cyclization by relying on di-*tert*-butylsilylene as a conformational lock (Scheme 3). Subsequent to the Kulinkovich cyclopropanation of



**Scheme 3.** Diastereoselective cyclization by using di-*tert*-butylsilylene. TBAF = tetrabutylammonium fluoride.

of **7**,<sup>[9]</sup> the resulting cyclopropanol **8** was converted into silylene **9** by standard methods. The key cyclization proceeded cleanly by the action of  $TiCl_4$  to deliver **10** as a single diastereomer, but as an inconsequential mixture of **10a** and **10b**. The stereochemistry of **10** was tentatively assigned by consideration of the most plausible transition state. As additional support, **10** was converted into **11**, which proved to be identical to the minor isomer from the cyclization of **3d** (Table 1, entry 3). Together with diastereoselective hydroxycyclopropanation of secondary homoallylic alcohols,<sup>[13b]</sup> this diastereoselective approach should be useful in a rapid increase in molecular complexity by the coupling of two large segments.

In conclusion, a concise synthesis of multifunctionalized seven-membered carbocycles has been achieved by sequential application of the Kulinkovich cyclopropanation of acetal-tethered esters and the Lewis acid mediated addition of the resulting cyclopropyl silyl ethers to the oxonium ion intermediates. Particularly noteworthy is the effective use of a *tert*-butylsilylene group for diastereoselective cyclization. Mechanistic studies and applications in natural product synthesis will be reported in due course.

Received: March 14, 2006

Published online: July 3, 2006

**Keywords:** carbocycles · cyclopropanation · cyclopropanols · homoenols

- [1] For reviews, see: a) C. H. DePuy, *Acc. Chem. Res.* **1968**, *1*, 33; b) D. H. Gibson, C. H. DePuy, *Chem. Rev.* **1974**, *74*, 605; c) I. Ryu, S. Murai, Houben-Weyl, *Houben-Weyl Methods of Organic Chemistry*, Vol. E17c, **1997**, p. 1985; d) O. G. Kulinkovich, *Chem. Rev.* **2003**, *103*, 2597; see also: e) H. N. C. Wong, M. Y. Hon, C. W. Tse, Y. C. Yip, J. Tanko, T. Hudlicky, *Chem. Rev.* **1989**, *89*, 165; f) H.-U. Reissig, R. Zimmer, *Chem. Rev.* **2003**, *103*, 1151; g) M. Yu, B. L. Pagenkopf, *Tetrahedron* **2005**, *61*, 321.
- [2] For reviews, see: a) B. M. Trost, *Top. Curr. Chem.* **1986**, *133*, 3; b) J. Salatin, *Top. Curr. Chem.* **1988**, *144*, 1; c) B. M. Trost, A. Brandi, *J. Am. Chem. Soc.* **1984**, *106*, 5041; d) B. M. Trost, D. C. Lee, *J. Am. Chem. Soc.* **1988**, *110*, 6556; e) B. M. Trost, D. W. C. Chen, *J. Am. Chem. Soc.* **1996**, *118*, 12541.
- [3] a) J.-H. Youn, J. Lee, J. K. Cha, *Org. Lett.* **2001**, *3*, 2935; b) H.-S. Oh, H. I. Lee, J. K. Cha, *Org. Lett.* **2002**, *4*, 3707; c) H.-S. Oh, J. K. Cha, *Tetrahedron: Asymmetry* **2003**, *14*, 2911.
- [4] I. Kuwajima, E. Nakamura, *Top. Curr. Chem.* **1990**, *155*, 1.
- [5] Cf. J. T. Carey, C. Knors, P. Helquist, *J. Am. Chem. Soc.* **1986**, *108*, 8313.
- [6] During the course of our own investigation, an elegant synthesis of oxepanes appeared: K. E. O'Neil, S. V. Kingree, K. P. C. Minbiole, *Org. Lett.* **2005**, *7*, 515.
- [7] a) O. G. Kulinkovich, S. V. Sviridov, D. A. Vasilevskii, T. S. Pritytskaya, *Zh. Org. Khim.* **1989**, *25*, 2244; b) O. G. Kulinkovich, S. V. Sviridov, D. A. Vasilevskii, *Synthesis* **1991**, 234; c) O. G. Kulinkovich, A. I. Savchenko, S. V. Sviridov, D. A. Vasilevski, *Mendeleev Commun.* **1993**, 230.
- [8] For reviews, see: a) O. G. Kulinkovich, A. de Meijere, *Chem. Rev.* **2000**, *100*, 2789; b) F. Sato, H. Urabe, S. Okamoto, *Chem. Rev.* **2000**, *100*, 2835; c) O. G. Kulinkovich, *Eur. J. Org. Chem.* **2004**, 4517.
- [9] Substrates **3d**, **e** were prepared from enantiomerically enriched **7** (> 95% ee) by adaptation of two reported procedures: a) G. P.-J.

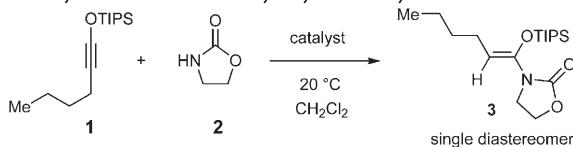


- Hareau, M. Koiwa, S. Hikichi, F. Sato, *J. Am. Chem. Soc.* **1999**, *121*, 3640; b) J. S. Panek, P. Liu, *J. Am. Chem. Soc.* **2000**, *122*, 11090; c) M. Tokunaga, J. F. Larrow, F. Kakiuchi, E. N. Jacobsen, *Science* **1997**, *277*, 936.
- [10] We thank Dr. Mary Jane Heeg for single-crystal X-ray analysis. CCDC 280875 contains the supplementary crystallographic data for this paper. These data can be obtained free of charge from The Cambridge Crystallographic Data Centre via [www.ccdc.cam.ac.uk/products/csd/request](http://www.ccdc.cam.ac.uk/products/csd/request).
- [11] Compare with: a) A. Alexakis, P. Mangeney, *Tetrahedron: Asymmetry* **1990**, *1*, 477; b) S. E. Denmark, N. G. Almstead, *J. Am. Chem. Soc.* **1991**, *113*, 8089; c) T. Sammakia, R. S. Smith, *J. Am. Chem. Soc.* **1992**, *114*, 10998.
- [12] This mode of addition might be considered as a formal “edge” attack, as conformational constraints preclude “corner” attack: C. Meyer, N. Blanchard, M. Defosseux, J. Cossy, *Acc. Chem. Res.* **2003**, *36*, 766.
- [13] Substrates **3g–i** were prepared diastereoselectively by previously reported methods: a) J. Lee, H. Kim, J. K. Cha, *J. Am. Chem. Soc.* **1996**, *118*, 4198; b) L. G. Quan, S.-H. Kim, J. C. Lee, J. K. Cha, *Angew. Chem.* **2002**, *41*, 2264; *Angew. Chem. Int. Ed.* **2002**, *41*, 2160.
- [14] Intervention of competing chair–boat pathways is known for similar cyclizations: a) A. B. Smith III, K. Minbirole, P. R. Verhoest, T. J. Beauchamp, *Org. Lett.* **1999**, *1*, 913; b) J. E. Dalgard, S. D. Rychnovsky, *J. Am. Chem. Soc.* **2004**, *126*, 15662; c) Q. Sun, J. S. Panek, *J. Am. Chem. Soc.* **2004**, *126*, 2425.

example of hydroamination of electron-rich alkynes by using a silver-based catalyst that enables *syn*-selective addition of secondary amides and carbamates to furnish the corresponding silyl ketene aminals with high efficiency and excellent diastereoselectivity. Our mechanistic studies demonstrate that the reaction proceeds by a fast and reversible silver-alkyne complexation, followed by a rate-determining C–N bond-forming step, which provides an important mechanistic platform for further development of  $d^{10}$  catalysts for alkyne and alkene hydroamination.

During our continuing investigation of the development of new catalytic C–C and C–X bond-forming reactions with electron-rich alkynes,<sup>[6]</sup> we discovered that treatment of siloxy alkyne **1** (TIPS =  $i\text{Pr}_3\text{Si}$ ) with carbamate **2** in the presence of either a silver- or a gold-based catalyst resulted in the formation of silyl ketene aminal **3** (Table 1). Initial inves-

**Table 1:** Hydroamination of siloxy alkynes: catalyst evaluation.



Entry	Catalyst	Catalyst loading	Reaction time	Yield [%] <sup>[a]</sup>
1	AuCl	5 mol %	1.5 h	51
2	AuCl <sub>3</sub>	5 mol %	30 min	75
3	AgNTf <sub>2</sub>	5 mol %	30 min	91 (82 <sup>[b]</sup> )
4	<b>AgNTf<sub>2</sub></b>	<b>1 mol %</b>	<b>30 min</b>	<b>95 (86<sup>[b]</sup>)</b>
5	AgNTf <sub>2</sub>	0.3 mol %	2 h	81
6	HNTf <sub>2</sub>	5 mol %	3 h	< 5
7	PdCl <sub>2</sub>	5 mol %	3 h	< 5 <sup>[c]</sup>
8	PtCl <sub>2</sub>	5 mol %	3 h	40 <sup>[c]</sup>

[a] Determined by NMR integration with respect to an internal standard. [b] Yield of isolated product (reaction giving best yield highlighted in bold). [c] The reaction was conducted in toluene at 80 °C.

## Hydroamination

DOI: 10.1002/anie.200601276

## Silver-Catalyzed Hydroamination of Siloxy Alkynes\*\*

Jianwei Sun and Sergey A. Kozmin\*

Transition-metal-catalyzed hydroamination of alkynes has emerged as a valuable method for C–N bond formation.<sup>[1]</sup> While significant progress in this area has been made,<sup>[2]</sup> several important limitations remain to be addressed. The majority of the previously developed catalytic processes employ highly nucleophilic primary amines that afford the corresponding imines as a result of tautomerization of the initially produced enamides.<sup>[3–5]</sup> We describe herein the first

tigations revealed that the use of AgNTf<sub>2</sub> (Tf = CF<sub>3</sub>SO<sub>2</sub>) proved to be superior to that of AuCl and AuCl<sub>3</sub> (Table 1, entries 1–3).<sup>[7]</sup> This finding is especially noteworthy as silver-based catalysts have not been used extensively for the hydroamination of alkynes and alkenes.<sup>[8]</sup> The hydroamination product, **3**, was obtained in 86% yield after 30 min at room temperature by using only 1 mol % of AgNTf<sub>2</sub> (Table 1, entry 4). The catalyst loading could be further decreased to 0.3 mol % without significant loss of efficiency (Table 1, entry 5). Furthermore, subjecting the reactants to HNTf<sub>2</sub> (5 mol %) produced only a trace of enol silane **3**, which ruled out a possible involvement of the conjugate Brønsted acid in the alkyne activation (Table 1, entry 6). Interestingly, PdCl<sub>2</sub> and PtCl<sub>2</sub> proved to be much less effective at catalyzing this reaction (Table 1, entries 7 and 8).

Having established a standard reaction protocol, we examined the scope of this catalytic process. The reaction of either 5- or 4-substituted oxazolidinones, **4** and **6**, with siloxy alkyne **1** afforded the desired products, **5** and **7**, respectively (Table 2, entries 1 and 2). Hydroamination of **1** with secondary amide **8** afforded silyl ketene aminal **9** with good efficiency (Table 2, entry 3), thus demonstrating that the

[\*] J. Sun, Prof. Dr. S. A. Kozmin  
Department of Chemistry  
University of Chicago  
5735 South Ellis Avenue, Chicago, IL 60637 (USA)  
Fax: (+1) 773-702-0805  
E-mail: skozmin@uchicago.edu

[\*\*] This work was supported by the NSF CAREER (CHE-0447751). S.A.K. thanks the Sloan Foundation, the Dreyfus Foundation, Amgen, and GlaxoSmithKline for additional funding.

Supporting information for this article is available on the WWW under <http://www.angewandte.org> or from the author.

**Table 2:** Ag-catalyzed hydroamination: nucleophile scope.<sup>[a]</sup>

Entry	Nucleophile	Product	Yield [%] <sup>[b]</sup>
1			72
2			86
3			71
4			80
5			86

[a] General reaction protocol: siloxy alkyne (0.40 mmol) and amide (0.36 mmol) were dissolved in  $\text{CH}_2\text{Cl}_2$  (5 mL) and treated with  $\text{AgNTf}_2$  (0.0036 mmol) at  $20^\circ\text{C}$ . The resulting solution was stirred for 30 min, then treated with one drop of  $\text{Et}_3\text{N}$ . The solvent was removed under reduced pressure and the crude product was purified by flash chromatography on silica gel. [b] Yield of isolated spectroscopically pure products that were fully characterized by NMR and IR spectroscopies and mass spectrometry.

reaction is not limited to the use of cyclic carbamates. Furthermore, lactams **10** and **12** were used to produce the corresponding enol silanes, **11** and **13** (Table 2, entries 4 and 5), thus illustrating the ability of this method to produce silyl ketene aminals that would not be available by using conventional silylation methods due to the problems associated with chemoselective generation of the required enols or enolates.

We next examined the scope of siloxy alkyne substitution (Table 3). Subjecting arene- or alkene-conjugated alkynes, **14** and **16**, to the standard reaction conditions with carbamate **2** afforded the corresponding ketene aminals, **15** and **17**, respectively (Table 3, entries 1 and 2). Hydroamination of diyne **18** proceeded to give enyne **19** with complete chemo- and diastereoselectivity (Table 3, entry 3). Other alkyl-substituted alkynes, **20** and **22**, gave the expected hydroamination products, **21** and **23** (Table 3, entries 4 and 5). The lower efficiency of the reaction in entry 5 of Table 3 is attributed to the significant increase in the steric bulk in direct proximity to the reaction site. While the current protocol is highly effective for hydroamination of a wide range of siloxy alkynes, ynamides and simple internal alkynes proved to be unreactive under its conditions.

To gain further insight into the mechanism of the Ag-catalyzed hydroamination and the nature of the observed

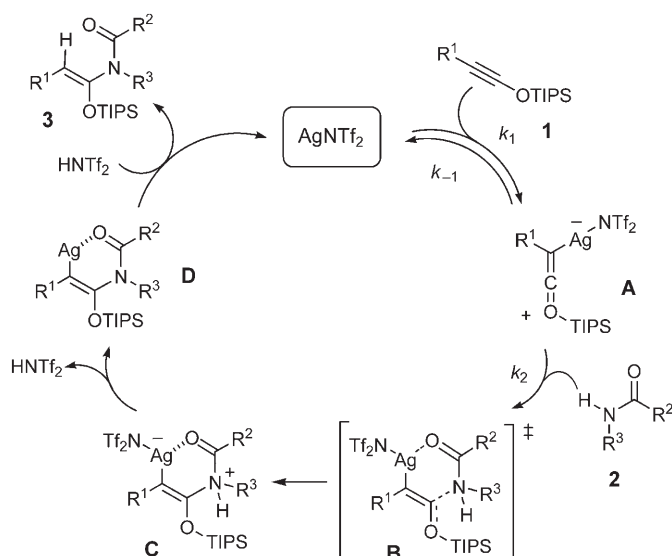
**Table 3:** Ag-catalyzed hydroamination: alkyne scope.

Entry	Alkyne	Product	Yield [%] <sup>[a]</sup>
1			86
2			81
3			76
4			73
5			45

[a] Refers to yields of isolated spectroscopically pure products that were fully characterized by NMR and IR spectroscopies and mass spectrometry.

high *syn* selectivity, we carried out a series of kinetic studies of the reaction of alkyne **1** with carbamate **2** in the presence of  $\text{AgNTf}_2$  at  $-20^\circ\text{C}$ . We found that the reaction was first-order with respect to both carbamate **2** and the silver catalyst, and zero-order with respect to alkyne **1**, thus providing the empirical rate law:  $r = k_{\text{obs}}[\text{AgNTf}_2][\text{2}]$ , in which  $k_{\text{obs}} = 1.52 \times 10^{-2} \text{ M}^{-1} \text{ s}^{-1}$ .<sup>[9]</sup> Furthermore, using deuterated oxazolidinone **2**, we found no primary deuterium isotope effect ( $k_{\text{H}}/k_{\text{D}} = 1.03$ ).

We propose that the reaction begins with a fast and reversible complexation between **1** and  $\text{AgNTf}_2$  to give silver-alkyne complex **A** (Scheme 1), which is supported by our previous stoichiometric studies.<sup>[6b]</sup> At high concentrations of alkyne, the catalyst is saturated with the alkyne and the equilibrium favors intermediate **A**, which explains why the reaction is zero-order with respect to the alkyne. The alkyne activation is followed by the rate-determining step, which entails the addition of the carbamate **2** to the silver-alkyne complex **A**. We believe that this reaction proceeds via a six-membered chelated transition state, **B**, which explains the high *syn* selectivity of the hydroamination process.<sup>[10]</sup> Subsequent release of the proton from intermediate **C**, followed by protodemetalation of the alkenyl-silver compound **D** affords the observed product, **3**, and regenerates the silver catalyst. The proposed rate-determining step is fully consistent with the absence of any primary deuterium isotope effect.



**Scheme 1.** Proposed catalytic cycle for the silver-catalyzed hydroamination of siloxy alkynes.

In summary, our study demonstrates for the first time the ability of a silver-based catalyst to promote a *syn*-selective hydroamination of electron-rich alkynes with either secondary amides or carbamates. This process represents an efficient method for the synthesis of a range of synthetically useful silyl ketene amins and provides an important mechanistic platform for further development of hydroamination reactions with late-transition-metal catalysts.<sup>[11]</sup>

Received: March 31, 2006

Published online: June 29, 2006

**Keywords:** alkynes · homogeneous catalysis · hydroamination · silver

- [1] For selected reviews, see: a) T. E. Müller, M. Beller, *Chem. Rev.* **1998**, *98*, 675–703; b) M. Nobis, B. Driessen-Hölscher, *Angew. Chem.* **2001**, *113*, 4105–4108; *Angew. Chem. Int. Ed.* **2001**, *40*, 3983–3985; c) F. Pohlki, S. Doye, *Chem. Soc. Rev.* **2003**, *32*, 104–114; d) M. Beller, J. Seayad, A. Tillack, H. Jiao, *Angew. Chem.* **2004**, *116*, 3448–3479; *Angew. Chem. Int. Ed.* **2004**, *43*, 3368–3398; e) F. Alonso, I. P. Beletskaya, M. Yus, *Chem. Rev.* **2004**, *104*, 3079–3159.
- [2] For representative examples, see: a) W. Reppe, *Justus Liebigs Ann. Chem.* **1956**, *601*, 81–138; b) M. Kimura, S. Kure, Z. Yoshida, S. Tanaka, K. Fugami, Y. Tamaru, *Tetrahedron Lett.* **1990**, *31*, 4887–4890; c) P. L. McGrane, T. Livinghouse, *J. Am. Chem. Soc.* **1992**, *114*, 1323–1324; d) P. J. Walsh, A. M. Baranger, R. G. Bergman, *J. Am. Chem. Soc.* **1992**, *114*, 1708–1719; e) Y. Li, T. J. Marks, *J. Am. Chem. Soc.* **1996**, *118*, 9295–9306; f) E. M. Campi, W. R. Jackson, *J. Organomet. Chem.* **1996**, *523*, 205–209; g) A. Haskell, T. Straub, M. S. Eisen, *Organometallics* **1996**, *15*, 3773–3775; h) T. E. Müller, *Tetrahedron Lett.* **1998**, *39*, 5961–5962; i) E. Haak, I. Bytschkov, S. Doye, *Angew. Chem.* **1999**, *111*, 3584–3586; *Angew. Chem. Int. Ed.* **1999**, *38*, 3389–3391; j) M. Tokunaga, M. Eckert, Y. Wakatsuki, *Angew. Chem.* **1999**, *111*, 3416–3419; *Angew. Chem. Int. Ed.* **1999**, *38*, 3222–3225; k) T. E. Müller, M. Grosche, E. Herdtweck, A.-P. Pleier, E. Walter, Y.-K. Yan, *Organometallics* **2000**, *19*, 170–183; l) C. G. Hartung, A. Tillack, H. Trauthwein, M. Beller, *J. Org. Chem.* **2001**, *66*, 6339–6343; m) A. Tillack, I. G. Castro, C. G. Hartung, M. Beller, *Angew. Chem.* **2002**, *114*, 2646–2648; *Angew. Chem. Int. Ed.* **2002**, *41*, 2541–2544; n) T. Shimada, Y. Yamamoto, *J. Am. Chem. Soc.* **2002**, *124*, 12670–12671; o) T. Shimada, Y. Yamamoto, *J. Am. Chem. Soc.* **2003**, *125*, 6646–6647; p) L. L. Anderson, J. Arnold, R. G. Bergman, *Org. Lett.* **2004**, *6*, 2519–2522; q) T. Shimada, G. B. Bajracharya, Y. Yamamoto, *Eur. J. Org. Chem.* **2005**, 59–62; r) L. D. Field, B. A. Messerle, K. Q. Vuong, P. Turner, *Organometallics* **2005**, *24*, 4241–4250; s) A. Zulys, M. Dochnahl, D. Hollmann, K. Lohnwitz, J.-S. Herrmann, P. W. Roesky, S. Blechert, *Angew. Chem.* **2005**, *117*, 7971–7976; *Angew. Chem. Int. Ed.* **2005**, *44*, 7794–7798; t) L. J. Gooßen, J. E. Rauhaus, G. Deng, *Angew. Chem.* **2005**, *117*, 4110–4113; *Angew. Chem. Int. Ed.* **2005**, *44*, 4042–4045.
- [3] For examples of intermolecular alkyne hydroamination with amides, see: T. Kondo, A. Tanaka, S. Kotachi, Y. Watanabe, *J. Chem. Soc. Chem. Commun.* **1995**, 413–414.
- [4] For use of secondary amines, see: a) Y. Uchamaru, *Chem. Commun.* **1999**, 1133–1134; b) J. Barluenga, F. Aznar, R. Liz, R. Rodes, *J. Chem. Soc. Perkin Trans. 1* **1980**, 2732–2737; c) J. Barluenga, F. Aznar, *Synthesis* **1977**, 195–197.
- [5] For Pd-catalyzed oxidative alkene amination with cyclic carbamates, see: V. I. Timokhin, S. S. Stahl, *J. Am. Chem. Soc.* **2005**, *127*, 17888–17893.
- [6] a) M. P. Schramm, D. S. Reddy, S. A. Kozmin, *Angew. Chem.* **2004**, *116*, 4404–4407; *Angew. Chem. Int. Ed.* **2001**, *40*, 4274–4277; b) R. F. Sweis, M. P. Schramm, S. A. Kozmin, *J. Am. Chem. Soc.* **2004**, *126*, 7442–7443; c) D. S. Reddy, S. A. Kozmin, *J. Org. Chem.* **2004**, *69*, 4860–4862; d) L. Zhang, S. A. Kozmin, *J. Am. Chem. Soc.* **2004**, *126*, 10204–10205; e) L. Zhang, S. A. Kozmin, *J. Am. Chem. Soc.* **2004**, *126*, 11806–11807; f) J. Sun, S. A. Kozmin, *J. Am. Chem. Soc.* **2005**, *127*, 13512–13513.
- [7] For examples of Au-catalyzed hydroamination of alkynes, alkenes, and dienes, see: a) Y. Fukuda, K. Utimoto, *Synthesis* **1991**, 975–978; b) A. Arcadi, S. Di Giuseppe, F. Marinelli, E. Rossi, *Adv. Synth. Catal.* **2001**, *343*, 443–446; c) E. Mizushima, T. Hayashi, M. Tanaka, *Org. Lett.* **2003**, *5*, 3349–3352; d) J. Zhang, C.-G. Yang, C. He, *J. Am. Chem. Soc.* **2006**, *128*, 1798–1799; e) C. Brouwer, C. He, *Angew. Chem.* **2006**, *118*, 1776–1779; *Angew. Chem. Int. Ed.* **2006**, *45*, 1744–1747; f) D. Kadzimirsz, D. Hildebrandt, K. Merz, G. Dyker, *Chem. Commun.* **2006**, 6, 661–662.
- [8] a) R. S. Robinson, M. C. Dovey, D. Gravestock, *Eur. J. Org. Chem.* **2005**, 505–511; b) Y. Luo, Z. Li, C. Li, *Org. Lett.* **2005**, *7*, 2675–2678; hydroamination was proposed to precede cyclization.
- [9] See the Supporting Information for detailed procedures.
- [10] For a proposed six-membered transition state in the Pd-catalyzed oxidative amination of alkenes, see: J. L. Brice, J. E. Harang, V. I. Timokhin, N. R. Anastasi, S. S. Stahl, *J. Am. Chem. Soc.* **2005**, *127*, 2868–2869.
- [11] For selected examples of the synthetic utility of silyl ketene acetals and amins, see: a) I. Fleming, A. Barbero, D. Walter, *Chem. Rev.* **1997**, *97*, 2063–2192; b) *Silicon in Organic, Organometallic, and Polymer Chemistry* (Ed.: M. A. Brook), Wiley-VCH, Weinheim, **2000**; c) I. F. Lutsenko, Y. I. Baukov, A. S. Kostyuk, N. I. Savelyeva, V. K. Krysin, *J. Organomet. Chem.* **1969**, *17*, 241–262; d) R. Zerrer, G. Simchen, *Synthesis* **1992**, 922–924; e) K. Neuschütz, J. Simone, T. Thyran, R. Neier, *Helv. Chim. Acta* **2000**, *83*, 2712–2737.



## The Roles of Hydrogen Bonding and Sterics in RNA Interference\*\*

Alvaro Somoza, Jijumon Chelliserrykattil, and Eric T. Kool\*

RNA interference (RNAi) has become one of the most important new tools for biological research in the past decade.<sup>[1–5]</sup> This methodology is used widely for “knocking down” (regulating) expression of specific genes in cell cultures, and it can be carried out conveniently by using synthetic RNA oligonucleotides (short interfering RNAs or siRNAs) that are complementary to a segment of a desired messenger RNA target. When the appropriate double-stranded 21mer RNAs (the sense and antisense strands) are added to a cell culture, they are taken up by the cellular RNA-induced silencing complex (RISC), which presents the separated antisense (“guide”) strand for binding and subsequent cleavage of the target mRNA.<sup>[1–5,6]</sup> One of the most useful features of this approach is that the resulting mRNA cleavage occurs with sequence selectivity<sup>[7,8]</sup> so that one gene can often be knocked down to low levels of activity with little effect on the rest of cellular gene expression.<sup>[9,10]</sup>

Recent RNA-interference studies with mismatched target RNAs have demonstrated sequence selectivity (at the single-nucleotide level) at many positions on the standard 21-nucleotide probe length.<sup>[8]</sup> The origins of this selectivity are not known; selectivity may arise from base-pair hydrogen bonding, which contributes to selective hybridization,<sup>[11]</sup> or from steric complementarity of nucleobases, which is important in replication by DNA polymerases.<sup>[12]</sup> Furthermore, selectivity could come chiefly from the RNA itself, or could be modulated by the RISC complex. Beyond this, it is not clear why responsiveness to mismatches varies along the siRNA strand.<sup>[8]</sup> Although recent structural studies of Piwi/Argonaute/Zwille (PAZ) domains<sup>[13]</sup> and *Argonaute* proteins<sup>[14]</sup> (parts of the RISC complex) have led to models of RNA cleavage, no structures of the RISC complex bound to siRNA and mRNA are yet available.

Herein, we describe experiments that give insights into the origins of RNAi activity and selectivity. We have evaluated this with a nonpolar, non-hydrogen-bonding ribonucleoside isostere (rF; Figure 1)<sup>[15,16]</sup> that we have incorpo-

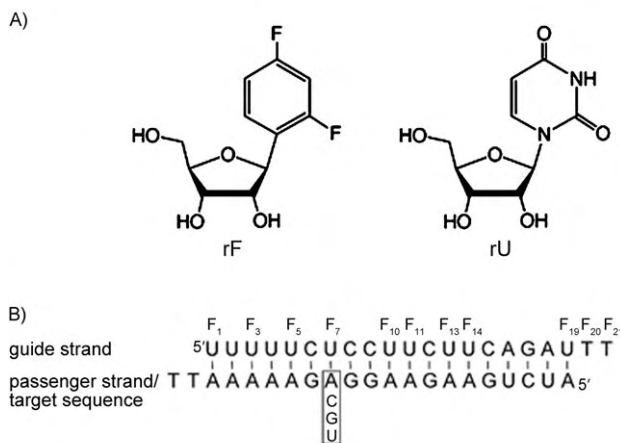


**Figure 1.** Modified RNA structures and sequences used in this study. A) 2,4-Difluorobenzene ribonucleoside rF, a uridine nonpolar isostere, is shown next to uridine (rU). B) Sequences of siRNA duplexes used in RNAi experiments. Sites of rF substitutions in various experiments are marked with “F<sub>n</sub>”. The “guide”-strand sequence (antisense to the mRNA) is above; “passenger” strands (corresponding to the target mRNA and mutants) are below. The shown sequence corresponds to nucleotides 501–519 in *Renilla* luciferase mRNA.

rated into a siRNA guide strand in place of natural uridine. We found that this analogue can maintain near-wild-type activity in human cells at a number of positions in the strand and importantly, we observe that it can retain and even enhance sequence selectivity.

The analogue rF contains difluorobenzene, a uracil isostere, in place of the earlier-used difluorotoluene deoxyriboside (dF) as a thymidine mimic in DNA.<sup>[17]</sup> This nonpolar structure serves as a probe for the importance of hydrogen bonding and electrostatics in the RNA context.<sup>[15,16,18]</sup> RNA hybridization studies have shown that rF pairs have little or no inherent selectivity and are destabilizing to the RNA duplex<sup>[15]</sup> consistent with its nonpolar properties; this is also consistent with the behavior of dF in DNA.<sup>[19]</sup> In separate experiments, we incorporated rF into eleven different positions in place of natural rU along an RNA guide strand that was complementary to a luciferase reporter gene in an A-rich site (Figure 1).

Thermal denaturation studies of synthetic RNA duplexes showed that rF is destabilizing to 21mer double-stranded siRNAs when it is placed near the center (see the Supporting Information). However, this destabilization lessened near the duplex ends (positions 1, 3, and 19), and virtually no destabilization was seen at unpaired positions 20 and 21. This is similar to the positional effects of mismatches on the helix stability of RNA duplexes,<sup>[20]</sup> and is reminiscent of the behavior of dF in DNA.<sup>[11]</sup> To measure selectivity, studies were also carried out with RNAs mismatched at a central position (position 7), where destabilization by rF is high. Results confirmed (see the Supporting Information) that this nonpolar nucleoside gives no pairing selectivity for adenine.<sup>[15,16,18,19]</sup> By comparison, natural uridine showed substantial pairing selectivity for adenine.

We then carried out separate RNA-interference studies in HeLa cells with the eleven modified guide-RNA strands

[\*] Dr. A. Somoza, Dr. J. Chelliserrykattil, Prof. Dr. E. T. Kool  
Department of Chemistry, Stanford University  
Stanford, CA 94305-5080 (USA)  
Fax: (+1) 650-725-0259  
E-mail: kool@stanford.edu

[\*\*] This work was supported by the US National Institutes of Health (GM072705), and by a Marie Curie OIF Fellowship (6th Framework Program, UE) to A.S.

Supporting information for this article is available on the WWW under <http://www.angewandte.org> or from the author.

containing single rF substitutions. Experiments were carried out in triplicate. The cells were first transfected with dual reporter plasmids that express *Renilla* luciferase and firefly luciferase, the activities of which could be separately quantitated by their luminescence.<sup>[21]</sup> The synthetic RNAs were complementary to positions 501–519 of *Renilla* luciferase mRNA<sup>[22]</sup> and not complementary to the firefly mRNA. The effects of the different RNAs on luciferase expression were evaluated after dosing with 0.21–21 ng of RNA in the cell media, and measuring relative luminescence responses after 22 h. The firefly luminescence is an internal control that rules out possible indirect effects of the different siRNAs, such as selective cell toxicity, variable cellular uptake, or differential enzymatic degradation.

Results showed that the rF substitution disrupted *Renilla* luciferase-specific RNA interference activity at two central positions of the guide RNA; surprisingly, however, a number of other positional substitutions retained near-wild-type activity (Figure 2). Substitutions of rF at positions 10 and 11

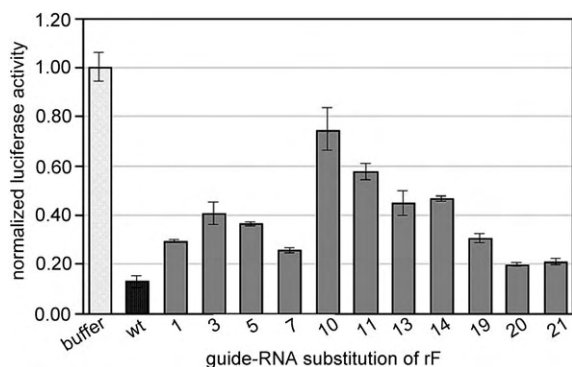


**Figure 2.** Histogram of gene-specific RNA interference activity for rF-substituted siRNAs at one site in the *Renilla* luciferase mRNA expressed in HeLa cells. The numbers refer to the position of rF in the guide-RNA strand. Data were normalized by an internal control of a noncomplementary firefly luciferase gene. Data are for the 2.1-ng RNA amount, and were measured in triplicate; standard deviations are as indicated. See the Supporting Information for the full data. wt = wild type.

caused loss of most of the interference activity even with a higher 21-ng dose of siRNA (see the Supporting Information); these positions flank the expected cleavage site in the target mRNA.<sup>[3]</sup> In contrast to this, all other substitutions retained substantial activity within 2–4-fold of the natural uracil-substituted strand. Especially remarkable is substitution at position 7, which showed near-wild-type activity despite the strong destabilization that this substitution causes (Figure 3). At the higher (21 ng) dose, guide RNAs containing rF at positions 1, 7, 19, 20, and 21 all showed near-wild-type activity (see the Supporting Information). Intermediate effects were found at positions 3, 5, 13, and 14. These results suggest that canonical hydrogen bonding is not necessary at several positions for the RISC complex to maintain high levels of RNA interference activity with the intended target.

The retention of strong activity at position 7 with the rF analogue, despite its central location in the siRNA, offers a

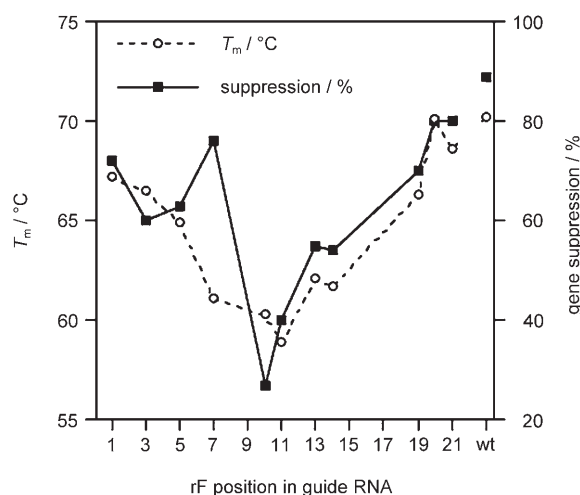


**Figure 3.** Dual plot comparing helix stability ( $T_m$ ) and RNA gene knockdown activity (% suppression) with rF substitution along the guide strand of siRNA duplexes at the positions shown. Data at the far right ("wt") are for the natural rU-substituted siRNA. See the Supporting Information for the original  $T_m$  data. Suppression data are from 2.1-ng siRNA amounts (see the Supporting Information).

unique opportunity to test the chemical origins of sequence selectivity in RNA interference. The corresponding position in the *Renilla* luciferase mRNA is universally variable in the gly171 codon. We therefore prepared three new mutant plasmids encoding *Renilla* luciferase with singly mismatched mRNAs. Measurement of activity with these four targets showed that the naturally substituted guide RNA did indeed distinguish single mismatches (Figure 4); the mismatches led to as much as a 2-fold drop in activity at a 2.1-ng RNA dose. This is consistent with a report for a different RNA target in which target mutations at position 7 led to significant selectivity.<sup>[8]</sup> In our experiments, a U–U mismatch was well tolerated, whereas a U–C mismatch was most disruptive to activity.

Remarkably, experiments with rF (position 7) showed that it also displayed selectivity, and more surprisingly, the level of selectivity was higher than that of the natural base. A selectivity of nearly threefold greater than the F–C mismatch was seen (Figure 4), and the rF-containing strand also showed significant selectivity for cleavage of the G mutant, which rU discriminated poorly. Thus, we conclude that, at least at position 7 of the RISC complex, mRNA–target–sequence selectivity does not require canonical Watson–Crick hydrogen bonding.

These experiments give new insight into the mechanism of RNA interference. We have shown that a nonpolar nucleobase analogue can maintain substantial cellular RNAi activity at nine of eleven sites tested, establishing clearly that canonical Watson–Crick hydrogen bonding is not crucial at all positions. We do note a general correspondence of  $T_m$  with mRNA-suppression activity, however (Figure 3), suggesting that not many simultaneous substitutions in guide RNA would be well tolerated. Notably, two positions tested (7 and 10) deviate markedly from this correlation, suggesting considerable changes in RNA–protein interactions across this

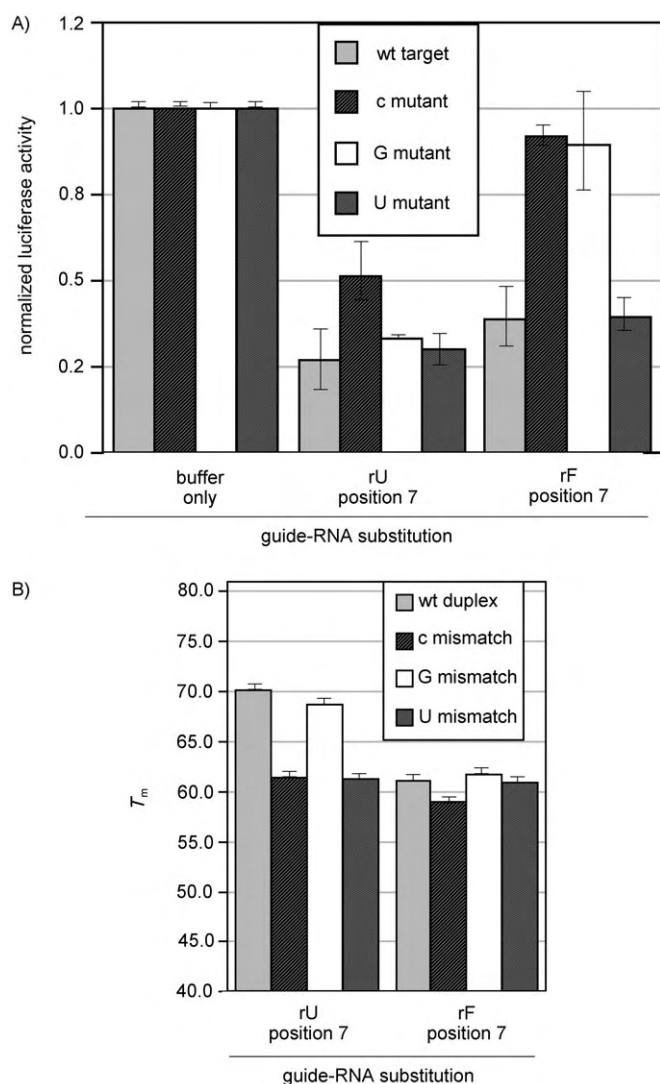


**Figure 4.** Selectivity of modified siRNA guide strands for singly mismatched RNA targets. The mismatch is opposite position 7 of the guide RNA and involves mutating the corresponding nucleotide in the complementary RNA. A) Histogram of RNAi activity showing rF-enhanced selectivity for adenine relative to mutations at position 513 in the luciferase target mRNA (position 513 is opposite position 7 on the guide RNA). B) Thermal stability histogram showing inherent hybridization selectivity of rU, and lack of selectivity of rF, as measured by thermal denaturation of the guide/passenger duplexes corresponding to the mutations in part (A). Raw data are given in the Supporting Information.  $T_m$  (melting temperature) represents the RNA duplex stability.

localized part of the RNA. The overall profile of rF-substitution responses suggests that guide-RNA positions 10 and 11, in particular, may require hydrogen bonding or base-pairing stability with the target (or both) for efficient RNA cleavage activity.

After submission of this manuscript, a report appeared testing difluorotoluene riboside, closely related to the current rF, in siRNA activity.<sup>[18]</sup> This study found similar positional effects on RNA interference, with the base analogue causing strong disruption of activity at positions 10 and 11, and little or no effect at position 7. The consistency of findings between

the two studies, carried out with different targets, suggests that these effects are general for the RISC complex. Sequence selectivity with mismatched targets was not examined in that study.

The current results strongly suggest that at position 7, the sequence selectivity of RNA interference arises not from the selectivity of hydrogen bonding, nor from selectivity caused by the RNA backbone alone. A possible hypothesis is that the selectivity arises instead from an enforced steric selection by the RISC complex (and *Argonaute* in particular<sup>[14]</sup>). Experiments with base analogues with varied size or shape could test this steric hypothesis explicitly. At this point, it is unknown whether selectivity at other positions depends on hydrogen bonding or not.

Finally, we note with interest the observation that use of rF in place of rU at position 7 appears to enhance sequence selectivity beyond that of the natural base. We suggest that this may be due to the general destabilization of the guide-target duplex by the nonpolar base analogue; it is known that a nearby mismatch can increase specificity of DNA hybridization,<sup>[23]</sup> perhaps by a similar destabilization mechanism. In any case, the result suggests a more-general practical utility of nonpolar isosteres in RNA interference studies.

### Experimental Section

**Nucleoside phosphoramidite synthesis:** The rF ribonucleoside was prepared as described.<sup>[15,16]</sup> For automated RNA synthesis, the previously unknown 5-dimethoxytrityl, 2'-*O*-TOM (TOM = [(triisopropylsilyl)oxy]methyl), 3'-*O*-phosphoramidite derivative was prepared. Details are given in the Supporting Information.

**Modified oligoribonucleotides:** RNA sequences were made following standard protocols for 2'-*O*-TOM-protected phosphoramidites<sup>[24]</sup> and were purified by polyacrylamide gel electrophoresis and characterized by MALDI-TOF mass spectrometry. Details are supplied in the Supporting Information.

**RNA interference studies and mismatched luciferase vectors:** The dual reporter Renilla/firefly assay was carried out by using HeLa cells transfected with reporter expression plasmids purchased from Promega (San Luis Obispo, CA). Sequence mutant plasmids were prepared following standard methods and were characterized by sequencing. Details are given in the Supporting Information.

Received: April 4, 2006

Revised: May 16, 2006

Published online: June 27, 2006

**Keywords:** base pairs · difluorobenzene · isosteres · protein structures · RNA structures

- [1] A. Fire, S. Xu, M. K. Montgomery, S. A. Kostas, S. E. Driver, C. C. Mello, *Nature* **1998**, *391*, 806–811.
- [2] S. M. Elbashir, J. Martinez, A. Patkaniowska, W. Lendeckel, T. Tuschl, *EMBO J.* **2001**, *20*, 6877–6888.
- [3] S. M. Elbashir, W. Lendeckel, T. Tuschl, *Genes Dev.* **2001**, *15*, 188–200.
- [4] G. Hutvagner, P. D. Zamore, *Curr. Opin. Genet. Dev.* **2002**, *12*, 225–232.
- [5] T. Tuschl, G. Meister, *Nature* **2004**, *431*, 343–349.
- [6] M. Manoharan, *Curr. Opin. Chem. Biol.* **2004**, *8*, 570–579.
- [7] B. L. Bass, *Cell* **2000**, *101*, 235–238.

- [8] Q. Du, H. Thonberg, J. Wang, C. Wahlestedt, Z. Liang, *Nucleic Acids Res.* **2005**, *33*, 1671–1677.
- [9] J.-T. Chi, H. Y. Chang, N. N. Wang, D. S. Chang, N. Dunphy, P. O. Brown, *Proc. Natl. Acad. Sci. USA* **2003**, *100*, 6343–6346.
- [10] D. Semizarov, L. Frost, A. Sarthy, P. Kroeger, D. N. Halbert, S. W. Fesik, *Proc. Natl. Acad. Sci. USA* **2003**, *100*, 6347–6352.
- [11] a) B. A. Schweitzer, E. T. Kool, *J. Am. Chem. Soc.* **1995**, *117*, 1863–1872; b) E. T. Kool, J. C. Morales, K. M. Guckian, *Angew. Chem.* **2000**, *112*, 1046–1068; *Angew. Chem. Int. Ed.* **2000**, *39*, 990–1009.
- [12] S. Moran, R. X.-F. Ren, E. T. Kool, *Proc. Natl. Acad. Sci. USA* **1997**, *94*, 10506–10511.
- [13] a) A. Lingel, B. Simon, E. Izaurralde, M. Sattler, *Nat. Struct. Mol. Biol.* **2004**, *11*, 576–577; b) J. B. Ma, K. Ye, D. J. Patel, *Nature* **2004**, *429*, 318–322; c) A. Lingel, M. Sattler, *Curr. Opin. Struct. Biol.* **2005**, *15*, 107–115.
- [14] a) J. J. Song, S. K. Smith, G. J. Hannon, L. Joshua-Tor, *Science* **2004**, *305*, 1434–1437; b) J. J. Song, L. Joshua-Tor, *Curr. Opin. Struct. Biol.* **2006**, *16*, 5–11.
- [15] J. Parsch, J. W. Engels, *Helv. Chim. Acta* **2000**, *83*, 1791–1808.
- [16] K. M. Guckian, Ph.D. Thesis, University of Rochester (NY), **1998**.
- [17] K. M. Guckian, E. T. Kool, *Angew. Chem.* **1997**, *109*, 2942–2945; *Angew. Chem. Int. Ed.* **1997**, *36*, 2825–2828.
- [18] J. Xia, A. Noronha, I. Toudjarska, F. Li, A. Akinc, R. Braich, M. Frank-Kamenetsky, K. G. Rajeev, M. Egli, M. Manoharan, *ACS Chem. Biol.* **2006**, *1*, 176–182.
- [19] S. Moran, R. X.-F. Ren, S. Rumney, E. T. Kool, *J. Am. Chem. Soc.* **1997**, *119*, 2056–2057.
- [20] Y. Xu, H.-Y. Zhang, D. Thormeyer, O. Larsson, Q. Du, J. Elmén, C. Wahlestedt, Z. Liang, *Biochem. Biophys. Res. Commun.* **2003**, *306*, 712–717.
- [21] R. Kierzek, M. E. Burkard, D. H. Turner, *Biochemistry* **1999**, *38*, 14214–14223.
- [22] G. Grentzmann, J. A. Ingram, P. J. Kelly, R. F. Gesteland, J. F. Atkins, *RNA* **1998**, *4*, 479–486.
- [23] Z. Guo, Q. Liu, L. M. Smith, *Nat. Biotechnol.* **1997**, *15*, 331–335.
- [24] a) S. Pitsch, P. A. Weiss, L. Jenny, A. Stutz, X. Wu, *Helv. Chim. Acta* **2001**, *84*, 3773–3795; b) S. Jin, C. V. Miduturu, D. C. McKinney, S. K. Silverman, *J. Org. Chem.* **2005**, *70*, 4284–4299.

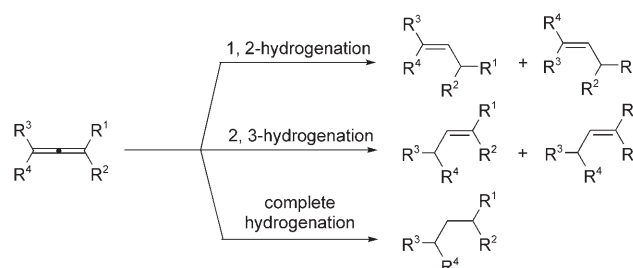


DOI: 10.1002/anie.200601366

# **[Pd(Ar-BIAN)(alkene)]-Catalyzed Highly Chemo-, Regio-, and Stereoselective Semihydrogenation of 1,2-Allenyl Phosphonates and Related Compounds\*\***

Hao Guo, Zilong Zheng, Fei Yu, Shengming Ma,\*  
Alexandre Holuigue, Dorette S. Tromp,  
Cornelis J. Elsevier,\* and Yihua Yu

Allenenes are an important class of compounds with many applications in organic chemistry.<sup>[1,2]</sup> However, the hydrogenation of allenenes is challenging, as there are issues of chemo-, regio-, and stereoselectivity to be addressed (Scheme 1).<sup>[2d]</sup> Only a very limited number of studies in this area have been reported, and the selectivity in the reported cases is low.<sup>[3]</sup>



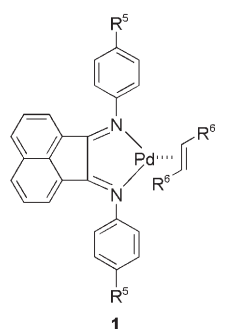
**Scheme 1.** The hydrogenation of allenenes.

[\*] H. Guo, Z. Zheng, F. Yu, Prof. S. Ma  
State Key Laboratory of Organometallic Chemistry  
Shanghai Institute of Organic Chemistry  
Chinese Academy of Sciences  
354 Fenglin Road, Shanghai 200032 (P. R. China)  
Fax: (+ 86) 21-6416-7510  
E-mail: masm@mail.sioc.ac.cn  
A. Holuigue, D. S. Tromp, Prof. C. J. Elsevier  
Van't Hoff Institute for Molecular Sciences  
University of Amsterdam  
Nieuwe Achtergracht 166, 1018 WV Amsterdam (The Netherlands)  
Fax: (+ 31) 20-525-6456  
E-mail: elsevier@science.uva.nl  
Y. Yu  
Key Laboratory of Optical and Magnetic Resonance Spectroscopy  
East China Normal University  
3663 Zhongshan Road, Shanghai 200062 (P. R. China)

[\*\*] The Chinese authors acknowledge financial support from the International Program of the National Natural Science Foundation of China. This research has also been partially funded by the National Research School Combination Catalysis (project number: 2000-14) and by the Universiteit van Amsterdam (grant SAP 2255). We thank Mr. Tao Bai of this group for independently reproducing representative examples of the work reported herein. Ar-BIAN = bis(arylimino)acenaphthene.



Supporting information for this article is available on the WWW under <http://www.angewandte.org> or from the author.

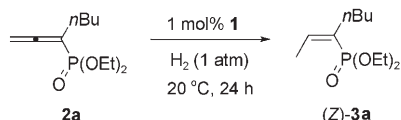


**1**  
**1a:** R<sup>5</sup> = Me, R<sup>6</sup> = CN  
**1b:** R<sup>5</sup> = OMe, R<sup>6</sup> = COOMe

One of the authors and co-workers have previously reported the hydrogenation of alkynes catalyzed by [Pd(Ar-BIAN)(alkene)] complexes **1** (Ar-BIAN = bis(aryl-imino)acenaphthene) to afford *Z*-alkenes in excellent yields with high stereoselectivity.<sup>[4]</sup> Herein we report a highly chemo-, regio-, and stereoselective hydrogenation of 1,2-allenyl phosphonates to give di- or trisubstituted (*Z*)-1-alkenyl phosphonates with the same catalysts. Such trisubstituted alkenes are otherwise difficult to obtain.

We first chose the 1,2-allenyl phosphonate **2a** as the model substrate to study the solvent effects of the reaction at 20 °C. In most solvents, such as diethyl ether, dioxane, *N,N*-dimethyl formamide, dimethyl sulfoxide, CH<sub>2</sub>Cl<sub>2</sub>, CH<sub>3</sub>CCl<sub>3</sub>, toluene, CH<sub>3</sub>NO<sub>2</sub>, CH<sub>3</sub>OH, AcOH, and Et<sub>3</sub>N, the hydrogenation did not proceed. Fortunately, when the reaction was conducted in CH<sub>3</sub>CN or THF, only the trisubstituted (*Z*)-1-alkenyl phosphonate (**Z**)-**3a** was formed, in excellent yield with excellent chemo-, regio-, and stereoselectivity (Table 1,

**Table 1:** [Pd(Ar-BIAN)(alkene)]-catalyzed hydrogenation of **2a** under various conditions.<sup>[a,b]</sup>



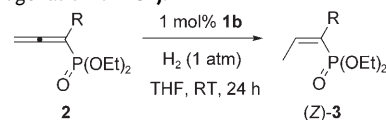
Entry	Solvent	Catalyst	T [°C]	Yield [%]
1	CH <sub>3</sub> CN	<b>1a</b>	20	92
2	THF	<b>1a</b>	20	94
3	THF	<b>1a</b>	30	94
4	THF	<b>1a</b>	50	92
5	THF	<b>1b</b>	20	94

[a] The reaction was carried out at the temperature stated with **2a** (0.2 mmol) and **1a** or **1b** (1 mol%) in 3 mL of solvent under H<sub>2</sub> (1 atm) for 24 h. [b] The chemo-, regio-, and stereoselectivities were determined by <sup>1</sup>H NMR spectroscopic analysis of the crude reaction product.

entries 1 and 2). As the yield in THF was slightly higher than that in CH<sub>3</sub>CN, THF was chosen as the solvent for this reaction. When we increased the reaction temperature, no obvious changes were observed (Table 1, entries 3 and 4). It was also found that the activity of catalyst **1b** was the same as that of **1a** for the hydrogenation of **2a** (Table 1, entry 5).

We next investigated the hydrogenation of various 1,2-allenyl phosphonates **2b–j** (Table 2). It was surprising to note that **1a** failed to catalyze the hydrogenation of the methyl-substituted 1,2-allenyl phosphonate **2b** (Table 2, entry 1). As the lack of hydrogenation activity may result from the stronger coordination of the fumaronitrile ligand, we decided to attempt the reaction with palladium complex **1b**, which has a more labile alkene ligand. Indeed, **1b** catalyzed the partial hydrogenation reaction to afford alkene (**Z**)-**3b** in 91 % yield (Table 2, entry 2). Therefore, the same conditions were used

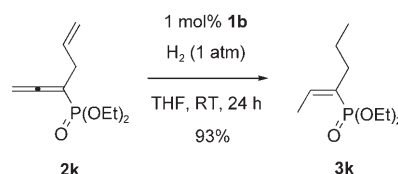
**Table 2:** Hydrogenation of **2b–j**.<sup>[a,b]</sup>



Entry	Allene	R	Product	Yield [%]
1 <sup>[c]</sup>	<b>2b</b>	Me	–	n.r.
2	<b>2b</b>	Me	( <i>Z</i> )- <b>3b</b>	91
3	<b>2c</b>	<i>t</i> Bu	( <i>Z</i> )- <b>3c</b>	90
4	<b>2d</b>	<i>n</i> -C <sub>7</sub> H <sub>15</sub>	( <i>Z</i> )- <b>3d</b>	94
5	<b>2e</b>	Ph	( <i>Z</i> )- <b>3e</b>	95
6	<b>2f</b>	<i>p</i> -MeOC <sub>6</sub> H <sub>4</sub>	( <i>Z</i> )- <b>3f</b>	99
7	<b>2g</b>	<i>p</i> -MeC <sub>6</sub> H <sub>4</sub>	( <i>Z</i> )- <b>3g</b>	93
8	<b>2h</b>	<i>p</i> -NO <sub>2</sub> C <sub>6</sub> H <sub>4</sub>	( <i>Z</i> )- <b>3h</b>	90
9	<b>2i</b>	<i>p</i> -MeO <sub>2</sub> CC <sub>6</sub> H <sub>4</sub>	( <i>Z</i> )- <b>3i</b>	93
10	<b>2j</b>	H	( <i>Z</i> )- <b>3j</b>	91

[a] The reaction was carried out at room temperature with **2** (0.2 mmol) and **1b** (1 mol%) in THF (3 mL) under H<sub>2</sub> (1 atm) for 24 h. [b] The chemo-, regio-, and stereoselectivities were determined by <sup>1</sup>H NMR spectroscopic analysis of the crude reaction product. [c] The reaction was conducted with **1a** (1 mol%) as the catalyst. n.r. = no reaction.

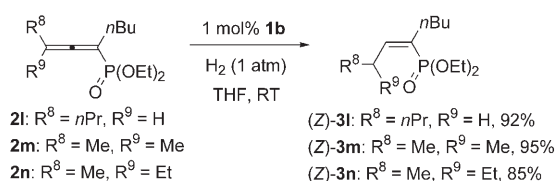
for the other substrates. Interestingly, the hydrogenation of **2k** under these conditions gave the (*Z*)-1-alkenyl phosphonate (**Z**)-**3k** in 93 % yield as the only product, in which the isolated allylic C=C bond in **2k** had also been hydrogenated, but the conjugated electron-deficient carbon–carbon double bond remained (Scheme 2). The configuration of the C=C bond in the products **3** was determined by analysis of the <sup>1</sup>H-<sup>1</sup>H NOESY spectra of (**Z**)-**3i**.



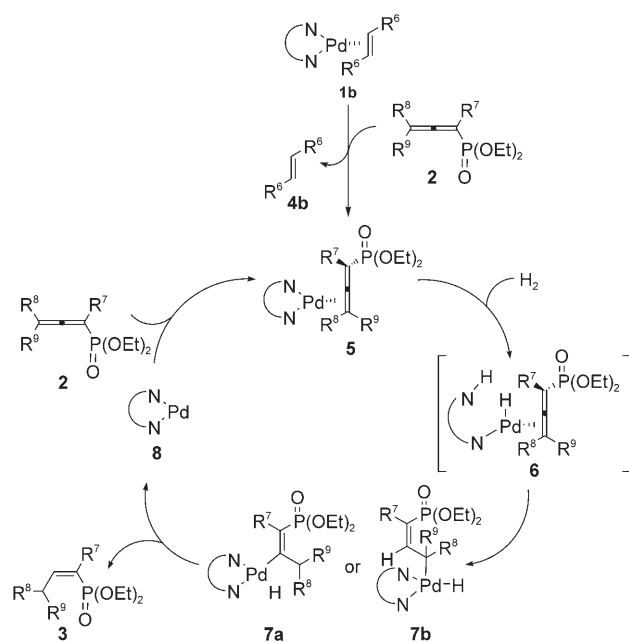
**Scheme 2.** The hydrogenation of **2k**.

The hydrogenation of the 1,3-disubstituted 1,2-allenyl phosphonate **2l** and 1,3,3-trisubstituted 1,2-allenyl phosphonates **2m** and **2n** under the conditions indicated in Table 2 was also studied. Compounds (**Z**)-**3l**, (**Z**)-**3m**, and (**Z**)-**3n** were formed highly selectively in 92, 95, and 85 % yield, respectively (Scheme 3).

On the basis of these and previous results, a mechanism for this reaction is proposed in Scheme 4. The catalytic cycle starts with the loss of the alkene ligand from **1b**. Next, the more electron rich C=C bond in **2** coordinates to palladium in



**Scheme 3.** The semihydrogenation of **2l–n**.



**Scheme 4.** A possible mechanism for this reaction.

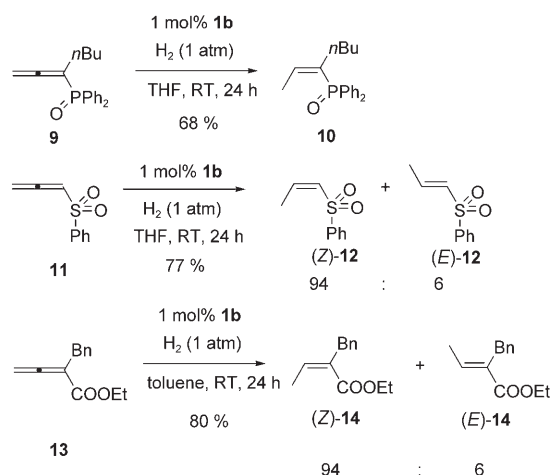
place of the alkene ligand to form a  $[\text{Pd}(\text{Ar-BIAN})(\text{allene})]$  complex **5**. In analogy with the mechanism for alkyne hydrogenation studied by one of us and co-workers,<sup>[4c]</sup> we propose the heterolytic hydrogen cleavage of **5** to afford the monohydridopalladium complex **6**, which may undergo highly stereoselective hydopalladation to generate the palladium hydride **7a** or **7b** after transfer of the N–H hydrogen atom to Pd.<sup>[5]</sup> The final product **3** is produced by reductive elimination from **7a** or **7b**. Meanwhile, the catalytically active  $[\text{Pd}(\text{Ar-BIAN})(\text{allene})]$  species **5** is regenerated through the interaction of **8** with the starting allene. On the basis of the stereoselectivity observed, we reason that the reaction most likely proceeds via the intermediate **7a**, in which the mutual *trans* orientation of the palladium and phosphonate moieties may determine the stereoselectivity.

This protocol was successfully extended to allenes substituted with other functionalities, namely, the 1,2-allenyl phosphine oxide **9**, the 1,2-allenyl sulfone **11**, and the 2,3-allenoate **13** (Scheme 5). In these cases the semihydrogenation also proceeds with very high chemo-, regio-, and stereoselectivity. Note that toluene should be used as the solvent for the 2,3-allenoate **13**.

In conclusion, we have demonstrated a novel, highly chemo-, regio-, and stereoselective  $[\text{Pd}(\text{Ar-BIAN})(\text{alkene})]$ -catalyzed hydrogenation of 1,2-allenyl phosphonates<sup>[6,7]</sup> and other 1,2-allenyl compounds to form di- or trisubstituted (*Z*)-1-alkenyl phosphonates, sulfones, and esters in excellent yields. Further studies in this field are being carried out in our laboratories, including investigations into synthetic applications of the reaction.

## Experimental Section

Typical procedure: Catalyst **1b** (1 mg, 0.002 mmol), **2a** (46 mg, 0.2 mmol), and anhydrous THF (3 mL) were added to a Schlenk



**Scheme 5.** The semihydrogenation of some related compounds.

tube under a nitrogen atmosphere. The nitrogen atmosphere was replaced with a hydrogen atmosphere (1 atm), and the solution was stirred at 20°C for 24 h. The reaction mixture was then filtered. Evaporation of the solvent and flash chromatography on silica gel (petroleum ether/diethyl ether 1:2) afforded (*Z*)-**3a** (44 mg, 94%) as a liquid. <sup>1</sup>H NMR (300 MHz, CDCl<sub>3</sub>): δ = 6.24 (dtq, *J* = 0.9, 7.2, 50.7 Hz, 1H), 4.13–3.96 (m, 4H), 2.22–2.12 (m, 2H), 2.03–1.98 (m, 3H), 1.48–1.38 (m, 2H), 1.35–1.23 (m, 8H), 0.88 ppm (t, *J* = 7.2 Hz, 3H); <sup>13</sup>C NMR (CDCl<sub>3</sub>, 75.4 MHz): δ = 142.2 (d, *J*<sub>PC</sub> = 11.8 Hz), 129.8 (d, *J*<sub>PC</sub> = 170.3 Hz), 61.0 (d, *J*<sub>PC</sub> = 5.8 Hz), 35.0 (d, *J*<sub>PC</sub> = 12.1 Hz), 31.7 (d, *J*<sub>PC</sub> = 3.0 Hz), 22.2, 16.3 (d, *J*<sub>PC</sub> = 4.4 Hz), 16.2 (d, *J*<sub>PC</sub> = 2.6 Hz), 13.8 ppm; <sup>31</sup>P NMR (121.5 MHz, CDCl<sub>3</sub>): δ = 21.0 ppm; IR (neat): ν̄ = 1632, 1444, 1391, 1245, 1026 cm<sup>−1</sup>; MS: *m/z*: 234 (*M*<sup>+</sup>, 9.87), 44 (100); HRMS (MALDI): *m/z* calcd for C<sub>11</sub>H<sub>23</sub>O<sub>3</sub>P<sup>+</sup> [*M*<sup>+</sup>]: 233.1385; found: 234.1400.

Received: April 6, 2006

Published online: June 29, 2006

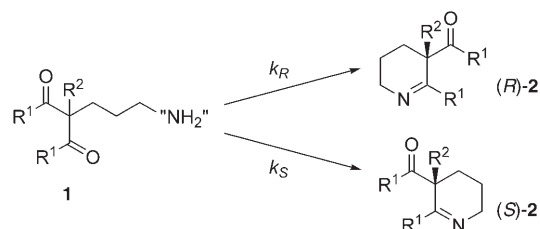
**Keywords:** alkenes · allenes · homogeneous catalysis · hydrogenation · palladium

- [1] a) *Allenes in Organic Synthesis* (Eds.: H. F. Schuster, G. M. Coppola), Wiley, New York, **1984**; b) *The Chemistry of Ketenes, Allenes, and Related Compounds, Part 1* (Ed.: S. Patai), Wiley, New York, **1980**; c) *Modern Allene Chemistry* (Eds.: N. Krause, A. S. K. Hashmi), Wiley-VCH, Weinheim, **2004**.
- [2] For reviews, see: a) K. K. Wang, *Chem. Rev.* **1996**, 96, 207; b) R. Zimmer, C. Dinesh, E. Nandan, F. Khan, *Chem. Rev.* **2000**, 100, 3067; c) J. Marshall, *Chem. Rev.* **2000**, 100, 3163; d) A. S. K. Hashmi, *Angew. Chem.* **2000**, 112, 3737; *Angew. Chem. Int. Ed.* **2000**, 39, 3590; e) X. Lu, C. Zhang, Z. Xu, *Acc. Chem. Res.* **2001**, 34, 535; f) R. Bates, V. Satcharoen, *Chem. Soc. Rev.* **2002**, 31, 12; g) S. Ma, *Handbook of Organopalladium Chemistry for Organic Synthesis* (Ed.: E. Negishi), Wiley, New York, **2002**, p. 1491; h) L. Sydnes, *Chem. Rev.* **2003**, 103, 1133; i) S. Ma, *Acc. Chem. Res.* **2003**, 36, 701; j) M. Tius, *Acc. Chem. Res.* **2003**, 36, 284; k) L.-L. Wei, H. Xiong, R. P. Hsung, *Acc. Chem. Res.* **2003**, 36, 773; l) L. Brandsma, N. A. Nedolya, *Synthesis* **2004**, 735; m) F. Pan, C. Fu, S. Ma, *Chin. J. Org. Chem.* **2004**, 24, 1168; n) S. Ma, *Chem. Rev.* **2005**, 105, 2829; o) S. Ma in *Topics in Organometallic Chemistry* (Ed.: J. Tsuji), Springer, Heidelberg, **2005**; p) C. J. Elsevier in *Houben-Weyl Methoden der Organischen Chemie, Stereoselective Synthesis, Vol. E 21a* (Eds.: G. Helmchen, R. W. Hoffmann, J. Mulzer, E. Schaumann), Thieme, Stuttgart, **1995**, pp. 537–566.

- [3] a) D. G. Pete, N. Munisamappa, *J. Org. Chem.* **1961**, 26, 3518; b) D. Devaprabhakara, P. D. Gardner, *J. Am. Chem. Soc.* **1963**, 85, 648; c) J. M. Brown, *Chem. Ind.* **1963**, 1689; d) P. Down, *J. Chem. Soc. Chem. Commun.* **1965**, 568; e) G. Nagendrappa, D. Devaprabhakara, *Tetrahedron Lett.* **1970**, 4243; f) R. Baudouy, J. Gore, *Tetrahedron* **1975**, 31, 383; g) L. Crombie, P. A. Jenkins, D. A. Mitchard, *J. Chem. Soc. Perkin Trans. 1* **1975**, 1081; h) F. Hammerschmidt, G. Bovermann, K. Bayer, *Liebigs Ann. Chem.* **1990**, 1055.
- [4] a) M. W. Laren, C. J. Elsevier, *Angew. Chem.* **1999**, 111, 3926; *Angew. Chem. Int. Ed.* **1999**, 38, 3715; b) J. W. Sprengers, J. Wassenaar, N. D. Clement, K. J. Cavell, C. J. Elsevier, *Angew. Chem.* **2005**, 117, 2062; *Angew. Chem. Int. Ed.* **2005**, 44, 2026; c) A. M. Kluwer, T. S. Koblenz, T. Jonischkeit, K. Woelk, C. J. Elsevier, *J. Am. Chem. Soc.* **2005**, 127, 15470.
- [5] A. Dedieu, S. Humbel, C. J. Elsevier, C. Grauffel, *Theor. Chem. Acc.* **2004**, 112, 305.
- [6] R. Asselt, C. J. Elsevier, W. J. J. Smeets, A. L. Spek, *Inorg. Chem.* **1994**, 33, 1521.
- [7] H. Altenbach, R. Korff, *Tetrahedron Lett.* **1981**, 22, 5175.

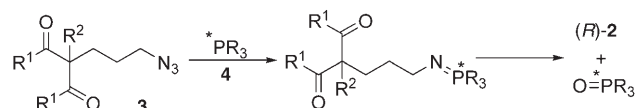


introduced from simple prochiral 1,3-dicarbonyl precursors **1** bearing an amine equivalent by the desymmetrizing formation of a keto imine **2** (Scheme 1).<sup>[2]</sup>



**Scheme 1.** Desymmetrizing imine formation by amine equivalent “NH<sub>2</sub>” for the construction of quaternary asymmetric centers.

Bonjoch and co-workers have demonstrated that a diastereoselective variant of this strategy is possible by using  $\alpha$ -chiral amines in their studies on reductive amination of 2-(2-oxooethyl)cycloalkyl 1,3-diones.<sup>[3,4]</sup> A conceptually much more powerful and general strategy would employ external chiral reagents in place of nonrecyclable chiral amines and further would leave the imine intact for subsequent derivatization. Given the rapid and reversible nature of imine formation, the potential for reagent-based acceleration of the reaction and/or retention of the stereochemical integrity of the products that are formed seems low. The aza-Wittig reaction of iminophosphoranes with carbonyl compounds,<sup>[5,6]</sup> however, is an irreversible imine-forming reaction and also allows for the introduction of external chirality through the use of chiral ligands on phosphorus. Thus, the Staudinger reaction of azidodiketones **3** with an appropriate chiral phosphorus reagent **4** would generate a chiral iminophosphorane, which undergoes selective meta-thesis with one of the two (now diastereotopic) carbonyl groups to yield, irreversibly, enantioenriched **2** and the corresponding phosphorus(V) oxide (Scheme 2). The anal-



**Scheme 2.** Asymmetric aza-Wittig reactions mediated by chiral phosphorus(III) reagents **4**.

Polysubstituted nitrogen heterocycles are prevalent in pharmaceuticals and biologically important natural product targets, and new approaches to these systems are in constant demand. A frequently occurring motif is the presence of an asymmetric all-carbon quaternary center in the 3-position of pyrrolidines, piperidines, and their polycyclic derivatives. All-carbon quaternary stereocenters are amongst the most challenging constructs in modern synthesis,<sup>[1]</sup> and a new approach to such functionality would be of considerable utility. It occurred to us that this moiety could potentially be

ogies with asymmetric variants of the carbon-based Wittig reaction are clear,<sup>[7,8]</sup> but to our knowledge there have been no reports of asymmetric variants of the aza-Wittig reaction. Herein we outline the successful demonstration of the first examples of this process.

The azido-1,3-diketone substrates **3a–d** were prepared in four steps commencing from either pentane-1,3-dione or cyclohexane-1,3-dione as shown in Scheme 3. For the chiral phosphorus(III) reagents, we chose the known and readily available proline-derived diazaphospholidine **4a**<sup>[9]</sup> and oxa-zaphospholidine **4b**,<sup>[10]</sup> and the cyclohexyldiamine-derived diazaphospholidine **4c** (Scheme 3).<sup>[11]</sup>

## Asymmetric Synthesis

DOI: 10.1002/anie.200601383

### Asymmetric Aza-Wittig Reactions: Enantioselective Synthesis of $\beta$ -Quaternary Azacycles\*\*

Duanpen Lertpibulpanya, Stephen P. Marsden,\*  
Ignacio Rodriguez-Garcia, and Colin A. Kilner

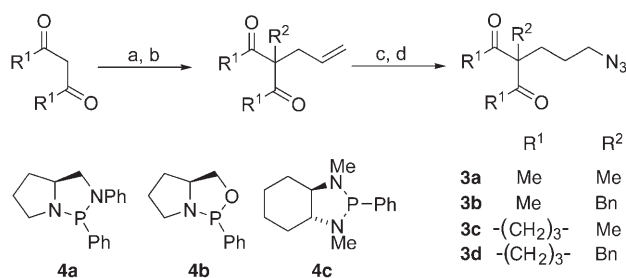
Polysubstituted nitrogen heterocycles are prevalent in pharmaceuticals and biologically important natural product targets, and new approaches to these systems are in constant demand. A frequently occurring motif is the presence of an asymmetric all-carbon quaternary center in the 3-position of pyrrolidines, piperidines, and their polycyclic derivatives. All-carbon quaternary stereocenters are amongst the most challenging constructs in modern synthesis,<sup>[1]</sup> and a new approach to such functionality would be of considerable utility. It occurred to us that this moiety could potentially be

[\*] Dr. S. P. Marsden, C. A. Kilner  
School of Chemistry  
University of Leeds  
Leeds, LS29JT (UK)  
Fax: (+44) 113-343-6425  
E-mail: s.p.marsden@leeds.ac.uk

D. Lertpibulpanya, Dr. I. Rodriguez-Garcia  
Department of Chemistry  
Imperial College London  
London SW72AY (UK)

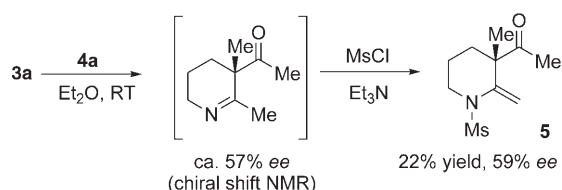
[\*\*] We thank the Royal Thai Government for Ph.D. support (D.L.) and the University of Almeria, Spain for research leave (I.R.-G.).

Supporting information for this article is available on the WWW under <http://www.angewandte.org> or from the author.



**Scheme 3.** Synthesis of substrates **3a–d**. Reagents and conditions: a) aqueous NaOH, MeI or BnBr; b) 1 M NaOH, allyl bromide, Bu<sub>4</sub>NI, room temperature; c) Cy<sub>2</sub>BH, THF, 0 °C, then NaOAc, I<sub>2</sub>; d) NaN<sub>3</sub>, Bu<sub>4</sub>NI, aqueous acetone, room temperature. Overall yields: **3a** 44%, **3b** 41%, **3c** 29%, **3d** 18%. Bn = benzyl; Cy = cyclohexyl.

Initial studies with diketo azide **3a** and diazaphospholidine **4a** showed that the reaction proceeded to conversion after about 56 hours at room temperature. Initially we attempted to assay the enantiomeric purity of the keto imine product from the crude reaction mixture by chiral shift NMR spectroscopic studies using BINOL as an additive. These studies showed that significant asymmetric induction was occurring (up to ca. 57% *ee*), but the values were found not to be reproducible between runs of identical experiments. We suspected that trace moisture was catalyzing racemization through imine hydrolysis to the achiral aminodiketone, and the viability of this pathway was verified by monitoring the *ee* value of a sample of the crude imine which was left exposed to atmospheric moisture. The enantiomeric purity decreased steadily from 50–60% to 0% over a period of three days. We therefore repeated the experiments with rigorous exclusion of water and further trapped the crude keto imine product as the stable *N*-methanesulfonyl enamine **5** by treatment with methanesulfonyl chloride and triethylamine (Scheme 4).



**Scheme 4.** Trapping of the initially formed keto imines leads to preservation of the enantiomeric integrity of the reaction. Ms = methanesulfonyl.

Upon chiral GC analysis of **5** we were delighted to find that the enantiomeric purity of the crude imine had been retained in the isolated product. It should be noted that the trapping strategy not only safeguards the enantiomeric integrity of the products but also further differentiates the two desymmetrized functional groups—the remaining ketone is electrophilic whereas the newly formed enamine is nucleophilic.

Encouraged by these results, we further optimized the reaction by a) utilizing the more reactive phosphorus(III) reagents **4b** and **4c** to shorten the reaction times and b) changing the trapping regime from mesylation to the higher-yielding and more reliable *N*-acetylation. These opti-

mized conditions were applied to the range of substrates **3a–d**, and the results are shown in Table 1.

The reproducibility of the reaction was verified by carrying out duplicate runs—the *ee* values shown are the

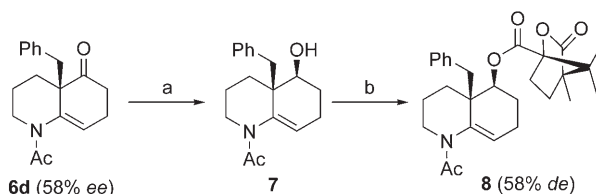
**Table 1:** Desymmetrization of diketo azides **3a–d** to yield **6a–d**.<sup>[a]</sup>

Entry	Azide	Reagent	Yield [%] <sup>[b]</sup>	<i>ee</i> [%] <sup>[c]</sup>
1	<b>3a</b>	<b>4b</b>	67	43.0
2	<b>3a</b>	<b>4c</b>	74	29.5
3	<b>3b</b>	<b>4b</b>	69	60.5
4	<b>3b</b>	<b>4c</b>	71	24.5
5	<b>3c</b>	<b>4b</b>	75	29.0
6	<b>3c</b>	<b>4c</b>	78	43.0
7	<b>3d</b>	<b>4b</b>	92	38.5
8	<b>3d</b>	<b>4c</b>	95	57.0

[a] Reactions carried out in Et<sub>2</sub>O or THF, at room temperature or elevated temperature; for individual reaction conditions, see the Supporting Information. [b] Yield of isolated purified product (average of two runs). [c] Average of two runs (all values ± 2%) as determined by chiral HPLC analysis on Chiralcel OD or OJ columns. Ac = acetyl.

average of the two runs with a maximum variance of ± 2%. In all cases the yields of the isolated products were good to excellent. In general the oxazaphospholidine **4b** gave higher asymmetric induction for the acyclic substrates whereas the diazaphospholidine **4c** gave higher asymmetric induction for the cyclic substrates. The maximum levels of asymmetric induction were around 60% *ee*. Though this value is not yet at the high levels observed in many modern asymmetric transformations, this result represents the first successful demonstration that the asymmetric aza-Wittig reaction is a viable process. We anticipate that further tuning of the reagents and/or substrates will lead to enhanced enantioselectivity.

The absolute sense of asymmetric induction was determined for keto enamide **6d**. We exploited the differentiated reactivity of the ketone and enamine by carrying out chemoselective reduction of the ketone with sodium borohydride to afford **7** (Scheme 5). Derivatization of the resulting equatorial alcohol with (1*S*)-camphanic chloride gave ester **8** (Scheme 5). The material that was formed had 58% *de* by <sup>1</sup>H NMR spectroscopy and HPLC, thus confirming the



**Scheme 5.** Chemoselective manipulation of keto enamides and proof of absolute stereochemistry. Reagents and conditions: a) NaBH<sub>4</sub>, room temperature (93% yield); b) (1*S*)-camphanic chloride, DMAP, DCE, reflux (98% yield). DMAP = 4-(dimethylamino)pyridine; DCE = 1,2-dichloroethane.

measured asymmetric induction. The major diastereoisomer was isolated by preparative HPLC, and crystals were grown for X-ray diffraction analysis.<sup>[12]</sup> The obtained crystal structure confirmed that the iminophosphorane had attacked the pro-*R* carbonyl group of **3d**.

In summary, we have disclosed the first example of a new class of asymmetric transformation, the asymmetric aza-Wittig reaction, in the context of the desymmetrization of prochiral azido-1,3-diketones. Further work to improve the levels of enantioselectivity, to extend the range of substrates for desymmetrization, and to apply this reaction in target synthesis is in progress.

## Experimental Section

A thoroughly flame-dried two-necked flask, fitted with a dry reflux condenser and connected to a Schlenk line through a rotaflo stopcock, was charged with an azidodiketone substrate **3a–d** (0.5 mmol, 1.0 equiv), and the apparatus was evacuated and then purged with a positive pressure of nitrogen. Freshly distilled dry solvent (see the Supporting Information for individual experimental details) was added to the flask by a septum, and a solution of the phosphane **4b** or **4c** (0.6 mmol, 1.2 equiv) was added, the total volume of solvent being 5 mL. The septum was replaced with a glass stopper, and the reaction was allowed to proceed either at room temperature or with heating (see the Supporting Information). At the end of the reaction, solvent was removed in vacuo to give the crude imine. The apparatus was then purged with a positive pressure of nitrogen, the glass stopper was replaced with a rubber septum, and DCE (5 mL), NEt<sub>3</sub> (4.0 equiv), Ac<sub>2</sub>O (2 equiv), and DMAP (0.1 equiv) were successively added to the flask. The septum was replaced with a glass stopper, and the mixture was heated in an oil bath at 85–90 °C for 5–9 h. The mixture was then cooled to room temperature, diluted with dichloromethane (40 mL), washed with water (50 mL) and brine (50 mL), and dried with MgSO<sub>4</sub>. The solvent was evaporated to give a residue, which was preadsorbed on silica gel and purified by flash column chromatography.

Received: April 7, 2006

Published online: July 3, 2006

**Keywords:** asymmetric synthesis · aza-Wittig reaction · azides · enantioselectivity · phosphanes

- Bosch, *Angew. Chem.* **1999**, *111*, 408–410; *Angew. Chem. Int. Ed.* **1999**, *38*, 395–397; d) D. Solé, J. Bonjoch, S. García-Rubio, E. Peidró, J. Bosch, *Chem. Eur. J.* **2000**, *6*, 655–665.
- [5] For reviews of aza-Wittig processes, see: a) Y. G. Gololobov, L. F. Kashukin, *Tetrahedron* **1992**, *48*, 1353–1406; b) A. W. Johnson, *Ylides and Imines of Phosphorus*, Wiley, New York, **1993**; c) S. Eguchi, Y. Matsushita, K. Yamashita, *Org. Prep. Proced. Int.* **1992**, *24*, 209–243; d) P. M. Fresneda, P. Molina, *Synlett* **2004**, 1–17; e) S. Eguchi, *ARKIVOC* **2005**, *2*, 98–119.
- [6] Synthesis of tetrahydropyridines by aza-Wittig reactions: a) M. Pailer, E. Haslinger, *Monatsh. Chem.* **1970**, *101*, 508–511; b) P. H. Lambert, M. Vaultier, R. Carrie, *J. Chem. Soc. Chem. Commun.* **1982**, 1224–1225; c) M. Vaultier, P. H. Lambert, R. Carrie, *Bull. Soc. Chim. Belg.* **1985**, *94*, 449–456; d) M. Vaultier, P. H. Lambert, R. Carrie, *Bull. Soc. Chim. Fr.* **1986**, 83–92.
- [7] For a review of asymmetric Wittig processes, see: T. Rein, T. M. Pedersen, *Synthesis* **2002**, 579–594.
- [8] For intramolecular desymmetrizing Wittig-type reactions of diketones, see: a) B. M. Trost, D. P. Curran, *J. Am. Chem. Soc.* **1980**, *102*, 5699–5700; b) B. M. Trost, D. P. Curran, *Tetrahedron Lett.* **1981**, *22*, 4929–4932; c) T. Mandai, Y. Kaihara, J. Tsuji, *J. Org. Chem.* **1994**, *59*, 5847–5849; d) A. V. Bedekar, T. Watanabe, K. Tanaka, K. Fuji, *Tetrahedron: Asymmetry* **2002**, *13*, 721–727; e) J. Yamazaki, A. V. Bedekar, T. Watanabe, K. Tanaka, J. Watanabe, K. Fuji, *Tetrahedron: Asymmetry* **2002**, *13*, 729–734.
- [9] J. M. Brunel, O. Legrand, S. Reymond, G. Buono, *J. Am. Chem. Soc.* **1999**, *121*, 5807–5808.
- [10] W. J. Richter, *Chem. Ber.* **1984**, *117*, 2328–2336.
- [11] D. Smyth, H. Tye, C. Eldred, N. W. Alcock, M. Wills, *J. Chem. Soc. Perkin Trans. 1* **2001**, 2840–2849.
- [12] CCDC-603132 contains the supplementary crystallographic data for this paper. These data can be obtained free of charge from The Cambridge Crystallographic Data Centre via [www.ccdc.cam.ac.uk/data\\_request/cif](http://www.ccdc.cam.ac.uk/data_request/cif).

- [1] For reviews, see: a) J. Christoffers, A. Baro, *Quaternary Stereocenters. Challenges and Solutions for Organic Synthesis*, VCH, Weinheim, **2005**; b) I. Denissova, L. Barriault, *Tetrahedron* **2003**, *59*, 10105–10146; c) J. Christoffers, A. Mann, *Angew. Chem.* **2001**, *113*, 4725–4732; *Angew. Chem. Int. Ed.* **2001**, *40*, 4591–4597; d) E. J. Corey, A. Guzman-Perez, *Angew. Chem.* **1998**, *110*, 402–415; *Angew. Chem. Int. Ed.* **1998**, *37*, 388–401; e) K. Fuji, *Chem. Rev.* **1993**, *93*, 2037–2066.
- [2] For reviews of desymmetrization processes in asymmetric synthesis, see: M. C. Willis, *J. Chem. Soc. Perkin Trans. 1* **1999**, 1765–1784.
- [3] a) D. Solé, J. Bonjoch, *Tetrahedron Lett.* **1991**, *32*, 5183–5186; b) D. Solé, J. Bosch, J. Bonjoch, *Tetrahedron* **1996**, *52*, 4013–4028; c) J. Bonjoch, D. Solé, R. Carrillo, E. Peidró, J. Bosch, *Tetrahedron* **2001**, *57*, 6011–6017.
- [4] For applications in total synthesis, see: a) D. Solé, J. Bonjoch, J. Bosch, *J. Org. Chem.* **1996**, *61*, 4194–4195; b) J. Bonjoch, D. Solé, S. García-Rubio, J. Bosch, *J. Am. Chem. Soc.* **1997**, *119*, 7230–7240; c) D. Solé, J. Bonjoch, S. García-Rubio, E. Peidró, J.

**Allylation**

DOI: 10.1002/anie.200601556

**Substituted Allyl Diphenylphosphine Oxides as Radical Allylating Agents\*\***

*Gilles Ouvry, Béatrice Quiclet-Sire, and Samir Z. Zard\**

Following its discovery nearly a quarter of a century ago,<sup>[1]</sup> the radical allylation using allylstannanes has proved to be a very powerful synthetic tool. Numerous applications attest to the

[\*] Dr. G. Ouvry, Dr. B. Quiclet-Sire, Prof. S. Z. Zard  
Laboratoire de Synthèse Organique Associé  
CNRS (UMR 7652), Département de Chimie  
Ecole Polytechnique, 91128 Palaiseau Cedex (France)  
Fax: (+ 33) 1-6933-3851  
E-mail: zard@poly.polytechnique.fr

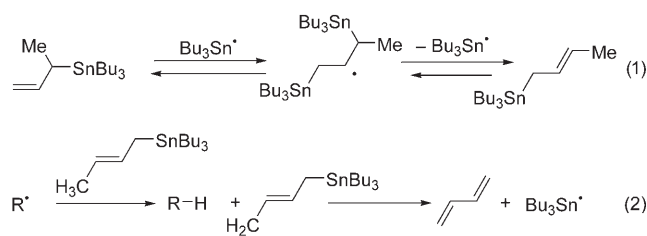
[\*\*] G.O. thanks the Ecole Polytechnique for a fellowship.



Supporting information for this article is available on the WWW under <http://www.angewandte.org> or from the author.



efficiency and compatibility of this methodology with a wide number of functional groups.<sup>[2]</sup> Nevertheless, the reaction suffers from some limitations, especially in respect to the substitution pattern around the allyl group.  $\gamma$ -Substituted allylstannanes rapidly rearrange under the reaction conditions into their more stable  $\alpha$ -isomers [Eq. (1)], and these were found to react mostly through abstraction of the allylic hydrogen atom [Eq. (2)] rather than by the desired addition fragmentation (Scheme 1).<sup>[2c,3,4]</sup>



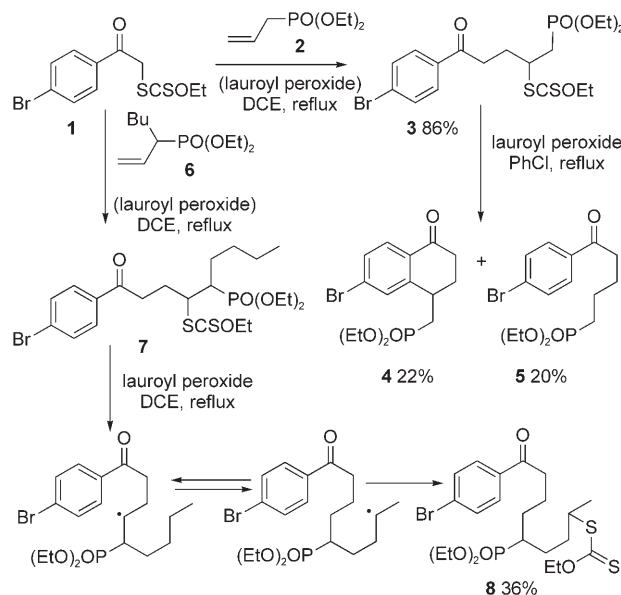
**Scheme 1.** Some side reactions during allylations with substituted allyltriorganotin reagents.

Several systems using allylcobalt,<sup>[5]</sup> allylgallium,<sup>[6]</sup> allylhalogen,<sup>[7]</sup> or allylsulfur<sup>[8]</sup> derivatives have been examined in an attempt to overcome these limitations. Nevertheless, most of these processes require a stoichiometric amount of a tin-based promoter<sup>[9]</sup> (or other heavy-metal derivatives) and have usually been applied to the introduction of simple allyl moieties.<sup>[10]</sup>

Our method to devise a new, tin-free allylation process was initially to separate the addition and fragmentation steps. This approach would eliminate the possibility of rearrangement of the allylating agent and thus obviate the shortcomings of the previous methods.<sup>[11]</sup> We thus needed an allylating agent substituted with a relatively poor leaving group (in the radical sense), which would undergo intermolecular addition and transfer of a dithiocarbonate unit and  $\beta$ -elimination in the second step.<sup>[12]</sup> In this respect, a phosphorus-centered leaving group appeared suitable. The reversible addition of phosphines to olefins is well known.<sup>[13]</sup> More recently, we and other groups found that a diethylphosphinyl group could be expelled when adjacent to nitrogen- or oxygen-centered radicals.<sup>[14]</sup> Other related observations include that of Clive and Kang, who reported the elimination of an aryl phosphinyl radical from a cyclohexadienyl system,<sup>[15]</sup> and the isolation of a minor (8% yield) by-product that arises from an apparent  $\beta$ -elimination of a methylphenylphosphinoyl radical located on a tertiary carbon atom, as reported by Malacria and co-workers.<sup>[16]</sup> All cases these were especially favorable, but did not foretell the generality of the elimination process in ordinary situations.

We initially envisaged the use of a simple diethyl phosphonate as the departing group and chose to study the behavior of phosphonate **3** derived from the addition of *p*-bromophenacyl dithiocarbonate **1** to diethyl allylphosphonate **2**. The choice was dictated by the possibility of the intermediate radical undergoing closure to the aromatic ring to give tetralone **4**, and this process, although unwanted in the present case, should act as an internal clock and give us an

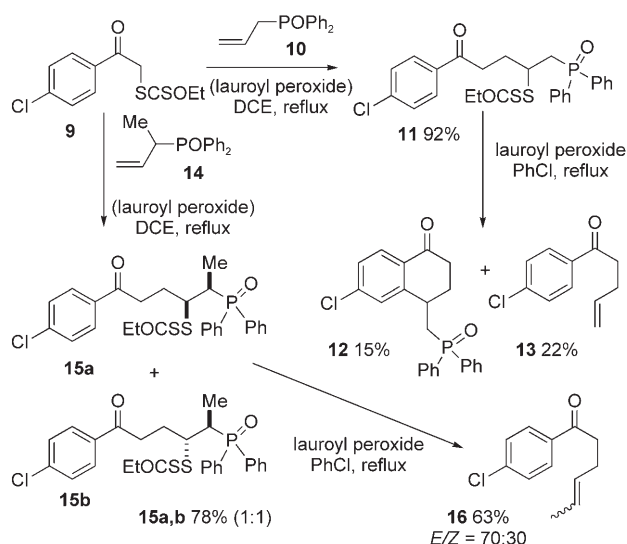
idea of the rate of  $\beta$ -elimination.<sup>[17]</sup> We also chose to use the higher-boiling chlorobenzene as the solvent to favor the fragmentation pathway, which has a large, positive entropy of activation. In the event, heating adduct **3** with lauroyl peroxide in chlorobenzene resulted in the formation of **4** and the reduced derivative **5** as the major products. No elimination of the phosphonate group was observed (Scheme 2).



**Scheme 2.** Negative experiments with allyl phosphonate reagents. DCE = 1,2-dichloroethane.

Weakening the carbon–phosphorus bond by substitution of the phosphonate group was the next logical step. Obtaining substituted derivatives was also more interesting synthetically and the purpose of our study in the first place. The radical addition of the same dithiocarbonate **1** to allylphosphonate **6** occurred fairly efficiently to give adduct **7** in 60% yield, but when this product was heated in 1,2-dichloroethane with lauroyl peroxide, neither elimination nor ring closure to the tetralone was observed. Instead, hydrogen abstraction from the side chain occurred to ultimately give compound **8** in 36% yield (Scheme 3). Steric hindrance in this case had clearly slowed down tetralone formation, and a Thorpe–Ingold effect had facilitated the 1,5-hydrogen shift. Switching to a higher-boiling solvent was obviously not going to overcome this unwanted radical translocation.

Decidedly, the phosphonate entity was too poor a leaving group for our objectives. It remained for us to examine the influence of the substituents around the phosphorus center on its leaving ability. The use of a diphenylphosphine oxide group seemed the most judicious choice as, in addition to ready availability, the bond we wanted to break would now acquire some benzylic character and perhaps be weakened sufficiently to undergo  $\beta$ -scission. Strain relief upon cleavage of such a bulky group should provide an extra driving force. Radical addition of dithiocarbonate **9** to allyl diphenylphosphine oxide **10** took place in high yield, and exposure to



**Scheme 3.** First successful allylations with allyl diphenylphosphine oxides.

peroxide in refluxing chlorobenzene gave the corresponding tetralone **12** and the desired elimination product **13**, both in low yield. The formation of allylated derivative **13** was nevertheless a good start, as it was expected that substitution would make the elimination step more efficient. Indeed, when substituted diphenylphosphine oxide **14** was employed as the radical trap, the intermolecular addition proceeded quite satisfactorily; more pleasing, it was observed that smooth elimination of the diphenylphosphinoyl group took place upon heating **15** with lauroyl peroxide in refluxing chlorobenzene to give unsaturated ketone **16** in 63% yield as a mixture of geometric isomers with the expected preponderance of the *E* isomer.<sup>[18]</sup>

The diphenylphosphine oxide group thus possessed the requisite properties we sought, and the desired allylation could at last be achieved. In principle, the process can be a chain reaction, propagated by the reaction of the diphenylphosphinoyl radical with the dithiocarbonate moiety. The addition–fragmentation of phosphorus-centered radicals on thiocarbonyl derivatives is well documented in the pioneering studies of Barton et al.<sup>[19]</sup> In practice, however, this approach did not turn out to be efficient, and nearly stoichiometric

amounts of the peroxide (0.5 equiv) were needed. It seems that the properties that make the diphenylphosphinoyl radical a good “leaving group” cause it to be a poor chain-propagating agent. All our attempts at determining the fate of the phosphorus species failed.

No elimination occurred in the absence of peroxide, so a purely thermal mechanism can be discarded. Furthermore, the mixture of the two diastereoisomers of **15** could be separated, and only one of the two was in fact subjected to the fragmentation process. Monitoring by thin layer chromatography (tlc) indicated that a rapid equilibration occurred between the two diastereoisomers **15a** and **15b** before elimination of the diphenylphosphinoyl group. Thus, the relative stereochemistry of the initial addition product will have no consequence on the elimination process. Finally, it turns out that it is not even necessary to isolate the addition product **15**, as the allylation can be accomplished directly by heating dithiocarbonate **9** and phosphine oxide **14** in chlorobenzene at reflux using the much longer lasting di-*tert*-butyl peroxide instead of lauroyl peroxide. The yield of enone **16** was 69%, based on **9**, thus representing a significant improvement on the two-step procedure.

We next explored the scope of this reaction by varying the dithiocarbonate and allylic diphenylphosphine oxide. The

**Table 1:** Examples of allylations with branched allyl diphenylphosphine oxides.

Dithiocarbonate	Phosphine oxide	Allylation product	Yield [%] <sup>[a]</sup>
<b>9</b>		<b>17</b>	<b>18</b> 58
<b>9</b>		<b>19</b>	<b>20</b> 52
	<b>19</b>	<b>22</b>	<b>22</b> 72
	<b>17</b>	<b>24</b>	<b>24</b> 68
<b>23</b>		<b>25</b>	<b>26</b> 67 (9:1)
	<b>25</b>	<b>28</b>	<b>28</b> 70
<b>27</b>		<b>30</b>	<b>31</b> 66
<b>27</b>		<b>30</b>	<b>32</b> 71 (83:17)

[a] Ratio of the *E/Z* isomers is given in brackets.

results are summarized in Table 1. It can be seen that prenylation is readily accomplished with phosphine oxide **17**, whereas allyl and homoallyl acetates can be introduced with the corresponding phosphine oxides **19**, **25**, and **30**. The dithiocarbonate moiety itself can bear a number of useful functional groups. Besides the initial phenacyl derivative **9**, substrates can contain a lactone (as in **21**), a protected aldehyde ester (as in **23**), or, perhaps most interestingly, a masked  $\alpha$ -aminoketone (as in **27**; Phth = phthalimido).  $\alpha$ -Aminoketones are at the centre of several classical syntheses of heteroaromatic rings, such as pyrroles and pyridines, and are not always readily accessible. Moreover, the introduction of many of these allylic fragments would not be trivial by the more common ionic processes, especially with the more functionalized substrates.

Our initial attempt to extend this approach to the formation of C–C bonds at the anomeric position of carbohydrates, such in the 2-deoxyglucose derivative **33**, was frustrated by the premature elimination of the dithiocarbonate group at the temperature of refluxing chlorobenzene to give glucal **34** as the major product (Scheme 4). The C–S bond

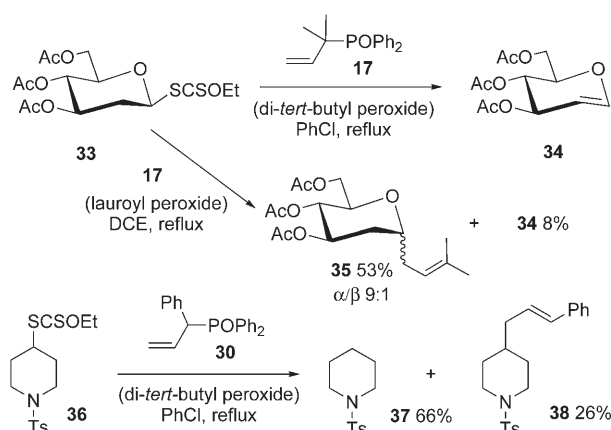
point, access to numerous substituted allyl diphenylphosphine oxides can be accomplished by direct reaction of the anion derived from the simplest member **10** with various electrophiles (alkylating agents, epoxides, aldehydes, and so forth).<sup>[20]</sup> Another powerful route is through the Arbuzov–Trippett rearrangement starting from allylic alcohols.<sup>[21]</sup> The radical reaction itself is flexible, convergent, and takes place under mild neutral conditions.

## Experimental Section

Typical procedure for the radical allylation: Di-*tert*-butyl peroxide (a few drops, ca. 100 mg) was added to a solution of the dithiocarbonate (1.0 mmol) and allyl phosphine oxide (2.0 mmol) in refluxing degassed chlorobenzene (10 mL) in a nitrogen atmosphere. A few more drops (ca. 100 mg) of di-*tert*-butyl peroxide were added after 4 h at reflux if the reaction is not yet complete (tlc). The reaction mixture was then cooled to room temperature, concentrated in vacuo, and purified by flash chromatography.

Received: April 20, 2006

**Keywords:**  $\beta$ -elimination · allylation · dithiocarbonates · phosphane oxides · radical reactions



**Scheme 4.** Two special cases. Ts = *p*-toluenesulfonyl.

is weakened by an anomeric effect of the lone pair of electrons on the oxygen atom and thus introduces an element of fragility into the substrate. This complication could be circumvented in a large measure by reverting to the lower-boiling 1,2-dichloroethane as the reaction solvent. In this unprecedented anomeric prenylation of a carbohydrate, the phosphine oxide is tertiary and therefore the addition–fragmentation occurs readily at 80°C.

A preliminary reaction that involved a simple secondary dithiocarbonate moiety gave rather disappointing results. Thus, the attempted allylation of dithiocarbonate **36** gave mostly reduced piperidine **37** and only a low yield of the normal product **38**. Hydrogen abstraction could take place from the solvent or from the benzylic position of the phosphine oxide reagent **30**. Further studies are needed to ascertain the source of the hydrogen atom.

These preliminary results represent a promising approach to a generalized allylation process and highlight the importance of the substitution around the phosphorus center in determining its leaving-group ability. From a synthetic stand-

- [1] a) J. Grignon, M. Pereyre, *J. Organomet. Chem.* **1973**, *61*, C33–C35; b) M. Kosugi, K. Kurino, K. Takayama, T. Migita, *J. Organomet. Chem.* **1973**, *56*, C11–C13.
- [2] a) G. E. Keck, J. B. Yates, *J. Am. Chem. Soc.* **1982**, *104*, 5829–5831; b) G. E. Keck, E. J. Enholm, D. F. Kachensky, *Tetrahedron Lett.* **1984**, *25*, 1867–1870; c) G. E. Keck, E. J. Enholm, J. B. Yates, M. R. Wiley, *Tetrahedron* **1985**, *41*, 4079–4094; d) G. E. Keck, D. F. Kachensky, E. J. Enholm, *J. Org. Chem.* **1985**, *50*, 4317–4325.
- [3] J. E. Baldwin, R. M. Adlington, D. J. Birch, J. A. Crawford, J. B. Sweeney, *J. Chem. Soc. Chem. Commun.* **1986**, 1339–1340.
- [4] For exceptions, see: a) G. A. Russell, L. L. Herold, *J. Org. Chem.* **1985**, *50*, 1037–1040; b) T. Migita, K. Nagai, M. Kosugi, *Bull. Chem. Soc. Jpn.* **1983**, *56*, 2480–2484; c) H. Fliri, C.-P. Mak, *J. Org. Chem.* **1985**, *50*, 3438–3442; d) C. J. Easton, I. M. Scharf-billig, *J. Org. Chem.* **1990**, *55*, 384–386; e) Y. Watanabe, T. Yoneda, T. Okumura, Y. Ueno, T. Toru, *Bull. Chem. Soc. Jpn.* **1993**, *66*, 3030–3033; f) Y. Yoshida, N. Ono, F. Sato, *J. Org. Chem.* **1994**, *59*, 6153–6155; g) I. Ryu, S. Kreimerman, T. Niguma, S. Minakata, M. Komatsu, Z. Luo, D. P. Curran, *Tetrahedron Lett.* **2001**, *42*, 947–950.
- [5] M. D. Johnson, *Acc. Chem. Res.* **1983**, *16*, 343–349.
- [6] S.-I. Usugi, H. Yorimitsu, K. Oshima, *Tetrahedron Lett.* **2001**, *42*, 4535–4538.
- [7] C. C. Huval, D. A. Singleton, *Tetrahedron Lett.* **1993**, *34*, 3041–3042.
- [8] a) G. E. Keck, J. H. Byers, *J. Org. Chem.* **1985**, *50*, 5442–5444; b) A. Yanagisawa, Y. Noritake, H. Yamamoto, *Chem. Lett.* **1988**, 1899–1902; c) P. Breuilles, D. Uguen, *Tetrahedron Lett.* **1990**, *31*, 357–360.
- [9] For emphasis on the problems linked with tin-mediated radical chemistry, see: P. A. Baguley, J. C. Walton, *Angew. Chem.* **1998**, *110*, 3272–3283; *Angew. Chem. Int. Ed.* **1998**, *37*, 3072–3082; for a review of tin-free allylations using allylsulfones, see: F. Bertrand, F. Le Guyader, L. Liguori, G. Ouvry, B. Quiclet-Sire, S. Seguin, S. Z. Zard, *C. R. Acad. Sci. Ser. II* **2001**, *4*, 547–555.
- [10] One notable exception is the elegant use of a branched allylsulfone in the total synthesis of (+)-pseudomonic acid C;

- see: G. E. Keck, A. M. Tafesh, *J. Org. Chem.* **1989**, *54*, 5845–5846.
- [11] It is possible to combine an atom- or group-transfer radical addition to allylsilanes with a fluoride-induced elimination; see: a) N. A. Porter, G. Zhang, A. D. Reed, *Tetrahedron Lett.* **2000**, *41*, 5773–5777; b) L. Chabaud, Y. Landais, P. Renaud, *Org. Lett.* **2002**, *4*, 425; c) M. E. Briggs, S. Z. Zard, *Synlett* **2005**, 334–336.
- [12] For reviews on dithiocarbonate chemistry, see: a) B. Quiclet-Sire, S. Z. Zard, *Top. Curr. Chem.* **2006**, *264*, 201–236; b) S. Z. Zard in *Radicals in Organic Synthesis, Vol. 1* (Eds.: P. Renaud, M. P. Sibi), Wiley-VCH, Weinheim, **2001**, pp. 90–108; c) B. Quiclet-Sire, S. Z. Zard, *Phosphorus Sulfur Silicon* **1999**, *153–154*, 137–154; d) B. Quiclet-Sire, S. Z. Zard, *J. Chin. Chem. Soc.* **1999**, *46*, 139–145; e) S. Z. Zard, *Angew. Chem.* **1997**, *109*, 724–737; *Angew. Chem. Int. Ed. Engl.* **1997**, *36*, 672–685.
- [13] J. Pellon, *J. Am. Chem. Soc.* **1961**, *83*, 1915–1916.
- [14] a) S. Kim, C. H. Cho, C. J. Lim, *J. Am. Chem. Soc.* **2003**, *125*, 9574–9575; b) B. Quiclet-Sire, S. Z. Zard, H. Zhang, *J. Organomet. Chem.* **2002**, *643–644*, 404–408; c) H. Zhang, PhD Thesis, Université Paris-Sud, Orsay, 2000.
- [15] D. L. J. Clive, S. Kang, *J. Org. Chem.* **2001**, *66*, 6083–6091.
- [16] S. Bogen, M. Gulea, L. Fensterbank, M. Malacria, *J. Org. Chem.* **1999**, *64*, 4920–4925.
- [17] For examples of  $\alpha$ -tetralone formation, see: a) A. Cordero Vargas, B. Quiclet-Sire, S. Z. Zard, *Org. Lett.* **2003**, *5*, 3717–3719; b) N. Legrand, B. Quiclet-Sire, S. Z. Zard, *Tetrahedron Lett.* **2000**, *41*, 9815–9818; c) A. Liard, B. Quiclet-Sire, R. N. Saicic, S. Z. Zard, *Tetrahedron Lett.* **1997**, *38*, 1759–1762.
- [18] The results reported herein are taken from chapter 4 of PhD thesis of G. Ouvry, which was defended on December 12th, 2002 (G. Ouvry, *Synthèses d'Oléfines par Voie Radicalaire*, Thèse, Ecole Polytechnique, **2002**); the use of the diphenylphosphinoyl entity as a “new” radical leaving group was recently reported by Malacria et al. (D. Leca, L. Fensterbank, E. Lacôte, M. Malacria, *Angew. Chem.* **2004**, *116*, 4316–4318; *Angew. Chem. Int. Ed.* **2004**, *43*, 4220–4222). One of the senior authors (L. Fensterbank) was a principal examiner of the thesis of G. Ouvry, yet no reference is made to the thesis in this paper, nor was there any acknowledgement in the full paper, which appeared shortly afterwards (D. Leca, K. Song, M. Albert, M. Grangeio Gonçalves, L. Fensterbank, E. Lacôte, M. Malacria, *Synthesis* **2005**, 1405–1420) despite a prior exchange of correspondence with the authors on the matter.
- [19] a) D. H. R. Barton, D. O. Jang, J. Jaszberenyi, *J. Org. Chem.* **1993**, *58*, 6838–6842; b) D. O. Jang, D. H. Cho, J. Kim, *Synth. Commun.* **1998**, *28*, 3559–3565.
- [20] J.-K. Erguden, E. Schaumann, *Synthesis* **1996**, 707–710; J. Ukai, Y. Ikeda, N. Ikeda, H. Yamamoto, *Tetrahedron Lett.* **1983**, *24*, 4029–4032.
- [21] For leading references, see: a) M. P. Savage, S. Tripett, *J. Chem. Soc. C* **1966**, 1842–1844; b) S. Demay, K. Harms, P. Knochel, *Tetrahedron Lett.* **1999**, *40*, 4981–4984.



# A Surface-Bound DNA Switch Driven by a Chemical Oscillator\*\*

Tim Liedl, Michael Olapinski, and Friedrich C. Simmel\*

The fabrication of autonomously moving molecular structures is one of the central challenges in the field of DNA nanodevices.<sup>[1]</sup> Some of the concepts introduced recently to achieve this goal rely on the sequence-dependent catalytic action of DNA-modifying enzymes such as restriction endonucleases or nicking enzymes<sup>[2]</sup> while others use the catalytic power of DNA itself by incorporating DNA enzyme sequences into DNA devices.<sup>[3]</sup> Both approaches have also been used to realize autonomous molecular computers.<sup>[4]</sup> Another strategy is based on controlled inhibition of DNA hybridization by formation of secondary structure and its acceleration by catalytic DNA strands.<sup>[5]</sup> These concepts were developed for the autonomous operation of DNA devices fueled by DNA hybridization. A different approach was recently taken by our research group<sup>[6]</sup> and we could show that the pH-sensitive conformational transition of a cytosine-rich DNA strand between a random conformation and the so-called “i motif” could be driven by the oscillating proton concentration generated by a chemical oscillator. In such a system, the temporal succession of the states of the DNA devices is determined by a nonlinear dynamical system rather than by an external operator. We report here how this system can be significantly improved by attaching the DNA conformational switches to a solid substrate. This attachment allows us to operate the chemical oscillator in a continuous flow stirred tank reactor (CSTR) into which a glass chip supporting the DNA devices is placed. In principle, the surface-bound DNA structures can undergo an infinite number of autonomous conformational switching events in this configuration.

We showed recently how proton-fueled DNA devices can be driven by an oscillating chemical reaction<sup>[6]</sup> by using a variant of the Landolt reaction to periodically change the pH value in a continuously fed reactor. To retain the DNA switches within the reaction solution, a reactor without an outlet had to be used. In such a configuration, one cannot reach a steady state since the continuous influx of reaction

solution means the average concentrations of the reactants vary. As a result, this dynamic chemical system is driven out of its oscillatory region, thus causing the oscillations to die away after a few periods.

To overcome this limitation in the present work we operated the oscillator in a CSTR with two inlets and one outlet. In principle, an infinite number of homogeneous pH oscillations can be generated by using a continuous filling combined with the simultaneous removal of waste materials. However, the DNA devices had to be attached to a solid substrate to prevent loss of the DNA through the reactor's outlet. For these experiments, we used thiol-modified, fluorescently labeled DNA switches bound to an ultrathin transparent gold layer on a glass substrate. This allowed a firm covalent attachment of the DNA to the surface while at the same time energy transfer between the fluorophores and the gold layer<sup>[7]</sup> could be used to characterize the conformational transitions of the switches.

Schematic representations of the surface-bound DNA switches in their two states at low and high pH values are shown in Figure 1 a. The switches consist of 21 nucleotide (nt)

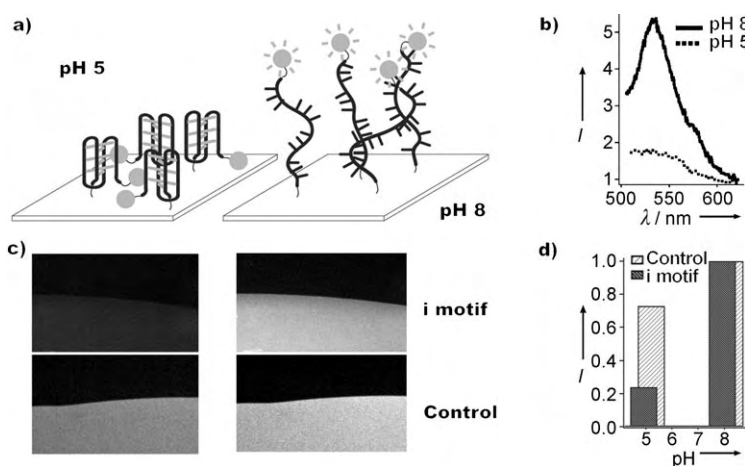


**Figure 1.** a) Schematic representation of single-stranded DNA bound to the gold/glass substrate through a 5'-thiol-C<sub>6</sub> spacer. In the closed i motif conformation at low pH values the dye attached to the 3' end is in proximity to the surface and is thus quenched. In contrast, the fluorescence strongly increases at higher pH values where the DNA strand adopts a random single-stranded conformation. b) Emission spectra recorded from the i motif attached to the substrate at pH 8 (random) and pH 5 (i motif). c) Fluorescence microscopy images of the i motif (top) and a control strand (bottom) at pH 5 (left) and pH 8 (right). d) Corresponding normalized fluorescence intensities.

long DNA strands with the sequence 5'-CCCTAACCC-TAACCCCTAACCC-3' (strand M). Below pH 6.5, DNA molecules of this sequence are known to undergo a conformational transition to the so-called “i motif”, in which four DNA strands are held together by a number of semiprotonated C-C<sup>+</sup> base pairs (in this case six intramolecular C-C<sup>+</sup> pairs). This particular DNA sequence has been utilized previously for the fabrication of other DNA-based nanodevices<sup>[8]</sup> and is also the same sequence as used in our previous bulk experiments.<sup>[6]</sup> The DNA strands were modified with a thiol-C<sub>6</sub>

[\*] T. Liedl, M. Olapinski, Dr. F. C. Simmel  
Department of Physics and Center for Nanoscience  
LMU Munich  
Geschwister Scholl Platz 1, 80539 Munich (Germany)  
Fax: (+49) 89-2180-3182  
E-mail: simmel@lmu.de

[\*\*] This work was supported by the Deutsche Forschungsgemeinschaft (Emmy Noether grant DFG SI 761/2-2). T.L. and M.O. are supported by the LMU International Graduate School “Nanobiotechnology”.

Supporting information for this article is available on the WWW under <http://www.angewandte.org> or from the author.

spacer at the 5' end and with the fluorescent dye Rhodamine Green (RG) at the 3' end. The fluorescence of RG is pH-insensitive between pH 4 and 9 (see the Supporting Information). At low pH values, the transition to the *i* motif brings the 3' end of the molecule into proximity to the 5' end (ca. 1.5 nm<sup>[9]</sup>). The fluorophore is brought closer to the substrate when the DNA switches are attached to a surface through the 5' end.

A glass coverslip with an ultrathin layer of gold was used as the substrate. To prepare the substrate, first a thin gold layer was evaporated onto a clean coverslip, and then nearly completely removed by sputtering with argon ions (experimental details are given in the Supporting Information). The substrate is then nearly transparent, but it is still possible to attach DNA strands to the remaining gold on the surface (see the Supporting Information). The modified coverslips were mounted on an epifluorescence microscope and the fluorescence was monitored while subsequently adding phosphate buffer of pH 8 and pH 5. Switching the DNA strands between a random conformation at high pH values and the *i* motif at low pH values resulted in strong changes in the fluorescence intensity (Figure 1 c,d). Such clear changes in the intensity could be monitored only at sites on the chip spotted with the *i* motif strand. Sites spotted with a control strand with a random sequence only showed a small change in intensity.

A fluorescence spectrometer was extended with a custom built module which allowed characterization of the sample when placed in a CSTR to allow for fluorescence spectroscopic and energy-transfer measurements during the operation of the pH oscillator. The setup is shown schematically in Figure 2. Fluorescence spectra recorded with this setup for the substrate-attached *i*-motif switches at low and high pH values are displayed in Figure 1 b.

The pH oscillator was operated by pumping two separate solutions at 150  $\mu\text{L min}^{-1}$  into the cuvette, which was initially filled with 20 mL H<sub>2</sub>O. One solution contained 19 mM NaIO<sub>3</sub> while the other contained 30 mM Na<sub>2</sub>SO<sub>3</sub>, 21 mM Na<sub>2</sub>S<sub>2</sub>O<sub>3</sub>, and 5 mM H<sub>2</sub>SO<sub>4</sub>. A second pump removed excess volume at 300  $\mu\text{L min}^{-1}$ . Typically, after a period of 4 h prior to oscillation, the pH value started to oscillate between pH 6.3 and pH 5.5 with a period of 20 minutes. The oscillations persisted until the reactant reservoirs were exhausted (typically after 24 h).

Figure 3 shows the fluorescence intensity recorded from the surface-immobilized DNA switches together with the oscillations in the pH value. The fluorescence strongly oscillates in concordance with the pH value, thus indicating that the chemical oscillator enforces the conformational transition of the switches as designed. We performed a variety of test experiments to verify that these fluorescence oscillations are indeed caused by the conformational transitions of the switches to the *i* motif and back. A conventional fluorescence titration experiment shows

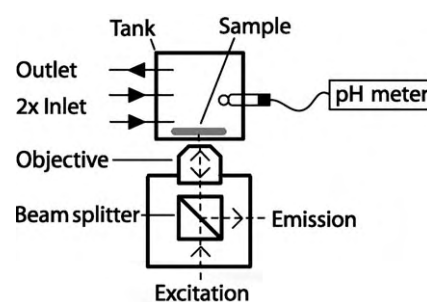


**Figure 2.** Experimental setup: Excitation light coming from a fluorescence spectrometer is focused onto the sample chip with a long working distance objective. Light emitted from the chip is collected by the same objective and reflected into the spectrometer with a beam splitter. The sample chip resides in a CSTR which consists of a large volume ( $V=25$  mL) fluorescence cuvette with two inlets and one outlet for the reactants. The pH value is monitored with a conventional pH meter.

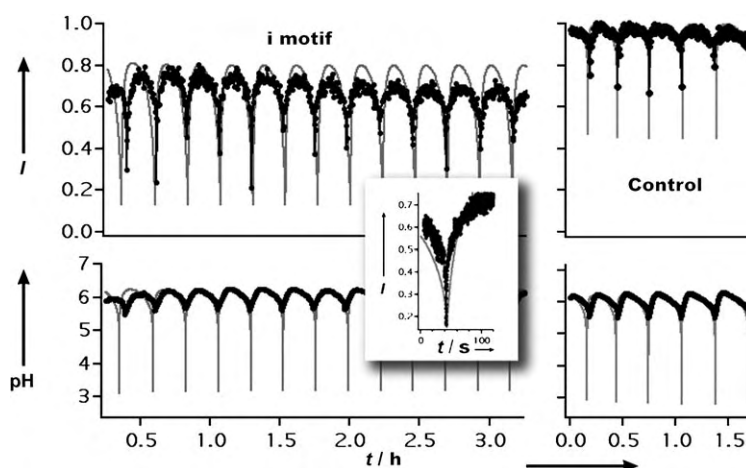


**Figure 3.** Left: In the CSTR setup, a large number of pH oscillations can be generated (bottom, black trace). The simultaneously recorded fluorescence intensity originating from the *i* motif bound to a gold/glass chip follows the pH oscillations (top, black trace). The simulated pH values (bottom, gray trace) coincide with the measured values except for regions where the low pH spikes occur. This deviation is caused by the slow response of the pH meter. The simulated fluorescence trace in the top graph (gray) is generated from data from a titration experiment (see the Supporting Information). Inset: In an experiment at higher time resolution it became apparent that the fluorescence intensity at the position of the low pH spikes indeed drops to 20% of its maximum value, as expected from the simulation. Right: Measured (bottom, black trace) and predicted (bottom, gray trace) pH oscillations and corresponding fluorescence intensity (top, black trace: experimental data, gray curve: calculated values) of the control strands. The fluorescence is normalized to the maximum value at pH 7.4 for both the device and control strand. In the case of the device strand, the *i* motif is already partly formed under the conditions of the oscillator, which results in a decreased fluorescence signal. The fluorescence values of both strands are in complete agreement with the titration experiments (see the Supporting Information), which shows that the strands essentially behave in the same way in the CSTR as under ordinary buffer conditions. The fluorescence of the device strand is consistent with its transition to the *i* motif, while the control strand does not show such a behavior.

that the immobilized DNA switches undergo a conformational change when the pH value is lowered below about 6.5, as expected (see the Supporting Information). A plot of the

fluorescence intensity obtained in the CSTR during the operation of the pH oscillator essentially shows the same transition (see the Supporting Information). By contrast, the immobilized control strands show a less pronounced response to pH changes, in particular no transition around pH 6 is observed. Accordingly, a different fluorescence trace is recorded when they are put under the influence of the oscillator (Figure 3). The fluorescence for the control strand only drops to about 50% of its maximum value, whereas the signal decreases to below 20% for the device strand. Both fluorescence traces are fully consistent with those obtained by conventional titration experiments, thus indicating that the immobilized DNA molecules undergo the same conformational changes when driven by the oscillator. It has to be noted, however, that when the pH is below 4 the fluorescence may not reflect conformational changes of the DNA alone, but can be influenced by a variety of other factors (see the Supporting information).

Simulated time traces of the pH oscillations based on a model developed by Rabai and Beck<sup>[10]</sup> are also shown in Figure 3. Experimentally obtained data agree well with the model's prediction at pH values above 5.5. However, the model also predicts sharp "spikes" down to pH values of about 3. In fact, these spikes also occur experimentally, but their short duration ( $t_{1/2} \approx 2$  s) means they cannot be resolved by our pH meter, which has a response time of 30 s. We independently checked the occurrence of the spikes at low pH values with the pH-sensitive dye methyl orange, which changes its color from yellow to pink at pH 4.4.<sup>[10]</sup> Indeed, during the operation of the oscillator we observed this color change for fractions of a second at the position of the low pH spikes. This also explains why we observe fluorescence values at the minima of the pH oscillations which are lower than those expected from the recorded pH values. For comparison, the upper panel of Figure 3 contains time traces calculated from the simulated pH values and the titration curves for DNA strand M and the control strand. The experimental intensities agree well with the simulated values, except that the experimental traces again do not follow the low intensity spikes. This is simply caused by "undersampling". Only a limited number of data points could be taken for observations over long times, because of excessive photobleaching, and therefore the spacing of the data points is not close enough to resolve the pH spikes. In the inset of Figure 3, a fluorescence trace recorded at a higher rate is shown which reproduces very well the predicted values. This also indicates that the response time of the immobilized switches is on the order of a second.

Further evidence for the formation of the i motif in the surface-bound DNA switches is obtained from temperature-dependent measurements: a sharp melting transition is observed for DNA switches immobilized on the chip surface and in solution, whereas no such transition is seen for the control strand (Figure 4). These observations are in agreement with previous circular dichroism studies on the i motif.<sup>[11]</sup>

In summary, a chemical oscillation generated in a continuous flow stirred tank reactor was utilized to periodically switch a DNA molecular structure immobilized on a

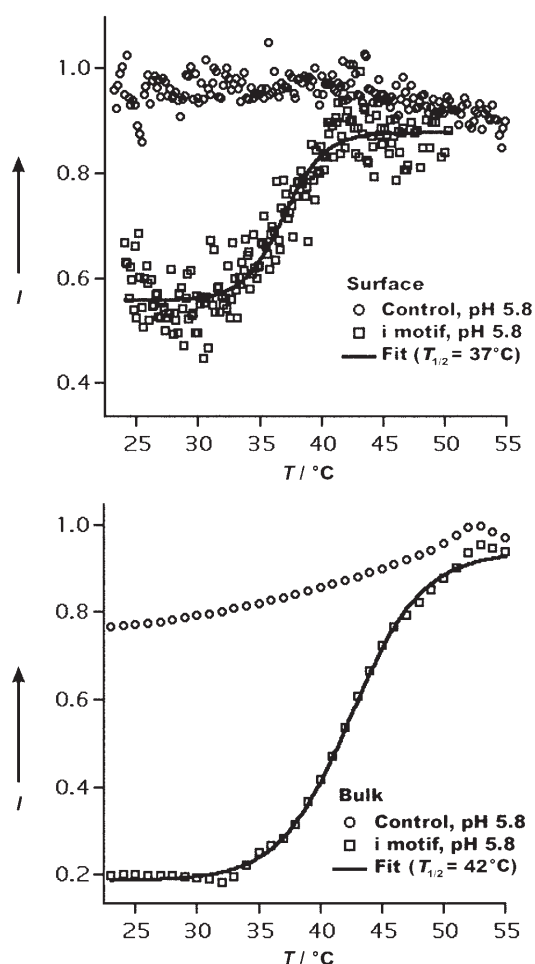


**Figure 4.** Fluorescence intensities of the i motif and the control strand in a melting experiment at pH 5.8 and comparison between surface-bound and solution-phase switches. Top: The surface-bound i motif unfolds at 37°C, while a surface-bound control strand does not show any change in fluorescence. Bottom: For the experiment in solution, the i motif strand labeled with a dye on one end and a quencher on the other end<sup>[10]</sup> displays essentially the same behavior and unfolds at a slightly higher temperature than on the surface. The control strand exhibits only a small change in the fluorescence in the solution experiment.

glass chip between two distinct conformations. In a CSTR, these oscillations occur with a regular period and can in principle occur infinitely often. To realize and characterize this molecular-switching system experimentally, the DNA oligonucleotides were immobilized on a glass surface covered with an ultrathin gold layer, which allowed characterization of the surface-bound switches within a CSTR in an epifluorescence setup. This system represents the first example of an autonomously driven DNA switch immobilized on a solid substrate. It was shown recently in a related study by Shu et al.<sup>[8b]</sup> that an immobilized DNA device based on the i motif can cyclically generate forces during the consumption of  $H^+$  ions and can thus even be construed as a periodically working motor. Such and similar systems may find application as actuators or sensors in biomolecular hybrid nanostructures. It is expected that surface-immobilized DNA switches could

also display spatiotemporal patterns and oscillations under the influence of chemical reaction waves.

Received: January 26, 2006

Revised: April 4, 2006

Published online: June 29, 2006

**Keywords:** chemical oscillations · DNA · molecular switches · nanotechnology

- 
- [1] a) N. C. Seeman, *Trends Biochem. Sci.* **2005**, *30*, 119–125; b) F. C. Simmel, W. U. Dittmer, *Small* **2005**, *1*, 284–299.
  - [2] a) P. Yin, H. Yan, X. G. Daniell, A. J. Turberfield, J. H. Reif, *Angew. Chem.* **2004**, *116*, 5014–5019; *Angew. Chem. Int. Ed.* **2004**, *43*, 4906–4911; ; b) J. Bath, S. J. Green, A. J. Turberfield, *Angew. Chem.* **2005**, *117*, 4432–4435; *Angew. Chem. Int. Ed.* **2005**, *44*, 4358–4361.
  - [3] a) Y. Chen, M. S. Wang, C. D. Mao, *Angew. Chem.* **2004**, *116*, 3638–3641; *Angew. Chem. Int. Ed.* **2004**, *43*, 3554–3557; b) Y. Tian, Y. He, Y. Chen, P. Yin, C. D. Mao, *Angew. Chem.* **2005**, *117*, 4429–4432; *Angew. Chem. Int. Ed.* **2005**, *44*, 4355–4358.
  - [4] a) Y. Benenson, T. Paz-Elizur, R. Adar, E. Keinan, Z. Livneh, E. Shapiro, *Nature* **2001**, *414*, 430–434; b) M. N. Stojanovic, D. Stefanovic, *Nat. Biotechnol.* **2003**, *21*, 1069–1074.
  - [5] A. J. Turberfield, J. C. Mitchell, B. Yurke, A. P. Mills, M. I. Blakey, F. C. Simmel, *Phys. Rev. Lett.* **2003**, *90*, 118102.
  - [6] T. Liedl, F. C. Simmel, *Nano Lett.* **2005**, *5*, 1894–1898.
  - [7] a) B. Dubertret, M. Calame, A. J. Libchaber, *Nat. Biotechnol.* **2001**, *19*, 365–370; b) H. Du, M. D. Disney, B. L. Miller, T. D. Krauss, *J. Am. Chem. Soc.* **2003**, *125*, 4012–4013; c) C. S. Yun, A. Javier, T. Jennings, M. Fisher, S. Hira, S. Peterson, B. Hopkins, N. O. Reich, G. F. Strouse, *J. Am. Chem. Soc.* **2005**, *127*, 3115–3119.
  - [8] a) D. S. Liu, S. Balasubramanian, *Angew. Chem.* **2003**, *115*, 5912–5914; *Angew. Chem. Int. Ed.* **2003**, *42*, 5734–5736; b) W. M. Shu, D. S. Liu, M. Watari, C. K. Riener, T. Strunz, M. E. Welland, S. Balasubramanian, R. A. McKendry, *J. Am. Chem. Soc.* **2005**, *127*, 17054–17060; c) D. Liu, A. Bruckbauer, C. Abell, S. Balasubramanian, D. Kang, D. Klenerman, D. Zhou, *J. Am. Chem. Soc.* **2006**, *128*, 2067–2071.
  - [9] K. Gehring, J. L. Leroy, M. Gueron, *Nature* **1993**, *363*, 561–565.
  - [10] a) G. Rabai, M. T. Beck, *J. Phys. Chem.* **1988**, *92*, 2804–2807; b) G. Rabai, M. T. Beck, *J. Phys. Chem.* **1988**, *92*, 4831–4835.
  - [11] G. Manzini, N. Yathindra, L. E. Xodo, *Nucleic Acids Res.* **1994**, *22*, 4634–4640.
-



DOI: 10.1002/anie.200600772

**Transition-Metal-Free Homocoupling of Organomagnesium Compounds\*\****Arkady Krasovskiy, Alexander Tishkov, Vicente del Amo, Herbert Mayr,\* and Paul Knochel\***Dedicated to Professor Siegfried Hünig on the occasion of his 85th birthday*

C–C coupling reactions are among the most powerful tools in modern organic chemistry.<sup>[1,2]</sup> For most types of cross-couplings, transition metals are required as mediators or catalysts.<sup>[3]</sup> Usually Cu<sup>I</sup> salts<sup>[4]</sup> (for Ullmann-type coupling reactions<sup>[5]</sup>), TiCl<sub>4</sub>,<sup>[6]</sup> or the addition of catalytic amounts of other transition metals is needed.<sup>[2,7]</sup> The importance of finding new catalytic systems<sup>[8]</sup> and using atmospheric oxygen<sup>[9]</sup> or its derivatives<sup>[10]</sup> for the performance of oxidation reactions is well-recognized. However, such oxidations are often unselective since they are governed by the chemistry of high-energy zwitterions, (di)radicals, or by electron-transfer reactions without stereochemical control.

Herein, we report a new concept which allows the performance of coupling reactions by using only main-group-metal derivatives. We have envisioned that the coordination of a main-group-metal center with a readily reducible ligand would function as an electron shuttle and would allow a reductive coupling to take place. Thus, the organic oxidant (Ox) converts the intermediate **A** to the key intermediate **B**, which can undergo an intramolecular redox process leading to C–C bond formation (oxidative coupling) and reduction of the ligand Ox, which is thereby converted into the reduced ligand (Red) by accepting two electrons (Scheme 1). The main-group metal keeps the same oxidation state during the entire process.

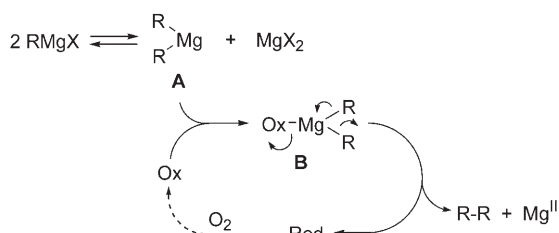
Thus, mono- and diorganomagnesium reagents that are complexed with lithium chloride<sup>[11]</sup> can be efficiently coupled by treatment with readily available 3,3',5,5'-tetra-*tert*-butyldi-phenoquinone (**1**),<sup>[12]</sup> which acts as a two-electron acceptor (Scheme 2 and Table 1).

[\*] Dr. A. Krasovskiy, Dr. A. Tishkov, Dr. V. del Amo, Prof. Dr. H. Mayr, Prof. Dr. P. Knochel  
Ludwig-Maximilians-Universität München  
Department Chemie und Biochemie  
Butenandtstrasse 5–13, Haus F, 81377 München (Germany)  
Fax: (+49) 89-21-80-776-80

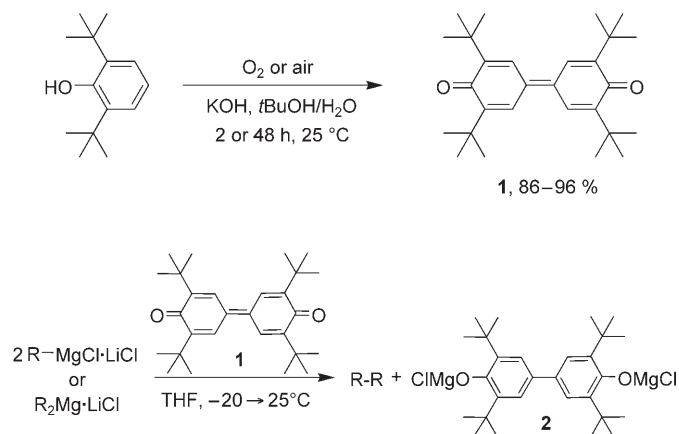
[\*\*] We thank the Fonds der Chemischen Industrie and Merck Research Laboratories (MSD) for financial support. We also thank V. Malakhov for the performance of some preliminary experiments as well as Chemetall GmbH (Frankfurt) and BASF AG (Ludwigshafen) for the generous gift of chemicals. V. del Amo thanks the Alexander von Humboldt Foundation for financial support.



Supporting information for this article is available on the WWW under <http://www.angewandte.org> or from the author.



**Scheme 1.** Coupling reactions of  $\text{Mg}^{\text{II}}$  reagents.



**Scheme 2.** Coupling of organomagnesium reagents with **1**.

The resulting biphenyldiolate **2** can be easily separated (>90% yield) from the reaction mixture by the addition of pentane and subsequent filtration. By oxidation of **2** with air, **1** can be recovered in nearly quantitative yield,<sup>[13]</sup> which makes this methodology especially attractive from ecological and economical standpoints.

The reaction of phenylmagnesium bromide with 0.5 equivalents of **1** at  $-20^\circ\text{C}$  led to the formation of biphenyl (**4a**; Table 1, entry 1) in quantitative yield. The reaction proceeded well with electron-rich (**3b**) and electron-poor (**3c**) arylmagnesium halides and afforded the corresponding biaryls **4b** and **4c**, respectively, in high yields (Table 1, entries 2 and 3). At low reaction temperature functionalized organomagnesium compounds that bear a nitrile (**3d**) or an ester group (**3e**) could be coupled in excellent yields (**4d** and **4e**; Table 1, entries 4 and 5). Functional groups in the *ortho* position do not disturb the reaction, and the corresponding *ortho,ortho'*-disubstituted biaryls **4f** and **4g** were formed in 85 and 88% yield, respectively (Table 1, entries 6 and 7). Even the sterically hindered *ortho-tert*-butyl- (**3h**) and mesitylmagnesium (**3i**) derivatives gave biaryls **4h** and **4i** in 83 and 88% yield, respectively (Table 1, entries 8 and 9). 1-Naphthylmagnesium reagents **3j** and **3k** are also suitable substrates and afforded the corresponding binaphthyls **4j** and **4k**, respectively, in good yields (Table 1, entries 10 and 11). Heterocyclic organomagnesium reagents could also be coupled by **1**. Thus, 5-bromopyridin-3-ylmagnesium chloride led to the corresponding dipyrindine **4l** in 80% yield (Table 1, entry 12). The organomagnesium reagent **3m**, which was generated from 1,1'-oxybis(2-iodobenzene), underwent selective intramolec-

**Table 1:** Formation of biaryls.

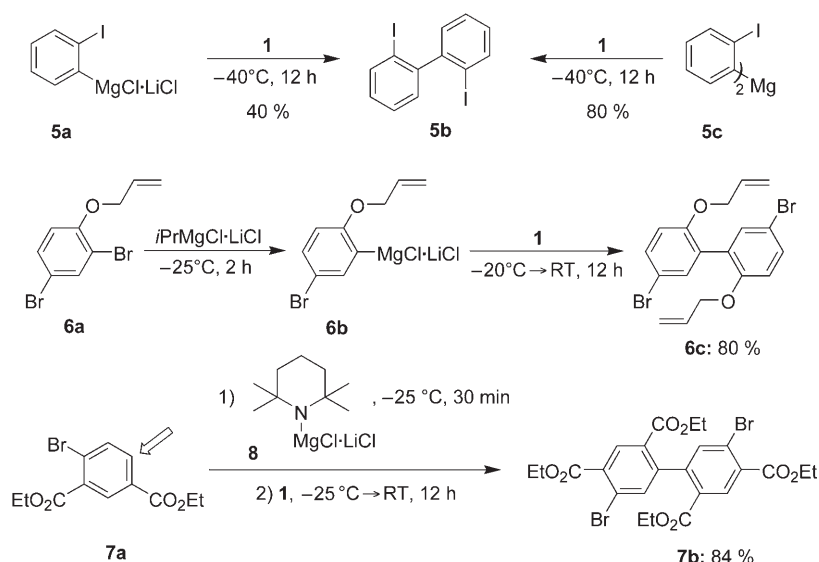
Entry	Grignard reagent	Biaryl ( <b>4</b> )	Yield [%] <sup>[a]</sup>
1	<b>3a</b> : FG = H, X = Br	<b>4a</b> : FG = H	96
2	<b>3b</b> : FG = MeO, X = Br	<b>4b</b> : FG = MeO	94
3	<b>3c</b> : FG = CF <sub>3</sub> , X = Cl	<b>4c</b> : FG = CF <sub>3</sub>	92
4	<b>3d</b> : FG = CN, X = Cl	<b>4d</b> : FG = CN	96
5	<b>3e</b> : FG = CO <sub>2</sub> Et, X = Cl	<b>4e</b> : FG = CO <sub>2</sub> Et	93
6	<b>3f</b> : FG = CN	<b>4f</b> : FG = CN	85
7	<b>3g</b> : FG = CO <sub>2</sub> Et	<b>4g</b> : FG = CO <sub>2</sub> Et	88
8	<b>3h</b> : FG = <i>t</i> Bu	<b>4h</b> : FG = <i>t</i> Bu	83
9	<b>3i</b>	<b>4i</b>	88
10	<b>3j</b> : FG = H	<b>4j</b> : FG = H	99
11	<b>3k</b> : FG = OMe	<b>4k</b> : FG = OMe	90
12	<b>3l</b>	<b>4l</b>	80
13	<b>3m</b>	<b>4m</b>	96

[a] Yield of isolated, analytically pure product.

ular coupling with quantitative formation of dibenzofuran (**4m**; Table 1, entry 13).

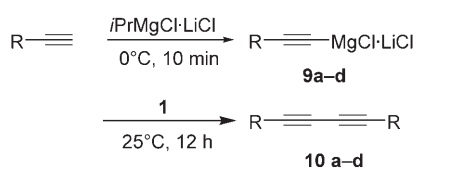
Although coupling of the *ortho*-iodophenyl Grignard reagent **5a** led only to a moderate yield of biaryl **5b**, compound **5b** was obtained in 80% yield when the diorganomagnesium reagent **5c** was used (Scheme 3). Coupling of the allyloxy-substituted organomagnesium reagent **6b**, which was prepared by selective Br/Mg exchange from the corresponding dibromide **6a** and *i*PrMgCl-LiCl,<sup>[14]</sup> gave rise to biaryl **6c**. We did not observe any ring-closure products arising from radical cyclization. The diester **7a** could be selectively deprotonated with the mixed Mg/Li base **8**<sup>[15]</sup> and coupled to form the highly substituted biaryl **7b**. This example shows that the presence of an NH group (2,2,6,6-tetramethylpiperidine) is tolerated.

We have also examined the coupling of alkynylmagnesium compounds, which are easily available by deprotonation of the corresponding acetylenes with *i*PrMgCl-LiCl. Although the Glaser coupling,<sup>[16]</sup> the Eglinton procedure,<sup>[17]</sup> and modifications thereof<sup>[18]</sup> are well-known, each of them necessitates the addition of a transition metal (usually Cu<sup>I</sup>) that requires subsequent recycling or disposal. Reactions of alkynylmagnesium reagents with **1** proceed cleanly with the formation of



**Scheme 3.** Formation of biaryls.

only the desired diacetylenes and easily recyclable **2**. Thus, phenyl- (**9a**), *n*-hexyl- (**9b**), trimethylsilyl- (**9c**), and cyclohexenylethynylmagnesium chloride (**9d**) react with **1** within 12 hours at 25°C to give the corresponding diynes **10a–d** in 80–90% yield (Scheme 4).



**a:** R = Ph, 80 %  
**b:** R = *n*-C<sub>6</sub>H<sub>13</sub>, 81 %  
**c:** R = SiMe<sub>3</sub>, 90 %  
**d:** R = , 88 %

**Scheme 4.** Formation of diynes.

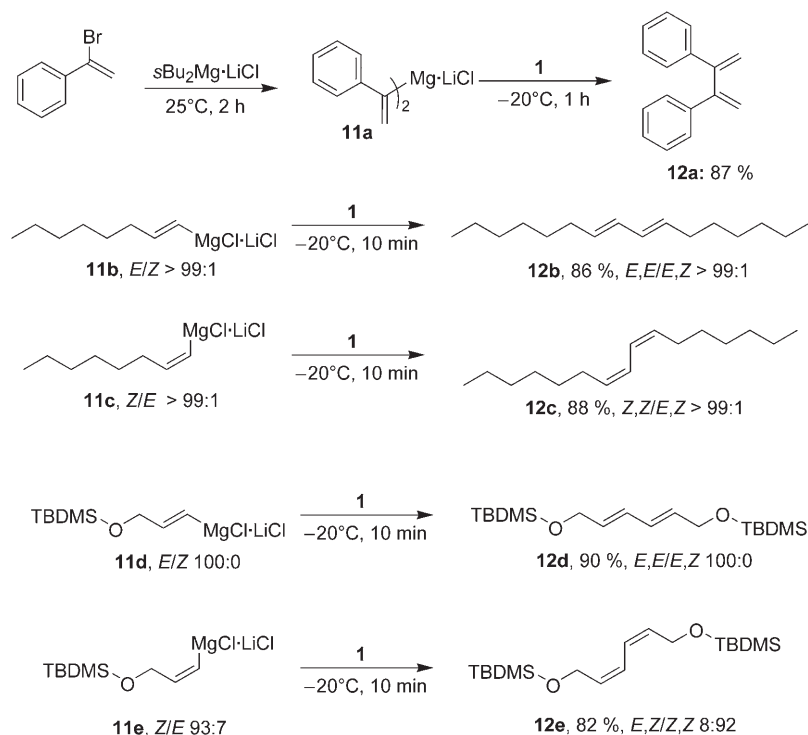
Alkenylmagnesium reagents also could be coupled in this way. Bis( $\alpha$ -styryl)magnesium (**11a**) reacted with **1** to afford 2,3-diphenyl-1,3-butadiene (**12a**) in 87% yield. Stereoselective couplings of terminal alkenes are of great interest since the resulting isomerically pure 1,3-dienes cannot be prepared by conventional Wittig reactions.<sup>[19]</sup> This methodology allows the coupling of *E*- (**11b**, **11d**) or *Z*-alkenylmagnesium reagents (**11c**, **11e**) with complete retention of the double-bond stereochemistry to afford the isomerically pure *E,E* (**12b**, **12d**) and *Z,Z* dienes (**12c**, **12e**), respectively (Scheme 5).

Interestingly, the coupling reaction could also be performed by using organozinc reagents. Thus, the reaction of 2,5-dibromothiophene (**13a**) with *i*PrMgCl-LiCl (25°C, 1 h) and subsequent transmetalation with ZnCl<sub>2</sub> produced the zinc reagent **13b**. The reaction of this thiophene–zinc species with

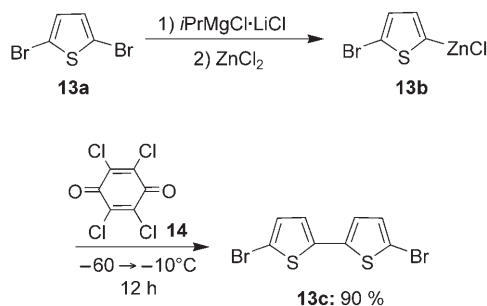
chloranil (**14**, 1.05 equiv,  $-60^{\circ}\text{C} \rightarrow -10^{\circ}\text{C}$ , 12 h) afforded the expected dimer **13c** in 90% yield (Scheme 6). The use of the zinc reagent in association with chloranil is complementary to the homocoupling of Grignard compounds, since attempts to perform the coupling with the Grignard reagent corresponding to **13b** and **1** did not lead to **13c**.

The mechanism of this reaction is still under investigation. By using a stopped-flow instrument with a UV/Vis detector, we were able to show that the interaction of **1** with Grignard reagents proceeds via the intermediate radical anion **1a** (Scheme 7).

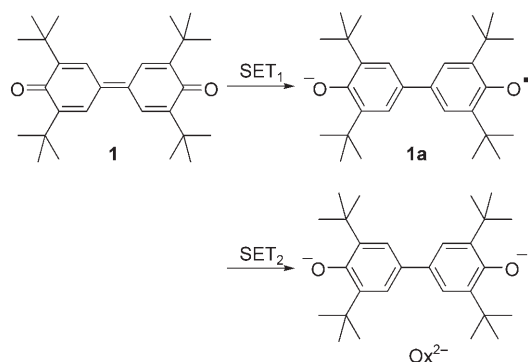
When **1** was mixed with a large excess of mesitylmagnesium bromide **3i**, the UV/Vis spectrum, which was taken 7 ms after mixing of the reagents, showed the complete consumption of **1** ( $\lambda_{\text{max}} = 423 \text{ nm}$ , Figure 1 b). A new species with an absorption maximum at  $\lambda_{\text{max}} = 459 \text{ nm}$  had appeared, which is assigned to **1a** (Scheme 7). Treatment of **1** with



**Scheme 5.** Stereoselective coupling of alkenylmagnesium reagents; TBDMS = *tert*-butyldimethylsilyl.



**Scheme 6.** Coupling of an organozinc compound.



**Scheme 7.** Stepwise reduction of **1** in the course of homocoupling of Grignard reagents; SET = single-electron transfer.

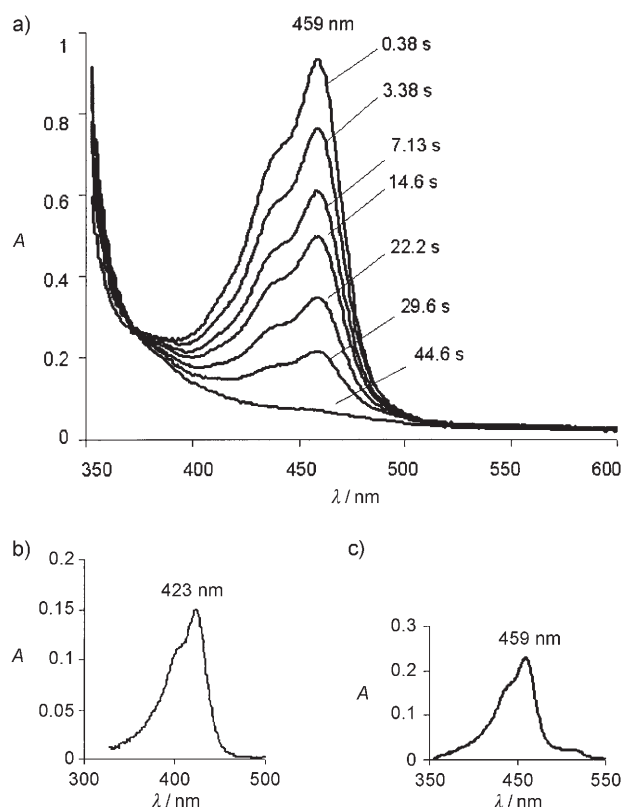


**Figure 1.** a) UV/Vis monitoring of the interaction of mesitylmagnesium bromide ( $c = 0.079$  M) with **1** ( $c = 1.25 \times 10^{-5}$  M). b) UV/Vis spectrum of **1** ( $c = 2.01 \times 10^{-6}$  M). c) UV/Vis spectrum of **1a**, obtained from the reduction of **1** ( $c = 5.12 \times 10^{-6}$  M) with Na in THF.

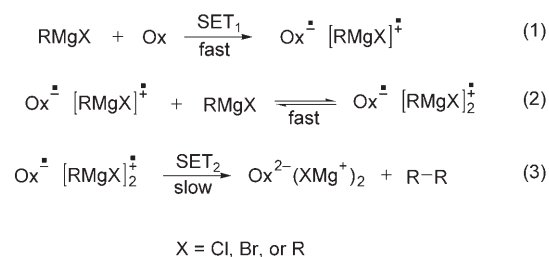
sodium metal in THF gave a green solution with a UV/Vis spectrum (Figure 1c) that was identical to that from the reaction of **1** with organomagnesium reagents (compare Figures 1a and 1c). Since both **1** and **1a** have previously been reported to have very similar absorption coefficients at  $\lambda_{\text{max}}$ ,<sup>[20]</sup> one can conclude that immediately after mixing, the concentration of **1a** is similar to the initial concentration of **1**.

In all cases studied, the formation of **1a** proceeded faster than the mixing of the reagents in the stopped-flow instrument. Assuming that the mixing time of the stopped-flow system (ca. 7 ms) corresponds to more than three half-lives of the substrate **1** in the presence of 0.08 M Grignard reagent, the

pseudo-first-order rate constant for SET<sub>1</sub> must be greater than  $300 \text{ s}^{-1}$ , thus corresponding to a second-order rate constant of greater than  $3700 \text{ M}^{-1} \text{ s}^{-1}$ . The consumption of **1a** is much slower and can be followed photometrically (Figure 1a). It was not possible, however, to find a simple rate law which describes SET<sub>2</sub> (Scheme 7).

The reaction of **1** ( $c = 1.25 \times 10^{-5}$  M) with 1-naphthylmagnesium bromide ( $c = 0.042$  M) also proceeded with immeasurably fast formation of **1a**, which disappeared within 3 s, which is much faster than in the corresponding experiment with mesitylmagnesium chloride (Figure 1). Since **1a**, generated from **1** and Na in THF, did not react with 1-naphthylmagnesium bromide, a mechanism in which the arylmagnesium reagents are oxidized by **1a** can be ruled out.<sup>[21]</sup>

The oxidation of the organomagnesium reagents does not yield a significant amount of free radicals as only traces of by-products, which emerge from the abstraction of H<sup>•</sup> from THF, are detected by GC–MS analysis of the crude reaction mixtures. Complete retention of the configuration of the C–C double bonds in the coupling of alkenylmagnesium reagents (Scheme 5) also indicates that free radicals are not involved in this homocoupling reaction. These findings are in line with the mechanism in Scheme 8.



**Scheme 8.** Mechanism of homocoupling of organomagnesium reagents; Ox = oxidizing agent, **1**.

The species that are formed by fast transfer of an electron from RMgX (or R<sub>2</sub>Mg) to **1** [Eq. (1)], Scheme 8) can be formally considered as radicals R<sup>•</sup> that are bound to the cationic magnesium center. The formation of analogous intermediates, in which the C–Mg bond is retained, was proposed in reactions of organomagnesium reagents with benzophenones and benzils.<sup>[22]</sup> These highly reactive species were reported to effect transfer of the R<sup>•</sup> group to a radical center of the reduced carbonyl group or form stable dimeric dications that contain two ketyl molecules as counterions.<sup>[23]</sup> Furthermore, it was reported that exchange of ligands in these intermediates (analogous to [Eq. (2)]) is fast and precedes the product-determining step.<sup>[24]</sup>

It is likely that the transfer of the R<sup>•</sup> group to the radical center of **1a** is hindered by the  $\alpha$ -tert-butyl groups. This hindrance may favor the consumption of the radical species through oxidative dimerization (SET<sub>2</sub>, [Eq. (3)]). Similar dimerization pathways that give rise to the formation of biaryls or biaryl anion radicals are known.<sup>[25]</sup>

In conclusion, we have shown that the use of 3,3',5,5'-tetra-tert-butylidiphenylquinone (**1**) as an electron acceptor allows a simple, high-yield preparation of a broad range of



functionalized biaryls, diynes, and dienes through coupling reactions of readily available organomagnesium reagents. The coupling of alkenylmagnesium reagents proceeds with high stereoselectivity. All of the reactions take place within a convenient range of temperatures ( $-20^{\circ}\text{C}$  to room temperature) and can be easily extended to large-scale preparations. We have performed for the first time an effective transition-metal-free coupling of a broad range of organomagnesium reagents by using a conceptually new process (Scheme 1). Extension of this work to other organometallic compounds, such as zinc reagents, has already been demonstrated (Scheme 6), and further such investigations are currently underway.

### Experimental Section

**Representative procedure:** Synthesis of **4e**: A dry and argon-flushed flask (10 mL), equipped with a magnetic stirrer and a septum, was charged with ethyl 4-iodobenzoate (552 mg, 2.0 mmol) in THF (2 mL). The reaction mixture was cooled to  $-20^{\circ}\text{C}$ , and  $i\text{PrMgCl}\cdot\text{LiCl}$  (2 mL, 1.05 M in THF, 2.1 mmol) was added dropwise. After 20 min at  $-20^{\circ}\text{C}$ , the I/Mg-exchange was complete (checked by GC analysis of reaction aliquots), and a solution of **1** (449 mg, 1.1 mmol) in THF (5 mL) was added dropwise. The reaction mixture was stirred for 2 h at  $0^{\circ}\text{C}$ . Conventional work up of the crude residue by flash chromatography (pentane/ $\text{CH}_2\text{Cl}_2$  1:1) yielded **4e** (184 mg, 93 %) as white crystals.

Received: February 28, 2006

Published online: July 3, 2006

**Keywords:** biaryls · C–C coupling · dienes · diynes · Grignard reagents

- [1] D. W. Knight in *Comprehensive Organic Synthesis*, Vol. 3 (Eds.: B. M. Trost, I. Fleming), Pergamon, Oxford, **1991**, chapt. 2.3.
- [2] *Metal-catalyzed Cross-coupling Reactions* (Eds.: F. Diederich, P. J. Stang), Wiley-VCH, Weinheim, **1998**.
- [3] a) J.-W. Cheng, F.-T. Luo, *Tetrahedron Lett.* **1988**, 29, 1293; b) S. K. Taylor, S. G. Bennett, K. J. Heinz, L. K. Lashley, *J. Org. Chem.* **1981**, 46, 2194; c) H. M. Relles, *J. Org. Chem.* **1969**, 34, 3687.
- [4] a) D. S. Surry, X. Su, D. J. Fox, V. Franckevicius, S. J. F. Macdonald, D. R. Spring, *Angew. Chem.* **2005**, 117, 1904; *Angew. Chem. Int. Ed.* **2005**, 44, 1870; b) Y. Miyake, M. Wu, M. J. Rahman, M. Iyoda, *Chem. Commun.* **2005**, 411.
- [5] a) F. Ullmann, J. Bielecki, *Ber. Dtsch. Chem. Ges.* **1901**, 34, 2174; b) P. E. Fanta, *Chem. Rev.* **1946**, 46, 139; c) P. E. Fanta, *Chem. Rev.* **1964**, 64, 613.
- [6] A. Inoue, K. Kitagawa, H. Shinokubo, K. Oshima, *Tetrahedron* **2000**, 56, 9601.
- [7] a) T. Nagano, T. Hayashi, *Org. Lett.* **2005**, 7, 491; b) G. Cahiez, C. Chaboche, F. Mahuteau-Betzer, M. Ahr, *Org. Lett.* **2005**, 7, 1943.
- [8] a) W. D. Jones, *Science* **2002**, 295, 289; b) J.-Y. Cho, M. K. Tse, D. Holmes, R. E. Maleczka, Jr., M. R. Smith III, *Science* **2002**, 295, 305.
- [9] S. Stahl, *Science* **2005**, 309, 1824.
- [10] A. Greer, *Science* **2003**, 302, 234.
- [11] Recently, we have found that mono- and diorganomagnesium reagents that are complexed with lithium chloride show exceptional reactivity towards electrophiles and can easily be prepared by I/Mg- or Br/Mg-exchange reactions; see: a) A. Krasovskiy, P. Knochel, *Angew. Chem.* **2004**, 116, 3396; *Angew. Chem. Int. Ed.* **2004**, 43, 3333; b) A. Krasovskiy, B. Straub, P. Knochel, *Angew. Chem.* **2006**, 118, 165; *Angew. Chem. Int. Ed.* **2006**, 45, 159; c) F. Kopp, A. Krasovskiy, P. Knochel, *Chem. Commun.* **2004**, 20, 2288; d) H. Ren, A. Krasovskiy, P. Knochel, *Org. Lett.* **2004**, 6, 4215; e) H. Ren, A. Krasovskiy, P. Knochel, *Chem. Commun.* **2005**, 4, 543.
- [12] M. S. Kharasch, B. S. Joshi, *J. Org. Chem.* **1957**, 22, 1439.
- [13] a) S. V. Bukharov, L. K. Fazlieva, N. A. Mukmeneva, R. M. Akhmadullin, V. I. Morozov, *Russ. J. Gen. Chem.* **2002**, 72, 1805; b) R. Rathore, E. Bosch, J. K. Kochi, *Tetrahedron Lett.* **1994**, 35, 1335.
- [14] A. L. J. Beckwith, W. B. Gara, *J. Chem. Soc. Perkin Trans. 2* **1975**, 795.
- [15] A. Krasovskiy, V. Krasovskaya, P. Knochel, *Angew. Chem.* **2006**, 118, 3024; *Angew. Chem. Int. Ed.* **2006**, 45, 2958.
- [16] a) C. Glaser, *Ber. Dtsch. Chem. Ges.* **1869**, 2, 422; b) C. Glaser, *Ber. Dtsch. Chem. Ges.* **1870**, 154, 159; c) G. W. Kabalka, L. Wang, R. M. Pagni, *Synlett* **2001**, 108.
- [17] a) G. Eglinton, A. R. Galbraith, *J. Chem. Soc.* **1959**, 889; b) R. Berschied, F. Vögtle, *Synthesis* **1992**, 58.
- [18] a) M. E. Krafft, C. Hirose, N. Dalal, C. Ramsey, A. Stieglman, *Tetrahedron Lett.* **2001**, 42, 7733; b) Y. Nishihara, K. Ikagashira, K. Hirabayashi, J.-i. Ando, A. Mori, T. Hiyama, *J. Org. Chem.* **2000**, 65, 1780; c) A. Lei, M. Srivastava, X. Zhang, *J. Org. Chem.* **2002**, 67, 1969; d) A. S. Hay, *J. Org. Chem.* **1962**, 27, 3320; e) G. E. Jones, D. A. Kendrick, A. B. Holmes, *Org. Synth.* **1987**, 65, 52; f) J. S. Yadav, B. V. S. Reddy, K. B. Reddy, K. U. Gayathri, A. R. Prasad, *Tetrahedron Lett.* **2003**, 44, 6493; g) C. H. Oh, V. R. Reddy, *Tetrahedron Lett.* **2004**, 45, 5221; h) I. J. S. Fairlamb, P. S. Bäuerlein, L. R. Marrison, J. M. Dickinson, *Chem. Commun.* **2003**, 632.
- [19] M. Arisawa, M. Yamaguchi, *Adv. Synth. Catal.* **2001**, 343, 27.
- [20] J. Zhou, A. Rieker, *J. Chem. Soc. Perkin Trans. 2* **1997**, 931.
- [21] M. Chanon, M. Rajzmann, F. Chanon, *Tetrahedron* **1990**, 46, 6193.
- [22] K. Maruyama, T. Katagiri, *J. Am. Chem. Soc.* **1986**, 108, 6263.
- [23] K. Maruyama, Y. Matano, T. Katagiri, *J. Phys. Org. Chem.* **1991**, 4, 501.
- [24] a) T. Holm, *J. Organomet. Chem.* **1971**, 29, C45; b) T. Holm, I. Crossland in *Grignard Reagents: New Developments* (Ed.: H. G. Richey, Jr.), Wiley, Chichester, **2000**.
- [25] T. L. Kurth, F. D. Lewis, C. M. Hattan, R. C. Reiter, C. D. Stevenson, *J. Am. Chem. Soc.* **2003**, 125, 1460.

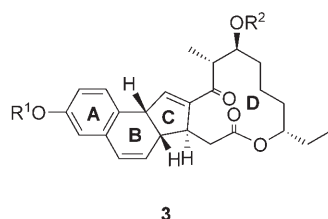
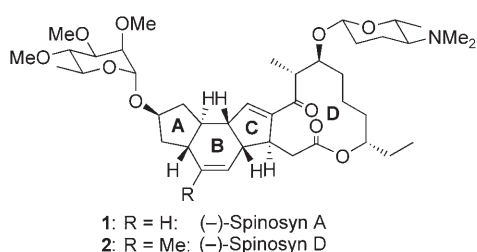
DOI: 10.1002/anie.200601003

# Multiple Palladium-Catalyzed Reactions for the Synthesis of Analogues of the Highly Potent Insecticide Spinosyn A\*\*

Lutz F. Tietze,\* Gordon Brasche, Christian Stadler, Alexander Grube, and Niels Böhnke

Dedicated to Professor Dieter Hoppe on the occasion of his 60th birthday

The natural product class of spinosyns comprises a group of more than 20 structurally related compounds that have been isolated from culture broths of the bacterium *Saccharopolyspora spinosa*.<sup>[1,2]</sup> These include spinosyn A (**1**) and D (**2**),



which are used world-wide in agriculture as extremely potent and highly selective insecticides<sup>[3]</sup> under the name Spinosad.<sup>[4]</sup> The spinosyns attack the neuronal activity of insects by a novel mechanism; interaction with the  $\gamma$ -aminobutyric acid (GABA) receptor plays a role, but it is the nicotinic acetylcholine receptors (n-AchR) that are mainly affected.<sup>[2a,5]</sup>

In 2000 the development of the first cases of resistance towards Spinosad was observed,<sup>[6]</sup> which has made the preparation of new, active spinosyn derivatives necessary.

[\*] Prof. Dr. L. F. Tietze, Dipl.-Chem. G. Brasche, Dipl.-Chem. C. Stadler, Dipl.-Chem. A. Grube, Dipl.-Chem. N. Böhnke  
Institut für Organische und Biomolekulare Chemie  
Georg-August-Universität Göttingen  
Tammannstrasse 2, 37077 Göttingen (Germany)  
Fax: +49 551-399476  
E-mail: ltietze@gwdg.de

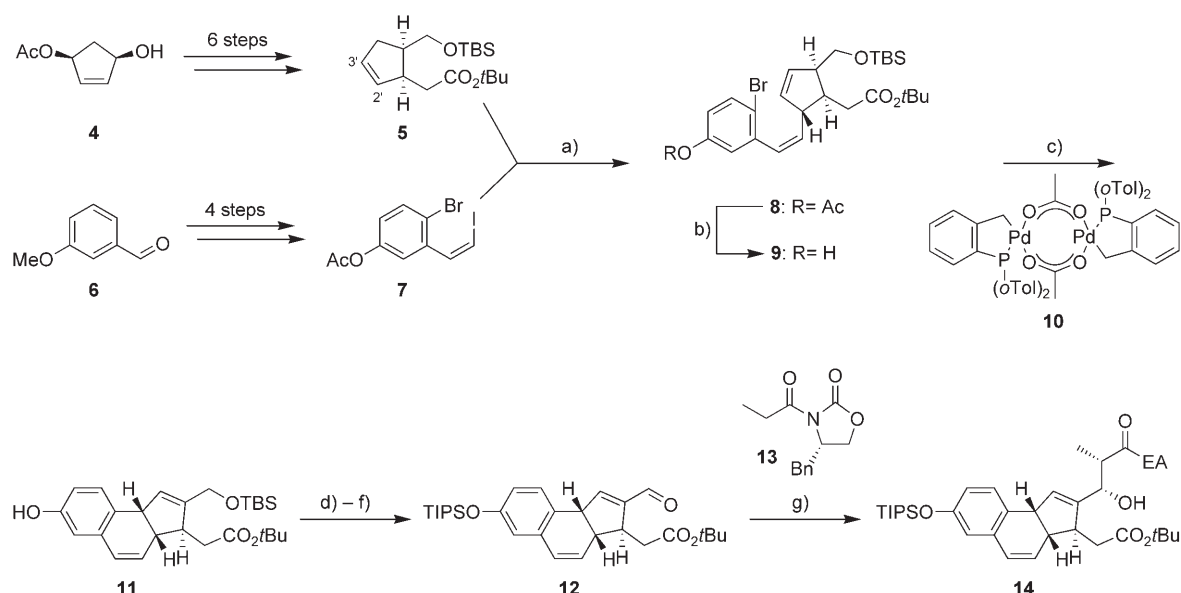
[\*\*] The investigations were supported by the Deutsche Forschungsgemeinschaft (SFB 416) and the Fonds der chemischen Industrie. We thank the companies BASF, Bayer, and Wacker-Chemie for gifts of chemicals.

The total syntheses of spinosyns<sup>[7]</sup> are, however, not very flexible, and are moreover very complex. Herein we report a convergent approach to the synthesis of structurally simplified analogues, such as **3**, which offers numerous variation possibilities and in whose key step ring B is constructed in a double Heck reaction.

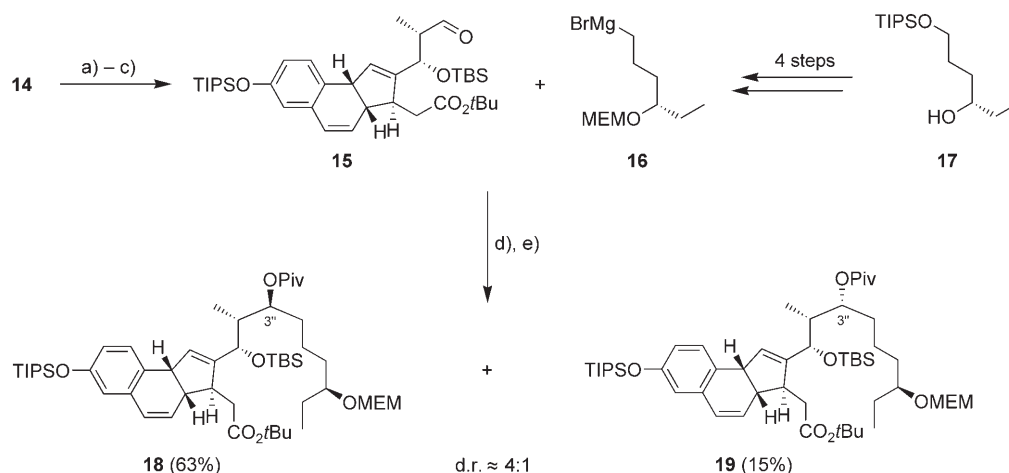
The decision to exchange the five-membered aliphatic ring A in **1** and **2** for a benzene ring was made on the basis of investigations into structure–activity relationships on **2**. It was shown that an additional C–C double bond in ring A of **2** hardly affects the biological activity, whereas in contrast, the *cis* linkage of rings B and C is important for insecticidal activity.<sup>[2]</sup> One strategy for the efficient construction of *cis*-annulated ring systems with the arrangement of the double bonds necessary in **3** comes from the double Heck reaction developed by us and first used in the total synthesis of estradiol.<sup>[8]</sup> As substrates for the synthesis of spinosyn analogues we used the bromoarene **7** (derived from 3-methoxybenzaldehyde (**6**)) with an iodovinyl side chain, and the enantiomerically pure cyclopentene derivative **5**, which was obtained in six steps starting from the monoacetate **4** (Scheme 1); **4** was accessible from 1,4-dihydroxycyclopentene with 99% *ee* by enzymatic acetylation.<sup>[9]</sup> The intermolecular Heck reaction of **5** and **7** with Pd(OAc)<sub>2</sub> in DMF provided the desired coupled product **8** diastereomerically pure in 51% yield.<sup>[10]</sup> A regioisomer of **5** with a coupling at the 3'-position and the corresponding compounds with an *E*-configured styrene double bond were isolated as further products. Carrying out the reaction at the unusually low temperature for Heck reactions of –25 °C gave the highest selectivity and yield. After cleavage of the acetate group, the tricyclic ring system **11** was constructed stereoselectively in 90% yield in an intramolecular Heck reaction with the cyclic palladium system **10**.<sup>[11,12]</sup> The *cis* connection of the rings in **11** was established by a NOESY-NMR spectroscopy experiment.

After protection of the phenolic hydroxy group in **11** as TIPS ether, cleavage of the TBS ether, and oxidation of the resulting primary alcohol the aldehyde **12** was obtained into which the C-3 fragment **13** was inserted as boron enolate in an Evans aldol addition.<sup>[13]</sup> The reaction took place with high diastereoselectivity, presumably through a closed six-membered transition state,<sup>[14]</sup> with exclusive formation of **14** in a yield of 89%. By use of a racemic mixture of aldehyde **12** in the aldol addition with **13**, two enantiomerically pure diastereoisomers were obtained as expected in a ratio of approximately 1:1 (in a total yield of 82%) and could be separated by chromatography on silica gel.

The secondary hydroxy group in **14** was then protected as a TBS ether and the imide converted into a primary alcohol with LiBH<sub>4</sub>/EtOH in Et<sub>2</sub>O (Scheme 2). Oxidation with Dess–Martin periodinane gave the aldehyde **15**. Reaction of **15** with the enantiomerically pure organomagnesium species **16** and subsequent transformation of the secondary alcohol thus formed into a pivaloyl ester provided the two coupled products **18** and **19** in a ratio of approximately 4:1 in a total yield of 78%. The preferred formation of diastereoisomer **18** with *S*-configuration at C-3' required for further synthesis can be explained by a Felkin–Anh transition state. Compound **16** can be prepared in four steps from the known alcohol **17**.<sup>[15]</sup>



**Scheme 1.** Synthesis of **14**: a) 5 Mol % Pd(OAc)<sub>2</sub>, 1.0 equiv. TBACl, 3.0 equiv. NaOAc, DMF, −25 °C, 6 days, 51%; b) 2.0 equiv. NaHCO<sub>3</sub>, MeOH, room temperature, 7 h, 99%; c) 7 Mol % **10**, 2.0 equiv. *n*Bu<sub>4</sub>NOAc, DMF/MeCN/H<sub>2</sub>O 5:5:1, 130 °C, 3.5 h, 90%; d) 1.5 equiv. TIPSOTf, 3.0 equiv. DMAP, CH<sub>2</sub>Cl<sub>2</sub>, 0 °C, 30 min, 96%; e) 10 mol % TsOH·H<sub>2</sub>O, MeOH, 0 °C, 4 h, 95%; f) 1.75 equiv. DMP, CH<sub>2</sub>Cl<sub>2</sub>, 0 °C, 2.5 h, 91%; g) 1.25 equiv. **13**, 1.3 equiv. *n*Bu<sub>2</sub>BOTf, 1.45 equiv. NEt<sub>3</sub>, CH<sub>2</sub>Cl<sub>2</sub>, −75 → −25 °C, 89%. TBS = *tert*-butyldimethylsilyl, TBACl = tetrabutylammonium chloride, *o*Tol = *ortho*-tolyl, TIPS = triisopropylsilyl, OTf = trifluoromethane sulfonate, DMAP = 4-dimethylaminopyridine, TsOH = toluene-4-sulfonic acid, DMP = Dess-Martin periodinane, Bn = benzyl, EA = Evans' auxiliary.



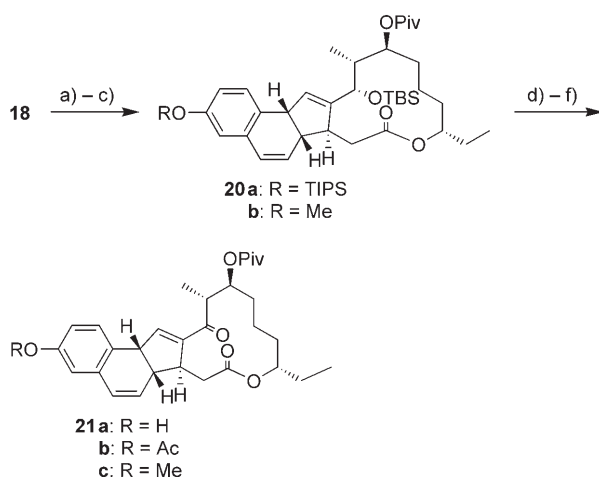
**Scheme 2.** Synthesis of **18**: a) 5.0 equiv. TBSOTf, 10 equiv. DMAP, CH<sub>2</sub>Cl<sub>2</sub>, room temperature, 20 h, 84%; b) 10 equiv. LiBH<sub>4</sub>, 20 equiv. EtOH, Et<sub>2</sub>O, room temperature, 15 min, 63%; c) 1.75 equiv. DMP, CH<sub>2</sub>Cl<sub>2</sub>, 0 °C, 2 h, 91%; d) 1.25 equiv. **16**, THF, −35 °C, 1.5 h; e) 10 equiv. PivCl, 1.0 equiv. DMAP, pyridine, 60 °C, 14 h, 63% (two steps). MEM = (2-methoxyethoxy)methyl, PivCl = pivaloyl chloride.

The MEM protecting group in **18** was removed with trimethylsilyl iodide (TMSI) prepared in situ, subsequently the *tert*-butyl ester group was cleaved with TMSOTf (Scheme 3). The hydroxy acid obtained was converted into the mixed anhydride with trichlorobenzoyl chloride (TCBzCl) by the method of Yamaguchi et al.,<sup>[16]</sup> from which the macrolactone **20a** was formed by slow addition to a solution of DMAP.

To conclude the synthesis of the analogues of Spinosyn-A aglycone the silyl protecting groups were cleaved and the enone unit constructed. The two silyl groups in **20a** were removed with HF·pyridine in pyridine at 60 °C. The subse-

quent oxidation of the secondary allylic alcohol by the method of Parikh and Doering<sup>[17]</sup> with SO<sub>3</sub>·pyridine in DMSO afforded the desired enone **21a** which, after protection of the phenolic hydroxy group as acetate **21b**, could be isolated over two steps in 34% yield. The low yield is attributed to the sensitivity of the phenolic hydroxy group towards oxidation. In contrast, by use of the methyl ether **20b** and DMP as the oxidizing agent the spinosyn analogue **21c** was obtained in 86% yield.

The synthesis described, with a double Heck reaction as the key step, allows rapid access to a structurally new spinosyn analogue. Future investigations will involve variation of



**Scheme 3.** Synthesis of the spinosyn analogues **21**: a) 4.0 equiv. TMSCl, 4.0 equiv. NaI, MeCN/CH<sub>2</sub>Cl<sub>2</sub> 4:1, -35°C, 1.5 h, 84%; b) 25 equiv. TMSOTf, 30 equiv. NEt<sub>3</sub>, THF, room temperature, 1 h; c) 4.0 equiv. TCBzCl, 6.0 equiv. NEt<sub>3</sub>, THF, room temperature, 1.5 h, then slow addition to 10 equiv. DMAP, toluene, 75°C, 5 h, 50% (two steps); **20a**: d) HF-pyridine/pyridine 1:3, 60°C, 14 h, 88%; e) 6.0 equiv. SO<sub>3</sub>-pyridine, 10 equiv. (iPr)<sub>2</sub>NEt, DMSO, room temperature, 1 h; f) 5.0 equiv. Ac<sub>2</sub>O, 10 equiv. NEt<sub>3</sub>, 0.5 equiv. DMAP, CH<sub>2</sub>Cl<sub>2</sub>, 0°C, 30 min, 34% **21b** (two steps); **20b**: d) HF-pyridine/pyridine 1:3, 60°C, 14 h, 91%; e) 1.5 equiv. DMP, CH<sub>2</sub>Cl<sub>2</sub>, room temperature, 20 min, 86% **21c**.

ring A, for example by use of five- and six-membered heteroarenes.

Received: March 14, 2006

Published online: July 3, 2006

**Keywords:** Heck reactions · macrocycles · palladium · plant protection agents · spinosyns

- [1] H. A. Kirst, K. H. Michel, J. W. Martin, L. C. Creemer, E. H. Chio, R. C. Yao, W. M. Nakatsukasa, L. V. D. Boeck, J. L. Occolowitz, J. W. Paschal, J. B. Deeter, N. D. Jones, G. D. Thompson, *Tetrahedron Lett.* **1991**, 32, 4839–4842.
- [2] Reviews: a) V. L. Salgado, T. C. Sparks in *Comprehensive Molecular Insect Science*, Vol. 6 (Eds.: L. J. Gilbert, K. Iatrou, S. S. Gill), Elsevier, Oxford, **2005**, p. 137–173; b) G. D. Crouse, T. C. Sparks, C. V. DeAmicis, H. A. Kirst, J. G. Martynow, L. C. Creemer, T. V. Worden, P. B. Anzeveno in *Pesticide Chemistry and Bioscience*, Vol. 233 (Eds.: G. T. Brooks, T. R. Roberts), RSC Special Publication, Royal Soc. Chem., Cambridge, **1999**, pp. 155–166.
- [3] a) T. C. Sparks, G. D. Thompson, H. A. Kirst, M. B. Hertlein, L. L. Larson, T. V. Worden, S. T. Thibault, *J. Econ. Entomol.* **1998**, 91, 1277–1283; b) G. D. Crouse, T. C. Sparks, *Rev. Toxicol.* **1998**, 2, 133–146.
- [4] H. Schmandke, *Ernährungs-Umschau* **2001**, 48, 402–406.
- [5] T. C. Sparks, G. D. Crouse, G. Durst, *Pest Manage. Sci.* **2001**, 57, 896–905.
- [6] a) A. H. Sayyed, D. Omar, D. J. Wright, *Pest Manage. Sci.* **2004**, 60, 827–832; b) T. Shono, J. G. Scott, *Pestic. Biochem. Physiol.* **2003**, 75, 1–7; c) C. F. Wyss, H. P. Young, J. Shukla, R. M. R. M. Roe, *Crop Prot.* **2003**, 22, 307–314; d) J.-Z. Zhao, Y.-X. Li, H. L. Collins, L. Gusukuma-Minuto, R. F. L. Mau, G. D. Thompson, A. M. Shelton, *J. Econ. Entomol.* **2002**, 95, 430–436; e) J. K. Moulton, D. A. Pepper, T. J. Dennehy, *Pest Manage. Sci.* **2000**, 56, 842–848.
- [7] a) D. J. Mergott, S. A. Frank, W. R. Roush, *Proc. Natl. Acad. Sci. USA* **2004**, 101, 11955–11959; b) L. A. Paquette, Z. Gao, Z. Ni, G. F. Smith, *J. Am. Chem. Soc.* **1998**, 120, 2543–2552; c) L. A. Paquette, I. Collado, M. Purdie, *J. Am. Chem. Soc.* **1998**, 120, 2553–2562; d) D. A. Evans, C. Black, *J. Am. Chem. Soc.* **1993**, 115, 4497–4513.
- [8] a) L. F. Tietze, M. Spescha, T. Nöbel, *J. Am. Chem. Soc.* **1998**, 120, 8971–8977; b) L. F. Tietze, M. Spescha, T. Nöbel, *Angew. Chem.* **1996**, 108, 2385–2386; *Angew. Chem. Int. Ed. Engl.* **1996**, 35, 2259–2261; for further work see: c) L. F. Tietze, L. P. Lücke, F. Major, P. Müller, *Aust. J. Chem.* **2004**, 57, 635–640; d) L. F. Tietze, W.-R. Krahnert, *Chem. Eur. J.* **2002**, 8, 2116–2125; e) L. F. Tietze, S. Petersen, *Eur. J. Org. Chem.* **2001**, 1619–1624.
- [9] F. Theil, H. Schick, G. Winter, G. Reck, *Tetrahedron Lett.* **1991**, 32, 7565–7582.
- [10] **8**: A degassed, light-protected solution of **7** (37 mg, 100 μmol) and **5** (82 mg, 250 μmol, 2.5 equiv.) in absolute DMF (1 mL) at -25°C under an argon atmosphere was treated with Pd(OAc)<sub>2</sub> (1.1 mg, 5 μmol, 5 mol %), NaOAc (25 mg, 300 μmol, 3.0 equiv.), and TBACl (28 mg, 100 μmol, 1.0 equiv.) and the mixture was stirred for 6 days at -25°C. The reaction mixture was taken up in Et<sub>2</sub>O (10 mL), washed with H<sub>2</sub>O (1 × 10 mL), and the aqueous phase then extracted with Et<sub>2</sub>O (2 × 10 mL). The combined organic extracts were then washed with saturated NaCl solution (1 × 20 mL), dried over Na<sub>2</sub>SO<sub>4</sub>, filtered, and the filtrate evaporated under reduced pressure. After preparative thin-layer chromatography (TLC; 1 plate, *n*-pentane(P)/ethyl acetate(E) 10:1) **8** (29 mg, 51 μmol, 51 %) was obtained as yellow oil. The regioisomer of **8** (14 mg, 25 μmol, 25 %, *R*<sub>f</sub> = 0.53 (P/EE 10:1)) and a fraction (11 mg, *R*<sub>f</sub> = 0.46 (P/EE 10:1)) which consisted to a large extent of the corresponding *E*-configured coupled products were isolated as further products. **8**: *R*<sub>f</sub> = 0.57 (P/EE 10:1); [*α*]<sub>D</sub><sup>20</sup> = -113.8° (*c* = 1.0 in CHCl<sub>3</sub>); UV (MeCN): λ<sub>max</sub>(lgε) = 194.5 (4.397), 213.0 nm (4.352); IR (Film): ν̄ = 2929, 1728, 1462, 1200 cm<sup>-1</sup>; <sup>1</sup>H NMR (300 MHz, CDCl<sub>3</sub>, 25°C TMS): δ = -0.06 (s, 3 H) and -0.04 (s, 3 H) (both Si(CH<sub>3</sub>)<sub>2</sub>), 0.77 (s, 9 H; Si(C(CH<sub>3</sub>)<sub>3</sub>)), 1.42 (s, 9 H; CO<sub>2</sub>(C(CH<sub>3</sub>)<sub>3</sub>)), 2.28 (s, 3 H; OC(O)CH<sub>3</sub>), 2.30–2.50 (m, 3 H; 2'-H, 1'-H), 2.81–2.90 (m, 1 H; 5'-H), 3.25–3.37 (m, 1 H; 2''-H), 3.54 (d, *J* = 4.5 Hz, 2 H; 5'-CH<sub>2</sub>-OTBS), 5.51 (t, *J* = 11.0 Hz, 1 H; 1''-H), 5.62–5.68 (m, 1 H) and 5.74–5.81 (m, 1 H) (3'-H, 4'-H), 6.45 (d, *J* = 11.4 Hz, 1 H; 2''-H), 6.88 (dd, *J* = 8.6, 2.6 Hz, 1 H; 4'''-H), 6.97 (d, *J* = 2.7 Hz, 1 H; 6'''-H), 7.54 ppm (d, *J* = 8.4 Hz, 1 H; 3'''-H); <sup>13</sup>C NMR (50 MHz, CDCl<sub>3</sub>, 25°C): δ = -5.7, -5.6 (Si(CH<sub>3</sub>)<sub>2</sub>), 18.0 (Si(C(CH<sub>3</sub>)<sub>3</sub>)), 21.1 (OC(O)CH<sub>3</sub>), 25.7 (Si(C(CH<sub>3</sub>)<sub>3</sub>)), 28.0 (CO<sub>2</sub>(C(CH<sub>3</sub>)<sub>3</sub>)), 34.6 (C-2), 44.7 (C-1'), 48.7 (C-5'), 49.4 (C-2'), 62.5 (C-5'-CH<sub>2</sub>-OTBS), 80.1 (CO<sub>2</sub>(C(CH<sub>3</sub>)<sub>3</sub>)), 120.4 (C-2''), 121.6 (C-4''), 123.5 (C-6''), 129.2 (C-2'), 133.2 (C-3''), 134.0, 134.1 (C-3', C-4'), 137.0 (C-1''), 138.7 (C-1'''), 149.4 (C-5''), 169.0, 172.9 ppm (C-1, OC(O)CH<sub>3</sub>); MS (DCI): *m/z* (%): 584.3 (42) [*M*+NH<sub>4</sub>]<sup>+</sup>, 567.3 (100) [*M*+H]<sup>+</sup>; HRMS (ESI): calcd for [*M*+Na]<sup>+</sup>: 587.17988; found: 587.17989; Elemental analysis (%) calcd for C<sub>28</sub>H<sub>41</sub>BrO<sub>5</sub>Si (565.61): C 59.46, H 7.31; found: C 59.60, H 7.23.
- [11] W. A. Herrmann, C. Broßmer, K. Öfele, C.-P. Reisinger, T. Priermeier, M. Beller, H. Fischer, *Angew. Chem.* **1995**, 107, 1989–1992; *Angew. Chem. Int. Ed. Engl.* **1995**, 34, 1844–1848.
- [12] **11**: A degassed mixture of **9** (4.55 g, 8.69 mmol), **10** (572 mg, 610 μmol, 7 mol %), and *n*Bu<sub>4</sub>NOAc (3.31 g, 17.4 mmol, 2.0 equiv.) in DMF/MeCN/H<sub>2</sub>O (220 mL, 5:5:1) was heated for 3.5 h in an oil bath pre-heated to 130°C under an argon atmosphere and with the exclusion of light. After cooling to room temperature Et<sub>2</sub>O (150 mL) and H<sub>2</sub>O (250 mL) were added after which the organic phase was separated and the aqueous phase extracted with Et<sub>2</sub>O (2 × 150 mL). The combined organic phases were dried over MgSO<sub>4</sub>, filtered, and the filtrate



evaporated under reduced pressure. After column chromatography on SiO<sub>2</sub> (60 g, 4.5 × 8 cm, P/Et<sub>2</sub>O 5:1) **11** was obtained as a yellow oil (3.45 g, 7.79 mmol, 90%). *R*<sub>f</sub> = 0.23 (P/EE 10:1); [ $\alpha$ ]<sub>D</sub><sup>20</sup> = −126.2° (*c* = 1.0 in CHCl<sub>3</sub>); UV (MeCN):  $\lambda_{\text{max}}$ (lg $\epsilon$ ) = 227.5 (4.425), 256.5 (3.656), 265.0 (3.735), 275.0 (3.668), 303.0 (3.368), 313.0 nm (3.307); IR (Film):  $\tilde{\nu}$  = 3392, 2929, 1727, 1462 cm<sup>−1</sup>; <sup>1</sup>H NMR (300 MHz, CDCl<sub>3</sub>, 25 °C TMS):  $\delta$  = 0.03 (s, 6H; Si(CH<sub>3</sub>)<sub>2</sub>), 0.88 (s, 9H; Si(C(CH<sub>3</sub>)<sub>3</sub>)), 1.47 (s, 9H; CO<sub>2</sub>(C(CH<sub>3</sub>)<sub>3</sub>)), 2.29 (dd, *J* = 15.3, 9.9 Hz, 1H; 2-H<sub>B</sub>), 2.61 (dd, *J* = 15.2, 4.4 Hz, 1H; 2-H<sub>A</sub>), 2.94–3.04 (m, 1H; 3'-H), 3.09 (m, 1H; 3a'-H), 4.02 (m, 1H; 9b'-H), 4.20 (s, 2H; 5'-CH<sub>2</sub>-OTBS), 5.38–5.45 (m, 2H; 1'-H, OH), 5.71 (dd, *J* = 9.8, 3.2 Hz, 1H; 4'-H), 6.18 (dd, *J* = 9.8, 2.0 Hz, 1H; 5'-H), 6.46 (d, *J* = 2.7 Hz, 1H; 6'-H), 6.62 (dd, *J* = 8.1, 2.7 Hz, 1H; 8'-H), 6.95 ppm (d, *J* = 8.1 Hz, 1H; 9'-H); <sup>13</sup>C NMR (75 MHz, CDCl<sub>3</sub>, 25 °C):  $\delta$  = −5.4, −5.4 (Si(CH<sub>3</sub>)<sub>2</sub>), 18.3 (Si(C(CH<sub>3</sub>)<sub>3</sub>)), 25.9 (Si(C(CH<sub>3</sub>)<sub>3</sub>)), 28.1 (CO<sub>2</sub>(C(CH<sub>3</sub>)<sub>3</sub>)), 39.3 (C-2), 44.2, 44.6 (C-3a', C-9b'), 50.5 (C-3'), 61.1 (C-

5'-CH<sub>2</sub>-OTBS), 80.7 (CO<sub>2</sub>(C(CH<sub>3</sub>)<sub>3</sub>)), 113.5, 114.0 (C-6', C-8'), 125.4 (C-5'), 126.7 (C-9a'), 128.9 (C-9'), 129.1 (C-1'), 131.9 (C-4'), 133.1 (C-5a'), 144.2 (C-2'), 154.3 (C-7'), 172.4 ppm (C-1); MS (ESI): *m/z* (%) = 467.1 (8), 466.2 (30), 465.2 (100) [*M*+Na]<sup>+</sup>; HRMS (ESI): calcd for [*M*+H]<sup>+</sup>: 443.26121; found: 443.26129; C<sub>26</sub>H<sub>38</sub>O<sub>4</sub>Si (442.66).

- [13] D. A. Evans, J. M. Takacs, L. R. McGee, M. D. Ennis, D. J. Mathre, J. Bartoli, *Pure Appl. Chem.* **1981**, 53, 1109–1127.
- [14] H. Danda, M. M. Hansen, C. H. Heathcock, *J. Org. Chem.* **1990**, 55, 173–181.
- [15] P. Knochel, W. Brieden, M. J. Rozema, C. Eisenberg, *Tetrahedron Lett.* **1993**, 34, 5881–5884.
- [16] J. Inanaga, K. Hirata, H. Saeki, T. Katsuki, M. Yamaguchi, *Bull. Chem. Soc. Jpn.* **1979**, 52, 1989–1993.
- [17] J. P. Parikh, W. E. Doering, *J. Am. Chem. Soc.* **1967**, 89, 5505–5507.